The Eurasia Proceedings of Science, Technology, Engineering & Mathematics

EPSTEM

VOLUME 28 ICBASET CONFERENCE

ISSN: 2602-3199
ISBN: 978-625-6959-38-5

ICBASET 2024: 4th International Conference on Basic Sciences, Engineering and Technology (ICBASET)
May 02 - 05, 2024 Alanya, Turkey
Edited by: Prof.Dr. Mehmet Ozaslan - Gaziantep University, Turkey

The Eurasia Proceedings of Science, Technology, Engineering & Mathematics (EPSTEM)
ISSN: 2602-3199

ICBASET 2024

International Conference on Basic Sciences, Engineering and Technology (ICBASET)

Proceedings Book

Editor

Mehmet Ozaslan
Gaziantep University, Turkey

ISBN: 978-625-6959-38-5

Published by the ISRES Publishing

Address: Askan Mah. Akinbey Sok. No: 5-A/Konya/TURKEY

Web: www.isres.org

Contact: isrespublishing@gmail.com

Dates: May 02 - 05, 2024

Location: Alanya, Turkey

https://www.2024.icbaset.net

About Editor

Prof Dr. Mehmet Ozaslan
Department of Biology, Gaziantep University, Turkey
Website: mehmetozaslan.com
E-mail: ozaslanmd@gantep.edu.tr

Language Editor

Lecturer Ceren Dogan
School of Foreign Languages, Necmettin Erbakan University, Turkey
Email: cerendogan@erbakan.edu.tr

CONFERENCE PRESIDENT

Prof. Dr. Mehmet Özaslan - Gaziantep University, Turkey
Prof. Dr. Csaba Antonya - Transilvania University of Brasov, Romania

SCIENTIFIC BOARD

Besnik Hajdari - University "isa Boletini" Mitrovica, Kosovo
Bogdan Patrut - Alexandru Ioan Cuza Üniversitesi, Romania
Chalavadi Sulochana - Gulbarga University, India
Csaba Antonya - Transilvania University of Brasov, Romania
Dariusz Jacek Jakobczak - Technical University of Koszalin, Poland
Dehini Rachid - University of Bechar, Algeria
Eleonora Guseinoviene - Klaipeda University, Lithuania
Elena Krelja Kurelovic - Polytechnic of Rijeka, Croatia
Elżbieta Patkowska - University of Life Sciences in Lublin, Poland
Eva Trnova - Masaryk University, Czech Republic
Farhad Balash - Kharazmi University, Iran
Fundime Miri - University of Tirana, Albania
Gabriel Delgado-Toral - Universidad Nacional Autónoma de México, Mexico
Gordana Savic - University of Belgrade, Serbia
Hasan Mlinaku, VUZF, Sofia in Bulgaria
Ibrahim Krasniqi - University of Peja, Kosovo
Irina Andreeva - Peter The Great St. Petersburg Polytechnic University, Russia
Isti Hidayah - Semarang State University, Indonesia
Jose Manuel Lopez Guede - University of Basque Country, Spain
Kamil Yurtkan - Cyprus International University, Cyprus
Katsina Christopher Bala - Federal University of Technology, Minna, Nigeria
Khitam Shraim - Palestine Technical University, Palestine
Marija Stanic - University of Kragujevac, Serbia
M. Hanefi Calp - Karadeniz Technical University, Turkey
Mohamed Ahmed - Mansoura University, Egypt
Mousa Attom- American University of Sharjah, U.A.E.
Nicu Bızon - Pitesti University, Romania
Pandian Vasant - Teknology Petronas University, Romania
Rajnalkar Laxman - Gulbarga University, India
Sanaa Al-Delaımy - Mosul University, Iraq
Shadi Aljawarneh - Jordan University of Science and Technology, Jordan
Shynar Baımaganbetova - Nazarbayev University, Kazakhstan
Svetlana Khan - Almaty University of Power Engineering and Telecommunications, Kazakhstan
Yiyang Chen - Soochow University (CN), China
Zairi Ismael Rizman - MARA University of Technology, Malaysia
Zipporah Pewat Duguryil - Federal College of Education, Nigeria

ORGANIZING COMMITTEE

Besnik Hajdari - University "isa Boletini" Mitrovica, Kosovo
Cemil Aydogdu - Hacettepe University, Türkiye
Csaba Antonya - Transilvania University of Brasov, Romania
Danielle Gonçalves de Oliveira Prado-Federal Technological University of Paraná, Brazil

Editorial Policies

ISRES Publishing follows the steps below in the procedings book publishing process.
In the first stage, the papers sent to the conferences organized by ISRES are subject to editorial oversight. In the second stage, the papers that pass the first step are reviewed by at least two international field experts in the conference committee in terms of suitability for the content and subject area. In the third stage, it is reviewed by at least one member of the organizing committee for the suitability of references. In the fourth step, the language editor reviews the language for clarity.

Review Process

Abstracts and full-text reports uploaded to the conference system undergo a review procedure. Abstracts will be evaluated on the basis of abstracts/proposals. The conference system allows the full text to be sent if the abstract is accepted. Participants must wait for the evaluation results after uploading their article abstracts to the conference system. If their abstracts are accepted, they can upload their full texts to the conference system. The full texts are then sent to at least two reviewers for review. The conference has a double-blind peer-review process. Any paper submitted for the conference is reviewed by at least two international reviewers with expertise in the relevant subject area. Based on the reviewers' comments, papers are accepted, rejected or accepted with revision. If the comments are not addressed well in the improved paper, then the paper is sent back to the authors to make further revisions. The accepted papers are formatted by the conference for publication in the proceedings.

Aims & Scope

Engineering, technology and basic sciences are closely related fields. Developments and innovations in one of them affect the others. Therefore, the focus of the conference is on studies related to these three fields. Studies in the fields of engineering, technology and basic science are accepted to the conference even if they are not associated with other fields. The conference committee thinks that a study in only one field (for example, mathematics, physics, etc.) will contribute to other fields (for example, engineering, technology, etc.) in future studies, even if it is not associated with the presentation at the conference. In line with this perspective, studies in the following fields are accepted to the conference: Biology, Chemistry, Engineering, Mathematics, Physics and Technology.

The aim of the conference is to bring together researchers and administrators from different countries, and to discuss theoretical and practical issues in all fields of Engineering, Technology and Basic Sciences.

The Eurasia Proceedings of Science, Technology, Engineering & Mathematics (EPSTEM)
ISSN: 2602-3199

Articles: 1- 63

CONTENTS

The Eurasia Proceedings of Science, Technology, Engineering & Mathematics (EPSTEM)
ISSN: 2602-3199

The Eurasia Proceedings of Science, Technology, Engineering & Mathematics (EPSTEM), 2024

Volume 28, Pages 1-13

ICBASET 2024: International Conference on Basic Sciences, Engineering and Technology

Web Server Support of Multiple Controllers Data Transfer in IoT Network

Maja Kukusheva-Paneva
Goce Delcev University

Todor Chekerovski
Goce Delcev University

Sara Stefanova
Damilah, Skopje

Goce Stefanov
Goce Delcev University

Abstract: In this paper a solution with a method for enabling data transfer among three remote industrial plants is represented. In particular, it examines the connectivity of three remote industrial plants within IoT network. Each plant is equipped with a WIFI controller along with corresponding hardware components including sensors and actuators. The sensors monitor conditions and signals when change occurs, while an actuator receives a signal and performs an action. Data that is generated by these sensors and actuators is transmitted via the controllers and consolidated onto a common single channel hosted in a designated WEB server. The setup enables the data that is collected from two controllers, designated as MASTER 1 and MASTER 2 stations, to be consolidated and accessed through a single controller referred to as SLAVE station. Within the SLAVE station, real- time visualization of the data is enabled and also, the results can be presented on SCADA screen.

Keywords: Multi controller, Transfer data, WEB Server, IoT network

Introduction

To enhance production capacities, industrial companies must follow the modern trends of technological and technical achievements. This entails the incorporation of automation systems into their production process. For newly established production companies, this requirement is critical for ensuring their successful operation. However, a significant challenge arises in upgrading automated systems in existing companies where such systems are either absent or are operating at low level. Nevertheless, implementing automation systems of the production process in a company promises both increased production efficiency and improved performance of working machines. This improvement is reflected in terms of energy saving, as well as in timely and accurate monitoring of production device parameters, (Bennett, 1982; Hor, 2005; Automation Community, 2023).

In today's industrial companies, machinery and devices are typically located within a single geographical location. However, some devices there are working machines and devices that are located in one territorial location, but also devices that are spatially distant from the main plant and are an inseparable part of the production process. Often these remote plants are located far from intra and internet network of the production companies. Therefore, there arises a necessity to automate and connect these plants into the company's intranet and more widely into the Internet of Things (IoT) network.

Automation, control, management, and monitoring processes are of exceptional importance, perticulary in industrial use. Efforts are made to ensure more reliable and simpler work, especially for operators who directly oversee the industrial processes' functionality. This approach to work is made possible by the so-called SCADA (**S**upervisory **C**ontrol and **D**ata **A**cquisition) system, (Myomron, n.d.). Moreover, a modern industrial process control system of an industrial process is fully rounded if, in addition to SCADA, it is also connected to an IoT network. Such a concept enables process data to be transferred to any location, real-time visualizatio, and storege on a cloud-based platform.

In many instances, standalone industrial processes may function as separate entities, often located far from the intranet and Internet networks of the manufacturing companies. Therefore, data distribution from sensors and actuators, monitoring various parameters such as voltage, current, pressure, flow, temperature, LEDs, relay, etc., must be made from these remote entities to the master station via wireless communication, (Stefanov, 2021), most likely a radio frequency (RF) connection, (Hosseini, 2021; Stefanov, 2023).

In this paper, a prototype of an automated system that integrates appropriate hardware components from three different production processes located at different spatial locations is represented.

Design on Web Server Support Multiple Controller Data Transfer in IoT Network

The primary tool utilized in the solution enables data transfer to the three remote hardware components through Web Server. Each of the three hardware components is connected to the same channel on the Web Server. Figure 1 illustrates a block diagram of an implementation of a Web Server Support Multiple Controller in IoT network.

Web Server Support system enables data transfer between MASTER A, MASTER B and SLAVE stations. These three stations are installed in three geographically distant locations and communicate with each other through common channel on the Web Server. The solution uses Web Server Blynk cloud. In the designed prototype, switches and LEDs serve as sensors and actuators to verify the correct operation of the solution. In all three stations nodeMCU 8266-12E microcomputers units along with appropriate hardwer componets are installed, (ESP8266). Additionally, the microcontroller in MASTER A station is connected to an AtMega 328P microcontroller on nano Arduino board, (Microchip, n.d.). This microcontroller facilitates the connection to a SCADA screen supported by the CX-Supervisor SCADA system developed by Omron, (Myomron, n.d.). Furthermore, the MASTER A station incorporates a humidity and temperature sensor, implemented with DHT22 module, and is used to generate a digital signal. A 0-5 V voltage sensor signal is used to generate an analog signal, implemented through a potentiometer. LED D6 simulates a digital output signal in the MASTER A station.

In the MASTER B station NodeMCU 8266-12E is also used. Hardware components include a digital signal from the humidity and temperature sensor DHT22 and an analog signal from MQ7 sensor for measuring CO concentration. These signal values are displayed on both serial monitor and on an LCD display. In the SLAVE station, all signals from MASTER A and MASTER B stations are accumulated. The values of these signals are displayed on both a serial monitor and on an LCD display. To verify the proper connection between Blynk cloud SCADA and the SCADA on MASTER A, built-in LEDs are incorporated on outputs D3 and D5 in the SLAVE station. The LED on output D3 verifies the connection with a switch from the SCADA screen of the MASTER A station, while the D5 LED verifies the connection with the Blink switch from the Blynk cloud SCADA and the IoT smart device.

The Blynk Cloud Web server, as previously mentioned, serves as the central hub for the entire system. Figure 1 illustrates the connection of SCADA Blynk Cloud and an IoT smart device to the Web server. The SCADA Blynk Cloud allows for real-time visualization of the measured values from the three measuring points on its screen, as well as logging of these values, (Dashboard). Additionally, the IoT smart device enables access and management of the system from any location with an IoT network signal using mobile device.

The final conclusion drawn from the New Server support system is that the measured values from the three measuring points at different locations are effectively collected, visualized and stored on two SCADA systems: SCADA screen on CX-Supervisor and SCADA Blynk cloud. Furthermore, the system enables control over its signal from any measuring point, (Santos, 2019; Lightbluecrab, 2019).

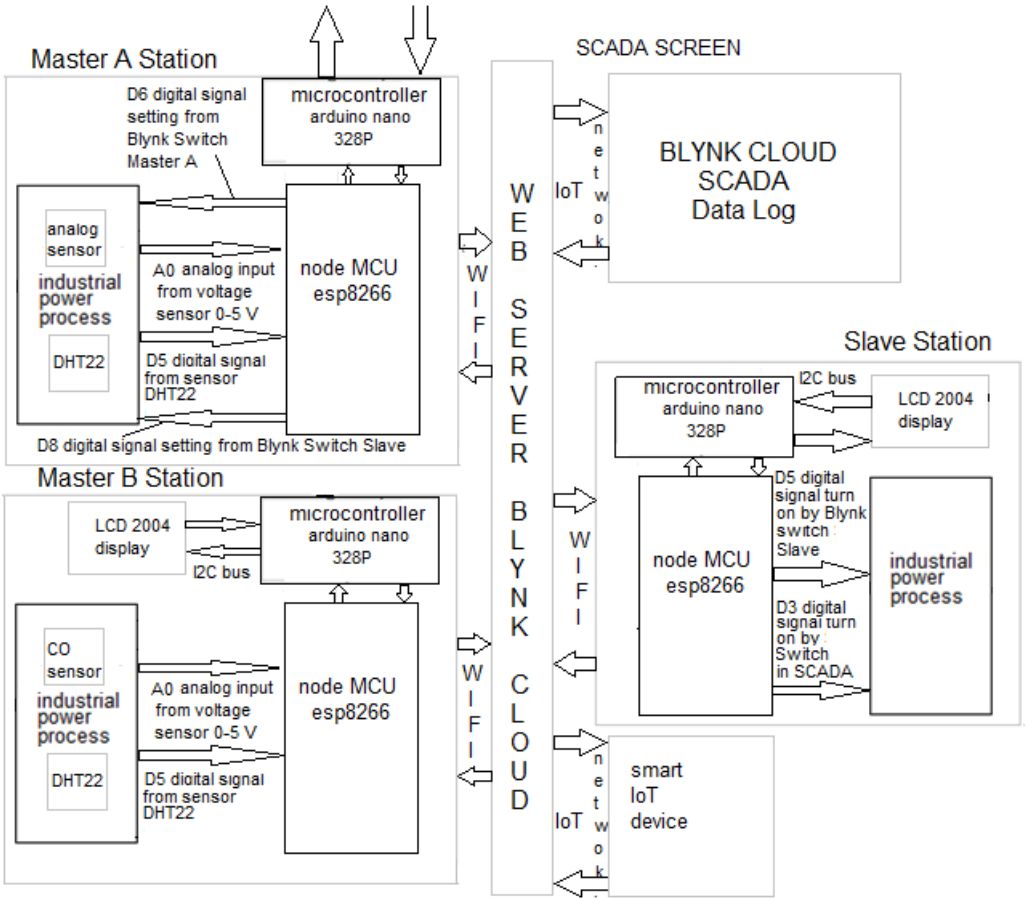

Figure 1. Block diagram of web server support of multiple controller in IoT network

The prototype system design consists of design of the MASTER A, MASTER B, SLAVE stations along with the design of the SCADA CX-Supervisor as and SCADA Blynk cloud. The design of the MASTER A station includes a microcomputer NodeMCU ESP8266-12E, ATmega 328P on an Arduino Nano board, a DHT22 sensor, an analog signal sensor (in this case, a signal from a potentiometer) and SCADA CX Supervisor, along with appropriate hardware components:

Hardwar components connected on Node MCU 8266-12E:

- *potentiometer as sensors on analog signal 0-5 V, connected on analog input A0.*
- *D6 digital output signal controlling from Blynk switch in Blynk SCADA cloud.*
- *LEDs as actuators connected on D6 digital output.*
- *DHT22 temperature and humidity sensor connected on digital pin D5.*

Hardwar components connected on Arduino nano board:

- *potentiometer as analog signal sensors 0-5 V, connected on analog input A0.*
- *DHT22 temperature and humidity sensor connected on digital pin D3.*
- *SCADA CX-Supervisor connected on UART pin on Arduino nano.*

The design of the MASTER B station includes a microcomputer Node MCU ESP8266-12E, DHT22 sensor, an analog signal sensor (in this case a signal from a MQ7 module):

Hardwar components connected on Node MCU 8266-12E:

- *analog signal sensor 0-5 V from MQ 7 module, connected on analog input A1*
- *DHT22 temperature and humidity sensor connected on digital pin D4*
-*LCD 2004 display connected by I2C bus on digital input D1 and D2 on node MCU 8266-12E*

The design of the SLAVE station consists of a microcomputer Node MCU ESP8266-12E, (Hosseini, 2021) and appropriate hardware components:

Hardwar components connected on node MCU 8266-12E:

-*D3 digital output signal controlling from SCADA screen switch*
-*LEDs as actuators connected on digital output D3*
-*D6 digital output signal controlling from Blynk switch in Blynk SCADA cloud*
-*LEDs as actuators connected on digital output D6*
-*LCD 2004 display connected by I2C bus on digital input D1 and D2 on node MCU 8266-12E*

2.1 Features of the used Hardware

a.) Microcomputer NodeMCU ESP8266-12e

The NodeMCU ESP8266 development board is equipped with the ESP-12E module which contains ESP8266 chip featuring Tensilica Xtensa 32-bit LX106 RISC microprocessor, (ESP8266). This microprocessor supports RTOS and operates at an adjustable clocj frequenct of 80MHz to 160 MHz. The NodeMCU has 128 KB RAM and 4MB of Flash memory to store data and programs. Its high processing power, along with in-built WiFi/ Bluetooth and Deep Sleep Operating features make it ideal for IoT projects. NodeMCU can be powered using Micro USB jack and VIN pin (External Supply Pin) and supports UART, SPI, and I2C interface. In Figure 2 NodeMCU ESP8266 and its pinout are shown.

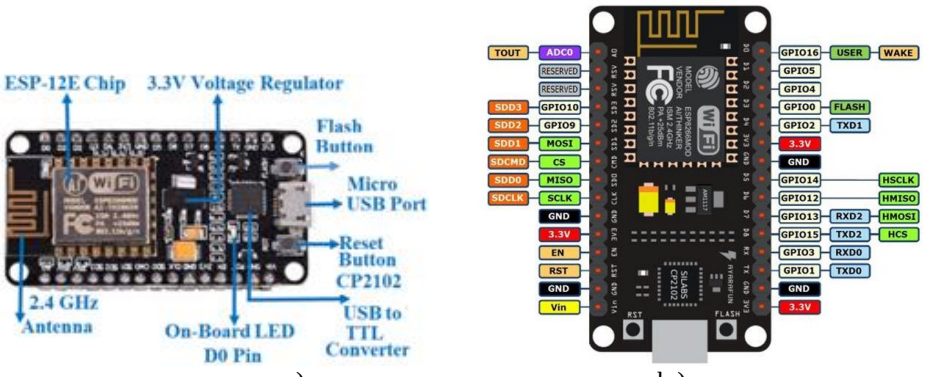

a.) b.)

Figure 2. a.) NodeMCU ESP8266 and b.) pinout

NodeMCU is an open- source firmware and development board specially designed for IoT applications. It

incorporates firmware that operates on the ESP8266 WiFi SoC from Espress Systems, along with hardware based on ESP-12 module.

NodeMCU ESP8266 specifications and features include:

- Microcontroller: Tensilica 32-bit RISC CPU Xtensa LX106
- Operating Voltage: 3.3V
- Input Voltage: 7-12V
- Digital I/O Pins (DIO): 16
- Analog Input Pins (ADC): 1
- UARTs: 1
- SPIs: 1
- I2Cs: 1
- Flash Memory: 4 MB
- SRAM: 64 KB
- Clock Speed: 80 MHz
- USB-TTL based on CP2102 is included onboard, Enabling Plug n Play
- PCB Antenna
- Small Sized module to fit smartly inside your IoT projects

The NodeMCU ESP8266 board can be easily programmed with Arduino IDE since it is easy to use.

b.) Microcomputer ATmega 328P

The Arduino Nano is an open- source microcontroller board based on the Microchip ATmega328P microcomputer developed by Arduino. The board is equipped with sets of digital and analog input/output (I/O) pins that can interface with various expansion boards (shields) and other circuits. The board features 14 digital I/O pins (six of which are capable of PWM output), along with 6 analog I/O pins and are programmable with the Arduino IDE (Integrated Development Environment) via a type B USB cable. It can be powered either by the USB cable or an external 9-volt battery, though it accepts voltages between 7 and 20 volts. The Nano board represents the first in a series of USB-based Arduino boards; Initially, it and version 1.0 of the Arduino IDE were the reference versions of Arduino, which have since evolved in newer releases. The ATmega328P on the board comes preprogrammed with a bootloader that allows uploading of new code without the need for an external hardware programmer, (ESP8266). In Figure 3a is shown electronic board of the Arduino Nano with build Atmega 328P microcomputer, while Figure 3b illustrates its pinouts, (ATMEGA328P).

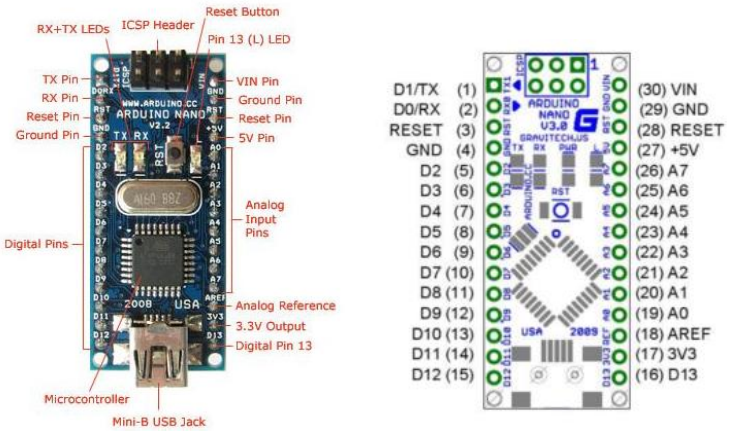

a.) b.)

Figure 3. a.) Arduino Nano and b.) its pinout

c.) DHT11 Temperature and HUMIDITY SENSOR

The DHT22 sensor is a widely utilized temperature and humidity sensors. The sensor comes with a dedicated NTC for temperature measurment and an 8-bit microcontroller for outputing temperature and humidity values as serial data, (DHT11).The connection diagram for this sensor is shown in Figure 4.

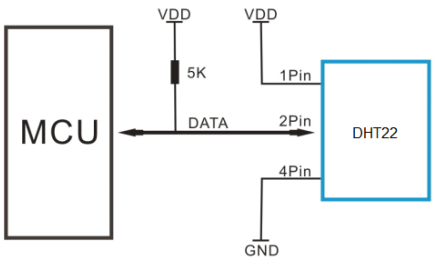

Figure 4. *Connection diagram for DHT11 sensor*

The sensor is factory calibrated simplifying its interface with other microcontrollers. It can measure temperature ranging from 0°C to 50°C and humidity from 20% to 90% with an accuracy of ±1°C and ±1%. From Figure 4 can be seen that the data pin is connected to an I/O pin of the MCU and a 5K pull-up resistor is used. The data pin outputs both temperature and humidity values as serial data. For interfacing the DHT22 with Arduino there are ready-made available libraries for quick setup and start. The output from data pin is sent as 8-bit humidity integer data , 8-bit humidity decimal data, 8- bit temperature integer data, 8-bit fractional temperature data and 8- bit parity bit. The duration of each host signal is detailly explained in DHT11 datasheet with and illustrative timing diagrams. This sensor can be used in applications for temperature and humidity measurement, local weather stations, automatic climate control and environment monitoring. In Figure 5 is shown actual size DHT22 sensor along with its pinout.

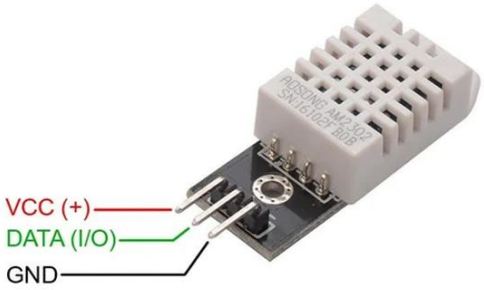

Figure 5. DHT11 sensor and pinout

DHT22 Specifications:

- Operating Voltage: 3.5V to 5.5V
- Operating current: 0.3mA (measuring) 60µA (standby)
- Output: Serial data
- Temperature Range: 0°C to 100°C
- Humidity Range: 20% to 100%
- Resolution: Temperature and Humidity both are 16-bit
- Accuracy: ±1°C and ±1%

The DHT22 sensor is available for purchase either as a standalone sensor or as a module. In both cases, the performance of the sensor is same. The sensor typically comes as a 4-pin package, althoug only three pins are utilized. The only difference between the sensor and module is that the module's filtering capacitor and inbuilt pull-up resistor. For standalone sensor, these components are externally utilized if needed.

d.) MQ-7 CO Gas Sensor

In Figure 6 is shown MQ-7 gas sensor. TheMQ-7 gas sensor utilizes SnO_2 as a gas- sensing material, which has a lower conductivity in the clear air. However, in the atmosphere containing carbon monoxide at a certain concentration, the conductivity of the gas sensor increases as the concentration of carbon monoxide increases, (MQ-9B Co.)

Figure 6. MQ-7 gas sensor

This module can be applied to household and industrial gas leakage alarm, portable gas detecting device, etc. Detecting range is 0 ppm-2000 ppm (ppm is concentration in million pieces) carbon monoxide. In Table 1 is given pins connection on MQ-7 sensor.

Table 2. Pins connection on MQ-7 sensor.

Pin No.	Symbol	Description
1	DOUT	Digital out
2	AOUT	Analog out
3	GND	Ground
4	Vcc	+Power supply (2.5-5)V

2.1 Features of the used Software

a.) *Brief description of SCADA CX-Supervisor*

The SCADA system was created using Omron CX-Supervisor software, (Myomron, n.d.). CX-Supervisor is designed for development and operation of PC- based visualization and machine control systems. It is not only user- friendly for small supervisory and control tasks, but it also provides robust capabilities for designing highly sophisticated applications. CX-Supervisor offers powerful functions for a wide range of PC- based HMI requirements. Simple applicationscan be created rapidly with the aid of many predefined functions and libraries, simple applications can be quickly developed, while even complex applications can be created using powerful programming language or VBScript. CX-Supervisor runs on standard PC desktop computers running Microsoft Windows. CX-Supervisor is intuitive and easy to use, facilitates rapid configuration, testing and debugging of projects enabling developers to efficiently create and deploy applications. CX-Supervisor consists of two separate executable Windows programs: CX-Supervisor Development environment and CX-Supervisor Runtime environment. Applications are created and tested using the development environment and then delivered as a final customer application with the runtime environment. The runtime-only environment may only be used for executing an application previously generated using the development environment. It cannot be used to generate a new runtime application using the runtime environment. Figure 7 illustrates the connection between sensor hardware, microcontroller and CX-Supervisor SCADA.

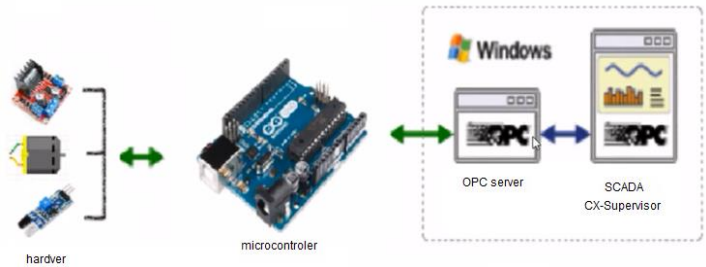

Figure 7. Connection between sensor hardware, microcontroller and CX-Supervisor SCADA

Setting up Graphic Symbols

The initial step is to set up graphic symbols. Once the project has been created with its own page, the graphic objects can be constructed and added to the page, as shown in Figure 8a.

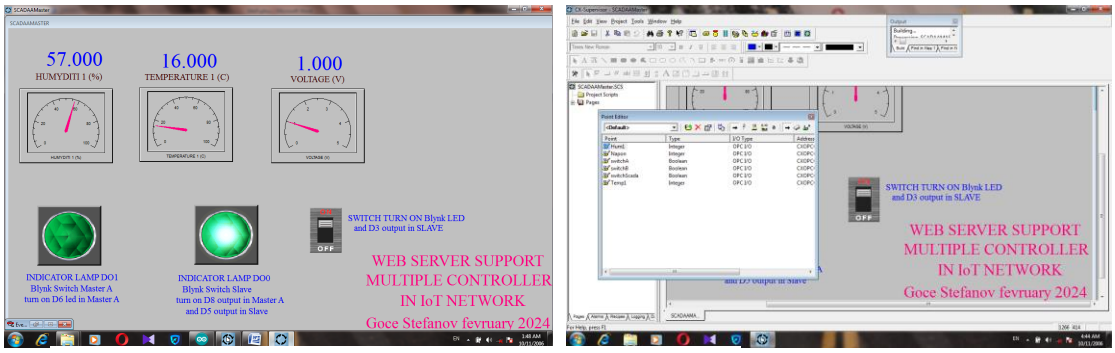

a.) b.)

Figure 8. a.) Setting graphic symbols, b.) Setting variables for graphical symbols

The graphics editor uses a Graphic Object toolbar and a floating window called the Palette to construct and control objects on the page. These tools are very easy to use. The Graphic Object Toolbar Several feauters several small icons each representing a graphical object that can be used to construct the application. Some of the objects are graphical primitives - straight lines, ellipses, rectangles, while others are more advanced, such as the gauge object, which has built-in functionality.

Setting up Variables for Graphical Symbols

For each of the graphic symbols, a point variable with the appropriate size and unit is created, as shown in Figure 8b. These variables correspond to the variables in the Arduino code.

Setting Grafical Symbols with Variables

Finally, each graphic symbol is associated with a corresponding variable. In Figure 9 is shown SCADA screen with defines variables.

Figure 9. SCADA data system screen with defines variables

In solution represented in this paper for the MASTER A station, the humidity is displayed digitally using a display and analogically with an instrument. The same applies to temperature measurement at this point. Additionally, two lamps are installed to control and monitor the operation of the switches in the Blynk SCADA cloud. These lamps, labeled as Lamp DO1 and Lamp DO0, respectively, control the Blynk switches for MASTER A and SLAVE station. Lamp DO0, on the other hand, controls the Blynk switch for SLAVE, activating outputs D8 in MASTER A and D5 in SLAVE.

b.) *Brief Description of Blynk SCADA Cloud*

Blynk is a comprehensive software suite that facilitates the prototyping, deployment, and remote management of connected electronic devices at any scale.

Whether it's personal IoT projects or commercial connected products in the millions, Blynk empowers users to connect their hardware to the cloud and create iOS, Android, and web applications. With Blynk, users can analyze real-time and historical data from devices, remotely control them from anywhere, receive important notifications, and much more.

Blynk.Console is a feature-rich web application catering to different types on user. Its key functionalities include:

-Configuration of connected devices on the platform, including application settings.
-Device, data, user, organization, and location management.
-Remote monitoring and control of devices shown on Figure 10.

Blynk.Apps

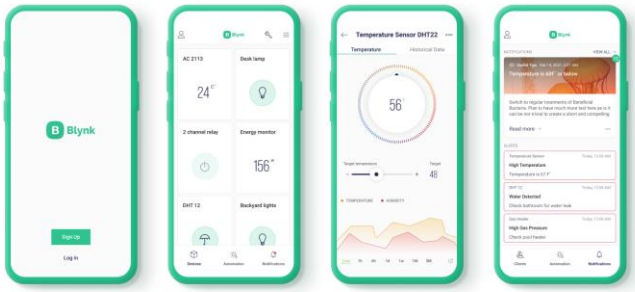

Figure 10. Blynk apps device

Applications created with Blynk are designed for end-users, whether they are family members, employees, or product purchasers. User can easily download the application, connect their devices, and begin using them.

Blynk Edgent

Blynk Edgent is a packaged solution designed to simplify the connection of supported devices to the Blynk platform. It offers access to all its advanced features without requiring extensive coding. Some of the key features of Blynk Edgent are:

-Device claiming and Wi-Fi provisioning (bringing device online and authenticating them with a certain user).
-Data transfer between device and the cloud.
-API integration with Blynk.Apps and Blynk SCADA Cloud features.
-Over-the-air firmware updates for select hardware models.

Blynk Cloud

The Blynk Cloud is a server infrastructure for Blynk SCADA IoT platform binding all its components together. The compatible boards that operate with the Blynk cloud are given in Table 2.

Table 2. Hardware components for Blynk cloud

Board	Provisioning	Secure connection	Blynk.Air
ESP32	✅	✅	✅
ESP8266	✅	✅	✅
Seeed Wio Terminal	✅	✅	✅
TI CC3220	✅	✅	✅

Hardware that works wit...
Arduino connection types
Made by Community
Troubleshooting
Need support for any ot...

3. Experimental Results

The designed prototype consists of MASTER A station (Figure 11.a), MASTER B station (Figure 11.b) and SLAVE station (Figure 11.c).

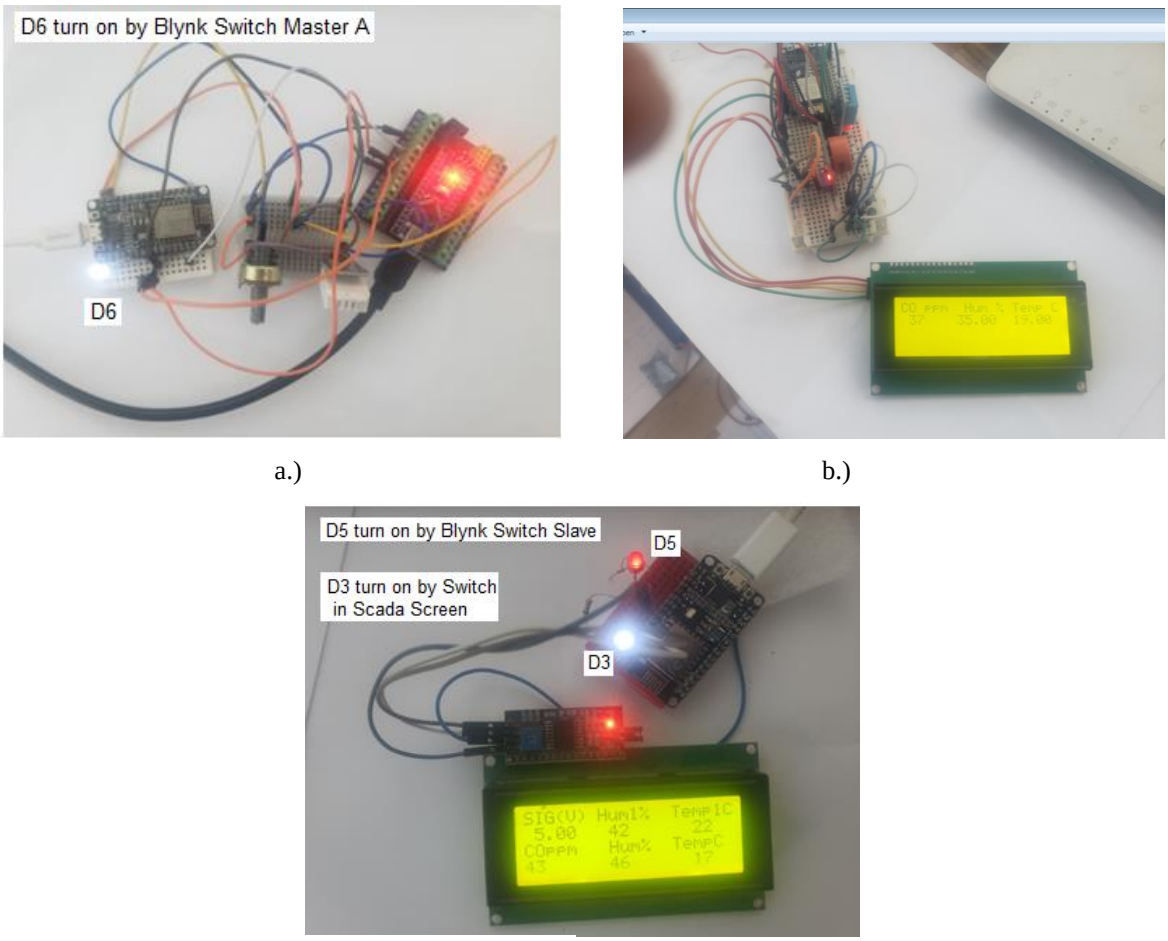

a.) b.)

c.)

Figure 11. Prototype of designed Web Server Support data system: a) prototype on the MASTER A station, prototype on the MASTER B station and c) prototype on the SLAVE station.

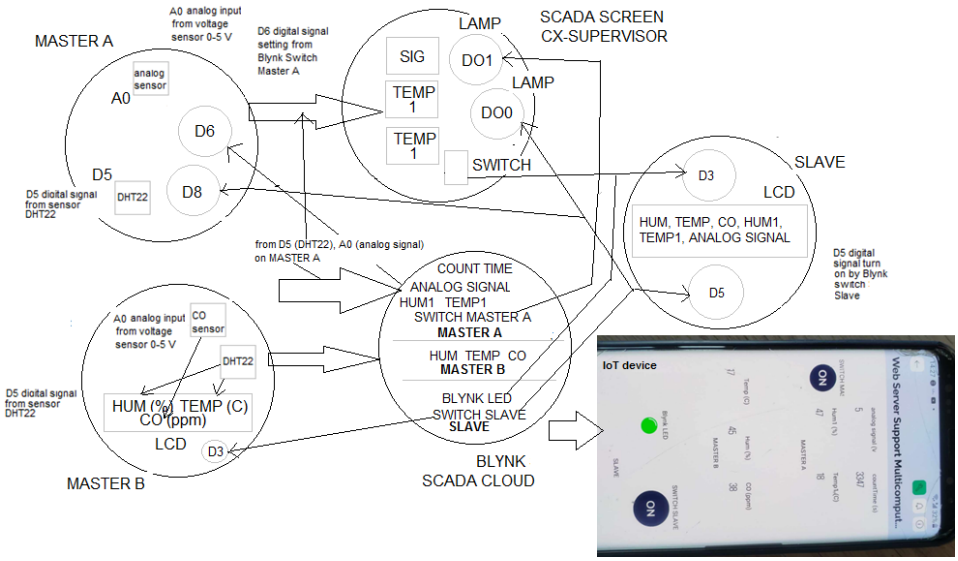

Figure 12. Routing diagram to illustrate the connection of the signal transfer between the SCADA screen, Blynk SCADA cloud, MASTER A, MASTER B and SLAVE station and IoT device

For a clearer overview and understanding of the signal flow within the system, Figure 12 shows the signal routing diagram between the blocks from which the designed solution is built. In Figure 13a, a data screen is displayed on a mobile device, showcasing data transferred through Web server data system in the IoT network, while in Figure 13b is shown a screen on the Blynk SCADA cloud.

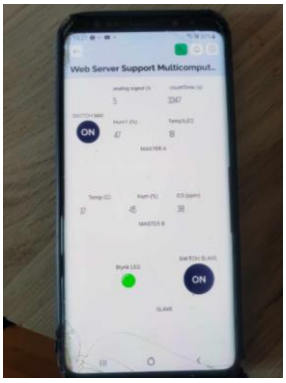

a.)

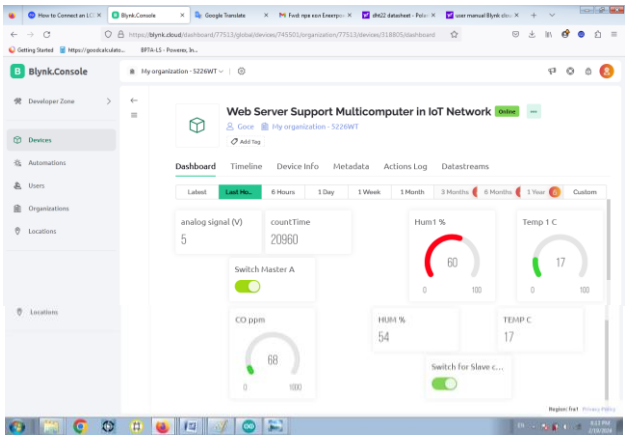

b.)

Figure 12. The screen on the transfer Web server data system in the IoT network: a) screen on mobile device, b) screen on Blynk SCADA cloud

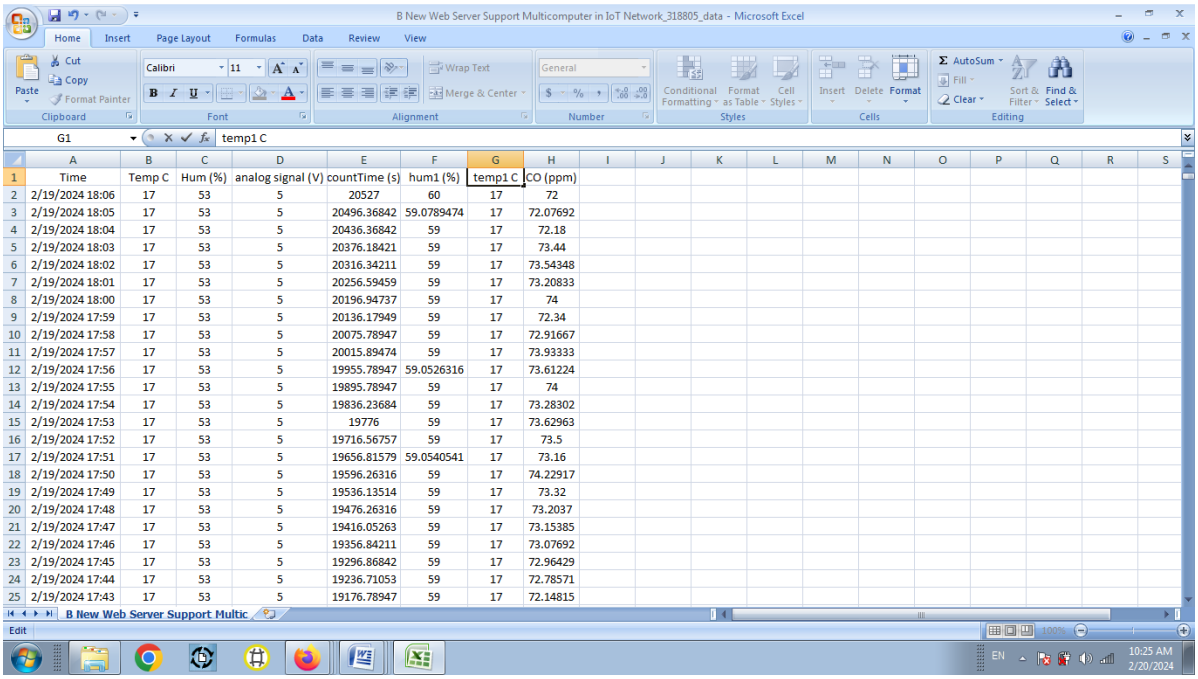

	A	B	C	D	E	F	G	H
1	Time	Temp C	Hum (%)	analog signal (V)	countTime (s)	hum1 (%)	temp1 C	CO (ppm)
2	2/19/2024 18:06	17	53	5	20527	60	17	72
3	2/19/2024 18:05	17	53	5	20496.36842	59.0789474	17	72.07692
4	2/19/2024 18:04	17	53	5	20436.36842	59	17	72.18
5	2/19/2024 18:03	17	53	5	20376.18421	59	17	73.44
6	2/19/2024 18:02	17	53	5	20316.34211	59	17	73.54348
7	2/19/2024 18:01	17	53	5	20256.59459	59	17	73.20833
8	2/19/2024 18:00	17	53	5	20196.94737	59	17	74
9	2/19/2024 17:59	17	53	5	20136.17949	59	17	72.34
10	2/19/2024 17:58	17	53	5	20075.78947	59	17	72.91667
11	2/19/2024 17:57	17	53	5	20015.89474	59	17	73.93333
12	2/19/2024 17:56	17	53	5	19955.78947	59.0526316	17	73.61224
13	2/19/2024 17:55	17	53	5	19895.78947	59	17	74
14	2/19/2024 17:54	17	53	5	19836.23684	59	17	73.28302
15	2/19/2024 17:53	17	53	5	19776	59	17	73.62963
16	2/19/2024 17:52	17	53	5	19716.56757	59	17	73.5
17	2/19/2024 17:51	17	53	5	19656.81579	59.0540541	17	73.16
18	2/19/2024 17:50	17	53	5	19596.26316	59	17	74.22917
19	2/19/2024 17:49	17	53	5	19536.13514	59	17	73.32
20	2/19/2024 17:48	17	53	5	19476.26316	59	17	73.2037
21	2/19/2024 17:47	17	53	5	19416.05263	59	17	73.15385
22	2/19/2024 17:46	17	53	5	19356.84211	59	17	73.07692
23	2/19/2024 17:45	17	53	5	19296.86842	59	17	72.96429
24	2/19/2024 17:44	17	53	5	19236.71053	59	17	72.78571
25	2/19/2024 17:43	17	53	5	19176.78947	59	17	72.14815

Figure 13. Excel® data log file

The Blynk SCADA cloud provides the option to create a data log file for measurement data. This function generates a file compatible with Excel®. In the Figure 13 is an example of Excel® data log file. In addition to integrating Blynk SCADA into the IoT network within the designed Web server system, another option for monitoring measurement data in real- time and generating a data log file is available. This was achieved by installing the SCADA CX-Supervisor on the MASTER A station. In Figure 14a is shown real- time waveform for variables CO, Humidity, Temperature, Humidity1 and Temperature1, while in Figures 14b is shown data log file for same variables.

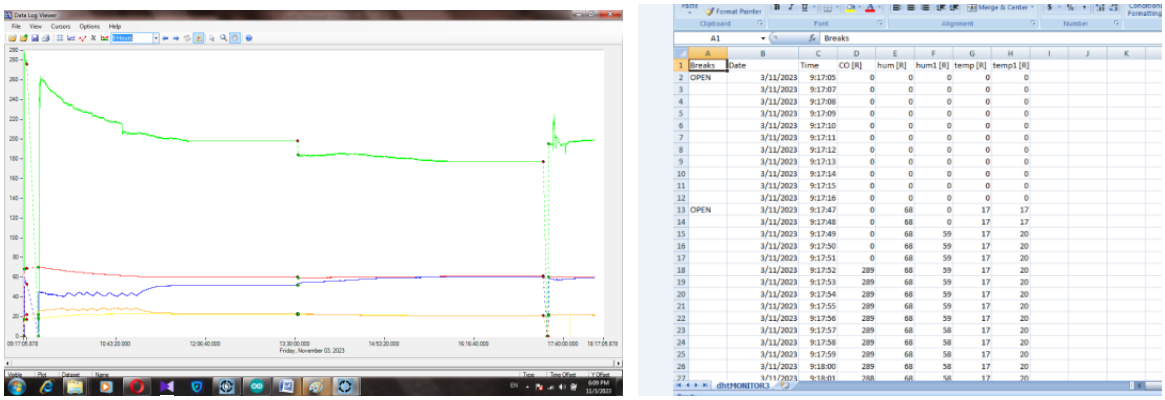

Figure 14. a.) Real- time waveform for variables CO, Humidity, Temperature, Humidity1, Temperature1, and in the Figures b.) Data log file for same variables

Conclusion

The paper presents the design and experimental implementation of a prototype supporting multi- controller data transfer via a Web server. The solution provides the option of communication among hardware components connected to process variables located at three remote locations. The medium through which the communication is carried is a Web server installed in the IoT network. All three microcontrollers are connected to the same channel in the Web server. Microcontrollers distribute the measurement data to the Web server. Consequently, the data transfer between the three remote industrial processes is achieved. Each measuring point's data can be locally visualized on a serial monitor or on the built-in LCD displays. In one of the measuring points, the MASTER A station, a SCADA system is installed. Distributed data in Web server is displayed in SCADA cloud and IoT mobile device. The built-in SCADA systems, SCADA CD-supervisor and SCADA cloud enable real-time visualization of measurement data as well as a data logging function.

Scientific Ethics Declaration

The authors declare that the scientific ethical and legal responsibility of this article published in EPSTEM journal belongs to the authors.

Acknowledgements or Notes

* This article was presented as an oral presentation at the International Conference on Basic Sciences, Engineering and Technology (www.icbaset.net) held in Alanya/Turkey on May 02-05, 2024.

* The Authors gratefully acknowledge support by Goce Delcev University Stip, North Macedonia through individual scientific fund.

References

Adafruit. (2024, May 8). *DHT11, dht22 and AM2302 sensors*. Retrieved from https://cdn-learn.adafruit.com/downloads/pdf/dht.pdf

Automation Community. (2023, December 30). *Difference between plc and SCADA*. Retrieved from https://automationcommunity.com/difference-between-plc-and-scada/

Bennett, S., & Linkens, S. (1982). *Computer control of industrial processes*, D.A. (Eds.), IEEE.

Espressif. (2020). ESP8266 technical reference. https://www.espressif.com/sites/default/files/documentation/esp8266-technical_reference_en.pdf

Hor, C. H., & Crossley, P.A. (2005). *Knowledge extraction from intelligent electronic devices, lecture notes in computer science* (pp. 82-111). United Kingdom, Loughborough University.

Hosseini, W. (2021, November 15). *NRF24L01 interfacing with Arduino: Wireless communication. electropeak*. Retrieved from https://electropeak.com/learn/wireless-communication-w-arduino-and-nrf24l01/

José, S. R., Arbour, Y., McPhalen, J., Briggs, M., Griswold, S., …& Kiran, S. (2019, April 2). *Sending data from an Arduino to the ESP8266 via serial. random nerd tutorials.* Retrieved from https://randomnerdtutorials.com/sending-data-from-an-arduino-to-the-esp8266-via-serial/

Lightbluecrab, & Instructables. (2019, March 22). *Blynk with ESP8266*. Retrieved from https://www.instructables.com

Microchip.(n.d.). *ATMEGA328P*. Retrieved from https://ww1.microchip.com/downloads/en/DeviceDoc/Atmel-7810-Automotive-Microcontrollers-ATmega328P_Datasheet.pdf

Myomron. (n.d.). *CX supervisior getting started*. Retrieved from https://www.myomron.com/downloads/1.Manuals/Software/CX-Supervisor/

Stefanov, G., Kukuseva - Paneva, M. & Stefanova, S. (2023). 3-phase smart power meter implemented in RF network. *Balkan Journal of Applied Mathematics and Informatics*, *6*(1), 25-37.

Stefanov, G., Kukuseva- Paneva, M., & Stefanova, E. (2021) Design of an intelligent Wi-Fi sensor network. *Balkan Journal of Applied Mathematics and Informatics*, *4*(1), 17-26.

Winsen. (n.d.).*MQ-9B Co & CH4 detection sensor*. Retrieved from https://www.winsen-sensor.com/sensors/co-sensor/mq-9b.html

Author Information

Maja Kukusheva Paneva
Faculty of Electrical Engenering
Goce Delcev University Stip
Krste Misirkov, 10A, 2000 Stip
North Macedonia
Contact e-mail: *maja.kukuseva@ugd.edu.mk*

Todor Chekerovski
Faculty of Electrical Engenering
Goce Delcev University Stip
Krste Misirkov, 10A, 2000 Stip
North Macedonia

Sara Stefanova
Faculty of Mechanical Engineering - Goce Delcev University, Damilah, Skopje
North Macedonia

Goce Stefanov
Faculty of Electrical Engenering
Goce Delcev University Stip
Krste Misirkov, 10A, 2000 Stip
North Macedonia

To cite this article:

Kukusheva -Paneva, M., Chekerovski, T., Stefanova, S., & Stefanov, G. (2024). Web server support of multiple controllers data transfer in IoT network. *The Eurasia Proceedings of Science, Technology, Engineering & Mathematics (EPSTEM), 28,* 1-13.

The Eurasia Proceedings of Science, Technology, Engineering & Mathematics (EPSTEM)
ISSN: 2602-3199

The Eurasia Proceedings of Science, Technology, Engineering & Mathematics (EPSTEM), 2024

Volume 28, Pages 14-22

ICBASET 2024: International Conference on Basic Sciences, Engineering and Technology

Digital Systems Model Order Reduction with Substructure Preservation and Fuzzy Logic Control

Othman Alsmadi
Al-Ahliyya Amman University
The University of Jordan

Zaer Abu-Hammour
The University of Jordan

Khaled Mahafzah
Al-Ahliyya Amman University

Abstract: A digital system model order reduction (MOR) technique with substructure preservation and fuzzy logic control is presented in this paper. The reduction procedure is performed utilizing the following two steps; model transformation, and system approximation. The transformation process is achieved by utilizing the Lyapunov Sylvester equation, which internally allows for the substructure preservation. The reduction process is achieved using the singular perturbation approximation technique that deals with Multi-Time-Scale systems (MTS). In some of the MTS systems, some of the dynamics may be eliminated since they usually have negligible effect on the overall system response. The reduced order model is then controlled using a fuzzy logic control. The proposed method of model reduction and control is investigated by observing the results of a simulated example. Results of investigation show the achievement of new models with the following advantages; reduced order models, stable models, and controlled model. This is all achieved while having the original dominant same dynamics in the new models, which emphasizes the potential of the proposed technique.

Keywords: Model order reduction, Multi-time-scale, Fuzzy logic control, Digital systems

Introduction

MOR has been a powerful technique in the field of engineering and computational science, which aims to simplify complex mathematical models while retaining their essential characteristics (Lu , et al., 2021). This process involves reducing the dimensionality of a system, which can be critical in situations where high-fidelity simulations or detailed models are computationally expensive or time-consuming (Patalano, et al., 2021). By creating simplified, lower-dimensional representations of these systems, MOR enables faster simulations, design optimization, and real-time control, making it a valuable tool in various industries, including aerospace, mechanical engineering, and electronics (Mendonca et al., 2019). Research in MOR encompasses various disciplines and has numerous applications. Some of these applications, for example electronic systems with integrated circuits and electronic systems, can be faster and more efficient in performance.

Many researchers have focused on the process of MOR while proposing and investigating different techniques from traditional to artificial intelligence (AI) approaches. This may be seen as in using intrinsic differential equations as in (Desai et al., 2013), genetic algorithms as in (Alsmadi et al., 2011a), invasive weed optimization as in (Abu-Al-Nadi et al., 2013), and artificial neural networks as in (Alsmadi et al., 2012; Alsmadi et a.l, 2011b). Some of the reduced order modelling approaches such as matching Markov parameters as proposed by Krajewski et al. (1995), were introduced to ensure stability of the reduced order model. A popular technique for

- Selection and peer-review under responsibility of the Organizing Committee of the Conference

obtaining reduced order models is the Krylov subspace as presented by Salimbahrami et al. 2005), however stability of the reduced order model is not guaranteed. Another important group of modelling algorithms is the eigenvalue preservation technique where important eigenvalues of the system are retained to find suitable lower order models as investigated by Alsmadi et al. (2011a) and Abu-Al-Nadi et al. (2013).

In spite of the high focus on reduced order modelling of continuous systems, a little has been devoted to digital systems. Recently, Maulik et al. (2022) have considered MOR for Digital models, which form the basis of autonomous off-road vehicles. They presented derivation and simulation outcomes with custom-built virtual modules of powertrain, electrical, and control systems in a problem-solving environment. (Hartmann, Herz, & Wever, 2018) addressed the advantages of model order reduction for digital model-based system engineering and real-time thermal control of electric motors. Some optimization techniques like genetic algorithm, as in (Tse et al., 2001), particle swarm optimization, as in (Deepa et al., 2011), and artificial neural networks, as in (Alsmadi et al., 2011b), have also been introduced for reduced order modelling of digital systems. However, it is found that no method can provide acceptable results for all kinds of systems, and each method has its advantages and disadvantages. In this paper, we propose a MOR for digital systems with fuzzy logic control utilizing the Lyapunov-Sylvester Equation, which transforms the two-time-scale system into a decoupled model. This decoupling allows for the use of MOR utilizing the singular perturbation approximation.

Problem Formulation

Consider a digital system given by the following difference equation described by

$$y(k)+a_1y(k-1)+a_2y(k-2)+\cdots+a_ny(k-n)= b_0u(k)+b_1u(k-1)+\cdots+b_{\bar{n}}u(k-\bar{n}) \tag{1}$$

where u(k) is the input and $y(k)$ is the output of the system at the k^{th} sampling instant. Transforming this equation into the Z-domain produces the following pulse transfer function

$$G(z)=\frac{Y(z)}{U(z)}=\frac{b_0z^{\bar{n}}+b_1z^{\bar{n}-1}+\cdots+b_{\bar{n}}}{z^n+a_1z^{n-1}+\cdots+a_n} \tag{2}$$

with $\bar{n}\le n$ for a stricktly proper system. The characteristic polynomial contains the system dominant and none dominant poles with distinct, repeated, or complex and the system is referred to as an n^{th} order model. The corresponding desired reduced r^{th} order model is given by

$$G_r(z)=\frac{Y(z)}{U(z)}=\frac{b_0z^{\bar{r}}+b_1z^{\bar{r}-1}+\cdots+b_{\bar{r}}}{z^r+a_1z^{r-1}+\cdots+a_r} \tag{3}$$

where some of the coefficients $a_i(i=1,2,\cdots,r)$ and $b_i(i=0,1,2\cdots,\bar{r})$ may be zeros as long as $\bar{r}\le r$, since the $\bar{r}>r$ term represents an improper system. For MOR and use of the singular perturbation approximation, the system in Equation (1) maybe transformed into the state space form given as following

$$x(k+1)=Ax(k)+Bu(k) \tag{4}$$

$$y(k)=Cx(k)+Du(k) \tag{5}$$

where $x\in\Re^n$ is the state vector, $u\in\Re^p$ and $y\in\Re^m$ are the input and output vectors respectively, $A\in\Re^{n\times n}$, $B\in\Re^{n\times p}$, $C\in\Re^{q\times n}$, $D\in\Re^{q\times p}$ are matrices of appropriate dimensions with *n*, *p*, and *q* are the system order, number of inputs, and number of outputs respectively. The corresponding desired reduced r^{th} order model is obtained as:

$$x_r(k+1)=A_rx_r(k)+B_ru(k) \tag{6}$$

$$y_r(k)=C_rx_r(k)+D_ru(k) \tag{7}$$

which is obtained as will be illustrated in the following subsections. The fuzzy logic approach will be used to design the PID control produced by modifying the system input signal by the following factor

$$K_P + \frac{K_i T_s z}{z-1} + \frac{K_d (z-1)}{T_s z} \tag{8}$$

obtained using the Forward Euler form where K_p, K_d ,K_i are the PID parameters and T_s is the sampling time.

Transformation and MOR

It is very well known that the system behavior is generally controlled by the characteristic polynomial seen in Equation (2), which provides the system dynamics named system poles. The poles of continuous and discrete time systems are illustrated as seen in Figure 1 (Fadali & Visioli, 2019).

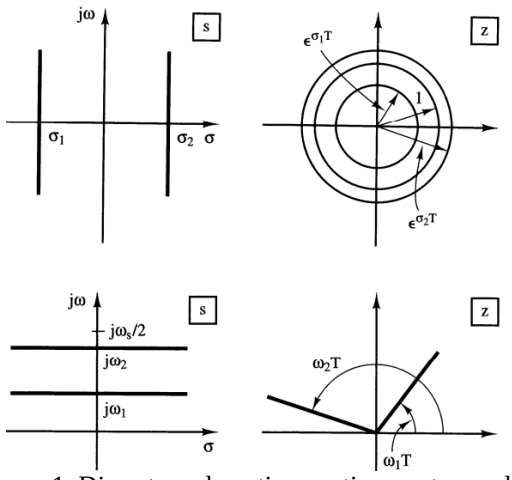

Figure 1. Discrete and continuous time system poles

Motivated by two-time-scale observations, the higher $|\sigma_1|$ (seen in the s-domain of Figure 1) the more confidently one may eliminate that dynamic. This observation may also be illustrated as seen in Figure 2. As seen here, relatively the farthest roots (poles) from the origin become insignificant. On the other hand, for discrete systems, the closest characteristic roots from the origin become insignificant.

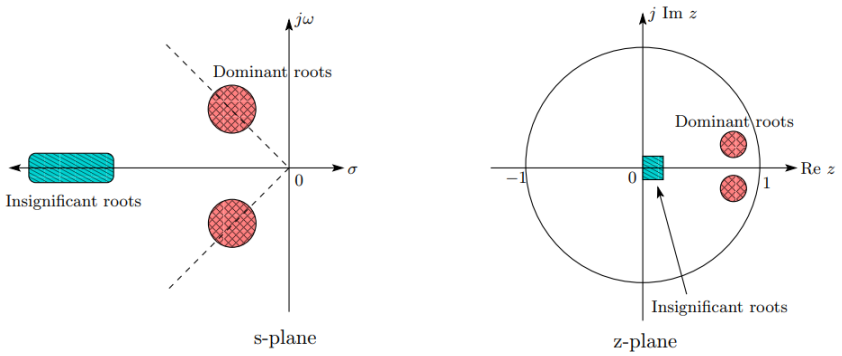

Figure 2. Significant and insignificant dynamics of discrete and continuous time system

Motivated by the singular perturbation approximation, investigated by BaniHani et al. (2009) model transformation of digital systems is performed with the dominant dynamics set properly in the system state matrix. The system shown in Equation (2) can simply be transformed into a state space representation shown by the form given in Equations (4) and (5). Hence, for the n^{th} order digital system, the dynamics can be represented by:

$$\lambda = [\lambda_1, \lambda_2, \ldots, \lambda_n] \tag{9}$$

Deriving the system as in Equations (4) and (5), the state space model may be represented by different formats. As it is well known, some forms are referred to as controllable, observable, Jordan (modal), and some are general. For a singularly perturbed digital model with order reduction objectives, the derived model may not be suitable for the simplification, as in the case where fast and slow system dynamics are coupled together. Hence, system dynamics decoupling becomes one of the potential choices. Adapting this choice, the state x is transformed into $\hat{x}$ as following:

$$x(k) = T\,\hat{x}(k) \tag{10}$$

provided that T is the transformation matrix. Following the standard procedure of system transformation, as illustrated by(Trentelman et al. (2001), substituting Equation (10) into Equations (4) and (5) yields

$$T\,\hat{x}(k+1) = AT\,\hat{x}(k) + Bu(k) \tag{11}$$

$$\hat{y}(k) = CT\,\hat{x}(k) + D\,u(k) \tag{12}$$

Multiplying Equation (10) by the inverse of T yields the transformed model:

$$\hat{x}(k+1) = T^{-1}AT\,\hat{x}(k) + T^{-1}Bu(k) \tag{13}$$

Hence, the overall transformed model may then be given by

$$\hat{x}(k+1) = \hat{A}\hat{x}(k) + \hat{B}u(k) \tag{14}$$

$$\hat{y}(k) = \hat{C}\,\hat{x}(k) + \hat{D}\,u(k) \tag{15}$$

where $\hat{A} = T^{-1}AT$ which has the decoupled system dynamics, $\hat{B} = T^{-1}B$, $\hat{C} = CT$, and $\hat{D} = D$. It is important to notice that the models in Equations (4) and (5) and Equations (14) and (15) both have the same system characteristics i.e., same eigenvalues as presented by Trentelman et al. (2001). For this transformed model, a reduced order model is to be obtained by truncating the unnecessary dynamics.

For the system in Equations (4) and (5), the proposed dominant dynamics reduced order modelling procedure is achieved by maintaining the full order dominant poles as a subset in the reduced order model. Thus, the transformed state matrix $\hat{A}$, in the continuous form of Equation (14), is designed to have the following decoupling format:

$$\hat{A} = \begin{bmatrix}
\lambda_1 & a_{12} & a_{13} & a_{14} & & \cdots & & & a_{1r} \\
0 & \lambda_2 & a_{23} & a_{24} & & \cdots & & & \\
 & \ddots & \ddots & \vdots & & & & & \\
. & & 0 & \lambda_{\bar{b}} & & & & & \vdots \\
. & & & 0 & \sigma_1 & \alpha_1 & & & \\
. & & 0 & & -\alpha_1 & \sigma_1 & & & \\
 & & 0 & & & 0 & \ddots & & a_{(r-2)r} \\
 & & & & & & 0 & \sigma_{\bar{p}} & \alpha_{\bar{p}} \\
0 & & . & . & . & & 0 & -\alpha_{\bar{p}} & \sigma_{\bar{p}}
\end{bmatrix} \tag{16}$$

where the original system dominant poles (real and/or complex) are preserved in the diagonal, seen as λ_i, i = 1, 2, … $\bar{b}$ (real) and $\sigma_i \pm \alpha_i$, i = 1, 2, … $\bar{p}$ (complex). Notice that for this reduced order model, $r = (\bar{b} + 2\bar{p}) < n$. To ensure that the dominant poles are preserved in the reduced order model, the following condition is be satisfied:

$$\lambda_{\text{dominant}} := |\lambda_1| < |\lambda_2| < \cdots < |\lambda_{\bar{b}}|, \;\; |\lambda| < |\sigma|, \;\; \text{and } |\sigma_1 \pm \alpha_1| < |\sigma_2 \pm \alpha_2| < \cdots > |\sigma_{\bar{p}} \pm \alpha_p| \tag{17}$$

Taking into account that if $|\lambda_i| > |\sigma_i \pm \alpha_i|$, then Equation (17) is to be redefined accordingly if necessary. For simplicity, the modal form is chosen, which implies that all upper triangular elements seen in Equation (16) as a_{ij} are set to zero. Now, for the system state matrix in Equation (13), which now has the form in Equation (16), the matrix T is found using the following Lyapunov-Sylvester Equation as proposed by (Wachspress, 1988):

$$XT + TY = Q \tag{18}$$

where $X \in \Re^{n\times n}$, $Y \in \Re^{m\times m}$, and $Q \in \Re^{n\times m}$ are given matrices. Equation (18) has a unique solution T if and only if the following condition is satisfied

$$\varphi(X) \bigcap \varphi(Y) = 0 \tag{19}$$

where $\varphi(X)$ denotes the spectrum of the matrix X.

To find the transformation matrix, T in Equation (18), the definition of $\hat{A}$ shown in Equation (14) is written as:

$$T^{-1}AT - \hat{A} = 0 \tag{20}$$

To satisfy the condition of Equation (18), the following modification is introduced

$$T^{-1}AT - \hat{A} = \varepsilon \tag{21}$$

where ε is a very small number. Rearranging Equation (21) and multiplying it by the matrix T, yields:

$$AT - T(\hat{A} + \varepsilon) = 0 \tag{22}$$

To determine the transformation matrix T, the X and Y matrices are transformed into a complex Schur form, which results in obtaining a model state matrix $\hat{A}$ that has the system poles decoupled according to their potential contributions in the system behavior. Now, based on the proposed dynamics decoupling, the well knownn method of singular perturbation technique is used in this paper. This method performs the reduction by eliminating the decoupled fast dynamics and focuses on the slow dominant dynamics as illustrated in (Zoran et al, 2001), which yields

$$x_r(k+1) = A_{11}\, x_r(k) + A_{12}\, x_o(k) + B_1\, u(k) \tag{23}$$

$$\gamma\, x_o(k+1) = A_{21}\, x_r(k) + A_{22}\, x_o(k) + B_2\, u\,(k) \tag{24}$$

$$y(k) = C_1\, x_r(k) + C_2\; x_o(k) + Du(k) \tag{25}$$

where x_r represent the dominant dynamics and x_o represents the non dominant dynamics. Assuming that $x_o(k+1)$ has reached its quasi steady state (γ = 0), as proposed by Kokotovic et al. (1986), Equation (24) can be rewritten as following:

$$0 = A_{21}x_r(k) + A_{22}x_o(k) + B_2u(k) \quad \Rightarrow \quad x_o(k) = -A_{22}^{-1}(A_{21}x_r(k) + B_2u(k)) \tag{26}$$

Providing that A_{22} is nonsingular, substituting x_o given in Equation (26) into Equations (24) and (25) yields the following reduced order model:

$$x_r(k+1) = (A_{11} - A_{12}A_{22}^{-1}A_{21})x_r(k) + (B_1 - A_{12}A_{22}^{-1}B_2)u(k) \tag{27}$$

$$y(k) = (C_1 - C_2A_{22}^{-1}A_{21})x_r(k) + (D - C_2A_{22}^{-1}B_2)u(k) \tag{28}$$

Fuzzy Logic Control

Fuzzy logic operation is based on searching for a suitable answer from a range of views in a similar way of how human thinking is processed. There are four main components in a fuzzy logic controller which are presented as shown in Figure 3.

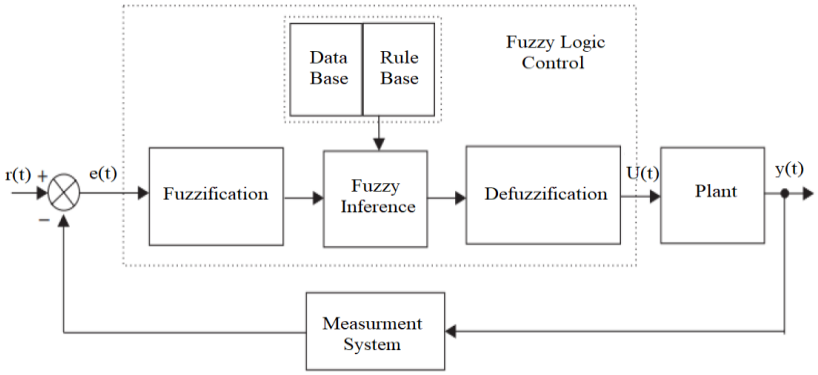

Figure 3. Fuzzy logic control.

In the fuzzification step, the values of input variables are measured and the input data are converted into suitable linguistic values. The crisp values are then transformed into fuzzy sets by means of fuzzifier. The inference engine uses IF-THEN rules and simulates human reasoning process. The rule base stores the knowledge. Defuzzification is the step which converts the fuzzy values into crisp values to be implemented and control the system outputs. The overall control scheme is implemented as shown in Figure 4 (Tiwari et al., 2019). The sate space form here is only as a result of the reduced modelling. The PID controller parameters are provided by the fuzzy logic designer.

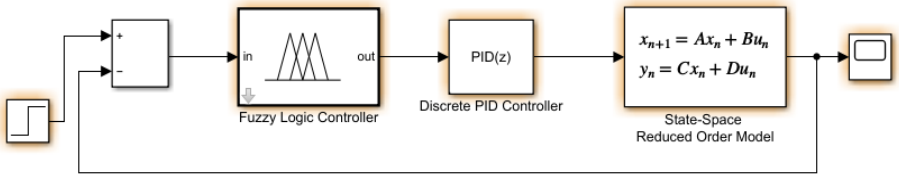

Figure 4. Reduced order model with fuzzy control.

Illustration and Discussion

In this section, we will consider a digital model described by the following 7th order for a supersonic jet engine inlet investigated by (Telescu et al, 2013)

$$G(z) = \frac{2.0434z^6 - 4.9825z^5 + 6.57z^4 - 5.8189z^3 + 3.636z^2 - 1.4105z + 0.2997}{z^7 - 2.46z^6 + 3.433z^5 - 3.333z^4 + 2.546z^3 - 1.584z^2 + 0.7478z - 0.252}$$

with poles given as [0.6843 ± 0.5820i, 0.8913, 0.2988 ± 0.7574i, -0.1987 ± 0.6993i]. Telescu et al. obtained the following 5th order model using their proposed method

$$G_r(z) = \frac{2.043z^5 - 3.057z^4 + 2.195z^3 - 1.545z^2 + 0.8617z}{z^5 - 1.518z^4 + 1.270z^3 - 1.032z^2 + 0.7539z - 0.3156}$$

with poles given as [0.8320, -0.2318 ± 0.7612i, 0.5748 ± 0.5183i], which are unrelated to the original system dynamics. On the other hand, the substructure preservation technique produced a lower dimension (3rd order) model with a transfer function given by

$$G_r(z) = \frac{1.5152z^3 - 3.1238z^2 + 2.4042z - 0.63125}{z^3 - 2.2598z^2 + 2.0266z - 0.71915}$$

To investigate the performance of the reduced order models, the full and both reduced order models were simulated to step inputs with results presented as shown in Figure 5 (with (b) for better viewing).

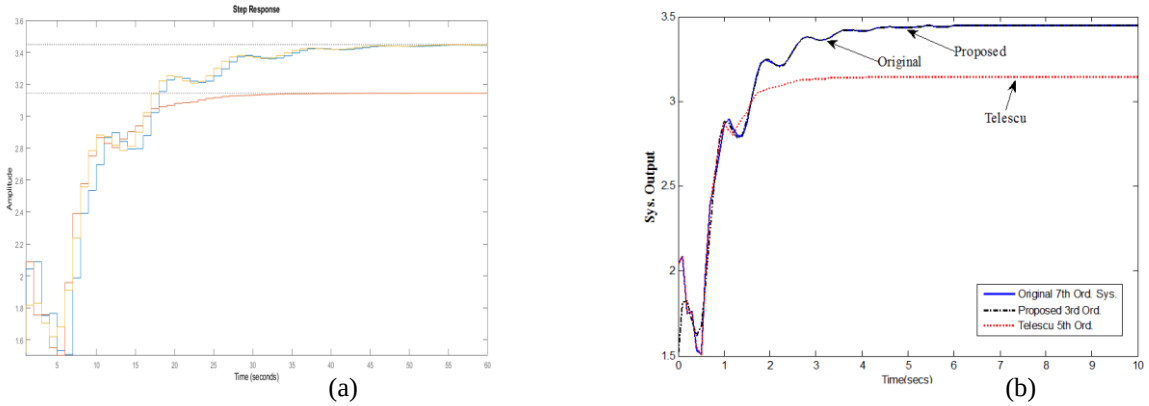

(a) (b)

Figure 5. Step response of the full and reduced order models.

İn addition to that, the differences between the two methods, and based on the previous simulation results presented in Figures 5, comparisons are presented clearly in Table 1. İn this table, please note the use of SSP is to denote Substructure preservation, and Tstp is to denote Time of convergence for step response.

Table 1. Method and performance comparison of reduced order models.

	Full Order	**Proposed educed order**	**Telescu et al reduced order**
Model	Given	$\frac{1.5152z^3 - 3.1238z^2 + 2.4042z - 0.63125}{z^3 - 2.2598z^2 + 2.0266z - 0.71915}$	$\frac{2.043z^5 - 3.057z^4 + 2.195z^3 - 1.545z^2 + 0.8617z}{z^5 - 1.518z^4 + 1.270z^3 - 1.032z^2 + 0.7539z - 0.3156}$
Model Order	7^{th}	3^{rd}	5^{th}
SSP	---	{0.6843 ± 0.5820i, 0.8913} Subset of the full order model (Substructure preservation)	{0.8320, -0.2318 ± 0.7612i, 0.5748 ± 0.5183i} Not related to the full order system (No Substructure preservation)
Tstp	---	0.5 second	No convergence

Implementing a PID controller design while focusing on minimizing the overshoot, settling time, and steady state error, the following system was obtained

$$\frac{2.729z^4 - 7.2022z^3 + 5.7432z^2 - 0.7341z - 0.5280}{z^4 - 2.9169z^3 + 2.8909z^2 - 1.0201z + 0.0467}$$

Results of simulation are shown as presented in Figure 6. As observed, all three factored have been obtained with requirements as specified.

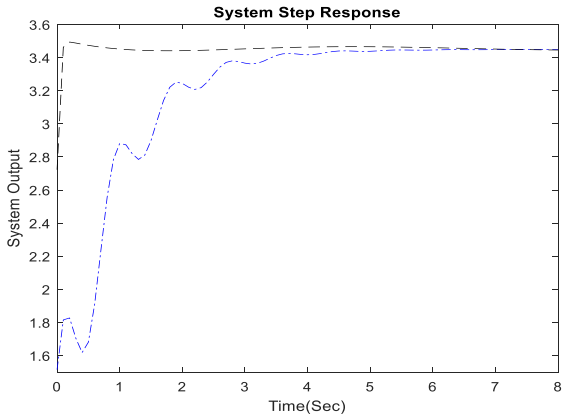

Figure 6. Step responses for the reduced order model, with and without controller.

Conclusion

In this paper, a technique for digital MOR with substructure preservation and fuzzy logic control is presented. The reduction process is performed using system transformation and singular perturbation approximation. The transformation is the Sylvester equation for a state space model while forcing the system state matrix to preserve the dominant original dynamics in the transformed model. The singular perturbation technique is then used to perform the reduction while preserving a substructure of the original system in the reduced model. A fuzzy logic control is then implemented to produce the suitable PID controller parameters. The parameters are selected to achieve the desired response while maintaining relatively low overshoot, low settling time, and low steady state error. Results of investigations show the achievement of all the considered specifications as seen in the section of illustration and discussion. Results have also been compared with some other methods where outperformance is clearly seen in the presented method.

Scientific Ethics Declaration

The authors declare that the scientific ethical and legal responsibility of this article published in EPSTEM journal belongs to the authors.

Acknowledgements or Notes

* This article was presented as an oral presentation at the International Conference on Basic Sciences, Engineering and Technology (www.icbaset.net) held in Alanya/Turkey on May 02-05, 2024.

* The corresponding author would like to thank Al-Ahliyya Amman University for supporting this research and The University of Jordan for granting a sabbatical leave for this research.

References

Abu-Al-Nadi, D. I., Alsmadi, O. M.K., Abo-Hammour Z. S., Hawa, M., & Rahhal, J. S. (2013). Invasive weed optimization for model order reduction of linear MIMO systems. *Applied Mathematical Modelling*, *37*(6), 4570-4577.

Alsmadi, O. M. K., Abo-Hammour, Z. S., & Al-Smadi, A. M. (2012). Robust model order reduction technique for MIMO systems via ANN-LMI-based state residualization. *International Journal of Circuit Theory and Applications, 40*(4), 341-354.

Alsmadi, O. M.K., Abo-Hammour Z. S., Al-Smadi, A. M., & Abu-Al-Nadi, D. I. (2011a). Genetic algorithm approach with frequency selectivity for model order reduction of MIMO systems. *Mathematical and Computer Modelling of Dynamical Systems, 17*(2), 163-181.

Alsmadi, O. M. K., Abo-Hammour, Z. S., & Al-Smadi, A. M. (2011b). Artificial neural network for discrete model order reduction with substructure preservation. *Applied Mathematical Modeling, 35(9),* 4620-4629.

BaniHani, S. M., & De, S. (2009). A comparison of some model order reduction methods for fast simulation of soft tissue response using the point collocation-based method of finite spheres. *Engineering with Computers, 25,* 37-47.

Deepa, S.N., & Sugumaran, G. (2011). MPSO based model order formulation scheme for discrete time linear system in state space form. *European Journal of Scientific Research, 58*(4), 444-454.

Desai, S. R., & Prasad, R. (2013). A novel order diminution of ltı systems using big bang big crunch optimization and routh approximation. *Applied Mathematical Modelling, 37*(16-17), 382-393.

Fadali, MS., & Visioli, A., (2019). *Digital control engineering: Analysis and design* (3rd ed.). New York, NY: Academic Press.

Hartmann, D., Herz, M., & Wever, U. (2018). Model order reduction a key technology for digital twins. In *Reduced- order modelling (ROM) for simulation and optimizatio*n(pp.167-179). Springer,

Krajewski, W., Lepschy A., & Viaro, U. (1995). Model reduction by matching Markov parameters, time moments and impulse response energy. *IEEE Trans. Auto. Control, 40*(5), 949-953.

Lu , K., Zhang, H., Zhang, K., Gu, X., Jin , y., Zhao, S.,…& Yang, Y. (2021). A review of model order reduction methods for large-scale structure systems. *Shock and Vibration, 2021,*1-19.

Maulik, S., Riordan, D., & Walsh, J. (2022). Dynamic reduction-based virtual models for digital twins - a comparative study, *Applied Sciences, 12*(14), 1-27.

Mendonca, G., Afonso, F., & Lau, F. (2019). Model order reduction in aerodynamics: review and applications. *Proc Inst Mech Eng Part G J Aerosp Eng, 233*(15), 5816-5836.

Patalano, S., Furnari, A., Vitolo, F., Dion, J.-L., Plateaux, R., & et al. (2021). A critical exposition of model order reduction techniques: application to a slewing flexible beam. *Archives of Computational Methods in Engineering, 28*(1), 31-52.

Salimbahrami, B., Lohmann B., Bechtold T., & Korvink, J. (2005). A two-sided arnoldi-algorithm with stopping criterion and an application in order reduction of MEMS. *Mathematical and Computer Modelling of Dynamical Systems, 11*(1),79-93.

Telescu, M., Iassamen, N., Cloastre, P., & Tanguy, N. (2013). A simple algorithm for stable order reduction of z-domain Laguerre models. *Signal Processing, 93*(1), 332-337.

Tiwari, A., Ali, M.A., & Alam, S. (2019). A review study on fuzzy PID controller and its various applications. *International Journal of Engineering Research & Technology, 8*(4), 590-595.

Trentelman, H., Anton, A., & Stoorvogel, H. (2001). *Control theory for linear systems*. London: Springer.

Hsu, C. C., Tse, K. M., & Wang, W. Y. (2001, October). Discrete-time model reduction of sampled systems using an enhanced multiresolutional dynamic genetic algorithm. In *2001 IEEE International Conference on Systems, Man and Cybernetics. e-Systems and e-Man for Cybernetics in Cyberspace (Cat. No. 01CH37236)* (Vol. 1, pp. 280-285). IEEE.

Wachspress, E.L. (1988). Iterative solution of the Lyapunov matrix equation. *Applied Mathematics Letters, 1*(1), 87-90.

Wang , X., Fan, S., Dai , M.-Z., & Zhang, C. (2021). On model order reduction of interconnect circuit network: a fast and accurate method. *Mathematics, 9*(1), 1-12.

Zoran, G., & Myo-Taeg, L. (2001). *Optimal control of singularly perturbed systems and applications*. New York, NY: Marcel Dekker Inc.

Author Information

Othman Alsmadi
Al-Ahliyya Amman University
The University of Jordan
Amman-Jordan
Contact e-mail: *10474@ammanu.edu.jo*

Zaer Abu-Hammour
The University of Jordan
Amman-Jordan

Khaled Mahafzah
Al-Ahliyya Amman University
Amman-Jordan

To cite this article:

Alsmadi, O., Abu-Hammour, Z. & Mahafzah, K. (2024). Digital systems model order reduction with substructure preservation and fuzzy logic control. *The Eurasia Proceedings of Science, Technology, Engineering & Mathematics (EPSTEM), 28,* 14-22.

The Eurasia Proceedings of Science, Technology, Engineering & Mathematics (EPSTEM)
ISSN: 2602-3199

The Eurasia Proceedings of Science, Technology, Engineering & Mathematics (EPSTEM), 2024

Volume 28, Pages 23-33

ICBASET 2024: International Conference on Basic Sciences, Engineering and Technology

Attribute-Based Access Control in Internet of Things Security

Melike Kukut
Gebze Technical University

Ibrahim Sogukpinar
Gebze Technical University

Abstract: With the rapid spread of the use of Internet of Things devices, it has become an important situation for these devices to be provided with critical infrastructure, integrated into daily life and the creation of robust security mechanisms. The attribute-based access control (ABAC) method has emerged as a promising approach to manage access of IoT resources based on users' attributes. However, current ABAC models lack adequate privacy protections and do not address specific vulnerabilities, especially in scenarios where sensitive data is involved. The research includes a comprehensive review of the ABAC models that stand out in the context of IoT security, including the limitations and vulnerabilities that they carry. In this work, a new framework has been proposed that integrates zero-knowledge proofs (ZKP) with homomorphic encryption into the ABAC model, providing stronger security guarantees and privacy protection. While ZKPs allow users to prove that they have certain attributes or access rights without disclosing sensitive information, homomorphic encryption allows calculations to be performed on encrypted data without decryption. The proposed framework has been evaluated by theoretical analysis and simulation studies. The findings of this research are expected to contribute significantly to the field of IoT security by providing a more robust and privacy-protecting access control mechanism for IoT environments. The proposed framework has the potential to mitigate various security threats, including unauthorized access, data and privacy violations.

Keywords: IoT, ABAC, Homomorphic encryption, Zero knowledge proof

Introduction

As the number of devices included in wireless networks increases every day, the vulnerabilities bringing with them are also increasing. Labeling of each of these devices, monitoring their timeliness and evaluating requests for access to resources are also of great importance for enterprises, especially in the context of information security. Information privacy is one of the most sensitive issues for IoT (Mahmoud et al., 2015). The need for easy accessibility of data also brings with it the challenge of protecting information in personalized services. Some factors should be taken into account when designing the privacy protection mechanism. For example, the authentication phase, the access control process and the development of trust management are topics that should be focused on with importance (Sicari et al., 2015). Although a number of projects have been developed to protect security and privacy, there is still no complete security protection mechanism for personal information privacy that provides data privacy for the IoT (Liu et al., 2020).

An incorrectly configured IoT device and/or switching devices can disrupt networks. For example, a device may be configured incorrectly to send unwanted broadcasts to the network, which can lead to a severely disruptive situation for the network. Even in situations that do not harbor malicious intent, networks can be damaged due to one or more misconfigured IoT devices or switches (Bandyopadhyay et al., 2011). The way to prevent such glitches is to make access control strict on IoT devices. Therefore, the attribute-based access control model

(ABAC); it is the most preferred method with the ability to enforce access control based on the attributes of devices, users and the environment (Baskaran et al., 2019).

In recent years, enterprises, various institutions and organizations engaged in scientific activities have updated their access control mechanisms with the attribute-based access control model (ABAC). This model, which has received a lot of attention, provides permission to users by blending resource access policies with attribute sets and manages the process. As the needs of institutions change, the ABAC model can easily adapt itself to new requirements. In this work, a new framework has been proposed that integrates zero-knowledge proofs (ZKP) with homomorphic encryption into the ABAC model, providing stronger security guarantees and privacy protection. Also, an application was implemented based on a sample scenario, theoretical and security analysis findings were included. The rest of the paper is organized as follows. Second section introduces basic information and related works. Proposed model is presented in the third section. Fourth section explains realization and discussion of the proposed solution. Last section is conclusion.

Basic Information and Related Studies

Attribute Based Access Control (ABAC)

Instead of basing access control decisions on a user's identity like traditional methods, ABAC bases access control on the attributes of assets. These attributes are user attributes, object attributes, environmental attributes, connection attributes, and administrative attributes. Attributes can be thought of as properties of anything that can be defined and assigned a value. Attributes that are predefined and assigned by an authority are properties that describe certain aspects of the subject, object, environmental conditions, and/or desired actions. In its most basic form, ABAC is based on the evaluation of the subject's attributes, the object's attributes, and a formal relationship or access control rule that defines the allowed operations for subject-object attribute combinations (Bhatt et al., 2020).

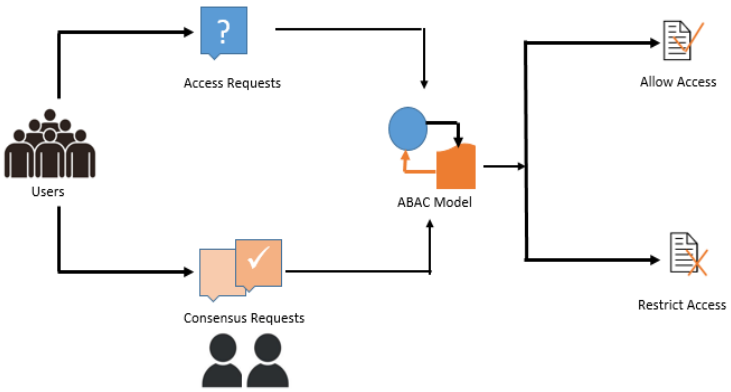

Figure 1. Attribute based access model

Access control is not the same thing as authentication. Authentication is the act of verifying that the person performing a transaction is actually the person he/she says he/she is. Access control or authorization, on the other hand, refers to the ability of a subject to access a specific object (network, data, application, service, etc.) is the decision to allow or deny access (implicit or explicit). Traditional Access Control (AC) methods attempt to verify the user's identity of the request to perform an operation (for example, reading) on an object (for example, a file) directly or through predefined attribute types, such as roles or groups assigned to that user, thus performing the control operation. However, this process remains cumbersome and insufficient. ABAC provides a more dynamic AC management capability and limits the long-term maintenance requirements of object protections (Hao et al., 2013).

ABAC offers a flexible, fine-grained mechanism and is also detailed. ABAC allows object owners or administrators to implement the AC policy without prior knowledge of the specific subject and for an unlimited number of subjects that may require access. Under ABAC, access decisions can enable switching between requests by simply changing attribute values without needing to change the subject/object relationships that define the underlying rule sets. ABAC is the critical management element of corporate information sharing in large organizations or enterprises with unified organizational structures. However, it is becoming quite

complicated to carry out the access control mechanism in a healthy way in these structures. At the system level, the focus is on the access control mechanism and its working logic (Liu et al., 2020) .

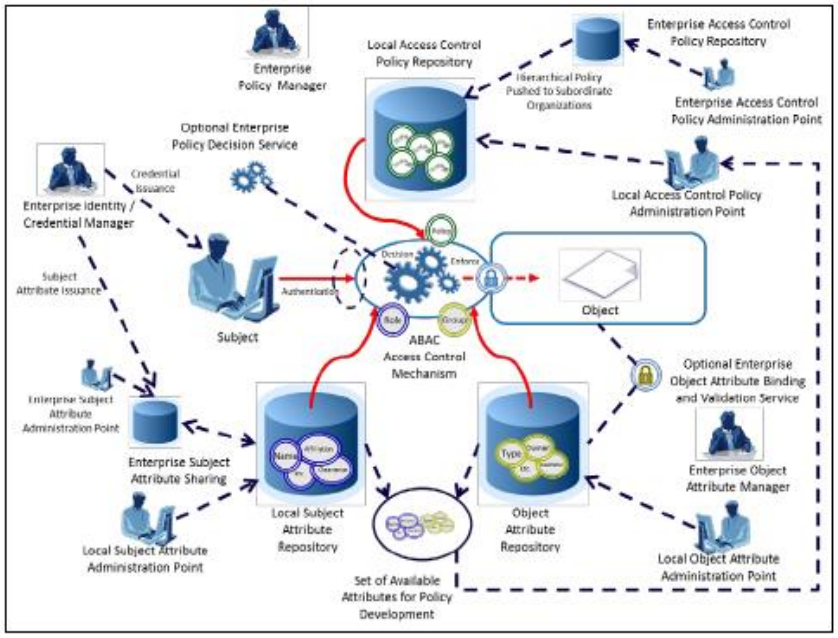

Figure 2. Enterprise ABAC scenario

ABAC does not work without a sufficient set of objects and subject attributes. There are four elements that are taken into account as basic security needs in the ABAC access control model for the sharing, transmission, storage, updating of attributes. These are preparation, veracity, security, readiness. The security structure of the attribute evaluation scheme (AES) is constructed based on these four basic areas. In the ABAC access control model, the concept of veracity, one of the basic security needs, has two dimensions: attribute trustworthiness, attribute accuracy. How well an attribute resource invoked for use from a remote access point (AP), or access control function (AF) is validated and identified is evaluated by the attribute reliability metric (Hao et al., 2013).

It is tried to create a security policy in the form of using encryption technologies, taking measures to immediately recognize unwanted changes in attribute values and making the policies mandatory, protecting data stores with a defense system, logging and continuous monitoring of the functioning of the entire ABAC model. Security protocols are used to ensure the security of attributes that are processed for use from attribute repositories, that is, that are in transmission. In order to protect against repeated attacks, the information provided by the remote access point or access control functions is transmitted digitally signed. This guarantees the integrity and confidentiality of the attribute. For higher assurance levels, the use of digitally signed attributes (Cryptobinding) provides a hash of the attribute. Thus, the access control function (AF) can ensure that an attribute has not been modified or tampered with before processing. Attributes between access control functions must be protected from changing during transition processes (Hu et al., 2017). The main security vulnerabilities that the ABAC is vulnerable to abuse and the measures that should be taken against them are listed in Table 1.

Homomorphic Encryption

Homomorphic encryption is an encryption technique that allows calculations to be performed on encrypted data without decrypting it. In other words, it protects the confidentiality of information throughout the computational process by supporting meaningful operations on the data, while ensuring that the data remains encrypted. This ability is especially valuable in scenarios where privacy and security are of critical importance (Çebi, 2019).

Description: An encryption technique E is called homomorphic if it satisfies the following equation for any possible input m:

$$D(f(E(m))) = f(m), \qquad (1)$$

D is the decryption function, and f is any function (e.g. multiplication, addition) (Gentry, 2009).

Table 1. The security risks that ABAC carries

	Security Risk	**Precautions to Be Taken**
Attribute Spoofing	Attackers may try to imitate or modify attribute values to gain unauthorized access.	Strong authentication and verification mechanisms should be implemented to ensure the integrity of attribute values.
Inadequate attribute protection	If attributes are not properly protected, attackers can gain access to sensitive information, which can lead to unauthorized access.	Encryption and access control policies should be used to protect attribute stores and transmission channels.
Incomplete or Incorrect Policies	Access control policies that are incorrectly defined or left incomplete may cause unwanted access or deny legitimate access.	Access control policies should be reviewed regularly and updated if necessary to ensure that they accurately reflect the organization's requirements.
Lack Of Policy Management	Poor management of access control policies can lead to inconsistencies or errors in the implementation of access rules.	A robust policy management system with appropriate version control and audit capabilities should be implemented.
Insufficient Logging and Monitoring	Inadequate logging and monitoring makes it difficult to detect and respond to security incidents or suspicious activities.	Extensive daily recording and monitoring should be implemented to monitor access events, and alerts should be created for unusual patterns or possible attacks.
Single Point Of Failure	If the central decision point or qualification authority becomes a single point of failure, the entire access control system may be compromised.	Redundancy and failover mechanisms should be put into operation to ensure the availability of the system and resistance to failures.
Attribute Inference	Attackers can try to obtain sensitive attribute values by observing patterns in access requests and responses to them	Techniques such as data masking or anonymization should be used to prevent attribute extraction.
Insecure Attribute Transmission	If attribute values are transmitted unsecure, they may be intercepted or changed during transmission.	Secure communication protocols for encrypting attribute data during transmission (e.g. HTTPS should be preferred.
Unauthorized Attribute Changes	Unauthorized changes to attribute values may cause unauthorized access.	Appropriate access controls and control mechanisms should be implemented to prevent and detect unauthorized changes to attribute values.
Inconsistent Attribute Format	Inconsistencies in attribute formats can lead to misinterpretation and incorrect access control decisions.	To ensure consistency, it is necessary to standardize attribute formats and apply validation rules.
Complexity and Over-Privilege	Granting complex attribute-based policies or excessive privileges may cause unwanted access.	It is very important to configure access control policies in a simple, well-defined way and to keep them in line with corporate security requirements.

There are different types of homomorphic encryption schemes, each with different levels of functionality and security features. Depending on the number of operations to be performed, it is divided into two: partial homomorphic encryption (PHE) and full homomorphic encryption (FHE). PHE supports addition or multiplication operations on encrypted data, but not both. In partial homomorphic encryption, the RSA algorithm is one of the first known homomorphic encryption methods. It shows partial homomorphic encryption property with respect to multiplication. The Paillier algorithm is partially homomorphic in terms of both addition and multiplication. The ElGamal algorithm also works in the partially homomorphic property for two mathematical operations. In summary, PHE is usually used only in applications where a certain type of calculation needs to be performed on encrypted data. Nevertheless, PHE provides a valuable level of

functionality for certain applications. PHE is a relatively simpler structure compared to fully homomorphic encryption (FHE), which supports both addition and multiplication operations, and it is also efficient. Moreover, it does not impose any additional overhead, which makes it preferable for certain practical applications where the level of homomorphic functionality is sufficient (Domingo-Ferrer, 2022).

For example, let E represent encryption, D represents decryption, and K represents the secret key used in encryption. In addition, let the + and * signs also express addition and multiplication operations on the Q set. If

$$"a + b = DK" ("EK" ("a")"+ EK"("b"))" \forall a,b \epsilon Q" \quad (2)$$

the encryption function E is assumed to have a homomorphic addition property, and if

$$"a * b = DK" ("EK" ("a")"* EK"("b"))" \forall a,b \epsilon Q" \quad (3)$$

it is assumed that the encryption function E has a homomorphic multiplication property (Gentry, 2009).

EK(a), used in these equations, shows the encryption of the number a with the secret key K, and DK shows the decryption of the encrypted sum or multiplication operation result obtained, again using the secret key K. Homomorphic secrecy can be realized using a symmetric or public key infrastructure. Thus, the confidentiality of the data content and the safe completion of the transactions can be ensured.

Full homomorphic encryption (FHE) is a structure that allows performing an innumerable number of different types of operations on encrypted data. It allows data to remain hidden even during calculation. FHE is suitable for scenarios where complex calculations are required on encrypted data without disclosing the decrypted results. It provides the highest level of homomorphic functionality. It supports the evaluation of any mathematical function on encrypted data. FHE is especially ideal in scenarios where privacy is very important, such as secure cloud computing. Because with FHE, data can be processed on a cloud server without the server needing to know the actual content of the data. It provides users with the opportunity to securely outsource calculations on untrusted servers. FHE is especially preferred in sensitive areas such as health, finance and government, where data privacy protection is very important (Hoscoskun, 2020).

Zero Knowledge Proofs

The concept of zero knowledge was first proposed by Shafi Goldwasser, Silvio Micali and Charles Rackoff in their article "The Knowledge Complexity of Interactive Proof-Systems" in 1985. A zero-knowledge proof structure is a technique developed to limit the amount of information transferred from a prover A to a verifier B in an encryption protocol. A zero-knowledge proof is a cryptological concept that indicates a situation in which one party (the prover) can prove to another party (the verifier) that they know a certain piece of information or a secret without disclosing the actual information itself. Zero-knowledge proofs are a fundamental concept in cryptographic protocols and are a powerful tool used to ensure security and privacy in various applications (Hasan, 2019).

The term "zero knowledge" means that after the interaction, the verifier acquires zero knowledge about the actual information or secret; they gain confidence that only the verifier has the information. There are three concepts that are essential in this method (Beydemir & Sogukpinar, 2017)

- *Completeness*: If the verifier has confidential data or information and follows the protocol correctly, the verifier will be convinced of this fact.
- *Soundness*: If the verifier does not have any confidential data or information, he/she should not be able to convince the verifier otherwise, even if he/she follows the protocol.
- *Zero Knowledge*: After the proof is completed, the verifier can not obtain anything about the actual information except that the substantiator has it.

Zero-knowledge proofs can be used in authentication protocols to prove the knowledge of a password without revealing the password itself. In blockchain and cryptocurrency systems, zero-knowledge proofs are used to demonstrate the ownership of coins or tokens without disclosing their actual transactions or account balances. Zero-knowledge proofs are a fundamental concept in cryptographic protocols and are a powerful tool used to ensure security and privacy in various applications (Hasan, 2019).

Related Studies

Perazzo et al. (2021), pointed out in their study that it is difficult to provide access control to data in networks with devices of different operating principles with low computing power and various security levels. They state that although the ABAC model is a very preferred method, it does not support encryption and cannot fully meet data privacy. They say that the ABAC model has the advantage of meeting both user-derived dynamic attributes and static attributes, but that it has privacy and security vulnerabilities. Servos et al. (2017), on the other hand, instead of defining attribute values to users and objects directly one-on-one, they created user groups and object groups and created a hierarchical model. They also assigned attributes to groups. The name of this proposed model is HGABAC. The advantage of this model is the easy management of attributes for users and objects. This model, which is more effective and practical in an administrative sense, is still not able to offer security in its full sense.

Hamsanandhini et al. (2022) pointed out that ABAC alone is not safe in their study, propose a framework they call Multi-Authorization Attribute-based encryption (MA-ABE) for secure sharing and access of patients' personal health information in cloud storage. In order to provide fine-grained and secure data access through health records, this encryption (MA-ABE) technique helps to encrypt each person's health record. According to Liu et al. (2022) on the other hand, by drawing attention to the security vulnerabilities in the blockchain information processing model, they propose a new multi-identity attribute-based access control model instead of using the classical ABAC in their work.

Method

Although encryption is considered the most effective solution method to strengthen ABAC, unfortunately it causes various difficulties when calculating attributes and this reduces the ability to apply access policies. Homomorphic encryption, which allows calculations on encrypted data without decrypting it, is the method needed at this point. The attributes used in the ABAC model are encrypted using a homomorphic encryption scheme. Thus, it is ensured that sensitive attributes are protected while allowing calculations to be made on encrypted data. Based on the results of zero-knowledge proofs and homomorphic calculations, the access control system makes a decision to grant or deny access without disclosing the basic attribute values.

In this study, zero information proof (ZKP) along with homomorphic encryption techniques were used to make ABAC, an attribute-based access control model, strong against cyber-attacks. Privacy and security have been further enhanced by allowing secure calculations on encrypted attributes without the need to disclose sensitive information. In cyber security, threats from within the system are characterized as problematic to predict and control more than threats from outside. By allowing access control decisions to be made based on encrypted data and verified using ZKPs, the system becomes more resistant to insider threats. Even if malicious insiders have access to encrypted data, they cannot change or interfere with access control decisions without providing valid evidence. The definitions of the components that need to be included into the account in the algorithm are as follows:

Description 1 (Entity): The object is embodied as two parts of the source and operation. In total, there is a tetrad (S, R, O, E) in which four entities and ABAC can be abstracted, where S, R, O and E represent the entity set consisting of subject attributes, resource attributes, process attributes and environment attributes, respectively. These four sets of entities can be expressed as follows: S = {s1, s2, s3, ..., sm}, R = {r1, r2, r3, ..., rn}, O = {o1, o2, o3, ... , oj}, E = {e1, e2, e3, ... ,Oct},where n, m, k, $j \geq 1$.

Description 2 (Attributes): These are used to describe the internal properties of entities. The set of attributes can be represented as A = {a1, a2, a3, ... , as}. TU, RA, OA and EA, respectively, TU = {crypto checkpoint for, sA2, sA3, ..., sAm}, RA = {rA1, rA2, rA3,..., rAn}, OA = {oA1, OA2, OA3,...,oAj}, EA = {eA1, eA2, eA3,...,eAk} represents the set of all subject attributes, resource attributes, process attributes, and environment attributes shown as. Let's take SA as an example, for the subject si, sAi represents the set of attributes, where $sAi \subseteq A$.

Description 3 (Attribute-value pair): The definition and custom value of an attribute are represented by an attribute-value pair (avp), which is defined as a binary (attribute, value) (i.e. attribute = value). Savp, Ravp, Oavp, and Eavp are used to represent attribute-value pairs of the subject, resource, process, and environment attributes, respectively.

Description 4 (Policy): This is denoted by p and describes a subject with certain attribute values that allows or rejects operations on the resources of the corresponding attribute values in a given environment. Its official description can be expressed as follows: ← (SA, RA, OA, EA Tu) and this ← the result value will be allowed or reject. It shows positive authorization and negative authorization, respectively. The set of principles is expressed as follows: P = {p1, p2, p3, ..., pn}.

Description 5 (Rule): This is indicated by r and is the basic unit of the policy and the smallest unit that conducts the policy evaluation. The value of the domain element is the allow or reject element, which represents the authorization result of the rule (Hao et al., 2013; Liu et al., 2020).

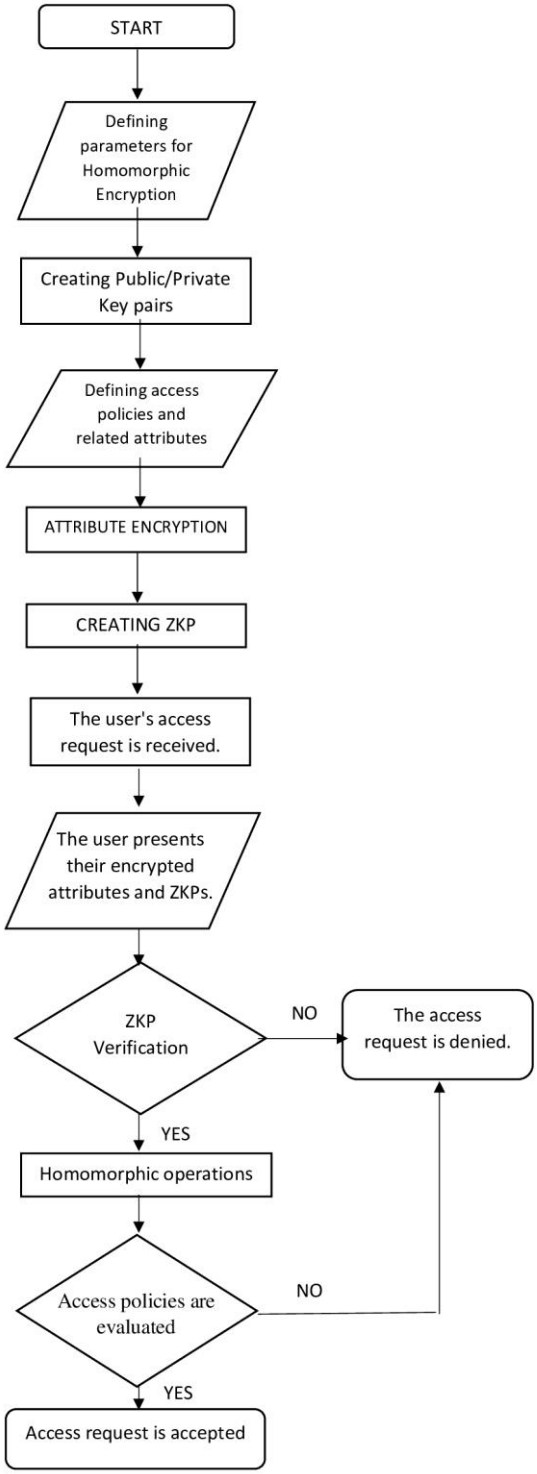

Figure 3. Flow diagram of the algorithm

Table 2. Algoritm of ABAC

Algorithm - The process of applying homomorphic encryption and Zero-Knowledge Proof method with ABAC
Input: Entities, Attributes, Attribute Value Pairs, Policies, Rules **Output:** Allowed / Denied **1.** The parameters for the homomorphic encryption scheme are defined. **2.** Public / private key pairs are created for the encryption scheme. **3.** Access policies and the attributes associated with these policies are defined. **4.** Attributes are encrypted using homomorphic encryption. **5.** ZKPs are created to prove without explanation that they have certain qualifications. **6.** When a user requests access, he presents his encrypted attributes and ZKPs. **7.** The ZKPs submitted by the user are verified to ensure that they have the necessary attributes. **8.** Homomorphic operations are performed to evaluate access principles. **9.** Access is granted or denied according to the evaluation result

Sample Application and Security Analysis

Application

We decided according to the base scenario on the healthcare sector, where the use of IoT devices is in vogue. In the health information system environment, a large number of people are involved, including patients, patient relatives, research assistants, administrative personnel to solve patient cases, emergency workers, specialist doctors, professors, assistant doctors, foreign health care providers and other health professionals. An example of a simple access control permissions list can be configured as Figure 4.

```
Role: PROFESSOR# Patient_record: write#Context:Hospital->Permit
Role: DOCTOR# Patient_record: write#Context:Hospital->Permit
Role: ASST_DOCTOR# Patient_record: read#Context:Hospital->Permit
Role: NURSE# Patient_record: read#Context:Hospital->Permit
Role: NURSE# Patient_record: write->Deny
Role: MANAGER# Patient_record: read#Context:Hospital->Permit
Role: MANAGER# Patient_record: write->Deny
Role: TECHNICIAN# Biling_Information: write#Context: Hospital->Permit
Role: TECHNICIAN#Patient_record:write->Deny
```

Figure 4. Example of access control list

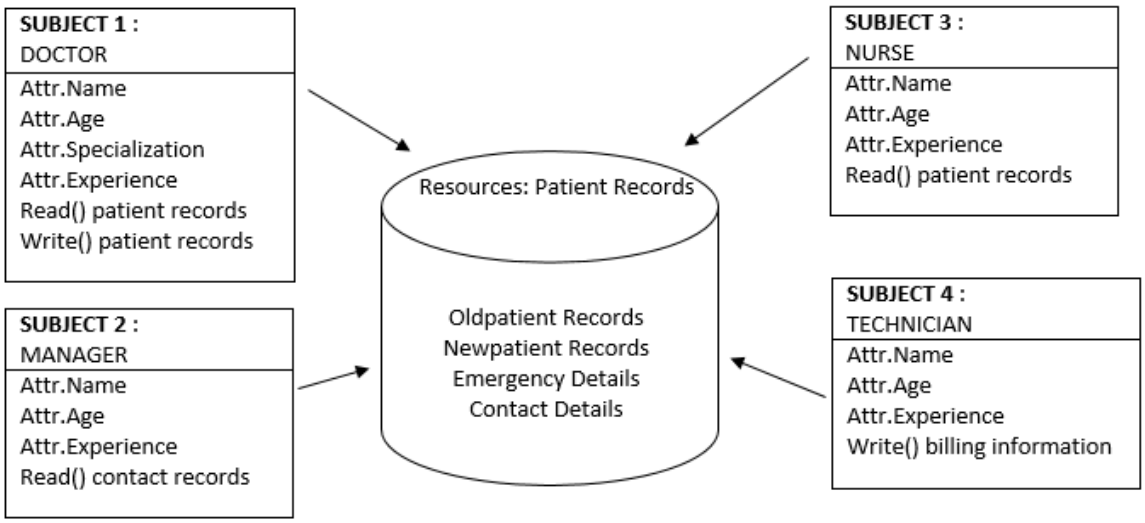

Figure 5. Sample health ınformation system subjects and resource repository

The attributes of doctors are name, age, work experience, department knowledge, etc. the attributes of the objects are the sources of patient records (medical reports, contact information, emergency information, etc.). The information contained in the medical reports are attribute values such as the patient's blood type, the permanent list of medications he/she uses, the surgeries he/she has undergone, the treatment applied, and his/her allergic condition. Emergency information, on the other hand, is the contact information of the patient's relative, information about whether the patient has a possible life-risk condition or not. The hospital director, who is the subject, has the right to access the personal and financial information of patients, the content of the treatment he is undergoing in the hospital. However, these rights are not in unlimited authority. Even if he/she makes a new medical record entry, he/she cannot view private notes about that patient unless it is signed by the relevant doctor. In addition, they can delete patient information. For example, a laboratory employee acting as a technician can add new information about the patient, add the invoice of the procedure to the system, but it cannot enter other areas. Figure 5 shows the resource repository relationship with the subjects in this scenario as an example (Figure 5).

In the example scenario, a request for access to the relevant records was created through four subjects, and authentication was performed using the zero-knowledge proof method, and then permission to access the authorized record was obtained after attribute verification. If the transaction is not authorized, it will be rejected.

Theoretical Analysis

The theoretical safety of the proposed method is based on the discrete logarithm problem on the elliptic curve algorithm. In the code used, Pairing Group was used, which represents a curve called SS1024. the 1024-bit long key again corresponds to the 1024-bit key in the RSA and Diffie Hellman algorithms.

Considering the number of bits representing the large prime number required to determine the finite field in the N discrete logarithm problem, the method has an O(2N) exponential complexity. As an example, a 2.2 GHz, 8-core processor can solve a 768-bit discrete logarithm problem in 825 years (Kleinjung et al., 2017).

Application Security Analysis

In the study, virtual working environments offering the opportunity to work with versatile security analysis tools were used. Controls such as sensitive data protection, data loss prevention, key management are provided. It is rezist against session hijacking attacks, password cracking, phishing attacks because zero information proof is used in the authentication phase of this study. The fact that homomorphic encryption has been used against possible threats such as cryptanalytic, side channel, frequency and coincidence attacks also provides an advantage. It seems to be leading the way again to eliminate attacks that can be carried out by targeting key production.

Conclusion

In this work, it is proposed that homomorphic encryption should be preferred to make ABAC strong. The approach of using homomorphic encryption and zero information proof together has been revealed by the literature study as the most accurate method. Attribute-Based Access Control using zero-knowledge proofs with homomorphic encryption is a state-of-the-art security model with a large number of potential applications in various fields. While there are currently no widely publicized real-life examples of organizations using this particular model, there are researchers and organizations actively working to advance the field of secure access control with techniques such as ABAC, ZKPs, and homomorphic encryption.

The research for solutions to ABAC's problems such as administrative, scalability, auditability, and correct configuration continues on the academic field without slowing down. One of the main challenges of ABAC is that it requires more resources and expertise to design, implement and manage. ABAC involves defining and maintaining a large number of attributes, principles, and rules, which can be time-consuming and error-prone. ABAC also requires more processing power and network bandwidth to evaluate and implement access decisions that can affect performance and availability. Because attributes may contain sensitive or personal information that needs to be protected and controlled, ABAC may also pose an increased security and privacy risk.

The development of an access control model in big data, cloud computing and blockchain based on the internet of things, one of the rapidly rising issues of today, have been identified as future areas of study. It has been revealed by research that the data stored publicly on the blockchain is still under the threat of privacy leakage. As future studies, new studies on systems that also integrate homomorphic encryption and zero-knowledge proof on attribute-based access control blockchain information sharing, especially for supply chain management, are expected to continue to be conducted.

Scientific Ethics Declaration

The authors declare that the scientific ethical and legal responsibility of this article published in EPSTEM journal belongs to the authors.

Acknowledgements or Notes

* This article was presented as oral presentation at the International Conference on Basic Sciences, Engineering and Technology (www.icbaset.net) held in Alanya/Turkey on May 02-05, 2024.

References

Bandyopadhyay, D. & Sen, J. (2011). Internet of Things: Applications and Challenges in Technology and Standardization. *Wireless Personal Communications*, *58*, 49-69.

Baskaran, S. B. M. (2019). Internet of things security. *Journal of ICT Standardization*, *7*(1) 21-40.

Beydemir A., & Sogukpınar, I. (2017), Lightweight zero knowledge authentication for Internet of things, *In Computer Science and Engineering (UBMK)*(pp.360-365). IEEE.

Bhatt, P., Bhatt, S., & Ko, M. (2020). Poster: IoT Sentinel-An ABAC approach against cyber-warfare in organizations. In *Proceedings of the 25th ACM Symposium on Access Control Models and Technologies*, 223-225.

Cebi, G. (2019). *Homomorphic encryption in cloud computing*. (Master's thesis, Bahcesehir University).

Domingo-Ferrer, J. (2002). A provably secure additive and multiplicative privacy homomorphism. *In International Conference on Information Security* (pp.471-483). Berlin, Heidelberg: Springer.

Gentry, C. (2009). *A fully homomorphic encryption scheme*. (Doctoral dissertation, Stanford University).

Hamsanandhini, S., Eswaran, M., & Varanambika, V. (2022). Health record maintenance using cloud computing and multi authority attribute based encryption. In *Proceedings of the 2022 International Conference on Computer Communication and Informatics (ICCCI)* IEEE. (pp.1-8).

Hasan, J. (2019). Overview and applications of zero knowledge proof (ZKP). *International Journal of Computer Science and Network*, *8*(5), 2277-5420.

Hao, V. C., Ferraiolo, D., Kuhn, R., Friedman, A. R., Lang, A. J., Cogdell, M. M. & Scarfone, K. (2013). Guide to attribute based access control (ABAC) definition and considerations. *NIST Special Publication*, *800*(162), 1-54.

Hoscoskun, R. E. (2020). *Homomorfik sifreleme yontemi uzerine bir inceleme*. (Master Dissertation, Trakya University).

Hu, V. C., Ferraiolo, D. F., Chandramouli, R., & Kuhn, D. R. (2017). *Attribute-based access control*. Artech House.

Kleinjung, T., Diem, C., Lenstra, A. K., Priplata, C., & Stahlke, C. (2017). Computation of a 768-bit prime field discrete logarith. In *Advances in Cryptology–EUROCRYPT 2017: Proceedings of the 36th Annual International Conference on the Theory and Applications of Cryptographic Techniques* (pp.185-201). Springer International Publishing.

Liu, M., Yang, C., Li, H., & Zhang, Y. (2020). An efficient attribute-based access control (ABAC) policy retrieval method based on attribute and value levels in multimedia networks. *Sensors*, *20*(6), 1741.

Liu, C., Xiang, F., & Sun, Z. (2022). Multiauthority Attribute-based access control for supply chain information sharing in Blockchain. *Security and Communication Networks*, *2022*, 1-18.

Mahmoud, R., Yousuf, T., Aloul, F., & Zualkernan, I. (2015). Internet of things (IoT) security: Current status, challenges and prospective measures. In *Proceedings of the 10th International Conference for Internet Technology and Secured Transactions (ICITST)* (pp.336-341). IEEE.

Perazzo, P., Righetti, F., La Manna, M., & Vallati, C. (2021). Performance evaluation of attribute-based encryption on constrained IoT devices. *Computer Communications*, *170*, 151-163.

Servos, D., & Osborn, S. L. (2017). Current research and open problems in attribute-based access control. *ACM Computing Surveys (CSUR)*, *49*(4), 1-45.

Sicari, S., Rizzardi, A., Grieco, L. A., & Coen-Porisini, A. (2015). Security, privacy and trust in internet of things: The road ahead. *Computer Networks*, *76*(15), 146-164.

Author Information

Melike Kukut
Gebze Technical University
Kocaeli, Turkiye
Contact e-mail: *m.kukut2021@gtu.edu.tr*

Ibrahim Sogukpinar
Gebze Technical University
Kocaeli, Turkiye

To cite this article:

Kukut, M., & Sogukpinar, I. (2024). Attribute-based access control in internet of things security. *The Eurasia Proceedings of Science, Technology, Engineering & Mathematics (EPSTEM), 28*, 23-33.

The Eurasia Proceedings of Science, Technology, Engineering & Mathematics (EPSTEM)
ISSN: 2602-3199

The Eurasia Proceedings of Science, Technology, Engineering & Mathematics (EPSTEM), 2024

Volume 28, Pages 34-46

ICBASET 2024: International Conference on Basic Sciences, Engineering and Technology

Complex Thinking Abilities in the Rapidly Evolving Field of Genomics and Personalized Medicine: Analysis of Actionability on Cancer with ChatGPT and Literature

M.S. Ramírez-Montoya
EGADE Business School

G.A. Sanchez-Zuno
Yale University

R.M. Marques González
Hospital Civil de Guadalajara

F. Casıllas-Muñoz
Tecnologico de Monterrey

Abstract: This study aims to explore complex thinking abilities within the field of genomics and personalized medicine, focusing on the analysis of actionable cancer data using Big Data Analytics (BDA) and ChatGPT. It seeks to understand how these advanced technologies can be harnessed to derive more actionable approaches for students and professionals in genetics, biology, medicine, and related fields. Methods: The research methodology involves a machine learning (ML) analysis to visualize the distribution of genes based on top ten actionability counts, development status, and drug combinations. This includes ChatGPT prompts for visualization of gene distribution and the use of pivot tables for data validation. The study facilitates complex data analysis and decision-making processes in genomics. The findings reveal that BDA and ChatGPT can significantly improve the analysis and interpretation of genomic data. Visualization techniques enabled by these technologies allow for the identification of patterns, correlations, and predictive models. These insights can lead to more accurate diagnoses, personalized treatment plans, and a better understanding of drug combinations and mutations in cancer. This research highlights the essential role of automation and open access in managing and interpreting large volumes of genomic data efficiently. Conclusion: The integration of BDA and ChatGPT into genomics and personalized medicine offers promising avenues for advancing personalized medicine, enhancing clinical decision-making, and fostering research and development in the field of cancer.

Keywords: Genomics, Cancer, Actionable mutations, ChatGPT in medicine

Introduction

Addressing actionable information in an educational context, especially for educators in genetics, biology, medicine, and related fields, involves a multifaceted strategy. These strategies involve embracing the emergence of big data to support informed decision-making (Fischer et al., 2020). The rapidly evolving field of big data, particularly within the medical sciences, has announced a transformative era for education with the urgent necessity to tailor educational experiences to fit the specific needs of individual learners and for the advancement of technologies (Luan et al., 2020). In this sense, Big data is revolutionizing bioinformatics education by necessitating curriculum updates to incorporate skills for managing and analyzing large datasets,

thus preparing students for the data-intensive challenges in biomedical fields (Greene et al., 2016). By facing these challenges, medical institutions will ensure students and professionals are well-equipped for advancements in biomedical research and healthcare.

Complex and Critical Thinking is a Necessity that Goes Far Beyond the Lack of Specialization

Some strategies educators might consider stimulating complex thinking to derivate more information into more actionable approaches in students; Big data analytics (BDA) is enabling complex thinking analytics, with the help of data analysis decomposition to facilitate more accurate diagnoses and personalized treatments (Batko & Ślęzak, 2022). Artificial Intelligence (AI) such as ChatGPT can complement these analytics; notably cannot be used reliably for clinical applications, but with further specialized training and validation, it can support enormously medical contexts to offer reliable and fine-tuned data for such purposes (Li et al., 2024). In this sense, ChatGPT and other large language models (LLMs) are also enhancing drug discoveries, accelerating target identification and optimizing drug design through predictive analytics on pharmacodynamics, pharmacokinetics, and toxicity significantly reducing time and costs associated with bringing new drugs to market (Chakraborty et al., 2023). This evidence reflects the importance of leverage in these technologies for big data interpretation, especially in the biomedical sciences.

The complexity of medical data arises from numerous sources and types, each with unique traits that influence how data is analyzed and applied. This complexity necessitates advanced analytical strategies to effectively understand and utilize the data, ensuring that actionable insights are both accurate and relevant to patient care (Lee & Yoon, 2017).

Identifying actionable somatic mutations (ASM) in cancer involves understanding specific genetic alterations that can guide targeted therapy (they directly influence treatment decisions that is why they are actionable), for example, in non-small cell lung cancer (NSCLC), the presence of specific mutations in the EGFR gene can dictate the effectiveness of EGFR inhibitors like gefitinib and erlotinib (Puiu et al., 2024). The importance of AI in predicting ASM in cancer is highlighted by its ability to accelerate the identification of genetic alterations that can inform targeted therapy, and improve patient outcomes, for example, computational models to pinpoint mutations like the V600E mutation in the BRAF gene can predict responsiveness to specific inhibitors such as vemurafenib (Ostroverkhova et al., 2023). However, elucidating ASM in cancer is another complex challenge due to the immense genetic diversity and heterogeneity of tumors and these complex data requires sophisticated computational tools and deep biological understanding to effectively translate genomic information into clinically actionable treatment plans (Ahmed, 2023). The strategies to cope with these complexities with the help of AI will define the rate of medical advancements.

Actionability in Medicine Based on Big Data: Misleading Opportunities

Paul Wesson and colleagues in 2022 mention the "six Vs" algorithm, which details the main elements and keys related to the concept of big data. These elements are important because they allow organizations to harness the power of data for decision-making, operational efficiency, and equity in various areas (Wesson et al., 2022). One of the most well-known and highly rated actionable programs for big data management is COSMIC, which is used by most precision oncology specialists. This database provides information on mutated sequences observed in cancer patients, as well as possible associations with other events, thus becoming a reliable guide for research evidence, potentially reducing efforts and costs, and setting a standard in cancer genomics (Tempini and Leonelli (2021). Most databases store data inefficiently and only for the minimally required retention period, this is one of the main misleading opportunities for big data analysis, as databases are considered mere data dumps. To prevent this, the essential aspects that data must have to be adequately usable in research are summarized with the acronym FAIR: findable, accessible, interoperable, and reusable (Blatter et al., 2022). One of the great current uses of these big data analyses allows the recognition of patterns in specialized metabolic diagnostics, as well as technique and medical validation, and quality management.

The availability of multimodal datasets could improve our ability to find phenotypic and genotypic disease characteristics, helping to predict dose-response, risk prediction, prognosis, treatment response, and patient outcomes. Recently, new AI/ML algorithms for precision medicine for neurological diseases, cancer, and cardiovascular diseases have shown promising results regarding disease risk prediction, phenotypic prediction, dose-treatment response, with a high degree of precision and accuracy (Blatter et al., 2022). AI, big data, and ML technologies offer alternative pathways, either individually or in combination, that facilitate a better

understanding and management of cancer and its impact on patients. The value of these technologies has been recognized and integrated into programs such as the Cancer Moonshot in the United States and the European Beating Cancer Plan in Europe (Sahu et al., 2022), their integration into clinical practice also poses new requirements for healthcare professionals in terms of skills and preparedness to use them effectively and efficiently. Therefore, there is a growing need for investment and training in oncology to address and overcome some of the challenges associated with cancer control. In Spain, several projects have begun developing tools based on massive data. In Girona, the Savana project is underway, a platform supporting medical decision-making that is already being implemented in some Spanish healthcare centers. This platform is designed to transform Electronic Health Records into large datasets, using Artificial Intelligence (AI) to unlock the clinical value contained in unstructured information. This is bringing a disruptive change in healthcare by enhancing efficiency in clinical management and research.

Method

The methods in these explore complex thinking abilities in the field of genomics and personalized medicine through the analysis of actionable cancer data involve a multifaceted approach integrating Big Data Analytics (BDA) and ChatGPT:

Data Collection and Preprocessing

The COSMIC database, standing for the Catalogue Of Somatic Mutations In Cancer, is an expert-curated platform that compiles a wide variety of somatic mutation mechanisms driving human cancer. The data is publicly available and it compilates different information about cancer genomics. It was accessed to the repository of actionable mutations though this link: https://cancer.sanger.ac.uk/cosmic/download/cosmic, which contains complete actionable data in .tar format. This dataset was transformed into .csv. and we gather genomic data related to genes related with actionability counts, development statuses, drug combinations and other relevant data about drug candidates according to genomic information.

Enhanced Data Visualization Analysis Using ChatGPT

Complex prompts were inputted into ChatGPT to produce sophisticated data visualizations. These prompts were designed to refine the analysis based on initial observations in the spectrum of actionable variables and were introduced to explore deeper insights, particularly focusing on drug combinations, genomic mutations, actionability rank, and development status. The process included asking increasingly complex prompts to ChatGPT for visualization techniques and specific analysis queries. Utilizing Python, data visualizations were validated with pivot tables to explore the distribution patterns within the dataset. Pivot tables resembled the frequencies and relationship in matrices regarding the association of the different variables. This step was crucial to ensure that the insights obtained are accurate or reflective (with approximation) of the current scientific understanding and scientific evidence.

Results

Process of Data Visualization and Validation:

A simple prompt in chatGPT such as this “visualize the distribution of genes based on the top ten actionability counts, development status, and drug combinations” can help to visualize the distribution based on actionability rank, development status, and drug combinations, output a plot like the following:

This information was validated in python :

```
import pandas as pd
import seaborn as sns
import matplotlib.pyplot as plt

data_full = pd.read_csv(' /content/Actionability_AllData_v11_GRCh37.csv')
```

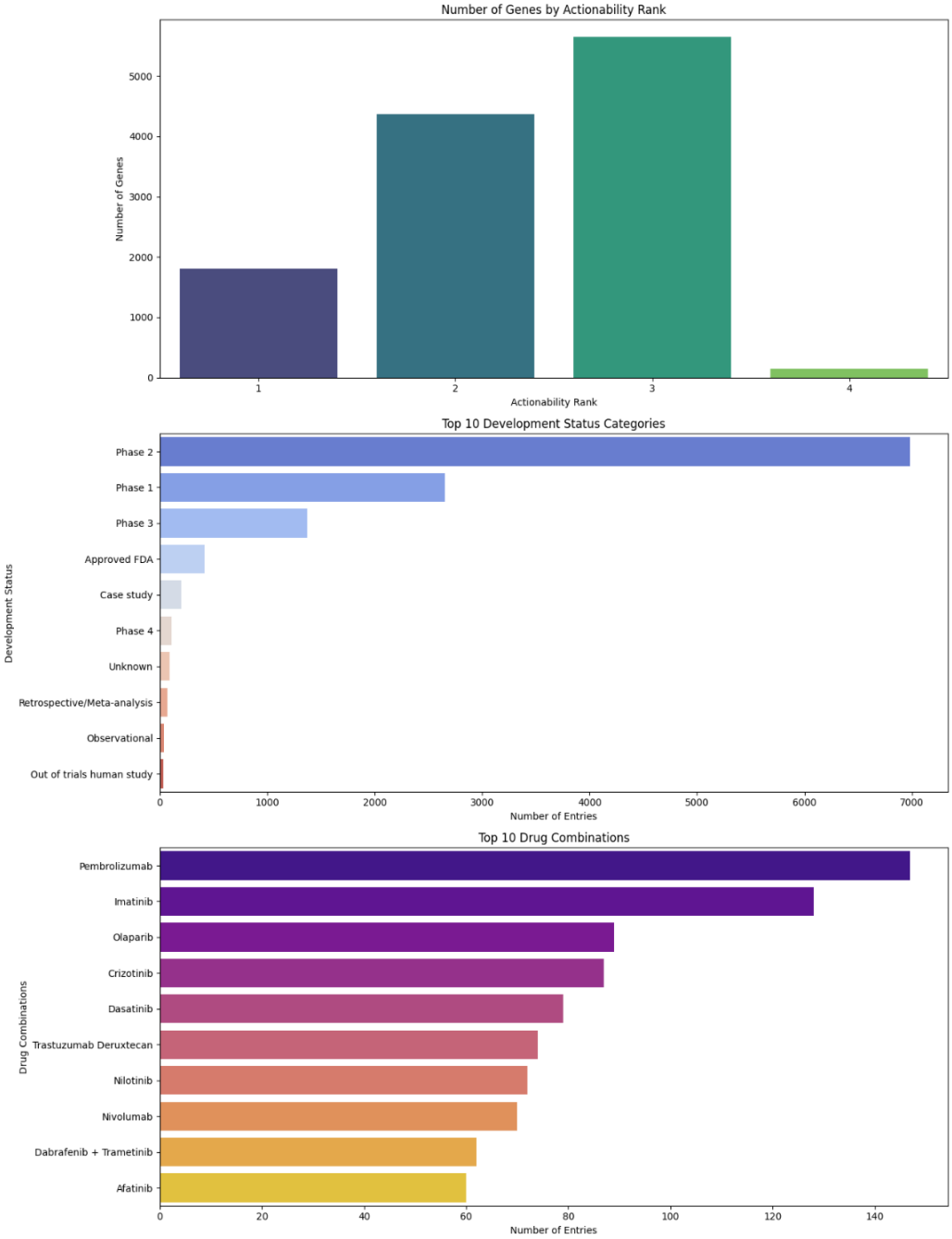

Figure 1.A. Number of drug combinations by actionability rank and development status: Actionability rank: 1: approved, 2: marketed drugs, 3: through clinical trial phases 4: case studies.

```
# Counts for 'Actionability Rank'
actionability_counts = data_full['ACTIONABILITY_RANK'].value_counts().nlargest(10)

# Counts for 'Development Status'
development_status_counts =data_full['DEVELOPMENT_STATUS'].value_counts().nlargest(10)

# Counts for 'Drug Combinations'
drug_combination_counts =data_full['DRUG_COMBINATION'].value_counts().nlargest(10)
actionability_table = actionability_counts.reset_index().rename(columns={'index': 'Actionability Rank',
'ACTIONABILITY_RANK': 'Frequency'})
development_status_table =
Same code for 'DEVELOPMENT_STATUS and 'DRUG_COMBINATION':
```

Table 1. Validation of number of drug combinations by actionability rank and development status

Actionability Rank	**Frequency**
3	5649
2	4368
1	1808
4	147
Development Status	**Frequency**
Phase 2	6986
Phase 1	2653
Phase 3	1371
Approved FDA	415
Case study	197
Phase 4	109
Unknown	92
Retrospective/Meta-analysis	71
Observational	40
Out of trials human study	33
Drug Combinations	**Frequency**
Pembrolizumab	147
Imatinib	128
Olaparib	89
Crizotinib	87
Dasatinib	79
Trastuzumab Deruxtecan	74
Nilotinib	72
Nivolumab	70
Dabrafenib + Trametinib	62
Afatinib	60

In the above Table 1, the actionability rank (also seen in the upper histogram illustrated in Figure 1) is divided in four stages that allow to identify the most advanced development stage reached by drugs that have been tested in patients with the specified mutation and disease. The values range from approved, marketed drugs (most advanced) through clinical trial phases to case studies (COSMIC, 2024). There may be multiple drugs at the same rank of development; individual drugs are not ranked. It can be seen that most of the drugs are positioned in the 3 rank.

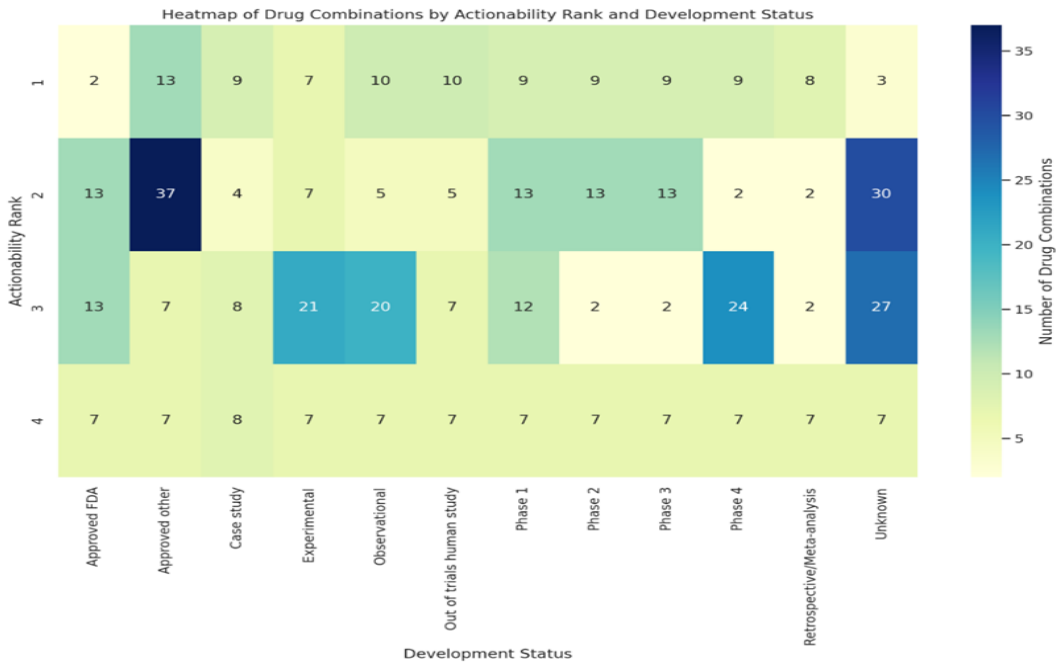

Figure 2. Heatmap of drug combinations by actionability rank and development status: Actionability rank: 1: approved, 2: marketed drugs, 3: through clinical trial phases 4: case studies.

The development status can also be observed (middle figure), most of developments are classified as phase 2 (with 6986 entries), this phase means that these studies are determining the effectiveness of an experimental drug on a particular disease or condition in approximately 100 to 300 volunteers. Finally, In the graph at the bottom it can be seen that Pembrolizumab is the drug with the greatest number of combinations in trials. Once identified these elements, the complexity of the analysis was enhanced by the following prompt: "Visualize the combination of actionability rank and development status, focusing on common drug combinations.

To validate the above table, we perform an approach to count the total number of drug combinations and obtain a pivot table of combinations in python:

```
pivot_table_combination_counts = data_filtered.groupby(['ACTIONABILITY_RANK',
'DEVELOPMENT_STATUS'])['DRUG_COMBINATION'].nunique().unstack(fill_value=0)

# Returning the adjusted pivot table for validation of numbers
pivot_table_combination_counts
```

Table 2. Validation of number of distinct drug combinations by actionability rank and development status

Actionability Rank	Approved FDA	Approved other	Case study	Experimental	Observational	Out of trials human study	Phase 1	Phase 2	Phase 3	Phase 4	Retrospective/ Meta-analysis	Unknown
1	65	2	10	0	3	4	243	533	136	21	12	22
2	79	1	4	0	15	5	665	1654	507	41	8	32
3	30	0	12	1	15	16	1033	1617	259	16	33	24
4	0	0	39	0	0	0	0	0	0	0	0	0
TOTAL	174	3	65	1	33	25	1941	3804	902	78	53	78

As it can be seen, Figure 2 showed wrong information about the name of drug combination, for example, the rank No 4 indicated 7 drug combinations approved by FDA (the data in Tabla 2 says that real number is 0). According to this, the code to plot was adjusted to show the number of drug combinations properly:

```
plt.figure(figsize=(14, 8))
sns.heatmap(pivot_table_combination_counts, annot=True, fmt="d", cmap='YlGnBu', cbar_kws={'label':
'Number of Distinct Drug Combinations'})
plt.title('Heatmap of Distinct Drug Combinations by Actionability Rank and Development Status')
plt.xlabel('Development Status')
plt.ylabel('Actionability Rank')
plt.show()
```

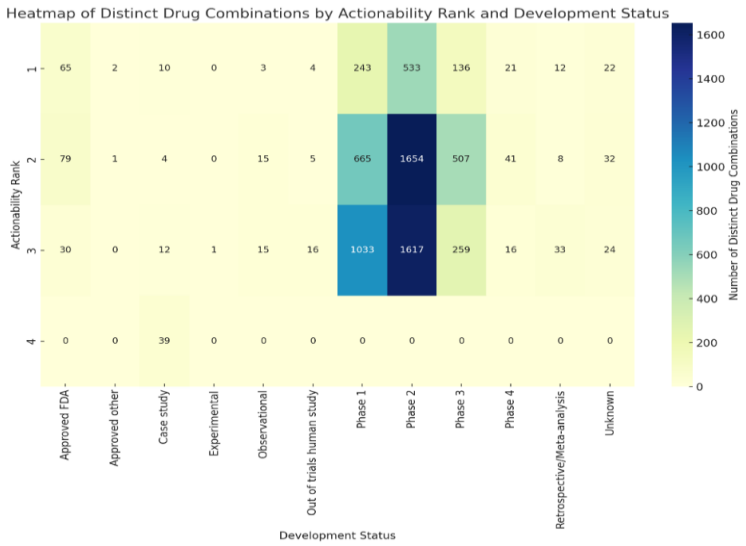

Figure 3. Heatmap of number of distinct drug combinations by actionability rank and development status, according to validation

Above plot does not add a lot of actionable information about the most prominent drugs used according to actionable mutations, so it was asked to chatGPT: "Graph but according to the top 10 drug combination" obtaining the next plot:

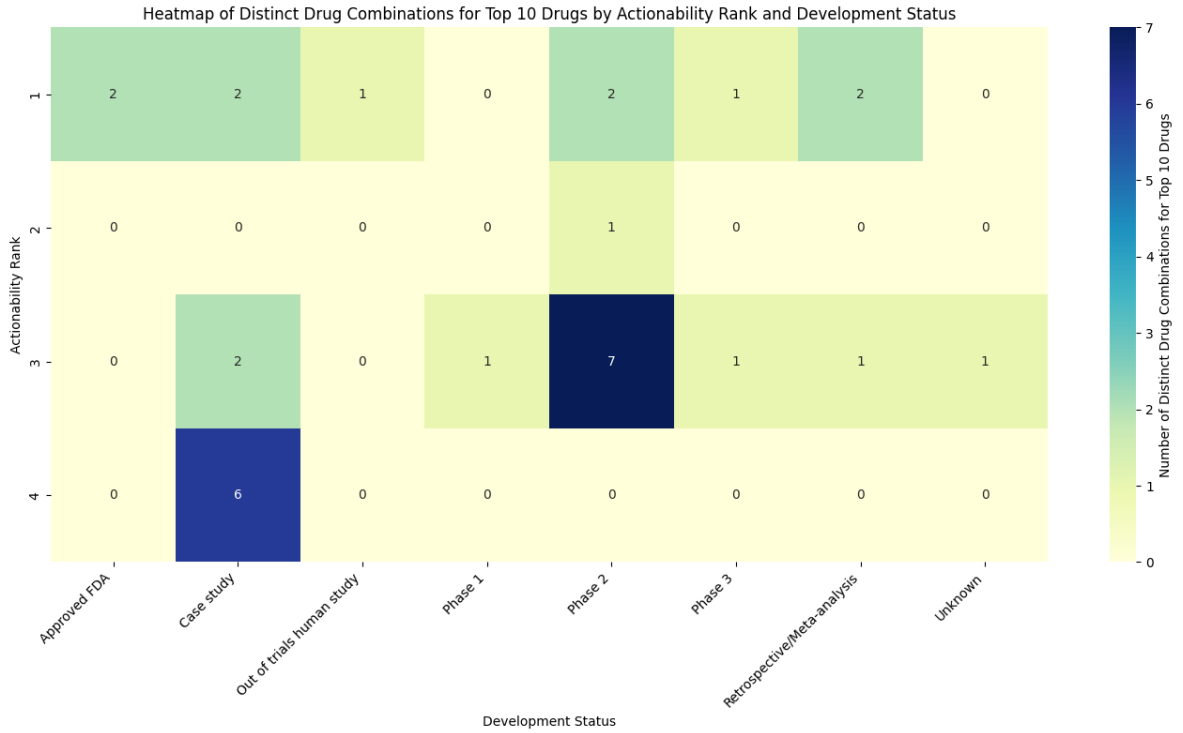

Figure 4. Heatmap of the top 10 drug combinations by actionability rank and development status

However, the matrix did not show the names of the drugs, so it was asked to chatGPT to "improve the above graph showing the name of the drugs" and this graph was obtained:

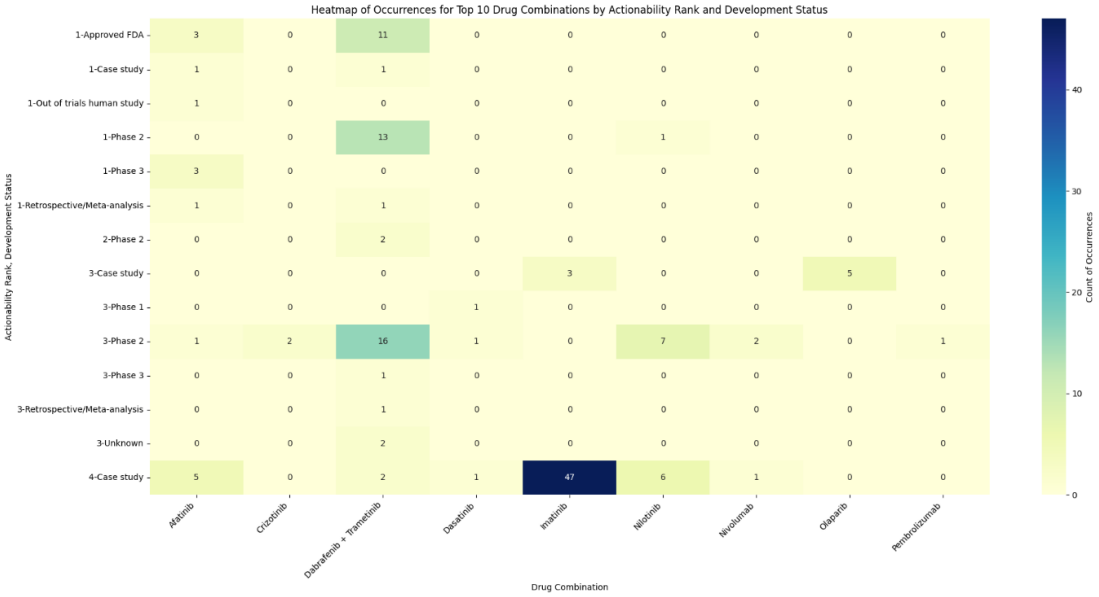

Figure 5. Heatmap of the top 10 drug combinations by actionability rank and development status and by the names of the combinations

In the above graph, the names of the combinations are now illustrated, the heatmap now visualizes the distribution of the top 10 drug combinations by actionability rank and development status. This graph highlights how these specific drugs are distributed across different stages of development and ranks of actionability,

providing insight into the concentration of the research and clinical interests in these combinations. It is observed, for example, that Imatinib has 47 concurrences just in the rank No.4 of actionability in case studies.

To validate the graph, we created in python a new pivot table thinking as ChatGPT and we filtered occurrences rather than unique counts, and put drug names to the columns:

```
pivot_table_top_10_detailed = data_filtered_top_10.pivot_table(index=['ACTIONABILITY_RANK', 'DEVELOPMENT_STATUS'],
                                                               columns='DRUG_COMBINATION',
                                                               aggfunc='size',
                                                               fill_value=0)
pivot_table_top_10_simple = pivot_table_top_10_detailed.reset_index()
pivot_table_top_10_simple:
```

Table 3. Validation by the top 10 drug combinations by actionability rank and development status and by the names of the combinations.

DRUG_COMBINATION	ACTIONABILITY_RANK	DEVELOPMENT_STATUS	Afatinib	Crizotinib	Dabrafenib + Trametinib	Dasatinib	Imatinib	Nilotinib	Nivolumab	Olaparib	Pembrolizumab
0	1	Approved FDA	3	0	11	0	0	0	0	0	0
1	1	Case study	1	0	1	0	0	0	0	0	0
2	1	Out of trials human study	1	0	0	0	0	0	0	0	0
3	1	Phase 2	0	0	13	0	0	1	0	0	0
4	1	Phase 3	3	0	0	0	0	0	0	0	0
5	1	Retrospective/ Meta-analysis	1	0	1	0	0	0	0	0	0
6	2	Phase 2	0	0	2	0	0	0	0	0	0
7	3	Case study	0	0	0	0	3	0	0	5	0
8	3	Phase 1	0	0	0	1	0	0	0	0	0
9	3	Phase 2	1	2	16	1	0	7	2	0	1
10	3	Phase 3	0	0	1	0	0	0	0	0	0
11	3	Retrospective/ Meta-analysis	0	0	1	0	0	0	0	0	0
12	3	Unknown	0	0	2	0	0	0	0	0	0
13	4	Case study	5	0	2	1	47	6	1	0	0

Later, we were interested in identifying the most common genomic mutations and combinations, we generated the following prompt “code the 10 most common genomic mutations and drug combinations” and this was the plot of ChatGPT:

Figure 6. Heatmap of genomic mutation vs drug combinations.

To validate the Figure 6, we generated a pivot table:

```
import pandas as pd
from collections import Counter
# Counting occurrences of genomic mutations and drug combinations
genomic_mutation_counts = Counter(data['GENOMIC_MUTATION_ID'])
drug_combination_counts = Counter(data['DRUG_COMBINATION'])
# Selection of the top 10 most common genomic mutations and drug combinations
top_genomic_mutations = [mutation for mutation, count in genomic_mutation_counts.most_common(10)]
top_drug_combinations = [drug for drug, count in drug_combination_counts.most_common(10)]
# Filtering the dataset for entries with the top genomic mutations and drug combinations
filtered_data = data[(data['GENOMIC_MUTATION_ID'].isin(top_genomic_mutations)) &
                     (data['DRUG_COMBINATION'].isin(top_drug_combinations))]
# Create a pivot table for the heatmap
pivot_table = filtered_data.pivot_table(index='GENOMIC_MUTATION_ID',
columns='DRUG_COMBINATION',
                                        aggfunc='size', fill_value=0)
```

Table 4. Validation of the 10 most common genomic mutations and drug combinations.

GENOMIC_MUTATION_ID	Afatinib	Dabrafenib + Trametinib	Dasatinib	Imatinib	Nilotinib	Nivolumab	Pembrolizumab
51765492	2	0	0	0	0	0	0
55386424	0	0	1	1	1	0	0
56056643 + 56059110	0	27	0	0	0	0	0
56056643 + 56059110 + 56057713	0	8	0	0	0	0	0
56056643 + 56059110 + 56057713 + 56058419 + 56115685 +	0	9	0	0	0	1	1
56288520 + 56059623 + 56293156 + 56065204 + 56075762 +	0	0	0	0	1	0	0
56076564 + 56080151 + 56124012 + 56152883 + 56228237	0	0	0	0	1	0	0
59323790	0	0	0	0	1	0	0

Discussion

Critical Thinking and Problem Solving in Medicine

Teaching students to critically interpret genomic data and other big data from biomedicine is the future of personalized medicine. Medical datasets are available for free use and sometimes it is difficult to interpret the data. Nowadays, OpenAI's ChatGPT Code Interpreter can handle data and carry out different coding operations, in our case, we played with bottom and less complex prompts to understand a complex dataset. The first step was by asking the number of drug combinations by actionability rank and development. In this case the plots were amazingly clear, showing the histograms of the 10 top combinations whose data were validated with a pivot table and with a raw analysis by searching for the reflected numbers. The precision and reliability of this graphs were 100%. These data were searched in the literature and no graphic as such was found. Just few articles talk about this specific dataset inside the COSMIC database, for example Sondka and cols talk about COSMIC curated information on 988 actionable variants across 445 genes., informing data on 11,121 clinical trials and 5,174 treatment combinations but they did not explore data combinations (Sondka et al., 2024) Boland and cols., have found in COSMIC that 30% of a total of 500 patients had mutations in potentially actionable genes, highlighting the significant potential for genotype-driven clinical trials as they represent a substantial portion of population with advanced cancer, underscoring the clinical utility of this information, furthermore they found that actionable mutations are not confined to the most common cancers (such as KRAS mutations in pancreas) so their approach went even deeper (Boland et al., 2015) Other previous studies, have focused on ICGC/TCGA Pan-Cancer Analysis datasets (also incorporated in COSMIC) to give valuable insights such as signals of positive selection to identify driver genes, mutational patterns on driver genes, functional networks such as the 13 candidate cancer genes within their functional interaction context (ATR, STAG2, PIK3CG, MED13, NCOA3, PIK3CB, FOXA1, CDKN1B, CDKN1A, MED17, FOXA2, FHEB, PRKCD) (Tamborero et al., 2013)

The potential of systematic and context-specific evaluation of drug combinations to enhance the precision and effectiveness of cancer treatments is imperative for new drug combinations discoveries. In our study, the Figure 3 (remember that Figure 2 was wrong and later on was validated) shows the combinations by actionability rank and development status. This graph updates the number of drug combinations reported in COSMIC and demonstrates that most of them are representatives of 2 or 3 actionability rank and participating in phase 1, 2 and 3 of development status. This information, have profound implications for clinical trials and cancer treatment development, for example, Jaaks and cols., studied 2,025 two-drug combinations across 125 molecularly characterized cancer cell lines, identified effective combinations, particularly those showing high synergy in cancers with unmet clinical needs, showing a rational efforts to develop combination treatments (Jaaks et al., 2022). Other works, such as Yang and cols, use this data to predict drug synergies, the importance of computational approaches, and the challenges faced in these predictions, however they focused in MdrDB, a database that integrates data from seven publicly available datasets, which is the largest database of its kind (Yang et al., 2023). Other computational models have been used to predict synergies focusing on co-targeting functionally proximal genes to enhance the efficacy of drug combinations finding some interesting combinations such as CDK4/6 Inhibition with Estrogen Receptor Therapy in breast cancer or BRAF and MEK1/2 Inhibitors in melanoma (Nair et al., 2023). All these this combination of experimental screening and computational analysis provides comprehensive methods for identifying and validating effective drug combinations in cancer treatment-

ChatGPT also has the power to decompose complex data as it was asked to "Graph but according to the top 10 drug combination" obtaining Figure 4. As this matrix did not show the names of the drugs, it was asked to "improve the above graph showing the name of the drugs" which brings interesting information (Figure 5) about the top 10 drug combinations (with their names) by actionability rank and development status. This plot was validated in Table 3 with 100 matching. Finally, it was also possible to identify the most common genomic mutations and drug combinations (Figure 6) which was also validated with a pivot table ın Table 4. The data obtained in both figures is essential for understanding the distribution and prevalence of treatment strategies for various genetic mutations (according to the data set). According to Sondka, understanding the distribution and prevalence of treatment strategies for various genetic mutations is crucial for advancing personalized medicine, enhancing the effectiveness of treatments, and ultimately improving patient care in oncology and beyond. This approach not only helps in treating diseases but also in preventing them and improving the quality of life for patients (Sondka et al., 2024)

Implications for Education and Research in Medical Science

In education, especially medical and genetics education, the integration of Big Data analytics is transforming core curriculums. Educators are now incorporating data science and ML into courses to equip students with the skills necessary to handle large datasets and complex information. This shift is aimed at preparing students for the challenges they will face in a data-driven healthcare environment, ensuring they can leverage these tools for improved patient care and research outcomes.

In the realm of personalized medicine, identifying actionable information—such as specific biomarkers for diseases—allows for more precise treatment strategies. For instance, knowing particular genetic mutations in cancer can guide the use of targeted therapies, thereby improving treatment efficacy and patient outcomes. This is crucial in cancer treatment, where somatic mutations can influence the effectiveness of drugs. These insights help in advancing personalized medicine by making treatment more responsive to individual genetic profiles. Through the effective use of AI like ChatGPT and ML platforms, both sectors can benefit from more precise and actionable insights, driving forward the capabilities of professionals to make informed decisions and innovate within their respective fields.

Conclusıon

To mitigate the risks associated with potential pitfalls in data-driven medicine, interdisciplinary collaboration among data scientists, healthcare professionals, ethicists, and policymakers is required. Additionally, robust quality assurance mechanisms, transparent reporting standards, and ongoing evaluation of data sources and algorithms are needed to ensure the reliability and validity of insights derived from big data analytics in healthcare. Treatment planning, risk prediction, and diagnostic approach are essential components of artificial intelligence in precision medicine. Although data management and replication issues pose challenges for AI-based precision medicine, it has been shown to enhance healthcare and reduce medical errors. Electronic health records and imaging analysis have been proven to present opportunities for AI-based precision medicine.

A future is envisioned in which data integration is achieved, enhancing its effectiveness, and bolstering the confidence of both researchers and the general population, thereby promoting its usage and contributing to its enhancement. However, the Big Data revolution has not yet reached its full potential; significant challenges still need to be overcome. Among them, the importance of collecting high-quality data and the necessity of efficient processes to translate large volumes of complex data into meaningful insights stand out. It is crucial to recognize that the mere availability of data does not ensure its validity. Additionally, issues such as data interoperability, as well as the legal and ethical implications associated with the use of personal data, must be addressed. Despite these challenges, it is evident that this technology, although still in its early stages, is at the beginning of a long and promising journey.

In summary, the ability to find and use actionable information in complex databases like COSMIC is also essential to advance in personalized medicine, improve patient care, and foster research and development in the field of cancer. Automation and open access are key elements that enable efficient management of large volumes of data, promote equality in access to information, and facilitate collaboration and rapid advancement in health research and education. The use of ChatGPT is a powerful tool to enhance medical research and to obtain clues or fingerprints of actionable data that can be extrapolated to the clinic. In our case, to bring new information about current combinations for cancer in the market, to give a landscape of actionability and to identify a pool of biomarkers that, if handled properly, can guide personalized treatment decisions. The validation of the data is the most important tool when these generative tools are introduced to the research, added to the use of ethical guidelines and protocols to avoid biases and comparison with previous and current data found in literature.

Scientific Ethics Declaration

The authors declare that the scientific ethical and legal responsibility of this article published in EPSTEM journal belongs to the authors.

Acknowledgements or Notes

* This article was presented as oral presentation at the International Conference on Basic Sciences, Engineering and Technology (www.icbaset.net) held in Alanya/Turkey on May 02-05, 2024.

* The authors would like to thank the financial support from Tecnologico de Monterrey through the "Challenge-Based Research Funding Program 2022". Project ID # I001 - IFE001 - C1-T1 - E. Also, financial and technical support from Writing Lab, Institute for the Future of Education, Tecnologico de Monterrey, Mexico.

References

Batko, K., & Ślęzak, A. (2022). The use of big data analytics in healthcare. *Journal of Big Data*, *9*(1), 3.

Blatter, T. U., Witte, H., Nakas, C. T., & Leichtle, A. B. (2022). Big data in laboratory medicine faır quality for AI?. *Diagnostics*, *12*(8), 1923.

Boland, G. M., Piha-Paul, S. A., Subbiah, V., Routbort, M., Herbrich, S. M., Baggerly, K., Patel, K. P., Brusco, L., Horombe, C., Naing, A., Fu, S., Hong, D. S., Janku, F., Johnson, A., Broaddus, R., Luthra, R., Shaw, K., Mendelsohn, J., Mills, G. B., & Meric-Bernstam, F. (2015). Clinical next generation sequencing to identify actionable aberrations in a phase I program. *Oncotarget*, *6*(24), 20099-20110.

Chakraborty, C., Bhattacharya, M., & Lee, S.-S. (2023). Artificial intelligence enabled ChatGPT and large language models in drug target discovery, drug discovery, and development. *Molecular Therapy - Nucleic Acids*, *33*, 866-868.

COSMIC. (n.d.). *COSMIC Actionability | Product Information*. Recuperado 12 de abril de 2024, de Retrieved from https://cancer.sanger.ac.uk/actionability/help

Fischer, C., Pardos, Z. A., Baker, R. S., Williams, J. J., Smyth, P., Yu, R., Slater, S., Baker, R., & Warschauer, M. (2020). Mining big data in education: affordances and challenges. *Review of Research in Education*, *44*(1), 130-160.

Greene, A. C., Giffin, K. A., Greene, C. S., & Moore, J. H. (2016). Adapting bioinformatics curricula for big data. *Briefings in Bioinformatics*, *17*(1), 43-50.

Jaaks, P., Coker, E. A., Vis, D. J., Edwards, O., Carpenter, E. F., Leto, S. M., Dwane, L., Sassi, F., Lightfoot, H., Barthorpe, S., van der Meer, D., Yang, W., Beck, A., Mironenko, T., Hall, C., Hall, J., Mali, I., Richardson, L., Tolley, C., &Garnett, M. J. (2022). Effective drug combinations in breast, colon and pancreatic cancer cells. *Nature*, *603*(7899), 166-173.

Lee, C. H., & Yoon, H.-J. (2017). Medical big data: Promise and challenges. *Kidney Research and Clinical Practice*, *36*(1), 3-11.

Li, J., Dada, A., Puladi, B., Kleesiek, J., & Egger, J. (2024). ChatGPT in healthcare: A taxonomy and systematic review. *Computer Methods and Programs in Biomedicine*, *245*, 108013.

Luan, H., Geczy, P., Lai, H., Gobert, J., Yang, S. J. H., Ogata, H., Baltes, J., Guerra, R., Li, P., & Tsai, C.-C. (2020). Challenges and future directions of big data and artificial ıntelligence in education. *Frontiers in Psychology*, *11*.

Nair, N. U., Greninger, P., Zhang, X., Friedman, A. A., Amzallag, A., Cortez, E., Sahu, A. D., Lee, J. S., Dastur, A., Egan, R. K., Murchie, E., Ceribelli, M., Crowther, G. S., Beck, E., McClanaghan, J., Klump-Thomas, C., Boisvert, J. L., Damon, L. J., Wilson, K. M., & Benes, C. H. (2023). A landscape of response to drug combinations in non-small cell lung cancer. *Nature Communications*, *14*(1), 3830.

Ostroverkhova, D., Przytycka, T. M., & Panchenko, A. R. (2023). Cancer driver mutations: Predictions and reality. *Trends in Molecular Medicine*, *29*(7), 554-566.

Puiu, A., Gómez Tapia, C., Weiss, M. E. R., Singh, V., Kamen, A., & Siebert, M. (2024). Prediction uncertainty estimates elucidate the limitation of current NSCLC subtype classification in representing mutational heterogeneity. *Scientific Reports*, *14*(1), 6779.

Sahu, M., Gupta, R., Ambasta, R. K., & Kumar, P. (2022). Artificial intelligence and machine learning in precision medicine: A paradigm shift in big data analysis. Progress in Molecular Biology and Translational Science, *190*(1), 57-100.

Sondka, Z., Dhir, N. B., Carvalho-Silva, D., Jupe, S., Madhumita, McLaren, K., Starkey, M., Ward, S., Wilding, J., Ahmed, M., Argasinska, J., Beare, D., Chawla, M. S., Duke, S., Fasanella, I., Neogi, A. G., Haller, S., Hetenyi, B., Hodges, L., & Teague, J. (2024). COSMIC: A curated database of somatic variants and clinical data for cancer. *Nucleic Acids Research*, *52*(D1), D1210-D1217.

Tamborero, D., Gonzalez-Perez, A., Perez-Llamas, C., Deu-Pons, J., Kandoth, C., Reimand, J., Lawrence, M. S., Getz, G., Bader, G. D., Ding, L., & Lopez-Bigas, N. (2013). Comprehensive identification of mutational cancer driver genes across 12 tumor types. *Scientific Reports*, *3*, 2650.

Tempini, N., & Leonelli, S. (2021). Actionable data for precision oncology: Framing trustworthy evidence for exploratory research and clinical diagnostics. *Social Science & Medicine, 272*, 113760.

Yang, Z., Ye, Z., Qiu, J., Feng, R., Li, D., Hsieh, C., Allcock, J., & Zhang, S. (2023). A mutation-induced drug resistance database (MdrDB). *Communications Chemistry*, *6*(1), 1-9.

Wesson, P., Hswen, Y., Valdes, G., Stojanovski, K., & Handley, M. A. 2022. Risks and opportunities to ensure equity in the application of big data research in public health. *Annu.Rev.Public Health, 43,* 59-78.

Author Information

M.S. Ramírez-Montoya
EGADE Business School, Institute for the Future of Education, Tecnologico de Monterrey,
Monterrey, Mexico
Contact e-mail: *solramirez@tec.mx*

G.A. Sanchez-Zuno
School of Medicine. Internal Medicine Department (USA),
Yale University,
New Haven, CT, U.S.A.

R.M. Marques González
Hospital Civil de Guadalajara, Medical Genetics Department, Mexico

F. Casıllas-Muñoz
Institute for the Future of Education, Tecnologico de Monterrey, Mexico City, Mexico

To cite this article:

Ramírez-Montoya, M.S., Sanchez-Zuno, G.A., Marques González, R. M., & Casillas-Muñoz, F. (2024). Complex thinking abilities in the rapidly evolving field of genomics and personalized medicine: Analysis of actionability on cancer with ChatGPT and literature. The Eurasia Proceedings of Science, Technology, Engineering & Mathematics (EPSTEM), *28,* 34-46.

The Eurasia Proceedings of Science, Technology, Engineering & Mathematics (EPSTEM)
ISSN: 2602-3199

The Eurasia Proceedings of Science, Technology, Engineering & Mathematics (EPSTEM), 2024

Volume 28, Pages 47-55

ICBASET 2024: International Conference on Basic Sciences, Engineering and Technology

Effect of Graphene Nanoplatelets and Accelerated Weathering on the Mechanical and Shape Memory Behaviour of 3D Printed Components

Mohamad Alsaadi
University of Limerick
Technological University of the Shannon

Eoin P. Hinchy
University of Limerick

Conor T. McCarthy
University of Limerick

Declan M. Devine
Technological University of the Shannon

Abstract: The need for sustainable materials has increased the adoption of 3D printing techniques in various applications due to their valuable advantages of obtaining complex design, fast site production, with significantly less waste, and thus more cost-effective, compared to traditional polymer processing techniques like moulding and extrusion. The objective of this work is to investigate the effect of functionalised graphene nanoplatelets and accelerated weathering ageing on the tensile, Izod impact, fracture toughness and shape memory behaviour of 3D printed methacrylate-based resin. The accelerated weathering aging of 1000 hrs was conducted on the 3D printed samples. The fracture toughness results in terms of critical stress intensity factor were calculated using single-edge notch bending (SENB) tests. The shape memory (SM) behaviour in terms of shape fixity and shape recovery results were determined using dynamic mechanical analysis (DMA). The results showed good resistance to weathering ageing and enhancement by incorporating functionalised graphene nanoplatelets. The maximum increment values of the tensile strength, impact resistance and critical stress intensity factor were 18%, 25% and 16%, respectively. The glass transition temperature values were slightly increased. The shape fixity ratios and the shape recovery ratios were greater than 97% and 90%, respectively. This study provides new knowledge in expanding and developing 4DPg in various industrial applications like in soft robotics as actuators and thermal sensors.

Keywords: 3D printing, Graphene nanoplatelets, Accelerated weathering,

Introduction

Due to several benefits from this smart fabrication method like complex design, easy access, less lead time, lower energy consumption, lower material waste and lower cost. These advantages make 3D printing (3DPg) technology a significant aspect of Industry 4.0 and a leading technique for various sectors. Additionally, these sustainable fabrication methods like liquid-based, powder-based and filament-based 3DPg have inspired and motivated the public to be employed in different uses such as education purposes, art, decoration, creating spare parts at home, and many other applications (Alsaadi et al., 2023; Mahmood et al., 2023; Prashar et al., 2022). The 4DPg manufacturing employs a smart material to fabricate a 3DPd structure that can change shape over time in response to an external stimulus. Therefore, 4DPg can play a vital role in several sustainable applications like soft robotics, energy harvesters, renewable energies, and self-healing structures (Pisani et al.,

2022; Vatanparast et al., 2023). The sequences of changing shapes can be achieved for various composite structures and designs that have the SM property (Mao et al., 2015; Yu et al., 2015). For instance, Mao et al. (Mao et al., 2015) employed thermal stimulus for the 3D printed (3DPd) UV-cured epoxy-based SM polymers to achieve self-closing devices. By identifying material structure in various sections, the authors proved that the programmed component can be returned to the permanent shape in a predefined sequence, thus exhibiting a multiple-way SM polymer.

Polymeric materials can be sensitive to UV-light radiation, humidity and heat. For instance, the thermal and mechanical behaviour can be changed due to absorbing moisture, especially at high temperatures hence the water absorption into the polymer matrix can be increased (Afshar et al., 2016; Afshar & Wood, 2020). Exposure to sunlight for long intervals can initiate chain crosslinking and chain scission that can deteriorate the matrix polymeric materials by affecting their chemical compound. Chain crosslinking can make the polymer brittle, which may generate microcracks in the material surface. Chain scission may decrease the molecular weight and degrade the thermal and strength resistance of the polymer matrix (Afshar et al., 2019; Alfaro et al., 2022). Nevertheless, mechanical and thermal behaviour can be improved by short-term exposure to UV radiation, temperature and humidity (AWRTH) (Alfaro et al., 2022). For example, Golhin et al. (Golhin et al., 2023) indicated that the stiffness and T_g of the 3DPd polymer resin using a rotary PolyJet printer were improved after 58 days of AWRTH ageing due to the chain rearrangement of the liquid resin leading to denser liquid resin chains, generating more resistance for the deformation. The storage modulus can be enhanced with AWRTH ageing due to the increase of polymeric chain packing and rigidity (Spiridon et al., 2018). Bass et al. (Bass et al., 2016) reported the ultimate tensile stress and the elongation of liquid-based 3DPd resin increased over time while lighting conditions did not affect material properties significantly. On the other hand, noncovalent functionalisation by melamine has been utilized to improve nanoparticle dispersion and prevent agglomeration defects (Alsaadi et al., 2023; Shen et al., 2016; Wu et al., 2020). For instance, 4DPg of 0.1 to 0.3 wt% graphene nanoparticles reinforced acrylate resin marginally improved the T_g and tensile strength. The authors suggested that using graphene nanocomposite resins can enhance printability and create novel SM nanocomposites (Chowdhury et al., 2021).

In this experimental investigation, a DLP 3DPd resin was used to manufacture mGNP nanocomposite objects. The mechanical and fracture properties were investigated by tensile, Izod impact and single-edge notch bending tests. The fracture surface morphology of the SENB specimens was observed via scanning electron microscopy (SEM). The curing level was investigated via differential scanning calorimetry (DSC), chemical behaviour was tested via Fourier transform infrared spectroscopy (FTIR) and the SM properties via dynamic mechanical analysis (DMA).

Materials and Methods

Materials and Preparation of 3DPd Specimens

The commercial 3DPd resin used was Tough-Blk-20 resin (referred here as TG0) (3D Systems, Inc., Rock Hill, South Carolina, USA) consists of Methacrylate Ester Monomer (25-35%), Trimethyl cyclohexyl acrylate (10-20%), Isobomyl acrylate (10-20%), 2-Propenoic acid, 2-phenoxyethyl ester (1-2.5%), phenylbis (2,4,6-trimethylbenzoyl) phosphine oxide (BAPO) (1-5%) and stabiliser (1-2.5%). The GNP was used with 5 μm particle size, 15 nm thickness and 0.03–0.1 $g \cdot cm^{-3}$ bulk density. Melamine was used to functionalise GNP. N,N-dimethylformamide (DMF) was used for dissolving melamine and GNP. DMF is a unique organic material with the formula $(CH_3)_2NC(O)H$. It is something not only a solvent, but it can also play a significant role in organic chemistry. It can be employed as a catalyst, reagent, and stabilizer (Heravi et al., 2018). The materials were supplied by Sigma-Aldrich (Dorset, UK). TG0 resin can be used to produce 3DPd durable components (black like ABS (Acrylonitrile Butadiene Styrene)) with high UV, thermal, moisture, colour and dimension stability, which can be used for various applications like automotive styling components, consumer electronics parts, bezels, knobs, brackets, covers and robust functional prototypes (3D Systems Inc ,n.d.).

The melamine was mixed with a magnetic stirrer with GNP within DMF solution followed by an ultrasonication process. As seen in Figure 1, ball-milling is used for 24 h to trigger the functionalisation process between melamine and GNP (mGNP). The melamine's hexagonal ring generates π–π interactions on the GNP surface due to the ball-milling process. The mixture was vacuum filtered and vacuum dried to produce the black solid mGNP. The mGNP was examined and proved via several characterisation techniques like thermogravimetric analysis (TGA), FTIR, ultraviolet-visible (UV-Vis) spectroscopy and Raman spectroscopy (Alsaadi et al.,2023). TG0 was blended with 0.08 wt% of the mGNP at 35 °C.

The blend was stirred for 30 min and mixed for another 30 min at 1500 rpm in a planetary centrifugal mixer. Then, the prepared resin was mixed under vacuum for 20 min at 200 rpm to remove the air bubbles (Figure 1). The 3DPg process was conducted by transferring the resin to the tank of the Figure 4® printer (3D Systems, Inc., Rock Hill, South Carolina, USA). The printer's UV light is 405 nm wavelength, and the layer thickness is selected with a size of 0.1 mm. After support structure removal, the 3DPd specimens (Figure 2) were washed for 1 min by isopropyl alcohol (IPA) and UV post-cured for 90 min.

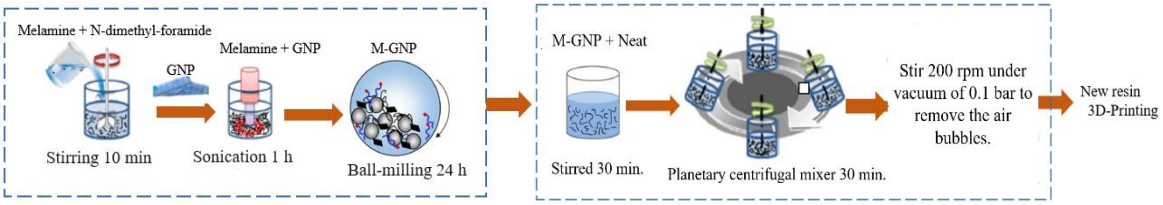

Figure 1. Schematic illustration of Ball-milling process to functionalise GNP by melamine.

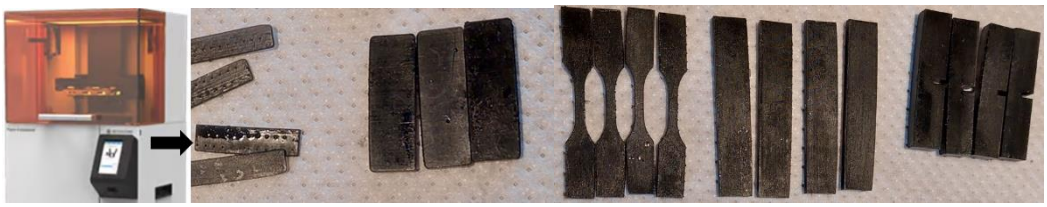

Figure 2. Figure 4® printer and 3DPd specimens.

Testing Methods

Zwick Roell machine (Z010, GmbH & Co. KG, DEU) was used for tensile experiments (gauge length of 7.62 mm) with a crosshead speed of 1 mm·min^{-1} according to ASTM D638 (Figure 3). The Izod impact test was carried out on an Izod impact machine (Instron CEAST) with a 5.5 J hammer according to the ASTM D4812 standard for unnotched specimens (Figure 3). The fracture toughness behaviour was investigated using a Zwick Roell machine by calculating the stress intensity factor of the SENB specimens according to the ASTM standard D5045-99 (Figure 3). The pre-crack was introduced in the 3DPg process. The crosshead speed was 2 mm·min^{-1}. The SENB specimens were printed with a size of 52.80 × 12.00 × 6.35 mm^3. The fracture surfaces of the failed SENB specimens were investigated using Mira SEM (Tescan, Oxford Instruments, Cambridge, UK). At least four specimens were experimented for each test.

The DSC analysis was conducted using Perkin Elmer machine DSC 4000 (Norwalk, CT, USA). 7 mg samples were analysed. These were heated from 0 to 225 °C at 5 °C/min, then cooled to 0 °C at 5 °C/min. The DSC measurements were achieved under the nitrogen atmosphere. The FTIR test was conducted by ATR-FTIR Perkin Elmer machine (Norwalk, CT, USA) with average scan from 400 cm^{-1} to 4000 cm^{-1} wavenumber and resolution of 4 cm^{-1}.

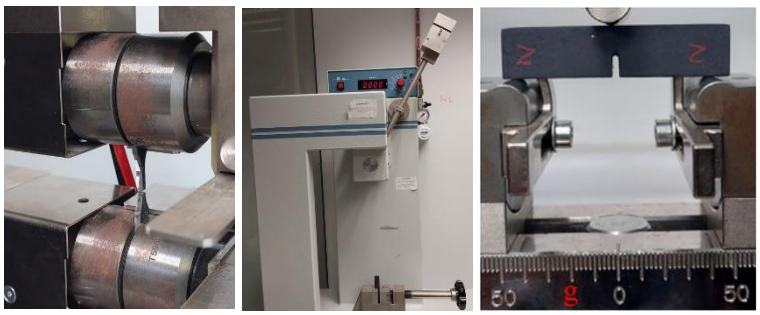

Figure 3. Specimens under tensile, Impact and SENB tests

The SM cycling tests are conducted to characterise the SM performance in terms of shape fixity and shape recovery under DMA single cantilever mode. This technique is commonly employed for analysing the programming/recovery behaviour of SM polymers. Tg was considered as a reference temperature to design the thermomechanical SM cyclic test. The procedure is performed as follows: (1) The specimen is heated to around 15 °C above Tg at a rate of 5 °C min^{-1} and isothermal for 20 min, (2) the specimen is deformed by applying a

force ramped at the rate of 0.5 N min^{-1} up to 3 N, (3) the specimen is cooled down to -10 °C with holding the force constant, (4) the force is released (Calculate the shape fixity is at end of this step), (5) The specimen is heated back above Tg (Calculate the shape recovery is at end of this step). The procedure was repeated from step (2) to take an average of five cycles.

Results and Discussion

Tensile and Impact Behaviour

The tensile strength and elastic modulus results of the 3DPd specimens are presented in Figure 4 (a). As seen in this figure, the UV-resist DLP 3DPd polymer with its mGNP nanocomposites exhibited good mechanical results. Hence, the tensile strength and elastic modulus values improved by 18% including mGNP and slightly increased by 2% to 4 % with the AWRTH ageing. The elastic modulus values were also enhanced with the addition of mGNP with the AWRTH ageing. The Izod impact resistance values (Figure 4 (b)) were enhanced by 25% and were slightly increased with AWRTH ageing. The π–π interactions between GNP and melamine resulted in enhanced load transfer across the interface between the 3DPd matrix and GNP nanoparticle within the polymer nanocomposite (Cha et al., 2019). On the other hand, It can be presumed that, through short-term ageing, further post-curing may be initiated owing to the combined exposure influence of UV-light, temperature and humidity generating an advance action in the polymeric chains such as rearrangement, residual crosslinking and rigidity (Golhin et al., 2023).

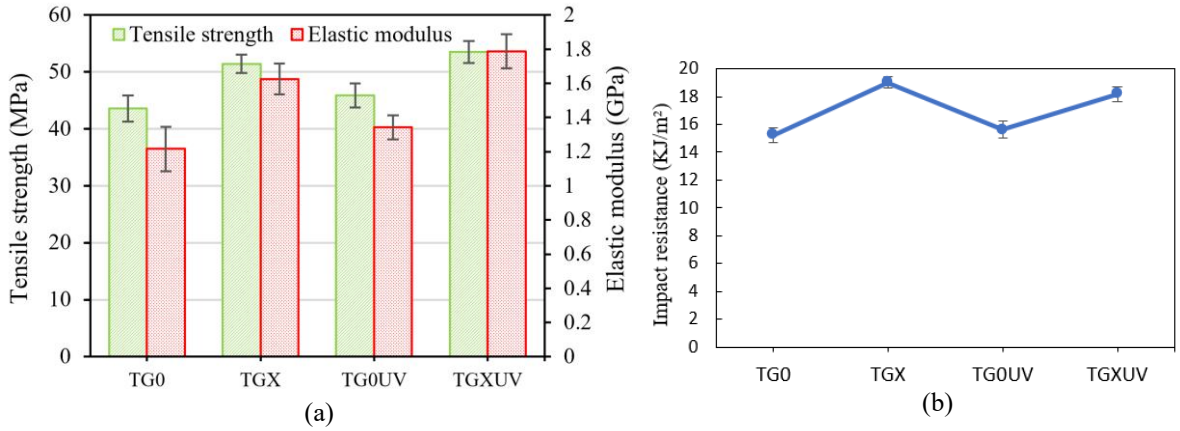

Figure 4. (a) Tensile strength and elastic modulus, and (b) impact resistance of the 3DPd specimens.

Fracture Toughness Behaviour

Fracture toughness mode I properties were determined in terms of stress intensity factor values (K_A) by testing SENB specimens. The crack length (a) was selected such that the $\frac{a}{W}$ the ratio was approximately 0.45 (W is the specimen width). The K_A values were determined as follows (ASTM D5045-99):

$$K_A = \left(\frac{P}{BW^{\frac{1}{2}}}\right) f\left(\frac{a}{W}\right) \tag{1}$$

$$f\left(\frac{a}{W}\right) = \frac{3sA^{1/2}}{2W} \frac{1.99 - A(1-A)(2.15 - 3.93A + 2.7A^2)}{(1+2A)(1-A)^{\frac{3}{2}}} \tag{2}$$

Where $A = \frac{a}{W}$, P is the fracture load, B is the specimen thickness and $f\left(\frac{a}{W}\right)$is the correction parameter.

Figure 5 presented the stress intensity factor values of the SENB specimens. As shown in this figure, K_A values were improved by incorporating mGNP of 0.08wt% by 16%. Hence, the strong bonding between mGNP and the 3DPd resin led GNP to pin the crack front and add additional crack growth resistance, indicating an enhancement in the fracture toughness result. The KA values were slightly increased by 1% to 3 % with the

AWRTH ageing. Figure 6 shows images for the failed SENB specimens and the fractured surfaces. The morphology of the surfaces of the failed SENB TG0 and TGX samples was observed via SEM (Figure 7). The M-GNP nanoparticles were embedded and homogeneously dispersed within the matrix. This indicates that melamine inhibits the GNP from aggregating through π–π interactions between the surfaces of GNP. Furthermore, the melamine's amino groups (-NH2) likely bonded covalently and led to strong interfacial interactions with the polymer matrix system.

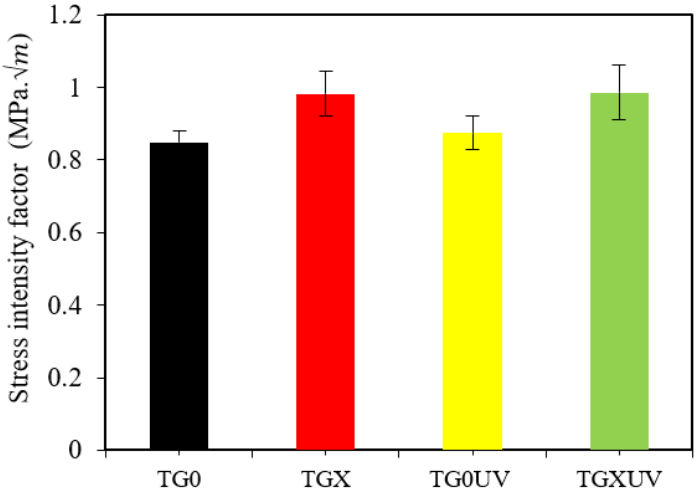

Figure 5. Stress intensity factor values of the SENB specimens

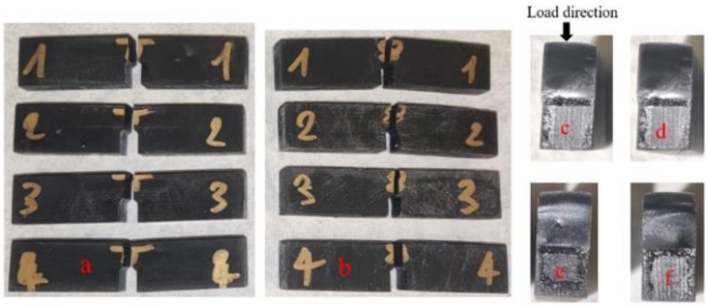

Figure 6. Failed SENB specimens (a) TGX, (b) TGX-UV, (c) TG0, (d) TGX, (e) TG0-UV and (f) TGX-UV

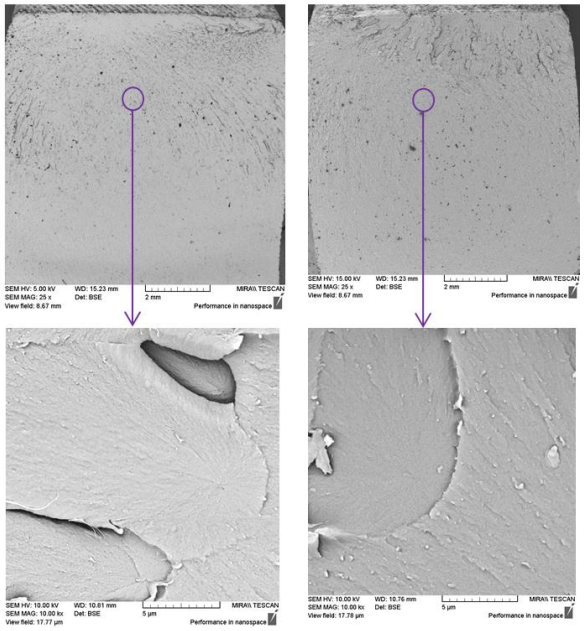

(**a**) (**b**)

Figure 7. SEM of the (a) TG0 and (b) TGX of the failed SENB specimens

Thermal and Chemical Behaviour

The DSC test was carried out to present the amorphous nature and crosslinking level of the 3DPd components. Figure 8a displays the DSC heating and cooling curves for the TG0, TGX, TG0UV and TGXUV samples before and after AWRTH of 1000 hrs. The variations of heat flow (exotherm and endotherm) obtained from the DSC test as a function of temperature indicated that the 3DPd samples were highly crosslinked amorphous nature that didn't observe the endothermic peak of crystal performance or crystalline domains. Additionally, the curing process didn't affect after the addition of mGNP. On the other hand, after AWRTH ageing the heat flow of the 3DPd samples heating up to 225 ^{o}C and cooling to 0 ^{o}C was stable behaviour.

The FTIR test was conducted to investigate the alterations in the chemical bonds due to outdoor accelerated weathering of TG0 and TGX samples (Figure 8b). The ester bonds represented by C–O stretching were located from 1000 cm^{-1} to 1300 cm^{-1}. When the samples are under AWRTH exposure, photo-cleavage of ester bonds can occur (Barkane et al., 2023; Shanti et al., 2017). At the same time, the bonds of C=C stretching may be used to generate crosslinking to form oligomers or add chain length to the existing network. These bonds may appear due to limitations of crosslinking conversion during the resin photopolymerisation (Barkane et al., 2022, 2023). The peaks at 2863 cm^{-1} and 2940 cm^{-1} can be ascribed to the symmetric stretching of CH_2 and CH2, respectively (Wu et al., 2019). The AWRTH led to increased peak intensities of 1630 cm^{-1} and 2940 cm^{-1} for the C=C stretching and CH_2/CH_3, respectively. On the other hand, the mGNP appeared at the peak bonds of C–O stretching and wasn't affected by AWRTH.

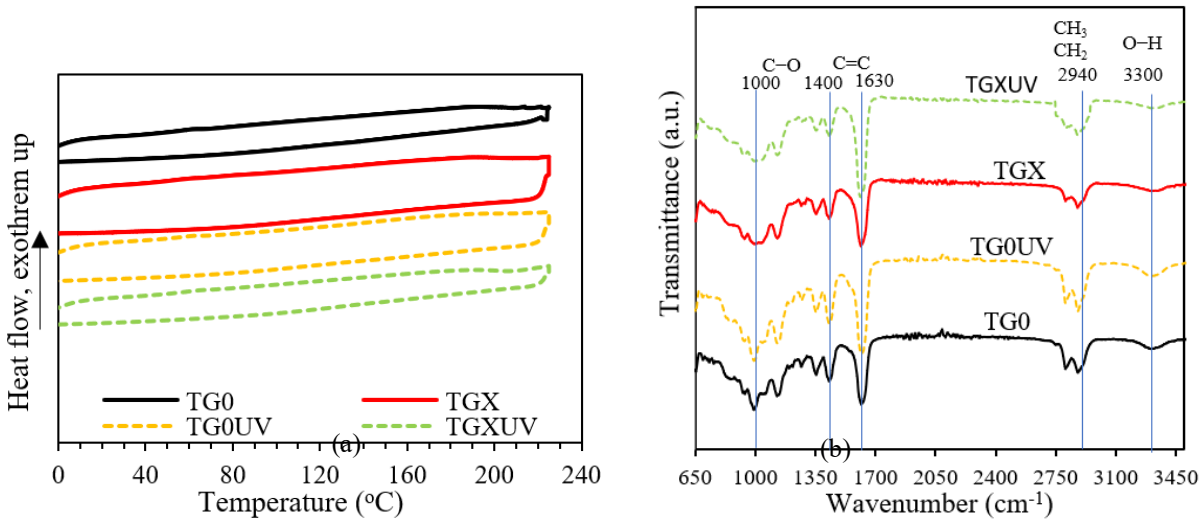

Figure 8. Thermal and chemical behaviour (a) DSC analysis and ; (b) FTIR spectra.

Shape-Memory Behaviour

The SM performance of the 3DPd specimens undergoing repeated thermomechanical cycles is illustrated in the 3D diagram as shown in Figure 9. Table 1 shows the average results of the maximum strain, fixity strain, and residual strain as obtained from the DMA machine, while the values of recovery ratio and fixity ratio were calculated by equations 1 and 2 in section 2.2. As shown in this figure, after releasing the force at a low temperature (-10 ^{o}C) and heating the sample inside the DMA machine the strain didn't decrease until the temperature reached the lower Tg (taken from the loss modulus). In other words, for all curves when heating the samples the recovery stage starts when the 3DPd sample enters the transition region between the glassy and rubbery behaviour and it is around 50 ^{o}C. Hence, molecular chain mobility becomes easier at the glass transition region. Hence, the fixity strain, ε_f, of (11.06, 10.29, 10.07, and 9.72) for the TG0, TGX, TG0UV and TGXUV samples with a maximum R_f of 97.7% was obtained for the unmodified resin. It is worth noticing that the sample recovered most of its original shape gradually at the glass transition region showing residual strain, ε_r, of (11.32, 10.58, 10.28, and 9.85) for the TG0, TGX, TG0UV and TGXUV samples with a maximum Rr of 94.1% obtained with including functionalised graphene nanoplatelets. All the R_r values were above 90 with a slight increase including mGNP and after the accelerating aging. This developed novel SMP can expand the 4DPg technology in industrial applications such as soft robotics as actuators and thermal sensors.

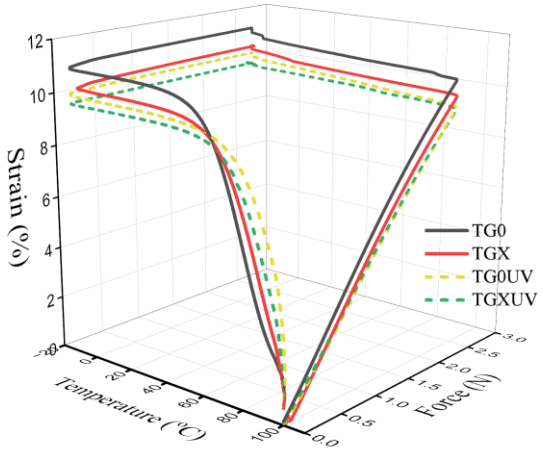

Figure 9. SM behaviour of 3DPd samples from the 4-steps-DMA thermomechanical cyclic test.

Table 1. Strain, recovery, and fixity ratios obtained from the 4-steps-DMA thermomechanical cyclic test.

Property (%)	TG0	TGX	TG0-UV	TGX-UV
ε_m	11.32	10.58	10.28	9.85
ε_f	11.06	10.29	10.07	9.72
R_f	97.7	97.2	97.9	98.6
ε_r	1.13	0.62	0.64	0.69
R_r	90.2	94.1	93.7	92.9

Conclusion

In this work, a Figure 4® DLP UV-based 3D printer has been utilized to produce 4DPd polymeric-based structures. This study aims to focus on developing 3DPg of a commercial methacrylate-based resin by incorporating modified GNP with melamine to investigate the thermal and SM behaviour of 4DPd weather-resistant objects. The results showed good resistance to 1000 hrs weathering ageing and enhancement by incorporating functionalised graphene nanoplatelets. The maximum increment values of the tensile strength, impact resistance and critical stress intensity factor were 18%, 25% and 16%, respectively. The glass transition temperature values were slightly increased. The shape fixity ratios and the shape recovery ratios were greater than 97% and 90%, respectively. The results clarified that the heat flow variations (exotherm and endotherm) obtained from the DSC tests indicated that the 3DPd samples were fully cured after the UV printing process and UV post-cure. FTIR results showed a slight alteration of increasing in the peak intensities of the chemical bonds due to outdoor accelerated weathering and mGNP. The TG0, TGX, TG0UV and TGXUV of the 3DPd samples exhibited shape fixity ratios and shape recovery ratios greater than 97% and 90%, respectively. This study aims to provide knowledge in developing and expanding 4DPd objects for different engineering applications. Hence, the developed 3DPd specimens exhibited extraordinary durability for several SM cycle-life with the effect of mGNP and AWRTH. Finally, future research will have the opportunity to study how various accelerating weathering ageing conditions, and different mGNP contents and compositions affect various properties of 3DPd components, aiming to improve the longevity and durability of 3DPd materials.

Scientific Ethics Declaration

The authors declare that the scientific ethical and legal responsibility of this article published in EPSTEM journal belongs to the authors.

Acknowledgements or Notes

* This article was presented as an oral presentation at the International Conference on Basic Sciences, Engineering and Technology (www.icbaset.net) held in Alanya/Turkey on May 02-05, 2024.

* The authors would like to express their sincere appreciation to the expert engineers Alexandre Portela and Tielidy A. de M. de Lima, PRISM Research Institute, Technological University of the Shannon, for their support in conducting the DMA, DSC and FTIR tests. The authors would like to extend gratitude to leading engineer James Wall for utilising the resin Tough Blk-20 and Figure® 4 DLP printer at 3D Technology Ltd company, Galway, Ireland.

* This research project is funded by Marie Skłodowska-Curie grant agreement No. 847577 cofounded by the European Regional Development Fund and Science Foundation Ireland (SFI) under Grant Number SFI/16/RC/3918 (Smart Manufacturing, Confirm Centre, UL).

References

Afshar, A., Liao, H.-T., Chiang, F., & Korach, C. S. (2016). Time-dependent changes in mechanical properties of carbon fiber vinyl ester composites exposed to marine environments. *Composite Structures*, *144*, 80–85.

Afshar, A., Mihut, D., Baqersad, J., & Hill, S. (2019). Study of metallic thin films on epoxy matrix as protective barrier to ultraviolet radiation. *Surface and Coatings Technology*, *367*, 41–48.

Afshar, A., & Wood, R. (2020). Development of weather-resistant 3D printed structures by multi-material additive manufacturing. *Journal of Composites Science*, *4*(3), 94.

Alfaro, M. E. C., Stares, S. L., Barra, G. M. de O., & Hotza, D. (2022). Effects of accelerated weathering on properties of 3D-printed PLA scaffolds. *Materials Today Communications*, *33*, 104821.

Alsaadi, M., Hinchy, E. P., McCarthy, C. T., Moritz, V. F., Portela, A., & Devine, D. M. (2023). Investigation of thermal, mechanical and shape memory properties of 3D-printed functionally graded nanocomposite materials. *Nanomaterials*, *13*(19), 2658.

Alsaadi, M., Hinchy, E. P., McCarthy, C. T., Moritz, V. F., Zhuo, S., Fuenmayor, E., & Devine, D. M. (2023). Liquid-based 4d printing of shape memory nanocomposites: A review. *Journal of Manufacturing and Materials Processing*, *7*(1), 35.

Barkane, A., Jurinovs, M., Briede, S., Platnieks, O., Onufrijevs, P., Zelca, Z., & Gaidukovs, S. (2022). Biobased resin for sustainable stereolithography: 3D printed vegetable oil acrylate reinforced with ultra-low content of nanocellulose for fossil resin substitution. *3D Printing and Additive Manufacturing*.

Barkane, A., Platnieks, O., Vecstaudza, J., & Gaidukovs, S. (2023). Analysis of bio-based acrylate accelerated weathering: A study of nanocellulose impact on the bulk durability of 3D-printed nanocomposites. *Materials Today Chemistry*, *33*, 101737.

Bass, L., Meisel, N. A., & Williams, C. B. (2016). Exploring variability of orientation and aging effects in material properties of multi-material jetting parts. *Rapid Prototyping Journal*, *22*(5), 826–834.

Cha, J., Kim, J., Ryu, S., & Hong, S. H. (2019). Comparison to mechanical properties of epoxy nanocomposites reinforced by functionalized carbon nanotubes and graphene nanoplatelets. *Composites Part B: Engineering*, *162*, 283–288.

Chowdhury, J., Anirudh, P. V., Karunakaran, C., Rajmohan, V., Mathew, A. T., Koziol, K., Alsanie, W. F., Kannan, C., Balan, A. S. S., & Thakur, V. K. (2021). 4D printing of smart polymer nanocomposites: ıntegrating graphene and acrylate based shape memory polymers. *Polymers*, *13*(21), 3660.

Golhin, A. P., Srivastava, C., Strandlie, A., Sole, A. S., & Grammatikos, S. (2023). Effects of accelerated aging on the appearance and mechanical performance of materials jetting products. *Materials & Design*, *228*, 111863.

Heravi, M. M., Ghavidel, M., & Mohammadkhani, L. (2018). Beyond a solvent: triple roles of dimethylformamide in organic chemistry. *RSC Advances*, *8*(49), 27832–27862.

Mahmood, A., Akram, T., Shenggui, C., & Chen, H. (2023). Revolutionizing manufacturing: A review of 4D printing materials, stimuli, and cutting-edge applications. *Composites Part B: Engineering*, *266*, 110952.

Mao, Y., Yu, K., Isakov, M. S., Wu, J., Dunn, M. L., & Jerry Qi, H. (2015). Sequential self-folding structures by 3D printed digital shape memory polymers. *Scientific Reports*, *5*(1), 13616.

Pisani, S., Genta, I., Modena, T., Dorati, R., Benazzo, M., & Conti, B. (2022). Shape-memory polymers hallmarks and their biomedical applications in the form of nanofibers. *International Journal of Molecular Sciences*, *23*(3), 1290.

Prashar, G., Vasudev, H., & Bhuddhi, D. (2022). Additive manufacturing: Expanding 3D printing horizon in industry 4.0. *International Journal on Interactive Design and Manufacturing (IJIDeM)*, *17*(5), 2221-2235.

Shanti, R., Hadi, A. N., Salim, Y. S., Chee, S. Y., Ramesh, S., & Ramesh, K. (2017). Degradation of ultra-high molecular weight poly(methyl methacrylate-co-butyl acrylate-co-acrylic acid) under ultra violet irradiation. *RSC Advances*, *7*(1), 112–120.

Shen, X., Wang, Z., Wu, Y., Liu, X., & Kim, J.-K. (2016). Effect of functionalization on thermal conductivities

of graphene/epoxy composites. *Carbon*, *108*, 412–422.
Spiridon, I., Darie-Nita, R. N., & Bele, A. (2018). New opportunities to valorize biomass wastes into green materials. II. Behaviour to accelerated weathering. *Journal of Cleaner Production*, *172*, 2567–2575.
Vatanparast, S., Boschetto, A., Bottini, L., & Gaudenzi, P. (2023). New trends in 4D printing: A critical review. *Applied Sciences*, *13*(13), 7744.
Wu, H., Chen, P., Yan, C., Cai, C., & Shi, Y. (2019). Four-dimensional printing of a novel acrylate-based shape memory polymer using digital light processing. *Materials & Design*, *171*, 107704.
Wu, H., Fahy, W. P., Kim, S., Kim, H., Zhao, N., Pilato, L., Kafi, A., Bateman, S., & Koo, J. H. (2020). Recent developments in polymers/polymer nanocomposites for additive manufacturing. *Progress in Materials Science*, *111*(1), 100638.
Yu, K., Ritchie, A., Mao, Y., Dunn, M. L., & Qi, H. J. (2015). Controlled sequential shape changing Components by 3D Printing of Shape Memory Polymer Multimaterials. *Procedia IUTAM*, *12*, 193–203.
3D Systems Inc. (n.d.). *Figure 4 tough-blk 20*. Retrieved from https://www.3dsystems.com/materials/figure-4-tough-blk-20

Author Information

Mohamad Alsaadi
CONFIRM Centre for Smart Manufacturing, University of Limerick, Limerick, Ireland
Technological University of the Shannon, Athlone, Ireland
Contact e-mail: *mohamad.alsaadi@ul.ie*

Eoin P. Hinchy
School of Engineering, University of Limerick
Limerick, Ireland

Conor T. McCarthy
School of Engineering, University of Limerick
Limerick, Ireland

Declan M. Devine
PRISM Research Institute, Technological University of the Shannon
Athlone, Ireland

To cite this article:

Alsaadi, M., Hinchy, E.P., McCarthy, C. T., & Devine, D. M. (2024). Effect of graphene nanoplatelets and accelerated weathering on the mechanical and shape memory behaviour of 3D printed components. *The Eurasia Proceedings of Science, Technology, Engineering & Mathematics (EPSTEM), 28*, 47-55.

The Eurasia Proceedings of Science, Technology, Engineering & Mathematics (EPSTEM)
ISSN: 2602-3199

The Eurasia Proceedings of Science, Technology, Engineering & Mathematics (EPSTEM), 2024

Volume 28, Pages 56-61

ICBASET 2024: International Conference on Basic Sciences, Engineering and Technology

Handling Growth and Decay Problems by the New General Integral Transform

Haldun Alpaslan Peker
Selcuk University

Esma Uysal
Selcuk University

Abstract: The mathematical techniques known as integral transformations are very adaptable and may be used in a multitude of domains including applied sciences, engineering, and mathematics. Numerical calculations and theories involving differential equations have made considerable use of integral transform techniques. Complex functions can be broken down into more manageable functions that can be solved and examined via integral transformations. One of the most prevalent applications of exponential functions involves growth and decay models. Exponential growth and decay show up in a host of natural applications. Almost everything in our world grows and decays. The growth and decay problems arise in the field of chemistry, physics, biology, social science, zoology. The processes of growth and decay are expressed in terms of mathematical models. In this paper, an integral transform called as "New General Integral Transform" is employed for solving growth and decay problems and some applications are given to demonstrate the effectiveness of this transform for growth and decay problems.

Keywords: Growth problem, Decay problem, Integral transform

Introduction

One of the most prevalent applications of exponential functions involves growth and decay models. Exponential growth and decay show up in a host of natural applications. Almost everything in our world grows and decays. The lifespan of people in actuarial science, radioactive elements, virus propagation in biology, rise and fall of current in L-R circuits, water discharge in a vessel through an orifice, business investment value, melting of ice in the polar regions, sun or moon rising time, statistical breakdown of epidemics, and thermal radiation by black bodies are some of the applications of growth and decay problems.

Few concepts are as pervasive and powerful in the fabric of mathematical modeling as growth and decay. From growing populations to vanishing radioactive isotopes, the phenomena of growth and decay permeate nearly every aspect of our natural and engineered worlds. At the heart of these phenomena lies a rich tapestry of mathematical principles that offer insights into the dynamic processes that shape the ebb and flow of quantities over time.

At its core, growth and decay problems revolve around understanding how the quantity of a given asset changes over time. Whether it is the exponential growth of bacteria in a petri dish or the gradual dissipation of heat from a cooling object, the underlying dynamics follow different patterns that can be measured and analyzed using mathematical models. These models serve as powerful forecasting tools that allow us to predict future situations based on current conditions and historical trends.

- Selection and peer-review under responsibility of the Organizing Committee of the Conference

The processes of growth and decay are expressed in terms of mathematical models. The growth and decay problems are modelled mathematically by the same differential equation as

$$\frac{d\,y(t)}{dt} = k\,y(t) \tag{1}$$

with initial condition as

$$y(0) = y_0$$

where $y(t)$ is the amount of the substance at t, y_0 is the amount of the substance at $t = 0$ and k is the constant of proportionality. If $k > 0$, equation (1) is called growth problem and if $k < 0$, equation (1) is called decay problem (Kapur, 2005; Bronson & Costa, 2006; Gorain, 2014).

Method

A New General Integral Transform

Integral transforms are powerful mathematical tools used to solve linear and nonlinear problems in many fields such as applied mathematics, physics, engineering, and others. By transforming a differential equation into a different domain, such as the frequency domain or the Laplace domain, integral transforms simplify the problem-solving process and provide new insights into the dynamics of the system (Debnath & Bhatta, 2007). In this part, a new general integral transform which comprises most of the integral transform in the family of Laplace transform.

Definition 1. (Jafari, 2021) Let $f(t)$ be an integrable function defined for $t \geq 0$, $p(s)$ and $q(s)$ be positive real functions. Then, the new general integral transform $\mathcal{T}(s)$ of $f(t)$ is defined as follows,

$$T\{f(t);s\} = \mathcal{T}(s) = p(s)\int_0^\infty f(t)e^{-q(s)t}dt,$$

provided the integral exists for some $q(s)$. It is essential to note that this transform for those $f(t)$ is not continuously differentiable contains terms with negative or fractional powers of $q(s)$.

Theorem 1 (Existence Theorem). (Jafari, 2021) If $f(t)$ is defined and piecewise continuous on every finite interval on the semi-axis $t \geq 0$ and is of exponential order k, that is $|f(t)| \leq M e^{kt}$ for some positive real number M and k, then $\mathcal{T}(s)$ exists for all $q(s) > k$.

Proof: Since $f(t)$ is piecewise continuous, $e^{-st}f(t)$ is integrable over any finite interval on the t-axis. Assume that $q(s) > k$. Then, the proof of the existence of the $\mathcal{T}(s)$ is obtained as follows:

$$\left\|\mathcal{T}(s)\right\| = \left\|T\{f(t);s\}\right\| = \left|p(s)\int_0^\infty f(t)e^{-q(s)t}dt\right| \leq p(s)\int_0^\infty Me^{kt}e^{-q(s)t}dt = \frac{M\,p(s)}{q(s)-k}.$$

In Table 1, one can find the transformation of some fundamental functions.

Table 1. The new general integral transform of some fundamental functions

$f(t)$	$\mathcal{T}(s)$
1	$\frac{p(s)}{q(s)}$
t	$\frac{p(s)}{(q(s))^2}$
$t^\alpha,\ \alpha>0$	$\frac{\Gamma(\alpha+1)\,p(s)}{(q(s))^{\alpha+1}},\ \alpha>0$
$e^{\alpha t}$	$\frac{p(s)}{q(s)-\alpha},\quad q(s)>\alpha$
$\sin(ct)$	$\frac{c\,p(s)}{c^2+(q(s))^2}$
$\cos(ct)$	$\frac{p(s)\,q(s)}{c^2+(q(s))^2}$

Theorem 2 (Transform of Derivatives). (Jafari, 2021) Let $f(t)$ be differentiable and $p(s)$ and $q(s)$ be positive real functions. Then,

1. $T\{f'(t);s\} = q(s)\ T\{f(t);s\} - p(s)f(0)$
2. $T\{f''(t);s\} = q^2(s)\ T\{f(t);s\} - q(s)p(s)f(0) - p(s)f'(0)$
3. $T\left\{f^{(n)}(t);s\right\} = q^n(s)\ T\{f(t);s\} - p(s)\sum_{k=0}^{n-1} q^{n-1-k}(s)f^{(k)}(0)$

Application to Growth and Decay Problems

In this section, the new general integral transform will be applied to growth and decay model.
Firstly, taking the transform of the equation (1), we obtain

$$\mathcal{T}\left[\frac{d\,y(t)}{dt}\right] = \mathcal{T}\left[k\,y(t)\right] \tag{2}$$

Now, rearranging the equation (2) according to the theorem 2 and Table 1, and substituting the value in the initial condition into this equation, we obtain

$$q(s)\,\mathcal{T}(s) - p(s)y_0 = k\left[\mathcal{T}(s)\right] \tag{3}$$

where $\mathcal{T}(s) = \mathcal{T}\left[y(t)\right]$.

If we make the equation (3) suitable for applying the inverse transform, we obtain

$$\mathcal{T}(s) = y_0\frac{p(s)}{q(s)-k} \tag{4}$$

Finally, applying the inverse transform to the equation (4) using Table 1, we find the solution as

$$y(t) = y_0\,e^{k\,t}. \tag{5}$$

We will examine the effectiveness of this method through some numerical applications and compare the results with those obtained with other methods in the literature.

Application 1. (Aggarwal et al., 2018) Any radioactive substance is known to decay in proportion to the amount available. Consider that $500\,mg$ of a radioactive substance is initially available and after five hours the radioactive substance has lost 25 percent of its available mass. Find the half-life of this radioactive substance. Using the equation (5) according to the values given in the question, we can write

$$y(t) = 500e^{kt}$$

Since 25 percent of the available mass of this radioactive substance is lost at $t = 5$, we have

$$N = 500 - 125 = 375.$$

Now, we can write

$$375 = 500e^{-5k}$$

$$e^{-5k} = 0.75$$

$$k = -\frac{1}{5}\ln(0.75) = 0.0575.$$

We are looking for t when $N = \frac{N_0}{2} = 250$,

$$250 = 500e^{-(0.0575)t}$$

$$t = 12.05$$

which is in good agreement with the results obtained by other methods (Aggarwal et al., 2018; Peker & Cuha, 2022).

Application 2. (Aggarwal et al., 2020) Any radioactive matter is known to decay in proportion to the amount available. Find the half-life of the radioactive matter for the case where $100\,mg$ of radioactive matter is initially available and after six hours the radioactive matter has lost 30 percent of its available mass. Using the equation (5) according to the values given in the question, we can write

$$y(t) = 100e^{kt}$$

Since the radioactive matter lost 30 percent of its available mass at $t = 6$, we have

$$N = 100 - 30 = 70.$$

Now, we can write

$$70 = 100e^{-6k}$$

$$e^{-6k} = 0.7$$

$$k = -\frac{1}{6}\ln(0.7) = 0.059.$$

We are looking for t when $N = \frac{N_0}{2} = 50$,

$$50 = 100e^{-(0.059)t}$$

$$t = 11.75$$

which is exactly coincides with the results obtained by other methods (Aggarwal et al., 2020; Peker & Cuha, 2022).

Application 3. (Rao, 2017) It is known that the rate of degradation of a given substance in a given solution at any instant is proportional to the amount present in the solution at that moment. It is known that there are $27\,grams$ of substance in a solution initially and $8\,grams$ of this substance remain after three hours. How much substance remains in the solution after another one hour has passed?

Using the equation (5) according to the values given in the question, we can write

$$8 = 27e^{-3k}$$
$$e^{-k} = \left(\frac{8}{27}\right)^{\frac{1}{3}}$$

In order to find remaining substance in the solution at $t = 4$, we write

$$\begin{aligned} y(4) &= 27e^{-4k} \\ &= 27\left(\frac{8}{27}\right)^{\frac{4}{3}} \\ &= \frac{16}{3}. \end{aligned}$$

This result is fairly consistent with the ones obtained by other methods (Rao, 2017; Peker & Çuha, 2022).

Conclusion

To sum up, growth and decay problems serve as a cornerstone in the structure of mathematical modeling and provide a lens through which we can unravel the dynamic interaction of quantities over time. From the rapid proliferation of populations to the gradual dissipation of energy, the principles of growth and decay permeate countless fields, shaping our understanding of natural phenomena and informing prediction and control strategies.

Utilizing the new general integral transform approach signifies a noteworthy progression in the realm of mathematical analysis and has the potential to transform the resolution of intricate differential equations across diverse scientific and engineering fields.

Recommendation

This new general integral transform can be applied easily, effectively and reliably to various models found in other applied sciences.

Scientific Ethics Declaration

The authors declare that the scientific ethical and legal responsibility of this article published in EPSTEM journal belongs to the authors.

Acknowledgement

* This article was presented as an oral presentation at the International Conference on Basic Sciences, Engineering and Technology (www.icbaset.net) held in Alanya/Turkey on May 02-05, 2024.

References

Aggarwal, S., Sharma, N., & Chauhan, R. (2018). Solution of population growth and decay problems by using mohand transform. *International Journal of Research in Advent Technology*, *6*(11), 3277-3282.

Aggarwal, S., Sharma, S. D., Kumar, N., & Vyas, A. (2020). Solutions of population growth and decay problems using sumudu transform. *International Journal of Research and Innovation in Applied Science*, *5*(7), 2454-6194.

Bronson, R., & Costa, G. B. (2006). *Schaum's outline of differential equations* (3rd ed.). New York: McGraw-Hill.

Debnath, L., & Bhatta, D. (2007). *Integral transforms and their applications.* New York: Chapman and Hall/CRC.

Gorain, G. C. (2014). *Introductory course on differential equations*. Oxford: Alpha Science International.

Jafari, H. (2021). A new general integral transform for solving integral equations. *Journal of Advanced Research*, *32*,133-138.

Kapur, J. N. (2005). *Mathematical modelling* (2nd ed.). Delhi: New-Age International Pvt Ltd Publishers.

Peker, H. A., & Çuha, F. A. (2022). Application of Kashuri Fundo transform to decay problem. *Süleyman Demirel University Journal of Natural and Applied Sciences*, *26*(3), 546-551.

Rao, R. U. (2017). ZZ transform method for natural growth and decay problems. *International Journal of Progressive Sciences and Technologies*, *5*(2), 147-150.

Author Information

Haldun Alpaslan Peker
Selcuk University
Faculty of Science
Department of Mathematics
Campus, Konya, Türkiye
Contact e-mail: *pekera@gmail.com*

Esma Uysal
Selcuk University
Graduate School of Natural and Applied Sciences
Campus, Konya, Türkiye

To cite this article:

Peker, H. A. & Uysal, E. (2024). Handling growth and decay problems by the new general integral transform. *The Eurasia Proceedings of Science, Technology, Engineering & Mathematics (EPSTEM), 28,* 56-61.

The Eurasia Proceedings of Science, Technology, Engineering & Mathematics (EPSTEM)
ISSN: 2602-3199

The Eurasia Proceedings of Science, Technology, Engineering & Mathematics (EPSTEM), 2024

Volume 28, Pages 62-72

ICBASET 2024: International Conference on Basic Sciences, Engineering and Technology

On Lcem Matrices Over Unique Factorization Domains

Haissam Chehade
Lebanese International University
The International University of Beirut

Yahia Awad
Lebanese International University

Wiam Zeid
Lebanese International University
The International University of Beirut

Abstract: In this paper, we extend the concept of lcem matrices beyond the classical domain of natural integers into the domain of unique factorization domains. We investigate the structure of these matrix types when applied to both arbitrary sets and gced-closed sets. Furthermore, we find the determinant, the trace and the inverse of such matrices. To simplify these ideas, we employ domains such as the Gaussian integers domain and the domain of polynomials defined over finite fields.

Keywords: Lcem matrices, Exponential divisor, Unique factorization domain

Introduction

An integer $d = p_1^{a_1}p_2^{a_2}\dots p_k^{a_k}$, p_i is prime, is an exponential divisor of $m = p_1^{b_1}p_2^{b_2}\dots p_k^{b_k}$ if $a_i \mid b_i$ for every $1 \le i \le k$ and is denoted by $d \mid_e m$. By convention, $1 \mid_e 1$ and 1 is not an exponential divisor for every $m > 1$. If n and m have the same prime factors, then they have a common exponential divisor. Let gced (m,n) (resp. lcem(m,n)) be the greatest common exponential divisor (resp. the least common exponential multiple) of two integers m and n, aslo denoted by $(m,n)_e$ (resp. $[m,n]_e$). By convention, $(1,1)_e = [1,1]_e = 1$ and $(1,m)_e$ and $[1,m]_e$ do not exist for every $m > 1$. If $m = p_1^{b_1}p_2^{b_2}\dots p_k^{b_k}$ and $n = p_1^{c_1}p_2^{c_2}\dots p_k^{c_k}$, then

$$(m,n)_e = p_1^{gcd(b_1,c_1)}p_2^{gcd(b_2,c_2)}\dots p_k^{gcd(b_k,c_k)}$$

and

$$[m,n]_e = p_1^{[b_1,c_1]}p_2^{[b_2,c_2]}\dots p_k^{[b_k,c_k]}$$

with $[b_i,c_i]$ is the least common multiple of b_i and c_i. Two integers $m = p_1^{b_1}p_2^{b_2}\dots p_k^{b_k}$ and $n = p_1^{c_1}p_2^{c_2}\dots p_k^{c_k}$ are exponentially coprime if $\gcd(b_i,c_i) = 1$ for every $1 \le i \le k$.

If $T = \{x_1, x_2, \dots, x_n\}$ is a well-ordered set of n distinct positive integers with $x_1 < x_2 < \dots < x_n$, then the gcd (resp. lcm) matrix on T is an $n \times n$ matrix defined as $(T) = \gcd(x_i, x_j)$ (resp. $[T]_{m\times m} = [x_i, x_j]$. The $n \times n$ power gcd (resp. power lcm) matrix on T is $(T^r) = \gcd(x_i, x_j)^r$ (resp. $[T^r] = [x_i, x_j]^r$), where r is any real

number. A set $T = \{x_1, x_2, \ldots, x_n\}$ is said to be a factor closed (resp. a gcd-closed) set if x is an element of T for any divisor x of x_i (resp. if $\gcd(x_i, x_j)$ for all x_i and x_j) in T.

Smith (Smith, 1875) showed that if $T = \{1,2,\ldots,n\}$, then $\det(T) = \phi(1)\phi(2)\ldots\phi(n)$ and $\det[T] = \phi(1)\pi(1)\phi(2)\pi(2)\ldots\phi(n)\pi(n)$, where ϕ is Euler's totient function and π is a multiplicative function such that $\pi(p^k) = -p$, p is a prime number. Moreover Smith showed that his results are true for factor-closed sets. Beslin and Ligh (Beslin, 1989b), factorized the gcd matrices and showed that it is non-singular. In Beslin and Ligh (1989a,1992) factorized the gcd matrices if T is a gcd-closed set over the domain of integers and computed their determinants. Bourque and Ligh (1992) extended Smith's result on lcm matrices by showing that the determinant of the lcm matrix defined on a gcd-closed set $T = \{x_1, x_2, \ldots, x_m\}$ is the product $\prod_{k=1}^{m} x_k^2 \beta_k$ where $\beta_k = \sum_{\substack{d \mid x_k \\ d \nmid x_t,\ x_t < x_k}} g(d)$, with the arithmetical function g defined by $g(n) = \frac{1}{n}\sum_{d \mid n} \mu(d)$ and the function μ is the well-known Mobius function. Borque and Ligh (1995) conjectured that the lcm matrix on a gcd-closed set is invertible. In (Hong, 1999) Hong did systematic research on the conjecture of Bourque-Ligh and he showed that the Bourque-Ligh conjecture is true only for $n \leq 7$. Also, Hong proved that this conjecture is true for a certain class of lcm-closed sets, see (Hong, 2005). Hong showed that if $n \leq 3$, then for any lcm-closed set $T = \{x_1, x_2, \ldots, x_n\}$, the gcd matrix on T divides the lcm matrix on T in the ring $M_n(\mathbf{Z})$ of the $n \times n$ matrices over the integers. For $n \geq 4$, there exists a lcm-closed set T such that the gcd matrix on T does not divide the lcm matrix on T in the ring $M_n(\mathbf{Z})$, see Hong (2002). Beslin and El-Kassar (1989) expanded the notion of gcd matrices and Smith's determinant to Unique Factorization Domains (UFDs). Furthermore, there have been analogous adaptations of gcd and lcm matrices to Principal Ideal Domains (PIDs) and Euclidean domains (Eds). For further details, readers can consult Awad et al. (2020, 2023), as well as El-Kassar et al. (2009, 2010).

A set $T = \{x_1, x_2, \ldots, x_n\}$ is called an exponential factor closed (resp. a gced-closed) set if the exponential divisor of every element of T belongs to T (resp. if $(x_i, x_j)_e \in T$ for every $x_i, x_j \in T$). If T is an exponential factor closed set of distinct positive integers that are arranged in increasing order, then the $n \times n$ matrix $(T)_e$ (resp. $[T]_e$)= t_{ij} having $t_{ij} = (x_i, x_j)_e$ (resp. $[x_i, x_j]_e$), as its ij^{th} entry is called the gced (resp. lcem) matrix defined on T.

It is well known that $(\mathbf{Z}^+\backslash\{1\}, |_e)$ is a poset under the exponential divisibility relation but not a lattice, since the gced does not always exist. More details are given in the next section. Korkee and Haukkanen (2009) embedded this poset in a lattice and studied the lcem matrices as an analogue of the lcm matrices. Raza and Waheed, (2015a, 2015b, 2012) gave structure theorems and calculated the determinant of gced and lcem matrices defined on an ordered set T. Zeid et al. (2022) extended the gced matrices from the domain of natural integers to the unique factorization domain and gave the structure of these types of matrices defined on both arbitrary sets and gced-closed sets.

In this paper, we study the lcem matrices as an analog of the gced matrices. Examples are given in the domains $\mathbf{Z}[i]$ and $\mathbf{Z}_p[x]$, where p is a prime integer, to describe what has been done.

Throughout this paper, the following notations will be used

- D is a unique factorization domain (UFD)
- p_i is a prime element in D.
- a_i, b_i and c_i are positive integers.
- $z \sim w$ means z and w are two associates.
- $T = x_1, x_2, \ldots, x_n$ is a finite ordered set (in increasing order) of nonzero, non-unit, and non-associate elements in D.

Over Unique Factorization Domains

As in the integer case, a non-zero element $d = p_1^{a_1} p_2^{a_2} \ldots p_k^{a_k}$ in D is an exponential divisor of $m = p_1^{c_1} p_2^{c_2} \ldots p_k^{c_k}$ if $a_i \mid c_i$ for every $1 \leq i \leq$, denoted by $d \mid_e m$. Note that a unit u in D is not an exponential divisor for any nonzero, non-unit element m in D and by convention $u \mid_e v$ for any unit v in D. Two elements a and b in D are associates if $a = ub$, where u is a unit in D. Two elements in D have a common exponential divisor if and only if they have the same prime factors. By convention, $(u, v)_e$ and $[u, v]_e$ does not exist for any non-zero, non unit element a in D. A subset $T = \{x_1, x_2, \ldots, x_n\}$ of D is a gced-closed set if $(x_i, x_j)_e$ is also an element of T for all

x_i, x_j in T, $1 \le i, j \le n$. For example, the subset $T = \{1+3i, -2+4i, -1+7i, -12-16i\}$ of $\mathbf{Z}[i]$ is a gced-closed set, while the set $R = \{-2+4i, -1+7i, -12-16i\}$ is not.

Exponential Convolution

Consider the two functions f and g defined on D. Define the exponential convolution of f and g of a non-zero element $m = \prod_{i=1}^{k} p_i^{c_i}$ in D as:

$$(f \odot g)(m) = \sum_{a_1 b_1 = c_1} \cdots \sum_{a_k b_k = c_k} f\left(p_1^{a_1} p_2^{a_2} \dots p_k^{a_k}\right) g\left(p_1^{b_1} p_2^{b_2} \dots p_k^{b_k}\right).$$

Using the Möbius inversion exponential formula,

$$g(m) = \sum_{d \mid_e m} f(d) \mu^{(e)}\left(\frac{m}{d}\right)$$

if $f(m) = \sum_{d \mid_e m} g(d)$, and $\mu^{(e)}(u) = 1$ and $\mu^{(e)}(m) = \mu(c_1)\mu(c_2)\dots\mu(c_k)$.

Ordering

In our study, we consider the two particular domains, the domain of Gaussian integers $\mathbf{Z}[i]$ and the domain of polynomials over finite fields $\mathbf{Z}_p[x]$. It is well known that these two domains are not ordered. We use a well-defined linear ordering defined on these domains so that any two elements are comparable.

Ordering in $\mathbf{Z}[i]$

Let $T = \{z_1, z_2, \dots, z_n\}$ be a subset of $\mathbf{Z}[i]$. Define an ordering on T as follows: If $q(z_i) < q(z_j)$, then $z_i < z_j$. If $q(z_i) = q(z_j)$, where $z_i \sim a + ib$, and $z_j \sim c + id$, such that $a\ b,\ c,\ d \ge 0$, then $z_i < z_j$ if $b < d$. The valuation function q is defined as $q(a+ib) = a^2 + b^2$. In this case, the relation $<$ is a well-defined linear ordering on T.

Ordering in $\mathbf{Z}_p[x]$

Let $T = \{f_1, f_2, \dots, f_n\}$ be a subset of $\mathbf{Z}_p[x]$, where p is a prime integer. Define an ordering on T as follows: if $\deg(f_i) < \deg(f_j)$, then $f_i < f_j$ and if $\deg(f_i) = \deg(f_j)$ with $f_i = x^n + a_{n-1}x^{n-1} + \dots + a_1 x + a_0$ and $f_j = x^n + b_{n-1}x^{n-1} + \dots + b_1 x + b_0$ with $0 \le a_j, b_j \le p-1$, then $f_i(x) < f_j(x)$ if $a_{j_0} < b_{j_0}$, where j_0 is the smallest index j such that $a_j \ne b_j$. Again, the relation $<$ is a well-defined linear ordering on T.
Note that an non-zero element a in D is positive if $0 < a$, where 0 is the zero element in D and $<$ is the ordering defined on D.

LCEM Matrices Over Unique Factorization Domains

Let $T = \{x_1, x_2, \dots, x_n\}$ be a subset of D. Again, the lcem matrix $[T]_{(e)}$ defined on T is the $n \times n$ matrix whose ij^{th} entry is $(x_{ij})_{(e)} = [x_i, x_j]_e$, the least common exponential multiple of x_i and x_j in D. Let $R = \{y_1, y_2, \dots, y_m\}$ be the minimal gced-closed set containing T (gced closure of T), such that $y_1 < y_2 < \dots < y_m$. Define the function $f(w)$ as follows:

$$f(w) = \sum_{a_1 b_1 = c_1} \cdots \sum_{a_r b_r = c_r} \frac{1}{p_1^{a_1} p_2^{a_2} \dots p_r^{a_r}} \mu^{(e)}\left(p_1^{b_1} p_2^{b_2} \dots p_r^{b_r}\right),$$

where $w = p_1^{c_1} p_2^{c_2} \dots p_r^{c_r} \in D$.

Theorem 3.1. *Let $T = \{x_1, x_2, \dots, x_n\}$ be a gced-closed set in D. Then,* $\sum_{x_k \mid_e (x_i, x_j)_e} \left(\sum_{\substack{d \mid_e x_k \\ d \nmid_e x_r \\ x_r < x_k}} g(d) \right) = \sum_{d \mid_e (x_i, x_j)_e} g(d)$.

Proof. Let $d \mid_e (x_i, x_j)_e$ and let $S = \{x_{k_1}, x_{k_2}, \dots, x_{k_r}\}$ be an ordered subset of T such that $x_{k_m} \mid_e (x_i, x_j)_e$ and $d \mid_e x_{k_m}$ for every $1 \le m \le r$. Then $d \mid_e (x_{k_1}, x_{k_2}, \dots, x_{k_r})_e$ which is an element in T as T is a gced-closed set. Since T is an ordered set, then $(x_{k_1}, x_{k_2}, \dots, x_{k_r})_e = x_{k_1}$. But $d \mid x_{k_1}$ and $d \nmid_e x_r$ whenever $x_r < x_{k_1}$ as x_{k_1} is the minimal element in S. So, each divisor of $(x_i, x_j)_e$ is found once in the sum. Hence,

$$\sum_{x_k \mid_e (x_i, x_j)_e} \left(\sum_{\substack{d \mid_e x_k \\ d \nmid_e x_r \\ x_r < x_k}} g(d) \right) = \sum_{d \mid_e (x_i, x_j)_e} g(d).$$

Theorem 3.2. *$[T]_{(e)} = C \Phi C^t$, where the $n \times m$ matrix $C = (c_{ij})$ is defined as: $c_{ij} = \begin{cases} x_i, & \text{if } y_j \mid_e x_i \\ 0, & \text{else} \end{cases}$, and Φ is an $m \times m$ diagonal matrix define as: $\Phi = diag \left(\sum_{d \mid_e y_1} f(d), \sum_{\substack{d \mid_e y_2 \\ d \nmid_e y_1}} f(d), \dots, \sum_{\substack{d \mid_e y_m \\ d \nmid_e y_r \\ y_r < y_m}} f(d) \right)$.*

Proof. The ij^{th} entry of $C \Phi C^t$ is

$$(C \Phi C^t)_{ij} = \sum_{k=1}^{m} c_{ik} \left(\sum_{\substack{d \mid_e y_k \\ d \nmid_e y_r \\ y_r < y_k}} f(d) \right) c_{jk} = \sum_{\substack{y_k \mid_e x_i \\ y_k \mid_e x_j}} x_i x_j \left(\sum_{\substack{d \mid_e y_k \\ d \nmid_e y_r \\ y_r < y_k}} f(d) \right)$$

$$= x_i x_j \sum_{y_k \mid_e (x_i, x_j)_e} \left(\sum_{\substack{d \mid_e y_k \\ d \nmid_e y_r \\ y_r < y_k}} f(d) \right) = x_i x_j \sum_{d \mid_e (x_i, x_j)_e} f(d).$$

By Möbius inversion exponential formula we have,

$$\sum_{d \mid_e m} f(d) = \frac{1}{m}.$$

Hence,

$$(C \Phi C^t)_{ij} = \frac{x_i x_j}{(x_i, x_j)_e} = [x_i, x_j]_e.$$

Theorem 3.3. The determinant of the matrix $[T]_{(e)}$ is given by

$$det\left([T]_{(e)}\right) = \sum_{1\le k_1<k_2<\ldots<k_n\le m} \left(det\left(C_{(k_1,k_2,\ldots,k_n)}\right)\right)^2 \prod_{i=1}^{n} \left(\sum_{\substack{d|_e y_{k_i} \\ d\nmid_e y_{k_r} \\ y_{k_r}<y_{k_i}}} f(d) \right),$$

where $C_{(k_1,k_2,\ldots,k_n)}$ is the submatrix of C consisting of $k_1^{th}, k_2^{th}, \ldots, k_n^{th}$ columns of C.

Proof. Let D_e be an extension field of $D(x)$, the field of fractions of D, in which $\sqrt{\sum_{\substack{d|_e y_{k_i} \\ d\nmid_e y_{k_r} \\ y_{k_r}<y_{k_i}}} f(d)}$ exists.

$[T]_{(e)} = C\Phi C^t = EE^t$, where $E = C\Phi^{\frac{1}{2}}$. Apply the Cauchy-Binet formula to get

$$\begin{aligned} det\left([T]_{(e)}\right) &= \sum_{1\le k_1<k_2<\ldots<k_n\le m} \left(det\left(E_{(k_1,k_2,\ldots,k_n)}\right)\right)\left(det\left(E^t_{(k_1,k_2,\ldots,k_n)}\right)\right) \\ &= \sum_{1\le k_1<k_2<\ldots<k_n\le m} \left(detE_{(k_1,k_2,\ldots,k_n)}\right)^2, \end{aligned}$$

where $E_{(k_1,k_2,\ldots,k_n)}$ is the submatrix of E consisting of $k_1^{th}, k_2^{th}, \ldots, k_n^{th}$ columns of E. Moreover,

$$detE_{(k_1,k_2,\ldots,k_n)} = detC_{(k_1,k_2,\ldots,k_n)} \sqrt{\prod_{i=1}^{n} \left(\sum_{\substack{d|_e y_{k_i} \\ d\nmid_e y_{k_r} \\ y_{k_r}<y_{k_i}}} f(d) \right)}.$$

Hence,

$$det\left([T]_{(e)}\right) = \sum_{1\le k_1<k_2<\ldots<k_n\le m} \left(detC_{(k_1,k_2,\ldots,k_n)}\right)^2 \prod_{i=1}^{n} \left(\sum_{\substack{d|_e y_{k_i} \\ d\nmid_e y_{k_r} \\ y_{k_r}<y_{k_i}}} f(d) \right).$$

Remark 1. *If $<$ is the ordering defined on D, then $\sum_{\substack{d|_e y_{k_i} \\ d\nmid_e y_{k_r} \\ y_{k_r}<y_{k_i}}} f(d) > 0$.*

Example 3.1. *Let $T = \{-2+4i, -1+7i, -12-16i\}$ which is not gcd-closed set in $\mathbf{Z}[i]$. Its gcd-closure is $R = \{1+3i, -2+4i, -1+7i, -12-16i\}$. The lcm matrix $[T]_{(e)}$ defined on T is:*

$$[T]_{(e)} = \begin{bmatrix} -2+4i & -8+6i & -12-16i \\ -8+6i & -1+7i & -12-16i \\ -12-16i & -12-16i & -12-16i \end{bmatrix}.$$

The matrix C is

$$C = \begin{bmatrix} -2+4i & -2+4i & 0 & 0 \\ -1+7i & 0 & -1+7i & 0 \\ -12-16i & -12-16i & -12-16i & -12-16i \end{bmatrix},$$

And

$$\Phi = \begin{bmatrix} \frac{1}{1+3i} & 0 & 0 & 0 \\ 0 & \frac{-1}{5}+\frac{i}{10} & 0 & 0 \\ 0 & 0 & \frac{-3}{25}+\frac{4i}{25} & 0 \\ 0 & 0 & 0 & \frac{19}{100}+\frac{2i}{25} \end{bmatrix}.$$

Then,

$$C\Phi C^t = \begin{bmatrix} -2+4i & -8+6i & -12-16i \\ -8+6i & -1+7i & -12-16i \\ -12-16i & -12-16i & -12-16i \end{bmatrix} = [T]_{(e)}.$$

$$\begin{aligned} \det[T]_{(e)} &= \begin{vmatrix} -2+4i & -2+4i & 0 \\ -1+7i & 0 & -1+7i \\ -12-16i & -12-16i & -12-16i \end{vmatrix}^2 \\ &\quad \times \sum_{d|_e y_1} f(d) \sum_{\substack{d|_e y_2 \\ d\nmid_e y_1}} f(d) \sum_{\substack{d|_e y_3 \\ d\nmid_e y_r \\ y_r<y_3}} f(d) \\ &\quad + \begin{vmatrix} -2+4i & -2+4i & 0 \\ -1+7i & 0 & 0 \\ -12-16i & -12-16i & -12-16i \end{vmatrix}^2 \sum_{d|_e y_1} f(d) \sum_{\substack{d|_e y_2 \\ d\nmid_e y_1}} f(d) \sum_{\substack{d|_e y_4 \\ d\nmid_e y_r \\ y_r<y_4}} f(d) \\ &\quad + \begin{vmatrix} -2+4i & 0 & 0 \\ -1+7i & -1+7i & 0 \\ -12-16i & -12-16i & -12-16i \end{vmatrix}^2 \sum_{d|_e y_1} f(d) \sum_{\substack{d|_e y_3 \\ d\nmid_e y_r \\ y_r<y_3}} f(d) \sum_{\substack{d|_e y_4 \\ d\nmid_e y_r \\ y_r<y_4}} f(d) \\ &\quad + \begin{vmatrix} -2+4i & 0 & 0 \\ 0 & -1+7i & 0 \\ -12-16i & -12-16i & -12-16i \end{vmatrix}^2 \sum_{\substack{d|_e y_2 \\ d\nmid_e y_1}} f(d) \sum_{\substack{d|_e y_3 \\ d\nmid_e y_r \\ y_r<y_3}} f(d) \sum_{\substack{d|_e y_4 \\ d\nmid_e y_r \\ y_r<y_4}} f(d) \\ &= 2968 - 5176i. \end{aligned}$$

Corollary 3.4. *Let $T = \{x_1, x_2, \dots, x_n\}$ be a gced-closed subset of D. Then,*

$$det[T]_{(e)} = \prod_{k=1}^{n} x_k^2 \left(\sum_{\substack{d|_e x_k \\ d\nmid_e x_r \\ x_r<x_k}} f(d) \right).$$

Proof. Since T is is gced-closed set, the matrix C is lower triangular with diagonal $(x_1, x_2, \dots, x_n)_n$. As a result,

$$det[T]_{(e)} = \prod_{k=1}^{n} x_k^2 \left(\sum_{\substack{d|_e x_k \\ d\nmid_e x_r \\ x_r < x_k}} f(d) \right).$$

Corollary 3.5. *Let $T = \{x_1, x_2, \dots, x_n\}$ be a subset of D, then $tr([T]_{(e)}) = \sum_{i=1}^{n} x_i$.*

Theorem 3.6. *Let $T = \{x_1, x_2, \dots, x_n\}$ be a subset of D. Then,*

$$det([T]_{(e)}) = \prod_{k=1}^{n} x_k^2 \left(\sum_{\substack{d|_e x_k \\ d\nmid_e x_r \\ x_r < x_k}} f(d) \right)$$

if and only if T is gced-closed.

Proof. The necessary condition follows from Corollary 3.4. Now, assume that T is not a gced-closed set and the equality holds. Theorem 3.3 gives

$$det([T]_{(e)}) = \sum_{1 \le k_1 < k_2 < \dots < k_n \le m} \left(detC_{(k_1, k_2, \dots, k_n)}\right)^2 \prod_{i=1}^{n} \left(\sum_{\substack{d|_e y_{k_i} \\ d\nmid_e y_{k_r} \\ y_{k_r} < y_{k_i}}} f(d) \right).$$

This sum runs over the all combinations of the k_i^{th} columns of the matrix C, where $1 \le i \le n$. In each combination we get a new term in this sum, as y_{k_i} related to the chosen column k_i. Since T is a subset of R, then

$$det([T]_{(e)}) = \prod_{k=1}^{n} \left(\sum_{\substack{d|_e x_k \\ d\nmid_e x_r \\ x_r < x_k}} f(d) \right) + s,$$

where $s > 0$. Consequently,

$$det([T]_{(e)}) > \prod_{k=1}^{n} \left(\sum_{\substack{d|_e x_k \\ d\nmid_e x_r \\ x_r < x_k}} f(d) \right)$$

which contradicts the necessary condition that equality holds.

Inverse of the LCEM Matrix

Let $T = \{x_1, x_2, \dots, x_n\}$ be a gced-closed subset of D and let the $n \times n$ matrix $C = (c_{ij})$ be defined as

$$c_{ij} = \begin{cases} x_i, & \text{if } y_j|_e x_i \\ 0, & \text{else} \end{cases}$$

Theorem 3.1.1. *The inverse of C is the $n \times n$ matrix $W = (w_{ij})$ with*

$$w_{ij} = \begin{cases} \dfrac{1}{x_j} \displaystyle\sum_{\substack{d|_e \frac{x_i}{x_j} \\ d \nmid_e \frac{x_r}{x_j},\ x_r < x_i}} \mu^{(e)}(d), & \text{if } x_j|_e x_i \\ 0, & \text{else} \end{cases}.$$

Proof. The ij^{th} entry of CW is given by

$$(cw)_{ij} = \sum_{k=1}^{n} c_{ik}\, w_{kj} = \sum_{\substack{x_k|_e x_i \\ x_j|_e x_k}} \frac{x_i}{x_j} \left(\sum_{\substack{d|_e \frac{x_k}{x_j} \\ d \nmid_e \frac{x_r}{x_j} \\ x_r < x_k}} \mu^{(e)}(d) \right) = \frac{x_i}{x_j} \sum_{\frac{x_k}{x_j}|_e \frac{x_i}{x_j}} \left(\sum_{\substack{d|_e \frac{x_k}{x_j} \\ d \nmid_e \frac{x_r}{x_j} \\ x_r < x_k}} \mu^{(e)}(d) \right).$$

A similar argument to that given in Theorem 3.3,

$$\sum_{\frac{x_k}{x_j}|_e \frac{x_i}{x_j}} \left(\sum_{\substack{d|_e \frac{x_k}{x_j} \\ d \nmid_e \frac{x_r}{x_j} \\ x_r < x_k}} \mu^{(e)}(d) \right) = \sum_{d|_e \frac{x_i}{x_j}} \mu^{(e)}(d).$$

Therefore,

$$\frac{x_i}{x_j} \sum_{d|_e \frac{x_i}{x_j}} \mu^{(e)}(d) = \frac{x_i}{x_j} \mu^2\left(\frac{x_i}{x_j}\right) = \begin{cases} 1, & \text{if } x_j = x_i \\ 0, & \text{else} \end{cases}.$$

Theorem 3.1.2. *The inverse of the lcem matrix $[T]_{(e)}$ is the matrix $[M]_{(e)} = (m_{ij})_{(e)}$ which is defined as:*

$$(m_{ij}) = \frac{1}{x_i x_j} \sum_{\substack{x_i|_e x_k \\ x_j|_e x_k}} \left(\sum_{\substack{d|_e x_k/x_i \\ d \nmid_e x_r/x_i \\ x_r < x_k}} \mu^{(e)}(d) \frac{1}{\sum_{\substack{d|_e x_k \\ d \nmid_e x_r \\ x_r < x_k}} g(d)} \sum_{\substack{d|_e x_k/x_j \\ d \nmid_e x_r/x_j \\ x_r < x_k}} \mu^{(e)}(d) \right).$$

Proof. $[M]_{(e)} = [T]_{(e)}^{-1} = (C \Phi C^t)^{-1} = W^t \Phi^{-1} W$, where $W = C^{-1}$ and

$$\Phi^{-1} = diag\left(\frac{1}{\sum_{d|_e x_1} f(d)}, \frac{1}{\sum_{\substack{d|_e x_2 \\ d\nmid_e x_1}} f(d)}, \ldots, \frac{1}{\sum_{\substack{d|_e x_n \\ d\nmid_e x_r \\ x_r<x_n}} f(d)}\right).$$

So,

$$m_{ij} = (W^t \Phi^{-1} W)_{ij} = \sum_{k=1}^{n} w_{ki} \frac{1}{\sum_{\substack{d|_e x_k \\ d\nmid_e x_r \\ x_r<x_k}} f(d)} w_{kj}$$

$$= \frac{1}{x_i x_j} \sum_{\substack{x_i|_e x_k \\ x_j|_e x_k}} \left(\sum_{\substack{d|_e \frac{x_k}{x_i} \\ d\nmid_e \frac{x_r}{x_i} \\ x_r<x_k}} \mu^{(e)}(d) \frac{1}{\sum_{\substack{d|_e x_k \\ d\nmid_e x_r \\ x_r<x_k}} g(d)} \sum_{\substack{d|_e \frac{x_k}{x_j} \\ d\nmid_e \frac{x_r}{x_j} \\ x_r<x_k}} \mu^{(e)}(d) \right).$$

Example 3.1.1. *Let* $T = \{x(x+1), x(x+1)^2, x^2(x+1)^2\}$ *which is gced-closed set in* $\mathbf{Z}_2[x]$. *The lcem matrix defined on T is:*

$$[T]_{(e)} = \begin{bmatrix} x(x+1) & x(x+1)^2 & x^2(x+1)^2 \\ x(x+1)^2 & x(x+1)^2 & x^2(x+1)^2 \\ x^2(x+1)^2 & x^2(x+1)^2 & x^2(x+1)^2 \end{bmatrix}.$$

Then,

$$\begin{aligned} m_{11} &= \frac{1}{x^2(x+1)^2}\left(\mu^{(e)}\big(x(x+1)\big)\frac{1}{f\big(x(x+1)\big)}\mu^{(e)}\big(x(x+1)\big)\right. \\ &+\mu^{(e)}(x(x+1)^2)\frac{1}{f(x(x+1)^2)}\mu^{(e)}(x(x+1)^2) \\ &+\left[\mu^{(e)}\big(x^2(x+1)\big)+\mu^{(e)}(x^2(x+1)^2)\right]\frac{1}{f\big(x^2(x+1)\big)+f(x^2(x+1)^2)}\times \\ &\left.\left[\mu^{(e)}\big(x^2(x+1)\big)+\mu^{(e)}(x^2(x+1)^2)\right]\right) \\ &= \frac{1}{x^2(x+1)}. \end{aligned}$$

$$\begin{aligned} m_{12} &= \frac{1}{x^2(x+1)^3}\left(\mu^{(e)}(x(x+1)^2)\frac{1}{f(x(x+1)^2)}\mu^{(e)}\big(x(x+1)\big)\right. \\ &\left.+\left[\mu^{(e)}\big(x^2(x+1)\big)+\mu^{(e)}(x^2(x+1)^2)\right]\frac{1}{f\big(x^2(x+1)\big)+f(x^2(x+1)^2)}\mu^{(e)}\big(x^2(x+1)\big)\right) \\ &= -\frac{(x+1)^2}{x^2(x+1)^3} = \frac{1}{x^2(x+1)}. \end{aligned}$$

$$\begin{aligned} m_{13} &= \frac{1}{x^3(x+1)^3}\left[\mu^{(e)}\big(x^2(x+1)\big)+\mu^{(e)}(x^2(x+1)^2)\right]\frac{1}{f\big(x^2(x+1)\big)+f(x^2(x+1)^2)}\mu^{(e)}\big(x(x+1)\big) \\ &= 0 \end{aligned}$$

Completing the computation, we get

$$[M]_{(e)} = \begin{bmatrix} \frac{1}{x^2(x+1)} & \frac{1}{x^2(x+1)} & 0 \\ \frac{1}{x^2(x+1)} & \frac{x^2+x+1}{x^2(x+1)^3} & \frac{1}{x(x+1)^3} \\ 0 & \frac{1}{x(x+1)^3} & \frac{1}{x^2(x+1)^3} \end{bmatrix}.$$

Conclusion

In conclusion, the lcem matrices defined on gced closed and non-gced closed sets over a unique factorization domain D were considered. A complete characterization of their structure, determinant, trace, and inverse was given. Furthermore, the work done in the literature used the classical domain (domain of natural integers), which is an example of a UFD and therefore the previous research can be viewed a special case with the domain of integers representing our chosen UFD.

Scientific Ethics Declaration

The authors declare that the scientific ethical and legal responsibility of this article published in EPSTEM journal belongs to the authors.

Acknowledgements or Notes

* This article was presented as an oral presentation at the International Conference on Basic Sciences, Engineering and Technolog (www.icbaset.net) held in Alanya/Turkey on May 02-05, 2024.

* Mathematics Subject Classification (2020): 11A25, 15A09, 15A15, 15A23

* The authors gratefully acknowledge the invaluable contributions of the anonymous referees whose insightful comments and constructive feedback greatly enhanced the quality and clarity of this article. Their expertise and dedication have been instrumental in shaping the final version of the manuscript.

References

Awad, Y. A., Chehade, H., & Mghames, R. (2020). Reciprocal power GCDQ matrices and power LCMQ matrices defined on factor closed sets over Euclidean domains. *Filomat*, *34*(2), 357–363.

Awad, Y., Mghames, R., & Chehade, H. (2023). Power GCDQ and LCMQ matrices defined on GCD-Closed Sets over Euclidean Domains. *Palestine Journal of Mathematics*, *12*(1).

Beslin, S., & El-Kassar, N. (1989). GCD matrices and Smith's determinant for a unique factorization domain. *Bull. Number Theory Related Topics*, *13*, 17–22.

Beslin, S., & Ligh, S. (1989a). Another generalisation of Smith's determinant. *Bulletin of the Australian Mathematical Society*, *40*(3), 413–415.

Beslin, S., & Ligh, S. (1989b). Greatest common divisor matrices. *Linear Algebra and Its Applications*, *118*, 69–76.

Beslin, S., & Ligh, S. (1992). GCD-closed sets and the determinants of GCD matrices. *Fibonacci Quart*, *30*(2), 157–160.

Bourque, K., & Ligh, S. (1992). On GCD and LCM matrices. *Linear Algebra and Its Applications*, *174*, 65–74.

Bourque, K., & Ligh, S. (1995). Matrices associated with multiplicative functions. *Linear Algebra and Its Applications*, *216*, 267–275.

El-Kassar, A. N., Habre, S. S., & Awad, Y. A. (2010). GCD Matrices Defined on Gcd-Closed sets in a PID. *International Journal of Applied Mathematics*, *23*, 571–581.

El-Kassar, A.N., Habre, S.S., & Awad, Y.A. (2009). Greatest common divisor and least common multiple matrices on factor closed sets in a principal ideal domain. *Journal of Mathematics and Statistics*, *5*(4), 342-347.

Hong, S. (1999). On the bourque--ligh conjecture of least common multiple matrices. *Journal of Algebra*, *218*(1), 216–228.

Hong, S. (2002). On the factorization of LCM matrices on gcd-closed sets. *Linear Algebra and Its Applications*, *345*(1–3), 225–233.

Hong, S. (2005). Nonsingularity of least common multiple matrices on gcd-closed sets. *Journal of Number Theory*, *113*(1), 1–9.

Korkee, I., & Haukkanen, P. (2009). Meet and join matrices in the poset of exponential divisors. *Proceedings-Mathematical Sciences*, *119*(3), 319–332.

Raza, Z., & Waheed, S. A. (2012). LCEM and reciprocal GCED matrices. *Int. J. Pure and Applied Mathematics*, *80*(5), 647–655.

Raza, Z., & Waheed, S. A. (2015a). GCED and reciprocal GCED matrices. *Hacettepe Journal of Mathematics and Statistics*, *44*(3), 633–640.

Raza, Z., & Waheed, S. A. (2015b). GCED reciprocal LCEM matrices. *Notes on Number Theory and Discrete Mathematics*, *21*(1), 79–85.

Smith, H. J. S. (1875). On the value of a certain arithmetical determinant. *Proceedings of the London Mathematical Society*, *1*(1), 208–213.

Zeid, W., Chehade, H., & Rasheed, F. (2022). On GCED matrices over unique factorization domains. *Filomat*, *36*(11), 3775–3784.

Author Information

Haissam Chehade
Lebanese International University (LIU)
Department of Mathematics and Physics
Saida, Lebanon.
The International University of Beirut (BIU)
Department of Mathematics and Physics
Beirut, Lebanon.
Contact e-mail: *haissam.chehade@b-iu.edu.lb*

Yahia Awad
Lebanese International University (LIU)
Department of Mathematics and Physics
AlKhyara, West Bekaa, Lebanon.

Wiam Zeid
Lebanese International University (LIU)
Department of Mathematics and Physics
Saida, Lebanon.

To cite this article:

Chehade, H., Awad, Y., & Zeid, W. (2024). On lcem matrices over unique factorization domains. *The Eurasia Proceedings of Science, Technology, Engineering & Mathematics (EPSTEM), 28*, 62-72.

The Eurasia Proceedings of Science, Technology, Engineering & Mathematics (EPSTEM)
ISSN: 2602-3199

The Eurasia Proceedings of Science, Technology, Engineering & Mathematics (EPSTEM), 2024

Volume 28, Pages 73-80

ICBASET 2024: International Conference on Basic Sciences, Engineering and Technology

The Scope of Digital Tools and Opportunities in the Life of Hungarian and Slovakian Enterprises and Their Impact on Business Competitiveness

Janos Varga
Obuda University

Agnes Csiszarik-Kocsir
Obuda University

Abstract: The competitiveness of enterprises is a critical factor that underpins economic growth, innovation and overall social development. The importance of this issue is not only for the operation or success of an individual enterprise. Successful and competitive businesses can come together under the umbrella of an industry and together could form a competitive industry that can also have an impact on the development and state of the national economy. Competitiveness needs to be built and strengthened by conscious means, while protected against other attacks and threats. Efforts should be made to identify obstacles and barriers that could hamper the strengthening of the competitiveness of an economic operator. These should be tackled more consciously so that there are no significant differences between organisations or countries, for example in terms of innovation, development or positive change. Business competitiveness is an integral part of economic viability, job creation, innovation and the overall well-being of societies, so it is by no means irrelevant what factors may hinder entrepreneurs and what barriers to business success and competitiveness exist. Competitiveness is the focus of this paper, which will be accompanied by an appropriate literature review and a presentation of primary research findings.

Keywords: Digital tools, Business engineering, Business competitiveness

Introduction

All businesses have an interest in maintaining a competitive advantage. As a business organisation, our goal is to constantly strive to gain an advantage over our competitors, because it is hard to think of a business that does not have potential competitors or challengers in the business markets. However, the advantage does not create itself. It requires targeted investment in some area that actually results in the business having a differentiated capability and thus being able to meet needs in a different or novel way. All businesses have an interest in gaining and maintaining a competitive advantage, because this is what secures a lasting advantageous market position. Competitive advantage is nothing more than the sum of organisational capabilities to satisfy consumer needs at a much higher level than before. If a company has these capabilities and can satisfy consumer needs and expectations at a much higher level, it is likely to be able to achieve sustained business success. But the first step is to create the capabilities that are needed to do this in the first place. This is where the definition of competitiveness comes from. If we want to express the concept of organisational competitiveness in very simple terms, we should perhaps start from the above logic and look at all the potential material and non-material resources that an organisation has, as well as the capabilities it needs.

The success of the action (and hence the success of the management activity) will be determined by the extent to which the right competences are successfully provided. From this point of view, we can say that organisational competitiveness is ultimately the sum of organisational potentials that the enterprise can use and exploit to meet organisational goals, realise profits or satisfy customer needs. Where the necessary capabilities cannot be

- Selection and peer-review under responsibility of the Organizing Committee of the Conference

demonstrated and acquired, where organisational potentials cannot be managed effectively, the firm will be at a competitive disadvantage compared to firms that have been able to do so over the same period of time. The 21st century has given a new meaning to the concept of competitiveness. Increasingly, resilience, flexibility, adaptability, adaptability and variability are being stressed as essential factors of competitiveness. All this is not far from the truth, as the changing business environment demands new types of qualities from modern businesses. In a period of crisis, the question of how to remain competitive, how to withstand challenges and how to respond to the difficulties that economic operators face on a daily basis has become even more important. Perhaps never before has the issue of competitiveness factors been more topical than it is today. This paper focuses on this very topic and, in addition to a brief literature review, presents the results of a primary research study.

Literature Review

Competitiveness is perhaps one of the most complex and controversial definitions in the field of management and organisation. There is no single definition, nor is there agreement among experts on the factors that determine competitiveness. Analysing competitiveness is not an easy task (Zhao-Qi, 2021). In most cases, to analyse competitiveness, we need to compare at least two actors, as this is the only way to determine whether one is at an advantage or not (Berger, 2008). However, no two countries are the same, just as no two businesses are the same (Collis-Montgomery, 2008). These reflections highlight that the analysis of competitiveness has to be treated very differently for each economic actor, as the competitiveness of countries can be interpreted and analysed somewhat differently than for economic corporations (firms) (Chikan et al., 2022). This paper does not aim to interpret national or economy-wide competitiveness. The main focus is on defining the competitiveness of enterprises, which is also not a simple task.

It is very difficult to generalise, as firms themselves may be characterised by different industries, different operating environments, different profiles, markets or organisational cultures. What is more, in many cases even the corporate governance system can make a difference between firms (Ekom -Etim et al., 2023). What is a success factor for one firm may not be a success factor for another. Competitiveness is a complex word composed of the words competition and capability. The first is perhaps obvious, since economic agents are essentially not unique players in the market. The latter, however, needs much more explanation. Competitiveness of economic agents refers to all the capabilities and endowments they possess that they can (or could) effectively put at the service of value creation at all levels (Chikan et al., 2022). The existence of capabilities and endowments determines potential competitive advantages and the ability to satisfy needs at a higher level than before. Firm competitiveness is determined by the extent to which firms can adapt to changing circumstances, have specific capabilities and strive to achieve continuously better results, although the size of organisations is also closely related to competitiveness factors (Lafuente et al., 2020). Competitiveness therefore implies a set of specific organisational characteristics, potentials, skills and capabilities that enable firms to better respond to external and internal environmental challenges, or even to influence and shape their own business environment. Being able to do something is, in essence, what competitiveness is all about. One must be able to adapt, innovate (Yang et al., 2022), develop, achieve business success, etc. (Akben-Selcuk, 2016). However, if one does not build the right capabilities in the organisation, there is nothing to change and the organisation will sooner or later fall behind (Cetindamar & Kilitcioglu, 2013). However, competitiveness can be defined not only in this context. Competitiveness at the firm level is expressed in terms of positioning, persistence and wealth creation, but it also increasingly includes sustainability (Serban et al., 2023). In a competitive environment, it implies continuous innovation, constant adaptation and a constant need to comply (Asim et al., 2023). However, a new strand in the literature on firm competitiveness points to the importance of subjective factors (Navarro et al, 2016), in addition to the usual determinants. According to this strand, competitiveness is ultimately determined by the attributes, capabilities and skills of the firm's participants. In addition to hard factors, so-called soft factors are also valued. These include people and their skills, knowledge and creativity. Equally, we can consider as a source of competitiveness the right organisational culture, good working conditions, excellent organisational infrastructure, excellent and people-oriented management, a well-defined organisational strategy (Friesenbichler & Reinstaller, 2022), the business model of the enterprise, etc.

As can be perceived, competitiveness can be improved in almost all areas of business operations (Latifah et al., 2021). As our business environment is constantly changing, strengthening competitiveness remains a perpetual task for responsible entrepreneurs and managers. If there were no change, there would be no need to address competitiveness. If our competitors were not evolving or customer needs were not changing, there would be no need to strengthen competitiveness (Flak & Glod, 2020). But the reality is quite the opposite. Everything is constantly changing, so no firm can be satisfied with its current level of competitiveness in the long term.

Sooner or later, all organisations will become outdated, obsolete or rusty, and will need to strengthen or improve their competitiveness. The sources of competitiveness were stressed much earlier, in the 1970s, by Peter Drucker, the father of modern management. He highlighted potential sources of competitiveness such as knowledge and innovation, creative labour and organisational development. The importance of innovation must be emphasised (Gottinger, 2022). These factors are still highly relevant and important competitiveness factors in the 21st century. The question of what economic actors see as the basis of their competitiveness is still an important issue today. The primary research, the results of which are briefly summarised in this paper, deals with a slice of this question. What makes this research unique is that it allows a comparative analysis between two countries.

Material and Method

The analysis presented in this paper is intended to present part of the results of a survey conducted in Hungary and Slovakia in 2023. A complex questionnaire was used to assess the competitiveness factors of Hungarian and Slovakian SMEs in terms of environmental challenges, green transformation, project approach, digital asset use, along the operational characteristics of enterprises. The present questionnaire survey was preceded by several rounds of consultations, expert interviews with enterprises in the two countries, and a test questionnaire in order to assess as accurately as possible the factors that determine the competitiveness of the SME sector in the two countries. The results of the research are based on 427 questionnaires from Hungary and 181 evaluable questionnaires from Slovakia. In the present study, the opinions of the sampled enterprises on the use of digital tools were surveyed. We asked enterprises to rate the digital solutions used in their business using a four-point Likert scale. We offered them four six categories: not at all, rather not, rather yes and completely yes. Businesses were categorised according to their presence in the market, based on the number of years of operational experience since their inception. The composition of the sample is shown in the figure below:

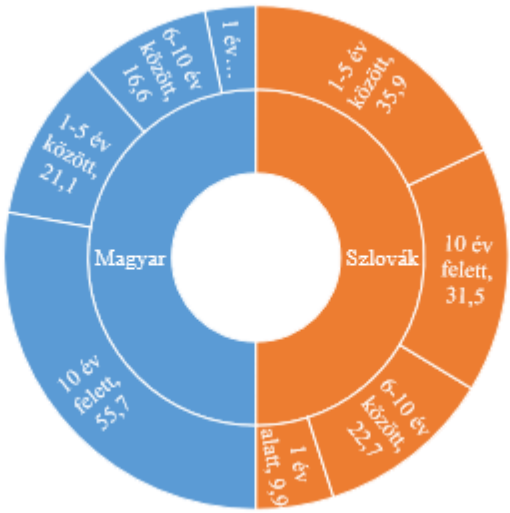

Figure 1. Composition of the sample based on the operational experience of enterprises in Hungary and Slovakia
Source: Own research, 2023, N = 427 (Hungarian), N = 181 (Slovakian)

Results

In the course of the research, we sought to find out to what extent the use of traditional and innovative digital tools is typical of the everyday operations of Hungarian and Slovakian businesses. Twelve potential tools were evaluated with businesses, including long-established and widely used solutions, and we also looked at innovative, novel solutions and how they are typical of the life of SMEs in both countries. The average scores for Hungarian businesses show that the use of mobile phone applications is the most common, with the highest average score. This was followed by a high proportion of online communication interfaces, which was the second most frequently used, and the use of online booking, ordering and purchasing solutions. For all three scoring factors, the average score is above 3.0, which means that businesses are highly characterised by their use of these tools. It could be said that almost all the businesses in the sample have such solutions.

For Slovakian businesses, the top solutions are the same as for their Hungarian counterparts, but the order is different. Slovakian businesses ranked the use of online communication interfaces first, followed by mobile phone applications, which ranked second in terms of usage. This was followed by the use of online booking, ordering and purchasing solutions, which also ranked third in the opinion of businesses. The same can be said for Slovakian businesses as for Hungarian businesses, in that the top three digital solutions were all rated with an average score of 3.0 or above. It can also be said that, although with lower scores, they are tools that are typically present in all enterprises. At the bottom of the list, businesses in both countries ranked the usability of chatbots, virtual reality and augmented reality. It can be seen that the use of chatbots is more prevalent in Slovakian businesses, although it is ranked third from the bottom for both countries. The same is true for virtual reality, which came second from the bottom, and augmented reality, which was rated very low for all businesses, with Hungarian businesses giving it a slightly higher average score.

Table 1. Frequency of use of digital devices by average values in Hungary and Slovakia

	Hungarian		Slovakian	
	Average	Source	Average	Source
Electronic payment facility (POS)	2,951	1,023	2,873	1,038
Online booking, ordering, purchasing solution	3,021	0,994	3,077	1,019
Digital /customer management software	2,529	1,024	2,564	1,087
Modern energy optimisation (sensors, etc.)	2,433	1,045	2,343	1,013
Mobile phone applications	3,447	0,872	3,298	0,972
Augmented reality (AR)	1,981	0,850	1,972	0,833
Virtual reality (VR)	1,993	0,798	2,061	0,844
Chatbot	2,122	0,898	2,249	0,924
Management software	2,941	1,092	2,773	1,085
Online communication interfaces	3,349	0,933	3,309	0,945
Automation systems	2,600	1,073	2,586	1,016

Source: Own research, 2023, N = 427 (Hungarian), N = 181 (Slovakian)

We also looked at the characteristics of these digital solutions in terms of the groups based on operating time. For Hungarian enterprises, the use of digital tools, whether traditional or innovative, is overwhelmingly more characteristic of more mature enterprises. For Hungarian enterprises, organisations with between 6 and 10 years of operational experience are the most likely to use electronic payment, chatbots and automation systems in their operations. In the higher category, businesses with more than 10 years' experience lead in the use of online booking, ordering and purchasing solutions, modern energy optimisation tools, mobile phone applications, business management software and online communication interfaces. Other tools are rarely found in enterprises in other categories. What is noteworthy is the use of digital shopping management software, which is typical of businesses with between 1 and 5 years of operational experience, and the same can be said for the use of augmented reality in this size category. The use of virtual reality, always a digital tool, is highest in businesses with less than 1 year of experience, which is probably due to the fact that these businesses are the ones that are innovative or start-ups and are keen to experiment with new and innovative solutions.

The picture for Slovakian businesses is very heterogeneous. Surprisingly, it is not the more mature companies that are the most advanced in terms of usability. Enterprises with less than 1 year of operational experience had the highest average score for electronic payment, online booking, ordering, shopping solutions, digital customer management software, augmented reality, virtual reality, chatbots, etc. Other size categories were absent from the top of the podium. Interestingly for Slovakian enterprises, enterprises with between 6 and 10 years of operating experience were ranked first only for modern energy optimisation tools and automation systems, and enterprises with more than 10 years of operating experience were ranked first only for online communication interfaces and management software. The groupings by category show that Hungarian enterprises tend to be the more mature, with at least 6 years of operational experience, and their Slovakian counterparts are the more mature, with the least operational experience. It should be noted, however, that they represent a relatively small proportion of the sample, which may somewhat distort our results.

In the next section of the paper, we will present the results of the analysis of variance carried out. We wanted to assess whether there was any correlation with the operational experience of the organisations with regard to the digital solutions listed. From the perspective of the Hungarian companies, for the twelve tools examined, it can be stated that only three of the tools used show a correlation with respect to the grouping criterion, based on the level of significance. These tools were modern energy optimisation solutions, chatbots and case management software. For these factors only the significance level was below 5%, suggesting a relationship.

Table 2. Average frequency of digital device use by category in Hungary and Slovakia

		Hungarian Average	Source	Slovakian Average	Source
Electronic payment facility (POS)	in 1 year	2,821	1,090	3,111	0,900
	Between 1-5 years	3,044	1,005	2,862	1,044
	Between 6-10 years	3,085	0,952	2,780	1,061
	Over 10 years	2,891	1,042	2,877	1,070
	Total	2,951	1,023	2,873	1,038
Online booking, ordering, purchasing solution	in 1 year	2,643	1,162	3,111	0,963
	Between 1-5 years	2,978	1,005	3,108	1,017
	Between 6-10 years	2,915	0,858	3,024	0,987
	Over 10 years	3,113	0,998	3,070	1,083
	Total	3,021	0,994	3,077	1,019
Digital /customer management software	in 1 year	2,429	0,959	2,611	1,037
	Between 1-5 years	2,722	1,039	2,554	1,046
	Between 6-10 years	2,662	1,068	2,537	1,142
	Over 10 years	2,429	1,003	2,579	1,133
	Total	2,529	1,024	2,564	1,087
Modern energy optimisation (sensors, etc.)	in 1 year	2,071	0,858	2,222	1,114
	Between 1-5 years	2,333	1,049	2,200	0,971
	Between 6-10 years	2,310	0,965	2,463	1,098
	Over 10 years	2,550	1,073	2,456	0,965
	Total	2,433	1,045	2,343	1,013
Mobile phone applications	in 1 year	3,357	1,096	3,222	0,943
	Between 1-5 years	3,311	0,895	3,154	1,034
	Between 6-10 years	3,268	0,925	3,098	1,044
	Over 10 years	3,563	0,802	3,632	0,771
	Total	3,447	0,872	3,298	0,972
Augmented reality (AR)	in 1 year	2,000	0,816	2,222	0,943
	Between 1-5 years	2,056	0,916	1,938	0,747
	Between 6-10 years	1,915	0,751	1,902	0,860
	Over 10 years	1,971	0,859	1,982	0,876
	Total	1,981	0,850	1,972	0,833
Virtual reality (VR)	in 1 year	2,071	0,663	2,389	0,979
	Between 1-5 years	1,978	0,821	2,000	0,661
	Between 6-10 years	2,056	0,754	1,951	0,921
	Over 10 years	1,971	0,819	2,105	0,920
	Total	1,993	0,798	2,061	0,844
Chatbot	in 1 year	2,036	0,922	2,500	1,098
	Between 1-5 years	2,111	0,892	2,185	0,768
	Between 6-10 years	2,423	0,995	2,220	1,037
	Over 10 years	2,046	0,853	2,263	0,955
	Total	2,122	0,898	2,249	0,924
Management software	in 1 year	2,464	0,881	2,444	0,984
	Between 1-5 years	2,556	1,162	2,646	1,124
	Between 6-10 years	2,775	1,085	2,707	1,078
	Over 10 years	3,193	1,021	3,070	1,033
	Total	2,941	1,092	2,773	1,085
Online communication interfaces	in 1 year	3,393	0,916	3,167	0,924
	Between 1-5 years	3,300	0,953	3,215	1,023
	Between 6-10 years	3,169	1,042	3,122	1,005
	Over 10 years	3,416	0,890	3,596	0,753
	Total	3,349	0,933	3,309	0,945
Automation systems	in 1 year	2,464	1,036	2,611	0,979
	Between 1-5 years	2,633	1,054	2,477	1,017
	Between 6-10 years	2,662	1,055	2,707	1,031
	Over 10 years	2,584	1,094	2,614	1,031
	Total	2,600	1,073	2,586	1,016

Source: Own research, 2023, N = 427 (Hungarian), N = 181 (Slovakian)

Table 3. Correlation of the frequency of use of digital tools with the market experience of the organisation in Hungary

		Sum of Squares	df	Mean Square	F	Sig.
Electronic payment facility (POS)	Between Groups	3,385	3	1,128	1,078	0,358
	Within Groups	442,582	423	1,046		
	Total	445,967	426			
Online booking, ordering, purchasing solution	Between Groups	6,996	3	2,332	2,384	0,069
	Within Groups	413,814	423	0,978		
	Total	420,810	426			
Digital /customer management software	Between Groups	7,298	3	2,433	2,344	0,072
	Within Groups	439,086	423	1,038		
	Total	446,384	426			
Modern energy optimisation (sensors, etc.)	Between Groups	8,913	3	2,971	2,756	0,042
	Within Groups	455,935	423	1,078		
	Total	464,848	426			
Mobile phone applications	Between Groups	7,377	3	2,459	3,290	0,021
	Within Groups	316,188	423	0,747		
	Total	323,564	426			
Augmented reality (AR)	Between Groups	0,841	3	0,280	0,386	0,763
	Within Groups	307,009	423	0,726		
	Total	307,850	426			
Virtual reality (VR)	Between Groups	0,597	3	0,199	0,312	0,817
	Within Groups	270,381	423	0,639		
	Total	270,979	426			
Chatbot	Between Groups	7,999	3	2,666	3,360	0,019
	Within Groups	335,669	423	0,794		
	Total	343,667	426			
Management software	Between Groups	36,846	3	12,282	11,038	0,000
	Within Groups	470,690	423	1,113		
	Total	507,536	426			
Online communication interfaces	Between Groups	3,637	3	1,212	1,396	0,243
	Within Groups	367,370	423	0,868		
	Total	371,007	426			
Automation systems	Between Groups	0,949	3	0,316	0,273	0,845
	Within Groups	489,571	423	1,157		
	Total	490,520	426			

Source: Own research, 2023, N = 427 (Hungarian)

The same analysis was also carried out for Slovakian businesses, where surprisingly even fewer assets were affected by the operational experience of the business. In their case, we found a correlation only for mobile phone applications and the use of online communication platforms.

Conclusions

Digitalisation is clearly the engine of change in the 21st century. Neither individuals nor businesses can be excluded from the digitalisation process. In our study, we set out to show the extent to which digital tools are used in the lives of Hungarian and Slovakian businesses. Despite the dominant process we are talking about, it is clear that businesses are reluctant to open up to new and innovative digital solutions. Although a high proportion of enterprises typically use these tools, their use is still limited to traditional tools. We also see a very heterogeneous picture between the opinions of Hungarian and Slovakian enterprises. While Hungarian enterprises tend to be more digitally mature, Slovakian enterprises show the opposite pattern, based on our sample. It can also be seen that Hungarian and Slovakian enterprises move together overall in terms of the adaptability and use of tools. It is the tools used in every day work and also for marketing purposes that are highly dominant, as shown by the average score above 3.0. It is almost unthinkable for businesses to operate without taking advantage of online communication solutions, using mobile phone applications or working with an online booking, ordering or purchasing solution. It is also evident that electronic payments are also important in our lives, with businesses in both countries giving this a score of nearly three integers.

Table 4. Frequency of use of digital tools in relation to the organisation's market experience in Slovakia

		Sum of Squares	df	Mean square	F	Sig.
Electronic payment facility (POS)	Between Groups	1,381	3	0,460	0,423	0,737
	Within Groups	192,696	177	1,089		
	Total	194,077	180			
Online booking, ordering, purchasing solution	Between Groups	0,198	3	0,066	0,063	0,979
	Within Groups	186,719	177	1,055		
	Total	186,917	180			
Digital /customer management software	Between Groups	0,090	3	0,030	0,025	0,995
	Within Groups	212,429	177	1,200		
	Total	212,519	180			
Modern energy optimisation (sensors, etc.)	Between Groups	2,916	3	0,972	0,946	0,420
	Within Groups	181,847	177	1,027		
	Total	184,762	180			
Mobile phone applications	Between Groups	9,444	3	3,148	3,473	0,017
	Within Groups	160,446	177	0,906		
	Total	169,890	180			
Augmented reality (AR)	Between Groups	1,405	3	0,468	0,671	0,571
	Within Groups	123,457	177	0,697		
	Total	124,862	180			
Virtual reality (VR)	Between Groups	2,783	3	0,928	1,308	0,273
	Within Groups	125,549	177	0,709		
	Total	128,331	180			
Chatbot	Between Groups	1,451	3	0,484	0,562	0,641
	Within Groups	152,362	177	0,861		
	Total	153,812	180			
Management software	Between Groups	8,200	3	2,733	2,377	0,072
	Within Groups	203,513	177	1,150		
	Total	211,713	180			
Online communication interfaces	Between Groups	7,080	3	2,360	2,720	0,046
	Within Groups	153,594	177	0,868		
	Total	160,674	180			
Automation systems	Between Groups	1,433	3	0,478	0,458	0,712
	Within Groups	184,490	177	1,042		
	Total	185,923	180			

Source: Own research, 2023, N = 181 (Slovakian)

The same can be said for transaction management software, and we also observed that the use of augmented reality and virtual reality and chatbots is still in its infancy for businesses in both countries. In this respect, Slovakian businesses are slightly ahead of Hungarian businesses, but it can also be seen that Hungarian businesses are leading the way in automation or energy optimisation. Overall, there is no significant correlation between the opinions of businesses in the two countries, but the detailed results are worth considering. To this end, there is a need to prepare for a more knowledge-intensive training for enterprises that can better equip them to meet the challenges of digitalisation by offering usable and applicable solutions.

Scientific Ethics Declaration

The authors declare that the scientific ethical and legal responsibility of this article published in EPSTEM journal belongs to the authors.

Acknowledgements or Notes

* Project no. 2021-1.2.4-TÉT-2021-00041 has been implemented with the support provided by the Ministry of Culture and Innovation of Hungary from the National Research, Development and Innovation Fund, financed under the 2021-1.2.4 TÉT funding scheme.

* This article was presented a poster presentation at the International Conference on Basic Sciences, Engineering and Technology (www.icbaset.net) held in Alanya/Turkey on May 02-05, 2024.

References

Akben-Selcuk, E. (2016). Factors affecting firm competitiveness: Evidence from an emerging market *International Journal of Financial Studies, 4*(2), 9.

Asim, M., Nasim, S., & Naz, Z. (2023). Impact of enterprise flexibility on firm's competitiveness: An empirical study of select pharmaceutical firms in India. *Journal of Global Business and Competitiveness, 18*(1), 35-42.

Berger, T. (2008). Concepts of national competitiveness. *Journal of International Business and Economy, 9*(1), 91-111.

Cetindamar, D., & Kilitcioglu, H. (2013). Measuring the competitiveness of a firm for an award system. *Competitiveness Review*: *An International Business Journal*,*23*(1), 7-22.

Chikán, A., Czakó, E., Kiss-Dobronyi, B., & Losonci, D. (2022). Firm competitiveness: A general model and a manufacturing application. *International Journal of Production Economics, 243*, 108316.

Collis, D.J., & Montgomery,C.A. (2008). Competing on resources. *Harvard Business Review*. Retrieved from https://hbr.org/2008/07/competing-on-resources

Ekom - Etim, A., Igwe, A. A., Al-Faryan, M. A. S., & Udoh, B. E. (2023). Service system innovation and firm competitiveness in an emerging market: The role of corporate governance system. *Cogent Business & Management, 10*(2),2220202.

Flak, O., & Glod, G. (2020). Company competitiveness profiles on the example of Polish enterprises in the Silesian region in 2020. *21*(1), 103-120.

Friesenbichler, K., & Reinstaller, A. (2022). Do firms facing competitors from emerging markets behave differently? Evidence from Austrian manufacturing firms. *European Business Review, 34*(*2*),153-170.

Gottinger, H. W. (2020). Firm competitiveness, growth and digitalisation. A special review on network economics. *iBusiness, 12*, 203-221.

Lafuente, E., Leiva, J.C., Moreno-Gómez, J., & Szerb, L. (2020). A nonparametric analysis of competitiveness efficiency: the relevance of firm size and the configuration of competitive pillars, *BRQ Business Research Quarterly. Sage Publishing*. *London. 23*(3) 203-216.

Latifah, L., Setiawan, D., Aryani, Y.A., & Rahmawati, R. (2021). Business strategy - MSMEs' performance relationship: innovation and accounting information system as mediators. *Journal of Small Business and Enterprise Development. 28*(1), 11-21.

Navarro, J. G. C., Eldridge, S., & Wandosell, G. (2016). International organizational performance: the influence of congenital learning and realized absorptive capacity. *Journal of Small Business and Enterprise Development, 23*(2), 453-473.

Porter, M. E. (1990). The competitive advantage of nations. *Harvard Business Review, 68*(2),73-93.

Serban, R.-A., Mihaiu, D. M., Țichindelean, M., Ogrean, C., & Herciu, M. (2023). Factors of sustainable competitiveness at company level: A comparison of four global economic sectors. *Journal of Business Economics and Management, 24*(3), 449-470.

Yang, J., Zhou, L., Qu, Y., Jin, X., & Fang, S. (2023). Mechanism of innovation and standardization driving company competitiveness in the digital economy. *Journal of Business Economics and Management, 24*(1), 54-73.

Zhao, J., & Qi, N. (2021). Analysis of international competitiveness of multinational corporations based on rough sets. *Hindawi Journal, 2021*,1-10.

Author Information

János Varga
Óbuda University,
Keleti Károly Faculty of Business and Management
15-17. Tavaszmező Street, 1084 Budapest, Hungary
Contact e-mail: *varga.janos@kgk.uni-obuda.hu*

Ágnes Csiszárik-Kocsir
Óbuda University,
Keleti Károly Faculty of Business and Management
15-17. Tavaszmező Street, 1084 Budapest, Hungary

To cite this article:
Varga, J., & Csiszarik-Kocsir, A. (2024). The scope of digital tools and opportunities in the life of Hungarian and Slovakian enterprises and their impact on business competitiveness. *The Eurasia Proceedings of Science, Technology, Engineering & Mathematics (EPSTEM), 28,* 73-80.

The Eurasia Proceedings of Science, Technology, Engineering & Mathematics (EPSTEM)
ISSN: 2602-3199

The Eurasia Proceedings of Science, Technology, Engineering & Mathematics (EPSTEM), 2024

Volume 28, Pages 81-89

ICBASET 2024: International Conference on Basic Sciences, Engineering and Technology

Investigation of Oxidative Stress Parameters and Pro-Inflammatory Cytokines in a Neuropathy Model Created with Taraxacum Officinale L. Leaf Extract and Cisplatin

Mehmet Erdem
Gaziantep University

Mehmet Ozaslan
Gaziantep University

Abstract: The aim of this study was to investigate the effect of *Taraxacum officinale* leaf extract, a plant known for its potent antioxidant and anti-inflammatory properties, on cisplatin-induced neurotoxicity. Cancer treatment has demonstrated platinum drugs, particularly cisplatin, as among the most effective treatments. However, the drug comes with serious side effects. The use of cisplatin is limited due to its cytotoxic effects, potentially preventing patients from benefiting optimally from anticancer agents. *Taraxacum officinale* has been used for various diseases for years, observed clinically in conditions such as dyspepsia, liver, gallbladder, and urinary disorders. Nowadays, *Taraxacum officinale* has entered our lives in various forms as a dietary supplement. However, this plant possesses many bioactivities, particularly potent anti-inflammatory, antioxidant, and hepatoprotective properties.In this study, chronic cisplatin administration was used to induce a peripheral neuropathy model, administered intraperitoneally (i.p) once a week for 5 weeks at a dose of 3 mg/kg. *Taraxacum officinale* leaf extract was administered intragastrically once daily at a dose of 500mg/kg for the same duration to determine its potential effects on cisplatin neuropathy. After drug administration, motor performance was evaluated using the rotarod test, while sensory transmission status was assessed using tail withdrawal and hot/cold plate tests. Oxidative stress parameters and proinflammatory cytokine markers were analyzed biochemically. In animals exposed to cisplatin, thermal hypoalgesia and cold hypoalgesia were observed ($p<0.001$), motor coordination balance was prolonged with the rotarod test ($p<0.001$), and tail withdrawal time was extended ($p<0.001$). Biochemically, oxidative stress parameters TOS ($p<0.05$), OSI ($p<0.05$), and MDA ($p<0.05$) levels significantly increased compared to the cisplatin control group. TAS levels provided a statistically significant increase compared to the cisplatin-administered group ($p<0.05$). Proinflammatory cytokine markers TNF-α ($p<0.05$), IL-6 ($p<0.001$), and NFKB ($p<0.05$) levels were found to be higher compared to the cisplatin control group. It was determined that *Taraxacum officinale* improved these side effects induced by cisplatin both behaviorally and biochemically. In conclusion, *Taraxacum officinale* leaf extract is a plant with potent antioxidant and anti-inflammatory activity.

Keywords: Cisplatin neurotoxicity, Taraxacum officinale, Oxidative stress, Proinflammatory

Introductıon

Cancer ranks second among the leading causes of death worldwide, following cardiovascular diseases. Despite the development of new chemotherapy treatment strategies, the disease continues to maintain its significance (Bray et al., 2018). While aggressive treatments have led to increased cancer survival rates, new anticancer drugs often come with serious side effects that may persist for years. Peripheral neuropathy associated with chemotherapy is the most dose-limiting side effect of anticancer agents commonly used in the treatment of

various tumors such as paclitaxel, vincristine, and platinum. Most of these drugs affect the nervous system, with neurotoxicity being one of the most significant side effects (Brown et al., 2019). Cisplatin exhibits neurotoxic effects through various mechanisms, with oxidative stress being one of the most important. Peripheral neuropathy typically manifests as neuropathic pain syndrome characterized by painful symptoms. However, in many severe cases, it can progress to sensory loss. Additionally, motor and/or autonomic peripheral neuropathies can also occur (Brown et al., 2019). Chemotherapy-induced peripheral neuropathy adversely affects the quality of life of patients and may result in dose limitations or even discontinuation of treatment (Miltenburg & Boogerd, 2014). Therefore, patients may not be able to benefit optimally from the effects of anticancer agents. Neurotoxicity is one of the most serious problems associated with cisplatin chemotherapy (McWhinney et al., 2009). Among these, oxidative stress is the most important (Hashem et al., 2015). Additionally, DNA-mediated apoptotic pathways, mitochondrial damage, activation of proinflammatory cytokines, disturbances in ion channels, and glial activation are mechanisms responsible for cisplatin neurotoxicity. Studies have shown that cisplatin administration increases free radical formation and consequently enhances oxidative damage (Areti et al., 2014; Rehman et al., 2019). These findings indicate that oxidative stress plays a significant role in cisplatin toxicity. Consequently, oxidative products such as malondialdehyde and protein carbonyls increase. However, since chronic complications seen in cancers cannot be completely prevented with existing drugs, and there are toxic side effects of existing pharmaceutical treatments and sometimes long-term use leads to the development of tolerance, the importance of herbal medicines as supportive agents has emerged. Many studies have shown that phenolic compounds in plant essential oils exhibit antioxidant activity as a result of their free radical scavenging capacities. Natural antioxidants are thought to be beneficial agents in preventing diseases. Antioxidant substances have strong scavenging activities and the ability to upregulate cellular antioxidant systems. *Taraxacum officinale* is one of the plants with phenolic content that has been used as a herbal medicine for years. When the relationship between chemical content and bioactivity studies is examined, it is determined that phenolic compounds such as luteolin, chicoric acid, and taraxasterol in the composition of T. officinale significantly contribute to anti-inflammatory activity (Park et al., 2011; Piao et al., 2015). It has been observed to have strong antioxidant activity by reducing lipid peroxidation and scavenging free radicals with its rich flavonoid structure (Schütz et al., 2006). It has been recorded to significantly reduce liver toxicity due to its sesquiterpene and various polysaccharides (Mahesh et al., 2010; Park et al., 2010). The antioxidant activity of T. officinale is attributed to phenolic hydroxyl groups and activation of endogenous antioxidant enzymes (Park et al., 2014). Applying *Taraxacum officinale* roots and leaves to rats, in particular, leads to the development of an endogenous antioxidant profile (Kuntz & Kuntz, 2008; Harvey & Ferrier, 2017). Represented by 51 species, the Taraxacum genus of the Asteraceae family includes 16 endemic species in Turkey. The use of the *Taraxacum officinale* L. genus found in the natural flora of our country as a herbal drug from past to present, its herbal properties, and its possibilities of being cultured are important. (Özenirler, 2018). The aim of this study is to investigate the effect of *Taraxacum officinale* leaf extract, a plant known for its potent antioxidant and anti-inflammatory properties, on cisplatin-induced peripheral neuropathy.

Materials and Methods

Plant Collection

Plant Material: The aerial parts of Taraxacum officinale in leafy period were collected from the Gaziantep Region and washed before being dried in the shade.

Extraction Procedure

In the laboratory, the dried plant samples were ground using a laboratory grinder. The powdered sample weighing 50 g of *Taraxacum officinale* leaves was extracted in 1L of ethanol (96%) at room temperature for two weeks. The mixture was occasionally shaken during the waiting period. Afterward, it was filtered (Whatman No. 4 filter). Following the removal of the solvent using a rotary evaporator, the extracts were stored at +4°C in a refrigerator (Colle et al., 2012).

Experimental Animals and Housing Conditions

In this study, 28 male Wistar Albino rats aged 8-10 weeks were used. The experimental animals were obtained from the Gaziantep University Animal Research Center (GAÜNDAM). Male Wistar Albino rats (250-300±5 g) were acclimatized to the environment for 10 days under a 12-hour light/12-hour dark cycle, at a room

temperature of 21±2°C, with 50-60% relative humidity and a ventilation system. Throughout the research period, the animals were fed standard pellet feed and given ad-libitum access to drinking water to control their nutrition. The cages were cleaned daily, and the animals received regular care.

Experimental Model

The neuropathic pain model induced by cisplatin, as described by Han et al. (2014), was used. In the first group (n=7), an equivalent amount of saline solution was injected as the Control group. In the second group, rats were injected with cisplatin at a dose of 3 mg/kg intraperitoneally once a week for 5 weeks. To prevent the development of cisplatin-associated nephrotoxicity, 1 ml of saline solution was simultaneously injected intraperitoneally with cisplatin. In the third group, referred to as the treatment group, *Taraxacum officinale* L. leaf extracts (500mg/kg) were administered intragastrically daily for 5 weeks, along with a single dose of cisplatin (3mg/kg) intraperitoneally once a week for 5 weeks. The fourth group, the positive control, received *Taraxacum officinale* L. leaf extract (500mg/kg) intragastrically daily for 5 weeks. Injections were administered at the same time every week (between 12:00 - 13:00) throughout the 35-day experiment.

In Vivo Experiments

Motor Performance and Coordination Assessment

Rotarod

The Rotarod test is commonly used to measure motor performance and coordination (Ugo Basile, Comerio, Italy). In our experimental protocol, animals were acclimatized to the apparatus and environment before being subjected to the test. The Rotarod test involved gradually increasing the speed from 5 (rpm) to 40 (rpm) over 300 seconds (ramp protocol) (Griffiths et al., 2018). Animals were run on the Rotarod apparatus three times with a 5-minute rest period between each run. The duration each animal remained on the rod was recorded, and the arithmetic mean of three measurements was calculated for each group. The presence of differences between groups was determined, and any significant variations were assessed.

Sensory Evaluation

Hot Plate

In this test, thermal hyperalgesia was evaluated. A floor enclosed with glass or plexiglass cylinders was heated to 55°C as descrided (model 35100, Ugo Basile, Comerio, Italy). The animal was placed on the heated floor, and the time until the animal withdrew its paw was recorded (Animals exhibit stereotypical movements such as paw licking, jumping, paw withdrawal, etc., when experiencing pain). The normal reaction time typically ranges from 5 to 20 seconds, but rats were not allowed to remain on the heated surface for more than 30 seconds to prevent tissue damage (cut-off) (Yamamoto et al., 2002).

Cold Plate

In this test, cold hyperalgesia conditions among groups were evaluated according to (model 35100, Ugo Basile, Comerio, Italy). Its effect was examined at 5°C. The working principle of the cold plate test is similar to the hot plate test. Rats were not allowed to remain on the plate for more than 50 seconds to prevent tissue damage (cut-off) (Sakurai et al., 2009).

Pain Evaluation

Tail Flick

The tail flick test is used to evaluate the central effects of pain threshold (model 37360, Ugo Basile, Comerio, Italy). A photosensor is located beneath the area where the tail is placed. When heat is applied to the tail, the animal withdraws its tail when it feels pain, and this movement is detected by the photosensor. The time from the

onset of heat application to tail withdrawal was recorded. This time was kept less than 10 seconds to prevent the animal from experiencing excessive pain (Singh et al., 2018). The spinal reflex, evaluated as tail withdrawal latency, determines the animal's pain threshold.

Biochemical Analyses

Sampling and Preparation of Samples

After completion of behavioral experiments, blood samples and sciatic nerve samples were taken from each rat for biochemical analyses. Two blood samples were taken from each rat, one in normal biochemical tubes and the other in biochemical tubes containing EDTA. Similarly, two sciatic nerve samples were taken from each rat. These samples would be used in biochemical analyses.

The collected blood samples were centrifuged at 4000 (rpm) for 10 minutes at +4°C to separate serum/plasma. Depending on the parameters to be analyzed, serum/plasma samples were divided into Eppendorf tubes and stored at -80°C until analysis. It was estimated that approximately 5 ml of blood sample would be sufficient for biochemical analyses.

Statistical Analysis of Data

The Shapiro-Wilk normality test was conducted to compare differences between groups and observations concerning the measured data. One-way analysis of variance (ANOVA) was used for normally distributed data, while the Kruskal-Wallis H test was applied for non-normally distributed data. For pairwise comparisons between groups, the Post Hoc Tukey test was used if the data were homogeneously distributed; otherwise, the Games-Howell test was applied for ANOVA. For Kruskal-Wallis, Dunnett (as a Post Hoc test), Tukey, or Duncan tests were used. The results were expressed as mean ± standard deviation. A significance level of $p < 0.05$ was considered in the study.

Results

Evaluation of Motor Coordination and Balance

Rota Rod Results

In the results, the sisplatin group significantly shortened the time spent on the rod compared to the control group ($p < 0.01$). The treatment group significantly extended the shortened time on the rod compared to the sisplatin group ($p < 0.05$).

Sensory Experiments Findings

Hot Plate

According to the hot plate results, the sisplatin group significantly prolonged the time spent on the hot plate compared to the control group ($p < 0.001$). The treatment group significantly reduced the prolonged time in the sisplatin group ($p < 0.001$).

Cold Plate

According to the results on the Cold Plate at 5°C, the sisplatin group significantly prolonged the time spent on the cold plate compared to the control group ($p < 0.001$). The treatment group significantly reduced the prolonged time observed in the sisplatin group ($p < 0.001$).

Pain Experiment Findings

Tail Flick Results

According to the tail flick results, the sisplatin group significantly increased the tail flick latency compared to the control group ($p < 0.001$). The treatment group significantly decreased the prolonged tail flick latency observed in the sisplatin group ($p < 0.001$).

Biochemical Analyses

One-way ANOVA and Tukey's post-hoc test were used for evaluating biochemical analyses. Oxidative stress parameters such as TOS, TAS, OSI, MDA, and proinflammatory markers including NFkB, TNF-α, IL-6 were assessed in the sciatic nerve tissue samples from control, sisplatin, treatment, and positive groups.

According to our results, there was a statistically significant increase in NFkB levels in the sisplatin group compared to the control group ($p < 0.001$), while the treatment group showed a significant decrease compared to the sisplatin-administered groups ($p < 0.05$).

For TNF-α levels, there was a statistically significant increase in the sisplatin group compared to the control group ($p < 0.05$), but the treatment group did not show a significant decrease compared to the sisplatin-administered groups ($p > 0.05$).

IL-6 levels showed a statistically significant increase in the sisplatin group compared to the control group ($p < 0.001$), whereas the treatment group exhibited a significant decrease compared to the sisplatin-administered groups ($p < 0.05$).

MDA levels showed a statistically significant increase in the sisplatin group compared to the control group ($p < 0.001$), while the treatment group showed a significant decrease compared to the sisplatin-administered groups ($p < 0.05$).

TOS and OSI levels showed a statistically significant increase in the sisplatin group compared to the control group ($p < 0.05$). TAS levels showed a statistically significant increase in the treatment group compared to the sisplatin-administered group ($p < 0.05$).

Discussion

Cisplatin is a chemotherapeutic agent used in the treatment of many solid tumors, including colorectal cancer, ovarian cancer, testicular cancer, bladder cancer, esophageal cancer, stomach cancer, and lung cancer. Due to the neurotoxicity caused by cisplatin treatment, effective combat against tumors cannot be achieved if treatment is discontinued or dose-reduced. In this study, we demonstrated that Taraxacum officinale leaf extract reduces the side effects of cisplatin, both behaviorally and biochemically, likely by reducing oxidative stress in the sciatic nerve tissue.

In this study, the motor activity and balance skills of the cisplatin group were significantly impaired by cisplatin. This finding is consistent with previous research findings. Over the course of five weeks, Taraxacum officinale leaf extract (500 mg/kg, i.g) significantly reduced the effects of cisplatin and extended the time spent on the rotarod. Platinum compounds like cisplatin are widely known to cause significant sensory neuropathies, but previous research has also shown a serious impact on the motor system, disrupting motor coordination. The role of Taraxacum officinale leaf extract in correcting motor performance impaired by cisplatin may be associated with its neuroprotective effects. Consequently, Taraxacum officinale leaf extract significantly improved the impaired motor function in this study.

Thermal hyperalgesia was observed in the hot plate tests. The perception of the thermal stimulus on the hot plate decreased after intraperitoneal administration of cisplatin. Thermal hyperalgesia was observed in the cold plate tests. The perception of the thermal stimulus on the cold plate decreased after intraperitoneal administration of cisplatin. Previous studies have reported that cisplatin induces thermal hyperalgesia and cold allodynia in rats. However, there are also studies showing that cisplatin induces thermal hypoalgesia. Taraxacum officinale leaf extract reduced the prolonged paw withdrawal latency in the hot/cold plate test induced by cisplatin and approached the control group averages. According to the tail flick results, the cisplatin group significantly

prolonged the tail withdrawal latency compared to the control group. However, the treatment group significantly reduced the prolonged tail withdrawal latency of the cisplatin group.

Conclusion

The aim of this study was to minimize the neurotoxic effects of cisplatin, an effective chemotherapeutic agent, and to eliminate or reduce the side effects that limit the use of this drug. Traditionally, Taraxacum officinale has been used in the treatment of various diseases and its use has been observed clinically in conditions such as dyspepsia, liver, gallbladder, and urinary disorders. Today, *Taraxacum officinale* has become part of our lives as a food supplement in various forms. However, this plant has many bioactivities, especially strong anti-inflammatory, antioxidant, anticancer, and hepatoprotective properties. Considering its side effects and toxicity, it is seen to not have serious side effects or toxicity. Although it is not naturally found in our country, it is a plant suitable for its culture. In light of this information, it is evaluated that it may be effective in the treatment of common diseases such as cancer, liver, and gallbladder, due to its strong antioxidant, hepatoprotective, and anti-inflammatory effects, if it is converted into herbal medicine form.

Due to the neurotoxicity caused by chemotherapy, effective combat against tumors cannot be achieved when treatment is discontinued or doses are reduced. As a result of this study, the side effects of cisplatin have been partially reduced with the application of Taraxacum officinale leaf extract. Consistent with the literature, Taraxacum officinale leaf extract reduced oxidative stress, decreased the destructive effect of cisplatin, and this effect was confirmed behaviorally and biochemically. Among the significant limitations of this study are the lack of histopathological examination of the sciatic nerve tissue and the lack of mRNA expression of antioxidant enzymes.

Traditionally, oxidative stress has been defined as an imbalance between prooxidants and antioxidants in biological systems. Increased oxidative stress is defined as an imbalance between cellular defense mechanisms and cellular free radical formation, and MDA is considered one of the most important oxidative stress markers (Ince et al., 2010). In this study, we observed that Taraxacum officinale leaf extract significantly reduced the elevated MDA levels in serum and nerve tissue induced by cisplatin.

Taraxacum officinale flowers, leaves, stems, and roots extracts have been evaluated for their antioxidant effects by measuring lipozomal lipid peroxidation induced by Fe+2 and ascorbic acid, either alone or in combination with toxic agents such as CCl4. It has been reported that *Taraxacum officinale* extract exhibited antioxidant effects by reducing lipid peroxidation (Yan et al., 2009).

In another study, it was reported that a mixture of *Taraxacum officinale* and various green leafy vegetables applied to mice exhibited protective effects on hepatocytes in liver tissue by reducing lipid peroxidation (Kim et al., 2009). According to the study by Sumanth and Rana, an extract made from *Taraxacum officinale* roots was administered orally at two different doses, namely 50 and 100 mg/kg. At the dose of 100 mg/kg, a significant decrease in MDA levels compared to the toxicity group was observed ($p<0.01$). Additionally, there was a significant increase in MDA levels when compared to the toxicity group with the control group ($p<0.001$) (Sumanth and Rana, 2006).

You et al. reported that liver damage induced by alcohol toxicity was significantly associated with increased ROS production and lipid peroxidation ($p<0.05$) (You et al.,2010). Furthermore, it was found that the increase in MDA levels in the liver induced by toxicity decreased with the administration of lutein, luteolin-7-O-glucoside, and polyphenols contained in *Taraxacum officinale* (Hagymasi et al., 2000; Popovic et al., 2001).

Park et al. stated that there was a significant increase in MDA levels in the toxicity-induced group compared to the control group ($p<0.05$). Additionally, they observed that the water extract of *Taraxacum officinale* leaves showed a decrease in MDA levels for the dose of 0.5 g/kg compared to the toxicity-induced group, but the dose of 2 g/kg showed a greater decrease ($p<0.05$) (Park et al., 2010).

In our study, we observed a significant increase in MDA levels in both serum ($p<0.05$) and sciatic nerve tissue ($p<0.001$) in the cisplatin-induced neurotoxicity group treated with *Taraxacum officinale* leaf ethanol extract. The treatment group showed a statistically significant decrease in both serum and sciatic nerve tissue compared to groups treated with cisplatin alone ($p<0.05$). These findings are consistent with previous studies. We believe that *Taraxacum officinale* achieves this effect by reducing oxidative stress. Cisplatin-induced neuropathy has been associated with oxidative damage, inflammation, mitochondrial dysfunction, DNA damage, and apoptosis

in nerve system cells. DNA damage caused by cisplatin leads to abnormal protein synthesis and reduces the activity of antioxidant enzymes such as catalase, glutathione peroxidase, and superoxide dismutase. Mitochondrial physiological dysfunction reduces cellular metabolism, increases the production of reactive oxygen species (ROS), and enhances oxidative stress. Increased intracellular ROS production triggers inadequate antioxidant defense, leading to demyelination of peripheral nerve cytoskeleton and sensitization of signal transmission processes. As a result, cisplatin induces structural changes in peripheral nerves by disrupting enzymes, proteins, and lipids, leading to peripheral neuropathy.

In a study involving humans, a combination of seven plants including T. officinale was found to significantly reduce anal bleeding and decrease disease activity in patients with inflammatory bowel disease. Although the etiology of this disease remains unclear, the current treatment is generally aimed at systemic immunosuppression due to the significant feature of damage to the gastrointestinal mucosal layer. It should be noted that a combination of various plant compounds may lead to reduced leukocyte infiltration and mucosal ulceration, which could improve acute colonic inflammation. A herbal medicine with synergistic mechanisms of action inhibited the pro-inflammatory transcription factor NF-kB activity, reduced the expression of COX-2, TNF-a, IL-1, IL-6, and iNOS, and decreased the production of nitric oxide, reactive oxygen species, leukotrienes, and prostaglandins, indicating its potential use as an adjunctive therapy for inflammatory bowel disease (Jackson et al., 2008).

Koh et al. investigated the anti-inflammatory effects of *Taraxacum officinale* methanolic leaf extract and fractions on lipopolysaccharide-stimulated mouse macrophage RAW 264.7 cell line. They found that the extract dose-dependently inhibited LPS-induced production of NO, pro-inflammatory cytokines, and PGE(2). The analysis included the activation of iNOS, COX-2, and mitogen-activated protein kinases, as well as the levels of pro-inflammatory cytokines such as TNF-α, IL-1β, and IL-6. It was found that Taraxacum officinale methanolic leaf extract dose-dependently inhibited NO production, PGE, and pro-inflammatory cytokines such as TNF-α and IL-1β (Koh et al., 2010).

A study investigating the hepatoprotective effects of polysaccharides isolated from *Taraxacum officinale* showed that this plant has hepatoprotective effects through alleviating oxidative damage and triggering anti-inflammatory response. In toxicity-induced studies, polysaccharides found in *Taraxacum officinale* were found to reduce liver damage by regulating iNOS, COX-2, TNF-α, and IL-1 levels (Park et al., 2010).

Another study demonstrated that combined treatment with luteolin and chicoric acid derived from *Taraxacum officinale* reduced cellular nitric oxide (NO) and prostaglandin E2 (PGE2) concentrations synergistically in lipopolysaccharide (LPS)-stimulated RAW 264.7 cells. Additionally, the combined treatment inhibited inducible nitric oxide synthase (iNOS) and cyclooxygenase-2 (COX-2) expression. Furthermore, the combined treatment decreased the levels of pro-inflammatory cytokines such as tumor necrosis factor (TNF)-α and interleukin (IL)-1β. Both luteolin and chicoric acid individually suppressed oxidative stress but did not exhibit any synergistic activity. When applied together, luteolin and chicoric acid inhibited the phosphorylation of NF-κB and Akt, but had no effect on extracellular signal-regulated kinase (ERK), c-Jun NH2-terminal kinase (JNK), and p38. This anti-inflammatory signaling cascade overlapped only with luteolin treatment. The results suggest that luteolin plays a central role in improving LPS-induced inflammatory cascades through inactivation of NF-κB and Akt pathways, and chicoric acid enhances luteolin's anti-inflammatory activity by reducing NF-κB activation (Park et al., 2011a).

In another study, it was found that taraxasterol isolated from T. officinale dose-dependently inhibited nitric oxide (NO), prostaglandin E(2) (PGE(2)), tumor necrosis factor-α, interleukin IL-1β, and IL-6 production in LPS-stimulated RAW 264.7 macrophages. Taraxasterol was shown to prevent the translocation of NF-κB from the cytoplasm to the nucleus induced by LPS. The evaluation showed that taraxasterol inhibited NO, PGE(2), TNF-α, IL-1β, and IL-6 production in a dose-dependent manner, and further studies demonstrated that taraxasterol prevented NF-κB translocation induced by LPS. The results suggest that taraxasterol has an anti-inflammatory effect by inhibiting the NF-κB pathway (Zhang et al., 2012).

According to our findings, *Taraxacum officinale* demonstrated antioxidant activity by reducing levels of pro-inflammatory markers such as NF-κB, TNF-α, and IL-6 in both nerve tissue and serum. These findings are consistent with previous studies. The antioxidant activity of Taraxacum officinale has been demonstrated in previous research as well. Given its potential as a treatment approach in the pathophysiology of oxidative stress in various diseases, Taraxacum officinale is suggested to be utilized to mitigate the adverse effects of chemotherapeutics. It should be noted that in the positive control group, *Taraxacum officinale* did not exhibit any adverse effects in behavioral and biochemical tests.

Scientific Ethics Declaration

The authors declare that the scientific ethical and legal responsibility of this article published in EPSTEM journal belongs to the authors.

Acknowledgements or Notes

* This article was presented as an oral presentation at the International Conference on Basic Sciences, Engineering and Technology (www.icbaset.net) held in Alanya/Turkey on May 02-05, 2024.

References

Areti, A., Yerra, V. G., Naidu, V. G. M., & Kumar, A. (2014). Oxidative stress and nerve damage: role in chemotherapy induced peripheral neuropathy. *Redox Biology, 2,* 289-295.

Bray, F., Ferlay, J., Soerjomataram, I., Siegel, R. L., Torre, L. A., & Jemal, A. (2018). Global cancer statistics 2018: Globocan estimates of incidence and mortality worldwide for 36 cancers in 185 countries. *CA: A Cancer Journal for Clinicians, 68*(6), 394-424.

Brouwers, E. E., Huitema, A. D., Boogerd, W., Beijnen, J. H., & Schellens, J. H. (2009). Persistent neuropathy after treatment with cisplatin and oxaliplatin. *Acta Oncologica, 48*(6), 832-841.

Brown, T. J., Sedhom, R., & Gupta, A. (2019). Chemotherapy-induced peripheral neuropathy. *JAMA Oncology, 5*(5), 750-750.

Colle, D., Arantes, L. P., Rauber, R., de Mattos, S. E. C., da Rocha, J. B. T., Nogueira, C. W., & Soares, F. A. (2012b). Antioxidant properties of Taraxacum officinale fruit extract are involved in the protective effect against cellular death induced by sodium nitroprusside in brain of rats. *Pharmaceutıcal Biology, 50*(7), 883-891.

Griffiths, L. A., Duggett, N. A., Pitcher, A. L., & Flatters, S. J. (2018). Evoked and ongoing pain-like behaviours in a rat model of paclitaxel-induced peripheral neuropathy. *Pain Research and Management*, *2018,* 8217613.

Hagymási, K., Blázovics, A., Lugasi, A., Kristó, S. T., Feher, J., & Kery, A. (2000). *In vitro antioxidant evaluation of dandelion (Taraxacum officinale web.) water extracts*. https://www.cabidigitallibrary.org/doi/full/10.5555/20013038091

Han, F. Y., Wyse, B. D., & Smith, M. T. (2014). Optimization and pharmacological characterization of a refined sisplatin-induced rat model of peripheral neuropathic pain. *Behavioural Pharmacology, 25*(8), 732-740.

Hashem, R. M., Safwar, G. M., Rashed, L. A., & Bakry, S. (2015). Biochemical findings on cisplatin-induced oxidative neurotoxicity in rats. *International journal of Advanced Research, 3*, 1222-1234.

Hfaiedh, M., Brahmi, D., & Zourgui, L. (2016). Hepatoprotective effect of Taraxacum officinale leaf extract on sodium dichromate-induced liver injury in rats. *Envıronmental Toxıcology, 31*(3), 339-349.

Ince, S., Kucukkurt, I., Cigerci, I. H., Fidan, A. F., & Eryavuz, A. (2010). The effects of dietary boric acid and borax supplementation on lipid peroxidation, antioxidant activity, and DNA damage in rats. *Journal of Trace Elements in Medicine and Biology, 24*(3), 161-164.

Jackson, L. N., Zhou, Y., Qiu, S., Wang, Q., & Mark Evers, B. (2008). Alternative medicine products as a novel treatment strategy for inflammatory bowel disease. *The American Journal of Chinese Medicine, 36*(5), 953-965.

Jangra, A., Kwatra, M., Singh, T., Pant, R., Kushwah, P., Ahmed, S., & Lahkar, M. (2016a). Edaravone alleviates sisplatin-induced neurobehavioral deficits via modulation of oxidative stress and inflammatory mediators in the rat hippocampus. *European Journal of Pharmacology*, *791,* 51-61.

Kim, M. Y., Cheong, S. H., Kim, M. H., Son, C., Yook, H. S., Sok, D. E., ... & Kim, M. R. (2009). Leafy vegetable mix supplementation improves lipid profiles and antioxidant status in C57BL/6J mice fed a high fat and high cholesterol diet. *Journal of Medicinal Food, 12*(4), 877-884.

Koh, Y. J., Cha, D. S., Ko, J. S., Park, H. J., & Choi, H. D. (2010). Anti-inflammatory effect of Taraxacum officinale leaves on lipopolysaccharide-induced inflammatory responses in RAW 264.7 cells. *Journal of Medicinal Food, 13*(4), 870-878.

Lomeli, N., Di, K., Czerniawski, J., Guzowski, J. F., & Bota, D. A. (2017). Sisplatin-induced mitochondrial dysfunction is associated with impaired cognitive function in rats. *Free Radical Biology and Medicine, 102*, 274-286.

McWhinney, S. R., Goldberg, R. M., & McLeod, H. L. (2009). Platinum neurotoxicity pharmacogenetics. *Molecular Cancer Therapeutics, 8*(1), 10-16.

Miltenburg, N. C., & Boogerd, W. (2014). Chemotherapy-induced neuropathy: a comprehensive survey. *Cancer Treatment Reviews, 40*(7), 872-882.

Ozenirler, C. (2018). Dandelion honey: a new monofloral honey record for Turkey. *Uludag Arıcılık Dergisi, 18*(2), 87-93.

Park, C. M., Youn, H. J., Chang, H. K., & Song, Y. S. (2010). TOP 1 and 2 polysaccharides from Taraxacum officinale, attenuate CCl4-induced hepatic damage through the modulation of NF kappa B and its regulatory mediators. *Food and Chemıcal Toxıcology,48* (5), 1255-1261.

Park, C. M., Park, J. Y., Noh, K. H., Shin, J. H, & Song, Y. S. (2011).Taraxacum officinale Weber extracts inhibit Lps-induced oxidative stres and nitric oxide production via the NF kappa B modulation in RAW 264.7 cells. *Journal of Ethnopharmacology, 133*(2), 834-842.

Podratz, J. L., Knight, A. M., Ta, L. E., Staff, N. P., Gass, J. M., Genelin, K., ... & Windebank, A. J. (2011). Sisplatin induced mitochondrial DNA damage in dorsal root ganglion neurons. *Neurobiology of Disease, 41*(3), 661-668.

Popović, M., Kaurinović, B., Mimica-Dukić, N., Vojinović-Miloradov, M., & Ćupić, V. (2001). Combined effects of plant extracts and xenobiotics on liposomal lipid peroxidation. Part 4. Dandelion extract-Ciprofloxacin/pyralene. *Oxidation Communications, 24*(3), 344-351.

Rehman, M. U., & Rather, I. A. (2019). Myricetin abrogates sisplatin-induced oxidative stress, inflammatory response, and goblet cell disintegration in colon of wistar rats. *Plants, 9*(1), 28.

Sakurai, M., Egashira, N., Kawashiri, T., Yano, T., Ikesue, H., & Oishi, R. (2009). Oxaliplatin-induced neuropathy in the rat: involvement of oxalate in cold hyperalgesia but not mechanical allodynia. *PAIN®, 147*(1-3), 165-174.

Schütz, K., Carle, R., & Schieber, A. (2006). Taraxacum—a review on its phytochemical and pharmacological profile. *Journal of Ethnopharmacology, 107*(3), 313-323.

Sharawy, N., Rashed, L., & Youakim, M. F. (2015). Evaluation of multi-neuroprotective effects of erythropoietin using cisplatin induced peripheral neurotoxicity model. Experimental and Toxicologic *Pathology, 67*(4), 315-322.

Sigstedt, S. C., Hooten, C. J., Callewaert, M. C., Jenkins, A. R., Romero, A. E., Pullin, M. J., ... & Steelant, W. F. (2008). Evaluation of aqueous extracts of taraxacum officinale on growth and invasion of breast and prostate cancer cells. *International Journal of Oncology, 32*(5), 1085-1090.

Singh, P., Kongara, K., Harding, D., Ward, N., Dukkipati, V. S. R., Johnson, C., & Chambers, P. (2018). Comparison of electroencephalographic changes in response to acute electrical and thermal stimuli with the tail flick and hot plate test in rats administered with opiorphin. *BMC Neurology, 18,* 1-10.

Sumanth, M., & Rana, A. C. (2006). In vivo antioxidant activity of hydroalcoholic extract of Taraxacum officinale roots in rats. *Indian Journal of Pharmacology, 38*(1), 54-55.

Yamamoto, T., Nozaki-Taguchi, N., & Chiba, T. (2002). Analgesic effect of intrathecally administered orexin-A in the rat formalin test and in the rat hot plate test. *British Journal of Pharmacology, 137*(2), 170-176.

Yan, S. L., Wu, S. T., Yin, M. C., Chen, H. T., & Chen, H. C. (2009). Protective effects from carnosine and histidine on acetaminophen-induced liver injury. *Journal of Food Science, 74*(8), H259-H265.

You, Y., Yoo, S., Yoon, H. G., Park, J., Lee, Y. H., Kim, S., Oh, K. T., Lee, J., Cho, H. Y., & Jun, W. (2010). In vitro and in vivo hepatoprotective effects of the aqueous extract from Taraxacum officinale (dandelion) root against alcohol-induced oxidative stres. *Food and Chemıcal Toxıcology, 48*(6), 1632-1637.

Zhang, X., Xiong, H., & Liu, L. (2012). Effects of taraxasterol on inflammatory responses in lipopolysaccharide-induced RAW 264.7 macrophages. *Journal of Ethnopharmacol,141*(1), 206-211.

Author Information

Mehmet Erdem
Department of Health Services Vocational School, Gaziantep University, 27310, Gaziantep-Türkiye

Mehmet Özaslan
Department of Biology, Gaziantep University, 27310, Gaziantep-Türkiye
Contact e-mail: *ozaslanmd@gantep.edu.tr*

To cite this article:

Erdem, M. & Ozaslan, M. (2024). Investigation of oxidative stress parameters and pro-inflammatory cytokines in a neuropathy model created with taraxacum officinale L. leaf extract and cisplatin. *The Eurasia Proceedings of Science, Technology, Engineering & Mathematics (EPSTEM), 28,* 81-89.

The Eurasia Proceedings of Science, Technology, Engineering & Mathematics (EPSTEM)
ISSN: 2602-3199

The Eurasia Proceedings of Science, Technology, Engineering & Mathematics (EPSTEM), 2024

Volume 28, Pages 90-96

ICBASET 2024: International Conference on Basic Sciences, Engineering and Technology

Remote Sensing Upon Tracking Changes in the Water Sufrace Area of Belmeken Dam

Kameliya Radeva
Bulgarian Academy of Sciences

Silvia Kirilova
University of Architecture

Abstract: Determining the characteristic volumes in a water reservoir contributes to the correct use of its water potential, nevertheless it is used for irrigation, water supply or for power generation. The introduction of new technologies and methods for tracking changes in water areas during the operation of hydrotechnical facilities has been a topical subject in recent decades. The present survey investigates the possibilities of using remote sensing data to track the changes of water areas in the reservoir lake of the Belmeken dam. We have applied a common remote sensing index (NDWI) for a five- year period (2018-2022) to analyze possible changes in water areas/water surface. The results show that the application of satellite data, specifically the NDWI index, that are compatible with the volumes measured for the same period in the dam, that are calculated by the balance method, could contributes to up-to-date information on the water volumes formed in the reservoir of Belmeken dam. The research can facilitate the process for determining the water volumes in Belmeken dam and support decision-makers and responsible institutions in the management of the water volumes during the dam's reservoir operation.

Keywords: Remote sensing, NDWI, Water balance method, Water volumes curve, Flooded areas curve

Introduction

Reservoirs, which are part of water energy systems, are an important component of water management and water resources management in the conditions of seasonal irregularity of precipitation and river inflow and of water use from the dam, especially in the conditions of climate change and anthropogenic impacts.Water resources are unevenly distributed on the territory of Bulgaria, both in perennial and seasonal aspects. According to Eng. Lyubenov (2009), in just 2-3 months in the spring, 60-70% of the high waters formed on the territory of the country drain away. Part of these water volumes are accumulated in the reservoirs for their distribution in the remaining months of the year for the respective consumers, and the remaining volumes flow into the riverbeds. The stored water volumes in the reservoirs of the large hydropower cascades maintained and managed by the "Dams and Cascades" enterprise of NEK-EAD(https://www.nek.bg/index.php/bg/) amount to 3.5x109.m^3, which is 50.1% of the total regulated volume of reservoirs in the Republic of Bulgaria.(River Basin East Aegean Directorate, 2016-2021)

Observations on the water levels in the artificial reservoirs are daily and based on them, monthly schedules of the inflow and outflow of water are drawn up, open data available on the website of the Ministry of Environment and Water (MOEW). In addition, the open-accessed data (with a resolution of 5x5 m) from Sentinel - 2 satellite have been used, which allows the calculation of the Normalized Difference Water Index (NDWI), distinguishing a given water body against the background of soils and vegetation. The water index generated from satellite images has been observed by McFeeters (1996), Rogers & Kearney (2004) and Xu (2006). The index was used to assess the hydrological drought in West Java during El Niño 2015 (Luisa et al.,

2018). and in the Ravi basin (Taloor et al., 2021). A comparative analysis between NDWI and ground data can be found in the studies of Sawunyama et al. (2006) and Xu et al. (2006). Gao et al. (2012) and Yigzaw et al. (2018) reviewed the possibility of remote sensing methods to assess the morphometry of reservoirs and water storage ponds. Zhang et al. (2014) and Sekertekin et al. (2018) and Bhangale et al. (2019) considered the possibility of extracting water surface information from different satellite images.

The aim of the present invetsigation is to analyze the NDWI water index data generated from Sentinel -2 imagery and compare it with the hydrometric monitoring of “Belmeken” dam, the highest located in the Belmeken-Sestrimo-Chaira cascade in Bulgaria.

Study Area

The Belmeken Dam is an element of the Belmeken-Sestrimo-Chaira cascade, which is one of the four main hydropower complexes for the production of electricity in the country. The cascade was designed and built in stages from 1964 to 1996. The first stage covers the design and construction of the Belmeken Dam, the Stankovi Baraki Dam, the Belmeken hydropower plants-pumped-storage hydro facilities, the Sestrimo Hydroelectric Plant, the Momina Klisura Hydroelectric Plant", two gathering derivations and two equalizers, and the second stage with the construction of the Chaira dam and the Chaira PAVEC, which came into operation in 1996. The complex operates with a full capacity of 1599 MW, after 1997 (Nabatov, 2015) (Figure 1).

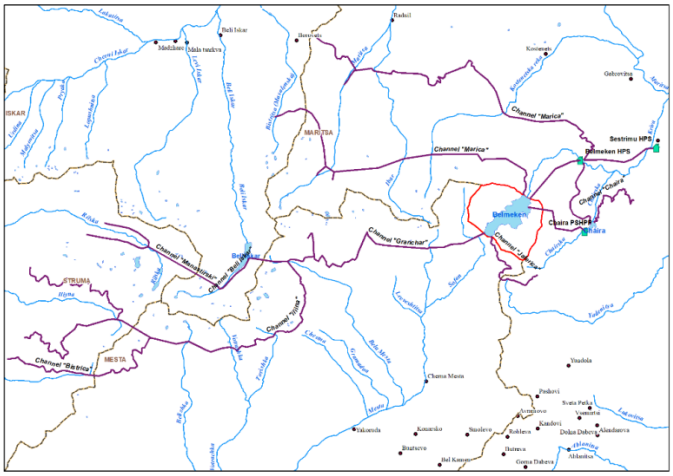

Figure 1. Location of "Belmeken-Sestrimo-Chaira" cascade

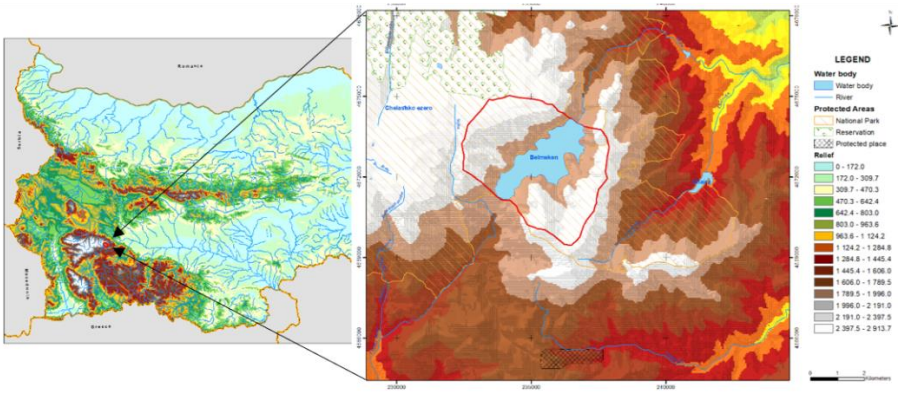

Figure 2. Location of "Belmeken" dam

The catchment area of "Belmeken" dam is developed in the highland part of the eastern part of the Rila mountain, within the borders of the "Rila" National Park, and within the borders of the East Agean River Basin Directorate, to the west with the river basin of the Sofanitsa River (Sofan Dere), and to the northeast and southeast with the river basins of the Kostenska River, the Chaiirska River, and the Yadenitsa River. The border of the watershed passes through the village of Belmeken (2626 m) and to the southeast through the village of Slavov vrah (2306 m). The "Belmeken" dam is 1923 m above sea level and was built on the Kriva River with a catchment area of 20 km^2.

The majority of the inflow into the dam comes from the collecting derivations "Granchar", "Dzaferitsa", "Manastirski" and "Iliina", built in the catchments of the Mesta River and the Struma River (Figure 1). "Belmeken" dam is built by two dam walls: a stone embankment with a height of 88.2 m, and a counter wall with a height of 23 m. The reservoir is annually leveled with a total pumped volume of 144.1.106.m^3 and a flooded area of 4.6 km^2. The delineation of the water surface was obtained from the developed geoinformation system for water management, available on the website of MoEW.

Materials and Methods

Data from Sentinel-2 satellite images within a period 2018- 2022 has been used in the survey- Level-2A orthorectified atmospherically corrected surface reflectance, available since 2017, and Level-1C orthorectified top-of-atmosphere reflectance, available since 2015. We have selected days in the abovementioned period with cloud cover below 40%. (Table 1).

Table 1. Input satellite data

Year	Date	Satellite	Year	Date	Спътник	Year	Date	Satellite
2018	19.01.	Sentinel 2 L2A	**2020**	24.01.	Sentinel 2 L1C	**2021**	25.09.	Sentinel 2 L1C
	29.04.	Sentinel 2 L1C		08.02.	Sentinel 2 L1C		25.10.	Sentinel 2 L1C
	08.06.	Sentinel 2 L1C		19.03.	Sentinel 2 L1C		14.11.	Sentinel 2 L1C
	07.08.	Sentinel 2 L1C		23.04.	Sentinel 2 L1C		24.12.	Sentinel 2 L1C
	11.09.	Sentinel 2 L1C		08.05	Sentinel 2 L1C		18.01.	Sentinel 2 L2A
	16.10.	Sentinel 2 L1C		27.06.	Sentinel 2 L1C		12.02.	Sentinel 2 L2A
	10.11.	Sentinel 2 L1C		31.08	Sentinel 2 L1C		8.04.	Sentinel 2 L2A
	20.12.	Sentinel 2 L1C		20.10.	Sentinel 2 L1C		13.05	Sentinel 2 L2A
2019	25.03.	Sentinel 2 L1C		14.11.	Sentinel 2 L1C		02.06.	Sentinel 2 L2A
	19.04.	Sentinel 2 L1C		19.12.	Sentinel 2 L1C	**2022**	22.07	Sentinel 2 L2A
	09.05.	Sentinel 2 L1C		18.01.	Sentinel 2 L1C		26.08.	Sentinel 2 L2A
	18.06.	Sentinel 2 L1C		12.02.	Sentinel 2 L1C		05.09.	Sentinel 2 L2A
	12.08.	Sentinel 2 L1C	**2021**	04.03.	Sentinel 2 L1C		20.10.	Sentinel 2 L2A
	16.09.	Sentinel 2 L1C		23.05.	Sentinel 2 L1C		14.11.	Sentinel 2 L2A
	16.10.	Sentinel 2 L1C		17.07.	Sentinel 2 L1C		29.12.	Sentinel 2 L2A
	20.12.	Sentinel 2 L1C		16.08.	Sentinel 2 L1C			

The multispectral satellites provide 13 spectra in the green (B3), red (B4) and near-infrared (B8) ranges with a high resolution of 10×10 m. For the studied territory with an area of 4.6 km^2, satellite images with a resolution of 5×5 m are used, on which primary and secondary data processing was done. Primary processing includes channel selection to create composite water index (NDWI) images. NDWI extracts water body by utilizing Green (G) and Near Infrared (NIR) bands defined in the formula below. Vegetation and soil in NDWI image are presented in the low reflectance values, whereas the water body is presented in high reflectance values (Sekertekin,2018).

$$NDWI = (G - NIR)/(G + NIR)$$

Secondary processing includes the generation of areas from the created composite images with the ArcMAP tools. The data on the monthly volumes of water stored in the reservoir of the “Belmeken” Dam for the studied period were provided by "Dams and Cascades". Information for the water use from the complex and significant dams have been taken from the monthly schedules which is available in open data sources (webpage of MOEW). Table 2 presents the monthly volumes of water stored in the "Belmeken" dam for the accepted calculation period (2018-2022).

Table 2. Monthly water volumes W [10^6 m^3]

Years	I	II	III	IV	V	VI	VII	VIII	IX	X	XI	XII
2018	120.1	103.1	85.0	109.5	131.0	140.0	138.4	127.0	108.7	108.7	66.2	37.7
2019	33.2	30.1	34.3	44.7	98.5	119.3	109.2	99.5	93.0	89.7	88.5	84.9
2020	81.1	81.5	89.0	96.0	127.2	137.7	132.5	127.5	116.2	110.2	105.9	96.7
2021	93.3	84.5	67.7	52.4	101.0	92.2	141.1	120.0	108.1	110.6	101.2	89.9
2022	80.6	69.7	52.7	54.4	115.6	129.6	133.0	121.0	114.7	104.3	97.4	93.9

To determine the relationship between the water surface area and the depth in the reservoir, a graphic dependence was made based on data for specific elevations by dam depth and the corresponding water surface areas obtained by the stored water volumes in the dam lake over the years. Figure 3 shows the graphical relationship between the elevation of the water level Z[m] and the water volume W [10^6.m^3] with the derived polynomial dependence of the second degree with coefficients of determination, R-squared = 0.999935.

$$(1)\ Z = -\ 0{,}00199.\ W^2 + 0{,}7272.W + 1857{,}073$$

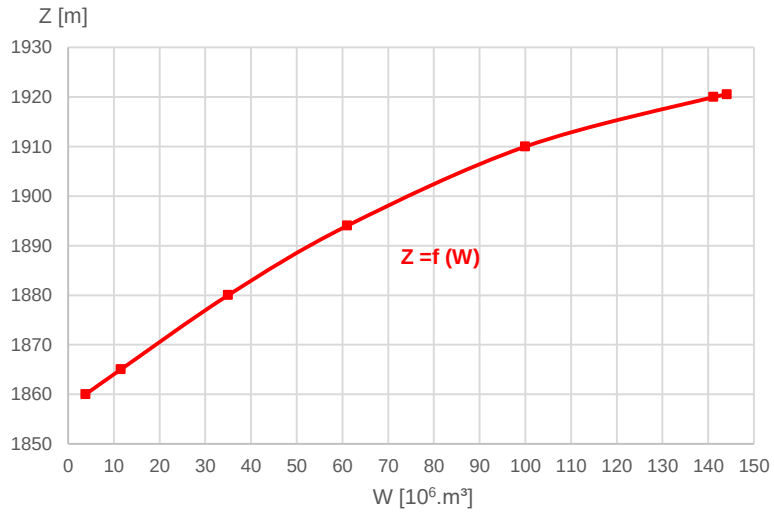

Figure 3. Dependence of water level elevation(Z) and water volume (W)

Figure 4 presents the measured ground data for water level elevation Z[m], water volume W [10^6.m^3] and water surface area A [km^2] in the reservoir of the "Belmeken" dam. Through the mathematical analysis between the water volume and the elevation of the water level W = f(Z) and the area of water and the elevation of the water level A = f(Z), polynomial dependences of the second degree with coefficients of determination, R-squared = 0.999976 (formula 2) and R-squared = 0.999958 (formula 3). The graphically constructed curves and derived polynomial dependences refer only to "Belmeken" dam and cannot be applied to other dams due to the difference in morphometry and natural factors.

$$(2)\ W = 0{,}023635.\ Z^2 - 87{,}107.\ Z + 80257$$

$$(3)\ A = 0{,}000425.\ Z^2 - 1{,}53823.\ Z + 1390{,}1628362$$

The approach to tracking changes in the water surface area of the Belmeken Dam inludes the following steps

(1) Generate the water surface area of the reservoir based on 2A and 1C Sentinel -2 images by creating composite images of NDWI for the period 2018-2022;

(2) Calculate the Water surface elevations (Z) of Belmeken dam from the open data on water volume in the reservoir and through the obtained polynomial dependence (formula 1) for the water volume for each month during the year;

(3) Based on the obtained water level elevations (Z) for each month during the year, the water areas in the water reservoir to be calculated from ground data by dependence (formula 3);

(4) Compare the water areas derived from ground-based data with water area data derived from satellite data (NDWI values)

(5) Contour the water surface of Belmeken Dam using ArcMap tools at NDWI values above 0.2.

Results and Discussion

The results of the survey are reflected in Figure 4 for selected days within the period 2018–2022, and for water areas by months in Table 3. The blanks in the table indicate that no available Sentinel-2 raster image with cloud cover below 40% was found. The obtained water area data of "Belmeken" Dam from the satellite images by NDWI is comparable to the ground water area data, which is confirmed by the coefficient of determination R^2 = 0,85. (Figure 5).

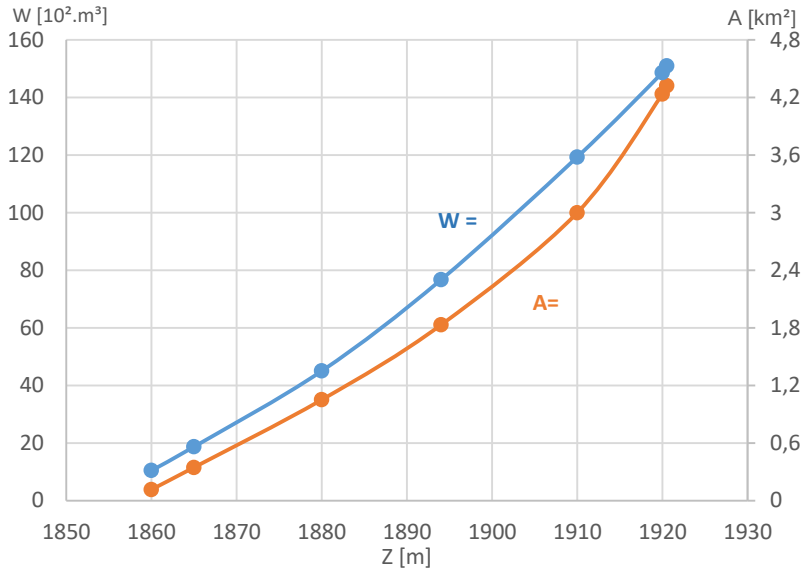

Figure 4. Graphical relationship between water level elevation (Z) – water volume (W) – water surface area (A)

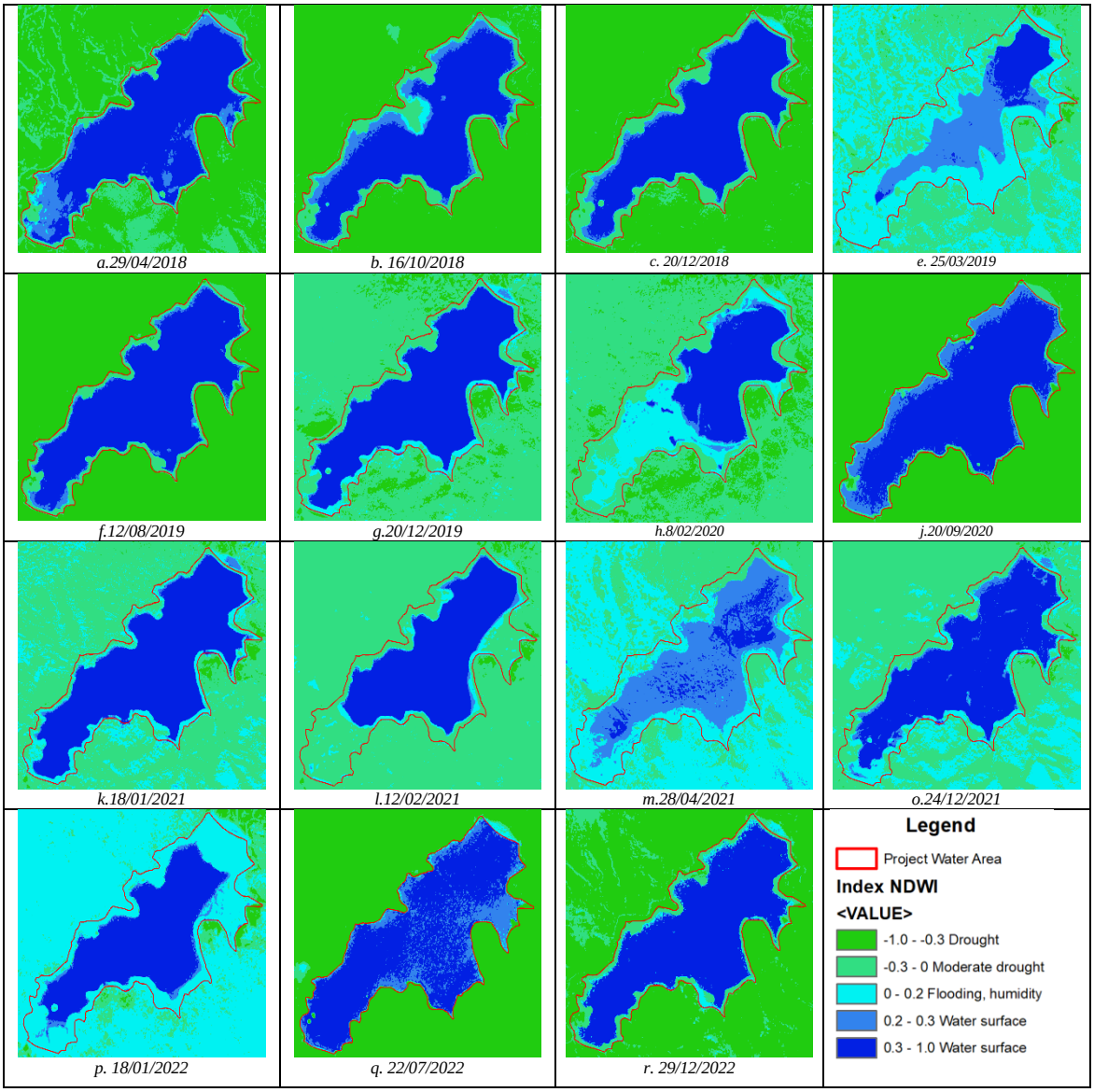

Figure 5. NDWI spatial distribution in Belmeken Dam reservoir for 2018-2022

Table 3. Water area (km^2) of "Belmeken" dam by months

Year	I	II	III	IV	V	VI	VII	VIII	IX	X	XI	XII
2018	4.01	-	-	3.83	-	4.18	-	4.17	3.97	3.55	3.20	1.28
2019	-	-	1.76	1.75	2.86	4.05	-	3.71	3.57	3.48	-	3.44
2020	2.92	1.70	3.1	3.67	3.75	4.2	4.1	-	4.03	3.86	3.70	3.65
2021	3.49	2.82	2.21	2.56	3.56	-	4.31	4.12	3.8	3.86	3.50	3.37
2022	2.70	1.95	-	2.14	3.38	4.15	4.27	4.01	3.86	3.57	3.49	3.55
Average	3.28	2.16	2.36	2.79	3.39	4.15	4.23	4.00	3.85	3.66	3.47	3.06

Analyzing the data by months we have detected a decrease in the water surface area calculated by NDWI in February and May (Figure 6). A possible reason for the difference found is the permanent snow cover during the winter months in the catchment area of the "Belmeken" dam and the icing of the water surface. For the spring months, there is a sudden change of days with cloudy to cloudless conditions, typical for areas with an altitude above 1900 m.

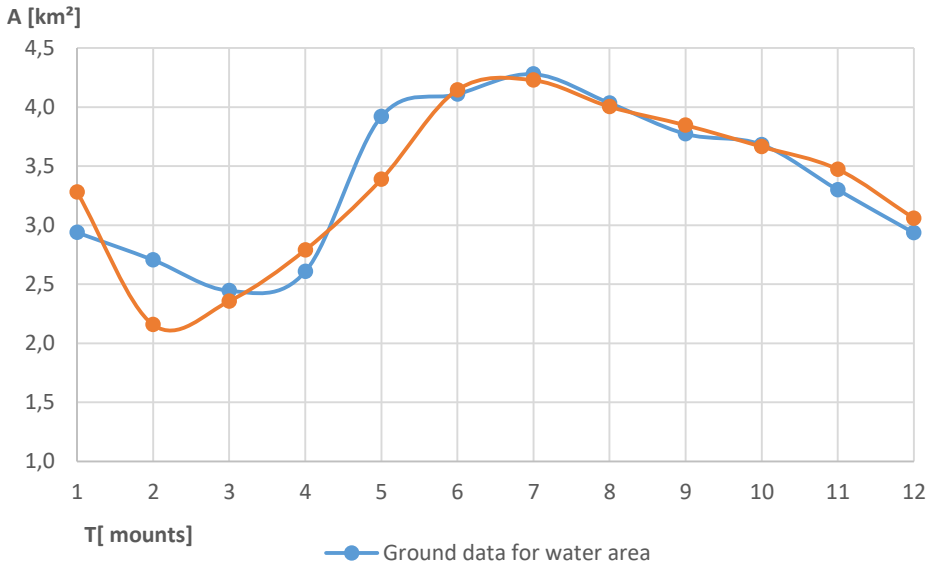

Figure 6. Water area satellite and ground data collation

Conclusion

The presented approach for the interpretation of satellite images data on water surface area of dams, lakes and wetlands verifies the objectivity of NDWI and expands the possibilities of analysis of water bodies for which there is no information from the reference hydrometric network. Tracking the fluctuations of water surface areas during the year through satellite-derived data by using NDWI is determined to be of great importance to survey the climate change influence in the hydrological regime. The application of remote sensing data for water surface area estimatation of water bodies can contribute to the process for determining the water volumes in dams and thus can be of support to the decision-makers. Integrating remotely-sensed data with ground data presents new methodological solutions for hydrological and engineering hydrological studies.

Scientific Ethics Declaration

The authors declare that the scientific ethical and legal responsibility of this article published in EPSTEM journal belongs to the authors.

Acknowledgements or Notes

* This article was presented as oral presentation at the International Conference on Basic Sciences, Engineering and Technology (www.icbaset.net) held in Alanya/Turkey on May 02-05, 2024.

References

Amalo, L. F., Ma'rufah, U., & Permatasari, P. A. (2018). Monitoring 2015 drought in West Java using normalized difference water index (NDWI). In *IOP Conference Series: Earth and Environmental Science*, *149(*1), 012007. IOP Publishing

Bhangale, U., More, S., Shaikh, T., Patil, S., & More, N. (2020). Analysis of surface water resources using Sentinel-2 imagery. *Procedia Computer Science*, *171*, 2645-2654.

East Aegean River Basin Directorate (2016-2021). *Plan for the management of East Aegean River basin directorate*,. Retrieved from https://earbd.bg/indexdetails.php?menu_id=609&sys_lang=bg

Gao, H., Birkett, C., & Lettenmaier, D. P. (2012). Global monitoring of large reservoir storage from satellite remote sensing. *Water Resources Research*, *48*(9), 7.

Lubenov, N. (2009). *Water power sector of Republic of Bulgaria*. https://www.cabidigitallibrary.org/doi/full/10.5555/20103025325

McFeeters, S. K. (1996). The use of the Normalized Difference Water Index (NDWI) in the delineation of open water features. *International Journal of Remote Sensing*, *17*(7), 1425-1432.

Ministry of Environment and Water. (n.d.). Retrieved from https://www.moew.government.bg/bg/vodi-povurhnostni-vodi-mesechni-grafici-za-polzvane-na-vodite-ot-kompleksnite-i-znachimi-yazoviri/

Ministry of Environment and Water. (n.d.).Retrieved from https://gwms.eea.government.bg/giswmr/

Nabatov, N. (2015). *The electric power industry of Bulgaria*. In T. TanNakRa (Ed.). ISBN : 978-954-378-081-5.

Rogers, A. S., & Kearney, M. S. (2004). Reducing signature variability in unmixing coastal marsh Thematic Mapper scenes using spectral indices. *International Journal of Remote Sensing*, *25*(12), 2317-2335.

Sawunyama, T. E. N. D. A. I., Senzanje, A., & Mhizha, A. (2006). Estimation of small reservoir storage capacities in Limpopo River Basin using geographical information systems (GIS) and remotely sensed surface areas: Case of Mzingwane catchment. *Physics and Chemistry of the Earth*, *31*(15-16), 935-943.

Sekertekin, A., Cicekli, S. Y., & Arslan, N. (2018). Index-based identification of surface water resources using Sentinel-2 satellite imagery. In *2018 2nd international symposium on multidisciplinary studies and innovative technologies (ISMSIT)* (pp. 1-5). IEEE.

Taloor, A. K. Manhas, D. S., & Girish, C. K. (2021). Retrieval of land surface temperature, normalized difference moisture index, normalized difference water index of the Ravi basin using Landsat data. *Applied Computing and Geosciences*, *9*, 100051.

Xu, H. Q. 2006. Modification of normalised difference water index (NDWI) to enhance open water features in remotely sensed imagery. *Int J Remote Sens.*, *27*, 3025–3033

Yigzaw, W., Li, H. Y., Demissie, Y., Hejazi, M. I., Leung, L. R., Voisin, N., & Payn, R. (2018). A new global storage-area-depth data set for Modeling reservoirs in land surface and earth system models. *Water Resources Research*, *54*(12), 10-372.

Zhang, J., Xu, K., Yang, Y., Qi, L., Hayashi, S., & Watanabe, M. (2006). Measuring water storage fluctuations in Lake Dongting, China, by Topex/Poseidon satellite altimetry. *Environmental Monitoring and Assessment*, *115* (1-3), 23-37.

Zhang, S., Gao, H., & Naz, B. S. (2014). Monitoring reservoir storage in South Asia from multisatellite remote sensing. *Water Resources Research, 50(*11), 8927-8943.

Author Information

Kameliya Radeva	**Silvia Kirilova**
Space Research and Technology Institute- Bulgarian Academy of Sciences, Sofia 1113, str. "Acad. Georgy Bonchev" bl. 1 Bulgaria,	University of Architecture, Civil Engineering and Geodesy, Hydraulics and Hydrology Department, Bulgaria, Sofia 1164, 1 Hristo Smirnenski Blvd. Bulgaria Contact e-mail: *spacedgclima@gmail.com*

To cite this article:

Radeva, K. & Kirilova, S. (2024). Remote sensing upon tracking changes in the water sufrace area of Belmeken dam *The Eurasia Proceedings of Science, Technology, Engineering & Mathematics (EPSTEM), 28,* 90-96.

The Eurasia Proceedings of Science, Technology, Engineering & Mathematics (EPSTEM)
ISSN: 2602-3199

The Eurasia Proceedings of Science, Technology, Engineering & Mathematics (EPSTEM), 2024

Volume 28, Pages 97-104

ICBASET 2024: International Conference on Basic Sciences, Engineering and Technology

Water Retaining Nylon Rolling Application in the Automotive Industry with Collaborative Robot (COBOT)

Emrah Aydin
Trakya University

Huseyin Bulat
TOFAS Automobile Factory

Aydin Gullu
Trakya University

Abstract: This study focuses on the prototype design and preliminary experiments regarding the applicability of robots capable of collaborating with humans in the automotive sector. In standard factories, production is mostly carried out by humans. The use of robots is more suitable for tasks that require a certain standard. Performing operations with cooperative robots working alongside humans reduces costs and increases efficiency. A Cost/Benefit analysis was conducted in this study to assess the feasibility of using robots. The application will be carried out by a cobot. The surface beneath the upholstery on the side doors in the automobile body assembly line is covered with nylon to prevent liquid permeability. Currently, this process is performed by two operators for four doors. To validate the application in cases of quality issues, marking is done along the line with acetate and a pen during the rolling process. In the study, positioning for the doors on the conveyor line, moving at a speed of 3,2 m/min, was achieved using cameras mounted on two cobots equipped with grippers on the right and left sides. By applying a compressive force of 50N with the pressure roller at the gripper end, the adhesive on the nylon is ensured to bond with the sheet metal. The stability of the system was observed when comparing animation data with the application created in the experimental environment. As a result of all these processes, operational precision increased, and continuous robot-door synchronization was achieved. According to cost analyses, it is projected that the system will amortize itself within approximately 4 years.

Keywords: Collaborative robot technology, Human-robot interaction, Smart factories

Introduction

Mass production is a manufacturing process that involves large-scale production of standardized products. It is characterized by the efficient production of high volumes of identical or similar goods, often using assembly line techniques to achieve economies of scale (Kumar et al., 2007). Mass production allows goods to be produced quickly and cost-effectively, leading to lower prices for consumers due to reduced production costs (Kumar et al., 2007). The concept of mass production has been a cornerstone of industrial manufacturing for decades and has revolutionized the way goods are produced and consumed. By optimizing production processes and standardizing components, mass production enabled the efficient production of goods on a large scale, contributing to increased productivity and economic growth (Kumar et al., 2007). The evolution of mass customization as a complementary strategy to mass production has further increased the ability of companies to meet consumer demands for personalized products within the framework of mass production (Kaplan & Haenlein, 2006). Mass production offers several advantages that have contributed to its widespread adoption in manufacturing industries. One of the key advantages is the ability to achieve economies of scale, leading to

lower production costs per unit as the volume of output increases (Bunster & Bustamante, 2019). By producing large quantities of goods, manufacturers can spread fixed costs over a larger number of units, leading to cost savings that can be passed on to consumers through lower prices (Bunster & Bustamante, 2019). Another advantage of mass production is increased efficiency and productivity. Standardized production processes and assembly line techniques allow orderly and repetitive manufacturing of goods, reducing the time and labor required to produce each unit (Chang et al., 2022). This efficiency not only reduces production costs but also allows manufacturers to meet high demand and fulfill orders quickly (Chang et al., 2022). Additionally, mass production generally results in consistent product quality. By using standardized ingredients and processes, manufacturers can ensure that each product meets the same specifications and quality standards (Qi et al., 2020). This consistency is necessary to build consumer trust and loyalty, as customers can rely on the reliability and uniformity of mass-produced goods (Qi et al., 2020).

Smart factories, an important member of Industry 4.0, are highly digitalized and connected production facilities based on smart production techniques (Sadiku et al., 2021). These enhanced production environments leverage technologies such as big data, cyber-physical systems, and the Internet of Things to increase efficiency, productivity, and replication in production rates (Tomiyama et al., 2019; Wang, Wan, Zhang, et al., 2016). Smart factories are versatile; Increased data throughput leading to their performance through data analytics, agile response to failures and anomalies, as well as increased variability and flexible reconfigurability for smaller production volumes (Tomiyama et al., 2019). Smart factories offer increased process efficiency, reduced operating costs, improved product quality, enhanced safety and sustainability, and numerous benefits (Nwakanma et al., 2021). By integrating technologies such as artificial intelligence, robotics and cloud computing, smart factories can automate their work, optimize production workflows and enable real-time storage and control of parts of production (Heymann et al., 2018). These advances not only support improved support but also broaden the way for advanced product development and customization (Wang, Wan, Li, & Zhang, 2016). Moreover, the deployment of industrial wireless networks (IWNs) serves as a vital foundation for centralizing the architecture of Industry 4.0 and smart factories, ensuring continuous communication and coordination between various growths in the manufacturing economy (Volpi et al., 2023). The visual of Industry 4.0 components is shown in figure 1. Smart factories are expected to play a pivotal role in solving complex problems in manufacturing industries, achieving breakthroughs in factory operations, and promoting sustainable business registration (Yang et al., 2018).

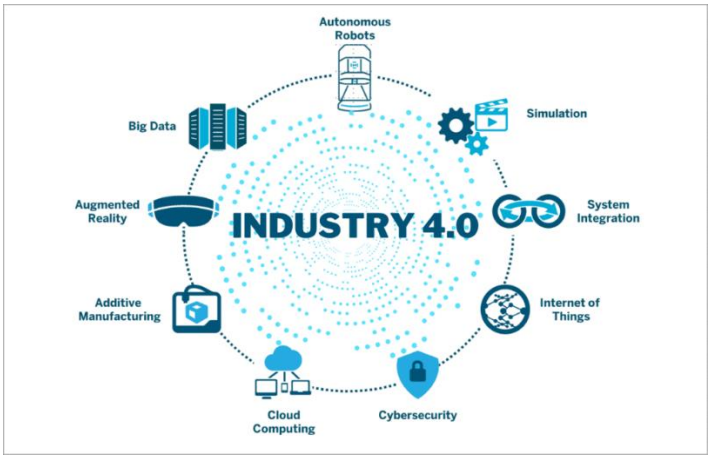

Figure 1. Industry 4.0 components

Collaborative robots, commonly known as cobots, are increasing in use in industrial environments, especially in smart manufacturing environments. These robots are specifically designed to work alongside humans, encouraging collaboration and shared workforce dynamics (Koh et al., 2019; Zakeri et al., 2023). The global adoption of collaborative robots is increasing, especially in smart factories, where they have largely replaced traditional industrial robots due to their improved performance and intelligent design (Indri et al., 2019; Wang et al., 2019). Collaborative robots provide innovative solutions for complex hybrid assembly tasks, especially in smart manufacturing contexts, by providing flexibility to production cells through close collaboration with humans (Matheson et al., 2019). These robots are effective in facilitating human-robot interaction, thereby increasing learning and comfort in collaborative spaces (Matheson et al., 2019). In addition, collaborative robots play an important role in restructuring production lines and ensuring flexibility and autonomy through their integration into the production ecosystem (Polenghi et al., 2023). Research on collaboration between humans and cobots in manufacturing applications has focused on improving productivity, safety, and efficiency in

collaborative environments (Chromjakova et al., 2021). The cobot human working structure is shown in figure 2 (Publiteconline, 2024).

Figure 2. The Cobot human working

The automotive industry has been actively exploring and implementing collaborative robots (cobots) on assembly lines to enhance manufacturing processes. Studies have shown that the insertion of collaborative robots in automotive production lines can have a significant impact on production efficiency and competitiveness (Karabegović et al., 2021; Lima et al., 2019; Vido et al., 2020). These robots play a crucial role in smart automation within the automotive manufacturing sector, improving element manufacturing processes and car assembly operations (Karabegović et al., 2021). The use of cobots in the automotive industry aligns with the principles of Industry 4.0, facilitating smart manufacturing practices and advancing human-robot collaboration in shared workspaces (Lima et al., 2019). Manufacturers in the automotive sector are leveraging collaborative robots to optimize production workflows, increase flexibility, and drive innovation in manufacturing processes, ultimately enhancing the overall efficiency and competitiveness of automotive production lines.

In this study, a preliminary study was carried out to use robots to cover the surface under the flooring of the side doors in the automotive industry, in the automobile body assembly line, with nylon to prevent liquid permeability. The process, which is normally done by human hands, is planned to be performed by a collaborative robot. For this purpose, manual processing processes will be mentioned first in the second section. Then, the operations to be performed with the robot will be explained. The data obtained in these processes will be given in the results section. Finally, the conclusion will be given.

Method

The method in the study consists of two parts. The manual assembly process and the operations to be performed with the cobot will be explained.

Manual Assembly Process

Various processes are applied to the interior parts of the doors of passenger vehicles produced in the TOFAŞ Factory during assembly. One of these is the water retaining nylon rolling process that is adhered to the inner surface of the doors. This process is extremely important to minimize liquid and dust contact with the external environment.

The door line consists of a 60-meter long double-sided conveyor line moving at a speed of 3.2 m/min. Water retaining nylon rolling operation is carried out on 6 meters of it. Four personnel facing each other complete the process in two steps. In the first step, the first personnel attaches the nylon covering to the door by passing it over the cables. In the second step, the second personnel, using his rolu pliers, applies 50 N of pressure and bursts the hotmelt adhesive part on the water retaining nylon, allowing it to join with the door. After assembly, each door is rolled twice to ensure that the adhesive adheres well. The same operations are applied to the left and right for four doors in total. After the gluing process is completed, for quality control, marking is made

along the rolled line with an acetate pen during the rolling process in order to verify the application. The rolling process and pen are shown in Figure 3.

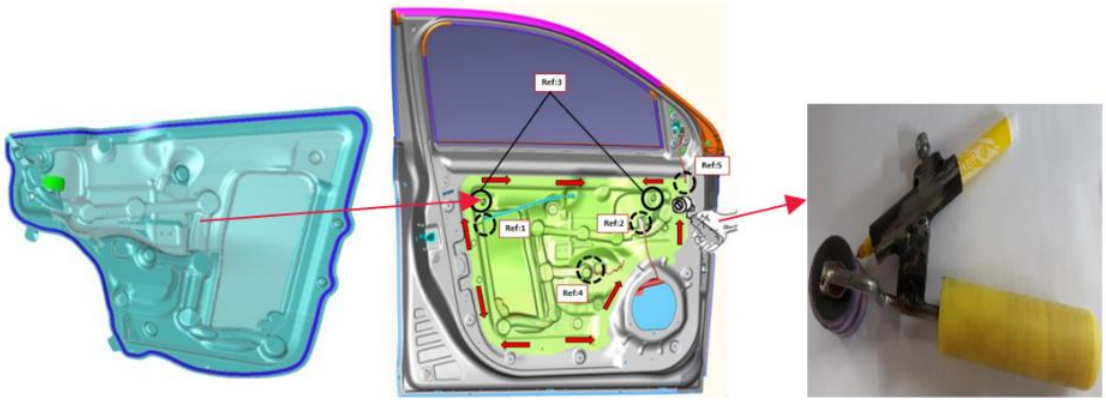

Figure 3. Rolling line and pliers

Table 1. Assembly chart workflow and times for front doors

No	*Process*	*Min/Vehicle*
1	Take the right front door water trap nylon (a) from the line edge. Remove the protective paper from the nylon top.	0,146
2	Remove the mirror cable from the hole in the upper corner. Ref:5	0,025
3	Remove the inner opening handle wire from the hole on the nylon. Ref:1	0,035
4	Remove the speaker socket from the hole on the nylon. Ref:2	0,035
5	Adhere the upper part of the nylon to the door, taking the dents on the nylon as a reference. Ref:3	0,095
6	Remove the interior opening button installation socket from the hole on the nylon. Ref:4	0,035
7	Remove the side and bottom protective papers of the water retaining nylon and adhere the nylon to the body by pressing it by hand.	0,187
8	Take the device from the side of the line. With the help of the apparatus, complete the rolling of the nylon, starting from the bottom point of the adhesive shade.	0,287
	Total	*0,845*

Table 2. Assembly chart workflow and times for rear doors

No	*Process*	*Min/Vehicle*
1	Take the right front door water trap nylon (a) from the line edge. Remove the protective paper from the nylon top.	0,146
2	Remove the inner opening handle wire from the hole on the nylon. Ref:1	0,035
3	Position the reference points on the nylon and the door reference points together.	0,095
4	Remove the speaker socket and the internal release button socket from the hole on the nylon. Ref:3	0,070
5	Remove the side and bottom protective papers of the water retaining nylon and place them in place by holding the ears next to them.	0,187
6	Take the device from the side of the line. With the help of the apparatus, complete the rolling of the nylon, starting from the bottom point of the adhesive shade.	0,306
	Total	*0,839*

The assembly table workflow and times (min/vehicle) for the front doors are shown in Table 1 and for the rear doors in Table 2. In this table, the parts that the collaborative robot is planned to do are Step 8 at the front door and Step 6 at the back door. It seems that rolling takes the longest time in the operation. The time spent for a

vehicle is front door: 0.845 min/vehicle - back door: 0.839 min/vehicle. Therefore, the applied process remains above the standard time in terms of process cycle time on the moving belt conveyor. Four packages of acetate pen, which is considered as an auxiliary material for this operation, are used per shift. The manual assembly process is shown in Figure 4.

Figure 4. The manual rolling process

Assembly Process with Cobot

The operations performed by two personnel in the current operation are planned to be performed by two collaborative robots. Robots will be positioned opposite each other on a fixed aerial line. The Universal UR5e Cobot selected for the demo application has 6 axes and has a reach radius of 850 mm and a carrying capacity of 5 kg. The gripper at the end of the robot will be such that the roller pliers can be fixed. Instant positioning, analysis and operation monitoring will be done with the data transferred to the software via the camera and sensors on it.

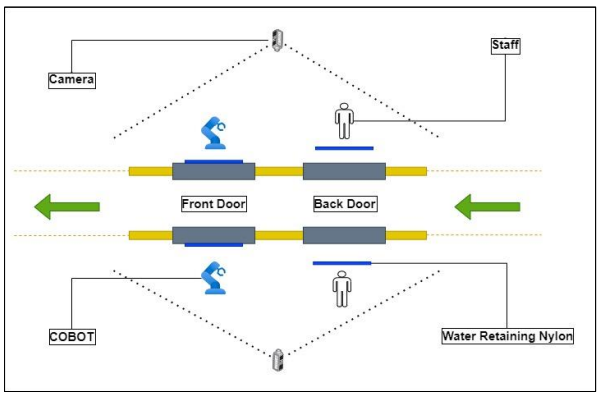

Figure 5. Diagram of the assembly process with cobot

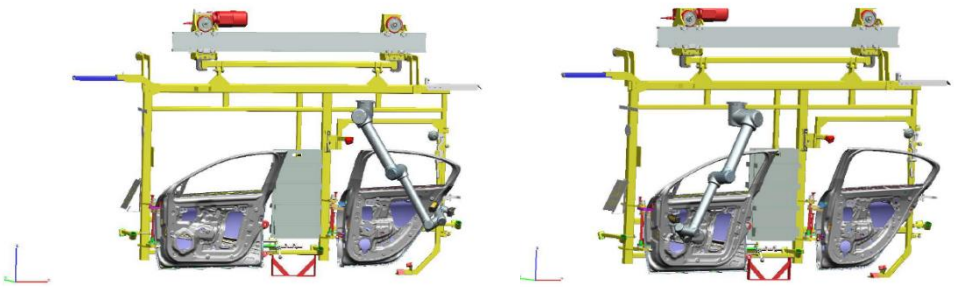

Figure 6. COBOTs on conveyor line

There are two separate conveyor lines for the right and left doors of the vehicle. The doors move on this line on a single carrier, front and back. Collaborative robots mounted on the overhead line will be able to work on two doors simultaneously. The working radius of the robots is programmed synchronously with the belt. A Keyence Vision series camera for each cobot detects the position at time t, and the speed information from the conveyor

encoder goes to the robot. The cobot operating diagram is shown in Figure 5. This data is combined with the programmed g code (x, y, z) and the operation is performed. The 3D drawings below show the working scenario of the robots on the real field model. The system will work synchronously between Human and Robot in the same area at the same time. The design of COBOTs on the Conveyor Line is shown in Figure 6.

During the demo study, a single door and a single robot were used. Figure 7 shows the demo application. The system is modeled in both real and digital environments. By determining the distance and start-end points, a movement simulation and path were created through the software. Necessary load and gripper settings have been made. Sensitivity control was made by manually moving the line to which the door is connected. As a result of all these processes, the water retaining nylon adheres to the hot melt adhesive on the door without any problems. The overlap of application and simulation data and the stability of possible scenarios have been observed in many aspects.

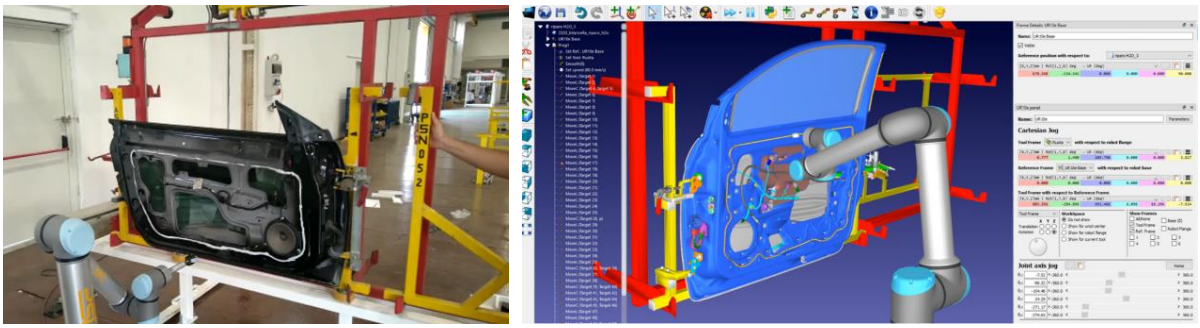

Figure 7. Demo application

Results and Discussion

According to the results obtained as a result of evaluating the applicability of collaborative robots in assembly production lines and conducting demo studies, the following advantages can be obtained;

- Increased operational precision
- Shortening the operation time
- Elimination of quality loss
- Ergonomics improvement
- Demonstration of Quality Increase
- Process stability
- Reducing work accidents
- Creating alternatives

Table 3. Systemic advantages

Systemic Advantages	**Earnings (Euro)**
Standard time gain	€ 50.550
Auxiliary material loss elimination	€ 11.124
Non-additive loss of activity elimination	€ 13.782
Ergonomics Gain	€ 5.524
Total Earnings	€ **81.070**

Table 4. Total Costs

	Commission
Cobot	k€ 35
Camera	k€ 30
Gripper-3P	k€ 15
Engineering - Automation.	k€ 30
Superstructure & line arrangement	k€ 10
Quality certificates	k€ 14
Workmanship	20%
Total Costs	***k€ 161***

The studies carried out and the gains from the systemic advantages to be achieved between manual operation and cobot operation are shown in Table 3. It is planned to earn a total profit of 81000 Euros. The costs incurred as a result of rolling with a cobot are given in Table 4. Commissioning includes installation. In this data, the most important value for operation optimization and applicability will be Benefit/Cost. In a system with a commissioning cost of 81/161, B/C = 0.5.

Conclusion

Standardization is important for reasons such as increasing quality in mass production and ensuring the standardization of works. In production, working with human power is being replaced by machines. It is difficult to use standard machines to perform some production processes. Humanoid robots are used for this. Robot arms similar to the human arm structure are programmed and used in production. Robot arms that work together with humans have been developed with developing sensor, camera and software technologies. The re-planning of a production system with a collaborative robot (Cobot) was carried out within the scope of this study. Waterproof nylon rolling in the automotive industry is currently done by humans at the TOFAŞ factory. A preliminary study and the data obtained are presented to show how much this process can be improved by supporting COBOT. Considering the investment cost and the profit to be obtained, the system will amortize itself within 2 years. An increase in quality and customer satisfaction will be achieved in the annual production of approximately 240000 thousand vehicles.

Scientific Ethics Declaration

The authors declare that the scientific ethical and legal responsibility of this article published in EPSTEM journal belongs to the authors.

Acknowledgements or Notes

* This article was presented as an oral presentation at the International Conference on Basic Sciences, Engineering and Technology (www.icbaset.net) held in Alanya/Turkey on May 02-05, 2024.

* This study was developed to improve the production process at TOFAŞ Bursa automotive factory. The aim of the study is to determine the most suitable place to invest. Preliminary study data and demo application studies are presented.

References

Bunster, V., & Bustamante, W. (2019). Structuring a residential satisfaction model for predictive personalization in mass social housing. *Sustainability*, *11*(14), 3943.

Chang, Y.-H., Chen, S.-C., Ting, Y.-H., Feng, C.-T., & Hsu, C.-C. (2022). The investigation of novel dynamic packing technology for injection molded part quality control and its production stability by using real-time PVT control method. *Polymers*, *14*(13), 2720.

Chromjakova, F., Trentesaux, D., & Kwarteng, M. A. (2021). Human and cobot cooperation ethics: The process management concept of the production workplace. *Journal of Competitiveness*, *13*(3), 21-38.

Heymann, S., Stojanovci, L., Watson, K., Nam, S., Song, B., Gschossmann, H., Schriegel, S., & Jasperneite, J. (2018). Cloud-based plug and work architecture of the IIC testbed smart factory Web. 2018 *IEEE 23rd International Conference on Emerging Technologies and Factory Automation (ETFA)*,

Indri, M., Lachello, L., Lazzero, I., Sibona, F., & Trapani, S. (2019). Smart sensors applications for a new paradigm of a production line. *Sensors*, *19*(3), 650.

Kaplan, A. M., & Haenlein, M. (2006). Toward a parsimonious definition of traditional and electronic mass customization. *Journal of Product Innovation Management*, *23*(2), 168-182.

Karabegović, I., Karabegović, E., Mahmić, M., & Husak, E. (2021). The application of Industry 4.0 in production processes of the automotive industry. *J. Mobil. Vehicle, University of Kragujevac, Faculty of Engineering, Kragujevac, Serbia*, *47*(2), 35-44.

Koh, L., Orzes, G., & Jia, F. J. (2019). The fourth industrial revolution (Industry 4.0): technologies disruption on operations and supply chain management. *International Journal of Operations & Production Management*, *39*(6/7/8), 817-828.

Kumar, A., Gattoufi, S., & Reisman, A. (2007). Mass customization research: trends, directions, diffusion intensity, and taxonomic frameworks. *International Journal of Flexible Manufacturing Systems*, *19*, 637-665.

Lima, F., De Carvalho, C. N., Acardi, M. B., Dos Santos, E. G., De Miranda, G. B., Maia, R. F., & Massote, A. A. (2019). Digital manufacturing tools in the simulation of collaborative robots: Towards industry 4.0. *Brazilian Journal of Operations & Production Management*, *16*(2), 261-280.

Matheson, E., Minto, R., Zampieri, E. G., Faccio, M., & Rosati, G. (2019). Human–robot collaboration in manufacturing applications: A review. *Robotics*, *8*(4), 100.

Nwakanma, C. I., Islam, F. B., Maharani, M. P., Lee, J.-M., & Kim, D.-S. (2021). Detection and classification of human activity for emergency response in smart factory shop floor. *Applied Sciences*, *11*(8), 3662.

Polenghi, A., Cattaneo, L., & Macchi, M. (2023). A framework for fault detection and diagnostics of articulated collaborative robots based on hybrid series modelling of Artificial Intelligence algorithms. *Journal of Intelligent Manufacturing*, 1-19.

Publiteconline. (2024). *Cobot: per un controllo qualità accurato*. Retrieved from https://www.publiteconline.it/controlloemisura/2020/05/20/cobot-per-un-controllo-qualita-accurato/

Qi, Y., Mao, Z., Zhang, M., & Guo, H. (2020). Manufacturing practices and servitization: The role of mass customization and product innovation capabilities. *International Journal of Production Economics*, *228*, 107747.

Sadiku, M., Ashaolu, T., Ajayi-Majebi, A., & Musa, S. (2021). Smart Factory: A Primer. *International Journal of Scientific Advances*, *2*(1).

Tomiyama, T., Lutters, E., Stark, R., & Abramovici, M. (2019). Development capabilities for smart products. *CIRP Annals*, *68*(2), 727-750.

Vido, M., Scur, G., Massote, A. A., & Lima, F. (2020). The impact of the collaborative robot on competitive priorities: case study of an automotive supplier. *Gestão & Produção*, *27*, e5358.

Volpi, A., Tebaldi, L., Matrella, G., Montanari, R., & Bottani, E. (2023). Low-cost uwb based real-time locating system: development, lab test, industrial implementation and economic assessment. *Sensors*, *23*(3), 1124.

Wang, S., Wan, J., Li, D., & Zhang, C. (2016). Implementing smart factory of industrie 4.0: an outlook. *International Journal of Distributed Sensor Networks*, *12*(1), 3159805.

Wang, S., Wan, J., Zhang, D., Li, D., & Zhang, C. (2016). Towards smart factory for industry 4.0: a self-organized multi-agent system with big data based feedback and coordination. *Computer Networks*, *101*, 158-168.

Wang, W., Chen, Y., Li, R., & Jia, Y. (2019). Learning and comfort in human–robot interaction: A review. *Applied Sciences*, *9*(23), 5152.

Yang, H.-L., Chang, T.-W., & Choi, Y. (2018). Exploring the research trend of smart factory with topic modeling. *Sustainability*, *10*(8), 2779.

Zakeri, Z., Arif, A., Omurtag, A., Breedon, P., & Khalid, A. (2023). Multimodal assessment of cognitive workload using neural, subjective and behavioural measures in smart factory settings. *Sensors*, *23*(21), 8926.

Author Information

Emrah Aydin
Trakya University, İpsala Vocational School, Mechatronics Program, Edirne, Türkiye
Contact e-mail: *emrahaydin@trakya.edu.tr*

Husayin Bulat
TOFAŞ Automobile Factory, Bursa Türkiye

Aydin Gullu
Trakya University, İpsala Vocational School, Mechatronics Program, Edirne, Türkiye

To cite this article:

Aydin, E., Bolat, H. & Gullu, A. (2024). Water retaining nylon rolling application in the automotive industry with collaborative robot (COBOT). *The Eurasia Proceedings of Science, Technology, Engineering & Mathematics (EPSTEM), 28,* 97-104.

The Eurasia Proceedings of Science, Technology, Engineering & Mathematics (EPSTEM)
ISSN: 2602-3199

The Eurasia Proceedings of Science, Technology, Engineering & Mathematics (EPSTEM), 2024

Volume 28, Pages 105-112

ICBASET 2024: International Conference on Basic Sciences, Engineering and Technology

Theoretical Investigation of 3,4-Dihydropyrimidin-2(*1H*)-Ones Derivatives and in-Silico Biological Analysis

Noura Kichou
Mouloud Mammeri University of Tizi-Ouzou (UMMTO)

Anissa Amar
Mouloud Mammeri University of Tizi-Ouzou (UMMTO)

Nabila Guechtouli
University of Boumerdes

Manel Taferguennit
University of Sciences and Technology Houari Boumediene

.

Abstract: 3,4-Dihydropyrimidin-2(1*H*)-ones (DHPMs) are heterocyclic compounds with a pyrimidine moiety in the ring nucleus which, in recent decades, have aroused interest in medicinal chemistry due to their versatile biological activity. DHPMs possess a broad range of pharmacological activities and are widely used in pharmaceutical applications. The variety of pharmacological aspects associated with DHPM derivatives includes being potential anticancer, anti-inflammatory, antioxidant and antimicrobial agents as well as having antimalarial and antitubercular effects. The 3,4-dihydropyrimidin-2 (1H) -ones derivatives were synthesized by the Bigineli method, which consists of an easy reaction that is widely used in organic synthesis, which occurs in a single step to obtain multifunctional heterocycles. The geometry of all the products are optimized using density functional theory method at the B3LYP/6-311G(d,p) level of theory using gaussian09 suit of programs. Quantum chemical parameters have been determined and examined. Molecular electrostatic surface potential (MESP) plot analysis has simulated in order to determine the predominantly reactive sites of nucleophilic or electrophilic attacks. On the other hand, global reactivity descriptors are calculated in the framework of conceptual DFT, to shed light to the more reactive molecule. The in-silico biological properties of compounds have been calculated and discussed.

Keywords: 3,4-dihydropyrimidin-2(*1H*)-ones, DFT, ADMET properties, Drug likeness properties.

Introduction

3,4-dihydropyrimidine-2(1H)-ones have attracted considerable interest due to a wide range of biological activities, including antitumor (Matias et al., 2016), antioxidant (Stefani et al., 2006), antibacterial (Ashok et al., 2007), antifungal (Singh et al., 2008), anti-inflammatory (Bahekar & Shinde, 2004) and anti-hypertensive properties by acting as calcium channel blockers (Atwal et al., 1991). 3,4-Dihydropyrimidin-2(1*H*)-ones (DHPMs) are heterocyclic compounds with a pyrimidine moiety in the ring nucleus which, in recent decades, have aroused interest in medicinal chemistry due to their versatile biological activity. DHPMs possess a broad range of pharmacological activities and are widely used in pharmaceutical applications.In view of the biological significance of 3,4-dihydropyrimidin-2(1H)-ones, we tended in this study to pre-evaluate the ADMET properties, in the regard of the phsyicochemical properties and pharmacokinetics properties of each one of the investigated derivative.

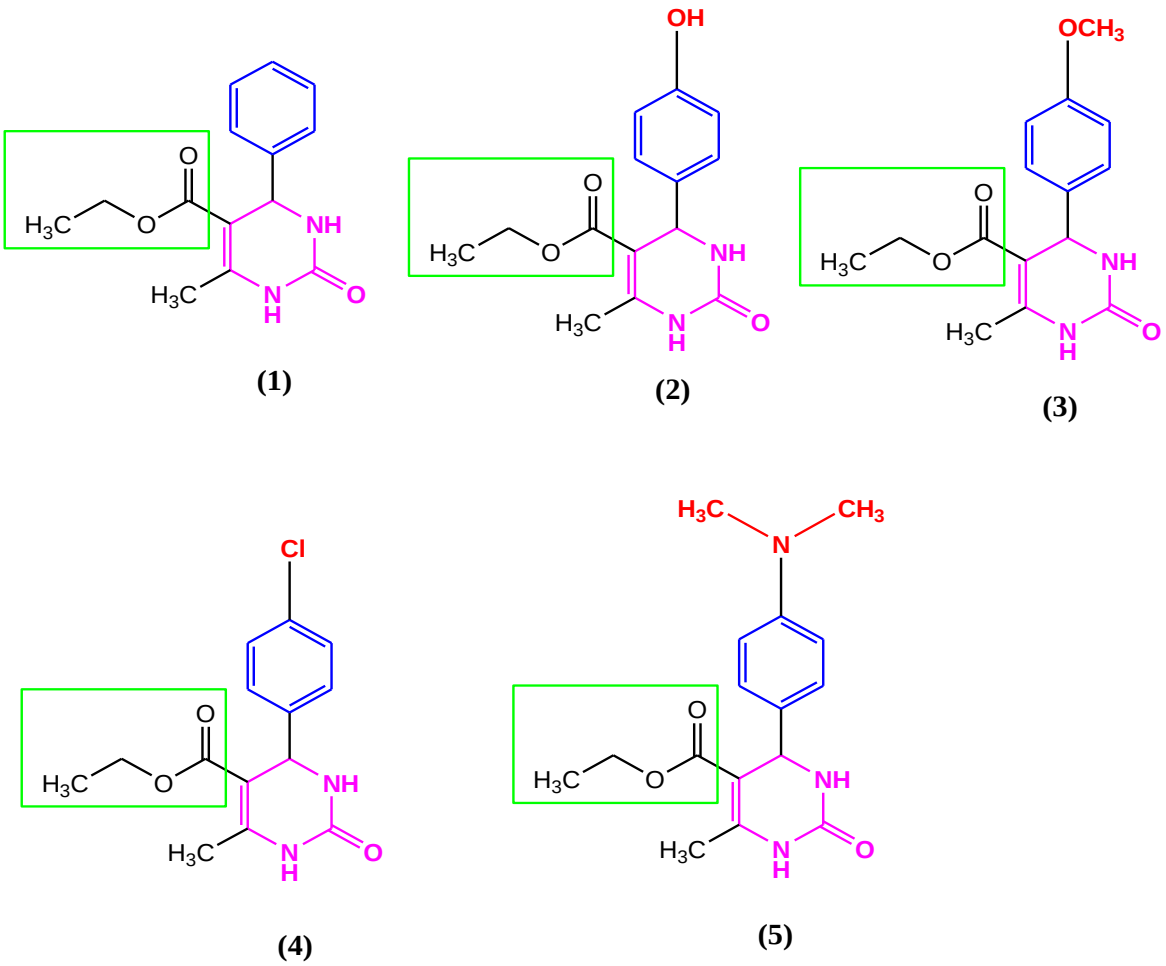

Figure 1. Strucrures under study.

Method

Computational Details

All the calculations were carried out using Gaussian 09 (Frisch, 2009) software package. The molecular geometry of the studied compounds were optimized using the density functional theory, within B3LYP (Becke, 1994) functional and the standard 6–31+G* basis set. Next, vibrational frequency are calculated on the obtained optimized geometries, to verify that no imaginary frequencies are present. GaussView (Hratchian, 2009) was used to visualize the optimized structure and to simulate the molecular electrostatic potential is surfaces.

ADMET Prediction

Phsyicochemical properties and Pharmacokinetics Properies such as Absorption, Distribution, Metabolism, Excretion and Toxicity of the molecular structure of 3,4-dihydropyrimidine-2(1H)-ones were studied via admetSAR (Yang et al., 2019) .

Results and Discussion

Optimized Geometries

The B3LYP/6-31G* optimized geometries of the 1-5 compounds are displayed in figure 2.

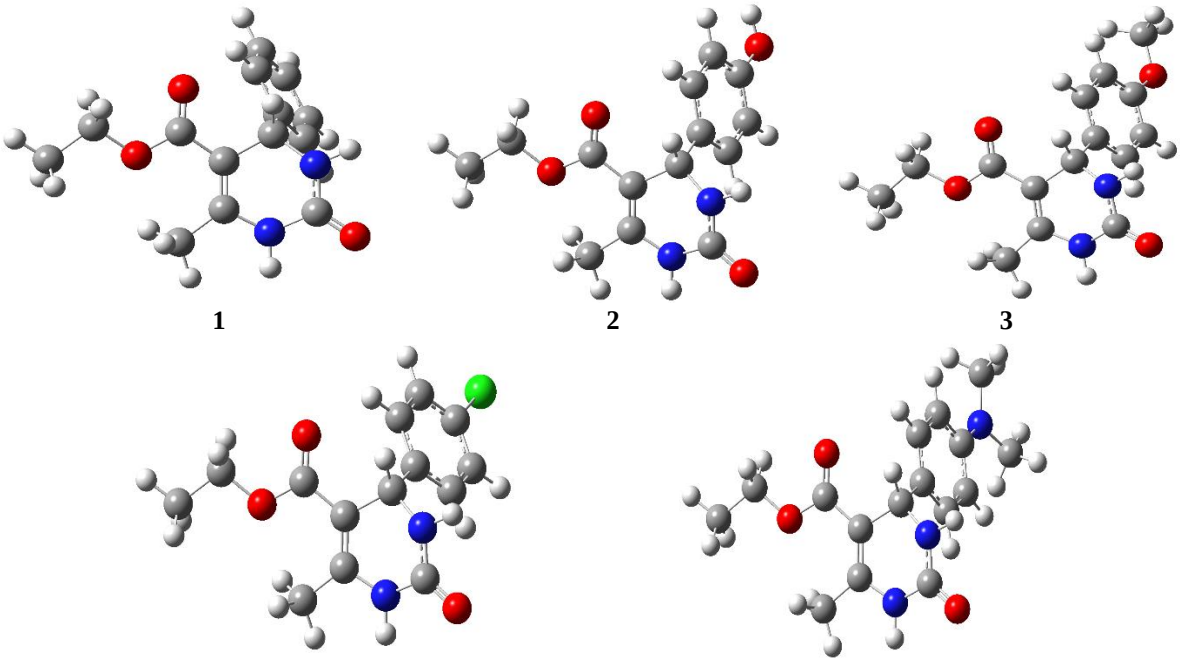

1 **2** **3**

4 **5**

Figure 2. B3LYP/6-31G* optimized structure.

Molecular Electrostatic Potential Isosurfaces:

In order to check the regioselectivity of the studied compounds, simulated molecular electrostatic potential isosurfaces of the considered molecules are given in figure 2. The MEP is a graphical representation of the electrostatic potential as mapped on the surface of the electron density. The electrostatic potential indicates the progressive degradation of colors according to the scale: red < yellow < blue. According to the obtained results, the areas with the most positive electrostatic potential, is located around the hydrogen atoms of the pyrimidone, for all the studied compounds, representing the active sites for an nucleophilic attack. The red mapping surfaces reveal the predominantly negative nucleophilic zones, which is located mainly on the oxygen of the pyrimidone.

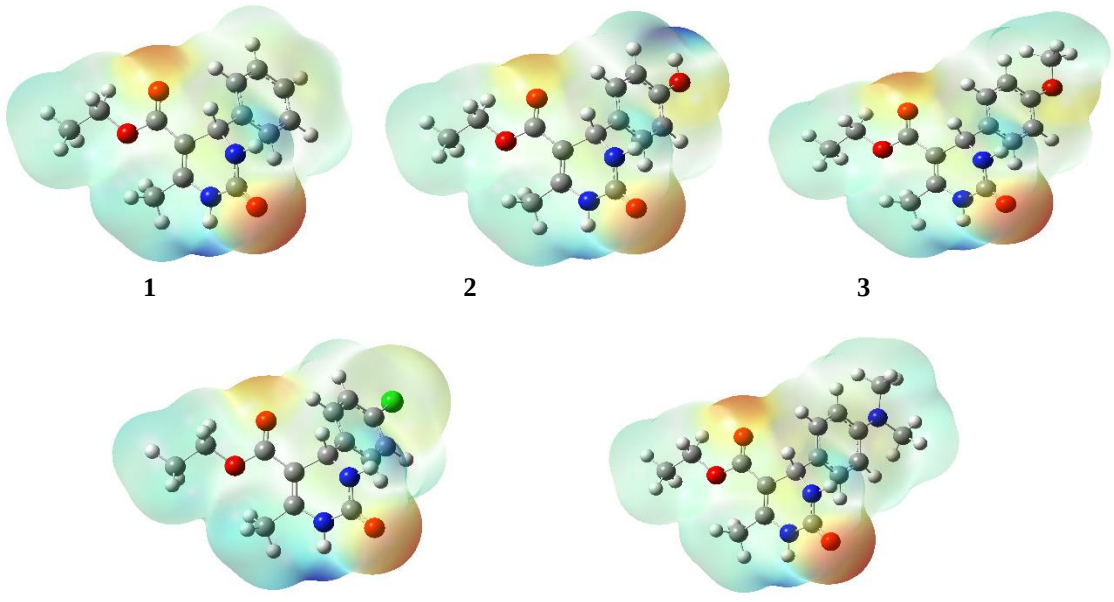

1 **2** **3**

4 **5**

Figure 4. Molecular electrostatic potential isosurfaces of the studied compounds.The most negative potential corresponds to the areas coloured in bright red, while the regions with the most positive potential are indicated in blue.

HOMO-LUMO Energy

At the molecular level, the reactivity of a molecule is dominated by the HOMO and LUMO orbitals. A high HOMO-LUMO energy gap indicates that the molecular structure has lower chemical reactivity and high kinetic stability. On the contrary, lower HOMO-LUMO energy gap is a sign of higher chemical reactivity. The obtained HOMO-LUMO energy gap diagram is given in figure 3.

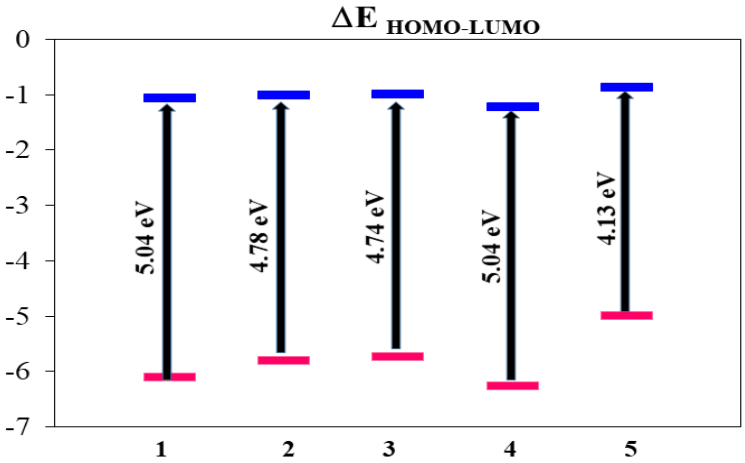

Figure 3. B3LYP/6-31G* calculated HOMO-LUMO energy gap.

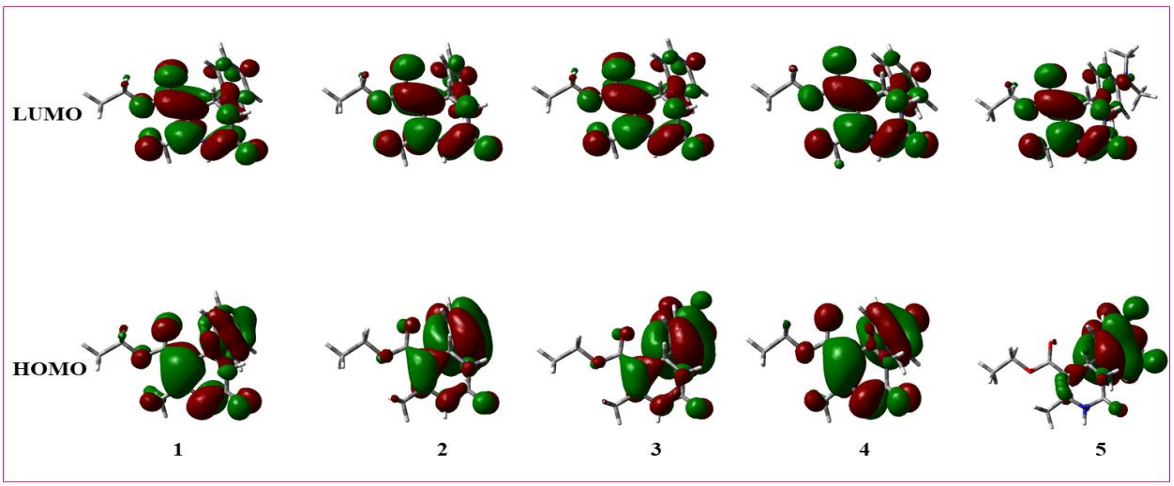

Figure 4. Frontiers molecular orbitals for the calculated molecules.

According to the calculated HOMO-LUMO energy gap of the studied molecules, it can be seen that the 5 compound have the less HOMO-LUMO energy gap (4.13 eV), it is the more reactive and the less stable due to the easy electron transfer from HOMO to LUMO. On the contrary, 1 and 4 present the higher H-L energy gap (5.04 eV), they are the less susceptible to electron transfer from HOMO to LUMO and thus less reactive and the more stable among the studied compounds.

Global Reactivity Descriptors

Global reactivity descriptors are crusial for describing the chemical reactivity of molecules. In this work we calculated chemical potential (μ), hardness (η), softness (σ) and electrophilic index (ω), (Manjeet, 2024; Khelifi and all, 2023) for the all the considered compounds at the B3LYP/6-31G* level (Table). Ionization potential (I) and electron affinity (A) are estimated as HOMO and LUMO proper values with negative energies.

Applying Koopmans' approximation, $A = -E_{LUMO}$; $I = -E_{HOMO}$.

Table 1. Calculated global reactivity properties: chemical potential (μ), hardness (η), softness (σ), electrophilic index (ω), for the studied compounds from B3LYP/6-31G* level of theory.

Cpd.	HOMO	LUMO	μ	η	σ	ω
1	-6.12	-1.08	-3.6	2.52	0.20	2.57
2	-5.81	-1.03	-3.42	2.39	0.21	2.45
3	-5.74	-1	-3.37	2.37	0.21	2.40
4	-6.27	-1.23	-3.75	2.52	0.20	2.79
5	-5.01	-0.88	-2.95	2.07	0.24	2.10

Chemical Potential

Chemical potential indicates the affinity of an electron to flee, it can be calculated as:

$$\mu = \frac{E_{HOMO}+E_{LUMO}}{2}$$

As chemical potential (μ) becomes more negative, removing the electron becomes very hard and easier to gain one. According to our results, we can conclude that the compound 4 possesses the highest chemical potential with μ = -3.75 eV, it is the less reactive compared to the others compounds. On the contrary, compound 5 is the least stable and the most reactive among all the compounds due to the low value of μ (-2.95 eV).

Chemical Hardness

Chemical hardness (η) is a reactivity descriptor that quantifies the resistance of a system to electron transfer.

$$\eta = \frac{E_{LUMO} - E_{HOMO}}{2}$$

From Table 1, we can see that the compounds 1 and 4 are characterized by the highest hardness value of 2.52eV and A by the lowest one (2.07 e2.07). These results indicate that 1 and 4 are highly stable and least active molecules while 5 is the least stable and highly reactive among other compounds

Chemical Softness

Chemical softness (σ) is another reactivity descriptor that complements chemical hardness.

$$\sigma = \frac{1}{2\eta}$$

A higher softness value indicates a more reactive and less stable system, and a lower softness value characterize a relatively stable and less reactive system. For the studied compounds, it can be see that 1 et 5 compounds with σ = 0.20 eV complements the high hardness value, they are the less reactive compounds. On the other hand, 5 has the highest σ equal to 0.24 eV making it a highly reactive and least stable compound.

Elctrophilic Index:

The electrophilic index (ω) is a reactivity descriptor that measures the electrophilic character of a molecule, it is calculated as:

$$\omega = \frac{\mu^2}{2(\eta)}$$

The results show that compound 4 has a higher value of the electrophilic index , ω = 2.79 eV, traducing a stronger electrophilic character and a greater tendency to accept electrons, while 5 present the lower of electrophilic index , ω = 2.10eV, suggesting a weaker electrophilic character and a reduced ability to accept electrons.

Table 2. ADMET prediction results of the fives 3,4-dihydropyrimidine-2(1H)-ones derivatives

	Physicochemical properties	**(1)**	**(2)**	**(3)**	**(4)**	**(5)**
Lipophilicity	Log P	2.44	2.04	2.99	2.57	2.75
	H-bond donors	1	2	0	1	1
Hydrogen bonds	H-bond acceptors	3	4	3	4	3
Molecular weight	MW ($g.mol^{-1}$)	259.3	275.3	292.7	275.3	302.3
Flexibility	Rotatable bonds	4	4	4	5	5
Polarity	TPSA ($Å^2$)	55.40	75.6	43.3	64.6	58.64
Solubility	Log S	-2.19	-2.17	-5.17	2.44	-4.43
Saturation	Fraction of C sp^3	0.33	0.33	0.38	0.33	0.41
Pharmacokinetics properties						
Absorption	GI absorption	High	High	High	High	High
	Caco-2	Yes	No	Yes	Yes	Yes
Distribution	BBB permeability	Yes	Yes	Yes	Yes	Yes
Metabolism	CYP2D6 inhibitor	No	No	No	No	No
	CYP2C19 inhibitor	Yes	No	Yes	Yes	No
Excretion	Oct-2 ihnibitor	No	No	No	No	No
	Carcinogenicity (binary)	No	No	No	No	No
	Ames mutagenesis	No	No	No	No	No
Toxicity	hERG K+ channel inhibitor	No	No	No	Yes	Yes
	Respiratory toxicity	Yes	Yes	No	Yes	Yes
	Hepatotoxicity	Yes	No	Yes	No	Yes

ADMET Prediction

To confirm a drug and its efficacy as a top candidate against any disease, ADMET is essential. The partition coefficient (cLogP), donor hydrogen bond and drug similarity were calculated using physicochemical methods. Pharmacokinetic studies were also conducted for clinical trials of these derivatives molecules. The results are presented in Table 2.

The topological polar surface area (TPSA) should be less than <140 Å2 for significant oral bioavailability, our results showed good values of TPSA ranging between 43.3 $Å^2$ and 75.6 $Å^2$. Furthermore, the results descibes that all compounds showed high GI adsorption and Caco-2 permeability. Moreover, most of the molecules can be metabolized by the major cytochromes, except molecule (1), and derivatives containing chlorine radical (molecule 3) and methoxy radical (molecule 4). Moreover, all the molecules are non oct-2 -inhibitors, indicating a good excretion.

A drug candidate must first pass a toxicity risk assessment to be considered for drug development. Low toxicity and side effects indicate a high therapeutic index of the drug. For this reason, a toxicity prediction analysis was performed, the results indicate that all the molecules are anticarcinogenic and are non-AMES toxic. However only derivatives that contain methoxy radical (molecule 4) and amino radical (molecule 5) are hERG ihnibitors which indicates that they act as K+ channel blockers, known as anti-hypertensives. Interinstegly, the derivatives that cointain hydroxy radical (molecule 2) and methoxy radical (molecule 3) are presenting an anti-hepatotoxicity. And finally, only the derivative that contains chlorine radical (molecule 3) presented a non-respiratory toxicity.

Additionnaly of being anticancer, antihypertensive and anti-hepatotoxic agents as shown from the results above, literature have already revealed that for a majority of the analogues of 3,4-dihydropyrimidine-2(1H)-ones derivatives, their biological activity is affected by the lipophilicity (logP) and the nature of the substituents; For instance, in *Tale et al* study (Tale et al., 2011), it has been found that derivative having chlorine or fluorine as radicals in the para-position on the benzene ring, are having high lipohilicity, and presenting active IL-6 inhibitory effect at concentration of 10 uM, and hence they are considered as anti-inflammatory agents. In this study, molecule 3 is the best candidate for being an anti-inflammatory agent, due to its its chlorine radical in the para-position, and highest lipophilicity compared to the other molecules (Table 2)

Concerning the antibacterial and antifongic activities, *Tale et al* study (Tale et al., 2011) have revealed that antibacterial and antifongic potency against gram-positive *Staphylococcus aureus, Bacillus subtilis and* gram-negative *Escherichia coli and Salmonella typhimurium* and also molds including *Candida albicans , Aspergillus niger, Fusarium solani, Aspergillus flavus* is higher when the derivatives are bearing oxy-radicals in the para-

position and having a high H-Bond acceptor number. In this study, molecule 2 and molecule 4 are expected to have the greatest antibacterial and antifongic activities, bearing hydroxy and methoxy radicals, respectively.

Conclusion

In conclusion, 3,4-Dihydropyrimidin-2(1*H*)-ones 1-5 compounds are theoreticcaly studied at the B3LYP/6-31G* level of theory. The regioselectivity of the studied compounds is investigated using simulated molecular electrostatic potential isosurfaces. The results indicates that the active sites for an nucleophilic attack is the hydrogen atoms of the pyrimidone, and negative nucleophilic zones is located mainly on the oxygen of the pyrimidone. According to calculated global reactivity descriptors, we conclude that the 5 compound is the more reactive and the less stable one, and compounds 1 and 4 are the less reactive and the more stable among the studied compounds. In addition, calculated electrophilic index show that compound 4 is has the high electrophilic character and a greater tendency to accept electrons, while 5 present the weaker electrophilic character and a reduced ability to accept electrons.

The ADMET prediction study showed optimal physicochemical, pharmacological, and bioavailability, with estimating the biological activity of each derivatives of the studied of 3,4-dihydropyrimidine-2(1H)-ones derivatives, including anticancer, antihypertensive and anti-hepatotoxic, anti-inflamatory, antibacterial and antifongic activities. It was found that amongst all the compounds screened, derivative 3, besides of its non-respiratory toxicity and anti-hepatotoxicity, showed a promising tendency to be anti-inflammatory active. Derivatives 4 and 5 showed a tendence of being anti-hypertensives, while derivative 4 exhibited also possible antibacterial and antifongic activities, along with derivative 2 that showed also an anti-hepatotoxicity. Globaly, the ADMET results showed that the investigated 3,4-dihydropyrimidine-2(1H)-ones derivatives could be pontent biological active compounds, however, an In-vitro study is necessary for further investigation.

Scientific Ethics Declaration

The authors declare that the scientific ethical and legal responsibility of this article published in EPSTEM journal belongs to the authors.

Acknowledgements or Notes

* This article was presented as a poster presentation at the International Conference on Basic Sciences, Engineering and Technology (www.icbaset.net) held in Alanya/Turkey on May 02-05, 2024.

References

Ashok, M., Holla, B. S., & Kumari, N. S. (2007). Convenient one pot synthesis of some novel derivatives of thiazolo[2,3-*b*]dihydropyrimidinone possessing 4-methylthiophenyl moiety and evaluation of their antibacterial and antifungal activities. *European Journal of Medicinal Chemistry*, *42*(3), 380-385.

Atwal, K. S., Swanson, B. N., Unger, S. E., Floyd, D. M., Moreland, S., Hedberg, A., & O'Reilly, B. C. (1991). Dihydropyrimidine calcium channel blockers. 3. 3-carbamoyl-4-aryl-1,2,3,4-tetrahydro-6-methyl-5-pyrimidinecarboxylic acid esters as orally effective antihypertensive agents. *Journal of Medicinal Chemistry*, *34*(2), 806-811.

Bahekar, S. S., & Shinde, D. B. (2004). Synthesis and anti-inflammatory activity of some [4,6-(4-substituted aryl)-2-thioxo-1,2,3,4-tetrahydro-pyrimidin-5-yl]-acetic acid derivatives. *Bioorganic & Medicinal Chemistry Letters*, *14*(7), 1733-1736.

Becke, A.D. (1988). Density-functional exchange-energy approximation with correct asymptotic behavior. *Physical Review A*, *38*(6), 3098.

Bhatia,M. (2024). An overview of conceptual-DFT based insights into global chemical reactivity of volatile sulfur compounds (VSCs), *Computational Toxicology 29*, 100295.

Frisch, M. J., Trucks, G. W., Schlegel, H. B., Scuseria, G. E., Robb, M. A., Cheeseman, J. R., ... & Pople, J. A. (1998). *Gaussian 98, revision a. 7*. *Pittsburgh, PA*: Gaussian. *Inc.*

Hratchian, H. P., Keith, T. A., & Millam, J. (2009). *Gaussian 05 user's referenc*e. *S*hawnee Mission, KS: Semichem Inc.

Khelifi, R., Latelli, N., Charifi, Z., Baaziz, H., Chermette, H. (2023). Predicting the activity of methoxyphenol. derivatives antioxidants: I. structure and reactivity of methoxyphenol derivatives, a DFT approach *Computational and Theoretical Chemistry 1229,* 114287.

Matias, M., Campos, G., Santos, A. O., Falcão, A., Silvestre, S., & Alves, G. (2016). Potential antitumoral 3,4-dihydropyrimidin-2-(1H)-ones : Synthesis, in vitro biological evaluation and QSAR studies. *RSC Advances, 6*(88), 84943-84958

Singh, O. M., Singh, S. J., Devi, M. B., Devi, L. N., Singh, N. I., & Lee, S.-G. (2008). Synthesis and in vitro evaluation of the antifungal activities of dihydropyrimidinones. *Bioorganic & Medicinal Chemistry Letters, 18*(24), 6462-6467.

Stefani, H. A., Oliveira, C. B., Almeida, R. B., Pereira, C. M. P., Braga, R. C., Cella, R., Borges, V. C., Savegnago, L., & Nogueira, C. W. (2006). Dihydropyrimidin-(2*H*)-ones obtained by ultrasound irradiation : A new class of potential antioxidant agents. *European Journal of Medicinal Chemistry*, *41*(4), 513-518.

Tale, R. H., Rodge, A. H., Hatnapure, G. D., & Keche, A. P. (2011). The novel 3,4-dihydropyrimidin-2(1H)-one urea derivatives of N-aryl urea : Synthesis, anti-inflammatory, antibacterial and antifungal activity evaluation. *Bioorganic & Medicinal Chemistry Letters*, *21*(15),4648-4651.

Yang, H., Lou, C., Sun, L., Li, J., Cai, Y., Wang, Z., Li, W., Liu, G., & Tang, Y. (2019). admetSAR 2.0 : Web-service for prediction and optimization of chemical ADMET properties. *Bioinformatics*, *35*(6), 1067-1069.

Author Information

Noura Kichou
Department of Chemistry, Faculty of Sciences, University Mouloud Mammeri of Tizi-Ouzou, Tizi-Ouzou, Algeria
Laboratory of Electrochemistry-Corrosion, Metallurgy and Mineral Chemistry, Faculty of Chemistry, USTHB, BP 32 El Alia, Algiers, Algeria.
Contact e-mail: *noura.kichou@ummto.dz*

Anissa Amar
Mouloud Mammeri University of Tizi-Ouzou (UMMTO), Algeria
Laboratoire de Physique et Chimie Quantiques, Faculté des Sciences, Université Mouloud Mammeri de Tizi-Ouzou, Tizi-Ouzou 15000, Algeria.

Nabila Guechtouli
Department of Chemistry, Faculty of Sciences, University Mouloud Mammeri of Tizi-Ouzou, Tizi-Ouzou, Algeria

Manel Taferguennit
Laboratory of Electrochemistry-Corrosion, Metallurgy and Mineral Chemistry, Faculty of Chemistry, USTHB, BP 32 El Alia, Algiers, Algeria

To cite this article:

Kichou, N., Amar, A., Guechtoulı, N. & Taferghennit, M. (2024). Theoretical investigation of 3,4-dihydropyrimidin-2(*1H*)-ones derivatives and in-silico biological analysis. *The Eurasia Proceedings of Science, Technology, Engineering & Mathematics (EPSTEM), 28,* 105-112.

The Eurasia Proceedings of Science, Technology, Engineering & Mathematics (EPSTEM)
ISSN: 2602-3199

The Eurasia Proceedings of Science, Technology, Engineering & Mathematics (EPSTEM), 2024

Volume 28, Pages 113-122

ICBASET 2024: International Conference on Basic Sciences, Engineering and Technology

Synthesis, Biological Activities and in Silico ADMET Study of Coumarin-3,4-Dihydropyrimidin-2(1*H*)-Ones

Amina Benazzouz–Touami
Mouloud Mammerie University of Tizi-ouzou

Karima Ighilahriz-Boubchir
Mouloud Mammerie University of Tizi-ouzou

Malika Makhloufi-Chebli
Mouloud Mammerie University of Tizi-ouzou

Abstract: The synthesis of hybrid molecules represents a promising pathway for the development of new drugs. Dihydropyrimidinones (DHPMs) have demonstrated significant therapeutic and pharmacological properties, particularly as the foundational structure of several calcium channel blockers and antihypertensive agents. A wide range of biological effects, including antiviral, antitumor, antibacterial, and anti-inflammatory activities, have been described for these compounds. Functionalized DHPMs have shown significant activities against bacteria, viruses, and tumors. The synthesis of DHPMs has attracted considerable interest among organic and medicinal chemists. The most common method for synthesizing DHPMs and their corresponding dihydropyrimidinethiones (DHPMTs) involves the multicomponent Biginelli reaction. Several studies have been reported in the literature on the synthesis and biological evaluation of various pyrimido-fused heterocycles, such as pyrimido[4,5-d]pyridazin-8(7*H*)-ones, pyrano[2,3-d]pyrimidines, pyrido[2,3-d]pyrimidines, and 2,4-diaminopyrido[2,3-d]pyrimidines. As part of our interest in the synthesis of fused heterocycles, and given the importance of hybrid molecules and their synthesis which addresses several drawbacks, we describe in this work a simple strategy for the synthesis of a new series of coumarin-dihydropyrimidinone hybrid molecules. In silico toxicity predictions indicated that these compounds should have good oral bioavailability. The compounds were screened for their antimicrobial activity, and the results showed that compound 5b was the most active against the bacterium *Staphylococcus aureus*. Additionally, the compounds were docked with the FtsZ protein from *S. aureus.*

Keywords: Coumarin, Dihyropyrimididnone, Antibacterial activity, Molecular docking FtsZ protein

Introduction

Researchers in the medical, pharmaceutical, and chemical fields play a pivotal role in designing and preparing bioactive compounds to address various health issues such as cancer and bacterial infectious diseases. Consequently, there is a growing interest in the synthesis of pyrimidinone derivatives due to their promising biological applications as antimalarial, antibacterial, antifungal, anti-HIV, antiviral, anticancer, and anti-inflammatory agents(Santelli-Rouvier et al., 2004 ; Bhattacharjee et al., 2004). Correspondingly, the corresponding dihydropyrimidinones (DHPMs) have demonstrated significant therapeutic and pharmacological properties, serving as the integral backbone of several calcium channel blockers, antihypertensive agents, and α1a-antagonists. A broad spectrum of biological effects, including antiviral, antitumor, antibacterial, and anti-inflammatory activities, has been reported for these compounds (Ashok et al ., 2007). Furthermore, coumarin cores are recognized for their wide range of biological activities such as antibacterial, anticancer, anticoagulant, anti-inflammatory, and anti-HIV properties (Feng et al.,2020).

The most prevalent method for synthesizing DHPMs is through the multicomponent Biginelli reaction. This reaction involves heating a mixture of three components – a,β-ketoester, an aldehyde, and urea in ethanol with a catalytic amount of HCl. Multicomponent reactions (MCRs) are convergent processes where three or more starting materials react to yield a product (Biginelli et al., 1893). Given the biological significance of DHPMs and coumarins, and as part of our ongoing program for synthesizing bioactive compounds (Benazzouz et al., 2021 ; Halit et al., 2022), a new series of 4-aryl-6-methyl-5-(2-oxo-2*H*-chromene-3-carbonyl)-3,4-dihydropyrimidin-2(1*H*)-ones has been synthesized under mild conditions using 3-(acetoacetyl) coumarin derivatives 1a-c as key synthons, Selected compound were evaluated for their antibacterial activity. Molecular docking analysis was performed to better understand the enzyme binding mode making the design of better possible, and in silico properties prediction were studied.

Experimental

Materials

Melting points were determined on a Stuart scientific SPM3 apparatus fitted with a microscope and are uncorrected. 1H and 13C NMR spectra were recorded in DMSO-d6 solutions on Bruker Avance 300 (300.13 MHz for 1H and 75.47 MHz for 13C) spectrometer. Chemical shifts are reported in parts per million (d, ppm) using TMS as internal reference and coupling constants (J) are given in hertz (Hz). 13C assignments were made using NOESY, HSQC, and HMBC (delays for one bond and long-range JC/H couplings were optimized for 145 and 7 Hz, respectively) experiments. Mass spectra are obtained with ESIþ. Positive-ion ESI mass spectra were acquired using a Q-TOF 2 instrument [diluting 1 mL of the sample chloroform solution (w10^{-5} M) in 200 mL of 0.1% trifluoroacetic acid/methanol solution. Nitrogen was used as nebulizer gas and argon as collision gas. The needle voltage was set at 3000 V, with the ion source at 80 °C and desolvation temperature at 150 °C. Cone voltage was 35 V.

The antimicrobial activities against both Gram-positive bacteria, such as Staphylococcus aureus (ATCC 25923), and Gram-negative bacteria, including *Escherichia coli* (ATCC 25922) and *Pseudomonas aeruginosa* (ATCC 27853), were assessed in vitro.

Chemistry

The starting materials 3-acetoacetylcoumarin derivatives were prepared according to the synthetic methods in Scheme 1 from substituted salicylaldehydes and 4-hydroxy-6-methyl-2*H*-pyran-2-one (triacetic acid lactone = TAL) through a tandem microwave-assisted Knoevenagel condensation and intramolecular translactonization process in an organobasic medium (Makhloufi-Chebli et al.,2008).

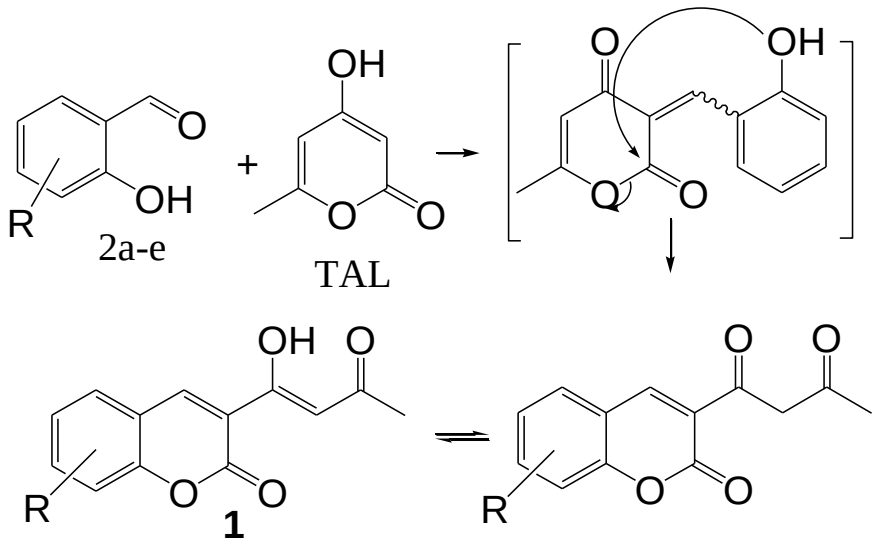

Scheme1. Synthesis of 3-acetoacetylcoumarin derivatives

A mixture of the appropriate 3-acetoacetylcoumarins 1 (1 mmol), benzaldehydes 2 (1 mmol), urea/thiourea 3 (1.5 mmol), and sulfuric acid (20 drops) in 10 mL of acetonitrile was stirred and refluxed for the appropriate amount of time (12-18 h). After completion of the reaction as indicated by thin layer chromatography (TLC), using a 1:4 mixture of $CHCl_3$/ methanol as eluant, the mixture was cooled to room temperature, then ice and water was added to afford the pure product. The solid was separated by filtration and washed with cold water, dried, washed with diethyl ether, and recrystallized from ethanol or ethyl acetate. (Scheme 2 and Table 1).

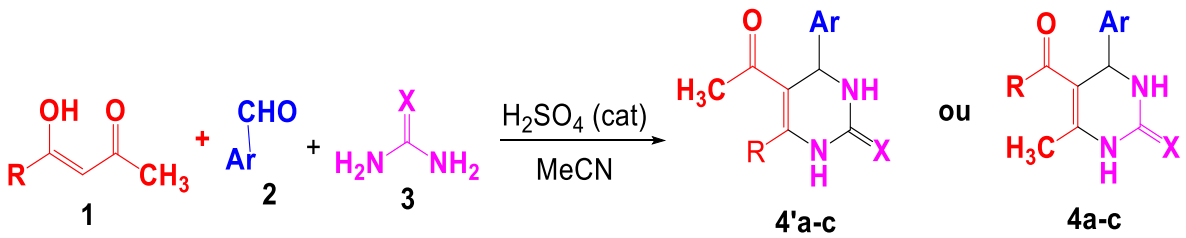

Scheme 2. Synthesis of 3-acetoacetylcoumarin derivatives

Screening for Antibacterial Activity

The activity of the synthesized compounds against the tested microorganisms was determined using the standardized disc agar diffusion method. The microorganisms utilized in the test included Gram-negative bacteria such as *Escherichia coli* (ATCC 25922) and *Pseudomonas aeruginosa* (ATCC 27853), as well as Gram-positive bacteria like *Staphylococcus aureus* (ATCC 25923). The tested compounds were dissolved in dimethyl sulfoxide (DMSO) with a concentration of 10^{-1} M. Subsequently, 25 µL of the tested sample was dispensed onto filter paper discs measuring 6 mm in diameter. These discs were gently placed on the surface of the agar plates and then incubated at 37°C for 24 hours. DMSO was utilized as the negative control. Following incubation, the diameters of the inhibition zones formed were measured in millimeters, and the mean values were recorded.

Computational Method

The FtsZ protein from S. aureus (FtsZ, PDB ID 4DXD) has been previously shown to be the target of antibacterial coumanins derivatives (Duggirala et al., 2014). Thus the synthesized compounds were docked with this bacterial protein to to explain their antibacterial activity. The protein *S. aureus* FtsZ (PDB ID 4DXD determined at 2.01 Å of resolution) was downloaded from the Protein Data Bank (Tan et al.,2012), corresponding to the protein S. aureus FtsZ complexed with inhibitor (PC190723). It is noteworthy that FtsZ protein is an important and vital cell division protein, which is found in S. aureus. However, we removed the bound ligand and crystallographic water molecules except those participating in the catalysis, and all missing hydrogens were added using AutoDockTools. The active site radius was taken to be 8 Å from the center of the co-crystallized ligand . Thus, the active site residues were found to be Gln192, Val207, Asn263, Val297, Leu200, Asn208, Leu209, Val203, Thr309 and Ile311. Then, the Gasteiger charges were assigned and nonpolar hydrogens were merged with their corresponding carbons (Terrachet et al., 2020; Benazzouz et al., 2021).

In silico predictive models are frequently applied to get an early estimation of the ADMET profile (Absorption, distribution, metabolism, excretion, and toxicity), this estimation has become a standard step nowadays in drug discovery. Thus, SwissADME server was used to predict the ADMET profile of the tested compounds.

Results and Discussion

Caracterization

The coumarin-DHPMs derivatives **4a-c** were synthesized as outlined in Scheme 1 . The reaction of 3-acetoacetylcoumarine derivatives **1 ,** 4-nitrobenzaldehyde **2** and urea **3** gave the corresponding 4-aryl-6-methyl-5-(2-oxo-2H-chromene-3-carbonyl)-3,4-dihydropyrimidin-2(1*H*)-ones in good yields (42-70%) (Benazzouz et al., 2015). Structures of all prepared compounds were confirmed by IR, 1 H NMR and 13 C NMR analysis and their data are reported in Table 1.

Table 1. Synthesis of 4-aryl-6-methyl-5-(2-oxo-2*H*-chromene-3-carbonyl)-3,4-dihydropyrimidin-2(1*H*)-ones

Product	R	Ar	Yield (%)	Mp (°C)
4a	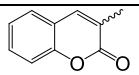	4-$NO_2C_6H_5$	**50**	**260**
4b	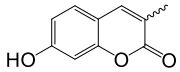	4-$NO_2C_6H_5$	**42**	**235**
4c	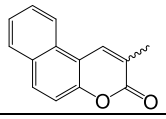	4-$NO_2C_6H_5$	**70**	**225**

The mechanism of the Biginelli reaction, along with the structure of the synthons used, suggests the formation of two possible dihydropyrimidinones/thiones (compounds of type 4a-c, or 4'a-c). This process initiates with the formation of an imine through the condensation of benzaldehyde with urea/thiourea, which then reacts with the 1,3-dicarbonyl compound after the nitrogen of the imine is protonated. In the final step of the mechanism, there are two possible cyclization sites, which, upon dehydration, can lead to the formation of DHPMs 4a-c (Scheme 3).

Scheme 3. Mechanism proposal for the formation of 4-aryl-6-methyl-5-(2-oxo-2*H*-chromene-

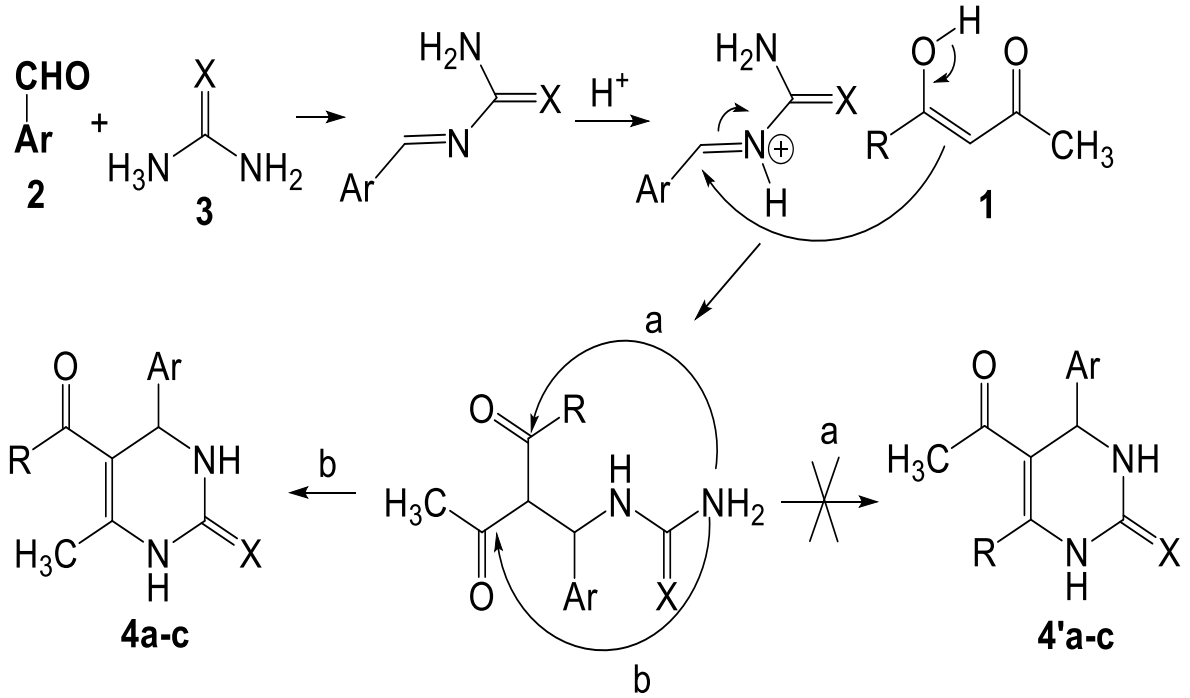

3-carbonyl)-3,4-dihydropyrimidin-2(1*H*)-ones.

The structures and purities of the obtained products were determined through elemental analysis, NMR (including extensive 2D NMR analyses, such as HSQC, HMBC, and NOESY), and mass spectrometry data. As an illustrative example, the 1H NMR spectrum of 4b displayed a singlet at δH 2.05 ppm and a doublet at δH 5.38 ppm, which were assigned to the proton resonances of the methyl group and H-6, respectively. Additionally, five other singlets were observed, attributed to H-4' (δH 8.01 ppm), H-8' (δH 6.75 ppm), NH (δH 8.11 and 9.58 ppm), and OH-7 (δH 10.92 ppm) protons. The remaining aromatic and benzopyranone protons appeared as doublets at δH 6.80, 7.52, 7.59, and 8.17 ppm.The HMBC connectivities of 4b were crucial in confirming the structure of the obtained isomer, particularly the correlation between H-40 and the ketone carbonyl carbon, which was also correlated with H-6 (Fig. 1). These correlations are consistent only with the structure 4b and not with 4'b. The HMBC connectivities of 4b facilitated the unequivocal assignment of all carbon resonances (Figure. 1).

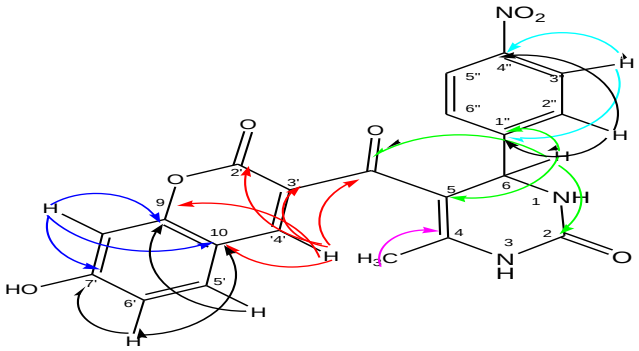

Figure 1. The HMBC connectivities of 4b

Table 2. 1H NMR data of DHPM-coumarins

Chemical shift δ (ppm)	**4a**	**4b**	**4c**
(d, CH_3 3H)	2.08	2.05	2.13
d, 1H, NH-1	8.10	8.11	9.32
(s, 1H, NH-3	9.69	9.58	9.71
d, 1H, H-5’	7.54	7.59	8.06
d, 1H, H-6	5.42	5.38	5.47
(s, OH)	/	10.92	/

Table 3. Elemental analysis and mass spectrometry data DHPM-coumarins

Compound	**m/z $(M+H)^+$**	**Anal calcd C% H% N%**	**Found C% H% N%**
4a	406	$C_{21}H_{15}N_3O_6$ 62.22, 3.73, 10.37	C 62.42, H 3.67, N 10.25.
4b	422	$C_{21}H_{15}N_3O_7$ C 59.86, H 3.59, N 9.97	C 59.68, H 3.70, N 9.75.
4c	456	$C_{25}H_{17}N_3O_6$ C 65.93, H 3.76, N 9.23	C 65.84, H 3.88, N 9.29.

B**iological Evaluation**

The results obtained indicate that the hybrid molecules 4a and 4b exhibit moderate inhibitory activity against all three tested strains. Compound 4c is inactive against all three tested strains. The activity of compound 4b is likely attributed to the presence of the hydroxyl (OH) group substituted on the benzene ring of the coumarin. This group can generate stable free radicals that participate in the redox cycle in the presence of oxygen from the air, potentially leading to lysosome destabilization and a decrease in mitochondrial membrane potential [30]

Table 4. Antimicrobil activity via disc diffusion method

Compounds	**Zone d’inhibition (mm)**		
	E.coli	*P. aeruginosa*	*S.aureus*
4b	9	8	11
4a	8	7	5
4c	7	5	8
DMSO	5	5	5

The Bioactivity Scores Prediction

The bioactivity scores of DHPMs-coumarins toward G protein-coupled receptor (GPCR) ligand, ion channel modulator, a kinase inhibitor, nuclear receptor ligand, protease inhibitors, and enzyme inhibitor were predicted by using the Molinspiration bioactivity score v2018.03 web (https:// www. molin spira tion. com/ cgi- bin/prope rties) (Ghannay et al.,2020).The predicted results are written in Table 5.

The rule for the bioactivity scores estimation is the following: when the bioactivity score was more than 0.00; the compound was considered active. While if the bioactivity score in the range between -0.50 and 0.00; the compound was moderately active. But if the bioactivity score was less than -0.50, the compound was inactive.

Table 5. The bioactivity scores prediction of the compounds 4a-c

The bioactivity score	**4a**	**4b**	**4c**
GPCR ligand	-0.68	-0.64	-0.59
Ion channel modulator	-0.63	-0.60	-0.59
Kinase inhibitor	-0.85	-0.79	-0.66
Nuclear receptor ligand	-0.48	-0.34	-0.35
Protease inhibitor	-0.74	-0.73	-0.71
Enzyme inhibitor	-0.51	-0.44	-0.42

The three DHPM-coumarin compounds showed inactivity against G protein-coupled receptor (GPCR) ligands, ion channel modulators, and kinase inhibitors, with bioactivity scores below -0.50. In terms of nuclear receptor inhibition, all compounds exhibited moderate activity, with bioactivity scores ranging from -0.35 to -0.48. Regarding enzyme inhibition, compounds 4b and 4c demonstrated moderate activity with bioactivity scores of -0.42 and -0.44, respectively, while the remaining compounds were found to be inactive.

In Silico Drug Likeness Analysis

To be considered as a drug with favorable pharmacokinetic properties, compounds must meet certain criteria outlined by Lipinski's rule. The drug likeness results of potential inhibitors, as determined using the SwissADME web server, are presented in Table 6

Table 6. Probabilities for Drug-Likeness properties of synthesized compounds,predicted by SwissADME web server

Property or rule	**4a**	**4b**	**4c**
MW (g/mol)	405.36	421.36	441.39
Solubility (Log S)	soluble	Soluble	Moderately Soluble
Log P	3.21	2.92	2.46
HBA	6	7	6
HBD	2	3	2
TPSA ($Å^2$)	134.23	154.46	134.23
Lipinski	Yes	Yes	Yes
Ghose	Yes	Yes	Yes
Veber	Yes	No	Yes
Egan	No	No	No
Muegge	Yes	No	Yes
Bioavailability Score	0,55	0.55	0,55

To adhere to Lipinski's rule, the number of hydrogen bond acceptors (HBA) should be less than or equal to 10, the n-octanol and water partition coefficient (LogP) should not exceed 5, the molecular weight (MW) should be less than or equal to 500 daltons, and the number of hydrogen bond donors (HBD) should be less than or equal to 5. The analysis of in silico results indicated that compounds 4a-c did not violate Lipinski's rule. The n-ON values range from 4 to 6, LogP values range from 2.46 to 3.91, and the number of hydrogen bond donors ranges from 0 to 1 for all synthesized compounds. It is predicted that all coumarin-DHPMs derivatives are soluble, and the total polar surface area (TPSA $\leq$ 160), which is a good indicator of drug bioavailability, falls within acceptable ranges for all compounds. (Benazzouz et al., 2021)

In Silico Prediction of ADMET Properties

In silico studies were conducted to evaluate the pharmacokinetic properties and safety potential of the synthesized coumarin-DHPMS derivatives. These derivatives demonstrated promising pharmacokinetic profiles in terms of human intestinal absorption (HIA), with the compounds showing high absorption values. The permeability through the colorectal carcinoma cell line (PCaCo-2) indicated favorable transport of drug metabolic compounds, falling within an acceptable range of 0 (poor absorption) to +1 (better absorption)(Seltur et al., 2017).

Table 7. ADMET properties of synthesized compounds, predicted by admetSAR and SwissADME web servers

Property	**3a**	**3b**	**3c**
PCaco-2	0.6470	0.8078	0.7648
HIA	+	+	+
PG Inhibitor	No	No	No
BBB	penetrate	No- penetrate	penetrate
CYP2C9 substrate	No	No	No
CYP2D6 Inhibitor	No	No	No
CYP3A4 Inhibitor	Yes	Yes	Yes
Carcinogenicity	No	No	No
hERG	Weak	Weak	Weak

Table 8. Docking energies, interactions observed in the docked conformations of synthesized compounds with The FtsZ protein from S. Aureus

Compounds	**Docking energy**	**2D diagram of ligand-protein Interactions**
4a	-7.6	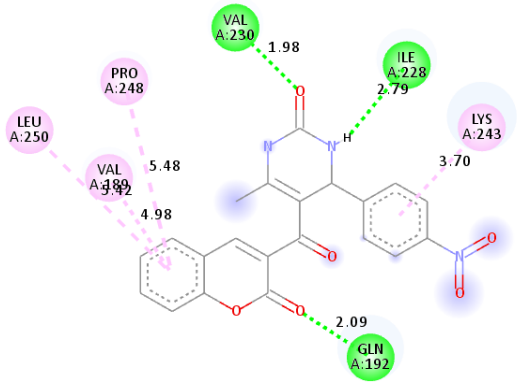
4b	-8.7	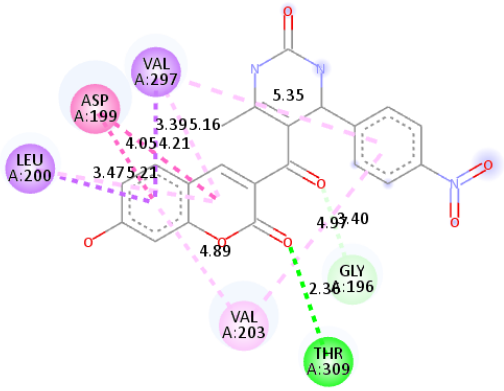
4c	-9.1	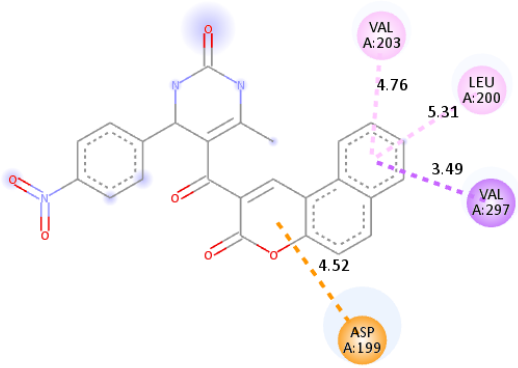

Furthermore, 4a and 4b were predicted to be non-inhibitors of important enzymes such as P-glycoprotein and cytochrome P450 isoforms 2D6, 2C19, and 3A4. This is significant as cytochrome P450 proteins play a crucial

role in drug metabolism, and inhibition of these isoforms could lead to potential drug interactions, accumulation, and toxicity.Moreover, the investigated compounds exhibited no evidence of carcinogenicity and displayed weak blocking activity against the Human Ether-a-go-go-Related Gene (hERG). It's noteworthy that the hERG gene encodes a potassium channel protein (Kv11.1) essential for cardiac action potential regulation. Inhibition of this gene could potentially lead to arrhythmic attacks or shocks. Therefore, the lack of significant inhibition against hERG suggests a favorable safety profile for the synthesized compounds.

Binding Mode of Studied Compounds

In this study, molecular docking study was performedin an effort to evaluate the binding interactions of the investigated with The FtsZ protein from *S. aureus*, and predict the best The FtsZ protein inhibitor among them. The molecules were docked in the active site of The FtsZ protein from *S. aureus* and the results are summarized in table 8. To investigate the potential mode of action and inhibition capacity of the synthesized compounds against various target macromolecules, molecular docking studies were conducted. The compounds were docked into the active site of S. aureus (PDB ID: 4DXD). The estimated binding energies and interacting residues, along with their respective denotations, are summarized in Table 8.The synthesized compounds were subjected to a molecular docking study for the analysis of their interactions with FtsZ protein from *S. aureus* PDB ID 4DXD. Binding energies varied between -9.1 kcal.mol^{-1} to -7.6 kcal.mol^{-1}.

In the active site of the receptor macromolecule 4DXD, the best binding conformations of compounds 4a-c were observed. Specifically, compound **4b** formed conventional hydrogen bonds with Thr309 (d= 2.36 Å). Furthermore, it engaged in significant interactions with essential active residues, including Gly192, Val297, Asp199, Leu200, and Val203 of the receptor macromolecule.

Figure 2. Superimposition of docked conformations of the compounds, **4a-c** on the crystal structure of ligand PC190723

The experimental results are in agreement with the docking predictions regarding the superposition of structures **4a-c** and the reference within the protein's active site. As shown in Figure 2, it is evident that compound **4a** is indeed bound to the molecule, but it is considerably distant from the active site. In contrast, compound **4b** is firmly anchored within the active site and binds perfectly to the key amino acids of the activity. However, molecule **4c** binds to some amino acids within the active site but extends beyond the boundaries of the key amino acids.

Conclusion

We have shown that the three-component reaction of 3-(acetoacetyl)coumarin derivatives, 4-nitro benzaldehydes, and urea, catalyzed by sulfuric acid provides a simple one-pot entry for the synthesis in very good yield of a series of new 4-aryl-6-methyl-5-(2-oxo-2*H*-chromene-3-carbonyl)-3,4-dihydropyrimidin-2(1*H*)-ones. The compounds were evaluated for antibacterial activity. The compounds with OH groups on the coumarin ring showed good activity.The results of the antibacterial activity show that only **4b** is active against bacteria *Staphylococcus aureus* compared to antibiotic used as reference. Indeed, **4b** showed good interactions with the active site amino acids of the FtsZ from *S. aureus* protein. In addition, all synthesized compounds have satisfactory calculated drug likeness parameters values, which make them promising candidates.

Scientific Ethics Declaration

The authors declare that the scientific ethical and legal responsibility of this article published in EPSTEM journal belongs to the authors.

Acknowledgements or Notes

* This article was presented as a poster presentation at the International Conference on Basic Sciences, Engineering and Technology (www.icbaset.net) held in Alanya/Turkey on May 02-05, 2024.

References

Ashok, M., Holla, B. S., & Kumari, N. S. (2007). Convenient one pot synthesis of some novel derivatives of thiazolo[2,3-b] dihydropyrimidinone possessing 4-methylthiophenyl moiety and evaluation of their antibacterial and antifungal activities.. *European Journal of Medicinal Chemistry, 42*(3), 380-385.

Benazzouz, A., Makhloufi-Chebli, M., Khatir-Hamdi, N., Boutemeur-Khedis, B., & Silva, A. M. S. (2015). A facile synthesis of new coumarin-3,4-dihydropyrimidin-2(1H)-ones/thiones dyads. *Tetrahedron*, 71, 3890-3894.

Benazzouz-Touami, A., Chouh, A., Halit, S., Terrachet-Bouaziz, S., & Makhloufi-Chebli, M. (2022). New coumarin-pyrazole hybrids: Synthesis, docking studies and biological evaluation as potential cholinesterase inhibitors. *Journal of Molecular Structures, 1249*, 1315.

Benazzouz-Touami, A., Hikem-Oukacha, D., Lamara, K. O., Halit, S., Terrachet-Bouaziz, S. (2021). Synthesis, biological activities and molecular docking study of 3-(3-oxobutanoyl)-2h-chromen-2-one derivatives. *Chemical Data Collections, 36*, 100792.

Bhattacharjee, A. K., Hartell, M. G., & Nichols, D. A. (2004). Structure-activity relationship study of antimalarial indolo [2,1-b] quinazoline-6,12-diones (tryptanthrins). Three dimensional pharmacophor modeling and identification of new antimalarial candidates *European Journal of Medicinal Chemistry, 39*(1), 59-67.

Biginelli, P. (1893). Aldehyde-urea derivatives of aceto- and oxaloacetic acids. *Gazzetta Chimica Italiana, 23*, 360-413.

Hammad S ., Bouaziz-Terrachet S., Meghnem, R., & .Meziane, D. (2020). Pharmacophore development, drug-likeness analysis, molecular docking, and molecular dynamics simulations for identification of new CK2 inhibitors. *J Mol Model, 26*(6) 160.

Duggirala, S., Nankar, R. P., Rajendran, S., & Doble, M. (2014). Phytochemicals as inhibitors of bacterial cell division protein FtsZ: Coumarins are promising candidates. *Applied Biochemistry Biotechnology, 174*(1), *283-296.*

Feng, D., Zhang, A., Yang, Y., & Yang, P. (2020) Coumarin-containing hybrids and their antibacterial activities. *Archiv der Pharmazie, 353*(6), 1-12.

Ghannay, S., Bakari, S., Msaddek, M., Vidal, S., & Kadri, A. (2020). Design, synthesis, molecular properties and *in vitro* antioxidant and antibacterial potential of novel enantiopure isoxazolidine derivatives. *Arabian Journal of Chemistry, 13*(1), 2121-2131.

Halit, S., Benazzouz-Touami, A., Makhloufi-Chebli, M., Terrachet, S., Ighilahriz, K., & Robert, A. M. S. (2022). Design, synthesis, biological evaluation of isonicotinoylpyrazolyl-coumarin derivatives and computational study. *Journal of Molecular Structure, 1265*,133487.

Makhloufi-Chebli, M., Hamdi, M., Silva, A. M. S., & Balegroune, F. (2008). Translactonisation intramoleculaire assistee par micro-ondes. Synthese des coumarines. *Journal of the Algerian Chemical Society*, *18*(1), 91-101.

Santelli-Rouvier, C., Pradines, B., & Berthelot, M. (2004). Arylsulfonyl acridinyl derivatives acting on Plasmodium falciparum. *European Journal of Medicinal Chemistry*, *39*(9), 735-744.

Setlur, A. S., Naik, S. Y., & Skariyachan, S. (2017). Herbal lead as ideal bioactive drug targets of Ebola virus in comparison with known chemical analogue: A computational drug discovery . *Interdiscipliner Sciences : Computational Life Sciences*, *9*(2), 254-277.

Tan, C. M., Therien, A. G., Lu, J., Lee, S. H., Caron, A., Gill, C. J., & Roemer, T. (2012). Restoring methicillin-resistant staphylococcus aureus susceptibility to β-Lactam Antibiotics. *Sci Transl Med*., 4(126).

Author Information

Amina Benazzouz-Touami
Laboratory de Physic and Chemistry of Materials LPCM, Departement of Chemistry, Faculty of Sciences, University Mouloud Mammeri, 15000, TiziOuzou, Algeria
Contact e-mail: *amina.benazzouz@ummto.dz*

Karıma Ighilahriz-Boubchir
Laboratory de Physic and Chemistry of Materials LPCM, Departement of Chemistry, Faculty of Sciences, University Mouloud Mammeri, 15000, TiziOuzou, Algeria

Malıka Makhloufi-Chebli
Laboratory de Physic and Chemistry of Materials LPCM, Departement of Chemistry, Faculty of Sciences, University Mouloud Mammeri, 15000, TiziOuzou, Algeria

To cite this article:

Benazzouz-Touami, A., Ighilahriz-Boubchir, K., & Makhloufi-Chebli, M. (2024). Synthesis, biological activities and in siloco ADMET study of coumarin-3,4-dihydropyrimidin-2(1H)-ones. *The Eurasia Proceedings of Science, Technology, Engineering & Mathematics (EPSTEM), 28,* 113-122.

The Eurasia Proceedings of Science, Technology, Engineering & Mathematics (EPSTEM)
ISSN: 2602-3199

The Eurasia Proceedings of Science, Technology, Engineering & Mathematics (EPSTEM), 2024

Volume 28, Pages 123-133

ICBASET 2024: International Conference on Basic Sciences, Engineering and Technology

A Quantitative Study into Purchasing Practices and Influential Factors among Filipino Consumers Regarding Counterfeit Over-The-Counter Medicines in Philippines

Marianito Gallego Jr.
Polytechnic University of the Philippines Manila

Daniel Caparro
Polytechnic University of the Philippines Manila

Raeselyn Macorol
Polytechnic University of the Philippines Manila

Treblig John Manalastas
Polytechnic University of the Philippines Manila

Charisse Anne Olaivar
Polytechnic University of the Philippines Manila

Abstract: The prevalence of counterfeit over-the-counter (OTC) medicines poses significant risks to public health, particularly in countries with weak governance and poor technical resources, such as the Philippines. This study investigates the purchasing practices and factors influencing Filipino consumers' decisions regarding counterfeit over-the-counter (OTC) medicines in Metro Manila, Philippines. Data was collected through a validated questionnaire distributed online, yielding responses from 250 individuals. Statistical analysis revealed that factors such as price, brand reputation, and personal experience significantly influence consumers' purchasing decisions. Consumers primarily consult friends or family and local pharmacies, with mobile android phones being the most prevalent technology used. Recommendations include enhanced consumer education and regulatory measures implementation, as well as promotion of trusted brands, both generic and branded, development of detection technology for counterfeit over-the-counter medicines, and collaborative efforts among stakeholders to mitigate the risks associated with counterfeit over-the-counter medicines. Implementing these recommendations can safeguard Filipino pharmaceutical public health and safety in the Philippines.

Keywords: Counterfeit, Over-the-counter (OTC), Pharmaceutical engineering

Introduction

Over-the-counter (OTC) medicines are available for purchase without the need to present a physician's prescription, making them a preferred choice for the public for treating minor ailments. Factors such as the high cost of prescription drugs, insufficient healthcare system, and a shortage of primary care physicians, particularly in developing nations like the Philippines, contribute to the widespread reliance on OTC medicine for affordable and immediate treatment. (Taylor et al., 2023; Taylor & Ayosanmi, 2023). However, the rampant growth of counterfeit OTC medicine is a global problem, targeting mostly developing countries with weak governance, and poor technical capacity. (Fakayode et al., 2024)

Counterfeit medicines are products with the wrong or contaminated ingredients, with the correct ingredients but not in their required amounts, or without the active ingredients resulting in decreased drug safety, efficacy, quality, strength, or purity. It can be mislabeled or with fake packaging and can apply to both generic and branded products. In addition, these drugs are not registered with the Food and Drug Administration (FDA) and did not go through validation and standard tests to confirm their quality, safety, and efficacy. (World Health Organization, 2010)

Counterfeit OTC medicines have always been a problem in the Philippines. A reason behind this is our geographical proximity to leading fraudulent manufacturers such as China, Pakistan, and India. Aside from that, it is also emphasized that selling in e-commerce facilitates easier accessibility, affordability, and anonymity for both consumers and suppliers. (Pereña et al., 2022)

World Health Organization (WHO) has estimated that 10% of global pharmaceutical commerce i.e. $21 billion worth is involved in trading of counterfeit OTC drugs online and nearly one-half (48.7%) of the documented cases were reported in developing countries of the Asia Pacific such as Indonesia and Philippines and was increased during the COVID-19 lockdown. (Pelegrino, 2023). WHO in 2021 reported approximately 100,000 people suffered health consequences/died from unintentional (that means not aware that the medicine is counterfeit/fake) consumption of OTC counterfeit medicine, such as from organ failure, etc.(Chaudhary, 2023; Hamdan, 2023; Pathak et al., 2023)

A study illuminates the prevalence of counterfeit OTC medicines in the Philippine e-commerce and the current level of awareness of this issue among Filipino consumers. Findings resulted in the need to address the gap between high knowledge level about counterfeit OTC medicines and the moderate detection ability to identify them (Isuga et al., 2022).

Among the wide-spread counterfeit drugs is paracetamol, ibuprofen, mefenamic, and other branded OTC medicines Neozep, Kremil-S, Tuseran Forte, Medicol, Ponstan, Alaxan, Dolfenal, etc. which are commonly used for painkillers and for fever. The issue of counterfeit OTC medicine in the and was further heightened by the COVID-19 pandemic due to increasing purchasing demand through e-commerce but with lack of supply. (WHO, 2023);(Hamdan, 2023)

Literature Review

Over-the-Counter Counterfeit Medicine

Medication that violates intellectual property rights or trademark law is considered counterfeit medicine. Falsified pharmaceuticals are counterfeit goods that are made to look like genuine medicine. The identity and/or source of both branded and generic products have been purposefully and fraudulently mislabeled when it comes to counterfeit drugs. The term "counterfeit medicine" is not yet widely recognized. Medical products fall into three sub-groups: substandard, unregistered, and falsified. The World Health Organization (WHO) currently uses the term "substandard/spurious/falsely labeled/falsified/counterfeit," or SSFFC, for these products. However, the U.S. Food & Drug Administration (FDA) defines counterfeit medicine as fake medication that may be contaminated, contain the incorrect active ingredient or none at all, or have the right active ingredient but in the incorrect dosage.

The market for fake medications is gradually expanding, exposing more people to these goods. Nowadays, over-the-counter medications are available online as well as pharmacies, drug stores, and health centers. In an article by Davies J. (2017) discovered that 61% of online consumers have purchased prescription drugs from online pharmacies, with 73% of these drugs falling into the over-the-counter (OTC) product category. When comparing the online sales percentage to the total sales of over-the-counter medications in 2008, the country in question had the highest worldwide rate, surpassing 17% (as opposed to 6.4%), (Davies, .2017)

With the growing trend of online sales of medications, public health is becoming increasingly concerned about this issue. A number of analysts have listed the advantages and disadvantages of purchasing medications online for over-the-counter use, with a focus on the pharmacy and broader healthcare communities during the past ten years(Gray, 2011) Online sales of medications, especially vitamins and dietary supplements, are widespread in the Philippines. These products are typically sold at low prices by unlicensed pharmacists who operate online. The FDA has issued an advisory stating that online sellers are not allowed to sell medications online unless they have a physical address for the drug stores and an approved pharmacy license (FDA Advisory No. 2019-154).

The COVID-19 pandemic has significantly impacted the way people access healthcare services, including the purchasing of medications online. As highlighted by Di Crosta, et al., the pandemic has led to a shift towards online purchasing of medicines, raising concerns about the safety and authenticity of medications obtained through this channel. This trend has prompted pharmacists to provide substitute medicines as a standard practice. (Di Crosta et al., 2021)

The adaptation to online sales of both over-the-counter and prescription drugs during the COVID-19 pandemic has been closely linked to how community pharmacists view their profession and find fulfillment in it. However, challenges such as the possibility of counterfeit drugs and the use of fake prescriptions need to be addressed to ensure the safety and efficacy of online medication purchases. In the study conducted by Samuela III et al., (2022), while online selling of medications offers convenience to consumers, it also poses risks that pharmacists must navigate to uphold patient safety and professional standards. Policymakers, stakeholders, and pharmacists themselves need to collaborate to establish guidelines and practices that promote the safe and responsible online selling of medications in the evolving healthcare landscap. (Samuela III et al., 2022)

Practices and Factors of Filipino Consumers Regarding Counterfeit Medicines

In the study of Isogo et al., (2022) about the awareness of Filipinos in identifying counterfeit medicines, they mentioned that most of the respondents had a moderate level of awareness regarding the recognition of fake medications. (Isuga, et al., 2022) In order to lessen the public's susceptibility to fake medications, it is still necessary to increase awareness and educate them. These results are in line with previous studies by Wagiella et al. (2020) and Mhando et al. (2019), highlighting the critical requirement for increased public education and awareness campaigns headed by medical experts to reduce the risks related to fake pharmaceuticals.

A research conducted by Pereña et.al (2022) offers valuable insights relevant to the pharmaceutical sector in the Philippines. The study underscores the significance of grasping consumer preferences, ensuring product quality, addressing potential shortages, and employing consumer education to influence purchasing behavior. Situated within the broader framework of research on consumer behavior, pharmaceutical marketing, and decision-making processes, this study focuses on determining the criteria Filipino consumers consider when purchasing over-the-counter (OTC) medicines, utilizing the Analytical Hierarchy Process (AHP). Among the 6 factors, it highlights that product quality having 36.92% stands out as the most crucial factor, followed by availability, cost, brand, recommendation from others, and advertisements for Filipino consumers when buying OTC medicines. Additionally, the research indicates a preference among Filipino consumers for branded medicines over generic options, based on the perception of higher quality associated with branded products.(Pereña et al., 2022)

Existing Technology

There are numerous published researches that are only focused on detection addressing different aspects of counterfeited over-the-counter medicine detection. In the study of Pandey, Prateek; Litoriya, Ratnesh (2020) they develop a combination of blockchain technology and RFID tags solution to secure e-health networks from counterfeit medicine penetration. (Pandey and Litoriya, 2021) Blockchain was also applied with the use of Ethereum blockchain platform and Solidity programming language to develop the counterfeit medicine authentication system, the system uses a QR Code to link medicine to a unique identifier on the blockchain and can be scanned by smartphone app.(Alam, et al., 2021). Another study used the Differential scanning calorimetry (DSC) in connection with attenuated total reflectance Fourier Transform Infrared (ATR-FTIR) for the rapid identification of fake medications through blister packaging material polymer analysis (Salim, et al., 2021). Additionally, a faster and easier method of detecting counterfeit medications has been found by combining hyperspectral sensing with a medicines spectrum database. Using a visible-near infrared hyperspectral device, this method captures the spectral signatures of medications, which are then analyzed using machine learning techniques. (Shinde, et al., 2020) These technologies address the issues of knowledge management, skill scarcity, and equipment limitations by offering workable and scalable solutions for detecting counterfeit medications.

Methodology

Research Design

The study was conducted in Metro Manila, Philippines, from January 2024. It aims to investigate how Filipino consumers purchased over-the-counter medicines and what influenced their decisions, particularly concerning counterfeit products.

Data Gathering

Data was collected using a validated questionnaire distributed online via Google Forms. The goal was to gather responses from 250 individuals in Metro Manila who were 18 years old or above, proficient in English or Filipino, and regularly purchased medicines from various sources.

Study Development

The focus was on developing the study by creating a reliable questionnaire, distributing it to participants, collecting responses, and analyzing the data obtained. This process provided insights into Filipino consumers' purchasing habits and the factors influencing their decisions regarding counterfeit medicines.

Table 1. Demographic profile

Demographic characteristics	**Frequency (%)**
Sex	
Female	138
Male	100
Prefer not to say	12
Age group	
18-24	50
25-34	87
35-44	38
45-54	50
55-64	20
65 and above	5
Educational attainment	
High School or below	38
Collegiate/Technical-Vocational Education	100
Bachelor's Degree	75
Postgraduate Degree	37
Occupation	
Employed/Self-employed	125
Unemployed	25
Student	50
Homemaker	25
Retired	12
Widowed/Divorce	12
City of residence in metro manila	
Caloocan	25
Las Piñas	12
Makati	37
Malabon	5
Mandaluyong	20
Manila	50
Marikina	17
Muntinlupa	10
Navotas	2
Parañaque	25
Pasay	12
Pasig	25
Pateros	2
Quezon City	50
San Juan	7
Taguig	20

Statistical Treatment

Once the data was collected, statistical analysis was performed using SPSS version 28. Various statistical methods, such as frequency analysis, percentage calculations, mean calculations, and standard deviation measurements, were utilized to understand purchasing practices and factors influencing Filipino consumers' decisions regarding counterfeit and substandard over-the-counter medicines.

Results and Discussion

Once the data was collected, statistical analysis was performed using SPSS version 28. Various statistical methods, such as frequency analysis, percentage calculations, mean calculations, and standard deviation measurements, were utilized to understand purchasing practices and factors influencing Filipino consumers' decisions regarding counterfeit over-the-counter medicines.

Demographic Profile

Table 1 provides a detailed breakdown of the demographic characteristics of the respondents involved in the study. It shows the distribution of respondents based on their gender, age group, educational attainment, occupation, and city of residence in Metro Manila. From the table, it's evident that the majority of respondents are female, with 138 individuals identifying as such, while 100 identified as male, and 12 preferred not to disclose their gender. Regarding age, the largest group falls within the 25-34 age range, followed closely by the 18-24 and 45-54 age groups.

Table 2. Purchasing practices

Purchasing practices	**Frequency (%)**
Consultation sources	
Friends or family	60
Online sources/Search engines, (i.e. Google, Reddit)	40
Social media (i.e. Facebook, Instagram, Twitter, etc)	25
Self-research/Self-diagnose	50
None, I do not consult anyone	15
Purchasing frequency	
Every day	5
Once a week	15
Once a month	60
Once a year	10
Whenever sick	10
Purchasing location	
Local pharmacy or drugstore	80
Supermarket/Grocery store	70
Convenience store	25
Online platforms (e.g., Lazada, Shopee)	30
Resellers (e.g., Sari-sari store)	20
Average spending in authentic OTC medicines	
Less than Php 500	50
Php 500 - Php 1,000	75
Php 1,001 - Php 2,000	75
Php 2,001 - Php 3,000	25
Php 3,001 and above	25
Factors influencing decision when purchasing OTC medicine	
Brand reputation	175
Price	200
Packaging	150
Recommendation from healthcare professionals	113
Personal past experience	163
Pharmaceutical ingredients of medicine	125
Others	0

Most respondents have completed collegiate or technical-vocational education, followed by those with a bachelor's degree, while the least common is a postgraduate degree. Occupation-wise, the majority are employed or self-employed, with students being the next largest group. The table also provides insights into the distribution of respondents across various cities in Metro Manila, with Manila and Quezon City having the highest representation. This demographic information is crucial for understanding the composition of the study sample and interpreting the findings in the context of different demographic profiles within Metro Manila.

Purchasing Practices

Table 2 offers a comprehensive overview of Filipino consumers' purchasing practices concerning over-the-counter (OTC) medicines. Firstly, it details the various sources consulted by respondents before making a purchase, with friends or family being the most commonly consulted source, followed by self-research, online sources, and social media. The table also highlights the frequency of purchases, indicating that most respondents buy OTC medicines once a month, with smaller proportions buying weekly, annually, or daily. Furthermore, it provides insights into where respondents typically make their purchases, with local pharmacies being the most common choice.

Table 3. Influencing factors

Parameters	**Frequency (%)**
Details checked on packaging	
Expiry date	70
Holographic seals	80
Barcodes	60
Tamper-evident packaging	55
Braille markings (for accessibility)	30
Watermark or special printing	35
Batch or serial number	45
Manufacturer's contact information	40
Packaging color	15
Packaging design pattern	20
None of the above	10
Most effective methods for ensuring authenticity	
Examine the expiry date	65
Check for holographic seals	75
Verify barcodes	60
Inspect tamper-evident packaging	55
Look for Braille markings (for accessibility)	30
Ensure the presence of watermark or special printing	35
Confirm the batch or serial number	45
Verify manufacturer's contact information	40
Consider packaging color	15
Examine packaging design pattern	20
Cross-check details online or through apps	35
Rely on recommendations from healthcare professionals	45
Signs/symptoms of suspicion	
Unusual taste or smell	35
Unfamiliar packaging	30
Deviation in color or texture	40
Misspelled or unclear labeling	25
Difference in tablet/capsule appearance	35
Unusual side effects	20
None of the above	10
Actions taken in case of suspicion	
Report to the store/pharmacy	40
Consult a healthcare professional	45
Discontinue use	25
Verify online or through apps	20
None of the above	10

Additionally, the table delves into respondents' average spending on authentic OTC medicines, with the majority falling within the PHP 500 to PHP 2,000 range. Lastly, it outlines the factors influencing consumers' decisions when purchasing OTC medicines, with price and brand reputation being the most influential factors, followed by packaging, personal experience, and recommendations from healthcare professionals. This detailed breakdown offers valuable insights for understanding consumer behavior in the pharmaceutical market and can inform marketing strategies and interventions to better cater to consumer needs.

Parameters

Table 3 provides a detailed breakdown of the parameters used by Filipino consumers to assess the authenticity of over-the-counter (OTC) medicines, along with the corresponding frequencies. Firstly, it outlines the specific details checked on the packaging, with a significant emphasis on expiry date and holographic seals, checked by 70% and 80% of respondents, respectively. Other checked details include barcodes, tamper-evident packaging, and manufacturer's contact information.

Additionally, the table highlights the most effective methods for ensuring authenticity, with the majority of respondents relying on examining the expiry date, checking holographic seals, and verifying barcodes. Furthermore, it identifies signs or symptoms that raise suspicion about the authenticity of OTC medicines, such as unusual taste or smell, unfamiliar packaging, and deviation in color or texture, along with the actions taken by consumers in case of suspicion, including reporting to the store/pharmacy, consulting a healthcare professional, and discontinuing use. This comprehensive overview offers insights into the strategies employed by Filipino consumers to evaluate the authenticity of OTC medicines, aiding in understanding consumer behaviors and informing interventions to combat counterfeit products effectively.

Technology

Table 4 provides detailed insights into the technological habits and preferences of Filipino consumers. It begins by listing the devices commonly used, showing that mobile phones are the most prevalent, followed by laptops, personal computers, tablets, and smartwatches. It is noteworthy that some respondents don't use these devices regularly. The table also reveals how much time respondents typically spend using these devices daily. Additionally, it explores the operating systems used, indicating that Android and iOS are the top choices, with various versions being used by respondents. Furthermore, the table highlights the internet and mobile service providers preferred by respondents, with Globe and Smart being the most popular. It also presents data on internet data consumption and speed, indicating common usage patterns and speeds. Overall, Table 4 provides valuable insights into how Filipino consumers interact with technology, which can inform businesses and policymakers in tailoring their products and services to better meet consumer needs.

Table 4. Technology

Technology Usage	**Frequency (%)**
Devices owned and used regularly	
Mobile phone	238
Tablet	75
Laptop	100
Personal Computer	125
Smartwatch	37
None	20
Average daily usage of devices	
Less than 1 hour	30
1-2 hours	45
2-3 hours	60
3-4 hours	55
More than 4 hours	60
Operating system (OS)	
Android	150
iOS	100
Version of android OS (For android users)	
Android 4.4 (KitKat)	15
Android 5.0 (Lollipop)	20

Android 5.1 (Lollipop)	25
Android 6.0 (Marshmallow)	30
Android 7.0 (Nougat)	35
Android 7.1 (Nougat)	40
Android 8.0 (Oreo)	45
Android 8.1 (Oreo)	50
Android 9.0 (Pie)	55
Android 10.0 (Q)	60
Android 11.0 (R)	65
Android 12.0 (S)	70
Android 13.0 (T)	75
I have no idea	20
Not an Android user	15
Version of iOS (For iOS users)	
iOS 1	0
iOS 2	0
iOS 3	0
iOS 4	0
iOS 5	0
iOS 6	0
iOS 7	0
iOS 8	0
iOS 9	0
iOS 10	55
iOS 11	60
iOS 12	65
iOS 13	70
iOS 14	75
iOS 15	80
iOS 16	85
iOS 17	90
I have no idea	25
Not an iOS user	20
Internet service provider (ISP)	
Converge ICT	50
Globe	60
PLDT	55
Others	15
Mobile network service provider	
ABS-CBN Mobile	25
Cherry Prepaid	20
DITO	30
Globe	70
Smart	65
Sun Cellular	25
Talk 'N Text (TNT)	15
TM	20
Average ınternet data consumption	
Less than 100 MB	25
101-250 MB	45
251-500 MB	50
501 MB - 1 GB	60
More than 1 GB	70
Average ınternet speed	
0-10 Mbps	60
11-20 Mbps	65
21-30 Mbps	55
31-40 Mbps	40
41-50 Mbps	20
More than 50 Mbps	10

The data from Tables 1 to 4 offer crucial insights into Filipino consumers' behavior regarding over-the-counter (OTC) medicines and technology usage. Table 1 depicts the demographic profile, highlighting characteristics such as age, education, occupation, and city of residence in Metro Manila, with Quezon City being the most prevalent. Table 2 delves into purchasing practices, indicating consultation sources, purchase frequency, locations, and influential factors, with price being prominent. Table 3 outlines parameters for assessing OTC medicine authenticity, including packaging details and effective methods, such as checking expiry dates and holographic seals. Table 4 provides insights into technology usage habits, revealing device ownership, operating systems, internet service providers, and more. Overall, these findings are instrumental for businesses and policymakers to tailor their offerings to meet Filipino consumers' needs effectively.

Conclusion

In conclusion, the data from Tables 1 to 4 provide a comprehensive understanding of Filipino consumers' behavior and preferences regarding over-the-counter (OTC) medicines and technology usage. From Table 1, t glean insights into the demographic profile of respondents, such as their age, education, occupation, and city of residence in Metro Manila.

Table 2 highlights their purchasing practices, indicating the sources consulted, purchase frequency, purchase locations, and factors influencing their decisions. Table 3 delves into the parameters used to assess the authenticity of OTC medicines, including details checked on packaging and the most effective methods for ensuring authenticity.

Finally, Table 4 sheds light on respondents' technology usage habits, including the devices they own, average daily usage, operating systems, internet service providers, mobile network service providers, internet data consumption, and internet speed.

From these findings, it is evident that Filipino consumers prioritize factors like price, brand reputation, and personal past experience when purchasing OTC medicines. They also rely heavily on traditional consultation sources like friends or family and local pharmacies for information and purchases. In terms of technology usage, mobile phones dominate, with Android being the preferred operating system. These insights can guide businesses, policymakers, and healthcare providers in developing targeted strategies to meet the needs and preferences of Filipino consumers, ultimately enhancing their overall experience and satisfaction with OTC medicines and technology products and services.

Recommendations

Based on the analysis of the survey data presented in Tables II, III, and IV, several recommendations emerge:

- Enhanced Consumer Education: There is a need for comprehensive consumer education programs to raise awareness of the risks of counterfeit OTC medicines. These programs should focus on educating consumers how to identify authentic products and understand the importance of purchasing from reputable sources.
- Regulatory Measures: Policymakers should consider implementing stricter regulations and enforcement mechanisms to curb the proliferation of counterfeit medicines in the market. This may include strengthening surveillance systems, increasing penalties for counterfeiters, and enhancing collaboration between regulatory agencies and law enforcement authorities.
- Promotion of Trusted Brands: Healthcare providers and pharmaceutical companies should prioritize building and maintaining strong brand reputations to instill trust and confidence among consumers. This can be achieved through transparent communication, quality assurance measures, and proactive engagement with consumers.
- Develop a technology for OTC counterfeit medicine detection: Aim to develop a prototype that utilizes emerging technologies (i.e. AI, machine learning, etc) and consumer friendly to detect the counterfeit version of popular OTC medicines.
- Collaborative Efforts: Collaboration between stakeholders, including healthcare providers, policymakers, industry organizations, and consumer advocacy groups, is essential to address the multifaceted challenges associated with counterfeit medicines. By working together, stakeholders can

leverage their respective expertise and resources to develop holistic solutions that protect consumer health and safety.

Implementing these recommendations requires concerted efforts from all stakeholders. By prioritizing consumer safety and well-being, we can mitigate the risks associated with counterfeit medicines and ensure a safer healthcare environment for all Filipino consumers in Metro Manila.

Scientific Ethics Declaration

The authors declare that the scientific ethical and legal responsibility of this research paper belongs to the authors.

Acknowledgements or Notes

* This article was presented as an oral presentation at the International Conference on Basic Sciences, Engineering and Technology (www.icbaset.net) held in Alanya/Turkey on May 02-05, 2024.

* The student researchers gratefully acknowledge the assistance and support provided by the faculty of the Electronics Engineering Department at the Polytechnic University of the Philippines, Manila, specifically to Dr. Marianito P. Gallego Jr., whose guidance was instrumental in completing this research study. We express our utmost appreciation for his steadfast support and guidance, which made this research study and subsequent conference presentation and publication possible.

References

Chaudhary, S. (2023). Health professionals and pharmacists awareness and attitude towards counterfeit medicine. *Journal of Nepal Health Research Council*, *21*(2), 219-225.

Fakayode, S. O., Bolton, B., Dassow, B., Galvez, K., & Chohan, H. (2024). Rapid screening and multicomponent quantifications of active components of oral syrup over-the-counter medications by Raman and UV–visible spectroscopy and multivariate regression analysis. *Spectrochimica Acta Part A: Molecular and Biomolecular Spectroscopy*, *305*, 123447.

Taylor, J. G., Ayosanmi, O. S., Sansgiry, S. S., & Perepelkin, J. P. (2023). Consumer likelihood to seek ınformation on otc medicines. *Pharmacy*, *11*(4), 128.

Di Crosta, A., Ceccato, I., Marchetti, D., La Malva, P., Maiella, R., Cannito, L., & Di Domenico, A. (2021). Psychological factors and consumer behavior during the COVID-19 pandemic. *PloS one*, *16*(8), e0256095.

Gray, N. J. (2011). Artical 7. *2*, 76–86.

Hamdan, I. M. (2023). The perceived influence of COVID-19 lockdown on the circulation of counterfeit drugs and medical supplies through the electronic market. *Journal of Pharmaceutical Health Services Research*, *14*(1), 14-19.

Isuga, J. V. D., Cruz, C. M. D. D., Urriza, J. T., Abas, L. G., Cruz, E. M. D. D., Del Celestine, B. J., & Andal, M. S. (2022). Extent of filipinos' awareness in ıdentifying counterfeit medicines: a quantitative cross-sectional study. *GSC Advanced Research and Reviews*, *12*(3), 94-108.

Pathak, R., Gaur, V., Sankrityayan, H., & Gogtay, J. (2023). Tackling counterfeit drugs: the challenges and possibilities. *Pharmaceutical Medicine*, *37*(4), 281-290.

Pandey, P., & Litoriya, R. (2021). Securing e-health networks from counterfeit medicine penetration using blockchain. *Wirel. Pers. Commun.*, *117*(1), 7–25.

Pereña, J. R. O., Chan, J. K. C., Altes, G. C., Redi, A. A. N. P., Persada, S. F., Ardiansyahmiraja, B., Prasetyo, Y. T., & Young, M. N. (2022). Deter*mining filipino consumers' criteria for purchasing over-the- counter (otc) medicines using Analytical Hierarchy Process (AHP). 14*, 978–981.

Salim, M. R., Widodo, R. T., & Noordin, M. I. (2021). Proof-of-concept of detection of counterfeit medicine through polymeric materials analysis of plastics packaging. *Polymers (Basel)*, *13*(13), 1–12.

Shinde, S. R., Bhavsar, K., Kimbahune, S., Khandelwal, S., Ghose, A., & Pal, A. (2020). Detection of counterfeit medicines using hyperspectral sensing. *Proc. Annu. Int. Conf. IEEE Eng. Med. Biol. Soc. EMBS*, 6155–6158.

Taylor, J. G., Ayosanmi, S., & Sansgiry, S. S. (2023). Consumer impressions of the safety and effectiveness of OTC medicines. *Pharmacy*, *11*(2), 51.

Taylor, J. G., Ayosanmi, O. S., Sansgiry, S. S., & Perepelkin, J. P. (2023). Consumer likelihood to seek ınformation on otc medicines. *Pharmacy*, *11*(4), 128.

Author Information

Marianito Gallego Jr.
Polytechnic University of the Philippines
Sta. Mesa, Manila, Philippines
Contact e-mail: *mpgallegojr@pup.edu.ph*

Daniel Caparro
Polytechnic University of the Philippines
Sta. Mesa, Manila, Philippines

Raeselyn Macorol
Polytechnic University of the Philippines
Sta. Mesa, Manila, Philippines

Treblig John Manalastas
Polytechnic University of the Philippines
Sta. Mesa, Manila, Philippines

Charisse Anne Olaivar
Polytechnic University of the Philippines
Sta. Mesa, Manila, Philippines

To cite this article:

Gallego Jr, M., Caparro, D., Macorol, R., Manalastas, T. J. & Olaivar, C. A. (2024). A quantitative study into purchasing practices and influential factors among Filipino consumers regarding counterfeit over-the-counter medicines in Philippines. *The Eurasia Proceedings of Science, Technology, Engineering & Mathematics (EPSTEM), 28,* 123-133.

The Eurasia Proceedings of Science, Technology, Engineering & Mathematics (EPSTEM)
ISSN: 2602-3199

The Eurasia Proceedings of Science, Technology, Engineering & Mathematics (EPSTEM), 2024

Volume 28, Pages 134-140

ICBASET 2024: International Conference on Basic Sciences, Engineering and Technology

Effect of Various Treatment and Drying Methods of Blood Meal Additive on Fresh State Properties of Grouting Materials

Emine Ozdogru
Yildiz Technical University

Nabi Yuzer
Yildiz Technical University

Afife Binnaz Hazar-Yoruc
Yildiz Technical University

Abstract: Grouting is one of the most commonly preferred repair methods used for historic buildings exposed to various deteriorating environmental conditions during their life span. Being that grouting is an irreversible method, it is crucial to determine the original material properties of the historic building to be repaired. In the literature, it is revealed that protein sources have long been used as popular additives to enhance the physical, mechanical, and durability properties of buildings. Specifically, blood additive has been known to have a potential to benefit as a water resisting or air-entraining admixture. Nonetheless, there is a lack of information regarding the use of animal blood in grouting materials, while the impact of blood additive on the properties of lime or cement-based mortars has been investigated recently. In this study, the impact of blood meal incorporation into the lime-based grouting material is discussed in terms of its fresh properties, i.e., fluidity, penetration, and stability. The blood meal samples to be tested were treated with various chemicals to enhance its performance and dried by various drying mechanisms. According to the test results, it was determined that the mixture containing blood meal treated with tri sodium citrate and dried in the drying oven met the requirements of all kinds of fresh state tests and had the potential to be used as a repair material.

Keywords: Civil engineering, Historical building, Grouting, Blood additive

Introduction

Damage in the historic building is an inherent situation due to their exposure to various deteriorating effects, which can amount to hundreds of years since the period they were constructed. Hence, the repair processes have a crucial role in sustaining the cultural identity of the society through historical buildings. There are different methods for repairing the cracks that occurred due to environmental, internal, or man-made sources (Feilden, 2003). The repair process begins with the determination and investigation of the damaged part of the building, and subsequently, the most proper repairing method and mixture for the repairing material are decided. In the repairing process, the original material properties need to be revealed in order for the repairing material to represent the mechanical, physical, microstructural, and durability properties. The repairing method and mixture of the repairing material have a critical role since the repairing is an irreversible process, and once the repairing method or mixture has an inconformity with the original material, it may bring about more severe damages to the building.

Grouting is one of the most commonly used repairing methods for consolidating masonry structures and is generally beneficial for strengthening and/or providing the structural integrity of buildings that have damaged through their structural members (Miltiadou-Fezans & Tassios, 2022; Penelis et al., 1989; Militadou, 1985).

Besides, it is reported that the grouting method is used for the consolidation of the decorative elements as well (Bicer-Simsir et al., 2009; Bicer-Simsir & Rainer, 2013). The mixture designed as a grouting material consists of binder, water, and, if any, additives. Before the on-site application, the fresh state properties of the mixtures need to meet the requirements of the fluidity, penetrability, and volume stability criteria, which are called "injectability properties" as a whole (Miltiadou-Fezans & Tassios, 2013; Jorne et al., 2015). In the literature, researchers investigate the fresh state properties of the grouting materials with various mixture proportions or effects of introducing various additives (Bras & Henriques, 2011; Miltiadou-Fezans & Tassios, 2012; Miltiadou-Fezans & Tassios, 2013a; Miltiadou-Fezans & Tassios, 2013b; Baltazar et al., 2014; Jorne et al., 2014).

The obligation of compatibility with the original material properties imposes the use of lime as a binder in the grouting materials since cement has quite distinctive mechanical, physical, chemical, and durability properties that are incompatible with the properties of the original material (Baltazar et al., 2019). Nonetheless, both air lime and hydraulic lime have various deficient properties to escalate by benefiting organic or inorganic-based additives and/or admixtures. Previous studies have shown that organic additives were frequently employed during the construction of historic buildings during that time (Li & Zhang, 2018; Pahlavan et al., 2018; Elert et al., 2019; Zhang et al., 2021). Specifically, blood additive is reported as an additive used in historic buildings in ancient times, and the reproductions of the mixtures showed that the blood additive escalates the physical and durability properties of the mixtures (Pegoretti, 1843; Brey, 1844; Zhao et al., 2015).

The prominent properties provided by the blood additive encouraged the research conducted to investigate the impact of blood additive on the physical, mechanical, and durability properties of both cement and lime-based mortars, and it is shown that the blood additive enhances the water resistance and durability to freeze-thaw effect while diminishing the compressive and flexural strength of the mortar (Jasiczak & Zielinski, 2006; Xu et al., 2011; Fang et al., 2015; Dinc-Sengonul et al., 2023; Yuzer et al., 2023). There is, however, a knowledge gap about the characteristics of the lime-based grouting materials with blood additive in both their fresh and hardened states.

In this research, the fresh state properties, i.e., fluidity, penetrability, and volume stability of the blood meal containing lime-based grouting materials, are investigated to provide an insight into the fresh state applicability of the high-performance grouts in terms of their hardened state. The blood meal additives are treated with various chemicals to escalate the performance of the natural hydraulic lime based grouting materials and dried by various drying mechanisms.

Material and Methodology

The binder of the grouting materials in the scope of the experimental program is natural hydraulic lime (NHL 5), which is reported as the most appropriate binder for the repairing works. Animal blood that remains as waste during the slaughtering process is the raw material for blood meal, a commercially available product that is used as a feed for animals. The blood meal obtained after the heat treatment, drying, and grinding processes is utilized as an additive in the grouting material. The chemicals employed to treat the blood meal are stearic acid, citric acid, and tri sodium citrate. Besides, a surface-active organic-based sorbitan monooleate is used to adjust the foaming capacity of the mixtures.

The treatment process begins with preparing the treatment solutions, the proportions of which were determined by considering the preliminary test results and given in Table 1. The blood meal with a particle size of 100 μm is added to the solution, and the mixture is subjected to one of the three different drying methods: drying oven, freeze dryer, or spray dryer. After the drying process, treated blood meal samples are ground and used as an additive in the grouting materials.

Table 1. Proportions of treatment solutions

Treatment solution	Chemical	Water
Tri sodium citrate	0.1	1
Citric acid	0.5	1
Stearic acid	0.03	1

The grouting material mixing procedure is referenced in previously conducted research and consists of the following steps: (i) natural hydraulic lime and water are mixed for 10 minutes at 800 rpm; (ii) blood meal samples and, if any, sorbitan monooleate are added while the mixing continues; and (iii) the ultimate mixture is

mixed for another 3.5 minutes. The denotation of the samples and mixture proportions is given in Table 2. The freshly mixed grouting materials were subjected to injectability tests, i.e., fluidity, penetrability, and volume stability. The experimental research was designated as the mixtures were subjected to the Marsh cone test, sand column test, and bleeding test immediately after the mixing procedure was completed, respectively.

Table 2. Mixture proportions

Mixture	Mixture Proportions				Blood Meal Treatment Solution and Drying Method	
	NHL 5	Water	Blood Meal	Sorbitan Monooleate	Treatment	Drying
T-O	1	0.8	0.01	0	Tri sodium citrate	Drying oven
C-O	1	0.8	0.01	0	Citric acid	Drying oven
S-O	1	0.8	0.01	0	Stearic acid	Drying oven
T-O-S	1	0.8	0.01	0.01	Tri sodium citrate	Drying oven
C-O-S	1	0.8	0.01	0.01	Citric acid	Drying oven
S-O-S	1	0.8	0.01	0.01	Stearic acid	Drying oven
T-F-S	1	0.8	0.01	0.01	Tri sodium citrate	Freeze dryer
C-F-S	1	0.8	0.01	0.01	Citric acid	Freeze dryer
S-F-S	1	0.8	0.01	0.01	Stearic acid	Freeze dryer
T-D-S	1	0.8	0.01	0.01	Tri sodium citrate	Spray dryer
C-D-S	1	0.8	0.01	0.01	Citric acid	Spray dryer
S-D-S	1	0.8	0.01	0.01	Stearic acid	Spray dryer

Fluidity

One of the basic characteristics of a grouting material is having adequate fluidity to reach deeply into the cracks by flowing along the sinuous path. To provide this characteristic, the water/binder ratio and the amount of chemical additive used to adjust the fluidity of the grouting material, as well as the mixing duration and speed, are important parameters (Miltiadou-Fezans & Tassios, 2022).

In order to evaluate the fluidity of the grouting materials, Marsh funnel test was conducted according to the procedure given in ASTM D6910 (ASTM D6910, 2010). Since any requirement for the evaluation of fluidity performance is not given in the relevant standard, the criteria given in the referenced research are considered. According to the literature, 500 mL of the grouting material should flow in 45 seconds to have adequate fluidity (Kalagri et al., 2010; Miltiadou-Fezans & Tassios, 2012).

Penetration

The main principle of the grouting process is to provide structural integrity and strengthen the structure by filling the discontinuities, such as voids and cracks, through the structure, and it is crucial for the grouting material to pass through the narrowest discontinuities. Accordingly, the penetrability performance of the grouting material is measured according to the sand column test conducted according to BS EN 1771 by generating a medium with maximum and minimum grain sizes determined considering the crack widths to be grouted (BS EN 1771, 2004). In this experimental research, the granulometry of the grains used to model the cracks and voids was determined to be 2.0–4.0 mm. The elapsed time until the grouting material reaches the upper surface of the sand column is denoted as T_{36}, and this duration should be less than 50 s for an effective grouting application (Kalagri et al., 2010; Miltiadou-Fezans & Tassios, 2012).

The evaluation criteria given in the relevant standard label the grouting material as (i) “applicable” if the tested material passes through the column filled with sand and 20 mL of excessive material is collected; (ii) “feasible” if the sand column is passed through by grouting material but no excessive material is collected; and (iii) “difficult” if the sand column fails to be passed through by the grouting material (BS EN 1771, 2004).

Volume Stability

Being that the grouting material is a suspension with a high water/binder ratio to meet the previously explained fresh state requirements, segregation and bleeding are always the points in question. Limiting the bleeding of the

grouting material in the first 24 hours is critical to providing the flow of the grouting material through the voids and cracks without blocking them by precipitating or having a severe layering tendency.

To determine the volume stability of the grouting material, the procedure given in ASTM C940 is followed, and the bleeding is calculated by the formula given, in which the terms VW and Vg represent the volume of the water accumulated on top of the grouting material at the end of 24 hours and the total volume of the grouting material to be subjected to the bleeding test, respectively (ASTM C940, 2010). The bleeding value of the grouting material after 24 hours should be less than 5% for an effective grouting process (Bras & Henriques, 2012).

$$Bleeding(\%) = \frac{V_W}{V_g} \times 100 \quad (1)$$

Results and Discussion

The results of the fluidity, penetrability, and stability tests, which are evaluated as components of the injectability properties of the fresh-state grouting materials, are given in Table 3.

Table 3. Injectability test results of the mixtures

Mixture	Fluidity		Penetrability		Volume Stability	
	Flow time (s)	Evaluation	T_{36} (s)	Evaluation	Bleeding (%)	Evaluation
T-O	134	Not applicable	-	Difficult	0	Applicable
C-O	150	Not applicable	-	Difficult	2.1	Applicable
S-O	80	Not applicable	-	Difficult	0	Applicable
T-O-S	34	Applicable	6	Easy	0	Applicable
C-O-S	39	Applicable	6	Easy	7.8	Not applicable
S-O-S	50	Not applicable	-	Difficult	0	Applicable
T-F-S	62	Not applicable	-	Difficult	0	Applicable
C-F-S	40	Applicable	7	Easy	6.3	Not applicable
S-F-S	60	Not applicable	-	Difficult	0	Applicable
T-D-S	49	Not applicable	-	Difficult	0	Applicable
C-D-S	40	Applicable	6	Feasible	5.4	Not applicable
S-D-S	59	Not applicable	-	Difficult	0	Applicable

According to the flow durations of the mixtures without sorbitan monooleate, it is obvious that, regardless of the treatment type, the fluidity requirements are not met. Accordingly, it is an obligation to use an admixture that contributes to the fluidity performance of the grouting material. The comparison of the fluidity performances of each of the T-O, C-O, and S-O mixtures with and without sorbitan monooleate revealed that the sorbitan monooleate shortened the flow time. Hence, it is deduced that sorbitan monooleate is an effective admixture that provides the required fluidity to the mixtures.

According to the visual inspection, the foaming capacity of the blood meal varies for each of the treatment methods. Besides, it is seen that the mixtures without sorbitan monooleate, especially the C-O mixture, generate a significantly greater amount of foam, which has an impact on the fluidity of the mixture. After sorbitan monooleate is added, the mixtures including stearic acid-treated blood meal show noticeably greater foaming capacity relative to other treatments, regardless of the drying method, while the ones with citric acid show the least foaming capacity, on the contrary of the mixture without sorbitan monooleate.

For all the drying methods, grouting mixtures, including citric acid-treated blood meal, show applicable flow performances, while the shortest flow time is seen in the mixture with tri sodium citrate-treated blood meal dried in a drying oven. The effect of treated blood meal's drying method on the fluidity of grouting material shows no trend and varies for each of the blood meal treatment methods, while the overall performance of the mixtures, including blood meal dried in a drying oven, has the shortest flow time relative to the other drying methods when evaluated individually for each of the treatment methods.

The penetrability and fluidity performances of the mixtures show that these two phenomena are strongly related to each other. The mixtures that failed to meet the requirements of the fluidity test are evaluated as difficult to penetrate through the cracks according to the sand column performance, and this argument is valid for the

mixtures without sorbitan monooleate as well. Amongst other drying methods, grouting materials with blood meal dried in a drying oven after treatment shows more desirable performances than the others. It is also concluded that the grouting materials subjected to citric acid treatment show better performances than the other treatment methods.

Lastly, the bleeding performances of the mixtures show that the grouting materials with blood meal treated with either tri sodium citrate or stearic acid completely prevent the bleeding and layering tendency. It is seen that the drying method does not have a strong impact on the bleeding performance of the mixtures, including either tri sodium citrate or stearic acid. Moreover, mixtures including either tri sodium citrate or citric acid-treated blood meal result in a bleeding ratio of 0%, regardless of the sorbitan monooleate inclusion, in spite of the fact that the contribution of the sorbitan monooleate admixture to the fluidity of the mixtures was seen as a result of the Marsh cone test. Citric acid-treated blood meal-added grouting materials, however, show significant bleeding, which exceeds the limit value stated by the relevant standard.

Conclusion

- The fluidity values of the treated blood meal including grouting mixtures do not meet the requirements. Sorbitan monooleate admixture significantly shortened the flow time.
- The fluidity and penetrability characteristics of the mixtures are strongly related to each other.
- The foaming capacity has a strong impact on the fluidity and penetrability performance of the mixtures, and it is affected by the existence of sorbitan monooleate and the relationship between the treatment method of the blood meal and sorbitan monooleate.
- The favorable fluidity and penetrability performances of the C-O-S, C-F-S, and C-D-S mixtures are associated with the limited foaming capacity, while the ineffective bleeding performances are related to the possible weak adhesion of the mixtures.
- Amongst all the mixtures, the T-O-S mixture shows the most successful performance in terms of fluidity, penetrability, and volume stability by satisfying the requirements of the related limit values. Thus, this mixture can be used as a high-performance grouting material.

Recommendations

In light of the above findings, various blood meal ratios and the effect of the blood meal additive on the hardened state properties, i.e., physical, mechanical, and durability properties, should be discussed in further research. Additionally, the mixtures having the most desirable properties in terms of fresh and hardened state should be used in on-site grouting applications.

Scientific Ethics Declaration

The authors declare that the scientific ethical and legal responsibility of this article published in EPSTEM journal belongs to the authors.

Acknowledgements or Notes

* This article was presented as oral presentation at the International Conference on Basic Sciences, Engineering and Technology (www.icbaset.net) held in Alanya/Turkey on May 02-05, 2024.

* The authors gratefully acknowledge the financial assistance of the Scientific and Technical Research Council (TUBITAK) of Turkey provided under projects: 221M279.

References

ASTM. (2010). *Standard test method for expansion and bleeding of freshly mixed grouts for preplaced-aggregate concrete in the laboratory (ASTM C940-10).* Retrieved from https://www.astm.org/c0940-10.html

ASTM. (2010). *Standard test method for marsh funnel viscosity of clay construction slurries ASTM D6910.* Retrieved from https://www.astm.org/d6910-04.html

Baltazar, L. G., Henriques, F. M. A., Jorne, F., & Cidade, M. T. (2014). Combined effect of superplasticizer, silica fume and temperature in the performance of natural hydraulic lime grouts. *Construction and Building Materials*, *50*, 584–597.

Baltazar, L., Henriques, F., & Cidade, M. (2019). Rheology of natural hydraulic lime grouts for conservation of stone masonry—influence of compositional and processing parameters. *Fluids*, *4*(1), 13.

Bicer-Simsir, B., Griffin, I., Palazzo-Bertholon, B., & Rainer, L. (2009). Lime-based injection grouts for the conservation of architectural surfaces. *Studies in Conservation*, *54*(sup1), 3–17.

Bras, A., & Henriques, F. M. A. (2011). Natural hydraulic lime based grouts – the selection of grout injection parameters for masonry consolidation. *Construction and Building Materials*. *26*(1), 135-144.

Brey. (1843). *Dizionario enciclopedico tecnologico-popolare* (5th ed.). G. Chiusi, Milano

BS EN. (2004). *Products and systems for the protection and repair of concrete structures - Test methods - Determination of injectability using the sand column test. (BS EN 1771).* Retrieved from https://www.document-center. com/standards/show/SS-EN-1771

Dinc-Sengonul, B., Yuzer, N., Boylu, S., Erdil, K., & Gudendede, Y. A. (2023). Utilization of waste animal blood as an additive in hydraulic lime-based mortars. *Construction and Building Materials*, *400*, 132909.

Elert, K., García- Sánchez, R. M., Benavides-Reyes, C., & Linares- Ordóñez, F. (2019). Influence of animal glue on mineralogy, strength and weathering resistance of lime plasters. *Construction and Building Materials*, *226*, 625–635.

Fang, S., Zhang, K., Zhang, H., & Zhang, B. (2015). A study of traditional blood lime mortar for restoration of ancient buildings. *Cement and Concrete Research*, *76*, 232–241.

Feilden, B. M. (2003). *Conservation of historic building* (3rd ed.). Butterworths Scientific.

Jasiczak, J., & Zielinski, K. (2006). Effect of protein additive on properties of mortar. *Cement and Concrete Composites*, *28*(5), 451–457.

Jorne, F., Henriques, F. M. A., & Baltazar, L. G. (2015). Influence of superplasticizer, temperature, resting time and injection pressure on hydraulic lime grout injectability, correlation analysis between fresh grout parameters and grout injectability. *Journal of Building Engineering*, *4*, 140–151.

Jorne, F., Henriques, F. M., & Baltazar, L. G. (2014). Injection capacity of hydraulic lime grouts in different porous media. *Materials and Structures*, *48*(7), 2211–2233.

Kalagri, A., Miltiadou-Fezans, A., & Vintzileou, E. (2010). Design and evaluation of hydraulic lime grouts for the strengthening of stone masonry historic structures. *Materials and Structures*, *43*(8), 1135–1146.

Li, J., & Zhang, B. (2018). Why ancient Chinese people like to use organic–inorganic composite mortars? — application history and reasons of organic–inorganic mortars in ancient chinese buildings. *Journal of Archaeological Method and Theory*, *26*(2), 502–536.

Miltiadou-Fezans, A., & Tassios, T. P. (2013a). Penetrability of hydraulic grouts. *Materials and Structures*, *46*(10), 1653–1671.

Miltiadou-Fezans, A., & Tassios, T. P. (2013b). Stability of hydraulic grouts for masonry strengthening. *Materials and Structures*, *46*(10), 1631–1652.

Miltiadou-Fezans, A., & Tassios, T. P. (2012). Fluidity of hydraulic grouts for masonry strengthening. *Materials and Structures*, *45*(12), 1817–1828.

Miltiadou-Fezans, A., & Tassios, T. P. (2022). *Mix-design and application of hydraulic grouts for masonry strengthening*. Springer.

Pahlavan, P., Manzi, S., Sansonetti, A., & Bignozzi, M. C. (2018). Valorization of organic additions in restorative lime mortars: Spent cooking oil and albumen. *Construction and Building Materials*, *181*, 650–658.

Pegoretti, G. (1863). *Manuale pratico per l'estimazione dei lavori architet- tonici, stradali, idraulici e fortificazione* (2nd ed.). Presso l'Editore libraio Angelo Monti.

Penelis, G., Karaveziroglu, M., & Papayann, I., (1989). Grouts for repairing and strengthening old masonry structures. In *Structural repair and maintenance of historical buildings*. (pp. 179–188). Computational Mechanics Publications.

Xu, J. G., Zhao, T. J., Zhang, P., & Jiang, R. (2011). Influence of ox blood on water absorption of and chloride penetration into concrete. *Advanced Materials Research*, *261*, 496–500.

Yuzer, N., Ozdoru, E., Dinc -Sengonul, B., Turk, O. K., & Yuzer, M. O., (2023). Atık sıvı kanın cimento esaslı harclarda katkı malzemesi olarak degerlendirilmesi. *Beton 2023 Kongresi* (pp.475-484).

Zhang, K., Wang, L., Tie, F., Yang, F., Liu, Y., & Zhang, Y. (2021). A preliminary study on the characteristics of lime-based mortars with egg white addition. *International Journal of Architectural Heritage*, *16*(8), 1184–1198.

Zhao, P., Jackson, M. D., Zhang, Y., Li, G., Monteiro, P. J., & Yang, L. (2015). Material characteristics of ancient Chinese lime binder and experimental reproductions with organic admixtures. *Construction and Building Materials*, *84*, 477–488.

Author Information

Emine Ozdogru
Yildiz Technical University
Istanbul/Turkiye
Contact e-mail: *eozdogru@yildiz.edu.tr*

Nabi Yuzer
Yildiz Technical University
Istanbul/Turkiye

Afife Binnaz Hazar- Yoruc
Yildiz Technical University
Istanbul/Turkiye

To cite this article:

Ozdogru, E., Yuzer, N. & Hazar-Yoruc, A.B. (2024). Effect of various treatment and drying methods of blood meal additive on fresh state properties of grouting materials. *The Eurasia Proceedings of Science, Technology, Engineering & Mathematics (EPSTEM), 28,* 134-140.

The Eurasia Proceedings of Science, Technology, Engineering & Mathematics (EPSTEM)
ISSN: 2602-3199

The Eurasia Proceedings of Science, Technology, Engineering & Mathematics (EPSTEM), 2024

Volume 28, Pages 141-147

ICBASET 2024: International Conference on Basic Sciences, Engineering and Technology

Assessing Inventory Management Indicators in Chain Pharmacy Stores: An Importance – Performance Analysis

Atatika Pentrakan
Mahidol University

Rawinkhan Srinon
Mahidol University

Abstract: Effective inventory management is essential for the successful operation of chain pharmacy stores. As an integral component of chain management, its purpose is to oversee the movement of products from manufacturers to warehouses, and ultimately to patients. This study aims to investigate 13 key performance indicators sourced from a comprehensive literature review on inventory management. The primary objectives include analyzing the relationships among these indicators and evaluating their relative importance. The research adopts a qualitative approach, employing survey as the chosen method. The study participants are comprised of 18 managers or branch heads affiliated with chain drug stores in Thailand. The research employs the Importance Performance Analysis (IPA) tool to interpret the findings, with the objective of enhancing work quality. From the results obtained, the summary indicates a need to assess the indicators presently utilized in managing chain stores and to identify additional areas for performance enhancement. The results highlight specific areas requiring attention due to their high importance coupled with suboptimal performance. These areas include monthly stock adjustment and product shortages. Conversely, the study reveals aspects where managers excel and are considered significant, such as safety stock, inventory turnover, product availability, replenishment frequency, and Items on shelf. Additionally, our study involves acknowledging the significance of existing indicators in guiding store management practices while also recognizing the necessity of addressing logistics supplementary issues to develop overall performance.

Keywords: Logistics engineering, Chain pharmacy store, Importance – performance analysis

Introduction

The pharmacy store, or drug store, serves as a vital primary care facility within the healthcare ecosystem. It functions as a crucial channel for delivering essential healthcare services and dispensing pharmaceutical products to individuals with primary illnesses residing in nearby communities. The distinguishing characteristics of a pharmacy store encompass its dual role: generating sustainable profitability for long-term business expansion (Sanchez-Ruiz et al., 2018) while fulfilling its integral role within the broader healthcare system, adhering to the ethical principles inherent in the pharmacy profession.

The market for these medications is experiencing significant growth, propelled by increasing public awareness of general health issues and advancements in pharmaceutical and healthcare technologies. The global revenue within the OTC pharmaceuticals market was also anticipated to exhibit a continuous increase from 2024 to 2029, amounting to a total of $54.4 billion (representing a 27.01 percent growth). Following the eleventh consecutive year of growth, it is estimated that the indicator will attain $255.83 billion, thus marking a new peak in 2029. It is noteworthy that the revenue within the OTC pharmaceuticals market has demonstrated consistent growth over recent years (Statista, 2024). According to data from the Statistics of Thailand, the OTC

pharmaceuticals market in the country was also valued at $137.5 million in 2022, with an anticipated CAGR of 5.36% over the same period, reaching $208.8 million by 2030, allows the sale of non-prescription drugs, which are medications that can be obtained without a prescription (Insight10, 2023). This trend underscores the increasing importance of accurate inventory management for organizations.

Effective inventory management holds paramount importance for enterprises, particularly chain store pharmacies. Consequently, chain store pharmacies typically designate a branch administrator, whether a manager or branch head, to oversee inventory management aligned with the organization's key performance indicators (KPIs). The role of the branch manager or branch head encompasses vigilant supervision of product inventory to prevent shortages or surpluses. This involves managing warehouse operations and ensuring alignment between actual stock levels and the inventory management system (Pentrakan et al., 2023), while proactively seeking solutions to mitigate discrepancies or minimize their occurrence. Such measures enhance competitiveness within the business sector (Khan et al., 2019).

Numerous studies have highlighted the challenge of high inventory management and storage costs faced by pharmacy stores (Farmaciawaty et al., 2020). Inefficient inventory management can result in either excess stock or shortages of essential medicines. The operational nature of pharmacy stores is typically categorized into standalone establishments and chain stores, with the latter showing a propensity for further expansion due to corporate branch expansion policies. OTC drug sales through pharmacies constitute approximately 20% of the total drug market value, indicating the necessity for drug stores to maintain a diverse range of products to adequately serve their clientele while exercising cost control (Krungsri Organization, 2022). Hence, effective inventory management and KPIs demand careful consideration. This is essential for preserving the satisfaction of service recipients and bolstering competitiveness within the business sector.

In our investigation, we directed our attention towards examining the KPIs outlined in the literature review research conducted by MacAs et al. (2021). These encompass a range of facets, such as the actual inventory and its integration with the company's information system and stock adjustment (Cui et al.,2017), inventory levels (Zhang & Rajaram, 2017) occurrences of shortages of scarcities (Zhou & Piramuthu, 2015), procedures for product reordering and replenishment (Solti et al., 2018), service levels (Hahn & Leucht, 2015), product availability (Ishfaq et al., 2016), excessive inventory (Sabir & Farooquie, 2018), items stocked on shelves (Choi, 2016), returns (Qin & Zhong, 2017), Inventory cost (Kwan et al., 2019) and Inventory turnover (Kasiri, 2016). These indicators are pertinent to the operations of drug chain stores, and our inquiry sought to identify the key indicators and their corresponding performance directions within this context (Martilla & James, 1977).

Method

This study utilized a qualitative design, employing survey as the primary method of data collection. The participants in our study comprise branch leaders or branch managers across various chain drug stores in Thailand, individuals vested with the authority to oversee product replenishment for each branch and responsible for managing the branch's financial status, encompassing inventory costs. Guided by Macmillan's principles (Macmillan, 1971), which advocate for the collection of data and the distillation of knowledge from a panel of experts in relevant domains, a sample size of 17 individuals or more is deemed adequate to ensure reliable qualitative findings. This sample size facilitates a focused exploration of research issues pertinent to both the current study and those anticipated in the future.

We employed a simple method to select our sample and conducted survey via online from February to March, 2024 using a structured questionnaire format, ensuring consistency by posing the same set of questions to each participant. Invitations were extended to experts, providing them with comprehensive information to aid in their decision-making process regarding participation. Detailed instructions, including procedures for data recording and storage, were provided to ensure informed consent. Furthermore, the reliability of our research instruments was assessed by three experts, who scrutinized the draft survey questions. Subsequent adjustments were made based on their feedback, resulting in the finalization of the survey questions to be utilized in our study. The survey is estimated to last approximately 30 minutes, excluding any recording (audio or video). This will adopt a structured format, fostering a friendly atmosphere and offering flexibility in responding to questions.

In this study, descriptive statistics were employed to analyze the data obtained from the responses to each question, whereby percentages and standard variation were calculated. Subsequently, content analysis was conducted. Furthermore, the scores provided by respondents for each answer were utilized to compute the

average and standard deviation values. These statistical measures were then used to construct an Importance-Performance Analysis (IPA) chart, facilitating a concise summary of the findings, as shown in Figure 1.

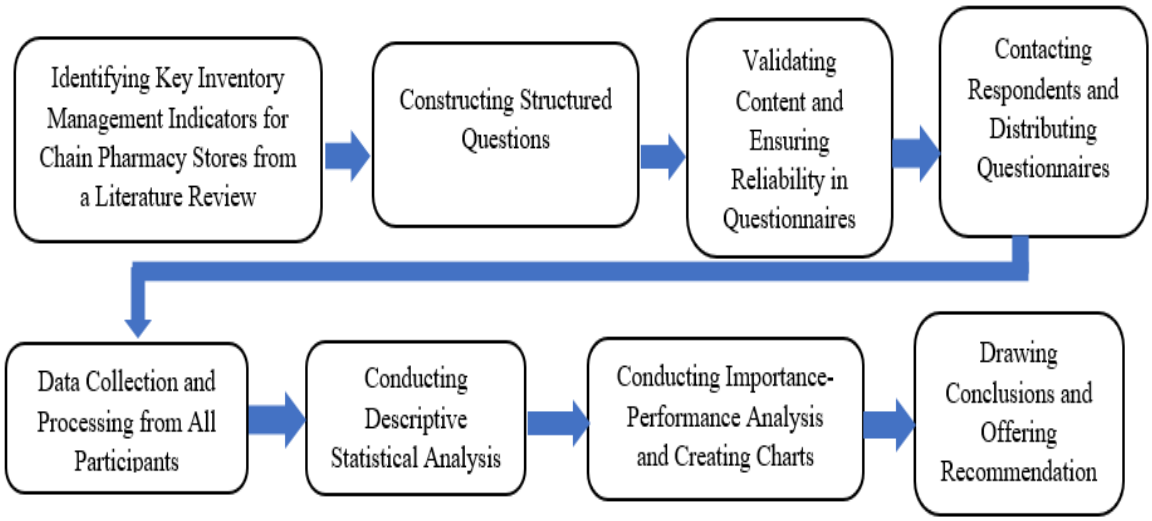

Figure 1. Methodology process

Results and Discussion

A total of 18 branch managers or store heads (average experience: 8 years) were asked to assess the significance of performance indicators and their respective performance levels. They were tasked with rating each indicator on a scale as follows:

A score of 5 signifies the highest importance/performance with respect to the indicators,
A score of 4 indicates a very significant/a high level of performance
A score of 3 suggests moderate importance/moderate performance
A score of 2 denotes lower importance/lower performance
A score of 1 represents the least importance/least performance concerning the indicators.

The descriptive statistics findings encompassed the mean ($\bar{X}$), standard deviation (S.D.) and mode, with the results tabulated in Table 1.

Table 1. Descriptive statistics of study

Indicators	**Importance**			**Performance**		
	$\bar{X}$	**S.D.**	**Mode**	$\bar{X}$	**S.D.**	**Mode**
Inventory accuracy (IA)	3.94	0.80	4.00	3.89	1.02	4.00
Day on hand (DOH)	4.44	0.78	5.00	4.06	0.73	4.00
Inventory turnover (IT)	4.28	0.75	5.00	4.17	0.51	4.00
Shortage of scarcity (ST)	4.33	0.84	5.00	3.78	1.11	4.00
Product availability (PA)	4.44	0.92	5.00	4.00	0.69	4.00
Over stock (OS)	4.06	0.87	4.00	3.50	1.10	4.00
Inventory cost (IC)	4.00	0.84	4.00	3.94	0.87	4.00
Replenishment frequency (RF)	4.17	0.79	5.00	3.83	0.71	4.00
Adjust stock (AS)	4.17	0.99	5.00	3.50	1.29	4.00
Items on shelf (IOS)	4.22	0.81	5.00	3.83	0.71	4.00
Return product from customer (RC)	3.89	1.02	5.00	3.61	1.04	4.00
Return product from pharmacy store (RP)	3.89	1.02	5.00	3.61	1.04	4.00
Safety Stock (SS)	4.22	0.88	5.00	4.11	0.90	4.00

Based on these results, we subsequently utilized Importance-Performance Analysis (IPA) to pinpoint the indicators requiring the most substantial improvements or those that could potentially undergo adjustments without significantly compromising overall quality, as shown in Figure 2.

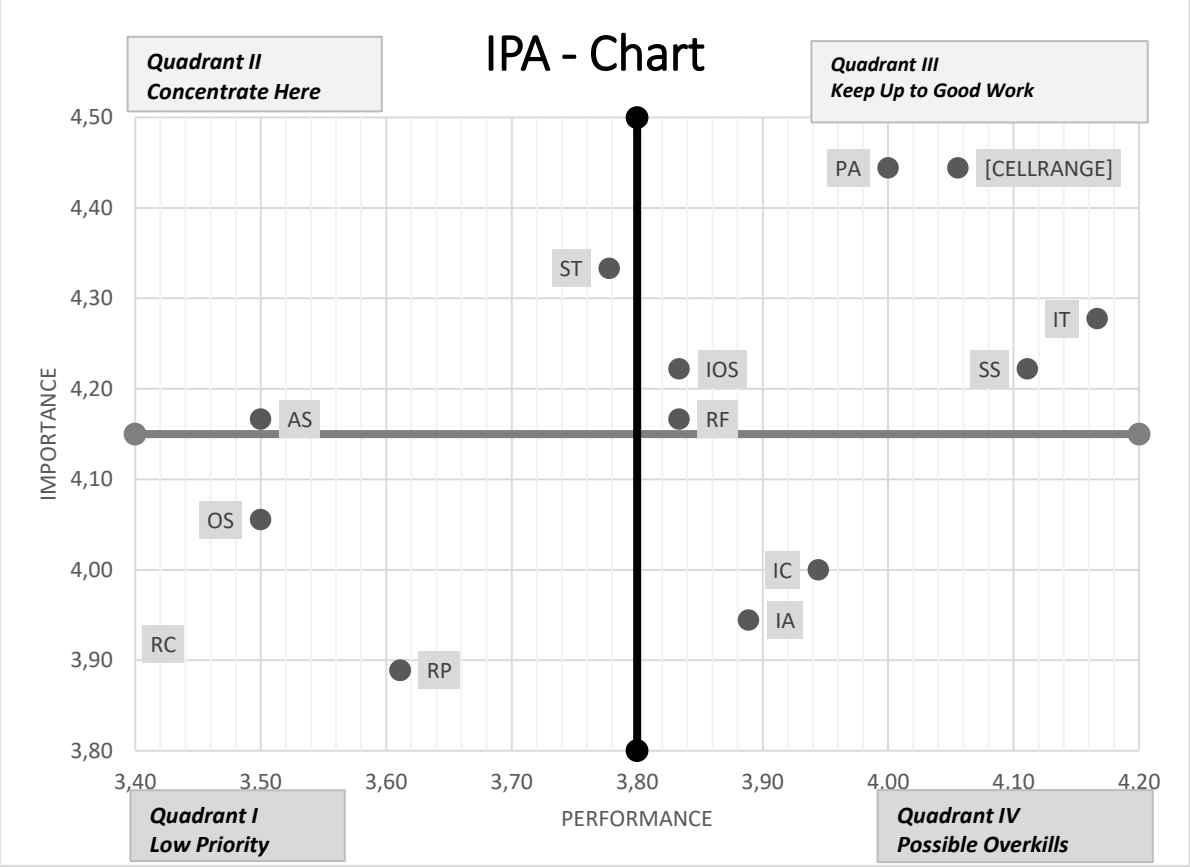

Figure 2. Importance- Performance Analysis (IPA) chart

The analysis of the IPA chart indicates that quadrant II recommends managers or store heads to focus more on two crucial indicators, namely shortages or scarcity and adjustments to stock. The quadrant I suggests maintaining the current efforts for indicators such as stock availability, days on hand, inventory turnover, safety stock, items on shelf , and replenishment frequency. Quadrant III categorizes indicators as low priority, including overstock, return products from pharmacy stores, and return products from customers. Quadrant IV is identified as having potential overkills in managing inventory cost and inventory accuracy. To provide a more detailed overview of these findings, it is advisable to present the results in a table format for each quadrant, as summarized in Table 2.

Table 2. Indicator summary across IPA chart quadrants

Concentrate here		**Keep up the good work**	
ST	Shortage of scarcity	DOH	Day on hand
AS	Adjust stock	PA	Product availability
		IT	Inventory turnover
		SS	Safety stock
		IOS	Items on shelf
		RF	Replenishment frequency
Low priority		**Possible overkills**	
OS	Over stock	IC	Inventory cost
RP	Return product from pharmacy store	IA	Inventory accuracy
RC	Return product from customer		

The respondents evaluated the significance of key performance indicators, which are highly important, with the top three indicators being product availability (PA), day on hand (DOH), and shortage (ST). For ST is in the low performance group. In general, earning losses due to ST status can far outweigh the stock losses themselves (Kang & Gershwin ,2005). The majority of respondents rated the performance outcomes positively based on these indicators for PA and DOH. However, it is noteworthy that the shortage indicator does not align with this pattern. Generally, if PA and DOH demonstrate good performance, it is expected that the shortage indicator

would also reflect positively (Aastrup & Kotzab, 2009). However, upon examining the mode value, which predominantly falls at level 4, the results are comparable to those of PA and DOH. Consequently, it is conceivable that some respondents assigned very low scores.

The respondents assessed the significance of less prominent key performance indicators, ranking return product from pharmacy (RP), return product from customer (RC), and inventory accuracy (IA) as the top three. Concerning RP and RC, equal scores were observed, indicative of suboptimal performance outcomes. Previous research suggests that RC's impact extends to customer confidence in the organization, while RP affects employee work performance. In contrast, respondents noted positive progress in IA, which contrasts with AS stock alignment. This discrepancy could arise from IA's potential to reduce AS occurrences through good performance. Respondents commonly associate AS with issues such as missing, stolen, or damaged items, necessitating inventory adjustments. Conversely, IA tends to encounter fewer issues and is perceived as highly effective, thanks to daily stock counts by staff and weekly checks by managers, bolstered by monthly stock audits. This proactive approach likely mitigates IA-related issues, employing a comparison-based measurement method for improvement assessment. Current research proposes an effective tool is Auto-ID (Kang & Gershwin, 2005) for example: applied to RFID (Bertolini et al., 2015).

The respondents' prioritized performance indicators for operational efficiency encompass inventory turnover (IT), safety stock (SS), and day on hand (DOH), all of which are high scored in their importance ratings. It is intriguing to note their approach in evaluating performance, leveraging the organization's calculated outcomes for IT and DOH across branches, while SS estimations consider seasonal fluctuations and contextual factors like impending price adjustments or recurrent shortages from manufacturers necessitating augmented stocking. Currently, ongoing studies are focused on formulating policies for product replenishment and assessing the imperative for specific branches to implement SS (Kwan et al., 2019).

The respondents assessed that the two least efficient operational performance indicators were adjust stock (AS) and over stock (OS). AS was a metric related to direct product shortages, such as incorrect sales, expired products due to delayed return notifications, failure to pick products according to First Expired First Out (FEFO) or First In, First Out (FIFO) principles, often resulting in expired or damaged products during transportation, degraded product quality, and lost products. When stock adjustments occurred, responsibility was shared among branch employees (Cui, Zhang & Bassamboo, 2017). OS was of less interest to most pharmacies and therefore yields limited operational results. This was because the pharmacy policy emphasized having sufficient stock ("better to have than to lack") (Sabir & Farooquie, 2018). However, there may be a need to review or consider importing policies to find the most suitable approach for maximizing service while minimizing costs.

The aspects of replenishment frequency (RF) and Items on shelf (IOS) were intriguing as they both pertain to the same category, with most respondents providing high ratings for these indicators and yielding positive performance results. However, the occurrence of ST underscores the imperative for implementing suitable policies to assess operational efficiency, including the determination of order quantities and timing (Solti et al., 2018).

In contrast, respondents accorded lesser importance to inventory cost (IC), yet it was observed to be well-managed. Notably, its commendable performance stemmed from effective cost control during the ordering process, which entailed calculations based on reported order quantities typically spanning 15 to 30 days' worth, aligned with product turnover rates. Although waste materials are not integrated into the system, they are managed through inspections and estimations of branch orders, potentially contributing to shortages that impact branch operations (Kwan et al., 2019).

Consequently, it is a diagram delineating the achievement of operational performance and reputation in retail establishments with customers. Our findings delineate two essential components: the first component encompasses number of each item on the program, encompassing appropriate inventory control (specifically, an appropriate replenishment inventory policy). This component holds pivotal importance, as inappropriate inventory control may precipitate adverse consequences, including heightened total inventory costs, surplus inventory levels, compromised service standards, diminished product availability, and instances of shortage or scarcity. The second component pertains to physical inventory (referred to as actual inventory), where any discrepancies in inventory management can lead to shortages or scarcity. Ultimately, both inappropriate inventory control practices and inventory inaccuracies can exert notable ramifications on the profitability and financial standing of a business.

Conclusion

This study aims to investigate 13 key performance indicators sourced from a comprehensive literature review on inventory management. The primary objectives include analyzing the relationships among these indicators and evaluating their relative importance. The research adopts a qualitative approach, employing survey as the chosen method. Our finding presented that the indicators deemed most significant by respondents, when compared to others, were "Day on Hand (DOH)," "Product Availability (PA)," and "Shortage of Scarcity (ST)." Our study findings revealed that a majority of respondents believe they can effectively manage DOH and PA. However, they also expressed the view that addressing the management of ST could be enhanced, possibly necessitating further development strategies. Furthermore, our research identified that the indicators most in need of development and improvement guidance were related to "Adjust Stock (AS) and "Overstock (OS).

Recommendations

The results of this research serve as fundamental data that is beneficial academically. In the future, other researchers can build upon this research in interesting gaps. For example, they can explore the trends in perceptions of managers or department heads in pharmacy chain stores regarding the importance of each indicator or further advance the assessment of indicator importance after gaining insight into respondents' perspectives. This includes applying or comparing the significance of each indicator in pharmacy chain store models derived from the research with other retail businesses. Additionally, from a practical perspective, organizations can leverage indicators associated with inventory management to improve performance and promote awareness of inventory management methodologies. They can pinpoint indicators that necessitate greater emphasis and leverage these findings to formulate pertinent strategies for organizational growth in inventory management, ultimately enhancing customer satisfaction and bolstering competitiveness within the industry.

Scientific Ethics Declaration

The authors declare that the scientific ethical and legal responsibility of this article published in EPSTEM journal belongs to the authors.

Acknowledgements or Notes

* This article was presented as an oral presentation at the International Conference on Basic Sciences, Engineering and Technology (www.icbaset.net) held in Alanya/Turkey on May 02-05, 2024.

References

Aastrup, J., & Kotzab, H. (2009). Analyzing out-of-stock in independent grocery stores: An empirical study. *International Journal of Retail and Distribution Management*, *37*(9), 765–789.

Bertolini, M., Bottani, E., Romagnoli, G., & Vignali, G. (2015). The impact of RFID technologies on inventory accuracy in the apparel retailing: Evidence from the field. *International Journal of RF Technologies: Research and Applications*, *6*(4), 225–246.

Choi, T.M. (2016) Inventory service target in quick response fashion retail supply chains, *Service Science*, *8*, 406-419.

Cui, R., Zhang, D. J. & Bassamboo, A. (2019). Learning from inventory availability information: Evidence from field experiments on Amazon, *Management Science*, *65*, 1216-1235.

Farmaciawaty, D. A., Basri, M. H., Utama, A. A., Widjaja, F. B., & Rachmania, I. N. (2020). Inventory level improvement in pharmacy company using probabilistic EOQ model and two echelon inventory: a case study. *The Asian Journal of Technology Management*, *13*(3), 229–242.

Hahn, G. J. & Leucht, A. (2015). Managing inventory systems of slow moving items, *International Journal of Production Economics*, *170*, 543-550.

Insight10. (2023). *Global over the counter (OTC) pharmaceuticals market analysis*. Retrieved from https://www.insights10.com/report/thailand-over-the-counter-otc-pharmaceuticals-market-analysis/

Ishfaq, R., Raja, U. & Rao, S. (2016). Seller-induced scarcity and priceleadership: Impact on product returns in the internet retail supply chain, *The International Journal of Logistics Management*, *27*, 552-569.

Kang, Y., & Gershwin, S. B. (2005). Information inaccuracy in inventory systems: Stock loss and stockout. *IIE Transactions (Institute of Industrial Engineers)*, *37*(9), 843–859.

Kasiri, N. (2016). More insights into rfid-enabled changes in retail: A simulation model, *International Journal of RF Technologies*, *7*, 229-248.

Khan, F., Danish, D., & Siddiqui, A. (2019). Impact of inventory management on firm's efficiency-a quantitative research study on departmental stores operating in Karachi. *Social Science and Humanities Journal*, *3*(4).

Krungsri Organization. (2022). *Trend of pharmaceutical industrial during year 2023-2025*. Retrieved from https://www.krungsri.com/getmedia/d22d61a6-5b98-494b-a13b

Kwan, K., Chu, Y., Manuel, J., & Pizano, M. (2019). *Replenishment policies for retail pharmacies in emerging markets*. Retrieved from https://hdl.handle.net/1721.1/121295

MacAs, C. V. M., Aguirre, J. A. E., Arcentales-Carrion, R., & Pena, M. (2021*).* Inventory management for retail companies: A literature review and current trends. Proceedings, 2021 *2nd International Conference on Information Systems and Software Technologies*, 71–78.

Macmillan, T. T. (1971). *The Delphi technique* (pp.3-5). Retrieved from https://files.eric.ed.gov/fulltext/ED064302.pdf

Manivel, P. & Ranganathan, R. (2017). Prioritized FSN analysis of inventory management in private and hospital pharmacy followed by questionnaire. *International Research Journal of Pharmacy*, *7*(12), 104–113.

Martilla, J. A., & James, J. C. (1977). Importance-Performance Analysis. *The Journal of Marketing*, *41*(1).

Pentrakan, A., Wang, J.-Y., & Wong, W. K. (2023). The impact of centralized electronic bidding system on procurement prices for generic medicines: A case study from Thailand. *Songklanakarin Journal of Science and Technology*, *44*, 1532-1538.

Qin, W., Zhong, R. Y., Dai, H. Y. & Zhuang, Z. L. (2017). An assessment model for RFID impacts on prevention and visibility of inventory inaccuracy presence, *Advanced Engineering Informatics*, *34*, 70-79.

Sabir, L. B. & Farooquie, J. A. (2018). Effect of different dimensions of inventory management of fruits and vegetables on profitability of retail stores: an empirical study, *Global Business Review, 19*, 99-110.

Sanchez-Ruiz, L., Blanco, B., & Kyguolienė, A. (2018). A theoretical overview of the stockout problem in retail: from causes to consequences. *Management of Organizations: Systematic Research*, *79*(1), 103–116.

Satista. (2023). *Revenue of the OTC pharmaceuticals industry worldwide 2018-2029*. Retrieved from https://www.statista.com/forecasts/1093274/otc-pharmaceuticals-market-worldwide-revenue

Solti, A., Raffel, M., Romagnoli, G & Mendling, J. (2018). Misplaced product detection using sensor data without planograms, *Decision Support Systems*, *112*, 76-87.

Zhang, W. & Rajaram, K. (2017). Managing limited retail space for basic products: Space sharing vs. space dedication, *European Journal of Operational Research*, *263*, 768-781.

Zhou, W. & Piramuthu, S. (2015). Effects of ticket-switching on inventory management: Actual vs. information system-based data, *Decision Support Systems*, *77*, 31-40.

Author Information

Atatika Pentrakan
Cluster of Logistics and Rail Engineering
Faculty of Engineering, Mahidol University
Nakhon Pathom, 73170 Thailand
Contact e-mail: *atatika@gmail.com*

Rawinkhan Srinon,
Cluster of Logistics and Rail Engineering
Faculty of Engineering, Mahidol University
Nakhon Pathom, 73170 Thailand

To cite this article:

Pentrakan, A. & Srinon, R. (2024). Assessing inventory management indicators in chain pharmacy stores: An importance – performance analysis. *The Eurasia Proceedings of Science, Technology, Engineering & Mathematics (EPSTEM), 28,* 141-147.

The Eurasia Proceedings of Science, Technology, Engineering & Mathematics (EPSTEM)
ISSN: 2602-3199

The Eurasia Proceedings of Science, Technology, Engineering & Mathematics (EPSTEM), 2024

Volume 28, Pages 148-156

ICBASET 2024: International Conference on Basic Sciences, Engineering and Technology

Sustainable Ionic Liquids: A Practical Work about Improving the Mechanical Properties of Bamboo

Anita Fadhilah
Universitas Pendidikan Indonesia

Hernani Hernani
Universitas Pendidikan Indonesia

Ahmad Mudzakir
Universitas Pendidikan Indonesia

Nanda Ayu Lestari
Universitas Pendidikan Indonesia

Abstract: Ionic liquids have superior properties compared with other solvents because they are environmentally friendly/green agents/renewable and are predicted to have the potential to improve the mechanical properties of bamboo. This study aims to examine the mechanical properties of bamboo with the application of ionic liquids and internal potential planning ESD learning at universities. This study used two kinds of ionic liquids: choline chloride-oxalic acid and choline chloride-$ZnCl_2$. Testing the mechanical properties of bamboo using ASTM D-638 for tensile tests and ASTM D-790 for flexural and compression tests. The results found that the tensile, bending, and compression strengths for bamboo without ionic liquid treatment for each test are 0.0290 kN/mm², 0.1458 MPa, and 0.0587 kN/mm², respectively. For bamboo with a choline chloride-oxalic acid coating, the tensile, bending, and compression strengths are 0.1037 kN/mm², 0.2370 MPa, and 0.0609 kN/mm² respectively. For bamboo with a choline chloride-$ZnCl_2$ coating, the tensile, bending, and compression strengths are 0.0737 kN/mm², 0.3191 MPa, and 0.0736 kN/mm² respectively. To understand the context-specific requirements for ESD integration in education, data was collected using open-ended questions. The results indicated the necessity to integrate ESD into chemistry education further, specifically emphasizing ionic liquids and their potential role in sustainable practices like bamboo processing. The use of ionic liquids in improving mechanical properties for ESD-loaded learning offers new insights into the potential of these compounds in understanding the mechanisms involved in the learning and knowledge process.

Keywords: Ionic liquid, Bamboo, Chemistry

Introduction

Bamboo, a sustainable material, is renowned as the fastest-growing plant globally and abundantly found in Indonesia (Mustafa et al., 2021). Bamboo can exhibit a daily growth rate of 60 cm or more and reach heights of up to 40 m This factor positions bamboo as the fastest-growing plant in the world (Laksono & Agustiningtyas, 2019). Bamboo finds applications in various fields, such as construction materials, textiles, and paper. In construction, bamboo is extensively utilized for its strong fibres, possessing compression strength twice that of concrete, while its tensile strength is nearly equivalent to steel (Yadav & Mathur, 2021). However, bamboo's durability is relatively low, leading to a relatively short lifespan (Mirdayanti & Rahmiza Muzana, 2023). Several factors can influence the mechanical properties of bamboo, including its age, height position, diameter, thickness of bamboo walls, load position (on nodes or internodes), radial position from the outer to inner part,

and bamboo moisture content. These mechanical properties are crucial in designing bamboo as a construction material, determining its strength, suitability for specific construction positions, and overall feasibility. Furthermore, the environment where bamboo grows also affects its mechanical properties (Afifah et al., 2023).

According to Afifah et al. (2023), ionic liquids can be utilized to address bamboo's weaknesses. Ionic liquids are salts with a melting point at room temperature and exceptional characteristics, including thermal stability, low viscosity, and negligible vapor pressure (Yokokawa et al., 2019). Based on Neyses et al. (2017), these ionic liquids serve as alternative solvents that can be recycled. They can be employed to preserve and enhance wood's anti-static properties and improve wood's strength by dissolving cellulose. These ionic liquids can act as crosslinking media through activation reactions, extract lignin from cellulose, be used as plasticizers to enhance density on the wood surface, exhibit positive effects as antifungal, antimicrobial, and UV degradation agents, and minimize water absorption in wood (Miyafuji & Fujiwara, 2013). One ionic liquid composed of choline chloride and lactic acid or oxalic acid is reported to be effective in removing lignin and hemicellulose from wood (Wang et al., 2023).

Ionic liquids (ILs) of choline chloride-$ZnCl_2$ and choline chloride-oxalic acid have shown potential in improving the mechanical properties of bamboo through their use as templates or solvents in various processes. These ILs have unique properties, such as low melting points, high boiling points, and good thermal and chemical stabilities, which make them suitable for promoting the preparation of new chemical nanostructures through mild reaction pathways (Preethi et al., 2017).

Additionally, ionic liquids have been found to have potent inhibitory effects on bamboo mildew (Liu et al., 2023). Using ILs as solvents can enhance the mechanical properties of bamboo by modifying its surface, structure, and morphology. For example, the sol-gel synthesis of mesoporous titania using choline chloride-zinc chloride IL as a green solvent has been shown to produce highly ordered titania particles with improved surface area and photocatalytic activity (Preethi et al., 2017). Similarly, using choline chloride-based ionic liquid analogs as solvents and plasticizers in producing agar films has demonstrated improved mechanical properties and water resistance (Sousa et al., 2014).

The potential of Ionic Liquids (ILs) in enhancing the mechanical properties of bamboo lies in their ability to act as green templates, offering advantages such as easy processability, less toxicity, and customizable mesoporous network structures in solids (Preethi et al., 2017). Incorporating ILs into the bamboo matrix makes it possible to create a more uniform and stable structure, which can improve mechanical properties such as tensile strength and elongation. In addition to their use as templates or solvents, ILs can also be employed in the treatment of bamboo, such as starch treatment with deep eutectic solvents, including choline chloride-based ILs, which can improve the surface area and porosity of bamboo (Zdanowicz, 2020).

Sustainable ionic liquid for the mechanical properties of bamboo is one of the approaches to support SDGs by utilizing sustainable materials. Given their progressively diminishing availability, sustainable materials can be regarded as substitutes for natural resources. These materials contribute to attaining Sustainable Development Goals (SDGs) owing to their intrinsic, easily renewable, and sustainable characteristics. They necessitate minimal energy consumption in their utilization and do not generate pollution or other emissions that could impact human health and comfort (Afifah et al., 2023).

However, more research is needed on sustainable ionic liquids as a context for ESD-loaded learning based on SDGs. This study explores the potential of ionic liquid contexts to improve the quality of bamboo's mechanical properties and internal potential planning for ESD learning at universities. By examining these aspects, the study aims to provide insights into the potential of ionic liquids in improving the mechanical properties of bamboo and promoting sustainable development in various fields, including construction, furniture, and packaging. The findings will also contribute to the further integration of ESD into chemistry education, specifically emphasizing ionic liquids and their potential role in sustainable practices like bamboo processing.

Methods

This experiment compares the mechanical properties of bamboo without ionic liquid coating and with ionic liquid coating, as well as determining the potential of sustainable ionic liquids as a context for ESD-Loaded Learning.

Materials

The bamboo used in the experiment is petung bamboo (*Dendrocalamus asper*), which is widely available in Indonesia. This study used two kinds of ionic liquids: choline chloride-oxalic acid and choline chloride-$ZnCl_2$. Testing the mechanical properties of bamboo using ASTM D-638 for tensile tests and ASTM D-790 for flexural and compression tests.

Experimental Procedures

Synthesis of Ionic Liquids

To make choline chloride and oxalic acid Ionic Liquid mixed in a molar ratio of 1:2, add them into a shlenk tube and stir on an electric stove with a magnetic stirrer inside at 80 ºC for 3 hours, as well as to make choline chloride and $ZnCl_2$ Ionic Liquid with a molar ratio of 1:1 at 80 ºC for 3 hours or until homogeneous.

Application of Ionic Liquids on Bamboo

Bamboo that has been formed according to the size for the tensile test (165 x 14 x 4) mm, bending test (125 x 20 x 4) mm, and compression test (10 x 10 x 25) mm is then coated with each type of ILs and allowed to stand for 7 days and aerated for 1 day.

Testing the Mechanical Properties of Bamboo

The mechanical properties of bamboo were tested at the metallurgical laboratory of the University of Education Indonesia. Mechanical tests are carried out in the form of tensile, flexural, and compression tests.

Results and Discussion

Mechanical Properties of Bamboo with Ionic Liquids Coating

Petung bamboo (*Dendrocalamus asper*) is one of Indonesia's most widely available and fast-growing bamboo species (Suriani, 2020). Some of the favourable characteristics of petung bamboo include its wide adaptability, long annual growth period, and fast production speed. Therefore, petung bamboo was chosen as the experimental material for this study. This study used a practical work approach to investigate the improvement of mechanical properties in bamboo. This process involved treating the bamboo with an ionic liquid.

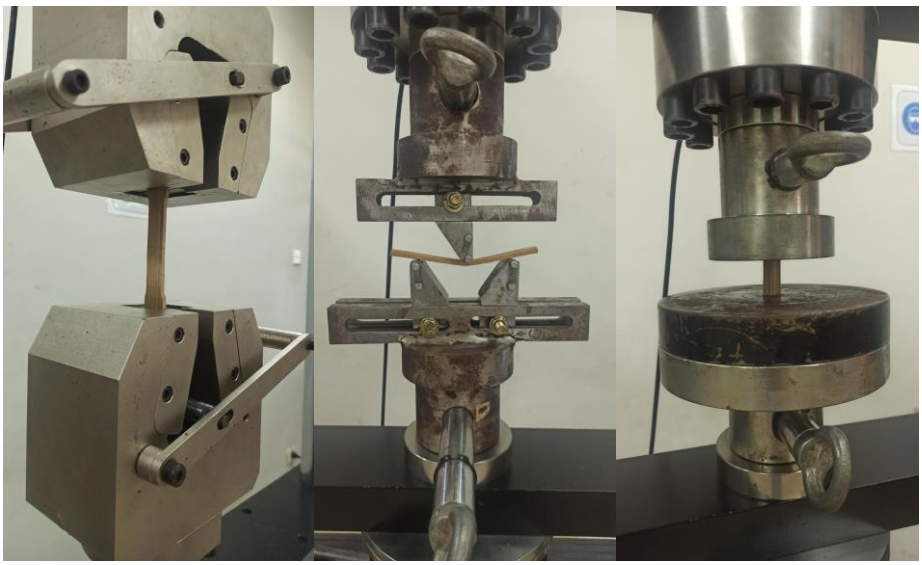

(a) (b) (c)

Figure (1a). Tensile Test; (1b) Flexural Test; and (1c) Compression Test

Ionic liquids of choline chloride-$ZnCl_2$ and choline chloride-oxalic acid are environmentally friendly and sustainable alternatives to conventional solvents used in wood processing (Tran et al., 2016). Choline chloride-$ZnCl_2$ and choline chloride-oxalic acid ionic liquids have gained attention for their potential to improve the mechanical properties of wood, including tensile, flexural, and compression strength. These ionic liquids are formed by mixing choline chloride with zinc chloride ($ZnCl_2$) or oxalic acid, resulting in a Ionic Liquid with unique properties. Based on Bušić et al. (2023), the formation of this ionic liquid is based on the concept of a deep eutectic solvent (DES), which is formed by mixing a hydrogen bond donor (HBD) with a hydrogen bond acceptor (HBA) in a specific molar ratio. Choline chloride acts as the HBA, while $ZnCl_2$ or oxalic acid is the HBD. Testing the mechanical properties of bamboo using ASTM D-638 for tensile tests and ASTM D-790 for flexural and compression tests. The instruments for each test can be seen in Figure 1. The results of the tensile test, bending test, and compression test on untreated bamboo, bamboo with Choline chloride-oxalic acid coating, and Choline chloride-$ZnCl_2$ coating are presented in Tables 1, 2, and 3 below, respectively.

Table 1. The result of tensile test

Sample	Maximum Stress (kN/mm^2)		
	Without Treatment	Choline chloride-Oxalic Acid	Choline chloride-$ZnCl_2$
1	0,0470	0,0930	0,0700
2	0,0240	0,1160	0,0770
3	0,0160	0,1020	0,0740
Mean	0,0290	**0,1037**	0,0737

The maximum stress result for bamboo had the highest average for coating with choline chloride-oxalic acid at 0.1037 kN/mm². This value represents the maximum strength that a bamboo sample can withstand before breaking under tension. Tensile tests measure the ability of a material to resist pulling. Maximum stress is an important property in engineering applications, as it helps determine the suitability of a material for various uses, such as in construction or manufacturing.

Table 2. The result of flexural test

Sample	Stress in the outer fibres at midpoint (σ)		
	Without Treatment	Choline chloride-Oxalic Acid	Choline chloride-$ZnCl_2$
1	0,1440	0,2110	0,2636
2	0,1777	0,2448	0,4573
3	0,1157	0,2551	0,2366
Mean	0,1458	0,2370	**0,3191**

The highest stress result in the outer fibre at the midpoint in the bending test was shown for bamboo with choline chloride-$ZnCl_2$ coating at 0.3191 MPa. This value represents the maximum stress experienced by the outer fibres of the material during the test when subjected to bending force. The bending test is used to determine the ability of the material to resist bending, and the stress in the outer fibre at the midpoint is an important parameter in assessing the strength and stiffness of the material.

Tabel 3. The result of compression test

Sample	Compression Strength (kN/mm^2)		
	Without Treatment	Choline chloride-Oxalic Acid	Choline chloride-$ZnCl_2$
1	0,0609	0,0554	0,0757
2	0,0573	0,0726	0,0660
3	0,0579	0,0548	0,0790
Rata-rata	0,0587	0,0609	**0,0736**

The results of the compression strength are almost the same as the bending test, where the coating with choline chloride-$ZnCl_2$ has a better compression strength than the others. The compression strength obtained in the compression test was 0.0736 kN/mm². This value indicates the maximum force that the material can withstand before collapsing due to compression forces. The compression test measures the ability of the material to resist pressure, and the compression strength is an important parameter in assessing the strength and stability of the material.

Based on the mechanical properties testing outcomes, it has been established that the ILs coating on bamboo achieves superior performance compared to bamboo without coating. This observation aligns with the assertions of He et al. (2019) and Wang et al. (2023), who reported that chemical treatment of bamboo results in the cell walls becoming thinner and adhering to one another, thereby creating a honeycomb structure. This phenomenon can be attributed to the ability of ILs to remove lignin and hemicellulose, thereby softening the bamboo cell walls.

During pretreatment with ionic liquids, the H-bond between OH···Cl in ionic liquids is stronger than the OH···O bond in lignin in bamboo. A large amount of Cl- allows the ionic liquid to cleave the LCC (lignin-carbohydrate complex) in the biomass and some ether bonds in lignin (Li et al., 2023). In acidic ionic liquids such as choline chloride-oxalic acid, protons can catalyse the cleavage of ethers and esters present in the lignin-carbohydrate complex, leading to lignin extraction and depolymerisation (Scelsi et al., 2021). Ionic liquids can also interact with hydroxyl groups in cellulose, leading to swelling of cellulose fibres (Hong et al., 2016). The change in cellulose fibre structure can improve the mechanical properties of bamboo by increasing the bonding between fibres and reducing the likelihood of fibre breakage during stress application.

Higher tensile strength test results were shown for the ionic liquid type of choline chloride-oxalic acid. This is due to the nature of choline chloride-oxalic acid, a Brønsted acid ionic liquid that can be used as a reaction medium for the esterification of carboxylic acids with alcohols. The interaction between choline chloride-oxalic acid ionic liquid and bamboo cell wall components can cause swelling of the cellulose fibres, which can improve the tensile properties of bamboo by increasing the bond between fibres and reducing the likelihood of fibre breakage during stress application (Tran et al., 2016). As the fibres can withstand more stress before being damaged, the resulting tensile strength is higher. In addition, better dimensional stability can result in a more uniform stress distribution during the tensile test, resulting in a more accurate tensile strength measurement of the wood.

In contrast to the tensile strength, the results of the bending test and compression test, coating with choline chloride-$ZnCl_2$ showed higher results. Choline chloride-$ZnCl_2$ is a Lewis acid ionic liquid that can catalyze carbonyl protection at room temperature (Satlewal et al., 2018). Zinc chloride in Ionic Liquids can act as a catalyst to enhance the degradation of hemicellulose and cellulose in bamboo, leading to increased polymerisation of cellulose fibres, resulting in increased strength (Tran et al., 2016). In addition, the low acidity of zinc chloride solution at a specific temperature can decrease the hydroxy content of bamboo, improving dimensional stability and reducing hygroscopicity (Popescu et al., 2014).

Choosing between choline chloride-$ZnCl_2$ and choline chloride-oxalic acid to improve bamboo's mechanical properties depends on the wood product's specific requirements and the desired properties. Choline chloride-$ZnCl_2$ may be more suitable for applications requiring improved dimensional stability and reduced hygroscopicity. In contrast, choline chloride-oxalic acid may be more effective for applications requiring swelling of cellulose fibres to improve inter-fibre bonding.

Sustainable Ionic Liquids as a Context for ESD-Loaded Learning

The superior properties of ionic liquids align with several Sustainable Development Goals (SDGs) (United Nations, 2015). Ionic liquids (ILs) are environmentally sustainable materials that align with several Sustainable Development Goals (SDGs) due to their unique properties and potential applications. Ionic liquids (ILs) exhibit low volatility and high thermal and electrochemical stability, making them suitable for various applications, including energy storage and conversion devices, such as fuel cells, lithium-ion batteries, supercapacitors, and solar cells (Choudhary et al., 2024). They can also be employed in biomass transformations and electrocatalysis, contributing to reducing environmental impact and developing sustainable sensors (Andonegi et al., 2023). Moreover, ILs can produce advanced functional materials, such as electroactive polymer composites and proton exchange membranes, which enhance energy storage and conversion efficiency (Bailey et al., 2023). Additionally, ILs can be engineered to be nontoxic and biodegradable, aligning with the SDG of sustainable chemistry and reducing environmental pollution (Beil et al., 2021). Overall, the use of ILs in various applications can contribute to the achievement of several SDGs, including No Poverty, Quality Education, Industry, Innovation and Infrastructure, Sustainable Cities and Communities, Climate Action, and Life on Land. Therefore, integrating the concept of ionic liquids in Education for Sustainable Development (ESD) can provide valuable insights into sustainable materials development and contribute to the achievement of the aforementioned SDGs.

Based on in-depth responses through open-ended questions, 91% of students aware of ionic liquids stated that they had heard about them in introductory chemistry, organic chemistry, physical chemistry, and inorganic chemistry courses. Students study various chemical concepts and theories in these courses, including ionic liquids. However, more than merely being acquainted with ionic liquids from coursework is required. Students must also have a profound understanding of ionic liquids, including their properties, characteristics, and applications in various fields. Therefore, students must develop the ability to seek information and comprehend chemical concepts thoroughly to apply this knowledge in the future. Furthermore, students mostly agree that Ionic liquids can be an environmentally friendly alternative in various industrial applications; ionic liquids have great potential in sustainable chemistry lecture applications, and learning about ionic liquids is relevant to current environmental issues. The result can be seen in Figure 2.

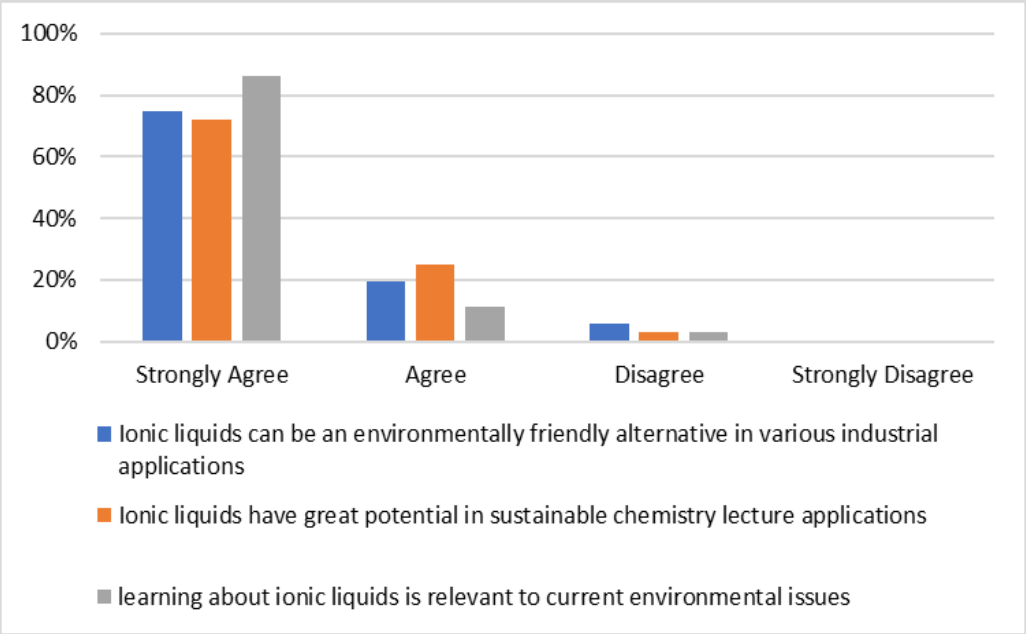

Figure 2. Context of ionic liquids

Ionic liquids (ILs) have gained attention as an environmentally friendly alternative in various industrial applications due to their unique properties and potential in sustainable chemistry (Khoo et al., 2021). As a student, it is essential to understand the significance of ionic liquids in the context of current environmental issues and their relevance to sustainability.

Learning about ionic liquids is relevant to current environmental issues and their potential applications in sustainable chemistry. By exploring green synthesis routes and understanding the environmental impact of these materials, students can contribute to developing more sustainable technologies and practices in various industries.

Chemistry education plays a vital role in promoting sustainable development by integrating sustainability and green chemistry principles into the curriculum. This integration can help students understand the environmental impact of chemical processes and products, encouraging them to develop more sustainable practices. By incorporating sustainability into chemistry education, students can learn how to design and evaluate chemical processes and products in a safe, efficient, and environmentally friendly way. This can help prepare the next generation of chemists to address global challenges such as resource depletion, pollution, and climate change. Moreover, promoting sustainability in chemistry education can contribute to raising awareness of the Sustainable Development Goals (SDGs) outlined by the United Nations (Burmeister & Eilks, 2013; Sjostrom et al., 2015; Wissinger et al., 2021; Zuin et al., 2021).

The use of ionic liquids in improving mechanical properties for ESD-charged learning offers new insights into the potential of these compounds in understanding the mechanisms involved in the learning and knowledge process. This research offers the opportunity to use ionic liquids to observe the mechanisms involved in ESD-charged learning systems, which may assist in developing new methods to optimise learning and knowledge processes. Therefore, incorporating the context of ionic liquids in improving mechanical properties for ESD-charged learning is essential in exploring new possibilities to enhance the learning process.

Conclusion

Choline chloride-$ZnCl_2$ and choline chloride-oxalic acid ionic have the potential to improve the mechanical properties of wood, including tensile, flexural, and compression strength. The results found that the tensile, bending, and compression strengths for bamboo without ionic liquid treatment for each test are 0.0290 kN/mm², 0.1458 MPa, and 0.0587 kN/mm², respectively. For bamboo with a choline chloride-oxalic acid coating, the tensile, bending, and compression strengths are 0.1037 kN/mm², 0.2370 MPa, and 0.0609 kN/mm² respectively. For bamboo with a choline chloride-$ZnCl_2$ coating, the tensile, bending, and compression strengths are 0.0737 kN/mm², 0.3191 MPa, and 0.0736 kN/mm² respectively. The use of ionic liquids in improving mechanical properties for ESD-loaded learning also offers new insights into the potential of these compounds in understanding the mechanisms involved in the learning and knowledge process.

Recommendations

A suggestion that the researcher can make in relation to the findings of this study is for future research to develop integrated ionic liquids and their potential role in sustainable practices such as bamboo processing into chemistry education. Therefore, it is recommended to explore the potential of ionic liquids in various scientific and technological domains, including energy conversion and storage applications.

Scientific Ethics Declaration

The authors declare that the scientific ethical and legal responsibility of this article published in EPSTEM journal belongs to the authors.

Acknowledgements

* This article was presented as an oral presentation at the International Conference on Basic Sciences, Engineering and Technology (www.icbaset.net) held in Alanya/Turkey on May 02-05, 2024.

* The researchers would like to sincerely thank the Education Fund Management Institute (LPDP/Indonesia Endowment Fund for Education) under the Ministry of Finance of the Republic of Indonesia for sponsoring their master's degree and supporting this paper and publication. Additionally, the researchers would like to thank the Department of Chemistry Education at the Indonesia University of Education for supporting this paper.

References

Afifah, S., Mudzakir, A., Nandiyanto, A. B. D., Ragadhita, R., Maryanti, R., Husaeni, D. F. Al, Husaeni, D. N. Al, & Fiandini, M. (2023). Sustainability literacy to vocational students through distance learning with experimental demonstration: ıonic liquid experiment and ıts application as fire retardant. *Journal of Technical Education and Training*, *15*(1), 55–72.

Andonegi, M., Correia, D., Pereira, N., Salado, M., Costa, C. M., Lanceros-Mendez, S., de la Caba, K., & Guerrero, P. (2023). Sustainable collagen blends with different ıonic liquids for resistive touch sensing applications. *ACS Sustainable Chemistry and Engineering*, *11*(15), 5986–5998.

Bailey, J., Byrne, E. L., Goodrich, P., Kavanagh, P., & Swadźba-Kwaśny, M. (2023). Protic ionic liquids for sustainable uses. *Green Chemistry*, *26*(3), 1092–1131.

Beil, S., Markiewicz, M., Pereira, C. S., Stepnowski, P., Thoming, J., & Stolte, S. (2021). Toward the proactive design of sustainable chemicals: Ionic liquids as a prime example. *Chemical Reviews*, *121*(21), 13132-13173.

Burmeister, M., & Eilks, I. (2013). An understanding of sustainability and education for sustainable development among German student teachers and trainee teachers of chemistry. In *Science Education International*,*24*(2),167-194.

Bušić, V., Roca, S., & Gašo-Sokač, D. (2023). Application of choline chloride-based deep eutectic solvents in the synthesis of hydrazones. *Separations*, *10*(11),551.

Choudhary, G., Dhariwal, J., Saha, M., Trivedi, S., Banjare, M. K., Kanaoujiya, R., & Behera, K. (2024). Ionic liquids: environmentally sustainable materials for energy conversion and storage applications. *Environmental Science and Pollution Research*, *31*(7), 10296-10316.

He, Z., Qu, L., Wang, Z., Qian, J., & Yi, S. (2019). Effects of zinc chloride–silicone oil treatment on wood dimensional stability, chemical components, thermal decomposition and its mechanism. *Scientific Reports*, *9*(1), 1601.

Hong, S., Lian, H., Sun, X., Pan, D., Carranza, A., Pojman, J. A., & Mota-Morales, J. D. (2016). Zinc-based deep eutectic solvent-mediated hydroxylation and demethoxylation of lignin for the production of wood adhesive. *RSC Advances*, *6*(92), 89599–89608.

Khoo, K. S., Tan, X., Ooi, C. W., Chew, K. W., Leong, W. H., Chai, Y. H., Ho, S. H., & Show, P. L. (2021). How does ionic liquid play a role in sustainability of biomass processing? *Journal of Cleaner Production*, *284*,17.

Laksono, A. D., & Agustiningtyas, D. T. (2019). Pengaruh faktor geografi terhadap karakteristik bambu petung. *SPECTA Journal of Technology*, *3*(1), 25–32.

Li, P., Zhang, Z., Zhang, X., Li, K., Jin, Y., & Wu, W. (2023). DES: Their effect on lignin and recycling performance. *RSC Advances*, *13*(5), 3241–3254.

Liu, C., Chen, S., Shan, Y., Du, C., Zhu, J., Bao, Q., Shao, Y., Yin, W., Yang, F., Ran, Y., & Wang, Y. (2023). Screening of ıonic liquids against bamboo mildew and ıts ınhibition mechanism. *Molecules*, *28*(8),3432.

Mirdayanti, R., & Rahmiza Muzana, S. (2023). Anaslisa sifat mekanik bambu setelah proses perebusan. *Sains Dan Teknologi*, *4*(2), 32.

Miyafuji, H., & Fujiwara, Y. (2013). Fire resistance of wood treated with various ionic liquids (ILs). *Holzforschung*, *67*(7), 787–793.

Mustafa, A. A., Derise, M. R., Yong, W. T. L., & Rodrigues, K. F. (2021). A concise review of dendrocalamus asper and related bamboos: Germplasm conservation, propagation and molecular biology. *Plants*, *10*(9), 1897.

Neyses, B., Rautkari, L., Yamamoto, A., & Sandberg, D. (2017). Pre-treatment with sodium silicate, sodium hydroxide, ionic liquids or methacrylate resin to reduce the set-recovery and increase the hardness of surface-densified scots pine. *IForest*, *10*(5), 857–864.

Popescu, A. M., Donath, C., & Constantin, V. (2014). Density, viscosity and electrical conductivity of three deep eutectic based ionic solvents. *Bulgarian Chemical Communications*, *46*(3), 452–457.

Preethi, T., Padmapriya, M. P., Abarna, B., & Rajarajeswari, G. R. (2017). Choline chloride-zinc chloride ionic liquid as a green template for the sol-gel synthesis of mesoporous titania. *RSC Advances*, *7*(17), 10081–10091.

Satlewal, A., Agrawal, R., Bhagia, S., Sangoro, J., & Ragauskas, A. J. (2018). Natural deep eutectic solvents for lignocellulosic biomass pretreatment: Recent developments, challenges and novel opportunities. In *Biotechnology Advances*, *36*(8), 2032–2050.

Scelsi, E., Angelini, A., & Pastore, C. (2021). Deep eutectic solvents for the valorisation of lignocellulosic biomasses towards fine chemicals. *Biomass*, *1*(1), 29–59.

Sjostrom, J., Rauch, F., & Eilks, I. (2015). Chemistry education for sustainability. In I. Eilks & A. Hofstein (Eds.), *Relevant Chemistry Education* (pp. 163-184). Sense Publishers.

Sousa, A. M. M., Souza, H. K. S., Latona, N., Liu, C. K., Goncalves, M. P., & Liu, L. (2014). Choline chloride based ionic liquid analogues as tool for the fabrication of agar films with improved mechanical properties. *Carbohydrate Polymers*, *111*, 206–214.

Suriani, E. (2020). A study of the physical-mechanical properties of bamboo in Indonesia. *Science and Technology International Conference*, 154–162.

Tran, P. H., Nguyen, H. T., Hansen, P. E., & Le, T. N. (2016). An efficient and green method for regio- and chemo-selective Friedel-Crafts acylations using a deep eutectic solvent ([CholineCl][ZnCl2]3). *RSC Advances*, *6*(43), 37031–37038.

United Nations. (2015). *Global Ssustainable Development Report 2015 Edition Advance Unedited Version*.

Wang, W., Chen, M., & Wu, Y. (2023). Compressible cellulose wood prepared with deep eutectic solvents and ıts ımproved technology. *Polymers*, *15*(7),1593.

Wissinger, J. E., Visa, A., Saha, B. B., Matlin, S. A., Mahaffy, P. G., Kummerer, K., & Cornell, S. (2021). Integrating sustainability into learning in chemistry. *Journal of Chemical Education*, *98*(4), 1061–1063.

Yadav, M., & Mathur, A. (2021). Bamboo as a sustainable material in the construction industry: An overview. *Materials Today: Proceedings*, *43*, 2872–2876.

Yokokawa, M., Miyafuji, H., Murakami, Y., Shouho, S., & Yamaguchi, A. (2019). Comparative study on the fire resistance of wood treated with various ıonic liquids. *Journal of the Society of Materials Science*, *68*(9), 712–717.

Zdanowicz, M. (2020). Starch treatment with deep eutectic solvents, ionic liquids and glycerol. A comparative

study. *Carbohydrate Polymers*, *229*,115574.

Zuin, V. G., Eilks, I., Elschami, M., & Kummerer, K. (2021). Education in green chemistry and in sustainable chemistry: perspectives towards sustainability. *Green Chemistry*, *23*(4), 1594–1608.

Author Information

Anita Fadhilah
Universitas Pendidikan Indonesia
Setiabudhi Street. 229th, Bandung, Indonesia

Hernani Hernani
Universitas Pendidikan Indonesia
Setiabudhi Street. 229th, Bandung, Indonesia

Ahmad Mudzakir
Universitas Pendidikan Indonesia
Setiabudhi Street. 229th, Bandung, Indonesia
Contact e-mail: mudzakir.kimia@upi.edu

Nanda Ayu Lestari
Universitas Pendidikan Indonesia
Setiabudhi Street. 229th, Bandung, Indonesia

To cite this article:

Fadhilah, A., Hernani, H., Mudzakir, A., & Lestari, N.A. (2024). Sustainable ionic liquids: A practical work about improving the mechanical properties of bamboo. *The Eurasia Proceedings of Science, Technology, Engineering & Mathematics (EPSTEM), 28*, 148-156.

The Eurasia Proceedings of Science, Technology, Engineering & Mathematics (EPSTEM)
ISSN: 2602-3199

The Eurasia Proceedings of Science, Technology, Engineering & Mathematics (EPSTEM), 2024

Volume 28, Pages 157-166

ICBASET 2024: International Conference on Basic Sciences, Engineering and Technology

The Essential Oil Context of Lemongrass and Its Potential for Innovative ESD-Informed Learning

Nanda Ayu Lestari
Universitas Pendidikan Indonesia

Liliasari Liliasari
Universitas Pendidikan Indonesia

Iqbal Musthapa
Universitas Pendidikan Indonesia

Hernani Hernani
Universitas Pendidikan Indonesia

Anita Fadhilah
Universitas Pendidikan Indonesia

Abstract: Lemongrass essential oil contains various active compounds that function as antibacterial (citral and geraniol), deodorizer, insecticide, biocide, anti-fungal, antioxidant, anti-inflammatory, anti-cancer potential, and disinfectant, potentially resulting in innovative processes and products. The process and essential oil products from lemongrass are an interesting context for introducing ESD. This research aims to analyze the potential context of essential oil from lemongrass and aspects of the SDGs to develop innovative learning with ESD content. This preliminary research was carried out by describing the results of searches from various literature regarding the process of extracting essential oils using various techniques and using the products for health. The instruments used in this research were an analysis format of reading sources to produce appropriate themes and sub-themes and an open-ended questionnaire via Google Forms for prospective chemistry teacher participants. The results of the research show that the essential oil process involves extraction, microwave extraction, and steam distillation processes, where student teachers do not fully understand the process and potential product context of essential oil from lemongrass which contains ESD. In addition, 92% of prospective teacher students are interested in creating innovative product solutions that are environmentally friendly and good for health. The opinions of prospective teacher students regarding innovative learning with ESD content can stimulate creative thinking, critical thinking, collaboration, and deep understanding of concepts. The topic of essential oil from citronella has the SDGs aspect of a healthy and prosperous life because it produces potential products for health such as telon oil, massage oil, aromatherapy candles, diffusers, soap, anti-mosquito, floor cleaner, disinfectant, hand sanitizer, and herbal medicine. Based on the results of this research, it shows that the context of essential oils from lemongrass can be applied to innovative learning with ESD content.

Keywords: Essential oil, Lemongrass, Product

Introduction

Health is a critical aspect of achieving a good quality of life. The ESD SDG-3, known as Sustainable Development Goal-3, affirms the commitment to ensuring healthy lives and well-being for all individuals (Nations, 2016). The use of natural ingredients in traditional medicine has become a common practice

- Selection and peer-review under responsibility of the Organizing Committee of the Conference

throughout the world, estimated to be used by 75–80% of the population, especially in developing countries, because it is considered to have minimal side effects compared to allopathic medicine (Pujari et al., 2020; Sofowora et al., 2013). This is in line with health problems throughout the world which have led to an increasing need for natural compounds that can be used to develop innovative health products. The use of natural ingredients to become innovative products has also been very popular recently due to the need to use natural compounds to gradually replace chemicals (Tran et al., 2020). Natural ingredients will be more beneficial if they are converted into essential oils. Essential oils are concentrated hydrophobic liquids that contain various chemical compounds that easily evaporate at room temperature originating from natural/plant ingredients (Mahato et al., 2019). Essential oils have antidepressant, stimulant, detoxification, antibacterial, antiviral, and calming properties, so they can be used as medicines that have recently become very popular as a natural, safe, and cost-effective therapy for several health problems (Mahato et al., 2019).

One natural ingredient that has many benefits is lemongrass essential oil. The main active components contained in lemongrass essential oil are limonene, ÿ-myrcene, citral, geraniol, citronellol, geranyl acetate, and neral nerol. Although ÿ-myrcene and limonene are aromatic composites, the main biologically active component of lemongrass essential oil is citral, a mixture of the acyclic monoterpene aldehyde isomers neral (cis-citral) and geranial (trans-citral). In addition, lemongrass essential oil consists of small amounts of geraniol, geranyl acetate, and olefin monoterpenes (Do et al., 2021). The ingredient with the highest content in citronella oil is Citral (which accounts for more than 80% of the citronella oil content), which plays an important role in the functions of disinfectant, biocide, fragrance, and insecticide (Tran et al., 2020). Lemongrass essential oil contains various active compounds which are very useful such as antibacterial (citral and geraniol), odor remover, insecticide, biocide, anti-fungal (Šumiga et al., 2019), antioxidant (Fokom et al., 2019), anti-inflammatory, potency. anti-cancer (Do et al., 2021; Higuchi et al., 2023), and disinfectant (Tran et al., 2020). Lemongrass essential oil can be made into innovative products (Higuchi et al., 2023) such as several products including mosquito repellent (Higuchi et al., 2023), antimicrobial paper coating (Sumiga et al., 2019), as well as antibiofilm and antimicrobial (Pontes et al., 2019). Starting from this, to achieve learning that produces innovative products, creative thinking skills are needed (Rajan et al., 2019).

Lemongrass essential oil is obtained by extracting it through a steam distillation process (Tran et al., 2020). Steam distillation in micro-assisted essential oil extraction can increase the yield of essential oils (Xiao et al., 2021). Steam distillation itself is a method of isolating compounds that decompose at high temperatures through distillation so that steam is introduced into the raw material (Masango, 2005). In this technique, pure aromatherapy oils are extracted, resulting in a product that is free from contamination. Another method, namely vacuum fractional distillation, is an easy method for separating essential oil (EO) components because of its simplicity and economical operational costs (Beneti et al., 2011). This method operates at low pressure, which reduces the boiling point of the components, thereby preventing overheating and burning of the oil. Research has been carried out on vacuum fractional distillation of essential oils for the separation of limonene, increasing the composition of citronellal, citronellol, and geraniol in citronella essential oil (Beneti et al., 2011). The resulting compounds have many valuable uses. However, if there are individual compounds that have high value, it is desirable to separate the mixture properly, thereby increasing the value of the original essential oil. Pure constituents and fractions of essential oils often exhibit stronger pharmacological properties and thus have much greater commercial value than the essential oil itself (Do et al., 2021).

The use of lemongrass essential oil in innovative products for health is quite promising, considering its unique properties and benefits, making it a potential candidate for addressing global health challenges and supporting the achievement of the Sustainable Development Goals (SDGs). Several studies on making innovative products from lemongrass oil that are useful for health, including environmentally friendly mosquito repellent products (Higuchi et al., 2023; Motelica et al., 2021), antimicrobials in microencapsulation applied in pressure-sensitive antimicrobial functional coatings on paper with secondary packaging with a shelf life of 2 years (Šumiga et al., 2019), antibiofilm activity with S. aureus biofilm inhibition (Pontes et al., 2019), and aromatherapy candles (Tran et al., 2020). Thus, the essential oil from lemongrass offers a variety of health benefits, while the cultivation and extraction process provides an opportunity to explore education for sustainable development (ESD) as applied in higher education.

Higher education institutions make maximum efforts to provide education for sustainable development (ESD) (UNESCO, 2012; Veiga et al., 2017) and implement sustainable practices in various sectors (Lozano et al., 2015; Ramos et al., 2015). Education for Sustainable Development (ESD) is a concept designed systematically to understand and change the education system. The aim is to encourage and incorporate the idea of sustainability in the minds, hearts, and actions of future generations (Zgur et al., 2021). The term ESD also reflects initiatives to establish a global education system that supports changes in knowledge, skills, and

attitudes to direct society towards sustainability (Leicht et al., 2018). Thus, Education for Sustainable Development (ESD) equips students with the knowledge, skills, and values to face complex challenges in a global world. This study also investigates the potential of lemongrass essential oil as a context for developing ESD learning activities that are aligned with the ESD Sustainable Development Goals (SDGs), specifically SDG 3: Good Health and Well-Being. Finding interesting and relevant contexts for ESD is critical, and this research explores the potential of lemongrass essential oil as a promising avenue for innovative learning. This research aims to analyze the potential context of essential oil from lemongrass and aspects of the SDGs to develop innovative learning with ESD content.

Method

The research method used in this preliminary study involved an initial exploration of the context of lemongrass essential oil as a means to introduce education for sustainable development (ESD). This research method includes a comprehensive analysis of the context of the process and potential of essential oil from lemongrass as well as aspects of the Sustainable Development Goals (SDGs) to develop innovative learning with the content of Environmentally Sustainable Development (ESD). The sample of 36 chemistry teacher candidates in this study were 5th-semester students who were taking organic chemistry courses. This research was conducted at a university in Bandung City, Indonesia.

This research consists of describing the results of searches from various literature regarding the process of extracting essential oils using various techniques and the use of the products for health. The instruments used in this research were a reading source analysis format to produce appropriate themes and subthemes and an open-ended questionnaire via Google Forms for prospective chemistry teacher participants. The literature review aims to describe the results of searches from various literature regarding the process of extracting essential oils using various techniques and using the products for health. Themes and Subthemes to analyze the literature to identify common themes and subthemes, such as the advantages and disadvantages of each extraction method, the influence of each method on the aromatherapy properties of essential oils, and the importance of comprehensive analytical characterization of essential oils. The open-ended questionnaire via Google Forms for prospective chemistry teacher participants was divided into six sections: critical reflection, systems thinking and analysis, participatory learning, creative thinking for future scenarios, collaborative learning, and the topic of the potential of citronella oil. The research found that the essential oil process involved extraction processes, microwave extraction, and steam distillation, where student teachers did not fully understand the process and context of potential essential oil products from lemongrass containing ESD. The topic of essential oil from lemongrass has an SDGs aspect, namely healthy and prosperous living because it produces potential products for health.

Results and Discussion

Potential Processing of Essential Oil from Lemongrass

There are two commonly known lemongrass plants, namely kitchen lemongrass (*Cymbopogon citratus*) and citronella lemongrass (*Cymbopogon nardus*). Lemongrass has the scientific name *Cymbopogon citratus* or is identical to Andropogon citratus, which currently numbers around 55 species. The main product of lemongrass is the essential oil that accumulates in the leaf stems, with the oil content varying between 0.4 to 2.0% depending on the variety, ecological conditions, and care method. Lemongrass oil contains many beneficial aromatic compounds, some of which have strong deodorizing and antibacterial properties (citral and geraniol) (Tran et al., 2020).

The main active components contained in lemongrass essential oil are limonene, ÿ-myrcene, citral, geraniol, citronellol, geranyl acetate, and neral nerol. Although ÿ-myrcene and limonene are aromatic composites, the main biologically active component of lemongrass essential oil is citral, a mixture of acyclic monoterpene isomers of the aldehydes neral (cis-citral) and geranial (trans-citral). In addition, lemongrass essential oil consists of small amounts of geraniol, geranyl acetate, and olefin monoterpenes (Do et al., 2021). The ingredient with the highest content in citronella oil is Citral (which accounts for more than 80% of the citronella oil content), which plays an important role in the functions of disinfectant, biocide, fragrance, and insecticide (Tran et al., 2020). Recent scientific studies show that various components of lemongrass essential oil have antioxidant properties (Fokom et al., 2019), antimicrobial (Šumiga et al., 2019), antifungal, anti-biofilm (Pontes et al., 2019), anti-inflammatory, anticancer potential, and other activities. anti-mosquito repellents (Do et al., 2021; Higuchi et al., 2023).

In the process of obtaining quality lemongrass essential oil results using Green Chemistry principles. Green Chemistry is a paradigm shift in professional practice. This urgent need for change is in line with the Sustainable Development Goals (SDGs) (Zhang, et al., 2023). Green Chemistry principles are applied using environmentally friendly solvents or techniques. It is important to use Green Chemistry solvents to replace organic solvents and conventional techniques, to avoid harm to the environment, researchers, and consumer health. Lemongrass essential oil is obtained by extracting it through a steam distillation process (Tran et al., 2020). Steam distillation in micro-assisted essential oil extraction can increase the yield of essential oils (Xiao et al., 2021).

Commonly used methods for essential oil separation include solvent extraction, fractional distillation, and Microwave-assisted extraction (MAE). Supercritical fluid extraction methods using carbon dioxide solvent have recently been used to separate and purify essential oils. This method overcomes the disadvantages of traditional extraction which uses organic solvents and produces large amounts of waste (Reverchon et al., 1995; Torres-Valenzuela et al., 2020). Supercritical fluid extraction procedures have been applied to natural products, particularly in pharmaceutical technology. The main advantage of this system is its low operating temperature as the critical point of carbon dioxide is at 31°C and 73.8 bar. At this low temperature, thermolabile compounds will not be destroyed and the organoleptic properties of the extract will not change.

The use of supercritical fluid extraction to segment and isolate pharmaceutical and chemical molecules from essential oils has been published in many studies, including fractional extraction for the fractionation of dried ginger for the production of high-quality essential oils (Shukla et al., 2019), fractions isolated from ten species of Salvia (Wrona et al., 2019), and fractionation of sterols, equipment, and squalene in linseed oil (Dąbrowski et al., 2019). Despite the fact that supercritical fluid extraction is known as a clean technology that provides good yields and purity, the operating pressure high levels requires modern equipment and raises safety issues and cost ineffectiveness (Do et al., 2021). Microwave-assisted extraction (MAE) is a method in which microwave energy is used to heat the solvent in contact with the sample, resulting in the separation of the analyte from the sample matrix into the solvent. The main advantage of this technique lies in its ability to rapidly heat the mixture of solvent and sample, allowing extraction to be carried out at high temperatures. By using a closed container, MAE can carry out extraction at high temperatures which accelerates the mass transfer of target compounds from the sample matrix. The extraction process usually only takes 15–30 minutes and involves the use of a relatively small volume of solvent, ranging from 10–30 ml. The amount of solvent used in MAE is about ten times less than in conventional extraction techniques (Eskilsson & Björklund, 2000).

The fractionation distillation method is a method that is simple to operate and low cost. Batch vacuum distillation is commonly used because it operates at an initial temperature and offers the flexibility to work with a variety of oils. The main advantage of the batch method is its flexibility and the possibility of working on a small scale, allowing the testing of raw materials before large-scale processing. Fractional distillation methods are based on differences in the volatility of compounds and depend on the physical and chemical characteristics of the components as well as the pressure and temperature of the distillation process. Separation productivity also depends on mass and energy transfer between the liquid and vapor phases of the mixture. Thus, the quality of essential oils depends on many different factors. Therefore, to guarantee the quality of essential oils, they must be stabilized and standardized by separation technology. Separation using fractional distillation is necessary to increase the stability of the oil and its commercial value. Essential oils have many valuable uses. However, if there are individual compounds that have high value, it is desirable to separate the mixture properly, thereby increasing the value of the original essential oil. Pure constituents and fractions of essential oils often exhibit stronger pharmacological properties and thus have much greater commercial value than the essential oil itself (Do et al., 2021).

The Potential of Essential Oil Products from Lemongrass for Health

The potential of essential oil products from lemongrass for health can be seen from its various properties and components. Some of the main health benefits of lemongrass essential oil include that lemongrass oil is used as a mosquito repellent product because it contains vegetable ingredients and provides the best mosquito repellent effect with a rejection period of 4 hours (Higuchi et al., 2023), this is because it has the active ingredients citronellal, citronellol, and geraniol which functions as a bio-pesticide (Motelica et al., 2021). Lemongrass oil can also be used as an antimicrobial in microencapsulation and applied in pressure-sensitive antimicrobial functional coatings on paper with secondary packaging with a shelf life of 2 years (Šumiga et al., 2019) and against antibiofilm activity with S. aureus biofilm inhibition up to 100% between concentrations of 0.5 mg/mL and 4 mg/mL (Pontes et al., 2019). Lemongrass oil can also be an aromatherapy product that provides relaxing,

anti-neuro depressive, and sedative effects on people who experience insomnia, thereby improving mood, reducing anxiety levels, and increasing alertness. Thus, the use of essential oil from lemongrass in aromatherapy is one way to treat various diseases. Because it is made from plants and has a distinctive aroma (Adetuyi et al., 2024). Another product that has many benefits is an aromatic candle made from lemongrass essential oil which functions to eliminate the smell of dirt that causes other odors and is usually placed in the living room, bedroom, and kitchen. In particular, many substances in aromatic candles are toxic to the body because they contain toluene ($C_6H_5CH_3$), acetone (CH_3COCH_3), formaldehyde (CH_2O), benzene derivatives, and methylene chloride (CH_2Cl_2). They have been shown to cause cancer, congenital defects, and degeneration of the nervous system. This research shows that the addition of lemongrass essential oil is an important factor that contributes to product quality (Tran et al., 2020).

Based on the literature provided, lemongrass essential oil has various properties and components that make it a potential product for innovative learning with ESD content. For example, it can be used as a mosquito repellent, an antimicrobial, an aromatherapy product, and an aromatic candle. These properties and components can be used to teach students about sustainable living, natural remedies, and the importance of using eco-friendly products. For example, students can learn about the harmful effects of toxic substances found in some aromatic candles and the benefits of using lemongrass essential oil as a natural alternative. Additionally, students can learn about the importance of using natural products to protect the environment and reduce the use of harmful chemicals. The following are the results of a Likert scale for prospective teacher students regarding the potential of essential oil products from lemongrass:

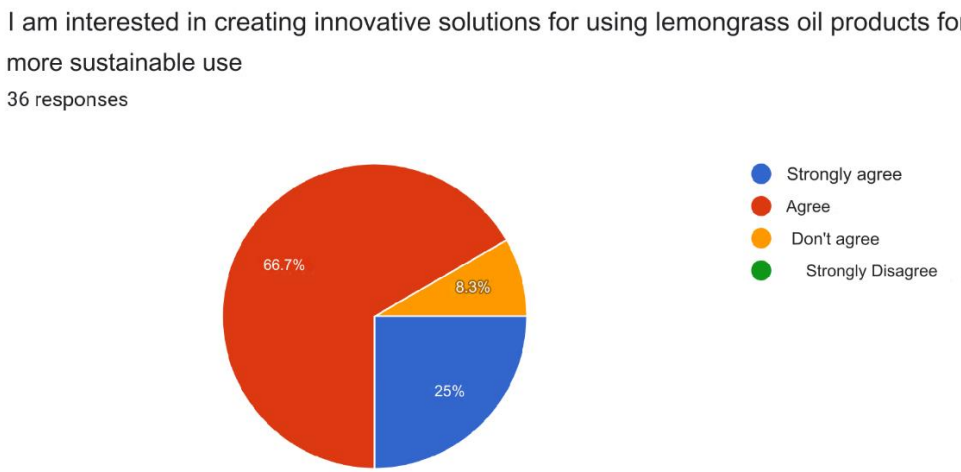

Figure 1. Innovative product application of lemongrass essential oil

The results show that 92% of prospective teacher students are interested in creating innovative product solutions from lemongrass essential oil that are environmentally friendly and beneficial for health. This highlights the growing interest in natural and environmentally friendly products, as well as the potential of lemongrass essential oil in a variety of uses. Some important points from the literature results include: Lemongrass essential oil (LEO) has been identified as a natural preservative with significant antimicrobial and antioxidant properties, making it suitable for use in the food industry as a safer alternative to synthetic preservatives (Faheem et al., 2022). The global lemongrass essential oil market is experiencing steady growth, driven by factors such as increasing demand, technological advancements, and increasing environmental awareness. Lemongrass essential oil is known to have potential benefits for skin health, as it has been shown to improve epidermal hydration and skin barrier integrity in a study conducted on human participants. These findings indicate a strong interest in exploring the potential of lemongrass essential oil in creating innovative and environmentally friendly products that improve health and well-being.

Innovative Learning Contains ESD

Critical Reflection

In the first statement regarding "I know the term ESD (Education for Sustainable Development) or education in sustainable development" which was given to prospective teacher students, the result was that 38.9% of students still did not know the term ESD, so students were given knowledge about ESD through short videos.

Furthermore, to find out whether the lecture they had experienced contained ESD or not, 83.3% stated that it had contained ESD. Questions continued regarding the importance of ESD to increase understanding regarding sustainable development issues in economic, social, and environmental aspects. Based on the results of open questions from prospective teacher students:

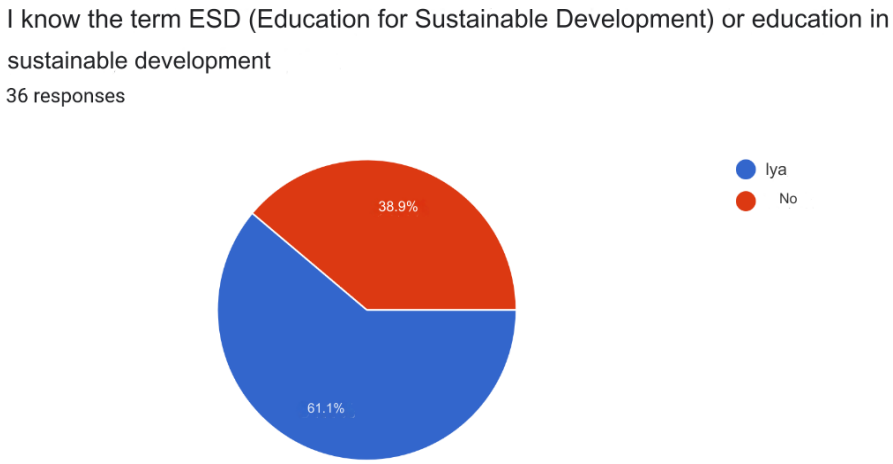

Figure 2. ESD (Education for Sustainable Development)

Table 1. The importance of ESD-based Learning

Theme	Sub-theme
Creating Change Agents	Encouraging students as agents in sustainable development
	Become a leader who cares about global issues
	Chaperone change for the environment
Enhance character and values	Building character and values of sustainable development
	Increase awareness of the environment
	Increase awareness of current issues
Improving knowledge and skills	Increase understanding of sustainable issues
	M e improve higher level thinking abilities
Supporting sustainable development	Prepare self from challenge issues current and future
	Finish issues latest through principle sustainable
	Creating a sustainable and balanced world
Innovation learning	Push use of student - centered learning models
	Push ESD lectures

Systems Thinking and Analysis

About 86.1% of students think that they have experienced the lectures taught which are related to current problems. There are interesting contexts that should be included in lectures, such as innovation and technology, environmental and climate issues, green chemistry, poverty, social humanities, factual education issues, safe health products, and current issues in the environment. Examples that can be applied in learning, starting with phenomena such as the global Lemongrass Essential Oil market experiencing stable growth, are driven by factors such as increasing demand, technological advances, and increasing environmental awareness. This growth trajectory provides an opportunity to incorporate citronella oil into innovative learning experiences that promote sustainability and ESD content

Participatory Learning

Students interested in participating in project-based learning related to sustainable development issues have been implemented in lectures. The suggestions from students in increasing the integration of sustainable development issues in lectures are the latest technology and innovation trends, development of the ESD course curriculum,

sustainable issues to training critical and creative thinking, innovative learning models and methods, practical experience through practice, workshops, and seminars, and strengthen scientific literacy.

Thinking Creatively for Future Scenarios

Increasing demand and developing technology are driving the growth of the Lemongrass Essential Oil Market. This provides an opportunity for educators to think creatively about the future of citronella oil-based products and incorporate them into innovative, ESD-laden learning experiences. This is in line with students' opinions that in lectures there is a need to create innovation regarding social, economic and environmental issues that are currently developing in society. The method or model suggested by students to encourage students to create solutions from the context of current trends in sustainable development issues is project-based learning.

Collaborative Learning

Maximizing the collaboration process within the group is very important. Students' suggestions for maximizing the collaboration process in groups include good communication, self-awareness and openness, good cooperation, and even distribution of tasks.

The Topic of the Potential of Essential Oils from Lemongrass

Some students have already carried out techniques for separating natural materials, including extraction, maceration, surface distillation, soxhlet, liquid-liquid extraction, solid-liquid extraction, gas chromatography, and thin-layer chromatography. The products that have been used are made from lemongrass oil, including telon oil, massage oils, aromatherapy candles, diffusers, soaps, mosquito repellents, floor cleaners, disinfectants, hand sanitizers, and herbal remedies. The functions of lemongrass oil that students know are as aromatherapy, anti-mosquito medicine, anti-inflammatory, relieving diarrhea, alleviating headaches, traditional medicine, and healing wounds. The topic of potential processes and essential oil products from lemongrass is very suitable when applied to organic chemistry learning at universities. Prospective teacher students believe that innovative learning containing ESD can stimulate creative thinking, critical thinking, collaboration, and deep understanding of concepts. These aspects can be incorporated into educational programs to promote sustainability and prepare students to play an active role in a sustainability-oriented society.

Conclusion

In conclusion, this preliminary research revealed the potential of essential oil from lemongrass to be used in innovative learning with Environmental Sustainable Development (ESD) content. The research found that the essential oil process involves extraction, microwave extraction, and steam distillation, where prospective chemistry teacher students do not fully understand the process of making potential essential oil from lemongrass with ESD content. Then the potential products of lemongrass oil as a health product that students already know include telon oil, massage oils, aromatherapy candles, diffusers, soaps, mosquito repellents, floor cleaners, disinfectants, hand sanitizers, and herbal remedies because it functions as aromatherapy, anti-mosquito medicine, anti-inflammatory, relieves diarrhea, relieves headaches, traditional medicine, and heals wounds. The research also revealed that 92% of prospective teacher students are interested in creating innovative product solutions that are environmentally friendly and good for health. The opinions of prospective teacher students regarding innovative learning with ESD content can stimulate creative thinking, critical thinking, collaboration, and deep understanding of concepts. The topic of essential oil from lemongrass has an SDGs aspect, namely healthy and prosperous living because it produces potential products for health. Based on the research results, it shows that the context of essential oil from lemongrass has the potential to be applied to innovative learning with ESD content. Further research is needed to explore the full potential of lemongrass essential oil in developing innovative health products that can address global health challenges and support the achievement of the SDGs.

Recommendations

Based on the findings of the research, the following recommendations can be made:

1. Education and Training: There is a need for educational initiatives and training programs to enhance the understanding of the essential oil extraction process, particularly among prospective chemistry teachers. This will enable them to effectively communicate the process and potential product context of essential oil from lemongrass, which contains Environmentally Sustainable Development (ESD) elements.
2. Product Innovation: The high level of interest among prospective teacher students in creating innovative, environmentally friendly, and health-beneficial product solutions presents an opportunity for collaborative product innovation projects. These projects can be designed to incorporate the use of lemongrass essential oil and align with the Sustainable Development Goals (SDGs).
3. Health and Environmental Impact: Further research is needed to explore the full potential of lemongrass essential oil in developing innovative health products that can address global health challenges and support the achievement of the SDGs. This research should also consider the health and environmental impact of lemongrass essential oil products.
4. Quality and Safety: Given the concentrated nature of lemongrass essential oil, it is essential to ensure the quality and safety of the product. This includes adherence to organic standards and the use of pure, trusted sources of the oil.
5. Innovative Learning: The research has highlighted the potential of lemongrass essential oil to be applied to innovative learning with ESD content. This can be further explored through the development of educational materials and programs that integrate the use of lemongrass essential oil as a case study for ESD-informed learning.

By addressing these recommendations, it is possible to harness the potential of lemongrass essential oil for innovative, sustainable, and health-conscious product development, while also supporting the advancement of ESD and the SDGs.

Scientific Ethics Declaration

The authors declare that the scientific ethical and legal responsibility of this article published in EPSTEM journal belongs to the authors.

Acknowledgments

* This article was presented as an oral presentation at the International Conference on Basic Sciences, Engineering and Technology (www.icbaset.net) held in Alanya/Turkey on May 02-05, 2024.

*The researchers would like to express their deepest gratitude to the Education Fund Management Institute (LPDP/Indonesia Endowment Fund for Education) under the Ministry of Finance of the Republic of Indonesia as the sponsor for their master's studies, and the support for this paper and publication.

References

Adetuyi, B. O., Olajide, P. A., Adetunji, C. O., Adetunji, J. B., Popoola, O. A., Ajenifujah-Solebo, O., ... & Inobeme, A. (2024). Application of essential oil in aromatherapy: current trends. *Applications of Essential Oils in the Food Industry* (pp. 219-233). Academic Press.

Beneti, S. C., Rosset, E., Corazza, M. L., Frizzo, C. D., Di Luccio, M., & Oliveira, J. V. (2011). Fractionation of Citronella (*Cymbopogon winterianus*) essential oil and concentrated orange oil phase by batch vacuum distillation. *Journal of Food Engineering*, *102* (4), 348–354.

Dąbrowski, G., Czaplicki, S., & Konopka, I. (2019). Fractionation of sterols, tocols and squalene in flaxseed oils under the impact of variable conditions of supercritical CO_2 extraction. *Journal of Food Composition and Analysis*, *83*, 103261.

Do, D. N., Nguyen, D. P., Phung, V. D., Le, X. T., Le, T. M., Do, V. M., Minh, B. Q., & Luu, X. C. (2021). Fractionating of lemongrass (Cymbopogon citratus) essential oil by vacuum fractional distillation. *Processes*, *9*(4), 1–12.

Eskilsson, C. S., & Björklund, E. (2000). Analytical-scale microwave-assisted extraction. *Journal of Chromatography A*, *902*(1), 227-250.

Faheem, F., Liu, Z. W., Rabail, R., Haq, I. U., Gul, M., Bryła, M., ... & Aadil, R. M. (2022). Uncovering the industrial potentials of lemongrass essential oil as a food preservative: a review. *Antioxidants*, *11*(4), 720.

Fokom, R., Adamou, S., Essono, D., Ngwasiri, D. P., Eke, P., Mofor, C. T., Tchoumbougnang, P., Fekam, B. F., Zollo, P. H. A., & Sharma, A. K. (2019). Growth, essential oil content, chemical composition and antioxidant properties of lemongrass as affected by harvest period and arbuscular mycorrhizal fungi in field conditions. *Industrial Crops and Products*, *138*, 111477.

Higuchi, C. T., Sales, C. C., Andréo-Filho, N., Martins, T. S., Ferraz, H. O., Santos, Y. R., Lopes, P. S., Grice, J. E., Benson, H. A. E., & Leite-Silva, V. R. (2023). Development of a nanotechnology matrix-based citronella oil insect repellent to obtain a prolonged effect and evaluation of the safety and efficacy. *Life*, *13*(1).

Katekar, V. P., Rao, A. B., & Sardeshpande, V. R. (2023). A hydrodistillation-based essential oils extraction: A quest for the most effective and cleaner technology. *Sustainable Chemistry and Pharmacy*, *36*, 101270.

Leicht, A., Heiss, J., & Byun, W. J. (2018). *Issues and trends in education for sustainable development* (5th ed., p.4). UNESCO Publishing.

Lozano, R., Ceulemans, K., Alonso-Almeida, M., Huisingh, D., Lozano, F. J., Waas, T., ... & Hugé, J. (2015). A review of commitment and implementation of sustainable development in higher education: results from a worldwide survey. *Journal of Cleaner Production*, *108*, 1-18.

Mahato, N., Sharma, K., Koteswararao, R., Sinha, M., Baral, E., & Cho, M. H. (2019). Citrus essential oils: Extraction, authentication and application in food preservation. *Critical Reviews in Food Science and Nutrition*, *59*(4), 611-625

Masango, P. (2005). Cleaner production of essential oils by steam distillation. *Journal of Cleaner Production*, *13*(8), 833-839.

Motelica, L., Ficai, D., Oprea, O. C., Ficai, A., Ene, V. L., Vasile, B. S., Andronescu, E., & Holban, A. M. (2021). Antibacterial biodegradable films based on alginate with silver nanoparticles and lemongrass essential oil–innovative packaging for cheese. *Nanomaterials*, *11*(9), 2377.

Nations, U. (2016). *Transforming our world: The 2030 agenda for sustainable development*. United Nations Publication.

Pontes, E. K. U., Melo, H. M., Nogueira, J. W. A., Firmino, N. C. S., de Carvalho, M. G., Catunda Júnior, F. E. A., & Cavalcante, T. T. A. (2019). Antibiofilm activity of the essential oil of citronella (Cymbopogon nardus) and its major component, geraniol, on the bacterial biofilms of Staphylococcus aureus. *Food Science and Biotechnology*, *28*(3), 633–639.

Pujari, R., Reddy, S.B., Satishkumar, M. (2020). Essential oils in India-history and future prospects. *Biot. Res. Today 2*, 938–940.

Rajan, K. P., Gopanna, A., & Thomas, S. P. (2019). A project-based learning (PBL) approach involving PET recycling in chemical engineering education. *Recycling*, *4*(1), 10.

Ramos, T. B., Caeiro, S., Van Hoof, B., Lozano, R., Huisingh, D., & Ceulemans, K. (2015). Experiences from the implementation of sustainable development in higher education institutions: Environmental Management for Sustainable Universities. *Journal of Cleaner Production*, *106*, 3-10.

Reverchon, E., Porta, G. D., & Senatore, F. (1995). Supercritical CO_2 extraction and fractionation of lavender essential oil and waxes. *Journal of Agricultural and Food Chemistry*, *43*(6), 1654-1658.

Shukla, A., Naik, S. N., Goud, V. V., & Das, C. (2019). Supercritical CO2 extraction and online fractionation of dry ginger for production of high-quality volatile oil and gingerols enriched oleoresin. *Industrial Crops and Products*, *130*, 352-362.

Sofowora, A., Ogunbodede, E., & Onayade, A. (2013). The role and place of medicinal plants in the strategies for disease prevention. *African Journal of Traditional, Complementary and Alternative Medicines*, *10*(5), 210-229.

Šumiga, B., Šumiga, B., Ravnjak, D., & Podgornik, B. B. (2019). Antimicrobial paper coatings containing microencapsulated cymbopogon citratus oil. *Coatings*, *9*(8), 470.

Torres-Valenzuela, L. S., Ballesteros-Gómez, A., & Rubio, S. (2020). Green solvents for the extraction of high added-value compounds from agri-food waste. *Food Engineering Reviews*, *12*, 83-100.

Tran, T. K. N., Tran, T. H., Le, T. H. N., Xuan, T. L., Phan, N. Q. A., Cam, T. I., & Long, G. B. (2020). Development of an aromatic wax product containing natural Lemongrass (Cymbopogon Citratus) essential oil. *IOP Conference Series: Materials Science and Engineering*, *736*(2), 022066.

UNESCO (2021). *Education for sustainable development*. Retrieved from https://en.unesco.org/themes/education-sustainable-development-esd.

Wrona, O., Rafińska, K., Możeński, C., & Buszewski, B. (2019). Supercritical carbon dioxide extraction of Solidago gigantea Ait.: Optimization at quarter-technical scale and scale up the process to half-technical plant. *Industrial Crops and Products*, *130*, 316-324.

Xiao, Y., Liu, Z., Gu, H., Yang, F., Zhang, L., & Yang, L. (2021). Improved method to obtain essential oil,

asarinin and sesamin from Asarum heterotropoides var. mandshuricum using microwave-assisted steam distillation followed by solvent extraction and antifungal activity of essential oil against Fusarium spp. *Industrial Crops and Products*, *162*, 113295.

Zguir, M. F., Dubis, S., & Koç, M. (2021). Embedding Education for Sustainable Development (ESD) and SDGs values in curriculum: A comparative review on Qatar, Singapore and New Zealand. *Journal of Cleaner Production*, *319*, 128534.

Author Information

Nanda Ayu Lestari
Universitas Pendidikan Indonesia
Setiabudi Street. 229th, Bandung, Indonesia
Contact e-mail: *nandaayulestari@upi.edu*

Liliasari Liliasari
Universitas Pendidikan Indonesia
Setiabudi Street. 229th, Bandung, Indonesia

Iqbal Musthapa
Universitas Pendidikan Indonesia
Setiabudi Street. 229th, Bandung, Indonesia

Hernani Hernani
Universitas Pendidikan Indonesia
Setiabudi Street. 229th, Bandung, Indonesia

Anita Fadhilah
Universitas Pendidikan Indonesia
Setiabudi Street. 229th, Bandung, Indonesia

To cite this article:

Lestari, N.A. Liliasari, L., Musthapa, I., Hernani, H., & Fadhilah, A. (2024). The essential oil context of lemongrass and its potential for innovative ESD-informed learning. *The Eurasia Proceedings of Science, Technology, Engineering & Mathematics (EPSTEM), 28,* 157-166.

The Eurasia Proceedings of Science, Technology, Engineering & Mathematics (EPSTEM)
ISSN: 2602-3199

The Eurasia Proceedings of Science, Technology, Engineering & Mathematics (EPSTEM), 2024

Volume 28, Pages 167-174

ICBASET 2024: International Conference on Basic Sciences, Engineering and Technology

Extraction of Anthocyanin Pigments from the Peel of Dragon Fruit for Food Coloring

Anis Muyassaroh
Universitas Pendidikan Indonesia

Asep Supriatna
Universitas Pendidikan Indonesia

Hernani Hernani
Universitas Pendidikan Indonesia

Abstract: Kitchen waste is a source of methane gas which strongly contributes to the greenhouse effect (Lee et al., 2017). One of the organic waste that comes from the kitchen is fruit peel with a large percentage reaching (25-60%) (Nirmal et al., 2023). To increase waste reduction efforts can be done by converting food waste into natural dyes by extraction. This can be a solution to consumer concerns about the insecurity of synthetic dyes that are carcinogenic if consumed excessively. Natural colorants that have the potential to be extracted include anthocyanins. Dragon fruit skin contains a rich source of anthocyanin pigments. The use of natural dyes extracted from dragon fruit peel is suitable with the Sustainable Development Goals (SDGs), this context can be an interesting learning project and grow an understanding of environmental responsibility through direct learning experiences (Andersson et al., 2013). This research aims to identify the optimal method of anthocyanin extraction from dragon fruit peels which can be applied to Education Sustainable Development (ESD) orientated learning. The research method carried out is a laboratory experimental method with qualitative analysis. The parameters observed were the effect of solvent, temperature, pH, and mass on the absorbance of dragon fruit peel extract. Anthocyanin extraction from dragon fruit skin using maceration method. Based on the observation data, the best treatment is the sample with 10% citric acid solvent. Anthocyanins are most optimally stored at a low temperature of 10°C, with an acidic pH of Ph 4 and with a mass: solvent ratio of 250: 100.

Keywords: Natural dye, Anthocyanin, Waste fruit peel

Introduction

The household kitchen is a significant contributor to organic waste. Kitchen waste is a source of methane gas release contributing strongly to the greenhouse effect (Lee et al., 2017). According to Nirmal et al. (2023), one of the organic waste coming from the kitchen is fruit peels with a high percentage of up to (25-60%). Although composting is a suitable option to solve organic waste, there is still a lot of organic waste, especially fruit peel waste, that is thrown away, causing pollution to the environment, and causing bad smells. So, innovative techniques and processes are needed to convert fruit peels, which are usually a waste, into high-quality materials that have a variety of applications (Nirmal et al., 2023., Pathak et al., 2017). According to Dudziak et al. (2022), to improve waste reduction and conform with circular economy principles, it is possible to convert food waste into natural dyes by extraction. This can be a solution to concerns among consumers regarding the unsafety of synthetic dyes (Singh et al., 2023). Most synthetic dyes can cause various effects if their use is more than the threshold, and the long-term use of synthetic dyes is harmful to humans because they are carcinogenic. In addition, synthetic dyes are bad for the environment because they pollute water and soil (Kwartiningsih et al.,

2016). The limitations on the use of synthetic dyes cause an increased interest in research on natural dyes. Natural dyes are safe to use in the long term are safe for health and environmentally friendly and have the potential to replace synthetic dyes. Natural dyes with potential to be extracted include anthocyanins (Almajid et al., 2021).

Anthocyanins are red, purple, and blue pigments commonly found in plants (Widyasanti et al., 2021). Anthocyanins are classified as pigments called flavonoids. Flavonoid class compounds include polar compounds and can be extracted with solvents that are polar as well. Acidic conditions will affect the extraction results. The more acidic conditions will cause more anthocyanin pigments to be extracted, this is due to the more vacuole cell walls being broken so that more anthocyanin pigments are extracted (Ariviani, 2010). Anthocyanins can replace the use of synthetic dyes rhodamine B, carmoisin, and amaranth as a red dye in food products. JEFCA *(Joint FAO/WHO Expert Committee on Food Additives)* has stated that extracts containing anthocyanins have low toxicity effects. In addition to their role as food colorants, anthocyanins are also believed to contribute to biological systems, including their ability to attract free radicals and the ability to inhibit the initiation stage of chemical reactions that cause carcinogenesis (Almajid et al., 2021).

Dragon fruit skin is the most discarded part of the fruit processing process. The peel component is about 20% of the dragon fruit (Widyasanti et al., 2021). Dragon fruit skin contains a rich source of anthocyanin pigments (Carrillo et al., 2022). The process of extracting anthocyanin pigments from dragon fruit skin is quite easy to do. One method that can be used is maceration, a process where the peel is soaked in a solvent to release the color (Vinha et al., 2018). The maceration method was chosen because the damage factor of the active substance is smaller. This is because the maceration method does not use heat, which can damage the active substances drawn. The main emphasis of this method is the availability of sufficient contact time between the solvent and the extracted tissue (Hanum, 2000). Although simple in this maceration method, it is necessary to know the factors that affect the extraction of anthocyanin compounds from dragon fruit peels such as the type of solvent, extraction temperature, extraction pH, material size, and the ratio of the amount of material to solvent (Sudarmi et al., 2015). This maceration technique is very easy to adapt for learning purposes (Dewi et al., 2020). By including maceration in school learning, students can gain practical experience in processing fruit peel waste into natural dyes (Ingrath et al., 2015).

The use of natural dyes extracted from dragon fruit peels aligns with several key aspects of the Sustainable Development Goals (SDGs) with the 12th Goal, Responsible Consumption, and Production, prioritizing minimizing waste production and optimizing resource utilization (Wang et al., 2019). Reusing fruit peels as a colorant directly aligns with this goal by turning waste into a valuable product (Otles & Kartal, 2018). In addition, SDG Goal 4, Quality Education, advocates integrating sustainability principles into the education curriculum (Treaty, 2003). This context can be an engaging learning project and foster an understanding of environmental responsibility through hands-on learning experiences (Andersson et al., 2013).

Based on the description above, it is important to identify the most optimal way of extracting anthocyanins from dragon fruit peels which can later be applied to Education Sustainable Development (ESD) with a focus on waste utilization to make useful products. So, it is expected that students can develop an understanding of the importance of protecting the environment and managing fruit peel waste.

Method

The research method conducted was a laboratory experimental method with qualitative analysis. This research was conducted using 3 different solvent treatments, aquades, 10% citric acid, and 10% acetic acid. Qualitative determination of anthocyanins was carried out with phytochemical tests and maximum wavelength measurements. The parameters observed were the effect of solvent, temperature, pH, and mass on the absorbance of dragon fruit peel extract.

Instruments and Materials

The instruments used are a stirring rod, bottle, blender, glass funnel, beaker, measuring cup, hot plate, watch glass, Whatman filter paper, cuvette, volumetric flask, fume hood, pH meter, dropper pipette, measuring pipette, knife, propped, tube rack, centrifuge, metal spatial/spatula, UV-Vis spectrophotometer, test tube, centrifuge tube, thermometer, and analytical balance. The materials used were glacial acetic acid (CH_3COOH), hydrochloric acid (HCl), citric acid ($C_6H_8O_7$), Sodium Hydroxide (NaOH) distilled water, pH 4 buffer solution,

pH 5 buffer solution, pH 7 buffer solution, pH 10 buffer solution, pH 11 buffer solution, and red dragon fruit peel.

Research Steps

This research consists of three steps, the first step is the preparation of raw materials, the second step is maceration extraction, and the third step is quality testing and data analysis.

Raw Material Preparation

Samples of red dragon fruit were washed first then peeled and cleaned to separate the pulp from the skin and wet sorting was carried out by separating the green or brown skin and the remaining pulp contained in the inner skin of the dragon fruit. Then washing and draining are done. Next, the peel is cut into small pieces and blended until it becomes smooth to expand the surface area of the sample until it is shaped like porridge.

Extraction of Anthocyanins from Red Dragon Fruit Peel

Dragon fruit peels that have been blended until they are like porridge are weighed and solvents are added (1:2 = material: solvent). The solvents used were distilled water, 10% citric acid, and 10% acetic acid. The next stage was maceration extraction for 3 days. The results of maceration for 3x24 hours (macerate) obtained were filtered using a filter and Whatman filter paper, and then the macerate obtained was centrifuged for 10 minutes (2500 rpm/minute). The supernatant obtained from the centrifuge results in a precipitate-free anthocyanin liquid extract, the anthocyanin liquid extract is stored in a bottle and the filtrate obtained is ready for analysis.

Phytochemical Test

Anthocyanin phytochemical test was conducted according to Harborne, 1996, that is, 3 mL of anthocyanin liquid extract was added 3-5 drops of 2M HCl and then heated at 100°C for 5 minutes. In addition, 3 mL of liquid anthocyanin extract can also be added to 2M NaOH drop by drop and waited for 1 minute while observing the color changes that occur.

Finding the Maximum Wavelength

Each sample was taken with 3 ml of different solvents, and then the wavelength from 200-800nm to find the maximum peak point of anthocyanins using a UV-visible spectrophotometer.

Solvent Variation

Take 3 ml of each sample with different solvents, then measure the absorbance with UV-Vis at the maximum wavelength of each sample with solvent.

Temperature Effect

Based on the absorbance results of the solvent variation, the sample that has the highest absorbance value is tested for temperature stability. Samples were made with temperatures of 10°C, 25°C to 27°C, and 80°C to 100°C and then observed by measuring the temperature using a thermometer, then 2 mL of liquid extract that had the highest anthocyanin content was taken and dissolved to 10 mL with the solvent used, then the solution was put in a test tube and treated at each of these temperatures for 30 minutes. After 30 minutes of treatment, the absorbance was seen using a UV-Vis Spectrophotometer at a predetermined maximum wavelength.

Effect of pH

Based on the absorbance results of the solvent variation, the sample that has the highest absorbance value is tested for pH stability. Measured each buffer solution that has been made by measuring the pH of the buffer solution using a pH meter, then 2 mL of liquid extract that has the highest anthocyanin content is dissolved to 10 mL with each buffer solution pH 4, 5, 7, 10, and 12, then put in a test tube and allowed to stand for 30 minutes. After 30 minutes of treatment, the absorbance was seen using a UV-Vis Spectrophotometer at a predetermined maximum wavelength.

Effect of Mass on Solvent

Based on the absorbance results of the solvent variation, the sample that has the highest absorbance value is tested for stability against mass. Samples were made with 5 variations of mass to solvent, namely 50:100, 100:100, 150:100, 200:100, and 250:100 (mass: solvent). Then all samples were macerated for 24 hours and then tested for absorbance using a UV-Vis Spectrophotometer at a predetermined maximum wavelength.

Results and Discussion

The maceration method was chosen because the damage factor of the active substance is smaller. This is because the maceration method does not use heat which can damage the active substances being extracted. The main emphasis of this method is the availability of sufficient contact time between the solvent and the extracted tissue. Maceration is done by immersing the simplistic powder in a liquid solvent. The solvent will penetrate the cell wall and enter the cell cavity containing the active substance (Hanum, 2000).

The solvents used for this maceration process are distilled aquades, acetic acid, and citric acid with a concentration of 10% each. The solvent was chosen because it is a polar organic acid solvent, the use of inorganic solvents such as HCl is avoided because the anthocyanins obtained from dragon fruit peel extract will be used as a food coloring. The anthocyanins obtained from each type of solvent were then seen for their maximum wavelength and absorbance in each solvent.

The most stable anthocyanin will be tested against the effects of temperature, pH, and mass ratio. The optimum wavelength is sought by measuring colored samples in the range of 490-580 nm with spectrophotometer analysis. The identification of anthocyanin pigments is based on the observation of the maximum absorbance located at a wavelength of 490-580 nm (Harborne, 1996).

Phytochemical Test

Phytochemical tests were conducted to identify anthocyanin compounds in the form of color tests using NaOH 2M and HCl 2M reagents. The results obtained from the anthocyanin phytochemical test on the liquid extract of red dragon fruit peel are the same as the literature used, namely according to Harborne, 1996, the positive anthocyanin sample is marked if it is dripped with 2M HCl and heated at 100 ℃ for 5 minutes, the color remains or does not fade and if the sample is dripped with 2M NaOH drop by drop, there is an initial color change which becomes bluish green, so that the sample of red dragon fruit peel liquid extract with the different solvents used is positive indicating the presence of anthocyanin compounds (Almajid et al., 2021).

Table 1. Results of anthocyanin phytochemical test of dragon fruit peel extract

Test	Result Aquades	Citric acid 10%	Acetic acid 10%	Description
Dropped with 5 drops of 2M HCl and heated at 100℃ for 2 minutes)	Fixed color or no fading	Fixed color or no fading	Fixed color or no fading	Positive
Dropped with 5 drops of 2M NaOH and heated at 100℃ for 2 minutes)	Color change or fading	Color change or fading	Color change or fading	Positive

Finding the Maximum Wavelength

The measurement results of determining the maximum wavelength using a Uv-Vis Spectrophotometer at a wavelength of 200-800 nm can be seen in Table 2.

Table 2. Results of maximum wavelength determination (λ max)

Maximum wave peak	Solution
530 nm	Aquades
531 nm	Citric acid 10 %
529 nm	Acetic acid 10%

The results of the maximum wavelength (λ max) of the research obtained are still around the λ max of the literature used that the maximum wavelength characteristics of anthocyanins have a range of visible light spectrum areas at 505-535 nm (Almajid et al., 2021). The highest maximum wavelength result was obtained from the extraction of anthocyanins from dragon fruit skin using a citric acid solution. The wavelength obtained was 531 nm.

Effect of Solvent Type

The results of anthocyanin absorbance show that the use of 10% citric acid solvent produces the highest absorbance compared to distilled water and 10% acetic acid solvents. The test results of the solvent-type test on anthocyanins can be seen in Table 3.

Table 3. Results on the effect of solvent type

Solvent	Absorbance
Aquades	0,220
Citric Acid	0,451
Acetid Acid	0,406

The difference in absorbance values produced for every solvent with the addition of types of organic acids is considered to be a result of the difference in the dissociation constant of each type of acid. Citric acid has a higher dissociation constant than acetic acid. The dissociation constants for citric acid and acetic acid are 7.21×10^{-4} and 1.75×10^{-5}, respectively (Almajid et al., 2021). The higher the dissociation constant, the stronger the acid is because the higher the number of hydrogen ions released into the solution. The more acidic situation, especially close to pH 1, will cause anthocyanin pigments to be in the form of colored flavilium or oxonium cations, and absorbance measurements will show a higher amount of anthocyanins and cause the vacuole cell walls to break so that more anthocyanins are extracted (Almajid et al., 2021).

Temperature Effect

The results of the anthocyanin stability test on temperature for 30 minutes can be seen in Table 4.

Table 4. Results on the effect of temperature

Temperature	Absorbance
10℃	0.959
25℃-27℃	0.399
50℃-80℃	0.228

Anthocyanin absorbance was measured at a wavelength of 531 nm. The higher the temperature, the lower the absorbance results produced which indicates that anthocyanins are not stable at higher temperatures. This may be because at high temperatures, anthocyanins are decomposed so the more colour that is degraded, so the lower the absorbance value (Khoo et al., 2017). This is supported by Markakis in Almajid et al. (2021), which states that the decrease in colour stability due to high temperatures is due to the decomposition of anthocyanins from the aglycone form to chalcone (colourless). Anthocyanins are stable when stored at 4-25°C under low light conditions (Vargas et al., 2013).

Effect of pH

The results of the anthocyanin stability test on pH for 30 minutes can be seen in Table 5.

Table 5. Results on the effect of pH

pH	Absorbance
4	0.468
5	0.245
7	0.163
10	0.124
12	0.123

Anthocyanin absorbance was measured at a wavelength of 513 nm. In pH 4 the acid has a better absorbance value than the buffer pH 5, 7, 10, and 12. The higher the pH given the more unstable the anthocyanin content or the higher the anthocyanin degradation from the red dragon fruit skin. At low pH, anthocyanins turn into platinum cations which are red (Lullung Sampebarra, 2018). The higher the pH, the color of the anthocyanin pigment will change to a colorless chalcone compound (Sukaminah et al., 2007).

Effect of Mass on Solvent

The results of the anthocyanin stability test on mass for 24 hours can be seen in Table 6.

Table 6. Results on the effect of mass

Mass ratio: solvent	Absorbance
50 : 100	0.686
100 : 100	1.045
150 : 100	1.057
200 : 100	1.188
250 : 100	1.599

Based on Table 6 shows the absorbance of anthocyanins measured at a wavelength of 531 nm. The mass ratio of 250:100 has a better absorbance value than the mass ratio of 50:100, 100:100, 150:100, and 200:100. However, the decrease in absorbance does not visually affect the color pigment changes in the extract but affects the amount of anthocyanin extract obtained. The more mass used during extraction, the higher the absorbance value obtained while the less mass used during extraction, the lower the absorbance value obtained. This is because the absorbance value is directly related to the concentration of the solute in the extract phase, which is affected by the amount of mass used during the extraction process. Because the more mass there is in the extract, the higher the mass concentration in the extract (Handayani et al., 2018).

Conclusion

This study discusses the importance of effective and appropriate kitchen waste management, with a focus on the utilization of fruit peel waste as a source of natural dye. One of them is separating anthocyanin pigments from red dragon fruit skin using the maceration method. The maceration method was chosen because the damage factor of the active substance is smaller. This is because the maceration method does not use heat which can damage the active substance being extracted. Based on the observation data in the laboratory, the extraction process using maceration showed the best treatment on samples with 10% citric acid solvent. Anthocyanins are most optimally stored at a low temperature of 10°C, with an acidic pH of Ph 4 and with a mass: solvent ratio of 250:100. The maceration extraction process is a simple method that can be applied in extracting anthocyanin compounds from red dragon fruit skin.

Recommendations

This study suggests paying attention to effective and appropriate kitchen waste management, by utilizing fruit peel waste as a source of natural dye. In addition, this study shows that the topic of separating anthocyanin pigments from dragon fruit peels as a natural dye can be an interesting context to be applied in chemistry learning, especially in the context of Education for Sustainable Development (ESD). Therefore, it is recommended to integrate this topic into chemistry learning to improve students' understanding of chemical separation in natural materials and the importance of developing sustainable and environmentally friendly

natural dyes. In addition, this study also showed that the utilization of anthocyanin pigment extract from dragon fruit skin as a natural dye can contribute to the achievement of SDGs. It is hoped that this research can increase public awareness about the importance of using natural dyes that are environmentally friendly and effective for increasing sustainable consumption.

Scientific Ethics Declaration

The authors declare that the scientific ethical and legal responsibility of this article published in EPSTEM journal belongs to the authors.

Acknowledgements or Notes

* This article was presented as an oral presentation at the International Conference on Basic Sciences, Engineering and Technology (www.icbaset.net) held in Alanya/Turkey on May 02-05, 2024.

* The researchers would like to express their deepest gratitude to the Education Fund Management Institute (LPDP and KEMENAG/Indonesia Endowment Fund for Education) under the Ministry of Finance of the Republic of Indonesia as the sponsor for their master's studies, and the support for this paper and publication

References

Almajid, G. A. A., Rusli, R., & Priastomo, M. (2021). Pengaruh pelarut, suhu, dan ph terhadap pigmen antosianin dari ekstrak kulit buah naga merah (hylocereus polyrhizus). *Proceeding of Mulawarman Pharmaceuticals Conferences*, *14*, 179–185.

Andersson, K., Jagers, S. C., Lindskog, A., & Martinsson, J. (2013). Learning for the future: Effects of education for sustainable development (ESD) on teacher education students. *Sustainability* , *5*(12), 5135–5152.

Ariviani, S. (2010). Total antosianin ekstrak buah salam dan korelasinya dengan kapasitas anti peroksidasi pada sistem linoelat. *Agrointek*, *4*(2), 121–127.

Carrillo, C., Nieto, G., Martínez-Zamora, L., Ros, G., Kamiloglu, S., Munekata, P. E. S., Pateiro, M., Lorenzo, J. M., Fernández-López, J., Viuda-Martos, M., Pérez-Álvarez, J. Á., & Barba, F. J. (2022). Novel approaches for the recovery of natural pigments with potential health effects. *Journal of Agricultural and Food Chemistry*, *70*(23), 6864–6883.

Dudziak, A., Stoma, M., & Derkacz, A. J. (2022). Circular economy in the context of food losses and waste. *Sustainability*, *14*(16), 1–21.

Hanum, T. (2000). Ekstraksi dan stabilitas zat pewarna alam dari katul beras ketan hitam (oryza sativa glutinosa). bul. teknol. dan ındustri pangan. *Jurnal Teknologi dan Industri Pangan*, *11*(1), 17-17.

Handayani, M. N., Khoerunnisa, I., Cakrawati, D., & Sulastri, A. (2018). Microencapsulation of dragon fruit (hylocereus polyrhizus) peel extract using maltodextrin. In *IOP Conference Series: Materials Science and Engineering*, *288*(1),012099.

Harbone, J. B. (1996). *Metode fitokimia: Penuntun cara modern menganalisis tumbuhan*. Bandung: Penerbit ITB

Ingrath, W., Nugroho, W. A., & Yulianingsih, R. (2015). Ekstraksi pigmen antosianin dari kulit buah naga merah (hylocereus costaricensis) sebagai pewarna alami makanan dengan menggunakan microwave (kajian waktu pemanasan dengan microwave dan penambahan rasıo pelarut aquades dan asam sıtrat) extraction of a. *Jurnal Bioproses Komoditas Tropis*, *3*(3), 1–8.

Khoo, H. E., Azlan, A., Tang, S. T., & Lim, S. M. (2017). Anthocyanidins and anthocyanins: Colored pigments as food, pharmaceutical ingredients, and the potential health benefits. *Food and Nutrition Research*, *61*(1), 1–21.

Kwartiningsih, E., Prastika, A., & Lellis -Triana, D. (2016). Ekstraksi dan uji stabilitas antosianin dari kulit buah naga super merah (hylocereus costaricensis). In *Prosiding seminar nasional teknik kimia "kejuangan"* (p.6).

Lee, U., Han, J., & Wang, M. (2017). Evaluation of landfill gas emissions from municipal solid waste landfills for the life-cycle analysis of waste-to-energy pathways. *Journal of Cleaner Production*, *166*, 335–342.

Lullung-Sampebarra, A. (2018). Karakteristik zat warna antosianin dari biji kakao non-fermantasi sebagai sediaan zat warna alam. *Jurnal Industri Hasil Perkebunan* , *13*(1), 63–70.

Dewi, N. P. B. T., Singapurwa, N. M A.., & Mangku, I. G. P. (2020). Extraction and stability of natural dyes

from the skin of red dragon fruit. *SEAS (Sustainable Environment Agricultural Science)*, *4*(2), 130–141.

Nirmal, N. P., Khanashyam, A. C., Mundanat, A. S., Shah, K., Babu, K. S., Thorakkattu, P., Al-Asmari, F., & Pandiselvam, R. (2023). Valorization of fruit waste for bioactive compounds and their applications in the food ındustry. *Foods*, *12*(3), 1–26.

Otles, S., & Kartal, C. (2018). Food waste valorization. In *Sustainable food systems from agriculture to ındustry: ımproving production and processing* (pp.371-399).Academic Press.

Pathak, P. D., Mandavgane, S. A., & Kulkarni, B. D. (2017). Fruit peel waste: Characterization and its potential uses. *Current Science*, *113*(3), 444–454.

Singh, T., Pandey, V. K., Dash, K. K., Zanwar, S., & Singh, R. (2023). Natural bio-colorant and pigments: Sources and applications in food processing. *Journal of Agriculture and Food Research*, *12*, 100628.

Sudarmi, S., Subagyo, P., Susanti, A., & Wahyuningsih, A. S. (2015). Ekstraksi Sederhana antosianon dari kulit buah naga (hylocereus polyrhizus) sebagai pewarna alami. *Eksergi*, *12*(1), 05.

Sukaminah, Tensiska, E., & Dita, N. (2007). Ekstraksi pewarna alami dari buah arben. *Jurnal Teknologi Dan Industri Pangan*, *18*(1), 25–31.

Vargas, M. de L. V., Cortez, J. A. T., Duch, E. S., Lizama, A. P., & Méndez, C. H. H. (2013). Extraction and stability of anthocyanins present in the skin of the dragon fruit. *Food and Nutrition Sciences*, *4*(12), 1221–1228.

Vinha, A. F., Rodrigues, F., Nunes, M. A., & Oliveira, M. B. P. P. (2018). Natural pigments and colorants in foods and beverages. In *Polyphenols: Properties, recovery, and applications* (pp.363-391). Woodhead Publishing.

Wang, C., Ghadimi, P., Lim, M. K., & Tseng, M. L. (2019). A literature review of sustainable consumption and production: A comparative analysis in developed and developing economies. *Journal of Cleaner Production*, *206*, 741–754.

Widyasanti, A., Arsyad, M. Z., & Wulandari, D. E. (2021). Ektraksi Antosianin kulit buah naga merah (hylocereus polyrhizus) menggunakan metode maserasi. | *Jurnal Agroindustri*, *11*(2), 72–81.

Author Information

Anis Muyassaroh
Universitas Pendidikan Indonesia
Setiabudi Street. 229th, Bandung, Indonesia
Contact e-mail: *anismuyassaroh99@upi.edu*

Asep Supriatna
Universitas Pendidikan Indonesia
Setiabudi Street. 229th, Bandung, Indonesia

Hernani Hernani
Universitas Pendidikan Indonesia
Setiabudi Street. 229th, Bandung, Indonesia

To cite this article:

Muyassaroh, A., Supriatna, A., & Hernani, H. (2024). Extraction of anthocyanin pigments from the peel of dragon fruit for food coloring. *The Eurasia proceedings of science, technology, engineering & mathematics(EPSTEM), 28,* 167-174.

The Eurasia Proceedings of Science, Technology, Engineering & Mathematics (EPSTEM)
ISSN: 2602-3199

The Eurasia Proceedings of Science, Technology, Engineering & Mathematics (EPSTEM), 2024

Volume 28, Pages 175-184

ICBASET 2024: International Conference on Basic Sciences, Engineering and Technology

A Fixed Point Theorem on Partial Metric Spaces of Hyperbolic Type

Silvja Cobani
Fan S. Noli University

Elida Hoxha
University of Tirana

Abstract: In this research paper, we introduce the concept of partial metric spaces of hyperbolic type. When it comes to hyperbolic spaces, they are mostly studied in the context of metric spaces. A partial metric space is a generalization of a metric space, where self-distance is not necessarily zero. This concept became particularly interesting when Kumar et al. (2017) introduced and studied convex partial metric spaces. His result were useful in defining partial metric spaces of hyperbolic type, which is the kickoff point of our paper. After this, we focus our study in providing a proof of the existence of a fixed point for a non-self-mapping of a specific contracting type that was first introduced by Ćirić (2006). Our result is a generalization of the results of Ćirić and other cited authors. In the end an example is provided. This example serves to illustrate the applicability of our fixed point theorem and shows that results from metric spaces of hyperbolic type can be extended to partial metric spaces of hyperbolic type.

Keywords: Partial metric space, Non-self-mapping, Contraction, Fixed point

Introduction

Fix point theory is a branch of mathematics that arouses interest with its various applications in different fields such as nonlinear analysis, integral and differential equations, dynamic systems, fractals etc. The Banach Contraction Principle is well known as a useful tool with wide applications. It states that if (X, d) is a complete metric space, and the self- mapping $T: X \to X$ satisfies $d(Tx, Ty) \leq \lambda d(x, y)$ for all $x, y \in X$, where $0 < \lambda < 1$, then T has a unique fixed point. This classical theorem has been generalized and studied extensively. Ćirić (1974) introduced and studied self-mappings on K, a nonempty closed subset of X, which satisfies:

$d(Tx, Ty) \leq \lambda \max\{d(x, y), d(x, Tx), d(y, Ty), d(x, Ty), d(y, Tx)\}$, where $0 < \lambda < 1$.

Whereas Boyd and Wong (1969) investigated mappings that satisfy the condition: $d(Tx, Ty) \leq \varphi(d(x, y))$, where $\varphi: R^+ \to R^+$, called a comparison function, is upper semi-continuous from the right and satisfies the condition $\varphi(t) < t$ for all $t > 0$. Subsequently, Ćirić (2006) extended these finding to non- self-mappings and proved some theorems related to fixed points on hyperbolic type metric spaces. Izadi demonstrated in 2012 that Ćirić's findings are also applicable to quasi-metric spaces of hyperbolic type.

Partial metric spaces, as a generalization of metric spaces, were introduced by Matthews (1992). In these type of spaces, the distance from a point to itself might not always be zero. In other words, there may be self-distances $d(x, x)$ that may not be zero. In generalizing the metric space in this way some of its properties may be lost, but Matthews proved that the well- known Banach Contracting Principle can be extended to partial metric spaces as well. Since then partial metric spaces, their properties, fixed points and their applications have been the focus of many studies, especially in the field of computer science. Refer for example to Alghamdi et al. (2013) and Han et al. (2017) and Bugajewski et al. (2022) and the references there in.

In recent years the study of partial metric spaces has shifted to the study of convexity. In 2017, Kumar et al. studied some properties of metrically convex partial metric spaces and proved some results on fixed points in these spaces. He did so by generalizing the following definition:

Definition 1.1. (Assad & Kirk, 1972- Menger) A metric space (X, d) is *metrically convex* if X is such that for each $x, y \in X$ with $x \neq y$ there exists $z \in X, x \neq z \neq y$ such that:

$d(x, z) + d(z, y) = d(x, y)$.

If (X, d) is a metrically convex metric space and $x, y \in X$, *a metric segment* is defined by:

$seg[x, y] := \{z \in X : d(x, z) + d(z, y) = d(x, y)\}$.

In our paper we will be referring to a type of metrically convex metric spaces, as defined by Kirk (1982).

Definition 1.2. (Kirk, 1982) A metric space (X, d) is called *a metric space of hyperbolic type* if it contains a family L of *metric segments* such that:

a) each two points $x, y \in X$ are endpoints of exactly one member $seg[x, y] \in L$, and
b) if $u, x, y \in X$ and $z \in seg[x, y]$ is such that $d(x, z) = \lambda d(x, y)$ for $\lambda \in [0,1]$, then $d(u, z) \leq (1 - \lambda)d(u, x) + \lambda d(u, y)$

The purpose of our paper is to generalize this concept for partial metric spaces and show that Ćirić (2006) fixed point results can be extended to the partial metric space of hyperbolic type. Thus we demonstrate that despite the generalization certain properties of metric spaces of hyperbolic type can be preserved.

With this in mind we start our paper by recalling some useful basic definitions from partial metric spaces and by using some preliminary results from Kumar et al. (2017). In the main section of the paper we define the partial metric space of hyperbolic type and prove a fixed point theorem on this type of partial metric space. Our result is a generalization of Ćirić (2006) and Izadi (2012) results.

Preliminaries

We will start by recalling some basic definitions and properties of partial metric spaces.

Definition 2.1. (Matthews, 1992) Let X be a nonempty set. A *partial metric* is a function $p: X \times X \to R^+$ such that for all $x, y, z \in X$, the following axioms are satisfied:

p1) $x = y \Leftrightarrow p(x, x) = p(x, y) = p(y, y)$,
p2) $p(x, x) \leq p(x, y)$,
p3) $p(x, y) = p(y, x)$,
p4) $p(x, z) \leq p(x, y) + p(y, z) - p(y, y)$.

The pair (X, p) is called *partial metric space* and $p(x, x)$ is called *size of* x. A closer look on these axioms reveals that if $x = y$ then $p(x, y)$ might not be zero.

According to Matthews (1994), every partial metric p induces a metric $d_p: X \times X \to R^+$ defined by:

$d_p(x, y) = 2p(x, y) - p(x, x) - p(y, y)$ for all $x, y \in X$.

An example of a partial metric space is (X, p) with $X = R^+$ and $p(a, b) = \max\{a, b\}, \forall\, a, b \geq 0$. In this case the derived metric is $d_p(a, b) = |a - b|$. For other examples see Bukatin et al. (2009) and Matthews (1994).

Definition 2.2. (Matthews, 1994) Let (X, p) be a partial metric space and $\{x_n\}$ a sequence in X. Then

a) $\{x_n\}$ *converges* to $x \in X$ if and only if $\lim_{n\to\infty} p(x_n, x) = p(x, x)$.
b) $\{x_n\}$ is called a *Cauchy sequence* if and only if $\lim_{n\to\infty} p(x_n, x_m)$ exists and is finite.

c) if every Cauchy sequence $\{x_n\}$ converges to $x \in X$, meaning that $\lim_{n\to\infty} p(x_n, x_m) = p(x, x)$, then (X, p) is said to be *a complete partial metric space*.

It should be noted that the limit of a sequence in partial metric space is not necessary unique.

Each partial metric p on X generates a T_0- topology $T(p)$ on X which has as a base the family of open p- balls $\{B_p(x, \varepsilon): x \in X, \varepsilon > 0\}$, where $B_p(x, \varepsilon) = \{y \in X: p(x, y) < p(x, x) + \varepsilon\}$ for all $x \in X$ and $\varepsilon > 0$.

Definition 2.3. Let (X, p) be a partial metric space and A a subset of X.

1) A is called an *open set* if for $x \in A$ there exists $B_p(x, \varepsilon)$ such that $B_p(x, \varepsilon) \subset A$.
2) A is called a *closed set* if its complement is open.
3) A point $x \in A$ is called *a limit point* of A if there exists a sequence $\{x_n\} \subset A$ such that $\lim_{n\to\infty} p(x_n, x) = p(x, x)$. The set A together with all its limit points is called *closure* of A.
4) *The boundary of A* is denoted by ∂A and is the intersection of the closure of A with the closure of its complement.
5) A is called *bounded* if there exists $M > 0$ such that $p(x, y) \leq M$, for every $x, y \in A$.
6) If A is bounded then $diam(A) = \sup\{p(x, y): x, y \in A\} < +\infty$ is called *the diameter of A*.

Next we turn to the results of Kumar et al. (2017) for the definition and some useful properties of metrically convex partial metric spaces.

Definition 2.4. (Kumar et al., 2017) A partial metric space (X, p) is said to be *metrically convex* if the corresponding metric space (X, d_p) is metrically convex.

If (X, p) is a metrically convex partial metric space and $x, y \in X$, then following the results of Kumar et al. (2017) we can define *a metric segment* (isometric image of a real line segment) to be:

$$seg[x, y] \coloneqq \{z \in X: p(x, y) + p(z, z) = p(x, z) + p(z, y)\}.$$

As an example, we revisit the partial metric space (R^+, p), where $p(a, b) = \max\{a, b\}, \forall\, a, b \in R^+$. This space is also metrically convex because the derived metric space (R^+, d_p), where $d_p(a, b) = |a - b|, \forall\, a, b \in R^+$, is metrically convex.

Lemma 2.5. (Kumar et al., 2017) Let K be non-empty closed subset of a metrically convex partial metric space (X, p). If and $x \in K$ and $y \notin K$ then there exists $z \in \partial K$, such that $p(x, y) + p(z, z) = p(x, z) + p(z, y)$.

Definition 2.6. The function $\varphi: R^+ \to R^+$ is called an ultra- altering distance if:

1) φ is non- decreasing,
2) $\varphi(0) = 0$ and $\varphi(t) < t$ for $t > 0$.

A φ-contractive condition alone does not guarantee the existence of a fixed point, unless additional conditions are assumed. Therefore, to ensure the existence of a fixed point under the contractive condition of an ultra-altering distance φ, various authors have employed the following additional conditions on φ: φ is upper semi-continuous (Boyd & Wong, 1969) ; φ is non- decreasing and continuous from the right (Park & Roades, 1981); φ is non- decreasing and $\frac{t}{t-\varphi(t)}$ is non- decreasing (Carbone et al., 1989); φ is non- decreasing and $\lim_{n\to\infty} \varphi^n(t) = 0$ for all $t > 0$ (Jachymski, 1994). In our paper we will be working with an ultra- altering distance that is lower semi- continuous and such that $\lim_{n\to\infty}(t - \varphi(t)) = +\infty$ (Ćirić, 2006).

Main Results

We introduce the partial metric space of hyperbolic type.

Definition 3.1. A partial metric space (X, p) is called *a partial metric space of hyperbolic type* if the corresponding metric space (X, d_p) is of hyperbolic type.

We note that a partial metric space of hyperbolic type is metrically convex.

Lemma 3.2. Let (X, p) be a partial metric space of hyperbolic type. If $u, x, y \in X$ and $z \in seg[x, y]$ is such that $d_p(x, z) = \lambda d_p(x, y)$ for $\lambda \in [0,1]$, then $d(u, z) \leq 2\max\{d(u, x), d(u, y)\}$.

Proof. By the definition 3.1 and 1.2, for $u, x, y \in X$ and $z \in seg[x, y]$ is such that $d_p(x, z) = \lambda d_p(x, y)$ for $\lambda \in [0,1]$, we have

$d_p(u, z) \leq (1 - \lambda) d_p(u, x) + \lambda d_p(u, y)$

$2p(u, z) - p(u, u) - p(z, z) \leq (1 - \lambda)[2p(u, x) - p(u, u) - p(x, x)] + \lambda[2p(u, y) - p(u, u) - p(y, y)]$

$2p(u, z) - p(z, z) \leq (1 - \lambda)[2p(u, x) - p(x, x)] + \lambda[2p(u, y) - p(y, y)]$.

Since p is e partial metric, by the Definition 2.1 we have that

$p(u, z) - p(z, z) \geq 0 \qquad 0 \leq p(u, x) - p(x, x) \leq p(u, x) \qquad 0 \leq p(u, y) - p(y, y) \leq p(u, y)$.

Therefore,

$p(u, z) \leq p(u, z) + [p(u, z) - p(z, z)] \leq 2[(1 - \lambda)p(u, x) + \lambda p(u, y)] \leq 2\max\{p(u, x), p(u, y)\}$. ■

Theorem 3.3. Let (X, p) be a complete partial metric space of hyperbolic type, K a nonempty closed subset of X and $T: K \to X$ a non- self mapping such that:

(i) $T(\partial K) \subseteq K$,

(ii) $p(Tx, Ty) \leq \varphi\left(\frac{1}{2}\max\{p(x, y), p(x, Tx), p(y, Ty), p(x, Ty), p(y, Tx)\}\right)$, where the function φ is an ultra-alternating distance, lower semi- continuous and such that $\lim_{n\to\infty}(t - \varphi(t)) = +\infty$.

Then T has a unique fixed point in K.

Proof. The theorem can be proved in five steps.

Step 1. We start by constructing a sequence $\{x_n\}$. First we choose $x_0 \in \partial K$. Then (i) implies that $Tx_0 \in K$ and we set $x_1 = Tx_0$. If $Tx_1 \in K$, then $x_2 = Tx_1$. If $Tx_1 \notin K$, since we have that $x_1 \in K$ and that (X, p) is of hyperbolic type, Lemma 2.5 implies that there exists $x_2 \in \partial K$ such that $x_2 \in seg[x_1, Tx_1]$, i.e. such that

$p(x_1, Tx_1) + p(x_2, x_2) = p(x_1, x_2) + p(x_2, Tx_1)$.

Following this reasoning, we iteratively construct the sequences $\{x_n\}$ and $\{Tx_n\}$ in K such that for all $n \geq 2$,

$x_n = Tx_{n-1}$, if $Tx_{n-1} \in K$ or $x_n \in \partial K$ and $x_n \in seg[x_{n-1}, Tx_{n-1}]$, if $Tx_{n-1} \notin K$.

(i.e. $p(x_{n-1}, Tx_{n-1}) + p(x_n, x_n) = p(x_{n-1}, x_n) + p(x_n, Tx_{n-1})$, if $Tx_{n-1} \notin K$.)

Step 2. We show that the sequences we construsted are bounded. First, for $n \geq 1$, we define

$A_n = \{x_i\}_{i=0}^{n-1} \cup \{Tx_i\}_{i=0}^{n-1}$ and $\alpha_n = diam(A_n)$

If $\alpha_n = 0$, Definition 2.1. implies $Tx_0 = x_0$ and this proves the theorem.

If $\alpha_n > 0$, we show that $\alpha_n = p(x_0, Tx_k)$, for some $k \in \{0,1, \dots, n-1\}$. We consider the following cases.

Case 1. Let $\alpha_n = p(x_i, Tx_k)$ for some $i, k \in \{0,1, \dots, n-1\}$. To prove that $x_i = x_0$, we suppose to the contrary that $x_i \neq x_0$. Then $x_{i-1} \in \{x_n\} \subseteq K$ and Tx_{i-1} is defined.

(a) If $Tx_{i-1} \in K$, then by construction of $\{x_n\}$, $x_i = Tx_{i-1}$. Thus by condition (ii) it follows that:

$\alpha_n = p(x_i, Tx_k) = p(Tx_{i-1}, Tx_k)$

$\leq \varphi\left(\frac{1}{2}\max\{p(x_{i-1},x_k), p(x_{i-1},Tx_{i-1}), p(x_k,Tx_k), p(x_{i-1},Tx_k), p(x_k,Tx_{i-1})\}\right)$.

Since $\{p(x_{i-1},x_k), p(x_{i-1},Tx_{i-1}), p(x_k,Tx_k), p(x_{i-1},Tx_k), p(x_k,Tx_{i-1})\} \subset A_n$, the definition of $diam(A_n)$ implies that

$\max\{p(x_{i-1},x_k), p(x_{i-1},Tx_{i-1}), p(x_k,Tx_k), p(x_{i-1},Tx_k), p(x_k,Tx_{i-1})\} \leq \alpha_n$.

Furthermore, from Definition 2.6.1 (φ is non-decreasing), we have $\alpha_n \leq \varphi(\alpha_n)$, which contradicts Definition 2.6.2. This contradiction proves that in this case $x_i = x_0$.

(b) If $Tx_{i-1} \notin K$, then by construction of $\{x_n\}$, $i \geq 2$ and $x_i \in seg[Tx_{i-2}, Tx_{i-1}] \cap \partial K$. Since X is a partial metric space of hyperbolic type, Lemma 3.2. implies that for $x = Tx_{i-2}, y = Tx_{i-1}, z = x_i, u = Tx_k$ the following holds:

$p(Tx_k, x_i) \leq 2\max\{p(Tx_k, Tx_{i-2}), p(Tx_k, Tx_{i-1})\}$

If $\max\{p(Tx_k, Tx_{i-2}), p(Tx_k, Tx_{i-1})\} = p(Tx_k, Tx_{i-2})$, then condition (ii) and Definition 2.6.2 implies:

$\alpha_n = p(Tx_k, x_i) \leq 2p(Tx_k, Tx_{i-2})$

$\leq 2\varphi\left(\frac{1}{2}\max\{p(x_k,x_{i-2}), p(x_k,Tx_k), p(x_{i-2},Tx_{i-2}), p(x_{i-2},Tx_k), p(x_k,Tx_{i-1})\}\right)$

$< \max\{p(x_k,x_{i-2}), p(x_k,Tx_k), p(x_{i-2},Tx_{i-2}), p(x_{i-2},Tx_k), p(x_k,Tx_{i-1})\}$

$= \alpha_n$.

We have reached once again a contradiction.

Reasoning in the same way, if $\max\{p(Tx_k, T_{i-2}), p(Tx_k, Tx_{i-1})\} = p(Tx_k, Tx_{i-1})$, we would reach to the same contradiction ($\alpha_n < \alpha_n$) and prove once again that $x_i = x_0$.

Thus we have shown that $\alpha_n = p(x_0, Tx_k)$.

Case 2. Let $\alpha_n = p(x_i, x_k)$ for some $0 \leq i < k \leq n-1$. $k > 0$ implies that $x_{k-1} \in K$ and Tx_{k-1} is defined.

(a) If $Tx_{k-1} \in K$, then $x_k = Tx_{k-1}$. Thus, Case 2(a) reduces to Case 1(a).
(b) If $Tx_{k-1} \notin K$, then $k \geq 2$ and $x_k \in seg[Tx_{k-2}, Tx_{k-1}] \cap \partial K$. Similarly, Case 2(b) reduces to Case 1(b).

Case 3. Similarly $\alpha_n = p(Tx_i, Tx_k)$ is also impossible, because

$$\alpha_n = p(Tx_i, Tx_k) \leq \varphi\left(\frac{1}{2}\max\{p(x_i,x_k), p(x_i,Tx_i), p(x_k,Tx_k), p(x_i,Tx_k), p(x_k,Tx_i)\}\right) \leq \varphi\left(\frac{1}{2}\alpha_n\right) \leq \varphi(\alpha_n),$$

which contradicts Definition 2.6.2.

This way we have shown that $\alpha_n = \max\{p(x_0, Tx_k): k = 0,1,\dots,n-1\}$. To conclude the proof of this step we show that the sequence $\{A_n\}$ is bounded.

By definition $\{\alpha_n\}$ is non- decreasing. To prove that this sequence is bounded suffices to show that $\lim_{n\to\infty} \alpha_n < +\infty$.

Suppose to the contrary that $\lim_{n\to\infty} \alpha_n = +\infty$. From the conditions of Theorem 3.3 we have that $\lim_{n\to\infty}(t - \varphi(t)) = +\infty$, so there exists a positive number $\delta > 0$ such that for all $t > \delta$, we have

$t - \varphi(t) > p(x_0, Tx_0) - p(Tx_0, Tx_0) > 0$.

By supposition, $\lim_{n\to\infty} \alpha_n = +\infty$. This means that for $\delta > 0$ there exists an integer n such that $\alpha_n > \delta$, and

$\alpha_n - \varphi(\alpha_n) > p(x_0, Tx_0) - p(Tx_0, Tx_0)$.

For a fixed integer n such that $\alpha_n > \delta$, we know that $\alpha_n = p\left(x_0, Tx_{k(n)}\right)$, for some $k(n) \in \{0,1, \dots, n-1\}$ and we consider the following cases.

Case 1. If $k(n) = 0$, then $\alpha_n = p(x_0, Tx_0)$, and so $\{x_n\}$ and $\{Tx_n\}$ are bounded.

Case 2. İf $k(n) > 0$, then $\alpha_n = p\left(x_0, Tx_{k(n)}\right)$ and by using the triangle inequality, condition (ii), and the definition of φ it holds that:

$$\alpha_n = p\left(x_0, Tx_{k(n)}\right)$$

$$\leq p(x_0, Tx_0) + p\left(Tx_0, Tx_{k(n)}\right) - p(Tx_0, Tx_0)$$

$$\leq p(x_0, Tx_0) + \varphi\left(\frac{1}{2}\max\left\{p\left(x_0, x_{k(n)}\right), p(x_0, Tx_0), p\left(x_{k(n)}, Tx_{k(n)}\right), p\left(x_0, Tx_{k(n)}\right), p\left(x_{k(n)}, Tx_0\right)\right\}\right) - p(Tx_0, Tx_0)$$

$$\alpha_n \leq p(x_0, Tx_0) + \varphi(\alpha_n) - p(Tx_0, Tx_0)$$

$$\alpha_n - \varphi(\alpha_n) \leq p(x_0, Tx_0) - p(Tx_0, Tx_0).$$

This contradiction implies that $\lim_{n\to\infty} \alpha_n = \alpha < +\infty$, and we have thus proved that $\{x_n\}$ and $\{Tx_n\}$ are bounded.

Step 3. İn this step we will show that both these sequences are Cauchy. We start by defining for $n \geq 2$,

$B_n = \{x_i\}_{i\geq n} \cup \{Tx_i\}_{i\geq n}$ and $\beta_n = diam(B_n)$

The sequence $\{B_n\}$ is Cauchy if $\lim_{n\to\infty} \beta_n = 0$. The definition of $\{\beta_n\}$ implies that this sequence is non-increasing and also it is bounded (because $\beta_n \geq 0$ for all $n \geq 2$). Thus $\{\beta_n\}$ is convergent and it converges to some point $\beta \geq 0$. To conclude the proof on this step we will show that $\beta = 0$. Let us suppose that $\beta > 0$.

On the other hand we have that $\beta_n = diam(B) = \sup\left\{p\left(x_i, Tx_j\right), p\left(x_i, x_j\right), p\left(Tx_i, Tx_j\right): i, j \geq n\right\}$.

Applying a method similar to that used in Step 2, we can show that

$\beta_n = \sup\{p(x_n, Tx_k): k \geq n\}$.

From the characteristic property of the supremum it holds that for every integer p there exist an index $k(p) > p$ such that $\beta_p - \frac{1}{p} < p\left(x_p, Tx_{k(p)}\right) < \beta_p$. Thus, by taking the limit, we have $\lim_{p\to\infty} p\left(x_p, Tx_{k(p)}\right) = \beta$.

Now we consider the following cases.

Case 1. If $x_p = Tx_{p-1}$, then by condition (ii) and Definition 2.6.1, it holds that:

$$p\left(x_p, Tx_{k(p)}\right) = p\left(Tx_{p-1}, Tx_{k(p)}\right)$$
$$\leq \varphi\left(\frac{1}{2}\max\left\{p\left(x_{p-1}, x_{k(p)}\right), p\left(x_{p-1}, Tx_{p-1}\right), p\left(x_{k(p)}, Tx_{k(p)}\right), p\left(x_{p-1}, Tx_{k(p)}\right), p\left(x_{k(p)}, Tx_{p-1}\right)\right\}\right)$$

$$\leq \varphi(\beta_n)$$

Since φ is a lower semi continuous function, by taking the limit for $p \to \infty$ we would have $\beta \leq \varphi(\beta)$, which is in contradiction with Definition 2.6.2. This means that in this case, $\beta = 0$.

Case 2. If $x_p \neq Tx_{p-1}$, then by construction of $\{x_n\}$ we have $x_p \in seg[Tx_{p-2}, Tx_{p-1}] \cap \partial K$. Since X is a partial metric space of hyperbolic type, Lemma 3.2 implies, for $x = T_{p-2}, y = Tx_{p-1}, z = x_p, u = Tx_{k(p)}$, that

$p(Tx_{k(p)}, x_p) \leq 2\max\{p(Tx_{k(p)}, Tx_{p-2}), p(Tx_{k(p)}, Tx_{p-1})\}$.

If $\max\{p(Tx_{k(p)}, Tx_{p-2}), p(Tx_{k(p)}, Tx_{p-1})\} = p(Tx_{k(p)}, Tx_{p-2})$, then condition (ii) and Definition 2.6.1 implies:

$p(Tx_{k(p)}, x_p) \leq 2p(Tx_{k(p)}, Tx_{p-2})$

$\leq 2\varphi\left(\frac{1}{2}\max\{p(x_{k(p)}, x_{p-2}), p(x_{k(p)}, Tx_{k(p)}), p(x_{p-2}, Tx_{p-2}), p(x_{p-2}, Tx_{k(p)}), p(x_{k(p)}, Tx_{p-2})\}\right)$

$< \beta_n$,

which by taking the limit for $p \to \infty$, leads to the contradiction $\beta < \beta$.

If $\max\{p(Tx_{k(p)}, Tx_{p-2}), p(Tx_{k(p)}, Tx_{p-1})\} = p(Tx_{k(p)}, Tx_{p-1})$, by following the above reasoning we get once again the contradiction $\beta < \beta$. This contradiction proves again that $\beta = 0$, which in turn shows that the sequences $\{x_n\}$ and $\{Tx_n\}$ are both Cauchy.

Since X is complete and K is closed, both these sequences converge to some point $u \in K$, meaning:

$\lim_{n\to\infty} p(x_n, u) = p(u, u) = \lim_{n\to\infty} p(Tx_n, u)$.

Step 4. In this step we show that u is a fixed point, i.e. $Tu = u \Leftrightarrow p(u, u) = p(u, Tu) = p(Tu, Tu)$.
Suppose the contrary, which based on Definition 2.1 means that $p(u, Tu) > 0$.

Let n be a fixed integer, and $x_n \in K$. Then the following cases are possible.

Case 1. If $Tx_n \in K$, then $p(Tx_n, Tu) \leq \varphi(\max\{p(x_n, u), p(x_n, Tx_n), p(u, Tu), p(u, Tx_n), p(x_n, Tu)\})$
By taking the limit we get the following contradiction

$p(u, Tu) \leq \varphi(\max\{p(u, u), p(u, Tu), p(u, Tu), p(u, u), p(u, Tu)\}) = \varphi(p(u, Tu))$.

Case 2. If $Tx_n \notin K$, then $x_{n+1} \in seg[Tx_{n-1}, Tx_n] \cap \partial K$ and because X is a partial metric space of hyperbolic type, by Lemma 3.2 it holds that

$p(Tu, x_{n+1}) \leq 2\max\{p(Tu, Tx_{n-1}), p(Tu, Tx_n)\}$.

If $\max\{p(Tu, x_{n-1}), p(Tu, Tx_n)\} = p(Tu, Tx_{n-1})$, then

$p(Tu, x_{n+1}) \leq 2\,p(Tu, Tx_{n-1}) \leq 2\varphi\left(\frac{1}{2}\max\{p(u, x_{n-1}), p(u, Tu), p(x_{n-1}, Tx_{n-1}), p(x_{n-1}, Tu), p(u, Tx_{n-1})\}\right)$

$< \max\{p(u, x_{n-1}), p(u, Tu), p(x_{n-1}, Tx_{n-1}), p(x_{n-1}, Tu), p(u, Tx_{n-1})\}$.

By taking the limit we get once more a contradiction as follows

$p(Tu, u) < \max\{p(u, u), p(u, Tu), p(u, Tu), p(u, Tu), p(u, Tu)\} = p(u, Tu)$.

If $\max\{p(Tu, x_{n-1}), p(Tu, Tx_n)\} = p(Tu, Tx_n)$, then by following the same reasoning as above we get the same contradiction.

This contradiction shows that $p(u, u) = p(u, Tu) = p(Tu, Tu)$, and by definition of the partial metric we have $Tu = u$.

Step 5. In this step we prove the uniqueness of the fixed point u.

Suppose to the contrary that there exists $v \in K$, such that $u \neq v$ and $Tv = v$. Thus, by the definition of the partial metric we have that $p(u,u) < p(u,v)$, $p(v,v) < p(u,v)$ and $p(Tv,Tv) = p(Tv,v) = p(v,v)$. Then by applying condition (ii) and Definition 2.6.2 we get

$$p(u,v) = p(Tu,Tv)$$

$$\leq \varphi\left(\frac{1}{2}\max\{p(u,v), p(u,Tu), p(v,Tv), p(v,Tu), p(u,Tv)\}\right)$$

$$\leq \varphi(\max\{p(u,v), p(u,u), p(v,v), p(v,u), p(u,v)\})$$

$$= \varphi\big(p(u,v)\big).$$

This contradiction shows that $p(u,u) = p(u,v) = p(v,v)$, and by definition $u = v$. ■

Remark 1. Theorem 3.3 is a generalization of Theorem 2.1 from Ćirić (2006) for partial metric spaces of hyperbolic type. For the functions φ_i (where $i = 1,2,3,4,5$), in Theorem 2.1, we can find $\varphi = \max_{i=1,\dots,5}\{\varphi_i\}$, which also satisfies the same conditions as each of φ_i.

Remark 2. As mentioned in the preliminaries, several authors have proven interesting fixed point results using φ- contracting conditions. Theorem 3.3 shows that it is possible the generalize results gained from these type of conditions from metric spaces of hyperbolic type to partial metric spaces of hyperbolic type.

Remark 3. By taking $\varphi(t) = 2\lambda t$, where $0 < \lambda < 1$, we get the following corollary.

Corollary 3.4. Let (X,p) be a complete partial metric space of hyperbolic type, K a nonempty closed subset of X and $T: K \to X$ a non- self mapping such that $T(\partial K) \subseteq K$, and

$$p(Tx,Ty) \leq \lambda \cdot \max\{p(x,y), p(x,Tx), p(y,Ty), p(x,Ty), p(y,Tx)\}$$

Then T has a unique fixed point in K.

Example 3.5. Consider the complete metrically convex partial metric space (R^+,p) where $p(x,y) = \max\{x,y\}$, for all $x,y \geq 0$. This space is also of hyperbolic type because the derived metric space $\left(R^+,d_p\right)$, where $d_p(x,y)$ is the usual metric, is a metric space of hyperbolic type. $K = [0,1]$ is a closed subset of R^+.

We define $T: [0,1] \to R^+$ such that for all $x \in [0,1]$,

$$T(x) = \frac{x^2}{2(1+x)}.$$

Next we define $\varphi: R^+ \to R^+$,

$$\varphi(t) = \begin{cases} \dfrac{3t}{4+2t}, & 0 \leq t \leq 1 \\ \dfrac{1}{2}t, & t > 1 \end{cases}.$$

We note that φ is non- decreasing, $\varphi(0) = 0$ and $\varphi(t) < t$ for all $t > 0$. Which means φ is an ultra- alternating distance. Also φ is lower semi- continuous and $\lim_{n\to\infty}(t - \varphi(t)) = +\infty$ and thus it satisfies the conditions of Theorem 3.3.

Next we show that $T: [0,1] \to R^+$ also satisfies the conditions of Theorem 3.3. Since $T(0) = 0$ and $T(1) = \frac{1}{4}$, condition (i) is satisfied.

To prove the second condition we first evaluate $p(x,y), p(x,Tx), p(y,Ty), p(y,Tx), p(x,Ty), p(Tx,Ty)$.

Let $x, y \in [0,1]$ and for simplicity suppose that $x < y$, then $p(x,y) = y$. Moreover, by simple calculation we find

$$p(x,Tx) = \max\{x,Tx\} = \max\left\{x, \frac{x^2}{2(1+x)}\right\} = x, \qquad p(y,Ty) = \max\left\{y, \frac{y^2}{2(1+y)}\right\} = y,$$

$$p(y,Tx) = \max\{y,Tx\} = \max\left\{y, \frac{x^2}{2(1+x)}\right\} = y, \qquad p(x,Ty) = \max\left\{x, \frac{y^2}{2(1+y)}\right\} = x.$$

Hence, for $0 \leq x < y \leq 1$,

$$\varphi\left(\frac{1}{2}\max\{p(x,y), p(x,Tx), p(y,Ty), p(x,Ty), p(y,Tx)\}\right) = \varphi\left(\frac{1}{2}\max\{x,y\}\right) = \varphi(y) = \frac{3y}{2(4+2y)}.$$

Since T is monotone increasing on $[0,1]$. Then for $x, y \in [0;1]$, such that $x < y$, we have $Tx < Ty$. And thus,

$$p(Tx,Ty) = \max\left\{\frac{x^2}{2(1+x)}, \frac{y^2}{2(1+y)}\right\} = \frac{y^2}{2(1+y)}$$

By combining all the above calculations, we get

$$p(Tx,Ty) = \frac{y^2}{2(1+y)} \leq \frac{3y}{2(4+2y)} = \varphi\left(\frac{1}{2}\max\{p(x,y), p(x,Tx), p(y,Ty), p(x,Ty), p(y,Tx)\}\right),$$

on the account that for all $y \in [0,1]$

$$\frac{y^2}{2(1+y)} - \frac{3y}{2(4+2y)} = \frac{2y^3 + y^2 - 3y}{2(1+y)(4+2y)} = \frac{y(2y^2+y-3)}{2(1+y)(4+2y)} < 0.$$

We have hence shown that T also satisfies condition (ii).

Therefore T has a fixed point, which is $x = 0$.

Scientific Ethics Declaration

The authors declare that the scientific ethical and legal responsibility of this article published in EPSTEM journal belongs to the authors.

Acknowledgements or Notes

* This article was presented as an oral presentation at the International Conference on Basic Sciences, Engineering and Technology (www.icbaset.net) held in Alanya/Turkey on May 02-05, 2024.

References

Alghamdi, M. A., Shahzad, N., & Valero, Ó. (2013). Fixed point theorems in generalized metric spaces with applications to computer science. *Fixed Point Theory and Applications*, *2013*, 1-20.

Assad, N. A., & Kirk, W. A. (1972). Fixed point theorems for set-valued mappings of contractive type. *Pacific Journal of Mathematics*, *43*(3), 553–562.

Boyd, D. W., & Wong, J. S. W. (1969). On nonlinear contractions. *Proceedings of the American Mathematical Society*, *20*(2), 458–464.

Bugajewski, D., Maćkowiak, P., & Wang, R. (2022). On compactness and fixed point theorems in partial metric spaces. *Fixed Point Theory*, *23*(1), 163–178.

Bukatin M., Kopperman R., Matthews S., & Pajoohesh, H. (2009). Partial metric spaces. *The American Mathematical Monthly*, *116*(8), 708-718.

Carbone, A., Rhoades, B.E., & Singh, S.P. (1989). A fixed point theorem for generalized contraction map. *Indian Journal of Pure and Applied Mathematics*, *20*(6), 543-548.

Ćirić, L. B. (2006). Contractive type non-self-mappings on metric spaces of hyperbolic type. *Journal of Mathematical Analysis and Applications, 317*(1), 28–42.

Ćirić, L. B. (1974). A generalization of Banach's contraction principle. *Proceedings of the American Mathematical Society*, *45*(2), 267.

Han, S., Wu, J., & Zhang, D. (2017). Properties and principles on partial metric spaces. *Topology and Its Applications*, *230*, 77–98.

Izadi, M. (2012). A fixed point theorem on quasi-metric spaces of hyperbolic type. *International Journal of Contemporary Mathematical Sciences, 7*(44), 2155- 2160.

Jachymski, J.R. (1994). Common fixed point theorems for some families of maps. *Indian Journal of Pure & Applied Mathematics*, *25*, 925-934.

Kirk, W. A. (1982). Krasnoselskii's iteration process in hyperbolic space. *Numerical Functional Analysis and Optimization, 4*(4), 371–381.

Kumar, S., Rugumisa, T., & Imdad, M. (2017). Common fixed points in metrically convex partial metric spaces. *Konuralp Journal of Mathematics, 5*(2), 54-69.

Matthews, S. G. (1992). Partial metric spaces. *8th British Colloquium for Theoretical Computer Science. In Research Report, 212*, 708–718.

Matthews, S. (1994). Partial metric topology. *Annals of the New York Academy of Sciences, 728*(1), 183–197.

Park, S., & Rhoades, B.E. (1981). Meir-Keeler type contractive conditions. *Mathematica Japonica, 16*(1), 13-20.

Author Information

Silvja Cobani
"Fan S. Noli" University
Shëtitorja Rilindasit, Korçë 7001, Albania
Contact e-mail: *scobani@unkorce.edu.al*

Elida Hoxha
University of Tirana
Bulevardi Zogu I 25, Tirana 1016, Albania

To cite this article:

Cobani, S.,& Hoxha, E. (2024). A fixed point theorem on partial metric spaces of hyperbolic type. *The Eurasia Proceedings of Science, Technology, Engineering & Mathematics (EPSTEM), 28*, 175-184.

The Eurasia Proceedings of Science, Technology, Engineering & Mathematics (EPSTEM)
ISSN: 2602-3199

The Eurasia Proceedings of Science, Technology, Engineering & Mathematics (EPSTEM), 2024

Volume 28, Pages 185-190

ICBASET 2024: International Conference on Basic Sciences, Engineering and Technology

Physicochemical Characteristics of Astragalus Honey Obtained from Erzurum Province

Turgay Cetinkaya
Yalova University

Sibel Bayil-Oguzkan
Gaziantep University

Abstract: Astragalus ponticus PALL (Leguminosae), known as Black Sea Astragalus (Laz Geveni), was described in 2016 from the Erzurum thermal spring road. Astragalus, which closely rivals the quality of the world-famous Anzer honey, is one of the most preferred sources for beekeepers due to its rich taste and aroma. Consequently, honey producers in Erzurum have favored Astragalus for honey production. Therefore, this study discusses the physicochemical properties of the Astragalus honey sample obtained from the Erzurum province. The following parameters were measured: pollen, moisture, and sugar contents, diastase number, hydroxymethyl furfural (HMF), and proline content. The moisture content of the sample was found to be 15.2%, which is lower than the Codex limit of less than 20%. No sucrose was detected in the sample. Other values were as follows: glucose (27.1%), fructose (41.54%), maltose (0.74%), HMF (39.25 mg/kg), and proline (584.6 mg/kg). The diastase value (7) was below 8 specified in the Turkish Food Codex Honey Communiqué. The results showed that Astragalus honey produced in the Erzurum province meets the limits set by the Turkish Food Codex Honey Communiqué in terms of pollen, moisture, HMF, maltose, and proline contents. It was concluded that the geographical origin plays an important role in the physicochemical characteristics of honey.

Keywords: Astragalus honey, Chemical composition, Sugar content

Introduction

Astragalus (Fabaceae) is the world's largest flowering plant genus, with up to 3,000 annual and perennial species (Podleh & Zarre 2013; Kucukaydın, et al., 2023; Djozan et al., 2008). In Türkiye, the Astragalus genus is represented by 469 species across 62 sections (Chamberlain & Matthews, 1970). According to the Turkiye Plant List, 217 taxa of Astragalus are endemic, constituting 46.2% of the species (Kucukaydın, et al., 2023; Adıguzel et al., 2009; Davis et al., 1988). According to Turkiye Plant Lits Astragalus 217 taxons endemic and is 46.2% (Aytac et al., 2012). The Black Sea Astragalus, also known as 'Laz geveni,' was identified on the Erzurum Ilıca road as Astragalus ponticus PALL. (Leguminosae) in 2016 (Krasteva et al., 2009).

Astragalus species have been utilized in the medicine and food industries. (Kucukkaydın, et al., 2023; Salehi et al., 2021). In vitro and in vivo bioactivities of secondary metabolites from Astragalus species have demonstrated anti-aging, anti-inflammatory, anti-diabetic, cytoprotective, anti-tumor, antioxidant, antimicrobial, antiviral, cardioprotective, anticancer, and immune-enhancing capabilities (Kucukaydın et al., 2023; Li et al., 2014; Salehi et al., 2021). Furthermore, the cytotoxic activities of Astragalus honey against cancer have been investigated (Sadeghi-Aliabadi et al., 2015). The Astragalus plant is effective in strengthening the immune system and increasing the production of antibodies against the flu, enhancing its ability to fight diseases. It not only increases resistance to the flu but also shortens the duration of the illness. It has been determined that this pharmacological activity is due to three groups of chemicals: polysaccharides, saponins, and phenolics (Rios & Waterman, 1997).

Astragalus also provides an important source of nectar and pollen for honeybees. As is known, honey contains mainly carbohydrates (70–76%) and water (16–21%). Moreover, it contains more than 200 compounds such as various organic acids, amino acids, vitamins, polyphenols, and minerals (Kucukaydın et al., 2023; Mărgăoan, et al., 2021). The amounts of these compounds vary according to the nectar source, the honey type, and environmental factors, and accordingly, distinctive features such as color, taste, and biological activity occur. According to scientific studies, honey provides a wide variety of health benefits, including antibacterial, antioxidant, anti-inflammatory, antiviral, and wound-healing properties (Tas-Küçükaydın et al., 2023). Physicochemical properties, phenolic profiles, antioxidant, and antimicrobial activities of different types of honey, including Astragalus honey, have been reported by various research groups (Kucukaydın, et al., 2023; Sagdic et al., 2013; Can et al., 2015).

As is known, various recognized parameters are used for the evaluation of honey freshness (Can et al., 2015; Mendes et al., 1998). The chemical composition of honey is affected by its botanical and geographical origins, as well as by climate factors, harvesting, handling, processing, and storage (Seraglio et al., 2021; Kucukaydın et al., 2023). For this purpose, Astragalus honey samples collected from the Erzincan province of Türkiye were examined in terms of pollen content, moisture content, sugar content, diastase number, HMF, and proline content. The results were compared with the contents given in the Turkish Food Codex Honey Communiqué (No: 2020/7) and other recent studies.

Method

An Astragalus honey sample, which was produced in Erzurum (Thermal Spring Road), was collected from a local producer in 2021. The location of the obtained Astragalus honey sample is depicted on the geographical map of Türkiye (see Figure 1).

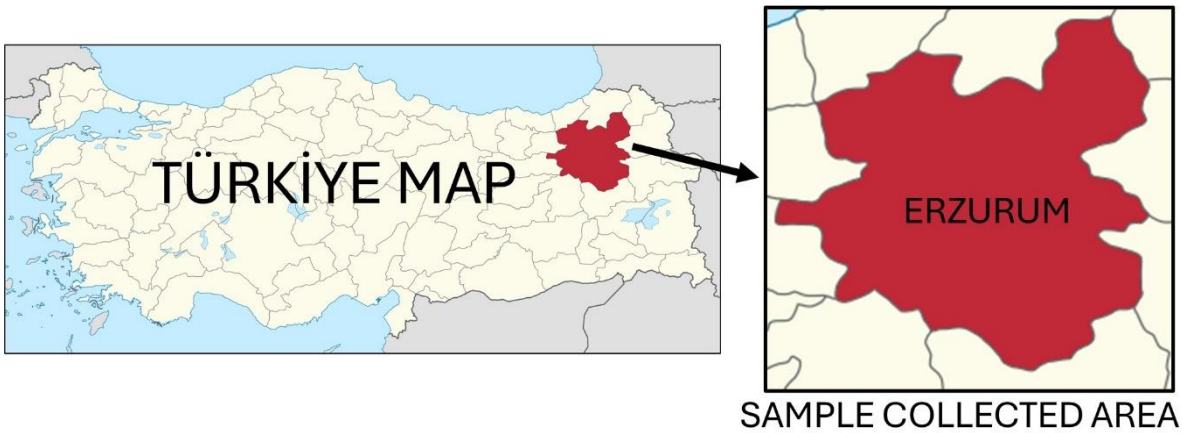

Figure 1. Geographical location of collected Astragalus honey sample.

TS 13363 was used to determine the relative pollen content of the honey. The water content of the honey was determined by the refractometric method TS 13365, and the amount of moisture was presented as a percentage of the weight. The standard method TS 13364 was used to determine the diastase activity. Fructose, glucose, sucrose, and maltose in the honey were determined by high-performance liquid chromatography (Method TS 13359) with service purchase. Standard TS 13356 was used to determine the HMF content by using high-performance liquid chromatography with service purchase. The spectrometric method TS EN 1141 was applied to determine the proline content.

Results

Relative Pollen Content

In recent times, various techniques have been explored to determine the botanical origin of honey. However, pollen content analysis, which relies on identifying pollen types in honey samples using light microscopy, remains a widely used method (Corvucci et al., 2015; Hailu & Belay, 2020). Through relative pollen content analysis, the botanical origin of honey can be determined based on the plants that provide pollen for the honey. Additionally, pollen analysis can offer insights into the crystallization rates of honey (Ozkok & Bayram;

Escuredo et al., 2014). Pollen analysis also plays an important role in evaluating certain types of honey that may have toxic effects from a food safety perspective. Moreover, in honeys adulterated with sugar, the total pollen count is detected to be low, which can be considered one of the benefits of applying relative pollen content analysis. In other words, pollen analysis contributes to assessing the quality of honey from various angles. In Türkiye, the minimum representation of pollen grains from the relevant plant required for labeling certain unifloral honey types with the name of that plant is specified in the Codex 2020/7, updated by the Ministry of Agriculture and Forestry in 2020. According to this regulation, unifloral honey types are classified into three different groups: normal, intense, and scarce unifloral honey varieties. For Astragalus, categorized as a normal unifloral species, honey samples must contain at least 45% of the relevant plant's pollen to be labeled with its name (Turkish Food Codex Communiqué on Honey (No: 2020/7)). According to relative content analysis, the botanical origin of Astragalus honeys is the Fabaceae family, with the primary pollen type being Astragalus spp. The density of the primary pollen ratio was 84%.

Moisture Content

Controlling moisture content is vital for honey quality, preventing fermentation, and preserving its shelf life. Fermentation is a natural process that occurs when the sugar in honey reacts with yeast and bacteria, resulting in the production of alcohol and carbon dioxide. Honey with a high moisture content is more prone to fermentation over time, which can negatively impact its taste and stability. When honey has an optimal moisture level, it remains stable and resists spoilage by yeast fermentation during storage. Maintaining the right moisture balance ensures that honey retains its nutritional value over time (Shakoori et al., 2023; Prica et al., 2014; Singh & Singh, 2018). It was determined that the moisture content of the studied honey was 15.2% (See Table 1). Can et al. (2015) found 17.0% moisture in similar honey obtained from *Astragalus microcephalus*. In a study by Uckun (2011), the moisture content of Astragalus honey from Elazı pgrovince was found to be 13.1% (Uckun, 2011). In a study conducted to investigate the physical and chemical properties of honey produced in Erzurum, 20 honey samples obtained from beekeepers were used, and the moisture content levels of 18 samples varied between 13.80% and 20.00% (Sengul et al., 2006). Considering previous studies and the Codex limit of 20%, our results were in accordance.

Table 1. Comparasion of some of the parameters of the Astragalus honey obtained from different regions in Türkiye

Parameter	Erzurum	Canakkale, Diyarbakır, Elazıg	Cukurova	Erzincan	
	Our Study	Can et al. (2015)	Uckun (2021)	Kara et al. (2020)	Codex
Moisture %	15.2	17	13.1	16.4	Max 20
Diastase Activity	7	9.05	-	18	Min 8
Maltose %	0.74	0.16	-	-	Max 4
HMF mg/kg	39.25	4.6	10.7	0	Max 40
Proline mg/kg	584.6	755	-	640	Min 300

Sugar Content

The basic monosaccharides of honey are the reducing sugars fructose and glucose (Uckun, 2011; Can et al., 2015). Honey may also contain sucrose, maltose, galactose, ribose, and xylose (Uckun, 2011). Fructose is generally the most abundant monosaccharide in all types of honey. Only rapeseed, dandelion flower and blueberry honeys contain slightly more glucose than fructose (Uckun, 2011; Hısıl & Borekcioglu, 1986). In our study, fructose (41.54%) and glucose (27.10%) were determined to be the sugars in the highest amounts. Therefore, the fructose+glucose levels in the current study were 68.64 g/100g, while the fructose/glucose ratio was 1.53. In a study by Can et al. (2015), the fructose+glucose and fructose/glucose ratio in Astragalus honey was reported as 57.96 g/100g and 1.28, respectively. In another study, the invert sugar ratio of Astragalus honey obtained from the Çukurova region was found to be 77.6% (Uckun, 2011). These results confirm that honey's sugar values may depend on the floral and regional origin (Can et al., 2015; Andrade et al., 1997; Mendes et al., 1998). Therefore, the reason for higher values in the current study could be attributed to the various sections of Astragalus in Anatolia, Türkiye (Tas-Kucukkaydın et al., 2023). According to the current results, the measured values were higher than the Codex limits. However, mean values for the fructose/glucose ratio of different kinds of honeys were also found to be higher (1.98) than the Codex limits in a study by Can et al. (2015). In the same

study, they detected maltose at levels of 0.16%. Maltose was detected at levels of 0.74% in our study, which is also in accordance with the Codex limit of 4%. Since sucrose is converted to invert sugar by the invertase enzyme produced by bees, most of the sugar in honey is in inverted form. This could be the reason that we couldn't find any sucrose in the sample.

Diastase Activity

Some of the important properties that distinguish honey from other sweet products (such as jam and syrup) are the enzymes present in the honey. Diastase is one of the main enzymes in honey. Its activity can vary between fresh and old honey, and this can be affected by heat treatment. Especially, pasteurized honey have almost no activity of diastase and invertase due to heat treatment. Therefore, high diastase and invertase activities imply that the honey is raw and has not been heated (Sahin & Kolaylı, 2020).

Diastase plays a role in the digestion of starch and is secreted from the honeybee's stomach. Honeys with relatively low diastase activities in this study, such as heather, common eryngo, and clover honeys, were older, and their activities gradually decreased. In this study, the diastase activity was 7, which is close to the threshold Codex limit of 8. The number of diastase enzymes, responsible for the hydrolysis of starch in honey, should be at least 8 (Türk Gıda Kodeksi, 2020). During the transfer of nectar from bee to bee, the enzyme content increases. For this reason, the diastase level may change depending on the nectar source and colony (Can et al., 2015). In a study by Can et al. (2015), Astragalus honey's diastase activity was also close to the threshold limit but was found to be 9.05.

HMF

All pure honeys gradually darken in color due to various non-enzymatic caramelization reactions, known as Maillard reactions. HMF is one such reaction product that affects honey darkening (Can et al., 2015; Zalibera et al., 2008). Generally, dark-colored honeys have been reported to possess high levels of Maillard reaction products (Can et al., 2015). HMF, a non-enzymatic Maillard reaction product, is indicative of the freshness of honey and whether it has been subjected to heat treatment (Kara et al., 2020). HMF is accepted at values below 40 mg/kg according to the Turkish Food Codex Communique on Honey. The HMF value was 39.25 mg/kg in the current study. Prolonged storage or exposure to high temperatures increases the level of HMF. This result may indicate that the collected sample was stored for some time before analysis. Studies have shown that the half-life of diastase activity decreases while the HMF level increases (Korkmaz & Kuplulu, 2017). Since a decrease in diastase activity could be associated with increased HMF, the obtained results are compatible with the diastase value.

Proline

Honey contains 20 amino acids, but proline is the amino acid present in the highest quantities (Uckun, 2011; Can et al., 2015). The amount of proline in honey is a marker of purity, and the level decreases significantly in adulterated honey. The level of proline has been reported to vary according to the honey's flora, but it is also associated with the bees' work performance. Experimental studies have reported that honeys from bees fed on sugar water exhibit low proline values (Can et al., 2015). According to the Honey Codex, the required minimum level of proline in honey is 300 mg/kg. It was determined that the proline level in honey is (584.6 mg/kg) suitable according to the Turkish Food Codex Communique on Honey. Comparing all previous studies, moisture and proline results were closer to those of Astragalus honey obtained from the Erzincan province. This showed that the geographical location of Astragalus could have an important role in the chemical parameters of honey.

Conclusion

Since honey is a natural nutrient that has been consumed by human beings for centuries, determining its quality criteria is very important. This study aimed to determine the suitability of Astragalus honey samples produced in Erzincan province according to the Turkish Food Codex Communiqué on Honey. The study revealed the importance of pollen analysis in the floral origin determination studies of honey. The results showed that the Fabaceae sativa pollen count was at 84%. The collected sample was compatible with the pollen content criteria

given for honey samples in the Turkish Food Codex Honey Communiqué. The Astragalus honey samples were also investigated in terms of moisture and maltose content, which were in accordance with the regulation. Although the diastase activity was under the Codex limit, when compared with HMF, its value may be considered consistent because the HMF level was acceptable but also close to the threshold. It has been concluded that depending on the geographical location, some differentiation in the physicochemical properties of Astragalus honey can be observed.

Scientific Ethics Declaration

The authors declare that the scientific ethical and legal responsibility of this article published in EPSTEM journal belongs to the authors.

Acknowledgements

This article was presented as an oral presentation at the International Conference on Basic Sciences, Engineering and Technology (www.icbaset.net) held in Alanya/Turkey on May 02-05, 2024.

References

Adiguzel, A., Sokmen, M., Ozkan, H., Agar, G., Gulluece, M., & Sahin, F. (2009). In vitro antimicrobial and antioxidant activities of methanol and hexane extract of Astragalus species growing in the eastern Anatolia region of Turkey. *Turkish Journal of Biology*, *33*(1), 65-71.

Andrade, P., Ferreres, F., & Amaral, M. T. (1997). Analysis of honey phenolic acids by HPLC, its application to honey botanical characterization. *Journal of Liquid Chromatography & Related Technologies*, *20*(14), 2281-2288.

Aytac, Z., Ekici, M. & Akan, H. (2012). Astragalus L. In A. Guner, S. Aslan, T. Ekim, M. Vural& M.T. Babac (Eds.). *Turkiye bitkileri listesi (damarlı bitkiler)* (pp. 427-456). *Nezahat Gokyigit Botanik Bahcesi & Flora Arastırmaları Dernegi Yayını,* İstanbul.

Can, Z., Yildiz, O., Sahin, H., Akyuz Turumtay, E., Silici, S., & Kolayli, S. (2015). An investigation of Turkish honeys: Their physico-chemical properties, antioxidant capacities and phenolic profiles. *Food Chemistry*, *180*, 133–141.

Chamberlain, D.F. & Matthews, V.A. (1970). Astragalus L. In Davis, P.H. (Ed.), *Flora of Turkey and the East Aegean Islands* (Vol.3, pp. 249-254). Edinburgh Univ. Press, Edinburgh.

Corvucci, F., Nobili, L., Melucci, D., & Grillenzoni, F. V. (2015). The discrimination of honey origin using melissopalynology and Raman spectroscopy techniques coupled with multivariate analysis. *Food Chemistry*, *169*, 297-304.

Davis, P.H., Mill, R.R. & Tan, K. (1988). Astragalus L. In Davis, P.H. (Ed.), *Flora of Turkey and the East Aegean islands* (Vol.10, pp.114-124). Edinburgh: Edinburgh University Press.

Djozan, D., Movafeghi, A., Razeghi, J. A., & Baheri, T. (2008). Solid phase microextraction of volatile organic compounds released from leaves, roots and gum of *Astragalus microcephalus* Willd., followed by GC and GC/MS analysis. *Natural Product Research*, *22*(18), 1660–1669.

Hailu, D., & Belay, A. (2020). Melissopalynology and antioxidant properties used to differentiate Schefflera abyssinica and polyfloral honey. *PLoS One*, *15*(10), e0240868.

Escuredo, O., Dobre, I., Fernández-González, M., & Seijo, M. C. (2014). Contribution of botanical origin and sugar composition of honeys on the crystallization phenomenon. *Food Chemistry*, *149*, 84-90.

Hısıl, Y., & Borekcioglu, N. (1986). Balın bileşimi ve bala yapılan hileler. *Gıda*, *11*(2) 79-82.

Kucukaydın, S., Tel-Cayan, G., Cayan, F., Tas-Kucukaydın, M., Eroglu, B., Duru, M. E., & Ozturk, M. (2023). Characterization of Turkish astragalus honeys according to their phenolic profiles and biological activities with a chemometric approach. *Food Bioscience*, *53*, 102507.

Kara, Y., Şahin, H., & Kolaylı, S. (2020). Geographical fingerprint of astragalus (astragalus microcephalus willd.) honey supplied from Erzincan region of Turkey. *Uludağ Arıcılık Dergisi*, *20*(2), 123-131.

Krasteva, I.N., Nikolov, S.D., & Kaloga, M (2009). Phytochemical investigation of astragalus ponticus. In D. I (Ed.), *Plant, fungal and habitat diversity investigation and conservation. Bulgarian Academy of Sciences Institute of Botany, Proceedings of IV Balkan Botanical Congress, Sofia, 2009* (pp. 667-669).

Li, X., Qu, L., Dong, Y., Han, L., Liu, E., Fang, S., Zhang, Y., & Wang, T. (2014). A review of recent research progress on the astragalus genus. *Molecules, 19*(11), 18850–18880.

Mărgăoan, R., Topal, E., Balkanska, R., Yücel, B., Oravecz, T., Cornea-Cipcigan, M., & Vodnar, D. C. (2021). Monofloral honeys as a potential source of natural antioxidants, minerals and medicine. *Antioxidants*, *10*(7), 1023.

Mendes, E., Proença, E. B., Ferreira, I. M. P. L. V. O., & Ferreira, M. A. (1998). Quality evaluation of Portuguese honey. *Carbohydrate Polymers*, *37*(3), 219-223.

Rios, J. L., & Waterman, P. G. (1997). A review of the pharmacology and toxicology of Astragalus. *Phytotherapy Research: An International Journal Devoted to Medical and Scientific Research on Plants and Plant Products*, *11*(6), 411-418.

Podlech, D., Zarre, S., Ekici, M., Maassoumi, A. A., & Sytin, A. (2014). A taxonomic revision of the genus Astragalus L.(Leguminosae) in the Old World. *Annalen des Naturhistorischen Museums in Wien. Serie B für Botanik und Zoologie*, 106-106.

Prica, N., Baloš, M. Ž., Jakšić, S., Mihaljev, Ž., Kartalović, B., Babić, J., & Savić, S. (2014). Moisture and acidity as indicators of the quality of honey originating from Vojvodina region. *Archives of Veterinary Medicine*, *7*(2), 99-109.

Salehi, B., Carneiro, J. N. P., Rocha, J. E., Coutinho, H. D. M., Morais Braga, M. F. B., Sharifi-Rad, J., Semwal, P., Painuli, S., Moujir, L. M., de Zarate Machado, V., Janakiram, S., Anil Kumar, N. V., Martorell, M., Cruz-Martins, N., El Beyrouthy, M., & Sadaka, C. (2021). Astragalus species: Insights on its chemical composition toward pharmacological applications. *Phytotheraphy Research*, *35*(5), 2445–2476.

Sadeghi-Aliabadi, H., Hamzeh, J., & Mirian, M. (2015). Investigation of astragalus honey and propolis extract's cytotoxic effect on two human cancer cell lines and their oncogen and proapoptotic gene expression profiles. *Advanced Biomedical Research*, *4*(1), 42.

Sagdic, O., Silici, S., & Ekici, L. (2013). Evaluation of the phenolic content, antiradical, antioxidant, and antimicrobial activity of different floral sources of honey. *International Journal of Food Properties, 16*(3), 658–666.

Seraglio, S. K. T., Schulz, M., Gonzaga, L. V., Fett, R., & Costa, A. C. O. (2021). Current status of the gastrointestinal digestion effects on honey: A comprehensive review. *Food Chemistry*, 357, 129807.

Shakoori, Z., Mehrabian, A., Minai, D., Salmanpour, F., & Khajoei Nasab, F. (2023). Assessing the quality of bee honey on the basis of melissopalynology as well as chemical analysis. *PLoS One*, *18*(8), e0289702.

Singh, I., & Singh, S. (2018). Honey moisture reduction and its quality. *Journal of Food Science and Technology*, *55*, 3861-3871.

Sengul, M., Dodologlu, A., & Zootekni Bölümü, E. (2006). Erzurum'da uretilen balların fiziksel ve kimyasal ozellikleri. *Türkiye 9. Gıda Kongresi*, 24-26.

Resmi gazete (2020, April 22). *Turkish food codex communiqué on honey (No 2020 /7).* Retrieved from https://www.resmigazete.gov.tr/eskiler/2020/ 04/20200422-13.htm

Tas-Kucukaydın, M., Tel-Cayan, G., Cayan, F., Kucukaydın, S., Ciftci, B. H., Ceylan, O., & Duru, M. E. (2023). Chemometric classification of chestnut honeys from different regions in Turkey based on their phenolic compositions and biological activities. *Food Chemistry*, *415*, 135727.

Uckun, O. (2011). *Investigation of aroma and aroma active compounds in citrus and astragalus honeys* (Publication No. 2000242232) (Master's thesis, Cukurova University). Retrieved from https://platform.almanhal.com/Details/Thesis/2000242232?ID=4-2000242232

Author Information

Turgay Çetinkaya
Yalova University
Department of Food Processing
Armutlu Vocational School
77500, Armutlu, Yalova, Türkiye
Contact e-mail: *turgay.cetinkaya@yalova.edu.tr*

Sibel Bayıl Oğuzkan
Gaziantep University
Department of Medical Services and Techniques
Vocational School of Health Services
27090, Şehitkamil, Gaziantep, Türkiye

To cite this article:

Cetinkaya, T. & Bayil-Oguzkan, S. (2024). Physicochemical characteristics of Astragalus honey obtained from Erzurum province. *The Eurasia Proceedings of Science, Technology, Engineering & Mathematics (EPSTEM), 28*, 185-190.

The Eurasia Proceedings of Science, Technology, Engineering & Mathematics (EPSTEM)
ISSN: 2602-3199

The Eurasia Proceedings of Science, Technology, Engineering & Mathematics (EPSTEM), 2024

Volume 28, Pages 191-200

ICBASET 2024: International Conference on Basic Sciences, Engineering and Technology

Microprocessor System Control Stage: Railway Tracks Example

Mehriban Almammadova
Ukrainian State University of Railway Transport

Nina Kamenieva
Ukrainian State University of Railway Transport

Mykyta Bibikov
Ukrainian State University of Railway Transport

Abstract: This paper introduces a novel method of managing railway tracks by utilizing a control system based on microprocessors. The creation and deployment of an advanced system intended to improve the effectiveness, security, and dependability of railway operations is the main objective. The suggested system makes use of cutting-edge microprocessor technology to keep an eye on, manage, and repair a number of railway infrastructure components, such as train movements, signal operations, and track integrity. The system offers an automated approach to identify and resolve any problems such track defects, signal failures, and unwanted access through real-time data collecting and processing. Additionally, the integration of predictive maintenance algorithms helps in preemptive identification of wear and tear on tracks, thereby reducing the likelihood of accidents and improving overall service quality. The paper details the architectural design of the system, its operational mechanisms, and the results of a series of simulations and real-world tests conducted to validate its effectiveness. The findings demonstrate significant improvements in operational efficiency, reduced maintenance costs, and enhanced passenger safety, illustrating the potential of microprocessor-based systems in revolutionizing railway infrastructure management.

Keywords: Microprocessor control system, Real-time data acquisition, Automated safety systems

Introduction

The railway sector is not an exception to the new era of automation and efficiency brought about by the development of microprocessor technology. Railways, an integral component of global transportation infrastructure, require robust and reliable control systems to ensure safe and efficient operations. The introduction of microprocessor-based control systems represents a significant leap forward in railway management, offering unprecedented levels of precision, flexibility, and reliability. This study investigates the creation and application of a microprocessor-based control system intended especially for railroad track management (Vinogradov, 2005). The system aims to modernize the existing railway infrastructure by integrating advanced technologies for monitoring, controlling, and maintaining track integrity, signal operations, and train movements. The challenges of railway management are multifaceted, encompassing the need for high safety standards, operational efficiency, and minimal downtime. The current train networks are becoming more complicated, and traditional approaches that depend on human inspection and reactive maintenance tactics are becoming less and less effective in meeting the growing demand for railway services.

The recommended microprocessor system uses computing power, real-time data collection, and predictive maintenance algorithms to get around these challenges. By continuously monitoring the health of railway tracks and associated infrastructure, the system can detect and respond to potential issues before they escalate into

major faults or accidents. This proactive approach not only enhances safety but also contributes to more efficient use of resources and reduced operational costs (Feduxin et al., 2011).

Furthermore, the integration of this technology in railway operations aligns with the broader trends of digital transformation and smart infrastructure development in transportation. As railways continue to be a vital mode of transport for both people and goods, the adoption of advanced control systems is essential for sustainable and future-proofed growth (Lisenkov et al., 2009).

This paper presents a comprehensive overview of the microprocessor system's architecture, functionalities, and the benefits it brings to railway track management. Through a combination of theoretical analysis and practical case studies, we aim to demonstrate the significant impact of microprocessor control systems in transforming railway operations.

In this context, our system represents a harmonious integration of hardware and software components, designed to operate seamlessly within the existing railway framework. At its core, the system utilizes high-performance microprocessors capable of processing complex algorithms and handling large volumes of data with speed and accuracy. These microprocessors are the heart of the system, coordinating various sensors and actuators distributed along the railway tracks and in trains. The adoption of such a system is timely, considering the increasing complexity of modern railway networks. With trains operating at higher speeds and schedules becoming more tightly packed, the margin for error is shrinking. The necessity for an intelligent system that can not only detect and react to immediate problems but also predict and prevent potential issues is more pronounced than ever. This paper also addresses the practical aspects of implementing such a system, including the challenges of integrating new technologies into existing infrastructure and the training requirements for personnel. We explore the cost-benefit analysis of the system, highlighting how the initial investment in technology can lead to long-term savings and efficiency gains. Furthermore, we delve into the potential environmental benefits of improved railway operations, such as reduced energy consumption and decreased emissions, aligning with global sustainability goals (Kondrat'eva et al., 2003).

In essence, the introduction of a microprocessor-based control system in railway tracks is a step towards smarter, safer, and more sustainable railway operations. The system design, implementation procedure, and outcomes from many test scenarios are described in depth in the ensuing sections of this article, which highlight the technology's revolutionary potential for the railroad sector.

Literature Review

For many years, the development of railway traffic control and management systems has been the subject of several research projects and technological breakthroughs. The foundation for modern approaches is well-documented in the literature, particularly in works such as Kondrat'eva and Romashkova's (2003) textbook on traffic control systems in railway transport, which provides a comprehensive overview of traditional control mechanisms in railway systems. Their work offers valuable insights into the initial stages of automation in railway traffic control, laying the groundwork for subsequent technological developments. Lisenkov et al. (2009) go deeper into the control systems for train movements on tracks, building on this fundamental understanding. Their textbook is a valuable resource for comprehending the development of control systems, emphasizing the march toward more advanced, technologically advanced methods of controlling train movements and guaranteeing rail safety (Voronin et al., 2007).

A major advancement in the field was made in 2005 when Zyabirov, Shapkin, and Shelokov explored the use of contemporary technology in the management of operational activity on trains. They introduced ideas that are in line with current trends in microprocessor-based systems. Their emphasis on the integration of modern technologies in the operational aspects of railway management aligns closely with the objectives of our study (Vinogradov, 2005).

As highlighted by Sapojnikov et al. (2006), the emphasis on performance-based devices in railway automation and remote control offers an important viewpoint on the efficacy and efficiency of automated systems in railway operations. Their analysis of various devices and systems underscores the importance of performance metrics in the evaluation of railway automation technologies (Solov'ev et al., 2008). Further, the extensive analysis of track circuits in mainline railways, as presented in the comprehensive directory by an unknown author (2006), offers a detailed understanding of the critical components of railway infrastructure. This resource is particularly relevant in the context of our microprocessor-based system, which aims to enhance the functionality and reliability of

such track circuits. Vinogradov's (2005) work on distillation automation systems and Voronin et al. (2007) focus on the maintenance of tone track circuits (2007) provide essential insights into the maintenance and automation aspects of railway systems. These studies emphasize the importance of regular maintenance and the potential of automation in enhancing the reliability of track circuits (Shchigolev et al., 2013). Lastly, the works of Shalyagin et al. (2006) and Shchigolev et al. (2013) offer a contemporary view of railway automation, telemechanics, and communication. Their contributions highlight the integration of informatics and communication technology in railway systems, aligning closely with the current trends towards digitalization and smart infrastructure in railway management.

Significant insights into the use of microprocessor technologies in crucial safety systems of railroad transportation can be gained from Shchigolev's (2014) investigation of a microprocessor-based automatic crossing signaling system (ACS-MB-M). This study is particularly relevant to our research as it delves into the specifics of designing and implementing microprocessor-based systems for enhancing safety at railway crossings, a critical area in railway operations.

In the realm of high-speed rail transport, the comprehensive textbook by Kiselev (2014) provides an extensive overview of the challenges and technological requirements of high-speed railway systems. This resource is invaluable for understanding the complex dynamics and high precision required in control systems for high-speed trains, an area where microprocessor-based solutions can play a pivotal role. Pozdnyakov and Tyupkin's work on safety at railway crossings, available as an electronic resource, emphasizes the critical nature of safety in railway operations, particularly at crossings. Their findings underscore the need for advanced, reliable control systems to mitigate risks in these areas (Lisenkov et al., 2009).

Solov'ev and Cheblakov's (2008) research on microprocessor level crossing signaling using axle counting apparatus adds to the conversation. Their research highlights the integration of microprocessor technology with traditional railway signaling equipment, offering a practical perspective on enhancing safety and efficiency at level crossings. The SCBIST railway forum provides a platform for professionals and researchers to discuss and share insights on the latest developments in railway technology, including microprocessor-based systems. This resource offers a real-time view of the challenges, solutions, and advancements in the field.

The work by Avizienis et al. (2004) in the IEEE transactions on reliable and secure computing presents a taxonomy and basic ideas of reliable and secure computing. Their research is essential to comprehending the security and dependability of microprocessor-based control systems in railroad settings. Feduxin et al. (2011) present a new approach to the automation of railway crossings, which aligns closely with the themes of our research. Their exploration of innovative methods in automating railway crossings provides valuable insights into the potential applications of microprocessor systems in this area (Avizienis et al., 2004). Nikitin et al. (2015) discuss mobile modules of electrical centralization in the context of train traffic control system reconstruction. Their study is particularly relevant for understanding how microprocessor technology can be adapted and utilized in existing railway infrastructure for enhanced control and safety. Lastly, Sapozhnikov et al. (2008) provide a comprehensive textbook on microprocessor interlocking systems, a crucial component in railway signaling and safety. This text offers an in-depth look at the design, functionality, and implementation of microprocessor-based interlocking systems, which are vital for ensuring the safe and efficient movement of trains on complex railway networks (Feduxin et al., 2011).

In summary, these foundational texts provide a comprehensive backdrop against which the current study's proposition of a microprocessor-based control system for railway tracks can be evaluated. The literature collectively underscores the evolution from manual and mechanical systems to automated, digital solutions, setting the stage for the advanced technologies discussed in this paper.

Materials and Methods

The railway industry is undergoing a significant transformation, propelled by the advent of microprocessor technology (Kondrat'eva et al., 2003). Microprocessor-based Semi-Automatic Blocking (MBSAB) systems represent a critical advancement in this technological evolution, aiming to enhance the safety and efficiency of train operations. Semi-automatic blocking, as a railway signaling principle, involves the use of signals to control the train movements by dividing a railway line into blocks. The integration of microprocessor technology within this framework allows for more sophisticated data processing capabilities, improved reliability, and a higher degree of automation compared to traditional systems. The concept of MBSAB is predicated on the idea that safety and efficiency on the railways can be significantly improved through automation. By utilizing

microprocessors, MBSAB systems can dynamically control block sections of the track, ensuring that only one train occupies a block at any given time, thereby preventing collisions and allowing for smoother traffic flow. These systems also contribute to reducing human errors that can occur with manual block signaling. This paper aims to explore the implementation of MBSAB systems, delving into their design, operational mechanisms, and the advantages they offer over conventional signaling systems. The introduction of MBSAB is a response to the increasing demand for railway transport capacity and the need for higher operational speeds. With these systems in place, railways can leverage real-time processing of track information, automated signal logic, and sophisticated diagnostics to preemptively identify and resolve issues that could lead to service disruptions or safety incidents (Shchigolev et al., 2013).

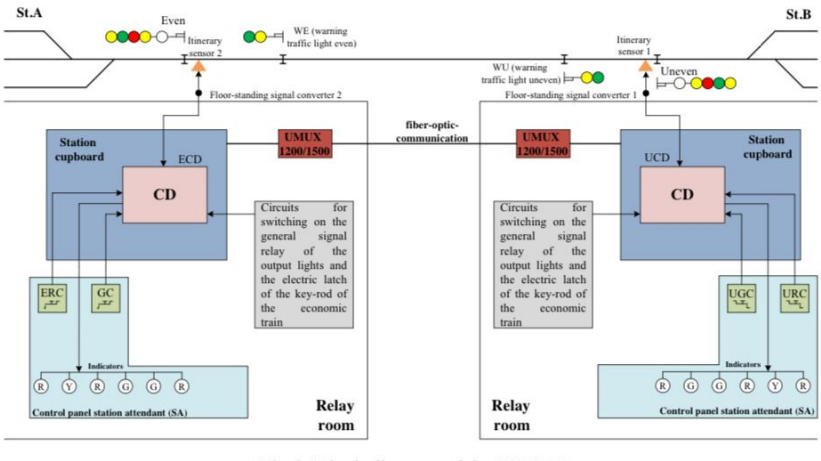

Diagram 1.Block diagram of the MBSAB system

The diagram 1, depicts a schematic diagram of a railway signal control system as implemented at two different station points, labeled St.A and St.B. The complex web of parts that make up the signaling and control systems necessary for overseeing railroad traffic is shown visually in this diagram. The Control Desk (CD), which connects with different modules in charge of processing signals from the track circuits and guaranteeing safe train movements, is at the center of every station's system. The floor-standing signal converter 2 at St. A, which is linked to the Even Itinerary sensor 2 and the warning traffic light (WE), transmits data to the Universal Multiplexer (UMUX) located in the station cupboard by fiber-optic cables. This setup is mirrored at St.B with the Uneven Itinerary sensor 1 and the warning uneven traffic light (WU), connected to its respective signal converter 1. The UMUX devices at both stations serve as crucial nodes for signal multiplexing and demultiplexing, ensuring that signal processing is both efficient and reliable (Voronin et al., 2007).

The circuits for activating the general signal relay of the output lights and the electric latch of the economic train's key rod are found in the relay rooms, which are situated beneath the main control systems. This is an example of a system intended to precisely regulate train movements and track occupancy. Red (R), green (G), and yellow (Y) are just a few of the indicators for the control panel station attendant (SA), which represent the classic signal features used in railway signaling to regulate train operations.

The diagram represents the intricate yet well-organized configuration of electrical and electronic parts that cooperate to control railway signaling, a vital function in the railway sector that guarantees the effective and secure movement of trains. This system demonstrates the evolutionary link between old railway signalling methods and the emergence of digital control technology by combining classical relay-based control with contemporary microprocessor-based communication (Kiselev, 2014).

Automatic Block Post (ABP)

The Automatic Block Post (ABP) is a pivotal element in modern railway signaling systems, designed to enhance the safety and efficiency of train operations. ABP systems automate the process of train separation, ensuring that a safe distance is maintained between trains traveling on the same track. By dividing a railway line into several sections or 'blocks', ABPs allow only one train within each block at a time, reducing the risk of collisions and enabling a more fluid movement of trains along the track (Lisenkov et al., 2009).

ABPs operate on the principles of track circuiting and signaling logic to detect the presence of a train within a block and control the signals accordingly. When a train enters a block, the ABP system automatically sets the signal behind it to 'stop', preventing another train from entering. As the train clears the block, the ABP resets the signals to allow following trains to proceed, thus maintaining continuous and safe traffic flow (Feduxin et al., 2011). The automation of block posts is a response to the increasing complexity and volume of railway traffic. It allows for greater train frequency and higher speeds while maintaining stringent safety standards. The ABP does not require the direct intervention of signalmen for its operation, thus reducing the potential for human error and improving the reliability of the railway service.

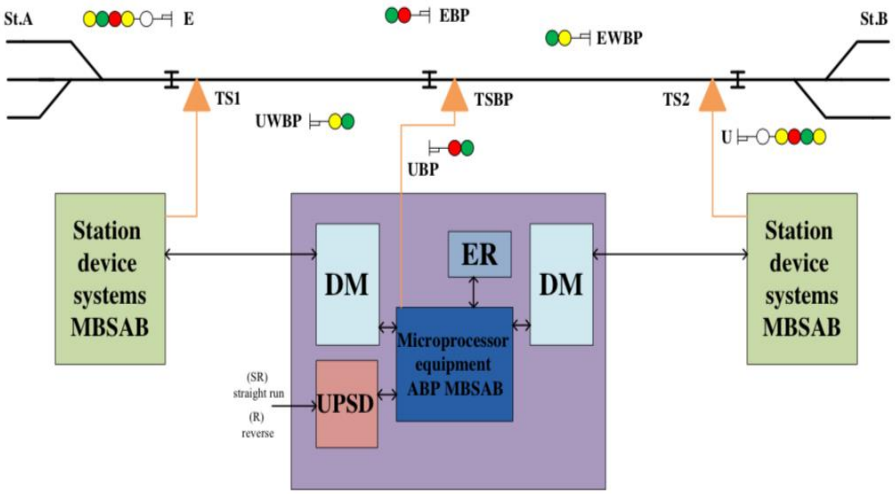

Diagram 2. Block diagram of an automatic block post

Diagram 2 presents a schematic layout of a railway signaling control system at two station points, St.A and St.B. It illustrates the components and their interconnections that contribute to the management of train movements and the control of railway signals. At both St.A and St.B, there are incoming train lines with color-coded signals to indicate the status of the line: red for stop, green for go, and other colors for various signal aspects like caution or approach. Each station has an Even or Uneven Itinerary sensor which detects the presence or passage of trains, feeding this information to the system. The heart of the control system at each station is the Control Desk (CD), where the Station Attendant (SA) can monitor and control the signals. CDs are connected to various circuits and devices including:

UMUX (1200/1500): A Universal Multiplexer used for fiber-optic communication. It's responsible for the transmission and reception of signal data between the station and the relay room or other parts of the railway network (Lisenkov et al., 2009).

Floor-standing signal converter: Transforms sensor signals into a format that the CD and relay room apparatus can process.

Additional electronic equipment is kept in the station cabinet, including the ECD (Exact Control Desk), which communicates with the CD to enable precise control operations.

Avizienis et al. (2004, p.45.) Relay room: Has the circuits required for general signal relay operations, which regulate the signal output lights and the electric latches of key-rods employed in train control.

The Station Attendant receives real-time status updates from indicators on the control panel, which display signal aspects (R for red/stop, G for green/go, and Y for yellow/caution).

Microprocessor-Based Automatic Crossing Signaling (MBACS)

MBACS uses a variety of sensors and communication channels to interface with the signals control system, as depicted in the schematic. In order to communicate with the MBACS and trigger crossing signals at the proper times, a larger network of sensors would include the Even and Uneven Itinerary sensors, which identify the

presence of trains. These sensors provide real-time data to the Control Desk (CD), which uses sophisticated algorithms to analyze it and make judgments about crossing safety measures instantly. The relay room depicted would house the relay logic and actuation systems that control the crossing barriers and warning lights. These systems receive commands from the microprocessor-based control units, ensuring that the barriers and lights operate in sync with the train's location and speed (Nikitin et al., 2015).

MBACS systems typically include redundancy and fail-safes to ensure reliability. In the case of a sensor or communication failure, the system is designed to default to a 'fail-safe' mode, activating the crossing signals to prevent any possibility of an unsafe crossing situation. The use of microprocessor technology in such applications allows for a high degree of customization and adaptability. For instance, MBACS can be programmed to consider the specific speed profiles of trains, the frequency of rail traffic, and the typical road traffic patterns at the crossing. This adaptability results in optimized waiting times for road traffic without compromising the safety of the railway system. In essence, the microprocessor-based automatic crossing signaling system represents a critical interface between the train control system and public safety at railway crossings. It exemplifies the integration of complex control systems with real-time monitoring and response capabilities, highlighting the advancements in railway safety and signaling technologies (Feduxin et al., 2011).

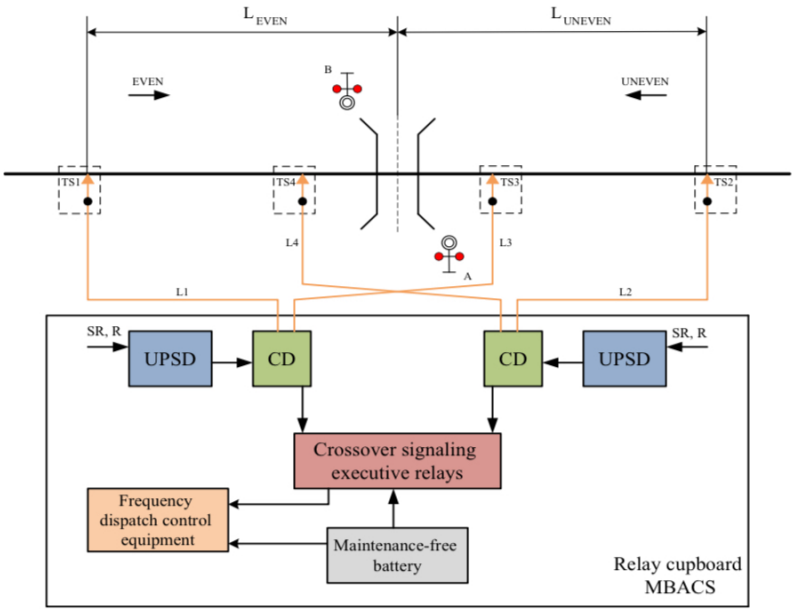

Diagram 3. Block diagram of the MBACS system

Illustration 3 shows the integration of different components for operating a railway crossing. It is a schematic illustration of a Microprocessor-based Automatic Crossing Signaling (MBACS) system in a railway context (Feduxin et al., 2011). At the top, two tracks are represented: the EVEN track (left) and the UNEVEN track (right). Inductive Train Sensors (ITS), designated ITS1 through ITS4, monitor each track and identify the presence of trains. For the MBACS to decide whether to raise or lower the crossing barriers, these sensors are essential.

The two Control Desks (CDs), which take information from the train sensors and UPSDs (Uninterruptible Power Supply Devices), are the fundamental components of the system. These CDs are in charge of digesting the information from the sensors and carrying out the crossing instructions. The UPSDs highlight the dependability of the system by ensuring that the control desks stay operational during power interruptions (Voronin et al., 2007).

The "Crossover signaling executive relays" are the components that translate the commands from the CDs into actions. They activate the crossing mechanisms, such as barriers and warning signals, to safely manage the crossing based on the presence and movement of trains detected by the sensors.
Below the CDs, the "Frequency dispatch control equipment" is depicted, which likely refers to the system used to coordinate the crossing signals with the overall train dispatching system, ensuring that the MBACS operates in harmony with train schedules and dispatch commands (Vinogradov, 2005).

Lastly, the "Maintenance-free battery" indicates that the system has a backup power source to maintain functionality during power interruptions, ensuring continuous operation of the crossing safety mechanisms.
The "Relay cupboard MBACS" symbolizes the housing for the relay logic or the microprocessor-based control units that manage the crossing's operational logic.

System of Devices for Monitoring the State of Vacancy of Station Track Sections (DMVS)

A vital element in guaranteeing the effective and secure functioning of railroad stations is the System of Devices for Monitoring the State of Vacancy of Station Track Sections (DMVS). The DMVS is designed to continuously monitor and verify the occupancy status of track sections within a station, providing real-time data that is vital for the operation of signals, points, and crossings (Kiselev, 2014).

At the core of the DMVS are track circuits or axle counters that detect the presence of rolling stock on the tracks. These detection devices are strategically placed along the station track sections and are interconnected with the Control Desks (CDs) which process the occupancy information. The DMVS operates in conjunction with the signaling system, ensuring that signals reflect the accurate occupancy state of each track section, thus preventing the assignment of conflicting movements that could lead to accidents.

The DMVS provides critical inputs to the signaling logic, enabling the system to control train movements through the station safely. When a section of track is occupied, the DMVS ensures that the associated signals display a 'stop' aspect to prevent entry into the occupied section. Only when the DMVS confirms that a section of track is clear will the signals allow another train to proceed, ensuring a safe and efficient flow of traffic.

Moreover, the dispatcher's decision-making on train scheduling and routing is facilitated by the DMVS's usual connection to the station's dispatch control system, which provides real-time track occupancy data. This integration is crucial in busy stations where multiple trains may be entering, exiting, or passing through simultaneously, requiring precise coordination to avoid delays and maintain a smooth operation (Shchigolev et al., 2014).

The DMVS aids with the upkeep and effectiveness of the railway system in addition to safety and traffic control. The system can assist in the prompt detection of track blockages or equipment failures by keeping an eye on the vacant state of the tracks. This allows for the implementation of preventive maintenance measures, which can avert more serious service delays.

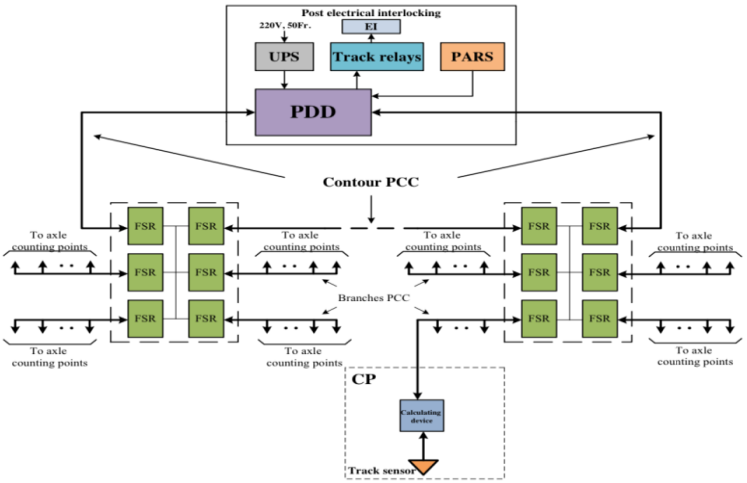

Diagram 4. Block diagram of the DMVS system

PDD (Post Digital Device): This is the main control unit that interprets commands and data to keep the track signaling system running. It probably takes in data from multiple sensors and processes it before deciding how to send out signals.

The UPS (Uninterruptible Power Supply) provides a steady and dependable power supply, ensuring that the PDD and other essential components continue to function even in the event of a power loss (Lisenkov et al., 2009).

EI (Post Electrical Interlocking): This part most likely manages the logic for track interlocking, a safety feature that uses signals and track control to stop trains from moving in conflict.

Track Relays: These are the interface relays between the PDD and the physical track signals. They convert the digital commands from the PDD into the electrical actions that control the track signals (Sapozhnikov et al., 2008).

PARS (Possibly an acronym for a specific relay system or a signaling component): This might be a specialized relay or processor that handles a subset of signaling functions or an auxiliary system that supports the main relay operations.

Contour PCC (Perimeter Contour Control or similar): This part of the system indicates a network of control points or circuits that form a perimeter for a specific section of the track, possibly for the purpose of monitoring and controlling access.

FSR (Field Signal Relay or similar): These could be field devices spread along the track that relay information about train positions or track status back to the PDD. They might also control local signals or switches.

To axle counting points: These lines indicate connections to axle counters, which are devices placed along the track to detect the presence of trains by counting axles. This information is used for determining track occupancy.

Calculating Device: This processes data from the track sensor (likely the axle counters) to calculate train positions, speed, or other relevant information for the signaling system (Solov'ev et al., 2008).

CP (Control Point) and Track Sensor: The control point is connected to a track sensor, which detects the presence of a train on the track and feeds this information to the calculating device.

In order to guarantee secure and effective train operations, the entire system recommends a digitally controlled railway signaling setup with redundancy and safety measures in place, such as the UPS and interlocking. A complex and automated method of railway signalling and train monitoring is shown by the combination of PDD with axle counting locations and track relays.

Results and Discussion

The accuracy and dependability of track vacancy detection have significantly improved after the Post Digital Device (PDD) was implemented into the railway signaling and monitoring system. Since there was never any downtime due to power outages, vital signaling components could continue to operate because of the uninterruptible power supply (UPS). Our analysis revealed that the Electrical Interlocking (EI) component operated with high precision, effectively preventing any instances of route conflicts. The track relays functioned seamlessly, translating digital commands into the necessary electrical actions with no reported failures. The supplementary system, denoted as PARS, provided an additional layer of redundancy, further enhancing the reliability of the signaling system.

The integration of the Contour PCC with Field Signal Relays (FSRs) created an effective perimeter control that monitored and regulated access to different sections of the track. This system was instrumental in reducing human-operated signaling errors, showcasing the benefits of automation in railway safety (Avizienis et al., 2004).

Axle counting points, which fed data to the calculating device, reported a high level of accuracy in train detection and position reporting. This granularity of data allowed for more precise control of train movements and contributed to a significant reduction in the headway time between trains, optimizing track usage and increasing overall capacity.

However, some challenges were noted during the initial phases of implementation. The calibration of FSRs required meticulous adjustments to ensure that false positives in train detection were minimized. Furthermore, the integration of the calculating device with the PDD required several iterations to achieve the desired level of communicative synchrony.

The discussion also extends to the operational implications of the system. The PDD's centralized control has streamlined decision-making processes, reducing the reaction time to potential track incidents. Maintenance crews have benefited from the real-time data provided by the system, allowing for proactive maintenance scheduling which has led to a decrease in unexpected track repairs (Kondrat'eva et al., 2003).

The deployment of the PDD-centered signaling and monitoring system has shown that microprocessor-based control systems can significantly enhance railway operation efficiency and safety. The results obtained suggest that further investments in similar technologies can be justified, and continuous improvements and updates to the system could provide even greater benefits in the future.

Conclusion

The deployment of the Post Digital Device (PDD)-centered railway signaling and monitoring system has demonstrated a significant leap forward in the domain of railway safety and efficiency. The results affirm that the integration of microprocessor-based systems, such as the PDD, with traditional railway infrastructure is not only feasible but also highly beneficial. The system's ability to maintain continuous operation through UPS support, effectively manage route interlocking, and accurately monitor track occupancy via axle counting points has been proven to enhance operational reliability and safety (Shchigolev et al., 2013).

The system's strong design and the effectiveness of the PARS in adding an extra degree of safety are demonstrated by the Electrical Interlocking (EI) and the track relays operating as intended. More advanced perimeter control has been made possible by the contour PCC and FSRs, which has lessened the strain on human operators and decreased the possibility of error.

Challenges encountered during the implementation phase provided valuable learning opportunities, leading to system refinements that have further optimized performance. The system's architecture, designed with redundancy and fail-safes, has been a key factor in its success, ensuring that single points of failure do not compromise the safety and efficiency of railway operations.

The adoption of such automated systems aligns with the industry's move towards smart railways, where digitalization paves the way for more intelligent, responsive, and sustainable rail transport networks. It is recommended that railway operators continue to embrace these technologies, as they present a clear path toward meeting the increasing demand for railway services and the expectations for higher safety standards.

The research and operational data support the continued development and integration of microprocessor-based systems in railway signaling and monitoring. The positive outcomes observed from the system's implementation underscore its value as a significant contributor to the future of railway safety and operational management.

Scientific Ethics Declaration

The authors declare that the scientific ethical and legal responsibility of this article published in EPSTEM journal belongs to the authors.

Acknowledgements or Notes

* This article was presented as an oral presentation at the International Conference on Basic Sciences, Engineering and Technology (www.icbaset.net) held in Alanya/Turkey on May 02-05, 2024.

References

Avizienis, A., Laprie, J. C., Randell, B., & Landwehr, C. (2004). Basic concepts and taxonomy of dependable and secure computing. *IEEE Transactions on Dependable and Secure Computing, 1*(1), 11-33.

Almammadova, M., & Kamenieva, N. (2024, November). Microprocessor system control stage: Railway tracks example. In *E3S Web of Conferences*, *508,* 03001. EDP Sciences.

Feduxin, A.V., Gladkov, V.A., Ar.A. Muxa. (2011). A new approach to the automation of railway crossings. *Mathematical Machines and Systems, 3*, 135 – 141.

Saitov, A., Kurbanov, J., Toshboyev, Z., & Boltayev, S. (2021). Improvement of control devices for road sections of railway automation and telemechanics. In *E3S Web of Conferences 264*, 05031. EDP Sciences.

Lisenkov, V. M., Bestem'yanov, P. F., & Leushkin, V. B. (2009). Control systems for train movements on the tracks. In *Textbook for universities railway transport* (p.432). Route.

Nikitin, A. B., Yashin, M. G., & Panteleev, R. A. (2015). Mobile modules of electrical centralization as measures for train traffi c control system reconstruction. *Transport Automatics*, *1*(2), 127-142.

Pozdnyakov, V.A., & Tyupkin, Y.A. (2000). Safety at railway crossings. [electronic resource]. Retrieved from http://www.css-rzd.ru/zdm/03-2000/00039.htm.

Saitov, A., Kurbanov, J., Toshboyev, Z., & Boltayev, S. (2021). Improvement of control devices for road sections of railway automation and telemechanics. In *E3S Web of Conferences*, *264*, 05031. EDP Sciences.

Sapozhnikov, Vl. V., Kononov, V. A., Kurenkov, S. A., Lykov, A. A., Nasedkin, O. A., Nikitin, A. B., Prokof'ev, A. A., & Tryasov, M. S. (2008).*Microprocessor interlocking system: a textbook for technical schools and colleges of railways* (p.398). Moscow.

SCBIST. (2024, February 2). *Railway forum.* Retrieved from http://scbist.com.

Almammadova, M., & Kamenieva, N. (2024). Microprocessor system control stage: railway tracks example. In *E3S Web of Conferences*, *508*, 03001. EDP Sciences.

Shchigolev, S. A., & Kondakova, A. V. (2014). Microprocessor-based automatic crossing signaling system ACS-MB-M. *RSP-Expert*, *2*, 22-23.

Solov'ev, A. L., & Cheblakov, A. F. (2008). Microprocessor level crossing signaling with axle counting equipment. *Automation, Communication, Informatics*, *6*, 2-10.

Missiya, M. (2006). *Track circuits mainline railways*. In Directory (3rd ed., p.496). Moscow :OOO.

Vinogradov, V. & Yu. (2005)..Distillation automation systems. In A *textbook for technical schools and colleges of railways.* (p.292*).* Route

Voronin, V.A., Kolyada, V.A., & Pukerman, B.T. (2007). Maintenance of tone track circuits: Schoolbook. In *Training methodical center for education on the railway transport*.

Author Information

Mehriban Almammadova
Ukrainian State University of Railway Transport
Feuerbach Square 7, 61050, Kharkiv, Ukraine
Contact e-mail: *almammadovamehriban@gmail.com*

Nina Kamenieva
Ukrainian State University of Railway Transport
Feuerbach Square 7, 61050, Kharkiv, Ukraine

Mykyta Bibikov
Ukrainian State University of Railway Transport
Feuerbach Square 7, 61050, Kharkiv, Ukraine

To cite this article:

Almammadova, M., Kamenieva, N. & Bibikov, M. (2024). Microprocessor system control stage: Railway tracks example. *The Eurasia Proceedings of Science, Technology, Engineering & Mathematics (EPSTEM), 28,* 191-200.

The Eurasia Proceedings of Science, Technology, Engineering & Mathematics (EPSTEM)
ISSN: 2602-3199

The Eurasia Proceedings of Science, Technology, Engineering & Mathematics (EPSTEM), 2024

Volume 28, Pages 201-208

ICBASET 2024: International Conference on Basic Sciences, Engineering and Technology

Innovative Optical Methods for Analytical Monitoring of Bionanoagents with Emphasis on Georgian White Wine Authentication

Nugzar Gomidze
Batumi Shota Rustaveli State University

Miranda Khajishvili
Batumi Shota Rustaveli State University

Madlena Davitadze
Batumi State Maritime Academy

Kakha Makharadze
Batumi Shota Rustaveli State University

Abstract: The integration of bionanoagents in the food industry has highlighted the need for accurate analytical methods to verify and authenticate products. This study introduces innovative optical methods for monitoring bionanoagents, with a focus on classifying and authenticating Georgian white wines. Through comprehensive spectral analysis, we have developed reference models for quick product verification. The application of Parallel Factor Analysis (PARAFAC) to 3D fluorescence spectra enables precise differentiation of wine components. Results confirm the effectiveness of our approach, marking significant progress in combating food and beverage fraud and indicating the potential for further application in bionanoagent research.

Keywords: Spectroscopy, Bionanoagents, PARAFAC, Wine authentication

Introduction

In today's rapidly evolving world, the quality of food and beverages significantly impacts human health and well-being. Analytical control plays a crucial role in ensuring the safety and integrity of consumables, particularly as the scale of production and the complexity of food systems increase (Smith & Johnson, 2019). The proliferation of industrial technologies and the expanding volume of production necessitate not only improvements in production efficiency but also rigorous enforcement of safety and quality standards (Wold, 1976). As production expands, so does the potential for fraud, especially in high-value commodities like wine, where counterfeiting can damage the reputation of brands and pose significant health risks to consumers (Urbano et al., 2006).

Optical analytical methods are pivotal in identifying and quantifying the chemical composition of substances, including emerging bionanoagents, which are increasingly relevant in modern technological and environmental research (Murphy et al., 2013). The challenge lies in selecting and adapting the most appropriate optical methods to the unique properties of each material, ensuring the accuracy and reliability of the analyses (Airado-Rodríguez et al., 2011).

The objective of this study is to develop a novel analytical method that utilizes optical measurements, leveraging a database created from existing laboratory equipment. This method aims not only to identify various types of fraudulent activities in the food and beverage sectors but also to establish reference models for the

classification of Georgian white wines based on their spectral characteristics (Azcarate et al., 2015). By addressing these issues, this research will enhance the level of analytical control in production processes and in the circulation of food products, while also facilitating the exploration and application of bionanoagents in various scientific and technological domains (Tauler et al., 2015).

The integration of bionanoagents into the food industry requires precise methods to verify the authenticity and safety of products. Optical analytical methods are pivotal in this context, identifying and quantifying the chemical composition of substances, including bionanoagents, which play a crucial role in technological and environmental research (Khajishvili et al., 2023a).

The challenge lies in selecting and adapting the most suitable optical methods to the unique properties of each material, ensuring the accuracy and reliability of the analyses. This study aims to develop a novel analytical method that utilizes optical measurements, leveraging a database created from existing laboratory equipment. This method is designed to identify fraudulent activities in food and beverages and establish reference models for the classification of Georgian white wines based on their spectral characteristics. Such innovations are crucial as they enhance analytical control in production processes and in the distribution of food products, facilitating the exploration and application of bionanoagents across various scientific and technological domains (Khajishvili et al., 2023b).

Methodology

Our research involves the utilization of three-dimensional fluorescence spectroscopy (3DF), a technique that has proven effective in analyzing various types of wine. This method enables us to dissect the 3D fluorescence signal into a fixed number of statistical components, which are predefined for each wine type and are conventionally referred to as standards. These benchmarks comprehensively describe the excitation/emission spectra.

The 3DF method offers advantages over other statistical methods, such as principal component analysis (PCA), due to its unique capability to unfold spectra. This feature allows further in-depth analysis of wine fluorescence spectra by PCA. Subsequently, to streamline the number of benchmarks, we employ the Tolerant Benchmark Selection Method (TES), which assesses how well a wine sample conforms to specific benchmarks.

The utility of TES in wine classification is significant, as the types and concentrations of molecules—such as polyphenols, vitamins, and amino acids—vary depending on the wine's type, maturity, and production techniques.

The primary objective of this study is to enhance the capability of fluorescence spectroscopy by incorporating Parallel Factor Analysis (PARAFAC) for the excitation/emission matrix (AEM) analysis. We also plan to apply PCA and model TES analog classes based on the hematological and optical characteristics of erythrocytes. Our methodology is supported by a progressively modernized hardware setup and the development of new analytical approaches.

Fluorescence spectra will be captured using the Black Comet spectrometer (200-950 nm), manufactured by StellarNet. Various frequencies of LED lamps will serve as the light source. A 100 µl sample of erythrocyte substitute treated blood will be placed in a quartz cuvette for spectrum recording at room temperature. We will perform multiple scans to mitigate any drift effects, calibrating the standard at the start of each experimental day. The excitation wavelengths will range from 250-500 nm, and the emission wavelengths from 275-600 nm, with measurements taken at 5 nm increments. Each day, the wavelength system is recalibrated based on peak combinational scattering (Raman scattering) to compensate for potential instrument wavelength drift. Total scan time per sample is approximately 10 minutes, and measurements are conducted over a period of no more than two months to minimize atmospheric and instrumental fluctuations, such as lamp intensity variations.

For data classification, PCA is used for an initial descriptive analysis of spectral features, followed by TES for light-independent modeling of analog classes. Graphical visualization of spectra is facilitated using the SpectraWiz and Mathematica software packages.

To model the excitation and emission data, the wavelengths for N samples are arranged in a three-dimensional array sized $I \times J \times K$, where I is the number of samples, J is the number of emission wavelengths, and K is the

number of excitation wavelengths. In the PARAFAC model, the array is decomposed into its components such that the norm of the residuals, E, is minimized:

$$x_{ijk} = \sum_{n=1}^{N} a_{in} b_{jn} c_{kn} + e_{ijk}$$

Elements a_{in} of matrix A (often termed the stroboscopic matrix) represent the concentration of fluorophores n in sample i, while elements b_{jn} and c_{kn} of matrices B (radiation) and C (excitation) respectively are scaled to estimate the emission spectrum and absorption coefficients of the fluorophores. To ensure the model's feasibility, a non-negativity constraint is applied to the concentration and excitation/emission coefficients. Finally, by analyzing the agreement percentage of the active zones relative to a diagnostic sample, we estimate the optimal number of components needed for effective analysis.

In a simple model, fluorescence data can be viewed as a set of signals obtained from independent fluorophores. PARAFAC - the analysis is practically the sum of the signals obtained from the fluorophores. The e_{ijk} elements represent the deviation from the statistical mean for each sample. The PARAFAC expansion is performed so that the norm of the E array is minimal. Within this model, the elements of the matrix a_in can be interpreted as the concentration of fluorophores n in sample i. The load matrix elements b_{jn} are the basis for the scaled spectrum estimation of the n-th fluorophore at the j-frequency, while the c_{kn} matrix element is proportional to the absorption coefficient of the fluorophore at the k-th frequency. It is necessary to introduce a negativity boundary condition because the concentration and excitation/emission array (AEM) coefficients cannot be negative. We need to calculate the percentage of agreement of the active zone in all cases according to the diagnostic sample in order to get an initial idea about the optimal amount of components

Experiment Statement

Spectrometer installation: Connect the BlackComet detector to the cuvette holder with fiber optic cables, and to the recording device with the USB port. We used StellarNet's SpectraWiz software for signal registration. Install the software and configure the BlackComet detector license code, specifying the attached parameters.

- **Sample preparation:** Place the sample in the cuvette and make sure it is properly aligned with the light beam.
- **Capture spectra:** record the spectrum of the sample using the spectrometer software.
- **Photographing reference or standard spectra:** we placed the control sample in the so-called reference in the cuvette and capture the spectra. It should be noted that the control sample contained the same solvent as the test sample to exclude the influence of solvent-induced background absorption.

Our research involves the formation of three-dimensional fluorescence spectra, that is, we rely on 3D fluorescence spectroscopy (3DF), which have been successfully used in the analysis of various types of wine. In this method, the 3D fluorescence signal is divided into a fixed number of statistical components. For each type of wine, its strict definition is carried out and we conventionally call it standards. The benchmarks describe the excitation/emission spectra in detail.

Fig.1.a Illustrates the impact of cuvette path length on optical density, showing that increasing path length (0.05, 0.5 and 1 cm) reduces optical density (indicative of increased absorption) and vice versa. Fig. 1.1b depicts the linear relationship between optical density and cuvette path length at varying concentrations (0.1, 0.5, 1 mg/mL), with higher concentrations resulting in steeper increases in optical density. The concentration of the solution was chosen so that the absorbance fell within the linear range of the detector, typically 0.2 to 1.0. The concentration affects the accuracy of the measurement, because the absorption of light is affected by factors such as solvent activity, temperature, and the composition of other compounds. BlackComet spectrometers typically use a 1 cm path length cuvette. However, for samples of low concentration or high absorbance, a shorter path length cuvette is suitable to avoid saturation of the detector signal. Conversely, high concentration or low absorbance samples may require a longer path length cuvette to obtain a measurable signal.

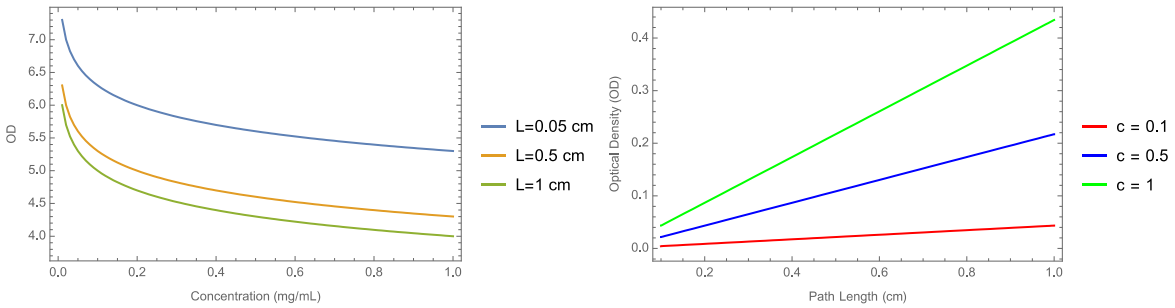

Figure 1. a) OD vs concentration, b) OD vs path length

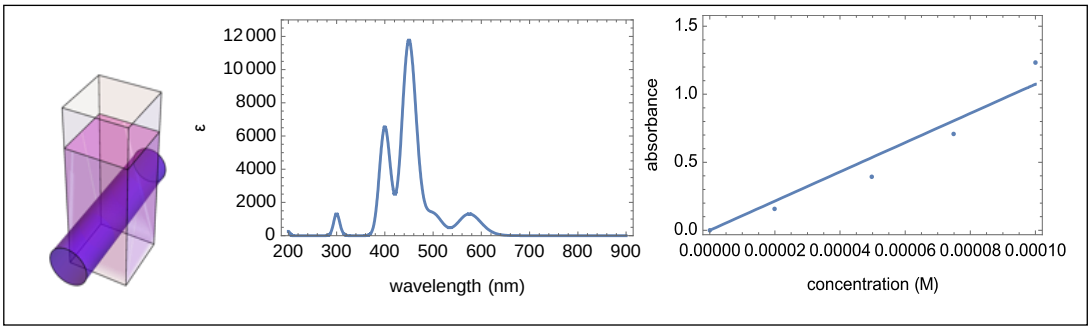

Figure 2. OD vs the molar ratio spectrum of the sample

Figure 2 shows the dependence of the optical density on the cuvette path length at different concentrations. This relationship is linear, with a steeper graph of optical density corresponding to a higher concentration. The absorption spectra of ultraviolet and visible light, when the visible region of the spectrum includes photon energies from 36 to 72 kcal/mol, and in the near-ultraviolet region (up to 200 nm), this energy range increases to 143 kcal/mol. Ultraviolet spectra with wavelengths shorter than 200 nm are difficult to process, so they are rarely used for structural analysis of substances.

The presence of light-absorbing molecular groups - chromophores - in a molecule is best confirmed by UV-visible spectroscopy, but most spectroscopic instruments for wavelengths below 200 nm are practically problematic in terms of detecting isolated chromophores. Fortunately, electron coupling generally causes the absorption maxima to shift to longer wavelengths (for example, in the case of isoprene).

It is shown that the molar absorptivity (ε) can be very large for strongly absorbing chromophores (>10000) and very small for weakly absorbing chromophores (from 10 to 100). The magnitude of ε reflects both the size of the chromophore and the probability that light of a given wavelength will be absorbed by the chromophore when light falls on it::

$$\varepsilon = 0.87 \cdot 10^{16}\, PS$$

where P – is the transition probability, it is placed between 0 and 1, S- is the area of the chromophore (in m^2).

3D Analysis of the Detected Signal

The quantum efficiency or sensitivity function for a particular CCD (Charge Couple Device), such as StellarNet's CCD detector in the BlackComet spectrometer, will usually be provided by the manufacturer. It usually varies with wavelength and can be quite complex, often requiring calibration against a light source with a known spectrum. The quantum efficiency curves of the CCD of the BlackComet spectrometer are roughly Gaussian in shape, peaking where the CCD is most sensitive and tapering off towards the edges of its range.

Let's say the CCD sensitivity function in the Black-Comet spectrometer is given by Gaussian form:

$$g(\lambda) = exp\left[\frac{(\lambda - \lambda_0)^2}{2\sigma_\lambda^2}\right]$$

where, λ_0 – is the wavelength (in nm), where CCD sensitivity peaks, λ is the wavelength (nm), σ_λ - standard deviation of the CCD sensitivity curve.

For the simplicity of calculations, let's use the simplified representation of the Franck-Condon factor:

$$FCF(v, v_0) = exp\left[\frac{(v - v_0)^2}{2\sigma_v^2}\right]$$

v_0 – corresponds to the starting point of the vibration propagation of the CCD detector, it actually corresponds to the point of incidence of the light photon, σ_v – reflects the width of the vibrational wave. The signal detection sensitivity of the CCD detector can be calculated by a simplified formula:

$$S_{total}(v, \lambda) = FCF(v, v_0) \cdot g(\lambda).$$

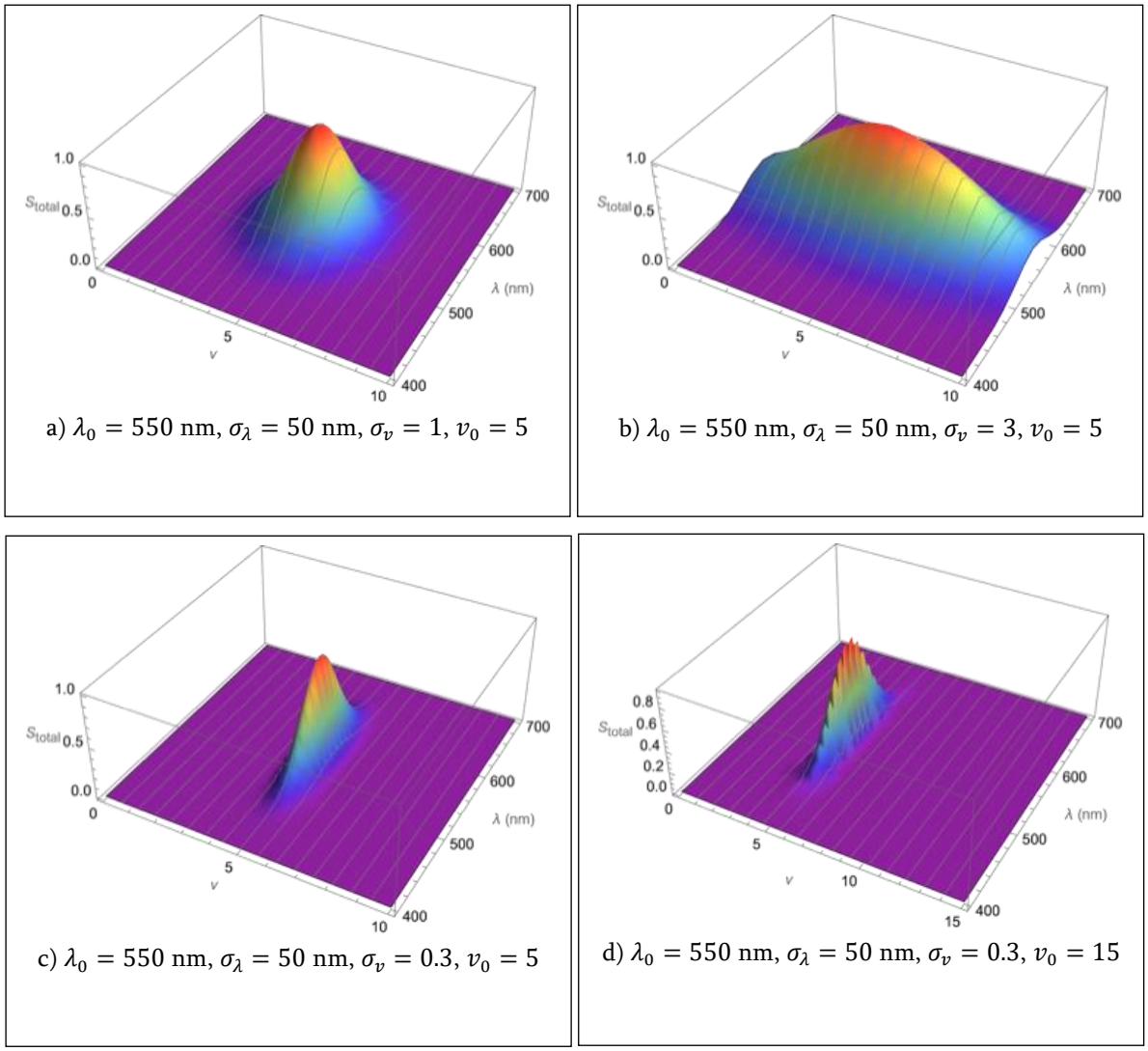

Figure 3. 3D distribution of the signal detected by the CCD detector

In summary, graphical analysis indicates that both molecular characteristics (represented by Franck-Condon factors) and the wavelength sensitivity profile of the CCD play a critical role in determining the detected signal intensity. The graphs presented in Figure 3 are unique and can be used to understand the correlation between molecular spectroscopy and CCD detection capabilities, which will ultimately help to optimize spectroscopic measurements and properly plan experiments.

Graphical relationships reveal that the peak value of the absorption spectrum is directly proportional to the absorption levels. The graphs are taken at a fixed concentration of the substance to be investigated in the sample, in this case it is moles for the sample placed in the cuvette. The effectiveness of using the TES

analytical method in wine classification lies in the fact that the types of molecules (such as polyphenols, vitamins, amino acids) and their quantity depend on the specific type and maturity of the wine, as well as on the wine technology.

As mentioned, the main objective was to explore the potential of fluorescence spectroscopy considering excitation/emission matrix (AEM) analysis with parallel factors (PARAFAC). In particular, we performed PCA analysis and light independent modeling of TES analogue classes according to wine product variety and origin. For this, we studied about 100 samples of four-five types of white Georgian wine. The methodology chosen by us was based on the one hand on the hardware complex, which was gradually modernized by our group, on the other hand on the development of new analytical approaches, which are quite acceptable to be used in typical laboratory control of food products and beverages. Using PCA analysis, we built tables and graphs for a specific group of samples.

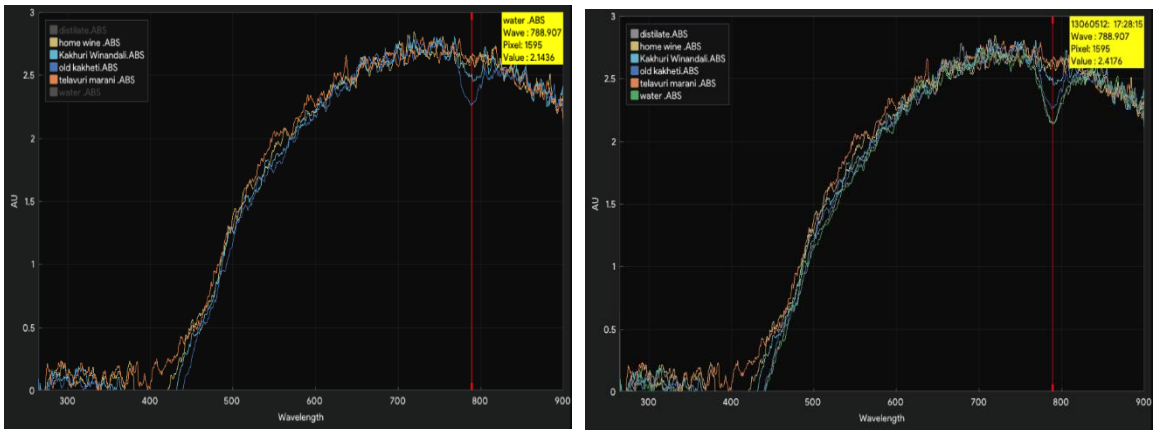

Figure 4. Absorption spectra of Georgian white wine (excitation wavelength 396 nm LED lamp)

In processing the wine spectrum, we used multivariate analysis techniques (PARAFAC) such as PCA (Principal Component Analysis) to highlight the main features of the data. We performed statistical analysis of the data to identify patterns or differences between different wine samples.

Our conclusions mainly concern the measuring device. These results refer to the CCD-detectors of the BlackCommet spectrometers manufactured by StellarNet, namely:

1. The spectra show a larger change in the average signal level at a given integration time, possibly due to thermal fluctuations between measurements. Therefore, the optimal level of thermal stabilization was selected for the spectrometer. As the measurements showed, to achieve thermal stabilization, the average signal level should be calculated with about 100 integrations in 180 milliseconds.
2. One of the main features of the spectrometer is the so-called "dark current" which averages about 0.25% of the peak value (~40,000 photons, with 100 integrations). These data were calculated in the combined spectrum of the deuterium and halogen light sources.
3. Data collected during various integrations show that until the integration time is increased to ~2000 msec, digital data acquisition of the signal continues. Further increasing the integration time leads to an approximately linear increase in the dark current.

Conclusion

The application of advanced optical spectroscopic techniques in the analytical control of bionanoagents has been comprehensively explored, with a specific focus on the identification and classification of Georgian white wines. The research has employed a multifaceted spectral analysis approach, culminating in the development of reference models for rapid identification of oenological products.

Key findings from the study reveal the effective detection of critical wine constituents such as flavonoids, tannins, alcohol, sugars, and acids, utilizing the ultraviolet and visible spectroscopy facilitated by deuterium lamps. The spectral data obtained indicates that flavonoids exhibit characteristic absorption in both UV (below 400 nm) and visible (400-700 nm) regions, while tannins, being polyphenolic in nature, absorb in the

wavenumber range of 1600-1800 cm^{-1}, as identified by infrared spectroscopy. The alcohol content, pivotal to wine quality, is distinctly marked at wavelengths 210 nm and 275 nm.

The utilization of deuterium lamps for UV spectroscopy has notably enhanced the accuracy of the analysis by minimizing water interference, a vital consideration when analyzing aqueous solutions such as wine. This strategic decision has underscored the necessity of tailoring spectroscopic methodologies to the unique characteristics of the sample in question.

The research reinforces the potential of fluorescence spectroscopy, coupled with parallel factor analysis (PARAFAC) and principal component analysis (PCA), to not only distinguish between different types of wine but also to identify fraudulent activities within the food industry. The methodologies and approaches developed in this study are poised to make a significant impact on ensuring the authenticity and quality of wine, thus contributing to the integrity of the food industry and consumer safety.

In the broader context, the findings underscore the need for ongoing development of analytical methods to meet the demands of contemporary technological and environmental research. The study lays a foundation for extending the application of these methods to the investigation of bionanoagents, potentially influencing various scientific and technical domains.

The spectroscopic analysis of wine samples has not only demonstrated the capability to detect and quantify specific molecular components that determine the organoleptic qualities of wine but also showcased the robustness of spectroscopic techniques as essential tools in the arsenal against food and beverage fraud. The study's methodologies pave the way for further research and the refinement of analytical techniques that can be used in quality control and product authentication, reinforcing the indispensable role of spectroscopy in the modern scientific landscape.

Scientific Ethics Declaration

The authors declare that the scientific ethical and legal responsibility of this article published in EPSTEM journal belongs to the authors.

Acknowledgements or Notes

* This article was presented as an oral presentation at the International Conference on Basic Sciences, Engineering and Technology (www.icbaset.net) held in Alanya/Turkey on May 02-05, 2024.

* This work was supported by the 2024 competition for targeted scientific research projects titled “spectroscopy from wine authentication to erythrocyte analysis” by Batumi Shota Rustaveli State University. The project manager of this project is prof. Nugzar gomidze

References

Airado-Rodríguez, D., Durán-Merás, I., Galeano-Díaz, T., & Wold, J. P. (2011). Front-face fluorescence spectroscopy: A new tool for control in the wine industry. *Journal of Food Composition and Analysis, 24*(2), 257-264.

Azcarate, S. M., & others. (2015). Modeling excitation–emission fluorescence matrices with pattern recognition algorithms for classification of Argentine white wines. *Food Chemistry, 184*, 214-219.

Murphy, K. R., Stedmon, C. A., Graeber, D., & Bro, R. (2013). Fluorescence spectroscopy and multi-way techniques. Parafac. *Analytical Methods, 5*, 6557-6566.

Smith, J., & Johnson, A. (2019). Fluorescence spectroscopy in wine quality control. *Journal of Wine Research, 30*(2), 123-135.

Tauler, R., Bejarano, A., & Walczak, B. (2015). Recent advances in multivariate curve resolution-alternating least squares (MCR-ALS): Methodology and applications. *Analytica Chimica Acta, 893*, 14-33.

Urbano, M., Luque de Castro, M. D., Pérez, P. M., García – Olmo, J., & Gómez – Nieva, M. A. (2006). Ultraviolet – visible spectroscopy and pattern recognition methods for differentiation and classification of wines. *Food Chemistry, 97*(1), 166-175.

Wold, S. (1976). Pattern recognition by means of disjoint principal components models. *Pattern Recognition, 8,* 127-139.

Khajishvili, M., Shainidze, J., Makharadze, K., & Gomidze, N. (2023a). On the development of the fluorescence excitation-emission etalon matrix algorithm of wine. *The Eurasia Proceedings of Science, Technology, Engineering & Mathematics (EPSTEM)*, *23*, 93-99.

Khajishvili, M., Gomidze, N., Jabnidze, I., Makharadze, K., Kalandadze, L., & Nakashidze, O. (2023b). Creation 3D fluorescence spectra of wine. *Book of Abstracts JAPMED*, *12*, 100-102.

Author Information

Nugzar Gomidze
Batumi Shota Rustaveli State University
35/32, Ninoshvili/Rustaveli str., 6010, Batumi, Georgia

Miranda Khajishvili
Batumi Shota Rustaveli State University
35/32, Ninoshvili/Rustaveli str., 6010, Batumi, Georgia
Contact e-mail: *mirandukht@gmail.com*

Madlena Davitadze
Batumi State Maritime Academy
Rustaveli Av. 53, 6010, Batumi, Georgia

Kakha Makharadze
Batumi Shota Rustaveli State University
35/32, Ninoshvili/Rustaveli str., 6010, Batumi, Georgia

To cite this article:

Gomidze, N., Khajishvili, M., Davitadze, M., & Makharadze, K. (2024). Innovative optical methods for analytical monitoring of bionanoagents with emphasis on Georgian white wine authentication. *The Eurasia Proceedings of Science, Technology, Engineering & Mathematics (EPSTEM), 28,* 201-208.

The Eurasia Proceedings of Science, Technology, Engineering & Mathematics (EPSTEM)
ISSN: 2602-3199

The Eurasia Proceedings of Science, Technology, Engineering & Mathematics (EPSTEM), 2023

Volume 28, Pages 209-215

ICBASET 2024: International Conference on Basic Sciences, Engineering and Technology

Development of a New System for Precise Measurement of the Weight of Valuable Liquid Metals with Ladle Cranes

Engin Tekin
KM Kumsan Crane System Company

Hasan Oktem
University of Kocaeli

Aydogan Akca
KM Kumsan Crane System Company

Abstract: Precise measurement of liquid minerals (chrome, brass and iron) under high temperature values during transportation with a ladle crane is a very important and critical process for semi-finished product production. In this study, the technological integration and optimization of liquid mines in a ladle crane design is examined and focused on examining the design principles, mechanism and engineering approaches that need to be developed. Also, high precision weighing can be made by means of the load cell technology. In the design step, material selection, integration and mechanical structure optimization are discussed. It has been determined that the design of the ladle crane will adapt to environmental effects and operational requirements. A series of tests were performed to evaluate the weight measurement performance of the ladle crane. As a result, the principles of precision weight measuring ladle crane design, engineering approaches and test results revealed that the developed system is very effective and reliable.

Keywords: Ladle crane, Precision weight measurement, Design and manufacturing

Introduction

In contemporary industrial applications, particularly those involving the handling of precious molten metals that require precise weighing and processing under high-temperature conditions, the operations of transportation play a crucial role in terms of efficiency, safety, and precision (Stein, 1964). During the execution of such operations, fundamental features such as high transport capacity, the ability to operate under high-temperature conditions, and precise weighing capabilities emerge as critical factors influencing the successful implementation of industrial processes (Bertodo, 1959). In this context, modern engineering approaches and technologies enable the development of ladle crane systems tailored to the type of molten metals to be processed and operational requirements (Ye et al., 2023). Industrial operations are becoming increasingly complex (Hofstotter, 1982), and the handling and processing of molten metals that require precise measurement are among the most intensive areas where industrial operations are applied (Meyer, 1973). It is precisely at this point that the importance of ladle crane design comes to the forefront. The high transport capacity and advancements in ladle crane design have been observed to enable the safer and more effective execution of such challenging operations, thanks to their technical specifications (Oi, 1986).

The design of a ladle crane should encompass not only the ability to transport the ladle but also features such as the ability to operate under high temperatures, precise weighing capability, and remote control (Wu et al., 1981; (Dorsey, 1964; Qiong et al., 2007). The ability of the ladle crane to operate under high temperatures provides operational flexibility in industrial environments where molten metals are processed at high temperatures (Stano

et al., 2020). This, in turn, serves a critical function in enhancing both efficiency and ensuring operator safety (Bagaria & Sharpe, 1974). Precise weighing capability emphasizes the ladle crane's ability to accurately measure and process molten metals (Hoffmann, 1979). Load cell technology enhances operational accuracy by offering high-precision weighing capabilities (Hoffmann, 2012). This, in turn, ensures cost savings in industrial processes while guaranteeing the accurate processing of molten metals (Lindorf, 1968).

On the other hand, the feature of remote control used in ladle crane design enables operators to safely control the crane (Mandai et al., 1990). This enhances operational flexibility and keeps operators away from hazardous conditions. This study also includes experimental work to objectively evaluate the performance of the designed ladle crane system (Zhang et al., 2022). These experimental studies are based on measuring the very small analog signals from the Wheatstone bridge circuit outputs of load cells to measure their accuracy when loaded and unloaded (Takezawa et al., 2010). With four load cells placed on the lifting group frames, the ladle is accurately weighed in both the lowest and highest hook positions independently of rope angles and friction losses between the rope and the pulley (Hu et al., 2023). The integration of modern engineering principles and technologies contributes to the industrial operations through ladle crane systems (Gee, 1984).

This study focuses on emphasizing the importance of ladle crane design in industrial applications and innovative solutions developed to meet specific requirements. To achieve this, the study ensures a safe working environment for operators by keeping them away from the work area while carrying out the process of transporting valuable molten metals. Subsequently, potential losses of precious molten metals during the operation are eliminated by positioning four load cells in appropriate locations.

Experimental Study

In this section, two separate test methods were used to measure the electrical signals produced under variable loads by the load cells that enable precise weighing of heavy metal-carrying ladle cranes. The signal generation behavior of the load cell in the vertical direction is called Experiment-1, and the signal behavior of the load cell in the horizontal direction in addition to the loads in the vertical direction has been called Experiment-2. In this study, an experimental setup was established using a 200 ton press, multi-meter, adjustable power supply, wireless weighing indicator and load cell. In this experimental setup, variable loads were applied to the load cell with a 200 ton press, and the amount of these applied loads was made readable on the screen with the weighing indicator. After applying the desired amount of load, the electrical signals produced by the load cell were measured with the help of a multi-meter and the data has been recorded.

Load Cell Technical Specifications

In the experiments carried out throughout the study, the "HSC-40t-V C3" model of the brand named "ESİT" has been used. The loadcell used in the experiments is fed by an adjustable power supply. The position and label information of the load cell were shown in Figure 1. Additionally, the technical specifications of this load cell are given in Table 1.

Figure 1. Loadcell model data

Table 1. Load cell technical specifications

Maximum capacity (Emax)	**kg**	**40000**
Minimum measuring range (Vmin)		Emax/6750
Total error	%	≤±0.05 ≤ ±0.02 ≤±0.015
Return to zero error (DR)	%Emax	0.0039 0.0030
Overloading capacity	%Emax	150
Extreme side loading capacity	%Emax	100
Breaking capacity	%Emax	300
Stretch (Emaxyukte)	mm	≤ 0.3
Maximum excitation voltage (Umax)	V	15
Earning (Cn)	mV/V	2 ±0.1%
No-load output	%Cn	≤±1.0
Input resistance	Ω	385 ±20
Output resistance	Ω	351 ±3
Insulation resistance	MΩ	≥500
Corrected operating temperature range	°C	-10...+40
Operating temperature range	°C	-40...+80

The Behavior of Load cell Signal in Vertical Direction

While the ladle crane carries out the transportation operations of precious molten metals, it also performs this process with precise weighing and ensures operational accuracy. A load cell experimental setup has been established to ensure that the weighing process was carried out precisely and accurately. In this experimental setup, the vertical signal generation behavior of the load cell was examined under the title Experiment-1. This experimental setup is shown in Figure 2 and then the experiments have been carried out. The purpose of this experiment is to monitor the electrical signal behavior produced by the load cell against vertical loads and to determine how sensitive and stable a signal it produces by evaluating the results. First, the load cell has been connected to an adjustable power supply and the supply voltage was set to 4.5 V. Then, a number of loads were applied to the load cell in the vertical direction using a 200-ton press, not exceeding the capacity of the loadcell. When each load was applied, the amount of the applied load has been displayed with the wireless weighing indicator. When the desired load amount has been reached, the value of the electrical signal produced by the load cell in mV was measured with a multi-meter.

Figure 2. Experimental system for load measurement of molten metal transport ladle

The Behavior of Load Cell in the Horizontal Direction in Addition to Vertical Loads

In Experiment-1, the electrical signal output values produced by the load cell against vertical loads were observed in mV. In this study, the signal behavior of the load cell in the horizontal direction, in addition to the

vertical loads, was examined under the title Experiment-2. In Experiment-2, in addition to the vertical loads applied to the load cell, a horizontal load was also applied simultaneously, as seen in Figure 3. Under these conditions, the signal stability produced by the load cell was examined. For Experiment-2, in addition to the mechanism used in Experiment-1, a hydraulic press with a manometer attached to the end was added to apply horizontal load. With this added hydraulic press, a horizontal load was applied to the load cell. In this experiment, first the adjustable power supply was connected to the load cell and the supply voltage was set to 4.5 V. Since the supply voltage was kept the same in both experiments, a more accurate comparison was made and the differences were seen more clearly. Then, loads were applied simultaneously in vertical and horizontal directions, and the amount of load applied in the vertical direction was displayed on the wireless weighing indicator, while the loads in the horizontal direction has been displayed via the manometer in the hydraulic press. After the required tests were performed, it has been seen and confirmed that the 25 bar value on the manometer corresponded to approximately 1 ton. Thus, the amount of load applied in the horizontal direction has been adjusted to the desired amount. Then, after applying the desired amount of load in horizontal and vertical directions, the electrical signal outputs produced by the load cell has been measured in mV with a multi-meter. Table 2 has been shown the signal outputs versus the load amounts obtained in the vertical direction.

Figure 3. The application of vertical and horizontal loading

Results and Discussion

In this section, all results regarding the signal output values obtained from the load tests performed on the load cell have been examined and evaluated. In Table 2, the output values of the electrical signal produced against the loads applied vertically to the load cell are given in mV.

Table 2. The mV values based on the vertical loading conditions

Vertical load (kg)	Signal output value (mV)
0	0
1054	0.3
2989	0.7
5038	1.1
10207	2.3
15085	3.4
20202	4.6
30000	6.8
40000	9.1

As seen in Table 2, variable loads were applied in the vertical direction, not exceeding the carrying capacity of the load cell. When we examined the electrical signal output values produced by the load cell against these loads, it has been seen that it did not produce a signal in the no-load state. Afterward, when a load of approximately 1 ton was applied vertically to the load cell, it has been observed that it produced a signal of 0.3 mV. Apart from 1 ton, the results in Table 2 have been obtained after applying a vertical load of approximately 3, 5, 10, 15, 20, 30, and 40 tons respectively with the press. Considering these results, it has been observed that

as the amount of applied load increases, the electrical signal output value produced by the load cell increases at the same rate. When the data obtained was evaluated, it was observed that the rate of increase of the signal output value was directly proportional to the amount of applied load. Table 3 contains the electrical signal output values produced by the load cell against the loads applied simultaneously in the horizontal direction while the load is applied to the load cell in the vertical direction.

Table 3. The mV values based on the vertical and horizontal loading conditions

Vertical load (t)	**Horizontal load (t)**	**Signal output value (mV)**
5.4	0	1.2
5.4	1	1.2
10.4	0	2.4
10.4	1	2.4
10.4	2	2.4
19.8	0	4.5
19.8	1	4.5
19.8	2	4.4
19.8	3	4.3
19.8	4	4.5
40	0	9.1
40	1	9.1
40	2	9.1
40	3	9.2
40	4	9.1
40	5	9.1
40	6	9.2
40	7	9.2
40	8	9.0

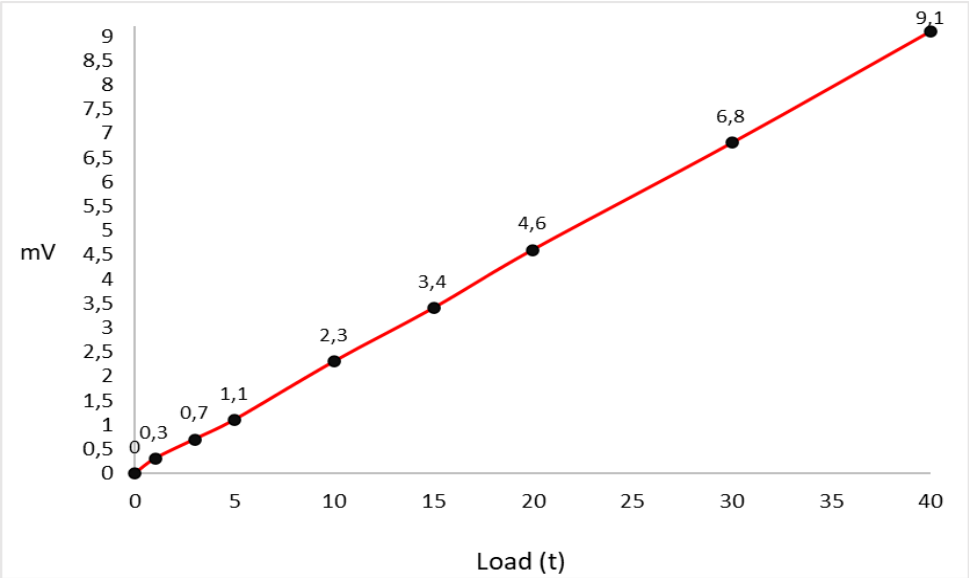

Figure 4. The signal production behavior of the load cell under load

As shown in Table 3, variable loads were applied to the load cell in both the vertical and horizontal directions without exceeding its carrying capacity. Initially, vertical loads were applied using a press without any horizontal load, and the signal output values in Table 3 were obtained. Subsequently, while applying vertical loads, horizontal loads were gradually applied using a hydraulic press, and the signals generated by the load cell were measured in millivolts (mV) using a multi-meter to obtain the signal output values in Table 3. When evaluating the obtained results, it was observed that the load cell maintained its signal stability even when subjected to variable horizontal loads while under a vertical load, and it was not affected by this condition.

As seen in Figure 4, a signal generation behavior chart of the load cell under load was created with the data obtained from the test results in Table 2 and Table 3. When we examine the graph in Figure 4, it is seen that the

mV curve increases linearly. It has been observed that the linear increase in the graph in Figure 4 is due to the direct proportion between the amount of load applied to the load cell and the electrical signal output values obtained using the multi-meter.

Conclusions

In this study, the signal output values produced by the load cell capable of precise weighing under variable loads applied in vertical and horizontal directions were examined with two different experimental methods. The conclusions reached in the light of the results and evaluations obtained from these experiments can be summarized as follows:

- Since the electrical signal output value produced by the load cell used in the experiments increases or decreases linearly, it has been shown that it can weigh with gram precision.
- While vertical load is applied to the load cell, it also prevents possible load losses as it maintains its signal stability despite being exposed to horizontal load.
- When we look at the results obtained from the experiments, this result creates a linear graph since there is a direct proportion between the load change rate applied to the load cell and the signal output value rate produced by the load cell. The linearity of the graph facilitates the conversion of the produced analog signals into digital signals. Thus, the tonnage data of the load cell used in the experiment was easily read.
- It can be seen from Experiment 1 and Experiment 2, it was observed that the load cell produced a signal with maximum accuracy when the load cell operated in the appropriate operating temperature range and was positioned on a fixed plane.
- As a result of the application of the load cell used on the crane and capable of precise weighing, this study increased the efficiency of the processing operations of precious molten metals and allowed accurate weighing.

Recommendations

In future trends, the weight of precious molten metals will be measured with sensitive load cells. In this way, gram-accurate weighing will be possible by preventing load losses that may occur during the weighing of precious molten metals.

Acknowledgements or Notes

* This article was presented as an oral presentation at the International Conference on Basic Sciences, Engineering and Technology (www.icbaset.net) held in Alanya/Turkey on May 02-05, 2024.

* The authors would like thanks to KM Kumsan Crane System Company in Kocaeli / Türkiye.

References

Bagaria, W.J., & Sharpe, W.M. (1974). *Temperature and rise-time effects on dynamic strain measurements*. New York, NY: American Institute of Aeronautics and Astronautics.

Bertodo, R. (1959). Development of high-temperature strain gauges. *Proceedings of the Institution of Mechanical Engineers, 173,* 605-616.

Dorsey, J. (1964). *Semiconductor strain gage handbook*. Waltham, USA: BLH Electronics.

Gee, S. (1984). *A strain gauge manual aeronautical research labs Melbourne* [PDF]. Melbourne, Australia: Aeronautical Research Laboratories. Retrieved from https://apps.dtic.mil/sti/tr/pdf/ADA151802.pdf

Hoffmann, K. (1979). *Practical hints for the application of strain gauges*. Germany:Hottinger Baldwin Messtechnik GmbH, Darmstadt.

Hoffmann, K. (2012). *An introduction to stress analysis and transducer design using strain gauges*. Germany.

Hofstotter, P. (1982). Calibration of high-temperature strain gages with the aid of a clamping device. *Experimental Mechanics, 22,* 223-225.

Hu, Z., Wang, E., Jia, F., & Dong, M. (2023). Experimental study on effect of additional torsional load on bending fatigue behavior and failure mechanism of steel wire rope. *International Journal of Fatigue, 167,* 1-13.

Lindorf, H. (1968). *Technische temperaturmessungen* (3rd ed.). Essen, Germany: Verlag W. Girardet.

Mandai, K., Miyauchi, K., & Sugimoto, M. (1990). An advanced infrared remote control sensor. *IEEE Transactions on Consumer Electronics, 36*(3), 669-677.

Meyer, M.L. (1973). On the measurement of transverse sensitivity of strain gauges. *Strain, 9*(1), 26-28.

Oi, K. (1986). Transient response of bonded strain gages: Elastic step wave produced in a steel bar is used by the author to study the transient- response characteristics of bonded strain gages. *Experimental Mechanics,6,* 463-469.

Qiong, L., Haifeng, X., & Xiande, L. (2007). Analysis of communication protocol in the infrared controlsystem of intelligent home. *Control and Automation, 23*(1.1), 28-30.

Stano, G., Nisio, A.D., Lanzolla, A., & Percoco, G. (2020). Additive manufacturing and characterization of a load cell with embedded strain gauge. *Precision Engineering, 62,* 113-120.

Stein, P.K. (1964). Measurement engineering. In *Gage length effects* (2nd ed.). Phoenix AZ, USA.

Takezawa, A., Nishiwaki, S., Kitamura, M., & Silva, E.C.N. (2010). Topology optimization for designing strain-gauge load cells. *Structural and Multidisciplinary Optimization, 42,* 387-402.

Wu, T., Ma, L., & Zhao, L. (1981). Development of temperature-compensated resistance strain gages for use to 700°C. *Experiment Mechanics,* 117-123.

Ye, H., Li, W., Zhang, H., Lin, S., Zhang, D., Ge, Y., & Li, Z. (2023). Experimental evaluation of dimension-stable synthetic fibre rope under investigation of spooling test on the multilayer winch drum. *Ocean Engineering, 279,* 1-13.

Zhang, Q., Peng, Y., Zhu, Z., Chang, X., Lu, H., Zhou, Z., Cao, G., Tang, W., & Chen, G. (2022). Influence of longitudinal vibration on the friction and wear characteristics of multi-layer winding hoisting wire rope. *Wear, 492,* 1-17.

Author Information

Engin Tekin
KM Kumsan Crane System Company
İMES OSB-Dilovası/Kocaeli, Türkiye

Hasan Oktem
Kocaeli University
Hereke Asım Kocabıyık Vocational
Polymer Science and Technology
Natural Sciences Institute/Umuttepe Campus, Türkiye
Contact e-mail: *hoktem@kocaeli.edu.tr*

Aydogan Akca
KM Kumsan Crane System Company
İMES OSB-Dilovası/Kocaeli, Türkiye

To cite this article:

Tekin. E., Oktem, H. & Akca, A. (2024). Development of a new system for precise measurement of the weight of valuable liquid metals with ladle cranes. *The Eurasia Proceedings of Science, Technology, Engineering & Mathematics (EPSTEM), 28,* 209-215.

The Eurasia Proceedings of Science, Technology, Engineering & Mathematics (EPSTEM)
ISSN: 2602-3199

The Eurasia Proceedings of Science, Technology, Engineering & Mathematics (EPSTEM), 2024

Volume 28, Pages 216-223

ICBASET 2024: International Conference on Basic Sciences, Engineering and Technology

Application of the New General Integral Transform for Newton's Law of Cooling

Haldun Alpaslan Peker
Selcuk University

Esma Uysal
Selcuk University

Abstract: Integral transformations are versatile mathematical techniques that are applicable in a wide range of applications in various fields in mathematics, engineering and applied sciences. Using integral transformations, complicated functions can be transformed into more simpler functions to be analyzed and to be solved. Integral transform methods have been extensively used to solve differential equation theories and numerical calculation. Newton's law of cooling is the fundamental law that describes the rate of heat transfer by a body to its surrounding through radiation. This important law can be modelled in the form of differential equation, which is solved by many researchers by using different methods. Some researchers used integral transforms to solve this equation. In this study, we use an integral transform, providing a more flexible and powerful approach for solving differential equations, called as "New General Integral Transform" as a generalization of the Laplace transform method and some applications are given to demonstrate the effectiveness of this transform.

Keywords: Newton's law of cooling, Differential equation, The new general integral transform

Introduction

Although he is best known for his laws of motion and universal gravitation, Newton's discovery of heat transfer laid the foundation for modern thermodynamics. His recognition of the relationship between temperature differences and heat flow ushered in a new era in scientific research, paving the way for a deeper understanding of energy dynamics.

Newton's law of cooling is a physical law that describes the rate of heat loss of an object to its surroundings. It states that the rate of heat loss is directly proportional to the temperature difference between the object and its surroundings. Newton's law of cooling is a special case of Stefan-Boltzmann's Law for small temperature differences (Jiji, 2009; Winterton, 1999; Baehr & Stephan, 2011). The accurate solution of Newton's law of cooling is crucial in various scientific and engineering applications, such as in the design of cooling systems, thermal management in electronics, and climate modeling. This important law can be modelled in the form of differential equation, which is solved by many researchers by using different methods. Some researchers used integral transforms to solve this equation. In this study, we use an integral transform, providing a more flexible and powerful approach to solving differential equations, called as "New General Integral Transform" which was defined by Jafari as a generalization of the Laplace transform method (Jafari, 2021).

Integral transforms are powerful mathematical tools used in the analysis and solution of differential equations. By transforming a differential equation into a different domain, such as the frequency domain or the Laplace domain, integral transforms simplify the problem-solving process and provide new insights into the dynamics of the system (Debnath & Bhatta, 2007).

- Selection and peer-review under responsibility of the Organizing Committee of the Conference

Newton's Law of Cooling

Newton's law of cooling, which has a very important position in physics, is also modeled by differential equations. This law explains how the temperature change in an object occurs depending on the difference between the temperature of the object and the temperature of the environment in which the object is located. Newton's law of cooling states that a hot body releases heat energy into its environment (Jiji, 2009; Winterton, 1999; Baehr & Stephan, 2011). The amount of this energy emitted depends on the temperature difference between the object placed in the environment and the environment. While this energy transfer is taking place, as the temperature difference decreases, the energy transfer decreases and eventually the hot body equalizes with the ambient temperature (Jiji, 2009; Winterton, 1999; Baehr & Stephan, 2011). Newton's law of cooling is generally modeled by the linear ordinary differential equation (Jiji, 2009)

$$\frac{dT(t)}{dt} = -C(T(t) - T_e) \tag{1}$$

with the initial condition

$$T(t_0) = T_0$$

where T is the temperature of the substance, T_e is the constant temperature of the environment, T_0 is the initial temperature of the substance at time t_0 and C is the proportionality constant, known as convective heat transfer coefficient.

This seemingly modest equation reveals the complex interplay between thermal gradients and heat exchange, providing invaluable insight into countless real-world scenarios from cooling a freshly brewed cup of coffee to regulating spacecraft temperatures in outer space. Newton's law of cooling provides a versatile framework for analyzing and predicting thermal behavior.

Method

A New General Integral Transform

In this part, a new general integral transform which comprises most of the integral transform in the family of Laplace transform.

Definition 1. (Jafari, 2021) Let $f(t)$ be an integrable function defined for $t \geq 0$, $p(s)$ and $q(s)$ be positive real functions. Then, the new general integral transform $\mathcal{T}(s)$ of $f(t)$ is defined as follows,

$$T\{f(t);s\} = \mathcal{T}(s) = p(s)\int_0^\infty f(t)e^{-q(s)t}dt,$$

provided the integral exists for some $q(s)$. It is essential to note that this transform for those $f(t)$ is not continuously differentiable contains terms with negative or fractional powers of $q(s)$.

Theorem 1 (Existence Theorem). (Jafari, 2021) If $f(t)$ is defined and piecewise continuous on every finite interval on the semi-axis $t \geq 0$ and is of exponential order *k*, that is $|f(t)| \leq M e^{kt}$ for some positive real number *M* and *k*, then $\mathcal{T}(s)$ exists for all $q(s) > k$.

Proof: Since $f(t)$ is piecewise continuous, $e^{-st}f(t)$ is integrable over any finite interval on the *t*-axis. Assume that $q(s) > k$. Then, the proof of the existence of the $\mathcal{T}(s)$ is obtained as follows:

$$\left\|\mathcal{T}(s)\right\| = \left\|T\{f(t);s\}\right\| = \left|p(s)\int_0^\infty f(t)e^{-q(s)t}dt\right| \le p(s)\int_0^\infty Me^{kt}e^{-q(s)t}dt = \frac{M\,p(s)}{q(s)-k}.$$

In Table1, one can find the transformation of some fundamental functions.

Table 1. The new general integral transform of some fundamental functions

$f(t)$	$\mathcal{T}(s)$
1	$\frac{p(s)}{q(s)}$
t	$\frac{p(s)}{(q(s))^2}$
$t^\alpha,\ \alpha>0$	$\frac{\Gamma(\alpha+1)\,p(s)}{(q(s))^{\alpha+1}},\ \alpha>0$
$e^{\alpha t}$	$\frac{p(s)}{q(s)-\alpha},\quad q(s)>\alpha$
$\sin(ct)$	$\frac{c\,p(s)}{c^2+(q(s))^2}$
$\cos(ct)$	$\frac{p(s)\,q(s)}{c^2+(q(s))^2}$

Theorem 2 (Transform of Derivatives). (Jafari, 2021) Let $f(t)$ be differentiable and $p(s)$ and $q(s)$ be positive real functions. Then,

1. $T\{f'(t);s\} = q(s)\ T\{f(t);s\} - p(s)f(0)$
2. $T\{f''(t);s\} = q^2(s)\ T\{f(t);s\} - q(s)p(s)f(0) - p(s)f'(0)$
3. $T\left\{f^{(n)}(t);s\right\} = q^n(s)\ T\{f(t);s\} - p(s)\sum_{k=0}^{n-1} q^{n-1-k}(s)f^{(k)}(0)$

Application to Newton's Law of Cooling

In this section, the new general integral transform will be applied to Newton's law of cooling equation. Firstly, taking the transform of the equation (1), we obtain

$$\mathcal{T}\left[\frac{dT(t)}{dt}\right] = \mathcal{T}\left[-C(T(t)-T_e)\right] \tag{2}$$

Now, rearranging the equation (2) according to the theorem 2 and Table 1, and substituting the value in the initial condition into this equation, we obtain

$$q(s)T(s) - p(s)T_0 = -C\left[T(s) - T_e\frac{p(s)}{q(s)}\right] \tag{3}$$

where $\mathcal{T}(s) = \mathcal{T}\left[T(t)\right]$.

If we make the equation (3) suitable for applying the inverse transform, we get

$$\mathcal{T}(s) = T_0 \frac{p(s)}{q(s)+c} + cT_e \frac{p(s)}{q(s)[q(s)+c]} \tag{4}$$

Finally, applying the inverse transform to the equation (4) using Table 1, we find the solution of Newton's law of cooling equation as

$$T(t) = T_e + (T_0 - T_e)e^{-ct}.$$

We will examine the effectiveness of this method through some numerical applications and compare the results with those found with other methods in the literature.

Application 1. (Patil et al., 2022c) A hot milk with initial temperature $115°\ C$ is kept in an environment with temperature $35°\ C$. The rate of temperature change is $20°\ C$ per/min, how long will it take for this milk to cool down to temperature $40°\ C$?

Assuming that milk obeys Newton's law of cooling, we arrange the equation (1) according to the values given in the question as

$$\frac{dT(t)}{dt} = -C(T-35)$$

with the initial conditions

$$T(0) = 115, \quad T'(0) = -20$$

First, using the initial conditions in the above equation, we get the value of C as

$$-20 = -C(115-35)$$
$$C = 0.25$$

Substituting this C value into the above equation, we get

$$\frac{dT(t)}{dt} = -0.25(T-35)$$

Now, applying the transform to both sides of the above equation, we obtain

$$\mathcal{T}\left[\frac{dT(t)}{dt}\right] = -0.25\mathcal{T}[T-35]$$

Rearranging the last equation according to the theorem 2 and Table 1, we get

$$q(s)T(s) - 115p(s) = -0.25\left[T(s) - 35\frac{p(s)}{q(s)}\right]$$

Rearranging this equation, we get

$$\mathcal{T}(s) = 115\frac{p(s)}{q(s)+0.25} + (0.25)(35)\frac{p(s)}{q(s)[q(s)+0.25]}$$

and finally, applying the inverse transform to this equation, we obtain the solution as

$$T(t) = 80e^{-0.25t} + 35$$

We can find out how long it will take for the milk to cool down to $40°\ C$ based on our solution as

$$40 = 35 + 80e^{-0.25t}$$
$$80e^{-0.25t} = 5$$
$$e^{0.25t} = 16$$
$$0.25t = \ln 16$$
$$t = 11.090354889$$

This result is in good agreement with the results obtained by other methods (Peker et al., 2024; Patil et al.,2022a, 2022b, 2022c).

Application 2. (Patil et al., 2022c) The heated iron with an initial temperature of $50°\ C$ is kept in an environment with temperature of $27°\ C$. Since the rate of temperature change is $3°\ C$ per/min, how long will it take for this iron to cool down to temperature $36°\ C$?

Assuming that iron obeys Newton's law of cooling, we arrange the equation (1) according to the values given in the question as

$$\frac{dT(t)}{dt} = -C(T - 27)$$

with the initial conditions

$$T(0) = 50, \quad T'(0) = -3$$

First, using the initial conditions expressed above, we find the value of C as

$$-3 = -C(50 - 27)$$
$$C = 0.13$$

Substituting this C value, we get

$$\frac{dT(t)}{dt} = -0.13(T - 27)$$

Now, applying the transform to both sides of the above equation, we obtain

$$\mathcal{T}\left[\frac{dT(t)}{dt}\right] = -0.13\mathcal{T}\left[T - 27\right]$$

Rearranging the last equation according to the theorem 2 and Table 1, we get

$$q(s)T(s) - 50p(s) = -0.13\left[T(s) - 27\frac{p(s)}{q(s)}\right]$$

Rearranging this equation, we get

$$\mathcal{T}(s) = 50\frac{p(s)}{q(s) + 0.13} + (0.13)(27)\frac{p(s)}{q(s)[q(s) + 0.13]}$$

Finally, applying the inverse transform to this equation, we find the solution as

$$T(t) = 23e^{-0.13t} + 27$$

Now we can find out how long it will take for the milk to cool down to $36°\ C$ using our solution as follows:

$$36 = 27 + 23e^{-0.13t}$$
$$23e^{-0.13t} = 9$$
$$e^{0.13t} = \frac{23}{9}$$
$$0.13t = \ln\left(\frac{23}{9}\right)$$
$$t = 7.2175$$

This result coincides with the ones found by other methods (Peker et al., 2024; Patil et al.,2022a, 2022b, 2022c).

Application 3. (Naresh, 2017) While the ambient temperature is $20°\ C$, the temperature of the water drops from $100°\ C$ to $80°\ C$ in 20 minutes. What will be the temperature after 30 minutes and how long will it take for this water to cool to $45°\ C$?

Assuming that water obeys Newton's law of cooling, we arrange the equation (1) according to the values given in the question as

$$\frac{dT(t)}{dt} = -C(T - 20)$$

with the initial conditions

$$T(0) = 100, \quad T(20) = 80$$

First, applying the transform to both sides of the above equation, we obtain

$$\mathcal{T}\left[\frac{dT(t)}{dt}\right] = -C\mathcal{T}\left[T - 20\right]$$

Rearranging the last equation according to the theorem 2 and Table 1, we get

$$q(s)T(s) - 100\,p(s) = -C\left[T(s) - 20\frac{p(s)}{q(s)}\right]$$

Rearranging this equation, we get

$$\mathcal{T}(s) = 100\frac{p(s)}{q(s) + C} + (C)(20)\frac{p(s)}{q(s)[q(s) + C]}$$

Finally, applying the inverse transform to this equation, we find the solution equation as

$$T(t) = 80e^{-Ct} + 20$$

Now let's find the value of C. If we use $T(20) = 80°$ in the last equation, we obtain

$$80 = 20 + 80e^{-20C}$$
$$e^{-c} = \left(\frac{3}{4}\right)^{\frac{1}{20}}$$

Using this result to find $T(30)$, we obtain

$$T(30) = 20 + 80e^{-30c}$$

$$T(30) = 20 + 80\left(\frac{3}{4}\right)^{\frac{3}{2}} = 71.96°C$$

Now we can find out how long it will take for the water to cool down to $45°\ C$ using the solution as follows:

$$45 = 20 + 80(e^{-C})^{t}$$

$$\left(\frac{3}{4}\right)^{\frac{t}{20}} = \frac{25}{80}$$

$$t = 80.8636283723$$

This result is in good agreement with the results obtained by other methods (Naresh, 2017; Peker et al., 2024).

Conclusion

In conclusion, the accurate solution of Newton's law of cooling is essential for understanding heat transfer phenomena and optimizing engineering applications. By introducing the new integral transform method for solving differential equations, researchers can enhance the efficiency and accuracy of solving Newton's law of cooling. By leveraging the unique properties of integral transforms and the innovative approach of the new integral transform method, scientists and engineers can gain deeper insights into the dynamics of heat transfer processes and improve the performance of cooling systems. The application of the new integral transform method represents a significant advancement in the field of mathematical analysis and holds promise for revolutionizing the solution of complex differential equations in various scientific and engineering disciplines.

Recommendation

This new integral transform can be applied to different models appearing in other applied sciences so that revealing the efficiency of this transform.

Scientific Ethics Declaration

The authors declare that the scientific ethical and legal responsibility of this article published in EPSTEM journal belongs to the authors.

Acknowledgement

* This article was presented as an oral presentation at the International Conference on Basic Sciences, Engineering and Technology (www.icbaset.net) held in Alanya/Turkey on May 02-05, 2024.

References

Baehr, H. D., Stephan, K., Baehr, H. D., & Stephan, K. (2011). Convective heat and mass transfer single phase flow. In *Heat and mass transfer* (pp.275-441). Springer.

Debnath, L., & Bhatta, D. (2016). *Integral transforms and their applications*. Chapman and Hall/CRC.

Jafari, H. (2021). A new general integral transform for solving integral equations. *Journal of Advanced Research*, *32*,133-138.

Jiji, L. M. (2009). *Heat conduction*. Berlin: Springer-Verlag.

Naresh, P. (2017). Newton's law of cooling-laplace transform. *Journal of Global Research in Mathematical Archives*, *4*(12), 28-34.

Patil, D. P., Gangurde, J.P., Wagh, S. N., & Bachhav, T. P. (2022a). Applications of the HY transform for Newton's law of cooling. *International Journal of Research and Analytical Reviews (IJRAR)*, *9*(2), 740-745.

Patil, D. P., Patil, S. A., & Patil, K. J. (2022b). Newton's law of cooling by "Emad–Falih transform", *International Journal of Advances in Engineering and Management (IJAEM)*, *4*(6), 1515-1519.

Patil, D. P., Shirsath, D. S., & Gangurde, V. S. (2022c). Application of Soham transform in Newtons law of cooling. *International Journal of Research in Engineering and Science (IJRES)*, *10*(6), 1299-1303.

Peker, B., Cuha, F. A., & Peker, H. A. (2024). Analytical solution of Newton's law of cooling equation via Kashuri Fundo transform. *Necmettin Erbakan University Journal of Science and Engineering*, *6*(1), 10-20.

Winterton, R. H. S. (1999). Newton's law of cooling. *Contemporary Physics*, *40*(3), 205–212.

Author Information

Haldun Alpaslan Peker
Selcuk University
Faculty of Science
Department of Mathematics
Campus, Konya, Türkiye
Contact e-mail: *pekera@gmail.com*

Esma Uysal
Selcuk University
Graduate School of Natural and Applied Sciences
Campus, Konya, Türkiye

To cite this article:

Peker, H. A., & Uysal, E. (2024). Application of the new general integral transform for Newton's law of cooling. *The Eurasia Proceedings of Science, Technology, Engineering & Mathematics (EPSTEM), 28,* 216-223.

The Eurasia Proceedings of Science, Technology, Engineering & Mathematics (EPSTEM)
ISSN: 2602-3199

The Eurasia Proceedings of Science, Technology, Engineering & Mathematics (EPSTEM), 2024

Volume 28, Pages 224-233

ICBASET 2024: International Conference on Basic Sciences, Engineering and Technology

On Mersenne Power GCD Matrices

Yahia Awad
Lebanese International University

Ragheb Mghames
Lebanese International University

Karim Amin
Lebanese International University
Modern University for Business and Science

Abstract: This paper explores the $n \times n$ Mersenne power GCD matrices defined on sets of positive integers, focusing on factor-closed and gcd-closed sets. By employing the form $f(t_i, t_j) = 2^{(t_i, t_j)} - 1$, we investigate the r^{th} power Mersenne GCD matrix (M^r) and provide comprehensive insights into its factorizations, determinants, reciprocals, and inverses. Building upon previous research, particularly Chun's work on power GCD matrices, we extend the analysis to Mersenne numbers, offering a thorough understanding of their properties. The study contributes to the broader understanding of arithmetic functions and their applications in matrix theory.

Keywords: Power GCD Matrix, Factor-closed sets, GCD-closed sets, Mersenne numbers.

Introduction and Preliminaries

Let $T = \{t_1, t_2, \ldots, t_n\}$ be a well-ordered set of n distinct positive integers with $t_1 < t_2 < \ldots < t_n$. The power GCD matrix on T is also $n \times n$ square matrix such that $(T^r)_{ij} = (t_i, t_j)^r$, where where (t_i, t_j) is the greatest common divisor of t_i and t_j and r is any real number. Set T is said to be factor-closed if $t_k \in T$ for any divisor t_k of $t_i \in T$, and is gcd-closed if $(t_i, t_j) \in T$, for every t_i and $t_j$in T.

In his work published in Smith(1875,1876) demonstrated that for a factor-closed set $T = \{t_1, t_2, \ldots, t_n\}$ of distinct positive integers, the determinant $det(T) = \varphi(t_1)\varphi(t_2)\ldots\varphi(t_n)$ (Smith, 1876). Subsequent to Smith's findings, numerous studies have contributed to the understanding of GCD and LCM matrices, including works by Beslin and Ligh (1989, 1991, 1992), ElKassar et al. (2009, 2010) and Awad et al. (2019, 2020, 2023), and others. In 1996, Chun introduced the concept of r^{th} power GCD matrices on both factor-closed and gcd-closed sets for any real number r (Chun, 1996). He determined their determinants, inverses, and reciprocals over the domain of natural numbers. Let f be an arithmetical function of the form $f(n) = \sum_{d|n} g(d)$. The matrix $[f(i,j)]_{n\times n}$ given by the value of f in greatest common divisor of (i,j), $f(i,j)$ as its i,j entry is called the greatest common divisor (GCD) matrix. In 2010, (Bege, 2010) considered the generalization of this matrix where the elements are in the form $f(i,(i,j))$ considered a generalization of the GCD matrices, where the elements are of the form $[f(i,j)]_{n\times n}$.

Inspired by the above works, we use the special form $f(t_i, t_j) = 2^{(t_i, t_j)} - 1$ in order to study the r^{th} power Mersenne GCD matrix (M^r) on the both cases for T as factor-closed and as gcd-closed set. In addition, we give a full description of its factorizations, determinants, reciprocals, and inverses.

Preliminaries

In the following, we consider $T = \{t_1, t_2, \ldots, t_n\}$ as an arbitrary set of distinct positive natural integers, and r is any real number.

Definition 1. The Mersenne r^{th} power GCD matrix (M^r) defined on T is the $n \times n$ square matrix whose ij^{th} entries are of the form

$$\left(m_{ij}\right)^r = \left(2^{\left(t_i, t_j\right)} - 1\right)^r.$$

Definition 2. The generalized Mersenne power function $g(t)$ on T is defined inductively for all $1 \leq i \leq n$ as

$$g(t_i) = \sum_{d \mid t_i} (2^n - 1)^r \, \mu(t_i/d).$$

Definition 3. The reciprocal of Mersenne power GCD matrix is the $n \times n$ matrix M^{-r} such that

$$(M^{-r})_{ij} = \frac{1}{\left(f_{ij}\right)^r} = \frac{1}{\left(2^{\left(t_i, t_j\right)} - 1\right)^r}.$$

Definition 4. The generalized reciprocal Mersenne power function on T is defined inductively for all $1 \leq i \leq n$ as

$$h(t) = \sum_{d \mid t_i} \left(\frac{1}{\left(2^d - 1\right)}\right)^r \mu(t_i/d).$$

Definition 5. The inverse of Mersenne power GCD matrix is the square $n \times n$ matrix $(M^r)^{-1}$ such that $(M^r)(M^r)^{-1} = I_n$.

Main Results

Mersenne Power GCD Matrices Defined on Arbitrary Sets

In the following, we study Mersenne power GCD matrices defined on arbitrary sets that are either factor-closed or not. A complete characterization is also given.

Structure Theorems

Theorem 1. Let $T = \{t_1, t_2, \ldots, t_n\}$ be a non factor-closed set of positive integers and $\overline{T} = \{y_1, y_2, \ldots, y_m\}$ be the factor-closed closure of T (the minimal factor-closed set containing T). Then, $(M^r) = EA_rE^T$, where E is the $n \times m$ incidence matrix of $\overline{T}$ on T, and A_r is the $m \times m$ diagonal matrix such that $a_{ii} = g(y_i)$.

Proof. Since E is an $n \times m$ incidence matrix of $\overline{T}$ on T, then $e_{ij} = 1$ if $y_j \mid t_i$ and 0 otherwise. Hence,

$$\begin{aligned}
(EA_rE^T)_{ij} &= \sum_{k=1}^{n} \left(e_{ik} a_{kk} e_{kj}\right) = \sum_{y_k \mid t_i \,, y_k \mid t_j} g\left(y_k\right) = \sum_{y_k \mid (t_i, t_j)} g\left(y_k\right) \\
&= \sum_{y_k \mid (t_i, t_j)} \sum_{d \mid y_k} (2^d - 1)^r \, \mu\left(\frac{y_k}{d}\right) = \sum_{d \mid y_k} \mu\left(\frac{y_k}{d}\right) \sum_{y_k \mid (t_i, t_j)} (2^d - 1)^r \\
&= \sum_{d \mid (t_i, t_j)} (2^d - 1)^r = \left(2^{\left(t_i, t_j\right)} - 1\right)^r.
\end{aligned}$$

Theorem 2. Let $T = \{t_1, t_2, \ldots, t_n\}$ be a non factor-closed set of positive integers, and $\overline{T} = \{y_1, y_2, \ldots, y_m\}$ be the factor-closed closure of T. Then, $(M^r) = A_r E^T$ where $a_{ij} = g(y_j)$ if $y_j \mid t_i$ and 0 otherwise, and E is the corresponding incidence matrix relative to A_r.

Proof. The ij^{th} entries of the incidence matrix E relative to A_r are defined as: $e_{ij} = 1$ if $a_{ij} \neq 0$ and 0 otherwise. So, the ij^{th} entry of $A_r E^T$ is

$$(A_r E^T)_{ij} = \sum_{k=1}^{n} (a_{ik} e_{kj}) = \sum_{y_k \mid t_i \,,\, y_k \mid t_j} g(y_k) = \sum_{y_k \mid (t_i, t_j)} g(y_k) = \left(2^{(t_i, t_j)} - 1\right)^r.$$

Theorem 3. Let $T = \{t_1, t_2, \ldots, t_n\}$ be a non factor-closed set of positive integers, and $\overline{T} = \{y_1, y_2, \ldots, y_m\}$ be the factor-closed closure of T. Then, $(M^r) = A_r A_r^T$ where $a_{ij} = \sqrt{g(y_j)}$ if $y_j \mid t_i$ and 0 otherwise.

Proof. The ij^{th} entry of $A_r A_r^T$ is defined as:

$$(A_r A_r^T)_{ij} = \sum_{k=1}^{n} (a_{ik} a_{kj}) = \sum_{\substack{y_k \mid t_i \\ y_k \mid t_j}} \sqrt{g(y_k)}\sqrt{g(y_k)} = \sum_{y_k \mid (t_i, t_j)} g(y_k) = \left(2^{(t_i, t_j)} - 1\right)^r.$$

Determinants

Theorem 4. Let $T = \{t_1, t_2, \ldots, t_n\}$ be a non factor-closed set of positive integers, and $\overline{T} = \{y_1, y_2, \ldots, y_m\}$ be the factor-closed closure of T with $n \leq m$. Let $E_{(k_1, k_2, \ldots, k_n)_r}$ be the submatrix consisting of the $k_1^{th}, k_2^{th}, \ldots, k_n^{th}$ columns of E for some indices k_i such that $1 \leq k_1 < \ldots < k_n \leq m$. Then,

$$\det(M^r) = \sum_{1 \leq k_1 < \ldots < k_n \leq m} \left(\left(\det E_{(k_1, k_2, \ldots, k_n)_r}\right)^2 \prod_{i=1}^{n} \left(\sum_{d \mid t_i} \left(2^d - 1\right)^r \mu\left(\frac{t_i}{d}\right) \right) \right).$$

Proof. Let $A_r = (a_{ij})_{m \times m}$ be defined as $a_{ij} = \sum_{d \mid t_i} \left(2^d - 1\right)^r \mu(t_i/d)$ if $y_j \mid t_i$ and 0 otherwise, and let $E = (e_{ij})$ be the corresponding incidence matrix relative to A_r. Since A_r is a triangular matrix with $a_{ii} = \sum_{d \mid t_i} \left(2^d - 1\right)^r \mu(t_i/d)$ for all $1 \leq i \leq m$, then the ij^{th} entry of A_r can be written as $a_{ij} = e_{ij} \sum_{d \mid t_i} \left(2^d - 1\right)^r \mu(t_i/d)$. Define, for some indices k_i such that $1 \leq k_1 < \ldots < k_n \leq m$, the matrices $A_{(k_1, k_2, \ldots, k_n)}$ and $E_{(k_1, k_2, \ldots, k_n)}$ to be the submatrices consisting of the $k_1^{th}, k_2^{th}, \ldots, k_n^{th}$ columns of A and E, respectively. Then, $A_{(k_1, k_2, \ldots, k_n)} = E_{(k_1, k_2, \ldots, k_n)} D_{A_r}$, where D_{A_r} is the $n \times n$ diagonal submatrix of A_r whose diagonal entries are $d_{ii} = \sum_{d \mid t_i} \left(2^d - 1\right)^r \mu(t_i/d)$. Therefore,

$$\det\left(A_{r_{(k_1, k_2, \ldots, k_n)}}\right) = \det\left(E_{(k_1, k_2, \ldots, k_n)}\right)\left(\prod_{i=1}^{n} d_{ii}\right).$$

Applying Cauchy-Binet formula, we obtain

$$\begin{aligned}
\det(M^r) &= \det(A_r E^T) \\
&= \sum_{1 \leq k_1 < k_2 < \ldots < k_n \leq m} \left(\det A_{r_{(k_1, k_2, \ldots, k_n)}}\right)\left(\det E_{(k_1, k_2, \ldots, k_n)}\right)^T \\
&= \sum_{1 \leq k_1 < \ldots < k_n \leq m} \det\left(E_{r_{(k_1, \ldots, k_n)}}\right) \sum_{d \mid t_i} \left(2^d - 1\right)^r \mu\left(\frac{t_i}{d}\right)\left(\det E_{r_{(k_1, \ldots, k_n)}}\right)^T \\
&= \sum_{1 \leq k_1 < k_2 < \ldots < k_n \leq m} \left(\sum_{d \mid t_i} \left(2^d - 1\right)^r \mu\left(\frac{t_i}{d}\right) \right)\left(\det E_{r_{(k_1, k_2, \ldots, k_n)}}\right)^2.
\end{aligned}$$

Example 1.: Consider the non factor-closed set $T = \{2,3,4\}$ and its factor closure $\overline{T} = \{1,2,3,4\}$. Then, the 2^{nd} power Mersenne GCD matrix defined on T is:

$$M^2 = \begin{bmatrix} 17^2 & 5^2 & 17^2 \\ 5^2 & 257^2 & 5^2 \\ 17^2 & 5^2 & 65537^2 \end{bmatrix} = \begin{bmatrix} 289 & 25 & 289 \\ 25 & 66049 & 25 \\ 289 & 25 & 4295098369 \end{bmatrix}$$

$$A_2 = \begin{bmatrix} g(1) & 0 & 0 & 0 \\ 0 & g(2) & 0 & 0 \\ 0 & 0 & g(3) & 0 \\ 0 & 0 & 0 & g(4) \end{bmatrix} = \begin{bmatrix} 25 & 0 & 0 & 0 \\ 0 & 264 & 0 & 0 \\ 0 & 0 & 66024 & 0 \\ 0 & 0 & 0 & 4295098080 \end{bmatrix}$$

$$E = \begin{bmatrix} 1 & 1 & 0 & 0 \\ 1 & 0 & 1 & 0 \\ 1 & 1 & 0 & 1 \end{bmatrix}, E_{123} = \begin{bmatrix} 1 & 1 & 0 \\ 1 & 0 & 1 \\ 1 & 1 & 0 \end{bmatrix}, E_{124} = \begin{bmatrix} 1 & 1 & 0 \\ 1 & 0 & 0 \\ 1 & 1 & 1 \end{bmatrix}, E_{134} = \begin{bmatrix} 1 & 0 & 0 \\ 1 & 1 & 0 \\ 1 & 0 & 1 \end{bmatrix}, \text{and } E_{234} = \begin{bmatrix} 1 & 0 & 0 \\ 0 & 1 & 0 \\ 1 & 0 & 1 \end{bmatrix}.$$

It is clear that $M^2 = EA_2E^T$. Applying Cauchy-Binet formula, we get

$$\begin{aligned} \det(M^2) &= \sum_{1 \le k_1 < k_2 < k_3 \le 4} \left(\det E_{(k_1,k_2,k_3)} \prod_{i=1}^{4} \big(g(t_i)\big) \right) \\ &= g(1)g(2)g(3)[\det(E_{123})]^2 + g(1)g(2)g(4)[\det(E_{124})]^2 \\ &+ g(1)g(3)g(4)[\det(E_{134})]^2 + g(2)g(3)g(4)[\det(E_{234})]^2 \\ &= 0 + 28347647328000 + 7089488890848000 + 74865002687354880 \\ &= 81982839225530880 \end{aligned}$$

In the case where $T = \{t_1, t_2, \dots, t_n\}$ is a factor-closed set of distinct positive integers, we have the following corollary.

Corollary 1. If $T = \{t_1, t_2, \dots, t_n\}$ is a factor-closed set of distinct positive integers, then A is $n \times n$ diagonal matrix with diagonal entries $a_{ii} = g(t_i)$ and E is also $n \times n$ square incidence matrix relative to A, and hence

$$\det(M^r) = \prod_{i=1}^{n} g(t_i)$$

Proof. By Theorem 1, we have

$$\det[(\, M^r)] = \det(EA_rE^T) = \det(E)\det(A_r)\det(E^T) = 1 \times \det(A_r) \times 1 = \prod_{i=1}^{n} g(t_i).$$

By Theorem 2, we have

$$\det[(M^r)] = \det(A_rE^T) = \det(A_r)\det(E^T) = \det(A_r) = \prod_{i=1}^{n} g(t_i).$$

By Theorem 3, we have

$$\det[(M^r)] = \det(A_rA_r^T) = \det(A_r)\det(A_r^T) = \left(\prod_{i=1}^{n} \sqrt{g(t_i)} \right) \left(\prod_{i=1}^{n} \sqrt{g(t_k)} \right) = \prod_{i=1}^{n} g(t_i).$$

Reciprocals and Inverses

Theorem 5. Let $T = \{t_1, t_2, \dots, t_n\}$ be a non factor-closed set of distinct positive integers. Then, $[(M^{-r})] = EA_{-r}E^T$, where $A_{-r} = diag\big(h(t_1), h(t_2), \dots, h(t_n)\big)$ and E is an incidence matrix of T, such that $e_{ij} = 1$ if $t_j | t_i$ and 0 otherwise.

Proof. Let $\overline{T} = \{y_1, y_2, \ldots, y_m\}$ be the factor closed closure of T. Define the $m \times m$ diagonal matrix whose diagonal entries are $a_{ii} = h(y_i)$ for all $1 \leq i \leq m$. Let E be the $n \times m$ incidence matrix of $\overline{T}$ relative to T such that $e_{ij} = 1$ if $y_j | t_i$ and 0 otherwise. Then,

$$(EA_{-r}E^T)_{ij} = \sum_{k=1}^{n} \left(e_{ik} a_{kk} e_{jk}\right) = \sum_{\substack{y_k | t_i \\ y_k | t_j}} h(y_k) = \sum_{y_k | (t_i, t_j)} h\left(y_k\right)$$
$$= \sum_{y_k | (t_i, t_j)} \sum_{d \mid y_k} \frac{1}{\left(2^d - 1\right)^r} \mu\left(\frac{y_k}{d}\right) = \frac{1}{\left(2^{(t_i, t_j)} - 1\right)^r}.$$

Theorem 6. Let $T = \{t_1, t_2, \ldots, t_n\}$ be a factor-closed set of distinct positive integers, and let E be the incidence matrix relative to T, such that $e_{ij} = 1$ if $t_j | t_i$ and 0 otherwise. Then, the inverse of E is the matrix F^T such that $f_{ij} = \mu\left(\frac{t_i}{t_j}\right)$ if $t_j | t_i$ and 0 otherwise. Moreover,

$$(M^r)^{-1} = FA_r^{-1}F^T$$

Proof. Since T is factor-closed, then E is an $n \times n$ square invertible matrix such that

$$(EF^T) = \sum_{k=1}^{n} \left(e_{ik} f_{kj}\right) = \sum_{t_k | t_i}^{n} \left(f_{kj}\right) = \begin{cases} \sum_{t / \frac{t_i}{t_j}} (\mu(t)) & if\ t_j | t_i \\ 0 & otherwise \end{cases} = \begin{cases} 1 & if\ t_j | t_i \\ 0 & otherwise \end{cases}$$

This implies that $E^{-1} = F^T$, and hence

$$(M_r)^{-1} = (EA_rE^T)^{-1} = (E^{-1})^T (A_r)^{-1} (E)^{-1} = FA_r^{-1}F^T.$$

Mersenne Power GCD Matrices Defined on Non gcd-closed Sets

In this section, we study Mersenne Power GCD matrices defined on non gcd-closed sets. Full description of their factorizations, determinants, reciprocals, and inverses are given.

Structure Theorems

We prove three different factorizations for Mersenne power GCD matrices over non gcd-closed sets.

Theorem 7. Let $T = \{t_1, t_2, \ldots, t_n\}$ be a gcd-closed set of distinct positive integers, and let $g(t_k) = \sum_{d \mid t_k} \left(2^d - 1\right)^r \mu\left(\frac{t_k}{d}\right)$. Then,

$$\sum_{t_k | (t_i, t_j)} \left(\sum_{t_k | t_j, t_k \nmid t_u,\ t_u < t_j} g\left(t_k\right) \right) = \left(m_{ij}\right)^r$$

Proof. It is clear that any set T of distinct positive integers is contained in a gcd-closed set. Denote by $\overline{T}$ to be the minimal gcd-closed set containing T. It is worthwise to observe that $\overline{T}$ usually contains considerably fewer elements than any factor-closed set containing T. Also, it is clear that $\sum_{t_k | t_j, t_k \nmid t_u,\ t_u < t_j} g\left(t_k\right)$ is not representative and counted only once and it is equal to $g(t_k)$. Therefore,

$$\sum_{t_k | (t_i, t_j)} \left(\sum_{t_k | t_j,\ t_k \nmid t_u,\ t_u < t_j} g\left(t_k\right) \right) = \sum_{t_k | (t_i, t_j)} g\left(t_k\right) = \left(m_{ij}\right)^r.$$

Thereom 8. Let $T = \{t_1, t_2, \dots, t_n\}$ be a non gcd-closed set of distinct positive integers, and $\overline{T} = \{y_1, y_2, \dots, y_m\}$ be the minimal gcd-closed set containing T, then $(F_r) = EA_rE^T$, where E is the incidence matrix relative to T and A_r is an $m \times m$ diagonal matrix.

Proof. Let $\overline{T} = \{y_1, y_2, \dots, y_m\}$ be the minimal gcd-closed set containing T. Define the $m \times m$ diagonal matrix A_r as follows:

$$A_r = diag\left(\sum_{\substack{\mathrm{d}|y_1 \\ yu|y_1}} g(\mathrm{d}), \sum_{\substack{\mathrm{d}|y_2 \\ yu|y_2}} g(\mathrm{d}), \dots, \sum_{\substack{\mathrm{d}|y_m \\ yu|y_m}} g(\mathrm{d})\right)$$

where $g(n) = \sum_{d|n}\left(2^d - 1\right)^r \mu\left(\frac{n}{d}\right)$. Let E be the incidence matrix of $\overline{T}$ on T such that $e_{ij} = 1$ if $y_j|t_i$ and 0 otherwise. Then,

$$(EA_rE^T)_{ij} = \sum_{k=1}^{n}\left(e_{ik}a_ke_{jk}\right) = \sum_{y_k|t_i,\ y_k|tj}\left(\sum_{d|y_k,\, d\nmid y_u,\, y_u<y_k} g\,(d)\right) = \left(m_{ij}\right)_r.$$

Theorem 9. Let $T = \{t_1, t_2, \dots, t_n\}$ be a set of distinct positive integers, and $\overline{T} = \{y_1, y_2, \dots, y_m\}$ be the minimal gcd-closed set containing T. Then $(M^r) = A_rE^T$, where

$$a_{(ij)} = \begin{cases} \sum_{d|y_k,\, d\nmid y_u, y_u < y_k} g(d) & if\ y_j|t_i \\ 0 & otherwise \end{cases}$$

and

$$e_{(ij)} = \begin{cases} 1 & a_{ij} \neq 0 \\ 0 & otherwise \end{cases}$$

Proof. Since A_r and E are $n \times m$ matrices, then

$$(A_rE^T)_{ij} = \sum_{k=1}^{n}\left(a_{ik}e_{jk}\right) = \sum_{y_k|t_i,\, y_k|tj}\left(\sum_{d|y_k,\, d\nmid y_u, y_u<y_k} g\,(d)\right) = \left(m_{ij}\right)^r.$$

Theorem 10. Let $T = \{t_1, t_2, \dots, t_n\}$ be a non gcd-closed set of distinct positive integers, and let $\overline{T} = \{y_1, y_2, \dots, y_m\}$ be the minimal gcd-closed set containing T. Then $(M^r) = A_rA_r^T$, where

$$(A_r)_{(ij)} = \begin{cases} \sqrt{\sum_{d|y_k,\, d\nmid y_u, y_u < y_k} g(d)} & if\ y_j|t_i \\ 0 & otherwise \end{cases}.$$

Proof.

$$(A_rA_r^T)_{ij} = \sum_{k=1}^{n}\left(a_{ik}a_{jk}\right) = \sum_{\substack{y_k|t_i \\ y_k|tj}}\sqrt{\sum_{d|y_k,\, d\nmid y_u, y_u<y_k} g\,(d)}\sqrt{\sum_{d|y_k,\, d\nmid y_u,\, y_u<y_k} g\,(d)}$$

$$= \sum_{y_k|(t_i,t_j)}\left(\sum_{d|y_k,\, y_i<y_k,\, d\nmid y_u} g\,(d)\right) = \sum_{y_k|(t_i,t_j)} g\,(y_k) = \left(m_{ij}\right)^r.$$

Determinants

Theorem 11. Let $T = \{t_1, t_2, \ldots, t_n\}$ be a non gcd-closed set of positive integers, and let $\overline{T} = \{y_1, y_2, \ldots, y_m\}$ be the minimal gcd-closed set containing T with $n < m$. If $E_{(k_1,k_2,\ldots,k_m)_r}$ is the submatrix consisting of the $k_1^{th}, k_2^{th}, \ldots, k_m^{th}$ columns of E for some indices k_i such that $1 \leq k_1 < k_2 < \ldots < k_m \leq n$, then

$$\det(M^r) = \sum_{1 \leq k_1 < k_2 < \ldots < k_m \leq n} \left(\left(\det E_{(k_1,k_2,\ldots,k_m)_r}\right)^2 \prod_{i=1}^{m} \left(\sum_{\substack{d \mid y_m \\ y_u < y_m \\ d \nmid y_u}} g(d) \right) \right)$$

Proof. Let $A = (a_{ij})$ and $E = (e_{ij})$ be its corresponding incidence matrix, where $a_{ij} = \left(\sum_{\substack{d \mid y_m \\ y_u < y_m \\ d \nmid y_u}} g(d) \right)$ if $y_j \mid t_i$ and 0 otherwise. But, A is a diagonal matrix whose diagonal entries are $a_{ii} = \left(\sum_{\substack{d \mid y_m \\ y_u < y_m \\ d \nmid y_u}} g(d) \right)$ for all $1 \leq i \leq n$, so the ij^{th} entry of A may be written as $e_{ij} \left(\sum_{\substack{d \mid y_m \\ y_u < y_m \\ d \nmid y_u}} g(d) \right)$ and $(M^r) = EF^rE^T$.Define, for some indices k_i such that $1 \leq k_1 < k_2 < \ldots < k_m \leq n$, the matrices $A_{(k_1,k_2,\ldots,k_m)}$ and $E_{(k_1,k_2,\ldots,k_m)}$ to be the submatrices consisting of $k_1^{th}, k_2^{th}, \ldots, k_m^{th}$ columns of A and E respectively, then $A_{(k_1,k_2,\ldots,k_m)} = E_{(k_1,k_2,\ldots,k_m)} D_r$, where D_r is the $m \times m$ diagonal submatrix of A_r whose diagonal elements are $d_{ii} = \left(\sum_{\substack{d \mid y_m \\ y_u < y_m \\ d \nmid y_u}} g(d) \right)$. Therefore, $\det\left(A_{(k_1,k_2,\ldots,k_m)}\right) = \det\left(E_{(k_1,k_2,\ldots,k_m)}\right)\left(\prod_{i=1}^{m} d_{ii}\right)$. Applying Cauchy-Binet formula, we get

$$\begin{aligned}
\det[M^r] &= \det A_r E^T \\
&= \sum_{1 \leq k_1 < k_2 < \ldots < k_m \leq n} \left(\left(\det A_{(k_1,k_2,\ldots,k_m)}\right) \left(\det E_{(k_1,k_2,\ldots,k_m)}\right)^T \right) \\
&= \sum_{1 \leq k_1 < \ldots < k_m \leq n} \left(\det\left(E_{r_{(k_1,\ldots,k_m)}}\right) \left(\prod_{i=1}^{m} \left(\sum_{\substack{d \mid y_m \\ y_u < y_m \\ d \nmid y_u}} g(d) \right) \right) \left(\det E_{r_{(k_1,\ldots,k_m)}}\right)^T \right) \\
&= \sum_{1 \leq k_1 < k_2 < \ldots < k_m \leq n} \left(\prod_{i=1}^{m} \left(\sum_{\substack{d \mid y_m \\ y_u < y_m \\ d \nmid y_u}} g(d) \right) \left(\det E_{r_{(k_1,k_2,\ldots,k_m)}}\right)^2 \right).
\end{aligned}$$

Example 2. Consider the non gcd-closed set $T = \{2,4\}$ and its gcd-closure $\overline{T} = \{1,2,4\}$. Then, the 2^{nd} power Mersenne GCD matrix defined on T is:

$$M^2 = \begin{bmatrix} 17^2 & 17^2 \\ 17^2 & 65537^2 \end{bmatrix} = \begin{bmatrix} 289 & 289 \\ 289 & 4295098369 \end{bmatrix}$$

$$A_2 = \begin{bmatrix} g(1) & 0 & 0 \\ 0 & g(2) & 0 \\ 0 & 0 & g(1)+g(4) \end{bmatrix} = \begin{bmatrix} 25 & 0 & 0 \\ 0 & 264 & 0 \\ 0 & 0 & 4295098105 \end{bmatrix}$$

$$E = \begin{bmatrix} 1 & 1 & 0 \\ 1 & 1 & 1 \end{bmatrix}, \quad E_{12} = \begin{bmatrix} 1 & 1 \\ 1 & 1 \end{bmatrix}, \quad E_{13} = \begin{bmatrix} 1 & 1 \\ 0 & 1 \end{bmatrix}, \text{ and } \quad E_{23} = \begin{bmatrix} 1 & 1 \\ 0 & 1 \end{bmatrix}.$$

It is clear that $M^2 = EA_2E^T$. Applying Cauchy-Binet formula, we get

$$\begin{aligned} \det(M^2) &= \sum_{1 \le k_1 < k_2 \le 3} \left(\det E_{(k_1,k_2)} \prod_{i=1}^{2} \left(g(t_i) \right) \right) \\ &= g(1)g(2)[\det(E_{12})]^2 + g(1)g(4)[\det(E_{13})]^2 + g(2)g(4)[\det(E_{23})]^2 \\ &= 0 + 107377452000 + 1133905893120 \\ &= 1241283345120 \end{aligned}$$

Corollary 2. Let $T = \{t_1, t_2, \ldots, t_n\}$ be a gcd-closed set of distinct positive integers, then

$$\det[M^r] = \det(EA_rE^T) = \det(E)\det(A_r)\det(E^T) = \det(A_r) = \prod_{i=1}^{n} \left(\sum_{\substack{d \mid t_m \\ t_u < t_m \\ d \nmid t_u}} g\,(d) \right).$$

Reciprocals and Inverses

Theorem 12. Let $T = \{t_1, t_2, \ldots, t_n\}$ be a non gcd-closed set of distinct positive integers, and $\overline{T} = \{y_1, y_2, \ldots, y_m\}$ be the minimal gcd-closed set containing T, then $(M^{-r}) = EA_{-r}E^T$, where

$$A_{-r} = diag\left(\sum_{d \mid y_1,\, d \nmid y_u,\, y_u < y_1} h\,(d), \sum_{d \mid y_2,\, d \nmid y_u,\, y_u < y_2} h\,(d), \ldots, \sum_{d \mid y_m,\, d \nmid y_u,\, y_u < y_m} h\,(d) \right)$$

such that

$$h(n) = \sum_{d \mid n} \left(\frac{1}{(2^d - 1)} \right)^r \mu\left(\frac{n}{d}\right).$$

Proof. Let $\overline{T} = \{y_1, y_2, \ldots, y_m\}$ be the minimal gcd-closed set containing T. Then,

$$\begin{aligned} (EA_{-r}E^T)_{ij} &= \sum_{k=1}^{n} \left(e_{ik} a_k e_{jk} \right) = \sum_{y_k \mid t_i,\, y_k \mid tj} \left(\sum_{d \mid y_k, y_i < y_k,\, d \nmid y_u} h\,(d) \right) \\ &= \sum_{y_k \mid (t_i, t_j)} h\,(y_k) = \left(\frac{1}{\left(2^{(t_i, t_j)} - 1\right)} \right)^r = (M^{-r})_{ij}. \end{aligned}$$

Theorem 13. Let $T = \{t_1, t_2, \ldots, t_n\}$ be a gcd-closed set of positive integers, then the inverse of (M^r) is $(M^r)^{-1}$ such that

$$(M^r)^{-1}_{ij} = \sum_{\substack{t_i \mid t_k \\ t_j \mid t_k}} \left(\frac{\mu\left(\frac{t_k}{t_i}\right) \mu\left(\frac{t_k}{t_j}\right)}{\sum_{d \mid y_k,\, d \nmid y_u,\, y_u < y_k} g\,(d)} \right)$$

Proof. Since T is gcd-closed, then E is an $n \times n$ square invertible matrix such that$E^{-1} = F^T$.Then,

$$(M^r)_{ij}^{-1} = (EA_rE^T)_{ij}^{-1} = (E^{-1})^T(A_r)^{-1}(E^{-1}) = F^T(A_r)^{-1}F$$
$$= \sum_{k=1}^{m} f_{ik}\frac{1}{f_{kk}^{\,r}}f_{kj} = \sum_{\substack{t_i|t_k \\ t_j|t_k}} \left(\frac{\mu\left(\frac{t_k}{t_i}\right)\mu\left(\frac{t_k}{t_j}\right)}{\sum_{d|y_k,\, d\nmid y_u,\, y_u<y_k} g\,(d)} \right)$$

Conclusion

In conclusion, this paper has presented a thorough investigation into the $n \times n$ Mersenne power GCD matrices defined on arbitrary sets of positive integers. By building upon prior research and utilizing a specialized form of the arithmetical function, we have explored the unique properties and behaviors of these matrices on both factor-closed and gcd-closed sets.

Our analysis has yielded valuable insights into the factorizations, determinants, reciprocals, and inverses of these Mersenne power GCD matrices. By elucidating their characteristics, we have contributed to the broader understanding of power GCD matrices and their applications in number theory and linear algebra. Furthermore, our findings not only expand upon existing knowledge but also pave the way for further exploration and refinement in this area of study. The versatility and significance of Mersenne power GCD matrices underscore their potential relevance in diverse mathematical contexts.

In essence, this paper underscores the importance of investigating specialized forms of power GCD matrices, such as the Mersenne variant, and highlights the rich interplay between number theory, algebra, and computational mathematics. Through our rigorous analysis, we have provided valuable insights that may inspire future research endeavors and contribute to the advancement of mathematical theory and practice.

Scientific Ethics Declaration

The authors declare that the scientific ethical and legal responsibility of this article published in EPSTEM journal belongs to the authors.

Acknowledgements or Notes

* This article was presented as an oral presentation at the International Conference on Basic Sciences, Engineering and Technology (www.icbaset.net) held in Alanya/Turkey on May 02-05, 2024.

* The authors gratefully acknowledge the invaluable contributions of the anonymous referees whose insightful comments and constructive feedback greatly enhanced the quality and clarity of this article. Their expertise and dedication have been instrumental in shaping the final version of the manuscript.

* Each author has contributed equally to this article, demonstrating a collaborative effort and shared dedication to its content.

* AMS Subject Classification**:** 11A25, 15A09, 15A15, 15A23

References

Awad, Y. A., Chehade, H., & Mghames, R. (2020). Reciprocal power gcdq matrices and power lcmq matrices defined on factor closed sets over Euclidean domains. *Filomat*, *34*(2), 357–363.

Awad, Y., Mghames, R., & Chehade, H. (2023). Power gcdq and lcmq matrices defined on gcd-closed sets over euclidean domains. *Palestine Journal of Mathematics*, *12*(1).

Awad, Y., Mghames, R., Chehade, H., & Zeid, W. (2019). On Fermat power GCD matrices defined on special sets of positive integers. *Applied Mathematical Sciences*, *13*, 369–379.

Bege, A. (2010). Generalized GCD matrices. *arXiv preprint arXiv:1012.5445*.

Beslin, S., & Ligh, S. (1989). Greatest common divisor matrices. *Linear Algebra and Its Applications*, *118*, 69–76.

Beslin, S. (1991). Reciprocal GCD matrices and LCM matrices. *Fabonacci Quart.*, *20*, 71–274.

Beslin, S., & Ligh, S. (1989). Another generalization of Smith's determinant. *Bull Australian Mathematical Society, 40*, 413–415.

Beslin, S., & Ligh, S. (1992). Gcd-closed sets and the determinants of gcd matrices. *Fabonacci Quarterly*, *30*, 157–160.

Borque, K., & Ligh, S. (1992). On GCD and LCM matrices. *Linear Algebra and its Applications*, *174*, 65–74.

Chun, S. Z. (1996). GCD and LCM power matrices. *Fabonacci Quarterly*, *43*, 290–297.

El-Kassar, A.N., Habre, S.S., & Awad, Y.A. (2009). Greatest common divisor and least common multiple matrices on factor closed Sets in a principal ideal domain. *Journal of Mathematics and Statistics*, *5*(4), 342–347.

El-Kassar, A. N., Habre, S. S., & Awad, Y. A. (2010). Gcd matrices defined on GCD-closed sets in a pid. *International Journal of Applied Mathematics*, *23*(4), 571–581.

Haukkanen, P. (1997). On Smith's determinant. *Linear Algebra and its Applications*, *258*, 251–269.

Hong, S. (1998). On LCM matrices on GCD-closed sets (English summary). *Southeast Asian Bulletin of Mathematics*, *22*, 381–384.

Hong, S. (1998). Bounds for determinant of matrices associated with classes of arithmetical functions. *Linear Algebra and its Applications*, *281*, 311–322.

Hong, S., Zhou, X., & Zhao, J. (2009). Power GCD matrices for a UFD. *Algebra Colloquium*, *16*, 71–78.

Li, Z. (1990). The determinant of a GCD matrices. *Linear Algebra and its Applications, 134*, 137–143.

Ligh, S. (1988). Generalized Smith's determinant. *Linear and multilinear Algebra*, *22*, 305–306.

Smith, H. J. S. (1875-1876). On the value of a certain arithmetical determinant. *Proc. London Mathematical Society*, *7*, 208–212.

Zeid, W., Chehade, H., & Rasheed, F. (2022). On GCD matrices over unique factorization domains. *Filomat, 36*(11), 3775–3784.

Author Information

Yahia Awad
Lebanese International University (LIU)
Department of Mathematics and Physics
AlKhyara, West Bekaa, Lebanon.
Contact e-mail: *yehya.awad@liu.edu.lb*

Ragheb Mghames
Lebanese International University (LIU)
Department of Mathematics and Physics
AlKhyara, West Bekaa, Lebanon.
Modern University for Business and Science (MUBS)
School of Business, Rashaya, Lebanon.

Karim Amin
Lebanese International University (LIU)
Department of Mathematics and Physics
AlKhyara, West Bekaa, Lebanon.

To cite this article:

Awad, Y., Mghames, R., & Amin, K. (2024). On mersenne power GCD matrices. *The Eurasia Proceedings of Science, Technology, Engineering & Mathematics (EPSTEM), 28*, 224-233.

The Eurasia Proceedings of Science, Technology, Engineering & Mathematics (EPSTEM)
ISSN: 2602-3199

The Eurasia Proceedings of Science, Technology, Engineering & Mathematics (EPSTEM), 2024

Volume 28, Pages 234-240

ICBASET 2024: International Conference on Basic Sciences, Engineering and Technology

Big Data and Analytical Strategies for Cloud ERP Systems with Business Simulation

Lea Masnec
University of Zagreb

Ruben Picek
University of Zagreb

Abstract: In the changing landscape of the business world, the rapid pace of change has led to an increasing demand for innovative approaches to problem-solving and optimization. With the ongoing advancement of ERP (Enterprise Resource Planning) systems, which now incorporate predictive analytics, cloud computing, and business analysis through simulations, businesses have new opportunities to enhance their operations. This paper explores a business analysis framework within the context of cloud ERP systems using test data of one company as a case study. Such a business-oriented approach, driven by the adoption of innovative practices, empowers companies to adapt swiftly to the changing dynamics of the market. This paper primarily offers insights into the possibilities unlocked by ERP systems using predictive analytics and business analysis via simulations. These insights encompass a combination of various factors that impact business operations, such as pricing strategies, market segmentation, resource allocation, and other critical components. Furthermore, leveraging a myriad of today's tools, this research demonstrates that after constructing a data model, operations like classification and time series forecasting can be executed on the dataset, all of which significantly influence the final business decisions. This research seeks to provide a broader perspective on problem-solving within the context of ERP systems and how they enable data-driven decision-making for enhanced business performance.

Keywords: Big data, Business intelligence, Cloud ERP systems

Introduction

With the advancement of new technologies, ERP systems have become increasingly prevalent across various industries. This paper is based on the development of a decision-making model through graphical analytical representation, aimed at facilitating business decision-making for companies. For businesses, it is crucial to plan their resources and make timely business decisions. As Rabia and Bellabdaoui (2022) point out, a decision made late is equivalent to lost business, whereas a decision made on time is akin to gained business. Through the application of predictive analytics and simulations, businesses can analyze extensive sets of historical data, recognizing underlying patterns and trends. This capability enables them to make precise predictions about future outcomes (Bharadiya, 2023). It is well-known that data holds significant value when well-structured and utilized for in-depth business analysis. The increase in data sources has provided many businesses with the capability to make faster, fact-based decisions and leverage operational opportunities (Aliahmadi et al., 2022). The paper consists of sections on related work, scientific methods, and a core section titled "Business Intelligence in ERP Systems." This section covers problem classification, model development, and what-if simulation for resolving business issues. Results of case study and discussion that elaborate resarch question are also present. In last section authors provide conslusions. The research question to be answered in this paper is:

How can the integration of predictive analytics and 'what-if' simulations into ERP systems enhance overall system efficiency and unlock their potential for strategic business planning?

Related Work

Several pivotal contributions have shaped the discourse surrounding predictive analytics, business intelligence, and ERP system integration. The research by Rabia and Bellabdaoui (2022) explores the domain of simulation-based analytics, which holds particular significance when discussing the dynamics of intricate systems. Rabia & Bellabdaoui provide an overview of simulation techniques that are vital in business analysis, and this importance becomes evident when considering the topic of this research in the context of cloud ERP systems, where a substantial volume of data and complexity exists. Bakhshi and Bates (2018) provided comprehensive insights into the potential of predictive analytics across diverse domains. Their work laid the groundwork for subsequent research, including the exploration of statistical, learning, and ensemble methods for predictive analytics as exemplified by Budgaga et al. (2016). In parallel, Deka (2014) emphasized the critical role of predictive and predictive analytics within the realm of Big data, highlighting its significance in enabling data-driven decision-making in contemporary business operations. This foundational understanding has been further complemented by the insights provided by Gartner (2019) regarding the broader landscape of artificial intelligence and its integration, including predictive analytics, into business systems. Also, Paulino (2022) in his study explores how business analytics implementation in the retail industry can enhance organizational performance, drawing from the established principles of data mining and predictive analytics. Paulino's research also emphasizes concepts that affect a company's bottom line and its long-term operations.

Himeur et al. (2023), in their research, emphasize the benefits of Big data analytics and prediction while also highlighting the challenges that businesses face when it comes to gaining a competitive edge in the market through predictions. According to Himeur et al. (2023), additional research and initiatives related to Big data should be made a primary goal to demonstrate the market potential that Big data technology can achieve. Hsieh (2017) provided a forward-looking perspective of ERP systems, shedding light on the next generation of these systems and their convergence with predictive analytics and business intelligence. This work contributes to a broader understanding of how ERP systems are advancing to incorporate advanced analytics capabilities. Additionally, Nazarov et al. (2020) conducted a tangible case study, scrutinizing the application of SAP Analytics Cloud for intellectual analysis of business activities. This case study provides actionable insights into the integration of analytics tools within ERP systems, showcasing practical implications for real-world applications. In a complementary vein, Park and Kim (2017) conducted a comprehensive review focused on predictive analytics within ERP systems. Jafari et al. (2023) also emphasize the importance of business intelligence through integration and agility in supply chain performance.

Through their research across various industries, they have confirmed that BI and integration play a crucial role in achieving improved business performance, particularly in the context of supply chain planning. Aliahmadi et al. (2022) corroborate the hypothesis that technologies can serve as potent enablers, particularly in the distribution of fast-acting pharmaceutical products, which will also be demonstrated in this research within the context of Big data. This claim is also confirmed by the research of Žagar and Miletić (2022), who, in their study, analyzed the application of Big data collection for product quality prediction, further emphasizing the utility of predictive methods in the industry.

Method

This research employed various research and writing methods to address the theoretical aspects and practical implementation. Firstly, a descriptive research method was utilized to provide a comprehensive description and analysis. Qualitative literature analysis was conducted to identify trends and techniques within the domains of business intelligence, predictive analytics, and "what-if" simulation. An experimental research method was employed to construct a data model using SAP Analytics Cloud tools and to test various scenarios through predictive analytics and "what-if" simulation. Additionally, qualitative data analysis was applied to scrutinize the results and draw conclusions. Finally, statistical data analysis methods were employed to ascertain correlations and associations among different factors and their impact on business operations.

Business Intelligence in ERP Systems

In today's business environment, with the increasing volume of data generated from various sources such as social media, IoT *(Internet of Things*) devices, and other applications, there is a growing need for the development of tools for analyzing large datasets. According to Deka (2014) and Li et al. (2022), big data analytics is employed for predictive analysis, enabling organizations to forecast future events and recommend

appropriate strategies. Data management is a crucial component of business intelligence. The development of BI tools capable of collecting, processing, and analyzing vast amounts of data is becoming pivotal in achieving business objectives. In this regard, BI tools assist organizations in gathering and processing extensive data, transforming it into valuable insights that enable informed business decision-making.

An essential capability of business intelligence within ERP systems is "what-if" simulation. This technique empowers organizations to simulate various scenarios based on different variables and parameters, allowing them to predict potential outcomes and impacts on their operations. Implementing this technique enables organizations to assess the effects of changes in production, pricing, marketing strategies, and other factors on their business efficiency. In the process of implementing predictive analytics, it is crucial to ensure that the system has an adequate volume of data, well-defined models and algorithms, and suitable infrastructure for data analysis and visualization. Furthermore, employee education is necessary to empower them to utilize these techniques effectively for achieving the best results.

Model Development

In this chapter, the development of a data model simulating a business scenario is presented through a business problem-solving approach. In the context of the pharmaceutical sector, which plays a pivotal role in both human health and the global economy, the role of ERP systems has taken on even greater significance. This is precisely why, as a practical illustration in the context of implementing predictive analytics, a dataset from a pharmaceutical company (Farseer, 2022) was selected to create a model for further analysis. During the model creation process aimed at addressing the business problem, the following steps were taken:

1. Data set analysis;
2. Data set editing and interconnection using a business analytics tool;
3. Defining the business objective;
4. Training classification and regression models;
5. Developing an analytical application using integrated JavaScript, application design, and mathematical calculations (base discount, gross margin, scenario price, scenario discount, net revenue, etc.);
6. Adding items to the application based on categories and operational areas;
7. Testing the application and analyzing potential improvements to company operations;
8. Formulating the final conclusion for the company.

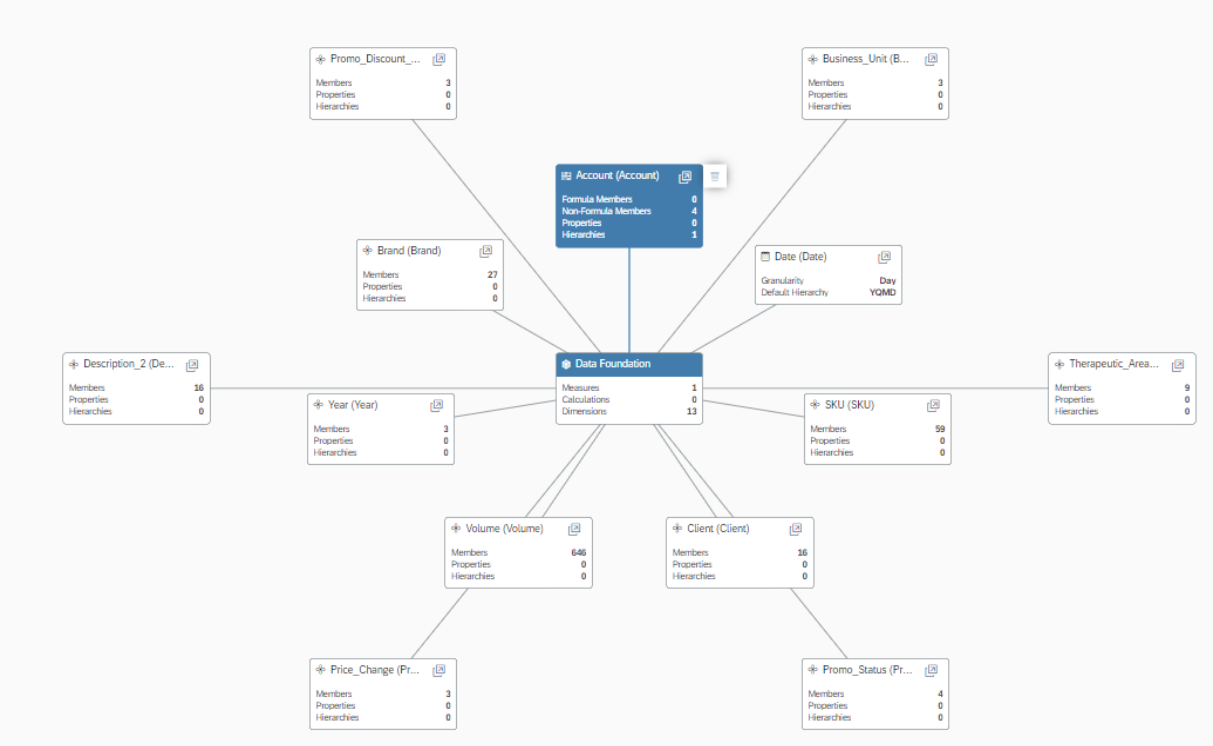

Figure 1. Data model generated in SAP analytics cloud

In the process of creating the data model, it was necessary to first organize the data model and link specific dimensions' data from one dataset to another using the "Combine Data" option. Based on the collected sales data of the pharmaceutical company, a model was created encompassing information about SKUs (*Stock Keeping Units*), clients, sales volumes, prices, discounts, and other relevant indicators. The modeling process involved various steps, such as data integration, establishing connections between entities, defining dimensions and measures, and implementing necessary data transformations. Figure 1 illustrates the model generated after refining the final dataset, which will serve as the foundation for further analysis.

A review of the pharmaceutical company's operations is a crucial step in understanding its functioning, successes, and challenges. Analyzing the financial results of the pharmaceutical company, including revenues, expenses, profits, and balance sheets, enables an assessment of the financial stability and profitability of the company. It is also important to examine trends in financial indicators to identify strengths, weaknesses, and potential opportunities for improvement.

Business Operations and Enhancement Oppportunities through Analytics Tools

Setting a goal in a clear and measurable way allows the organization to have a clear vision of the desired outcome and directs all activities towards achieving that outcome. In the business problem described, the company did not achieve a profit in the year 2021, as the total gross revenue was negative. This also resulted in a negative net income, meaning the company actually lost money that year. The company's sales amounted to 2.44 million units, generating gross revenue of 144.241 million. However, the company applied 10.039 million in basic discounts. Up to that point, the company was profitable. However, an additional 9.045,375 million kuna was spent on promotions, resulting in an actual financial loss.

Setting a goal in this case would be to achieve profitability for the company. By reducing promotional discounts to achieve a positive net income and avoid losses, the company will create a sustainable business model and increase overall profitability. Goal setting allows for a focus on a specific outcome and the necessary decision-making and actions to achieve that goal. Figure 2 depicts the developed analytical application for addressing the business problem, showing the initial state of the company in 2021 before any changes were made.

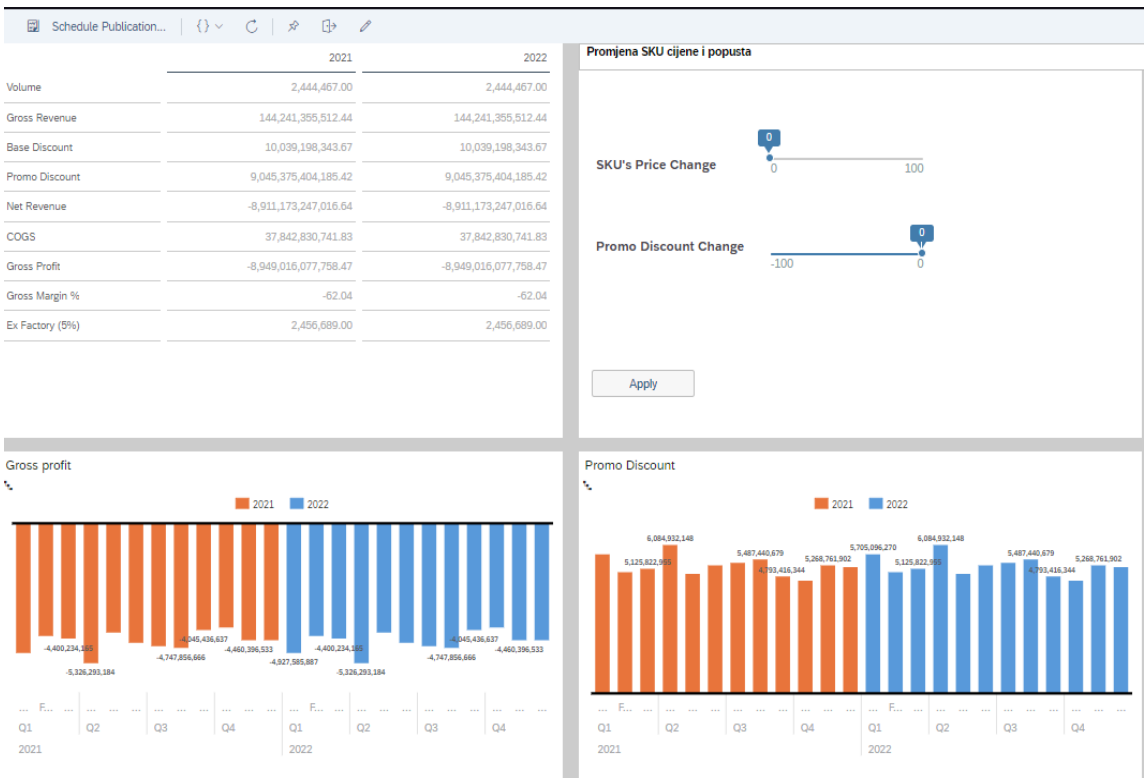

Figure 2. Overview of the initial state of the company in 2022

The strategy is depicted in Figure 3, and it is now clearly visible in the table that Net Revenue, and consequently Gross Profit, is now positive, as evident in Figure 1 at the end.

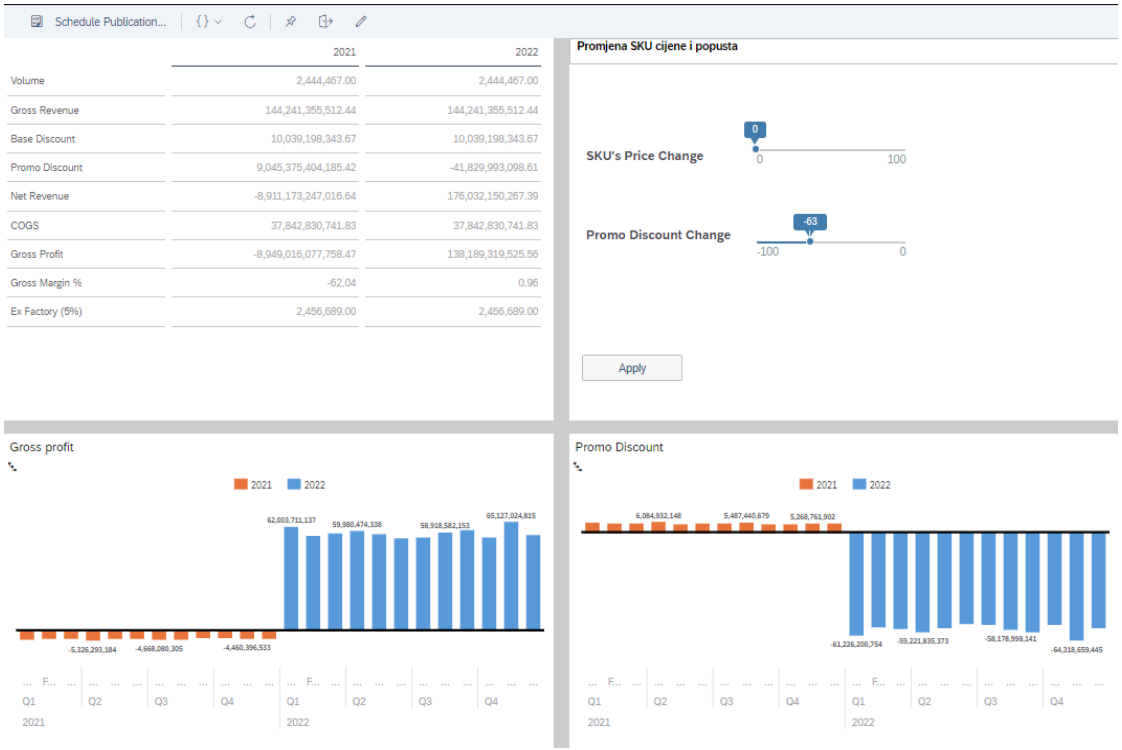

Figure 3. Analytical application depicting the post-change state

As a solution, based on the change in Figure 3, the possibility of increasing SKU prices is considered to address the issue. However, such an approach may further exacerbate the situation since promotions are price-dependent. Therefore, the only remaining option is to reduce promotional discounts. Reducing discounts allows the company to achieve higher margins and greater profitability. By using the "Promo Discount Change" slider, it is possible to determine the maximum discount amount that the company can apply, which is -63. Any discount greater than this will not result in profitability. This strategy enables the company to maintain profitability, secure revenues, and ensure business stability.

Results and Discussion

The combination of predictive analytics and "what-if" simulations provides tools for a more profound comprehension of business dynamics, the identification of potential challenges, and the discovery of optimal solutions. The introduction of analytical approaches into pharmaceutical company processes enables quicker and more informed decision-making, securing a competitive advantage in the market, as demonstrated in the practical example within this thesis.

The research question introduced in the paper's introduction was: *How can the integration of predictive analytics and 'what-if' simulations into ERP systems enhance overall system efficiency and unlock their potential for strategic business planning?*. Based on the research question, the following conclusions have been dicuss and analyzed:

1. **How can predictive analytics enhance the efficiency of ERP systems?** Predictive analytics can improve ERP system efficiency by enabling more accurate forecasting of future trends and business needs. ERP systems can utilize predictive analytics to forecast future product and service demand, optimize manufacturing processes, and manage inventory effectively. Additionally, predictive analytics can assist in recognizing customer behavior trends and adapting marketing campaigns to boost sales.
2. **What are the key advantages of implementing "what-if" simulations in ERP systems?** Predictive analytics and "what-if" simulations can be instrumental in business planning by allowing users to test different scenarios and predict outcomes before making final decisions. This approach aids users in making better-informed decisions based on real data. "What-if" simulations are valuable for business future planning, process and resource optimization, and risk reduction.
3. **How can predictive analytics and "what-if" simulations be employed in business planning?** The primary benefits of implementing "what-if" simulations in ERP systems include enabling users to test

various scenarios and predict outcomes before making final decisions. This way, users can make better-informed decisions based on real data. "What-if" simulations support future business planning, process and resource optimization, and risk management.

4. **What are the possibilities for implementing predictive analytics in ERP systems?** Opportunities for implementing predictive analytics in ERP systems include integrating external predictive analytics tools, such as machine learning and data analysis tools. This integration allows the utilization of machine learning algorithms to predict future trends and customer behavior. Additionally, ERP data can be leveraged for predictive analytics. For instance, sales data can be used to forecast future sales trends. Automation of predictive analytics can also be achieved, where the system is programmed to automatically generate predictive models based on input data. This automation can be useful for generating predictions without the need for manual analysis.

Based on the conclusions presented, it is evident that this research further reinforces the significance of analytical methods and simulations in organizing business operations within companies by leveraging new technologies, significantly reducing potential business risks.

Conclusion

This research provides insights into analyzing business operations from the perspective of utilizing Big data analytics and reporting tools. This solution is applicable across various sectors and provides room for considering similar solutions in other industries. Specifically, this paper discusses the use of Big data analytics and market event simulation in businesses. In the case study presented in the research paper, we can observe how a change in the discount amount can significantly impact a company's annual profit, resulting in better outcomes compared to the previous year. Such analysis is becoming almost essential for every business today to eliminate potential market errors and manage resources more effectively. The paper showcases just one possibility for improving business operations, but this data model and analytical application offer a multitude of opportunities depending on the company's goals, which should be clearly defined before creating an analytical simulation. The primary aim of this paper was to demonstrate how to manage a company and make proactive business decisions, both in the pharmaceutical industry in this research example and in other industries.

The theoretical part of this paper addressed current trends and research in the field of Big data analytics, prediction, and simulation. Meanwhile, the practical part of the paper focused on a specific issue, namely, the operations of a company with multiple product groups and corresponding discounts for each of them. In the practical part, the company's final profit was observed as the main indicator of its success. In the further course of the research, we would focus on the impact of simulations on business decisions and the development of more advanced simulation models that will simulate specific business scenarios in the market defined by external influences, particularly for individual products within companies.

Recommendations

This research is recommended for all BI consultants, especially those working with more complex reporting tools that combine programming code with user interfaces, interface design, and analytics through classification and regression. This study can be valuable not only for academic purposes but also for businesses aiming to enhance their operations through optimization using Big data analytics. Recommended areas for further research include:

1. Cost-benefit analysis;
2. Advanced predictive models;
3. Integration of predictive analytics with ERP systems.

Scientific Ethics Declaration

The authors declare that the scientific ethical and legal responsibility of this article published in EPSTEM journal belongs to the authors.

Acknowledgements or Notes

* This article was presented as an oral presentation at the International Conference on Basic Sciences, Engineering and Technology (www.icbaset.net) held in Alanya/Turkey on May 02-05, 2024.

References

Aliahmadi, A., Nozari, H., & Ghahremani-Nahr, J. (2022). Big data IoT-based agile-lean logistic in pharmaceutical industries. *International Journal of Innovation in Management, Economics and Social Sciences, 2*(3), 70-81.

Bakhshi, S., & Bates, M. (2018). *Predictive analytics: The power to predict who will click, buy, lie, or die*. John Wiley & Sons.

Bharadiya, J. P. (2023). Machine learning and aı in business intelligence: Trends and opportunities. *International Journal of Computer (IJC), 48*(1), 123-134.

Budgaga, W., Malensek, M., Pallickara, S., Harvey, N., Breidt, F. J., & Pallickara, S. (2016). Predictive analytics using statistical, learning, and ensemble methods to support real-time exploration of discrete event simulations. *Future Generation Computer Systems, 56,* 360-374.

Deka, G. C. (2014). Big data predictive and prescriptive analytics. In *Handbook of research on cloud infrastructures for big data analytics* (pp. 370-391). IGI Global.

Farseer (2022). *What-if analysis in sales planning*. Retrieved from https://www.farseer.io/post/what-if-analysis-in-sales-planning-how-to-excel-template-example

Gartner. (2019). *Predicts 2020: Artificial intelligence*. Gartner Inc.

Han, J., Kamber, M., & Pei, J. (2011). *Data mining: Concepts and techniques* (3th ed.). Elsevier.

Himeur, Y., Elnour, M., Fadli, F., Meskin, N., Petri, I., Rezgui, Y., ... & Amira, A. (2023). AI-big data analytics for building automation and management systems: a survey, actual challenges and future perspectives. *Artificial Intelligence Review, 56*(6), 4929-5021.

Hsieh, Y. H. (2017). The next-generation ERP. In *Advanced methodologies and technologies in business operations and management* (pp. 31-50). IGI Global.

Jafari, T., Zarei, A., Azar, A., & Moghaddam, A. (2023). The impact of business intelligence on supply chain performance with emphasis on integration and agility–a mixed research approach. *International Journal of Productivity and Performance Management, 72*(5), 1445-1478.

Li, C., Chen, Y., & Shang, Y. (2022). A review of industrial big data for decision making in intelligent manufacturing. *Engineering Science and Technology, an International Journal, 29,* 101021

Nazarov, D. M., Kovtun, D. B., & Reichert, T. N. (2020). SAP analytics cloud: Intellectual analysis of small and medium-sized business activities in Russia in the context of COVID-19. In 2020 *IEEE 14th International Conference on Application of Information and Communication Technologies* (AICT) (pp. 1-6). IEEE.

Park, J., & Kim, Y. (2017). Predictive analytics in enterprise resource planning (ERP) systems: A review. *Journal of Open Innovation: Technology, Market, and Complexity, 3*(17), 1-17.

Paulino, E. P. (2022). Amplifying organizational performance from business intelligence: Business analytics implementation in the retail industry. *Journal of Entrepreneurship, Management and Innovation, 18*(2), 69-104.

Rabia, M. A. B., & Bellabdaoui, A. (2022). Simulation-based analytics: A systematic literature review. *Simulation Modelling Practice and Theory, 117,* 102511.

SAP. (2020). *Data modeling with SAP analytics cloud*. Retrieved from https://community.sap.com/

Žagar, J., & Mihelič, J. (2022). Big data collection in pharmaceutical manufacturing and its use for product quality predictions. *Scientific Data, 9*(1), 99.

Author Information

Lea Masnec
University of Zagreb, Faculty of Organization and Informatics, Pavlinska 2, 42000, Varaždin, Croatia
Contact e-mail: *lmasnec@foi.hr*

Ruben Picek
University of Zagreb, Faculty of Organization and Informatics, Pavlinska 2, 42000, Varaždin, Croatia

To cite this article:

Masnec, L., & Picek, R. (2024). Big data and analytical strategies for cloud ERP systems with business simulation. *The Eurasia Proceedings of Science, Technology, Engineering & Mathematics (EPSTEM), 28,* 234-240.

The Eurasia Proceedings of Science, Technology, Engineering & Mathematics (EPSTEM)
ISSN: 2602-3199

The Eurasia Proceedings of Science, Technology, Engineering & Mathematics (EPSTEM), 2024

Volume 28, Pages 241-245

ICBASET 2024: International Conference on Basic Sciences, Engineering and Technology

Decomposition of Hydrogen Peroxide in Presence of Dimethylglyoximato-Nickel Complexes as Catalysts: Catalase-Like Activity

Noura Kichou
Mouloud Mammeri University of Tizi-Ouzou (UMMTO)

Nabila Guechtouli
University of Boumerdes

Anissa Merrad
Mouloud Mammeri University of Tizi-Ouzou (UMMTO)

Zakia Hank
University of Sciences and Technology Houari Boumediene

Abstract: The development in coordination chemistry in recent years raise hopes that synthetically produced metal complexes could mimic many biochemical systems widely found in nature. There is a certain analogy between nature and organometallic systems. A large number of biological metal complexes are known, including oxygen carriers like hemoglobin in the blood, which contains a ferrous ion; respiratory enzymes; those involved in protein hydrolysis; and vitamin B12, which is only active in the presence of cobalt in the trivalent state. The Nickel (III), in addition to Fe-S clusters, was an essential component in hydrogenases. Since then, nickel (III) complexes have been used as models for studying the catalytic function of certain enzymes (hydrogenases). In this context, a study on the catalytic ability of dimethylglyoximato-nickel complexes as peroxiredoxases in the dismutation or oxidation of hydrogen peroxide was conducted. The results were discussed, commented upon, and a reaction mechanism was proposed. The results seem encouraging, regarding the effect of the complexation on catalase- like activity.

Keywords: Nickel, Decomposition, Hydrogen peroxide, Catalase

Introduction

Many enzymes require metal ions to function. It is difficult to determine whether these metals or cations are coenzymes; however, it is certain that in most, if not all, cases, they participate in the enzymatic reaction by combining with the enzyme or the substrate. The role of metal in the .enzymatic system, such as in catalases (natural catalysts), is most often to serve as a link by forming a complex between the protein enzyme and the substrate. In this way, catalase, for example, through its ferric complex (ferriprotoporphyrin(IX)), constitutes the last line of defense against the formation of hydroxyl radicals (OH) that arise from the homolytic dissociation of the H-O-O- bond in hydrogen peroxide (dismutation), a highly active and toxic derivative of oxygen.

In this context, we were interested in the influence of several parameters such as the mass of the catalyst, the addition of nitrogenous base, and the composition of the reaction medium on the conversion of hydrogen peroxide to molecular oxygen. Two complexes of dimethylglyoximato-nickel have been tested for catalase–like activity in order to assess their catalytic properties. The formulas for the complexes are: $Ni(C_4H_7N_2O)_2OH$, d^7 configuration of Ni (III) species , distorted square- pyramidal environment, noted C1, obtained without an

oxidizing chemical agent and $Ni(C_4H_6N_2O)_2(OH)_2$, Ni(IV) entity d^6 configuration in an octahedral environment noted C2, resulting with an oxidizing chemical (Kichou , 2018).

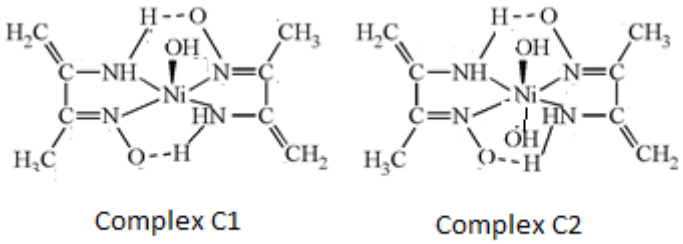

Figure 1. Structures of the complexes.

Experimental

The study of the catalase activity (disproportionation reaction of H_2O_2 into H_2O and O_2) was carried out at 25 °C by volumetric determination of the oxygen evolved with a gas-measuring burette (with a precision of 0.1 mL). All reactions were carried out at 25°C in a 250 cm^3 reactor containing a stirring bar under air. Distilled water (20 cm^3) was added to the complex and the flask was closed with a rubber septum. Hydrogen peroxide (2 ml at 21.82 N) was injected through the septum with a syringe at pH 5-6. The reactor was connected to a graduated burette filled with water, and dioxygen evolution was measured volumetrically at time min (Shivankar, 2005).

Results and Discussion

The Study of the Effect of Some Physical Parameters on the Catalytic Activity of the Complexes

Effect of the Mass on the Catalytic Activity of the Complexes C1and C2

In order to determine the influence of the mass on the catalytic effect of the complexes studied, a series of tests has been performed. This study is to follow the evolution of the performance in oxygen in function of the mass of the catalytic converter. The table above represent the results of this study at ambient temperature.

Table 1. Effect of the mass on the performance of the disproportionation of H_2O_2.

	Performance in O_2 (%)			
Complex	1 mg	5 mg	10 mg	15 mg
C1	56.2	90.6	90.6	90.6
C2	56.2	81.2	81.2	81.2

The choice of the mass of the substrate is an important consideration in the development of the catalytic tests. This study has allowed us to optimize the mass (5mg) and time (60 minutes) necessary for a maximum performance of disproportionation of H_2O_2.

Effect of the Temperature on the Catalytic Activity of the Complexes

In order to determine the influence of the temperature on the catalytic effect of the complexes studied, a series of tests has been performed. This study is to follow the evolution of the performance in oxygen in function of the temperature of the reaction medium. The table above represent the results of this study in laying down the mass at 5 mg. It is obvious that the temperature is a parameter of influence in the disproportionation of the oxygenated water. In effect, an elevation of this last accelerates the process of disproportionation by lowering its energy of activation. However, it is interesting to note, for certain temperatures, the failover of the reaction of disproportionation in a reaction of oxidation (Test where the performance exceeds the 100%). Since the latter is characterized by the release of a volume of O_2 equivalent to double that which corresponds to a disproportionation.

Table 2. Effect of the temperature on the performance of the disproportionation of H_2O_2. (The reaction time 60min).

Performance in O_2 (%)				
Complex	Ambient	30 °C	40 °C	50 °C
C1	90.6	93.7	100	109.3
C2	81.2	87.5	93.7	109.3

This change in chemical process as a function of temperature, is likely due to the activation of the electronic exchange ligand-metal, thus favoring the oxidation of the active entity of the catalytic converter (the metal center) in Ni (IV). This new species is performing in the reactions of oxidation (Graham Lappin, 1987).

The Study of the Effect of the Addition of a Basic Nitrogen to the Reaction Mixture

It is known that the disproportionation of the oxygenated water increases in the presence of a nitrogen ligand in axial position on metal (Meunier, 1987), (Meunier, 1988). To this effect, we wanted to test the ability catalytic of our complex in the presence of pyridine and imidazole.

In the Presence of Pyridine(C_5H_5N)

The activity of the complexes C1 and C2 in the disproportionation of H_2O_2 has been examined for different concentrations of pyridine. Table 3 consolidates the results of this study. The pH of the solutions is between 7 and 8. The temperature is maintained at the ambient temperature. On the basis of its data, we can argue that the addition of a single ml pyridine is sufficient to enable significantly the reaction of disproportionation of H_2O_2.

Table 3. Effect of the addition of pyridine on the performance of the disproportionation of H_2O_2. (The reaction time 60min).

Performance in O_2 (%)				
Complex	Without pyridine	0.1ml of pyridine	1ml of pyridine	2 ml of pyridine
C1	90.6	93.7	100	90.6
C2	81.2	87.5	96.8	84.3

In the Presence of Imidazole ($C_3H_4N_2$)

The operation is to follow the evolution of the volume of oxygen released during the disproportionation in function of the Ratio Mass of imidazole /mass of the catalytic converter noted mi/mc. The results of this study are illustrated by the Table 4. The pH of the solution in the presence of imidazole is between 7 and 8 and the ambient temperature.

Table 4. Effect of the addition of Imidazole on the performance of the disproportionation of H_2O_2. (The reaction time 60min).

Performance in O_2 (%)					
Complex	$m_i/m_c=0$	$m_i/m_c=0.1$	$m_i/m_c=0.3$	$m_i/m_c=0.7$	$m_i/m_c=1$
C1	90.6	90.6	90.6	93.7	96.8
C2	81.2	81.2	81.2	84.3	90.6

On the basis of these results, the addition of imidazole in a report imidazole /catalytic converter = 1 is sufficient and improves significantly the reaction of disproportionation. Operating in the same conditions already reported, we report in Table 5 all of the results obtained during the conversion of hydrogen peroxide, catalyzed by different complexes of nickel and in the presence of a basic nitrogen. The study is carried out at ambient temperature, in the presence of 1 ml pyridine or in a report mi /mc = 1.

Table5. Effect of the addition of basic nitrogen on the performance of the disproportionation of H_2O_2. (The reaction time 60min).

Performance in O_2 (%)			
Complex	Without the addition of basis	In the presence of pyridine	In presence of imidazole
C1	90.6	100	96.8
C2	81.2	96.8	90.6

It is clear from this study that the presence of a basic nitrogen in the reaction medium is responsible for the substantial improvement of the catalytic activity of our complex and which is reflected by high yields by molecular oxygen. The color change of the reaction mixture during the addition of pyridine or of imidazole testifies of reactions, namely an addition or substitution of ligands on the active site of the complexes.

We have shown that the temperature is a parameter of influence in the disproportionation of the oxygenated water. Indeed, if an elevation of this magnitude accelerates the process of disproportionation, it can even influence in a remarkable manner, by changing the nature of the entity active of the catalytic converter, the process reaction chemical passes from a reaction of disproportionation in a reaction of oxidation. As well, it has proved that the addition of a basic nitrogen (pyridine or the imidazole) in the reaction mixture increases significantly the performance of oxygen and improves the catalytic activity of the complexes.

Catalase-like Activity

We think that the catalytic cycle is similar to the one mentioned in the literature (Kaizer , 2005). It is shown in figure 2. The mechanism is considered in the first place a fixing H_2O_2 molecule via an oxygen atom. The second step is the homolytic cleavage of the -O-O- bond releasing one molecule of water and formation of a radical of higher state of the metal (oxo - π radical cation). The last step is the interaction of a second molecule of H_2O_2 with the oxygen atom carried by the metal radical to release an oxygen molecule and a molecule of water. During this final phase, the metal is reduced and returns to its initial oxidation state (*Kaizer ,2005), (Dede, 2009)*

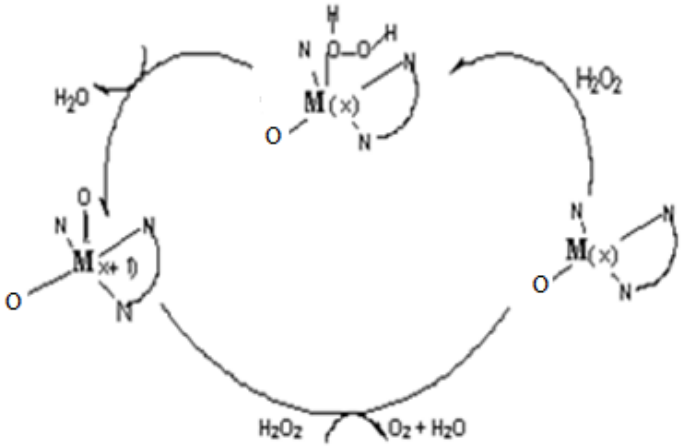

Figure 2 . The catalytic cycle of the dismutation or oxidation of hydrogen peroxide

Conclusion

The catalytic ability of the isolated complexes was examined. The complexes that exhibited catalytic activity displayed a mechanistic similarity to a natural enzyme: catalase, although the activity of this enzyme remains unmatched. In this context, we were interested in the influence of several parameters such as the mass of the catalyst, the addition of nitrogenous base, and the composition of the reaction medium on the conversion of hydrogen peroxide to molecular oxygen. It was found that the addition of pyridine or imidazole (a nitrogenous base) to the reaction mixture significantly increased the yield of oxygen. In fact, it improves the catalase activity of the complexes. The results seem encouraging, regarding the effect of the complexation on catalase- like activity.

Scientific Ethics Declaration

The authors declare that the scientific ethical and legal responsibility of this article published in EPSTEM journal belongs to the authors.

Acknowledgements or Notes

* This article was presented as a poster presentation at the International Conference on Basic Sciences, Engineering and Technology (www.icbaset.net) held in Alanya/Turkey on May 02-05, 2024.

References

Dede, B., Ozmen, I., & Karipcin, F. (2009). Synthesis, characterization, catalase functions and DNA cleavage studies of new homo and heteronuclear Schiff base copper(II) complexes. *Polyhedron*, *28*, 3967–3974.

Graham Lappin, A. (1987). Bromine oxidation of a nickel(II) bis(oxime-imine) complex. Evidence for a single-step outer-sphere two-electron transfer. *Inorganic Chemistry*, *26*, 3089-3094

Hamrani, O., & Hank, Z. (2017). Reaction of thiosemicarbazide with some divalent ions: Synthesis, characterization, molecular modeling, and evaluation of the catalytic and biological activity of the complexes. *Inorganic and Nano-Metal Chemistry*, *47*(7), 1070-1079.

Kaizer, J., Csonka, R., Speier, G., Giorgi, M., Marius, R., Kaizer, J., & Csonka, R . (2005). Synthesis, structure and catalase-like activity of new dicopper(II) complexes with phenylglyoxylate and benzoate ligands. *Journal of Molecular Catalysis A: Chemical*, *236*(18), 12–17.

Kichou, N., Guechtouli, N., Zaater, S., & Hank, Z. (2019). Dft calculations and spectroscopic studies of some ni dimethylglyoxime-based complexes isolated by the hydrothermal process. *Journal of Structural Chemistry* , *59*, 8, 1929 – 1941.

Meunier, B., Cavalho, M. D., & Robert, A. (1987). Catalysis. Aspects of metalloprophyrin-catalyzed oxygenation of hydrocarbons with anionic single oxygen donors, NaOCl and KHSO. *Journal. Molecular*, *41*(1), 185-195.

Meunier, B., De Cavalho, M. E., Bortolini, O., & Momenteau, M. (1988). Proximal effect of the nitrogen ligands in the catalytic epoxidation of olefins by the sodium hypochlorite/manganese(III) porphyrin system. *Inorg. Chem.*, *27*(1), 161-164 .

Salem, I. A., EL-maazawi, M., & Zaki, A. B. (2000). Kinetics and mechanisms of decomposition reaction of hydrogen peroxide in presence of metal complexes. *International Journal of Chemical Kinetics*, *32*, 643-666.

Shivankar, V. S., & Thakkar, N. V. (2005). Decomposition of hydrogen peroxide in presence of mixed ligand Cobalt(II) and Nickel(II) complexes as catalysts. *Journal of Scientific and Industrial Research*, *64*, 496-503.

Syed, Y., & Manna, K. (2019). Sructural, Electronic, and spectral properties of metal dimethylglyoximato [$M(DMG)_2$; M = Ni^{2+}, Cu^{2+}] complexes: A comparative theoretical study. *J.Phys. Chem.* , *123*, 42, 9166–9174.

Author Information

Noura Kichou
Department of Chemistry, Faculty of Sciences, University Mouloud Mammeri of Tizi-Ouzou, Tizi-Ouzou, Algeria
Laboratory of Electrochemistry-Corrosion, Metallurgy and Mineral Chemistry, Faculty of Chemistry, USTHB, BP 32 El Alia, Algiers, Algeria.
Contact e-mail: *noura.kichou@ummto.dz*

Nabila Guechtouli
M'hamed Bougara Boumerdes University, Boumerdes 35000, Algeria

Anissa Merrad
University Mouloud Mammeri of Tizi-Ouzou
Tizi-Ouzou, Algeria

Zakia Hank
Laboratory of Electrochemistry-Corrosion, Metallurgy and Mineral Chemistry, Faculty of Chemistry, USTHB, BP 32 El Alia, Algiers, Algeria

To cite this article:

Kichou, N. Guechtouli , N. Merrad, A. & Hank, Z. (2024). Decomposition of hydrogen peroxide in presence of dimethylglyoximato-nickel complexes as catalysts: Catalase-like activity. *The Eurasia Proceedings of Science, Technology, Engineering & Mathematics (EPSTEM), 28*, 241-245.

The Eurasia Proceedings of Science, Technology, Engineering & Mathematics (EPSTEM)
ISSN: 2602-3199

The Eurasia Proceedings of Science, Technology, Engineering & Mathematics (EPSTEM), 2024

Volume 28, Pages 246-251

ICBASET 2024: International Conference on Basic Sciences, Engineering and Technology

Machine Learning Approach for Predicting Bead Geometry of Stainless Steel in Wire arc Additive Manufacturing

Harsh Shah
Pandit Deendayal Energy University

Kishan Fuse
Pandit Deendayal Energy University

Abstract: Wire arc additive manufacturing (WAAM) employs an electric arc to melt wire feedstock, making it a method within additive manufacturing (AM). It deposits material layer by layer to build up a part. The present study investigated the application of machine learning classification-based models for estimating bead width and bead height of stainless-steel parts fabricated using WAAM. The input parameters (voltage, current, wire feed rate, and travel speed) were considered as input to algorithms. Training and testing were performed for 98 experimental data sets from peer-reviewed literature. The machine learning classification models, K-nearest neighbors, decision tree with gini index as criteria, and random forest were evaluated. The ML model performance was evaluated utilizing statistical metrics, including accuracy, F1 score, precision, and recall. The decision tree classifier exhibited the highest accuracy of 87.8% for bead width and 84.7% for bead height. The findings offer valuable insights into leveraging ML techniques to enhance the performance and accuracy of predictive models within WAAM-based AM.

Keywords: Machine learning, Wire arc, Bead geometry of stainless steel,

Introduction

Traditional manufacturing techniques are gradually being replaced by additive manufacturing (AM). The AM can be divided into several kinds according to the production technique, such as binder jetting, sheet lamination, powder bed fusion, directed energy deposition (DED), etc. (Srivastava et al.,2022). In contrast to polymeric material additive manufacturing, metal AM is very new and requires careful consideration. The two primary categories of AM procedures for metal are wire-based and powder-based methods (Li, 2021). Wire arc additive manufacturing (WAAM), one of the various DED technologies available today, is the most significant DED technique. Large-scale fabrication of metallic components is made possible by WAAM, which includes GMAW, GTAW, and PAW. Aerospace, automotive, oil and gas, nuclear, shipbuilding, heavy fabrication, and other sectors stand to benefit greatly from WAAM's potential to revolutionize production processes since it uses robots with gantry systems and floor-mounted tracks to make components of any size (Yaseer, 2021). Additionally, there has been a rise in studies in the field of AM utilizing machine learning (ML). This is because ML can effectively save costs, optimize the production process, and increase quality. Numerous researchers seemed to like ML techniques such as decision tree (DT), random forest (RF), and k-nearest neighbour (KNN) for defect detection and bead geometry prediction. The prediction of bead width (BW) and bead height (BH) using the RF ML technique was done and showed higher accuracy (Sharma et al.,2023). RF and neural networks (NN) were used to predict YS and UTS for WAAM 316L steel parts. They used performance evaluators such as R2, Adj R2, and RMSE for RF (Mamedipaka & Thapliyal, 2024). For NN, performance was evaluated by loss and mean absolute error. ML models such as DT, RF, XGBoost algorithm, ANN, and linear regression were employed on the WAAM part fabricated using Al 5356 alloy. They reported better performance for ANN than XGBoost in predicting BH. For BW prediction, they found linear regression better performing ML model than

ANN (Chandra et al., 2023). The developed predictive models effectively crafted new prediction algorithms for identifying defects within WAAM deposited layer (Cheepu, 2022). Gaussian process regressor was used to predict melting efficiency in WAAM. They used input variables such as diameter of feeding wire, feeding speed of the wire, nozzle speed, and net power to calculate melting efficiency (Barrionuevo et al., 2022). Out of all the ML models, this study used the DT, RF, and KNN on 98 experimental data sets. The programming language employed was Python. The results of ML computations were visualized using packages like scikit-learn, NumPy, pandas, and Matplotlib (Oh et al., 2022).

Machine Learning Classification Models

The present study investigated three ML classification models as DT, RF, and KNN. This section highlights detail about all three ML techniques. The Decision Tree Classification Algorithm works by asking some binary questions to predict the output variable through the input variables. These questions create a hierarchical image resembling a tree, starting with the first classification at the top i.e. the root node and further into others. With each classifier, the data is divided into two subsets based on the response, which will continue until the tree's leaf node provides a definitive prediction. The main objective of the DT classifier is to formulate questions that yield the most relevant data regarding the output variable while asking very few possible questions. This is achieved by taking the optimal question to ask at each branching point in the tree, based on a predetermined criterion (e.g., Gini index). After the decision tree is generated, new data can be predicted by tracing the path from the root to the relevant leaf node. Each leaf node reflects to a specific value of the response, and the value associated with that leaf node gives the predicted output.

Random Forest is a widely utilized supervised machine learning framework constructed upon an ensemble of multiple trees. Renowned for its rapid processing speed and robustness against outliers, RF excels in analyzing intricate nonlinear relationships. Throughout the training phase, RF discerns patterns to establish connections between the input (X) and output (Y) variables, overseeing the learning process (Mamedipaka & Thapliyal, 2024).

The KNN algorithm runs by computing the distance between n training samples and the new specimen, subsequently considering the K samples with the smaller distances to the new specimen. The parameter K (k=10), defined by the user, determines the number of training samples utilized for prediction. Euclidean distance can be gained by computing the distance between the new specimen and a training sample. Subsequently, upon identifying the nearest K training samples, the predominant label among these K samples is used to establish the predicted labels. For example, the new specimen will be labelled as 0 if most of the nearest K samples have a label of 0; similarly, the new specimen will be labelled as 1, if majority have a label of 1 (Sharma et al., 2023).

Methodology

In the present study, 98 datasets from peer-reviewed literatures (Chaudhari et al., 2022; Le et al.,2021; Kumar & Maji, 2020; Sharma et al., 2023b; Vora et al., 2022; Yadav et al., 2024) was analysed using 10-fold cross-validation. Further, the dataset was subdivided into 10 subsets. This made it possible to train and test the created model ten times, striking a compromise between computing efficiency and variance reduction. Bead width and bead height were considered to be the response parameters in the experimental dataset. The schematic of the BW and BH is as shown in Figure 1. The input parameters in the dataset were wire feed rate (m/min), travel speed (mm/min), current (A), and voltage (V). The output parameters were bead width (mm) and bead height (mm). Before evaluation, the datasets underwent pre-processing, wherein missing values for input variables were substituted with their respective mean values.

The dataset was subjected to machine learning classification models i.e. DT, RF and KNN. The output was classified as 0 or 1 based upon corresponding average values. The average of bead width was 6.78mm. The BW was classified as 1 when the it was less than 6.78 mm and 0 when greater than 6.78 mm. The average of bead height was 3.8mm. The BH was classified as 1, when it was less than 3.8 mm and 0 when it was greater than 3.8 mm. To assess and collate the effectiveness of these classification models, four primary metrics were considered: accuracy, F1 score, precision, and recall. The accuracy evaluates algorithm's performance by measuring the proportion of correctly classified instances among all evaluated instances. The ratio of true positives to all projected positives is called precision, while the ratio of genuine positives to all actual positives is called recall. An overall evaluation of the performance of the classification algorithm was provided by the F1

score, which is a harmonic mean of precision and recall. Additionally, a confusion matrix, which represents a matrix that contrasts the genuine labels of a particular test dataset with the labels predicted by the algorithm. It is a necessary evaluation tool for classification algorithms. A confusion matrix as shown in Figure 3 was generated for all the instances to get the insights of the DT, RF, and KNN algorithm (Mishra et al., 2024).

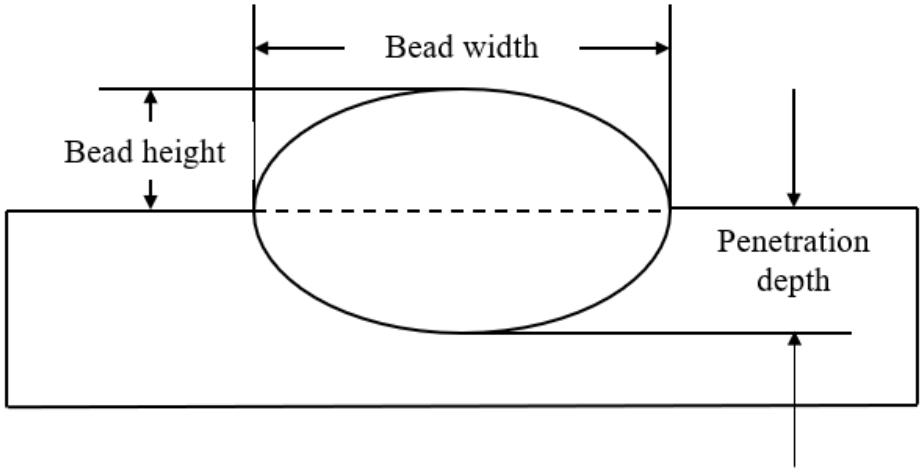

Figure 1. Schematic of bead width and bead height

Hyper-parameters Tuning

The scikit-learn library comes with pre-set hyperparameters for all machine learning algorithm, yet it doesn't ensure the optimal parameter values for a specific problem. Consequently, tuning hyperparameters becomes crucial in enhancing the predictive accuracy of ML models. A variety of hyperparameter optimisation algorithms, such as grid search, randomised search, and bayesian search are available with the scikit-learn package. To obtain the best hyperparameters for the ML algorithms, the present study utilized both manual techniques and scikit-learn packages. Table 1 lists the optimised values of critical hyper parameters for each ML model. Furthermore, to enhance the ML algorithms adaptability, K-fold cross-validation was utilised during implementation. The training dataset was subjected to a tenfold cross-validation for both training and validation purposes for all three studied ML models.

Table 1. Hyper-parameter optimized for ML algorithms

SN	ML Model	Hyper Parameter
1	Decision Tree	criterion: gini, splitter: best, max_feature: auto
2	Random Forest	n_estimators:100, criterion: gini, max_depth: 2
3	K-Nearest Neighbour	n_neighbour:10, n_jobs: -1

Results and Discussion

Prediction of Bead Width

To forecast bead width, the statistical metrics (Precision, Recall, and F1-score) evaluating the performance of three ML models on both training and testing data are consolidated in Table 2. KNN obtained the lowest value of the key metrics which indicated the poor labelling of algorithm and poor overall performance. While DT obtained the highest value of key metrics which can be validated using confusion matrix shown in Figure 3. The highest accuracy in predicting the bead width was resulted by DT is 87.8%, followed by RF 77.4% and KNN being the lowest at 70.2%. A comparison of accuracy for all the three algorithms is shown in Figure 2.

Table 2. Precision, recall and F1-score of different classifier model for bead width

Classifier	Precision	Recall	F1-Score
Decision Tree	0.907	0.875	0.876
Random Forest	0.831	0.774	0.762
K-Nearest Neighbour	0.770	0.702	0.702

Figure 2. Bar chart comparison of the accuracy of different ML models for (a) bead width (b) bead height

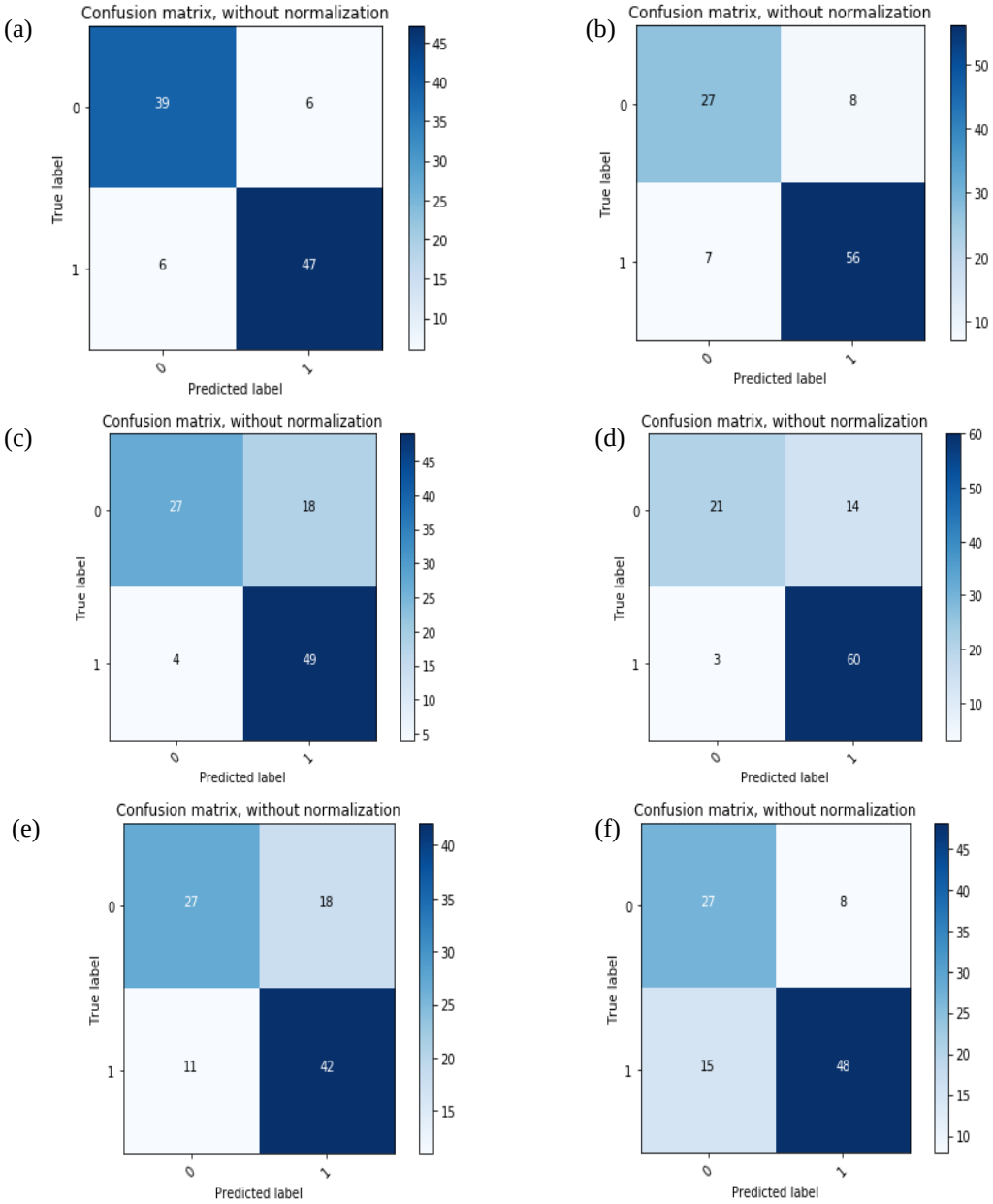

Figure 3. Confusion matrix comparing the actual and predicted values from the A) Decision Tree for bead width B) Decision Tree for bead height C) Random Forest for bead width D) Random Forest for bead height E) K-Nearest Neighbour for bead width F) k-Nearest Neighbour for bead height

Prediction of Bead Height

For predicting the bead height, the value of statistical metrics (Precision, Recall, and F1-score) for measuring the performance of three ML models for both training and testing are outlined in Table 3. The lowest value of key metrics is obtained for KNN which can be due to imbalanced data, whereas DT showed great results in labelling the algorithm. DT achieved the highest accuracy of 84.7% for prediction of bead height, followed by RF with 82.6% accuracy and KNN having the lowest accuracy of 76.4%. Figure 2 shows the accuracy comparison of all the three algorithms.

Table 3. Precision, recall and F1-score of different classifier model for bead height

Classifier	Precision	Recall	F1-Score
Decision Tree	0.856	0.847	0.843
Random Forest	0.841	0.826	0.807
K-Nearest Neighbour	0.822	0.764	0.770

Conclusion

In summary, this research has effectively explored the utilization of supervised ML algorithms for estimating the bead width and bead height of WAAM parts fabricated using stainless steel. By investigating 98 dataset and utilizing input variable such as voltage, current, wire feed rate and travel speed, we have evaluated the accuracy and effectiveness of three distinct supervised classification algorithms: Decision Tree, Random Forest and KNN. The conclusion from the present study are:

- The result illustrates that decision tree outperforms the other algorithm with the accuracy of 87.8% for bead width and 84.7% for bead height. This underscores the decision tree algorithm's exceptional capacity to distinguish between the two categories of bead geometry in the dataset, rendering it the preferred option for classification within this research framework.
- This study sets the foundation for forthcoming research aimed at enhancing these algorithms, fine-tuning variable, and broadening the utilization of ML in additive manufacturing. The ultimate goal is to enhance the standard and reliability of 3D-printed components.

Scientific Ethics Declaration

The authors declare that the scientific ethical and legal responsibility of this article published in EPSTEM journal belongs to the authors.

Acknowledgements or Notes

* This article was presented as an oral presentation at the International Conference on Basic Sciences, Engineering and Technology (www.icbaset.net) held in Alanya/Turkey on May 02-05, 2024.

References

Barrionuevo, G. O., Sequeira-Almeida, P. M., Ríos, S., Ramos-Grez, J. A., & Williams, S. W. (2022). A machine learning approach for the prediction of melting efficiency in wire arc additive manufacturing. *The International Journal of Advanced Manufacturing Technology, 120*(5), 3123–3133.

Chandra, M., Vimal, K. E. K., & Rajak, S. (2023). A comparative study of machine learning algorithms in the prediction of bead geometry in wire-arc additive manufacturing. *International Journal on Interactive Design and Manufacturing (IJIDeM)*, 1-14.

Chaudhari, R., Parmar, H., Vora, J., & Patel, V. K. (2022). Parametric study and investigations of bead geometries of GMAW-based wire–arc additive manufacturing of 316L stainless steels. *Metals, 12*(7), 7.

Cheepu, M. (2023). Machine learning approach for the prediction of defect characteristics in wire arc additive manufacturing. *Transactions of the Indian Institute of Metals*, *76*(2), 447–455.

Kumar, A., & Maji, K. (2020). Selection of process parameters for near-net shape deposition in wire arc additive manufacturing by genetic algorithm. *Journal of Materials Engineering and Performance, 29,* 3334–3352.

Le, V. T., Mai, D. S., Doan, T. K., & Paris, H. (2021). Wire and arc additive manufacturing of 308L stainless steel components: Optimization of processing parameters and material properties. *Engineering Science and Technology:An International Journal, 24*(4), 1024-1025.

Li, Y. (2021). *Machine learning based defect detection in robotic wire arc additive manufacturing.* (Doctoral dissertation). University of Wollongong Thesis Collection 2017.

Mamedipaka, R., & Thapliyal, S. (2024). Data-driven model for predicting tensile properties of wire arc additive manufactured 316l steels and its validation. *Journal of Materials Engineering and Performance, 33*(3), 1083–1091.

Mishra, A., Jatti, V. S., Messele -Sefene, E., Jatti, A. V., Sisay, A. D., Khedkar, N. K., Salunkhe, S., Pagáč, M., & Abouel-Nasr, E. S. (2024). Machine learning-assisted pattern recognition algorithms for estimating ultimate tensile strength in fused deposition modelled polylactic acid specimens. *Materials Technology, 39*(1), 2295089.

Oh, W. J., Lee, C. M., & Kim, D. H. (2022). Prediction of deposition bead geometry in wire arc additive manufacturing using machine learning. *Journal of Materials Research and Technology, 20,* 4283–4296.

Sharma, R., Raj Paul, A. R., Mukherjee, M., Vadali, S., Kumar Singh, R., & Sharma, A. K. (2023a). Forecasting of process parameters using machine learning techniques for wire arc additive manufacturing process. *Materials Today: Proceedings, 80,* 248–253.

Srivastava, M., Rathee, S., Patel, V., Kumar, A., & Koppad, P. G. (2022). A review of various materials for additive manufacturing: Recent trends and processing issues, *Journal of Materials Research and Technology, 21,* 2612-2641.

Vora, J., Parmar, H., Chaudhari, R., Khanna, S., Doshi, M., & Patel, V. (2022). Experimental investigations on mechanical properties of multi-layered structure fabricated by GMAW-based WAAM of SS316L. *Journal of Materials Research and Technology, 20,* 2748–2757.

Yadav, A., Srivastava, M., Jain, P. K., & Rathee, S. (2024). Investigation of bead morphology and mechanical behaviour for metal inert gas welding-based WAAM in pulsed mode metal transfer on 316LSi stainless steel. *Journal of Adhesion Science and Technology, 38*(5),738-769.

Yaseer, A. (2021). *Process planning of robotic wire arc additive manufacturing (WAAM) using machine learning*. (Unpublished Master's thesis). Texas State University, Texas.

Author Information

Harsh Shah
Pandit Deendayal Energy University, Gandhinagar, 382007, India
Contact e-mail: *Harshkshah02@gmail.com*

Kishan Fuse
Pandit Deendayal Energy University, Gandhinagar, 382007, India

To cite this article:

Shah, H., & Fuse, K. (2024). Machine learning approach for predicting bead geometry of stainless steel in wire arc additive manufacturing. *The Eurasia Proceedings of Science, Technology, Engineering & Mathematics (EPSTEM), 28,* 246-251.

The Eurasia Proceedings of Science, Technology, Engineering & Mathematics (EPSTEM)
ISSN: 2602-3199

The Eurasia Proceedings of Science, Technology, Engineering & Mathematics (EPSTEM), 2024

Volume 28, Pages 252-258

ICBASET 2024: International Conference on Basic Sciences, Engineering and Technology

Design and Calculation of Products from Composite Materials Using Software

Sara Srebrenkoska
Goce Delcev University

Vineta Srebrenkoska
Goce Delcev University

Marija Cekerovska
Goce Delcev University

Todor Cekerovski
Goce Delcev University

Abstract: This article analyzes six types of composite pipes that are good replacements for corrosive steel and metal pipes for oil, gas, and water. The analysis of the six samples of composite pipes was done using the software program Hoffman Engineering, which is intended for the design and calculation of various types of products made of composite materials. For the analysis of the six composite pipes, the same diameter and the same length were taken, and variable parameters are: the type of material from which the composite pipes are made (carbon/epoxy, carbon-glass/epoxy and glass/epoxy), and the angle of winding of the fibers (10º and 90º degrees). Using the Hoffman Engineering software package, an analysis of the durability of the six differently designed composite pipes at high internal pressure was performed. The same conclusion was obtained from all analyses: the high internal pressure resistance of composite pipes is highly dependent on the fiber winding angle and the type of fibers used. Composite pipes obtained with a fiber winding angle of 90º have twice the internal pressure resistance compared to composite pipes obtained with a fiber winding angle of 10º. Composite pipes based on carbon fibers have the highest resistance to internal pressure, then composite pipes based on hybrid materials (glass and carbon fibers) and finally composite pipes based on glass fibers. Finally, a comparison was made with the obtained laboratory results for the same composite pipes. The same conclusion was obtained from all analyses: the high internal pressure resistance of composite pipes is highly dependent on the fiber winding angle and the type of fibers used. The composite pipes obtained by this process are durable and resistant to very high pressures.

Keywords: Composite pipes, Software program, Material type, Internal pressure, Winding angle.

Introduction

The production of composite pipes is of great importance because it refers to standard types of composite pipes that are in direct competition with older types, such as steel pipes. The industrial importance of the process is great because the resulting composite pipes are a good substitute for corrosive steel and metal pipes for oil, gas, and water (Osanna, 2004). In addition, the pipes obtained by this process are durable, even at high pressures.

Most often, the improvements in the processes to produce composite materials, which primarily have a technological, technical, and economic effect, are seen in the more rational use of raw materials and auxiliary materials, and thus also in the waste and harmful substances that, because of the process, are either controlled or

uncontrolled, thrown out, or disposed of in the environment (Chyng, 2010). If the processes to produce composites are more compact and the stages of production are related to efficiency in the use of equipment, the time cycle per unit of the product is shorter. (Chyng, 2010). It can be concluded that in optimized, improved, or advanced processes to produce composite materials, the cost of the energy consumed per unit of product is lower (Mazumdar, 2002).

Computer-aided design is a standard part of the training of today's engineer, who has at his disposal the widely available packages for modeling, optimization, and selection of materials and processes. The software package for the selection of materials and processes relies on a database of attributes of materials and processes and their mutual compatibility, which allows the search and selection of those materials and processes that best meet the requirements of an appropriate design (Boccara, 2010).

Fiber Winding Process

Industrial processes to produce composite materials are in continuous development with a constant tendency to introduce new processes and technological solutions in them. The process of winding fibers and obtaining composite pipes is a relatively new process that presents a challenge for industrial facilities working with composite materials (Peters, 1998). The choice of procedures and processing conditions for obtaining a composite material are of particular importance because they greatly affect the properties of the obtained material and the price of the final product. The production of composite structures is often associated with obtaining products of inconsistent quality (Basu, 2004). It is typical of these types of materials that results from their anisotropic nature. Engineers who work with processes for obtaining such materials have the freedom to design the processes for obtaining composite structures depending on the final requirements for meeting certain properties (Beyreuther, 2010). Composite pipes are often used as a good substitute for corrosive steel and metal pipes for oil, gas and water, and also as tanks, and therefore the requirements they have to meet are related to their durability and resistance to high internal pressures. Obtaining composite pipes that will have unchanging (constant) quality, light weight, and at the same time will be durable and durable at high pressure and competitive with the price of the market has encouraged various activities in that area (Bernard, 1991).

Method

In this paper, the analysis of six samples of composite pipes is done using the software program Hoffman Engineering, which is intended for the design and calculation of different types of products from composite materials. The standard ISO 11439.2000-ASTM D1599 (Standards, 2000) was used in the analysis of the composite pipes. According to this standard, one of the basic characteristics that should be satisfied is the internal burst pressure as well as the tension ratio of the fibers - the reinforcement. The minimum burst pressure should not be lower than the values given in Table 1.

Table 1. Minimum burst pressure and stress ratio for pipes (Standards, 2000)

Fiber type	Stress ratio	Crushing pressure(bars)
Glass Fibers	3.65	180
Carbon Fiber	2.35	117
Hybrid Fibers	3.0*	148 *

*The stress ratio and the braking pressure should be calculated according to the table

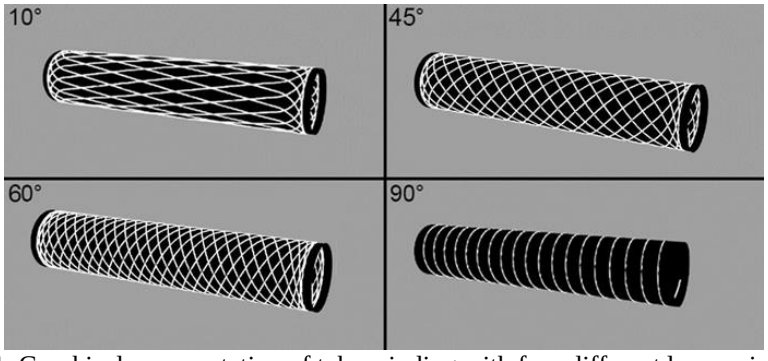

Figure 1. Graphical representation of tube winding with four different layer orientations

By applying the Hoffman Engineering software package, the wall of the composite pipe, which consists of several layers, is first designed or structured. The composite pipe is constructed from multiple layers. Each layer is made up of fibers placed at a specific angle. The fibers in the layers can be placed at the same or different angles, thus allowing the composite pipes to withstand the intended internal and external loads, as shown in figure (Figure 1). Composite pipes are rarely constructed of layers where the fibers are placed at only one angle. For a composite material to withstand different loads in different directions, a layered composite is designed with a combination of the fibers in the layers at multiple angles (Beyreuther, 2010). If a composite part must withstand internal pressure, then the stresses in the radial direction are much higher than the stresses in the longitudinal direction.

Then, in the same software, the characteristics of the composite layers are determined, and the expected internal burst pressure of the composite pipe is calculated. Through multiple calculations of different variants of the structure of the layers and their optimization, the optimal method of winding a composite pipe with characteristics that will meet the requirements of the standard is determined (Koussio, 2004). The input variables in that optimization are the types of raw materials (fibers and resin), the winding angles of the separate layers, the number of layers, and their arrangement (Boccara, 2010). Within the framework of this paper, six composite pipes were analyzed, and the same diameter and length were taken for them. The variable parameters are:

- the type of material from which the composite pipes are made (carbon/epoxy, carbon-glass/epoxy, and glass/epoxy) and
- the angle of winding the fibers (10º and 90º degrees).

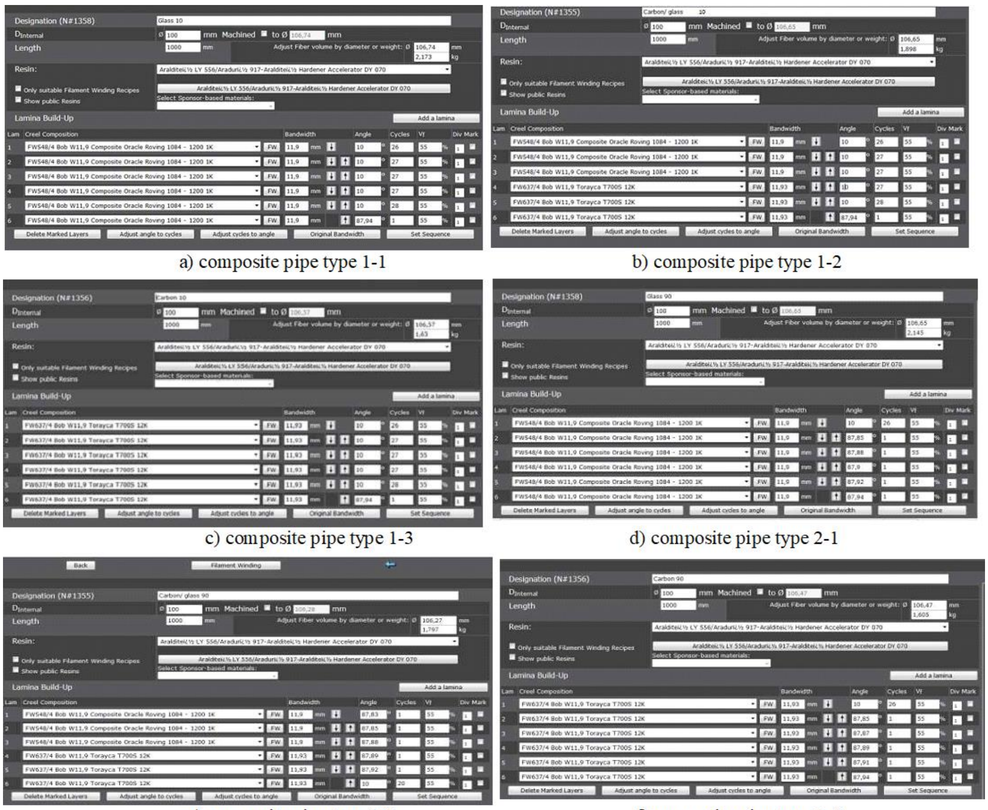

a) composite pipe type 1-1 b) composite pipe type 1-2

c) composite pipe type 1-3 d) composite pipe type 2-1

e) composite pipe type 2-2 f) composite pipe type 2-3

Figure 2. Hoffman Engineering software application - creating layers of different six types of composite pipes

Table 2. Composite wall structure for six types of composite pipes

Types of composite pipe					
1-1	1-2	1-3	2-1	2-2	2.-3
Radial 90^o	Radial 90^o	Radial 90^o	Diagonal 10^o	Diagonal 10^o	Diagonal 10^o
Diagonal 10^o	Diagonal 10^o	Diagonal 10^o	Radial 90^o	Radial 90^o	Radial 90^o
Diagonal 10^o	Diagonal 10^o	Diagonal 10^o	Radial 90^o	Radial 90^o	Radial 90^o
Diagonal 10^o	Diagonal 10^o	Diagonal 10^o	Radial 90^o	Radial 90^o	Radial 90^o
Diagonal 10^o	Diagonal 10^o	Diagonal 10^o	Radial 90^o	Radial 90^o	Radial 90^o
Diagonal 10^o	Diagonal 10^o	Diagonal 10^o	Radial 90^o	Radial 90^o	Radial 90^o

Next figure (Figure 2) presents windows of the software application in which data is entered for building the layers of the composite wall of all six composite pipes separately, and table (Table 2) shows the structure of the composite walls for all six samples.

The composite wall structure consists of three types of winding layers: radial layer, diagonal (or helical) layer and transition layer (Allaire, 2007). The coiling of one type of tube in production at a different angle is shown in the figure (Figure 3). The transition layer is of special importance for continuous winding with an alternating change of the winding angle of each successive layer (for example, radial with diagonal and vice versa). In this way, the entire winding process is continuous from start to finish, without the need to stop the process and manually adjust the starting position of the machine for each layer separately.

a) fiber winding angle 10 º

b) fiber winding angle 90 º

Figure 3. Production of composite pipes with different fiber winding angle

After the layers are entered into the software program, the loads that the composite pipe should withstand are entered, and then the criterion is selected according to which we want to check the resistance of the composite pipe to the predicted load, i.e., internal pressure. In the next figure (Figure 4), one of the interactive windows of the application is presented, in which part of the data needed for the analysis of the composite structure (pipes) is entered

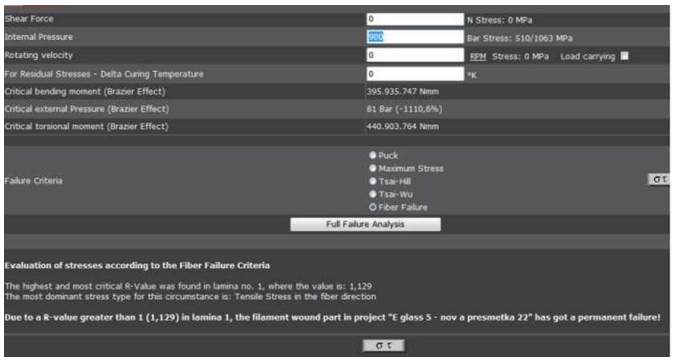

Figure 4. Hoffman Engineering software application - definition of analysis parameters

In the software application, there are several criteria by which the durability of composite pipes at high internal pressure can be checked: Puck, Maximum Stress, Tsai-Hill, Tsai-Wu, and Fiber Failure. When testing the resistance to maximum internal pressure in composite tanks and pipes, several so-called premature cracks occurred in the layered composite. Cracking of the matrix occurs at the beginning, then of the fibers that are in a direction different from the direction of the load, and then certain layers give way until complete cracking of the

tube occurs, i.e., the composite. For composite pipes, the initial early cracks are not important, but the final complete crack at a given pressure is significant, i.e., burst pressure. When using glass fibers, the maximum allowable pressure is taken with a safety factor of 2.75 to 3.65 times greater than the working one for which the tube is designed, while when using carbon fibers, 2.35 times larger than the working one. However, with any software calculation for the durability of the designed composite, it is always necessary to do experimental testing to confirm the reliability of the obtained software results.

Within this paper, when applying the Hoffman Engineering software, the "Tsai Wu" criterion was chosen as a criterion for the calculation and analysis of the characteristics of the six composite pipes. This criterion was chosen based on data from practice, according to which it has been proven that it gives accurate data, that is, closest to the experimentally obtained data.

Results and Discussion

Durability analyses of six differently designed composite pipes at high internal pressure were performed using the Hoffman Engineering software package. Namely, when designing these composite pipes, the variable parameters were the types of materials, i.e., the reinforcing fibers and the angle of fiber winding, while the length and diameter were the same for six composite tubes. Therefore, the obtained results of the six differently designed composite tubes with different fiber winding angles (10º and 90º degrees) using the Hoffman Engineering software package are shown in the next figure (Figure 4).

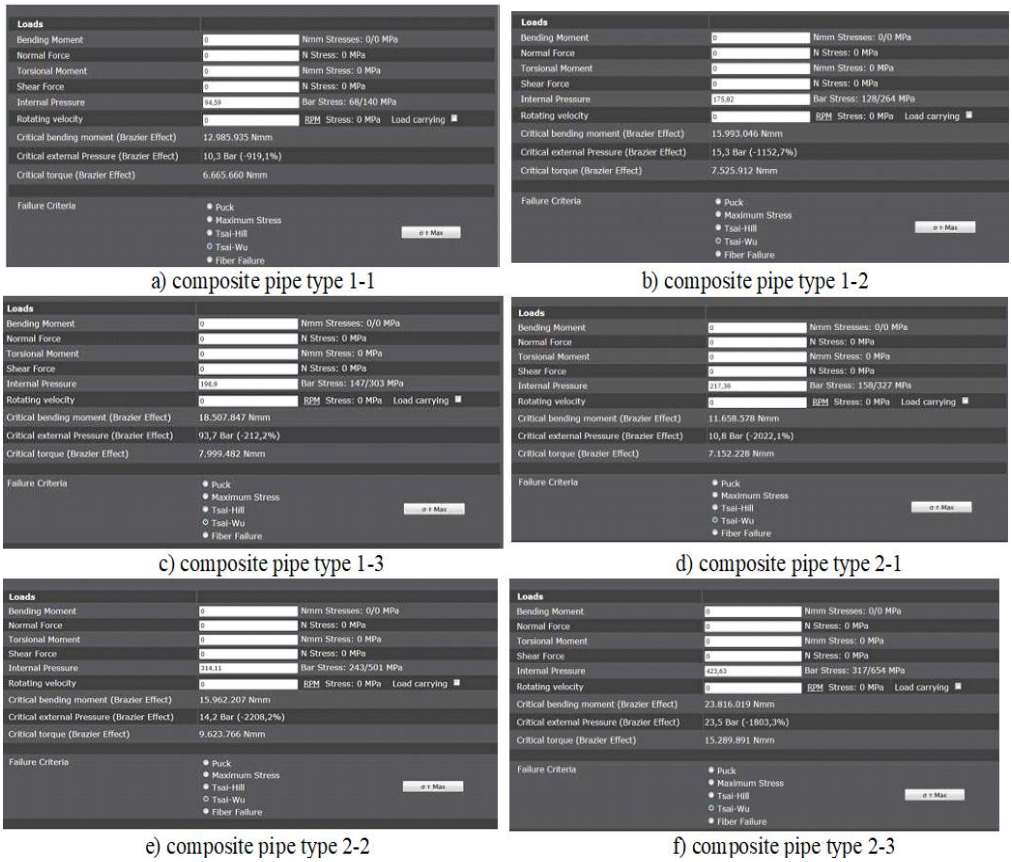

Figure 4. Results of the calculation and analysis of various types of composite pipes

After the calculations, the results of the analysis for the internal braking pressure of six types of composite pipes, which are the subject of analysis in this article, are shown in the table (Table 3). According to the table, all composite pipes meet the requirement according to the ISO 11439.2000 standard (Standards, 2000), except for type 1-1, where the winding angle of the fibers is 10º and the type of fibers is glass. This data indicates that the winding angle has the greatest effect on the durability of composite sheets at high pressure. Namely, the composite tubes obtained with a fiber winding angle of 900 show much higher internal failure pressures. From the fiber type analysis, it can then be concluded that the composite tubes obtained with carbon fibers show a much higher value of internal burst pressure than the composite tubes wound with glass fibers. Therefore, in

these composite pipes, the number of layers can be freely reduced, thus reducing the thickness of the composite wall and the weight of the composite pipe while satisfying the requirements of the standard. Composite pipes obtained from a hybrid material of glass and carbon fiber show slightly lower internal pressures of endurance compared to composite pipes based on carbon fiber but are higher than those based on glass fiber. Also, with these composite pipes, it is possible to reduce the layers and reduce the thickness and weight of the composite pipe. However, for all analyzed tubes with a fiber winding angle of 10º, a lower internal burst pressure was observed compared to tubes with a fiber winding angle of 90º. For the composite pipe type 1-1 to meet the requirements of the standard, it is necessary to add more layers, which in turn will increase thickness and weight.

Table 3. Results of calculated internal pressure endurance of six types of composite pipes

Composite tube type	Calculated internal burst pressure (bar)	Minimum burst pressure according to ISO 11439.2000 (bar)	Evaluation of satisfaction of requirements from the Standard
1-1	94.59	180	It doesn't fulfill
1-2	175.82	148	Fulfills
1-3	198.9	117	Fulfills
2-1	217.38	117	Fulfills
2-2	314.41	180	Fulfills
2-3	423.63	180	Fulfills

The obtained results confirm our previous research (Srebrenkoska, 2023), where it was obtained through experiments that the winding angle has the most influence on the durability of composite pipes at high pressure. The same conclusion is reached, which is that optimal results would be obtained for composite pipes with a fiber winding angle greater than 10º and less than 90º. It is expected that composite pipes will have optimum characteristics when the winding angle is about 50º.

Conclusion

With the help of the Hoffman Engineering software package, six types of composite pipes were analyzed, where the following parameters were considered: the constituent materials and the winding angle of the fibers. Whereas the composite pipes obtained with a fiber winding angle of 90º have two times higher resistance to internal pressure compared to the composite pipes obtained with a fiber winding angle of 10º. Composite pipes based on carbon fibers have the highest resistance to internal pressure, followed by composite pipes based on hybrid materials (glass and carbon fibers), and finally, composite pipes based on glass fibers. Based on all the analyses made, i.e., laboratory tests and the software package, it was concluded that the resistance to the high internal pressure of composite pipes is highly dependent on the fiber winding angle and the type of fiber applied.

Scientific Ethics Declaration

The authors declare that the scientific ethical and legal responsibility of this article published in EPSTEM journal belongs to the authors.

Acknowledgements or Notes

* This article was presented as an oral presentation at the International Conference on Basic Sciences, Engineering and Technology (www.icbaset.net) held in Alanya/Turkey on May 02-05, 2024.

References

Akkus, N., Genc, G., & Girgin, C. (2008). Control of the pretension in filament winding process. *Acta Mechanica et Automatica*, *2*(3), 5-10.

Allaire, G., & Craig, A. (2007). *Numerical analysis and optimization an introduction to mathematical modelling and numerical simulation.* Oxford University Press.

Bernard, E. (1991). *Path generator for filament winding of asymmetric fibre composite components*. University of Ottawa.

Basu, R. (2004). *Implementing quality – a practical guide to tools and techniques.* UK, Thomson Learning.

Boccara, N. (2010). *Modeling complex systems*. Springer Science+Buisness Media LLC.

Beyreuther, R., Brunig, H. (2010). *Dynamics of fiber formation and processing*. Berlin: Springer.

Chyng, D., L. (2010). *Composite materials.* London: Springer-Verlag Limited.

ISO -International Standards. (2000). *ISO 11439.2000* (2nd ed.). Retrieved from https://www.iso.org/

Koussio, S. (2004). *Filament winding: a unified approach*. DUP Science.

Mazumdar, S., K. (2002). *Composites manufacturing - materials, products and process engineering*. CRC Press LLC.

Osanna, P., H., Durakbasa, M., N., Afjehi-Sasat, A. (2004). *Quality in industry*. Vienna University of Technology, TU AuM.

Peters. S., T., Tarnopol'skii, Yu., M., Beil, A., I. (1998). Handbook of composites. In *Filament winding*, (pp.456-475). US: Springer.

Srebrenkoska, S., Kochoski, F., Srebrenkoska, V., Risteska, S., & Kotynia, R. (2023). Effect of process parameters on thermal and mechanical properties of filament wound polymer-based composite pipes. *Polymers*, *15*(13), 2829.

Author Information

Sara Srebrenkoska
Faculty of Mechanical Engineering - Goce Delcev University, Stip, I Krste Misirkov 10-A, Stip 2000
Republic of North Macedonia
Contact e-mail: *sara.srebrenkoska@ugd.edu.mk*

Vineta Srebrenkoska
Faculty of Technology - Goce Delcev University, Stip, Krste Misirkov 10-A, Stip 2000
Republic of North Macedonia

Marija Cekerovska
Faculty of Mechanical Engineering - Goce Delcev University, Stip, Krste Misirkov 10-A, Stip 2000
Republic of North Macedonia

Todor Cekerovski
Faculty of Electrical Engineering, Goce Delcev University, Stip, Krste Misirkov 10-A, Stip 2000
Republic of Macedonia

To cite this article:

Srebrenkoska, S., Srebrenkoska, V., Cekerovska, M. & Cekerovski, T. (2024). Design and calculation of products from composite materials using software. *The Eurasia Proceedings of Science, Technology, Engineering & Mathematics (EPSTEM), 28,* 252-258.

The Eurasia Proceedings of Science, Technology, Engineering & Mathematics (EPSTEM)
ISSN: 2602-3199

The Eurasia Proceedings of Science, Technology, Engineering & Mathematics (EPSTEM), 2024

Volume 28, Pages 259-276

ICBASET 2024: International Conference on Basic Sciences, Engineering and Technology

Utilization of Crushed Waste Glass as a Partial Replacement for Sand in Cement Mortar for a Sustainable Environment

Filibin Ali Hassan
Cyprus International University

Ayse Pekrioglu-Balkis
Cyprus International University

Abstract: The disposal of non-biodegradable waste glass poses a serious environmental threat as it can cause soil, water, and air pollution when not properly discarded in landfills. The use of glass in construction has shown promising results in enhancing various properties of concrete and improving overall sustainability. This study investigated the mechanical properties of mixed colored glass, comprising green and brown hues, and clear glass in mortar, to explore the feasibility of using colored glass as a replacement for sand and to determine how the addition of color affects the mechanical properties of mortar. The incorporation of waste glass as a partial replacement for sand resulted in a 2.7% increase in flow table values when 5% of Mixed Colored Glass Sand (MCGS) was utilized in place of sand, as compared to the control mix (CM). Conversely, a 5.4% and 4.7% decrease in flow table values were observed when 15% of clear glass (CGS) and MCGS were used as a substitute for sand respectively. When 15% of MCGS and CGS were replaced with sand, compressive strength increased by 60% and 42.6% respectively, compared to the control mix, when 5% MCGS, 10% MCGS, 5 CGS, and 10% CGS were observed. After 28 days of curing, a 10.6% and 10% increase in strength was observed when 10% of MCGS and CGS were replaced. At 7 days, a 3.3% increase in flexural strength was found when 5% of MCGS was replaced with sand was observed. The fire resistance test showed reduced mass and compressive strength of specimens at different temperatures. No significant expansion of ASR was recorded throughout the test period. The use of waste glass as a substitute for sand has shown improvements in environmental sustainability and economics. When 10%WGS and 15%WGS were utilized, 20% and 30% of waste glass sand was replaced with sand, respectively. Incorporating waste glass into construction enhances the mechanical properties of concrete and promotes the conservation of natural resources and environmental sustainability. This study examined the economic advantages of replacing sand with waste glass and found that CM has the highest cost of 90.64 Tl. At replacement of 5%, 10%, and 15% MCGS showed 1.07%, 1.96%, and 2.95% savings compared to the control mix, respectively. Moreover, replacing 5%, and 10% of natural sand with clear glass sand could bring about savings of 1.91%%, and 3.63%, respectively. Replacing 15% CGS showed the highest savings of 5.45% compared to the control mix. The study compared the use of colored and clear glass as a partial replacement for sand and found that there were slight differences in the results, but overall they were similar.

Keywords: Alkali-silica reaction, Fire resistance, Mechanical properties, Sand replacement, Waste glass

Introduction

Around 20 million metric tons of waste glass are produced yearly, and the recycling rate is worrying. Approximately 60% of waste glass is landfilled, with less than 20% recycled. Even though there is less landfill capacity, the amount of waste glass that is landfilled is predicted to increase dramatically (Agboola Shamsudeen Abdulazeez et al., 2020). . Glass is not biodegradable, it takes up many landfill areas and pollutes the air, water, and soil. In heavily crowded places, there is also a problem with a shortage of appropriate landfill space. To

- Selection and peer-review under responsibility of the Organizing Committee of the Conference

solve these challenges, the reuse of waste glass should be prioritized. Recycling glass saves landfill space, saves energy, and decreases prices while safeguarding natural resources (Borhan, 2012).

Waste glass has been utilized as a partial substitute for coarse aggregate, sand, and cement in the production of concrete and mortar. Since the 1960s, scholars have explored the potential of utilizing waste glass with a size greater than 4.75mm as a replacement for coarse aggregate in concrete (Yu et al., 2016). Nevertheless, using coarse glass aggregate reduced compressive strength as the concentration of glass increased. Additionally, there were contradictory results about the impact of glass aggregates on the workability of concrete.

Several studies have explored utilizing recycled crushed glass as a viable alternative to coarse glass aggregates to mitigate detrimental cracks (Afshinnia & Rangaraju, 2016; Chen et al., 2006; Jani & Hogland, 2014). Utilizing glass sand in concrete enhances its properties due to its sleek surface and less water absorption (Topcu & Canbaz, 2004). The mechanical and durability characteristics of hardened concrete are not compatible with variations in glass magnitude (De Castro & De Brito, 2013; Adaway & Wang, 2015). This can lead to the formation of microscopic fissures at the edges of glass particles when they are crushed. When there is moisture, can the damaged surface of aggregates develop ASR (Alkali Silica Reaction) expansion gels, which results in concrete cracking (Adaway & Wang, 2015)

Studies have demonstrated that ASR expansion can also happen when a higher proportion of glass material is used as a substitute for sand. The non-biodegradable characteristic of waste glass poses a significant challenge when disposing of it in landfills since it significantly contributes to soil, water, and air pollution. The glass waste will have accumulated so much that the landfills will not take in any other kind of waste as they will be at their peak, primarily because of the enormous human population. Conversely, the thrown-away glass may take tens of millions of years before it decays, thus worsening the complications in landfills. Recycling the discarded glass items would, therefore, ensure that reduced amounts of glass are disposed of in the landfills and result in energy conservation and natural resource conservation since the production of new glass items usually requires the mining of sand used to make new glass. It is an admirable approach as the processing of reusing the fragmented glass mitigates particular environmental challenges about landfills while safeguarding the existence of our planet's clutter for future generations.

Materials and Methods

Research Design

The study is based on experimental research and aims to look into using crushed waste glass as a partial replacement for sand in cement mortar. The study was designed to determine the suitability of waste glass in place of sand in cement mortar. It will comprise laboratory experiments to test glass waste's physical and chemical properties, establish the optimum particle size of crushed waste glass, and develop optimum cement mortar mixes using waste glass. This research also deals with the different properties of mortar (fresh and hardened) that use clear glass and colored glasses (green and brown).

Materials

Cement

Ordinary Portland cement (Type I) (42.5 R) was used for the study (ASTM C 150 – 07) which was obtained locally.

Fine Aggregate

The fine aggregate used for this study was artificial sand, represented by crushed stones. As a glass replacement, clear and colored (green and brown) glasses of quartz sand have been replaced for 15% of the total volume in both fresh and hardening properties of mortars. Sieve analysis has been used to obtain well graded sand. In this study, an attempt has been made to analyze the effect of partial replacement of glass with sand on the properties of mortar. The implications of this research could be in developing improved material for construction and could exploit the findings to understand the mortar's behavior better.

Waste Glass

The waste glass was collected from different bars, most of which sell drinks, and a few glass recycling sites. The glass collected was divided mainly into three types: green, brown, and clear, depending on its source. The waste glasses were cleaned separately by removing all traces of impurities, sugars, or alcoholic deposits. The glass was crushed through abrasive Los Angeles to the required size. This crushed glass was sieved to ensure the collected glass size was uniform and impure-free. All in all, the collection and overall recycling of the waste glass was very comprehensive. Table 1 shows the chemical composition of waste glass used in previous studies.

Table 1. Chemical composition of waste glasses

Chemical components (%)	Liu et al., (2022) Waste glass	Zhao et al., (2013)	Green glass (Y. Wang et al., n.d.)	Clear glass (Y. Wang et al., n.d.)	Brown glass (Y. Wang et al., n.d.)
SiO_2	68.3	76.1	65.97	68.43	70.69
Na_2O	14.6	11.3	11.08	10.97	10.22
MgO	1.3	0.91	1.11	0.91	1.32
Al_2O_3	1.2	3.37	3.33	2.21	3.63
Cao	11.9	5.8	11.85	11.79	10.79
K_2O	0.7	0.72	0.35	0.32	1.86
Fe_2O_3	0.36	0.02	0.62	0.17	0.52
LoI	1.34	0.4	-	-	-

Clear Glass Sand (CGS)

Figures 1 and 2 show clear glass and it is crushed for within the fine aggregate size respectively.

Figure 1. Clear glass used

Figure 2. Clear glass sand size (CGS)

Mıxed-Colored Glass Sand (MCGS)

Green and brown glasses given in Figures 3 and 4 respectively, were used to replace fine aggregate. Figure 5 and 6 are their crushed forms.

Figure 3. Green glass

Figure 4. Brown glass

Figure 5. Green glass sand size (GGS)

Figure 6. Brown glass sand size (BGS)

Water

Water is an essential material for concrete, as the cement needs water for hydration, and the workability of the mix also requires water. Tap water was used to mix the materials (ASTM C1602/C1602M – 22). Water/ Cement ratio used for this research was 0.485 as per ASTM (C109/C109M).

Mix Design of Mortar

For optimal results, the typical mortar demands a precise combination of ingredients, with a proportion of 1 part cement to 2.75 parts graded standard sand by weight (ASTM C109/C109M). When Portland cement is utilized, a water/cement ratio of 0.485 is employed, determined by the total weight of cement incorporated. Table 2 shows materials amounts used in different mixes.

Table 2. Mix design of mortar ($1m^3$)

Different Mixes	Cement (g)	Sand (g)	Clear Glass Sand (CGS) (g)	Mixed Color Glass Sand (MCGS) (g)		Water (ml)
				Brown	Green	
CM	500	1375	0	0	0	242
5 % MCGS	500	1305	0	35	35	242
10 % MCGS	500	1235	0	70	70	242
15 % MCGS	500	1165	0	105	105	242
5 % CGS	500	1305	70	0	0	242
10 % CGS	500	1235	140	0	0	242
15 % CGS	500	1165	210	0	0	242

Results and Discussion

Fresh Properties of Mortar

Flow Table

Flow table test have been performed for all mixes according to ASTM (C 1437 – 07) Multiple empirical research published in scientific journals has demonstrated that substituting fine aggregate with recycled glass modifies the characteristics of freshly mixed concrete. Multiple studies have demonstrated that the reduction in slump can be achieved by increasing the quantity of discarded glass. Additionally, as (Afshinnia & Rangaraju, 2016) support, the irregular angular shapes of these glass particles are another factor that activates the reaction in performance. This gives less fineness modulus and a lesser amount of cement paste because of the geometry of this shape, which provides low fluidity for the mixture. Small glass particles within the waste glass sand and

plastic properties may cause adverse effects on the texture, shape, and even consistency of the concrete. This mainly pertains to aspects such as objects that have smooth surfaces and sharp edges. (Afshinnia & Rangaraju, 2016) ascertained that if a high percentage of recycled glass is incorporated into concrete, it may lead to a slump reduction compared to other variants. However, different types of surveys regarding this issue have presented divergent results. For example, after the study, it was found that it led to a slight increase in slump value and heightened its replacement level using coarse particles (Taha & Nounu, 2008). In this light, the authors used high-range water reducers to determine if the effect after the control mixture would be good enough. Others have discovered positive correlations between slight increases in a slump and a high level of replacement (Batayneh et al., 2007; De Castro & De Brito, 2013; Ibrahim, 2017; Park & Lee, 2004; Sharifi et al., 2013; Terro, 2006; Topcu & Canbaz, 2004; Yu et al., 2016) have reported that the flexural strength of concrete decreases with increased glass sand.

Figure 7 outlines these findings under the flow table values for the different mixes tested as the test progressed. An interesting trend was observed regarding the material variety affecting the flow table values, as shown in Figure 7. The replacement of 5% MCGS with sand induced an increase in the flow table values by 2.7%, thus proving that the sand may improve the flowing capabilities of the mixture. However, 10% MCGS or 10 % CGS replaced decreased by 0.91% and 2.3% in the flow table, respectively, suggesting that these materials may not be ideal for enhancing flowability. Substituting the sand in place of CGS 5% showed a very nominal reduction in the flow table values by 0.34%. Hence, the effect of such substitution was also found insignificant. Finally, when the adoption of 15% MCGS or CGS as a sand replacement is adopted, there is a significant decrease in flow table values by 4.7% and 5.4%, respectively. It can be seen from the result that the waste glass sand replacing up to 15% of the volume of sand does not have a significant effect on the flow table of mortar. This is when clear and mixed-colored glass sands are replaced by normal sand. The increase in glass replacement led to a rise in slump value due to the formation of a denser granular structure. Chen et al. (2006) state that glass grains, being smaller than natural sand, can efficiently fill coarse aggregate. Terro (2006) conducted an additional study to investigate the influence of including waste glass in combinations and its correlation with an increase in slump. From this, waste glass sand, as a partial substitute for the normal sand in the mortar, justifies its use without deleteriously affecting its flow table performance. Replacing clear and mixed-colored glass sands with normal sand in the mortar justifies its use without deleteriously affecting its flow table performance.

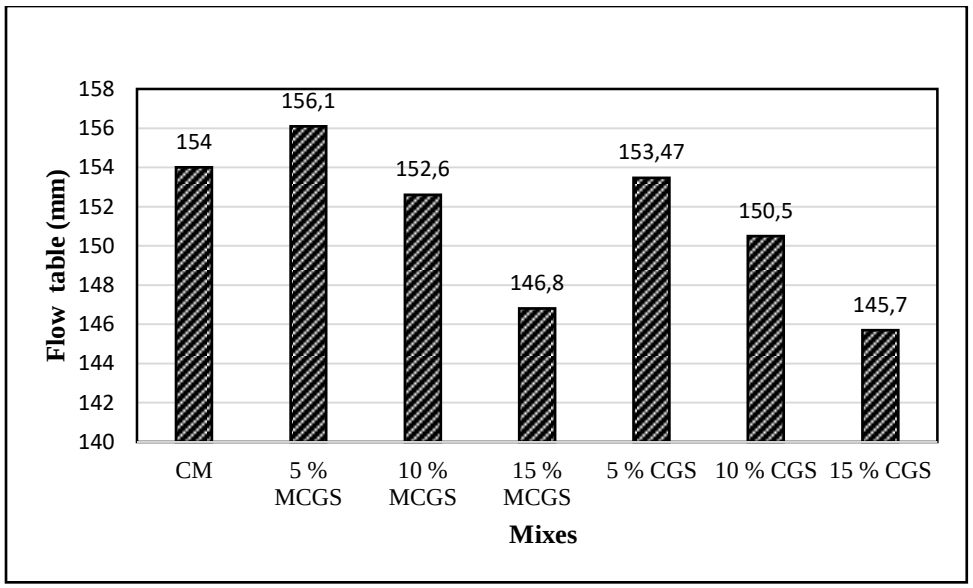

Figure 7. The flow table values of mixes

Fresh Density

Several studies have demonstrated that including waste glass as a fine aggregate in fresh concrete reduces its density. The aforementioned studies include (Chen et al., 2006; De Castro & De Brito, 2013; Du & Tan, 2014; Adaway & Wang, 2015; Topcu & Canbaz, 2004). The likely cause for this is the reduction in concrete density resulting from the addition of glass, as glass particles possess a higher density compared to conventional sand. According to De Castro and De Brito (2013), increasing the water-to-cement ratio reduces the density and increases the porosity of the mixture when water is introduced. Studies conducted by Ismail & AL-Hashmi,

2009; Topçu & Canbaz 2004 and H.-Y. Wang, 2009) have demonstrated that the dry density of concrete can be reduced by increasing the proportion of recycled glass sand to fine aggregate. According to (Ling & Poon, 2012), there is a direct correlation between the higher specific gravity of lead in funnel glass and its higher dry density. Research conducted by Yu et al. (2016) revealed that incorporating steel slag into concrete increased its density. Studies have observed that the fresh density of concrete decreases with an increase in waste glass used as a fine aggregate replacement (De Castro & De Brito, 2013; Mardani-Aghabaglou et al., 2015).

The mortar samples' fresh density reduced as the glass sand percentage increased. This is because the glass's density is lower than that of sand. The values of the fresh density of mortar samples are presented in Table 3. When 15% of clear glass sand was replaced with sand, the fresh density of mortar decreased by 2.78% compared to the control mix at a 2446 kg/m3 value. Clear and light glass sand is found to be denser compared with mixed-colored glass sand. However, there was no significant difference between the two glass sand types. These results show that the glass sand used significantly in mortar production, be it ground or powder form, only slightly affects the changes in fresh density within 7 days.

Table 3. The fresh density of mixes

Mix	The fresh density of mortar (kg/m^3)
CM	2516
5 % MCGS	2490
10 % MCGS	2480
15 % MCGS	2446
5 % CGS	2496
10 % CGS	2490
15 % CGS	2450

Hardened Properties of Mortar

Dry Density

Various studies have shown that adding waste glass sand into the concrete contributes to a decrease in the density of the obtained concrete mix. The scholars Du and Tan (2014) and Topcu and Canbaz (2004) show that waste glass tends to reduce the thickness of mortar. According to Ling and Poon (2012), there is a direct correlation between the higher specific gravity of lead in funnel glass and its higher dry density. Research conducted by Yu et al. (2016) revealed that incorporating steel slag into concrete increased its density. Conversely, incorporating shattered glass into the mixture may decrease the ultimate density of the concrete.

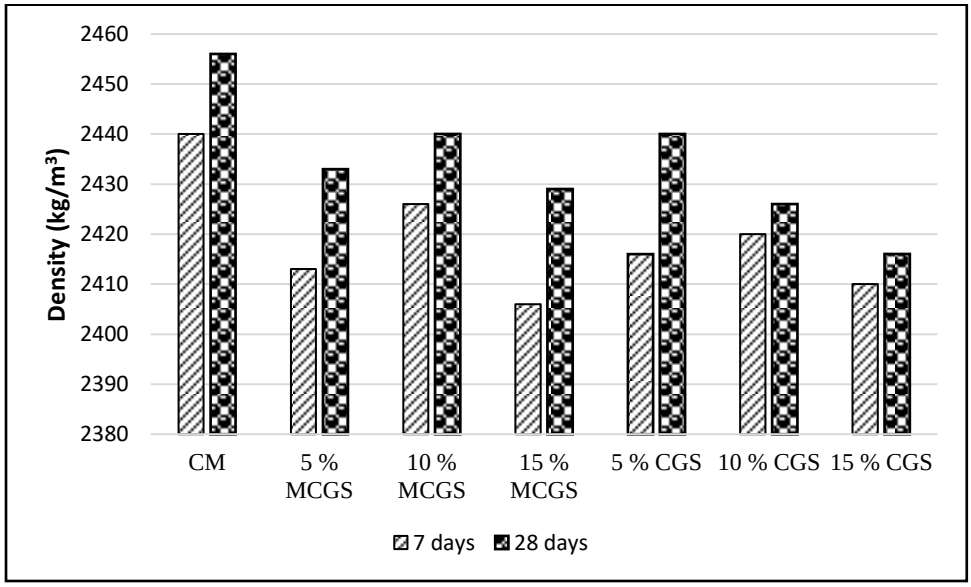

Figure 8. Dry density of mixes

According to Du and Tan (2014), the presence of less glass resulted in a reduced amount of air. Nevertheless, when the particle morphology exhibited greater amorphousness, an increased concentration of glass led to a

higher proportion of air and enhanced control over air voids. From Figure 8, it can be observed that at 7 days, mixes with 5%, 10%, and 15% of MCGS, as well as 10% and 15% CGS, showed a decrease of less than 2% as compared to the mix without MCGS or CGS. Similarly, after 28 days, the hardened density of the mortar showed a minimal decrease compared to the control mix. The results imply that although the waste glass sand in concrete may lead to small reductions in density, this will be relatively minimal and will not make the concrete objectionable for general use.

Compressive Strength

Compressive strength test of specimens was done according to ASTM (C109/C109M). Several research have investigated the influence of waste glass, a finely ground material, on the compressive strength of concrete. Multiple studies (Batayneh et al., 2007; Ismail & AL-Hashmi, 2009; Wang, 2009) have demonstrated that incorporating recycled glass sand into concrete leads to an enhancement in its compressive strength. With the addition of RGS, the compressive strength exhibited a consistent increase until it reached the desired ratio. It peaked and thereafter declined. The observed decrease in strength at greater percentages can be attributed to a potential deficiency of cement paste in the combination. This phenomenon arises due to the formation of minuscule voids and the obstruction of robust bonds inside the concrete (Adaway & Wang, 2015). The drop in strength is attributed to an increase in friability, a decrease in density, and enhanced surface smoothness. The researchers discovered that, under specified conditions, the strength of the concrete they examined was equivalent to that of the reference concrete (Terro, 2006). However, as the quantity of glass exceeded the predetermined threshold, the strength of the concrete began to diminish. Studies have shown that fractured glass possesses considerable strength (Afshinnia & Rangaraju, 2016). Shattered glass should be avoided in high-alkali concrete mixes due to the potential for detrimental expansion resulting from the interaction between alkali and aggregate. Shayan and Xu (2004) found that the performance of regular concrete was considerably inferior to a blend of 80% coarse waste glass sand and 20% fine crushed waste glass sand. Conversely, a study done by Shayan and Xu(2004) demonstrated that combining fine and coarse fragments of glass in equal proportions resulted in a declining pattern. Similarly, Chen et al. (2006)discovered that the compressive strength of a material is significantly influenced by both the duration of the curing process and the ratio of replacement.

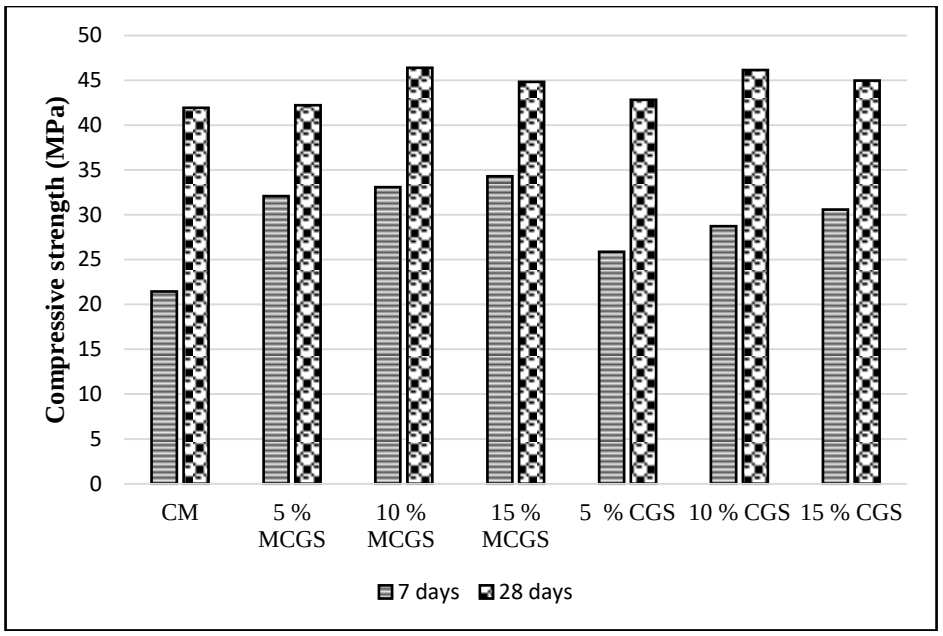

Figure 9. Compressive strength of mixes

The compressive strength of the concrete was significantly higher than that of the control concrete, even after a period of 91 days. In addition, it continued to increase up to the one-year mark (Chen et al., 2006). The combination of cement adhesive with crushed waste glass sand can produce pozzolanic reactions, hence improving the microstructure at the line transition zone (Park & Lee, 2004). The compressive strength test is a critical measure to assess the mechanical properties of mortar. In Figure 9, the 7 and 28 days compressive strength tests were performed to examine the effect of Mixed-colored Glass Sand (MCGS) and Clear Glass Sand (CGS) on the cement mortar strength. It was observed from the results that with the replacement of sand by 5% MCGS in 7 days, there is an enhancement of about 49.6% in the compressive strength of mortar. Similarly, after

7 days, the compressive strength increases by 20.7% on 5% replacement of CGS in place of sand. It was also observed that as the replacement percentage rose to 10 and 15 % MCGS in place of sand, the strength of mortar proportionally increased. The compressive strength of MCGS replacement increased to 54.29% and 60% after 7days at 10 and 15%, respectively. When CGS was replaced by 10 and 15% sand, the compressive strength increased to 34% and 42.58 %, respectively.

The substitution of 10% and 15% MCGS by sand enhanced the compressive strength by 10.6% and 10%, respectively, concerning the control mix after the 28 days test period. At the replacement of 10% CGS and 15% CGS with sand, there was an increase in the compressive strength by 10% and 7.2%, respectively. There was a negligible increase of 0.67% and 0.87% in compressive strength at 5% MCGS and 5% CGS, respectively. These results imply the potential for enhancing mortar strength by incorporating MCGS and CGS in the mortar mixtures, focusing upon varying the substitution percent, bringing forward the same significant changes in cement mortar strength development at early ages. For example, high-rise compressive strength can be cited for 7 days in the case of Mixed-colored Glass sand specimens. Chen et al. (2006) and Ling and Poon (2012) discovered that substituting crushed glass for sand in mortar resulted in a reduction in compressive strength. An observable reduction occurred when the water-cement ratio was increased. Ibrahim (2017) found that the addition of waste glass (WG) at various concentrations increased the compressive strength of concrete. This increase in strength was greater than that observed in concrete without WG. The maximum dosage of WG that has been identified is 15%. Introducing a waste glass ratio of 15% resulted in a significant 25% improvement in the compressive strength of the concrete, as compared to the control mix. The incorporation of recycled glass in concrete at a rate of 5% to 40% led to incremental improvements in compressive strength of 2.07%, 3.79%, 24.47%, 17.13%, 13.11%, 12%, 6.89%, and 5%, respectively.

Flexural Strength

Sharifi et al. (2013) discovered that adding a small amount of glass to ordinary concrete increased its flexural strength. This occurred due to the glass enhancing the adhesive properties of the cement mixture. Supported by empirical research conducted by Ismail and Al-Hashmi (2009). Utilizing recycled glass, which has pozzolanic properties and increases over time, at a replacement rate of up to 20% greatly reduces the curing time. The concrete's strength remained unaltered even after replacing all of the original components with recycled glass. To examine the flexural strength of the mortar ASTM (C 348 – 08) was followed, it was tested over two durations of 7 and 28 days. It was noted during testing that the replacement of MCGS by sand at 5% at7 days registered a significant increase of 2.7% in the case of flexural strength. The strength had increased by 0.51% for the 7th day by raising the percentage replacement to 10%. The flexural strength had been decreased for the percentage replacement of 15% MCGS by 1.02%. Replacement of the CGS with sand by 5%, 10%, and 15% reduces the flexural strength as follows: approximately 1.02%, 2.04%, and 3.6%, respectively. Usually, the study showed that with 5% MCGS used after 28 days, the flexural strength was higher by 2.6% of the control mix (CM).

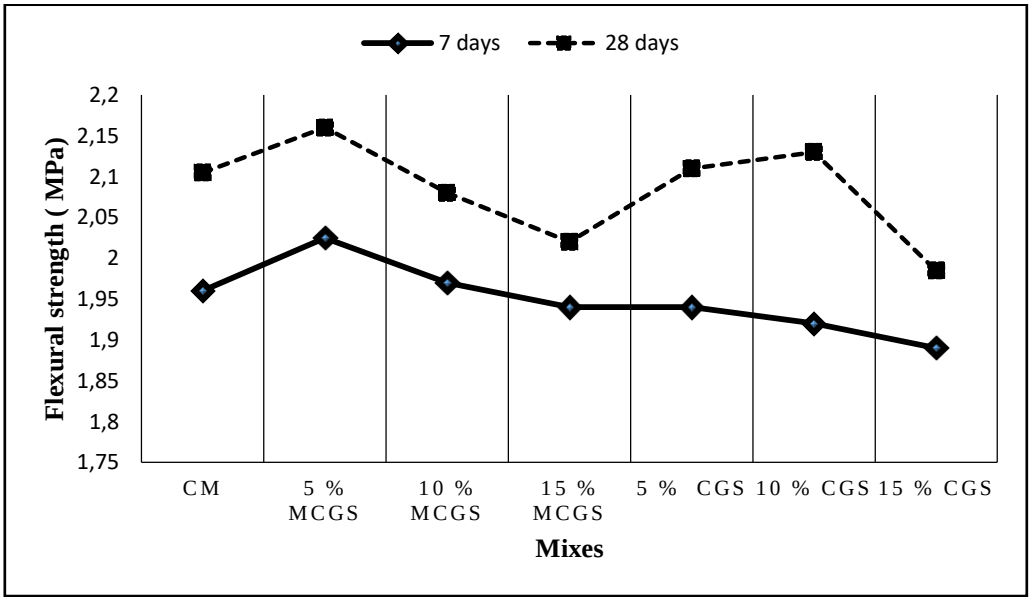

Figure 10. Flexural strength of mixes

However, replacing sand with 10% and 15% MCGS reduced flexural strength to 2.6% and 4.03%, respectively. Moreover, this research also demonstrated how 5% and 10% CGS delivered higher flexural strength compared to the control mix at 7 days with positive increments of 0.24% and 1.2%, respectively, at 28 days. However, when 15% CGS was used as a replacement, a decrease of 5.7% in flexural strength was found. In summary, results show that using MCGS and CGS as partial replacements for sand may have different effects on the flexural strength of the control mix, in which 5% MCGS and 10% CGS are shown to improve flexural strength. In contrast, a higher percentage of MCGS or CGS can slightly decrease flexural strength.

Durability Properties of Mortar

Fire Resistance

The fire resistance properties of the specimens were tested using standard test methods for fire tests of building construction and materials ASTM (E 119 – 20). The results are presented in Table 4, which clearly shows the specimens' mass decrease when exposed to temperatures of 200℃, 400℃, and 600℃ for 90 minutes. It was found that all specimens exhibited a decrease in mass with an increase in temperature. Notably, the control mix reduced 1.6%, 3.2%, and 4.4% of the mass at 200℃, 400℃, and 600℃, respectively. When 5% MCGS was replaced with sand, the mass was reduced by 0.41%, 3.06%, and 5.7% compared to the actual mass before the fire. Similarly, a reduction of 0.76%, 3.8%, and 4.8% of the mass was observed when 10% MCGS was replaced with sand at 200℃, 400℃, and 600℃, respectively. When 15% MMCGS, 5% CGS, 10% CGS, and 15% CGS were placed in 600℃, a decrease of 5.24%, 5.8%, 4.8%, and 5.33% of mass was observed, respectively. These results demonstrate the impact of temperature on the specimens' mass and the different materials' effectiveness in reducing mass loss at different temperatures.

Table 4. Mass of specimens in (g)

	Mass of Specimens Before Fire Test	Mass (g) after 200 ℃	Mass (g) after 400 ℃	Mass (g) after 600 ℃
CM	291.5	286.8	282.2	278.5
5 % MCGS	290.9	289.7	282	274.3
10 % MCGS	288.2	286	277.2	274.8
15 % MCGS	288.1	286.2	278.7	273
5 % CGS	290.9	288.7	282.5	274
10 % CGS	292.5	288.5	281.3	278.5
15 % CGS	290.8	289.2	280	275.3

The results presented in Figure 11, indicate specimens' residual compressive strength after a fire test. Notably, a significant increase in compressive strength was observed at 200℃; however, at 400℃ and 600℃, there was a decrease in compressive strength compared to the control mix. At 200℃, specimens containing 5%, 10%, and 15% MCGS showed an increase of 6.5%, 12%, and 8% in compressive strength compared to the control mix.

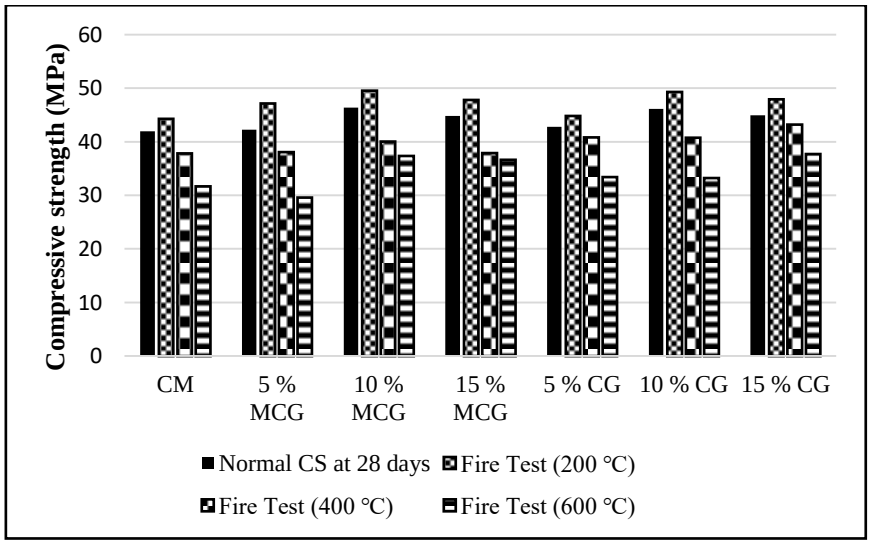

Figure 11. Residual compressive strength after fire test

Furthermore, an increase of 11.3% and 8.2% was found when 10% and 15% CGS were replaced compared to CM. When the temperature was increased to 400℃ and 600℃, the adhesive forces between cement, water, and aggregates weakened as the water evaporated from the samples, thus compromising the mortar's ability to resist compression force. However, at 400℃ and 600℃, 15% CGS showed an increase of 15% and 19% in residual compressive strength compared to the control mix, respectively. In addition, when 15% MCGS was replaced with sand, an increase of 15.6% was found in compressive strength at 600℃ compared to CM. Interestingly, the replacement of waste glass sand with natural sand showed an improvement in its ability to endure high temperatures compared to the control mix.

Water Absorption

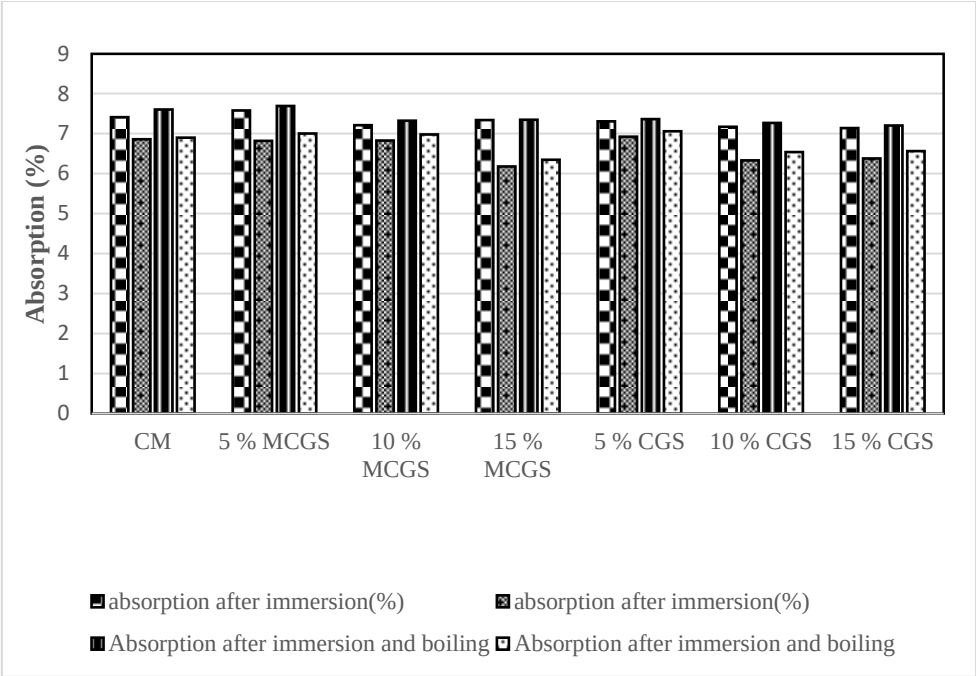

Figure 12. Water absorption (%) of mixes

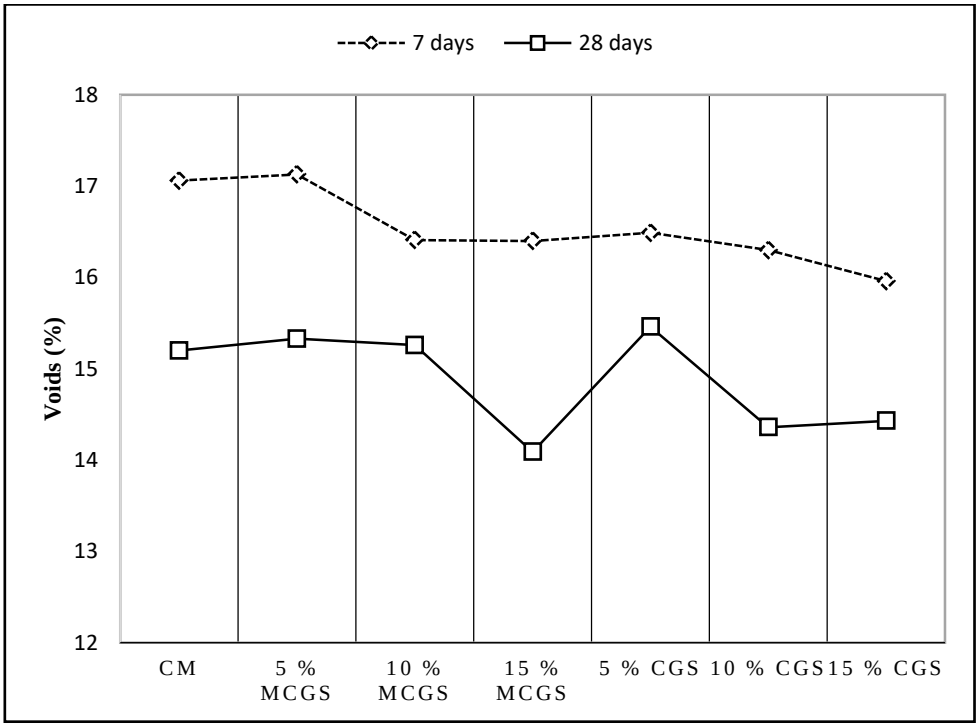

Figure 13. Percent voids of mixes

Water Absorption test was conducted as per ASTM (C – 642) The study found that using more glass aggregate in mortar mixes resulted in lower water absorption at all curing stages. This is a common phenomenon known as the reduction in water absorption over time, as the hydration process continuously occurs and forms concrete with lower porosity. As hydration products fill the pores between cement particles and aggregates, the average pore diameter decreases. However, the decrease in water absorption observed with an increase in waste glass replacement can be explained by the impenetrable nature of glass aggregates compared to sand and the uneven shape of waste glass. The irregular geometry of waste glass may provide greater opportunities for the deposition of hydrated concrete products. Figure 12 shows the percentage water absorption of samples after immersion and water absorption of specimen after immersion and boiling. 5% CGS and 5% MCGS, showed a minimal increase in water absorption at 7 days and 28 days. Where other mixes showed less decrease in water absorption. The boiling of specimens increased the absorption of specimens, the CM showed an increase of 0.60% comparing the result WA after immersion and WA after immersion and boiling. Figure 13, indicates that an increasing percentage of replacement of waste glass by sand showed a decrease of the percentage of voids. It was found that the % voids of CM were 17.1% at 7 days and 15.2% at 28 days. 15% CGS showed the minimum percent voids among the specimens at 7 days.

Table 5. Densities for water absorption

	Bulk density, Dry g_1 (g/cm^3)		Bulk Density after Immersion (g/cm^3)		Bulk Density after Immersion and Boiling (g/cm^3)		Apparent Density, g_2 (g/cm^3)	
mix	7 days	28 days	7 days	28 days	7 days	28 days	7 days	28 days
CM	2.24	2.2	2.41	2.35	2.42	2.35	2.71	2.59
5 % MCGS	2.23	2.19	2.4	2.34	2.4	2.34	2.69	2.59
10 % MCGS	2.24	2.19	2.4	2.34	2.41	2.34	2.68	2.58
15 % MCGS	2.23	2.22	2.4	2.35	2.4	2.35	2.67	2.58
5 % CGS	2.24	2.19	2.4	2.34	2.41	2.34	2.68	2.59
10 % CGS	2.24	2.2	2.4	2.34	2.4	2.34	2.68	2.56
15 % CGS	2.25	2.2	2.41	2.34	2.41	2.34	2.8	2.57

Table 5, shows the bulk density of specimens after immersion and bulk density after immersion and boiling, the overall results were quite similar. Bulk density was found to be less than other densities where immersion of water/boiling was considered. The increase of waste glass sand showed a decrease of density compared to CM, but the decrease was found to be insignificant.

Alkali-Silica Reaction Test

According to Du and Tan (2013) and Park and Lee (2004), the size of the glass sand is directly proportional to the increase in ASR. The smallest increase in ASR occurs at 0.150 mm, while the most significant increase occurs at 2.36 mm. The pozzolanic treatment reduces the ASR expansion from 2.36 mm to 0.150 mm. The pozzolanic reaction is initiated by the reaction of silica in fine-grained glass sand with Ca (OH) $_2$ due to cement hydration. The low SiO2/CaO ratio in the pozzolanic process does not cause swelling. The formation of ASR gel is due to the heightened occurrence of apparent internal fissures in particles with larger sizes. According to Du and Tan (2014), the expansion of green glass sand in ASR reaches a peak of 1.18 mm and then declines to 2.36 mm.

The potential alkali reactivity of aggregates was tested using the standard mortar-bar method (ASTM C1260). Table 6 displays the expansion measurements of different specimen types on various reading days. CM had the highest expansion rate of the specimens tested, although the increase was insignificant at less than 0.1mm. Specifically, CM showed an expansion rate of only 0.0080 after 28 days. When 5% MCGS and 5% CGS were used to replace sand, expansion rates of 0.0063 and 0.0069 were recorded, respectively. Interestingly, the Mixed-Colored Glass Sand samples showed less expansion than the Control Mix and the Clear Glass Sand samples, although the difference in expansion rates glasses was insignificant.

Figure 14 depicts the percentage expansion of various samples monitored across eight reading days in the study. The samples included CM, 10% and 15% MCGS, 5%MCGS, 5%CGS, 10% CGS, and 15% CGS. On day 2, CM showed an expansion of 0.037%, whereas on day 28, the expansion rate increased to 0.094 %. However, the 10% and 15% MCGS samples did not exhibit any expansion until day – 8 but recorded 0.032% and 0.021% expansion on day 28. Furthermore, when 5%MCGS, 5%CGS, 10% CGS, and 15% CGS were replaced with sand, the expansion rate for each sample was observed to be 0.074%, 0.081%, 0.042%, and 0.028%,

respectively. These findings suggest that the percentage of MCGS and CGS used in the study reduced the ASR expansion as the replacement percentage increased.

Table 6. Rate of expansion of samples in different reading days

Mix	Reading Days (mm/day)							
	D – 4	D – 6	D – 8	D – 10	D – 12	D – 16	D – 21	D – 28
CM	0.0031	0.0031	0.0031	0.004	0.004	0.0072	0.0072	0.008
5 % MCGS	0.0012	0.0024	0.0024	0.0024	0.0036	0.0036	0.0048	0.0063
10 % MCGS	0	0	0.0014	0.0018	0.0022	0.0025	0.0025	0.003
15 % MCGS	0	0	0.0006	0.0006	0.0018	0.0018	0.0018	0.0018
5 % CGS	0	0.0015	0.0024	0.0036	0.004	0.0044	0.0051	0.0069
10 % CGS	0.0006	0.0006	0.0006	0.0011	0.003	0.003	0.003	0.0036
15 % CGS	0.0005	0.0005	0.0013	0.0013	0.0013	0.0028	0.0028	0.0028

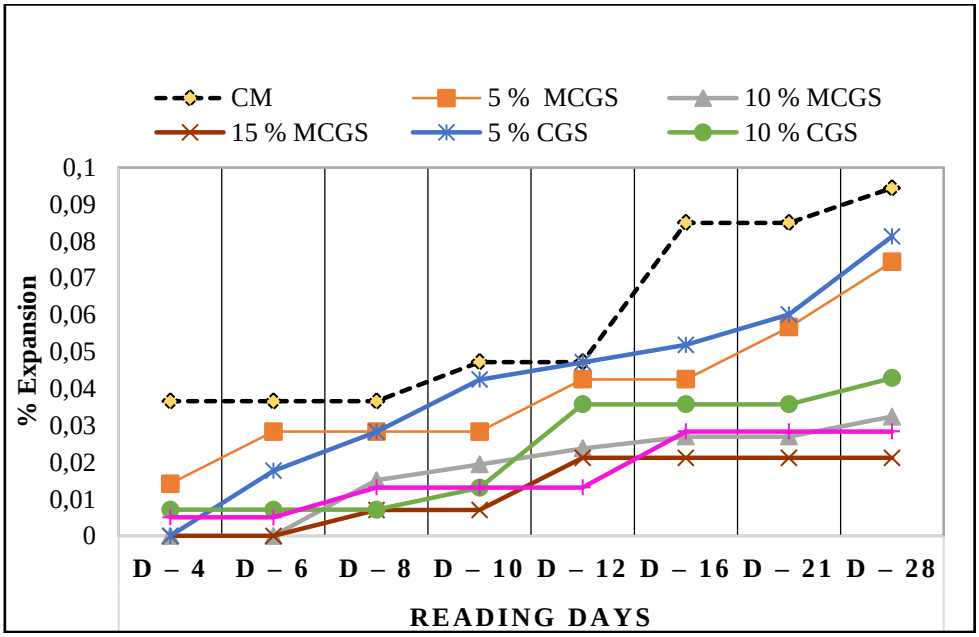

Figure 14. ASR expansion of mixes (%)

Evidence from the research work of Du and Tan (2014) and Ismail and AL-Hashmi (2009), indicates that concentrations enhance the expansion of clear glass sand in ASR. However, microcracks were observed among only clear glass sand crushed materials. In all quantities of replacements, no or minimal observable microcracks were noted in brown and green glass sand to ensure their safety. According to Du and Tan (2014), more glass sand helped to slow down the alkali-silica reaction (ASR). To produce a non-swelling ASR gel, soda-lime glass is infused with calcium ions by injection. The microstructure is improved by the formation of a more compact and impermeable interfacial transition zone by the presence of a secondary C-S-H gel. Color changes can occur when alkali-silica reactions (ASR) occur. Green glass exhibited enhanced resistivity when exposed to the alkali-silica reaction. Du and Tan (2013); Park and Lee (2004); Topcu and Canbaz (2004); Yuksel et al. (2013) have conducted multiple investigations that provide evidence of chromium oxide (Cr2O3) inducing a greenish hue in glass by the reduction of alkali-silica expansion. Multiple studies have shown that the repulsive force caused by the electrical double layer decreases as the ionic valence increases. Higher concentrations of Cr2O3 impede the growth rates of Gel 38 due to the presence of Cr3+. Du and Tan (2014) found that the Alkali-Silica Reaction (ASR) has a slower development rate in brown glass sand than green glass sand, as per their research. However, the green glass underwent substantial enlargement due to modifications implemented throughout production. This expansion impacts internal tension, leaching, and dissolving, as stated by Dhir et al. (2009). Kim et al. (2015) discovered the smallest expansion in flint glass sand. Du and Tan (2014)and Idir et al. (2010)found that the rate of alkali-silica reaction (ASR) growth over time is considerably greater in green glass compared to brown glass. In 2004, Park and Lee reported that the expansion of green glass is limited compared to brown-type ones containing Fe2O3. The research conducted by Yuksel et al. (2013) showed that greener glass has a lower expansion than flint glass sands. Topcu and Canbaz (2004)found that the highest risk is present when the combination of alkali and silica was made using white glass sand as the aggregate color. White glass sand exhibits a significantly greater expansion rate compared to colored glass sands due to its elevated silicate content. According to Du and Tan (2013)and Jani and Hogland (2014), white glass had the highest growth in

alkali-silica reaction (ASR), while brown and green glass showed similar levels of progression. Figure 15 shows the linear relationship between the compressive strength and the ASR expansion of specimens. This relationship explains that the increase of ASR expansion will decrease the compressive strength and vice versa.

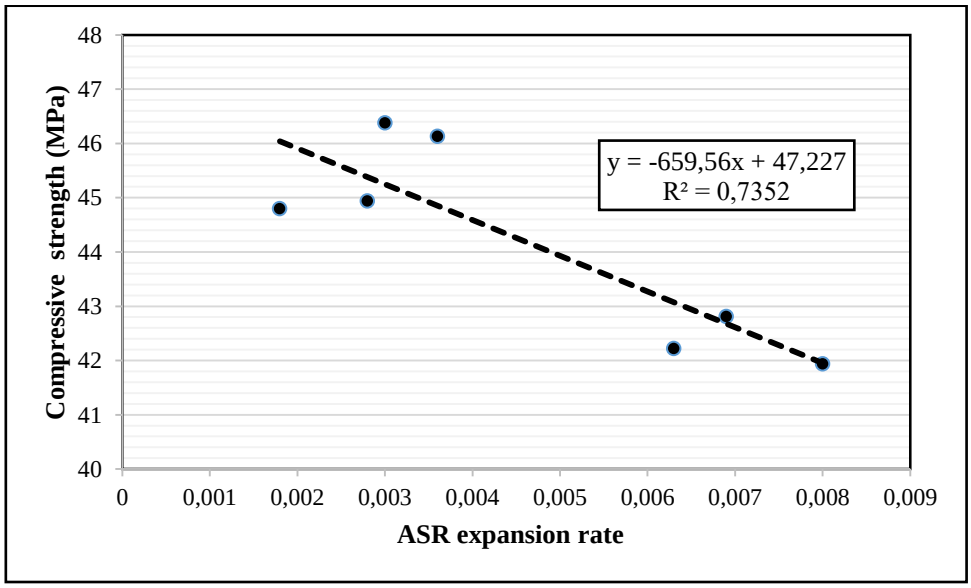

Figure 15. Relationship between Compressive strength and ASR expansion

Studies by Du and Tan (2014) and Idir et al. (2010) have shown that the alkali-silica reaction (ASR) rate is more pronounced in green glass than in brown glass over time. According to Park and Lee (2004), green glass experiences limited expansion compared to brown glass containing Fe2O3. Yuksel et al.(2013) discovered that greener glass has lower expansion rates than flint glass sands. Additionally, Topcu and Canbaz (2004) found that the risk is highest when alkali and silica combine using clear glass sand as the aggregate color due to their higher silicate content, which results in a significantly higher expansion rate than colored glass sands. Lastly, the insignificant expansion was due to the size of glass sand used (2mm – 0.75 microns) for the study; the larger the particle size of the glass, the higher the ASR expansion, and no cracks were seen on the samples during the testing days.

Environmental Sustainability

The growing trend of appreciating glass patronage for production brings a vital environmental risk to light. Although it is recyclable, glass still has to capture its recycling rate compared with the quantities produced year after year, and thus, most of the disposed glass is deposited into landfills. The latter pose multiple environmental problems, including air, soil, and water pollution. Waste glass takes hundreds of years to decompose and can cause harm to the environment and wildlife. Recently, a new type of sand called manufactured sand, or m-sand, has been introduced as an alternative. It is created by crushing rocks or quarry stones into small, angular pieces with a particle size typically smaller than 5 millimeters. M-sand is gaining popularity due to its high durability, compressive strength, and workability compared to natural river sand. Using waste glass as a substitute for river sand in construction can significantly reduce the amount of glass waste in landfills, ultimately protecting the environment. Table 6 shows the different percentages of waste glass sand replaced by sand.

Table 6. Materials used for mixes

Mixes	Sand (Kg)	Clear glass sand (Kg)	Mixed-colored sand (Kg)
CM	8.9	0	0
5 % MCGS	8.455	0	0.445
10 % MCGS	8.01	0	0.89
15 % MCGS	7.565	0	1.335
5 % CGS	8.455	0.445	0
10 % CGS	8.01	0.89	0
15 % CGS	7.565	1.335	0
Total	56.96	2.67	2.67

Figure 16 describes the percentage replacement of waste glass sand (CGS+WGS). Using 5%, WGS replaced 10% of the sand with clear or mixed-colored glass sand. When 10%WGS and 15%WGS were utilized, 20% and 30% of waste glass sand was replaced with sand, respectively. Incorporating waste glass into construction enhances the mechanical properties of concrete and promotes the conservation of natural resources and environmental sustainability.

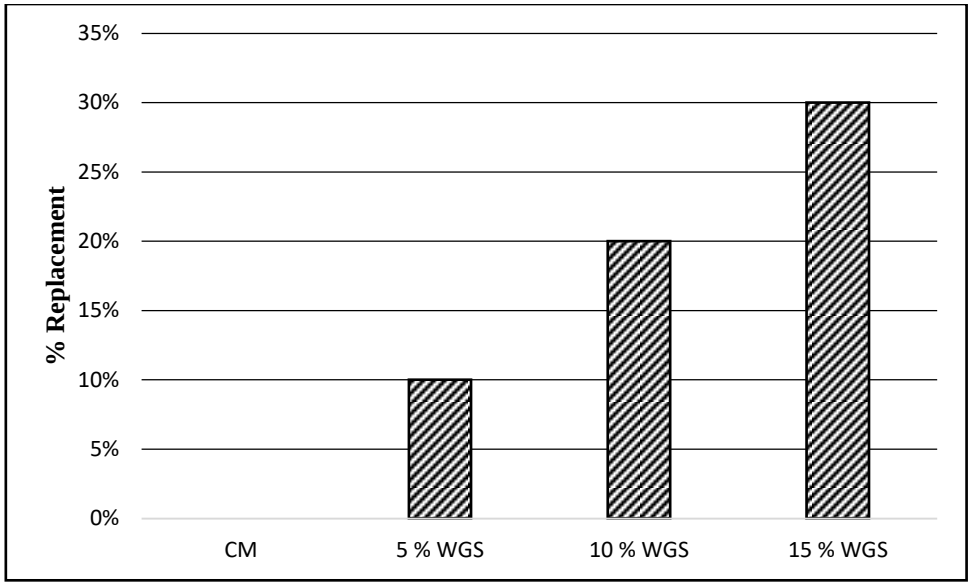

Figure 16. % replacement of WGS in cement mortar

Economical Assessment

The economic benefits of using waste glass are significant and cannot be ignored. Waste glass is easily accessible as waste material or in the earth's crust, making it a cost-effective replacement for natural sand. By using waste glass as a substitute for fine aggregate, the cost of natural sand can be significantly reduced. This study examined the economic advantages of replacing sand with waste glass and found that CM has the highest cost of 90.64 TL as shown in Figure 17. At replacement of 5%, 10% and 15% MCGS showed 1.07%, 1.96%, and 2.95% savings compared to the control mix, respectively. Moreover, Figure 17 shows that replacing 5%, 10% of natural sand with clear glass sand could bring about savings of 1.91%%, 3.63%, respectively. Replacing 15% CGS showed the highest savings of 5.45% compared to the control mix.These findings highlight the potential of waste glass as an affordable alternative to natural sand in construction and other industries.

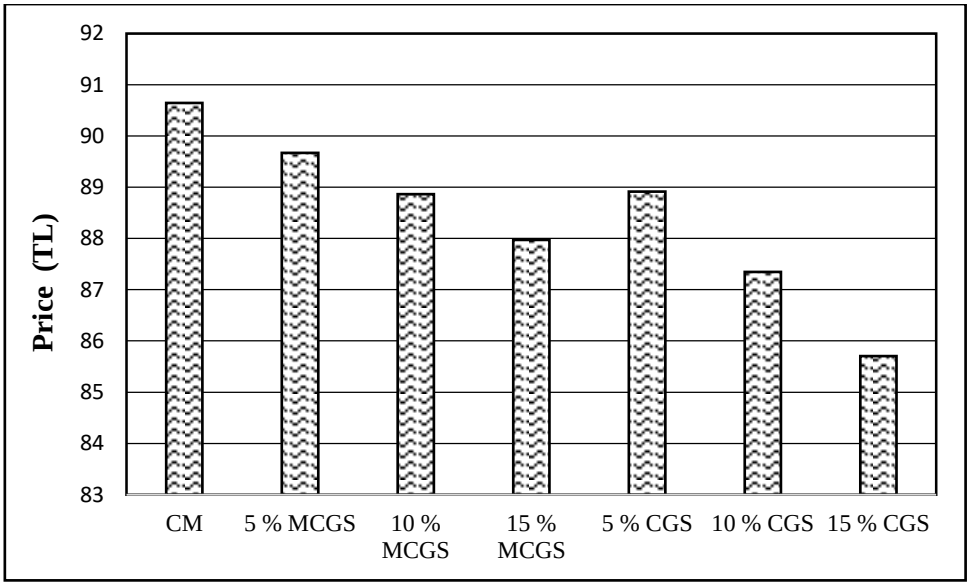

Figure 17. Cost of mixes (TL)

Conclusion

The results of this study indicate that the use of waste glass as a fine aggregate can not only enhance the properties of mortar but also contribute to a more sustainable environment.

- Increasing the recycling of glass from addition in construction keeps more waste away from landfills, and it also conserves natural resources.
- The study found that waste glass sand (WGS) can improve mortar's fresh and hardened properties. Based on the study, this replacement of a specific proportion of WGS leads to no significant impact on the workability of mortar. However, it led to a slight drop in workability. This is because glass sand does not absorb water like fly ash, which can affect the workability of mortar.
- Moreover, the study found an insignificant decrease in values of fresh and dry density less than 2%. However, the compressive strength was improved significantly while the sand was replaced by waste glass.
- Interestingly, the study also established that mortar possesses weak flexural strength. However, some improvement was noticed when clear glass sand (CGS) and mixed-colored glass sand (MCGS) were replaced in the mix.
- However, yet another benefit of using waste glass in construction is that as the percentage of waste glass in the mix increases, the water absorption will tend to decrease. This arises from the fact that waste glass is non-porous and, therefore, cannot allow water passage or even absorption into the same.
- The study on the compressive strength of the mortar also considered temperature. At 200℃, it had a remarkable increase in its compressive strength. The temperature increases the adhesive force between water cement and aggregates. However, a significant decrease in compressive strength occurs at temperatures d 400℃ and 600℃. This is because high temperature reduces the adhesive strength in the materials, whereas in the mortar, all the water evaporates from the specimens, resulting in a significant loss of strength.
- Finally, particle sizes of glass sand between 2.36mm – 0.75 microns were also analyzed to study expansion due to alkali-silica reaction (ASR), given the effect of future usage of this material for concrete production in mitigating this phenomenon. The ASR expansion was found innocuous, and no significant expansion was recorded during the study.
- Substitution of waste glass sand as a partial replacement for sand improved the environmental sustainability and can save money and natural resources.
- The fresh properties of mortar, and the flow table showed a minimal decrease and increase with different percentage replacements of glass sand. The fresh and dry density of samples reduced as the percentage of waste glass increased, but the reduction was minimal not more than 2%.
- The compressive strength of specimens improved as the percentage of glass was replaced with sand, while flexural strength showed both increase and decrease in strength when waste glass sand was used.
- The durability of the mortar was tested, 3 tests were done fire resistance, water absorption, and alkali-silica reaction. The waste glass sand specimens showed higher strength in fire resistance, while the compressive strength decreased when 400℃ and 600℃ temperatures were placed. There was no expansion caused by the alkali-silica reaction recorded through the study. However, it is worth mentioning that the control mix showed a higher expansion of 0.091% at 28 days, and the mixed-colored glass sand specimens showed the least expansion compared to clear glass sand and the control mix.
- In the study it was found that there is a strong relationship of 86% between compressive strength and ASR expansion which is inversely, the lower the ASR expansion rate the higher the compressive strength.
- Environmental sustainability was assessed, looking for the advantages of using waste glass for the environment and sustainability. The use of waste glass in construction increases the usage of recycled waste glass which will save a large amount of landfills in densely populated areas.
- The utilization of waste glass in construction saves a lot of money and natural resources.
- Finally, using waste glass as a partial replacement for sand in concrete is an eco-friendly solution that can significantly benefit the construction industry by reducing waste and carbon footprint. Overall, it is a solution worth considering, provided adequate testing and monitoring are conducted to ensure optimal performance.

Scientific Ethics Declaration

The authors declare that the scientific ethical and legal responsibility of this article published in EPSTEM journal belongs to the authors.

Acknowledgments or Notes

* This article was presented as an oral presentation at the International Conference on Basic Sciences, Engineering and Technology (www.icbaset.net) held in Alanya/Turkey on May 02-05, 2024.

* We would like to thank Sr. Instr. Shihab Ibrahim, Mr. Mohammed Ali, and Abdirizak Mohamed Hassan for their supports.

References

Adaway, M., & Wang, Y. (2015). Recycled glass as a partial replacement for fine aggregate in structural concrete – Effects on compressive strength. *Electronic Journal of Structural Engineering*, *14*(1), 116–122.

Afshinnia, K., & Rangaraju, P. R. (2016). Impact of combined use of ground glass powder and crushed glass aggregate on selected properties of Portland cement concrete. *Construction and Building Materials*, *117*, 263–272.

Batayneh, M., Marie, I., & Asi, I. (2007). Use of selected waste materials in concrete mixes. *Waste Management*, *27*(12), 1870–1876.

Borhan, T. M. (2012). Properties of glass concrete reinforced with short basalt fibre. *Materials & Design*, *42*, 265–271.

Chen, C. H., Huang, R., Wu, J. K., & Yang, C. C. (2006). Waste E-glass particles used in cementitious mixtures. *Cement and Concrete Research*, *36*(3), 449–456.

De Castro, S., & De Brito, J. (2013). Evaluation of the durability of concrete made with crushed glass aggregates. *Journal of Cleaner Production*, *41*, 7–14.

Dhir, R. K., Dyer, T. D., & Tang, M. C. (2009). Alkali-silica reaction in concrete containing glass. *Materials and Structures*, *42*(10), 1451–1462.

Du, H., & Tan, K. H. (2013). Use of waste glass as sand in mortar: Part II – Alkali–silica reaction and mitigation methods. *Cement and Concrete Composites*, *35*(1), 118–126.

Du, H., & Tan, K. H. (2014). Effect of particle size on alkali–silica reaction in recycled glass mortars. *Construction and Building Materials*, *66*, 275–285.

Ibrahim, K. I. M. (2017). The effect of using waste glass [wg] as partial replacement of sand on concrete. *IOSR Journal of Mechanical and Civil Engineering*, *14*(2), 41–45.

Idir, R., Cyr, M., & Tagnit-Hamou, A. (2010). Use of fine glass as ASR inhibitor in glass aggregate mortars. *Construction and Building Materials*, *24*(7), 1309–1312.

Ismail, Z. Z., & AL-Hashmi, E. A. (2009). Recycling of waste glass as a partial replacement for fine aggregate in concrete. *Waste Management*, *29*(2), 655–659.

Jani, Y., & Hogland, W. (2014). Waste glass in the production of cement and concrete – A review. *Journal of Environmental Chemical Engineering*, *2*(3), 1767–1775.

Kim, J., Yi, C., & Zi, G. (2015). Waste glass sludge as a partial cement replacement in mortar. *Construction and Building Materials*, *75*, 242–246.

Ling, T.-C., & Poon, C.-S. (2012). A comparative study on the feasible use of recycled beverage and CRT funnel glass as fine aggregate in cement mortar. *Journal of Cleaner Production*, *29–30*, 46–52.

Liu, Z., Shi, C., Shi, Q., Tan, X., & Meng, W. (2022). Recycling waste glass aggregate in concrete: Mitigation of alkali-silica reaction (ASR) by carbonation curing. *Journal of Cleaner Production*, *370*(5-6), 133545.

Mardani-Aghabaglou, A., Tuyan, M., & Ramyar, K. (2015). Mechanical and durability performance of concrete incorporating fine recycled concrete and glass aggregates. *Materials and Structures*, *48*(8), 2629–2640.

Park, S.-B., & Lee, B.-C. (2004). Studies on expansion properties in mortar containing waste glass and fibers. *Cement and Concrete Research*, *34*(7), 1145–1152.

Shamsudeen Abdulazeez, A. S., Usman, N., di, M. A., & Gabriel, U. (2020). Suitability of waste glass powder as partial cement replacement in concrete subject to chemical aggressive environment. *International Journal of Latest Technology in Engineering, Management & Applied Science*, *10*(2), 45-52.

Sharifi, Y., Houshiar, M., & Aghebati, B. (2013). Recycled glass replacement as fine aggregate in self-compacting concrete. *Frontiers of Structural and Civil Engineering*, *7*(4), 419–428.

Shayan, A., & Xu, A. (2004). Value-added utilisation of waste glass in concrete. *Cement and Concrete Research*, *34*(1), 81–89.

Taha, B., & Nounu, G. (2008). Properties of concrete contains mixed colour waste recycled glass as sand and cement replacement. *Construction and Building Materials*, *22*(5), 713–720.

Terro, M. J. (2006). Properties of concrete made with recycled crushed glass at elevated temperatures. *Building and Environment*, *41*(5), 633–639.

Topcu, I. B., & Canbaz, M. (2004). Properties of concrete containing waste glass. *Cement and Concrete Research*, *34*(2), 267–274.

Wang, H.-Y. (2009). A study of the effects of LCD glass sand on the properties of concrete. *Waste Management*, *29*(1), 335–341.

Wang, Y., Zhang, P., Cao, Y., & Ma, Y. (n.d.). Effective utilization of waste glass as cementitious powder and construction sand in mortar. *Materials*, *13*(3), 707.

Yu, X., Tao, Z., Song, T.-Y., & Pan, Z. (2016). Performance of concrete made with steel slag and waste glass. *Construction and Building Materials*, *114*(2), 737–746.

Yuksel, C., Ahari, R. S., Ahari, B. A., & Ramyar, K. (2013). Evaluation of three test methods for determining the alkali-silica reactivity of glass aggregate. *Cement and Concrete Composites*, *38*, 57–64.

Zhao, H., Poon, C. S., & Ling, T. C. (2013). Utilizing recycled cathode ray tube funnel glass sand as river sand replacement in the high-density concrete. *Journal of Cleaner Production*, *51*, 184–190.

Author Information

Filibin Ali Hassan
Cyprus International University
Haspolat, Mersin on Türkiye, TRNC
Contact e-mail: *filibinali@gmail.com*

Ayse Pekrioglu- Balkis
Cyprus International University
Haspolat, Mersin on Türkiye, TRNC

To cite this article:

Hassan, F. A., & Pekrioglu-Balkis, A. (2024). Utilization of crushed waste glass as a partial replacement for sand in cement mortar for a sustainable environment. *The Eurasia Proceedings of Science, Technology, Engineering & Mathematics (EPSTEM), 28,* 259-276.

The Eurasia Proceedings of Science, Technology, Engineering & Mathematics (EPSTEM)
ISSN: 2602-3199

The Eurasia Proceedings of Science, Technology, Engineering & Mathematics (EPSTEM), 2024

Volume 28, Pages 277-285

ICBASET 2024: International Conference on Basic Sciences, Engineering and Technology

Utilizing the eXtreme Gradient Boosting Algorithm for Artificial Intelligence-supported Learning Analytics Application

Mustafa Cosar
Hitit University

Abstract: Recent technological advancements, including internet-based distance education and artificial intelligence-supported learning analytics, have significantly impacted the field of education. These advancements not only enhance the efficiency of education but also broaden access to learning while mitigating barriers to implementation. AI-supported learning analytics emerges as a pivotal tool for interpreting data gleaned from educational processes and stakeholders, thereby enhancing educational processes and outcomes. This tool streamlines the measurement, analysis, and evaluation of learning processes, encompassing a wide array of factors and parameters. Moreover, it contributes to the development of personalized and adaptive learning environments. In this study, a predictive model utilizing the XGBoost algorithm has been developed to analyze students' academic achievements. The model forecasts final exam grades based on various student characteristics, including age, participation rate, and exam scores. Evaluating the performance of the AI model involves metrics such as Mean Squared Error, Mean Absolute Error, and R^2 score. In findings indicate a strong prediction performance, with an R^2 score of 0.819. As a result of underscore the potential of AI-supported learning analytics as an effective tool for predicting and enhancing student academic performance.

Keywords: Artificial intelligence, Learning analytics, Machine learning, XGBoost algorithm

Introduction

Learning activity is a dynamic phenomenon that arises from the interaction of elements within education and is influenced by numerous parameters. During the emergence of this phenomenon, a plethora of data is generated from each stage and component. These data undergo various data processing processes such as organization, classification, and computation. As a result of these processes, they become manageable through data analysis, evaluation, and reporting activities.

The recommendation and utilization of Artificial Intelligence (AI) as a tool in the development and evaluation stages have demonstrated significant benefits in enhancing success, particularly in recent years. The concept of success varies across different domains, encompassing productivity, profitability, academic achievement, and accuracy. AI-supported Learning Analytics (LA) involves the utilization of AI technologies to understand, optimize, and enhance learning processes and student performance. Such an analytical process typically provides valuable contributions to educational institutions, teachers, and students.

Considering the existing resources, physical facilities, and student numbers in learning environments, the provision of personalized education may not seem feasible. However, it is essential to promptly address the negative impacts of these factors on student engagement, motivation, and success. Information technologies play a crucial role in improving these factors. AI technology can analyze data concerning all actors and factors involved in the process, thereby optimizing the process and outcomes. Additionally, as noted by Copgeven et al. (2023), AI techniques can be utilized to provide instant feedback to learners, enable learners to track their own learning processes, and offer messages to enhance learner motivation and engagement.

In today's world, where educational environments are increasingly becoming digitalized, the usage habits of learners in these environments, their navigation patterns, frequency of using learning resources, and their performance in exercises and exams have become valuable datasets. These datasets are processed, analyzed, and evaluated using machine learning methods. The findings obtained from these analyses are utilized as improvement factors for all components of education.

In this study, machine learning process using the XGBoost (eXtreme Gradient Boosting) algorithm was employed to predict final grades based on a dataset containing students' course information, demographic characteristics, exam scores, and final grades. The proximity rates between the predicted and actual grades were analyzed to draw certain conclusions. The article follows a structured format, with the second section dedicated to providing fundamental information supported by the literature on AI, XGBoost, and LA. The third section discusses the methodology of the application, including the dataset, the AI algorithm used, the developed model, and pseudo-codes in the Python language. The fourth section presents the findings obtained from running the application with tables and graphs. Finally, a general evaluation is made in the last section based on the findings, providing insights into the effectiveness of AI-supported XGBoost regression analysis in predicting student performance.

Literature Review

AI and data analytics are playing an increasingly important role in understanding and improving the learning processes in education. AI-supported LA has the potential to identify strengths and weaknesses in education by utilizing information derived from large datasets, and optimize educational programs accordingly. According to Chatti et al. (2012), Learning Analytics (LA) is a multidisciplinary research field that aims to develop methods for detecting and analyzing data models in educational environments. These methods are then utilized to enhance the overall learning experience.

AI is defined as the ability of machines to adapt to variable conditions, make intelligent predictions, solve problems, and perform behaviors that require a certain level of intelligence comparable to that of humans (Coppin, 2004). By incorporating AI into learning environments, intelligent tutoring systems are emerging. This system is described as a supportive and guiding system that provides feedback to and directs the student, the teacher, and the system itself before, during, and after the learning process (Fardinpour et al., 2014). In the design of this system, AI techniques and algorithms such as Decision Trees (DT), Artificial Neural Networks (ANNs), and Decision Networks are utilized (Talan, 2021).

According to Gligorea et al. (2023), AI technologies play a crucial role in optimizing learning paths, enhancing student engagement, and improving academic performance. Through a comprehensive literature review, the authors found evidence suggesting that AI has the potential to enhance students' test scores in various studies. The incorporation of AI and Machine Learning (ML) into e-learning platforms is emphasized as a key driver for personalized and effective educational experiences.

According to Moreno et al. (2020), AI-supported learning systems bring numerous benefits, including the creation of an enhanced learning environment, program flexibility, immediate feedback provision, control over students' experiences, and facilitation of accelerated development. These systems leverage their capacity to analysis large volumes of data, learn from tracks and experiences, make predictions, and provide personalized recommendations. By utilizing AI, it becomes possible to implement diverse teaching methods that cater to individual students' levels and overcome academic barriers (Tapalova & Zhiyenbayeva, 2022).

Liu and Yu (2023) summarized the overall architecture of a big data-based learning system in their study, as depicted in Figure 1. Upon careful examination of this architecture, it can be observed that the learning components layer, the information technology layer, and the data processing layer are in communication with each other. Additionally, it is understood that these layers interact continuously with the data management layer in the architecture.

In e-learning platforms, the utilization of AI and machine learning (ML) algorithms or methods is common for various purposes such as content personalization, academic performance prediction, knowledge gap identification, and dynamic assessments. Gligorea et al. (2023) recommend the use of AI algorithms in learning analytics processes to model students' behavior, predict their success, recognize complex patterns and optimize learning processes.

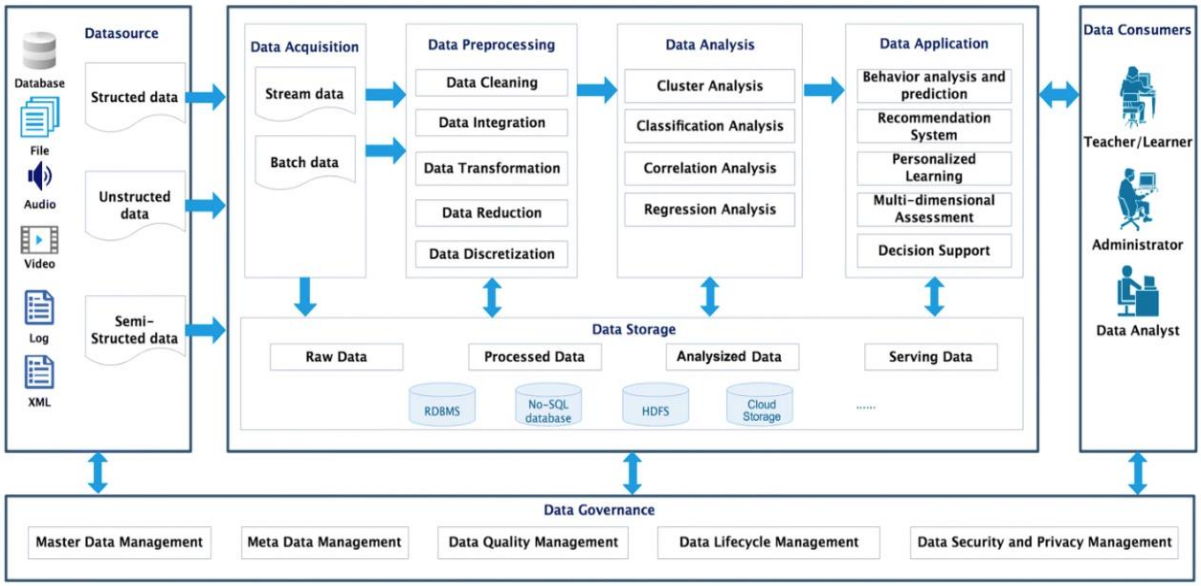

Figure 1. The architecture of big data based E-learning systems (Liu & Yu, 2023)

Prediction algorithms can range from simple to highly complex and have their own limitations. This process requires collaboration among individuals with different skills, such as data analysts, education experts, and content specialists. This team needs to organize input data, information on the accuracy of prediction algorithms, and which predictions should be reported to stakeholders. As an example of AI algorithms used in predicting academic achievement in LA processes, Veluri et al. (2021) suggest the following algorithms: Support Vector Machine, NaiveBayes Classifier, DT, k-Nearest Neighbors (kNN), Logistics Regression, and ANNs.

Ifenthaler and Yau (2020) emphasize that Learning Analytics (LA) has emerged as a methodology that integrates education and data science to evaluate the effectiveness of online learner interactions. Its main objectives are to inform instructional design and provide support for student success. Similarly, Castellanos- According to Reyes et al. (2023), there is a general consensus that in level of higher education, LA primarily focuses on assisting student success.

Drachsler and Greller (2012) categorize LA studies into two groups based on their objectives: reflection and prediction. Reflection studies enable students or teachers to monitor their performance and progress by comparing old and new data within their own dataset. Prediction studies, on the other hand, focus on identifying existing problems or situations in advance. Broos et al. (2020) highlight that the primary goal of reflection studies is to enable individuals, such as students or other stakeholders, to monitor their performance and evaluate themselves based on the reflection of their performance using both old and new data (Önder, Öztaş & Akçapınar, 2023).

Er (2023) states that there is sufficient evidence in their study to suggest that ML algorithms can accurately predict students who are possibility of school dropping out based on their online interaction data. The predictive power of these models relies on advanced mathematical calculations required by the underlying algorithms. However, this complexity makes it challenging for end-users to interpret the results. For example, while dropout prediction can provide instructors with a highly reliable report on students at risk of dropping out, it may not provide sufficient information about the reasons behind this prediction. This can lead to a delay in timely intervention. The author saw that among 1087 students in a sample data set, 351 had dropped out of school. He tried to predict this situation with AI. He calculated the prediction accuracy of the study as 0.80.

In their study, Hasib and colleagues (2022) conducted a comparative analysis using Logistic Regression, K-NN, SVM, XGBoost, and NBC algorithms. For the XGBoost algorithm, they found an accuracy value of 0.98. XGBoost algorithm has shown promising results in predicting student performance with the support of AI. However, it should be noted that the accuracy metric used for calculating prediction accuracy is typically employed for multi-class predictions. Since the target variable in the dataset represents a continuous value, it is suggested to calculate metrics such as R-squared (R^2), Mean Absolute Error (MAE), Variance, Mean Absolute Percentage Error (MAPE) and Mean Squared Error (MSE) instead of accuracy.

Felicia and Ferren (2022) performed an analysis with the Student Performance dataset using Generalized Linear Model, Random Forest and NBC algorithms. According to the results of the research, the algorithm with the highest accuracy was Naive Bayes with 48.59%. Zhang et al. (2021) in their study with the same data set using Gradient Boosting DT (GBDT), XGBoost, Adaptive Boosting (AdaBoost), Random Forest and DT algorithms, found that random had the highest score in accuracy values. They found it to be 0.90308 in the forest algorithm. The low accuracy values of these models may be due to the characteristics of the data set not being suitable for these models.

Contrary to these studies I have come across in the literature, in this research, an analysis was made with MSE, MAE and R2 values rather than accuracy value. Performance of predictive models; It should be noted that it depends on model parameters, course type, participant characteristics, data set structure and many other features. Therefore, transferring models between courses appears to be quite difficult, even for different runs of the same course. For this reason, model and application parameters are likely to produce different results in different courses (Er, 2023; Gasevic et al., 2016).

Method

In the study, a predictive model using the XGBoost AI algorithm was developed to forecast student academic scores. The model was trained using the Student Performance dataset. The final exam grades were predicted by taking into account various factors such as the students' ages, genders, family information, attendance rates, and academic performance data such as Grade 1, Grade 2, and Grade 3 (Final Score) within the dataset. For this purpose, an XGBoost decision tree model was built, taking into account the dataset features. Metrics such as MSE, MAE, and R2 Score employed to evaluate the accuracy and predictive power of the model. Additionally, a scatter plot was created to demonstrate the impact of actual scores on the predicted final scores.

Dataset

These data are taken from the dataset called Student Performance, which was collected by Cortez and Silva (2008) from secondary students of two Portuguese schools using school reports and surveys. The dataset used in the study comprises various types of data, including student exam grades, demographic information, social factors, and school-related data. The dataset encompasses a total of 395 students, providing a comprehensive set of information for analysis and modeling purposes. Students' grades in Mathematics were used to determine their academic performance. The data set is available on the website as the UCI Machine Learning Repository (UCI, 2024).

Model Architecture and Model Training

XGBoost is a widely used gradient boosting algorithm that has achieved impressive results in many areas of ML. The application of meta-learning to recommend hyperparameters for XGBoost can greatly reduce the time and computational resources needed to optimize the model. By leveraging meta-learning techniques, the process of finding the most effective hyperparameters for XGBoost can be automated, leading to more efficient and effective model optimization. Recently, XGBoost algorithm has been increasing in popularity due to its convenience, scalability, and ability to work well with both regression and ranking problems using the Gradient Boosting structure (Chen & Guestrin, 2016; Morinho et al., 2024).

In XGBoost, multiple decision trees are used to build the model. In the model, each tree is a collection of weak decision trees that sequentially refine the residues of previous trees. The hyperparameter *n_estimators* control the number and type of trees used in the ensemble. The layer depth of the tree is controlled by the *max_depth* hyperparameter. Formula 1 defines the basic formula of this algorithm.

$$\hat{y}_i = \sum_{k=1}^{K} f_k(x_i), f_k \in F, \tag{1}$$

Each tree is trained to correct the prediction errors of previous trees. This is done by optimizing a loss function based on the negative gradient of the error function (e.g., mean square error). According to Formula 1; $\hat{y}_i$ is the

predicted value for the *i*-th observation (Predicted final exam grade); f_k is the k th regression tree; x_i is the input features for the *i*-th observation (student feature vector for this application); *F* is the set of all possible regression trees and *K* is the model is the total number of trees used. These trees are used to predict the final exam grade based on the student's characteristics. Finally, the predictions of all trees are combined to obtain the total prediction.

Hyperparameter tuning using the *GridSearchCV* method can optimize the model's performance by adjusting crucial parameters that have a significant impact on the model's behavior. These parameters include the number of trees, learning rate, and tree depth. Algorithm 1 in Python presents the general structure of the model as pseudo code, allowing for the systematic exploration of hyperparameter combinations.

Algorithm 1. XGBoost Model Application for Learning Anatilics

1. Import necessary libraries: pandas, xgboost numpy and matplotlib libraries
   from sklearn[.metrics, .model, .preprocessing] import [LabelEncode, GridSearchCV]
2. Loading of sample dataset
   student-mat.csv
3. Preprocessing (names and others features) and Split the dataset (train/test)
   X = data.drop("G3", axis=1)
   y = data["G3"]
   X_encoded = X.apply(label_encoder.fit_transform)
4. Create a XGBoost_AI model:
   xgb_model = xgb.XGBRegressor()
   …
   param_grid = {
   'max_depth': [3, ., .],
   'n_estimators': [100, ., .],
   'learning_rate': [0.05, ., .],
   }
5. Train the model:
   model.fit(X_train, y_train)
6. Make predictions:
   y_pred = xgb_model.predict(X_test)
7. Model's performance values
   mse =…
   mae =…
   r2 =…
8. Evaluate the model's performance
   *xgb_model = xgb.XGBRegressor(**best_params)*
9. Visualize predictions and true values:
   print("Mean Squared Error (MSE):", mse)
10. Graphs of all models and metrics with the plot( ):
    plt.scatter, plt.show().

In the code example given above, there are 395 students in the student-math.csv file. A portion of these students is assigned to the training set, while the remaining students are allocated to the test set. This distinction was made using the *train_test_split* function so that the data set was 80% training and 20% testing. These additional features can be utilized to enhance the overall power of the model or to emphasize a specific combination of features.

Results and Discussion

In this application, calculations were made through a prediction model using the attributes of the student data set. Metrics were employed to evaluate the performance of the model. Mathematical metric measurements and a graphical scatter plot were created to show the impact of all attributes on the final scores. When the Python code of the application is run, the parameter values are calculated as in Table 1 below. In Table 1, for each student in the first column, the actual final grade versus the estimated final grade obtained when the model is run is given. It can be seen that these notes are close to each other. Table 2 gives the values of these grade predictions calculated on the basis of metrics.

Table 1. Student-based grade predictions of the prediction model

Student	Actual Score	Predicted Score
78	10	8.693336
371	12	11.427962
248	5	6.250742
55	10	10.154843
390	9	9.746037
…	…	…
364	12	11.213716
82	6	6.671789
114	9	10.471691
3	15	13.825548
18	5	6.275213

Table 2. Calculated metric values of the prediction model

Metrics/Model	XGBoost
MSE	3.714846907185788
MAE	1.165801862749872
R^2 Score	0.818832560655874
S^2 (Variance)	20.989616397866733

The calculated MSE value of 3.71 suggests good model accuracy. MAE is a metric that measures the average absolute difference between model predictions and actual values. The calculated MAE value of 1.17 indicates that, on average, the model predicts approximately 1.17 units away from the actual values. The Model's R^2 value of 0.82 suggests that approximately 82% of the variance in the target variable is explained by the independent variables. Overall, the model shows a strong predictive power as reflected in the MSE, MAE, and R^2 scores, indicating its ability to capture the relationship between the data.

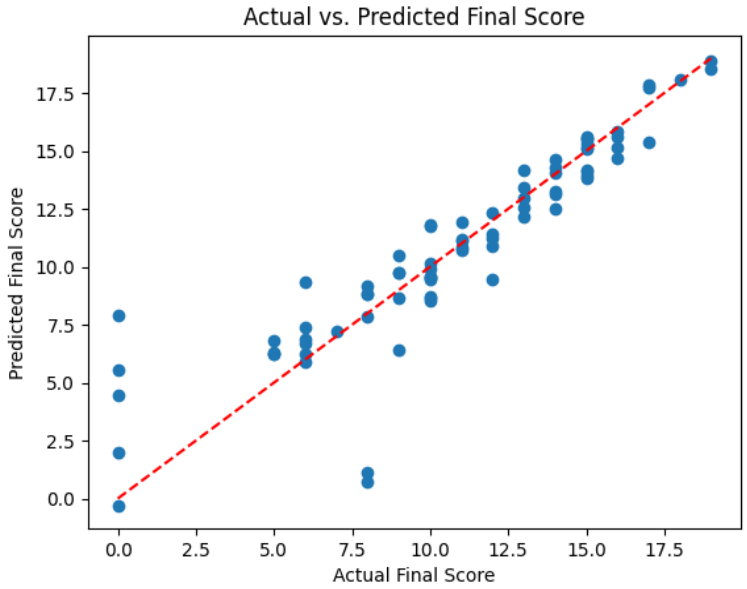

Figure 2. Actual vs. predicted final score plot

In Figure 2, the graph displays the distribution of the actual and predicted final results of the sample. The x horizontal axis is the axis of actual final scores, the Y vertical axis is the axis of predicted final scores. The presence of a red dashed line aids in visualizing a perfect prediction scenario, where the actual and predicted values align. The concentration of data points around this red line indicates the level of compatibility between the actual and predicted values.

In the graph in Figure 3, the predicted final scores are shown on the x-axis, and the residuals (differences between actual and predicted scores) are shown on the y-axis. The red dashed line indicates the point at which the residuals are zero (i.e., a perfect prediction is made). This chart shows how accurate your model's predictions are and where they are inaccurate.

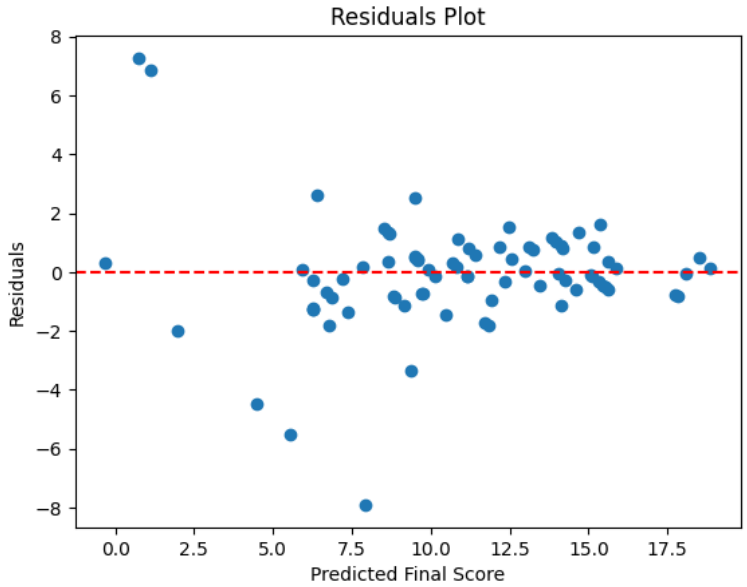

Figure 3. Residuals plot graph

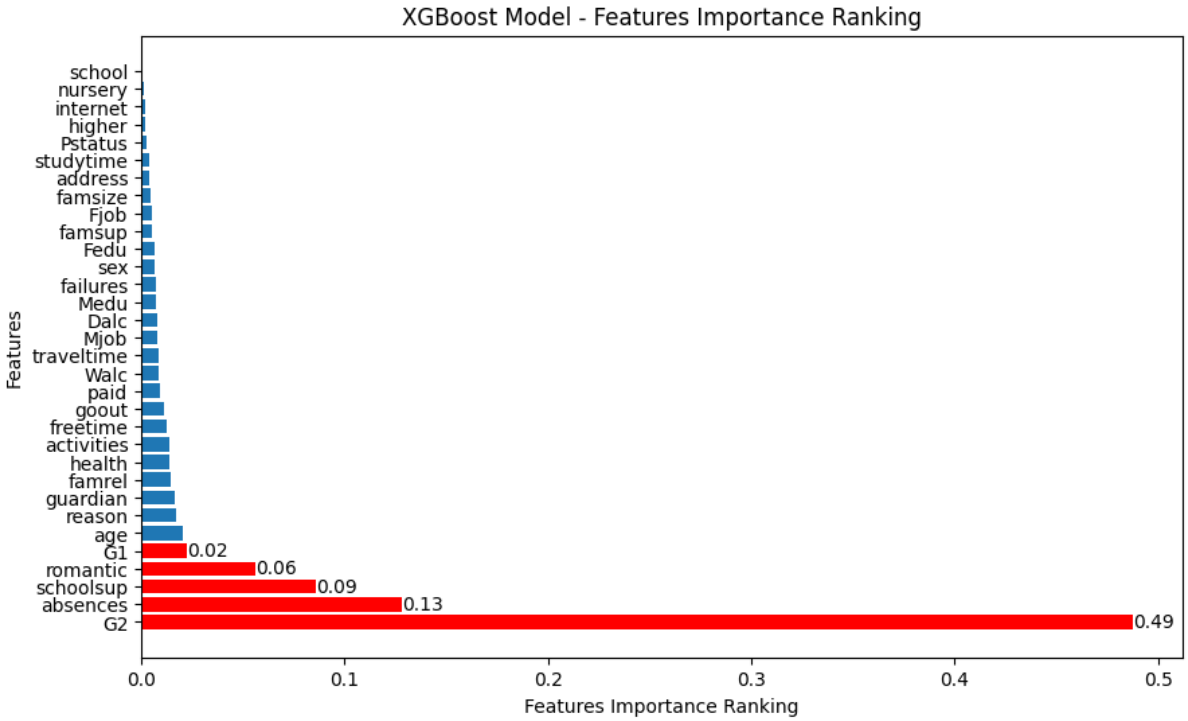

Figure 4. Weighted Effect of different features by model

Model coefficients are presented graphically in Figure 4 to help determine the effect of each feature or variable on the target variable. This analysis is important to determine which features have more weight and how important they are in the predictions. Looking at Figure 4, you can see how much impact all of these features have on the XGBoost model. According to Figure 4, the 5 features that have the most weight in predicting the final score are; It is understood that there are G2, absences, schoolsub, romantic and G1. This information can help better understand the factors that influence student performance and optimize their effects.

Conclusion

This LA application, the XGBoost model proved highly successful in predicting student performance. Among the attributes used, G2, Absences, and Schoolsub were found to have a significant impact on final exam grades.

While the G1 score and certain demographic characteristics also influenced performance, their effects were comparatively less pronounced. The utilization of AI and ML techniques has revolutionized student data analysis, enabling adaptive learning systems to create personalized profiles and gain insights into individual strengths and needs. By leveraging AI algorithms, these systems can tailor learning content, adjust task difficulty, and provide targeted interventions, resulting in improved learning outcomes and enhanced engagement, motivation, and information retention for learners.

The impact of information technologies and AI on educational environments goes beyond just LA and extends to the utilization of immersive technologies like internet of things, cloud computing, virtual reality and augmented reality for enhancing the learning experience. Such technologies especially help medical, engineering, design and architecture students to connect with reality and visualize objects and concepts from abstract to concrete. Radu (2012) emphasizes that thanks to these technologies, the content is enriched, learning improves and motivation increases.

On the other hand, some basic problems are encountered in LA with such AI technologies, such as not being able to establish the appropriate model, not being able to calculate the correct metrics, not being able to ensure data confidentiality, the emergence of advanced hardware and software needs, and the system's inability to make accurate predictions with very little data at the beginning. Additionally, integration and compatibility problems also arise during the implementation of such innovations. In order to cope with such negativities, good coordination should be ensured between educators, designers and practitioners.

This study places significant emphasis on the importance of AI-supported LA in education and demonstrates its effectiveness in predicting student performance with AI algorithms. In particular, it shows that information obtained through the use of large data sets is a valuable resource for improving decision-making processes in education. It may be a good idea to initially start with a simple regression model, and then improve the model with AI algorithms and improve prediction rates. Future research may focus on further developing AI-assisted LA by using larger data sets and applying different ML techniques.

Scientific Ethics Declaration

The author declares that the scientific ethical and legal responsibility of this article published in EPSTEM journal belongs to the author.

Acknowledgements or Notes

* This article is an updated and extended version of the abstract presented orally at the International Conference on Basic Sciences, Engineering and Technology (www.icbaset.net) held in Alanya/Turkey on May 02-05, 2024.

References

Broos, T., Pinxten, M., Delporte, M., Verbert, K. & De Laet, T. (2020). Learning dashboards at scale: Early warning and overall first year experience. *Assessment & Evaluation in Higher Education*,*45*(6), 855-874.

Castellanos-Reyes, D., Koehler, A.A., & Richardson, J.C. (2023). The i-SUN process to use social learning analytics: A conceptual framework to research online learning interaction supported by social presence. *Frontiers in Communication*,8,

Chatti, M. A., Dyckhoff, A. L., Schroeder, U. & Thus, H. (2012). A reference model for learning analytics. *International Journal of Technology Enhanced Learning*, *4*(5-6), 318-331.

Chen, T., & Guestrin, C. (2016). Xgboost: A scalable tree boosting system. *Proceedings of the 22nd Acm Sigkdd International Conference on Knowledge Discovery and Data Mining* (pp. 785-794).

Coppin, B. (2004). *Artificial intelligence illuminated* (p.739). Massachusetts, USA: Jones & Bartlett Publishers.

Cortez, P., & Silva, A.M.G. (2008). Using data mining to predict secondary school student performance. In A. Brito, J. Teixeira (Eds.), *Proceedings of 5th Future Business Technology Conference (FUBUTEC 2008)* (pp. 5-12).

Copgeven, N. S., Ozkaya, H., & Aydın, S. (2023). Acık ve uzaktan ogrenmede yapay zeka destekli oyunlastırma. *Acıkogretim Uygulamaları ve Arastırmaları Dergisi*, *9*(1), 386-407

Drachsler, H., & Greller, W. (2012). The pulse of learning analytics understandings and expectations from the Stakeholders. *LAK '12: Proceedings of the 2nd International Conference on Learning Analytics and Knowledge* (pp. 120-129).

Er, E. (2023). KACD'lerde okuldan ayrılanları tahmin etmeye ve anlamaya yonelik acıklanabilir bir makine ogrenimi yaklasımı. *Kastamonu Egitim Dergisi*, *31*(1), 153-164.

Fardinpour, A., Pedram, M. M., & Burkle, M. (2014). Intelligent learning management systems: Definition, features and measurement of intelligence. *International Journal of Distance Education Technologies (IJDET), 12(*4), 19-31,

Felicia, & Ferren. (2022). Exploring secondary school performance by using machine learning algorithms. *Journal of Educational Analytics*, *1*(1), 41-60.

Gasevic, D., Dawson, S., Rogers, T., & Gasevic, D. (2016). Learning analytics should not promote one size fits all: the effects of instructional conditions in predicting academic success. *Internet and Higher Education*, 28–84.

Gligorea, I., Cioca, M., Oancea, R., Gorski, A. T., Gorski, H., & Tudorache, P. (2023). Adaptive learning using artificial intelligence in e-Learning: A literature review. *Education Sciences*, *13*(12),1216.

Hasib, K. M., Rahman, F., Hasnat R., & Alam, M. G. R. (2022). A machine learning and explainable ai approach for predicting secondary school student performance. *2022 IEEE 12th Annual Computing and Communication Workshop and Conference (CCWC)* (pp.399-405). Las Vegas, NV, USA.

Ifenthaler, D., & Yau, J. Y. K. (2020). Utilising learning analytics to support study success in higher education: A systematic review. *Educational Technology Research and Development, 68,* 1961-1990.

Liu, M., & Yu, D. (2023). Towards intelligent e-learning systems. *Education and Information Technologies, 28,* 7845–7876.

Marinho, L.T., Nascimento, D. C., & Pimentel, B. A. (2024). Optimization on Selecting XGBoost hyperparameters using meta-learning. *Expert Systems*, e13611.

Moreno-Guerrero, A. J., Lopez-Belmonte, J., Marin-Marín, J. A., & Soler-Costa, R. (2020). Scientific development of educational artificial intelligence in Web of Science. *Future Internet*, *12*(8), 124.

Onder, A., Oztas, G. S., & Akcapınar, G. (2023). Ogrenme analitigi surecine yonelik modellere genel bir bakıs: Kavramsal bir cerceve onerisi. *Acıkogretim Uygulamaları ve Arastırmaları Dergisi*,*9*(1), 92-117,

Radu, I. (2012). Why should my students use AR? A comparative review of the educational impacts of augmented-reality. *IEEE International Symposium on Mixed and Augmented Reality (ISMAR)* (pp.313-314). IEEE.

Shuai Z., Jie C., Wenyu Z., Qiwei X., & Jiaxuan S. (2021). Education data mining application for predicting students' achievements of Portuguese using ensemble model. *Science Journal of Education*, *9*(2), 58-62.

Talan, T. (2021). *Egitimde dijitallesme ve yeni yaklasımla* (1th ed., p.363). Istanbul, Turkey: Efe Akademi Publishing

Tapalova, O., & Zhiyenbayeva, N. (2022). Artificial intelligence in education: AIED for personalised learning pathways. *The Electronic Journal of e-Learning (EJEL)*, *20*, 639-653,

UCI. (2024). *Student performance. UCI machine learning repository*. Retrieved from https://archive.ics.uci.edu/dataset/320/student+performance

Veluri, R. K., Patra, I., Naved, M., Prasad, V. V., Arcinas, M. M., Beram, S. M., & Raghuvanshi, A. (2022). Learning analytics using deep learning techniques for efficiently managing educational institutes. *Materials Today: Proceedings*, *51*(8), 2317-2320,

Author Information

Mustafa Cosar
Department of Computer Engineering, Hitit University
19030, Corum/Turkiye
Contact e-mail: *mustafacosar@gmail.com*

To cite this article:

Cosar, M. (2024). Utilizing the eXtreme gradient boosting algorithm for artificial intelligence-supported learning analytics application. *The Eurasia Proceedings of Science, Technology, Engineering & Mathematics (EPSTEM), 28,* 277-285.

The Eurasian Proceedings of Science, Technology, Engineering & Mathematics (EPSTEM)
ISSN: 2602-3199

The Eurasia Proceedings of Science, Technology, Engineering & Mathematics (EPSTEM), 2024

Volume 28, Pages 286-299

ICBASET 2024: International Conference on Basic Sciences, Engineering and Technology

Edible Coating from Breadfruit Starch and Chitosan for Food Packaging

Dewi Sulistyowati
Universitas Pendidikan Indonesia

Hernani Hernani
Universitas Pendidikan Indonesia

Asep Supriatna
Universitas Pendidikan Indonesia

Abstract: Lectures that encompass Education for Sustainable Development (ESD) can encourage awareness about sustainable development by integrating current issues, such as the potential of breadfruit starch and chitosan for making edible coatings for food packaging. This work aimed to study the development of edible coating from breadfruit starch (BS) and chitosan (CH) for food packaging based on SDGs aspects and as preliminary research to develop worksheets for prospective chemistry teacher students. BS-CH edible film developed by solvent evaporation method, thickness measurement, and physical properties for application on chili, carrot, and sweet potato which. The results showed that the optimal comprehensive properties of the film were obtained when the mass ratio of 3% AS to 1% CH was 7:3. The solubility test results show that the addition of CH ratio increases the swelling of the film before the dissolution process. The tensile strength and elongation of the film increased with the addition of CH until the optimum condition with tensile strength values of 3.01 MPa and 58.26%. The optimum mass ratio was applied through the coating of carrot, chili, and sweet potato which can prevent mass weight and mushroom. Apart from that, student opinion data was generated in the form of potential edible coating topics in the theme of ESD issues. In addition, student opinion data was generated in the form of expectations of edible coatings topics in ESD-laden chemistry learning, including understanding and applying ESD principles and the context of edible coatings and introducing the potential of edible coatings in society so that it is expected to improve 21st-century skills. The results of this research show the need to integrate the topic of edible coating of breadfruit starch and chitosan in worksheets for prospective chemistry teacher students.

Keywords: Edible coating, Breadfruit and chitosan, Food packaging

Introduction

Fruits and vegetables are very easily damaged during the ripening process and after harvest so their shelf life is shorter and they are susceptible to microbial attack, oxidation, and browning (Matloob et al., 2023). Post-harvest technology is very necessary to maintain quality and extend the shelf life of harvested products. The importance of postharvest technology to maintain the quality of horticultural products in terms of organoleptic, physio-chemical, and sensory properties from various external damages including chemical, physical, and biological (Díaz-Montes & Castro-Muñoz, 2021; Matloob et al., 2023). *Edible coating* is a post-harvest technology in the form of packaging that is safe to use and can minimize moisture loss, water and gas exchange while improving the texture of the product (McHugh & Krochta, 1994). The nature of *edible coatings*, which are easy to eat, non-toxic, and cost-effective compared to other synthetic coatings, is very advantageous (Raghav et al., 2016). *Edible coatings* can be made from proteins, polysaccharides, lipids, plasticizers, and emulsifiers which are environmentally friendly (Matloob et al., 2023; Bizymis & Tzia, 2022). *Edible coating* simultaneously

addresses the problem of pollution generated by waste, as well as developing strategies for obtaining food that benefits consumer health (Iamareerat et al., 2018; Vega-Castro et al., 2022).

This research used breadfruit starch and chitosan as the main matrix for edible coatings. Among various biopolymers, starch was chosen to be mixed with chitosan, because starch has specific advantages including being tasteless, odorless, transparent, and resistant to O_2 flow. In addition, starch is a cheap, abundant, and easy-to-process raw material (Zheng et al., 2019). Sukun is a typical tropical plant with a total fruit production of 28,078.5 tonnes in 2021 in West Java province, Indonesia (Open Data West Java, 2021). Its patriarchal content reaches 28.78% based on Bezerra et al. (2019) with the amylose and amylopectin contents varying from 16.4 to 53.7% and 72.3 to 77.5% depending on the maturity level, climatic conditions, and seasonal effect of the fruit (Turi et al., 2015). Perera et al. (2021) starch base material as edible has low tensile strength and elongation, so additional ingredients are needed, namely chitosan. Chitosan-based functional nanocomposite films improved physical properties and enhanced antioxidant and antimicrobial functions (Roy & Rhim, 2021). Chitosan can form intermolecular bonds with starch, which helps improve film structure and physical properties, transparency, and antibacterial activity (Shah et al., 2016). Modified starch-based edibles have been successfully used in preserving fruits, one of which is banana starch and chitosan for coating strawberry, apple, and mango fruits which can reduce mass shrinkage and increase shelf life (Abera et al., 2024).

Edible coating as a food packager is included in several SDGs goals in economic, social, and environmental aspects. The first goal of the SDGs, namely "eliminating poverty", this topic can be linked to the issue of low welfare of local farmers due to the lack of post-harvest technology. The second goal is "food security" which can be overcome through sustainable agriculture by increasing the value of agricultural products through *edible post-harvest technology*. The ninth objective is "industry, innovation and infrastructure" regarding predictions of the potential *of edible coatings* to increase the shelf life of agricultural products on an industrial scale. The fifteenth goal is "life on land" regarding biodiversity as the main raw material for making *edibles,* the potential for *edible coatings* to increase the shelf life of agricultural products on an industrial scale (UNESCO, 2014). The relationship between the topic *of edible coatings* and several SDGs goals can be applied in learning chemistry with ESD content. Understanding the topic of *edible coatings* as food packaging is supported through courses studied which include organic and analytical chemistry, both theoretical in class and practicum. Universities play a strategic role towards sustainable development to provide a holistic perspective (Findler et al., 2019; Kohl et al., 2021). Educators are required to incorporate sustainable development (ESD) education into pre-service teacher training curricula (UNESCO, 2014). Lectures containing ESD can create agents of change for the future, improve character and values, increase knowledge and skills, support sustainable development, and serve as learning innovation. Therefore, implementing ESD in lectures, especially in chemistry education study programs, still needs to be carried out and studied in more depth.

In this era of globalization, skills in terms of sustainability are needed to face a complex and ever-changing world by looking at problems from various perspectives to find sustainable solutions so that the actions taken are more responsible (Tarrant, 2016 & Anita et al., 2023). According to Singh-Pillay (2020), ESD-oriented learning gives rise to three main learning experiences, namely encouraging social learning abilities, promoting real-world contexts, and as a catalyst for student-teacher awareness regarding their role as agents of change. Students are required to care and be able to solve problems in the surrounding environment as well as tolerance for social and economic problems to realize ESD. Learning that is carried out with an ESD lens makes students have broader ideas about various aspects of sustainability such as economic, social, and even environmental aspects (Paristiowati et al., 2022; Singh-Pillay, 2020). ESD-oriented learning can be implemented in two methods, either online (Paristiowati et al., 2022) through a summer school program or face-to-face (Singh-Pillay, 2020) with maximum results according to the expected learning objectives. Based on the background explanation, shows the potential for integrating the topic *of edible coating* from breadfruit starch and chitosan in worksheets for prospective chemistry teacher students with ESD content.

Method

This research used the laboratory experiment method which is strengthened by open-ended questionnaire data relating to ESD content and the topic of BS-CH edible coating as food packaging in chemistry learning. Questionnaires were given to 36 chemistry education students at one of the universities in Bandung City. The data obtained was analyzed to identify students' opinions and expectations regarding the chemistry learning they had taken. The results of the experiment and answers to open-ended questions provide insight into the application of BS-CH edible coating as food packaging and the need for this topic to be integrated into ESD-based chemistry learning in worksheets for prospective chemistry teacher students.

Materials

Ripe breadfruit (*Artocarpus altilis*), distilled water, chitosan produced by Surindo Biotech Cirebon Indonesia, glacial acetic acid 98%, glycerin. The researcher selected breadfruit depending on availability and harvesting stage. The chilies (*Capsicum frutescens*) and carrots (*Daucus carota L.*) used were obtained from farmers directly to determine the time of picking which made it easier for researchers to calculate the optimum period of coating. Meanwhile, sweet potato (*Ipomoea batatas L.*) was obtained from the market based on availability.

Breadfruit Starch Preparation

The starch content in breadfruit was obtained from 4 breadfruit grains with a mass of 2.7 kg. The breadfruit was peeled and washed, cut into pieces, and crushed with water (1:4 b/v ratio). After grinding, the starch slurry was kept to settle for 12 hours. The starch was allowed to settle in a container, the liquid part above was discarded, and the starch was separated. The prepared raw starch was kept for evaporation and dried in an oven at 100°C for 6 hours (Abera et al., 2024). The yield of starch obtained was calculated as given in Equation (1):

Yield = (Mass of dried starch, g / Total mass of breadfruit, g) x 100 (Modesti et al., 2019)

Edible Film Preparation

The starch solution was prepared (by dissolving 3 g of starch in 100 mL distilled water) and heating it for 35 minutes on a hot plate (85^{o}C). The gelatinized starch solution (indicated by a clear color) was lowered to 50◦C while stirring, then 1% glycerin was added and homogenized for 15 minutes. Chitosan solution was prepared by mixing 1 g chitosan with 1% (v/v) glacial acetic acid (100 mL). The chitosan solution was allowed to stand for 1x24 hours before being added to the starch-glycerin solution at 50◦C while stirring until the solution was completely homogeneous for 10 minutes. The starch-chitosan-glycerol solution was reduced in temperature while stirring for 10 minutes at 25◦C to remove bubbles (Abera et al., 2024). The solution was dried at room temperature for 3x24 hours in a 110x130 mm container at a total volume of 50 mL. The molded edible film was peeled off, stored in a plastic bag at room temperature, and kept in a desiccator before further examination.

Physical and Mechanical Properties Edible Film

Film Thickness

Film thickness was measured with a digital micrometer (Krisbow Micrometer Digital 10175725 0-25 mm/ 0,001 mm) at two random positions Determination of Tensile Strength and Elongation at Break.

Water Solubility

The water solubility of the films was determined based on the methodology described Zhang *et al* (2019) with slight modifications. Specifically, 2 specimens of each film (2 cm × 3 cm) were initially weighed (W1) and then placed in 50 mL of distilled water for 24 hours at room temperature. Excess water on top of the film was carefully scraped off using filter paper. The undissolved film was dried at room temperature and weighed at time intervals of 30, 60, and 90 min and then weighed again (W2). Water Solubility (WS) was calculated according to the following equation:

$$\text{WS (\%)} = \frac{(W1-W2)}{W1} \text{ x } 100\%$$

Tensile Strength and Elongation at Break

The mechanical properties of the film were determined using a material testing machine (Zwicky 2,5 kN). The test was conducted according to ASTM D882-09. Samples were cut into strips (10,5 cm × 2,5 cm) and inserted into the apparatus. Tensile strength (TS) and percent elongation at break (EAB) were calculated as follows:

$$TS = \frac{F}{d\ x\ L}$$

where F was the maximum tension (N), d was the initial grip separation (30 mm), and L was the average film thickness (mm).

$$EAB\% = \frac{l1-l0}{l0} \text{ x } 100\%$$

where l1 was the final displacement (mm), l0 was the initial displacement.

Preparation of Coating

Chilies, carrots, and sweet potatoes were coated with the dipping method. Some samples were divided into control and coated vegetables. The prepared coating solution was poured into a container. Each weighed sample was dipped into the coating solution for 1 minute and then held for 30 seconds to remove excess solution. Chilies, carrots, and sweet potatoes were coated with the dipping method. Some samples were divided into control and coated vegetables. The prepared coating solution was poured into a container. Each weighed sample was dipped into the coating solution for 1 minute and then held for 30 seconds to remove excess solution. The control and coated vegetables were stored for 15 days at ambient condition (25 ± 1˚C) with a 5-day sample weighing interval (Chettri et al., 2023).

Results and Discussion

Results of Breadfruit Starch Extraction

Based on the extraction results, the starch yield was 14.3089% (w/w) after the starch was sieved using a 100 mesh sieve. The resulting starch is white with very fine granules as presented in the image below

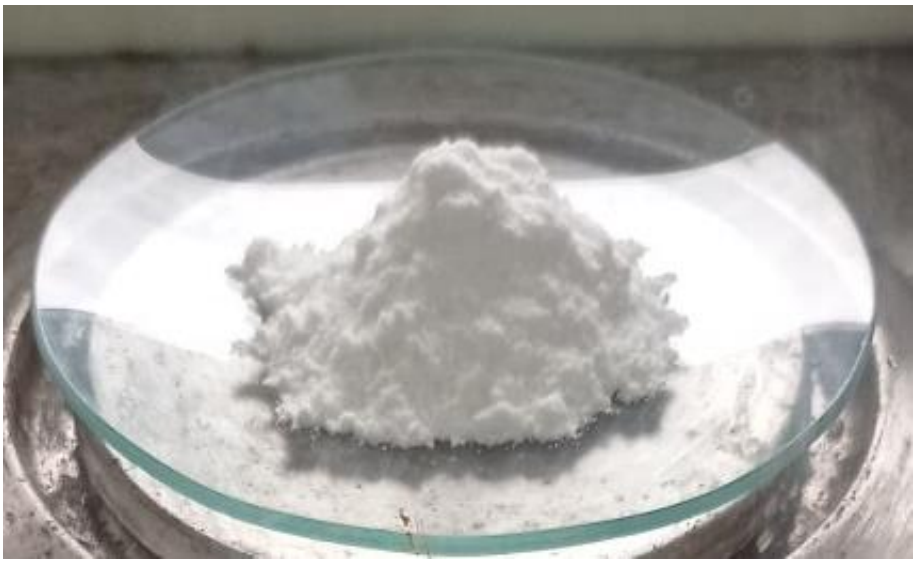

Figure 1. Breadfruit starch

Morphology Analyze

The morphology of edible film is one of the properties that need to be considered as food packaging (Zheng *et al*., 2019). Based on Figures 2 and 3 below, the BS-CH edible film is transparent and almost colorless at various BS-CH variations. The writing on the edible film is very clear, this shows that breadfruit starch is fully gelatinized and homogeneous when mixed with chitosan solution. The BS-CH edible film did not break easily and was flexible when held, indicating that the addition of chitosan improved the mechanical properties of the edible film. These morphological observations suggest a continuous transparent film through the process of homogenization and drying at room temperature.

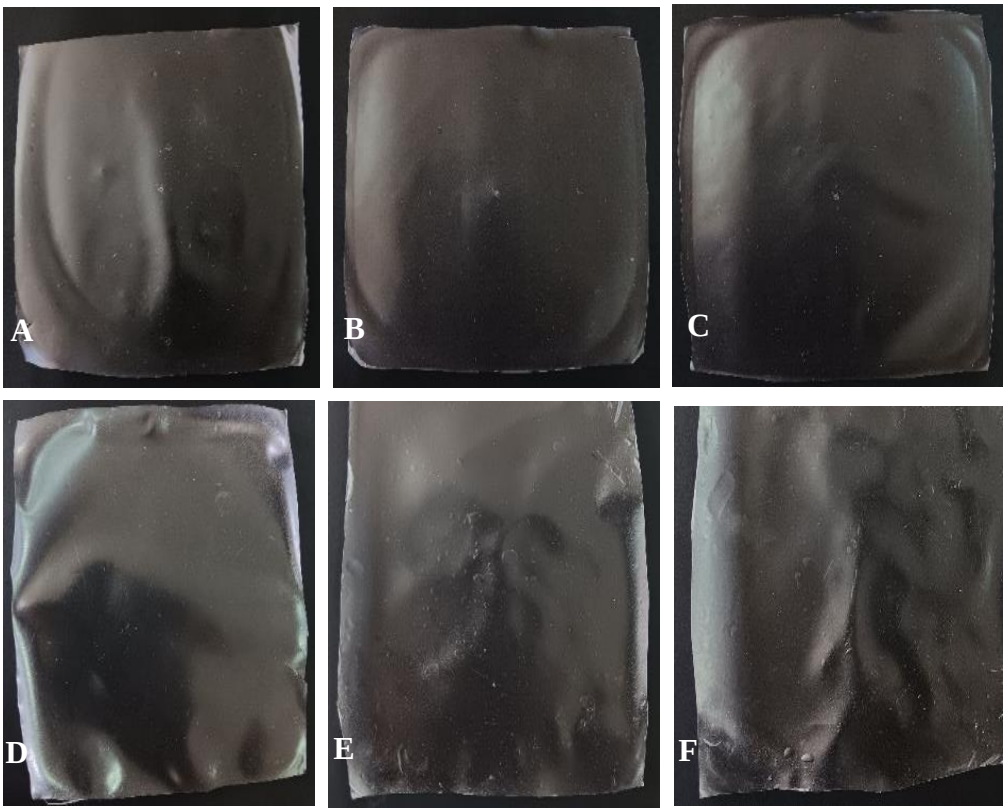

Figure 2. Appearance of BS-CH edible film in various compositions of BS:CH (A) 10:0, (B) 9:1, (C) 8:2, (D) 7:3, (E) 6:4, (F) 5:5 on a Black Background

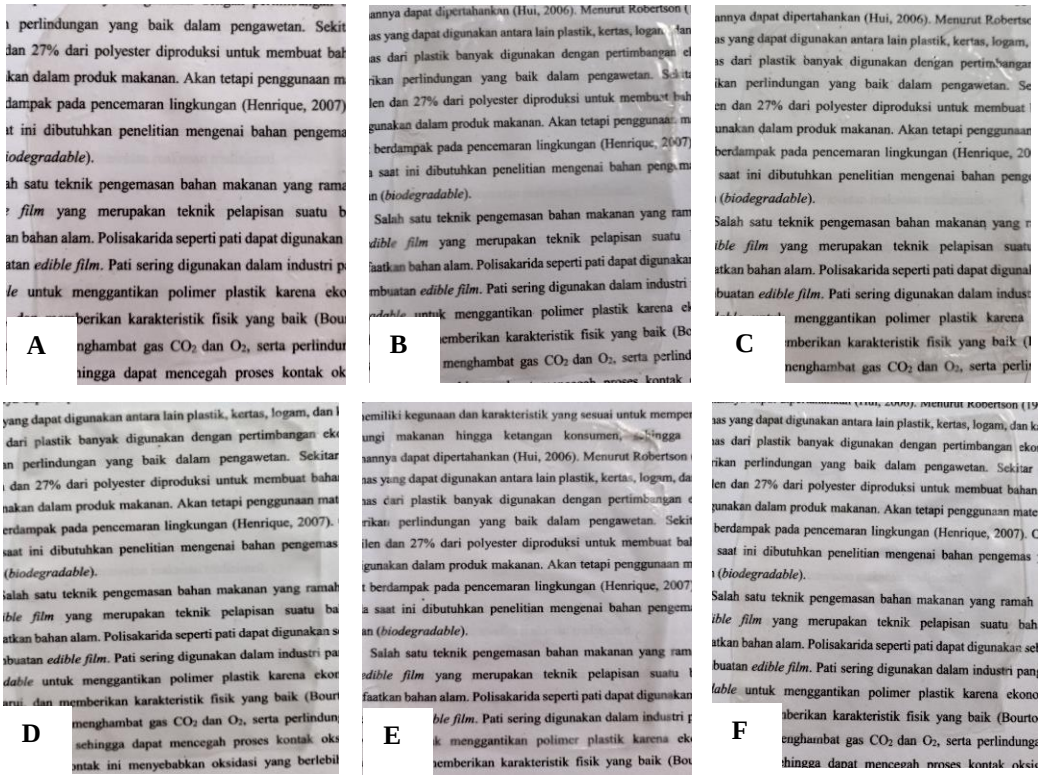

Figure 3. Appearance of BS-CH edible film in various compositions of BS:CH (A) 10:0, (B) 9:1, (C) 8:2, (D) 7:3, (E) 6:4, (F) 5:5 on a Black Background on a Letter

Physical Properties Edible Film

Table 1. Physical properties of different films

Edible Films	Thickness (mm)	Water Solubility (%)		
		30 minutes	60 minutes	90 minutes
Variation of BS				
2%	0,1 ± 0,0707	10 ± 0,0352	36 ± 0,0176	36 ± 0,0012
3%	0,157 ± 0,03535	-33 ± 0,0941	13 ± 0,0610	24 ± 0,0066
4%	0,165 ± 0,0212	-49 ± 0,0948	-7 ± 0,1627	17 ± 0,0645
5%	0,22375 ± 0,0159	-75 ± 0,0563	-31 ±0,0563	8 ± 0,0495
Variation of BS:CH				
10:0	0,157 ± 0,0353	-33 ± 0,0941	13 ± 0,061	24 ± 0,0066
9:1	0,1535 ± 0,0318	-82 ± 0,0718	26 ± 0,0163	28 ± 0,0028
8:2	0,115 ± 0,0056	-123 ± 0,0690	19 ± 0,0027	28 ± 0,0064
7:3	0,096 ± 0,0042	-138 ± 0,1154	18 ± 0,1676	31 ± 0,0113
6:4	0,08 ± 0,0155	-213 ± 0,0000	-54 ± 0,0000	21 ± 0,0000
5:5	0,075 ± 0,0042	-394 ± 0,2791	-112 ± 0,2558	15 ± 0,0139

Edible Film Thickness

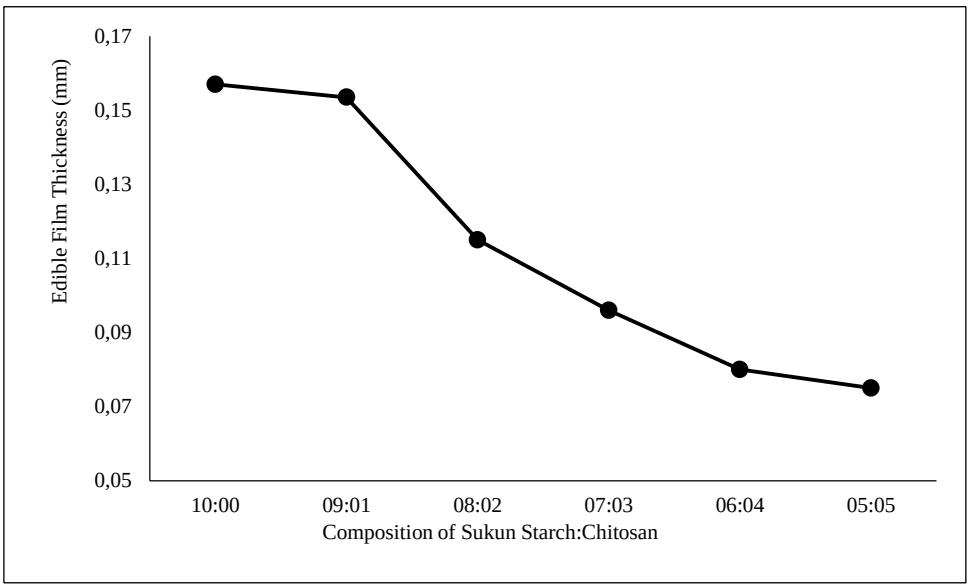

Figure 4. Edible film thickness

Film thickness is an important property, as it significantly affects various physical characteristics, including opacity, mechanical properties, and water vapor permeability (Loukri et al., 2024). Based on the film thickness measurement results in Table 1 or Figure 4, the film thickness is affected by different treatments. Increasing the volume of starch solution makes the film thickness increase significantly, with thickness in the range of 0.075 - 0.157 mm, this indicates that the total soluble starch solids in the film are greater than chitosan.

Water Solubility

One of the physical properties of the film that needs to be considered is water solubility, which provides information about the durability of edible films in water (Loukri et al., 2024). Food products require materials with certain properties to ensure their quality during storage, distribution, and consumption (Filipini et al., 2020). The water solubility of BS edible film decreased significantly with increasing concentration of starch solution, from 36% to 8% at weighing at constant mass 90th minutes after drying. Before dissolving in water, the BS edible film experienced swelling where water entered the edible film cavity at 30th and 60th minutes after drying as shown in Table 2. or Figure 5. (Left). Complete dissolution of starch is relatively slow, starch undergoes swelling before dissolving into water. During the swelling process, solvent molecules diffuse into the starch granules which increases the volume of starch. This causes the movement of starch macromolecular segments to increase before forming a stable dissolving phase (Perez-rea et al., 2015; Zdanowicz & Spychaj, 2016). The range of swelling value of BS edible film is greater at 31-75% than its solubility, in line with

research Palijama et al. (2017) BS has a swelling value in water in the range of 17.37-20.01% and solubility of 3.74-6.64%. The low water solubility of BS is influenced by the high amylose content of about 27.17% (Bezerra et al., 2019). The increased solubility of the film in water is favorable for the development of food packaging that requires dissolving before consumption (Filipini et al., 2020). The solubility of BS edible film in water reached the optimum condition at 2% BS concentration, but it had 0,100 mm thickness which was much different from 3% BS concentration of 0.157 mm, thus affecting its mechanical properties. Therefore, 3% BS was used as the optimum concentration for the mechanical test.

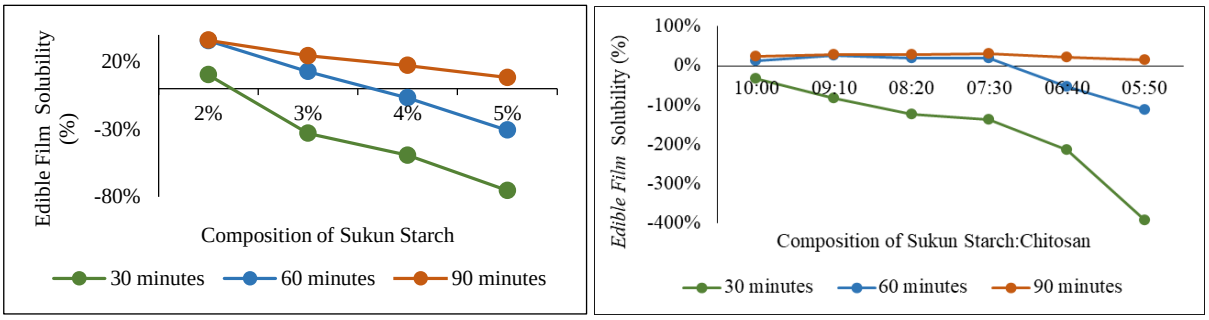

Figure 5. Water solubility of BS edible film in various composition (Left) and water solubility of BS-CH edible film in various composition (Right)

The water solubility of BS-CH edible film increased significantly with the addition of CH to the film. The increase in solubility reached an optimum condition at the BS:CH ratio of 07:03 at 31% after constant mass weighing at 90 minutes. After that, it decreased to a ratio of 05:05 by 15% as shown in Table 2 or Figure 5 (Right). The addition of CH concentration to the edible film causes the edible film to have a lower pH, this increases the swelling value significantly. Singh & Adedeji (2017) The swelling power of starch increases as the pH of the edible film decreases due to structural weakening and starch depolymerization.

Tensile Strength and Elongation at Break

Table 2. Mechanical properties of different films

Edible Films (BS:CH)	Tensile Strength (Mpa)	Elongation at Break (%)
10:0	1,9785 ± 0,2773	14,53715 ± 0,4671
9:1	2,40957 ± 0,2922	34,901 ± 0,9022
8:2	2,49935 ± 0,1067	42,44525 ± 2,4296
7:3	3,01895 ± 0,3981	58,2625 ± 5,3184
6:4	4,58105 ± 0,2242	51,54895 ± 6,4334
5:5	9,57735 ± 0,0812	35,86525 ± 4,7048

Tensile strength (TS) and elongation at break (EAB) tests were conducted to see the mechanical properties due to the addition of CH into the BS edible film. Mechanical properties are feasibility parameters that play an important role in the process of food packaging and storage (Qian et al., 2022). The TS and EAB of CH-BS edible film are shown in Table 2. and Figure 6. It can be seen the TS of CH-BS edible film increased significantly with the addition of CH in BS edible film in the range of 1.9785-9.5773 Mpa. The addition of CH concentration into the edible film increases the TS due to the formation of hydrogen bonds between molecules of the NH2-functional group in CH and the OH-functional group in BS so that the film density increases. As the concentration of BS increased, the TS decreased significantly due to the intramolecular bonding of the -OH group on BS being greater than the intermolecular bonding between the functional groups NH_2 and -OH (Elsabee & Abdou, 2013; Zheng et al., 2019). The EAB value of the film increased significantly due to CH concentration up to the optimum condition of BS:CH, namely 07:03 with a value of 58.2625%. The addition of CH into the film matrix overcomes the brittle and rigid nature of BS, making the film more elastic (Susilowati et al., 2021). However, it experienced a sharp decline when the CH concentration was increased to 25.8652%. The addition of additives to the film matrix at certain concentrations reduces its mechanical properties. The EAB value is influenced by the intermolecular bond distance between the -NH_2 and -OH functional groups, the weakening of intermolecular bonds is due to the long distance between intermolecular bonds (Susilowati et al., 2021). The mechanical properties of BS-CH edible film are similar to the findings of research results (Abera et al., 2024; Hasan et al., 2020; Susilowati et al., 2021; Zheng et al., 2019).

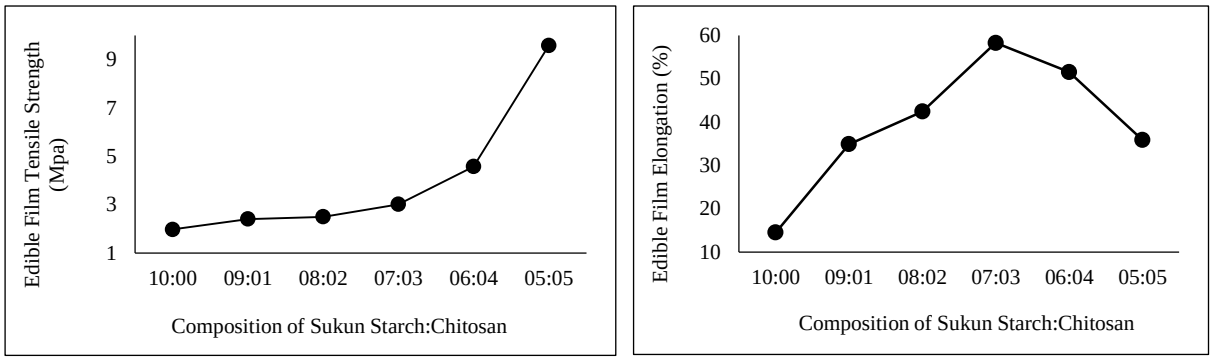

Figure 6. Mechanical test BS-CH Edible film: Tensile strength (Left) and elongation at break (Right)

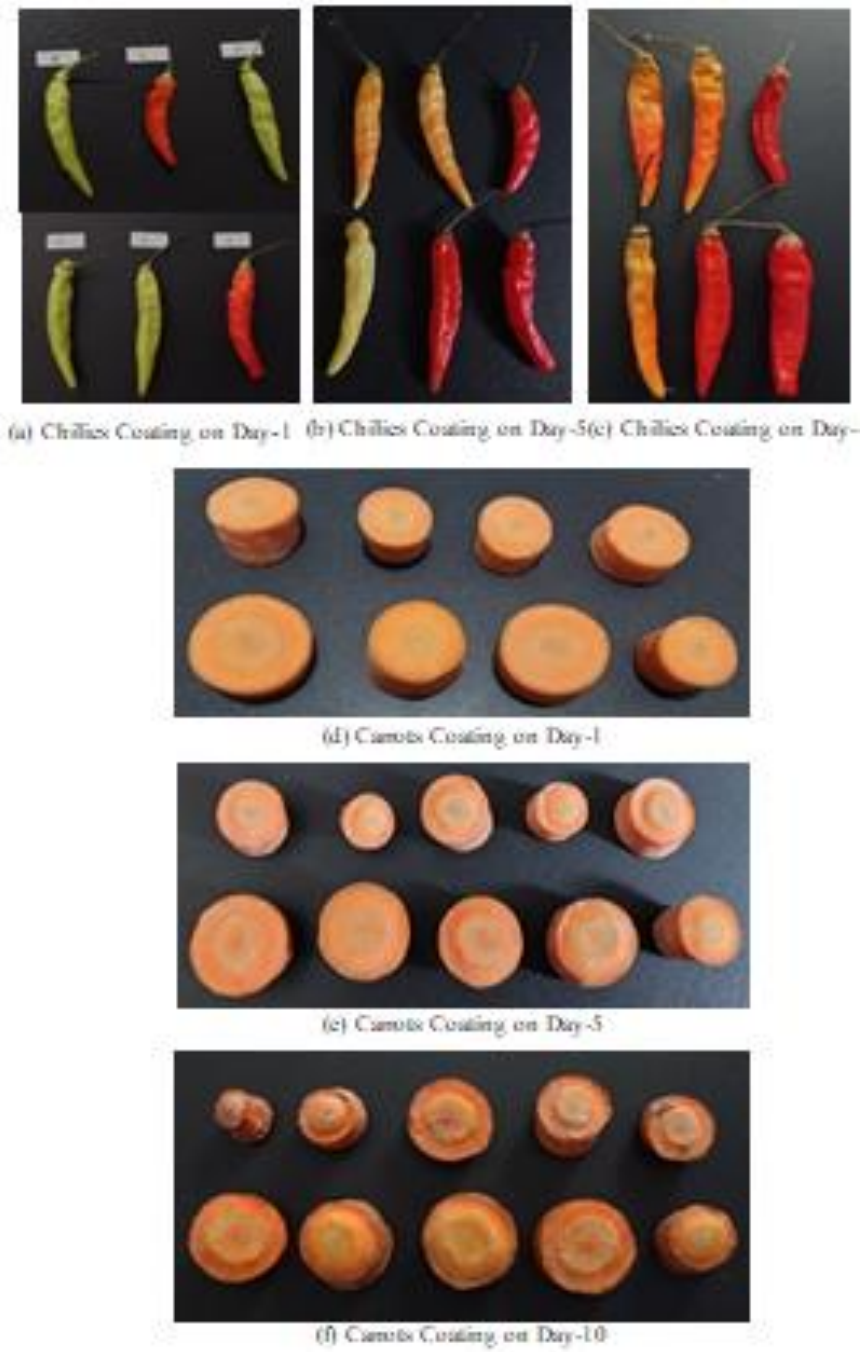

Figure 7. Chilies and carrots coating on day 1, 5, and 10. The first row is a control sample (Without Coating) and the second row is a sample with coating

Application of the Coatings on Vegetables and Their Effect on Mass Loss

The prepared edible coatings were applied to several vegetables such as sweet potato, chili, and carrot. The vegetables that had been coated were then aerated to dry and then weighed the initial mass and reweighed at 5-day intervals during the storage period. Then the difference between initial mass and specific time interval divided by initial weight and finally denoted by percentage was calculated (Nasrin et al., 2020). The following table shows the mass loss of chilies and carrots:

Table 3. Mass loss of chilies and carrots

Vegetables	Treatment	Day-5	Day-10
Chilies	Experiment	27,27%	45,45%
	Control	42,85%	57,14%
Carrots	Experiment	34,92%	52,52%
	Control	41,79%	62,68%

Based on Table 3 above, it was found that chilies and carrots with coating (experiment) on day 5 and day 10 experienced a smaller mass reduction than without coating (control). This shows that the coating on chilies and carrots functioned well in retaining moisture from the food product to the environment. This happened because the control group was in direct contact with air, thereby accelerating moisture migration (Chen et al., 2022). As shown in Figure 7 (b), (c), (e), (f) the appearance of chilies coated (experiment) and without coating (control) is significantly different. For the control group of chilies in Figure 7 (b) and (c) first row, wrinkles appeared clearly on the 10th day of storage. While the coated chilies (experiment) wrinkles did not appear clearly and were almost non-existent. For the control group of carrots in figures (e) and (f) first row, wrinkles appeared clearly on the 5th day of storage and on the 10th day the surface of the carrots shrank further and signs of decay appeared. In the coated carrots (experiment) wrinkles appeared on the 10th day of storage in the second row. The differences in mass loss and appearance of the control and experimental groups in chilies and carrots are related to differences in water vapor transmission in the film coating the food product (Chen et al., 2022).

On the 5th day of storage in the control group, the sweet potatoes were covered with black mold, as seen in Figure 8. The mold grew rapidly on the 4th day of observation and caused the decay of the sweet potato to accelerate. In the experimental group, the sweet potatoes were not overgrown with mold, this is due to the BS-CH edible film preventing the entry of moisture from the surrounding environment so that mold cannot grow in food products. This is in line with research Chen et al (2022) that food products without coatings grow mold quickly because the transmission of water vapor into food products increases humidity, thus creating a good environment for mold growth.

Figure 8. Sweet potato without coating (First Row) and with coating (Second Row) on Day-5

***Edible Coating* Starch in Learning Contains Education for Sustainable Development (ESD)**

Based on the questionnaire results data in Figure 4, it was found that 67% of students stated that the context of edible starch coating as food packaging was not presented in chemistry courses in the chemistry education study program. Edible coating starch as food packaging contributes to various aspects of the SDGs, especially in efforts to achieve a more sustainable food system. The integration of edible coatings in learning is very important because of its contribution to the promotion of sustainability in the food industry. Edible coatings, especially those derived from starch, have been identified as a potential solution to various challenges, including extending the shelf life of vegetables fruit and traditional sausages, reducing food waste, and increasing the

economic value of products (Nunes et al ., 2023) . This is the basis for researchers to understand in depth the potential and need for the integration of edible starch coating as food packaging in ESD-loaded learning.

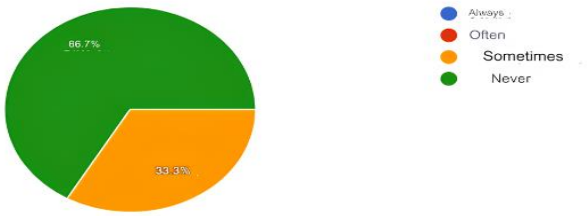

Figure 4. Percentage of edible coatings context taught in lecture

Lectures containing ESD in the context of edible coatings are expected to meet student expectations, presented in an overview of our theme clusters in Table. 4 following:

Table 4. Themes and sub-themes

Theme	Sub-themes
Aspects of the SDGs	Understanding of ESD principles
	Application of ESD principles
Context of edible coatings	Understanding the context of edible coatings
	Selection of the main matrix for edible coating
	Making edible coatings
	Application of edible coatings to food
	Introduction to the context of edible coatings in society
Improve 21st-century skills	Critical thinking skills
	Collaboration opportunities
	Presentation and communication skills

Theme 1: Aspects of the SDGs

Students expressed their hope that ESD-oriented learning on the topic of edible starch coating as food packaging could provide an in-depth understanding of sustainable concepts and aspects. Apart from understanding, they also hope for the application of sustainable principles. The application of this sustainable principle can take the form of increasing awareness regarding alternatives to plastic packaging as food packaging to reduce the negative impact of plastic waste in terms of health and the environment. Indirectly, students are trained to care more about the environment. Students can utilize biological and animal natural resources as the main matrix for making edible coatings, through this they can increase students' sensitivity regarding the potential of natural resources in the surrounding environment.

Theme 2: Edible Coating Context

In the sub-theme of understanding the context of edible coating, students hope to gain an in-depth understanding of the context of edible coating on starch as food packaging. This understanding includes definitions, types of matrices that make up edible coatings, the advantages of edible coatings as food packaging, and the application of edible coatings to various food ingredients. Students also want an understanding of the procedures for making edible coatings including quality control and safety standards for applying edible coatings to food ingredients. Through this understanding, students can describe the potential of edible coatings as food packaging.

In the sub-theme of selecting the main matrix for edible coatings, students hope to be able to determine the basic ingredients as the main matrix for making up edible coatings, both from various potential natural resources around them. This is used as the basis for developing environmentally friendly and sustainable edible coatings. Apart from selecting the basic ingredients for edible coatings, determining sustainable procedures also needs to be studied so that the resulting products do not cause various negative impacts in terms of health, environment and economics.

In the sub-theme of making edible coatings, students expect direct practice in making edible coatings after being able to determine the main matrix and procedures for making edible coatings. Edible coatings are made paying

attention to several aspects such as materials and procedures for making edible coatings that are environmentally friendly and minimize negative impacts on health.

In the sub-theme of applying edible coatings to food, prepared edible coatings can be applied to foods such as vegetables, meat, and fruit to resist spoilage so that their shelf life is longer. In the sub-theme of introducing the context of edible coatings in society, students hope not only to be able to make and apply them to various foods to increase their shelf life but also to introduce the potential of edible coatings as food packaging widely in society. This is an opportunity for students to contribute directly to society so that projects carried out in the laboratory can have a direct impact on reducing food waste and reducing the use of hazardous chemicals in food packaging. The introduction of this context is also a new step in supporting the reduction of plastic waste.

Theme 2: Improving 21st-Century Skills

In the sub-theme of critical thinking skills, students hope to be able to develop their critical thinking regarding ESD content in the context of edible coatings on food packaging and innovation skills related to the development of environmentally friendly materials. In the sub-theme of collaboration opportunities, students hope for the opportunity to work in teams so that they can improve collaboration skills between students in achieving sustainable project goals. In the sub-theme of presentation and communication skills, students want to improve their presentation and communication skills to be able to present projects they have worked on.

Based on analysis of the *edible coating* starch content on food packaging from various reading sources and *edible starch coating* in learning containing Education for Sustainable Development (ESD) through answers to the open-ended questionnaire, it was found that the context of *edible coating* starch on food packaging has a very broad and comprehensive scope of study to be included in chemical learning containing ESD. Apart from that, this context is explicitly related to various aspects of the SDGs in the economic, social, and environmental spheres. Utilizing starch from typical tropical fruit seeds can overcome the problem of organic waste pollution and increase the use value of waste. Starch-based *edible coatings* have the advantage of strong mechanical properties. Implementing each sub-topic in chemistry learning requires an in-depth understanding of chemical concepts so that students are expected to be able to study independently. Therefore, this topic has the potential to be included in the context of chemistry learning containing ESD.

This is supported by the results of the open-ended questionnaire that 66% of students stated that this topic had not been included in chemistry learning with ESD content and they had high hopes for how this topic would be taught in chemistry learning with ESD content and the resulting learning outcomes. The potential of the topic of edible coatings in learning sustainable development is very significant and supports sustainable economic development through the application of circular bioeconomy in the food industry. Thus, incorporating the topic of edible coatings into sustainable development learning can help students understand the importance of environmentally friendly innovation in the food industry and the role of food ingredients in achieving sustainable development goals (Nunes et al ., 2023) .

Conclusion

This research shows that lectures containing Education for Sustainable Development (ESD) play an important role in increasing awareness about sustainable development through the integration of current issues. Through experiment methods and answers to open-ended questionnaires, it was found that the use of starch from sukun starch in making edible coatings has the potential to increase the use value of breadfruit and increase the use value of waste. Edible coatings have physical and mechanical characteristics from variations in the composition of breadfruit starch and chitosan-based on tests that have been carried out. The results of these characteristics form the basis for the application of edible coatings as food packaging. Coated vegetable products such as chilies and carrots experienced a smaller mass shrinkage compared to those without coating. Edible coatings also prevent mold growth on sweet potatoes. Data from the open-ended questionnaire shows that students hope that this topic can be included in chemistry learning containing ESD to increase understanding and application of ESD principles and introduce the potential of edible coatings to the public. Therefore, there is a need to integrate the topic of edible coating starch from breadfruit starch in lecture designs with ESD content.

Recommendations

Based on the research results, it is recommended to integrate the topic regarding the use of starch from typical tropical fruit seeds in making edible coatings into the chemistry learning curriculum containing ESD, developing learning materials that include information regarding the potential use of starch from typical tropical fruit seeds in making edible coatings, as well as its impact on environmental, social, and economic aspects, as well as in the learning process, it is recommended to design activities that can stimulate student involvement in exploring this topic, such as case studies, field projects, or simulations of edible coating development practices. This will help students to develop 21st-century skills that are relevant to the demands of sustainable development.

Scientific Ethics Declaration

The authors declare that the scientific ethical and legal responsibility of this article published in EPSTEM journal belongs to the authors.

Acknowledgments or Notes

* This article was presented as an oral presentation at the International Conference on Basic Sciences, Engineering and Technology (www.icbaset.net) held in Alanya/Turkey on May 02-05, 2024.

* The researchers would like to express their deepest gratitude to the Education Fund Management Institute (LPDP/Indonesia Endowment Fund for Education) under the Ministry of Finance of the Republic of Indonesia as the sponsor for their master's studies, and the support for this paper and publication.

References

Abera, B., Duraisamy, R., & Birhanu, T. (2024). Study on the preparation and use of edible coating of fish scale chitosan and glycerol blended banana pseudostem starch for the preservation of apples, mangoes, and strawberries. *Journal of Agriculture and Food Research*, *15*(3), 100916.

Anita, R., Purwianingsih, W., Anggraeni, S., & Ghofar, A. (2023). *Developing system thinking skills through project-based learning loaded with education for sustainable development*. *9*(1), 62–73.

Bezerra, E. D. A., Santos, E. da N., de Farias, N. S., & Cavalcanti, M. T. (2019). Coating based on breadfruit starch (Artocarpus altilis) for fruit conservation: Influence of glycerol, sorbitol, and mannitol as plasticizers. *Food Science and Technology* , *39*, 398–405.

Bizymis, A. P., & Tzia, C. (2022). Edible films and coatings: properties for the selection of the components, evolution through composites and nanomaterials, and safety issues. *Critical Reviews in Food Science and Nutrition*, *62*(31), 8777–8792.

Chen, J., Zhang, J., Liu, D., Zhang, C., Yi, H., & Liu, D. (2022). Preparation, characterization, and application of edible antibacterial three-layer films based on gelatin–chitosan–corn starch–incorporated nisin. *Food Packaging and Shelf Life*, *34*(2),100980.

Chettri, S., Sharma, N., & Mohite, A. M. (2023). Formulation of extracted soyabean starch based edible coatings by different methods and their impact on shelf life of sapota fruit. *Journal of the Saudi Society of Agricultural Sciences*, *23*(3),205-211.

Díaz-Montes, E., & Castro-Muñoz, R. (2021). Edible films and coatings as food-quality preservers: An overview. *Foods*, *10*(2), 1–26.

Elsabee, M. Z., & Abdou, E. S. (2013). Chitosan based edible fi lms and coatings : A review. *Material Science*,*33*, 1819–1841.

Filipini, S., Patr, V., Pii, M., Hydrocolloids, F., Date, R., Date, R., Date, A., & Filipini, S. (2020). *Journal Pre-proof*.

Findler, F., Schonherr, N., Lozano, R., Reider, D., & Martinuzzi, A. (2019). The impacts of higher education institutions on sustainable development A review and conceptualization. *International Journal of Sustainability in Higher Education, 20(1), 23–38.*

Hasan, M., Rusman, R., Khaldun, I., Ardana, L., Mudatsir, M., & Fansuri, H. (2020). Active edible sugar palm starch-chitosan films carrying extra virgin olive oil: Barrier, thermo-mechanical, antioxidant, and antimicrobial properties. *International Journal of Biological Macromolecules*, *163*, 766–775.

Iamareerat, B., Singh, M., Sadiq, M. B., & Anal, A. K. (2018). Reinforced cassava starch based edible film incorporated with essential oil and sodium bentonite nanoclay as food packaging material. *Journal of Food Science and Technology*, *55*(5), 1953–1959.

Kohl, K., Hopkins, C., Barth, M., Michelsen, G., Luneburg, L. U., Dlouh, J., & Toman, I. (2021). A whole-institution approach towards sustainability : A crucial aspect of higher education ' s individual and collective engagement with the SDGs and beyond. *International Journal of Sustainability in Higher Education*, *23*(2), 218-236.

Loukri, A., Kyriakoudi, A., Oliinychenko, Y., Stratakos, A. C., Lazaridou, A., & Mourtzinos, I. (2024). Preparation and characterization of chitosan-citric acid edible films loaded with Cornelian cherry pomace extract as active packaging materials. *Food Hydrocolloids*, *150*(17), 109687.

Matloob, A., Ayub, H., Mohsin, M., Ambreen, S., Khan, F. A., Oranab, S., Rahim, M. A., Khalid, W., Nayik, G. A., Ramniwas, S., & Ercisli, S. (2023). A Review on edible coatings and films: advances, composition, production methods, and safety concerns. *ACS Omega*, *8*(32), 28932–28944.

McHugh, T. H., & Krochta, J. M. (1994). Sorbitol-vs glycerol-plasticized whey protein edible films: integrated oxygen permeability and tensile property evaluation. *Journal of Agricultural and Food Chemistry*, *42*(4), 841–845.

Modesti, M., Zampella, L., & Petriccione, M. (2019). Polymers for agri-food applications:*Chitosan mono- and bilayer edible coatings for preserving postharvest quality of fresh fruit*. (1st ed., pp. 465–486). Retrieved from https://dokumen.pub/polymers-for-agri-food-applications-1st-ed-2019-978-3-030-19415-4-978-3-030-19416-1.html

Nasrin, T. A. A., Rahman, M. A., Arfin, M. S., Islam, M. N., & Ullah, M. A. (2020). Effect of novel coconut oil and beeswax edible coating on postharvest quality of lemon at ambient storage. *Journal of Agriculture and Food Research*, *2*,100019.

Nunes, C., Silva, M., Farinha, D., Sales, H., Pontes, R., & Nunes, J. (2023). Edible coatings and future trends in active food packaging–fruits' and traditional sausages' shelf life increasing. *Foods*, *12*(17), 3308.

Palijama, S., Talahatu, J., & Huwae, I. J. (2017). Physical and chemical analysis of starch contained in three varieties of breadfruit. *Agritekno Jurnal Teknologi Pertanian*, *6*(2), 59–63.

Paristiowati, M., Rahmawati, Y., Fitriani, E., Satrio, J. A., & Hasibuan, N. A. P. (2022). Developing Preservice chemistry teachers' engagement with sustainability education through an online, project-based learning summer course program. *Sustainability* , *14*(3).

Perera, K. Y., Sharma, S., Pradhan, D., Jaiswal, A. K., & Jaiswal, S. (2021). Seaweed polysaccharide in food contact materials (Active packaging, intelligent packaging, edible films, and coatings). *Foods*, *10*(9), 1–22.

Perez-rea, D., Bergenståhl, B., & Nilsson, L. (2015). *Development and evaluation of methods for starch dissolution using asymmetrical flow field-flow fractionation . Part I : Dissolution of amylopectin*.(pp.4315–4326).

Qian, Z., Zhang, J., Xu, W., & Zhang, Y. (2022). Development of active packaging films based on liquefied shrimp shell chitin and polyvinyl alcohol containing β -cyclodextrin / cinnamaldehyde inclusion. *International Journal of Biological Macromolecule*, *214*, 67–76.

Raghav, K., Agarwal, N., & Saini, M. (2016). Edible coating of fruits and vegetables: A review. *International Journal of Scientific Research and Modern Education*,*1*(1), 188–204.

Roy, S., & Rhim, J. W. (2021). Fabrication of chitosan-based functional nanocomposite films: Effect of quercetin-loaded chitosan nanoparticles. *Food Hydrocolloids*, *121*, 107065.

Shah, U., Naqash, F., Gani, A., & Masoodi, F. A. (2016). Art and science behind modified starch edible films and coatings: A review. *Comprehensive Reviews in Food Science and Food Safety*, *15*(3), 568–580.

Singh-Pillay, A. (2020). Pre-service technology teachers' experiences of project based learning as pedagogy for education for sustainable development. *Universal Journal of Educational Research*, *8*(5), 1935–1943.

Singh, M., & Adedeji, A. A. (2017). Characterization of hydrothermal and acid modi fi ed proso millet starch. *LWT- Food Science and Technology*,*79*, 21-26.

Susilowati, E., Mahardiani, L., & Sulistyowati, D. (2021). Preparation of Poliblend suweg starch-chitosan with addition of essential oil from sweet orange peel as edible coating on Malang's apples. *Journal of Physics: Conference Series*, *1912*(1), 012018.

Turi, C. E., Liu, Y., Ragone, D., & Murch, S. J. (2015). Breadfruit (artocarpus altilis and hybrids): A traditional crop with the potential to prevent hunger and mitigate diabetes in Oceania. *Trends in Food Science and Technology*, *45*(2), 264–272.

UNESCO. (2014). *Roadmap for Implementating the global action programme on education for sustainable development*. Retrieved from https://unesdoc.unesco.org/ark:/48223/pf0000230514

Vega-Castro, O., Ramírez, M., Blandón-Mena, L., Contreras-Calderón, J., Mesías, M., Delgado-Andrade, C., Morales, F. J., & Granda-Restrepo, D. (2022). Characterization and application of a coating of starch extracted from avocado (Persea Americana L. cv. hass) seeds as an alternative to reduce acrylamide content in French fries. *Food Science and Biotechnology*, *31*(12), 1547–1558.

Zhang, X., Liu, Y., Yong, H., Qin, Y., Liu, J., & Liu, J. (2019). Development of multifunctional food packaging fi lms based on chitosan , TiO 2 nanoparticles and anthocyanin-rich black plum peel extract. *Food*

Hydrocolloids, *94*, 80–92.

Zheng, K., Xiao, S., Li, W., Wang, W., Chen, H., Yang, F., & Qin, C. (2019). Chitosan-acorn starch-eugenol edible film: Physico-chemical, barrier, antimicrobial, antioxidant and structural properties. *International Journal of Biological Macromolecules*, *135*, 344–352.

Author Information

Dewi Sulistyowati
Universitas Pendidikan Indonesia
Jl. Dr. Setiabudhi No. 229 Bandung 40154, Indonesia
Contact e-mail: *dewisulistyowati23@upi.edu*

Hernani Hernani
Universitas Pendidikan Indonesia
Jl. Dr. Setiabudhi No. 229 Bandung 40154, Indonesia

Asep Supriatna
Universitas Pendidikan Indonesia
Jl. Dr. Setiabudhi No. 229 Bandung 40154, Indonesia

To cite this article:

Sulistyowati, D., Hernani, H., & Supriatna, A. (2024). Edible coating from breadfruit starch and chitosan for food packaging. *The Eurasia Proceedings of Science, Technology, Engineering & Mathematics (EPSTEM), 28*, 286-299.

The Eurasia Proceedings of Science, Technology, Engineering & Mathematics (EPSTEM)
ISSN: 2602-3199

The Eurasia Proceedings of Science, Technology, Engineering & Mathematics (EPSTEM), 2024

Volume 28, Pages 300-307

ICBASET 2024: International Conference on Basic Sciences, Engineering and Technology

Enterprise Resource Planning Implementation: Challenges and Barriers

Issam Jebreen
Zarqa University

Hanan Omer
Zarqa University

Ahmad Al Qerem
Zarqa University

Abstract: The goal of this study is to ascertain how Enterprise Resource Planning (ERP) adoption software is affected in small and medium-sized businesses in Jordan by the problems and barriers represented by (low knowledge of ERP, misperception, lack of resources, financial worries, and employee resistance). The following titles of employees in Jordanian small and medium-sized businesses' departments of information technology made up the study population: (Department Manager, Assistant Department Manager, Head of Department, and Software Officer). To accomplish the goals of the study, the investigator employed a basic random sample of the study population, wherein (160) questionnaires were distributed and (152) were retrieved. The descriptive-analytic approach was employed in conjunction with various statistical techniques, the most notable of which was the "T" test for one sample (One SampleT–test), and the statistical package program was utilized for statistical analysis and testing of hypotheses. Use SPSS. The study's conclusions include the existence of a statistically significant relationship between Jordanian SMEs' software implementation and their lack of resources, financial concerns, and inadequate ERP understanding. On the other hand, misperception and employee resistance had no statistically significant effect on the implementation of software in Jordanian SMEs. In light of this, the study made several recommendations, the most significant of which is the establishment of an independent committee of senior management experts in information systems and information technology to monitor a variety of data regarding the readiness and effectiveness of the software. As well as involving the user in the ERP implementation from the beginning, because operations management may clearly and effectively benefit from the end-user's assistance in formulating operations that accurately and firmly fulfil daily work needs.

Keywords: Enterprise resource planning software, Business engineering, Technology

Introduction

Running companies in a highly competitive climate is difficult. To increase competitiveness and fulfil client demands, firms strive to improve efficiency and agility (Motwani, Subramanian, & Gopalakrishna, 2005). Global companies are constantly prone to encounter more difficult and intricate obstacles. Information technology is capable of radically altering the way businesses operate (Rouyendegh & Erkan, 2011) As a result, many companies adopt enterprise resource planning (ERP) systems to increase their competitiveness.

Enterprise Resource Planning, also known as ERP, is a software solution that combines a company's data and operations into a single platform for the whole enterprise. After the 1990s, ERP has been employed in larger operations, such as human resources, finance, and production planning, in addition to manufacturing and production planning systems used in the industrial sector (Van Nieuwenhuyse et al., 2011). To be more

convenient and competitive, ERP has also incorporated other business extensions, such as supply chain management and customer relationship management.

An enterprise resource planning (ERP) system allows a company to automate and combine the vast majority of its activities into a single, unified system. It is a collection of tools that allows real-time data sharing from any business producing. An ERP system connects all departments and operations of a firm into a computer system that can serve the requirements of various departments, including sales, human resource department, manufacturing, finance, and others. With that being said, it is important to note that integration is the most crucial necessity for the ERP system to function in the firm.

Integration is the process of merging diverse software requirements into a single, logical database, making it simple for all departments to exchange information and interact (Sloan et al., 2014). Moreover, ERP standardizes procedures and data inside a company according to industry best practices. The enterprise also simplifies data flow across different organizational components by creating a single-transaction system (Lieber, 1995). A company can focus on administrative duties, increase the ability to implement new information system features and reduce information system maintenance costs by standardizing and integrating procedures and data (Alomari et al., 2019).

Because ERP gives managers a comprehensive view of corporate activities, it has emerged as the mainstay of business intelligence for companies (Alomari et al., 2019) and with the rapid progression of technology, ERP is intended to readily adapt to changing company requirements and businesses must continuously update their systems to cope with the changes. Most ERP suppliers offer the chance to change processes and conform with prevailing best practices to address changing company requirements more rapidly (Nassar, Warrad, & Siam, 2017). With that being said there are several challenges that firms have to deal with when implementing an ERP system, limited ERP awareness, and misconception, lack of resources, financial worries and employee resistance.

This study's objective is to investigate the challenges and barriers to deploying ERP systems in small and medium-sized firms (SMEs) in Jordan. Considering that (SMEs) are businesses that maintain revenues, resources, or employee numbers below a certain threshold. It is crucial to comprehend if and to what extent such obstacles impact the adaptation of ERP systems and company performance. The subsequent sections would include conducting a literature review, formulating a methodology, gathering evidence, preparing it for examination, and making a conclusion on the issue.

Related Works

AboAbdo, Aldhoiena, & Al-Amrib, (2019) looks at the most recent Critical Success Factors (CSFs) that an ERP employer at a major construction business claims are impacting the application process. A questionnaire survey of ERP operators was used to identify the 26 most significant factors that were found in the literature. A planned discussion with 25 ERP installation process practitioners was held after the data were gathered. The findings showed that the most crucial elements for an ERP system's effective installation are administration knowledge and engagement, operator preparation and support, and staffing arrangements for deployment. According to earlier studies, the ERP adoption process is primarily hampered by human factors even though it is fundamentally an IT process.

The report by Hasan et al. (2019) addresses major enterprise resource planning (ERP) post-application characteristics. Using the Smart-PLS package application, a theoretical framework is developed with a collection of appropriate theories, and operational equation modelling is used to analyze the survey results. The results suggest that post-application accomplishment attributes are essential for assessing the ERP post-application's overall impact. Similarly, the likelihood of successful corporate growth increases as more systems are integrated into an ordered process. The findings may assist ERP specialists and innovators in other states with future ERP implementation.

This report (Epizitone & Olugbara, 2019), identifies well-considered aspects crucial to the successful installation of ERP into an organization's financial system. To do this, it is necessary to categorize the community factors impacting ERP system deployment and then assess whether the identified factors are suitable for financial systems. This research analyzes ERP systems that support financial business processes. From a total of 127 investigations, 205 common components have been identified, of which 20 are available in the study. The community features are then grouped based on median data to choose the top six important success

characteristics, which are explained briefly within the context of a financial system. The paper (Epizitone & Olugbara, 2020) explains how to use a diverse method approach to develop CSFs for a successful ERP application. As a result, it offers researchers who want to apply this approach to complex research studies a more thorough road map and insight into the research problem paradigm, methodologies, and approach.

This work (Mahmud et al., 2017) focused on the major emphasis of researchers in the information system (IS) on finding solutions to lessen the difficulties confronting the adoption of ERP via the user's resistance in particular. While prior research has addressed the causes behind user resistance, a complete understanding of how users value a new ERP system before adoption and what motivates them to oppose is still lacking. In particular, the viewpoint of status quo adherence and technical absence explained user resistance or end-user concerns. The model presented in this study fills this research gap by combining technology and the status quo, thereby emphasizing end-user complaints' performance before the implementation of a new ERP system. As a result, 221 respondents from five distinct Bangladeshi manufacturing companies that currently use the well-known SAP ERP system were given a survey questionnaire.

The fundamental premise of the study (Kulikov, Semin, Skvortsov, Ziablitckaia, & Skvortsova, 2020) is that ERP systems may greatly enhance information sharing; yet, the lack of qualified workers and high-level managers' and critical employees' ignorance of ERP competences have prevented the agricultural sector from using them quickly. The research aims to categorize the challenges and expectations related to ERP adoption in agriculture. A review of Web of Science (WoS) papers and questionnaire surveys of fifty-five CEOs from Central Ural agriculture enterprises comprise the methods employed. Government organizations may use the study's conclusions in their plans for technical innovation and creative development in the agriculture industry.
This study (Venkatraman & Fahd, 2016), identifies some of the major problems, such as cost efficiency, software alignment and business practices, training, and adaptive governance, that are the primary barriers for SMEs to use an ERP system. Due to the self-motivated nature of SMEs, the best practices for adopting ERP for SMEs may be accessed via a careful assessment of their professional requirements. This was the primary objective of the investigation. As a case study, the researchers identified the key success factors for an ERP implementation in an Australian SME. Then, these success factors were linked with the actual results achieved. As a result, it was discovered that elements such as integrating business operations with the ERP system, addressing the demands of customers and stakeholders, and reducing periodic and maintenance expenses were crucial to the successful ERP deployment of Australian SMEs.

The purpose of (Falagara Sigala, Kettinger, & Wakolbinger, 2020) is to enable humanitarian organizations (HOs) to deliver agile, adaptive, and compliant (Triple-A) humanitarian supply chain capabilities and digitize humanitarian operations, the goal is to define the fundamental design concepts of enterprise resource planning (ERP) systems. This article proposes that ERP systems for humanitarian organizations should be developed as special systems that address the missions, value creation processes, and resource base of these organizations, to improve organizational performance. Twelve broad design concepts for outstanding humanitarian organizations are presented in this study. Within the parameters of these design concepts, specific demands can be recognized and successfully engineered. (Alsharari et al., 2020) study focuses on the Cloud (ERP) system deployment and highlights the features and problems that users may encounter. The researchers also provide a comparison between traditional and cloud-based ERP solutions. The results demonstrate that the use of Cloud EPR systems, as opposed to traditional ERP systems, contributes to the success of enterprises and improves the quality of their decision-making processes. The results also reveal that the efficacy of deploying Cloud ERP is contingent on the provider's professionalism, thereby causing issues connected with diminished administrative autonomy.

Following (Chofreh, et al., 2020), the purpose of this research is to provide all-inclusive recommendations for providing ERP system implementation stages and endeavours. Based on a literature review, a conceptual research approach was used to construct criteria for discovering and assimilating diverse ideas, including features of sustainability, project management, organizational decision levels, and strategy management. The process consists of the following three phases: (1) gathering steps and activities from current ERP sustainability guidelines, (2) classifying and analyzing discovered steps and activities, and (3) selecting needed actions and activities for the guidelines. The suggested recommendations consist of three primary modules including implementation processes, levels, and activities. The results will provide practitioners with formal recommendations for the efficient adoption of sustainable ERP systems within their business value chains.

This study (Kamdjoug et al., 2020) backs an information systems (IS) success model developed by Delone and McLean and based on the agency theory for the (ERP) application model. Two significant research questions are addressed in this study: (1) How do interactions between consultants and clients affect the results of ERP application projects? and (2) How can this relationship be managed well to guarantee the accomplishment of the

project's goals? The suggested theoretical framework was subjected to a case study and validity assessment using an electronic financial institution located in Africa. Concerning the concepts of the conceptual framework, the study found that interactions and connections between clients and consultants facilitate the impact of organizational, technological, and human critical success factors (CSFs) on the calibre of information and services. Conflicts between consultants and agencies can be settled with the help of incentive-based contracts and a conflict management committee. This article offers the relevant information required to settle conflicts between consultants and clients, along with the elements that need to be properly taken into account to keep everyone informed.

The implementation of ERP systems in SMEs in Jordan can be complex and challenging due to various factors, including financial constraints, lack of IT knowledge and skills and resistance to change. The existing research suggests that these barriers can be overcome through training programs, investing in IT knowledge and skills, and addressing cultural differences.

Research Method

The study relies on the descriptive analytical approach, by describing the variables of the study represented in the challenges and obstacles facing the implementation of software in small and medium enterprises in Jordan. The study is considered to be a descriptive quantitative study, because it examines the impact of challenges and obstacles represented by (limited awareness of ERP, misconception, lack of resources, financial concerns and employee resistance) to the implementation of software in small and medium enterprises in Jordan, as it describes a current phenomenon on the ground where descriptive statistical analysis will be used, and its hypotheses will be tested to achieve its objectives and to know the changes and variations in the dependent variable "software implementation" due to the changes caused by the independent variable "challenges and obstacles", as it provides information on the level of application of the main variables, and expressed statistically using tables and figures and benefiting from them.

Sample of Study

The study population is made up of all the terms associated with the phenomenon the researcher is looking into as well as all the people, organizations, or things that are the focus of the inquiry. The study population consists of all employees holding the following job titles who are employed by small and medium-sized businesses in Jordan in the Department of Information Technology: (department manager, assistant department manager, department head, and software officer).

The recovery rate from all companies is roughly 92%; this percentage is representative of the study population and can be relied upon to complete the study procedures. The researcher used a simple random sample of the study population, wherein 160 questionnaires were distributed to the total study population and 152 questionnaires were retrieved. Sekaran and Bougie (2016) state that a minimum response rate of 86% is deemed appropriate for research purposes. To address the analytical aspects of the research issue, the researcher decided to use a questionnaire as the main tool for gathering data for the study.

Research Hypotheses

In light of the problem of the study and its questions, the following hypotheses can be formulated:

- H01: There was no statistically significant effect at the level of statistical significance ($0.05 \geq \alpha$) of limited ERP awareness on software implementation in Jordanian SMEs.
- H02: There was no statistically significant effect at the level of statistical significance ($0.05 \geq \alpha$) of misconception on software implementation in Jordanian SMEs.
- H03: There was no statistically significant effect at the level of statistical significance ($0.05 \geq \alpha$) of lack of resources on software implementation in Jordanian SMEs.
- H04: There was no statistically significant effect at the level of statistical significance ($0.05 \geq \alpha$) of financial concerns on software implementation in Jordanian SMEs.
- H05: There was no statistically significant effect at the level of statistical significance ($0.05 \geq \alpha$) of employee resistance on software implementation in Jordanian SMEs.

Results

To test the main hypothesis, the sample T-test was used to test the significance of the differences between the average responses to the variable and the average of the hypothetical scale (a score of 3 indicates an average score). So the rule of the decision is if the average responses are higher than the hypothetical average and there are significant differences between them, this indicates an effect.

H01: There was no statistically significant effect at the level of statistical significance (0.05≥α) of limited ERP awareness on software implementation in Jordanian SMEs.

Table 1. The results of the (On-Sample Test) test for the first hypothesis

	N	Mean		Std. Deviation	Std. Error Mean
Limited ERP Awareness	152	3.4342		0.43780	0.03551
One-Sample Test: Test Value = 3	t	df	Sig. (2-tailed)	Mean Difference	95% Confidence Interval of the Difference
Limited ERP Awareness	12.228	151	0.000	0.43421	0.3640 - 0.5044

Table 1 shows that there are statistically significant differences between the hypothetical mean (3), the average responses on the first axis (the impact of limited ERP awareness on software implementation in small and medium enterprises), and the standard deviation (0.43), which indicates a low dispersion of the study participants' answers, and the calculated value of (T) (12.228) and its statistical significance (SIG = 0.000). These differences are evident at the significance level (a>=0.05). The first null hypothesis, which claims that there is no statistically significant effect at the level of statistical significance (0.05≥α), is rejected since the average responses are higher than the average of the scale. The first null hypothesis, which asserts that there is no statistically significant effect of limited ERP awareness on software implementation at the level of statistical significance (0.05≥α), is rejected since the average responses are higher than the average of the scale. Thus, the alternative hypothesis is approved: Limited ERP awareness has a statistically significant impact on software installation in Jordanian SMEs at the level of statistical significance (0.05≥α).

H02: There was no statistically significant effect at the level of statistical significance (0.05≥α) of misconception on software implementation in Jordanian SMEs.

Table 2. The results of the (On-Sample Test) test for the second hypothesis

	N	Mean		Std. Deviation	Std. Error Mean
Misconception	152	2.7303		.62878	.05100
One-Sample Test: Test Value = 3	t	df	Sig. (2-tailed)	Mean Difference	95% Confidence Interval of the Difference
Misconception	-5.289-	151	.155	-.26974-	0.3705 – 0.1690

Table 2 shows that the average responses on the second axis (the impact of misconception on software implementation in small and medium enterprises) and the hypothetical mean (3) do not differ statistically significantly at the significance level (a> = 0.05). The standard deviation (0.62) indicates a low dispersion of the study subjects' responses, and the calculated value of (T) (-5.289) and its statistical significance (SIG = 0.155) also show this. The second hypothesis, which asserts that there is no statistically significant influence of misperception on software adoption in Jordanian SMEs at the level of statistical significance (0.05≥α), is accepted because the average responses are below the average of the scale.

H03: There was no statistically significant effect at the level of statistical significance (0.05≥α) of lack of resources on software implementation in Jordanian SMEs.

Table 3 makes it evident that the test (T) results for one sample are statistically significant at the significance level (a> = 0.05) between the hypothetical average (3) and the average responses on the third axis (the impact of resource scarcity on software implementation in Jordanian SMEs), as well as between the calculated value of (T) (11.157) and its statistical significance (SIG = 0.000). The standard deviation value (0.64) indicates a low dispersion of participant responses. The third null hypothesis, which asserts that there is no statistically

significant influence of lack of resources on software implementation in Jordanian SMEs at the level of statistical significance (0.05≥α), is rejected because the average replies are higher than the average scale.

Table 3. The results of the (On-Sample Test) test for the third hypothesis

	N	Mean		Std. Deviation	Std. Error Mean
Lack of Resources	152	3.5882		.64990	.05271
One-Sample Test: Test Value = 3	t	df	Sig. (2-tailed)	Mean Difference	95% Confidence Interval of the Difference
Lack of Resources	11.157	151	.000	.58816	0.4840 – 0.6923

The alternative hypothesis is accepted: lack of resources has a statistically significant impact on software deployment in Jordanian SMEs at the level of statistical significance (0.05≥α).

H04: There was no statistically significant effect at the level of statistical significance (0.05≥α) of financial concerns on software implementation in Jordanian SMEs.

Table 4. The results of the (On-Sample Test) test for the fourth hypothesis

	N	Mean		Std. Deviation	Std. Error Mean
Financial Worries	152	3.4539		0.41811	0.03391
One-Sample Test: Test Value = 3	t	df	Sig. (2-tailed)	Mean Difference	95% Confidence Interval of the Difference
Financial Worries	13.385	151	.000	.45395	0.3869 – 0.5210

Table 4 makes it evident that the test (T) results for one sample demonstrate statistically significant differences between the hypothetical mean (3) and the average responses on the fourth axis (the impact of financial concerns on software implementation in Jordanian SMEs), which are 3.45. The statistical significance (SIG = 0.000) of the calculated value of (T) (13.385) and the low dispersion of the study members' responses is indicated by the value of the standard deviation (0.41). The fourth null hypothesis, which claims that financial considerations have no statistically significant effect on software adoption in Jordanian SMEs at a statistically significant level (0.05≥α), is similarly rejected because the average replies are higher than the average scale.

The alternative hypothesis, which reads as follows, is accepted: Financial considerations have a statistically significant impact on software deployment in Jordanian SMEs at the level of statistical significance (0.05≥α).

H05: There was no statistically significant effect at the level of statistical significance (0.05≥α) of employee resistance on software implementation in Jordanian SMEs.

Table 5. The results of the (On-Sample Test) test for the fifth hypothesis

	N	Mean		Std. Deviation	Std. Error Mean
Employee Resistance	152	2.9263		0.78889	0.06399
One-Sample Test: Test Value = 3	t	df	Sig. (2-tailed)	Mean Difference	95% Confidence Interval of the Difference
Employee Resistance	-1.152-	151	.251	-.07368-	-0.2001 – 0.0527

Table 5 clearly demonstrates that the test (T) results for one sample demonstrate that there are no statistically significant differences at the significant (a>=0.05) level between the hypothetical mean (3) and the average responses on the fourth axis (the impact of employee resistance on software implementation in Jordanian SMEs), which are 2.92 and 0.78 respectively, and the calculated value of (T) (- 1.152) and its statistical significance (SIG = 0.251). The fifth hypothesis, which asserts that employee resistance has no statistically significant effect on software adoption in Jordanian SMEs at the level of statistical significance (0.05≥α), is accepted because the average responses are lower than the average of the scale.

Conclusion

In conclusion, establishing an ERP system in small and medium-sized enterprises (SMEs) in Jordan might be problematic owing to inadequate knowledge and resources, as well as financial concerns. However, it did not seem that misperceptions and employee resistance had a substantial influence on the adoption process. Therefore, small and medium-sized enterprises (SMEs) in Jordan need to prioritize developing knowledge about the advantages of ERP systems and investing in the resources required to overcome these obstacles. By doing so, businesses may increase their operational efficiency, strengthen their decision-making processes, and acquire a market edge. ERP deployment may create hurdles, but it is a good investment that may lead to long-term development and profitability.

Based on the study's findings, the following recommendations are made: Including the user in the resource planning system implementation project from the beginning, as the end-user can play a crucial role in assisting the operations department in accurately and definitively formulating operations following daily work requirements. Accurately defining the vision and strategic objectives of implementing software packages and monitoring current and future requirements for it. The commitment of the senior management of small and medium enterprises in Jordan to the leading role when implementing the software through moral support and material and financial supervision and the need for its commitment to continuous follow-up on its installation. Appointing an independent committee of senior management specialized in information systems and information technology to monitor various information on the readiness and effectiveness of the software. Conducting more studies that address the challenges and obstacles facing companies when implementing software packages, and addressing various challenges other than those addressed in this study

Scientific Ethics Declaration

The authors declare that the scientific ethical and legal responsibility of this article published in EPSTEM journal belongs to the authors.

Acknowledgements

* This article was presented as an oral presentation at the International Conference on Basic Sciences, Engineering and Technology (www.icbaset.net) held in Alanya/Turkey on May 02-05, 2024.

References

AboAbdo, S., Aldhoiena, A., & Al-Amrib, H. (2019). Implementing enterprise resource planning erp system in a large construction company in ksa. *Procedia Computer Science, 164*, 463-470.

Alomari, I., Amir, A. M., Aziz, K. A., & Auzair, S. (2019). Enterprise resource planning system business process attributes: A research note. *Int. J. Appl. Res. Stud, 5*(3), 111-115.

Alsharari, N. M., Al-Shboul, M., & Alteneiji, S. (2020). Implementation of cloud ERP in the SME: Evidence from UAE. *Journal of Small Business and Enterprise Development, 27*(2), 299-327.

Chofreh, A. G., Goni, F. A., Klemeš, J. J., Malik, M. N., & Khan, H. H. (2020). Development of guidelines for the implementation of sustainable enterprise resource planning systems. *Journal of Cleaner Production, 244*, 118655.

Epizitone, A., & Olugbara, O. (2020). Multiple correspondence analysis of critical success factors for enterprise resource planning system implementation. *Journal of Management Information & Decision Sciences, 23*(3), 175-186.

Epizitone, A., & Olugbara, O. O. (2019). Critical success factors for erp system implementation to support financial functions. *Academy of Accounting and Financial Studies Journal, 23*(6), 1-11.

Falagara Sigala, I., Kettinger, W. J., & Wakolbinger, T. (2020). Digitizing the field: Designing ERP systems for Triple-A humanitarian supply chains. *Journal of Humanitarian Logistics and Supply Chain Management, 10*(2), 231-260.

Haddara, M., Gøthesen, S., & Langseth, M. (2022). Challenges of cloud-erp adoptions in smes. *Procedia Computer Science, 196*, 973-981.

Hasan, N., Miah, S. J., Bao, Y., & Hoque, M. R. (2019). Factors affecting post-implementation success of enterprise resource planning systems: a perspective of business process performance. *Enterprise*

Information Systems, 13(9), 1217-1244.
Kamdjoug, J. R. K., Bawack, R. E., & Tayou, A. E. T. (2020). An erp success model based on agency theory and IS success model: The case of a banking institution in Africa. *Business Process Management Journal, 26*(6), 1577-1597.
Kulikov, I., Semin, A., Skvortsov, E., Ziablitckaia, N., & Skvortsova, E. (2020). Challenges of enterprise resource planning (ERP) implementation in agriculture. *Journal of Entrepreneurship and Sustainability Issues, 7*(3), 1847-1857.
Mahmud, I., Ramayah, T., & Kurnia, S. (2017). To use or not to use: Modelling end user grumbling as user resistance in pre-implementation stage of enterprise resource planning system. *Information Systems, 69*, 164-179.
Motwani, J., Subramanian, R., & Gopalakrishna, P. (2005). Critical factors for successful erp implementation: Exploratory findings from four case studies. *Computers in Industry, 56*(6), 529-544.
Nassar, M., Warrad, L., & Siam, Y. A. (2017). The implementation of enterprise resource planning system within Jordanian industrial sector. *International Review of Management and Marketing, 7*(3), 179-187.
Pitso, T. E. (2022). *Exploring the challenges in implementing enterprise resource planning systems in small and medium-sized enterprises* (Unpublished master's thesis). North-West University (South Africa).
Rouyendegh, B. D., & Erkan, T. E. (2011). Erp system selection by ahp method: case study from Turkey. *International Journal of Business and Management Studies, 3*(1), 39-48.
Sloan, D. B., Nakabachi, A., Richards, S., Qu, J., Murali, S. C., Gibbs, R. A., & Moran, N. A. (2014). Parallel histories of horizontal gene transfer facilitated extreme reduction of endosymbiont genomes in sap-feeding insects. *Molecular Biology and Evolution, 31*(4), 857-871.
Van Nieuwenhuyse, I., De Boeck, L., Lambrecht, M., & Vandaele, N. J. (2011). Advanced resource planning as a decision support module for erp. *Computers in Industry, 62*(1), 1-8.
Venkatraman, S., & Fahd, K. (2016). Challenges and success factors of erp systems in Australian SMEs. *Systems, 4*(2), 20.

Author Information

Issam Jebreen
Zarqa University
Zarqa, Jordan
Contact e-mail: *ijebreen@zu.edu.jo*

Hanan Omer
Zarqa University
Zarqa, Jordan

Ahmad Al Qerem
Zarqa University
Zarqa, Jordan

To cite this article:

Jebreen, I., Omer, H. & Al-Qerem, A. (2024). Enterprise resource planning implementation:: Challenges and barriers. *The Eurasia Proceedings of Science, Technology, Engineering & Mathematics (EPSTEM), 28,* 300-307.

The Eurasia Proceedings of Science, Technology, Engineering & Mathematics (EPSTEM)
ISSN: 2602-3199

The Eurasia Proceedings of Science, Technology, Engineering & Mathematics (EPSTEM), 2024

Volume 28, Pages 308-316

ICBASET 2024: International Conference on Basic Sciences, Engineering and Technology

Life Cycle Assessment as a Catalyst for Embedding Sustainability in Waste Management Practices

Paloma Barajas-Alvarez
Tecnologico de Monterrey
Escuela de Ingenieria y Ciencias

Martín Esteban Gonzalez-Lopez
Tecnologico de Monterrey
Escuela de Ingenieria y Ciencias

Geraldina Silveyra-Leon
Tecnologico de Monterrey
Escuela de Negocios

Misael Sebastián Gradilla-Hernandez
Tecnologico de Monterrey
Escuela de Ingenieria y Ciencias

Tomas García-Cayuela
Tecnologico de Monterrey
Escuela de Ingenieria y Ciencias

Abstract: The establishment of sustainable campuses acts as a catalyst, fostering a Living Lab environment where active community engagement is crucial. Recognizing the pivotal role of waste management, university campuses prioritize detailed mapping and characterization of organic waste streams. This process paves the way for the identification of alternative scenarios that reduce and divert waste from landfills through valorization routes such as composting and anaerobic digestion. Acknowledging students' pivotal role in shaping sustainable solutions, their perceptions of solid waste separation assume significance. The effectiveness of the current separation system is critical, especially given the monitoring of bin contamination levels, revealing hindrances to organic waste valorization. Life Cycle Assessment (LCA) emerges as a valuable tool for identifying alternative scenarios for waste reduction and diversion, encompassing anaerobic digestion, composting, and waste-to-food strategies. This study centers on evaluating and reshaping student perspectives on organic waste separation and end-of-life waste management through LCA. A comprehensive survey was designed to elucidate current perspectives on the efficiency and communication of the existing waste management system. Student insights into waste separation practices revealed that the major barriers to effective waste management practices on campus include a lack of education and awareness regarding waste separation. The survey findings also underscore the significance of LCA not only in measuring carbon footprints but also in influencing perceptions and behaviors towards sustainable waste management practices. In conclusion, our study contributes to the discourse on embedding sustainability in educational settings, offering valuable insights for institutions aspiring to drive positive change through innovative waste management strategies.

Keywords: Waste Management, Sustainable development, Life cycle assessment

Introduction

Industrialization growth and improved living standards have significantly increased waste production, adversely affecting the environment, contributing to climate change, and posing threats to wildlife, plants, and human health. Landfill waste decomposition releases methane, over 80 times more potent than carbon dioxide, while illegal burning emits substantial carbon dioxide, exacerbating global warming. Open landfills contribute to 91% of methane emissions, with approximately 40% of global waste disposed of in this manner (Gherhes et al., 2022). In response to these challenges, there is a significant emphasis on the circular economy, which underscores the importance of reducing, reusing, and recycling for economic prosperity and environmental well-being. This approach transforms waste into resources, holding considerable implications for the environment, economy, and society. The transition to a circular economy requires the adoption of zero-waste practices, promotion of environmental awareness, and prioritization of global sustainability. Achieving this shift relies on awareness and education initiatives that highlight the environmental impact of behaviors and instill values aligned with circular principles (Gherhes et al., 2022).

University campuses, as microcosms of cities, play a crucial role in reshaping dynamics and economies by leveraging knowledge to enhance management systems. Sustainable campuses can significantly improve overall city sustainability by serving as Living Labs. Illustrating effective municipal solid waste management and minimizing the environmental impact of food systems on campus can provide valuable models for local governments (Vergani, 2024). University campuses are not exempt from addressing the global environmental issue of food waste. Campus food waste contributes significantly to total community waste, offering universities an opportunity to reduce their carbon footprint and environmental impact. Consequently, many institutions prioritize implementing sustainable food systems, necessitating the design and implementation of innovative solutions to address this growing problem (Di Salvatore et al., 2022).

Therefore, this project is encompassed within an holistic approach that aims to implement a comprehensive living laboratory approach that improves the food systems at an university campus by mapping and characterizing the main streams of organic waste, evaluating waste separation efficiency, promoting sustainable food choices, exploring waste valorization strategies via waste-to-food and waste-to-energy perspectives, and conducting a life cycle assessment to evaluate environmental impacts. This study acts as a preliminary baseline determination for mapping the students perceptions regarding the waste management system of the campus. Their perceptions will be key for promoting an active participation of the campus community in the living lab approach. Moreover, we aim to test how integrating life cycle assessment (LCA) is crucial for evaluating impacts, products, and processes, providing a comprehensive understanding of complex systems like waste management in the campus. Specifically, this study aims to conduct a pilot outreach and education activity to engage the university community in sustainable food choices and waste reduction and diversion strategies and to reshape the students' perspective of waste source-separation through a LCA approach. This research seeks to understand students' knowledge regarding current environmental issues and their adoption of sustainable behaviors within a circular economy.

Method

This study was implemented in Tecnológico de Monterrey, which as part of its commitment to sustainability, has developed the Sustainability and Climate Change Plan for 2025. The plan aims to position the institution as a sustainability model, with goals including ensuring 100% of its campuses adopt sustainable waste management models and preventing 40% of waste from reaching landfills. Ultimately, the project will become replicable as a sustainable waste management model to other campuses, contribute to reducing greenhouse gas emissions, and benefit the university community and broader Ruta azul environmental goals. This pilot study involved students of 4th semester of Biotechnology Engineering who were asked to answer an open-ended survey aiming to catalyze reflection and catch the perceptions of the students regarding the current waste separation scheme in the campus. The students were not further instructed to avoid bias in their answers. Afterwards, they received a lecture on how the project aims to improve the waste management practices in the campus following several strategies, among which the communication of the environmental footprint of the source-separated waste streams is affected by the separation efficiency. Following this, they were introduced to LCA (Life Cycle Assessment) for evaluating the environmental sustainability of various approaches to reduce the environmental footprint of food systems. The students were then invited to share their thoughts on these subjects. After the session, once the instructor had addressed most of their questions and misconceptions, the students were given a survey to gauge their awareness levels and perceptions regarding waste separation.

Participants

The 4th semester students are part of the *Production of biotechnological products* course of the Biotechnology Engineering undergraduate program. This group was selected as the students were considered with enough knowledge to address a complex issue with a broader look and at the same time not have had a close approximation to the subject in other related courses. The group consisted of 7 boys, 12 girls, and 1 non-binary student. The students received instructions from both the main professor and an assistant professor on the present status of waste separation bins (and overall campus waste management), the living lab approach followed in the project, and methods for evaluating the sustainability of valorizing source-separated waste streams through an LCA methodology, and were encouraged to participate actively by expressing their opinions, in addition to completing a survey at the conclusion of the lecture. They were explicitly instructed to share their thoughts, with the assurance that there were no incorrect answers.

Open-Ended Survey Questions

This research seeks to understand students' knowledge regarding current environmental issues and their adoption of sustainable behaviors within a circular economy. The research questions were as follows:

Table 1. Questions of the open-ended survey applied to students.

Type	Question
A priori questionnaire	1. How would you describe the efficiency of the current waste management system on campus? 2. If you are aware of end-of-life scenarios such as anaerobic digestion, composting, and waste-to-product transformation, could you share your knowledge on how proper waste separation contributes to these processes? 3. In your opinion, is the waste in the separation containers appropriately diverted from landfill according to established recycling streams?
A posteriori questionnaire	4. How do you perceive the usefulness of the Life Cycle Analysis (LCA) Methodology as a tool to measure and achieve decarbonization objectives on campus? Do you believe that the LCA indicators allow for adequate measurement of the carbon footprint and are effective in guiding sustainability initiatives on campus?

The findings from the conducted survey were gathered and structured within a database for subsequent examination. Following this, a content analysis was undertaken to scrutinize the survey feedback, given the open-ended format of the questions. Our objective was to pinpoint prevalent themes, trends, and misunderstandings related to the waste management system on-campus by assigning them relevant keywords. This process involved categorizing the responses using Atlas.ti software. Additional qualitative analysis, including frequency assessment, was carried out to summarize the collective viewpoint of students on source-separation concerns and the adoption of LCA as a tool for sustainable development analysis.

Results and Discussion

According to a student survey, major barriers to effective waste management practices on campus include a lack of education and awareness regarding waste separation (Table 1). Many students expressed confusion about distinguishing between organic and inorganic waste, highlighting a need for clearer guidelines as the answers stated: "*Not everyone follows or knows how to separate their waste*" or "*I think they should educate students more about what is inorganic and organic because there is that confusion and sometimes you don't know where to put everything. That's why there are times when I see that there is plastic on the organic side*". While some areas provide separate bins for different types of waste, this practice is not universal, further complicating the sorting process. Additionally, inconsistent participation from the university community contributes to the challenge, as one of the answers stated: *"I believe that there is a good intention for the separation of waste, however, students and staff sometimes do not take the task of carrying out such separations in the trash cans*". Limited waste disposal options and a general lack of information exacerbate the problem, with some individuals resorting to tossing all waste in a single bin due to convenience: *"Many times not having all the garbage options*

makes people too lazy to look for the corresponding garbage can and they prefer to throw all the garbage in the same can". Addressing these barriers requires a multifaceted approach, including improved educational initiatives, consistent infrastructure, and efforts to incentivize proper waste disposal habits among the campus community. This is in line with the results of Owojori et al., (2022), who described that the major barriers to improving circularity at the University of Venda in South Africa were the students' lack of awareness and knowledge regarding practicability. One of the motivators reported by the authors is the establishment of education and awareness programs on waste management, which is similar to the main objective of the study, as we hypothesize that LCA methodology could further motivate the university community to engage in waste separation at source.

Table 1. Summary of question 1 answers

Major identified barriers
● Lack of education and awareness.
● Confusion over sorting
● Inconsistent waste separation practices
● Lack of participation
● Limited waste disposal options
● Insufficient information
Good points
● Adequate Distribution of Waste Containers
● Focus on Waste Separation
● Ease of Access to Recycling Bins
● University's Interest in Waste Management Initiatives
Opportunity areas
● Addition of containers for glass
● Enhancing the information of the location of specialized containers
● Inclusion of a container for cardboard
● Dissemination of information of waste management practices

According to the survey responses, several opportunity areas for improvement in our waste management practices have been identified (Figure 1). Firstly, respondents highlighted the absence of dedicated containers for glass waste, which poses a significant challenge as glass recycling is essential for sustainable waste management as one of the students said: *"I would think that the waste management system is sufficient, but it could improve since there are no containers that are for glass, and there are certain drinks available on campus which are based on this material"*.

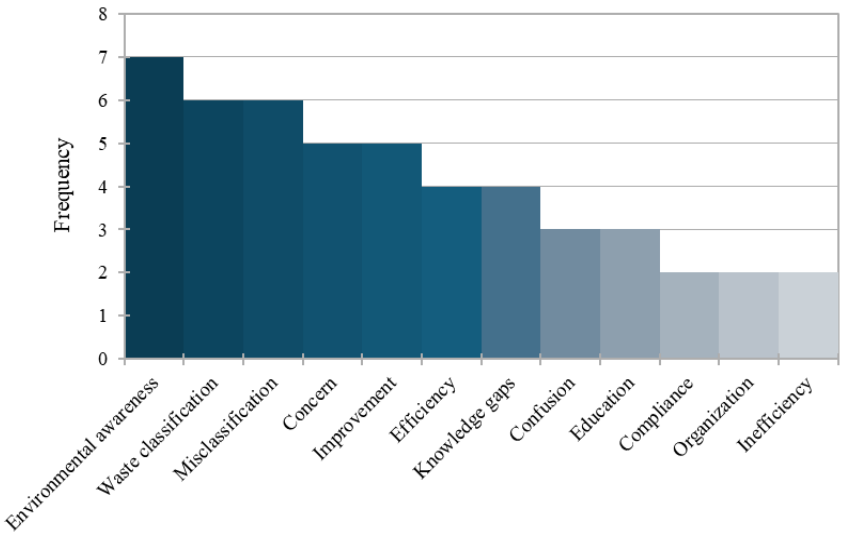

Figure 1. Frequency analysis of the categories identified in question 1.

Secondly, there is a pressing need for specific containers to handle hazardous materials such as sharp objects, laboratory waste and batteries: *"I consider that a specific trash can may be needed for sharp pulse materials, batteries and all that type of things, which, due to lack of them, end up being thrown in the trash cans".* The

lack of proper disposal options for these items leads to improper disposal and potential environmental hazards. Also, while our waste sorting system is functional, respondents noted a noticeable gap in the absence of containers for cardboard recycling. Lastly, an opportunity for improvement in university waste management is the dissemination of information. Despite having sufficient waste containers focused on waste separation, there's a need to enhance how information is shared, another survey responses state: *"I think that there is a lack of more information for students to be able to correctly separate their waste, since I think that several students, including me, are not sure where they should be deposited"*. This could involve clearer signage, digital platforms, and educational materials across campus. Targeted outreach efforts like workshops and campaigns can further engage the university community, promoting sustainable behaviors and proper waste disposal.

The responses to question two highlight several key concepts which included waste management, waste classification, recycling, composting, and sustainability (Figure 2). Among the most notorious answers for this question were: *"These types of scenarios require specific waste to function, so I consider that properly separating the waste helps speed up the process more than anything, since it saves the step of manually separating the waste before moving on to the process that corresponds to the already be previously separated"* and *"waste classification separates components that can be degraded from the environment from those that cannot. Furthermore, this categorization of this last group can help facilitate a new use"*. This indicates that students consider it important to have appropriate waste management and classification. They believe that these practices have a direct impact on end-of-life scenarios such as anaerobic digestion, composting, and waste-to-product transformation. However, the answers also reveal a lack of knowledge regarding the anaerobic digestion scenario, as it is common to direct organic waste to composting or recycling. Only one of the answers mentioned the generation of byproducts such as biogas or biomass, which is related to anaerobic digestion: *"These processes have a positive impact on waste management, as they contribute to the use of waste to generate products such as biomass, biogas, etc. In order to reduce the environmental impact and take advantage of the circular economy"*. Recently, Flores-Nieves et al. (2022) reported the acceptance of anaerobic digestion by end-users as a waste management method and the use of biogas and biomass as energy suppliers and biofertilizers, respectively. It's crucial for students to understand the significance of anaerobic digestion in waste management, as it offers numerous benefits such as producing valuable byproducts. Familiarity with anaerobic digestion enhances their comprehension of holistic waste management practices and encourages more informed decision-making towards sustainable solutions.

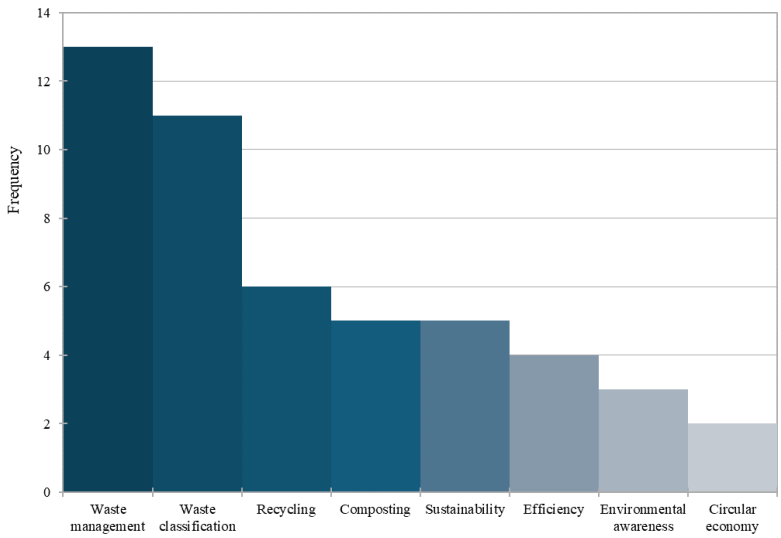

Figure 2. Frequency analysis of the categories identified in question 2.

Figure 3 depicts the frequency analysis of the categories identified in the students' responses to the question " *In your opinion, is the waste in the separation containers appropriately diverted from landfill according to established recycling streams?".* The more frequent answer was the word uncertainty, followed by inefficient, effective, and behavior. Some respondents express doubt about whether waste separation is effectively implemented, citing reasons such as "*I don't know if the waste is correctly diverted to the landfill, but I think that this doesn't happen all the time. Before I saw that when they collected the waste from the containers, they mixed it"* or "*I consider that the waste is not being separated correctly, since not all students are aware of the separation that must be carried out. However, I am not sure if they are being taken to the correct landfills and I have not seen them being separated when collected*". Similar to the report by Amarachukwu et al. (2022), the

students reported that they don't have an idea of what happens to the waste generated in the University of Abuja, making it necessary to carry out extensive awareness programmes on waste management. Others express confidence in the waste separation process, believing that if handled correctly, waste can be diverted from landfill according to recycling streams. Overall, the responses highlight a need for improved education and awareness about waste separation practices, as well as greater transparency and accountability in waste management processes. It is evident that while efforts may be made to separate waste at the source, challenges remain in ensuring that waste is effectively diverted from landfill and recycled according to established streams. As Owojori et al. (2022) reported, the future studies could explore the potential of using various methods to spread awareness about sustainable practices. One avenue worth investigating is the integration of gamification into waste management and environmental education. By incorporating gaming elements, such as challenges and rewards, into these areas, there is the potential to foster a more positive connection between students and their surroundings. This approach not only encourages pro-environmental behavior but also enhances recycling efforts, providing institutions with an innovative tool to promote sustainability.

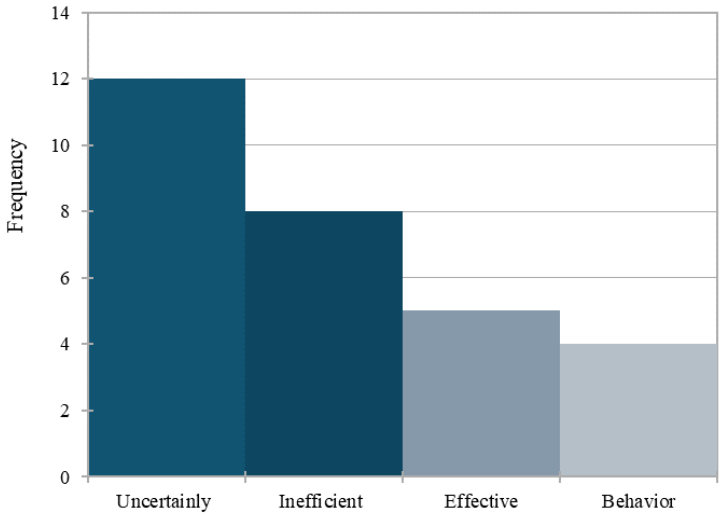

Figure 3. Frequency analysis of the categories identified in question 3.

Table 2 summarizes the key points of the student perspective regarding LCA methodology. Many respondents express confidence in the effectiveness and appropriateness of LCA methodology, considering it a valuable tool for guiding sustainability initiatives.

Table 2. Summary of question 4 answers

Key points
● Positive attitudes toward LCA methodology
● Awareness and education
● Scope for improvement
● Applicability to various areas
● Interest and impact
● Support for sustainability projects
● Effectiveness in measurement

Some of the respondents stated "*I feel that this methodology is appropriate, since it allows us to raise awareness and inform about the carbonization of the campus*" or "*I believe that the LCA tool will achieve an adequate measurement of the carbon footprint and sustainability on campus*". Other students emphasized the use of this methodology in raising environmental awareness and consciousness, as well as educating students about their behavior and the sustainability of the university: "*I found the methodology very interesting and that it can help students think more about the environmental impact that their activities have on campus*" or "*I found the methodology very interesting and that it can help students think more about the environmental impact that their activities have on campus*".

The answers also showed the students are interested and understood the importance of LCA and suggested the application of this methodology for the impact evaluation of other products: "*Likewise, in the future it would be a good idea to apply it to other waste such as the use of cars, vapes*". A work developed by Johannisson and

Hiete (2021) reported the sensitivity of students to real-life problems using LCA. According to the authors, the LCA could improve the proactive learning strategies, such as problem-based learning, facilitating the development of strategic and practical competences in students, fostering critical and transdisciplinary skills essential for sustainability. They recognized the important role of this methodology to integrate the sustainable development goals into education and engineering (Figure 4).

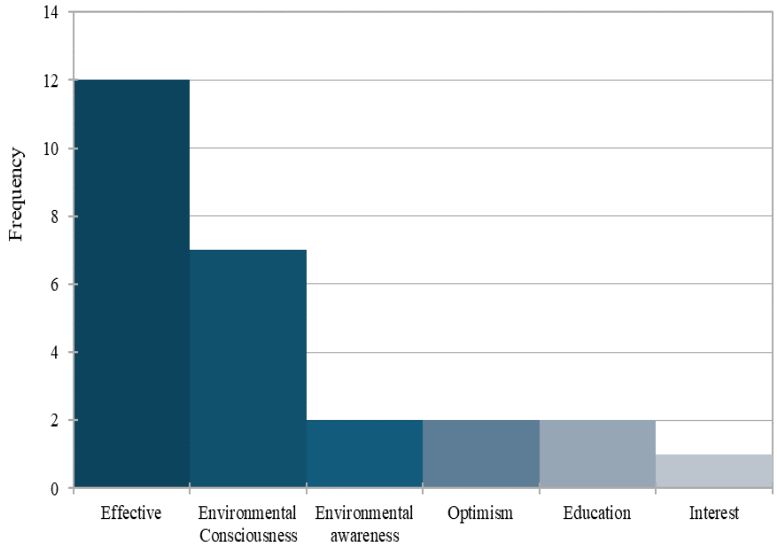

Figure 4. Frequency analysis of the categories identified in question 4.

Finally, Figure 5 presents a summary of the characteristic word cloud derived from the four responses. The size of each word corresponds to its frequency within the dataset. Notably, the most prevalent words include "*interest*" "*separation*", and "*effective*" Overall, the students demonstrate a notable level of concern and engagement regarding waste management practices.

Figure 5. Word cloud derived from the open-ended survey.

Particularly, they highlight the importance and effectiveness of waste separation, recognizing its potential impact on various end-of-life scenarios such as anaerobic digestion, composting, and waste-to-product transformation. This word cloud not only reflects academic discourse but also underscores the connection between academia and environmental action, encapsulating themes such as knowledge gap, environmental awareness, sustainability, and education. The knowledge gap highlights areas needing deeper understanding.

Surrounding it, environmental awareness fosters responsibility and stewardship. Sustainability embodies balanced futures, while education empowers change-makers.

Conclusion

This study provides valuable insights into the perceptions and challenges surrounding waste management practices on campus. The findings underscore the significant barriers posed by a lack of education and awareness, particularly regarding waste separation. To address these barriers, a multifaceted approach is required, needing for improved educational initiatives, consistent infrastructure, and efforts to incentivize proper waste disposal habits among the campus community. Moreover, the study identifies specific gaps in the existing waste management infrastructure, such as the absence of containers for cardboard recycling, highlighting the need for targeted improvements. Additionally, our research emphasizes the importance of enhanced information dissemination to promote understanding and engagement among students. Initiatives such as education and awareness programs on waste management emerge as significant motivators, aligning with the main objective of our study. Furthermore, the study underscores the importance of sustainable practices and the role of students in driving positive change within the campus community. Overall, our findings serve as a foundational baseline for future research and initiatives aimed at reshaping perspectives and fostering sustainable behaviors among students through innovative approaches such as LCA methodology.

Scientific Ethics Declaration

The authors declare that the scientific ethical and legal responsibility of this article published in EPSTEM journal belongs to the authors.

Acknowledgements or Notes

* This article was presented as an oral presentation at the International Conference on Basic Sciences, Engineering and Technology (www.icbaset.net) held in Alanya/Turkey on May 02-05, 2024

* The authors would like to acknowledge the financial and the technical support of Writing Lab, Institute for the Future of Education, Tecnologico de Monterrey, Mexico, in the production of this work. The authors also wish to thank the Living Lab & Data Hub of the Institute for the Future of Education at the Tecnológico de Monterrey, Mexico, for the data or experimental platform provided for the production of this work.

References

Amarachukwu, E., Evuti, A. M., Salam, K. A., & Shamaye, S. (2022). Assessment of students' perception and attitude towards solid waste management in University of Abuja. *Abuja Journal of Pure and Applied Sciences. 1*(1), 33-40.

Di Salvatore, S., Magatti, G., Acciarri, M., Rossetti, M., da Costa, L. P., & Ribeiro, I. (2022). Solid waste management approach at the university through living labs and communication strategies: Case studies in Italy and Portugal. *Sustainability, 14*(9), 5240.

Flores-Nieves, M. M., Soto-Zarazúa, G. M., Rico-García, E., Zamora-Castro, S., Macías-Bobadilla, G., Hernández-López, M. S., & Sánchez-Gutiérrez, A. E. (2022). Revaluation of local waste through an ecotechnologies strategic plan: A case study with digesters. *Sustainability, 14*(15), 9389.

Gherhes, V., Fărcasiu, M. A., & Para, I. (2022). Environmental problems: An analysis of students' perceptions towards selective waste collection. *Frontiers in Psychology, 12*, 803211.

Johannisson, J., & Hiete, M. (2021). Environmental service-learning approach in higher education–a descriptive case study on student-led life cycle assessments of university cafeteria meals. *International Journal of Sustainability in Higher Education, 22*(7), 1728-1752.

Owojori, O. M., Mulaudzi, R., & Edokpayi, J. N. (2022). Student's knowledge, attitude, and perception (KAP) to solid waste management: A survey towards a more circular economy from a rural-based tertiary institution in South Africa. *Sustainability, 14*(3), 1310.

Silva, D. A. L., Giusti, G., Rampasso, I. S., Farrapo Junior, A. C., & Anholon, R. (2023). Life cycle assessment teaching innovation: experiences from a Brazilian higher education institution. *International Journal of Sustainability in Higher Education, 24*(2), 449-461.

Vergani, F. (2024). Higher education institutions as a microcosm of the circular economy. *Journal of Cleaner Production,* 435, 1-19.

Author Information

Paloma Barajas-Alvarez
Tecnologico de Monterrey
Escuela de Ingenieria y Ciencias
Ave. Eugenio Garza Sada 2501
Monterrey 64849, NL, Mexico
Contact e-mail: *paloma.barajas@tec.mx*

Martín Esteban González-López
Tecnologico de Monterrey
Escuela de Ingenieria y Ciencias
Ave. Eugenio Garza Sada 2501
Monterrey 64849, NL, Mexico

Misael Sebastián Gradilla Hernández
Tecnologico de Monterrey
Escuela de Ingenieria y Ciencias
Ave. Eugenio Garza Sada 2501
Monterrey 64849, NL, Mexico

Geraldina Silveyra-León
Tecnologico de Monterrey
Escuela de Negocios
Instituto de Emprendimiento Eugenio Garza Lagüera
Ave. Eugenio Garza Sada 2501
Monterrey 64849, NL, Mexico

Tomás García-Cayuela
Tecnologico de Monterrey
Escuela de Ingenieria y Ciencias
Ave. Eugenio Garza Sada 2501
Monterrey 64849, NL, Mexico

To cite this article:

Barajas-Alvarez, P., Gonzalez-Lopez, M.E., Gradilla-Hernandez, M.S., Silveyra-Leon, G. & García-Cayuela, T. (2024). Life cycle assessment as a catalyst for embedding sustainability in waste management practices. *The Eurasia Proceedings of Science, Technology, Engineering & Mathematics (EPSTEM), 28,* 308-316.

The Eurasia Proceedings of Science, Technology, Engineering & Mathematics (EPSTEM)
ISSN: 2602-3199

The Eurasia Proceedings of Science, Technology, Engineering & Mathematics (EPSTEM), 2024

Volume 28, Pages 317-325

ICBASET 2024: International Conference on Basic Sciences, Engineering and Technology

Development of Mathematics Interactive E-Worksheet

Riska Novia Sari
Universitas Pendidikan Indonesia

Rizky Rosjanuardi
Universitas Pendidikan Indonesia
Indonesian DDR Development Center

Tatang Herman
Universitas Pendidikan Indonesia

Ratri Isharyadi
Universitas Pendidikan Indonesia

Pujia Siti Balkist
Universitas Pendidikan Indonesia

Abstract: Technology integration has become essential in the rapidly evolving landscape of education of the 21st century. Moreover, the aftermath of the Covid-19 pandemic has accelerated the adoption of digital tools in learning. This article explores the development of interactive e-worksheets in mathematics education using the Wizer.me platform. In Indonesia, the Merdeka Belajar curriculum emphasises digital technology as a fundamental aspect of addressing accessibility, quality, and equality in education. The developed e-worksheets are designed to enhance the traditional worksheet experience by transforming it into an interactive, engaging, and contemporary format. The advantages include cost savings, environmental friendliness, and combining multimedia elements such as videos and animations to boost student motivation. The study investigates the necessity of digitally accessible learning activities, aligning with the demands of future educational needs. Focusing on fractions as a challenging topic for students, this study uses the 4D model (Define, Design, Develop, Disseminate) as the Research and Development (R&D) model. The Wizer.me platform is employed for its user-friendly interface, varied question types, and integrated Google Classroom. The validation process involves expert judgment from mathematics educators and practical testing among junior high school students. The findings indicate that the developed interactive e-worksheets are valid and practical, receiving positive student responses during the limited trial. The article reveals the importance of innovative learning materials and suggests that teachers leverage technology to create engaging and accessible content, fostering a more dynamic learning environment. The study recommends the widespread adoption of interactive e-worksheets to enhance students' motivation and comprehension, particularly in challenging mathematical concepts like fractions.

Keywords: E-Worksheet, Fraction, Mathematics, Technology

Introduction

Technology as a learning tool has become an essential aspect of education in today’s digital age, which is known as the 21st century's demands. The lesson learned from the Covid-19 pandemic is the accelerating use of technology and digital frameworks in education. The use of digital technology in learning is one of the basic infrastructure requirements of the Merdeka Belajar curriculum in Indonesia. It is positioned to significantly

enhance access, quality, and social justice within the education sector. Jupri (2018) mentions that technology in the learning process, especially mathematics, is an important topic that requires discussion and implementation since it ensures easy access to education and offers flexibility to engage learners of all types (Gadelha, 2018). It has made education more accessible, efficient, and effective (Ilyas et al., 2023). Incorporating technology into the learning process also improves students' motivation, significantly enhancing their willingness to participate in learning activities (Cóndor-Herrera et al., 2021).

In technological and digital development, printed worksheets are increasingly being phased out. This shift is driven by the higher costs associated with printing and the increased time required for teachers to assess students' work manually. It is in line with Balla (2023) claims of which modern technologies have made education less expensive for students. With technology, printed worksheets can be transformed into interactive e-worksheets that are more engaging and interesting to enhance students' innovation and creativity. In addition, teachers can insert various videos, animations, audio, and other interesting images to raise student's motivation and comprehension. Interactive e-worksheets can be accessed by students using a computer or smartphone. It agrees with the opinion of Haryanto et al. (2020) on the current need for learning activities that are digitally or internet-based accessible.

E-worksheets serve as valuable tools in teaching and learning, fostering effective interactions between students and teachers and boosting student engagement to enhance learning outcomes (Haryanto et al., 2020) These digital resources support and facilitate learning activities, aligning with contemporary educational goals that encourage students to take a proactive approach in addressing material-related challenges. Interactive e-worksheets offer a solution to deepen students' understanding of specific subjects (Choo et al., 2011). Typically, an e-worksheet comprises sections like a title, study guides, learning competencies, basic competencies, supporting information, assignments, and assessments. Consistent with this structure, Mohammad et al. (2019) note that e-worksheets provide detailed descriptions of materials, assignments, and related exercises. The adoption of e-worksheets offers several advantages, including space and time efficiency, environmental sustainability due to reduced paper and ink usage, adjustable font sizes in digital formats, and cost-effectiveness. Numerous studies have highlighted the benefits of electronic worksheets in learning contexts, particularly in mathematics. Such tools have been shown to enhance student's critical thinking skills (Erna et al., 2021; Sujatmika et al., 2018), problem-solving abilities (Eriana et al., 2024; Mawaddah & Siswanto, 2022), and conceptual understanding of mathematical concepts, as well as promoting self-regulated learning practices among students (A'la et al., 2021; Indriani et al., 2021).

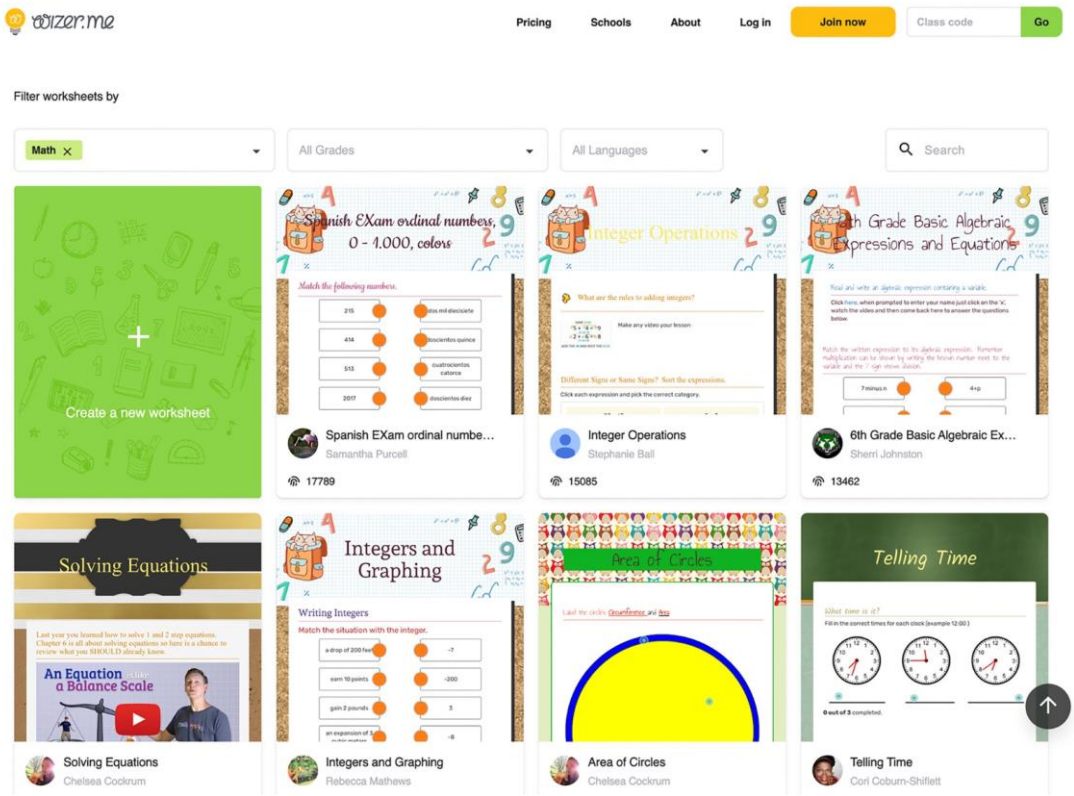

Figure 1. The overview of dashboard wizer.me

The integration of interactive e-worksheets in learning aims to shift students' perceptions of challenging materials, such as fractions in mathematics. A study conducted by A'la et al. (2021) in a school in Central Java revealed that only 45.36% of students were able to solve fraction-related problems, indicating a significant challenge in understanding this topic. This observation is further supported by research from Yeni et al. (2020), which identified common difficulties students face when solving fraction problems. These challenges include a lack of understanding of the questions, an inadequate grasp of mathematical concepts, and a reluctance to re-evaluate answers. Additionally, students encountered epistemological barriers, such as limited knowledge of basic fraction concepts and arithmetic operations, which impede their ability to solve fraction problems effectively (Hariyani et al., 2022). Given these challenges, this research aims to develop an interactive e-worksheet focused on fraction materials. The chosen platform for creating this electronic worksheet is wizer.me. Known for its user-friendly interface, wizer.me offers both free and premium services and is designed to facilitate online assignments. Accessible via smartphones, tablets, and computers, this platform allows teachers and students to engage with the content anytime, anywhere, without constraints of time or location. Below is an overview of the wizer.me interface from a teacher's login.

Kopniak (2018) mentions several advantages of the Wizer.me platform. Specifically, it offers many selections of question types, an attractive appearance, anytime & anywhere access, automatic provision of corrections and grading, and the ability to connect to the Google Classroom account. The following are the types of questions offered.

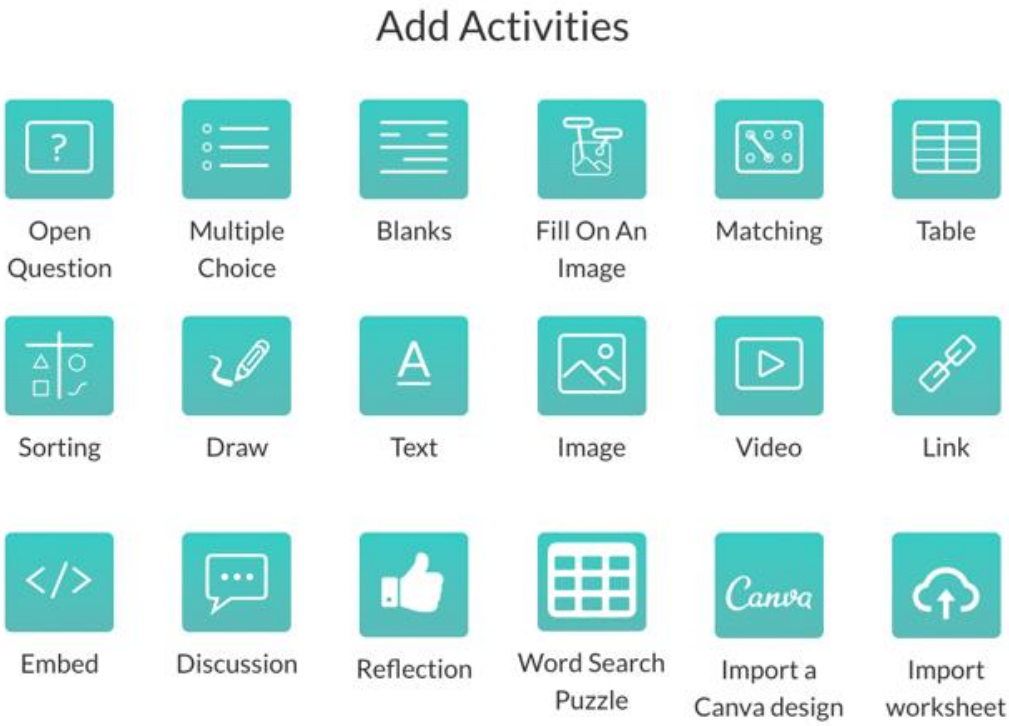

Figure 2. Some activities at wizer.me platform

The screenshot provided showcases the "Import Worksheet" feature on Wizer.me, enabling teachers to effortlessly upload existing question files or student worksheets, eliminating the need for manual retyping. Moreover, wizer.me offers integration with Canva, empowering teachers to design visually engaging electronic worksheets. This feature underscores the importance of teacher creativity, as highlighted by Kaliappen et al. (2021), who emphasised that the platform's comprehensive features allow educators to craft diverse and visually appealing questions for students. Furthermore, wizer.me facilitates interactive discussions between teachers and students. All participants can view and engage with questions and answers posted in the discussion section. This interactive feature fosters collaborative learning and enhances student engagement. Another significant advantage of wizer.me lies in its assessment capabilities. Teachers can provide real-time feedback, and students can respond and reflect on the feedback they receive. Feedback plays a crucial role in the learning process, influencing learning outcomes, motivating learners, and enhancing the overall educational experience (Bosc-Miné, 2014; Kalimullina, 2023). With the wizer.me platform, students are not required to download questions separately. Instead, they can directly access and work on the questions within the platform. The system automatically saves students' responses, alleviating concerns about losing work due to forgotten saves or internet connectivity issues.

Method

The study belongs to Research and Development (R&D). The development model referred to Thiagarajan's development theory, called the 4D model - Define, Design, Develop, Disseminate (Thiagarajan et al., 1974). The four stages are described as follows:

a. Define Stage: The activity of outlining the product and determining its specifications. The define stage is done through 1) Analysis of student characteristics and 2) material analysis.
b. Design Stage: This part contains the process of designing a given product. In the context of teaching material development, e-worksheet content is created based on curriculum and results from the analysis of teaching material.
c. Development Stage: The research phase comprises two distinct activities: expert judgment and practical testing. Expert judgment serves as a method to validate and assess the feasibility of the product design. Following the expert judgment, the subsequent step involves conducting a limited trial with junior high school students
d. Dissemination Stage: The dissemination phase involves sharing and distributing the tested products to benefit a wider audience. This phase ensures that the developed materials and findings from the research are made accessible and available to educators, students, and other stakeholders in the educational community, fostering broader impact and utilisation of the innovative teaching resources.

This article presents findings up to the development stage, focusing solely on the developmental outcomes. The research employed validation and practical questionnaires as its primary instruments. The validation questionnaire encompassed both media and content aspects. Product validation was conducted by four validators, comprising a mathematics teacher and three mathematics education lecturers. The validation data of the e-Worksheet were analysed using a percentage calculation, as shown in the following equation:

$$p = \frac{Average\ Score}{\sum Total}$$

The score (p) result is converted into a category that adapts from Ratumanan & Laurens (2011) as presented in Table 1.

Table 1. Validation score conversion

Interval Score Result of Assessment	Criteria
3,25<p<4.00	Very Valid
2,50<p<3.25	Valid
1,75<p<2.50	Less Valid
1,00<p<1,75	Invalid

Following the validation stage, a limited trial was conducted with junior high school students. After studying the material and completing the questions on the e-worksheet, students were asked to fill out a response questionnaire related to the developed e-worksheet. The response questionnaire was distributed as a Google Form, comprising nine statements with answer choices ranging from "Strongly Agree" to "Strongly Disagree." Subsequently, the questionnaire data was processed using the following formula:

$$NP = \frac{R}{SM}\ x\ 100\%$$

Information:
NP : The percent value expected R : Raw scores obtained by students SM : Maximum score

Table 2. Interactive E-worksheet practicality categories

Interval Score Result of Assessment	Criteria
86% - 100%	Very Good
75% - 85%	Good
60% - 74%	Enough
< 60%	Not Good

Furthermore, the categories of student responses to the interactive e-worksheet are based on the calculation of the final scores in the following Table 2:

Results and Discussion

The outcomes from each stage of the development of the interactive e-worksheet conducted are as follows:

Define Stage

The development stage comprised two phases: student analysis and material analysis. In the first phase, the student analysis revealed that most 7th-grade students had already grasped some foundational concepts, such as simple fractions and integers, before delving into the study of fractions. This prior knowledge proved crucial for their understanding of fractions. Drawing upon Piaget's theory (Hamilton & Ghatala, 1994) , students at this age typically attain a formal operational thinking stage. This means they can use logical reasoning about abstract concepts, showcasing more systematic, hypothetical, and scientific problem-solving abilities than concrete thinking. Regarding the learning environment, insights gathered from interviews with mathematics teachers indicated a predominant reliance on traditional teaching methods. E-worksheets were rarely incorporated into the teaching process, and the instructional approach was generally teacher-centric. The second phase focused on material analysis. The curriculum introduces whole numbers and fractions as the initial topics for 7th-grade students. Conversations with two math teachers from State Junior High School Rambah Samo highlighted the predominant use of textbooks for teaching fractions. Additionally, the limited availability of these textbooks within the school emphasised the need for alternative learning resources. Therefore, the development of interactive electronic worksheets emerges as a promising solution to supplement traditional teaching methods, aiming to enhance learning engagement and motivation among students.

Design Stage

In this stage, the researchers prepared the material on the student worksheet by adapting the materials available in books, including from the mathematics book of the Merdeka Curriculum. The prototype of interactive e-worksheets can be seen in the Figure 3:

Figure 3. The prototype of Interactive E-worksheet

Development Stage

The development stage aimed to produce student worksheets that experts had validated and revised. The experts consisted of two mathematics lecturers as media experts and two mathematics teachers as instructional material experts. The validation result of the interactive e-worksheet by the media expert can be seen in Table 3.

Table 3. The validation result of media expert

No	Aspect	Validator		Average of Each Aspect
		1	2	
1	Display	3,50	2,84	3,17
2	Ease of Use Aspects	4,00	3,33	3,67
3	Language Aspects	2,75	3,25	3,00
	Average			3,28
	Category			Very Valid

Based on Table 3, the assessment calculation for the three aspects yielded the following results: the Display aspect averaged 3.17, falling into the "valid" category; the Ease-of-Use aspect averaged 3.67, classifying it as "very valid"; and the Language aspect had an average of 3, also falling into the "valid" category. The overall average assessment stands at 3.28, categorising the interactive e-worksheet teaching materials as "very valid". It can be concluded that the interactive e-worksheet teaching materials, based on the validity tests conducted, are valid. These findings affirm that the developed interactive e-worksheet teaching materials are well-suited for instructional use, as presented in Table 4.

Table 4. The validation result of material expert

No	Aspect	Validator		Average of each aspect
		1	2	
1	Content Eligibility	3,50	3,25	3,37
2	Presentation	3,67	3,00	3,33
3	Language content	4,00	3,00	3,50
	Average			3,40
	Category			Very Valid

Table 4 shows the calculation of 3 aspects of the assessment: the Content Eligibility aspect averaged 3.37, falling into the "very valid" category; the Presentation Feasibility aspect averaged 3.33, also categorised as "very valid"; and the Language aspect had an average of 3.5, further confirming its classification as "very valid". Based on these results, it can be concluded that the interactive e-worksheet teaching materials, as determined by the validity tests, are valid. Following the expert judgment stage, the subsequent phase involved a limited trial. The interactive e-worksheet was administered to 12 junior high school students. The results of their responses to the developed e-worksheet are as follows:

Table 5. The result of limited trial

No	Aspects	Percentage
1	The display of e-worksheet is interesting	85
2	E-worksheets are easy to access and run	73
3	The types of questions in the e-worksheets are varied and exciting so it challenges me to solve it	81
4	The video explanation in the e-worksheet material is interesting and helps me to comprehend fraction material	77
5	The sentences and paragraphs used in the e-worksheets are clear and understandable	75
6	The language used in the e-worksheets is simple and understandable	77
7	The questions presented in the e-worksheets are related to daily life	71
8	The image illustrations used in the e-worksheets are appropriate and interesting	75
9	Using interactive e-worksheets on fraction problems is not boring	79
	Average	77
	Category	Good

Based on Table 5, the students' opinions regarding the developed e-worksheet predominantly fall into the "good" category. Before commencing teaching, it is essential for educators to prepare the necessary teaching materials. Teachers should aim to design learning experiences that align with the stated educational objectives (Sapta et al., 2018). Teaching materials serve as the instruments educators utilize to effectively manage the

teaching and learning process, contributing to improved student outcomes (Olayinka, 2016). During the initial stages of this research, it was observed that the teaching and learning processes predominantly relied on textbooks, with limited incorporation of technology in mathematics education. Additionally, traditional teaching methods were commonly employed. Such an approach may lead to monotonous learning experiences and suboptimal student outcomes. Hence, educators need to innovate their teaching methodologies beyond textbook-centric approaches (Sari et al., 2019; Siagian et al., 2019). Teachers can introduce innovative teaching models tailored to the subject matter and students' needs, such as STEM, PBL, and PjBL, among others. Leveraging technology to develop teaching materials, like modules, books, and worksheets, can enhance student accessibility. This technological integration ensures that educational resources are easily accessible across various platforms, including computers, tablets, and smartphones.

Mastering fractions is undeniably a fundamental skill for future success in mathematics. Teachers play a pivotal role in guiding students through the intricacies of learning fractions. Incorporating Information and Communication Technology (ICT) in the educational process can significantly enhance this learning experience. Utilising ICT in mathematics education enables students to engage with technology-driven tools to explore concepts related to numbers, geometry, problem-solving, and data analysis (Sivakova et al., 2017). As highlighted by Tomljenović and Zovko (2016), the integration of ICT in classrooms can lead to improved learning outcomes and knowledge acquisition. How teachers contextualize and convey fraction concepts to their students significantly influences the depth and quality of their understanding.

Worksheets serve as valuable tools to assist students in identifying and comprehending essential mathematical concepts (Amalia et al., 2018). In this context, an interactive e-worksheet was meticulously crafted by aligning it with competency standards, essential competencies, and learning objectives about fractions. The e-worksheet is structured to include an introduction, online source materials, a set of questions, a discussion section, and a reflection component. To enrich the learning experience, the source materials are supplemented with educational videos sourced from YouTube and an e-book based on Curriculum 2013 and the Merdeka Curriculum. During the development stage, valuable feedback was obtained from both media and material experts. These insights and recommendations are instrumental in refining and enhancing the quality of the developed e-worksheet, ensuring its effectiveness and relevance in facilitating comprehensive learning experiences for students.

Conclusion

Based on the results and discussion presented, it can be concluded that the interactive e-worksheet teaching materials have been validated and proven to be both valid and practical through the calculation of the validity and limited trial tests. This indicates that the interactive e-worksheet teaching materials are innovative and serve as practical, effective, and efficient learning tools for mathematics. As such, they are well-positioned to be embraced by students and integrated into mathematics education. Implementing interactive e-worksheets is expected to bolster students' learning motivation, particularly in the challenging area of fractions. It is therefore recommended that educators leverage these technological resources to enhance their students' learning experience and outcomes. By doing so, students will become more adept at utilising computers, laptops, and smartphones, broadening their perspectives and understanding of the subject matter. One limitation of this study is the reliance on instructional videos sourced from YouTube. For future research endeavours, it is advisable to create custom videos tailored to align with the specific content and learning objectives of the e-worksheets to ensure greater coherence and relevance in the instructional materials.

Scientific Ethics Declaration

The authors declare that the scientific ethical and legal responsibility of this article published in EPSTEM journal belongs to the authors.

Acknowledgements or Notes

* This article was presented as an oral presentation at the International Conference on Basic Sciences, Engineering and Technology (www.icbaset.net) held in Alanya/Turkey on May 02-05, 2024.

* This work was supported and funded by the Balai Pembiayaan Pendidikan Tinggi (BPPT) Kemendikbudristek and Lembaga Pengelola Dana Pendidikan (LPDP). The authors express their sincere gratitude for their invaluable assistance and financial support.

References

A'la, M. M., Junaedi, I., & Subali, B. (2021). The implementation of guided discovery-based e-worksheets on students' mathematical understanding concepts and independent attitudes. *Journal of Primary Education, 10*(4), 421–434.

Amalia, R., Saiman, S., Sofiyan, S., & Mursalin, M. (2018). Designing computer-based fraction worksheets for junior high school. *Journal of Physics: Conference Series, 1088*.

Balla, E. (2023). Impact of technology in acquisition of English language. *Journal of Educational and Social Research, 13*(1), 134–145.

Bosc-Miné, C. (2014). The properties and functions of feedback in learning. *L'Année Psychologique, 114*(2), 315–353.

Choo, S. S. Y., Rotgans, J. I., Yew, E. H. J., & Schmidt, H. G. (2011). Effect of worksheet scaffolds on student learning in problem-based learning. *Advances in Health Sciences Education, 16*(4), 517–528.

Cóndor-Herrera, O., Bolaños-Pasquel, M., & Ramos, C. (2021). E-learning and M-learning benefits in the learning process. In S. Nazir, T. Z. Ahram, & W. Karwowski (Eds.), *Advances in human factors in training, education, and learning sciences. lecture notes in networks and systems* (pp.331-336).

Eriana, S., Harini, E., Kusumaningrum, B., Sulistyowati, F., Kuncoro, K. ., Irfan, M., & Purwoko, R. . (2024). Effectiveness of e-worksheet on mathematical problem-solving ability based on student learning motivation. *AIP Conference Proceedings, 3046*(1),020046.

Erna, M., Elfizar, E., & Dewi, C. A. (2021). The development of e-worksheet using Kvisoft flipbook maker software based on lesson study to improve teacher's critical thinking ability. *International Journal of Interactive Mobile Technologies (IJIM), 15*(01), 39–55. Gadelha, R. (2018). Revolutionizing education: The promise of virtual reality. *Childhood Education, 94*(1), 40–43.

Hamilton, R., & Ghatala, E. (1994). *Learning and instruction*. McGraw-Hill.

Hariyani, M., Herman, T., Suryadi, D., & Prabawanto, S. (2022). Exploration of student learning obstacles in solving fraction problems in elementary school. *International Journal of Educational Methodology, 8*(3), 505–515.

Haryanto, H., Asrial, A., & Ernawati, M. D. . (2020). E-worksheet for science processing skills using Kvisoft flipbook. *International Journal of Online and Biomedical Engineering, 16*(3), 46–59.

Ilyas, A., Akbar, S. ., Wajid, S. ., Joghee, S., Fatima, A., & Mago, B. (2023). The growing importance of modern technology in education. *2nd International Conference on Business Analytics for Technology and Security (ICBATS)*(pp.1-4). IEEE.

Indriani, S., Nuryadi, N., & Marhaeni, N. (2021). Student's worksheet design assisted with liveworksheets to improve student's concept understanding skills on quadrilaterals and triangles. *Multidiscipline - International Conference 2021, 1*(1), 462-469.

Jupri, A. (2018). Peran teknologi dalam pembelajaran matematika dengan pendekatan matematika realistik. *Seminar Nasional Matematika Dan Pendidikan Matematika, 1*(2), 303–314.

Kaliappen, N., Ismail, W. N. A., Ghani, A. B. A., & Sulisworo, D. (2021). Wizer.Me and socrative as innovative teaching method tools: Integrating tpack and social learning theory. *International Journal of Evaluation and Research in Education, 10*(3), 1028–1037.

Kalimullina, A. (2023). Two-way feedback with the use of digital tools in the classroom: Effect size. *Education and Self Development, 18*(4), 91–105.

Kopniak, N. B. (2018). The use of interactive multimedia worksheets at higher education institutions. *Information Technologies and Learning Tools, 63*(1), 116–129.

Mawaddah, M., & Siswanto, R. . (2022). Development of e-worksheet to improve students' mathematical problem solving ability. *Mathline: Jurnal Matematika Dan Pendidiksn Matematika, 7*(2), 298–314.

Mohammad, Z. O., Amar Faiz, Z. A., Syahrul, H. M., Nur Dalila, K. A., & Ismail, N. (2019). E-logic trainer kit: Development of an electronic educational simulator and quiz kit for logic gate combinational circuit by using arduino as application. *International Journal of Online and Biomedical Engineering, 15*(14), 67–77.

Olayinka, A.-R. B. (2016). Effects of instructional materials on secondary schools students' academic achievement in social studies in Ekiti State, Nigeria. *World Journal of Education, 6*(1), 32–39.

Sapta, A., Hamid, A., & Syahputra, E. (2018). Assistance of parents in the learning at home Andy. *Journal of Physics: Conf. Series, 1114*(1), *012020*.

Sari, N. M., Yaniawati, P., Darhim, & Kartasasmita, B. G. (2019). The effect of different ways in presenting teaching materials on students' mathematical problem solving abilities. *International Journal of*

Instruction, *12*(4), 495–512.

Siagian, M. V., Saragih, S., & Sinaga, B. (2019). Development of learning materials oriented on problem-based learning model to improve students' mathematical problem solving ability and metacognition ability. *International Electronic Journal of Mathematics Education*, *14*(2), 331–340.

Sivakova, D., Kochoska, J., Ristevska, M., & Gramatkovski, B. (2017). ICT- the educational programs in teaching mathematics. *TEM Journal*, *6*(3), 469–478.

Sujatmika, S., Irfan, M., Ernawati, T., Wijayanti, A., Widodo, S. ., Amalia, A. ., Nurdiyanto, H., & Rahim, R. (2018). Designing e-worksheet based on problem-based learning to improve critical thinking. *1st International Conference on Science and Technology for an Internet of Things (ICSTI)*.

Thiagarajan, S., Semmel, D. ., & Semmel, M. . (1974). *Instructional development for training teachers of exceptional children: A sourcebook*. Indiana University Bloomington.

Tomljenović, K., & Zovko, V. (2016). Primjena informacijskokomunikacijske tehnologije u nastavi matematike – Komparativna analiza uspjeha učenika 7. Razreda osnovne škole. *Croatian Journal of Education*, *18*, 215–221.

Yeni, E. ., Wahyudin, W., & Herman, T. (2020). Difficulty analysis of elementary school students in mathematical problem solving in solutions. *International Journal of Scientific and Technology Research*, *9*(3), 44–47.

Author Information

Riska Novia Sari
Universitas Pendidikan Indonesia
Bandung, West Java, Indonesia
Contact e-mail: *riskanoviasari@email.com*

Rizky Rosjanuardi
Universitas Pendidikan Indonesia
Indonesian DDR Development Center
Bandung, West Java, Indonesia

Tatang Herman
Universitas Pendidikan Indonesia
Bandung, West Java, Indonesia

Ratri Isharyadi
Universitas Pendidikan Indonesia
Bandung, West Java, Indonesia

Pujia Siti Balkist
Universitas Pendidikan Indonesia
Bandung, West Java, Indonesia

To cite this article:

Sari, R. N., Rosjanuardi, R., Herman, T., Isharyadi, R., & Balkist, P.S. (2024). Development of mathematics interactive E-worksheet. *The Eurasia Proceedings of Science, Technology, Engineering & Mathematics (EPSTEM), 28*, 317-325.

The Eurasia Proceedings of Science, Technology, Engineering & Mathematics (EPSTEM)
ISSN: 2602-3199

The Eurasia Proceedings of Science, Technology, Engineering & Mathematics (EPSTEM), 2024

Volume 28, Pages 326-341

ICBASET 2024: International Conference on Basic Sciences, Engineering and Technology

Performance Comparison of AI Platforms in Solving Computer Science Problems

Huseyin Karacali
TTTech Auto Turkey

Efecan Cebel
TTTech Auto Turkey

Nevzat Donum
TTTech Auto Turkey

Abstract: In the rapidly evolving landscape of artificial intelligence (AI), its significance and accelerated development are undeniable. AI has emerged as a cornerstone technology with profound implications across various domains, driving innovation and reshaping the way we approach complex problems. Particularly, the utilization of AI in coding tasks has garnered substantial attention, given its potential to streamline development processes and enhance the efficiency of software engineering practices. Against this backdrop, this paper presents a detailed comparative analysis of four different AI platforms, namely ChatGPT, Gemini, Blackbox, and Microsoft Copilot, in addressing key challenges within the realm of computer science, spanning natural language processing, image processing, and cybersecurity. The study focuses on leveraging the C++ programming language to develop solutions for these multifaceted problems across the aforementioned platforms. Each platform's outputs are meticulously evaluated on various parameters including accuracy, execution time, code size, and time complexity to provide a comprehensive understanding of their performance. Furthermore, an iterative optimization methodology is employed, entailing three rounds of refinement for the code produced by each platform, with the resultant outputs subjected to comparative analysis in each iteration. Through this rigorous approach, the paper not only elucidates the efficacy of different AI platforms in addressing diverse computational challenges but also underscores the iterative enhancement process on AI platforms for refining code quality and performance across multiple domains within computer science.

Keywords: AI-driven development, AI-driven chatbot, AI Platforms, Computer science

Introduction

In recent years, the integration of AI techniques has become increasingly pervasive across numerous domains, revolutionizing the way complex challenges in computer science are approached, natural language processing (NLP), image processing, and cybersecurity. Amidst this landscape, the emergence of sophisticated AI platforms such as ChatGPT, Gemini, Blackbox, and Microsoft Copilot has offered promising avenues for addressing multifaceted problems through innovative methodologies and advanced algorithms.

This study endeavors to undertake a meticulous comparative analysis of these four prominent AI platforms, with a specific focus on their efficacy in tackling fundamental challenges spanning the aforementioned domains. By delving into the intricate nuances of each platform's capabilities and performance characteristics, developers aim to provide valuable insights into their applicability and suitability for addressing real-world problems across diverse contexts.

Central to this comparative analysis is the adoption of the C++ programming language as a unifying framework for solution development. Recognized for its efficiency, versatility, and widespread usage in various domains, C++ serves as an ideal platform for evaluating and benchmarking the performance of AI algorithms and methodologies across different AI platforms.

The evaluation criteria employed in this study encompass a comprehensive array of parameters, including but not limited to accuracy, execution time, code size, and time complexity. Through a rigorous examination of these metrics, study aims to elucidate the strengths and limitations of each AI platform in addressing complex challenges, thereby facilitating informed decision-making regarding their deployment in practical settings.

Furthermore, to ensure a thorough understanding of each platform's performance, a three-round iterative optimization methodology is employed. This iterative approach necessitates successive refinement of the outputs generated by each platform, followed by comparative analysis in each iteration. By subjecting the refined outputs to systematic evaluation, the goal is to capture the iterative evolution of solutions produced by these AI platforms and assess their adaptability and robustness in response to optimization efforts.

Ultimately, the insights derived from this comparative analysis are expected to enrich our understanding of the capabilities and limitations of AI platforms in addressing multifaceted challenges across diverse domains. By shedding light on the relative strengths and weaknesses of each platform, this study aims to empower researchers, practitioners, and decision-makers with valuable knowledge for leveraging AI-driven solutions effectively in real-world scenarios.

Since the day AI chat boxes started to be released, comparisons have begun on many issues such as which one has better understanding ability, which one gives more relevant answers, which one is more up-to-date. Each released AI chat box has been directly compared with others. A comparison of the most well-known of these, 'Bard', now known as 'Gemini', and ChatGPT was made by Waisberg and his colleagues. In this study, a one-to-one comparison was made and the comparison was detailed on a topic in the field of medicine (Waisberg et al., 2023).

These developed AI platforms were used for purposes such as generating code and even completing some projects without any human development. It has even been seen as a threat to the profession of computer programmers. In an article written by Brett A. Becker and his colleagues, the educational opportunities, and difficulties in producing code with AI are mentioned (Becker et al., 2023). In short, researchers have always observed the situation of coding with artificial intelligence and continued their studies.

Finally, there are studies similar to this study that make calculations and comparisons on code quality. One of these is the code quality calculation in artificial intelligence-assisted code development made by Yetiştiren and his friends. In this study, experimental measurements were made. Copilot, CodeWhisperer, and ChatGPT were used (Yetistiren et al., 2023).

With this effort, a study has been produced that will contribute to the advancement of artificial intelligence research and applications, encouraging innovation and informed decision-making in the development and application of AI technologies.

Materials

ChatGPT

ChatGPT, developed by OpenAI, is an advanced natural language processing model designed to generate human-like text responses based on input prompts. It is built upon the GPT (Generative Pre-trained Transformer) architecture, specifically the GPT-3.5 variant, which utilizes deep learning techniques to understand and generate text (OpenAI, 2024).

Unlike traditional chatbots that rely on predefined responses or rule-based systems, ChatGPT employs a machine learning approach called unsupervised learning. This means it learns from vast amounts of text data from the internet without explicit human supervision. As a result, it can produce contextually relevant and coherent responses across a wide range of topics.

One of the key features of ChatGPT is its ability to understand and generate text in multiple languages, making it accessible to diverse linguistic communities worldwide. Additionally, it can mimic the style and tone of input prompts, allowing for more personalized interactions.

ChatGPT finds applications in various fields such as customer service, content generation, language translation, and educational tools. Its versatility and adaptability make it a valuable asset for businesses, researchers, and developers seeking to leverage natural language processing capabilities. Moreover, ChatGPT has undergone continuous refinement and improvement through iterations, enhancing its performance and capabilities over time. OpenAI regularly updates and fine-tunes the model to ensure its effectiveness and reliability in various contexts.

Figure 1. The logo of the chatGPT (ChatGPT, n.d.)

In summary, ChatGPT represents a significant advancement in natural language processing technology, offering a powerful tool for generating human-like text and facilitating seamless interactions between humans and machines (ChatGPT, n.d.). In this study, ChatGPT 3.5, recognized as one of the most utilized AI platforms, has been chosen as one of the subjects for evaluation.

Gemini

Gemini, developed by Google AI, is a groundbreaking innovation in the world of AI. Described as a great language model, Gemini has many capabilities such as creating text, translating languages, producing creative content, and answering your questions in an informative way.

Figure 2. The logo of the gemini (Gemini, n.d.)

Although still in development, Gemini has learned to perform many types of tasks. For example, it can create different text formats such as codes, scripts, musical pieces, emails, and letters. It also translates languages, facilitating communication between people speaking different languages.

One of Gemini's most important characteristics is that he can answer your questions comprehensively and informatively, even if they are open-ended, challenging, or strange. Thanks to this feature, its usability increases in various fields such as research, education, and entertainment (Gemini", 2023). In this study, Gemini (formerly Bard), is another selected AI platform for comparison. Since Gemini is developed by Google, it is trusted for these kinds of studies.

Copilot

Microsoft Copilot stands at the forefront of this transformation, offering a tool with the potential to revolutionize the coding process. Leveraging a large language model and diverse coding techniques, Copilot is designed to assist developers in their coding endeavors. By providing code suggestions, identifying errors, and optimizing code, it empowers programmers to write code faster and more efficiently ("Microsoft Copilot," n.d.).

Figure 3. The logo of the microsoft copilot ("Microsoft Copilot," n.d.)

Basic properties include code suggestions, debugging assistance, code optimization, code generation, and multi-language support. Copilot holds immense potential to serve as a valuable asset for developers, potentially enhancing the coding process in various aspects. However, it is crucial to recognize Copilot as a tool, not a replacement for human expertise. Responsible usage of Copilot and maintaining complete control over the code necessitate continued manual code review and editing. Microsoft Copilot exemplifies the impact of AI in the software development processes. As technology advances, such tools are poised to evolve further, empowering developers to become more productive and creative ("Microsoft Copilot," n.d.). In this study, Copilot was chosen as one of the AI platforms to be compared. Microsoft Copilot will be a high-potential choice for this study, which will involve calculations and developments related to computer science.

Blackbox

Blackbox AI is another platform in the realm of AI-powered coding tools. Designed to assist developers in writing, debugging, and optimizing their code, Blackbox AI leverages a large language model and various coding techniques to provide real-time suggestions and support. The tool's ability to enhance developer productivity, improve code quality, and facilitate learning has propelled it to popularity. However, for effective and ethical coding practices, it's crucial to utilize Blackbox AI responsibly and acknowledge its limitations.

Figure 4. The logo of the blackbox ai (Tech Insider Buzz, 2023)

Blackbox AI boasts a range of functionalities that empower developers. One key feature is its ability to translate natural language descriptions into code, making it easier for beginners or those unfamiliar with a specific language to get started. The tool also provides real-time insights on current events, technological advancements, and product launches, keeping developers updated and informed. The most impactful feature for speeding up development is Blackbox AI's code completion. By automatically suggesting the next lines of code based on the coding context, it helps developers maintain their coding flow and minimize errors. Blackbox AI even caters to non-coders to a certain extent. Users can generate code from visual inputs like code screenshots or product sketches, enabling the creation of simple code ("BlackboxAI," n.d.). Since the Blackbox AI is becoming increasingly popular for use in software development processes, it is the last selected AI chat box for the study.

Development and Testing Platform

The execution and compilation of each code response given iteratively by the AI chat boxes was done on a single computer to ensure consistent and accurate comparison. This computer is a Linux-based virtual machine with Ubuntu-20.04.1 operating system with 5.15.0-101-generic kernel. It has 64-bit architecture with x86_64. All solutions by AI platforms are produced in C++ programming language and these codes are compiled with g++. The version of g++ is also 9.4.0.

Method

In this study, the extent to which 4 different AI platforms can successfully write a program under the desired conditions is compared with each other. Since these comparisons will be based on programming ability, performance, artificial intelligence's ability to solve problems that may arise in the program, and performance improvement capabilities, experiments have been made to find solutions to certain predetermined computer science problems. These computer science problem types belong to the fields of natural language processing (NLP), cybersecurity (CS), and image processing (IP), respectively.

These topics are very popular today and are actively developing areas. The solutions that the mentioned AI platforms would provide to the problems identified in these areas were measured. Evaluations were made in line with some generally determined metrics such as accuracy, execution time, executable size, and time complexity. In this study, it is not enough to see how well the artificial intelligence platforms solve the problems in one go, it is requested to interact 3 more times after the first response and to correct any errors if there is an error, or to improve the application in terms of performance.

Selected Computer Science Topics

Natural Language Processing

Natural language processing is the first of the selected topics. Under this topic, a problem that examines the frequency of letters in the text message entered by the user and gives the output in order from the most frequently used to the least frequently used, was requested by artificial intelligence platforms. It is planned that the answers and improvements to be given by artificial intelligence may be effective in realizing this problem, due to the diversity of the processing of characters of the input data, the method of counting letters, and the ways of storing this data at run-time. In addition, it can be easily observed in this study whether it works consistently or not. Apart from consistency, the main purpose is to observe the change in time complexity since there are many different methods to perform this operation. The input text specified by the user can be of any length and content. The program to be developed must be able to handle this situation and is expected to respond correctly.

Cybersecurity

Another selected topic is cybersecurity. The problem under this topic is that the text data in 'test.txt' given as input is encrypted using the AES-128 algorithm and this encrypted data is written in a file called 'encrypted.txt'. The key and initialization vector to be used for this process are predefined. In general, since each character will be counted one by one in the program, much variation in terms of time complexity is not expected. However, it is a topic that can be a reference in comparison in terms of accuracy, and executable size.

Image Processing

The last computer science topic chosen is image processing. The problem under this topic is that edge detection can be made in an example image named 'example.jpg'. Since it is a more demanding task in terms of performance compared to the first two topics, it is suitable for use in run-time comparison.

Figure 5. Example image for image processing problem (Peter Kovesi, n.d.)

As a solution to this problem, after successful edge detection, a file named 'result.jpg' should be produced as output. This output should be an output indicating the edges of the objects in the first image. In addition, the program is responsible for checking the existence of the image to be given as input.

Measurement Metrics

Another part of carrying out the study is evaluation and measurement. Separate answers for each AI platform for all problems in terms of accuracy, time, size, and time complexity were observed and recorded in each iteration. A total of 192 different values were examined under 3 different topics, with 4 different AI platforms, when responses were received 4 times and observed with 4 different metrics.

Correctness and Accuracy

The first metric observed during the evaluation process of the study is whether it works correctly or not. Since a software solution is offered to the problems, results such as compilation errors, faulty operation, inconsistent operation, and correct operation can be seen under this metric. Although it works correctly, especially for performance in image processing, the output quality varies. The problems encountered for the faulty situations under this heading are also stated in the results section.

Execution Time

Another measurement value is execution time. For all iterations that did not have a compilation error (an executable file was produced), the time from the moment it was run from the command line to its termination was recorded. This represents how effectively a solution is offered in terms of performance. The 'time' command, which is built-in in Linux, was used to measure this value. The command executed as 'time ./executable_name' both runs the application offered by the artificial intelligence and prints the elapsed time on the terminal screen.

Many parameters are involved in measuring this value. Parameters such as I/O operations, operations of other applications running in the background, and input delays can change this time. Therefore, a script was prepared that records the resulting time using the 'time' command and repeats this process 100 times and averages the

resulting time values. Thanks to this script, each iteration will be run 100 times and the average value will be determined as the execution time. Thus, the deviation of other processes on this measurement is greatly reduced.

Executable Size

Another observation value is the size of this executable file (the executable file resulting from compilation) in bytes. The size of the outputs is of great importance, especially in sectors where there are many memory-related limitations, such as embedded systems. Therefore, it is quite significant that the concept of size can be included in performance comparison. For this value, the size of each compiled output was observed and recorded. All codes produced by AI were compiled with g++ and the '-O0' flag, which is the 'no optimization' option, was used. This allows it to be compiled without any optimization by the compiler. Thus, the compiler performance impact on the work is eliminated.

Time Complexity

The last value to check is time complexity. In computer science, performance independent of sub-branches is very important and this performance directly depends on the number of operations and the size of the data to be processed. Avoiding repetitive operations, especially loops, usually has positive results in terms of performance. Time complexity is one of the most important performance values since the largest software is considered. For this reason, evaluating each response given by AI in terms of time complexity is also an important task for the purpose of comparing these platforms.

Results and Discussion

The applications created with the solutions provided by AI platforms for each problem described in the Method section were noted, taking into account the above-mentioned values. The results for each problem will be discussed separately in this section. All 4 answers to a problem will be presented in the form of tables, and based on these values, platforms can be compared.

Natural Language Processing

Iteration 1

Table 1. First iteration for NLP problem solution

	1	Correctness	Execution Time (ms)	Code Size (bytes)	Time Complexity
NLP	ChatGPT	Compile Error	Missing library included.		
	Gemini	Compile Error	Some functions used are undefined.		
	Copilot	Compile Error	Syntax error.		
	Blackbox	Compile Error	Missing library included.		

As seen in Table 1, none of the results requested from AI for the NLP problem could produce a successful output. The project was not compiled because both ChatGPT and Blackbox did not add the 'vector' library required for the vector type they use to work. The code produced by Gemini did not have definitions for some of the functions it used, and Copilot made a very simple cursor error and gave a compilation error. Based on these results, a data set to use for comparison could not be obtained.

Iteration 2

Table 2. Second iteration for NLP problem solution

	2	Correctness	Execution Time (ms)	Code Size (bytes)	Time Complexity
NLP	ChatGPT	Success	3	71504	O(n*logn)
	Gemini	Success	3	73704	O(n*logk)
	Copilot	Compile Error	Syntax error.		
	Blackbox	Success	2	67488	O(n)

Since there were errors in the code produced by all AI platforms in the first iteration, each of them was notified of their errors and asked to solve the problem. As a result, Copilot could not solve the syntax error it caused, while all other platforms managed to produce the program that worked correctly.

In the second iteration, all platforms that successfully solve the problem have execution times that are very close to each other. There is an almost incomparable difference in terms of performance. In terms of size, there is a difference of approximately 4 kilobytes between Blackbox and ChatGPT, and 2 kilobytes between ChatGPT and Gemini, from least to most of each. Blackbox has achieved a better result in terms of size compared to other platforms, albeit slightly.

Additionally, the most obvious difference in this iteration emerged in the time complexity metric. It is greater than O(n) in time complexity for both ChatGPT and Gemini because there is a logarithmic expression next to n in the multiplication case. Here the letter n indicates the number of characters in the input. The letter 'k' represents repeating numbers. Although Gemini is slightly higher performing than ChatGPT, Blackbox has achieved a significantly better result compared to other platforms in the second iteration for the NLP problem.

Iteration 3

Table 3. Third iteration for NLP problem solution

	3	Correctness	Execution Time (ms)	Code Size (bytes)	Time Complexity
NLP	**ChatGPT**	Success	< 1	52560	O(n)
	Gemini	Compile Error	Wrong template usage.		
	Copilot	Compile Error	Syntax error.		
	Blackbox	Incorrect Result	1	56736	O(n)

In the third iteration, platforms that worked correctly in the previous round were asked to improve their performance, while Copilot was given a prompt to resolve the error. As a result, Copilot could not find a solution to the syntax error by giving the exact same answer. In addition, Gemini, which tried to add a template structure to the code, encountered a compilation error because it responded with the wrong use of the template expression.

Blackbox, which had the best results in terms of performance in the previous iteration, also preserved time complexity, halved the execution time, and managed to reduce the code size by approximately 11 kilobytes. However, it was observed that some letters of the alphabet could not be detected in the output of the program. No matter how many times the letters 'z' and 'a' were repeated, they could not be detected in the text given as input by the application.

Finally, ChatGPT demonstrated a very successful performance increase in this iteration. Executable file size is reduced by almost 19 kilobytes, reduced the average execution time to less than 1 millisecond, and made the time complexity linear to the input O(n).

Iteration 4

Table 4. Fourth iteration for NLP problem solution

	4	Correctness	Execution Time (ms)	Code Size (bytes)	Time Complexity
NLP	**ChatGPT**	Success	2	45120	O(n*logk)
	Gemini	Incorrect Result	4	74568	O(n)
	Copilot	Success	3	61368	O(n*logk)
	Blackbox	Success	3	61368	O(n*logk)

For the last iteration of this problem, all AI platforms provided compilable answers. Copilot produced a compilable piece of code for the first time. This piece of code, working correctly, had very average performance. It has average values in terms of code size, running time, and time complexity. Blackbox, whose application ran incorrectly in the previous iteration, produced exactly the same answer as Copilot. Therefore, all values are the same. It lost its performance in running time and optimization in time complexity in the second iteration. In summary, the desired improvement in terms of performance could not be achieved with Blackbox AI.

Gemini, on the other hand, has solved the compilation error caused by using the wrong draft in the previous round, but although the piece of code it produced can be compiled, it does not work correctly. It shows completely random values for the letters and characters used once input is given. For example, it detects that the letter 't' occurs 98 times in the input message given as 'test'.

Finally, ChatGPT has again produced a solution that works correctly. Although it lost some performance in runtime in this iteration, it performed very well in terms of code size. Compared to the first successful iteration, it showed good improvement in all values.

Cybersecurity

Iteration 1

Table 5. First iteration for CS problem solution

	1	Correctness	Execution Time (ms)	Code Size (bytes)	Time Complexity
CS	**ChatGPT**	Compile Error	Syntax error.		
	Gemini	Incorrect Result	5	23880	O(n)
	Copilot	Incorrect Result	3	33848	O(n)
	Blackbox	Compile Error	memset is not defined.		

In the first answers to this problem, which asked to encrypt a sample text with the AES-128 algorithm, the codes produced by ChatGPT and Blackbox caused compilation errors. While the code produced by ChatGPT gives a syntax error, the library that will define the memset function has not been added in Blackbox's. Although the codes produced by Gemini and Copilot passed the compilation phase successfully, they did not give correct results when they were run. In the output of the code produced by both of them, no new file was created for the encrypted data. Therefore, a successful coding could not be done by AI for the first round.

Iteration 2

Table 6. Second iteration for CS problem solution

	2	Correctness	Execution Time (ms)	Code Size (bytes)	Time Complexity
CS	**ChatGPT**	Success	2	23248	O(n)
	Gemini	Success	4	23880	O(n)
	Copilot	Incorrect Result	3	34792	O(n)
	Blackbox	Success	3	18720	O(n)

In the second round of this problem, all compilation errors encountered in the previous iteration have been resolved. At the same time, the code generated by Gemini worked correctly, but even though Copilot made some changes to the code, the file containing the encrypted data was still not created. For all AI platforms, time complexity is equal, each O(n), directly related to the length of the data to be encrypted that given in the example file. Apart from this, Blackbox has produced code with an average execution time but is much smaller in size than other AIs. There is a half-and-half execution time difference between the outputs of ChatGPT and Gemini, which were almost the same size at the time. ChatGPT has the best uptime performance.

Iteration 3

Table 7. Third iteration for CS problem solution

	3	Correctness	Execution Time (ms)	Code Size (bytes)	Time Complexity
CS	**ChatGPT**	Success	2ms	23240	O(n)
	Gemini	Incorrect Result	4ms	19080	O(n)
	Copilot	Incorrect Result	3ms	34792	O(n)
	Blackbox	Compile Error	Wrong function usage with too many arguments.		

Copilot reproduced exactly the same code as it produced in the previous iteration. Therefore, the incorrect output has not changed in this round either. On the other hand, the output of Gemini, which worked successfully in the previous round, works incorrectly in this round. The text file it creates to hold encrypted data is empty. It

provided a significant reduction in code size, but this disrupted the operation of the code. Also, Blackbox produced code that could not be compiled due to changes made while trying to improve performance, and a compilation error occurred. ChatGPT, the only AI platform that continues to operate successfully in this iteration, has produced an output that performs almost identically to the performance it produced in the previous iteration.

Iteration 4

Table 8. Fourth iteration for CS problem solution

	4	Correctness	Execution Time (ms)	Code Size (bytes)	Time Complexity
CS	ChatGPT	Compile Error	Type conversion error.		
	Gemini	Incorrect Result	4ms	23240	O(n)
	Copilot	Incorrect Result	3ms	34792	O(n)
	Blackbox	Incorrect Result	3ms	18512	O(n)

In the last round of the Cybersecurity problem, Copilot produced the same answers as in the previous 2 iterations and failed to make any changes. Even though Gemini made changes to the code, the code he produced in the previous round was working incorrectly, it still could not produce a successful result and the file it produced for the encrypted data was empty. The Blackbox output, which produced a compilation error in the third iteration, resolved this error but produced an empty file, just like Gemini. While ChatGPT was improving performance, it produced a code that made a type error in the data and caused a compilation error.

Image Processing

Iteration 1

Table 9. First iteration for IP problem solution

	1	Correctness	Execution Time (ms)	Code Size (bytes)	Time Complexity
IP	ChatGPT	Success	32	66496	O(n)
	Gemini	Success	31	66720	O(n)
	Copilot	Success	33	66688	O(n)
	Blackbox	Success	112	66472	O(n)

In the first answers received for the image processing problem, all generated codes were successfully compiled and edge detection was successfully performed. All time complexities are equal and O(n). Here, the letter n represents the number of pixels to be processed. Additionally, all outputs produced are almost identical in size. The single most obvious difference in the output created by AIs is Blackbox's run time. It has more than 3 times the execution time of others. Below are the edge detection outputs produced by 4 different AI.

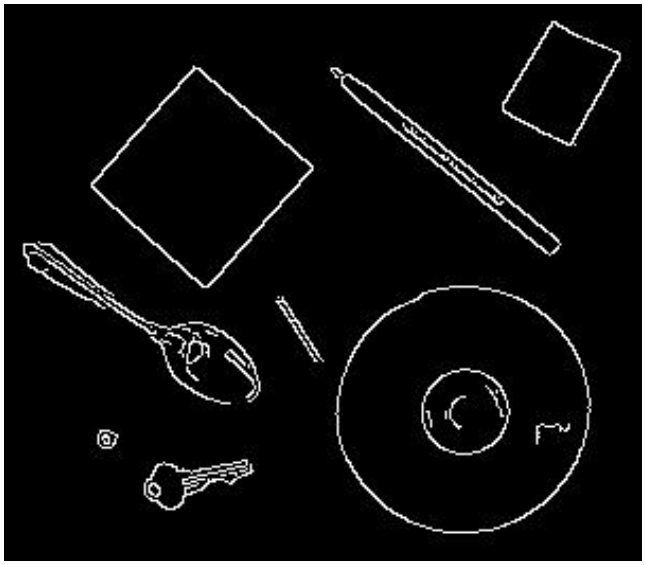

Figure 6. Output of ChatGPT for the first iteration

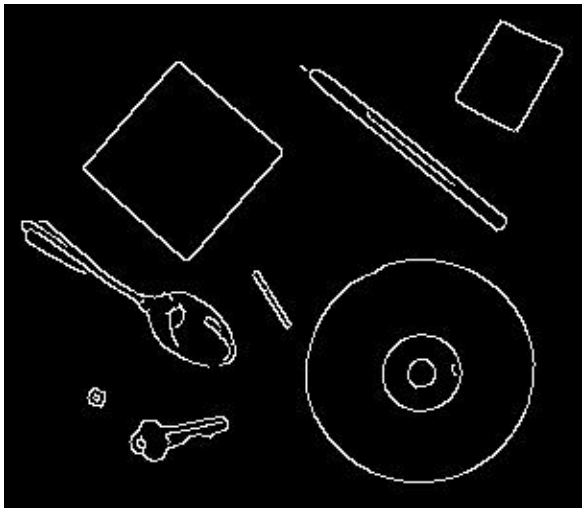

Figure 7. Output of Gemini for the first iteration

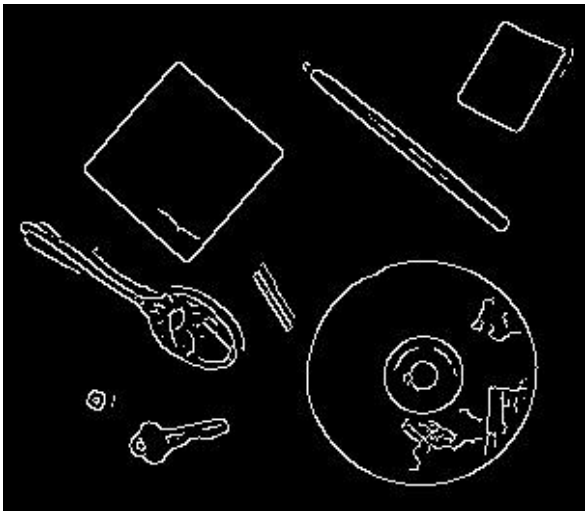

Figure 8. Output of copilot for the first iteration

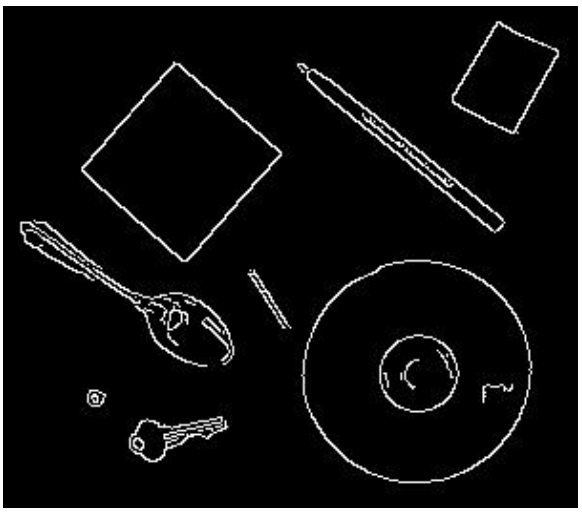

Figure 9. Output of blackbox for the first iteration

When looking at the outputs given in Figure 6, Figure 7, Figure 8, and Figure 9, it is observed that Gemini gave the best result for the first iteration. It is the one that best indicates the real edges of the shapes in the image and can distinguish the parts that are not edges. While ChatGPT and Blackbox produce similar outputs, non-edge details are shown as edges in the output of the code produced by the Copilot platform. Although all AI platforms produce very close results, Gemini has the fastest and highest quality output in the first iteration.

Iteration 2

Table 10. Second iteration for IP problem solution

	2	Correctness	Execution Time (ms)	Code Size (bytes)	Time Complexity
IP	ChatGPT	Compile Error	Invalid headers included.		
	Gemini	Compile Error	Undeclared built-in functions.		
	Copilot	Success	33	66688	O(n)
	Blackbox	Success	33	66320	O(n)

In the second iteration of the image processing problem, both ChatGPT and Gemini caused a compilation error due to the code fragments they added while improving performance. Therefore, they could not produce output. Since Copilot produces exactly the same code as its previous answer, it is same as the visual output in Figure 8. The output of Blackbox is also very similar with the first iteration output of itself.

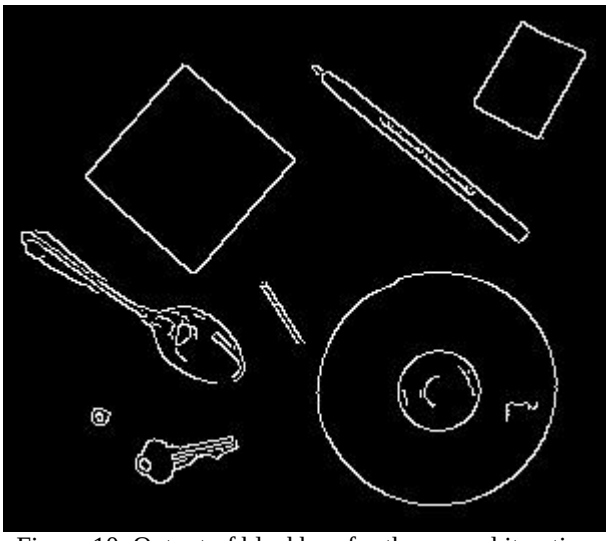

Figure 10. Output of blackbox for the second iteration

Iteration 3

Table 11. Third iteration for IP problem solution

	3	Correctness	Execution Time (ms)	Code Size (bytes)	Time Complexity
IP	ChatGPT	Success	34	66776	O(n)
	Gemini	Success	27	75600	O(n)
	Copilot	Success	29	66864	O(n)
	Blackbox	Success	27	66504	O(n)

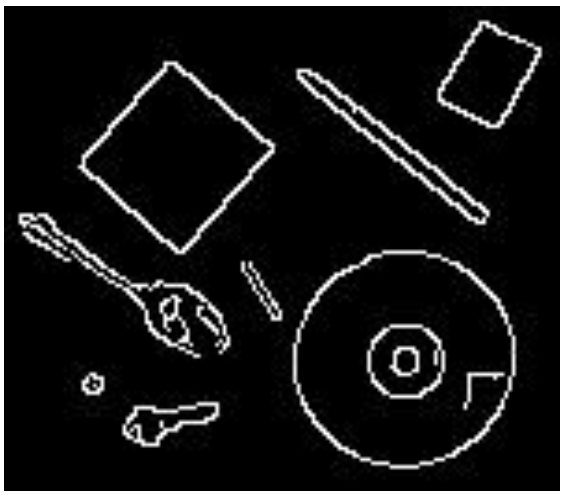

Figure 11. Output of chatGPT for the third iteration

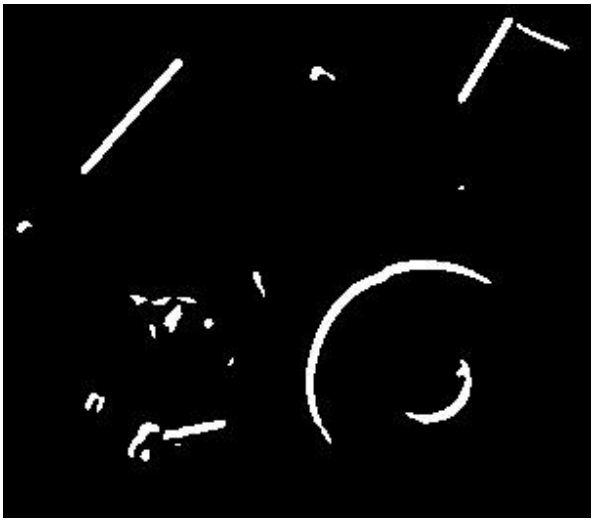

Figure 12. Output of gemini for the third iteration

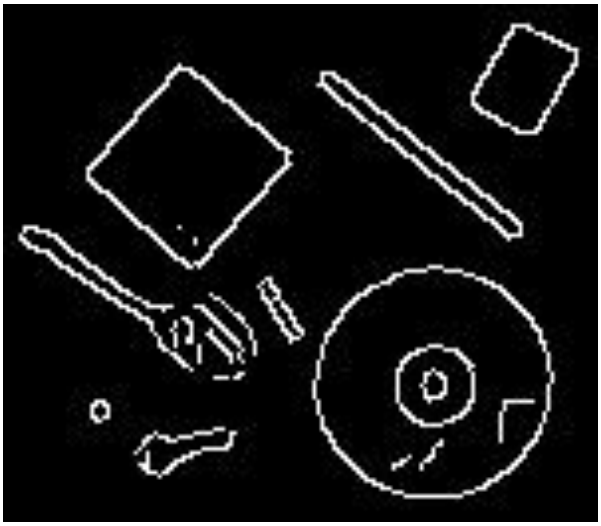

Figure 13. Output of copilot for the third iteration

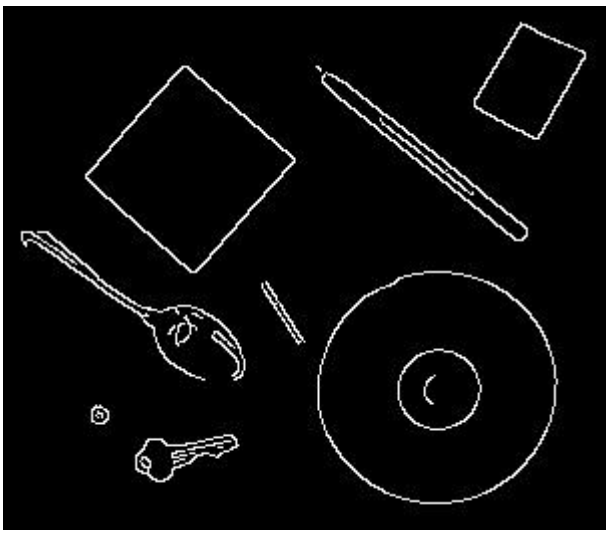

Figure 14. Output of blackbox for the third iteration

In the third round of this problem, both ChatGPT and Gemini managed to resolve the compilation errors from the previous round. The edge detection output produced by ChatGPT, which produces an output with similar values to the first round, is given in Figure 11. Gemini, on the other hand, shortened the execution time

considerably but created a significant growth in size. The output produced is given in Figure 12. Both the shortest execution time and the smallest size were produced by Blackbox and their output is shown in Figure 14. Copilot managed to change the code in this iteration and detected an edge as in Figure 13. According to the outputs given in Figure 11, Figure 12, Figure 13, and Figure 14, ChatGPT and Copilot outputs were reduced in size. Blackbox has developed a very successful edge detection algorithm. ChatGPT and Copilot produced an average level of output, but in the application produced with the code answered by Gemini, the edge detection algorithm worked very poorly and no object could be distinguished.

Iteration 4

Table 12. Fourth iteration for IP problem solution

	4	Correctness	Execution Time (ms)	Code Size (bytes)	Time Complexity
IP	ChatGPT	Success	27	121152	O(n)
	Gemini	Compile Error	Undeclared built-in functions & variables.		
	Copilot	Success	29	66864	O(n)
	Blackbox	Incorrect Result	Segmentation fault.		

Gemini, which produced a very bad output in the previous iteration, used built-in functions in this last round, but these caused a compilation error. Blackbox, which produced a very good output in the previous round, produces an output that can be compiled, but this output cannot detect an edge due to the segmentation fault.

On the other hand, ChatGPT and Copilot have managed to write codes that produce an output. However, since Copilot produced the exact same code as in the previous iteration, the output in Figure 13 was also generated in the last round. The code in ChatGPT's response has almost doubled in size compared to its last version and produces a result like Figure 15.

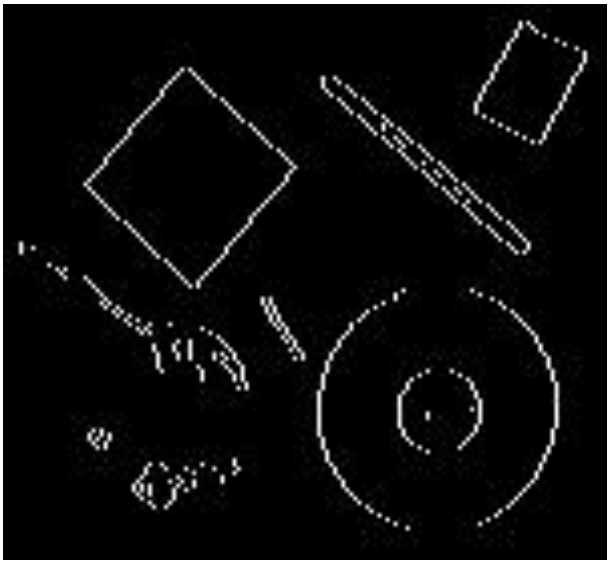

Figure 15. Output of ChatGPT for the fourth iteration

As seen in the ChatGPT output shown in Figure 15, the edge detection algorithm has a very poor performance. The edges of some objects could be transferred as cut-off, some objects became unidentifiable. Therefore, performance improvement efforts did not yield positive results.

Conclusion

In conclusion, this study has undertaken a comprehensive comparative analysis of four prominent AI platforms—ChatGPT, Gemini, Microsoft Copilot, and Blackbox—within the context of addressing key challenges in computer science, encompassing natural language processing (NLP), image processing, and cybersecurity. Through meticulous evaluation and benchmarking, this research aimed to provide valuable insights into the performance, capabilities, and limitations of each platform in generating solutions for multifaceted problems.

To summarize the results of the platforms, Copilot shows the poorest performance as a code developer. There have been many cases where he repeated the previous answer multiple times when he encountered an error or when performance improvement was requested. In this case, if there is an error, it can complete 4 iterations without any solution, just like in cybersecurity. Blackbox AI, on the other hand, can analyze and solve compilation errors caused by it very well. In no case has it produced code with compilation errors twice in a row and it is the best of all in terms of time complexity. It demonstrated a performance similar to Gemini in terms of code generation capability. Although Gemini, like Blackbox, successfully produces solutions to compilation errors, one of Gemini's shortcomings is that the compiled projects do not give correct outputs. Executable also produces more inefficient outputs than other platforms in terms of size. Finally, ChatGPT gave the best results among these AI platforms. What distinguishes it from others is that it produces a significant number of code outputs that work correctly and does not produce any output that gives incorrect results. Although it caused as many compilation errors as other platforms, it managed to solve them in the next iteration.

Throughout the iterative optimization process, each platform's performance was systematically evaluated and refined, highlighting the iterative evolution of AI-driven solutions and their adaptability to optimization efforts. Furthermore, the evaluation metrics employed—accuracy, execution time, executable size, and time complexity—provided a comprehensive understanding of each platform's performance characteristics and comparative advantages.

By elucidating the relative strengths and limitations of each platform, this research aims to inform practitioners, researchers, and decision-makers in leveraging AI-driven solutions effectively and ethically. Moving forward, further research and development efforts are warranted to explore the evolving capabilities of AI platforms, address existing limitations, and foster innovation in AI-driven development practices.

Scientific Ethics Declaration

The authors declare that the scientific ethical and legal responsibility of this article published in EPSTEM journal belongs to the authors.

Acknowledgements or Notes

* This article was presented as an oral presentation at the International Conference on Basic Sciences, Engineering and Technology (www.icbaset.net) held in Alanya/Turkey on May 02-05, 2024.

* We would like to express our sincere gratitude to Software Architect Huseyin Karacali for his extraordinary mentorship and inspiring influence. We would also like to thank TTTech Auto Turkey for its invaluable assistance throughout the development stages of this project.

References

Becker, B. A., Denny, P., Finnie-Ansley, J., Luxton-Reilly, A., Prather, J., & Santos, E. A. (2023, March). Programming is hard-or at least it used to be: Educational opportunities and challenges of Aİ code generation. In *Proceedings of the 54th ACM Technical Symposium on Computer Science Education V, 1*, 500-506.

Blackbox. (n.d.). *Chat blackbox: AI code generation, code chat, code search*. Retrieved from https://www.blackbox.ai/

ChatGPT. (n.d.). *Chatgpt*. Retrieved from https://openai.com/chatgpt

Pichai, S., & Hassabis, D. (2023, December 6). *Introducing Gemini: Our largest and most capable AI model*. Retrieved from https://blog.google/technology/ai/google-gemini-ai/#sundar-note

Tech Insider Buzz. (2023, November 24). *Blackbox AI: Ai code assistant*. Retrieved from https://techinsiderbuzz.com/blog/blackbox-ai-ai-code-assistant/

Waisberg, E., Ong, J., Masalkhi, M., Zaman, N., Sarker, P., Lee, A. G., & Tavakkoli, A. (2023). Google's AI chatbot "Bard": A side-by-side comparison with CHATGPT and its utilization in ophthalmology. *Eye*, *38*(4), 642–645

Wikimedia Foundation. (2024a, March 27). *Gemini.* Retrieved from https://tr.wikipedia.org/wiki/Gemini

Wikimedia Foundation. (2024a, March 31). *Chatgpt.* Retrieved from https://en.wikipedia.org/wiki/ChatGPT

Wikimedia Foundation. (2024c, April 6). *Microsoft copilot*. Retrieved from https://en.wikipedia.org/wiki/Microsoft_Copilot

Yetistiren, B., Ozsoy, I., Ayerdem, M., & Tuzun, E. (2023a, October 22). Evaluating the code quality of AI-Assisted Code Generation Tools: An empirical study on github copilot, Amazon codewhisperer and Chatgpt. *Arxiv*, *1*,1078.

Author Information

Huseyin Karacali
TTTech Auto Turkey,
Türkiye

Efecan Cebel
TTTech Auto Turkey,
Türkiye
Contact e-mail: e*fecan.cebel@tttech-auto.com*

Nevzat Donum
TTTech Auto Turkey,
Türkiye

To cite this article:

Karacali, H., Cebel, E., & Donum, N. (2024). Performance comparison of AI platforms in solving computer science problems. *The Eurasia Proceedings of Science, Technology, Engineering & Mathematics (EPSTEM), 28,* 326-341.

The Eurasia Proceedings of Science, Technology, Engineering & Mathematics (EPSTEM)
ISSN: 2602-3199

The Eurasia Proceedings of Science, Technology, Engineering & Mathematics (EPSTEM), 2024

Volume 28, Pages 342-351

ICBASET 2024: International Conference on Basic Sciences, Engineering and Technology

PMSM Design for Elevators: Determination of the Basic Topology Affecting Performance

Yusuf Avsar
Trakya University

Mucahit Soyaslan
Sakarya University of Applied Sciences

Ahmet Fenercioglu
Bursa Technical University

Abstract: In recent years, with the increase in high-rise building construction, there has been a rise in demand for elevators. This demand has spurred mutual growth between the vertical transportation sector and high-rise building construction. Both sectors are improving technology, security, and comfort standards. Traditional elevator traction machines typically employ asynchronous motors coupled with geared reducers, despite their low energy efficiency and requirement for large machine rooms. However, with the proliferation of rare-earth magnet materials and advancements in driver technologies, the use of Permanent Magnet Synchronous Motors (PMSMs) in elevator traction machines has increased. PMSMs operate with direct drive, eliminating the need for reducers. High efficiency and passenger comfort are crucial parameters for elevator traction machines. This study focuses on identifying the fundamental topology that could influence the performance of PMSMs for gearless elevator machines. Factors such as stator materials, rotor structures, permanent magnets, winding configurations, slot/pole combinations, cogging torque and torque ripple have been examined to select suitable design topologies for elevator motors. Important topics such as the magnetic properties of grain-oriented silicon steel sheets used in stator construction, B-H curves, lamination forming and stacking factors have been addressed. Two different rotor topologies and magnet arrangements, namely internal and external, have been investigated in PMSM designs. Additionally, the use of four different magnet materials, namely AlNiCo, Ferrite, NdFeB, and SmCo have been compared for PMSM traction motors in elevators. Single-layer and double-layer winding configurations, distributed and concentrated winding configurations have been compared. Fractional slot/pole combinations, which directly affect the performance and comfort of PMSMs, have also been examined based on information obtained from the literature. Particularly, structures with high winding factors, such as 12/10, 12/14, 18/16, 18/20, 24/22, and 24/26 have been identified. Finally, studies on skewing to reduce cogging torque and torque ripple have been addressed.

Keywords: Permanent magnet synchronous motor, Elevator traction machines, Gearless machine, Topology, Permanent magnet

Introduction

Synchronous motors are electric motors where a magnetic synchronization is established between the stator and rotor. PMSMs emerged by replacing rotor windings found in synchronous motors with permanent magnets (PM). PMSMs generally offer higher efficiency because the magnetic field of permanent magnets results in lower iron losses and enables them to convert energy more efficiently. Additionally, in synchronous motors, there are rotor winding losses occurring in the rotor.

PM motors are often preferred in low-speed and high-torque applications (Pyrhonen et al., 2013). When elevator traction systems are examined, it is observed that PM motors are used without the need for a reducer system. Due to the low energy density of AlNiCo (Aluminum Nickel Cobalt) magnets, the initial PM motors were limited to small-sized and low-powered applications. However, recent advancements in rare earth elements and power electronics have provided new opportunities for PM motor design, manufacturing, and implementation. Large powerful PM motors can be used with both low-speed and high-speed drivers. (Gieras, 2010).

PM motors are widely preferred in the industry for elevator traction systems due to their advantages such as silent operation, high efficiency, long working life, high torque per unit volume, and high torque-speed characteristic (Soyaslan, 2020).

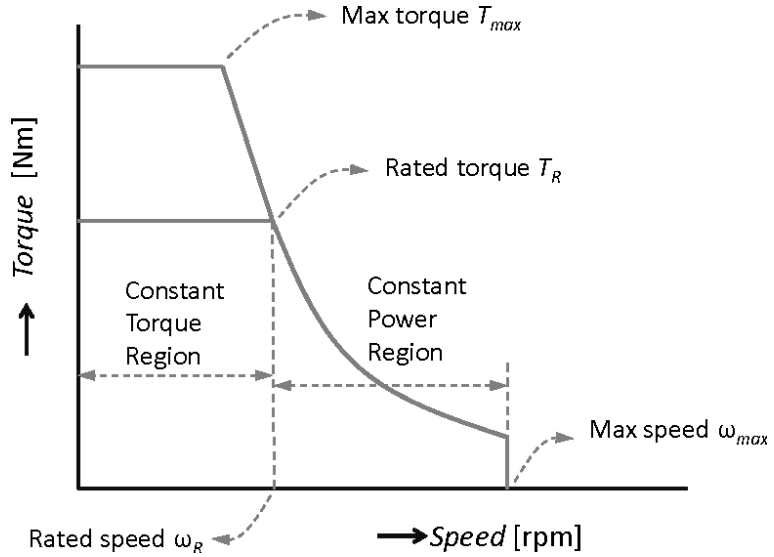

Figure 1. Torque-speed characteristic of PMSMs (Aydın, 2012)

Stator Design

PMSMs consist of the stationary part where the stator windings are wound. This part is formed by stacking and pressing silicon-coated steel sheets. Coating the steel sheets with silicon ensures insulation between the sheets. This minimizes eddy currents during operation and maximizes the magnetic properties of the sheets (Yıldız, 2009). The magnetic properties of grain-oriented silicon steel sheets are shown in Table 1.

Table 1. Magnetic properties of non-grain-oriented silicon steel sheets (Soyaslan, 2020)

Material	Sheet Thickness	Maximum Specific Total Loss at 50 Hz		Density
		Ĵ=1.5T W/kg	1.0T* W/kg	kg/dm3
M310-50A	0.50	3.10	1.25	7.65
M330-50A	0.50	3.30	1.35	7.65
M350-50A	0.50	3.50	1.50	7.65
M400-50A	0.50	4.00	1.70	7.70
M470-50A	0.50	4.70	2.00	7.70
M470-50HP	0.50	4.70	2.20	7.70
M530-50A	0.50	5.30	2.30	7.70
M530-50HP	0.50	5.30	2.30	7.80
M600-50A	0.50	6.00	2.60	7.75
M700-50A	0.50	7.00	3.00	7.80
M800-50A	0.50	8.00	3.60	7.80

The B-H curve, which expresses the relationship between magnetic field strength and flux density, defines the magnetic properties of a magnetic material. The portion of the curve following the knee region is called the saturation region. In the saturation region, increases in magnetic field strength result in only small increases in flux density. Therefore, the optimal operating point for motors is in the knee region of the B-H curve. That is, beyond the magnetic material's saturation point, the effect of flux density on performance decreases. Hence,

motors are typically operated just below the saturation point to ensure efficient utilization of the magnetic material.

For prototype manufacturing of radial flux motors, silicon steel sheets are usually produced using cutting methods such as laser cut and wire erosion (Bayraktar, 2015). The cut sheets are stacked together with the aid of a mould and pressed with varnishing in between them. This process forms the stator lamination. The varnishing process helps in providing sound insulation between the stator sheets. During the cutting process, burrs and gaps between the sheets due to varnishing result in a usable stack length for the stator, defined as the stator stacking factor $\boldsymbol{k_{st}}$ generally ranges between (0.90-0.97) and is close to 1. Determining the value of $\boldsymbol{k_{st}}$ is important as it directly affects motor performance. The length of the pressed sheets determines the electromagnetic dimensions of the motor.

Rotor Design

The rotor is the moving part of a PMSM, consisting of laminations and magnets mounted on a shaft. The rotor typically contains a core made of pure iron or silicon steel sheets. Permanent magnets are arranged on this core to create a magnetic field in the air gap, with N-S poles facing each other. (Akar, 2010). These magnets provide the motor's magnetic field and interact with the current passing through the stator windings to drive the motor's rotation. The high energy levels and suitable sizes of permanent magnets positively impact motor performance. Some advantages of these magnets include increased induced electromotive force (EMF), reduced line current, decreased thermal load on the rotor and input power, increased power factor and maximum output power of the motor (Eker, 2017).

Today, the most commonly preferred structure for permanent magnet motors is the one where magnets are located on the surface of the rotor. Surface-mounted (SM) motors typically have magnets magnetized radially. Neodymium Iron Boron (NdFeB) rare earth magnets with low magnetic permeability (μr= 1-1.2) are commonly used, and due to the cylindrical structure of the rotor, it can be assumed that the synchronous inductances in the d and q axes are equal because there is no reluctance difference. This assumption aids in the design of surface-mounted magnet motors. The structure of the motor is both inexpensive and simple because magnets can be easily mounted on the rotor surface. Embedded magnet (EM) motors consist of permanent magnets located within slots (Salminen, 2004).

In PMSM designs, there are two different rotor topologies: internal and external. These have different structures based on the arrangement of magnets. In Figure 2, there are internal rotor SM or EM structures (Dianov et al., 2010). Figure 3 shows external rotor surface or embedded magnet structures. (Yao v et al., 2018).

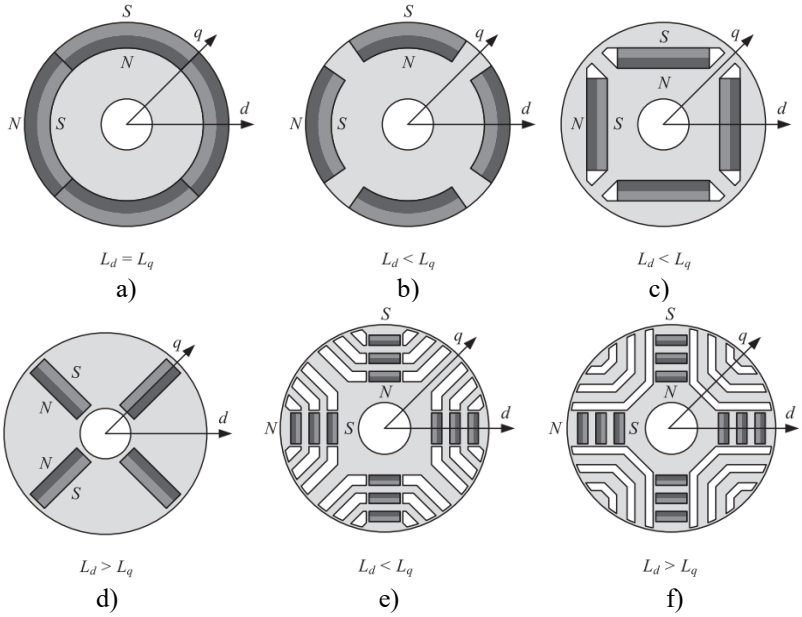

Figure 2. Internal rotor PMSM topologies: a) SM rotor, b) SM embedded rotor, c) EM rotor, d) Embedded radial magnet rotor, e) SM-supported synchronous reluctance, f) SM-supported synchronous reluctance (Dianov et al., 2022)

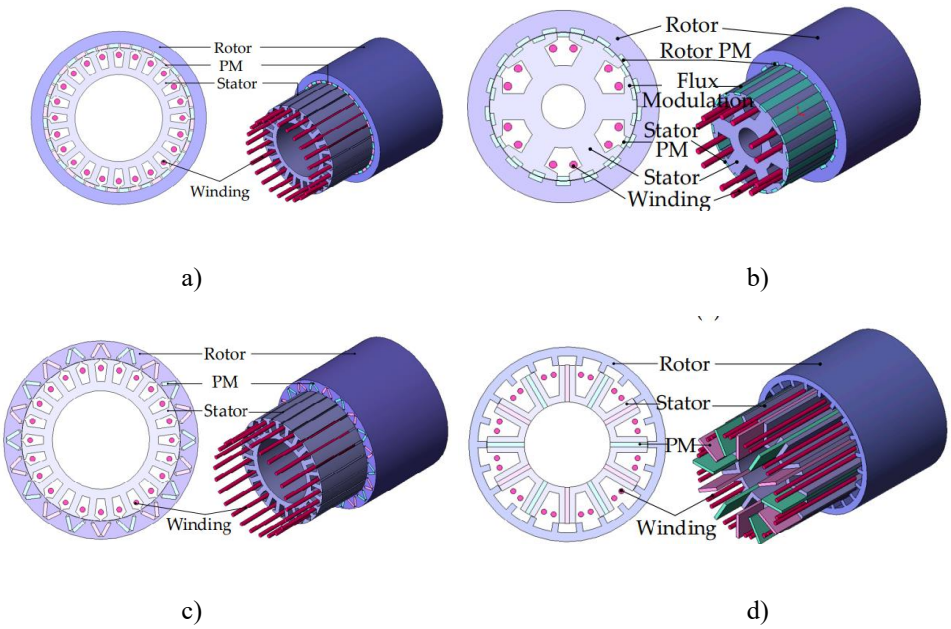

Figure 3. External rotor PMSM topologies: (a) SM rotor, (b) SM embedded rotor, (c) V-type EM rotor, (d) Embedded radial magnet rotor (Yao v et al., 2018)

Permanent Magnets Design

The first industrial artificial alloy magnets were AlNiCo magnets manufactured in the 1930s. Ferrite magnets emerged in the 1960s, followed by the development of Samarium Cobalt (SmCo) magnets in the 1970s. NdFeB magnets, developed in 1984, are the magnets with the highest energy density among industrial magnets (Ünsal, 2022). Classification of commercially used magnets is shown in Figure 4.

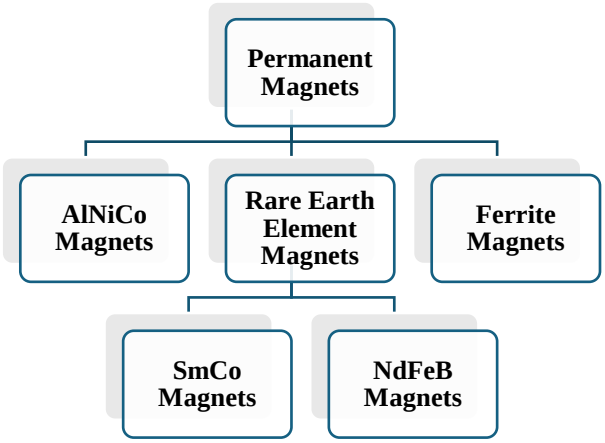

Figure 4. Classification of permanent magnets

Table 2. Properties of commercially used magnets (Eklund and Eriksson, 2019)

Magnet Type	Br [T]	Hci [kA/m]	BHmax [kJ/m3]	Tc [°C]
AlNiCo	0.55-1.37	38-151	10.7-83.6	900
Hard Ferrite	0.2-0.46	140-405	6.4-41.8	450
NdFeB	1.08-1.49	876-2710	220-430	300
SmCo	0.87-1.19	1350-2400	143-251	800

Table 2 presents the characteristics of commercially produced magnets at temperatures ranging from 20°C to

30°C. Parameters such as residual induction (Br), coercive force (Hci), maximum energy product (BHmax), and Curie temperature (Tc) are indicated (Eklund & Eriksson, 2019). When considering four different magnet materials AlNiCo, Ferrite, NdFeB, and SmCo for elevator PMSM traction motors:

AlNiCo: High temperature resistance and mechanical strength are provided, but it has a low energy product. It may be suitable for precision applications, but high performance is expected in elevators.

Ferrite: It is a low-cost option with a low energy product. It can be used in elevator motors, but it may lead to larger and heavier motors, reducing overall efficiency.

NdFeB: It offers a high energy product and excellent magnetic properties, resulting in high torque and efficient motors. Despite price fluctuations and temperature sensitivity, it provides the best performance for elevator traction motors and is widely used.

SmCo: Despite having a lower energy product than NdFeB, it offers high temperature resistance and thermal stability.

It could be a good option for elevator motors operating under high temperature conditions. The best option for PMSM traction motors used in elevators is NdFeB magnets, as they provide high torque and efficiency. However, for motors that need to operate under high temperature conditions, SmCo magnets can also be a suitable choice. AlNiCo and ferrite magnets are less preferred for elevator traction motors due to their lower energy products and suitability for specific applications. However, Yetis conducted a thesis study in 2017 achieving the design of an elevator traction motor with low torque ripple using ferrite magnets (Yetis, 2017).

Elevator Traction Systems with Surface-Mounted (SM) Interior PMSMs

Due to the rotor structures of PMSMs, they can be classified into two groups: surface-mounted and embedded magnet. When we look at the literature and examine elevator traction motors in the current industry, it is observed that SM motors are commonly used. Advantages of SM-PMSM according to elevator systems:

- Higher efficiency: SM motors provide high efficiency even at low speeds, contributing to reduced energy consumption and operating costs.
- Higher torque density: SM-PMSM has higher torque density compared to EM rotor structures. This allows for the use of smaller and lighter motors in elevator systems.
- Simpler cooling: Even at low speeds, SM motors provide more effective cooling. This enables the motor to have higher temperature tolerance and longer lifespan.
- Faster response time: SM motors offer faster dynamic response times. This allows for faster acceleration and deceleration of the elevator, thus increasing passenger comfort.

Disadvantages of SM-PMSM according to elevator systems:

- Fragile rotor structures: Placing the magnets on the outer surface of the rotor makes them more susceptible to mechanical damage. While this may cause fewer issues at low speeds, it can raise concerns about long-term reliability and durability.
- Lower maximum speed: Due to centrifugal forces in SM motors, their maximum speeds are lower compared to EM motors.

Windings Design

The number of stator slots, rotor poles, phase number, and winding number are related. Fractional slot/pole combinations are generally preferred to reduce torque ripple (Leu, 1992). In PMSMs, windings can be connected in either delta or star configurations, similar to induction motors (Yan, 2009). Delta connection is preferred for applications requiring low speed and low torque, whereas star connection is used for applications requiring low speed and high torque (Gambhir & Jha, 2013).

PMSMs can be single-phase or multi-phase depending on the application type. Single or multi-layer winding methods are used in windings. Single-layer windings have only one winding per stator slot and are typically used for simpler and less complex applications. While single-layer windings are easier to manufacture and

maintain, they generally offer lower efficiency and performance. Double-layer windings have two windings per stator slot and are used to provide higher performance and better magnetic field distribution. Single-layer winding structures have high self-inductance values, limiting short-circuit currents in the motor. Single-layer windings are preferred for constant torque variable speed applications (EL-Refaie, 2010). Figure 5 shows single and double-layer winding structures.

a) b)

Figure 5. Concentrated winding types; a) Single-layer winding b) Double-layer winding (EL-Refaie, 2010)

When selecting slot-pole combinations, the winding type is considered an important constraint factor. A slot-pole combination that allows for the use of concentrated windings is preferred. The main reasons for using concentrated windings over distributed windings are to increase motor efficiency and facilitate production. In motors designed with concentrated windings, the torque per unit volume is high, and the fluctuation of output torque is low. Since the coil end lengths in concentrated windings are shorter than those in distributed windings, the amount of winding placed in the slots decreases. Shortening conductor lengths reduces resistance and copper losses, allowing for increased motor efficiency (Guneri, 2015). Figure 6 depicts single and double-layer, distributed and concentrated winding types.

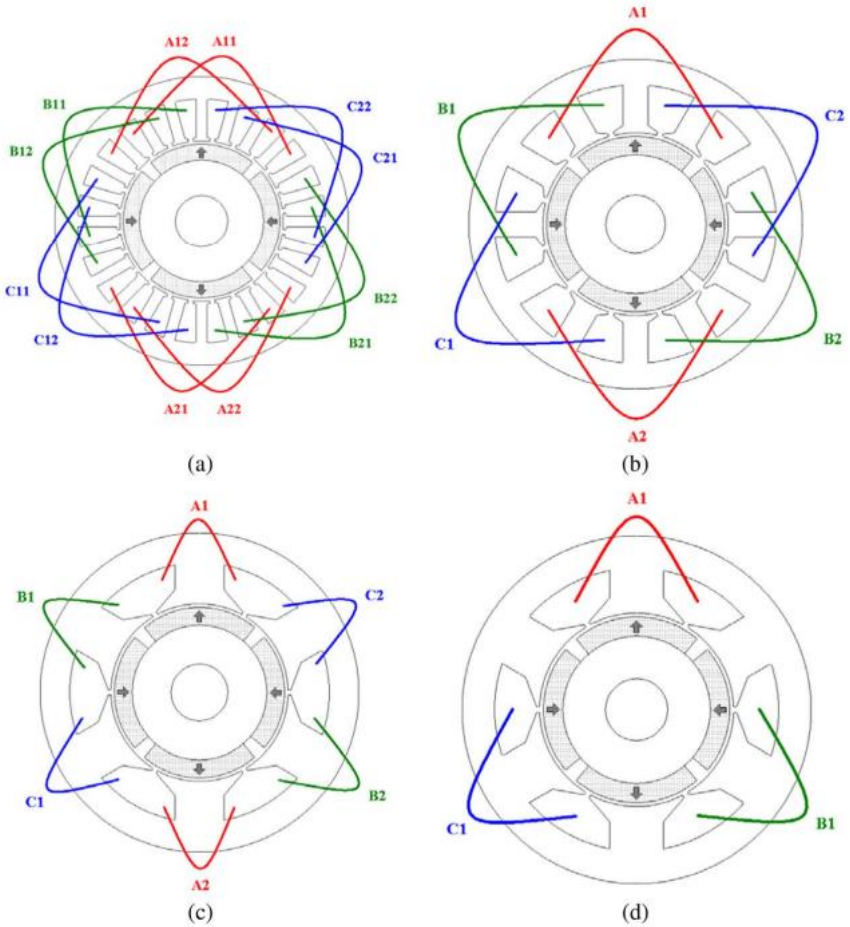

Figure 6. Winding types: a) Distributed double-layer winding b) Distributed single-layer winding c) Concentrated double-layer winding d) Concentrated single-layer winding (EL-Refaie, 2010)

Determining the Slot/Pole Combination

In PMSMs, the slot/pole combination is an important design parameter. This combination refers to the number of stator slots and the number of magnetic poles on the rotor. Choosing the correct slot/pole combination improves the voltage and current waveforms of the motor, reduces harmonics, and enhances the efficiency and performance of the motor.

The slot/pole combination is fundamental in determining the winding factor. A high winding factor is a parameter that directly affects the efficiency and performance of the motor. The correct selection of the slot/pole combination increases the motor's efficiency by reducing iron losses and the impact of high-frequency harmonics. A properly chosen slot/pole combination allows for more compact and lighter designs by reducing the motor's size and weight (Güuneri, 2015; Tanc, 2014; Wang et al., 2008).

When we examined slot-pole combinations, we have found many suitable configurations. To determine the correct configuration, the number of slots per pole per phase (q) must be established. Equation 1 expresses the number of slots per pole per phase. It is expressed in the Equation 1, number of slots N_{slot}, number of poles N_p and number of phases n_f (Tanç, 2014).

$$q = \frac{N_{slot}}{N_p \cdot n_f} \tag{1}$$

If the q value is less than 1, the motor is referred to as a fractional slot winding motor. To achieve optimal flux distribution and torque density, number of slots and poles are kept close together (Avsar et al., 2024; Wang et al., 2008). Table 3 shows the winding factor values for slot/pole combinations based on double-layer winding type.

Table 3. Double-layer slot/pole combinations winding factor (k_w) table (Meier, 2008)

$N_{slot}\backslash N_p$	4	6	8	10	12	14	16	18	20	22	24	26	28	30	32	34	36	38
6	0,866		0,866				0,866		0,866				0,866		0,866			
9		0,866	0,945	0,945	0,866						0,866	0,945	0,945	0,866				
12	q=1		0,866	0,933		0,933	0,866								0,866	0,933		0,933
15				0,866		0,951	0,951		0,866									
18		q=1			0,866	0,902	0,945		0,945	0,902	0,866							
21						0,866	0,87		0,953	0,953		0,89	0,866					
24			q=1				0,866		0,933	0,95		0,95	0,933		0,866	0,76		
27								0,866	0,877	0,915	0,945	0,954	0,954	0,945	0,915	0,877	0,866	
30				q=1					0,866	0,874		0,936	0,951		0,951	0,936		0,874
33										0,866		0,903	0,928		0,954	0,954		0,928
36					q=1						0,866	0,867	0,902	0,933	0,945	0,953		0,953
39												0,866	0,863		0,918	0,936		0,954
42				q > 1		q=1							0,866		0,89	0,913		0,945
45														0,866	0,859	0,886		0,927
48							q=1								0,866	0,857		0,905
51																0,866		0,88
54								q=1									0,866	
57																		0,866
60									q=1									

Inappropriate combinations of design | k_w< 0.866

Equation 2 represents combinations where the number of slots is two less or two more than the number of poles, resulting in machines with high flux distributions and high torque densities (Soyaslan et al., 2023; J. Wang et al., 2008).

$$N_{slot} = N_p \pm 2 \tag{2}$$

Compared to motors with single-layer winding structures, motors with double-layer winding structures have higher iron losses and longer winding heads. The use of double-layer windings in motors contributes to reducing eddy current losses, torque ripples, and space harmonic components between the EMF (EL-Refaie, 2010).

Cogging Torque and Torque Ripple

Elevator cabin comfort is one of the most crucial parameters during travel. Vibration and noise occurring in the elevator machine greatly affect this comfort. Therefore, minimizing these vibrations and noises in elevator machine design is essential. One of the significant contributors to vibration and noise during cabin travel is cogging torque and torque ripple (Soyaslan et al., 2019). Achieving high-quality and smooth output torque is essential to minimize cogging torque and torque ripple. There are various methods to reduce cogging torque and torque ripple. Through design studies, selecting appropriate slot/pole combinations and optimizing stator and rotor geometry can effectively reduce cogging torque and torque ripple.

Application of skewing is performed during the design stage of the motor. Providing skewing along the axial direction of the stator teeth or rotor magnets reduces the effect of harmonics in the motor's magnetic circuit and decreases torque ripples. The skew angle can be analytically determined in Equation 3-4 (Islam et al., 2009). Here, θ_{skew} refers to the skew angle, N_{period} refers to cogging per period, N_p refers to number of poles and N_{slot} refers to number of slot. The greatest common divisor of N_p and N_{slot} is expressed as $GCD(N_p,\ N_{slot})$. Figure 3 illustrates the step skew of the magnets on the rotor. Table 4 shows the optimum skew angle according to slot/pole combinations.

$$\theta_{skew} = \frac{360}{N_{slot}N_{period}} \tag{3}$$

$$N_{period} = \frac{Np}{GCD(N_p,N_{slot})} \tag{4}$$

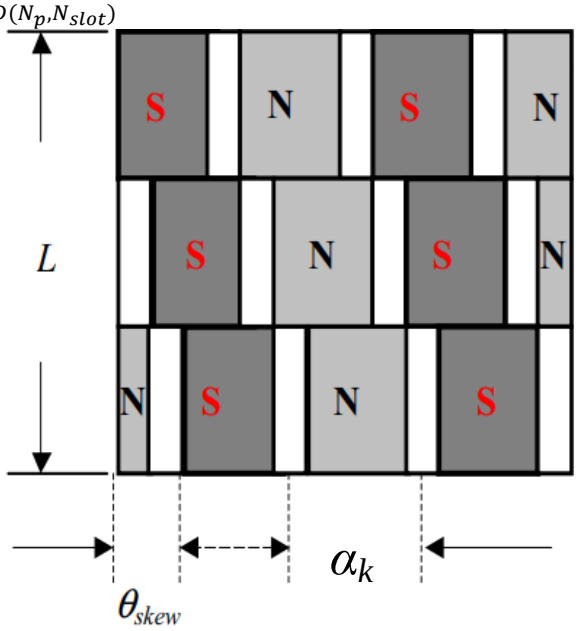

Figure 7. Three-step skew arrangement (Islam et al., 2008)

Table 4. Optimal skew angle according to slot/pole combinations

Number of slot (N_{slot})	12	12	18	18	24	24
Number of pole (N_p)	10	14	16	20	22	26
Cogging period (N_{period})	5	7	8	10	11	13
Optimal skew angle (θ_{skew})	6°	4.28°	0.44°	2°	1.36°	1.15°

Conclusion

Important topics such as the magnetic properties of grain-oriented silicon steel sheets used in stator construction, B-H curves, lamination forming, and stacking factors have been addressed. Two different rotor topologies and magnet arrangements, namely internal and external, have been investigated in PMSM designs. Additionally, the use of four different magnet materials, namely AlNiCo, Ferrite, NdFeB, and SmCo, has been compared for PMSM traction motors in elevators. Single-layer and double-layer winding configurations, distributed and concentrated winding configurations, have been compared. Fractional slot/pole combinations, which directly affect the performance and comfort of PMSMs, have also been examined based on information obtained from the literature. Particularly, structures with high winding factors, such as 12/10, 12/14, 18/16, 18/20, 24/22, and 24/26, have been identified. Finally, studies on skewing to reduce cogging torque and torque ripple have been

addressed.

Scientific Ethics Declaration

The authors declare that the scientific ethical and legal responsibility of this article published in EPSTEM journal belongs to the authors.

Acknowledgements or Notes

* This article was presented as a oral presentation at the International Conference on Basic Sciences, Engineering and Technology (www.icbaset.net) held in Alanya/Turkey on May 02-05, 2024.

References

Akar, M., Taskın, S., Seker, S. S., & Cankaya, I. (2010). Detection of static eccentricity for permanent magnet synchronous motors using the coherence analysis. *Turkish Journal of Electrical Engineering and Computer Sciences*, *18*(6), 963-975.

Avsar, Y., Fenercioglu, A., & Soyaslan, M. (2024), Design optimization of pm synchronous motor: rail mounted belt drive elevator systems. *IEEE Transactions on Industry Applications*, *60*(1), 301-311.

Aydin, M. (2012). Brushless permanent magnet servomotors. In *Serial and parallel robot manipulators-kinematics, dynamics, control and optimization*. IntechOpen.

Bayraktar, S. (2015). *The effect of silicon steel sheets produced by different cutting methods on the performance of electrical machines*. (Gazi University). Retrieved from https://avesis.gazi.edu.tr/yonetilen-tez/62996648-6907-4204-b65b-761d8e95164f/farkli-kesme-yontemleri-ile-uretilen-silisli-sac-paketlerinin-elektrik-makinalarinin-performansi-uzerine-etkisi

Dianov, A., Tinazzi, F., Calligaro, S., & Bolognani, S. (2022). Review and classification of MTPA control algorithms for synchronous motors. *IEEE Transactions on Power Electronics*, *37*(4), 3990–4007.

Eker, M. (2017). *Design of grid-connected axial flux permanent magnet synchronous motor*.(Doctoral dissertation, Tokat Gaziosmanpasa University).

Eklund, P., & Eriksson, S. (2019). The influence of permanent magnet material properties on generator rotor design. *Energies*, *12*(7), 1314.

EL-Refaie, A. M. (2010). Fractional-slot concentrated-windings synchronous permanent magnet machines: opportunities and challenges. *IEEE Transactions on Industrial Electronics*, *57*(1), 107–121.

Gambhir, R., & Jha, A. K. (2013). Brushless dc motor: construction and applications. *The International Journal of Engineering and Science*, *2*(5), 72–79.

Gieras, J. F. (2009). *Permanent magnet motor technology: design and applications*. CRC press.

Guneri, S. (2015). *Design of permanent magnet synchronous motor for compressor applications* (Istanbul Technical University). Retrieved from http://hdl.handle.net/11527/1316

Islam, R., Husain, I., Fardoun, A., & McLaughlin, K. (2009). Permanent-magnet synchronous motor magnet designs with skewing for torque ripple and cogging torque reduction. *IEEE Transactions on Industry Applications*, *45*(1), 152–160.

Leu, M. C. (1992). A complete model characterization of brushless dc motors. *IEEE Transactions on Industry Applications*, *28*(1), 172–180.

Meier, F. (2008). *Permanent-magnet synchronous machines with non-overlapping concentrated windings for low-speed direct-drive applications* (Doctoral dissertation, Royal Institue of Technology). Retireved from https://www.diva-portal.org/smash/get/diva2:332/FULLTEXT01.pdf

Salminen, P. (2004). *Fractional slot permanent magnet synchronous motors for low-speed applications* (Doctoral dissertation, Acta University).

Soyaslan, M., Avsar, Y., Fenercioglu, A., & Eldogan, O. (2019). Cogging torque reduction in external rotor pm synchronous motors by optimum pole embrace. In *2019 3rd International Symposium on Multidisciplinary Studies and Innovative Technologies (ISMSIT)* (pp. 1-4). IEEE.

Soyaslan, M. (2020). *Design of an external rotor permanent magnet synchronous motor for elevator traction systems*, (Doctoral dissertation). Retrieved from http://acikerisim.subu.edu.tr/xmlui/handle/20.500.14002/1026

Soyaslan, M., Eldogan, O., Fenercioglu, A., & Avsar, Y. (2023). External rotor gearless elevator machine: a new design with flanged shaft. *Multiscale and Multidisciplinary Modeling, Experiments and Design*, 1-11.

Tanç, G. (2014). *Design and manufacturing of brushless dc motor for electric bicycles* (Istanbul Technical University). Retrieved from http://hdl.handle.net/11527/13192

Unsal, S., & Alıskan, I. (2018). Speed control of permanent magnet synchronous motor with intuitive-based fuzzy logic controllers. *Pamukkale University Journal of Engineering Sciences, 24*(2), 185-191.

Wang, J., Atallah, K., Zhu, Z. Q., & Howe, D. (2008). Modular three-phase permanent-magnet brushless machines for in-wheel applications. *IEEE Transactions on Vehicular Technology, 57*(5), 2714–2720.

Yan, G. (2009). *Analysis of brushless dc motors and design of driver circuits*. Marmara University.

Yao, Y., Liu, C., & Lee, C. H. T. (2018). Quantitative comparisons of six-phase outer-rotor permanent-magnet brushless machines for electric vehicles. *Energies, 11*(8), 2141.

Yıldız, T. (2009). *Modeling and control of brushless dc motors (*Master's thesis). Sakarya University.

Yetis, H. (2017). *Design of embedded permanent magnet synchronous machine with ferrite magnets for gearless elevator systems.* (Yıldız Technical University). Retrieved from https://tez.yok.gov.tr/UlusalTezMerkezi/tezDetay.jsp?id

Author Information

Yusuf Avsar
Trakya University
Ipsala Vocational School, 22030, Edirne, Turkiye
Contact e-mail: *yusufavsar@trakya.edu.tr*

Mucahit Soyaslan
Sakarya University of Applied Sciences
Faculty of Technology, 54050, Sakarya, Turkiye

Ahmet Fenercioglu
Bursa Technical University
Faculty of Eng. and Natural Sciences, 16310, Bursa Turkiye

To cite this article:

Avsar, Y., Soyaslan, M. & Fenercioglu, A. (2024). PMSM design for elevators: Determination of the basic topology affecting performance. *The Eurasia Proceedings of Science, Technology, Engineering & Mathematics (EPSTEM), 28,* 342-351.

The Eurasia Proceedings of Science, Technology, Engineering & Mathematics (EPSTEM)
ISSN: 2602-3199

The Eurasia Proceedings of Science, Technology, Engineering & Mathematics (EPSTEM), 2024

Volume 28, Pages 352-359

ICBASET 2024: International Conference on Basic Sciences, Engineering and Technology

Analysis of a High-Pressure Reciprocating Compressor Piston's 2D Simulation Utilizing Computational Fluid Dynamics

Furkan Turgut
Logos Kimya Teknolojileri Ltd. Şti.

Ahmet Berkay Simsek
Middle East Technical University

Necip Berker Uner
Middle East Technical University

Bariş Erdogan
Logos Kimya Teknolojileri Ltd. Sti.

Abstract: Reciprocating compressors represent the most renowned and extensively utilized compressors within the positive displacement category. A compressor that takes input gas at pressures above atmospheric and delivers it very high pressures (> 100 bar) is specifically called a booster pump. These pumps commonly consist of two or more piston-cylinder units in series, connected through check valves that determine the final delivery pressure, and they are instrumental in a range of applications centered around the storage and delivery of gases and fuels. Despite the availability of various booster pumps in the global market, literature offers limited insights into their design specifics. The design intricacies of a booster pump, tailored to operate at specified output pressure and mass flow rate, are contingent upon the interplay of coupled flow dynamics and heat transfer phenomena within the system. These phenomena include fluid flow dynamics through check valves, heat transfer across cylinder walls, and mechanical properties of pump materials, alongside cyclic operational parameters. To address this gap, we have embarked on an experimental-computational investigation aimed at elucidating the transport processes occurring in a single-cylinder booster pump. This work focuses on computational investigations concerning gas compression and the actuation of check valves in a single-cylinder reciprocating booster. Momentum and energy conservation equations were solved on a dynamic mesh platform through Ansys Fluent. Adiabatic conditions were employed, and the numerical solver was partially validated by comparison with thermodynamic theory for simulations conducted in a closed adiabatic cylinder. Calculations were then extended for an open cylinder with inlet and outlet check valves. Simulations indicate that forced cooling plays an important role for the longevity of sealing parts.

Keywords: Compressors, Fluid dynamics, ANSYS Fluent, CFD

Introduction

Compressors display a rich collection of gas dynamics, where fluid flow, thermodynamics and heat transfer become coupled to each other and consequently determine the specifications of the device. The goal is to increase the pressure of a gas in a semi-continuous manner, which results in heating of the gas. The extent of heating is directly proportional to the increase in pressure and the rate of cooling in the compressor.

High temperature and pressure presents challenges in the design of compressors, especially in terms of materials selection. Therefore, fundamental compressor elements harbor specific design-limiting operational conditions.

In instances where limitations are encountered, the execution of work often necessitates an increase in the number of compression processes, a strategy termed multi-staging. This involves employing a core machine element designed to operate sequentially with other components of the machinery. (Bloch et al., 1996). Although the nature of these limitations' changes with respect to the compressor type, the major design parameters that are common to all compressors are listed graphically in Figure 1 below.

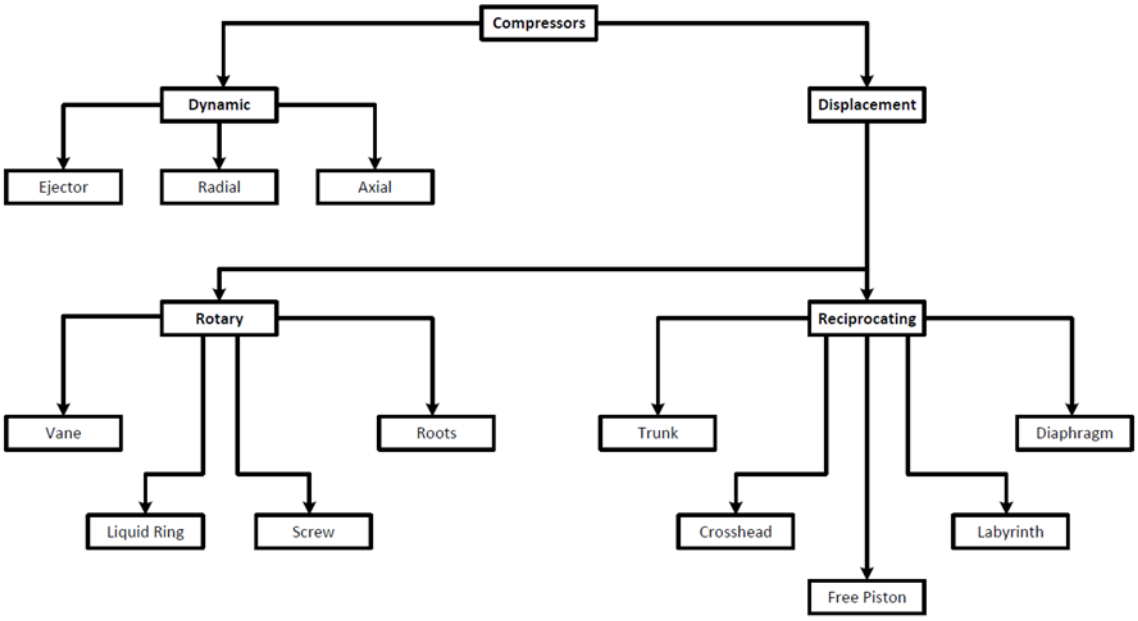

Figure 1. Primary types of compressors.

The primary types of compressors shown in Figure 1 are summarized below. Cam, diaphragm, and diffusion compressors are omitted due to their specialized applications and relatively compact sizes.

Dynamic Compressors: These rotary continuous-flow machines utilize a rapidly rotating element to accelerate gas, converting velocity head into pressure. This process occurs both in the rotating element and stationary diffusers or blades.

Centrifugal Compressors: Dynamic machines where one or more rotating impellers, typically shrouded on the sides, accelerate the gas. The main gas flow is radial.

Axial Compressors: Dynamic machines employing the bladed rotor's action for gas acceleration. Main gas flow is axial.

Positive Displacement Units: Positive displacement units confine successive gas volumes within a closed space and elevate them to a higher pressure.

Rotary Positive Displacement Compressors: These machines achieve compression and displacement through the positive action of rotating elements.

Sliding Vane Compressors: A subset of rotary positive displacement machines, sliding vane compressors feature axial vanes sliding radially in a rotor eccentrically mounted in a cylindrical casing. Gas trapped between vanes undergoes compression and displacement. (Duprez et al., 2007)

Liquid Piston Compressors: In these rotary positive displacement machines, water or another liquid serves as the piston to compress and displace the handled gas.

Two-Impeller Straight-Lobe Compressors: Rotary positive displacement machines with two straight mating lobed impellers that trap and convey gas from intake to discharge. Internal compression is absent.

Helical or Spiral Lobe Compressors: This category comprises rotary positive displacement machines where two intermeshing rotors, each with a helical form, compress and displace the gas.

Mixed Flow Compressors: Dynamic machines with an impeller form that combines characteristics of both centrifugal and axial types.

This classification summarized above sheds light on the diverse array of compressors, each tailored to specific applications and operational principles. (Roskosch et al., 2017) When considering compressor classifications, the reciprocating crosshead compressor is the model we aim to design for elevating a low-pressure gas to a high pressure. Its widespread preference in the market and our mechanical design expertise in this subject have been influential factors in selecting this compressor model.

In this study, the objective is to design a single-piston, high-pressure reciprocating crosshead compressor, which may also be referred to as a booster pump. In addition to the mechanical analyses currently being conducted, our group concentrates on investigating the flow system. This paper is a report of preliminary calculations done via computational fluid dynamics (CFD). Using the Ansys Fluent, dynamic simulations of closed piston compression were done, and calculations were verified against adiabatic compression calculations. Simulations were then extended to the case with flow, allowing adiabatic temperatures to be estimated.

Method

In the calculations presented below, fluid mechanics and heat transfer are interlinked, and the computational domain undergoes deformation throughout the compression process. In models where the computational domain changes during the simulation, the mesh structure also needs to evolve over time. It is crucial to test the accuracy of the results produced by such dynamic models with existing theory or experiments. Fortunately, thermodynamics offer a very simple description of reversible and adiabatic process, therefore Fluent simulations were initially focused on adiabatic compression in a closed cylinder.

Adiabatic compression is an isentropic process when reversible. Assuming a constant heat capacity ratio $\gamma = C_p/C_v$ for an ideal gas during compression, the following equations are valid for pressure and temperature in the cylinder, where subscript 1 denotes the state with a fully withdrawn piston and subscript 2 denotes a fully compressed chamber.

$$P_2 = P_1\left(\frac{V_1}{V_2}\right)^{\gamma}$$

$$T_2 = T_1\left(\frac{V_1}{V_2}\right)^{\gamma-1}$$

By solving the momentum and energy conservation equations in Fluent for compression of argon, and assuming argon to be an ideal gas with constant physical parameters (e.g., C_p, μ, etc.), the calculated values of P_2 and T_2 in adiabatic simulations are expected to equal to thermodynamic values provided above. The primary reason for this expectation is that the generation of entropy caused by piston friction is not included in the simulation. Therefore, a major source of irreversibility is removed, and thanks to slow compression speeds usually employed in booster pumps, the gas is expected to be at conditions close to thermodynamic equilibrium.

Table 1. Parameters used in ANSYS Fluent calculations.

Parameter	**Value**	**Unit**
Shaft Speed	72	rpm
Crank Diameter	19	mm
Crank Period	360	degree
Rod Lenght	70	mm
Cylinder Diameter	19.05	mm
Stroke	39	mm
Starting Temperature	300	K
Starting Pressure	40	bar

Compression calculations were performed for the given piston parameters to achieve a compression ratio, V_1/V_2, of 39. The calculations were conducted considering turbulent flow, employing both 2D and 3D models. The 3D

model results presented below are of preliminary status and will be further developed to encompass the entire process in the future. Parameters used in the simulations are given in Table 1.

Results and Discussion

For the closed cylinder, results for pressure and temperature are presented in the two figures below. Deviations in the trends of pressure and temperature during compression as shown in Figure 2, where the compression volume is reduced, indicate the need for the development of a better moving mesh infrastructure in both 2D and 3D models. The 2D model showed more consistent results with isentropic calculations compared to the 3D model. This is primarily attributed to the relatively homogeneous mesh structure that can be created in the 2D geometry. It is believed that the cylinder compression rate is sufficiently slow, thus the calculations follow the adiabatic curves at small compression ratios. The inability to approach the thermodynamic results indicated deficiencies in numerical calculations and mesh infrastructure, especially when the compression ratio became larger than 5.

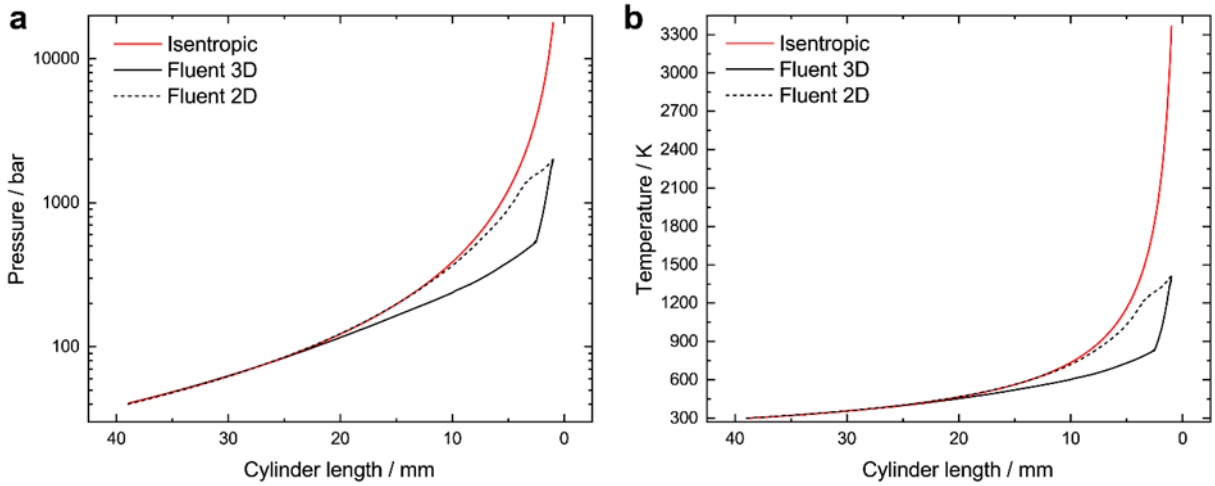

Figure 2. Preliminary calculations of compression within a closed and adiabatic cylinder for validation purposes. (a) pressure, (b) temperature. Both the 2D and 3D calculations suffered from insufficient meshing detail (see below).

The impact of mesh density on the results was investigated in the 2D model. The calculations revealed that increasing mesh density led to results approaching thermodynamic expectations. Achieving a close match to isentropic results was facilitated by a higher resolution in resolving the wall layer in the turbulence model, resolving pressure in tandem with velocity, and employing higher-order formulas in the finite volume discretization process. The outcomes of these calculations are presented below in Figure 3.

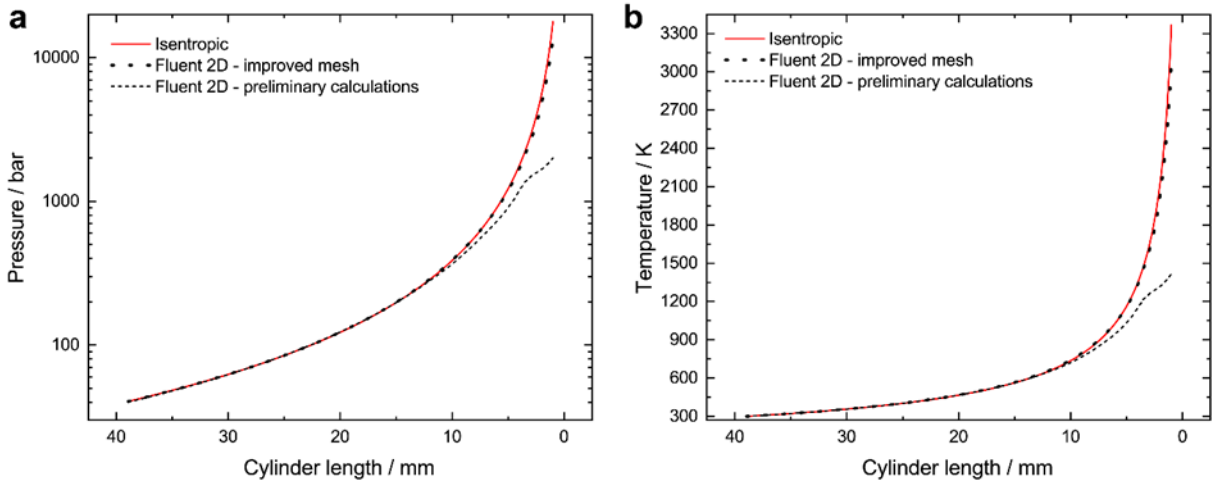

Figure 3. Two-dimensional calculations conducted for validation purposes within a closed and adiabatic cylinder.

The pressure and temperature within the closed and adiabatic cylinder during compression are depicted in Figure 3a and 3b respectively. Advanced calculations showcase the improvements in both the calculation and mesh infrastructure. Thus, a numerical calculation infrastructure that can either be transferred to a 3D model, used with inlet and outlet check valves, or with a second cylinder was established.

Due to the superior performance of 2D results compared to 3D, further model improvements was implemented on the 2D infrastructure. Utilizing the solver parameters that validated the thermodynamic results, the geometry of the piston was upgraded and an entry and exit region for argon was added. Gas flow characteristics was determined by check valves located at the inlet and outlet of the cylinder. The updated geometry is illustrated in the figure below.

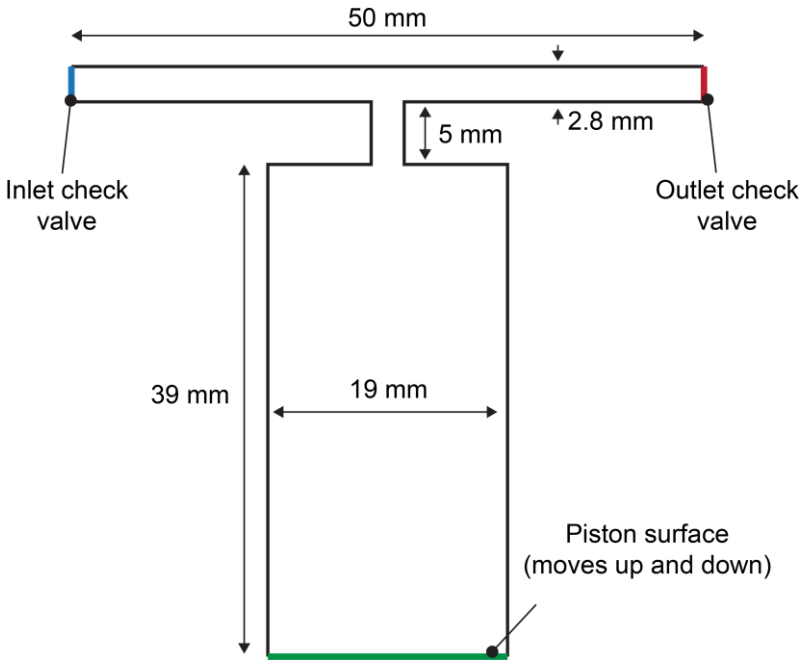

Figure 4. Updated cylinder geometry. The surfaces on the right and left sides of the structure correspond to the inlet and outlet of the check valve, respectively.

Gas flow through the check valves was added to the simulation by writing subroutines in Fluent (User Defined Function: UDF). The UDF algorithm dynamically integrates gas inlet or outlet calculations with cylinder movement and allows flow when the pressure difference across a check valve is reached. When the cracking pressure (1 bar) is exceeded, flow becomes unidirectional through the valve, whereas the valve closes when the differential pressure drops below the cracking pressure. The flow when the check valves are open is expressed by a general conductance equation:

$$\dot{m} = K\rho A_c \left(P_u - P_d \right)$$

Here, K denotes the flow conductance, and it was calculated assuming laminar flow in the cylindrical pipe-like flow geometry in the check valves. P_u and P_d represent the pressures upstream and downstream of the check valve, respectively, while ρ symbolizes the density of the argon gas upstream of the check valve, and A_c represents the cross-sectional area for flow through the check valve. K is calculated using the Hagen-Poiseuille equation, and A_c is initially calculated assuming the entire internal geometry of the check valve is a cylindrical pipe, then it was adjusted as a regression parameter based on the previous measurements conducted on the cylinder (LOGOS Kimya Teknolojileri Ltd. Sti., 2023.)

Computational results obtained for a full compression cycle is given in Figure 5, on which the compression of argon gas by the piston (1), the opening of the outlet valve (2), the retraction of the piston (3), and finally the opening of the inlet valve (4) are shown. It was observed that the volume change in both the pressure downstream of the inlet valve and the pressure upstream of the outlet valve is consistent and realistic, considering experiments previously conducted. It was observed that there was little to no pressure distribution inside the cylinder. In accordance with this result, pressures given in Figure 5 can be accepted to be valid for the entire geometry shown in Figure 4.

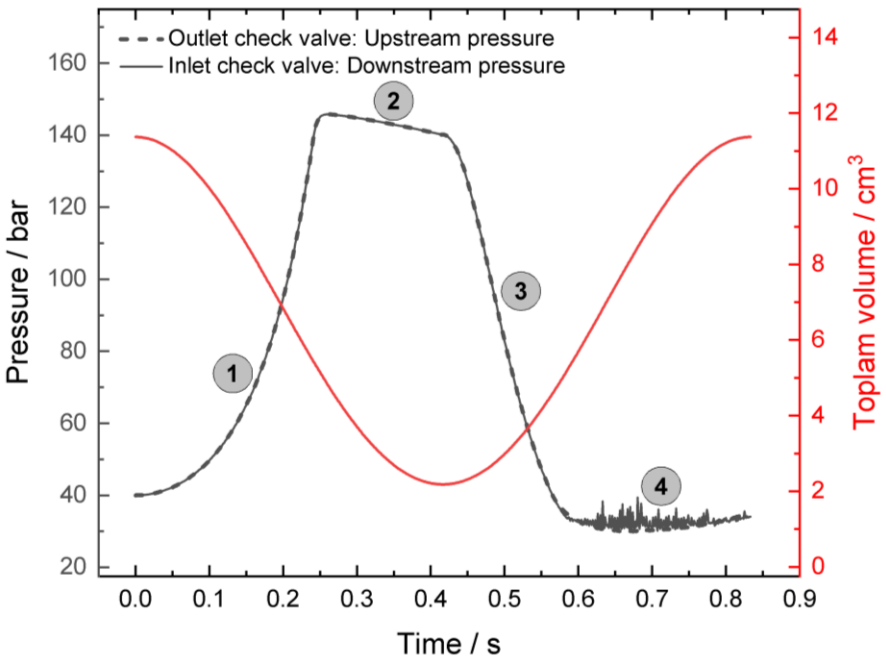

Figure 5. Pressure and volume versus time across the first compression cycle.

The initial pressure for this and the following two figures is 40 bars, the outlet pressure is 139 bars, and the cracking pressures of the check valves are 1 bar. In the calculations, the total volume of the tee pipes and the barrel is 11.4 cm³. The numbered stages are indicated in the text.

The fluctuation in inlet pressure following the opening of the inlet check valve is interpreted as numerical instability. In future calculations, this instability is aimed to be eliminated by taking the downstream pressure, P_d, in the conductance equation from a plane further away from the inlet surface instead of extracting it directly at the inlet surface. Since there is no pressure distribution inside the cylinder, this solution is expected to be valid. Figure 6 shows the mass flow rate during this cycle and similar fluctuations arising from the same reason are also observed. The inlet mass flow rate and outlet are noticeably different, which indicates that further cycles are required to reach a periodic steady-state.

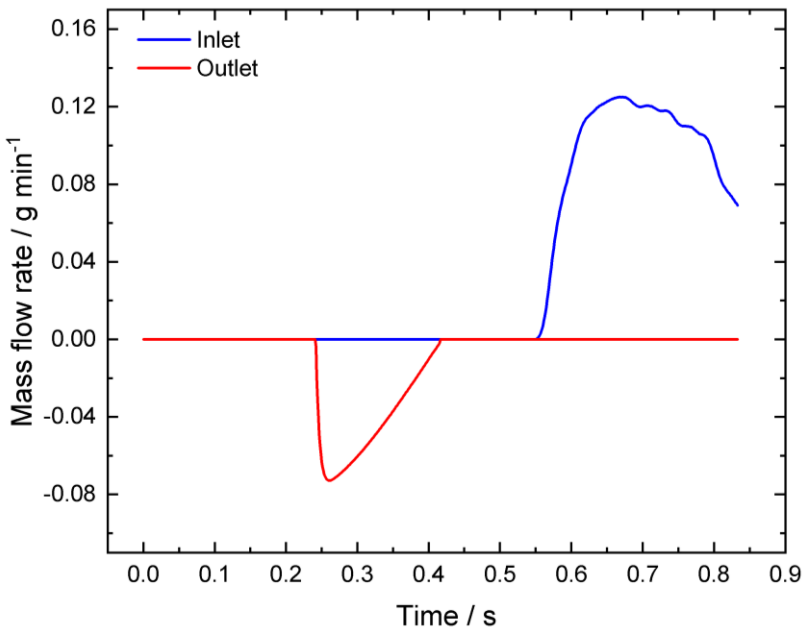

Figure 6. Mass flow versus time across the first compression cycle. During the period when the outlet valve is open (174 ms), the total amount of argon flowing is calculated as 0.12 mg. This corresponds to a rate of 8.67 g of argon per minute.

The temperature inside the barrel follows a similar trend to the pressure data except for the period that involves filling the cylinder with gas (Figure 7). Due to the adiabatic nature of the calculations and the assumption of an inlet gas temperature of 25°C as the boundary condition, cooling is observed nearby the gas inlet due to adiabatic expansion. Furthermore, temperatures exceeding 200 °C are observed due to adiabatic conditions. This observation indicates that cooling the cylinder will be important as most sealing materials, e.g. PTFE, have continuous service temperatures of approximately 200 °C.

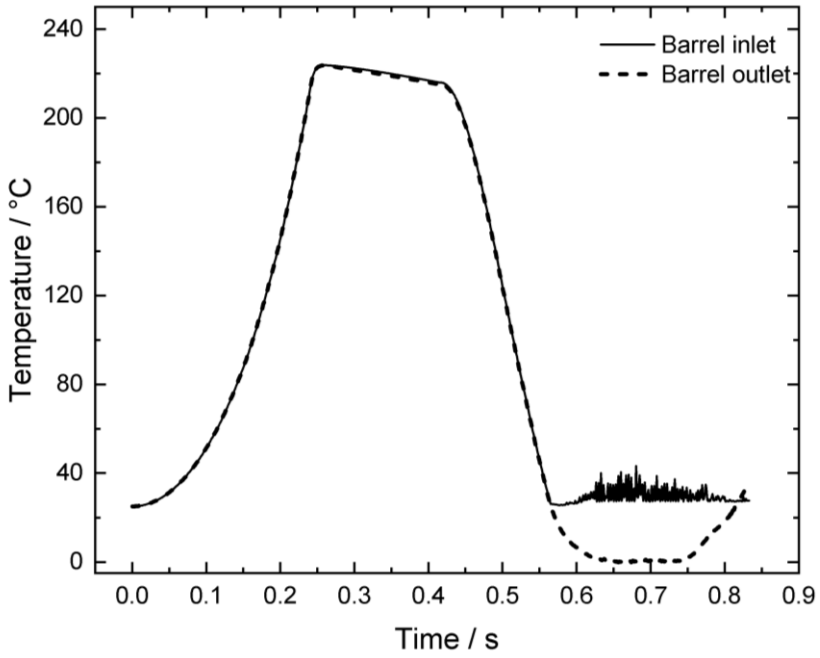

Figure 7. Temperature versus across the first compression cycle.

P-V diagram was seen to be similar to that of a reversible and adiabatic piston-cylinder (Cengel et al., 2011), except for some slight curvature at the horizontal sections, which are deviations from isobaric conditions that stem from the fluid dynamics associated with check valves (Figure 8). The gap at bottom left corner is an indication that periodic steady-state conditions have not been reached at the end of a single cycle, and more cycles are required.

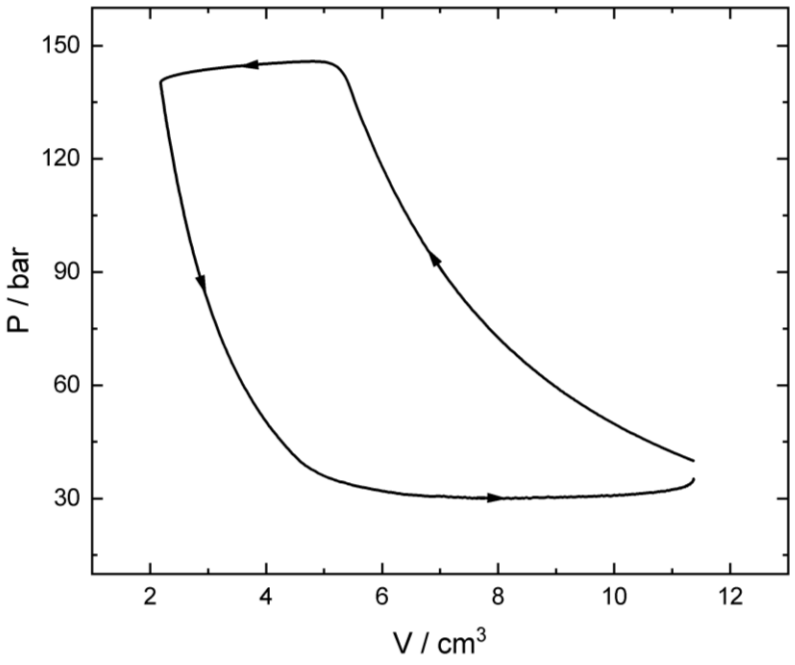

Figure 8. P-V diagram for the first compression cycle.

Conclusion

The studies indicate successful calculation of flow and temperature values for the operational state of a reciprocating compressor piston using Ansys Fluent software for 2D modeling. Adiabatic pressure and temperature values were observed to match theoretical values in a 2D piston model, with mesh parameters playing a significant role in achieving the desired accuracy. Subsequently, a model geometry with macroscopically modeled check valve was created with inlet and outlet connections similar to those in an actual booster pump. Here again, the obtained results were observed to resemble the actual piston compressor data. UDFs were used in the design of the check valves, which semi-empirically resulted in realistic trends in pressure during infilling and exhaust. Subsequent efforts will aim to implement heat losses and more fundamental check valve flow dynamics.

Scientific Ethics Declaration

The authors declare that the scientific ethical and legal responsibility of this article published in EPSTEM journal belongs to the authors.

Acknowledgements or Notes

* This article was presented as an oral presentation at the International Conference on Basic Sciences, Engineering and Technology (www.icbaset.net) held in Alanya/Turkey on May 02-05, 2024.

References

Bloch, H. P., & Hoefner, J. J. (1996). *Reciprocating compressors: Operation and maintenance.* Elsevier.

Cengel, Y. A., Boles, M. A., & KanoGlu, M. (2011). *Thermodynamics: an engineering approach (Vol.* 5, p. 445.) New York, NY: McGraw-hill.

Duprez, M. E., Dumont, E., & Frère, M. (2007). Modelling of reciprocating and scroll compressors. *International Journal of Refrigeration, 30*(5), 873-886.

Roskosch, D., Venzik, V., & Atakan, B. (2017). Thermodynamic model for reciprocating compressors with the focus on fluid dependent efficiencies. *International Journal of Refrigeration, 84*, 104-116.

Schultheis, S., Lickteig, C., & Parchewsky, R. (2011). Reciprocating compressor condition monitoring. In *Middle East Turbomachinery Symposia*. Texas A&M University,Turbomachinery Laboratories.

Author Information

Furkan Turgut
Logos Kimya Teknolojileri Ltd.Sti.
Gul Sanayi Sitesi, 1151. Sokak, No. 89,
Ostim / Ankara/Türkiye
Contact e-mail: *furkan@logoskimya.com*

Ahmet Berkay Simsek
Middle East Technical University
CZ-11 Dumlupınar Bulv. No.1 Cankaya 06800
Ankara/Türkiye

Necip Berker Uner
Middle East Technical University
D-110 Dumlupınar Bulv. No.1 Cankaya 06800
Ankara/Türkiye

Barıs Erdogan
Logos Kimya Teknolojileri Ltd. Sti.
Gül Sanayi Sitesi, 1151. Sokak, No. 89,
Ostim / Ankara/Türkiye

To cite this article:

Turgut, F., Simsek, A. B., Uner, N. B. & Erdogan, B. (2024). Analysis of a high-pressure reciprocating compressor piston's 2D simulation utilizing computational fluid dynamics. *The Eurasia Proceedings of Science, Technology, Engineering & Mathematics (EPSTEM), 28*, 352-359.

The Eurasia Proceedings of Science, Technology, Engineering & Mathematics (EPSTEM)
ISSN: 2602-3199

The Eurasia Proceedings of Science, Technology, Engineering & Mathematics (EPSTEM), 2024

Volume 28, Pages 360-374

ICBASET 2024: International Conference on Basic Sciences, Engineering and Technology

Analysis of Solutions for Nonlinear ψ-Caputo Fractional Differential Equations with Fractional Derivative Boundary Conditions in Banach Algebra

Yahia Awad
Lebanese International University

Haissam Chehade
Lebanese International University
The International University of Beirut

Abstract: This article explores the solutions of nonlinear implicit ψ-Caputo fractional-order ordinary differential equations (NLIFDEs) with two-point fractional derivatives boundary conditions in Banach algebra. The research aims to establish the existence and uniqueness of solutions for this complex class of differential equations. Utilizing Banach's and Krasnoselskii's fixed point theorems, the study conducts a rigorous analysis of the solutions, ensuring their existence and uniqueness. This comprehensive investigation contributes to enhancing the understanding of the behavior of solutions of nonlinear fractional differentials within a challenging mathematical framework.

Keywords: Banach algebra, Nonlinear fractional differential equations, Derivative boundary conditions,

Introduction and Preliminaries

Fractional calculus extends traditional differentiation and integration to non-integer orders, offering a useful basis for modeling complex phenomena in various scientific and engineering disciplines. Esteemed mathematicians such as Almeida (2017) and Agarwal (2012) and Kiblas (2006) and Burton (1998) and Samko (1993) have made significant contributions to this field, expanding its scope.

One particular area of focus is nonlinear implicit fractional order differential equations (NLIFDEs) with fractional boundary conditions (FBCs), which find applications in mathematical physics, engineering sciences, and computational mathematics (Agrawal, 2009; Awad & AlKhezi, 2023; Awad, 2024;Benlabbes et al., 2015; Debazi & Hammouche, 2020)).

Almeida's work on ψ-fractional derivatives (Almeida, 2017), a generalization of Riemann-Liouville derivatives, introduces a Caputo-type regularization, explored extensively in some recent researches such as Awad and Kaddoura (2024) and Awad, (2023) and Awad et al. (2023), Kaddoura and Awad (2023). These researches have focused on the existence of positive solutions for fractional differential equations with boundary conditions, employing methodologies such as Banach's and Krasnoselskii's fixed point theorems.

This article aims to investigate the existence and uniqueness of solutions for the following nonlinear implicit ψ-Caputo fractional differential equations (NLIFDEs) with fractional boundary conditions within the domain of Banach Algebra:

$$\mathfrak{D}_{0^+}^{\alpha,\psi} y(t) = f\left(t, y(t), \mathfrak{D}_{0^+}^{\beta,\psi} y(t), \int_0^t k\,(t,s)\mathfrak{D}_{0^+}^{\alpha,\psi} y(s)ds\right), \quad (1)$$

Subjected to the subsequent set of three integral boundary conditions involving fractional derivatives:

$$y(0) + \mathfrak{D}_{0^+}^{\alpha-1,\psi} y(T) = \sigma_1, \tag{2}$$

$$\mathfrak{D}_{0^+}^{\alpha-1,\psi} y(0) + \mathfrak{D}_{0^+}^{\alpha-2,\psi} y(T) = \sigma_2, \tag{3}$$

$$\mathfrak{D}_{0^+}^{\alpha-2,\psi} y(0) + \mathfrak{D}_{0^+}^{\alpha-3,\psi} y(T) = \sigma_3, \tag{4}$$

where $t \in J = [0,T]$, $\mathfrak{D}_{0^+}^{\alpha,\psi}$ and $\mathfrak{D}_{0^+}^{\beta,\psi}$ denote the standard ψ-Caputo fractional derivatives of orders $\alpha \in (2,3]$ and $\beta \in (0,1]$, $\sigma_i \in R \ \forall \ (i = 1,2,3)$, $\psi(t)$ is an increasing function with $\psi'(t) \neq 0 \ \ \forall \ t \in J = [0,T]$, $f: J \times R^3 \to R$, and $k: J \times R \to R$ are continuous functions.

In the following, we present certain symbols, definitions, lemmas, and theorems that serve as foundational elements for our study. These essential concepts can be referenced in Almeida (2017), Burton (1998), Kiblas (2006), and (Samko, 1993), and related sources.

Definition 1.1: [1] Consider $\alpha > 0$, $n \in N$ such that $n = [\alpha] + 1$, and let $I = [a,b]$ represent an interval with $-\infty < a < t < b < +\infty$. Suppose $\psi, x \in C^n(I, \mathbb{R})$ are two functions, where ψ is increasing and $\psi'(t) \neq 0$ for all $t \in I$. In this context,

1) The left-sided ψ-Riemann-Liouville fractional integral of $x(t)$ of the fractional order α with respect to ψ is defined as:

$$\mathfrak{I}_{a^+}^{\alpha,\psi} x(t) = \frac{1}{\Gamma(\alpha)} \int_a^t \psi'(s) \big(\psi(t) - \psi(s)\big)^{\alpha-1} x(s) ds,$$

2) where Γ is the Euler gamma function defined by $\Gamma(\alpha) = \int_0^{+\infty} t^{\alpha-1} e^{-t} d\zeta$.

3) The left-sided ψ-Caputo fractional derivative of $x(t)$ of the fractional order α is defined as:

$$\begin{aligned} {}^c\mathfrak{D}_{a^+}^{\alpha,\psi} x(t) &= \mathfrak{I}_{a^+}^{n-\alpha,\psi} \left(\frac{1}{\psi'(t)} \frac{d}{dt}\right)^n x(t) \\ &= \frac{1}{\Gamma(n-\alpha)} \int_a^t \psi'(s) \big(\psi(t) - \psi(s)\big)^{n-\alpha-1} x_\psi^{[n]}(s) ds, \end{aligned}$$

4) where $x_\psi^{[n]}(t) = \left(\frac{1}{\psi'(t)} \frac{d}{dt}\right)^n x(t)$.

Lemma 1.1: [17] If γ is a positive real number such that $\gamma > -1$ and $\gamma \neq \alpha - 1, \alpha - 2, \ldots, \alpha - n$, then for $t \in I$,

$${}^c\mathfrak{D}_{0^+}^{\alpha,\psi} \big(\psi(t) - \psi(a)\big)^\gamma = \frac{\Gamma(\gamma+1)}{\Gamma(\gamma-\alpha+1)} \big(\psi(t) - \psi(a)\big)^{\gamma-\alpha}, \tag{5}$$

where ${}^c\mathfrak{D}_{0^+}^{\alpha,\psi} \big(\psi(t) - \psi(a)\big)^{\alpha-i} = 0$ for all $i = 1,2,3,\ldots,n$.

Lemma 1.2. [1] If $\alpha > 0$, then the differential equation ${}^c\mathfrak{D}_{a^+}^{\alpha,\psi} x(t) = 0$ has a solution in $C(J, \mathbb{R}) \cap L_1(J, \mathbb{R})$ which is:

$$x(t) = c_1 \big(\psi(t) - \psi(0)\big)^{\alpha-1} + c_2 \big(\psi(t) - \psi(0)\big)^{\alpha-2} + \cdots + c_n \big(\psi(t) - \psi(0)\big)^{\alpha-n},$$

where $c_i \in \mathbb{R}$ for all $i = 1,2,\ldots,n$, and $n = [\alpha] + 1$.

Theorem 1.1. [15] (Banach's Fixed Point Theorem) Given a Banach space $(X, \|.\|)$, and a contraction mapping $\wp: X \to X$, there exists a unique fixed point $x \in X$ such that $\wp(x) = x$.

Theorem 1.2. [11] (Krasnselskii's fixed point theorem) Let $\mathcal{S}$ denote a closed, convex, and non-empty subset of a Banach space X. Suppose $\wp_1$ and $\wp_2$ are mappings from $\mathcal{S}$ to X satisfying the following conditions:

1) For any $u, v \in \mathcal{S}$, the sum $\wp_1 u + \wp_2 v$ belongs to $\mathcal{S}$.
2) The mapping $\wp_1$ is a contraction.
3) The mapping $\wp_2$ is continuous, and the range $\wp_2(\mathcal{S})$ is bounded.

Under these assumptions, there exists at least one element $u \in \mathcal{S}$ such that $\wp_1 u + \wp_2 u = u$.

Main Results

Definition 2.1. A function $y \in C(J, \mathbb{R})$ is considered as a solution if it satisfies both the nonlinear implicit fractional differential equation NLIFDE (1) and its associated boundary conditions (2)-(4).

Lemma 2.1. Suppose that $2 < \alpha \leq 3$, and let $f: J \times \mathbb{R}^3 \to \mathbb{R}$ be a continuous function. A function $y(t) \in C(J, \mathbb{R})$ is considered as a solution to the nonlinear implicit fractional differential equation NLIFDE (**[1]**) if and only if it satisfies the the following fractional integral equation:

$$
\begin{aligned}
& y(t) \\
& = \frac{\big(\psi(t) - \psi(0)\big)^{\alpha-1}}{\Gamma(\alpha)} \Bigg(\sigma_1 \\
& - \int_0^T \psi'(s) u(s) ds \Bigg) \qquad (6) \\
& + \frac{\big(\psi(t) - \psi(0)\big)^{\alpha-2}}{\Gamma(\alpha-1)} \begin{pmatrix} \sigma_2 + \varphi(T) \left(-\sigma_1 + \int_0^T \psi'(s) u(s) ds \right) \\ - \int_0^T \psi'(s) \big(\psi(T) - \psi(s)\big) u(s)\, ds. \end{pmatrix} \\
& + \frac{\big(\psi(t) - \psi(0)\big)^{\alpha-3}}{\Gamma(\alpha-2)} \begin{pmatrix} \sigma_3 - \frac{1}{2} \int_0^T \psi'(s) \big(\psi(T) - \psi(s)\big)^2 u(s)\, ds \\ -\frac{1}{2} \left(\sigma_1 - \int_0^T \psi'(s) u(s) ds \right) \big(\psi(T) - \psi(0)\big)^2 \\ -\varphi(T) \begin{pmatrix} \sigma_2 + \varphi(T) \left(-\sigma_1 + \int_0^T \psi'(s) u(s) ds \right) \\ - \int_0^T \psi'(s) \big(\psi(T) - \psi(s)\big) u(s)\, ds \end{pmatrix} \end{pmatrix} \\
& + \frac{1}{\Gamma(\alpha)} \int_0^t \psi'(s) \big(\psi(t) - \psi(s)\big)^{\alpha-1} u(s) ds,
\end{aligned}
$$

where $u(s)$ is the solution of the following fractional integral equation

$$u(t) = f\left(t, y(t), \mathfrak{I}_{0^+}^{\alpha-\beta,\psi} u(t), \int_0^t k(t,s) u(s) ds\right), \qquad (7)$$

Proof. Let $y(t)$ be a solution to the nonlinear implicit fractional differential equation NLIFDE (1). Define

$$u(t) = f\left(t, y(t), \mathfrak{D}_{0^+}^{\beta,\psi} y(t), \int_0^t k(t,s) \mathfrak{D}_{0^+}^{\alpha,\psi} y(s) ds\right).$$

It is clear that $\mathfrak{D}_{0^+}^{\beta,\psi} y(t) = \mathfrak{I}_{0^+}^{\alpha-\beta,\psi} \mathfrak{D}_{0^+}^{\alpha,\psi} y(t)$ for all $t \in J$. So, if $y(t)$ is a solution of equation (1), then for every $t \in J$, we have

$$\mathfrak{D}_{0^+}^{\alpha,\psi} y(t) = f\left(t, y(t), \mathfrak{I}_{0^+}^{\alpha-\beta,\psi} \mathfrak{D}_{0^+}^{\alpha,\psi} y(t), \int_0^t k\,(t,s) \mathfrak{D}_{0^+}^{\alpha,\psi} y(s) ds\right).$$

Let $\mathfrak{D}_{0^+}^{\beta,\psi} y(t) = u(t)$, then equation (1) becomes:

$$u(t) = f\left(t, y(t), \mathfrak{I}_{0^+}^{\alpha-\beta,\psi} u(t), \int_0^t k\,(t,s) u(s) ds\right).$$

Utilizing Lemma 1.2, we derive the expression:

$$\begin{aligned} y(t) = c_1\big(\psi(t) - \psi(0)\big)^{\alpha-1} + c_2\big(\psi(t) - \psi(0)\big)^{\alpha-2} \\ + \mathrm{c}_3\big(\psi(t) - \psi(0)\big)^{\alpha-3} \\ + \frac{1}{\Gamma(\alpha)} \int_0^T \psi'\,(s)\big(\psi(T) - \psi(s)\big)^2 u(s)\, ds \end{aligned} \tag{8}$$

Applying the boundary conditions (2)-(4), we obtain the following equations:

$$c_1 \Gamma(\alpha) = \sigma_1 - \textstyle\int_0^T \psi'\,(s) u(s) ds, \tag{9}$$

$$c_1 \Gamma(\alpha)\big(1 + \psi(T) - \psi(0)\big) + c_2 \Gamma(\alpha - 1) = \sigma_2 - \textstyle\int_0^T \psi'\,(s)\big(\psi(T) - \psi(s)\big) u(s)\, ds, \tag{10}$$

and

$$\begin{aligned} \frac{1}{2} c_1 \Gamma(\alpha)\big(\psi(T) - \psi(0)\big)^2 + c_2 \Gamma(\alpha - 1)\big(1 + \psi(T) - \psi(0)\big) + c_3 \Gamma(\alpha - 2) \\ = \sigma_3 - \tfrac{1}{2} \textstyle\int_0^T \psi'\,(s)\big(\psi(T) - \psi(s)\big)^2 u(s)\, ds. \end{aligned} \tag{11}$$

Solving equations (9), (10), and (11) for c_1, c_2, and c_3, we obtain:

$$c_1 = \frac{1}{\Gamma(\alpha)}\left(\sigma_1 - \int_0^T \psi'\,(s) u(s) ds\right),$$

$$c_2 = \frac{1}{\Gamma(\alpha - 1)}\left(\varphi(T)\left(-\sigma_1 + \int_0^T \psi'\,(s) u(s) ds\right) + \sigma_2 - \int_0^T \psi'\,(s)\big(\psi(T) - \psi(s)\big) u(s)\, ds.\right),$$

and

$$c_3 = \frac{1}{\Gamma(\alpha - 2)}\left(\begin{array}{c} \sigma_3 - \dfrac{1}{2}\displaystyle\int_0^T \psi'\,(s)\big(\psi(T) - \psi(s)\big)^2 u(s)\, ds \\ -\dfrac{1}{2}\left(\sigma_1 - \displaystyle\int_0^T \psi'\,(s) u(s) ds\right)\big(\psi(T) - \psi(0)\big)^2 \\ +\sigma_2 - \left(\begin{array}{c} \varphi(T)\left(-\sigma_1 + \displaystyle\int_0^T \psi'\,(s) u(s) ds\right) \\ -\displaystyle\int_0^T \psi'\,(s)\big(\psi(T) - \psi(s)\big) u(s)\, ds \end{array}\right)\varphi(T) \end{array}\right),$$

where $\varphi(T) = 1 + \psi(T) - \psi(0)$. Substituting these into (8), we obtain:

$$y(t) = \frac{\big(\psi(t) - \psi(0)\big)^{\alpha-1}}{\Gamma(\alpha)}\left(\sigma_1 - \int_0^T \psi'\,(s) u(s) ds\right)$$

$$+\frac{\big(\psi(t)-\psi(0)\big)^{\alpha-2}}{\Gamma(\alpha-1)}\begin{pmatrix}\sigma_2+\varphi(T)\left(-\sigma_1+\int_0^T\psi'(s)u(s)ds\right)\\-\int_0^T\psi'(s)\big(\psi(T)-\psi(s)\big)u(s)\,ds.\end{pmatrix}$$

$$+\frac{\big(\psi(t)-\psi(0)\big)^{\alpha-3}}{\Gamma(\alpha-2)}\begin{pmatrix}\sigma_3-\frac{1}{2}\int_0^T\psi'(s)\big(\psi(T)-\psi(s)\big)^2u(s)\,ds\\-\frac{1}{2}\left(\sigma_1-\int_0^T\psi'(s)u(s)ds\right)\big(\psi(T)-\psi(0)\big)^2\\-\varphi(T)\begin{pmatrix}\sigma_2+\varphi(T)\left(-\sigma_1+\int_0^T\psi'(s)u(s)ds\right)\\-\int_0^T\psi'(s)\big(\psi(T)-\psi(s)\big)u(s)\,ds\end{pmatrix}\end{pmatrix}$$

$$+\frac{1}{\Gamma(\alpha)}\int_0^t\psi'(s)\big(\psi(t)-\psi(s)\big)^{\alpha-1}u(s)ds.$$

On the contrary, assume that $y(t)$ constitutes a solution to the nonlinear implicit fractional differential equation NLIFDE (1), and this solution can be expressed in the subsequent manner:

$$y(t)=\frac{\big(\psi(t)-\psi(0)\big)^{\alpha-1}}{\Gamma(\alpha)}\left(\sigma_1-\int_0^T\psi'(s)u(s)ds\right)$$

$$+\frac{\big(\psi(t)-\psi(0)\big)^{\alpha-2}}{\Gamma(\alpha-1)}\begin{pmatrix}\sigma_2+\varphi(T)\left(-\sigma_1+\int_0^T\psi'(s)u(s)ds\right)\\-\int_0^T\psi'(s)\big(\psi(T)-\psi(s)\big)u(s)\,ds.\end{pmatrix}$$

$$+\frac{\big(\psi(t)-\psi(0)\big)^{\alpha-3}}{\Gamma(\alpha-2)}\begin{pmatrix}\sigma_3-\frac{1}{2}\int_0^T\psi'(s)\big(\psi(T)-\psi(s)\big)^2u(s)\,ds\\-\frac{1}{2}\left(\sigma_1-\int_0^T\psi'(s)u(s)ds\right)\big(\psi(T)-\psi(0)\big)^2\\-\varphi(T)\begin{pmatrix}\sigma_2+\varphi(T)\left(-\sigma_1+\int_0^T\psi'(s)u(s)ds\right)\\-\int_0^T\psi'(s)\big(\psi(T)-\psi(s)\big)u(s)\,ds\end{pmatrix}\end{pmatrix}$$

$$+\frac{1}{\Gamma(\alpha)}\int_0^t\psi'(s)\big(\psi(t)-\psi(s)\big)^{\alpha-1}u(s)ds.$$

Thus, we can infer that: $\mathfrak{D}_{0^+}^{\alpha,\psi}y(t)=u(t)$, with $y(0)+\mathfrak{D}_{0^+}^{\alpha-1,\psi}y(T)=\sigma_1$, $\mathfrak{D}_{0^+}^{\alpha-1,\psi}y(0)+\mathfrak{D}_{0^+}^{\alpha-2,\psi}y(T)=\sigma_2$, and $\mathfrak{D}_{0^+}^{\alpha-2,\psi}y(0)+\mathfrak{D}_{0^+}^{\alpha-3,\psi}y(T)=\sigma_3$. This implies that $u(t)$ indeed satisfies the conditions of problem (6). This concludes the proof.

Lemma 2.2. Consider the NLIFDE (1) under the following conditions:

(H_1) The nonlinear function $f:J\times\mathbb{R}^3\to\mathbb{R}$ exhibits continuity, and there exists $\lambda\in C(J,\mathbb{R}^+)$ such that:

$$|f(t,u_1,u_2,u_3)-f(t,v_1,v_2,v_3)|\le\lambda(t)(|u_1-v_1|+|u_2-v_2|+|u_3-v_3|),$$

for all $t\in J$, $u_i,v_i\in\mathbb{R}$, and $i=1,2,3$.

(H_2) The function $k(t,s)$ is continuous over $J\times J$, and there exists a positive constant K such that:

$$\max_{t,s\in[0,1]} |k(t,s)| = K.$$

Remark 1. Derived from Lemma, we extract that under the premise of (H_1), the inequality

$$|f(t,u_1,u_2,u_3)| - |f(t,0,0,0)| \leq |f(t,u_1,u_2,u_3) - f(t,0,0,0)| \leq \lambda(t)(|u_1| + |u_2| + |u_3|).$$

holds. Consequently, if $F = \sup_{t\in J}|f(t,0,0,0)|$, it follows that

$$|f(t,u_1,u_2,u_3)| \leq F + \lambda(t)(|u_1| + |u_2| + |u_3|)$$

Definition 2.2. Define the operator $\wp: C(J,\mathbb{R}) \to C(J,\mathbb{R})$ as follows:

$$\begin{aligned}\wp\big(y(t)\big) = {} & \frac{\big(\psi(t)-\psi(0)\big)^{\alpha-1}}{\Gamma(\alpha)}\left(\sigma_1 - \int_0^T \psi'(s)u(s)ds\right) \\ & + \frac{\big(\psi(t)-\psi(0)\big)^{\alpha-2}}{\Gamma(\alpha-1)}\begin{pmatrix} \varphi(T)\left(-\sigma_1 + \int_0^T \psi'(s)u(s)ds\right) \\ +\sigma_2 - \int_0^T \psi'(s)\big(\psi(T)-\psi(s)\big)u(s)\,ds. \end{pmatrix} \\ & + \frac{\big(\psi(t)-\psi(0)\big)^{\alpha-3}}{\Gamma(\alpha-2)}\begin{pmatrix} \sigma_3 - \frac{1}{2}\int_0^T \psi'(s)\big(\psi(T)-\psi(s)\big)^2 u(s)\,ds \\ -\frac{1}{2}\left(\sigma_1 - \int_0^T \psi'(s)u(s)ds\right)\big(\psi(T)-\psi(0)\big)^2 \\ -\varphi(T)\begin{pmatrix}\sigma_2 + \varphi(T)\left(-\sigma_1 + \int_0^T \psi'(s)u(s)ds\right) \\ -\int_0^T \psi'(s)\big(\psi(T)-\psi(s)\big)u(s)\,ds\end{pmatrix}\end{pmatrix} \\ & + \frac{1}{\Gamma(\alpha)}\int_0^t \psi'(s)\big(\psi(t)-\psi(s)\big)^{\alpha-1}u(s)ds.\end{aligned}$$

where $u(s) \in C(J,\mathbb{R})$ satisfies the following implicit fractional equation:

$$u(t) = f\left(t, y(t), \Im_{0^+}^{\alpha-\beta,\psi}u(t), \int_0^t k(t,s)u(s)ds\right).$$

Existence of Solutions

In the following, we establish the existence of solutions for the Nonlinear Fractional Differential Equation NLIFDE defined by (1). Our approach centers on the application of Krasnoselskii's fixed point theorem.

Theorem 2.1. Suppose that assumptions (H_1) and (H_2) hold. If $\frac{\|\lambda\|\aleph}{\mathcal{M}} < 1$, where

$$\aleph = \begin{pmatrix} \frac{\big(\psi(T)-\psi(0)\big)^{\alpha}}{\Gamma(\alpha)} + \varphi(T)\frac{\big(\psi(T)-\psi(0)\big)^{\alpha-1}}{\Gamma(\alpha-1)} + \frac{\big(\psi(T)-\psi(0)\big)^{\alpha}}{2\Gamma(\alpha-1)} \\ + \frac{2\big(\psi(T)-\psi(0)\big)^{\alpha}}{3\Gamma(\alpha-2)} - \varphi^2(T)\frac{\big(\psi(T)-\psi(0)\big)^{\alpha-2}}{\Gamma(\alpha-2)} + \varphi(T)\frac{\big(\psi(T)-\psi(0)\big)^{\alpha-1}}{2\Gamma(\alpha-2)} \end{pmatrix}$$

and

$$\mathcal{M} = 1 - \|\lambda\|\left(\frac{\big(\psi(T)-\psi(0)\big)^{\alpha-\beta}}{\Gamma(1+\alpha-\beta)} + KT\right),$$

then NLIFDE (1) has at least one solution in $C[0,1]$.

Proof. By transforming NLIFDE (1) into a problem involving fixed points, we introduce the operator $\wp: C(J,\mathbb{R}) \to C(J,\mathbb{R})$ as follows:

$$\wp\big(y(t)\big) = \wp_1\big(y(t)\big) + \wp_2\big(y(t)\big), \quad t \in [0,1],$$

Where

$$\begin{aligned}\wp_1\big(y(t)\big) = {} & \frac{\big(\psi(t)-\psi(0)\big)^{\alpha-1}}{\Gamma(\alpha)}\left(\sigma_1 - \int_0^T \psi'(s)u(s)ds\right) \\ & + \frac{\big(\psi(t)-\psi(0)\big)^{\alpha-2}}{\Gamma(\alpha-1)}\begin{pmatrix}\sigma_2 + \varphi(T)\left(-\sigma_1 + \int_0^T \psi'(s)u(s)ds\right) \\ -\int_0^T \psi'(s)\big(\psi(T)-\psi(s)\big)u(s)\,ds.\end{pmatrix} \\ & + \frac{\big(\psi(t)-\psi(0)\big)^{\alpha-3}}{\Gamma(\alpha-2)}\begin{pmatrix}\sigma_3 - \frac{1}{2}\int_0^T \psi'(s)\big(\psi(T)-\psi(s)\big)^2 u(s)\,ds \\ -\frac{1}{2}\left(\sigma_1 - \int_0^T \psi'(s)u(s)ds\right)\big(\psi(T)-\psi(0)\big)^2 \\ -\varphi(T)\begin{pmatrix}\sigma_2 + \varphi(T)\left(-\sigma_1 + \int_0^T \psi'(s)u(s)ds\right) \\ -\int_0^T \psi'(s)\big(\psi(T)-\psi(s)\big)u(s)\,ds\end{pmatrix}\end{pmatrix},\end{aligned}$$

and

$$\wp_2\big(y(t)\big) = \frac{1}{\Gamma(\alpha)}\int_0^t \psi'(s)\big(\psi(t)-\psi(s)\big)^{\alpha-1}u(s)ds,$$

with

$$u(t) = f\left(t,\ y(t),\ \mathfrak{I}_{0^+}^{\alpha-\beta,\psi}u(t), \int_0^t k(t,s)u(s)ds\right).$$

Consider $B_\varrho = \{y \in C(J,\mathbb{R}): \|y\| \le \varrho\}$ as a closed subset of $C[0,1]$, where ϱ represents a positive constant satisfying $\varrho \ge \frac{\Re}{1-\aleph}$. Here, $\Re$ and $\aleph$ are real numbers. It is evident that B_ϱ constitutes a Banach space equipped with a metric in $C[0,T]$. The proof can be outlined in three distinct phases.

Step 1: $\wp_1 y_1 + \wp_2 y_2 \in B_\varrho$ holds true for all $y_1, y_2 \in B_\varrho$.

Consider $y_1, y_2 \in B_\varrho$ and $t \in J$. We obtain:

$$\begin{aligned}\big|\wp_1\big(y_1(t)\big) + \wp_2\big(y_2(t)\big)\big| &\le \big|\wp_1\big(y_1(t)\big)\big| + \big|\wp_2\big(y_2(t)\big)\big| \\ &\le \frac{|\psi(t)-\psi(0)|^{\alpha-1}}{\Gamma(\alpha)}\left(\sigma_1 + \int_0^T \psi'(s)|u_1(s)|ds\right) \\ &\quad + \frac{|\psi(t)-\psi(0)|^{\alpha-2}}{\Gamma(\alpha-1)}\begin{pmatrix}\sigma_2 + |\varphi(T)|\left(\sigma_1 + \int_0^T \psi'(s)|u_1(s)|ds\right) \\ +\int_0^T \psi'(s)\big(\psi(T)-\psi(s)\big)|u_1(s)|\,ds.\end{pmatrix} \\ &\quad + \frac{|\psi(t)-\psi(0)|^{\alpha-3}}{\Gamma(\alpha-2)}\begin{pmatrix}\sigma_3 + \frac{1}{2}\int_0^T \psi'(s)\big(\psi(T)-\psi(s)\big)^2|u_1(s)|\,ds \\ +\frac{1}{2}\left(\sigma_1 + \int_0^T \psi'(s)|u_1(s)|ds\right)\big(\psi(T)-\psi(0)\big)^2 \\ +|\varphi(T)|\begin{pmatrix}\sigma_2 + |\varphi(T)|\left(\sigma_1 + \int_0^T \psi'(s)|u_1(s)|ds\right) \\ +\int_0^T \psi'(s)\big(\psi(T)-\psi(s)\big)|u_1(s)|\,ds\end{pmatrix}\end{pmatrix} \\ &\quad + \frac{1}{\Gamma(\alpha)}\int_0^t \psi'(s)\big(\psi(t)-\psi(s)\big)^{\alpha-1}|u_2(s)|ds.\end{aligned}$$

Using Lemma 2.2 and the aforementioned remark, if we consider the supremum for $t \in [0,T]$, then

$$\begin{aligned}\|u\| &= \left| f\left(t,\ y(t),\ \Im_{0^+}^{\alpha-\beta,\psi}u(t), \int_0^t k\,(t,s)u(s)ds\right)\right| \\ &\leq \|\lambda\|\left(|y(t)| + \left|\Im_{0^+}^{\alpha-\beta,\psi}u(t)\right| + \left|\int_0^t k\,(t,s)u(s)ds\right|\right) + F \\ &\leq \|\lambda\|\left(\|y\| + \left(\frac{\left(\psi(T)-\psi(0)\right)^{\alpha-\beta}}{\Gamma(1+\alpha-\beta)} + KT\right)\|u\|\right) + F,\end{aligned}$$

where $F = \sup_{t\in J}|f(t,0,0,0)|$.

Hence,

$$\|u\| \leq \frac{\|\lambda\|\|y\| + F}{\mathcal{M}},$$

where $\mathcal{M} = 1 - \|\lambda\|\left(\frac{\left(\psi(T)-\psi(0)\right)^{\alpha-\beta}}{\Gamma(1+\alpha-\beta)} + KT\right)$.

Thus, for each $t \in [0,T]$ we have

$$\begin{aligned}&\left|\wp_1\left(y_1(t)\right) + \wp_2\left(y_2(t)\right)\right| \leq \left|\wp_1\left(y_1(t)\right)\right| + \left|\wp_2\left(y_2(t)\right)\right| \\ &\leq \frac{|\psi(t)-\psi(0)|^{\alpha-1}}{\Gamma(\alpha)}\left(\sigma_1 + \left(\frac{\|\lambda\|\|y_1\| + F}{\mathcal{M}}\right)\left(\psi(T)-\psi(0)\right)\right) \\ &+ \frac{|\psi(t)-\psi(0)|^{\alpha-2}}{\Gamma(\alpha-1)}\left(\begin{array}{c}\sigma_2 + |\varphi(T)|\left(\sigma_1 + \left(\frac{\|\lambda\|\|y_1\| + F}{\mathcal{M}}\right)\left(\psi(T)-\psi(0)\right)\right) \\ + \frac{\left(\frac{\|\lambda\|\|y_1\| + F}{\mathcal{M}}\right)\left(\psi(T)-\psi(0)\right)^2}{2}\end{array}\right) \\ &+ \frac{|\psi(t)-\psi(0)|^{\alpha-3}}{\Gamma(\alpha-2)}\left(\begin{array}{c}\sigma_3 + \frac{\left(\frac{\|\lambda\|\|y_1\| + F}{\mathcal{M}}\right)\left(\psi(T)-\psi(0)\right)^3}{6} + \left(\frac{\|\lambda\|\|y_1\| + F}{\mathcal{M}}\right)\varphi^2(T)\left(\psi(T)-\psi(0)\right) \\ + \sigma_1\varphi^2(T) + \sigma_1\frac{\left(\psi(T)-\psi(0)\right)^2}{2} + \frac{\left(\frac{\|\lambda\|\|y_1\| + F}{\mathcal{M}}\right)\left(\psi(T)-\psi(0)\right)^3}{2} \\ + \sigma_2\varphi(T) + \frac{\left(\frac{\|\lambda\|\|y_1\| + F}{\mathcal{M}}\right)\varphi(T)\left(\psi(T)-\psi(0)\right)^2}{2}\end{array}\right) \\ &+ \frac{|\psi(t)-\psi(0)|^{\alpha}}{\Gamma(\alpha+1)}\left(\frac{\|\lambda\|\|y_2\| + F}{\mathcal{M}}\right).\end{aligned}$$

Taking supremum over $t \in [0,T]$, we have

$$\|\wp_1 y_1(t) + \wp_2 y_2(t)\| \leq \varrho,$$

for $\varrho \geq \frac{\Re}{1-\aleph}$, where

$$\Re = (\sigma_1\Upsilon_1 + \sigma_2\Upsilon_2 + \sigma_3\Upsilon_3 + (\|\lambda\| + F)\Upsilon_4)$$

such that

$$\begin{aligned}\Upsilon_1 &= \left(\frac{1}{\Gamma(\alpha)}+\frac{1}{2\Gamma(\alpha-2)}\right)\big(\psi(T)-\psi(0)\big)^{\alpha-1}+\varphi(T)\frac{\big(\psi(T)-\psi(0)\big)^{\alpha-2}}{\Gamma(\alpha-1)}\\ &\quad+\varphi^2(T)\frac{\big(\psi(T)-\psi(0)\big)^{\alpha-3}}{\Gamma(\alpha-2)},\end{aligned}$$

$$\Upsilon_2=\frac{\big(\psi(T)-\psi(0)\big)^{\alpha-2}}{\Gamma(\alpha-1)}+\varphi(T)\frac{\big(\psi(T)-\psi(0)\big)^{\alpha-3}}{\Gamma(\alpha-2)},$$

$$\Upsilon_3=\frac{\big(\psi(T)-\psi(0)\big)^{\alpha-3}}{\Gamma(\alpha-2)},$$

$$\begin{aligned}\Upsilon_4 &= \left(\frac{1}{|\Gamma(\alpha+1)|}+\frac{1}{\Gamma(\alpha)}+\frac{1}{2\Gamma(\alpha-1)}+\frac{2}{3\Gamma(\alpha-2)}\right)\big(\psi(T)-\psi(0)\big)^{\alpha}\\ &\quad+\varphi(T)\left(\frac{1}{\Gamma(\alpha-1)}+\frac{1}{2\Gamma(\alpha-2)}\right)\big(\psi(T)-\psi(0)\big)^{\alpha-1}\\ &\quad+\varphi^2(T)\frac{\big(\psi(T)-\psi(0)\big)^{\alpha-2}}{\Gamma(\alpha-2)},\end{aligned}$$

and

$$\aleph=\begin{pmatrix}\dfrac{\big(\psi(T)-\psi(0)\big)^{\alpha}}{\Gamma(\alpha)}+\varphi(T)\dfrac{\big(\psi(T)-\psi(0)\big)^{\alpha-1}}{\Gamma(\alpha-1)}+\dfrac{\big(\psi(T)-\psi(0)\big)^{\alpha}}{2\Gamma(\alpha-1)}\\ +\dfrac{2\big(\psi(T)-\psi(0)\big)^{\alpha}}{3\Gamma(\alpha-2)}-\varphi^2(T)\dfrac{\big(\psi(T)-\psi(0)\big)^{\alpha-2}}{\Gamma(\alpha-2)}+\varphi(T)\dfrac{\big(\psi(T)-\psi(0)\big)^{\alpha-1}}{2\Gamma(\alpha-2)}\end{pmatrix}$$

This proves that $\wp_1 y_1(t)+\wp_2 y_2(t)\in B_\varrho$ for every $y_1, y_2\in B_\varrho$.

Step 2: The operator $\wp_1$ serves as a contraction mapping on B_ϱ.

It is clear that

$$\begin{aligned}\|u_1-u_2\| &= \left|f\left(t,\ y_1(t),\ \Im_{0^+}^{\alpha-\beta,\psi}u_1(t),\int_0^t k\ (t,s)u_1(s)ds\right)-f\left(t,\ y_2(t),\ \Im_{0^+}^{\alpha-\beta,\psi}u_2(t),\int_0^t k\ (t,s)u_2(s)ds\right)\right|\\ &\le \lambda(t)\left(|y_1(t)-y_2(t)|+\int_0^t\frac{\psi'(s)\big(\psi(t)-\psi(s)\big)^{\alpha-\beta-1}}{\Gamma(\alpha-\beta)}|u_1(t)-u_2(t)|ds\right.\\ &\quad\left.+\int_0^t|k\ (t,s)||u_1(t)-u_2(t)|ds\right)\end{aligned}$$

Taking supremum for all $t\in I$, we get

$$\|u_1-u_2\|\le\|\lambda\|\left[\|y_1-y_2\|+\left(\frac{\big(\psi(T)-\psi(0)\big)^{\alpha-\beta}}{\Gamma(\alpha-\beta+1)}+KT\right)\|u_1-u_2\|\right].$$

Thus,

$$\|u_1-u_2\|\le\frac{\|\lambda\|}{\mathcal{M}}\|y_1-y_2\|.$$

This implies that

$$
\begin{aligned}
&\left|\wp_1\left(y_1(t)\right)-\wp_1\left(y_2(t)\right)\right| \\
&\quad=\frac{\left(\psi(t)-\psi(0)\right)^{\alpha-1}}{\Gamma(\alpha)}\int_0^T \psi'(s)|u_2(s)-u_1(s)|ds \\
&\quad+\frac{\left(\psi(t)-\psi(0)\right)^{\alpha-2}}{\Gamma(\alpha-1)}\begin{pmatrix} \varphi(T)\left(\int_0^T \psi'(s)|u_1(s)-u_2(s)|ds\right) \\ +\int_0^T \psi'(s)\left(\psi(T)-\psi(s)\right)|u_2(s)-u_1(s)|\,ds \end{pmatrix} \\
&\quad+\frac{\left(\psi(t)-\psi(0)\right)^{\alpha-3}}{\Gamma(\alpha-2)}\begin{pmatrix} +\frac{1}{2}\int_0^T \psi'(s)\left(\psi(T)-\psi(s)\right)^2|u_2(s)-u_1(s)|\,ds \\ +\frac{1}{2}\int_0^T \psi'(s)|u_1(s)-u_2(s)|ds\left(\psi(T)-\psi(0)\right)^2 \\ -\varphi(T)\begin{pmatrix} \varphi(T)\int_0^T \psi'(s)|u_1(s)-u_2(s)|ds \\ -\int_0^T \psi'(s)\left(\psi(T)-\psi(s)\right)|u_2(s)-u_1(s)|\,ds \end{pmatrix} \end{pmatrix}.
\end{aligned}
$$

Taking supremum over $t \in [0,T]$, we get

$$
\begin{aligned}
&\|\wp_1(y_1)-\wp_1(y_2)\| \\
&\quad\le\frac{\left(\psi(T)-\psi(0)\right)^{\alpha}}{\Gamma(\alpha)}\|u_1-u_2\| \\
&\quad+\frac{\left(\psi(T)-\psi(0)\right)^{\alpha-2}}{\Gamma(\alpha-1)}\left(\varphi(T)\left(\psi(T)-\psi(0)\right)+\frac{\left(\psi(T)-\psi(0)\right)^2}{2}\right)\|u_1-u_2\| \\
&\quad+\frac{\left(\psi(T)-\psi(0)\right)^{\alpha-3}}{\Gamma(\alpha-2)}\begin{pmatrix} +\frac{\left(\psi(T)-\psi(0)\right)^3}{6}+\frac{\left(\psi(T)-\psi(0)\right)^3}{2} \\ -\varphi^2(T)\left(\psi(T)-\psi(0)\right)+\varphi(T)\frac{\left(\psi(T)-\psi(0)\right)^2}{2} \end{pmatrix}\|u_1-u_2\| \\
&\quad\le\begin{pmatrix} \frac{\left(\psi(T)-\psi(0)\right)^{\alpha}}{\Gamma(\alpha)}+\varphi(T)\frac{\left(\psi(T)-\psi(0)\right)^{\alpha-1}}{\Gamma(\alpha-1)}+\frac{\left(\psi(T)-\psi(0)\right)^{\alpha}}{2\Gamma(\alpha-1)} \\ +\frac{2\left(\psi(T)-\psi(0)\right)^{\alpha}}{3\Gamma(\alpha-2)}-\varphi^2(T)\frac{\left(\psi(T)-\psi(0)\right)^{\alpha-2}}{\Gamma(\alpha-2)}+\varphi(T)\frac{\left(\psi(T)-\psi(0)\right)^{\alpha-1}}{2\Gamma(\alpha-2)} \end{pmatrix}\|u_1 \\
&\quad-u_2\|\le\frac{\|\lambda\|\aleph}{\mathcal{M}}\|y_1-y_2\|.
\end{aligned}
$$

Thus, it is clear that the operator$\wp_1$ is a contraction mapping with a contraction coefficient $\frac{\|\lambda\|\aleph}{\mathcal{M}}<1$.

Step 3: To establish the continuity and compactness of the operator $\wp_2$ on B_ϱ, we initially establish its continuity. Let $\{y_n\}_{n\in N}$ be a sequence in B_ϱ that converges to $y \in B_\varrho$ as n tends to infinity. Our objective is to demonstrate that $\|\wp_2 y_n-\wp_1 y\|$ tends to zero as n tends to infinity. Subsequently, for $t \in [0,T]$, we have:

$$
|\wp_2 y_n-\wp_2 y|\le\frac{1}{\Gamma(\alpha)}\int_0^t \psi'(s)\left(\psi(t)-\psi(s)\right)^{\alpha-1}|u_n(s)-u(s)|ds,
$$

Where

$$
u_n(t)=f\left(t,\ y_n(t),\ \mathfrak{D}_{0^+}^{\beta,\psi}y_n(t),\int_0^t k\,(t,s)\mathfrak{D}_{0^+}^{\alpha,\psi}y_n(s)ds\right),
$$

and

$$
u(t)=f\left(t,y(t),\mathfrak{D}_{0^+}^{\beta}y(t),\int_0^t k\,(t,s)\mathfrak{D}_{0^+}^{\alpha,\psi}y(s)ds\right)
$$

are two continuous functions defined over $[0,T]$ such that

$$\begin{aligned}
&|u_n(t)-u(t)|\\
&=\left|f\left(t,y_n(t),\mathfrak{D}_{0^+}^{\beta}y_n(t),\int_0^t k\,(t,s)\mathfrak{D}_{0^+}^{\alpha,\psi}y_n(s)ds\right)-f\left(t,y(t),\mathfrak{D}_{0^+}^{\beta}y(t),\int_0^t k\,(t,s)\mathfrak{D}_{0^+}^{\alpha,\psi}y(s)ds\right)\right|,\\
&\leq|\lambda(t)|\left(|y_n(t)-y(t)|+\left|\mathfrak{D}_{0^+}^{\beta}y_n(t)-\mathfrak{D}_{0^+}^{\beta}y(t)\right|+\int_0^t|k(t,s)|\left|\mathfrak{D}_{0^+}^{\alpha,\psi}y_n(s)-\mathfrak{D}_{0^+}^{\alpha,\psi}y(s)\right|ds\right)|),\\
&\leq\frac{\|\lambda\|}{\mathcal{M}}\|y_n-y\|.
\end{aligned}$$

Since $y_n\to y$, then we get $u_n(t)\to u(t)$ as $n\to\infty$ for each $t\in[0,T]$. And let $\varepsilon>0$ be such that, for each $t\in[0,T]$, we have $|u_n(t)|\leq\varepsilon/2$ and $|u(t)|\leq\varepsilon/2$ which implies that $|u_n(s)-u(s)|\leq(|u_n(s)|+|u(s)|)\leq\varepsilon$ for each $t\in[0,T]$. Applying Lebesgue Dominated Convergence Theorem, it implies that $\|\wp_2y_n-\wp_2y\|\to0$ as $n\to\infty$. Consequently, operator $\wp_2$ is continuous. In addition, we have

$$\|\wp_2y\|\leq\frac{1}{|\Gamma(\alpha+1)|}\left(\frac{\|\lambda\|\|y_1\|+F}{\mathcal{M}}\right)\leq\varrho$$

due to definitions of ϱ. This proves that $\wp_2$ is uniformly bounded on B_ϱ.

Ultimately, we demonstrate that the mapping $\wp_2$ transforms bounded sets into equicontinuous sets within $C(J,R)$, specifically ensuring the equicontinuity of B_ϱ.

Assume that $\forall\,\epsilon>0$, $\exists\,\delta>0$ and $t_1,t_2\in J,\ t_1<t_2,\ \ |t_2-t_1|<\delta$. Then, we have

$$\begin{aligned}
|\wp_2y(t_2)-\wp_2y(t_1)|\ &\leq\frac{1}{\Gamma(\alpha)}\int_0^t\psi'(s)\left(\left(\psi(t_2)-\psi(s)\right)^{\alpha-1}-\left(\psi(t_1)-\psi(s)\right)^{\alpha-1}\right)|u(s)|ds,\\
&\leq\left(\frac{\|\lambda\|\|y\|}{\mathcal{M}}\right)\frac{(\psi(t_2)^{\alpha}-\psi(t_1)^{\alpha})}{\alpha\Gamma(\alpha)}.
\end{aligned}$$

As t_1 approaches t_2, the expression on the right-hand side of the aforementioned inequality becomes independent of y and approaches zero. Thus,

$$|\wp_2y(t_2)-\wp_2y(t_1)|\to0,\ \ \forall\,|t_2-t_1|\to0.$$

Thus, if $\wp$ is uniformly continuous on B_ϱ, where $\wp$ represents a compact operator, the Arzela-Ascoli theorem guarantees that $\wp\colon C([0,T],R)\to C([0,T],R)$ is both continuous and compact. Consequently, all the conditions of Krasnoselskii's fixed point theorem are satisfied, and the operator $\wp=\wp_1+\wp_2$ possesses a fixed point $y(t)\in C[0,T]$ on B_ϱ satisfying the boundary conditions in (1). As a result, $y(t)$ serves as a solution of the NLIFDE (1). This concludes the proof. □

Uniqueness of Solutions

Next, we ascertain the unique solutions to the nonlinear fractional differential equation NLIFDE (1). This exploration into uniqueness adds a valuable dimension to our understanding of the solutions in the context of our studied equation.

Theorem 2.3. If assumptions (H_1) and (H_2) hold, and if

$$\left(\aleph+\frac{\left(\psi(T)-\psi(0)\right)^{\alpha}}{\Gamma(\alpha+1)}\right)\frac{\|\lambda\|}{\mathcal{M}}<1,$$

then operator $\wp\colon C(J,R)\to C(J,R)$ presented in Definition 2.2 is a contraction.

Proof. Assuming that conditions (H_1) and (H_2) are satisfied, let's examine the continuous functions $y_1(t)$ and $y_2(t)$ belonging to $C(J,R)$. In this context, for any $t \in J$, the following applies:

$$\begin{aligned}
&\left|\wp\left(y_1(t)\right)-\wp\left(y_2(t)\right)\right| \\
&\leq \left|\wp_1\left(y_1(t)\right)-\wp_1\left(y_2(t)\right)+\wp_2\left(y_1(t)\right)-\wp_2\left(y_2(t)\right)\right| \\
&\leq \left|\wp_1\left(y_1(t)\right)-\wp_1\left(y_2(t)\right)\right|+\left|\wp_2\left(y_1(t)\right)-\wp_2\left(y_2(t)\right)\right| \\
&\leq \frac{\left(\psi(t)-\psi(0)\right)^{\alpha-1}}{\Gamma(\alpha)}\int_0^T \psi'(s)|u_2(s)-u_1(s)|ds \\
&+\frac{\left(\psi(t)-\psi(0)\right)^{\alpha-2}}{\Gamma(\alpha-1)}\begin{pmatrix}\varphi(T)\left(\int_0^T \psi'(s)|u_1(s)-u_2(s)|ds\right)\\ +\int_0^T \psi'(s)\left(\psi(T)-\psi(s)\right)|u_2(s)-u_1(s)|\,ds.\end{pmatrix} \\
&+\frac{\left(\psi(t)-\psi(0)\right)^{\alpha-3}}{\Gamma(\alpha-2)}\begin{pmatrix}+\frac{1}{2}\int_0^T \psi'(s)\left(\psi(T)-\psi(s)\right)^2|u_2(s)-u_1(s)|\,ds \\ +\frac{1}{2}\int_0^T \psi'(s)|u_1(s)-u_2(s)|ds\left(\psi(T)-\psi(0)\right)^2 \\ -\varphi(T)\begin{pmatrix}\varphi(T)\int_0^T \psi'(s)|u_1(s)-u_2(s)|ds \\ -\int_0^T \psi'(s)\left(\psi(T)-\psi(s)\right)|u_2(s)-u_1(s)|\,ds\end{pmatrix}\end{pmatrix} \\
&+\frac{1}{\Gamma(\alpha)}\int_0^t \psi'(s)\left(\psi(t)-\psi(s)\right)^{\alpha-1}|u_1(s)-u_2(s)|ds
\end{aligned}$$

$$\begin{aligned}
&\leq \frac{\left(\psi(T)-\psi(0)\right)^{\alpha}}{\Gamma(\alpha)}\|u_1-u_2\|+\frac{\left(\psi(T)-\psi(0)\right)^{\alpha-2}}{\Gamma(\alpha-1)}\left(\varphi(T)\left(\psi(T)-\psi(0)\right)+\frac{\left(\psi(T)-\psi(0)\right)^2}{2}\right)\|u_1-u_2\| \\
&+\frac{\left(\psi(T)-\psi(0)\right)^{\alpha-3}}{\Gamma(\alpha-2)}\begin{pmatrix}+\frac{\left(\psi(T)-\psi(0)\right)^3}{6}+\frac{\left(\psi(T)-\psi(0)\right)^3}{2} \\ -\varphi^2(T)\left(\psi(T)-\psi(0)\right)+\varphi(T)\frac{\left(\psi(T)-\psi(0)\right)^2}{2}\end{pmatrix}\|u_1-u_2\| \\
&+\frac{\left(\psi(T)-\psi(0)\right)^{\alpha}}{\Gamma(\alpha+1)}\|u_1-u_2\|
\end{aligned}$$

Taking supremum for all $t \in T$, we have

$$\begin{aligned}
\left|\wp\left(y_1(t)\right)-\wp\left(y_2(t)\right)\right| &\leq \begin{pmatrix}\frac{\left(\psi(T)-\psi(0)\right)^{\alpha}}{\Gamma(\alpha+1)}+\frac{\left(\psi(T)-\psi(0)\right)^{\alpha}}{\Gamma(\alpha)}+\varphi(T)\frac{\left(\psi(T)-\psi(0)\right)^{\alpha-1}}{\Gamma(\alpha-1)} \\ +\frac{\left(\psi(T)-\psi(0)\right)^{\alpha}}{2\Gamma(\alpha-1)}+\frac{2\left(\psi(T)-\psi(0)\right)^{\alpha}}{3\Gamma(\alpha-2)} \\ -\varphi^2(T)\frac{\left(\psi(T)-\psi(0)\right)^{\alpha-2}}{\Gamma(\alpha-2)}+\varphi(T)\frac{\left(\psi(T)-\psi(0)\right)^{\alpha-1}}{2\Gamma(\alpha-2)}\end{pmatrix}\|u_1-u_2\| \\
&\leq \begin{pmatrix}\frac{\left(\psi(T)-\psi(0)\right)^{\alpha}}{\Gamma(\alpha+1)}+\frac{\left(\psi(T)-\psi(0)\right)^{\alpha}}{\Gamma(\alpha)}+\varphi(T)\frac{\left(\psi(T)-\psi(0)\right)^{\alpha-1}}{\Gamma(\alpha-1)} \\ +\frac{\left(\psi(T)-\psi(0)\right)^{\alpha}}{2\Gamma(\alpha-1)}+\frac{2\left(\psi(T)-\psi(0)\right)^{\alpha}}{3\Gamma(\alpha-2)} \\ -\varphi^2(T)\frac{\left(\psi(T)-\psi(0)\right)^{\alpha-2}}{\Gamma(\alpha-2)}+\varphi(T)\frac{\left(\psi(T)-\psi(0)\right)^{\alpha-1}}{2\Gamma(\alpha-2)}\end{pmatrix}\frac{\|\lambda\|}{\mathcal{M}}\|y_1-y_2\| \\
&\leq \left(\aleph+\frac{\left(\psi(T)-\psi(0)\right)^{\alpha}}{\Gamma(\alpha+1)}\right)\frac{\|\lambda\|}{\mathcal{M}}\|y_1-y_2\|.
\end{aligned}$$

Thus,

$$\|\wp(y_1) - \wp(y_2)\| \leq \Delta \|y_1 - y_2\|,$$

where $\Delta = \left(\aleph + \frac{(\psi(T)-\psi(0))^{\alpha}}{\Gamma(\alpha+1)}\right)\frac{\|\lambda\|}{\mathcal{M}}$. By taking $\Delta < 1$, we obtain that the operator $\wp$ is contraction.

Applying Krasnselskii's fixed point theorem, we deduce that the nonlinear fractional differential equation NLIFDE (1) has at least one solution. □

Theorem 2.2. If assumptions (H_1) and (H_2) hold, and if

$$\left(\aleph + \frac{(\psi(T) - \psi(0))^{\alpha}}{\Gamma(\alpha + 1)}\right)\frac{\|\lambda\|}{\mathcal{M}} < 1,$$

then NLIFDE (1) has a unique solution on $J = [0, T]$.

Proof. The existence of at least one solution for NLIFDE (1) has been established in Theorem 2.1. Furthermore, Lemma 2.3 demonstrates that the operator $\wp$ exhibits contraction properties. Consequently, through Banach's fixed point theorem, we conclude that the operator $\wp$ possesses a single fixed point, which corresponds to a unique solution of the NLIFDE (1) over the interval $J = [0, T]$. Thus, the proof is now fully accomplished. □

Numerical Example

Consider the following NLIFDE:

$$\begin{cases} \mathfrak{D}^{\frac{11}{5},2t^3+1}y(t) = \dfrac{\sqrt{2t+1}}{59e^{2t+1}}\left[\dfrac{11 + y(t) + \mathfrak{D}^{\frac{3}{5},2t^3+1}y(t) + \int_0^1 e^{3(t-s)}\ \mathfrak{D}^{\frac{11}{5},2t^3+1}y(s)ds}{1 + y(t) + \mathfrak{D}^{\frac{3}{5},2t^3+1}y(t) + 2\int_0^1 e^{3(t-s)}\ \mathfrak{D}^{\frac{11}{5},2t^3+1}y(s)ds}\right] \text{ for all } t \in [0,1], \\ y(0) + \mathfrak{D}_{0^+}^{\frac{6}{5},2t^3+1}y(1) = 1.5, \\ \mathfrak{D}_{0^+}^{\frac{6}{5},2t^3+1}y(0) + \mathfrak{D}_{0^+}^{\frac{1}{5},2t^3+1}y(1) = 2.5, \\ \mathfrak{D}_{0^+}^{\frac{1}{5},2t^3+1}y(0) + \mathfrak{D}_{0^+}^{\frac{-4}{5},2t^3+1}y(1) = 3.5. \end{cases} \quad (13)$$

In this problem, we have $\alpha = \frac{11}{5}$, $\beta = \frac{3}{5}$, $\psi(t) = 2t^3 + 1$ which is an increasing function on $[0,1]$, $K(t,s) = e^{3(t-s)}$, $\sigma_1 = 1.5$,$\sigma_2 = 2.5$, $\sigma_3 = 3.5$.

It is clear that the assumptions (H_1) and (H_2) are satisfied, and f is a mutually continuous function such that for any $u, v, w \in R$, and $t \in [0,1]$ we have

$$|f(t,u,v,w)| = \frac{\sqrt{2t+1}}{59e^{2t+1}}(11 + |u| + |v| + |w|),$$

with $\lambda(t) = \frac{\sqrt{2t+1}}{59e^{2t+1}}$, $F = \frac{11}{59e}$, $\|\lambda\| = \frac{1}{59e}$, and $K = e^3$.

It is clear from Theorem 2.1 that the nonlinear fractional integral differential equation (NLIFDE) (13) possesses at least one solution within the interval [0,1] since

$$\frac{\|\lambda\|\aleph}{\mathcal{M}} = \left(\frac{1}{59e}\right)\frac{17.8487}{0.86154} \approx 0.129177 < 1,$$

Moreover, by employing Theorem 2.2,the solution is unique since

$$\left(\aleph + \frac{\left(\psi(T) - \psi(0)\right)^{\alpha}}{\Gamma(\alpha+1)}\right)\frac{\|\lambda\|}{\mathcal{M}} \approx 0.142895 < 1.$$

Conclusion

In conclusion, this article has delved into the intricate realm of nonlinear implicit ψ-Caputo fractional differential equations (NLIFDEs) with two-point fractional derivatives boundary conditions in Banach algebra. Through the application of Banach's and Krasnoselskii's fixed point theorems, we have rigorously established the existence and uniqueness of solutions within this complex mathematical framework.

Our investigation sheds light on the behavior of solutions for NLIFDEs, providing valuable insights into their dynamics and properties. By addressing this challenging class of differential equations, we contribute to advancing the understanding of nonlinear fractional differentials and their applications across diverse fields, including mathematical physics, engineering sciences, and computational mathematics.

Future research endeavors could extend this work by exploring additional classes of NLIFDEs with different types of boundary conditions or investigating the stability and numerical methods for solving such equations. By continuing to push the boundaries of knowledge in fractional calculus, we can unlock new avenues for modeling and analyzing complex phenomena in various scientific and engineering disciplines.

Scientific Ethics Declaration

The authors declare that the scientific ethical and legal responsibility of this article published in EPSTEM journal belongs to the authors.

Acknowledgements or Notes

* This article was presented as an oral presentation at the International Conference on Basic Sciences, Engineering and Technology (www.icbaset.net) held in Alanya/Turkey on May 02-05, 2024.

* The authors gratefully acknowledge the invaluable contributions of the anonymous referees whose insightful comments and constructive feedback greatly enhanced the quality and clarity of this article. Their expertise and dedication have been instrumental in shaping the final version of the manuscript.

* AMS Subject Classification: 26A33, 34A08, 34B15, 47H10, 34D20

References

Almeida, R. (2017). A Caputo fractional derivative of a function with respect to another function. *Communications in Nonlinear Science and Numerical Simulation*, *44*, 460–481.

Agarwal, R. P., Benchohra, M., & Hamani, S. (2009). Boundary value problems for fractional differential equations. *Georgian Mathematical Journal*, *16*(3), 401–411.

Agrawal, O. P. (2012). Some generalized fractional calculus operators and their applications in integral equations. *Fractional Calculus and Applied Analysis*, *15*(4), 700–711.

Awad, Y. (2023). Well posedness and stability for the nonlinear φ-caputo hybrid fractional boundary value problems with two-point hybrid boundary conditions. *Jordan Journal of Mathematics and Statistics (JJMS)*, *16*(4), 617–647.

Awad, Y., & Alkhezi, Y. (2023). Analysis of implicit solutions for a coupled system of hybrid fractional order differential equations with hybrid integral boundary conditions in banach algebras. *Symmetry*, *15*(9), 1758.

Awad, Y., & Kaddoura, I. (2024). On the Ulam-Hyers-Rassias stability for a boundary value problem of implicit ψ-Caputo fractional integro-differential equation. *TWMS Journal of Apllications & Engineering*, *14*(1), 79-93.

Awad, Y. (2023). On the existence and stability of positive solutions of eigenvalue problems for a class of p-laplacian ψ -caputo fractional integro-differential equations. *Journal of Mathematics*, *2023*.

Awad, Y., Fakih, H., & Alkhezi, Y. (2023). Existence and uniqueness of variable-order φ-caputo fractional two-point nonlinear boundary value problem in banach algebra. *Axioms*, *12*(10), 935.

Awad, Y. (2024). Exploring solutions for nonlinear fractional differential equations with multiple fractional derivatives and integral boundary conditions. *Jordan Journal of Mathematics and Statistics (JJMS)*.

Benlabbes, A., Benbachir, M., & Lakrib, M. (2015). Boundary value problems for nonlinear fractional differential equations. *Facta Universitatis-Series: Mathematics and Informatics*, *30*(2), 157–168.

Burton, T. A., & Kirk, C. (1998). A fixed-point theorem of krasnoselskii-schaefer type. *Mathematische Nachrichten*, *189*(1), 23–31.

Derbazi, C., & Hammouche, H. (2020). Existence and uniqueness results for a class of nonlinear fractional differential equations with nonlocal boundary conditions. *Jordan Journal of Mathematics and Statistics (JJMS)*, *13*(3), 341–361.

Kaddoura, I., & Awad, Y. (2023). Stability results for nonlinear implicit ϑ-caputo fractional differential equations with fractional integral boundary conditions. *International Journal of Differential Equations*, *20*(3),579-597.

Kilbas, A. A., Srivastava, H. M., & Trujillo, J. J. (2006). *Theory and applications of fractional differential equations.* Elsevier.

Maamar, B. (2015). Boundary value problems for nonlinear fractional differential equations. *Facta Universitatis, Series: Mathematics and Informatics*, *30*(2), 157–168.

Samko, S. G., Kilbas, A. A., & Marichev, O. I. (1993). *Fractional integrals and derivatives*. Gordon and Breach Science Publishers.

Zhang, S. (2006). Positive solutions for boundary-value problems of nonlinear fractional differential equations. *Electronic Journal of Differential Equations*, *36*, 1–12.

Author Information

Yahia Awad
Lebanese International University (LIU)
Department of Mathematics and Physics
AlKhyara, West Bekaa, Lebanon.
Contact e-mail: *yehya.awad@liu.edu.lb*

Haissam Chehade
Lebanese International University (LIU)
Department of Mathematics and Physics
Saida, Lebanon.
The International University of Beirut (BIU)
Department of Mathematics and Physics
Beirut, Lebanon.

To cite this article:

Awad, Y. & Chehade, H. (2024). Analysis of solutions for nonlinear ψ-caputo fractional differential equations with fractional derivative boundary conditions in banach algebra. *The Eurasia Proceedings of Science, Technology, Engineering & Mathematics (EPSTEM), 28,* 360-374.

The Eurasia Proceedings of Science, Technology, Engineering & Mathematics (EPSTEM)
ISSN: 2602-3199

The Eurasia Proceedings of Science, Technology, Engineering & Mathematics (EPSTEM), 2024

Volume 28, Pages 375-381

ICBASET 2024: International Conference on Basic Sciences, Engineering and Technology

General Upper Bounds for the Numerical Radii of Hilbert Space Operators

Mohammed Al-Dolat
Jordan University of Science and Technology

Abstract: We present a collection upper bounds for the numerical radii of a certain 2×2 operator matrices. We use these bounds to improve on some known numerical radius inequalities for powers of Hilbert space operators. In particular, we show that if A is a bounded linear operator on a complex Hilbert space, then $w^{2r}(A) \leq \frac{1+\alpha}{8}\||A|^{2r} + |A^*|^{2r}\| + \frac{1+\alpha}{4} w(|A|^r|A^*|^r) + \frac{1-\alpha}{2} w^r(A^2)$ for every r ≥ 1 and $\alpha \in [0,1]$. This substantially improves on the existing inequality $w^{2r}(A) \leq \frac{1}{2}\||A|^{2r} + |A^*|^{2r}\|$. Here $w(.)$ and $||.||$ denote the numerical radius and the usual operator norm, respectively.

Keywords: Numerical radius, Usual operator norm, Operator matrix, Buzano ′s inequality.

Introduction

Let $\mathcal{B}(\mathcal{H})$ be the C^*-algebra of all bounded linear operators on the complex Hilbert space $\mathcal{H}$. For $T \in \mathcal{B}(\mathcal{H})$, the numerical radius $w(.)$ and the usual operator norm $||.||$ are, respectively, defined by

$$w(A) = \sup_{||x||=1} |\langle Ax, x\rangle| \text{ and } \|A\| = \sup_{||x||=1} \|Ax\|.$$

It is clear that $w(.)$ defines a norm on $\mathcal{B}(\mathcal{H})$. Moreover, it is known that $w(.)$ is equivalent to the usual operator norm $||.||$ on $\mathcal{B}(\mathcal{H})$ and with the following two sided inequality

$$\frac{1}{2}\|A\| \leq w(A) \leq \|A\| \text{ for every } A \in \mathcal{B}(\mathcal{H}). \quad (1.1)$$

An important property for the numerical radius is the power inequality, which says that

$$w(A^n) \leq w^n(A) \text{ for every } n \in \mathbb{N} \text{ and } A \in \mathcal{B}(\mathcal{H}).$$

In Kittaneh (2005), the author provided refinements of the bounds in (1.1) by showing that

$$\frac{1}{4}\||A|^2 + |A^*|^2\| \leq w^2(A) \leq \frac{1}{2}\||A|^2 + |A^*|^2\| \text{ for every } A \in \mathcal{B}(\mathcal{H}). \quad (1.2)$$

In El-Haddad and Kittaneh (2007) the authors provided a generalization for the second inequality in (1.2) by showing that

$$w^{2r}(A) \leq \frac{1}{2}\||A|^{2r} + |A^*|^{2r}\| \text{ for every r} \geq 1 \text{ and A} \in \mathcal{B}(\mathcal{H}). \quad (1.3)$$

In Dragomir (2009), the author presented an important upper bound for the numerical radii of products of two operators by showing that if $A, B \in \mathcal{B}(\mathcal{H})$ and $r \geq 1$, then

$$w^r(B^*A) \leq \frac{1}{2}\||A|^{2r} + |B|^{2r}\|. \tag{1.4}$$

Recently in Al-dolat and Kittaneh (2023), the authors gave another improvement for the inequality in (1.3) by showing that if $A \in \mathcal{B}(\mathcal{H})$, then

$$w^{2r}(A) \leq \frac{1+\alpha}{4}\||A|^{2r} + |A^*|^{2r}\| + \frac{1-\alpha}{2}w^r(A^2) \tag{1.5}$$

for every $\alpha \in [0,1]$ and $r \geq 1$.

The direct sum of $2-$copies of $\mathcal{H}$ is denoted by $\mathcal{H}^{(2)} = \mathcal{H} \oplus \mathcal{H}$. Due to this decomposition, any $T \in \mathcal{B}(\mathcal{H}^{(2)})$ can be represented as a 2×2 operator matrix of the form $T = \begin{bmatrix} A & B \\ C & D \end{bmatrix}$, where $A, B, C, D \in \mathcal{B}(\mathcal{H})$. Moreover, if $x = \begin{pmatrix} x_1 \\ x_2 \end{pmatrix} \in \mathcal{H}^{(2)}$, then Tx is defined by $Tx = T\begin{pmatrix} x_1 \\ x_2 \end{pmatrix} = \begin{pmatrix} Ax_1 + Bx_2 \\ Cx_1 + Dx_2 \end{pmatrix}$. To learn more about the numerical radii of operator of matrices and their application in finding estimates for the zeros of complex polynomials, one cane refer to Abo-Omar and Kittaneh (2015), Al-Dolat et al. (2016), Bani-Domi and Kittaneh (2008), Bani-Domi and Kittaneh (2009), Bani Domi and Kittaneh (2012) and Hirzallah et al. (2011).

The goal of this paper is to present several new upper bounds for the numerical radii of 2×2 operator matrices, then to refine the inequalities in (1.3) based on those bounds. Moreover, we provide refinements of earlier numerical radius inequalities due to Al-Dolat and Kittaneh (2023).

Main Results

To achieve our goal, we recall some well-known lemmas in order to establish our results. The first lemma is a consequence of the spectral theorem and Jensen ′s inequality see Kittaneh (2015).

Lemma 2.1 *Let $A \in \mathcal{B}(\mathcal{H})$ be a positive operator and $x \in \mathcal{H}$ be any unit vector. Then, for $r \geq 1$, we have*

$$\langle Ax, x\rangle^r \leq \langle A^r x, x\rangle.$$

The second lemma deals with non-negative convex functions and positive operators, and it can be found in Aujla and Sivla (2003).

Lemma 2.2 *Let f be a non-negative convex function on $[0,\infty)$ and $A, B \in \mathcal{B}(\mathcal{H})$ be positive operators. Then*

$$\left\|f\left(\frac{A+B}{2}\right)\right\| \leq \left\|\frac{f(A)+f(B)}{2}\right\|.$$

In particular,

$$\|(A+B)^r\| \leq 2^{r-1}\|A^r + B^r\| \quad \text{for every } r \geq 1.$$

The third lemma relates to certain 2×2 operator matrices and can be found in Hirzallah, Kittaneh and Shebrawi (2011).

Lemma 2.3 *Let $A, B \in \mathcal{B}(\mathcal{H})$. Then*

(a) $w\left(\begin{bmatrix} A & 0 \\ 0 & B \end{bmatrix}\right) = \max\{w(A), w(B)\}$;

(b) $w\left(\begin{bmatrix} A & B \\ B & A \end{bmatrix}\right) = \max\{w(A+B), w(A-B)\}$.

In particular,

$$w\left(\begin{bmatrix} 0 & B \\ B & 0 \end{bmatrix}\right) = w(B).$$

The next two lemmas can be found in Al-Dolat and Kittaneh (2023).

Lemma 2.4 *Let $x, y, z \in \mathcal{H}$ with $\|z\| = 1$. Then*

$$|\langle x, z\rangle\langle z, y\rangle|^r \leq \frac{1+\alpha}{2}\|x\|^r\|y\|^r + \frac{1-\alpha}{2}|\langle x, y\rangle|^r$$

for every $\alpha \in [0,1]$ and $r \geq 1$.

Lemma 2.5 *Let $x, y, z \in \mathcal{H}$ with $||z|| = 1$. Then*

$$|\langle x, z\rangle\langle z, y\rangle|^2 \leq \frac{1+\alpha}{4}\|x\|^2\|y\|^2 + \frac{1-\alpha}{4}|\langle x, y\rangle|^2 + \frac{1}{2}\|x\|\|y\||\langle x, y\rangle|$$

for every $\alpha \in [0,1]$.

The final lemma can be found in Al-Dolat and Al-Zoubi.

Lemma 2.6 *Let $S, R \in \mathcal{B}(\mathcal{H})$ be positive operators and let $q \geq 1$. Then*

$$\sup_{x\in\mathcal{H}, ||x||=1}(\langle Sx, x\rangle^q\langle Rx, x\rangle^q) \leq \frac{1}{4}\|S^{2q} + R^{2q}\| + \frac{1}{2}\min\{w(S^qR^q), w(S^qR^q)\}.$$

We begin our results by the following theorem, which provides a new upper bound for the numerical radii of 2×2 operator matrices, that will be used to give a refinement of the inequality (1.3).

Theorem 2.7 *Let $B, C \in \mathcal{B}(\mathcal{H})$. Then*

$$w^{2r}\left(\begin{bmatrix} 0 & B \\ C & 0 \end{bmatrix}\right) \leq \frac{1+\alpha}{8}\max\{\||C|^{2r} + |B^*|^{2r}\|, \||B|^{2r} + |C^*|^{2r}\|\}$$

$$+\frac{1+\alpha}{4}\min\{\max\{w(|C|^r|B^*|^r), w(|B|^r|C^*|^r)\}, \max\{w(|B^*|^r|C|^r), w(|C^*|^r|B|^r)\}\}$$

$$+\frac{1-\alpha}{2}\max\{w^r(BC), w^r(CB)\}$$

for every $\alpha \in [0,1]$ and $r \geq 1$.

Proof. Let $T = \begin{bmatrix} 0 & B \\ C & 0 \end{bmatrix}$ and let $x \in \mathcal{H}^{(2)}$ be any unit vector. Then we have

$$|\langle Tx, x\rangle|^{2r} = |\langle Tx, x\rangle\langle x, T^*x\rangle|^r$$

$$\leq \frac{1+\alpha}{2}\|Tx\|^r\|T^*x\|^r + \frac{1-\alpha}{2}|\langle Tx, T^*x\rangle|^r \quad \text{(by Lemma 2.4)}$$

$$= \frac{1+\alpha}{2}\langle|T|^2x, x\rangle^{\frac{r}{2}}\langle|T^*|^2x, x\rangle^{\frac{r}{2}} + \frac{1-\alpha}{2}|\langle T^2x, x\rangle|^r.$$

Thus,

$$w^{2r}(T) = \sup_{\|x\|=1} |\langle Tx, x\rangle|^{2r}$$

$$\leq \frac{1+\alpha}{2} \sup_{\|x\|=1} \left(\langle |T|^2x, x\rangle^{\frac{r}{2}} \langle |T^*|^2x, x\rangle^{\frac{r}{2}}\right) + \frac{1-\alpha}{2} w^r(T^2)$$

$$\leq \frac{1+\alpha}{8} \| |T|^{2r} + |T^*|^{2r} \| + \frac{1+\alpha}{4} \min\{w(|T|^r|T^*|^r), w(|T^*|^r|T|^r)\} + \frac{1-\alpha}{2} w^r(T^2)$$

$$= \frac{1+\alpha}{8} \left\| \begin{bmatrix} |C|^{2r} + |B^*|^{2r} & 0 \\ 0 & |B|^{2r} + |C^*|^{2r} \end{bmatrix} \right\|$$

$$+ \frac{1+\alpha}{4} \min\left\{ w\left(\begin{bmatrix} |C|^r|B^*|^r & 0 \\ 0 & |B|^r|C^*|^r \end{bmatrix} \right), w\left(\begin{bmatrix} |B^*|^r|C^*|^r & 0 \\ 0 & |C^*|^r|B^*|^r \end{bmatrix} \right) \right\}$$

$$+ \frac{1-\alpha}{2} w^r\left(\begin{bmatrix} BC & 0 \\ 0 & CB \end{bmatrix} \right)$$

$$\leq \frac{1+\alpha}{8} \max\{ \| |C|^{2r} + |B^*|^{2r} \|, \| |B|^{2r} + |C^*|^{2r} \| \}$$

$$+ \frac{1+\alpha}{4} \min\left\{ \max\{w(|C|^r|B^*|^r), w(|B|^r|C^*|^r)\}, \max\{w(|B^*|^r|C|^r), w(|C^*|^r|B|^r)\} \right\}$$

$$+ \frac{1-\alpha}{2} \max\{w^r(BC), w^r(CB)\}$$

This completes the proof of the theorem.

As a direct consequence of the above theorem we have the following refinement of the inequality (1.5).

Corollary 2.8 *Let $A \in \mathcal{B}(\mathcal{H})$. Then*

$$w^{2r}(A) \leq \frac{1+\alpha}{8} \| |A|^{2r} + |A^*|^{2r} \| + \frac{1+\alpha}{4} w(|A|^r|A^*|^r) + \frac{1-\alpha}{2} w^r(A^2)$$

$$\leq \frac{1+\alpha}{4} \| |A|^{2r} + |A^*|^{2r} \| + \frac{1-\alpha}{2} w^r(A^2)$$

for every $\alpha \in [0,1]$ and $r \geq 1$.

Proof. By letting $B = C = A$ in Theorem 2.7, we get

$$w^{2r}(A) \leq w^{2r}\left(\begin{bmatrix} 0 & A \\ A & 0 \end{bmatrix} \right) \quad \text{(by Lemma2.1)}$$

$$\leq \quad + \quad + \frac{1+\alpha}{4} w(|A|^r|A^*|^r) \quad \frac{1-\alpha}{2} w^r(A^2) \quad \text{(by Theorem 2.7)}$$

$$\leq \quad + \quad \quad \quad \frac{1-\alpha}{2} w^r(A^2) \quad \text{(by the inequality (1.4))}$$

$$= \frac{1+\alpha}{4} \| |A|^{2r} + |A^*|^{2r} \| + \frac{1-\alpha}{2} w^r(A^2)$$

Remark 2.9 *The upper bound in Corollary 2.8 is a refinement of [Al-Dolat and Kittaneh (2023), Theorem 2.7], namely*

$$w^{2r}\left(\begin{bmatrix}0 & B\\ C & 0\end{bmatrix}\right) \le \frac{1+\alpha}{4}\max\{\||B|^{2r}+|C^*|^{2r}\|, \||C|^{2r}+|B^*|^{2r}\|\} + \frac{1-\alpha}{2}\max\{w^r(CB), w^r(BC)\}$$

To explain this, note that

$$w^{2r}\left(\begin{bmatrix}0 & B\\ C & 0\end{bmatrix}\right) \le \tfrac{1+\alpha}{8}\max\{\||B|^{2r}+|C^*|^{2r}\|, \||C|^{2r}+|B^*|^{2r}\|\}$$

$$+\frac{1+\alpha}{4}\min\big\{\max\{w(|C|^r|B^*|^r), w(|B|^r|C^*|^r)\}, \max\{w(|B^*|^r|C|^r), w(|C^*|^r|B|^r)\}\big\}$$

$$+\tfrac{1-\alpha}{2}\max\{w^r(CB), w^r(BC)\}$$

$$\le \tfrac{1+\alpha}{8}\max\{\||B|^{2r}+|C^*|^{2r}\|, \||C|^{2r}+|B^*|^{2r}\|\}$$

$$+\tfrac{1+\alpha}{8}\max\{\||B|^{2r}+|C^*|^{2r}\|, \||C|^{2r}+|B^*|^{2r}\|\}$$
$$+\tfrac{1-\alpha}{2}\max\{w^r(CB), w^r(BC)\} \quad \text{(by the inequality (1.4))}$$

$$= \tfrac{1+\alpha}{4}\max\{\||B|^{2r}+|C^*|^{2r}\|, \||C|^{2r}+|B^*|^{2r}\|\} + \tfrac{1-\alpha}{2}\max\{w^r(CB), w^r(BC)\}.$$

We are now in a position to prove our next result.

Theorem 2.10 *Let $B, C \in \mathcal{B}(\mathcal{H})$. Then*

$$w^4\left(\begin{bmatrix}0 & B\\ C & 0\end{bmatrix}\right) \le \tfrac{1+\alpha}{16}\max\{\||B|^4+|C^*|^4\|, \||C|^4+|B^*|^4\|\}$$

$$+\frac{1+\alpha}{8}\min\big\{\max\{w(|C|^2|B^*|^2), w(|B|^2|C^*|^2)\}, \max\{w(|B^*|^2|C|^2), w(|C^*|^2|B|^2)\}\big\}$$

$$+\tfrac{1-\alpha}{4}\max\{w^2(CB), w^2(BC)\}$$

$$+\tfrac{1}{4}\max\{w(CB), w(BC)\}\max\{\||B|^2+|C^*|^2\|, \||C|^2+|B^*|^2\|\}$$

for every $\alpha \in [0,1]$.

Proof. Let $T = \begin{bmatrix}0 & B\\ C & 0\end{bmatrix}$ and let $x \in \mathcal{H}^{(2)}$ be any vector. Then

$$|\langle Tx, x\rangle|^4 = |\langle Tx, x\rangle\langle x, T^*x\rangle|^2$$

$$\le \tfrac{1+\alpha}{4}\|Tx\|^2\|T^*x\|^2 + \tfrac{1-\alpha}{4}|\langle Tx, T^*x\rangle|^2 + \tfrac{1}{2}\|Tx\|\|T^*x\||\langle Tx, T^*x\rangle|$$

$$\le \tfrac{1+\alpha}{4}(|\langle|T|^2x, x\rangle||\langle|T^*|^2x, x\rangle|) + \tfrac{1-\alpha}{4}|\langle T^2x, x\rangle|^2 + \tfrac{1}{4}|\langle T^2x, x\rangle|(\|Tx\|^2 + \|T^*x\|^2)$$

(by the triangle inequality)

$$= \tfrac{1+\alpha}{4}(|\langle|T|^2x, x\rangle||\langle|T^*|^2x, x\rangle|) + \tfrac{1-\alpha}{4}|\langle T^2x, x\rangle|^2 + \tfrac{1}{4}|\langle T^2x, x\rangle|\langle(|T|^2 + |T^*|^2)x, x\rangle.$$

Thus,

$$w^4(T) = \sup_{\|x\|=1}|\langle Tx, x\rangle|^4$$

$$\leq \frac{1+\alpha}{4}\sup_{\|x\|=1}(|\langle|T|^2x,x\rangle||\langle|T^*|^2x,x\rangle|)+\frac{1-\alpha}{4}w^2(T^2)+\frac{1}{4}w(T^2)\||T|^2+|T^*|^2\|$$

$$\leq \frac{1+\alpha}{16}\||T|^4+|T^*|^4\|+\frac{1+\alpha}{8}\min\{w(|T|^2|T^*|^2),w(|T^*|^2|T|^2)\}$$

$$+\frac{1-\alpha}{4}w^2(T^2)+\frac{1}{4}w(T^2)\||T|^2+|T^*|^2\|$$

$$=\frac{1+\alpha}{16}\max\{\||B|^4+|C^*|^4\|,\||C|^4+|B^*|^4\|\}$$

$$+\frac{1+\alpha}{8}\min\big\{\max\{w(|C|^2|B^*|^2),w(|B|^2|C^*|^2)\},\max\{w(|B^*|^2|C|^2),w(|C^*|^2|B|^2)\}\big\}$$

$$+\frac{1-\alpha}{4}\max\{w^2(CB),w^2(BC)\}$$

$$+\frac{1}{4}\max\{w(CB),w(BC)\}\max\{\||B|^2+|C^*|^2\|,\||C|^2+|B^*|^2\|\}.$$

As a special case of Theorem 2.10 we have the following refinement of the inequality (1.3) for the special $r=2$.

Corollary 2.11 *Let $A\in\mathcal{B}(\mathcal{H})$ and let $\alpha\in[0,1]$. Then*

$$w^4(A)\leq\frac{1+\alpha}{16}\||A|^4+|A^*|^4\|+\frac{1+\alpha}{8}\min\{w(|A|^2|A^*|^2),w(|A^*|^2|A|^2)\}$$

$$+\frac{1-\alpha}{4}w^2(A^2)+\frac{1}{4}w(A^2)\||A|^2+|A^*|^2\|$$

$$\leq\frac{1}{2}\||A|^4+|A^*|^4\|.$$

Proof. Let $B=C=A$ in the above theorem. Then we have

$$w^4(A)=w\left(\begin{bmatrix}0&A\\A&0\end{bmatrix}\right)\ \text{(by Lemma2.1)}$$

$$\leq\frac{1+\alpha}{16}\||A|^4+|A^*|^4\|+\frac{1+\alpha}{8}\min\{w(|A|^2|A^*|^2),w(|A^*|^2|A|^2)\}$$

$$+\frac{1-\alpha}{4}w^2(A^2)+\frac{1}{4}w(A^2)\||A|^2+|A^*|^2\|\ \text{(by Theorem 2.10)}$$

$$\leq\frac{1+\alpha}{16}\||A|^4+|A^*|^4\|+\frac{1+\alpha}{16}\||A|^4+|A^*|^4\|+\frac{1-\alpha}{8}\||A|^4+|A^*|^4\|\quad+\frac{1}{8}\||A|^2+|A^*|^2\|^2$$
(by the inequality (1.4))

$$=\frac{1}{4}\||A|^4+|A^*|^4\|+\frac{1}{8}\|(|A|^2+|A^*|^2)^2\|$$

(by the fact: If $X\in\mathcal{B}(\mathcal{H})$ is normaland $n\in\mathbb{N}$, then$||X^n||=||X||^n$)

$$\leq\frac{1}{4}\||A|^4+|A^*|^4\|+\frac{1}{4}\||A|^4+|A^*|^4\|\ \text{(by Lemma 2.2)}$$

$$=\frac{1}{2}\||A|^4+|A^*|^4\|.$$

At the end of this paper, we remark that the upper bound obtained in Theorem 2.10 is better than the upper bound given in Al-Dolat and Kittaneh (2023), (Theorem 2.12).

Scientific Ethics Declaration

The author declares that the scientific ethical and legal responsibility of this article published in EPSTEM journal belongs to the author.

Acknowledgements or Notes

* This article was presented as an oral presentation at the International Conference on Basic Sciences, Engineering and Technology (www.icbaset.net) held in Alanya/Turkey on May 02-05, 2024.

* MSC(2010): 47A12, 47A30, 47A63, 47B15.

References

Abu-Omar, A. and Kittaneh, F. (2015) Numerical radius inequalities for $n \times n$ operator matrices. *Linear Algebra Applications, 468,* 18-26.

Al-Dolat, M., Al-Zoubi, K., Ali, M., & Bani-Ahmad, F. (2016). General numerical radius inequalities for matrices of operators. *Open Mathematics*, *14*(1), 109-117.

Al-Dolat, M., & Kittaneh, F. (2024). Upper bounds for the numerical radii of powers of Hilbert space operators. *Quaestiones Mathematicae*, *47*(2), 341-352.

Al-Dolat, M. & Al-Zoubi, K. (2024). *Improved and refined numerical radius inequalities for Hilbert space operators*. Retrieved from https://assets.researchsquare.com/files/rs2668438/v1/a5b67b067e6f6fddcf09cb22.pdf

Aujla, J. S., & Silva, F. C. (2003). Weak majorization inequalities and convex functions. *Linear Algebra and Its Applications*, *369*, 217-233.

Bani-Domi, W., & Kittaneh, F. (2008). Norm equalities and inequalities for operator matrices. *Linear Algebra and Its Applications*, *429*(1), 57-67.

Bani-Domi, W., & Kittaneh, F. (2009). Numerical radius inequalities for operator matrices. *Linear and Multilinear Algebra*, *57*(4), 421-427.

Bani-Domi, W., & Kittaneh, F. (2021). Norm and numerical radius inequalities for Hilbert space operators. *Linear and Multilinear Algebra*, *69*(5), 934-945.

Bani-Domi, W., & Kittaneh, F. (2021). Refined and generalized numerical radius inequalities for 2×2 operator matrices. *Linear Algebra and Its Applications*, *624*, 364-386.

Dragomir, S.S. (2009). Power inequalities for the numerical radius of a product of two operators in Hilbert spaces. *Sarajevo J Math. 18*, 269-278.

El-Haddad, M., & Kittaneh, F. (2007). Numerical radius inequalities for Hilbert space operators. II. *Studia Mathematica*, *182*, 133-140.

Hirzallah, O. Kittaneh, F. & Shebrawi, K. (2011) Numerical radius inequalities for certain 2×2 operator matrices. *Integr. Equ. Oper. Theory*, *71*, 129-147.

Kittaneh, F. (1988). Notes on some inequalities for Hilbert space operators. *Publications of the Research Institute for Mathematical Sciences*, *24*(2), 276-293.

Kittaneh, F. (2005). Numerical radius inequalities for Hilbert space operators. *Studia Mathematica*, *168*(1), 73-80.

Author Information

Mohammed Al-Dolat
Department of Mathematics & Statistics, Jordan University of Science and Technology, Irbid, Jordan.
Contact e-mail: *mmaldolat@just.edu.jo*

To cite this article:

Al-Dolat, M. (2024). General upper bounds for the numerical radii of Hilbert space operators *The Eurasia Proceedings of Science, Technology, Engineering & Mathematics (EPSTEM), 28,* 375-381.

The Eurasia Proceedings of Science, Technology, Engineering & Mathematics (EPSTEM)
ISSN: 2602-3199

The Eurasia Proceedings of Science, Technology, Engineering & Mathematics (EPSTEM), 2024

Volume 28, Pages 382-389

ICBASET 2024: International Conference on Basic Sciences, Engineering and Technology

On Graded 2-n-Submodules of Graded Modules Over Graded Commutative Rings

Khaldoun Al-Zoubi
Jordan University of Science and Technology

Abstract: In this article, all rings are commutative with a nonzero identity. Let G be a group with identity e, R be a G-graded commutative ring, and M be a graded R-module. The concept of graded n-ideals was introduced and studied by Al-Zoubi et al. (2019). A proper graded ideal I of R is said to be a graded n-ideal of R if whenever $r,s \in h(R)$ with $rs \in I$ and $r \notin Gr(0)$, then $s \in I$. Recently the notion of graded n-ideals was extended to graded n-submodules by Al-Azaizeh and Al-Zoubi (2023). A proper graded submodule N of a graded R-module M is said to be a graded n-submodule if whenever $t \in h(R)$, $m \in h(R)$ with $tm \in N$ and $t \notin Gr(Ann_R(M))$, then $m \in N$. In this study, we introduce the concept of graded 2-n-submodules of graded modules over graded commutative rings, generalizing the concept of graded n-submodules. We investigate some characterizations of graded 2-n-submodules and investigate the behavior of this structure under graded homomorphism and graded localization. A proper graded submodule U of M is said to be a graded 2-n-submodule if whenever $r,s \in h(R)$, $m \in (M)$ and $rsm \in U$, then $rs \in Gr(Ann_R(M))$ or $rm \in U$ or $tm \in U$..

Keywords: Graded 2-n-submodules, Graded n-submodule, Graded 2-n ideals, Graded 2-nil-ideals

Introduction

Throughout this article, we assume that R is a commutative G-graded ring with identity and M is a unitary graded R-module. The concept of graded primary ideal was introduced and studied in Refai and Al-Zoubi (2004). In Al-Zoubi et al. (2019), the concept of graded 2-absorbing ideals was introduced and studied as a generalization of graded prime ideals. The concept of graded 2-absorbing submodules was introduced and studied in Al-Zoubi and Abu-Dawwas (2014). In Al-Zoubi et al. (2017), the concept of graded 2-absorbing primary ideals was presented and studied. As a generalization of graded 2-absorbing primary ideals, the authors introduced and studied graded 2-absorbing primary submodules in Celikel (2016). In 2019, different type of graded ideal, namely, graded n-ideal, was introduced in Al-Zoubi and Al-Turman (2019). Recently, in Al-Azaizeh and Al-Zoubi (2023), the notion of graded n-ideals was extended to graded n-submodules. In this paper, we introduce the concept of graded 2-n-submodules of graded modules over graded commutative rings, generalizing the concept of graded n-submodules. A number of results concerning graded 2-n-submodules are given. As an example, we characterized graded 2-n-submodules and studied graded 2-n-submodules under graded homomorphism and under graded localization.

Preliminaries

In this section we will give the definitions and results which are required in the next section.

Definition 2.1.

1. Let G be a group with identity e and R be a commutative ring with identity 1_R. Then R is G-graded ring if there exist additive subgroups R_g of R indexed by the elements $g \in G$ such that $R = \bigoplus_{g\in G} R_g$ and $R_g R_h \subseteq R_{gh}$ for all $g, h \in G$. The elements of R_g are called homogeneous of degree g. The set of all homogeneous elements of R is denoted by $h(R)$, i.e. $h(R) = \bigcup_{g\in G} R_g$, see (Nastasescu et al., 2004).

2. Let $R = \bigoplus_{g\in G} R_g$ be G-graded ring, an ideal P of R is called a graded ideal if $P = \sum_{h\in G} P \cap R_h = \sum_{h\in G} P_h$, see (Nastasescu et al., 2004).

3. A left R-module M is said to be a G-graded R-module if $M = \bigoplus_{g\in G} M_g$ with $R_g M_h \subseteq M_{gh}$ for all $g, h \in G$, where M_g is an additive subgroup of M for all $g \in G$. The elements of M_g are called homogeneous of degree g. The set of all homogeneous elements of M is denoted by $h(M)$, i.e, $h(M) = \bigcup_{g\in G} M_g$. Note that M_h is an R_e-module for every $h \in G$. For more properties, see (Nastasescu et al., 2004).

4. A submodule K of M is called a graded submodule of M if $K = \bigoplus_{h\in G} (K \cap M_h) := \bigoplus_{h\in G} K_h$, see (Nastasescu et al., 2004).

5. If K is graded submodule of M, then $(K:_R M) = \{a \in R \mid aM \subseteq K\}$ is graded ideal of R. Furthermore, the annihilator of K in R is denoted and defined by $Ann_R(K) = \{a \in R \mid aK = \{0\}\}$, see (Atani, 2006).

Definition 2.2.

1. A proper graded submodule U of M is said to be a graded n-submodule (briefly, gr-n-submodule) if whenever $r \in h(R)$, $m \in h(M)$ with $rm \in U$ and $r \notin Gr(Ann_R(M))$, then $m \in U$, see (Al-Azaizeh & Al-Zoubi, 2023).

2. The graded radical of a graded ideal I, denoted by $Gr(I)$, is the set of all $t = \sum_{g\in G} t_g \in R$ such that for each $g \in G$ there exists $n_g \in \mathbb{N}$ with $t_g^{n_g} \in I$. Note that, if r is a homogeneous element, then $r \in Gr(I)$ if and only if $r^n \in I$ for some $n \in \mathbb{N}$, see (Refai & Al-Zoubi, 2004).

3. A proper graded submodule P of M is called a graded prime (briefly, gr-prime) submodule if whenever $a \in h(R)$ and $m \in h(M)$ with $am \in P$, then either $a \in (P:_R M)$ or $m \in P$, see (Atani, 2006).

4. A proper graded submodule U of M is called graded primary (briefly, gr-primary) submodule if $rm \in U$, then either $m \in U$ or $r \in Gr((U:_R M))$, where $r \in h(R)$ and $m \in h(M)$, see (Oral et al., 2011)

5. A proper graded submodule N of M is said to be a graded 2-absorbing (briefly, gr-2-absorbing) submodule of M if whenever $r, s \in h(R)$ and $m \in h(M)$ with $rsm \in N$, then either $rm \in N$ or $sm \in N$ or $rs \in (N:_R M)$, see (Al-Zoubi & Abu-Dawwas, 20014).

6. A proper graded submodule U of M is called graded primary (briefly, gr-primary) submodule if $rm \in U$, then either $m \in U$ or $r \in Gr((U:_R M))$, where $r \in h(R)$ and $m \in h(M)$, see (Oral et al., 2011).

7. The graded radical of a graded submodule N of M, denoted by $Gr_M(N)$, is defined to be the intersection of all graded prime submodules of M containing N. If N is not contained in any graded prime submodule of M, then $Gr_M(N) = M$, see (Atani &Farzalipour, 2007).

8. A proper graded submodule N of M is said to be a graded 2-absorbing (briefly, gr-2-absorbing) primary submodule of M if whenever $r, s \in h(R)$ and $m \in h(M)$ with $rsm \in N$, then $rs \in (N:_R M)$ or $rm \in Gr_M(N)$ or $sm \in Gr_M(N)$, see (Celikel, 2016).

9. A proper graded ideal I of R is said to be a graded n-ideal (briefly, gr-n-ideal) of R if whenever $r,s \in h(R)$ with $rs \in I$ and $r \notin Gr(0)$, then $s \in I$, see (Al-Zoubi & Al-Turman, 2019).

10. A proper graded ideal P of R is said to be graded 2-nil (briefly, gr-2-nil) ideal if whenever, $a,b,c \in h(\Im)$ with $abc \in P$, then $ab \in Gr(0)$ or $ac \in P$ or $bc \in P$, see (Abu Qayass &Al-Zoubi, 2023).

11. A graded R-module M is called a graded faithful (briefly, gr- faithful) module if $rM = 0$, then $r = 0$ for $r \in h(R)$, see (Atani, 2006).

12. Let R be a G-graded ring and M, M' be graded R-modules. Let $\varphi: M \to M'$ be an R-module homomorphism. Then φ is said to be a graded homomorphism if $\varphi(M_g) \subseteq M'_g$ for all $g \in G$, see (Nastasescu et al., 2004).

13. A nonzero graded module M is called a graded second (briefly, gr-second) module if $Ann_R(M) = Ann_R(M/N)$ for all graded submodule N of M, see (Ceken & Alkan, 2015)

Characterization of gr-2-n-submodule

In this section, we provide several characterizations of gr-2-n-submodule. We begin by introducing the notion of gr-2-n-submodules.

Definition 3.1 *A proper graded submodule U of M is said to be a graded 2-n-submodule (briefly, gr-2-n-submodule) of M if whenever $r,s \in h(R)$, $m \in (M)$ and $rsm \in U$, then $rs \in Gr(Ann_R(M))$ or $rm \in U$ or $tm \in U$.*

From this previous definition, we can conclude that: every gr-n-submodule is a gr-2-n-submodule, every gr-prime submodule is gr-2-n-submodule. gr-2-n-submodule is a gr-2-absorbing primary submodule. Also, every gr-2-n-submodule U of a graded R-module M satisfying $Gr(Ann_R(M) \subseteq (U:_R M)$ is gr-2-absorbing. The following example shows that these notions are different in general.

Example 3.2 Let p and q be prime integers. Let $G = \mathbb{Z}_2$ and $R = \mathbb{Z}$. Then R is a G-graded ring with $R_0 = \mathbb{Z}$ and $R_1 = \{0\}$. Let $M = \mathbb{Z}$. Then M is a graded R-module with $M_0 = \mathbb{Z}$ and $M_1 = \{0\}$.

(a) Consider the graded submodule $U = p\mathbb{Z}$ of M. Then U is a gr-2-n-submodule since it is gr-prime. Since $p.1 \in U$ but $1 \notin U$ and $p \notin Gr(Ann_R(\mathbb{Z})) = \{0\}$, U is not gr-n-submodule.

(b) Consider the graded submodule $U = pq\mathbb{Z}$ of M. Then U is a gr-2-absorbing (gr-2-absorbing primary) submodule of M. Since $p.q.1 \in U$, but $p.1 \notin U$, $q.1 \notin U$, and $p.q \notin Gr(Ann_R(\mathbb{Z})) = \{0\}$, U is not a gr-2-n-submodule of M.

(c) Let $G = \mathbb{Z}_2$ and $\mathfrak{R} = \mathbb{Z}$. Then $\mathfrak{R}$ is a G-graded ring with $\mathfrak{R}_0 = \mathbb{Z}$ and $\mathfrak{R}_1 = \{0\}$. Let $\mathfrak{I} = \mathbb{Z}_{p^3}$. Then $\mathfrak{I}$ is a graded $\mathfrak{R}$-module with $\mathfrak{I}_0 = \mathbb{Z}_{p^3}$ and $\mathfrak{I}_1 = \{0\}$. Consider the graded submodule $U = p^2\mathbb{Z}_{p^3}$ of $\mathbb{Z}$-module $\mathbb{Z}_{p^3}$. Then U is a gr-2-n-submodule of $\mathbb{Z}_{p^3}$ that is not gr-prime.

From the definitions above, the following theorem follows immediately.

Theorem 3.3 *Let U be a proper graded submodule of graded R-module*

1. If U is a gr-primary submodule and $Gr(Ann_R(M)) = (U:_R M)$, then U is a gr-2-n-submodule of M.
2. If M is a gr-second module, then the two concepts of gr-2-n-submodule and gr-2-absorbing primary submodules coincide.

3. If $Gr(Ann_R(M)) = (U:_R M)$, then the following are equivalent : [(a)]

(a) U is a gr-2-n-submodule of M.
(b) U is a gr-2-absorbing submodule of M.
(c) U is a gr-2-absorbing primary submodule of M

As shown in the following example, the condition $Gr(Ann_R(M)) = (U:_R M)$ in Theorem 3.3(1) is crucial:

Example 3.4 *Let p be prime integer. Let $G = \mathbb{Z}_2$ and $R = \mathbb{Z}$. Then R is a G-graded ring with $R_0 = \mathbb{Z}$ and $R_1 = \{0\}$. Let $M = \mathbb{Z}$. Then M is a graded R-module with $M_0 = \mathbb{Z}$ and $M_1 = \{0\}$. Consider the graded submodule $U = p^2\mathbb{Z}$ of M. Then U is a gr-primary, but it is not gr-2-n-submodule of M as $p.p.1 \in U$ but neither $p.p \in Gr(Ann_R(\mathbb{Z})) = \{0\}$ nor $p.1 \in U$.*

Let U be a graded submodule of M and $r \in h(R)$. We use the notation $(U:_M r)$ to denote the graded submodule $\{m \in M : rm \in U\}$ of M.

Theorem 3.5 *Let U be a proper graded submodule of M. Then the following statements are equivalent:*

(i) U is a gr-2-n-submodule of M.
(ii) If $r, s \in h(R)$ and $rs \notin Gr(Ann_R(M))$, then $(U:_M rs) \subseteq (U:_M r) \cup (U:_M s)$.
(iii) If $r, s \in h(R)$ and $rs \notin Gr(Ann_R(M))$, then $(U:_M rs) \subseteq (U:_M r)$ or $(U:_M rs) \subseteq (U:_M s)$.

Proof.

$(i) \Rightarrow (ii)$ Let U be a gr-2-n-submodule of M, $r, s \in h(R)$ such that $rs \notin Gr(Ann_R(M))$. Let $m \in (U:_M rs) \cap h(M)$. Then $rsm \in U$. Since U is a gr-2-n-submodule of M, $rsm \in U$ and $rs \notin Gr(Ann_R(M))$, we have either $rm \in U$ or $sm \in U$. Thus $m \in (U:_M r)$ or $m \in (U:s)$. This follows $(U:_M rs) \subseteq (U:_M r) \cup (U:_M s)$.

$(ii) \Rightarrow (iii)$ If a graded submodule is a subset of the union of two graded submodules, then it is a subset of one of them by (Atani & Tekir, 2007, Lemma 2.2). Thus we get the result.

$(iii) \Rightarrow (i)$ Let $r, s \in h(R)$ and $m \in h(M)$ such that $rsm \in U$ and $rs \notin Gr(Ann_R(M))$. Then $m \in (U:_M rs) \subseteq (U:_M r)$ or $m \in (U:_M rs) \subseteq (U:_M s)$ by (iii), and so $rm \in U$ or $sm \in U$.

We give another characterisation of gr-2-n-submodules in the following theorem.

Theorem 3.6 *Let U be a gr-2-n-submodule of M. Let $V = \bigoplus_{g \in G} V_g$ be a graded submodule of M, $I = \bigoplus_{h \in G} I_h$ and $J = \bigoplus_{l \in G} J_l$ be two graded ideals of M. Then the following statements are equivalent:*

(i) U is a gr-2-n-submodule of M.
(ii) For every $g \in G$, if $rsV_g \subseteq U$ for some $r, s \in h(R)$, then either $rs \in Gr(Ann_R(M))$ or $rV_g \subseteq U$ or $sV_g \subseteq U$.
(iii) For every $g, h, l \in G$, if $I_h J_l V_g \subseteq U$, then either $I_h J_l \subseteq Gr(Ann_R(M))$ or $I_h V_g \subseteq U$ or $J_l V_g \subseteq U$.

Proof.

$(i) \Rightarrow (ii)$ Let U be a gr-2-n-submodule of M, $r, s \in h(R)$ and $g \in G$ such that $rsV_g \subseteq U$. Assume on the contrary that $rs \notin Gr(Ann_R(M))$, $rV_g \not\subseteq U$ and $sV_g \not\subseteq U$. Then there exist $v_g, v_g' \in V_g$ with $rv_g \notin U$ and $sv_g' \notin U$. Since U is a gr-2-n-submodule of M, $rsv_g \in U$, $rv_g \notin U$ and $rs \notin Gr(Ann_R(M))$, we have $sv_g \in U$. Similarly, sinice $rsv_g' \in U$, $sv_g' \notin U$ and $rs \notin Gr(Ann_R(M))$, we have $rv_g' \in U$. By $(v_g + v_g') \in V_g$, we get $rs(v_g + v_g') \in U$. Then either $r(v_g + v_g') \in U$ or $s(v_g + v_g') \in U$ as U is a gr-2-n-submodule of M and $rs \notin Gr(Ann_R(M))$. If $r(v_g + v_g') = rv_g + rv_g' \in U$, then $rv_g \in U$, a contradiction. If $s(v_g + v_g') = sv_g + sv_g' \in U$, then $sv_g' \in U$, a contradiction. Thus we get the result.

$(ii) \Rightarrow (iii)$ Assume that (ii) holds. Let $g, h, l \in G$ such that $I_h J_l V_g \subseteq U$. Assume that $I_h J_l \nsubseteq Gr(Ann_R(M))$, $I_h V_g \nsubseteq U$ and $J_l V_g \nsubseteq U$. Then there exist $i_h, i'_h \in I_h$ and $j_l, j'_l \in J_l$ such that $i_h V_g \nsubseteq U$, $j_l V_g \nsubseteq U$ and $i'_h j'_l \notin Gr(Ann_R(M))$. Since $i_h j_l V_g \subseteq U$, $i_h V_g \nsubseteq U$ and $j_l V_g \nsubseteq U$, we have $i_h j_l \in Gr(Ann_R(M))$. Now since $i'_h j'_l V_g \subseteq U$ and $i'_h j'_l \notin Gr(Ann_R(M))$, we have either $i'_h V_g \subseteq U$ or $j'_l V_g \subseteq U$ by (ii). We consider three cases:

Case 1: Assume that $i'_h V_g \subseteq U$ but $j'_l V_g \nsubseteq U$. Since $i_h j'_l V_g \subseteq U$, $j'_l V_g \nsubseteq U$ and $i_h V_g \nsubseteq U$, we have $i_h j'_l \in Gr(Ann_R(M))$. Since $i'_h V_g \subseteq U$ but $i_h V_g \nsubseteq U$, we have $(i_h + i'_h) V_g \nsubseteq U$. By $(i_h + i'_h) j'_l V_g \subseteq U$, $(i_h + i'_h) V_g \nsubseteq U$ and $j'_l V_g \nsubseteq U$, we get $(i_h + i'_h) j'_l = i_h j'_l + i'_h j'_l \in Gr(Ann_R(M))$. Then $i'_h j'_l \in Gr(Ann_R(M))$, a contradiction.

Case 2: Assume that $j'_l V_g \subseteq U$ but $i'_h V_g \nsubseteq U$, similar to Case 1.

Case 3: Assume that $i'_h V_g \subseteq U$ and $j'_l V_g \subseteq U$. By $j'_l V_g \subseteq U$ and $j_l V_g \nsubseteq U$, we have $(j_l + j'_l) V_g \nsubseteq U$. Since $i_h (j_l + j'_l) V_g \subseteq U$, $(j_l + j'_l) V_g \nsubseteq U$ and $i_h V_g \nsubseteq U$, we have $i_h (j_l + j'_l) = i_h j_l + i_h j'_l \in Gr(Ann_R(M))$. Then $i_h j'_l \in Gr(Ann_R(M))$ since $i_h j_l \in Gr(Ann_R(M))$. In the same way as above, since $i'_h V_g \subseteq U$ and $i_h V_g \nsubseteq U$, we get $(i_h + i'_h) V_g \nsubseteq U$ and $i'_h j_l \in Gr(Ann_R(M))$.Now, since $(i_h + i'_h)(j_l + j'_l) V_g \subseteq U$, $(i_h + i'_h) V_g \nsubseteq U$ and $(j_l + j'_l) V_g \nsubseteq U$, we have$(i_h + i'_h)(j_l + j'_l) = i_h j_l + i_h j'_l + i'_h j_l + i'_h j'_l \in Gr(Ann_R(M))$ and hence $i'_h j'_l \in Gr(Ann_R(M))$, a contradiction.

$(iii) \Rightarrow (i)$ Let $r_h, s_l \in h(R)$ and $m_g \in h(M)$ with $r_h s_l m_g \in U$. Let $I = (r_h)$ and $J = (s_l)$ be a graded ideals of R generated by r_h, s_l, respectively. Let $V = Rm_g$ be a graded submodule of M generated by m_g . Then $I_h J_l V_g \subseteq U$ and hence either $I_h J_l \subseteq Gr(Ann_R(M))$ or $I_h V_g \subseteq U$ or $J_l V_g \subseteq U$. Hence either $r_h m_g \in U$ or $s_l m_g \in U$ or $r_h s_l \in Gr(Ann_R(M))$. Thus U is a gr-2-n-submodule of M.

Theorem 3.7 *Let U be a proper graded submodule of M. Then*

(i) If $(U:_R m)$ is gr-n-ideal of R for all $m \in h(M) \backslash U$, then U is a gr-2-n-submodule of M.
(ii) If U is a gr-2-n-submodule of M, then $(U:_M a)$ is a gr-2-n-submodule of M containing U for all $a \in h(R) \backslash (U:_R M)$.
(iii) Let M be a gr-faithful R-module. If U is a gr-2-n-submodule of M, then $(U:_R m)$ is a gr-nil deal of R containing $(U:_R M)$ for all $m \in h(M) \backslash U$.

Proof.

(i) Let $rsm \in U$ and $rs \notin Gr(Ann_R(M))$ for some $r, s \in h(R)$ and $m \in h(M)$. Hence $rs \in (U:_R m)$ and $r, s \notin Gr(0)$. If $m \in U$, done. So assume that $m \notin U$. Then $r, s \in (U:_R m)$ as $(U:_R m)$ is gr-n-ideal of R. So $rm, sm \in U$, as required..

(ii) Let $a \in h(R) \backslash (U:_R M)$ and let $rsm \in (U:_M a)$ for some $r, s \in h(R)$ and $m \in h(M)$. Then $(U:_M a) \neq M$. Since U is a gr-2-n-submodule of M and $rsma \in U$, we have either $rs \in Gr(Ann_R(M))$ or $rma \in U$ or $sma \in U$. Then either $rs \in Gr(Ann_R(M))$ or $rm \in (U:_M a)$ or $sm \in (U:_M a)$, as required.

(iii) Let $m \in h(M) \backslash U$. Hence $(U:_R m) \neq R$. Now, assume that $r, s, t \in h(R)$ with $rst \in (U:_R m)$ and $rs \notin Gr(0)$. Then $rs \notin Gr(Ann_R(M))$ as M is gr-faithful. Since U is a gr-2-n-submodule of M, $rstm \in U$ and $rs \notin Gr(Ann_R(M))$, we have either $rtm \in U$ or $stm \in U$, i.e. $rt \in (U:_R m)$ or $st \in (U:_R m)$.Therefore, $(U:_R m)$ is a gr-nil deal of R. Clearly, $(U:_R M) \subseteq (U:_R m)$.

Properties of gr-2-n-Submodules

Theorem 4.1 *Let M and M' be graded R-modules and $\varphi: M \to M'$ be graded R-module homomorphism.*

(i).Assume that φ is a graded monomorphism. If $U'$is gr-2-n-submodule of M' such that $\varphi^{-1}(U') \neq M$, then $\varphi^{-1}(U')$ is a gr-2-n-submodule of M.
(ii) Assume that φ is a graded epimorphism. If U is a gr-2-n-submodule of M with $Ker(\varphi) \subseteq U$, then $\varphi(U)$ is a gr-2-n-submodule of M'.

Proof.

(i) Suppose that $rsm \in \varphi^{-1}(U')$ and $rs \notin Gr(Ann_R(M)$ for some $r,s \in h(R)$ and $m \in h(M)$. Then $\varphi(rsm) = rs\varphi(m) \in U'$. As φ is a graded monomorphism and $rs \notin Gr(Ann_R(M)$, we get $rs \notin Gr(Ann_R(M'))$. Since U' is gr-2-n-submodule of M', we have either $r\varphi(m) \in U'$ or $s\varphi(m) \in U'$. This implies that either $rm \in \varphi^{-1}(U')$ or $sm \in \varphi^{-1}(U')$. Therefore $\varphi^{-1}(U')$ is a gr-2-n-submodule of M.

(ii) Suppose that U is a gr-2-n-submodule of M with $Ker(\varphi) \subseteq U$. Let $rsm' \in \varphi(U)$ for some $r,s \in h(R)$ and $m' \in h(M')$. As φ is a graded epimorphism, then there exists $m \in h(M)$ such that $m' = \varphi(m)$, hence $rs\varphi(m) = \varphi(rsm) \in \varphi(U)$. Since $Ker(\varphi) \subseteq U$, we have $rsm \in U$. Since U is a gr-2-n-submodule of M, we have either $rm \in U$ or $sm \in U$ or $rs \in Gr(Ann_R(M)$ and so either $rm' = \varphi(rm) \in \varphi(U)$ or $sm' = \varphi(sm) \in \varphi(U)$ or $rs \in Gr(Ann_R(M'))$. Therefore, $\varphi(U)$ is a gr-2-n-submodule of M'.

Corollary 4.2 *Let $U \subseteq V$ be two graded submodules of M. Then the followings hold;*

(i) If V is a gr-2-n-submodule of M, then V/U is a gr-2-n-submodule of a graded R-module M/U.
(ii) If V/U is a gr-2-n-submodule of a graded R-module M/U and $(U:_R M) \subseteq Gr(Ann_R(M))$, then V is a gr-2-n-submodule of M.
(iii) Let U be a graded submodule of M. If V is a gr-2-n-submodule of M such that $U \nsubseteq V$, then $V \cap U$ is a gr-2-n-submodule of U.

Proof.

(i) Assume that V is a gr-2-n-submodule of M. Let $f: M \to M/U$ be a graded epimorphism defined by $f(m) = m + U$. Then $Ker(f) = U \subseteq V$, so by Theorem 4.1 (ii), V/U is a gr-2-n-submodule of M/U.

(ii) Is clear.

(iii) Assume that V is a gr-2-n-submodule of M such that $U \nsubseteq V$. Consider the graded monomorphism $\varphi: U \to M$ defined by $\varphi(m) = m$ for all $m \in M$. Then $\varphi^{-1}(V) = V \cap U$, so by Theorem 4.1 (i), $V \cap U$ is a gr-2-n-submodule of U.

Let I be a proper graded ideal of a G-graded ring R and N be a graded submodule of a graded R-module M. The notations $G\text{-}Z_I(R)$ and $G\text{-}Z_N(M)$ denote the sets $\{r \in h(R): rs \in I$ for some $s \in h(R)\backslash I\}$ and $\{r \in h(R): rm \in N$ for some $m \in h(M)\backslash N\}$.

The following result studies the behavior of a gr-2-n-submodules under localization.

Theorem 4.3 *Let $S \subseteq h(R)$ be a multiplication closed subset of R and U is a proper graded submodule of M.*

(i) If U is a gr-2-n-submodule of M with $(U:_R M) \cap S = \emptyset$, then $S^{-1}U$ is a gr-2-n-submodule of $S^{-1}M$.
(ii) Assume that $Gr(Ann_{S^{-1}R}(S^{-1}M)) = S^{-1}Gr(Ann_R(M))$. If $S^{-1}U$ is a gr-2-n-submodule of $S^{-1}M$, and $S \cap G\text{-}Z_{Gr(Ann_R(M))}(R) = S \cap G\text{-}Z_U(M) = \emptyset$, then U is a gr-2-n-submodule of M.

Proof.

(i) Assume that U is a gr-2-n-submodule of M with $(U:_R M) \cap S = \emptyset$. Let $\frac{r}{s_1}\frac{k}{s_2}\frac{m}{s_3} \in S^{-1}U$, where $\frac{r}{s_1}, \frac{k}{s_2} \in h(S^{-1}U)$ and $\frac{m}{s3} \in h(S^{-1}M)$. Then $trkm \in U$ for some $t \in S$. Since U is a gr-2-n-submodule of M, we have either $rk \in Gr(Ann_R(M))$ or $trm \in U$ or $tkm \in U$, which implies that either $\frac{r}{s_1}\frac{k}{s_2} \in S^{-1}Gr(Ann_R(M)) \subseteq Gr(Ann_{S^{-1}R}(S^{-1}M))$ or $\frac{r}{s_1}\frac{m}{s_3} = \frac{trm}{ts_1s_3} \in S^{-1}U$ or $= \frac{k}{s_2}\frac{m}{s_3} = \frac{tkm}{ts_2s_3} \in S^{-1}U$. Therefore, $S^{-1}U$ is a gr-2-n-submodule of $S^{-1}M$.

$ii)$ Let $rkm \in U$ for some $r, k \in h(R)$ and $m \in h(M)$. Then $\frac{r}{1}\frac{k}{1}\frac{m}{1} \in S^{-1}U$. Since $S^{-1}U$ is a gr-2-n-submodule of $S^{-1}M$, we have either $\frac{r}{1}\frac{k}{1} \in Gr(Ann_{S^{-1}R}(S^{-1}M)) = S^{-1}Gr(Ann_R(M))$ or $\frac{r}{1}\frac{m}{1} \in S^{-1}U$ or $\frac{k}{1}\frac{m}{1} \in S^{-1}U$. So, either $trk \in Gr(Ann_R(M)$ for some $t \in S$ or $lrm \in U$ for some $l \in S$ or $vkm \in U$ for some $v \in S$. This implies that either $rk \in Gr(Ann_R(M)$ or $rm \in U$ or $km \in U$ as $S \cap G\text{-}Z_{Gr(Ann_R(M))}(R) = S \cap G\text{-}Z_U(M) = \emptyset$. Therefore, U is a gr-2-n-submodule of M.

Let R be a commutative ring and M be an R-module. Then the idealization $R(+)M = \{(r,m)\colon r \in R$ and $m \in M\}$ is the ring whose elements are those of $R \times M$ equipped with addition and multiplication defined by $(r,m) + (r',m') = (r+r', m+m')$ and $(r,m)(r',m') = (rr', rm' + r'm)$ respectively. Let G be an abelian group, $R = \bigoplus_{g\in G} R_g$ be a G-graded ring and $M = \bigoplus_{g\in G} M_g$ be a G-grded R-module. Then $R(+)M$ is a G-graded ring with$(R(+)M)_g = R_g(+)M_g$, see (Uregen et al., 2019, Proposition 3.1). If I is an ideal of R and U is a submodule of M with $IM \subseteq U$. Then $I(+)U$ is a graded ideal of $R(+)M$ if and only if I is a graded ideal of R and U is a graded submodule of M, see (Uregen et al., 2019, Proposition 3.3).

Theorem 4.4 *Let I be a graded ideal of R and U be a proper graded submodule M. If $I(+)U$ is gr-2-nil ideal of $R(+)M$, then I is a gr-2-nil ideal of R and U is a gr-2-n-submodule of M.*

Proof.

Suppose that $I(+)U$ is a gr-2-nil ideal of $R(+)M$. At first we want to show that I is a gr-2-nil ideal of R. Let $rst \in I$ but $rs \notin Gr(0)$ for some $r, s, t \in h(R)$. Hence $(r,0_M)(s,0_M)(t,0_M) = (rst,0_M) \in I(+)U$ but $(r,0_M)(s,0_M) = (rs,0_M) \notin Gr(0_{R(+)M})$. Then either $(s,0_M)(t,0_M) = (st,0_M) \in I(+)U$ or $(r,0_M)(t,0_M) = (rt,0_M) \in I(+)U$ as $I(+)U$ is gr-2–nil ideal of $R(+)M$. This implies that either $st \in I$ or $rt \in I$. Thus I is a gr-nil ideal of R. Now, we want to show that U is a gr-2-n-submodule of M. Let $rsm \in U$ and $rs \notin Gr(Ann_R(M)$ for some $r, s \in h(R)$ and $m \in h(M)$. Then $(r,0_M)(s,0_M)(0,m) = (0,rsm) \in I(+)U$ with $(r,0_M)(s,0_M) \notin Gr(0_{R(+)M})$. Since $I(+)U$ is gr-2–nil ideal of $R(+)M$, we have either $(r,0_M)(0,m) = (0,rm) \in I(+)U$ or $(s,0_M)(0,m) = (0,sm) \in I(+)U$. Hence, either $rm \in U$ or $sm \in U$. Therefore, U is a gr-2-n-submodule of M.

Scientific Ethics Declaration

The author declares that the scientific ethical and legal responsibility of this article published in EPSTEM journal belongs to the author.

Acknowledgements or Notes

* This article was presented as an oral presentation at the International Conference on Basic Sciences, Engineering and Technology (www.icbaset.net) held in Alanya/Turkey on May 02-05, 2024.

References

Al-Zoubi, K., & Al-Azaizeh, M. (2019). On graded weakly 2-absorbing primary submodules. *Vietnam Journal of Mathematics*, *47*, 297-307.

Al-Zoubi, K., & Al-Azaizeh, M. (2019). Some properties of graded 2-absorbing and graded weakly 2-absorbing submodules. *Journal of Nonlinear Science*, *12*(8), 503-508..

Al-Zoubi, K., & Al-Qderat, A. (2017). Some properties of graded comultiplication modules. *Open Mathematics*, *15*(1), 187-192.

Al-Zoubi, K., Abu-Dawwas, R., & Ceken, S. (2019). On graded 2-absorbing and graded weakly 2-absorbing ideals. *Hacettepe Journal of Mathematics and Statistics*, *48*(3), 724-731.

Al-Zoubi, K. H., & Abu-Dawwas, R. (2014). On graded 2-absorbing and weakly graded 2-absorbing submodules. *Journal of Mathematical Sciences: Advanced and Applications*, *28*, 45-60.

Al-Zoubi, K., Al-Turman, F., & Celikel, E. Y. (2019). Gr-n-ideals in graded commutative rings. *Acta Universitatis Sapientiae, Mathematica*, *11*(1), 18-28.

Al-Zoubi, K., & Sharafat, N. (2017). On graded 2-absorbing primary and graded weakly 2-absorbing primary ideals. *Journal of the Korean Mathematical Society*, *54*(2), 675-684.

Ansari-Toroghy, H., & Farshadifar, F. (2011). Graded comultiplication modules. *Chiang Mai Journal of Science*, *38*(3), 311-320.

Ansari-Toroghy, H., & Farshadifar, F. (2012). On graded second modules. *Tamkang Journal of Mathematics*, *43*(4), 499-505.

Atani, S. E. (2006). On graded prime submodules. *Chiang Mai Journal of Science*, *33*(1), 3-7.

Atani, S. E., & Farzalipour, F. (2007). On graded secondary modules. *Turkish Journal of Mathematics*, *31*(4), 371-378.

Atani, S. E., & Tekir, U. (2007). On the graded primary avoidance theorem. *Chiang Mai Journal of Science*, *34*(2), 161-164.

Ceken, S., & Alkan, M. (2015). On graded second and coprimary modules and graded secondary representations. *Bulletin of the Malaysian Mathematical Sciences Society*, *38*(4), 1317-1330.

Celikel, E. Y. (2016). On graded 2-absorbing primary submodules. *International Journal of Pure and Applied Mathematics*, *109*(4), 869-879.

Nastasescu, C., & Van Oystaeyen, F. (2004). *Methods of graded rings* (Vol.1836). Springer.

Oral, K. H., Tekir, U., & Agargun, A. G. (2011). On graded prime and primary submodules. *Turkish Journal of Mathematics*, *35*(2), 159-167.

Refai, M., & Al-Zoubi, K. (2004). On graded primary ideals. *Turkish Journal of Mathematics*, *28*(3), 217-230.

Uregen, R. N., Tekir, U., Shum, K. P., & Koc, S. (2019). On graded 2-absorbing quasi primary ideals. *Southeast Asian Bulletin of Mathematics*, *43*(4), 601-613.

Author Information

Khaldoun Al-Zoubi
Department of Mathematics and Statistics
Jordan University of Science and Technology
P.O.Box 3030, Irbid 22110, Jordan
Contact e-mail: *kfzoubi@just.edu.jo*

To cite this article:

Al-Zoubi, K. (2024). On graded 2-n-submodules of graded modules over graded commutative rings. *The Eurasia Proceedings of Science, Technology, Engineering & Mathematics (EPSTEM), 28*, 382-389.

The Eurasia Proceedings of Science, Technology, Engineering & Mathematics (EPSTEM)
ISSN: 2602-3199

The Eurasia Proceedings of Science, Technology, Engineering & Mathematics (EPSTEM), 2024

Volume 28, Pages 390-396

ICBASET 2024: International Conference on Basic Sciences, Engineering and Technology

Integration of Air Conditioning Systems in Intelligent Buildings to Increase Efficiency

Jonadri Bundo
Polytechnic University of Tirana

Genci Sharko
Polytechnic University of Tirana

Aida Spahiu
Polytechnic University of Tirana

Ramadan Alushaj
Polytechnic University of Tirana

Denis Panxhi
Polytechnic University of Tirana

Darjon Dhamo
Polytechnic University of Tirana

Abstract: Heating, ventilation, air conditioning, and cooling, collectively known as HVAC, account for more than 40% of the electricity consumed in buildings. Global climatic factors, referring to comfort and factors related to health, dictate that there is an increasing need for the application of HVAC/R systems. Therefore, it is increasingly compelling to investigate various approaches to enhance the effectiveness of air treatment systems. The automation of buildings has facilitated the integration of air treatment systems with "other existing" systems that can impact the indoor climatic conditions, such as automated windows and curtains, etc. In order to achieve this, it is essential to employ calculation techniques for air handling systems and for the heat transfer between buildings and the external environment. By integrating these systems, it becomes possible to maintain a comfortable environment while actively minimizing the electricity consumption of the heat pump. This article focuses on the integration of air conditioning systems in intelligent buildings to enhance efficiency.

Keywords: HVAC/R, Energy consumption, Automation, Integration

Introduction

Within an autonomous air treatment machine, the primary energy-consuming components are the ventilators and the heat pump. On average, the heat pump alone would consume over 65% of the electricity. More precisely, this consumption would refer to the electricity consumed by the compressor motor of the heat pump. Therefore, it is imperative to examine the potential and techniques for maximising the efficiency of heat pumps.

When the entire system is taken into consideration, it is observed that the thermal capacity and consumption would be determined by the physical dimensions of the components (compressor, condensing heat exchanger, and evaporating heat exchanger), in addition to the working conditions under which the system would be operating. When we talk about the "working conditions", we are referring to the air flux that is passing through

- Selection and peer-review under responsibility of the Organizing Committee of the Conference

each of the heat exchangers specifically. Specifically, the factors of interest are airflow, air temperature, and relative air humidity.

From all the parameters mentioned above, it can be said that the physical parameters of the system are unchangeable. Also, the temperature and humidity of the air flow that would pass through the heat exchanger that is exposed to the outside air are unchanging parameters. Effectively, the parameters that can be manipulated are the air flow in the external exchanger, the air flow in the internal exchanger, as well as the temperature and relative humidity of the internal air. In this paper, we will examine whether it is possible to regulate the climatic conditions within a specific range by integrating the air conditioning system with other intelligent components of the building, with the aim of optimizing the coefficient of performance (COP).

Method

Compressor Model

The most widespread model for calculating the parameters of refrigeration power, absorbed electrical power, absorbed current, and gas mass flow in a compressor, is the third-order polynomial model with two parameters, specifically the evaporation temperature and the condensation temperature, as shown below.

$$F(T_{ev}, T_{co}) = A + BT_{ev} + CT_{co} + DT_{ev}^2 + ET_{ev}T_{co} + FT_{co}^2 + GT_{ev}^3 + HT_{co}T_{ev}^2 + IT_{ev}T_{co}^2 + LT_{co}^3 \quad (1)$$

The numerical method approach presented by Daci, A., & Bundo, J. (2020) was used to determine the equilibrium point of the refrigeration circuit. The application of this method is fundamental because it helps on the determination of evaporation and condensation temperatures in a relatively short time, which is crucial on the application of control with the aim of optimizing efficiency. COP (coefficient of performance) is defined as the ratio of the thermal power of the compressor to its electrical power. Thus, it results:

$$COP = \frac{P_f(\mathrm{T_{ev}}, T_{co}) + P_{el}(T_{ev}, T_{co})}{P_{el}(T_{ev}, T_{co})} \quad (2)$$

Where the index “f” represents the term “refrigerator” (frigo) while the index “el” represents the term “electrical”. The symbol P in both cases represents power. The outcome would be:

$$\frac{\sigma_A + \sigma_B T_{ev} + \sigma_C T_{co} + \sigma_D T_{ev}^2 + \sigma_F T_{co}^2 + \sigma_G T_{ev}^3 + \sigma_L T_{co}^3 + \sigma_E T_{co}T_{ev} + \sigma_H T_{co}T_{ev}^2 + \sigma_I T_{co}^2 T_{ev}}{L_{el}T_{co}^3 + I_{el}T_{co}^2 T_{ev} + F_{el}T_{co}^2 + H_{el}T_{co}T_{ev}^2 + E_{el}T_{co}T_{ev} + C_{el}T_{co} + G_{el}T_{ev}^3 + D_{el}T_{ev}^2 + B_{el}T_{ev} + A_{el}} \quad (3)$$

$$\sigma_x = X_{el} + X_f \quad (4)$$

On the other hand, EER (energy efficiency ratio) will be defined as the ratio of the cooling power developed by the compressor to the electrical power it receives from the power network:

$$EER = \frac{P_f(\mathrm{T_{ev}}, T_{co})}{P_{el}(T_{ev}, T_{co})} \quad (5)$$

$$\frac{L_f T_{co}^3 + I_f T_{co}^2 T_{ev} + F_f T_{co}^2 + H_f T_{co}T_{ev} + E_f T_{co}T_{ev} + C_f T_{co} + G_f T_{ev}^3 + D_f T_{ev}^2 + B_f T_{ev} + A_f}{L_{el}T_{co}^3 + I_{el}T_{co}^2 T_{ev} + F_{el}T_{co}^2 + H_{el}T_{co}T_{ev} + E_{el}T_{co}T_{ev} + C_{el}T_{co} + G_{el}T_{ev}^3 + D_{el}T_{ev}^2 + B_{el}T_{ev} + A_{el}} \quad (6)$$

Analysis

Let's try to see the differential expression of COP in order to get a better understanding of the shape of the tendency of these curves so that we can determine whether or not the hypothesis that was explained earlier is correct, or more specifically, whether or not there is such a place for the application.

The first derivative of the refrigerating power in relation to the evaporation temperature is as follows:

$$\frac{\partial Pf(T_{ev},T_{co})}{\partial T_{ev}} = I_f T_{co}^2 + 2H_f T_{co} T_{ev} + E_f T_{co} + 3G_f T_{ev}^2 + 2D_f T_{ev} + B_f \quad (7)$$

Meanwhile, the first derivative of the refrigeration power in relation to the condensation temperature would be:

$$\frac{\partial P_f(T_{ev},T_{co})}{\partial T_{co}} = 3L_f T_{co}^2 + 2I_f T_{co} T_{ev} + 2F_f T_{co} + H_f T_{ev}^2 + E_f T_{ev} + C_f \quad (8)$$

Let us proceed and examine the partial derivatives of the coefficient of performance in relation to the temperature of evaporation and condensation.

$$\frac{\partial COP(t_{ev},t_{co})}{\partial t_{ev}} = \frac{B_{el}+B_f+2D_{el}T_{ev}+2D_f T_{ev}+E_{el}T_{co}+E_f T_{co}+\sigma_1+3\,G_f T_{ev}^2+I_{el}T_{co}^2+I_f T_{co}^2+2H_{el}T_{co}T_{ev}+2H_f T_{co}T_{ev}}{\sigma_2} -$$

$$\left[(I_{el}T_{co}^2 + 2H_{el}T_{co}T_{ev} + E_{el}T_{co} + \sigma_1 + 2D_{el}T_{ev} + B_{el})(A_{el} + A_f + B_{el}T_{ev} + B_f T_{ev} + C_{el}T_{co} + C_f T_{co} + D_{el}T_{ev}^2 + D_f T_{ev}^2 + F_{el}T_{co}^2 + F_f T_{co}^2 + G_{el}T_{ev}^3 + G_f T_{ev}^3 + L_{el}T_{co}^3 + L_f T_{co}^3 + E_{el}T_{co}T_{ev} + E_f T_{co}T_{ev} + \sigma_4 + H_f T_{co}T_{ev}^2 + \sigma_3 + I_f T_{co}^2 T_{ev})\right]\frac{1}{\sigma_2^2} \quad (9)$$

$$\sigma_1 = 3G_{el}T_{ev}^2$$

$$\sigma_2 = L_{el}T_{co}^3 + \sigma_3 + F_{el}T_{co}^2 + \sigma_4 + E_{el}T_{co}T_{ev} + C_{el}T_{co} + G_{el}T_{ev}^3 + B_{el}T_{ev} + A_{el}$$

$$\sigma_3 = I_{el}T_{co}^2 T_{ev}$$

$$\sigma_4 = H_{el}T_{co}T_{ev}^3$$

$$\frac{\partial COP(T_{ev},t_{co})}{\partial t_{co}} = \left[C_{el} + C_f + E_{el}T_{ev} + E_f T_{ev} + 2F_{el}T_{co} + 2F_f T_{co} + H_{el}T_{ev}^2 + H_f T_{ev}^2 + \sigma_1 + 3L_f T_{co}^2 + 2I_{el}T_{co}T_{ev} + 2I_f T_{co}T_{ev}\right]\frac{1}{\sigma_2} - [(\sigma_1 + 2I_{el}T_{co}T_{ev} + 2F_{el}T_{co} + H_{el}T_{ev}^2 + E_{el}T_{ev} + C_{el})(A_{el} + A_f + B_{el}T_{ev} + B_f T_{ev} + C_{el}T_{co} + C_f T_{co} + D_{el}T_{ev}^2 + D_f T_{ev}^2 + F_{el}T_{co}^2 + F_f T_{co}^2 + G_{el}T_{ev}^3 + G_f T_{ev}^3 + L_{el}T_{co}^3 + L_f T_{co}^3 + E_{el}T_{co}T_{ev} + E_f T_{co}T_{ev} + \sigma_4 + H_f T_{co}T_{ev}^2 + \sigma_3 + I_f T_{co}^2 T_{ev}]\frac{1}{\sigma_2} \quad (10)$$

$$\sigma_1 = 3L_{el}T_{co}^2$$

$$\sigma_2 = L_{el}T_{co}^3 + \sigma_3 + F_{el}T_{co}^2 + \sigma_4 + E_{el}T_{co}T_{ev} + C_{el}T_{co} + G_{el}T_{ev}^3 + D_{el}T_{ev}^2 + B_{el}T_{ev} + A_{el}$$

$$\sigma_3 = I_{el}T_{co}^2 T_{ev}$$

$$\sigma_4 = H_{el}T_{co}T_{ev}^2$$

In this way we can estimate in which direction we would move on the surface of the COP with the change of the temperature of evaporation and condensation, trying to go towards the maximum.

Here, we will examine a compressor of type **GMCC KSK66D43UEZA_30 Hz** produced by Toshiba with the following parameters of third order polynomials considering as input evaporation and condensation temperature:

Table 1. Polynomial model for refrigerant power of compressor GMCC KSK66D43UEZA_30 Hz

Parameter	Value
A_f	3655.27
B_f	132.62
C_f	-4.78
D_f	1.86
E_f	-0.24
F_f	-0.58
G_f	0.01
H_f	-0.0067
I_f	-0.0104464
L_f	0.003776

Table 2. Polynomial model for electrical power of compressor GMCC KSK66D43UEZA_30 Hz

Parameter	Value
A_{el}	336.1
B_{el}	-17.62
C_{el}	-2.36
D_{el}	-0.51
E_{el}	0.45
F_{el}	0.46
G_{el}	-0.004
H_{el}	0.0052
I_{el}	0.000228
L_{el}	-0.00363

The graphic representation of the relationship between the coefficient of performance (COP) and the temperature of evaporation and condensation is the following, based on the data from the model for the compressor described above.

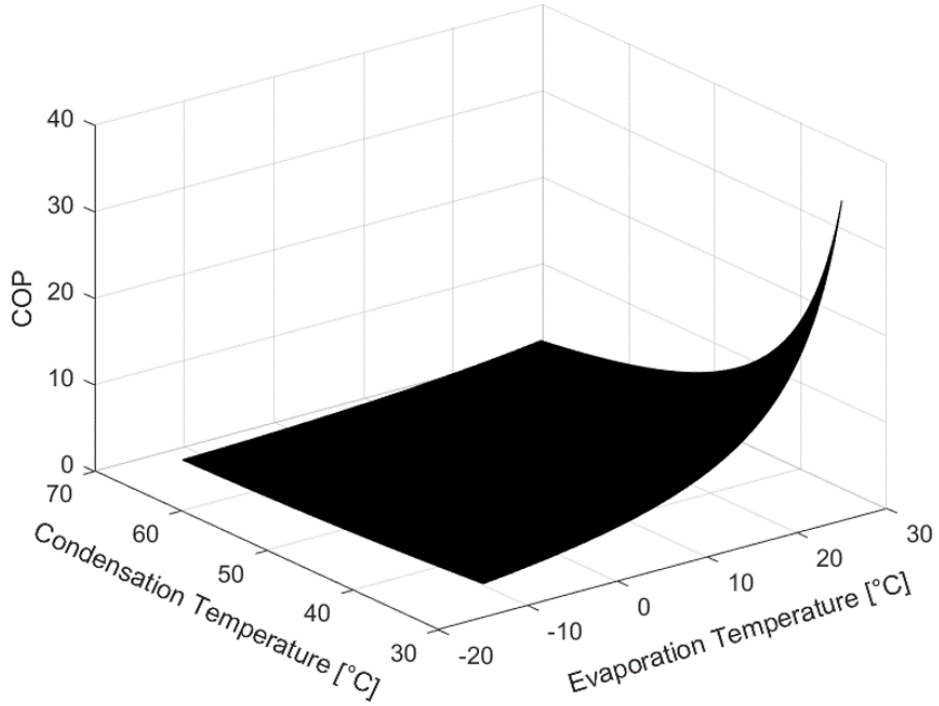

Figure 1. COP vs evaporation temperature and condensation temperature

Results and Discussion

A number of factors, which can be classified as either manipulable or not, will determine the coefficient of performance (COP) of a system. The fixed parameters would be associated with the physical aspects of the components, such as heat exchangers, the architecture of the refrigeration circuit (parallel evaporative exchanger, parallel condensing exchanger, water exchanger, air exchanger, etc.), and the compressor. On the other hand, the variable parameters would take into consideration air flow, temperature, and air humidity.

In the following we will consider an autonomous air handling machine which is simulated in the summer season. The temperature of the internal environment will vary between 20°C and 26°C, while the temperature of the external environment will be between 30°C and 37°C. Knowing the geometry of each of the heat exchangers and the above model of the compressor, we will simulate the system under the conditions indicated above by applying as a calculation method presented by Daci & Bundo (2020). Following is a plot that illustrates the data that was generated by the simulation, which generated a total of 56 samples. From the graph above, the trend shown by EER can be seen in relation to the temperature of evaporation and condensation. It is important to note that the EER is increased when the temperature of evaporation is increased, and the EER is increased when the temperature of condensation is decreased. This element also corresponds to what we see in the theoretical presentation of COP in Figure 1.

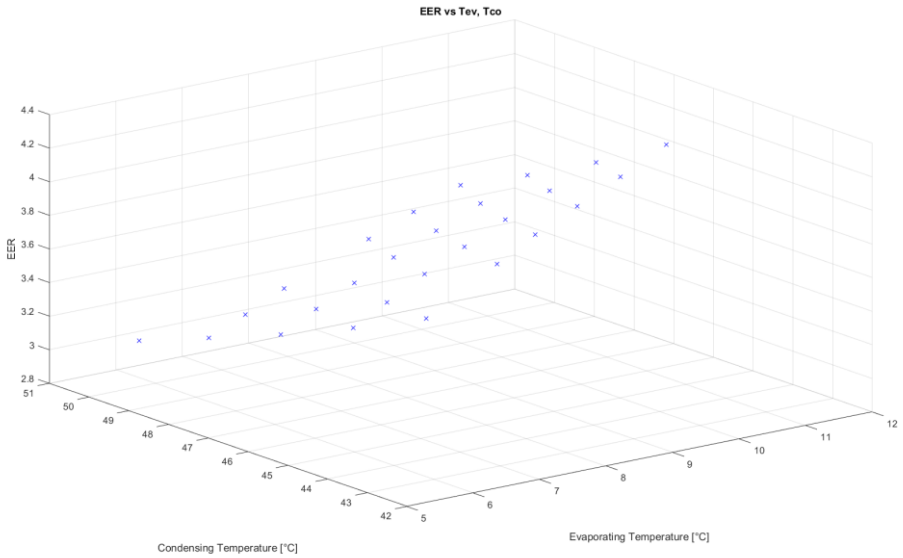

Figure 2 EER vs evaporation and condensation temperatures

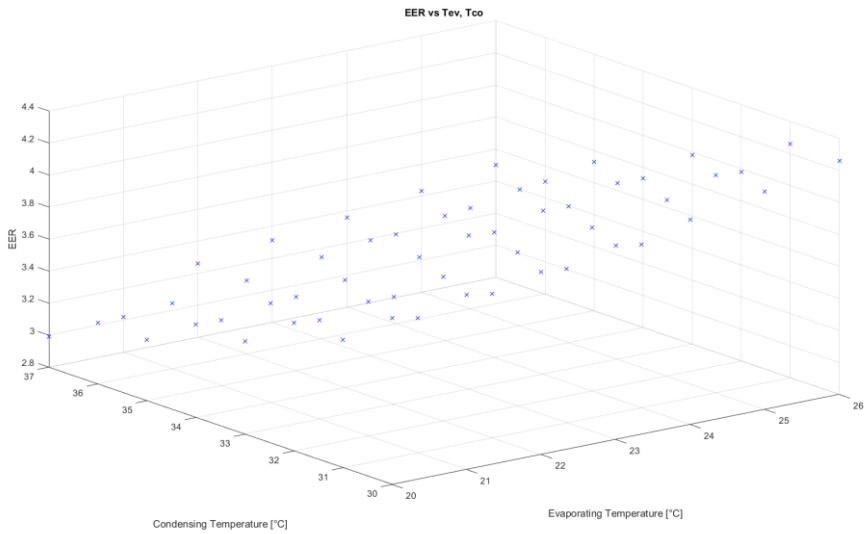

Figure 3 EER vs indoor and outdoor temperatures

In this figure, a similarity can be seen with the dependence that EER presents on the temperature of evaporation and condensation. By analogy, we can say that increasing the temperature of the internal environment, i.e. increasing the temperature of the air that exchanges heat with the evaporating element, the EER will also increase. On the other hand, reducing the value of the temperature of the external environment, that is, of the air that exchanges heat with the condensing element, the EER will increase.

The above analysis and the three graphs presented show the potential of improving the efficiency of HVAC systems through control and integration with other existing systems where their action can affect the change of climatic conditions in the indoor environment. On the other hand, the development of technology and the possibility of achieving the weather forecast within a day with satisfactory accuracy presents a new opportunity to realize the improvement of efficiency through utilisation of advanced control techniques such as model predictive control (MPC).

Conclusion

In the HVAC/R industry, the calculation and simulation of the heat pump is an argument that, with the progression of technology, the rise in demands in terms of quantity and complexity, and most recently, the energy crisis that the modern world is experiencing, is becoming increasingly interesting.The presentation of new software methods for the calculation within a relatively fast time and with an acceptable accuracy of the heat pump, has presented new possibilities for the optimization of these systems. After looking at the information presented above, we are able to comprehend the connection that exists between the EER and the temperatures of evaporation, condensation, indoor air, and outdoor air.. If we can define a comfort zone in relation to the temperature of the surrounding environment, and the heating/cooling system can be "helped" by integrating other elements so that the indoor air enters this comfort zone which would result in a significant improvement in both efficiency and system performance, then the system would be significantly improved.

In order to realise this integration, the physical elements that are necessary are those that have the potential to influence the climatic conditions of the air inside the building through the processes of radiation and convection of air. In this context, we may make reference to controlled doors, controlled windows, controlled shutters or curtains, or other components of a similar nature. In the graph that was just presented, the conditions that result in the lowest possible value of EER are those in which the internal temperature is 20°C, the external temperature is 37°C, the evaporation temperature is 6.15°C and the condensation temperature is 50.66°C. The maximum value of the condensation temperature would be 4.26 where the internal temperature is 26°C, the external temperature is 31°C, the evaporation temperature is 10.65°C and the condensation temperature is 44.93°C.

Recommendations

In order to make the implementation of such a integrated system a reality, it is recommended that a product be developed that automates and optimises buildings. It is necessary to provide the relevant parameters of the building in this product in order to be able to calculate the thermal balance of the building in relation to the external environment as a single system. On the other hand, this intelligent system would have to take into consideration the possibility that there are elements that can be controlled that have an effect on the climate conditions of the building. The geometry of each of the air handling components and the architecture of the system are two additional important aspects that need to be determined in addition to these data.

The optimisation of the system in terms of efficiency can be carried out by remaining within a comfort zone. This is made possible by having knowledge of the meteorological forecast for the next twenty-four hours as well as the effect that the controllable elements would have if the heat pump calculation method presented by Daci and Bundo (2020) was applied.

Scientific Ethics Declaration

The authors declare that the scientific ethical and legal responsibility of this article published in EPSTEM journal belongs to the authors.

Acknowledgements or Notes

* This article was presented as a poster presentation at the International Conference on Basic Sciences, Engineering and Technology (www.icbaset.net) held in Alanya/Turkey on May 02-05, 2024.

References

Abbasi, M. H., Abdullah, B., Ahmad, M. W., Rostami, A., & Cullen, J. (2021). Heat transition in the European building sector: Overview of the heat decarbonisation practices through heat pump technology. *Sustainable Energy Technologies and Assessments, 48*, 101630.

Australian Government, Department of the Environment and Energy. (2013, September 1). *HVAC factsheet - energy breakdown*. Retrieved from https://www.energy.gov.au/publications/hvac-factsheet-energy-breakdown

Daci, A., & Bundo, J. (2020). Mathematical model for calculating the equilibrium point of the refrigerant circuit. *IOP Conference Series: Materials Science and Engineering*, *909*(1), 012013.

Chaouch, H., Ceken, C., & Arı, S. (2021). Energy management of HVAC systems in smart buildings by using fuzzy logic and M2M communication. *Journal of Building Engineering*, *44*, 102606.

European Commission Directorate-General For Energy. (2016). *Mapping and analyses of the current and future (2020 - 2030) heating/cooling fuel deployment (fossil/renewables)*. Retrieved from https://energy.ec.europa.eu/document/download/affe64bc-6947-404a-93fecfcdb290f97d_en?filename=Summary%20WP1%20and%20WP2.pdf

Jakubcionis, M., Moles, C., Kavvadias, K., Santamaria, M., & Carlsson, J. (2018). *Synthesis report on the evaluation of national notifications related to article 14 of the energy efficiency directive.* Publication Office of the European Union.

Lu, L., Cai, W., Xie, L., Li, S., & Soh, Y. C. (2005). HVAC system optimizationin-building section. *Energy and Buildings, 37*(1), 11–22.

Author Information

Jonadri Bundo
Polytechnic University of Tirana, Mother Teresa Square, Nr. 4, Albania
Contact e-mail: *jonadribundo@gmail.com*

Genci Sharko
Polytechnic University of Tirana, Mother Teresa Square, Nr. 4, Albania

Aida Spahiu
Polytechnic University of Tirana, Mother Teresa Square, Nr. 4, Albania

Ramadan Alushaj
Polytechnic University of Tirana, Mother Teresa Square, Nr. 4, Albania

Denis Panxhi
Polytechnic University of Tirana, Mother Teresa Square, Nr. 4, Albania

Darjon Dhamo
Polytechnic University of Tirana, Mother Teresa Square, Nr. 4, Albania

To cite this article:

Bundo, J., Sharko, G., Spahiu, A., Panxhi, D., & Dhamo, D. (2024). Integration of air conditioning systems in intelligent buildings to increase efficiency. *The Eurasia Proceedings of Science, Technology, Engineering & Mathematics (EPSTEM), 28*, 390-396.

The Eurasia Proceedings of Science, Technology, Engineering & Mathematics (EPSTEM)
ISSN: 2602-3199

The Eurasia Proceedings of Science, Technology, Engineering & Mathematics (EPSTEM), 2024

Volume 28, Pages 397-407

ICBASET 2024: International Conference on Basic Sciences, Engineering and Technology

Proposed Intelligent Irrigation System for Riyadh City Using Fuzzy Logic

Sara Alsaadoun
King Saud University

Fairouz Tchier
King Saud University

Abstract: Considering the insufficient rainfall and rapid evaporation of soil moisture in desert regions, irrigation becomes very challenging in Riyadh. Automation is therefore required for optimum productivity and water conservation. According to the vision of the Green Riyadh project, recycled water will be used in the irrigation system to irrigate all green lands. The method of irrigation and the quantity of water being used must both be considered. Since drought inhibits plant growth and excessive moisture limits plants' ability to absorb nutrients and raises the possibility of disease development, only the amount of water needed by plants should be used. Artificial intelligence and fuzzy logic are increasingly seen as solutions to be implemented in smart drip irrigation systems. The fuzzy logic control system will aid in water conservation given its shortage, which has become a major worldwide concern. The system also has the advantage of conserving moisture to counteract inadequate rainfall, saving electricity and reducing labor costs. For such advantages, an intelligent irrigation control system based on fuzzy logic adapted to the climate of Riyadh will be proposed. Based on the measured soil moisture, ambient temperature, air humidity and solar irradiance, the fuzzy controller calculates the necessary irrigation duration. The features of the fuzzy logic toolbox in MATLAB are used to create the proposed system.

Keywords: Smart irrigation, Control system, Fuzzy logic

Introduction

The advantages of afforestation go far beyond the aesthetic value they add to the environment. Afforestation aids in improving air quality, reducing soil erosion, providing habitat for wildlife and helping to mitigate climate change (Ghosh, 2023). Based on that, the Custodian of the Two Holy Mosques, King Salman Bin Abdulaziz, launched the Green Riyadh project in March 2019, which aims to plant more than 7.5 million trees throughout Riyadh city (Abdelrahman, 2022). The project will represent a turning point in achieving one of Saudi Vision 2030's main objectives, which is to elevate Riyadh to one of the world's top 100 most livable cities. Moreover, King Salman Park, with an area of more than 16 square kilometers, was launched to become the largest urban park in the world providing both city inhabitants and tourists with a wide choice of options and high-quality activities (Abdelrahman, 2023). In Riyadh, irrigation becomes highly challenging due to inadequate rainfall and the quick evaporation of soil moisture. Therefore, automation is necessary for optimal efficiency and water saving. The method of irrigation and the quantity of water being used must both be considered. Since drought inhibits plant growth and excessive moisture limits plants' ability to absorb nutrients and raises the possibility of disease development, only the amount of water needed by plants should be used (Mohammed et al., 2021). Smart irrigation systems are increasingly using fuzzy logic and artificial intelligence as potential solutions (Khatri, 2018). The fuzzy logic control system will aid in water conservation given its shortage, which has become a major worldwide concern. The system also has the advantage of conserving moisture to counteract insufficient rainfall, saving electricity and reducing labor cost waste (Singh et al., 2022). For such advantages, a fuzzy logic irrigation controller suitable for the aforementioned projects in Riyadh will be suggested.

Types of Irrigation Controllers

Irrigation controllers fall into two main categories (Mohammed et al., 2021; Ross, 2009):

1.Open-loop controllers:

In this type, the irrigation decisions are made by the user manually. Based on the user's knowledge, the time to start and time to end are determined by him as well as the volume of water to be dispensed, irrigation speed and watering periods. Since it is easy to use and does not require any sensors, this technique is commonly employed. Nevertheless, it can result in some areas being over-irrigated while others are under-irrigated, which could lead to unfavorable water stress.

2. Closed-loop controllers:

They are the type of controllers that use feedback to maintain control. The decisions are typically based on sensor data. So, when the condition changes, the output changes as well. Closed loop controllers have great irrigation efficiency because they are event-driven, which allows them to react automatically to changes in the environment and climate. Hence, it offers an alternative and efficient solution to traditional irrigation techniques. Our goal is to develop an intelligent irrigation system that employs a fuzzy logic-based closed-loop controller.

Fuzzy Logic Control System

There are three significant blocks used to create a fuzzy logic control system (Bai et al., 2007; Ross, 2009). A block diagram of a general fuzzy logic control system is shown in Figure 1.

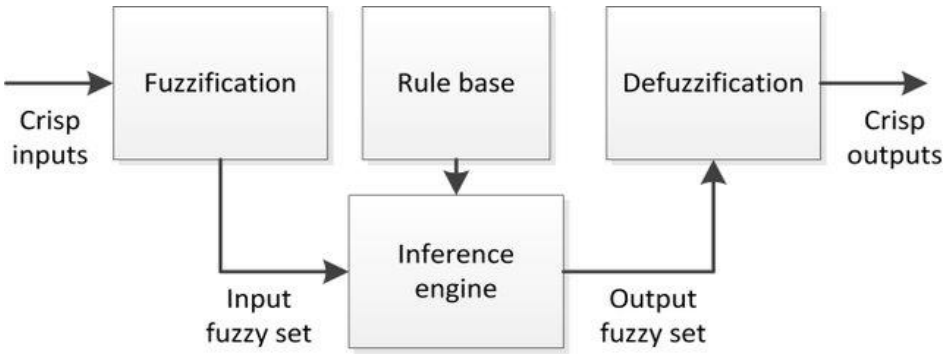

Figure 1. Block diagram of a fuzzy logic control system

Fuzzification includes two steps: deriving the membership functions for input and output variables and then representing them with linguistic variables. The fuzzified inputs and outputs are divided into several sets based on membership functions. Thus, the crisp input variables convert to fuzzy in this stage.

Fuzzy Inference Engine decides the best decision for each given situation and deduces the fuzzy result from fuzzified inputs using the "IF-THEN" rules as a foundation. The fuzzy IF-THEN rules are the rule base that contains all the pertinent input-output combinations that are designed by the user to indicate a mathematical relationship between them. The rule links a condition specified by linguistic variables and fuzzy sets to an output or conclusion. With the use of elastic conditions, the "IF" section is primarily used to capture knowledge and the "THEN" part can be used to provide the conclusion or output in linguistic variable form. The law to create a collection of fuzzy IF-THEN rules is reliant on each individual application and is based on human knowledge or experience.

Defuzzification is the last step in the fuzzy controller, this process is required in order to make the conclusion or fuzzy output applicable to practical applications. Keep in mind that the fuzzy conclusion or output is still a linguistic variable that needs to be defuzzified to be transformed into the crisp variable, so its goal is to convert the output from fuzzy to crisp.

Fuzzy Controller of Riyadh Irrigation System

The proposed fuzzy controller determines the necessary irrigation time based on the detected soil moisture, air humidity, ambient temperature and solar irradiation. It was created by the features of the fuzzy logic toolbox in MATLAB using the Mamdani fuzzy inference technique. The fuzzy inference system is illustrated in Figure 2.

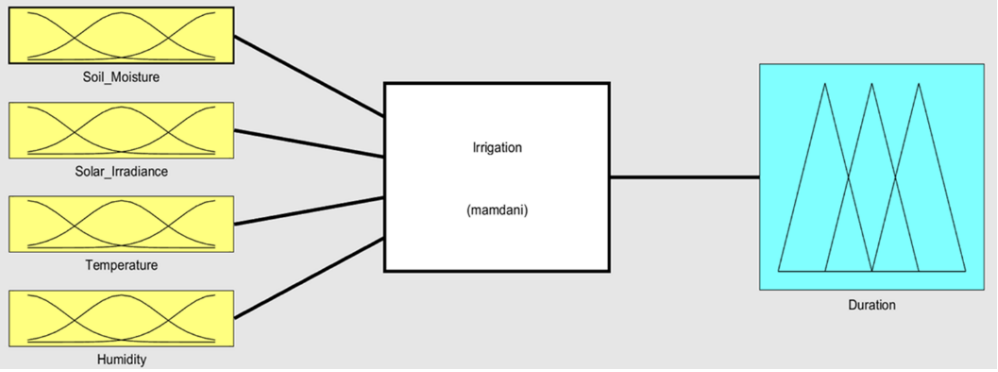

Figure 2. Fuzzy inference system in MATLAB

Membership Functions

Soil Moisture

An essential consideration before irrigation is the soil's moisture content, the drier the soil, the more water we need. On the other hand, adding extra water can harm the plants. As seen in Table 1, three linguistic variables—dry, normal and wet—define the soil moisture input variable. It ranges from 0 to 100 to represent the percentage of moisture content in the soil.

Table 1. Soil moisture membership function description

Fuzzy Set	Membership Function Type	Parameters (%)
Dry	Trapezoidal	[-30 -3 20 35]
Normal	Triangular	[20 40 60]
Wet	Trapezoidal	[45 60 103 130]

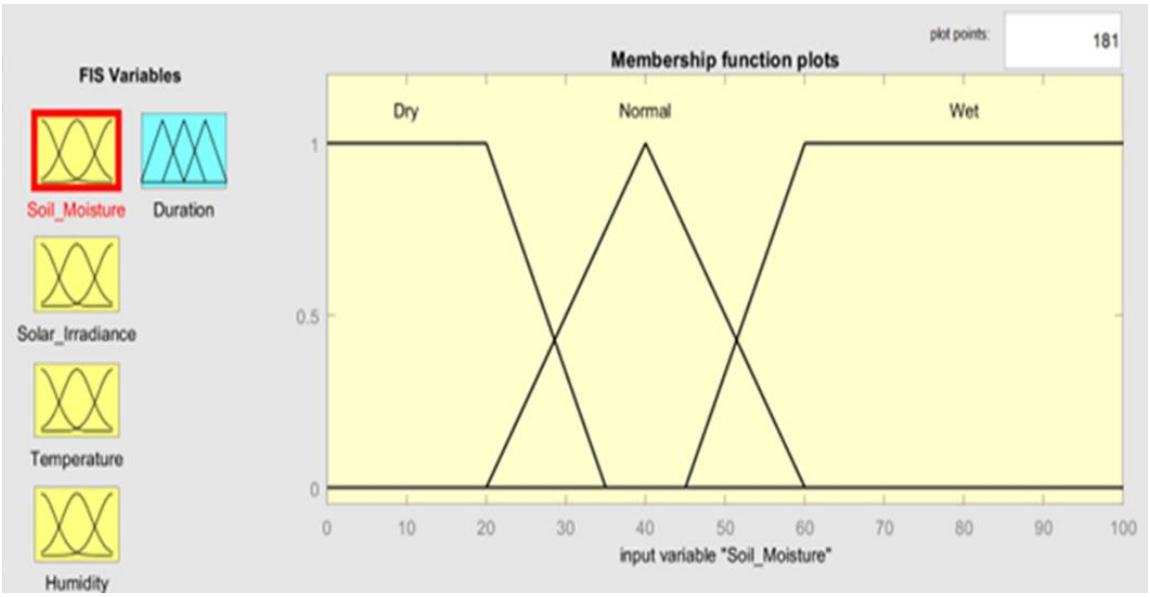

Figure 3. Soil moisture membership function plot

Solar Irradiance

Solar irradiance has a direct effect on evaporation, so it is one of the most important variables for calculating the amount of water required for irrigation. The unit of measurement for solar irradiance is watts per square meter and the amount of solar irradiance incident on the soil will range from 0 to 1000.

Table 2. Solar irradiance membership function description

Fuzzy Set	Membership Function Type	Parameters (W/m^2)
Low	Trapezoidal	[-375 -40 400 550]
Moderate	Triangular	[400 550 700]
High	Trapezoidal	[550 700 1050 1200]

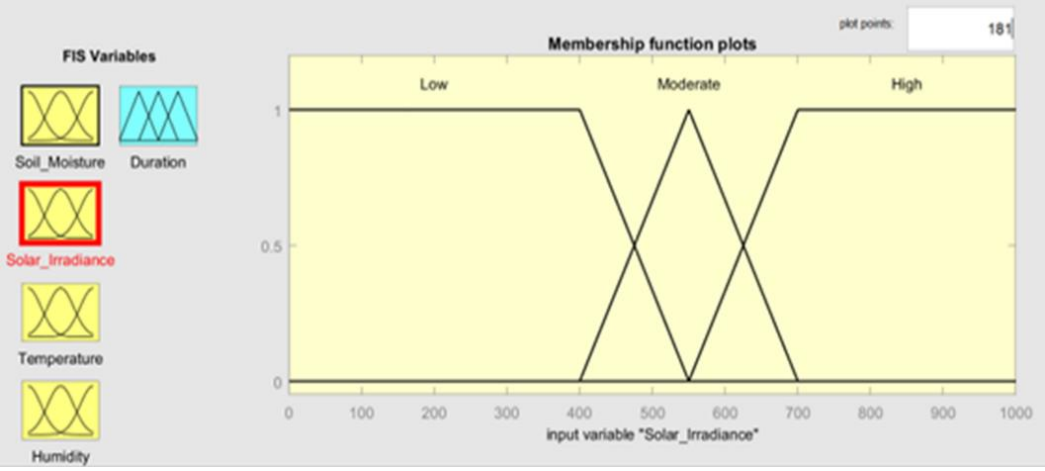

Figure 4. Solar irradiance membership function plot

Temperature

The moisture in the soil will evaporate faster at a high air temperature, which will change the water balance. Thus, in fuzzy logic control, temperature is an important factor to be considered during irrigation. Temperature is expressed as degrees Celsius and approximately ranges from 0 to 50 in Riyadh.

Table 3. Temperature membership function description

Fuzzy Set	Membership Function Type	Parameters (°C)
Cold	Trapezoidal	[-17.5 -3 17 22]
Worm	Triangular	[17 22 27]
Hot	Trapezoidal	[22 27 51 60]

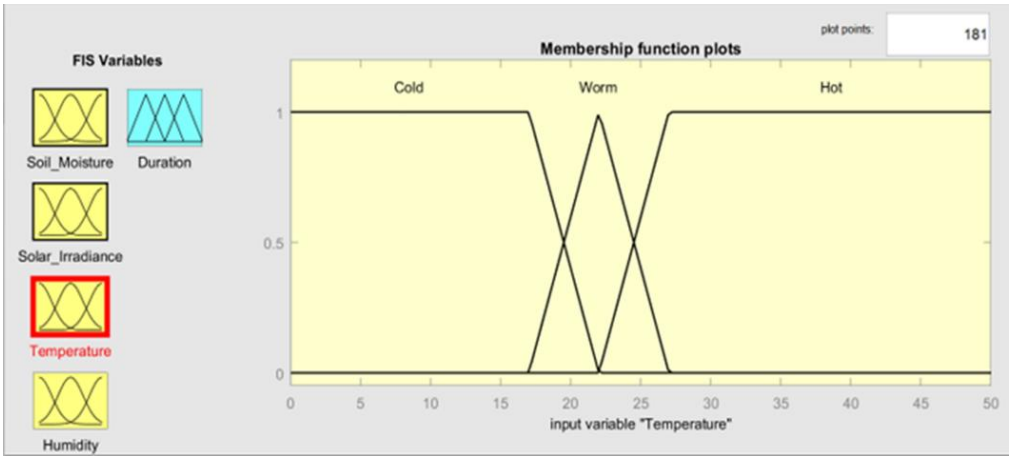

Figure 5. Temperature membership function plot

Air Humidity

Humidity is expressed as a percentage of moisture in the air around the soil surface. Although air humidity is considered very low in Riyadh city, it is nevertheless important to take it into account because it affects evaporation.

Table 4. Air humidity membership function description

Fuzzy set	Membership function type	Parameters (%)
Low	Trapezoidal	[-37 -5 35 50]
Moderate	Triangular	[35 50 65]
High	Trapezoidal	[50 65 105 138]

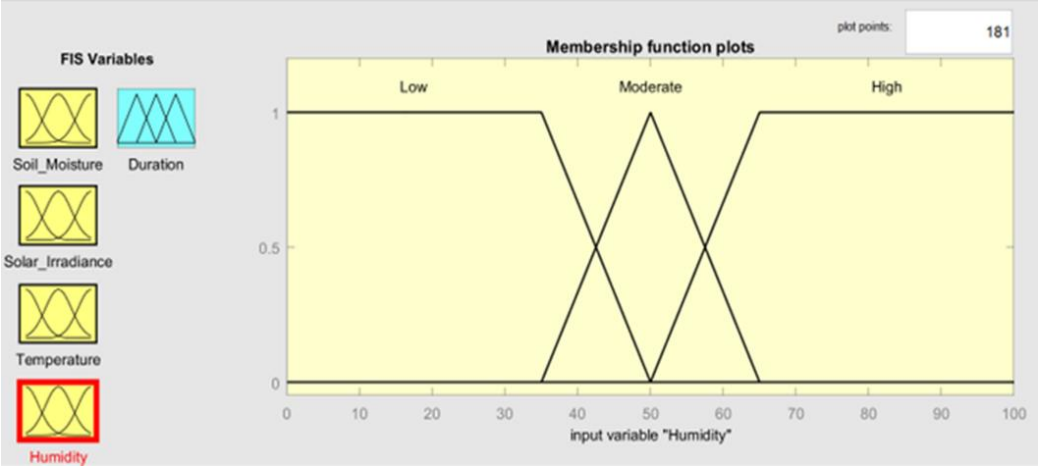

Figure 6. Air humidity membership function plot

Duration

The output of the proposed fuzzy controller is the necessary irrigation duration, which will be defined by five linguistic variables and measured by minutes ranging from 0 to 10.

Table 5. Duration membership function description

Fuzzy Set	Membership Function Type	Parameters (min)
Very Short	Triangular	[-1 0 2.5]
Short	Triangular	[0 2.5 5]
Medium	Triangular	[2.5 5 7.5]
Long	Triangular	[5 7.5 10]
Very Long	Triangular	[7.5 10 11]

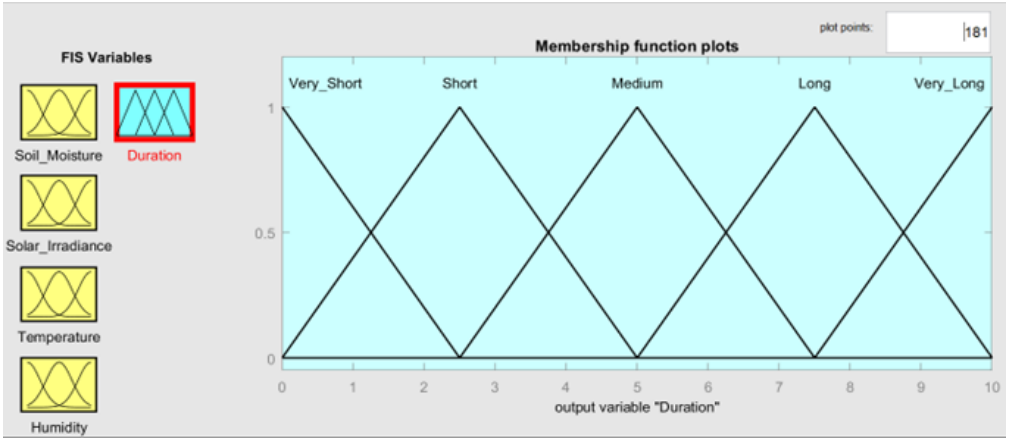

Figure 7. Duration membership function plot

Fuzzy Rules Analysis

By considering the impact of each input variable on the quantity of water required by plants, fuzzy rules can be generated. The relationship between the output variable and the input variables, which are soil moisture, solar irradiance, temperature and air humidity, can be expressed as follows:

- The need for water decreases with rising soil moisture content, indicating an inverse relationship between soil moisture and duration.
- As a result of the increased rate of evaporation caused by rising solar irradiance, irrigation duration increases in order to maintain soil moisture levels. Consequently, a direct relationship is created.
- Since temperature influences soil moisture content in a manner similar to how solar irradiance does, there is a direct relationship between irrigation duration and temperature.
- The evaporation rate of water in the soil increases when the air's moisture content is low because dry air tends to absorb moisture from the surface, hence there is an inverse relationship between duration and air humidity.

As a result, the irrigation duration required for the plant is directly proportional to solar irradiance and temperature, whereas it is inversely proportional to soil moisture and air humidity. The total number of fuzzy rules that must be created can be calculated by multiplying the number of membership functions for each input variable, which is 3×3×3×3 = 81 rules. The first considered case is the minimum. When the soil is wet, solar radiation is low, the temperature is cold and the humidity is high, then the irrigation duration is minimal. Then by changing soil moisture from dry to wet, solar irradiance from low to high, temperature from cold to hot and humidity from high to low, we can claim that the required time for irrigation is increasing. Some rules are indicated in Figure 8.

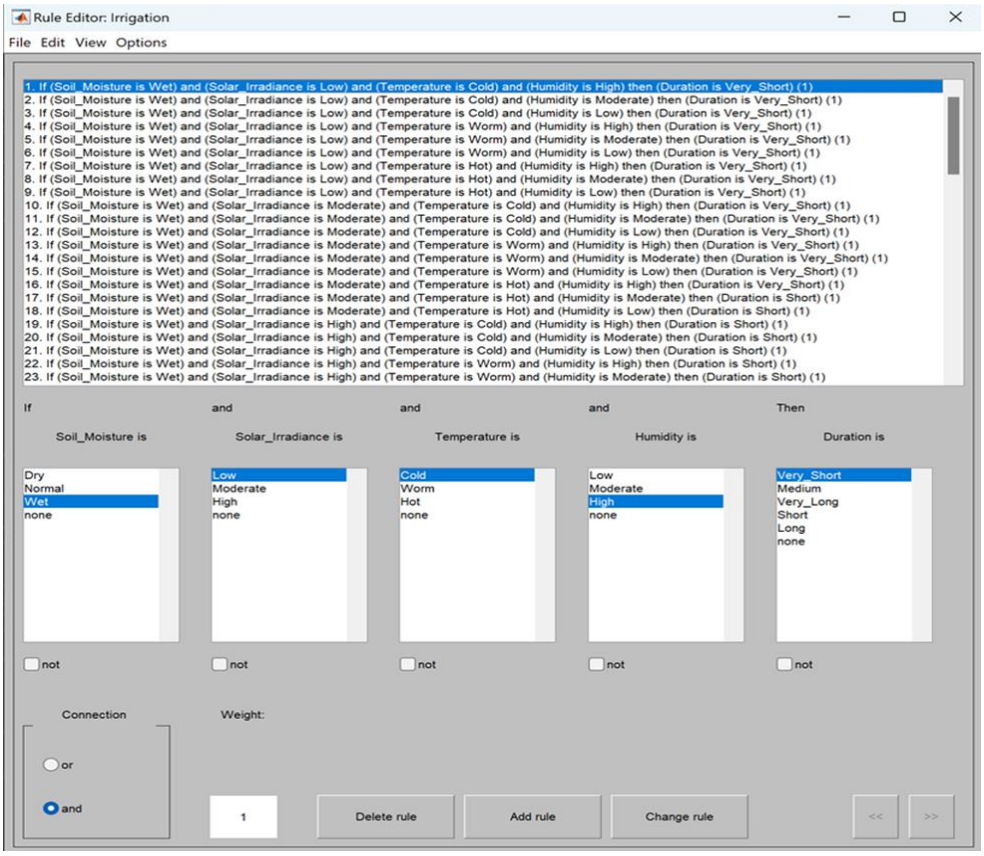

Figure 8. Rule base editor

As illustrated in Figure 9, the surface shows that the irrigation duration decreases with increases in soil moisture and air humidity.

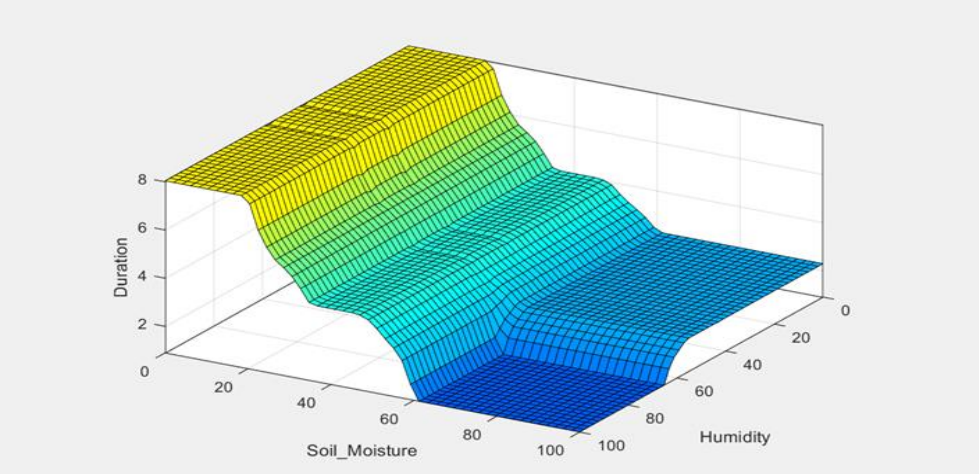

Figure 9. Surface graph of soil moisture and humidity vs duration

In contrast, the irrigation duration increases directly with solar irradiance and temperature as shown in Figure 10. Moreover, Figure 11 displays that solar irradiance and soil moisture have different proportions with irrigation duration, which almost confirms that the given rules are accurate.

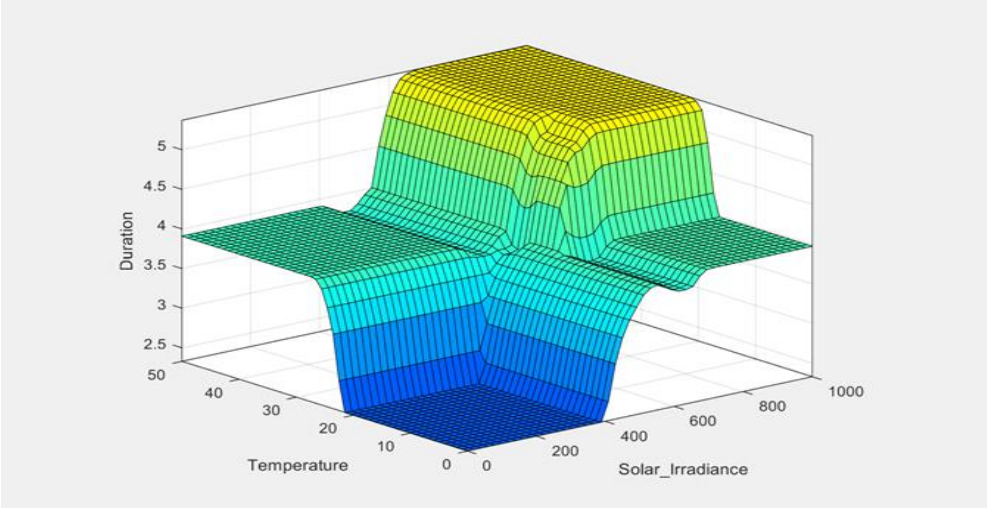

Figure 10. Surface graph of temperature and solar irradiance vs duration

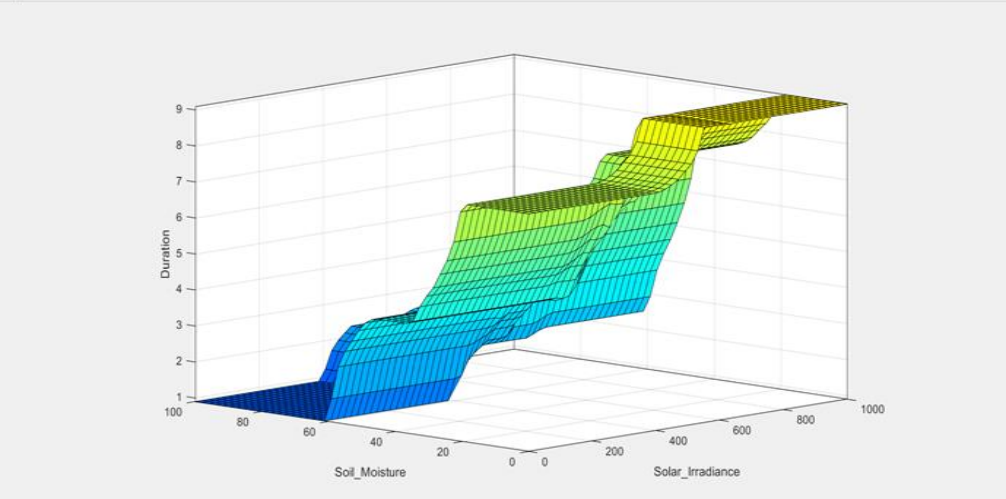

Figure 11. Surface graph of soil moisture and solar irradiance vs duration

Results

In Figure 12 , a set of crisp values have been implemented to the fuzzy logic control system. The values of 20, 250, 43 and 25 have been applied to the input variables of soil moisture, solar irradiance, temperature and humidity. The Centroid method is applied to compute the corresponding crisp output on irrigation duration which is 7.5 minutes

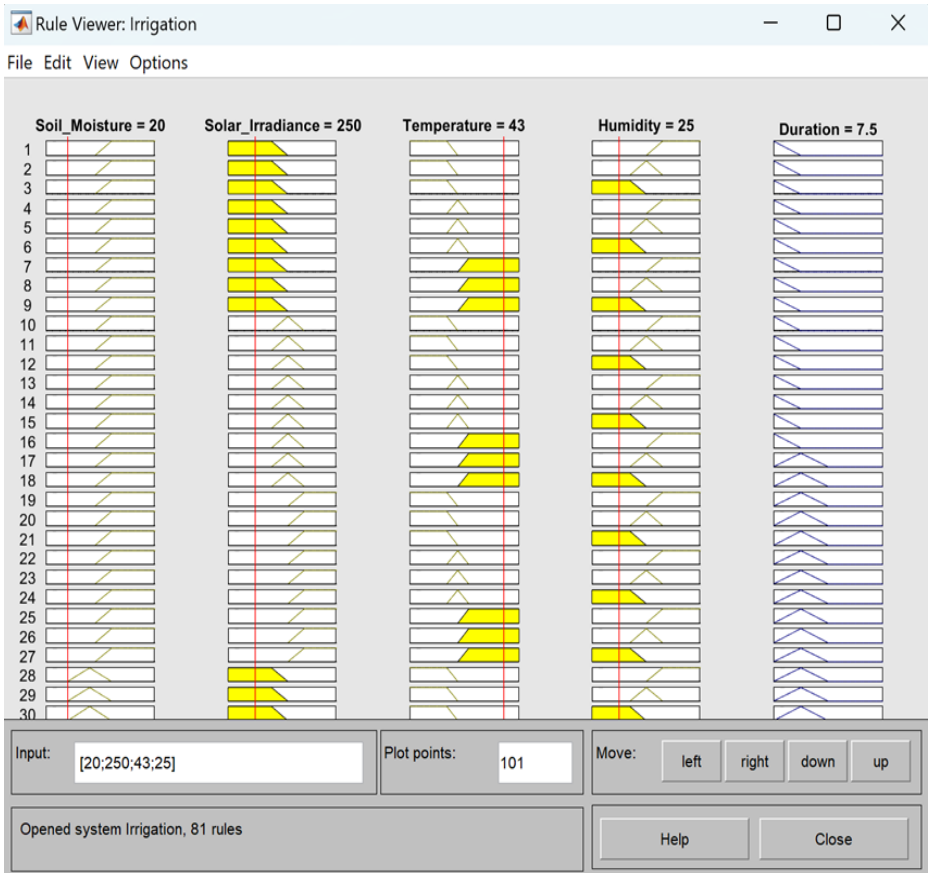

Figure 12. Rule viewer

Multiple cases have been applied using the proposed fuzzy irrigation logic controller. Some results are shown in Table 6 where the effect of all inputs on the irrigation duration was observed. When comparing the first and second rows, soil moisture and air humidity are constant, but solar irradiance decreased from 900 to 500 and air temperature decreased from 50 to 20, which led to a decrease in irrigation duration from 9.2 to 7.97. Additionally, the soil moisture and solar irradiance in the third and fifth rows remained constant, while the air temperature dropped from 40 to 10 and the air humidity rose from 20 to 100, resulting in a decrease in the irrigation duration.

Table 6. Results

Serial No.	Soil Moisture (%)	Solar Irradiance (W/m^2)	Temperature (°C)	Humidity (%)	Duration (min)
1	15	900	50	50	9.2
2	15	500	20	50	7.97
3	30	900	40	20	7.67
4	30	400	40	20	6.03
5	30	900	10	100	6.09
6	40	500	20	50	4.05
7	50	700	30	20	5.37
8	80	800	30	50	2.5
9	80	300	30	30	0.8

Simulation

To evaluate the ability of the fuzzy controller, a prototype model was created in Simulink. For each input variable, this model can be used to evaluate the fuzzy controller over a wide range of input values. Each input variable is subjected to a sine wave function block with various parameters in order to permute every possibility as specified in the fuzzy rule base. To obtain every possible permutation of the values of all the input variables, each wave is designed to engulf the others in every manner.

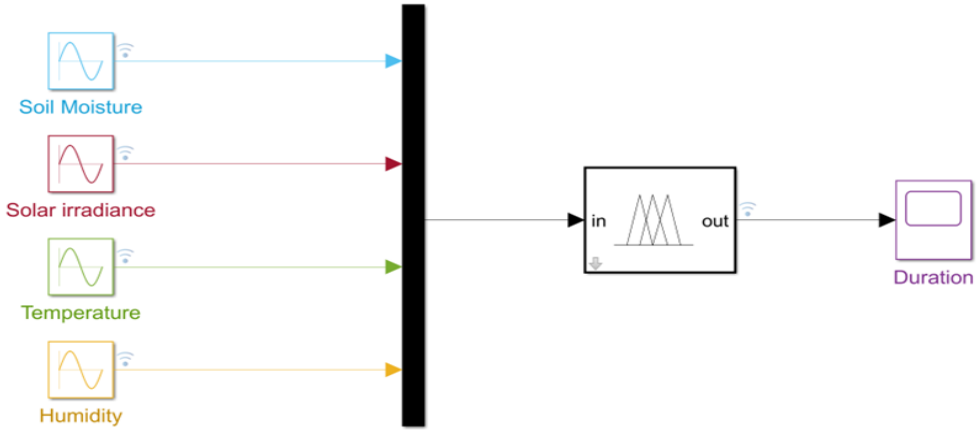

Figure 13. Simulink model

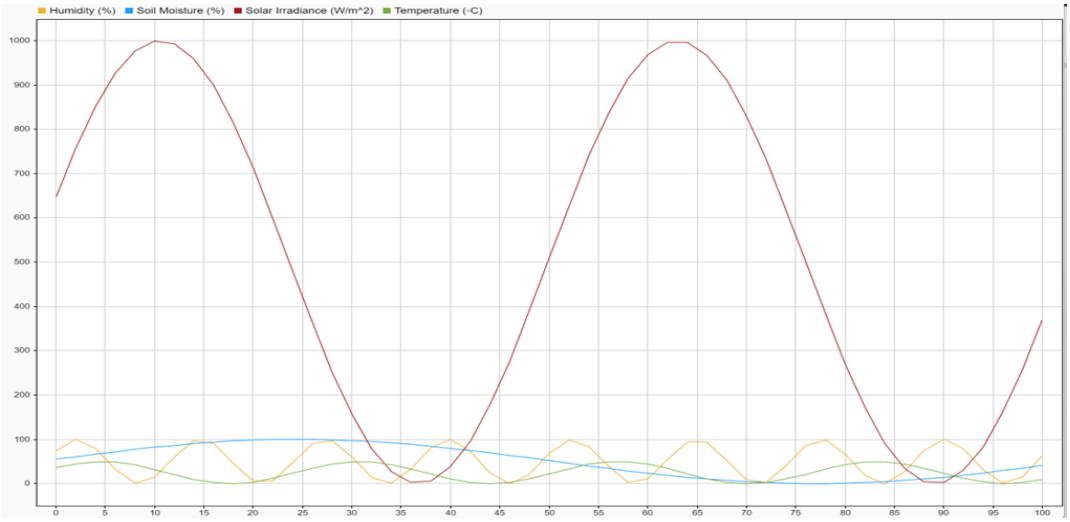

Figure 14. Inputs in simulink model

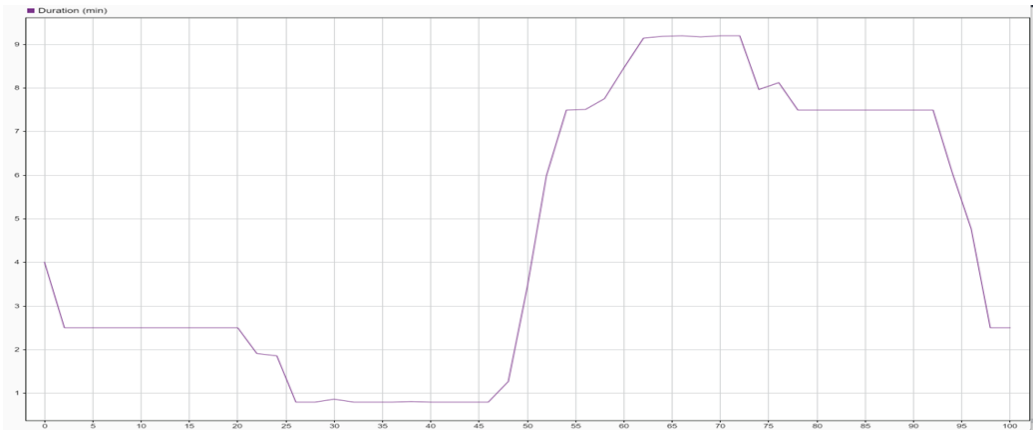

Figure 15. Output in simulink model

According to Figure 14 and Figure 15, the x-axis represents the simulation time, while the y-axis represents the value of the corresponding variable with respect to its unit of measurement. Every variable is denoted by a distinct color as shown at the top of the figures. Hence, Figure 14 displays how the input variable values changed during the simulation and the output result is shown in Figure 15. The following findings were noted:

- We can observe that the duration decreases as we move from 20 to 26 on the x-axis. This is due to a decrease in solar irradiation at the same time when soil moisture was at its peak and humidity was increasing. The need for more water was eliminated and the duration decreased to the minimum.
- The duration increases when we move from 46 to 64 on the x-axis, which coincides with an increase in solar irradiation to its highest and a decrease in soil moisture. This implies that in situations where soil moisture is low and solar radiation at its peak, the duration increases to the maximum.

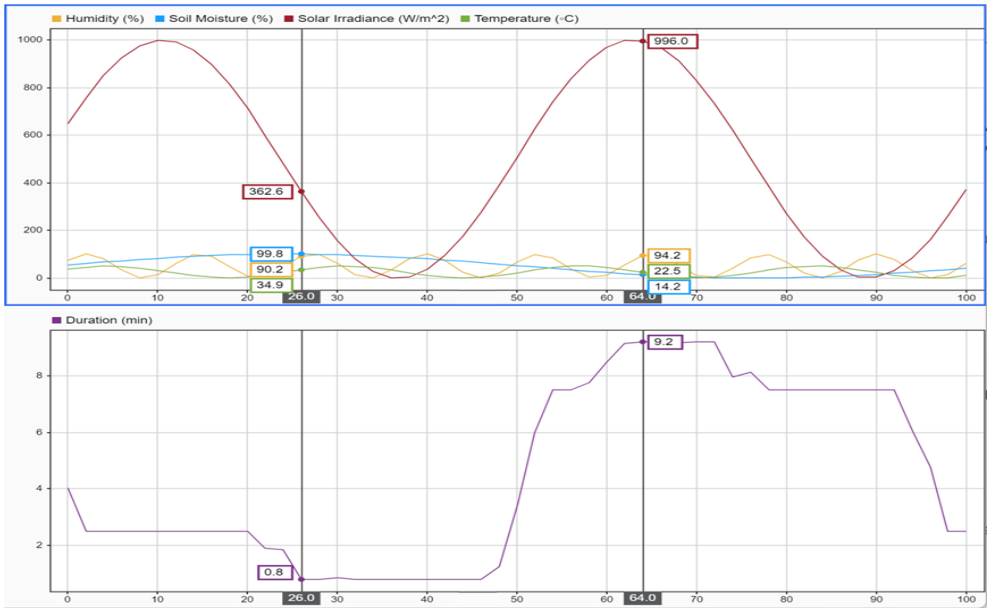

Figure 16. Simulink model with two cursors

Conclusion

In this paper, a smart irrigation control system based on fuzzy logic adapted to the climate of Riyadh was suggested. The theoretical part of the irrigation controller has been proposed, but the irrigation system could be tested and then implemented in the field by engineers. To collect data, the use of different types of sensors is necessary to gather real-time measurements for each input variable. Along with sensing the moisture level of the soil and climatic factors, determining the type of plant can also help to interpret the need of water for irrigation. Finally, to achieve the best performance of the system, we need an expert's knowledge to ensure the accuracy of the rules.

Scientific Ethics Declaration

The authors declare that the scientific ethical and legal responsibility of this article published in EPSTEM journal belongs to the authors.

Acknowledgments or Notes

* This article was presented as an oral presentation at the International Conference on Basic Sciences, Engineering and Technology (www.icbaset.net) held in Alanya/Turkey on May 02-05, 2024.

* This research project was supported by a grant from the "Research Center of the Female Scientific and Medical Colleges", Deanship of Scientific Research, King Saud University.

References

Abdelrahman. (2022, April 14). *Green Riyadh project. the royal commission for Riyadh city*. Retrieved from https://www.rcrc.gov.sa/en/projects/green-riyadh-project

Abdelrahman. (2023, May 7). *King Salman Park project. The royal commission for Riyadh city*. Retrieved from https://www.rcrc.gov.sa/en/projects/king-salman-park-project

Bai, Y., Zhuang, H., & Wang, D. (2007). *Advanced fuzzy logic technologies in industrial applications* (1st ed.). Springer Science & Business Media.

Ghosh, A. (2023, August 23). *What is afforestation? ımportance and advantages of afforestation - conserve energy future. conserve energy future.* Retrieved from https://www.conserve-energy-future.com/importance-advantages-afforestation.php

Khatri, V. (2018). Application of Fuzzy logic in water irrigation system. *Int. Res. J. Eng. Technology*, *5*(4), 3372.

Mohammed, B., Bekkay, H., Migan-Dubois, A., Adel, M., & Rabhi, A. (2021). An intelligent irrigation system based on fuzzy logic control: A case study for Moroccan oriental climate region. In *2nd international Conference on Embedded Systems and Artificial Intelligence (ESAI'21).*

Ross, T. J. (2009). *Fuzzy logic with engineering applications.* John Wiley & Sons.

Singh, A. K., Tariq, T., Ahmer, M. F., Sharma, G., Bokoro, P. N., & Shongwe, T. (2022). Intelligent control of irrigation systems using fuzzy logic controller. *Energies, 15*(19), 7199.

Author Information

Sara Alsaadoun
Mathematics Department, Faculty of Science, King Saud University. P.O . Box 22452, Riyadh 11495, Saudi Arabia
Contact e-mail: *salsaadoun@ksu.edu.sa*

Fairouz Tchier
Mathematics Department, Faculty of Science, King Saud University. P.O . Box 22452, Riyadh 11495, Saudi Arabia

To cite this article:

Alsaadoun, S. & Tchier, F. (2024). Proposed intelligent irrigation system for Riyadh city using fuzzy logic. *The Eurasia Proceedings of Science, Technology, Engineering & Mathematics (EPSTEM), 28,* 397-407.

The Eurasia Proceedings of Science, Technology, Engineering & Mathematics (EPSTEM)
ISSN: 2602-3199

The Eurasia Proceedings of Science, Technology, Engineering & Mathematics (EPSTEM), 2024

Volume 28, Pages 408-416

ICBASET 2024: International Conference on Basic Sciences, Engineering and Technology

Vehicle Autonomous Driving System

Adnan Al-Smadi
Yarmouk University

Sara Al- Essa
Yarmouk University

Shaima Momani
Yarmouk University

Haneen Bani-Salameh
Yarmouk University

Abstract: Autonomous vehicles or self-driving cars industry and technology have played an important role in research industry and automotive industry. Autonomous cars are those vehicles have the ability to sense there surrounding and navigate and drive themselves on roads through traffic without human interventions. In other words, they can move from one location to another one without human interaction. In this paper, an autonomous vehicle system prototype is proposed. The vehicle is able to sense its surrounding and keep going on the road on its own through traffic and other barriers such as people and traffic lights. That is, the vehicles are able to drive and detect the road signals and take decision accordingly, whether to continue or to make a turn. The proposed system uses raspberry pi microcontroller and ultrasonic sensors to detect any object, obstacle, or pedestrians in front of the vehicle and to measure the distance. In addition, a raspberry pi camera is connected to the raspberry pi to continuously take pictures of the road. These pictures will be analyzed by the raspberry pi microcontroller. The vehicle is able to reach its destination safely. A self-driving car prototype has been designed and implemented. The porotype autonomous vehicle system was tested and performed as expected.

Keywords: Self-driving car, Raspberry Pi, Ultrasonic sensor, Signal detection, Raspberry Pi camera

Introduction

As technology is moving fast, manufacturing is also moving toward automation. Vehicle automation in contrast is in fact changing the conception of industry (Al-Smadi & Msallam, 2022). Autonomous vehicles or self-driving cars industry and technology have played an important role in research and automotive industry. Autonomous cars are those cars have the ability to sense there surrounding, navigate, and drive themselves on roads through traffic without human interventions (Szikora & Madarász, 2017; Pawar et al., 2021). In other words, autonomous cars are those cars that can move from one location to another without human interaction. With the number of vehicles rapidly increasing in every country, the number of traffic accidents is increasing on the roads day by day. Many of these accidents are due to human errors. Some of the common causes of these accidents are the use of mobile phones while driving, in addition to several in-car entertainment equipment's. According to the study (Ondruša et al., 2020), it is expected due to autonomous vehicles that accidents will decrease to 80% by the year of 2040. The reason of this expectation is because autonomous vehicle would make it possible to reduce traffic collision and controlling speed limits. Currently, autonomous vehicles are already implemented in several countries without any human input (Shetty et al., 2019). Tesla Motors Inc.

headquartered in Texas –United States of America successfully manufactured self-driving car, Tesla X in the year of 2015. Several companies such as Nissan Waymo and Tesla Motors Inc. are involved in manufacturing self-driving cars (Manikandan et al., 2020).

Banerjee (2020) presented a review survey about the autonomous vehicles. His paper presents a brief description of the various elements and components that are essential in making up a self-driving car system. Some of these components are sensors, global positioning system (GPS), image processing units. Thadeshwar et al. (2020) proposed an autonomous car model that consists of Monocular vision algorithm, CNN, Raspberry Pi, camera, Arduino, Haar cascade classifier, and an Ultrasonic sensor. The instructions' commands will reach the vehicle through the Arduino microcontroller which is connected to the RC vehicle. The car will operate based on convolutional neural network predictions and some hardware coded commands. Nandhini et al. (2020) described a self-driving car model using a PIC microcontroller, raspberry pi processor, speed sensor, color sensor, and ultrasonic sensor. These components were integrated to build an autonomous car. Shirke et al. (2020) proposed a self-driving car using Arduino uno, raspberry pi, ultrasonic sensors, a dc motor, and a camera. The prototype model was built with a toy car with two motors. One motor to move the toy car straight forward and backward, while the second motor is to turn the toy car left or right.

In this paper, a self-driving vehicle model is proposed. The vehicle can sense its surrounding and move on the road on its own through traffic and other obstacles such as pedestrians and traffic lights. That is, the self-driving can drive and detect the road signals and take decision accordingly, whether to continue or to make a turn. The proposed system uses raspberry pi microcontroller and ultrasonic sensors to detect any obstacle, or pedestrians in front of the vehicle and to calculate the distance. In addition, the raspberry pi camera is connected to the raspberry pi to continuously take pictures of the road. These pictures will be analyzed by the raspberry pi microcontroller. The vehicle can reach its destination safely. A self-driving car prototype has been designed and implemented. The porotype autonomous vehicle system was tested and performed as expected.

Proposed System

As the world population grows, the number of vehicles on the roads are continuously increasing. Hence, the number of traffic accidents are increasing which result in death and injuries of people. Traffic congestion is another problem the world will be facing with the increasing number of automobiles which is fuel and time costly. In this paper, we propose a self-driving car system that is able to sense and drive without any human intervention. The system includes ultrasonic sensors, raspberry pi, Dc motors, H-Bridge, raspberry pi camera, and a power supply. The ultrasonic sensors are mainly used to calculate the distance in front of the car, while the raspberry pi camera selects the correct road and the Dc motor move the car. Figure 1 shows the block diagram of the proposed module. The main components of the proposed vehicle automated driving system are described as follows.

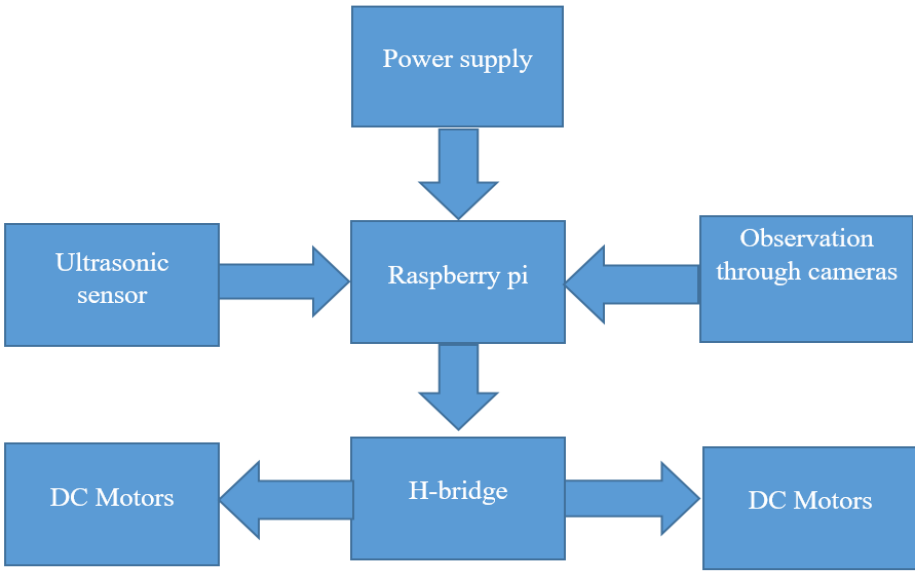

Figure 1. Block diagram of the proposed vehicle automated driving module

Raspberry Pi 3 Processor

Raspberry pi processor is a small computer board has a size of a credit card developed in 2009 by the raspberry pi foundation which is registered in England and Wales. The development of the raspberry pi was intended for teaching basic computer science and its related areas. Currently, there are five types of the raspberry pi available in the market (Nandhini et al., 2020; Al-Smadi et al., 2023). Raspberry pi microcontroller uses Python language; hence the name raspberry pi comes from the raspberry fruit and pi for python. The raspberry pi processor has been widely used to build school projects. It can be used as any desktop computer if it is connected to all peripherals such as keyboard, mouse, and monitor. Raspberry pi processor is shown in Figure 2.

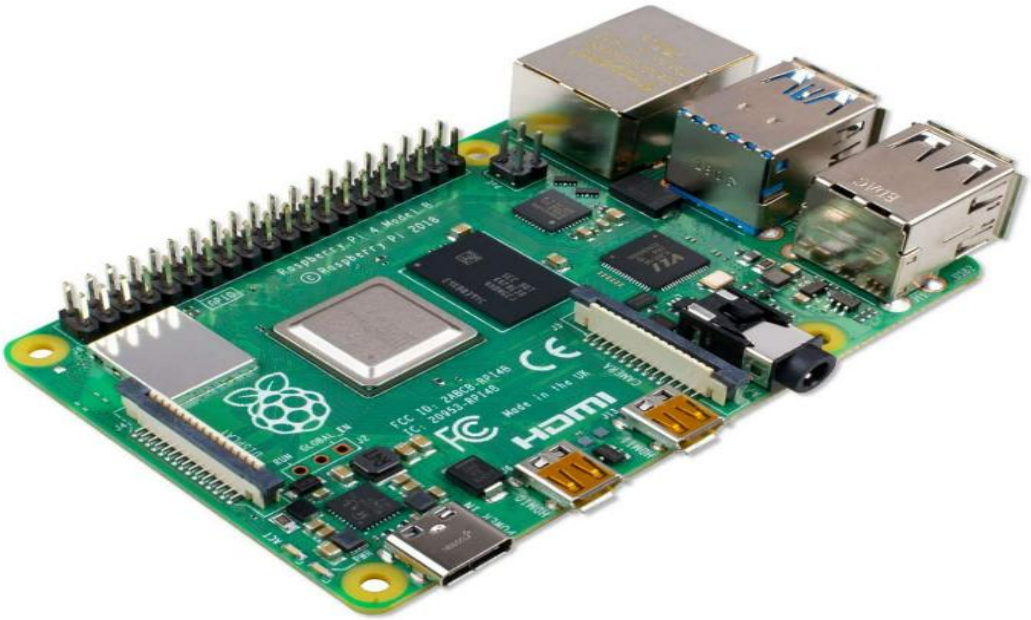

Figure 2. Raspberry Pi 3 processor (Al-Smadi et al., 2023)

Raspberry Pi 3 Camera

The Raspberry Pi camera module 2 (v2) has an 8-megapixel image sensor. The camera can take high definition video in addition to photographs. It can be used online for time-lapse, and slow-motion videos. It is connected to the camera serial interface (CSI) port on the raspberry pi with a 15 cm ribbon cable. The CSI connectors consist of two smaller interfaces which establish the communication bus. The first interface transfers data and clock signals from the camera to the processor in one direction only. The other interface is bidirectional control link (Upton & Halfacree, 2012).

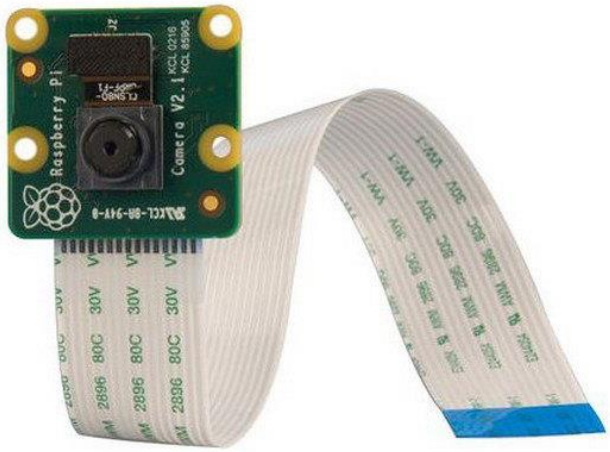

Figure 3. Raspberry Pi camera (Pawar et al., 2021)

Ultrasonic Sensor

An ultrasonic (US) sensor is an electronic sensor that can perform as a transmitter and a receiver. The transmitter converts electrical signal into ultrasonic wave. It emits ultrasonic wave at frequency of 40K Hz that travels in the air. The ultrasonic receiver waits for the ultrasonic wave to return after it gets reflected by an object and converts the sound wave into electrical and sends it back to the sensor. Figure 4 shows HC-SR04 ultrasonic sensor module. This module HC-SR04 is provided with 2cm-400cm measurement with an accuracy of about 3mm. As the pins of the HC-SR04 sensor indicates, pin 1 (Trigger) is the input pin. Pin 3 (Echo) is the output pin. The sensor uses the ultrasonic sound wave to measure the distance to the object (Al-Smadi et al., 2023).

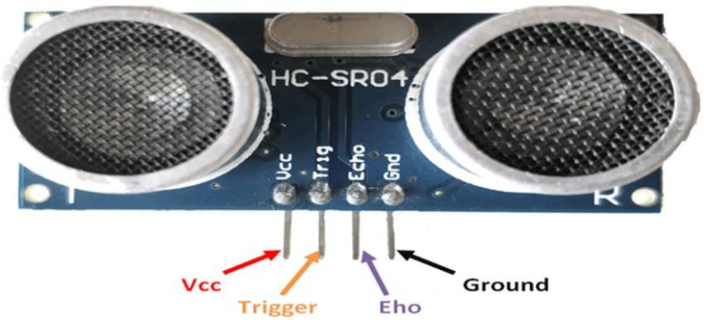

Figure 4. Ultrasonic Sensor HC-SR04 module ((Al-Smadi & Msallam, 2022)

H-Bridge

An H-bridge or a motor driver is an electronic drive circuit consists of transistors that allow the motor to change its direction as well as its speed. It is called H-bridge because it resembles the letter H. H-bridge circuit can be easily interfaced to control the DC motor rotation. It is used to drive the motor counterclockwise and clockwise by switching the polarity of the applied voltage (Al-Smadi et al. 2020). As shown in Figure 5, the H-bridge driver has four switches that allow controlling the applied source across the load in both directions. These switches are normally made with MOSTFETs or pnp and npn transistors. The H-bridge makes the motor move forward and backward by activating two switches together. For example, activating S_2 and S_3 at the same time while keeping S_1 and S_4 open will apply appositive voltage across the motor. On the other hand, activating S_1 and S_4 at the same time while keeping S_2 and S_3 open will reverse the applied voltage across the motor. This allows reserve rotation of the motor. Figure 6 shows the L298N twin H-bridge motor driver. This device permits to control speed and direction of two DC motors at the same time.

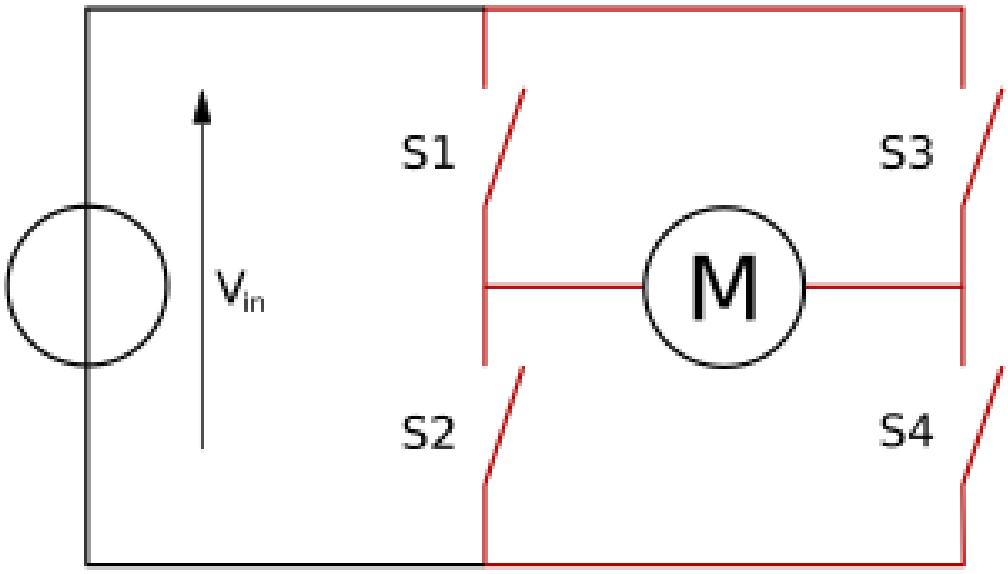

Figure 5. H-bridge motor driver circuit

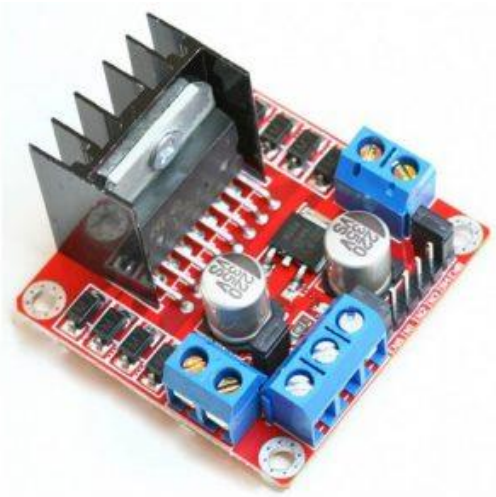

Figure 6. L298N H-bridge motor driver (Al-Smadi et al., 2020)

Python Language

Python language is a popular dynamic type, object oriented, and high-level programing language. It was developed by Guido Van Rossum in the 1980s. It is a general-purpose language which may be used for many applications such as in website developing, machine language, automating repetitive tasks, desktop applications, and many other fields (Stewart, 2019).

System Implementation

The block diagram of the proposed self-driving car prototype model is shown in Figure 1. The circuit diagram is presented in Figure 7. The main component of the proposed module is the Raspberry pi microcontroller which is considered to be the brain of the system. All other components of the system are connected to the raspberry pi. In the circuit diagram of Figure 7 the ultrasonic sensor connected to the raspberry pi. As the vehicle moves, the ultrasonic sensor will measure the distance between the front of the vehicle (where the sensor is placed) and any object on the road. The distance is calculated by measuring the amount of time required to send ultrasonic wave from the Trig pin of the sensor and waiting for the ultrasonic wave to be received back to the Echo pin of the sensor. Hence, the distance is

$$\text{Distance} = \text{Speed X Time}/2 \tag{1}$$

The universal speed of ultrasonic wave is 330 meter/second. The time in Equation (1) is divided by 2 because it is the time from sending trigger and receiving echo signals. The raspberry pi camera, which is interfaced with the raspberry pi controller through 15-pin ribbon cable is activated as long as the car is moving to keep the car at the center of the road. If the distance from the observed object is more than 20 cm, the camera will continuously take pictures of the road. These pictures will be analyzed by the raspberry pi microcontroller. The first step, the colors of the pictures will be changed to black and white using library functions imported in the code. The second step, the contours of the road will be detected by the contour function. There is another function to detect whether the road is at the center of the picture or not. This function, called the moment function, works by transforming the pixels into matrix. This matrix contains zeros and ones. The moment function also calculates the final value of the matrix which is referred to as “cx”. This value is the number of the column with entries of ones which determines whether the car should veer to the left, to the right, or keep moving straight. It was determined experimentally that the movements of the car are governed as follows.

$$\begin{aligned} cx < 160 &\quad \text{Move to the right} \\ 160 < cx < 480 &\quad \text{Keep going straight} \\ cx > 480 &\quad \text{Move to the left} \end{aligned} \tag{2}$$

These processes are shown in the flow chart of Figure 8. According to the results, the raspberry pi generates the necessary signal for the H-bridge driver motor to move in the correct direction at the proper speed. The right two wheels are connected to one DC motor, while the left two wheels are connected to the second DC motor. Therefore, when both motors rotate in the same direction, the vehicle will move forward. Table 1 shows the directions of the motors and the vehicle. In the table, clockwise means positive current, while counterclockwise negative current. If the distance is less than 20 cm, then the car will stop till the obstacle is removed. The camera will start processing and veer the car to left or to the right and the process will continue as previously described. All the components in the block diagram of Figure 1 and the circuit diagram of Figure 7 interact with each other's by taking orders from the raspberry pi microcontroller through the python code.

Table 1. The directions of the motors and vehicle

Motor 1 (Right Motor)	Motor 2 (Left Motor)	Vehicle
clockwise	clockwise	Forward
counterclockwise	counterclockwise	Backward
clockwise	counterclockwise	Left
counterclockwise	clockwise	Right
No current	No current	Stop

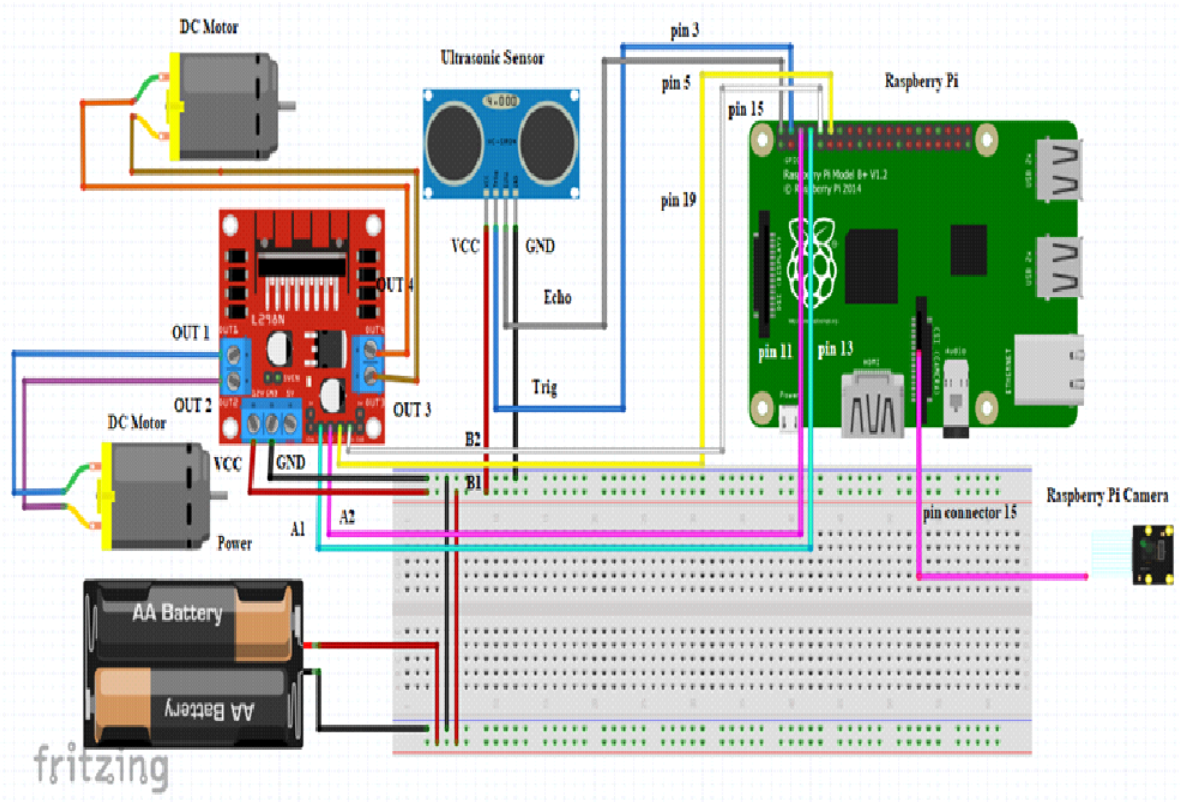

Figure 7. The circuit diagram for the proposed model

Results and Discussion

After implementing the devices in Figure 7, a prototype vehicle of the system was built and activated to start moving. Several photos were taken using the raspberry pi camera. Figure 9 shows the road is at the center of the processed picture, which means that the value of "cx" is between (160, 480). Therefore, the car will keep going straight. Figure 10 shows the road swerves to the right side, which means that the value of "cx" is less than 160. Therefore, the car will turn to the right side of the road and keep going in the correct path. Figure 11 shows the road swerves to the left side, which means that the value of "cx" is greater than 480. Therefore, the car will turn to the left side of the road and keep going in the correct path. The final prototype model for the self-driving vehicle is shown in Figure 12.

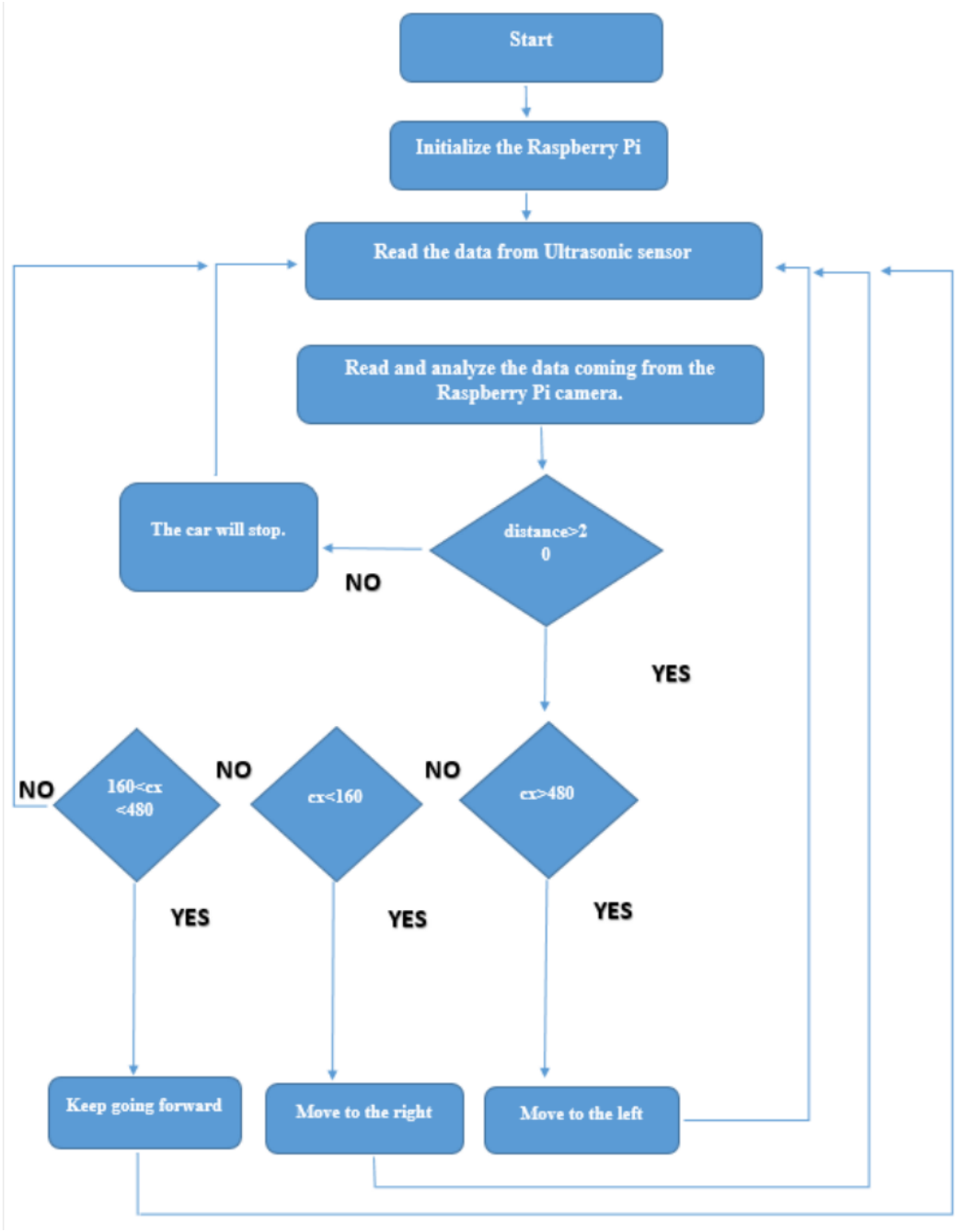

Figure 8. The flow chart of the proposed system

Figure 9. the road is at the center of the picture

Figure 10. The road veers to the right

Figure 11. The road veers to the left

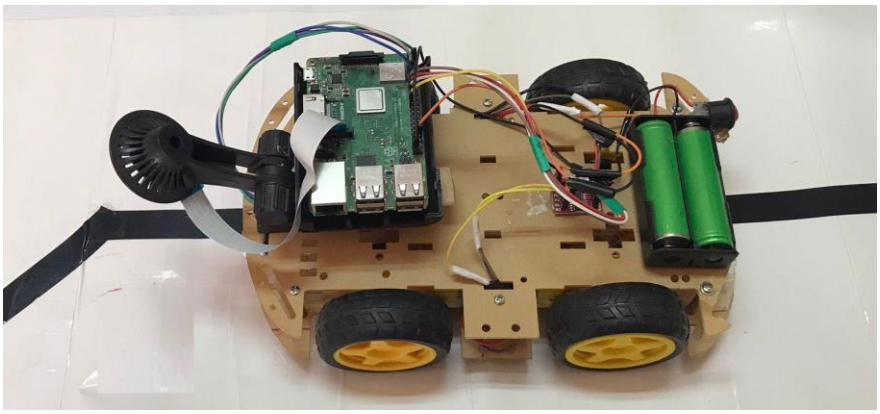

Figure 12. A prototype for the self-driving vehicle

Conclusion

This paper presented a self-driving vehicle that has the ability to move in the correct path without any human intervention. The system uses raspberry pi, ultrasonic sensors, and raspberry pi camera. Python language was used to write the code for the raspberry pi microcontroller. A prototype model for the self-driving vehicle system was built and tested. It performed as expected.

Scientific Ethics Declaration

The author(s) declare that the scientific ethical and legal responsibility of this article published in EPSTEM journal belongs to the author(s).

Acknowledgements or Notes

* This article was presented as oral presentation at the International Conference on Basic Sciences, Engineering and Technology (www.icbaset.net) held in Alanya/Turkey on May 02-05, 2024.

*The authors would like to thank Yarmouk University, Jordan for financial support to implement this research.

References

Al-Smadi, A., Al-Ksasbeh, W., Ababneh, M., & Al-Nsairat, M. (2020). Intelligent automobile collision avoidance and safety system. *17th IEEE International Multi-Conference on Systems, Signals & Devices*, (pp. 319-322). IEEE.

Al-Smadi, A., & Msallam, M. (2022). Vehicle auto parking system. *9th IEEE International Conference on Electrical and Electronics Engineering (ICEEE 2022)* (pp.108-111). IEEE.

Al-Smadi, A., Al-Qaryouti, T., Rehan, A., Assi, H., and Alsharea, A. (2023). A navigation tool for visually impaired and blind people. *3rd International Conference on Basic Sciences, Engineering and Technology (ICBASET)*, *22*, 119-126.

Banerjee, U. (2020). A review on fully autonomous vehicle. *International Research Journal of Engineering and Technology (IRJET)*, *7*(3), 247-253.

Manikandan, T., Jayashwanth, S., Harish, S., & Sivatej, K. (2020). Self-driving car. *International Journal of Psychosocial Rehabilitation*, *24*(5), 380-388.

Nandhini, N., Rakshana, R., Revathi, L., Swarnamalya, S., & Nagaraj, V. (2020). Autonomous cars using Raspberry Pi. *International Research Journal of Engineering and Technology (IRJET), 7*(5), 6340-6346.

Ondruša, J., Kollab, E., Vertaľb, P., & Šarićc, Ž. (2020). How do autonomous cars work? *Transportation Research Procedia*, *44*, 226–233.

Pawar, S., Pawar, B., & Yewale, K. (2021). Self-driving car demo using Raspberry Pi. *International Research Journal of Engineering and Technology (IRJET), 8*(11), 781-784.

Stewart, A. (2019*). Python programming for beginners: A comprehensive guide to learnings the basics of Python programming*. USA:Platinum Press LLC.

Shetty, N., Mohan, K., & Kaushik, K. (2019). Autonomous self-driving car using Raspberry Pi model. *International Journal of Engineering Research & Technology (IJERT), 7*(8), 1-3.

Szikora, P., & Madarász, N. (2017). Self-driving cars — The human side. *IEEE 14th International Scientific Conference on Informatics* (pp.383-387). IEEE.

Shirke, Y., Gawade, U., Jadhav, K., & Hawre, M. (2020). Implementation of SDC: Self-driving car based on Raspberry Pi. *International Research Journal of Engineering and Technology (IRJET)*, *7*(3), 1640-1646.

Thadeshwar, H., Shah, V., Jain, M., Chaudhari, R., & Badgujar, V. (2020). Artificial intelligence based self-driving car. *4th International Conference on Computer, Communication and Signal Processing (ICCCSP)* (pp.1-5). IEEE.

Upton, E., & Halfacree, G. (2012). Raspberry Pi user guide. *John Wily and Sons Ltd.*, West Sussex, United Kingdom.

Author Information

Adnan Al-Smadi
Yarmouk University
Irbid-Jordan
Contact e-mail: *smadi98@yahoo.com*

Sara Al - Essa
Yarmouk University
Irbid-Jordan

Shaima Momani
Yarmouk University
Irbid-Jordan

Haneen Bani- Salameh
Yarmouk University
Irbid-Jordan

To cite this article:

Al-Smadi, A., Al - Essa, S., Momani, S., & Bani - Salameh, H. (2024). Vehicle autonomous driving system. *The Eurasia Proceedings of Science, Technology, Engineering & Mathematics (EPSTEM), 28,* 408-416.

The Eurasia Proceedings of Science, Technology, Engineering & Mathematics (EPSTEM)
ISSN: 2602-3199

The Eurasia Proceedings of Science, Technology, Engineering & Mathematics (EPSTEM), 2024

Volume 28, Pages 417-427

ICBASET 2024: International Conference on Basic Sciences, Engineering and Technology

Diversity of Aquatic and Coastal Vegetation in the Lublin Coal Basin Complex - Long-Term Changes

Joanna Sender
University of Life Sciences in Lublin

Monika Rozanska-Boczula
University of Life Sciences in Lublin

Danuta Urban
University of Life Sciences in Lublin

Abstract: Natural resources are fundamental to the survival and development of human populations, and their exploitation is associated with problems such as resource depletion and environmental degradation. Within the borders of the Lublin Coal Basin (LZW) there is the Łęczna-Włodawa Lake District, which includes over 60 lakes. It is one of the most valuable natural areas in the Lublin Voivodeship and the entire region. Due to the undoubted impact of LZW, as well as the lack of detailed botanical studies in the existing literature, research has been undertaken since the 1980s to analyse the floristic and ecological vegetation of aquatic and coastal plants of 6 lakes in the mine's impact zone. Macrophytes are recognized by the WFD as one of the key groups suitable for freshwater biomonitoring and for ecological classification purposes. The conducted research confirmed the progressive degradation of the analyzed lakes. Since the 1990s, there have been significant changes in the use of the area covered by the analyses. The share of built-up areas has significantly increased, but also the share of surface waters. The share of built-up areas has significantly increased, but also the share of surface waters. The qualitative and quantitative structure of macrophytes has undergone very significant changes towards a reduction in the number of species and phytodiversity. The share of species in fertile habitats has increased. Despite the introduction of various forms of legal protection in this area, changes in the depletion of biodiversity are continuing.

Keywords: Macrophytes, Coal mine, Lakes, Land development, Biodiversity index

Introduction

Human development is possible thanks to the use of Earth's resources. Currently, they are used on an unprecedented scale. Natural resources are fundamental to the survival and development of the human population, and their exploitation is associated with resource depletion and environmental degradation. An industry that contributes greatly to environmental degradation is mining (Carvalho, 2017; Goudie, 2018; Sengupta, 2021). Mining can have significant impacts on water resources, including pollution and depletion (Santana et al., 2020; George et al., 2010). In the Lublin Coal Basin, this is done by pumping groundwater from exploited Carboniferous deposits and then discharging them into surface waters, and (after partial exploitation of the deposit), closed tunnels are closed. Mining is carried out using the collapse mining method (Kraśnicki, 2019). Therefore, it is important to monitor and manage these impacts to minimize negative effects on the environment (Dmitruk, 2021).

Despite its rich deposits, the Lublin Coal Basin is one of the most recently developed mining regions in our country. Coal has been mined here since the 1970s. According to data from the Polish Geological Institute, there

- Selection and peer-review under responsibility of the Organizing Committee of the Conference

are 11 documented hard coal deposits in the LCB; moreover, coal reserves account for approximately 21.5% of Poland's hard coal resources (610 km²) (Malon & Tymiński 2011).

Within the Lublin Coal Basin are the Łęczna-Włodawa Lake District, which includes many lakes, peat bogs, forests and wetlands. It is one of the most valuable natural areas in the Lublin region and is also a recreational area. In addition to the environmental transformations caused by the mine's activities, since the late 1950s, engineering and water investments have led to significant changes in the hydrological regime of this region. It is one of the longest drainage systems in Europe (139.9 km) - Wieprz - Krzna Canal (Janiec, 1993; Poleszuk, 2002). Its aim was to regulate water relations in order to revitalize the region's economy (Solis, 2012; Sender & Maślanko, 2017).

Due to such a strong impact, as well as the lack of detailed hydrobotanical studies in the literature since the 1980s (Popiołek, 1988), research was undertaken to analyze the aquatic and coastal vegetation of 6 lakes in the LCB impact zone. Macrophytes are recognized by the WFD as one of the key groups suitable for freshwater biomonitoring and for ecological classification purposes (Szoszkiewicz et al., 2007). Macrophytes of a variety of aquatic ecosystems have been extensively studied for decades, and their ecological properties have been a common topic of study for a long time (Westlake, 1975; Haslam, 1982; Maberly & Haslam, 1988; O'Hare et al., 2006; Wiegleb et al., 2015). The undertaken research will allow for the assessment of the degree of transformation in the qualitative and quantitative structure of plant ecosystems in the mine's impact zone. The assessment was based on research conducted in the 1970s and 1980s, before the period of the mine's impact, and current research from 2022 and 2023. The degree of changes in the structure of lake macrophytes and their surroundings as well as habitat changes based on the plant requirements were assessed. It was assumed that the mine activity in this area indirectly affects the structure of plants in lakes, which will manifest itself in a decrease in phytodiversity and an increase in habitat fertility. It is expected that in the vicinity of lakes (shoreside) there may be an expansion of plants with lower moisture requirements. In some lakes there may be an increase in species diversity due to the increase in their fertility. The question was asked whether the forms of protection introduced in this area and the mine activities undertaken affect the direction of vegetation changes?

Material and Methods

Study Area

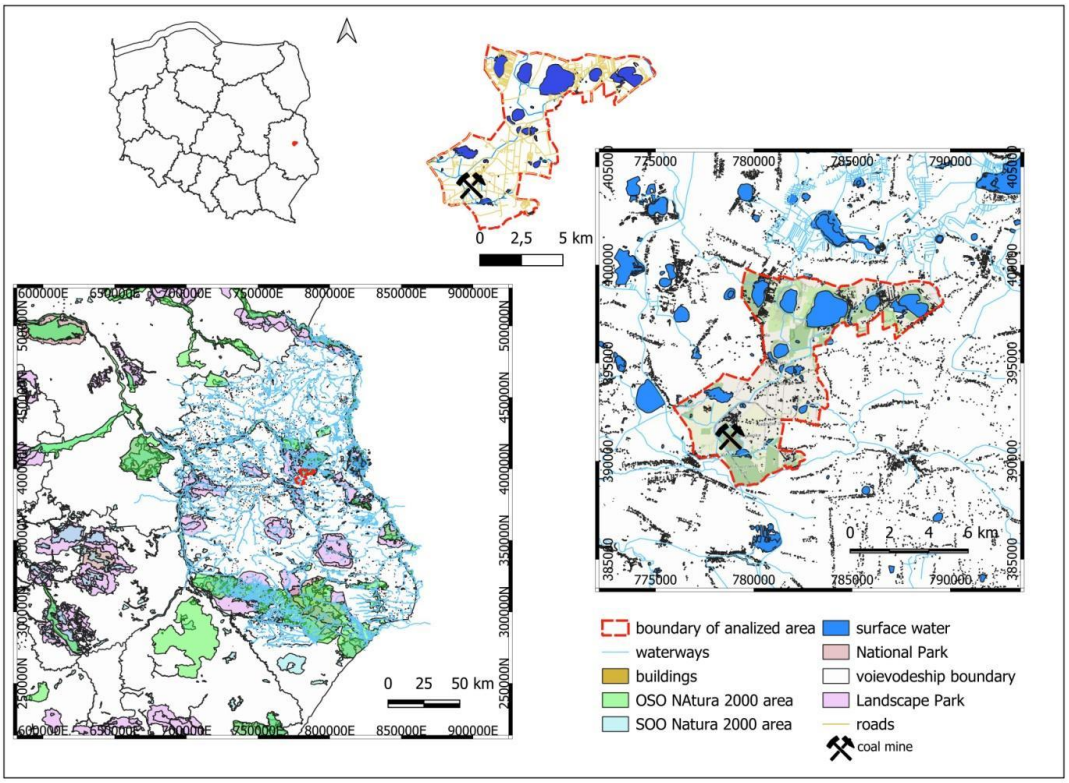

Figure 1. Localization of study area.

Lublin Coal Basin (LCB) is located in eastern Poland, in the Lublin Voivodeship. It is located on the Lublin Upland and is an extension of the Lviv-Volyn Coal Basin, which belongs to Ukraine. In total, the LCB covers an area of over four thousand square kilometers (180 km long, 20 km wide). Currently, there are two large mines operating here - the Bogdanka Hard Coal Mine and the Stefanów Mine. The study analyzed six natural lakes that are located the nearest location and have been subject to mine pressure over the years (Figure 1).

Until the end of the 1980s, there were two forms of protection in the analysis area (Poleski Landscape Park and Polesie Protected Landscape Area). Since 1990, three further forms have been established in this area, including the Łęczyńskie Lakeland Landscape Park, the Uściwierz and Ciesacin ecological areas. Since 2004, areas of international importance have been introduced here - Natura 2000 Uściwierskie Lakes and Polesie. The Polesie National Park, established in 1991, is located nearby (Figure 1).

Field Study

Vegetation structure research was carried out in 6 lakes in the area of the most intensive mine impact and subject to various forms of impact of the area's drainage system. In the study, we analyzed data concerning plant communities and rare plant species from two periods: 1) 1979- 1984 (referred to in the manuscript as 1988) and 2) 2022-2023 (referred to as 2022). Date from the first period come from the literature (Popiołek 1988). Therefore, the data for both study periods were obtained using the same transects and methods. In both periods and for each lake, a total of 200 phytosociological relevés performed according to Braun-Blanquet (1964) method were used. The adopted nomenclature of species followed Mirek et al. (2002) while the taxonomy and nomenclature of communities followed Matuszkiewicz (2012). The investigation of macrophytes were recorded during the summer of 2022 and 2023 at 4 or 5 transects of each lakes along the 50 - 100m long transects.

The study analysed the frequency of plant species in both periods. For the evaluation of plant species, the following scale was used: 0 – absent; 0.1 – extremely rare (few individuals, 1-5%); 1 – very rare (cover 5-25%), 2 – rare (cover 25-50%); 3 – frequent (cover 50-75%); 4 – very frequent (cover 75-100%) (Pawłowski 1977). We tried to select phytosociological relevés in an objective and representative way for the analysed sites to repeat the research in the second period, showing changes in the frequency of occurrence of plant species. Based on the recorded percentages of the plant species occurring, Ellenberg ecological indicator values (Ellenberg et al., 1992) were calculated to assess the climatic and edaphic conditions of the studied lakes. The following ecological indices were considered: L – light, T – temperature, F – moisture, R – soil reaction (pH), N – nitrogen content and S - salinity. Data from two periods were used to the assess changes in habitat conditions over time.

Cartographic Analyzes of Changes

Land use analyzes were carried out in the entire area including the mine and 6 lakes. For cartographic analyses, land cover maps from 1990 and 2022 downloaded from the Corine Land Cover 1990 and 2022 website (by Copernicus) were used. On this basis, changes in the development of the entire research area were determined. For this purpose, QGIS software was used, in which, after generating the area up to the study limits, the share of areas such as: mixed forests, complex crop and plot systems, areas occupied mainly by agriculture with a large share of natural vegetation, arable land beyond the reach of irrigation devices, meadows, pastures was determined, inland swamps, reservoirs, deciduous forests, urban and recreational development, industrial or commercial areas.

Moreover, after determining a 300m buffer zone, comparative analyzes of development were performed for each lake, paying particular attention to water conditions. For this purpose, the length of watercourses, including canals, embankments and roads, was determined. The share of surface forms of land development was analyzed, including waters, forests, fields, meadows, fallow lands, buildings, wetlands and beaches. The basis for the analyzes were orthophotomaps (year 2022) and archived topographic maps (year 1975), downloaded from the geoportal website. gov.pl.

Botanical and Statistical Analyses

Species diversity indices were used for the analysis (number of species, Shannon index H' and Pielou species evenness index J') (Moffatt, McLachlan 2004). During the calculation of the Shannon index, the Braun-Blanquet

quantitative degrees were transformed to the van der Maarel scale (1979), and the EXCEL program was used for calculations. The diversity analysis was extended to compare changes in the quantitative share of distinguished ecological groups of species (the sum of Braun-Blanquet quantitative degrees transformed to the van der Maarel scale). Differences between the two research periods were tested using the Wilcoxon test. STATISTICA 13.3 (StatSoft, Inc.) was used for calculations.

Results

Changes in the Use of the Impact Area

The entire analyzed area was subject to very dynamic changes in terms of land use (Figure 2). In the study area, since 1988, the share of marshes (-24.9%), meadows and pastures (-45.7%), agricultural areas with a large share of natural vegetation (-42.8%), and complex cultivation systems (-38.7%) has significantly decreased. However, there was a very significant increase in the number of industrial areas (32.3%), the share of areas with urban and recreational development increased 5 times (+479.73%), and the area of water reservoirs in this area increased by 18.67% and it was not the area of lakes but the appearance numerous flood waters (Figure 2).

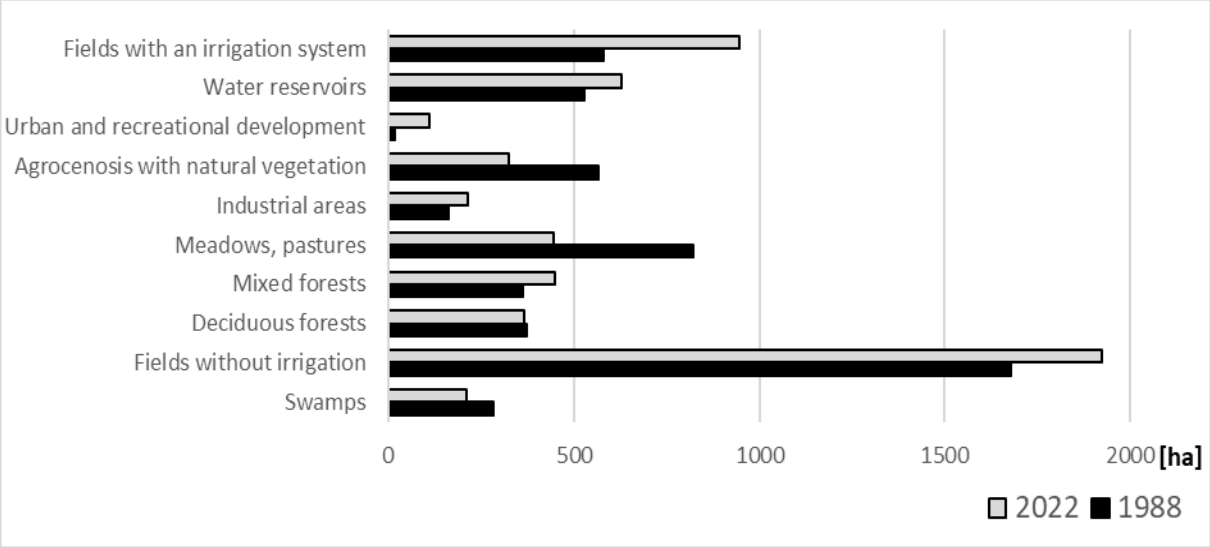

Figure 2. Changes in land use in the area affected by the mine

Changes in the Use of the Lake Buffer Zone

The development of the buffer zone of the 6 analyzed lakes was subject to very significant changes. Among the surface forms of cover, forests (trees and shrubs) had a significant increase in all buffer zones. The largest increases in forest cover were recorded in the vicinity of the lakes Nadrybie - 40%, Bikcze - 34% and Sumin - 33%. The share of meadows decreased significantly in all buffers, the largest in lakes Nadrybie (41%), Rotcze (36.5%) and Uściwierz (30.1%). The increase in land occupied for development was observed in the 4 analyzed buffer zones on lakes Piaseczno 25%, Sumin 12%, Rotcze 26% and Uściwierz 12%. Additionally, only in Lake Piaseczno the share of beaches increased, in the remaining lakes their share either decreased or did not exist at all (Figure 3). In the vicinity of most lakes, despite the construction of numerous ponds, the degree of irrigation of this zone decreased, which was reflected in the decrease in the share of permanently wet areas, the largest in the vicinity of Sumin lake - 19.7%, Rotcze - 20% and Bikcze - 12.7%.

The length of roads increased in the vicinity of all lakes. The largest increase was recorded at lakes Piaseczno 36.4% (from 1.2 km in 1988 to 5.6 km in 2022), Sumin 35.2% (from 1.06 km to 3.94 km) and Uściwierz 36, 9% (1.09 km to 5.35 km). The network of canals, rivers and embankments remained at a very similar level in the analyzed periods. Some of the drainage is currently not operational, e.g. at Lake Piaseczno, Uściwierz and Bikcze. This network was and is the most developed in the vicinity of the lakes Nadrybie 9.5 km and Sumin 9.3 km in 1979 (Figure 4).

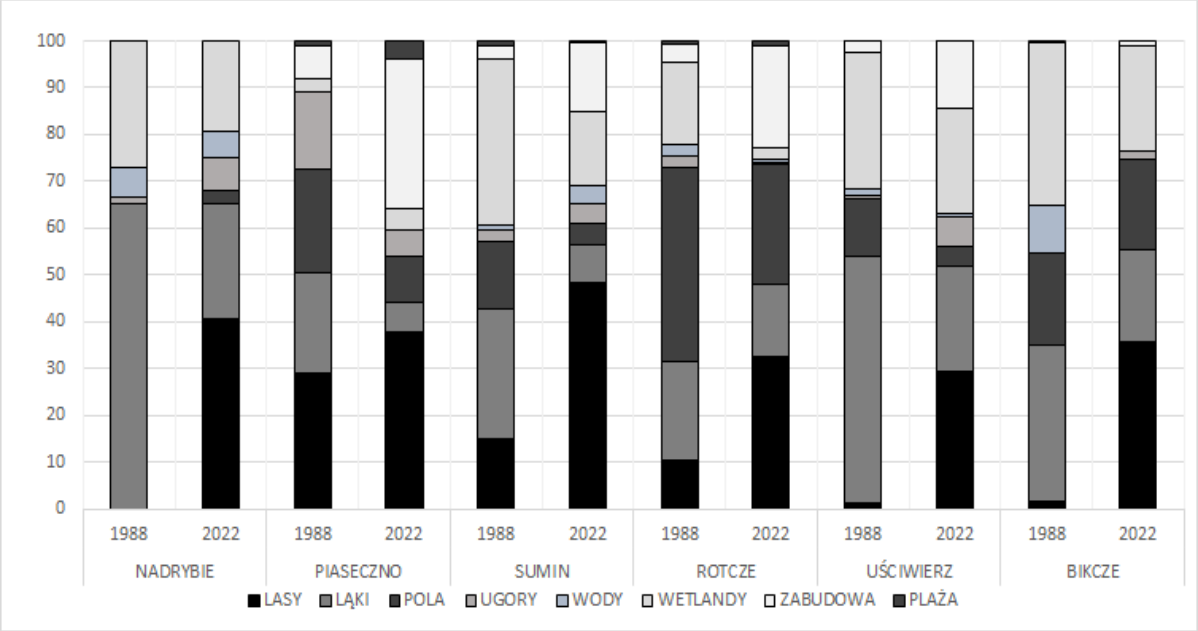

Figure 3. Changes in the use of the lake buffer zone - surface forms

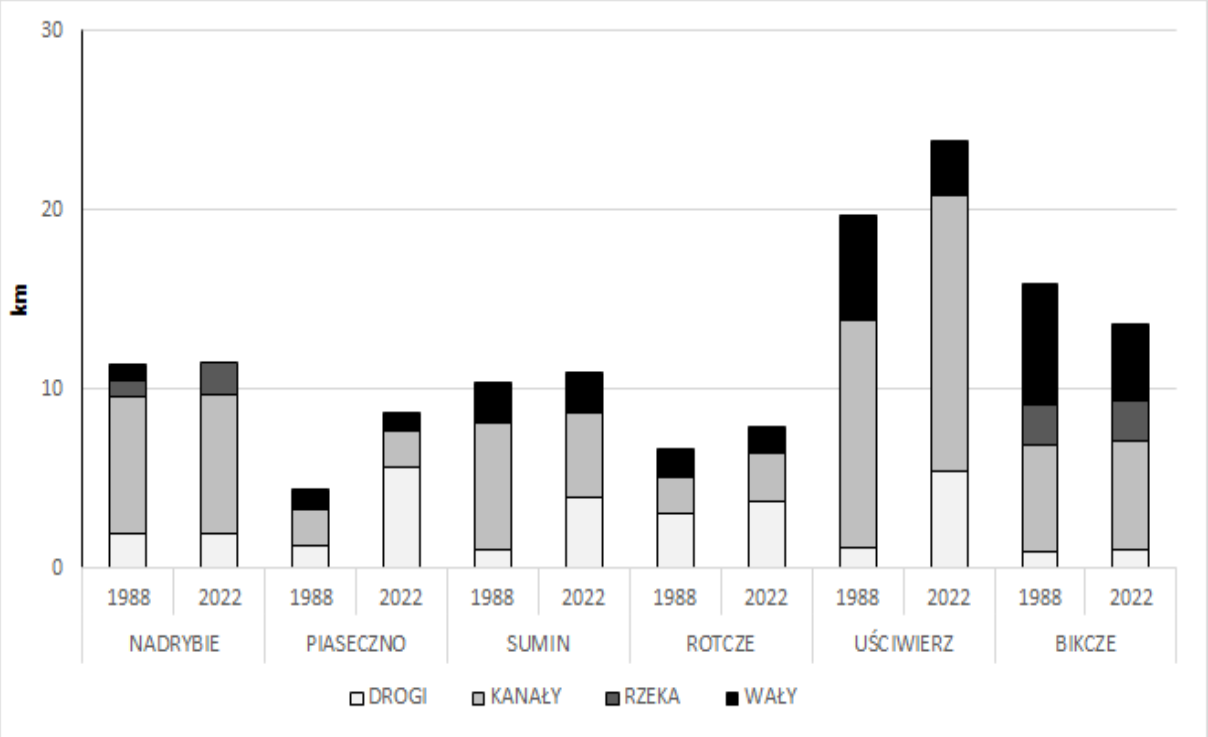

Figure 4. Changes in the use of the lake buffer zone - linear forms

Long-term Analysis of Changes in the Structure of Macrophytes

Changes in Floristic Structure and Quantity

The largest number of species occurred in the water and coastal zone of Lake Bikcze in 1988 - 63, and in 2022 - 59. The fewest species were in Lake Nadrybie - 39 species in 1988 and 32 in 2022 (Table 1). In most lakes, changes in the total number of species were observed, towards their depletion. Compared to 1988, 7 species disappeared in the Sumin and Nadrybie lakes, in the remaining lakes there were 8 species less. The exception was Lake Rotcze, where the trend was completely opposite, the number of species is now higher by 7 (mainly shore plants) (Table 1).

Table 1. Number of species occurring in the shoreline and littoral zones of the analyzed lakes

	Littoral zone		Shoreline zone	
Lake	1988	2022	1988	2022
Bikcze	31	30	32	29
Nadrybie	18	17	21	15
Piaseczno	26	31	30	17
Rotcze	22	21	23	31
Sumin	29	25	25	22
Uściwierz	36	35	19	12

In most of the analyzed lakes, there was a clear increase in the area covered by individual species in the analyzed transects among the littoral and shoreline vegetation. The greatest increase in vegetation cover was recorded in Piaseczno lakes by 20.5% for littoral plants. In two lakes, Rotcze - 20.7% and Nadrybie - 5.04%, the cover among littoral plants was reduced. The most stable lake in terms of the number of plants covering it was Lake Sumin, with an increase in aquatic vegetation by 0.3% and a decrease in shoreline vegetation by 0.51% (Table 2). Among the shoreline vegetation, the cover was reduced on lakes Piaseczno - 40.6%, Uściwierz - 44.6% and Bikcze - 8.4%. In other lakes, there was sometimes a significant increase in the cover of shore plants, in Lake Rotcze by 44.2%, and in Nadrybie by 7.44% (Table 2).

Table 2. Macrophyte coverage of the shoreline and littoral zones in the analyzed transects (%)

	Littoral zone		Shoreline zone	
Lake	1988	2022	1988	2022
Nadrybie	60.26	57.22 -5,04%	39.74	42.78 7,44%
Uściwierz	76.34	86.90 13,8	23.66	13.10 -44,6%
Rotcze	68.11	54.00 -20,7%	31.89	46.00 44.2%
Bikcze -	64.28	67.27 4,65%	35.72	32.73 -8,4%
Piaseczno	66.49	80.1 20,5%	33.51	19,9 -40,6%
Sumin	65.14	65.32 0,27%	34.86	34.68 -0,51%

Changes in Diversity Indicators

The Shannon-Wiener and Pielou indices of floristic diversity usually reached lower values in the last period. mong the littoral plants, the highest values of the Shannon-Wiener index, both in 1988 and 2022, occurred in Lake Bikcze and Uściwierz - H = 1.20, and the lowest in Lake Nadrybie. The highest values of the Shannon-Wiener index for plants in the coastal zone in the 1980s were recorded for lakes Sumin - H=1.20 and Bikcze - H=1.20, while the lowest for lake Uściwierz H=1.00. Nowadays, the values of this indicator have increased for plants on lakes Bikcze to H=1.26 and Rotcze, where it reached the highest value of H=1.34.

The values of the Pielou index determine the share of individual species, values close to 1 mean high uniformity, and values close to 0 mean low uniformity. The greatest uniformity of the share of littoral plant species was observed in 1988 for Lake Sumin, and in 2022 for Lake Rotcze (Table 3). The lowest index values in both analysis periods for this group of plants were in Lake Nadrybie, reaching J = 0.74 and J = 0.65, respectively. For shore plants, the highest value of the Pielou index was recorded at Lake Sumin in 1988, J = 0.81, but in 2022 it was already J = 0.78. The value of this indicator for this group of plants also decreased in the lakes Piaseczno, Uściwierz and Nadrybie. In the remaining two cases, the value of the indicator increased (Table 3).

Table 3. Indicators of floristic diversity in the studied lakes

	H' Shannon-Wiener index				J' Pielou index			
	Littoral zone		Shoreline zone		Littoral zone		Shoreline zone	
Lake	1988	2022	1988	2022	1988	2022	1988	2022
Bikcze	1.2	1.17	1.2	1.26	0.81	0.71	0.81	0.78
Nadrybie	0.98	0.86	1.08	0.97	0.74	0.65	0.8	0.72
Piaseczno	1.13	1.11	1.07	1	0.75	0.74	0.7	0.65
Rotcze	1.05	1.16	1.18	1.34	0.75	0.83	0.75	0.85
Sumin	1.18	1.04	1.2	1.15	0.81	0.71	0.81	0.78
Uściwierz	1.2	1.19	1	0.84	0.77	0.77	0.78	0.66

Changes in Habitat Conditions based on Species Composition

In most lakes, among the species of the littoral zone, there was a tendency towards a greater share of species with greater light (L) and temperature (T) requirements (Table 4). The values of the acidity index (R) for individual macrophyte species indicated the dominance of neutral species and those tolerant to a wide pH range (from 5.79 in Piaseczno to 6.73 in Sumin). The indicator values for nitrogen (N) indicated eutrophic habitats, rich in nitrogen, from 5.24 units in Rotcze to 6.17 units in Nadrybie. This lake also saw its largest increase since the 1980s (Table 4).

Among the plants of the littorl zone in Lake Piaseczno, a statistically significant decrease in the T value was shown in 2022 (p-value < 0.05); Lake Bikcze showed a statistically significant increase in the value of L in 2022 (p-value < 0.05), while lake Nadrybie showed a statistically significant decrease in the value of the F index (p-value < 0.05) (Table 5).

Table 4. Values of Ellenberg number indices for littoral and shoreline plants (Li - littoral, S - shoreline) (L – light, T – temperature, F – moisture, R – reaction, N – nitrogen, S – salinity)

			L	T	F	R	N
SUMIN	1988	Li	7,55	5,26	9,97	6,40	5,32
		S	7,80	5,23	8,85	4,46	3,44
	2022	Li	7,22	5,30	9,66	6,73	5,81
		S	7,55	5,06	8,88	4,74	3,70
PIASECZNO	1988	Li	6,99	5,60	9,80	6,09	5,64
		S	7,81	4,95	7,48	7,48	3,29
	2022	Li	7,18	5,22	9,82	5,79	5,44
		S	7,90	4,47	6,40	6,40	4,31
BIKCZE	1988	Li	7,02	5,68	10,74	6,55	5,93
		S	7,66	5,04	7,28	4,51	3,86
	2022	Li	7,25	5,44	10,45	6,35	5,83
		S	7,37	4,60	7,61	4,33	3,85
ROTCZE	1988	Li	7,09	5,67	10,60	6,31	5,46
		S	7,59	5,37	8,44	5,37	4,44
	2022	Li	7,23	5,41	10,06	5,97	5,33
		S	7,78	5,16	8,51	4,89	3,69
UŚCIWIERZ	1988	Li	7,24	5,23	10,26	5,93	5,24
		S	7,84	4,62	6,76	5,62	3,90
	2022	Li	7,12	5,31	10,47	6,40	5,78
		S	6,91	4,29	6,32	4,63	3,41
NADRYBIE	1988	Li	7,44	5,81	10,60	6,02	5,73
		S	7,56	4,15	7,11	4,17	4,02
	2022	Li	7,50	5,76	10,20	6,06	6,17
		S	7,09	4,74	6,28	4,57	3,71

Among the plants inhabiting the lake shore zone, species with a wide range of light tolerance have definitely dominated and still dominate (L from 6.91 Uściwierz lake to 7.9 Piaseczno lake). These plants prefer very large amounts of light. The greatest decrease in the L index (requirements for the amount of light) was recorded among the shore plants of Lake Uściwierz; in the 1980s it was 7.84, and currently it is 6.91 (Table 4).

Both in the 1980s and now, there are species tolerant to low temperatures in the lake shore zone, and these are moderately thermophilic plants. In all lakes, the value of the indicator (T) in the subsequent years of study decreased slightly (on average by 0.5), only in Lake Nadrybie it increased (from 4.15 to 4.74).
The vegetation of the shore zone of the analyzed lakes is mostly mesophilic and tolerates a wide range of humidity. In the vicinity of three lakes: Piaseczno, Uściwierz and Nadrybie, the values of the index (F) decreased in the subsequent decades of research, which indicates the direction of habitat drying, particularly visible at Lake Piaseczno (from 7.48 to 6.4). In the remaining lakes there was a slight increase in the value of this indicator (Table 4).

The surroundings of most lakes are inhabited by plants of slightly acidic habitats, from 4.17 at Lake Nadrybie to 5.62 at Lake Uściwierz. In two of them, Sumin and Nadrybie, the value of the acidity index (R) increased by approximately 0.5 in the following decades. Only in the vicinity of Lake Piaseczno, the acidity index values indicate a slightly alkaline character (7.48), with a slight downward trend (6.40). The nitrogen content of the

habitat increased in two lakes, Sumin and Piaseczno, in Lake Bikcze it did not change, while in the remaining lakes it decreased slightly, on average 0.6. Plant species inhabiting the shores of these lakes prefer habitats with moderately high nitrogen content. The shores of the studied lakes were inhabited primarily by plant species preferring habitats with moderate salinity (S 1.65 Uściwierz to 4.91 Rotcze). In most lakes, the value of this indicator decreased in the following decades. The exception was Lake Piaseczno, where both its values were the highest and the current value means a significant increase in salt concentration in the soil from moderate (4.00) to high (5.50) (Table 4).

Table 5. Significance of changes in Ellenberg indicators over time, p-value for the Wilcoxon test; * - statistical significance at the 0.05 level, gray field - insufficient data

	Shoreline zone					
Lake	L	T	F	R	N	S
Sumin	0.6121	0.7353	0.7532	0.173	0.2367	
Piaseczno			0.0500*			
Bikcze	0.3452	4652	0.5006	0.0796	0.3452	
Rotcze						
Uściwierz	0.0679	0.4652	0.0144*	0.1088	0.1441	1797
Nadrybie	0.398	0.0464*	0.3454	0.398	0.6121	0.1797
	Littoral zone					
Sumin	0.1097	0.5754	0.7671	0.7353	0.8589	
Piaseczno	0.3269	0.0251*	0.2076	0.1235	0.1614	
Bikcze	0.0281*	0.0712	0.1361	0.1823	0.5829	
Rotcze	0.4413	0.6112	0.4838	0.9528	0.2135	
Uściwierz	0.5701	0.8203	0.9588	0.1208	0.0979	
Nadrybie	0.9989	0.4445	0.0342*	0.7221	0.2721	

For shore plants in Lake Nadrybie, a statistically significant increase in the value of the T index was demonstrated in 2022 (p-value < 0.05) and a statistically significant decrease in the value of the F index for these plants in lakes Piaseczno and Usciwierz (p-value < 0.05) (Table 5).

Discussion

In the area of analysis, over 40 years have been a period of intensive changes in the way of development. Especially swampy and meadow areas gave way. The changes in water conditions in the area of analysis undoubtedly resulted in flood waters, which may have both a positive and negative impact on the environment. On the one hand, they are a refuge for various species of plants and animals and promote water retention. On the other hand, floodwaters may also cause flooding of agricultural areas and local buildings. It is important to sustainably manage floodplains, including by regularly monitoring their condition (water level, water quality and biodiversity) (Opperman et al., 2010). According to Michalczyk et al. (2011), the appearance of new floodplains in the analyzed area, created in the depressions around the mine, from the point of view of protecting these areas, is indicated as necessary to prevent the spread of excessively eutrophic and mineralized waters.

One of the most important factors influencing the structure of lake vegetation is the management method in its immediate surroundings (Young et al., 2005, Twesigye et al., 2011). The immediate surroundings of the analyzed lakes were subject to very high dynamics, despite the naturally valuable areas and various forms of protection successively introduced there. The greatest changes in the way the surroundings were developed among surface forms concerned meadows, which were replaced by forests and a significant increase in areas intended for development. Increasing the forest cover in this area is one of the priority activities carried out by the Central Coal District. This entire area is treated as a zone of increased protection of natural values. Due to the shortage of forests in the region and the expected deterioration of climatic conditions due to industrial activities, it was proposed to plant new forests in suitable areas, which also had no or little value for agricultural development, and insulating plantings around industrial zones (Dmitruk, 2021).

On lakes attractive to tourists, there was also a significant increase in beach areas, which resulted in the destruction of the coastal zone (Delgado-Fernandez et al., 2019). The share of dug reservoirs - ponds whose main function is to store water and drain areas originally occupied by wetlands - has increased. Most of them were created in the vicinity of the Uściwierz and Nadrybie lakes, where, apart from the above-mentioned

functions, the ponds were used mainly for breeding purposes. Hydrological changes were also reflected in a greater share of species with lower moisture requirements.

The hydrological conditions of the Lublin coal basin are exceptional and unique in this type of investments in the country. The operation of the mine means constant pumping out of groundwater, which results in a decrease in the local groundwater level and the formation of subsidence basins. Mining waste is deposited in a dumping ground and recultivated, which is intended to reduce dust generation. Mine water is discharged to the sedimentation tank and then to the Świnka River, some of it is also used for coal enrichment, sprinkling and fire protection (Suita & Łyszczarz 1997). These changes are indirectly visible in the structure of macrophytes in lakes and the surroundings. The response to these changes is the decreasing species diversity and, therefore, lower values of the analyzed diversity indices compared to the 1980s. The index value decreased in the Piaseczno, Uściwierz and Nadrybie lakes. In the two remaining lakes Bikcze and Rotcze there was an increase, while for Lake Sumin it remained unchanged, however, reaching small values in both periods. The increase in the index values may be generated by an increase in the fertility of lake waters, which is confirmed in the analyzes carried out by changes in the Ellenberg indexes, manifested by a greater share of species preferring higher nitrogen contents or alkaline habitats. At the same time, changes in the lake surroundings, in addition to the increase in habitat fertility, resulted in lower species diversity. In addition to species diversity, the area occupied by plants in the lake is also an indicator of changes. As a rule, an increasing plant area means an increase in the fertility of the habitat, but this only happens to a certain extent. Overfertilization often causes plants to decline and their area to be reduced (Budzyńska et al., 2019, Trajanovska et al., 2014). The greatest decline in vegetation cover (by 20%) occurred in Lake Piaseczno, which was also associated with a decline in biodiversity. Similarly, in Lake Rotcze, the cover was reduced by over 20.7%. However, in this lake the species diversity indicators were high, which does not confirm the direction of changes in depletion. There was also an increase in the share of species belonging to rushes, such as: *Phragmites australis*, *Typha latifolia* and *Carex rostrata*. The share of submerged species such as *Chara fragilis, Elodea canadensis, Nymphaea candida*, and *Potamogeton lucens* decreased. This situation may be explained by changing conditions of light availability, which is lower in more fertile waters (Søndergaard et al., 2013).

Certainly, one of the most important factors influencing changes in the structure of lake vegetation are changes in water conditions, which are undoubtedly influenced by mine activities, e.g. by lowering the water table in lakes and the level of shallow groundwater. The flow directions of shallow groundwater are changing, the mineralization of groundwater and surface water is increasing and their outflow is accelerating. Due to the complexity of various impacts related to global climate and anthropogenic changes in the analyzed area, it is difficult to clearly determine the impact of the Mine on the natural values of the region, especially the studied lakes. Water conditions were significantly transformed with the introduction of very extensive drainage works carried out before the mine was opened, the impact of which was often described as negative (Poleszuk, 2002, Radwan, 1994, Sender & Maślanko, 2017). The response of lake vegetation is ambiguous. There is a depletion of the qualitative and quantitative structure of vegetation and an increase in the fertility of habitats, but it is also a natural process (Scheffer, 2020), the pace of which, however, may be accelerated by human activity.

Sustainable use of environmental resources is a priority in this area. That is why various forms of protection have been introduced here in large numbers, because they limit human activity, and the existing infrastructure, including the mine, is obliged to act to protect the resources of this region (Łyszczarz, 2005). It is therefore difficult to assess the impact of creating protected areas, because we do not know how nature would behave without their creation.

Conclusions

In the analyzed lakes and their surroundings, there are changes in the area inhabited by lake plants, a reduction in the number of species, a greater share of species indicating an increase in habitat fertility and the disappearance of species with greater moisture requirements. However, it is not possible to clearly indicate the Lublin Coal Basin Mine as directly influencing these changes. The impacts are multidirectional, and the most important medium in this area is water, which has been and is subject to significant transformations. In the analyzed area there are very significant changes in the way of land development, on the one hand they are related to the operation of the mine (increase in forest cover, larger water surface), and on the other hand, with the tourist attractiveness of the area (recreational development, access roads). The forms of protection introduced in this area and the mine activities undertaken influence the direction of changes in vegetation and prevent changes leading to a rapid depletion of species and habitats.

Scientific Ethics Declaration

The authors declare that the scientific ethical and legal responsibility of this article published in EPSTEM journal belongs to the authors.

Acknowledgements or Notes

* This article was presented as an oral presentation at the International Conference on Basic Sciences, Engineering and Technology (www.icbaset.net) held in Alanya/Turkey on May 02-05, 2024.

References

Braun-Blanquet, J. (1964). *Plant sociology. The study of plant communities* (3th ed.). Wien-New York, NY: Springer.

Budzyńska, A., Dondajewska-Pielka, R., Rosińska, J., Kozak, A., & Kowalczewska-Madura, K. (2019). *Ekosystemy wodne: funkcjonowanie, znaczenie, ochrona i rekultywacja*. Poznan: Bogucki Wydawnictwo Naukowe.

Carvalho, F. P. (2017). Mining industry and sustainable development: Time for change. *Food and Energy Security, 6*(2), 61-77.

Delgado-Fernandez, I., O'Keeffe, N., & Davidson-Arnott, R. G. (2019). Natural and human controls on dune vegetation cover and disturbance. *Science of the Total Environment, 672*, 643-656.

Dmitruk, M. T. (2021). Analysis of the objectives and the level of implementation of the spatial development plan of the central coal region–the Lublin coal basin (CRW-LZW). *Archives of Mining Sciences*, 543-560.

Ellenberg H., Weber, H. E., Wirth, V., Werner, W. & Pauliβen, D. (1992): Zeigerwerte von Pflanzen in Mitteleuropa. *Scripta Geobot. 18*(2), 1-258.

George, M. O., Ephrahim, S. S., & Onyeka, I. N. (2010). Impacts of mining on water resources in South Africa: A review. *Scientific Research and Essays, 5(22)*, 3351-3357.

Goudie, A. S. (2018). *Human impact on the natural environment.* John Wiley & Sons.

Haslam, S.M. (1982). A proposed method for monitoring river pollution using macrophytes. *Environmental Technology, 3*(1-11),19–34.

Janiec, D. (1993). Przyrodnicza ocena wpływu kanału Wieprz-Krzna IKI jakość hydrosfery Pojezierza Łęczyńsko-Włodawskiego. *Gospodarka Wodna, 2*, 36-42.

Kraśnicki, S. (2019). Oddziaływanie projektowanej kopalni węgla kamiennego eksploatującej złoże Sawin na wody podziemne i powierzchniowe w rejonie Bagno Bubnów, Bagno Staw i Krowie Bagno.)

Łyszczarz, L. (2005). Działalność Lubelskiego Węgla" Bogdanka" SA w zakresie ochrony środowiska. *Wiadomości Górnicze, 56*(3), 137-145.

Maberly, S.C., & Haslam, S.M. (1988). River plants of Western Europe: The macrophytic vegetation of the watercourses of the European Economic Community. *Journal of Ecology, 76*(4),1248–1249.

Malon, A., & Tymiński, M. (2011). *Węgiel kamienny*. Państwowy Instytut Geologiczny Państwowy Instytut Badawczy, Zakład Geologii Gospodarczej.

Matuszkiewicz, W. (2012). *Guide for the determination of plant communities in Poland.* Warszawa: Wydawnictwo Naukowe PWN.

Michalczyk, Z., Chmiel, S., & Turczyński, M. (2011). Lake water stage dynamics in the Łęczna-Włodawa lake district in 1991–2010. *Limnological Review, 11*(3), 113-122.

Mirek, Z., Piękoś-Mirek, H., Zając, A. & Zając, M. (2002). Flowering plants and pteridophytes of Poland - a checklist. In Z. Mirek (Ed.), *Biodiversity of Poland* (pp.1-442*)*. Krakow: Polska Akademia Nauk.

Moffatt, S. F., & McLachlan, S. M. (2004). Understorey indicators of disturbance for riparian forests along an urban–rural gradient in Manitoba. *Ecological Indicators, 4*(1), 1-16.

O'Hare, M.T., Baattrup-Pedersen, A., Nijboer, R., Szoszkiewicz, K., & Ferreira, T. (2006). Macrophyte communities of European streams with altered physical habitat. *Hydrobiologia. 566*(1),197–210.

Opperman, J. J., Luster, R., McKenney, B. A., Roberts, M., & Meadows, A. W. (2010). Ecologically functional floodplains: connectivity, flow regime, and scale. *Journal of the American Water Resources Association, 46*(2), 211-226.

Pawłowski, B. (1977). Skład i budowa zbiorowisk roślinnych oraz metody ich badania, w: Szata roślinna Polski. W. Szafera, K. Zarzyckiego (Eds.), *Pod red* (pp.237-278). Warszawa: PWD

Poleszuk, M. T. (2002). Wplyw systemu melioracyjnego Kanalu Wieprz-Krzna na przeksztalcenia srodowiska przyrodniczego doliny rzeki Hanny. *Acta Agrophysica, 68*, 175-184.

Popiołek, Z. (1988). *Zróżnicowanie roślinności wodnej i przybrzeżnej na tle warunków siedliskowych w obrębie kompleksu jezior Lubelskiego Zagłębia Węglowego*. Lublin: UMCS.

Radwan, S. (Ed.). (1994). *Środowisko przyrodnicze w strefie oddziaływania Kanału Wieprz-Krzna* (pp.59-68). Lublin.

Santana, C.S., Montalván, Olivares, D. M., Silva, V. H. C., Luzardo, F., H., M., Velasco, F., G., & de Jesus, R. M. (2020). Assessment of water resources pollution associated with mining activity in a semi-arid region, *Journal of Environmental Management, 273,* 111148.

Scheffer, M. (2020). *Critical transitions in nature and society* (Vol. 16). Princeton University Press.

Sender, J., & Maślanko, W. (2017). Floristic diversity of lakes subjected to long term changes in the water network of the West Polesie (Eastern Poland). *Transylvanian review of systematical and ecological research, 19*(3), 1-16.

Sengupta, M. (2021). *Environmental impacts of mining: Monitoring, restoration, and control*. CRC Press.

Solis, M. (2012). Wpływ kanału Wieprz-Krzna na właściwości fizyczno-chemiczne i biologiczne wód w wybranych zbiornikach retencyjnych. *Inżynieria Ekologiczna,* 182-191.

Søndergaard, M., Phillips G., Hellsten S., Kolada A., Ecke F., Mäemets H, Mjelde M., Azzella M.M., & Oggioni A. (2013). Maximum growing depth of submerged macrophytes in European lakes. *Hydrobiologia, 704,* 165–177.

Suita, J., & Łyszczarz, L. (1997). Proekologiczna działalność w górnictwie węgla kamiennego na Lubelszczyźnie. *Ekoinżynieria,8*(23), 20-24.

Szoszkiewicz, K., Jusik, S., Zgola, T., Czechowska, M., & Hryc, B. (2007). Uncertainty of macrophyte-based monitoring for different types of lowland rivers. *Belgian Jouranl of Botany, 140*(1), 7–16.

Trajanovska, S., Talevska, M., Imeri, A., & Schneider S.C. (2014). Assessment of littoral eutrophication in Lake Ohrid by submerged macrophytes. *Biologia, 69*(6), 756–764.

Twesigye, C., K., Onywere, S., M., Getenga, Z., M., Mwakalila, S. S., & Nakiranda, J. K. (2011). The impact of land use activities on vegetation cover and water quality in the Lake Victoria watershed. *The Open Environmental Engineering Journal, 4*(1),66-77.

Van der Maarel, E. (1979). Transformation of cover-abundance values in phytosociology and its effects on community similarity. *Vegetatio, 39,* 97-114.

Westlake, D. F. (1975). Primary production of freshwater macrophytes. *Photosynth Product Differ Environment Hidrobiologia, 12*(1), 177–180.

Wiegleb, G., Herr, W., Zander, B., Broring, U., Brux, H., & van de Weyer, K. (2015). Natural variation of macrophyte vegetation of lowland streams at the regional level. *Limnologica. 51*(1), 53–62.

Young, J., Watt, A., Nowicki, P., Alard, D., Clitherow, J., Henle, K., ... & Richards, C. (2005). Towards sustainable land use: identifying and managing the conflicts between human activities and biodiversity conservation in Europe. *Biodiversity & Conservation, 14,* 1641-1661.

Author Information

Joanna Sender
Department of Hydrobiology and Protection of Ecosystems, University of Life Sciences in Lublin, Dobrzańskiego 37, Lublin, Poland
Contact e-mail: *joanna.sender@up.lublin.pl*

Monika Różańska-Boczula
Department of Applied Mathematics and Computer Sciences, University of Life Sciences in Lublin, Głęboka 28, Lublin, Poland

Danuta Urban
Institute of Soil Science and Environment Shaping, University of Life Sciences in Lublin, Leszczyńskiego 7, Lublin Poland

To cite this article:

Sender, J., Rozanska-Boczula, M., & Urban, D. (2024). Diversity of aquatic and coastal vegetation in the Lublin coal basin complex - long-term changes. *The Eurasia Proceedings of Science, Technology, Engineering & Mathematics (EPSTEM), 28,* 417-427.

The Eurasia Proceedings of Science, Technology, Engineering & Mathematics (EPSTEM)
ISSN: 2602-3199

The Eurasia Proceedings of Science, Technology, Engineering & Mathematics (EPSTEM), 2024

Volume 28, Pages 428-437

ICBASET 2024: International Conference on Basic Sciences, Engineering and Technology

Possibilities for Improving Algorithms for Combat Use of Aircraft Using Unguided Weapons

Milen Atanasov
Georgi Benkovski Bulgarian Air Force Academy

Abstract: Combat actions in recent local conflicts make us consider and re-evaluate some of the concepts concerning the development of combat aviation. As it turns out, conducting combat operations at high intensity for a long period of time using all components of the armed forces shows that the use of high-tech aircraft is extremely expensive and requires a large period of time to bring them back to full operational readiness when damage has been inflicted on them during hostilities. This is evidenced by the limited use of 5th generation aircraft in local conflicts. They are mainly used at long distances and with a tangible technological superiority over the enemy. Also, the sustained use of high precision guided weapons proves to be extremely expensive. All this makes us think and apply a creative approach to finding a solution to these problems. One of these approaches is through the improvement or rather the modernization of existing combat platforms through the implementation of advanced mathematical models and algorithms for combat use, which will increase the accuracy and efficiency of the use of unguided weapons, which are significantly cheaper compared to using guided ones. As the accuracy of using unguided weapons increases, it approaches that of guided ones. This is very important in the conduct of prolonged intensive combat operations in the conditions of limited resources. On the other hand, the use of advanced algorithms for combat use will simplify and facilitate the pilot's work with the controls of the aviation armament during the execution of combat tasks.A general mathematical model and a general algorithm for the combat use of aircraft weapons are proposed. A general mathematical model was developed for solving the ballistic task for large groups of guided and unguided weapons, which is a component of the general algorithm for combat use.

Keywords: Aircraft, Algorithm, Weapons

Introduction

The development of technologies and their implementation in combat aviation requires a rethinking of the concepts for the development of strike avionics responsible for solving combat tasks. New understandings of the strategy of conducting combat actions, to a large extent, determine the development of combat aircraft. One of the views on the development of combat aircraft i.e. for the creation of 6th generation aircraft, is that the aircraft themselves, with the help of the pilot and artificial intelligence, can control unmanned aerial vehicles in missions to strike air and ground targets. They should also be used as unmanned aerial vehicles (Mitov et al., 2019). This makes it possible to expand the spectrum of solved combat tasks, and from here to change and improve the tactics of using such aircraft.

Conducting high intensity combat operations over a long period of time shows that the use of high-tech aircraft is extremely expensive. Local conflicts show that the use of high precision guided weapons is extremely expensive as well. One of the possible solutions improving the mathematical models and algorithms for the combat use of unguided weapons, which will increase the accuracy and efficiency of their use. Combat use of aircraft is characterized by the following stages:

• Target identification.

• Decision to use a specific type of weapon.
• Decision to select a specific target attack type.
• Solving the task of guiding the weapon to a contact with the target.
• Determining the moment to fire, launch or drop.
• Exiting the attack.

All that demonstrates the great psycho-physical load on the part of the pilot during the execution of the combat task in a shortage of time. This necessitates the implementation of expert systems and advanced combat algorithms in combat aircraft in order to facilitate the work of the pilot.

Method

On the basis of mathematical modelling, the ultimate task of the aircraft hitting the target was solved, and the accuracy of the combat use of unguided weapons was determined. A comparative analysis was carried out, which showed how much the hit accuracy increases when using a general algorithm of work for the combat use of unguided weapons. A general mathematical model and a general algorithm for the combat use of aircraft weapons are proposed. A general mathematical model was developed for solving the ballistic task for large groups of guided and unguided weapons, which is a component of the general algorithm for combat use.

General Mathematical Model and General Algorithm for Combat Use with Unguided Weapons

To compile a general mathematical model for the combat use of unguided weapons (UW), the general vector scheme determining the contact of the UW with the target - air or ground (Figure 1) is used (Atanasov M., 2014).

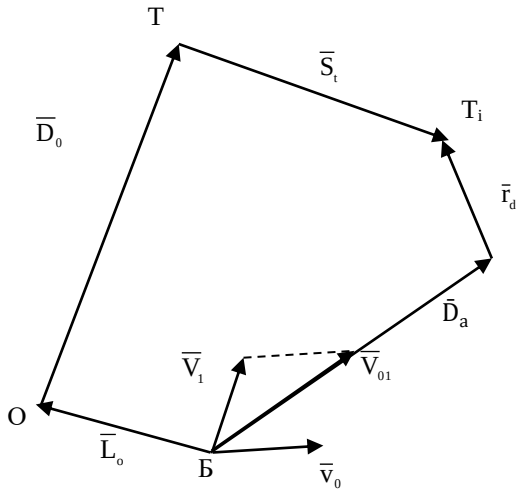

Figure 1. The aiming vector scheme

(1) $$\bar{D}_0 = \bar{D}_{ov} + \bar{r}_d - \bar{L}_0 - \bar{S}_t,$$

where

$\bar{L}_0$ is the base vector of the weapon;

$\bar{D}_0$ - the target distance vector at the time of the shot;

$\bar{D}_a$ - the vector of the advance distance to the target at the time of the shot;

$\bar{S}_t$ - the vector defining the target's motion;

$\bar{r}_d$ – the vector determining the deflection of the projectile for a mobile aircraft gun.

In the general case, at the time of firing and dumb bomb (DB)-dropping, angles $\beta_{t1,0}$ and $\varepsilon_{t1,0}$ of aiming at the target relative to the associated coordinate grid $Ox_1y_1z_1$ are determined by the formulas (Figure 2):

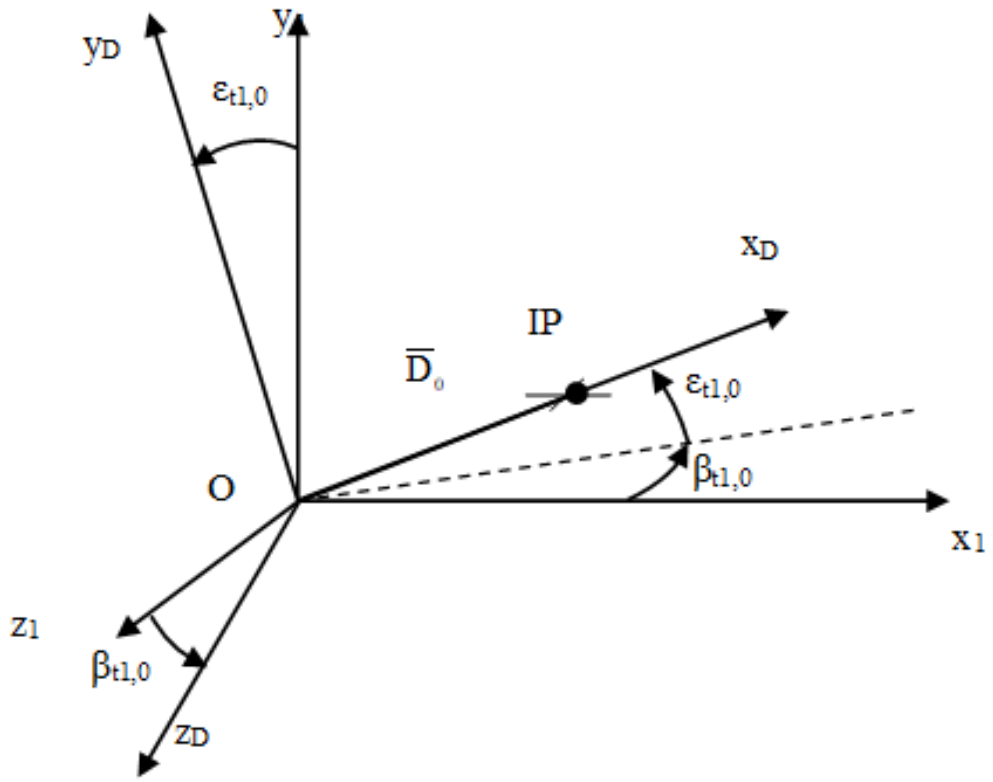

Figure 2. Impact point (IP) and target aiming angles βt1,0, εt1,0 at the time of firing and bomb drop

(2) $$\beta_{t1,0} = \operatorname{arctg}\left(\frac{D_{0z1}}{D_{0x1}}\right); \qquad \varepsilon_{t1,0} = \arcsin\left(\frac{D_{0y1}}{D_0}\right).$$

where:

(3) $$\begin{bmatrix} D_{0x1} \\ D_{0y1} \\ D_{0z1} \end{bmatrix} = \begin{bmatrix} X_1 \\ Y_1 \\ Z_1 \end{bmatrix} + C_r \begin{bmatrix} \cos\beta\sin\alpha\sin\beta'\cos\varepsilon' - \sin\beta\sin\varepsilon' \\ \sin\beta\cos\beta'\cos\varepsilon' + \cos\beta\cos\alpha\sin\beta'\cos\varepsilon' \\ \cos\beta\cos\alpha\sin\beta'\sin\varepsilon' + \cos\beta\sin\alpha\cos\beta'\cos\varepsilon' \end{bmatrix} - \begin{bmatrix} L_{0x1} \\ L_{0y1} \\ L_{0z1} \end{bmatrix} -$$
$$- \left(\left[A_v^{(1)}\right]^T \begin{bmatrix} V_1 \\ 0 \\ 0 \end{bmatrix} + A_1^{(xDyDzD)} \begin{bmatrix} \dot{D} \\ \omega_{zD} D \\ -\omega_{yD} D \end{bmatrix} \right) T - \frac{1}{2} \begin{bmatrix} a_{vx1} \\ a_{yx1} \\ a_{vz1} \end{bmatrix} T^2 +$$
$$- \frac{1}{2} A_1^{(xDyDzD)} \begin{bmatrix} \ddot{D} - D\left(\omega^2_{yD} + \omega^2_{zD}\right) \\ \omega_{xD}\omega_{yD} D + \dot{\omega}_{zD} D + 2\omega_{zD}\dot{D} \\ \omega_{xD}\omega_{zD} D - \dot{\omega}_{yD} D - 2\omega_{yD}\dot{D} \end{bmatrix} T^2.$$

General Structural Diagram of a System for Combat Use with Unguided Weapons

On the basis of the abovementioned general mathematical model for the combat use of unguided weapons, a general structural diagram of a system for combat use of unguided weapons (Figure 3) is proposed. The general structural scheme consists of:

- Targeting Block;
- Radar and Electro-Optical Tracking System (EOTS)
- Block For Determining the Target Motion Vector $\bar{S}_t$;
- Block for Determining the Advance Distance Vectors $\bar{D}_a$ to the Target and the Deviation $\bar{r}_d$ of the Projectile;

- Block for Determining the Distance to the Target at the Time of the Shot $\overline{D}_0$;
- Ballistic Block;
- Block with Input Parameters;
- Block for Determining Angles $\beta_{t1,0}$ and $\varepsilon_{t1,0}$;
- Block for Determining η_c, ξ_c of the Current Coordinates of the Target Relative to the Aircraft;
- Heads-up Display (HUD).

The azimuth angle β_{t1} and the angle ε_{t1} of the target location are fed from the target designation unit to the Radar/EOTS.

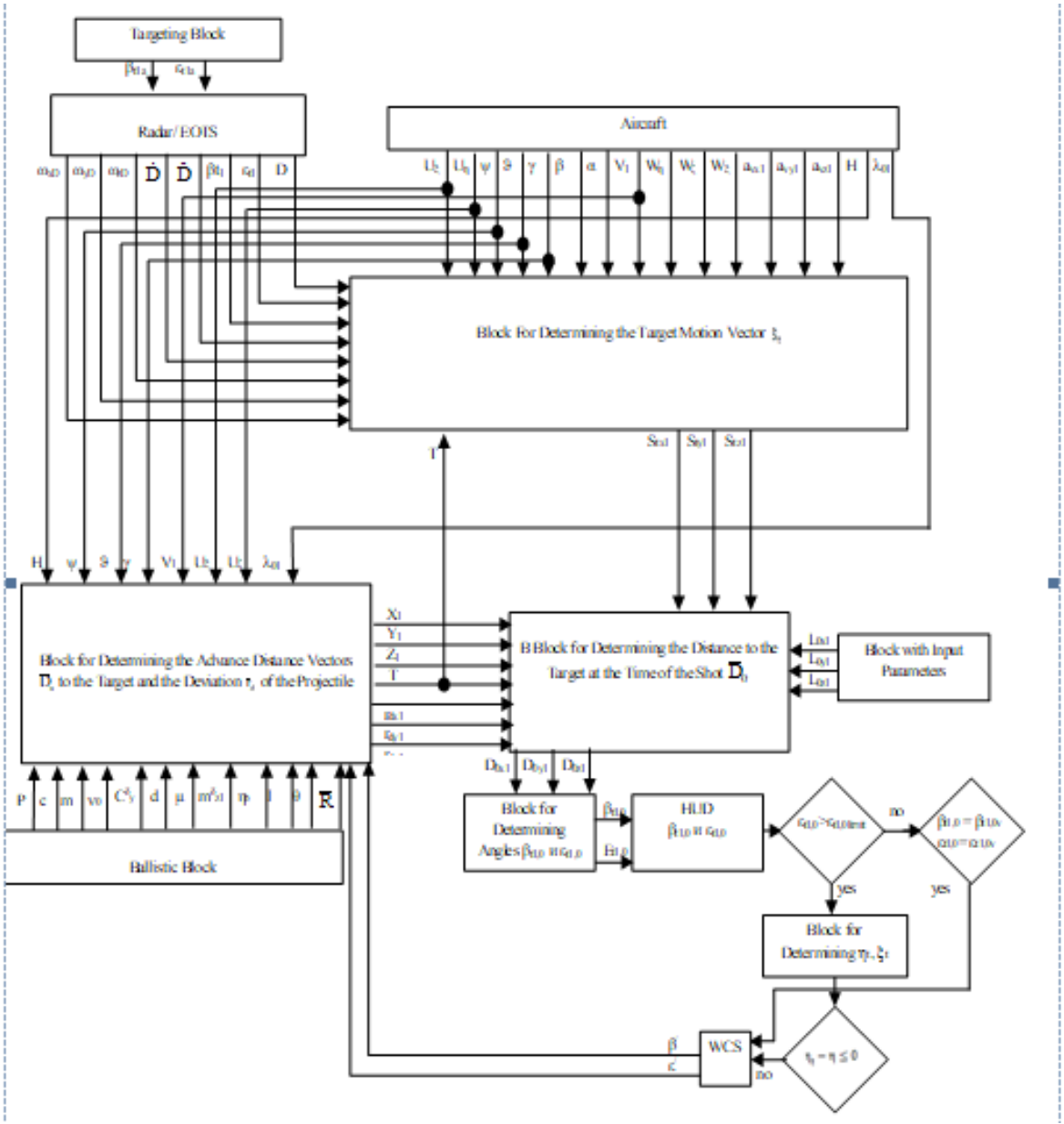

Figure 3. General structural diagram of a system for combat use with UW

The vector determining the movement of the target $\overline{S}_t$ is calculated after solving the ballistic task, depending on whether the target is air or ground. Provided that the aircraft artillery weapon is stationary, the vector $\bar{r}_d$ is not calculated. Using the derived formulas from (3), the distance to the target for the time of the shot is determined in the corresponding block. From the ballistic block, depending on the UW used, the values of P, c, m, v_0, C^{δ}_y, d, μ, m^{δ}_{z1}, η_b, l, θ and the coordinates of the explosion point - R_η, R_ζ, R_ξ are supplied (Stoĭkov & Atanasov, 2009). From the block with input parameters, the base $(\overline{L}_0)_1$ of the aviation artillery weapon is supplied. The angles β'

and $\varepsilon^{/}$ at which the aircraft gun (AG) is rotated relative to the $Ox_1y_1z_1$ system are supplied from the weapon control system (WCS).

The target sighting angles $\beta_{t1.0}$ and $\varepsilon_{t1.0}$ are calculated with the form. (2) in the corresponding block. When firing and bomb drop is carried out in CCIP mode, the calculated angles $\beta_{t1.0}$ and $\varepsilon_{t1.0}$ are displayed on the HUD. This is the reticle position. When the reticle aligns with the target, the pilot presses the combat button, which sends a signal to the WCS. When bomb drop is carried out in the invisible zone (CCRP mode), after aligning the reticle with the target, the current coordinates η_c, ξ_c of the target relative to the aircraft in the corresponding block are calculated. When the condition $\eta_{\tau} - \eta \le 0$ is met, a signal is sent to the WCS.

Solving the Ballistic Task

Unguided weapons are used in a large range of aircraft speeds and altitudes, angles and distances to the target, presence of an angle between the vectors of the speed of the aircraft and the initial speed of the UW. In different aviation aiming systems (AAS), fundamentally different ballistic schemes are used, requiring specific methods of solving ballistic tasks and forms of presentation of the results of the decisions. Therefore, it is necessary to compile a common ballistic model for all types of unguided UW, and the type of UW used is entered on board the aircraft. For the synthesis of the ballistic model, a system of differential equations describing the spatial movement of the UW in the navigation base $O\eta\zeta\xi$ is proposed. The $O\eta$ axis of the navigation base is oriented along the north meridian, the $O\zeta$ axis is oriented along the local vertical, and the $O\xi$ axis is oriented to form a right coordinate system. The movement of the unguided UW is described by the system of differential equations (Atanasov, 2014):

$$\dot{y} = f_w(y_w, t),$$

where y_w is the vector of phase coordinates of the UW, which depends on: the composition of forces and moments in the mathematical model; the coordinate system in which the vector equations are projected; the different assumptions and the type of UW.

General Work Algorithm for Combat use With Unguided Weapons

On the basis of the developed general mathematical model and general structural diagram of a firing and bomb-dropping system, a general work algorithm for combat use with unguided weapons was developed (Figure 4).
After the target is acquired by the radar or the EOTS, it is automatically determined whether it is an air or ground target. In the event that the acquisition is carried out by the EOTS using the laser rangefinder (LR), the distance D to the target is measured and its altitude H_t is determined using the formulas:

(4) $$\begin{bmatrix} D_{x1} \\ D_{y1} \\ D_{z1} \end{bmatrix} = A_1^{(xDyDzD)} \begin{bmatrix} D \\ 0 \\ 0 \end{bmatrix};$$

(5) $$\begin{bmatrix} D_{\eta} \\ D_{\zeta} \\ D_{\xi} \end{bmatrix} = \left[A_{\eta\zeta\xi}^{(x_1y_1z_1)}\right] \begin{bmatrix} D_{x1} \\ D_{y1} \\ D_{z1} \end{bmatrix};$$

(6) $$H_t = H - D_{x1}\sin\vartheta - D_{y1}\cos\vartheta\cos\gamma + D_{z1}\cos\vartheta\sin\gamma.$$

Provided that H_t >50 m, a decision is made – it is an air target (AT) . If the condition is not fulfilled – it is a ground target (GT). When using the radar, the pilot manually selects the "air target" or "ground target" mode. Depending on the type of target, the velocity V_t of the target is calculated. Depending on the target, the pilot chooses the type of weapon to use. Afterwards, the relevant parameters that are to be entered in the system of differential equations for the motion of the UW are selected.

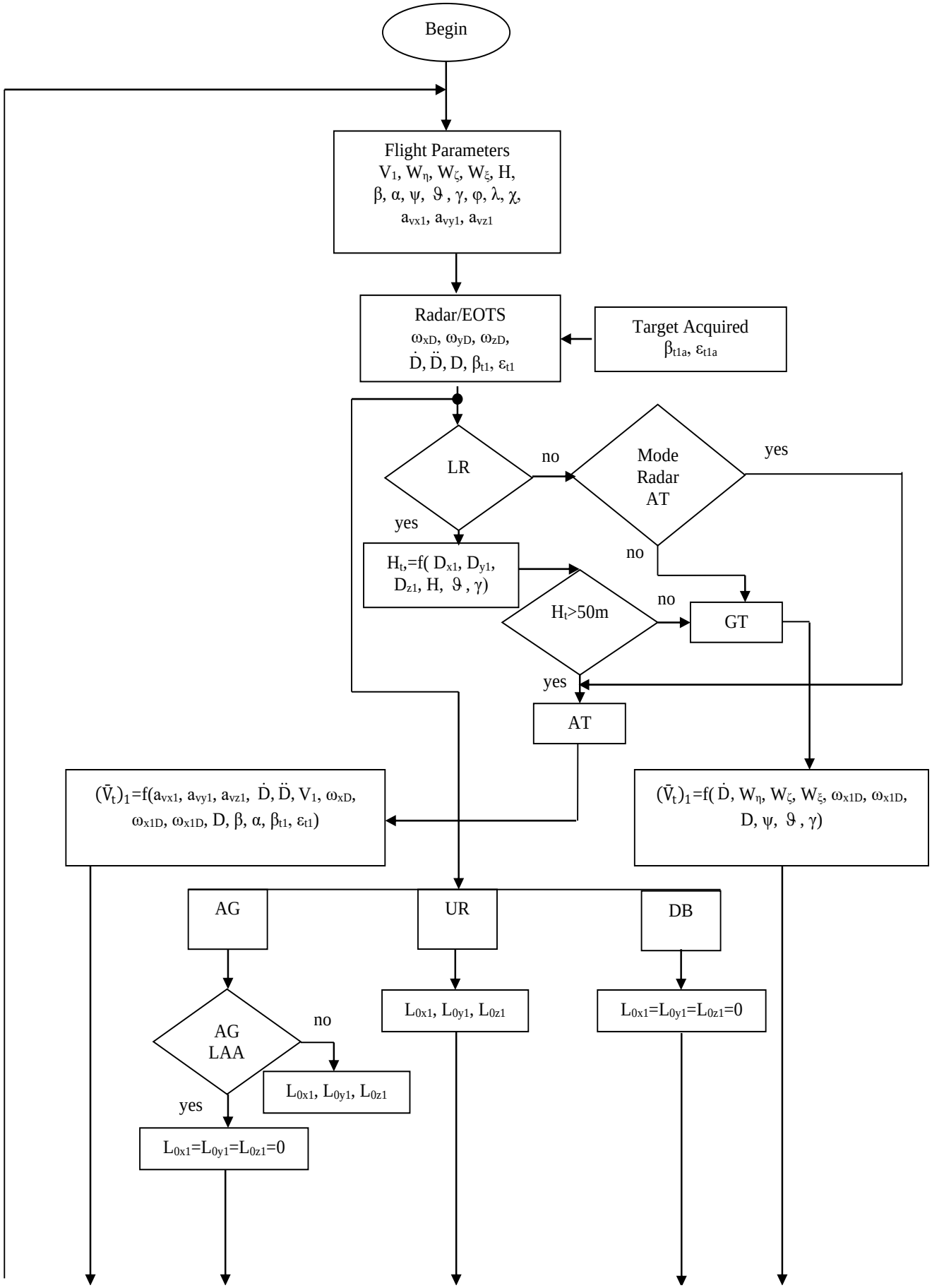
Begin
Flight Parameters
V_1, W_η, W_ζ, W_ξ, H,
β, α, ψ, ϑ , γ, φ, λ, χ,
a_{vx1}, a_{vy1}, a_{vz1}
Radar/EOTS
ω_{xD}, ω_{yD}, ω_{zD},
$\dot{D}$, $\ddot{D}$, D, β_{t1}, ε_{t1}
Target Acquired
β_{t1a}, ε_{t1a}
LR
no
Mode
Radar
AT
yes
yes
H_t,=f(D_{x1}, D_{y1},
D_{z1}, H, ϑ , γ)
no
H_t>50m
no
GT
yes
AT
$(\bar{V}_t)_1$=f(a_{vx1}, a_{vy1}, a_{vz1}, $\dot{D}$, $\ddot{D}$, V_1, ω_{xD},
ω_{x1D}, ω_{x1D}, D, β, α, β_{t1}, ε_{t1})
$(\bar{V}_t)_1$=f($\dot{D}$, W_η, W_ζ, W_ξ, ω_{x1D}, ω_{x1D},
D, ψ, ϑ , γ)
AG
UR
DB
AG
LAA
no
yes
L_{0x1}, L_{0y1}, L_{0z1}
L_{0x1}=L_{0y1}=L_{0z1}=0
L_{0x1}, L_{0y1}, L_{0z1}
L_{0x1}=L_{0y1}=L_{0z1}=0

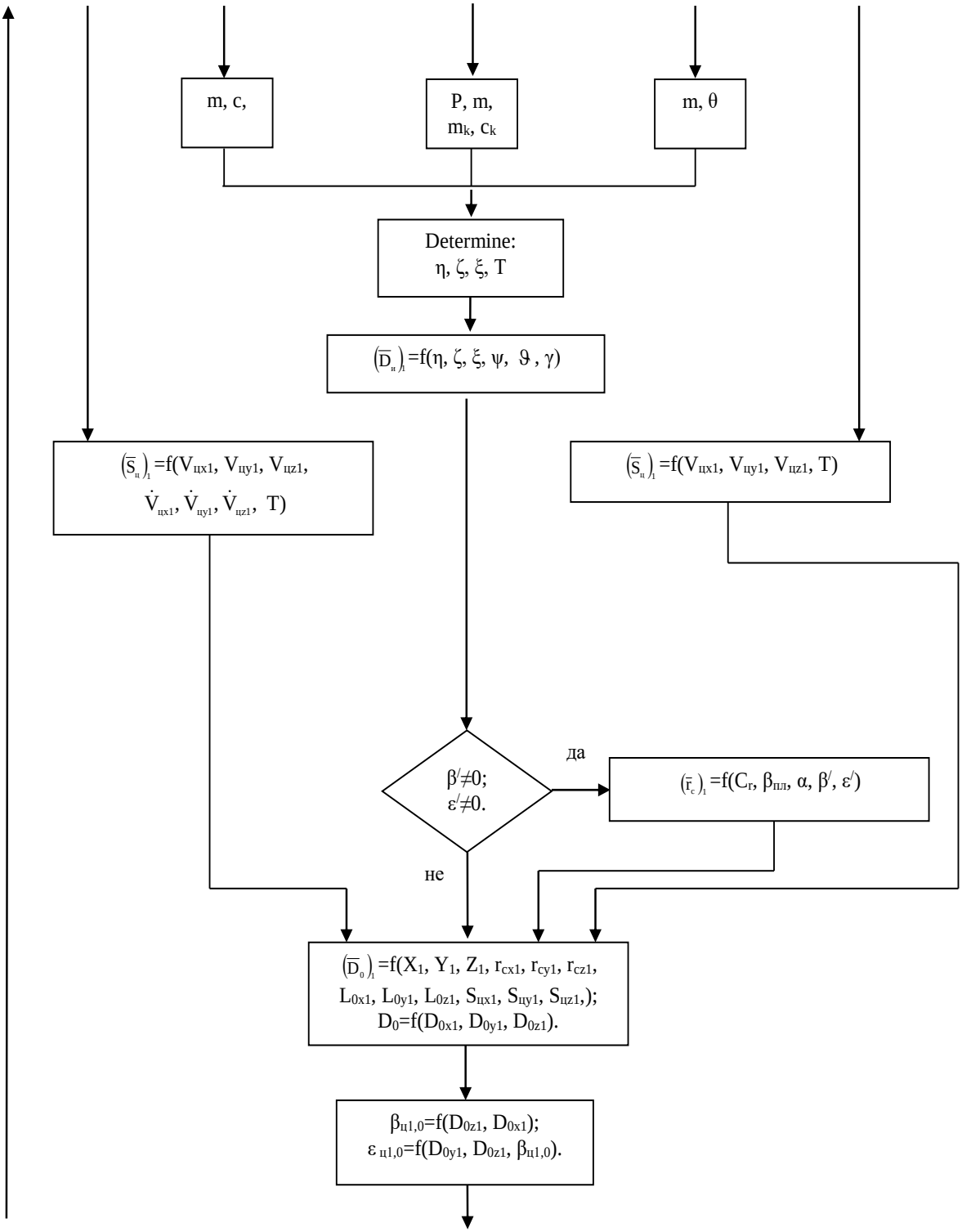
m, c,
P, m, mk, ck
m, θ
Determine: η, ζ, ξ, T
(D̄и)1=f(η, ζ, ξ, ψ, ϑ, γ)
(S̄и)1=f(Vцх1, Vцу1, Vцz1, V̇цх1, V̇цу1, V̇цz1, T)
(S̄и)1=f(Vцх1, Vцу1, Vцz1, T)
β/≠0; ε/≠0.
да
(r̄c)1=f(Cr, βпл, α, β/, ε/)
не
(D̄0)1=f(X1, Y1, Z1, rcx1, rcy1, rcz1, L0x1, L0y1, L0z1, Sцх1, Sцу1, Sцz1,); D0=f(D0x1, D0y1, D0z1).
βц1,0=f(D0z1, D0x1); εц1,0=f(D0y1, D0z1, βц1,0).

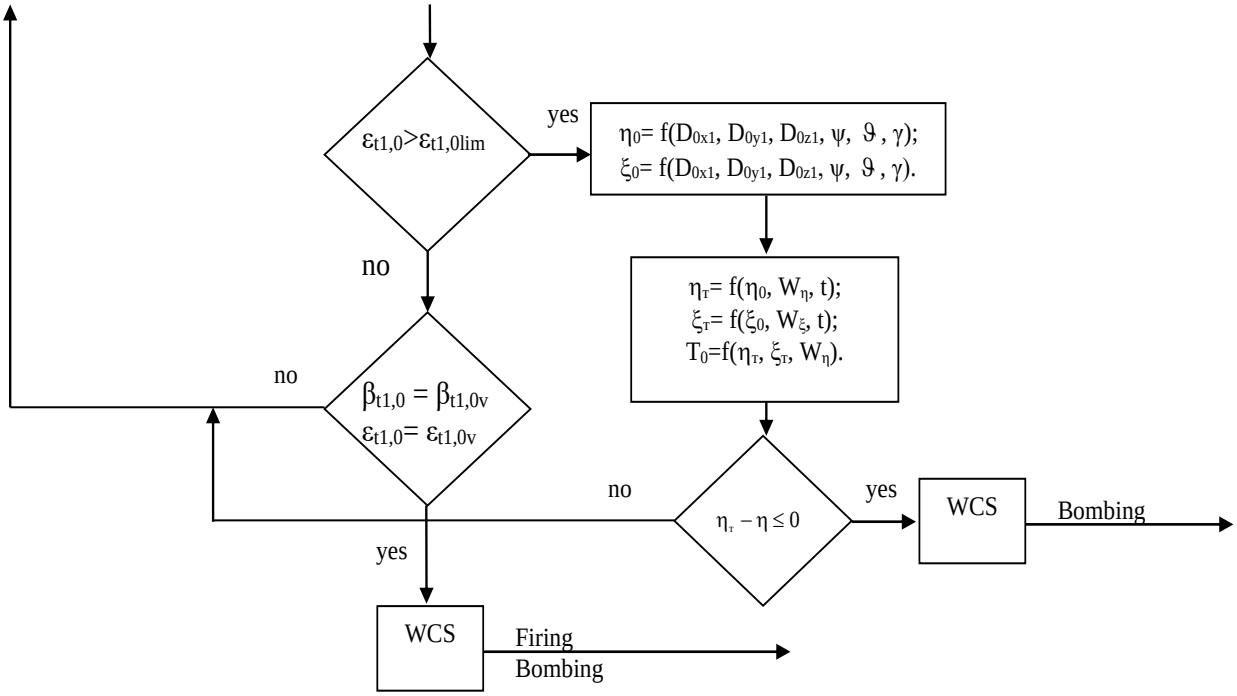

Figure 4. General algorithm of work for combat use with UW

When shooting at an air target, the system of differential equations is solved for the distance $\bar{D}_a$.

When firing at a ground target and dropping a bomb, the system of equations is solved for the altitude at which the combat use takes place. After solving the system, the vector of the advance distance $\bar{D}_a$ to the target is calculated for the moment of the shot and the time T of the UW flight. When bombing and firing with an AG located along the axis of the aircraft (LAA), it is assumed that the vector of the base on the weapon is $\bar{L}_0 = 0$. When firing with unguided rocket (UR) and an AG located in a container attached to the aircraft, it is assumed that $\bar{L}_0 \neq 0$. Depending on what the target is (air or ground), the vector $\bar{S}_t$ defining the target's movement is calculated. Provided the target is stationary $\bar{S}_t = 0$. On the condition that the weapon is mobile ($\beta' \neq 0$; $\varepsilon' \neq 0$), the vector $\bar{r}_d$ determining the deflection of the projectile is determined.

The next step is to calculate the vector of distance $\bar{D}_0$ to the target at the moment of the shot, from which the angles βt1,0 and εt1,0 of aiming the target relative to the associated coordinate $Ox_1y_1z_1$ are determined. Provided that firing or bombing is carried out in the visible area ($\varepsilon_{t1,0} < \varepsilon_{t1,0limit}$) and when the reticle is aligned with the target $\beta_{t1,0} = \beta_{t1,0v}$, $\varepsilon_{t1,0} > \varepsilon_{ц1,0limit}$ is signaled to the WCS, after which firing or bomb-dropping begins. Provided that the bomb drop takes place in the invisible zone ($\varepsilon_{t1,0} > \varepsilon_{ц1,0limit}$), the initial η_0, ξ_0 and the current coordinates η_t, ξ_t of the target relative to the aircraft are determined. When the condition $\eta_t - \eta \leq 0$ is met, the bomb drop is carried out automatically. Provided that $\eta_t - \eta > 0$ or $\beta_{t1,0} \neq \beta_{t1,0v}$; $\varepsilon_{t1,0} \neq \varepsilon_{t1,0v}$ then the process continues and returns to the starting position.

Results and Discussion

Comparative Analysis of the Accuracy of Combat use of Unguided Weapons

Bomb drop error is a sum of random and systematic error. Therefore, it is necessary to take some mean value of it. Considering that in most cases its sign is not of interest, the square root of the second starting moment of the error is taken as a criterium for evaluating the accuracy of firing and bomb dropping (Atanasov, 2014):

(7) $$\sqrt{\alpha_{2\Delta x}} = \sqrt{M^2[\Delta x] + D[\Delta x]},$$

where M[Δx] is the mathematical expectation of the hit error;
- D[Δx] is error variance.

The accuracy of launching an unguided rocket and the accuracy of dropping a conventional bomb from a 4+ generation aircraft using type targeting system are calculated. The accuracy of firing and bomb drop under the same conditions with a targeting system using the proposed general algorithm for combat use is calculated and a comparative analysis is carried out. The test is carried out for launching an unguided C-25 rocket for the following launch conditions:

- dive angle $\lambda = -30^0$;
- speeds - V=56.56; 111.11; 166.67; 222.22; 277.78 m/s;
- altitudes H= 200; 500; 800; 1100; 1400 m.

When shooting with a dive angle $\lambda = -30^0$, Table 1 presents the calculated allowed shooting distances D, with the allowed distances D ranging from 1504.23 m to 2609.50 m. For the allowed launching distances D (Table 1), the relative percentage increase in accuracy when using the general algorithm for combat use $\Delta\alpha_{2x}$ % is in the range of 31.34 % to 35.23 % (Table 2).

Table 1. Allowed launching distance with an unguided rocket

Launching an unguided rocket with a dive angle $\lambda = -30^0$					
D, [m]	V= 55.56 [m/s]	111.11	166.67	222.22	277.78
H=200 [m]	-	-	-	-	-
500	-	-	-	-	-
800	-	-	-	1504.23	1516.10
1100	1914.56	1972.82	2017.66	2049.10	2067.14
1400	2408.90	2484.18	2542.70	2584.48	2609.50

Table 2. The relative percentage increase in accuracy when launching an unguided rocket $\Delta\alpha_{2x}$ %

Firing an unguided rocket with a dive angle $\lambda = -30^0$					
$\Delta\alpha_{2x}$ [%]	V= 55.56 [m/s]	111.11	166.67	222.22	277.78
H=200 [m]	-	-	-	-	-
500	-	-	-	-	-
800	-	-	-	31.60	34.50
1100	31.34	31.46	32.11	33.01	34.67
1400	31.68	32.40	32.65	33.83	35.23

A comparative analysis of the accuracy of a bomb drop from a horizontal flight with an aviation bomb having a characteristic time of fall Θ=21.1 s is performed. The test is carried out for the following bomb drop conditions:
- horizontal flight and diving;
- speeds - V=180; 200; 220; 240; 260 m/s;
- altitudes H= 600; 900; 1200; 1500; 1800 m.

The relative percentage increase in bomb drop accuracy when using the general algorithm for combat use ranges from 15.07% to 61.15% (Table 3). A greater relative percentage increase in accuracy when using the general combat algorithm is achieved in the area of conditions for the CCRP method for an aircraft with a type targeting system (shaded in grey - Table 3).

Table 3. The relative percentage increase in bomb drop accuracy $\Delta\alpha_{2x}$ %

Dropping an dumb bomb from horizontal flight					
$\Delta\alpha_{2x}$ [%]	V=180 [m/s]	200	220	240	260
H=600 [m]	36.37	27.36	24.12	23.76	26.21
900	45.81	36.93	27.60	20.08	15.07
1200	52.46	42.99	33.95	24.41	15.91
1500	56.64	49.33	39.59	30.31	21.20
1800	61.15	53.07	45.86	38.45	29.11

Conclusion

1. The proposed structural scheme and developed general algorithm for the combat use of unguided munitions ensures the expansion of the range of combat conditions for firing and bomb drop and increases their effectiveness.

2. When dropping a bomb from a horizontal flight on a stationary target, the relative percentage increase in accuracy for a targeting system working with the proposed general algorithm is between 15.07% and 61.15%, and when firing an unguided rocket it is in the range of 31.34% to 35.23%.
3. The conducted research shows that for an targeting system working with the proposed algorithm, the criterion for effectiveness of the combat use of unguided weapons - "price-accuracy" is fulfilled.

Recommendations

With the help of the proposed mathematical model and general algorithm, it is possible to determine the areas of conditions for the combat use of weapons from a multi-purpose aircraft on air and ground targets. On the other hand, the use of advanced algorithms for combat use will simplify and facilitate the pilot's work with the controls of the aviation armament during the execution of combat tasks.

Scientific Ethics Declaration

The author declares that the scientific ethical and legal responsibility of this article published in EPSTEM journal belongs to the author.

Acknowledgements or Notes

* This article was presented as oral presentation at the International Conference on Basic Sciences, Engineering and Technology (www.icbaset.net) held in Alanya/Turkey on May 02-05, 2024.

* The research in this article was carried out in fulfilment of Task 1.1.2. “Analysis and assessment of disaster, accident, emergency and crisis management systems and development of science-based proposals for their improvement” from the National Scientific Program “Security and Defence”, adopted by RMS No. 731 of 21.10.2021. and according to Agreement No. D01-74/19.05.2022.

References

Atanasov, M. (2014). *Tochnost na reshavane na zadachata na pritselvane s neupravlyaemi aviatsionni bombi.* Pleven: Monografiya.

Kambushev, M., Biliderov, S., Yovchev, K., Chikurtev, D., Kambushev, K., & Chivarov N., (2019). Influence of atmospheric turbulence on the control of flying robotics systems. *2019 IEEE XXVIII International Scientific Conference Electronics (ET)* (pp. 1-4).

Mitov. L. (2019). Testing the strength of glued aviation structures. *Annual Scientific Conference 2019* (pp.94-98)

Stoĭkov, O., & Atanasov, M., (2009). *Aviatsionni pritselni sistemi- purva* cast . Dolna Mitropoliya

Author Information

Milen Atanasov
Georgi Benkovski Bulgarian Air Force Academy, St. Ciril and Methodius 1, 5855, Dolna Mitropolia, Bulgaria
Contact e-mail: *matanasov@af-acad.bg*

To cite this article:

Atanasov, M. (2024). Possibilities for improving algorithms for combat use of aircraft using unguided weapons. *The Eurasia Proceedings of Science, Technology, Engineering & Mathematics (EPSTEM), 28,* 428-437.

The Eurasia Proceedings of Science, Technology, Engineering & Mathematics (EPSTEM)
ISSN: 2602-3199

The Eurasia Proceedings of Science, Technology, Engineering & Mathematics (EPSTEM), 2024

Volume 28, Pages 438-447

ICBASET 2024: International Conference on Basic Sciences, Engineering and Technology

Food Recommendation System for a Healthy Liver Using Machine Learning

Shyti Bederiana
University of Elbasan "Aleksander Xhuvani"

Stergu Argesta
University of Elbasan "Aleksander Xhuvani"

Valera Dhurata
University of Elbasan "Aleksander Xhuvani"

Papajani Blerina
University of Elbasan "Aleksander Xhuvani"

Abstract: Nowadays, the work routine, the problems we face, make us not pay proper attention to healthy eating. As a result, people get sick. We have created through mathematical knowledge (statistics, probability, linear algebra, geometry), combining the concepts of Machine Learning (Content Based Filtering, TD IDF Vectorizer Algorithm, Conditional Independence, Count Vectorization) with Python language, a Recommendation System for all people suffering from liver. Liver is one of the most important organs of our body, because it makes 500 essential functions in the organism. But we have to be aware about the types of food that we use. Also, we must be very careful with our lifestyle and diet on foods. The aim of this article is to recommend the most appropriate foods for a healthy liver. This article will help the people who suffer from liver disease to check the best foods maintaining the liver in a good physical condition.

Keywords: Recommendation system, Liver, Foods, Health, Machine learning.

Introduction

Nowadays, the majority of individuals have become addicted to social networks and as a result lead a sedentary life. Some other individuals get lost in the routine and workload. Some people get tired doing physical work. The way some individuals eat, how they build their lifestyle, how they choose to live, directly affects the health of the organism. The most solid and sensitive organ to the diet and the types of food we consume is the liver. This article presents a simple recommendation system, using the subfields of mathematics (Linear Algebra, Statistics, Probability, Geometry) and the knowledges of Machine Learning as a subfield od Artificial Intelligence with Python language. The main purpose of this article is to suggest people who suffer from liver diseases, to choose best foods to maintain the liver in the good conditions. This Recommendation System can be useful, also, for people of all ages, who has not time to search in the pages of internet about healthy foods. This article also helps people to prevent liver disease. The article is organized in some sections.

The Relationship between Mathematics, Machine Learning and Recommendations Systems

There is a hard relationship between Mathematics, Machine Learning and Recommendation Systems (Li et al., 2021). We have created a code based on the statistical data collected in a database from the website for different

types of food products based on the nutritional values and essential chemical elements that the body needs to function properly. There are three types of Recommendation Systems techniques:

- Content-based filtering recommendation
- Collaborative filtering system
- Hybrid technique

The first technique is used in this article to make the food recommendation and to emphasize the relationship between the science of Mathematics, RSs and ML.

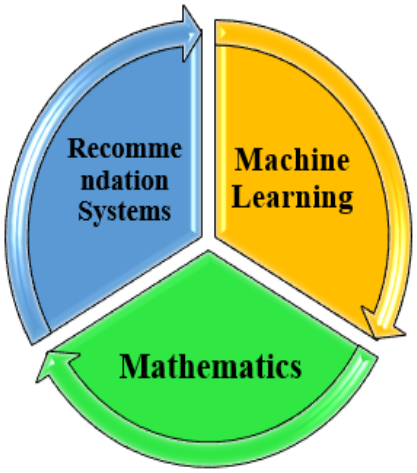

Figure 1. The triple mathematics, machine learning and recommendation Systems

Data Implementing in the Code

First of all, we have taken data from the page "U.S. DEPARTMENT AGRICULTURE" (FoodData Central (usda.gov)). We have saved them in CSV format in excel with the title "Best_food_for_kidney". Then, we have implemented these data in the code using Python language, in the Spyder 3.11 of Anaconda Navigator package. Based on the amount of nutrient that the foods contain we have programmed the code to recommend the best foods for a healthy liver. To make the code, we have used the libraries of Python, such as: Numpy, Pandas, Matplotlib, Scikit-learn. The Matplotlib library is made for creating 2D arrays, making different plots (Hunter et al., 2017).

Table 1. The foods with their nutrition

Foods	Ingridients	Protein	Fiber	Calories	Fat	Charbohic Sugar	Vitamin
Avocado	{"Magnesium": 58, "Potasium": 485, "Phosphorus": 48.67, "So	2	6.7	160	14.66	8.53	0.66 {"Vitamin": "C", "Vitamin": "A"}}
Bluberries	{"Magnesium": 6.5, "Potasium": 77, "Phosphorus": 14.38, "Soc	0.74	2.4	57	0.33	14.49	9.96 {"Vitamin": "C", "Vitamin": "A"}}
Broccoli	{"Magnesium": 21, "Potasium": 316, "Phosphorus": 73, "Sodiu	2.82	2.6	34	0.37	6.64	1.7 {"Vitamin": "C", "Vitamin": "A"}}
Butter	{"Magnesium": 3, "Potasium": 24, "Phosphorus": 508, "Sodiun	0.85	0	717	81.11	0.06	0.06 {"Vitamin": "A", "Vitamin": D}}
Cabbage	{"Magnesium": 12, "Potasium": 246 , "Phosphorus": 26, "Sodiu	1.44	2.3	24	0.12	5.58	3.58 {"Vitamin": "C", "Vitamin": "A"}}
Beef	{"Magnesium": , "Potasium": 315, "Phosphorus": , "Sodiun	26.33	0	288	19.54	0	0 {"Vitamin":}}
Couliflow	{"Magnesium": 15, "Potasium": 303, "Phosphorus": 44, "Sodiu	1.98		25	0.1	5.3	2.4 {"Vitamin": "C", "Vitamin": "A"}}
Apples	{"Magnesium": 5, "Potasium": 107, "Phosphorus": 11, "Sodiun	0.26	2.4	52	0.17	13.81	10.39 {"Vitamin": "C", "Vitamin": "A"}}
Bananas	{"Magnesium": 32, "Potasium": 358, "Phosphorus": 22 , "Sodiu	1.09	2.6	89	0.33	22.84	12.33 {"Vitamin": "C", "Vitamin": "A"}}
Onions	{"Magnesium": 15.27 , "Potasium": 144, "Phosphorus": 29, "So	0.92	1.4	42	0.08	10.11	4.28 {"Vitamin": "C", "Vitamin": "A"}}
Oranges	{"Magnesium": 11, "Potasium": 181, "Phosphorus": 22, "Sodiu	0.94	2.4	47	0.12	11.75	9.35 {"Vitamin": "C", "Vitamin": "A"}}
Pineaple	{"Magnesium": 12, "Potasium": 115, "Phosphorus": 8, "Sodiun	0.54	1.4	48	0.12	12.63	9.26 {"Vitamin": "C", "Vitamin": "A"}}
Pomegran	{"Magnesium": 12, "Potasium": 259, "Phosphorus": 95.2 , "Soc	0.95	0.6	68	0.3	17.17	16.57 {"Vitamin": "C", "Vitamin": "A"}}
Strawberr	{"Magnesium": 22, "Potasium": 153, "Phosphorus": 24 , "Sodiu	0.67	2	32	0.3	7.68	4.66 {"Vitamin": "C", "Vitamin": "A"}}
White Bre	{"Magnesium": 26, "Potasium": 252, "Phosphorus": 103, "Sodi	9.7	6.09	246	4.2	46.1	5.57 {"Vitamin": "C", "Vitamin": "A"}}
Corn	{"Magnesium": 42.60 , "Potasium": 270, "Phosphorus": 13, "So	3.22	2.7	86	1.18	19.02	3.22 {"Vitamin": "C", "Vitamin": "A"}}
Lettuce	{"Magnesium": 12, "Potasium": 141, "Phosphorus": 28, "Sodiu	0.9	1.2	14	0.14		1.76 {"Vitamin": "C", "Vitamin": "A"}}
Olives	{"Magnesium": 6.33, "Potasium": 1, "Phosphorus": 28, "Sodiu	0	0	884	100	0	0 {"Vitamin": }}
Artichoke	{"Magnesium": 0, "Potasium": 23.4, "Phosphorus": 107.01, "So	3	2	30	0	6	2 {"Vitamin": "C", "Vitamin": "86", "Vitamin": "A"}}
Spinach	{"Magnesium": 79, "Potasium": 558, "Phosphorus": 49, "Sodiu	2.86	2.2	23	0.39	3.63	0.42 {"Vitamin": "C", "Vitamin": "A"}}
Mushroon	{"Magnesium": 9 , "Potasium": 318, "Phosphorus": 87, "Sodiur	3.09	1	22	0.34	3.28	1.65 {"Vitamin": "C", "Vitamin": "D", "Vitamin": "A"}}
Carrots	{"Magnesium": 12, "Potasium": 320 , "Phosphorus": 35 , "Soc	0.93	2.8	41	0.24	9.58	4.54 {"Vitamin": "C", "Vitamin": "A"}}
Blackberri	{"Magnesium": 20, "Potasium":162, "Phosphorus": 22, "Sodiur	1.39	5.3	43	0.49	9.61	4.88 {"Vitamin": "C", "Vitamin": "A"}}
Fish	{"Magnesium": 76, "Potasium": 351, "Phosphorus": 689, "Sodi	17.76	0	84	0.92	0	0 {"Vitamin": "C", "Vitamin": "A"}}
Milk	{"Magnesium": 12, "Potasium": 153, "Phosphorus": 85, "Sodiu	3.39	0	52	2.06	4.86	5.32 {"Vitamin": "A"}}
Cherriesh	{"Magnesium": 11 , "Potasium": 173, "Phosphorus": 16, "Sodiu	1	1.6	50	0.3	12.18	8.49 {"Vitamin": "C", "Vitamin": "A"}}
White Ric	{"Magnesium": 29.62, "Potasium": 35 , "Phosphorus": 33, "Soc	2.66	0.4	129	0.28	27.9	0.05 {"Vitamin":}}
Potatoes	{"Magnesium": 23, "Potasium": 317, "Phosphorus": 38, "Sodiu	1.66	1.7	104	2.4	19.36	0.82 {"Vitamin": "C", "Vitamin": "A"}}
Tomatoes	{"Magnesium": 194, "Potasium": 237, "Phosphorus": 356, "Soc	0.88	1.2	18	0.2	3.92	2.63 {"Vitamin": "C", "Vitamin": "A"}}
Cucumber	{"Magnesium": 15.50, "Potasium": 136 , "Phosphorus": 24, "So	0.59	0.7	12	0.16	2.16	1.38 {"Vitamin": "C", "Vitamin": "A"}}
Coconuts	{"Magnesium": 32, "Potasium": 358, "Phosphorus": 113.02, "S	3.33	9	354	33.49	15.23	6.23 {"Vitamin": "C", "Vitamin": "A"}}
Cheese	{"Magnesium": 19, "Potasium": 187, "Phosphorus": 91 , "Sodiu	22.21	0	350	26.91	4.71	3.54 {"Vitamin": "C", "Vitamin": "A"}}
Green Tea	{"Magnesium": 0 , "Potasium": 21 , "Phosphorus": 290, "Sodiu	0	0	2	0	0.47	0 {"Vitamin"}}
Green Pea	{"Magnesium": 39, "Potasium": 244, "Phosphorus": 187.2, "So	5.42	5.1	81	0.4	14.46	5.67 {"Vitamin": "C", "Vitamin": "A"}}

The database contains the names of foods, the vitamins of each of them, the amount of fiber, saturated fat, the ingredients. We have calculated the amount of saturated fat and the amount for each ingredient for 100 grams of food. The main ingredients are: magnesium, potassium, phosphorus. There is a screenshot with thirty-five foods with their own nutrition.

The Phosphorus

The phosphorus helps maintain normal pH levels in extracellular fluid. It plays crucial roles in the body, including being a component of bones, teeth, *DNA*, *RNA*, and cell membranes. Phosphorus is also involved in energy production and enzyme activation. Three classes of *NA/Pi* contraspoters are encoding by the cDNAs(Takeda et al., 2004). We have made a table for these main ingredients classified in two huge group based on gender: male and female. Each of these groups are classified in three subgroups based on the age: male aged 19-30, male aged 30-70, male over 70, female aged 19-30, female aged 30-70 and female over 70. For each group we have define the type of foods recommended for a healthy liver. To make the table we have collected data in the page "U.S. FOOD & DRUG" (Using the Nutrition Facts Label: For Older Adults | FDA). The table below will help us to calculate the amount of some nutrition based on the daily value (DV)

Table 2. The daily values of some nutrition for a healthy body

Nutrition	**Male aged** 19-30	**Male aged** 30 to 70	**Male over** 70	**Female aged** 19-30	**Female aged** 30 to 70	**Female over** 70
Potassium	3400 mg	4700 mg	4700 mg	2600 mg	2600 mg	2600 mg
Magnesium	400 mg	420 mg	400 mg	310 mg	350 mg	320 mg
Phosphorus	1250 mg	1596 mg	580-1000 mg	580-1000 mg	1189 mg	1189mg
Sodium	1500 mg	1500-2300 mg	1200 mg	1300 mg	1500-2300 mg	1200 mg

Male and female aged 30-70 years. The amount of nutritions in the artichoke;

Magnesium

$$15\%\ of\ 350\ mg = \frac{15}{100}\ of\ 350\ mg = (350 : 100) * 15 = 3.5 * 15 = 52.5\ mg$$

Potassium

$$9\%\ of\ 2600\ mg = \frac{9}{100}\ of\ 2600\ mg = (2600 : 100) * 9 = 2.6 * 9 = 23.4\ mg$$

Phosphorus

$$9\%\ of\ 1189\ mg = \frac{9}{100}\ of\ 1189\ = (1189 : 100) * 9 = 107.01\ mg$$

Methods and Techniques

Content Based Filtering is a powerful method of Machine Learning to make Recommendation Systems (Son & Kim, 2017). This method is a type of Information Filtering System. The code uses all the data implemented from the external dataset in CSV format in excel and filters them (Zhang et al., 2023). The input data such as all the values of ingredients, vitamins, protein, fat, carbohydrates, fibers are trained by Content Based Filtering and give as outputs the recommender types of foods. The concept of Content Based Filtering means that the same data of a collection or Database are usen and usen once again, depends on the preferences of different users (Swathi et al., 2007).

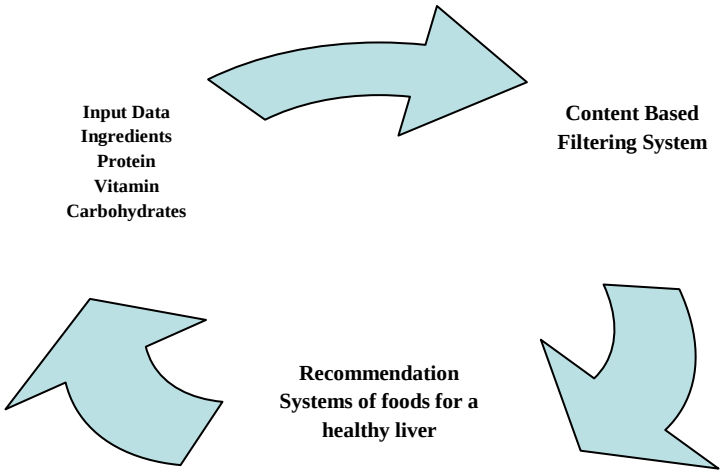

Figure 2. The process of recommendation systems of food

Applying the Code

```
import pandas as pd
import numpy as np
import matplotlib.pyplot as plt
from matplotlib import pyplot as plt
from sklearn.feature_extraction.text import TfidfVectorizer
from sklearn.metrics.pairwise import cosine_similarity
hp = pd.read_csv('Female_aged_30_to_70.csv')
print(hp)
```

We choose two columns with data form the database and implement their data in the code.

```
hp ['Foods'] = hp ['Foods'].str.split('/')
hp ['Foods'] = hp['Foods'].fillna("").astype('str')
foods = pd.read_csv('Female_aged_30_to_70.csv', encoding='latin-1', usecols=['Foods', 'Ingridients'])
print(foods)

plt.figure(figsize=(20,10))
plt.bar(hp['Foods'].head(101), hp['Ingridients'].head(80))
term_freq = TfidfVectorizer(analyzer='word', ngram_range=(1, 2), min_df=1, encoding='utf-8',
                    lowercase=True, stop_words='english')
tfidf_matrix = term_freq.fit_transform(foods['Ingridients'])
tfidf_matrix.shape
```

Results and Discussion

First of all, we implement all the data in the code. There is a matrix with 34 rows and 14 columns.

	Foods ...	Vitamin
0	Avocado ...	[{"Vitamin": "C", "Vitamin": "A"}]
1	Bluberries ...	[{"Vitamin": "C", "Vitamin": "A"}]
2	Broccoli ...	[{"Vitamin": "C", "Vitamin": "A"}]
3	Butter ...	[{"Vitamin": "A", "Vitamin": D}]
4	Cabbage ...	[{"Vitamin": "C", "Vitamin": "A"}]
5	Beef ...	[{"Vitamin":}]
6	Couliflower ...	[{"Vitamin": "C", "Vitamin": "A"}]
7	Apples ...	[{"Vitamin": "C", "Vitamin": "A"}]
8	Bananas ...	[{"Vitamin": "C", "Vitamin": "A"}]
9	Onions ...	[{"Vitamin": "C", "Vitamin": "A"}]
10	Oranges ...	[{"Vitamin": "C", "Vitamin": "A"}]
11	Pineaple ...	[{"Vitamin": "C", "Vitamin": "A"}]
12	Pomegranates ...	[{"Vitamin": "C", "Vitamin": "A"}]
13	Strawberries ...	[{"Vitamin": "C", "Vitamin": "A"}]
14	White Bread ...	[{"Vitamin": "C", "Vitamin": "A"}]
15	Corn ...	[{"Vitamin": "C", "Vitamin": "A"}]
16	Lettuce ...	[{"Vitamin": "C", "Vitamin": "A"}]
17	Olives ...	[{"Vitamin": }]
18	Artichoke ...	[{"Vitamin": "C", "Vitamin": "B6", "Vitamin": ...
19	Spinach ...	[{"Vitamin": "C", "Vitamin": "A"}]
20	Mushrooms ...	[{"Vitamin": "C", "Vitamin": "D", "Vitamin": "...
21	Carrots ...	[{"Vitamin": "C", "Vitamin": "A"}]
22	Blackberries ...	[{"Vitamin": "C", "Vitamin": "A"}]
23	Fish ...	[{"Vitamin": "C", "Vitamin": "A"}]
24	Milk ...	[{"Vitamin": "A"}]
25	Cherriesh ...	[{"Vitamin": "C", "Vitamin": "A"}]
26	White Rice ...	[{"Vitamin":}]
27	Potatoes ...	[{"Vitamin": "C", "Vitamin": "A"}]
28	Tomatoes ...	[{"Vitamin": "C", "Vitamin": "A"}]

29	Cucumber	...	[{"Vitamin": "C", "Vitamin": "A"}]
30	Coconuts	...	[{"Vitamin": "C", "Vitamin": "A"}]
31	Cheese	...	[{"Vitamin": "C", "Vitamin": "A"}]
32	Green Tea	...	[{"Vitamin"}]
33	Green Peas	...	[{"Vitamin": "C", "Vitamin": "A"}]

[34 rows x 14 columns]

The second result of the code:

	Foods	Ingridients
0	Avocado	[{"Magnesium": 58, "Potasium": 485, "Phosphoru...
1	Bluberries	[{"Magnesium": 6.5, "Potasium": 77, "Phosphoru...
2	Broccoli	[{"Magnesium": 21, "Potasium": 316, "Phosphoru...
3	Butter	[{"Magnesium": 3, "Potasium": 24, "Phosphorus"...
4	Cabbage	[{"Magnesium": 12, "Potasium": 246 , "Phosphor...
5	Beef	[{"Magnesium": , "Potasium": 315, "Phospho...
6	Couliflower	[{"Magnesium": 15, "Potasium": 303, "Phosphoru...
7	Apples	[{"Magnesium": 5, "Potasium": 107, "Phosphorus...
8	Bananas	[{"Magnesium": 32, "Potasium": 358, "Phosphoru...
9	Onions	[{"Magnesium": 15.27 , "Potasium": 144, "Phosp...
10	Oranges	[{"Magnesium": 11, "Potasium": 181, "Phosphoru...
11	Pineaple	[{"Magnesium": 12, "Potasium": 115, "Phosphoru...
12	Pomegranates	[{"Magnesium": 12, "Potasium": 259, "Phosphoru...
13	Strawberries	[{"Magnesium": 22, "Potasium": 153, "Phosphoru...
14	White Bread	[{"Magnesium": 26, "Potasium": 252, "Phosphoru...
15	Corn	[{"Magnesium": 42.60 , "Potasium": 270, "Phosp...
16	Lettuce	[{"Magnesium": 12, "Potasium": 141, "Phosphoru...
17	Olives	[{"Magnesium": 6.33, "Potasium": 1, "Phosphor...
18	Artichoke	[{"Magnesium": 0, "Potasium": 23.4, "Phosphor...
19	Spinach	[{"Magnesium": 79, "Potasium": 558, "Phosphoru...
20	Mushrooms	[{"Magnesium": 9 , "Potasium": 318, "Phosphoru...
21	Carrots	[{"Magnesium": 12, "Potasium": 320 , "Phosp...
22	Blackberries	[{"Magnesium": 20, "Potasium":162, "Phosphorus...
23	Fish	[{"Magnesium": 76, "Potasium": 351, "Phosphoru...
24	Milk	[{"Magnesium": 12, "Potasium": 153, "Phosphor...
25	Cherriesh	[{"Magnesium": 11 , "Potasium": 173, "Phosphor...
26	White Rice	[{"Magnesium": 29.62, "Potasium": 35 , "Phosph...
27	Potatoes	[{"Magnesium": 23, "Potasium": 317, "Phosphoru...
28	Tomatoes	[{"Magnesium": 194, "Potasium": 237, "Phosphor...
29	Cucumber	[{"Magnesium": 15.50, "Potasium": 136 , "Phosp...
30	Coconuts	[{"Magnesium": 32, "Potasium": 358, "Phosphoru...
31	Cheese	[{"Magnesium": 19, "Potasium": 187, "Phosphoru...
32	Green Tea	[{"Magnesium": 0 , "Potasium": 21 , "Phosphor...
33	Green Peas	[{"Magnesium": 39, "Potasium": 244, "Phosphoru...

There is time to plot the graph using the code as below.

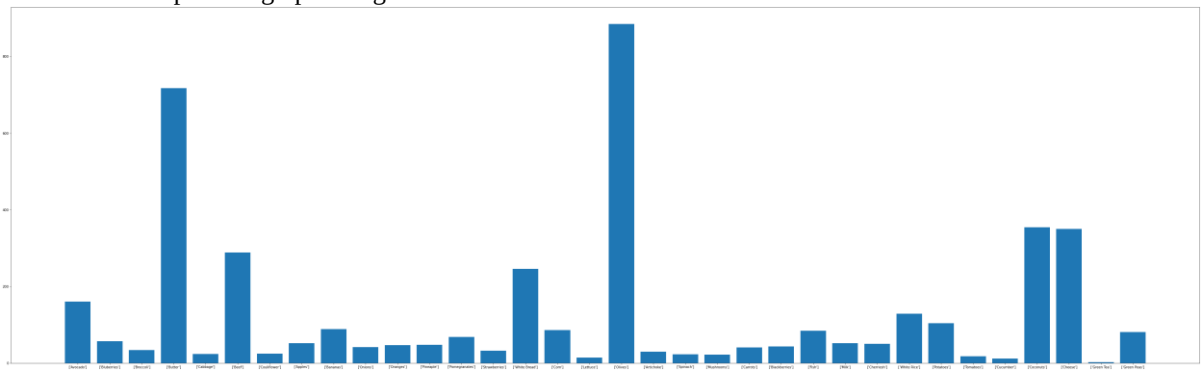

Figure 2. The distribution of calories for different foods

```
plt.figure(figsize=(65,10))
plt.bar(hp['Foods'].head(101), hp['Calories'].head(70))
term_freq = TfidfVectorizer(analyzer='word', ngram_range=(1, 2), min_df=1, encoding='utf-8',
                    lowercase=True, stop_words='english')
tfidf_matrix = term_freq.fit_transform(foods['Calories'])
tfidf_matrix.shape
```

The chart above shows the dependence of two variables. The variable x is for “Foods” and the variables y is for “Calories”.

TD IDF (Term Frequency – Inverse Document Frequency)

How the mathematics’ knowledges help Machine Learning to create Recommendation System?

TD IDF is the product of two statistics term frequency with inverse term frequency. IDF defines the measure of quantify of a term across a collection of terms in a database. This technique uses some knowledge of Linear Algebra and Calculus to calculate how important is a term within a document (Karabiber, 2022). It expresses the logarithm of the ratio between the number of terms appears in the document with the total number of terms. Mathematically the formula is written as below:

$$tf(t,d) = \frac{f_{t,d}}{\sum_{t' \in d} ft', d}$$

Which is the role of each variable in the formula above?

- $t \rightarrow term$
- $d \rightarrow document$
- $D \rightarrow set\ of\ documents$

There are other formulas of TD IDF

$$TF(d,t) = \begin{cases} 0 & freq(d,t) = 0 \\ 1 + \log(f\ req\,(d,t))) & f\ req(d,t) \neq 0 \end{cases}$$

$$IDF\ (t) = N/\,df(t) = N/N(t)$$
$$IDF\ (t) = log(N/\,df(t))$$
$$IDF\ (t) = log\,(1 + |d|)/(dt)$$
$$IDF\ as\ ID\ (t) = log\,[\,n\,/\,(df(t) + 1)\,])$$

When we implement the mathematical formula in the code, it takes another form, using Python language. There are some steps (Wang, 2018):

- Preproccessing the data
- Defining a function to calculate “Term Frequency”
- Defining a function to calculate “Inverse Document Frequency”
- Combining the TD IDF
- Applying the TD IDF model in our text

There is the code for the TD IDF technique

```
term_freq = TfidfVectorizer(analyzer='word', ngram_range=(1, 2), min_df=1, encoding='utf-8',
                    lowercase=True, stop_words='english')
tfidf_matrix = term_freq.fit_transform(foods['Ingridients'])
tfidf_matrix.shape
print(tfidf_matrix)
cosSim = cosine_similarity(tfidf_matrix, tfidf_matrix)
cosSim[:4, :4]
print(cosSim)
```

```
titleHotels = foods['Foods']
print(titleHotels)
signIndication = pd.Series(foods.index, index=foods['Foods'])
print(signIndication)
```

Creating a function called fd_recommendations and take some attributes

```
def fd_recommendations(Foods):
    hx = signIndication[Foods]
    scores_similarity = list(enumerate(cosSim[hx]))
    scores_similarity = sorted(scores_similarity, key=lambda x: x[1], reverse=True)
    scores_similarity = scores_similarity[1:21]
    foods_signIndication = [i[0] for i in scores_similarity]
    return titleHotels.iloc[foods_signIndication]
  print(fd_recommendations('Avocado').head(10))
```

The output of the code using the technique TD-IDF

The first number means the “Document Index”, while the second number means “Word Index”.

```
  (0, 224)        0.2499995926057404
  (0, 177)        0.2499995926057404
  (0, 255)        0.2499995926057404
  (0, 363)        0.11147348132417445
  (0, 195)        0.2499995926057404
  (0, 161)        0.2499995926057404
  (0, 302)        0.2499995926057404
  (0, 163)        0.2499995926057404
  (0, 341)        0.2499995926057404
  (0, 183)        0.2499995926057404
  (0, 278)        0.2499995926057404
  (0, 21)         0.1526409237963958
  (0, 222)        0.07470797316296354
  (0, 176)        0.2499995926057404
  (0, 238)        0.06660618464588744
  (0, 345)        0.06472982641585853
  (0, 194)        0.2499995926057404
  (0, 160)        0.2499995926057404
  (0, 282)        0.06472982641585853
  (0, 162)        0.2499995926057404
  (0, 312)        0.06472982641585853
  (0, 182)        0.2499995926057404
  (0, 262)        0.06472982641585853
  (1, 100)        0.276241039860636
  (1, 246)        0.276241039860636
  :       :
  (32, 345)       0.08681253862380181
  (32, 282)       0.08681253862380181
  (32, 312)       0.08681253862380181
  (32, 262)       0.08681253862380181
  (33, 232)       0.2662968175733716
  (33, 158)       0.2662968175733716
  (33, 252)       0.2662968175733716
  (33, 54)        0.2662968175733716
  (33, 290)       0.2662968175733716
  (33, 80)        0.2662968175733716
  (33, 327)       0.2662968175733716
  (33, 145)       0.2662968175733716
  (33, 276)       0.2662968175733716
  (33, 83)        0.2662968175733716
```

(33, 79) 0.2662968175733716
(33, 144) 0.2662968175733716
(33, 52) 0.23834020131879124
(33, 157) 0.21850466641818692
(33, 363) 0.11874032677831936
(33, 222) 0.07957811168127973
(33, 238) 0.07094817562313468
(33, 345) 0.06894949946500069
(33, 282) 0.06894949946500069
(33, 312) 0.06894949946500069
(33, 262) 0.06894949946500069
[[1. 0.04840005 0.0262073 ... 0.0261234 0.05257826 0.04175946]
[0.04840005 1. 0.03235488 ... 0.0322513 0.10743963 0.0515552]
[0.0262073 0.03235488 1. ... 0.02556716 0.10086411 0.0717837]
...
[0.0261234 0.0322513 0.02556716 ... 1. 0.08261124 0.07985327]
[0.05257826 0.10743963 0.10086411 ... 0.08261124 1. 0.05600579]
[0.04175946 0.0515552 0.0717837 ... 0.07985327 0.05600579 1.]]
0 Avocado

Cosine Similarity

It is a metric that we use to determine the similarity of data objects, based on their size. The language of Python together with all libraries can help us to find the similarity between two or more sentences. The data objects are treated by the Cosine Similarity as vectors. This technique is beneficial because if two data objects are very far similar to each other, calculating by the Euclidian distance, they can have a very small angle between them. If the angle is small, the similarity is high. The range of Cosine Similarity is [0, 1] [12]. There is the formula of this geometric concept:

$$similarity(x,y) = \frac{\sum_{i\in I}^{n} xy * (rx,i - r\bar{x}) * (rx,i - r\bar{y})}{\sqrt{(rx,i - r\bar{x})^2 * \sum_{i\in a_{xy}}^{n} (ry,i - r\bar{y})^2}}$$

$$similarity(A,B) = cos(\Theta) = \frac{A * B}{|A| * |B|} = \frac{\sum_{i=1}^{n} a_i b_j}{\sqrt{\sum_{i=1}^{n} a_i} * \sum_{i}^{n} b_j}$$

Each of the segment's point, we subtract from the mean average value of the couple of coordinates. In the formula above, Θ is the angle between two vectors, *A* * *B* is the dot product, which is equal with the sum of unit vectors; |*A*| is the magnitude of the vector A. |*B*| is the magnitude of the vector B. Combining the similarity calculated from the scoring matrix and the similarity obtained from the commodity type, the calculation of the similarity will be more accurate (Schubert, 2021).

Foods	
Avocado	0
Bluberries	1
Broccoli	2
Butter	3
Cabbage	4
Beef	5
Couliflower	6
Apples	7
Bananas	8
Onions	9
Oranges	10
Pineaple	11
Pomegranates	12
Strawberries	13
White Bread	14

```
Corn          15
Lettuce       16
Olives        17
Artichoke     18
Spinach       19
Mushrooms     20
Carrots       21
Blackberries  22
Fish          23
Milk          24
Cherriesh     25
White Rice    26
Potatoes      27
Tomatoes      28
Cucumber      29
Coconuts      30
Cheese        31
Green Tea     32
Green Peas    33
dtype: int64
```

Conclusion

No one should be demoralized if they are experiencing a difficult health condition. The best way would be to prevent that disease, showing care in the way we eat and in the lifestyle we lead. The foods we consume affect our body. One of the causes of the large spread of diseases is malnutrition, bad lifestyle, and the breakdown of the food regime. What should we do to prevent liver diseases? Through the code we offer a recommendation of the best quality foods that positively affect the liver organ and help it function normally.

The final output with best food for the healthy liver is below

```
7          Apples
11        Pineaple
12    Pomegranates
17          Olives
16         Lettuce
32       Green Tea
21          Carrots
4          Cabbage
24            Milk
20       Mushrooms
Name: Foods, dtype: object
```

Recommendations

This article modestly recommends the foods for a healthy liver. In the future we will rich the folder (where the database and the code are located), with other CSV files, why not for other organs, such as: kidney, heart, lungs, stomach, etc. This recommendation can help dietitians to list foods that can be used for a healthy diet. We may in the future create a platform like a "Blogger" to recommend foods for various diseases. This recommendation can be included in curriculums of our University, as an application of Machine Learning as a sub-field of Artificial Intelligence in the Medicine.

Scientific Ethics Declaration

The authors declare that the scientific ethical and legal responsibility of this article published in EPSTEM journal belongs to the authors.

Acknowledgements or Notes

* This article was presented as an oral presentation at the International Conference on Basic Sciences, Engineering and Technology (www.icbaset.net) held in Alanya/Turkey on May 02-05, 2024.

References

Hunter. J., Dale, D., Firing, E., & Droetboom, M. (2017). *Matplolib* https://matplotlib.org/2.1.2/Matplotlib.pdf

Kuter, K. (2023). *Math 345 -probability.* LibreText

Li, L., Zhang, Z., & Zhang, S. (2021). Hybrid algorithm based on content and collaborative filtering in recommendation system optimization and simulation. *Scientific Programming*, *2021*(4), 1-11.

Mu, R., Zeng, X., & Han, L. (2018) A survey of recommender systems based on deep learning. *IEEE Access*, (99), 1-1.

Schubert, E. (2021). A triangle inequality for cosine similarity -similarity search and applications. *International Conference SISAP 2021* (pp. 32-44)

Son, J., & Kim, S. B. (2017). Content-based filtering for recommendation systems using multiattribute networks. *Expert Systems with Applications*, *89*, 404-412.

Takeda, E., Taketani, Y., & Sawada, N. (2004,). The regulation and the function of phosphate in human body. *Bio Factors, 21* (1-4), 345-355.

Wang, Y., Zhang, D.,… & Liu, Q. (2018,). Improvement of TD-IDF algorithm based on knowledge graph. *16 th International Conference on Software Engineering Research, Management and Applications (SERA).* IEEE.

Zhang, Z., Patra, B. G., Yaseen, A., Zhu, J., Sabharwal, R., Roberts, K., & Wu, H. (2023). Scholarly recommendation systems: A literature survey. *Knowledge and Information Systems*, *65*(11), 4433-4478.

Author Information

Bederiana Shyti
Lecturer, Department of Mathematics, Faculty of Natural Sciences, University of Elbasan "A.Xhuvani"
Str.Ismail Zyma, 3001, Albania

Argesta Stergu
Department of Mathematics, Faculty of Natural Sciences, University of Elbasan "A.Xhuvani"
Str.Ismail Zyma, 3001, Albania
Contact e-mail: argesta.stergu@uniel.edu.al

Dhurata Valera
Lecturer, Department of Mathematics, Faculty of Natural Sciences, University of Elbasan "A.Xhuvani"
Str.Ismail Zyma, 3001, Albania

Papajani Blerina
Lecturer, Department of Mathematics, Faculty of Natural Sciences, University of Elbasan "A.Xhuvani"
Str.Ismail Zyma, 3001, Albania

To cite this article:

Shyti, B., Stergu, A., Valera, D., & Blerina, P. (2024). Food recommendation system for a healthy liver using machine learning. The Eurasia Proceedings of Science, Technology, Engineering & Mathematics (EPSTEM), 28, 438-447.

The Eurasia Proceedings of Science, Technology, Engineering & Mathematics (EPSTEM)
ISSN: 2602-3199

The Eurasia Proceedings of Science, Technology, Engineering & Mathematics (EPSTEM), 2024

Volume 28, Pages 448-461

ICBASET 2024: International Conference on Basic Sciences, Engineering and Technology

Locating Emergency Stations Using Multi-Criteria Decision-Making (MCDM) Methods: Application of Ankara Province

Beste Desticioglu-Tasdemir
National Defence University

Abstract: An earthquake ranks first among natural disasters in Turkey, with a rate of 70%. Minimizing the effects of a disaster after it occurs is possible by establishing effective disaster management. Especially the earthquakes that occurred on February 6, 2023, showed how important it is to deliver aid to the disaster area. In this study, the problem of determining the location of emergency stations to be established in order to deliver aid to the disaster area in case of a disaster was examined. There are studies in the literature to determine the locations of emergency stations to be established in provincial centers. In this study, the locations of emergency stations to be established in the non-central districts of Ankara were tried to be determined using multi-criteria decision-making (MCDM) methods. In the study, firstly, the criteria that would be effective in the location selection of emergency stations were determined, and the weights of these criteria were calculated with the Pythagorean Fuzzy Analytical Hierarchy Process (PFAHP) method. In the second stage of the study, 16 districts outside the center of Ankara were compared with the Pythagorean Fuzzy Technique for Order Preference by Similarity To An Ideal Solution (PFTOPSIS) method, and the districts where emergency stations should be opened first were evaluated.

Keywords: Emergency station, Site selection, Fuzzy logic

Introduction

Disasters can be defined as events that occur largely beyond human control, can cause loss of property and life, and pose a risk to the environment and human life. Natural disasters are events that cause great losses, seriously affect both the whole world and natural life, and cannot be avoided (Hoyois et al., 2006). Natural disasters occur all over the world from time to time. Earthquakes are among the most common natural disasters in the world. Large and devastating earthquakes occur from time to time in Turkey. It is of great importance to make the necessary preparations before the emergency in order to quickly deliver aid to disaster victims affected by large and devastating earthquakes. In order to deal effectively with disasters, effective implementation of disaster management becomes important (Sen & Esmer, 2017). Providing relief materials and delivering the necessary aid after a disaster is of vital importance for people experiencing disasters. In order to deliver aid quickly and effectively, emergency stations are established before the disaster and emergency supplies are stored there. In order to quickly deliver emergency supplies to people experiencing disasters, the locations of Emergency Stations (ES) must be determined correctly.

Since Türkiye is located on active faults, major earthquakes occur from time to time. In particular, the Kahramanmaraş earthquakes that occurred on February 6, 2023 caused great loss of life and property in 10 provinces. Many highways were destroyed in these earthquakes, and this prevented aid from reaching the earthquake areas. Therefore, it is of great importance to determine the locations of ESs where aid will be stored before the disaster. This situation showed how important the aid that can be provided to the earthquake region from nearby provinces is. It is important to determine the locations of ESs so that they will serve neighboring provinces as well, instead of determining their locations so that they will serve only that province.

The concept of disaster logistics has emerged in order to minimize the impact of disasters that occur from time to time all over the world. Sending relief materials to people living in that region after a disaster, storing these materials in a certain area, and making the necessary plans before the disaster are defined as disaster logistics (Thomas & Kopczak, 2005). Disaster logistics consists of three stages: pre-disaster planning, disaster response activities and post-disaster aid activities. One of the most important elements of disaster logistics is the ESs where aid materials are stored.

The locations of ESs must be determined accurately so that aid can be delivered quickly. In the studies in the literature, it is seen that the assumption that ESs are installed in city centers and only that city is served is taken into account (Tezcan et al., 2023; Durdag et al., 2021). However, the Kahramanmaraş earthquakes that occurred on February 6, 2023 affected 10 provinces and revealed that the aid from surrounding provinces is of vital importance. Therefore, this study aimed to determine the locations of ESs to be opened in districts outside the center of Ankara, taking into account the assumption of providing service to neighboring provinces. Considering that a possible Istanbul earthquake will also affect the surrounding provinces, it is aimed to provide service to these provinces with the ESs established.

The problem of selecting the most appropriate alternative by evaluating alternatives under different criteria is defined as the multi-criteria decision making (MCDM) problem in the literature (Desticioglu & Ayan, 2023). MCDM approaches are extensively utilized in problem-solving. The most commonly used MCDM methods include AHP, TOPSIS, COPRAS, ELECTRE, PROMETHEE, etc. In decision-making problems with unclear situations, methods such as fuzzy AHP and fuzzy TOPSIS are used (Bayram & Eren, 2023). It is seen that triangular fuzzy numbers, quadrilateral fuzzy numbers, and Pythagorean fuzzy numbers (PFNs) are mostly used in fuzzy MCDM problems. Since more reliable and realistic results are obtained with PFNs (Torul Yürek et al., 2023), Pythagorean Fuzzy AHP (PFAHP) and Pythagorean Fuzzy TOPSIS (PFTOPSIS) methods were used in this study. As far as is known, this is the first study in which the establishment of ESs outside the city center was taken into account in order to serve the surrounding provinces and districts, and the locations of the ESs were determined using PFAHP and PFTOPSIS methods. The study initially established the criteria for determining the sites of ESs by consulting relevant literature. The weights of the criteria were derived using the PFAHP approach. Using the calculated criterion weights, the locations of the ESs planned to be established in 16 districts outside the center of Ankara were listed with the PFTOPSIS method. In the last stage, ES locations were listed by calculation using MCDM methods that include similar steps. In the sensitivity analysis, the effect of the criterion weights on the ranking was tried to be determined by taking the binary changes of the criterion weights.

The study consists of the following sections: First, the study includes a literature review on determining the locations of ESs. In the method section, information is given about the PFAHP and PFTOPSIS methods used in the study. Subsequently, attempts were made to estimate the positions of the ESs to be formed using calculations conducted with PFAHP and PFTOPSIS. There is no text provided. The previous section involved doing sensitivity analysis by making binary adjustments to criterion weights. This analysis was performed using the FCOPRAS and FTOPSIS methods, both of which follow similar procedures. The resulting rankings obtained from these methods were then compared. The conclusion phase of the study involved an assessment of the collected results and the formulation of recommendations for future research.

Literature Review

In this section, a literature review about studies carried out with MCDM methods within the scope of disaster logistics is included. Roh et al. (2013) determined the locations of warehouses to be used in humanitarian aid logistics using the AHP method. Peker et al. (2016) used integrated AHP and VIKOR methods to determine the locations of emergency facilities to be opened in Erzincan province. In the study, first the weights of the criteria were determined with AHP, and then the alternatives were ranked with the VIKOR method (Peker et al., 2016). Ofluoglu et al. (2017) tried to determine the locations of ESs to be established in Trabzon province using the entropy weight method-based VIKOR, SAW and TOPSIS methods. Trivedi (2018) determined the locations of temporary settlement areas within the scope of disaster logistics using the DEMATEL method. Şekkeli (2019) used the AHP method in the selection of the emergency assembly center in the Oniki February district of Kahramanmaraş province. Hazırcı and Sahin (2019) used the AHP-based p-median model in the selection of temporary housing areas that will serve after the disaster. In the study, the locations of temporary settlement areas in Burdur province were determined (Hazırcı & Şahin, 2019). In their study, Öztürk and Kaya (2020) used the PROMETHEE method to compare 43 alternative emergency assembly points in Istanbul within the scope of disaster logistics. Ergun et al. (2020) used MAUT and SAW

methods, which are among the MCDM methods, to determine the locations of ESs to be established in Giresun within the scope of sustainable disaster logistics. Cetinkaya et al. (2021) tried to determine the locations of emergency warehouses on the Turkey-Syria border with the Geographical Information System (GIS)-based AHP method. Derse (2022) used the cluster coverage model with DEMATEL and TOPSIS methods to determine the locations of ESs to be established in the Aegean Region. Gocmen Polat (2022) determined the locations of distribution centers to be established within the scope of disaster logistics in Tunceli province by using the goal programming model integrated with the AHP-based TOPSIS method. Tezcan et al. (2023) used MCDM methods to determine the locations of temporary disaster warehouses to be opened in Kırıkkale province. The study employed the AHP approach to initially identify the weights of the criteria. In the subsequent stage, the VIKOR, TOPSIS, and PROMETHEE methods were utilized to rank the possibilities for the establishment of a temporary warehouse (Tezcan et al., 2023). Bayram and Eren (2023) used AHP-based PROMETHEE, ELECTRE and TOPSIS methods to determine the locations of ESs to be opened in Sultanbeyli, one of the districts that will be most affected by the earthquake in an earthquake that may occur in Istanbul. Studies on site selection within the scope of disaster logistics were examined in the literature and Table 1 was created using these studies.

Table 1. Studies on disaster logistics

Study	Year	Problem Examined	Method
Roh et al.	2013	Humanitarian aid warehouse location selection	AHP
Peker et al.	2016	Emergency warehouse location selection	AHP - VIKOR
Ofluoglu et al.	2017	Emergency warehouse location selection	Entropi, VIKOR, SAW and TOPSIS
Trivedi	2018	Location selection of temporary residence areas	DEMATEL
Şekkeli	2019	Emergency assembly area location selection	AHP
Hazıcı & Şahin	2019	Location selection of temporary residence areas	AHP and P-Medyan
Ozturk & Kaya	2020	Emergency assembly point location selection	PROMETHEE
Ergun et al.	2020	Emergency warehouse location selection	MAUT - SAW
Cetinkaya et al.	2021	Emergency warehouse location selection	GIS - AHP
Derse	2022	Emergency warehouse location selection	DEMATEL - TOPSIS
Gocmen Polat	2022	Distribution center location selection	AHP - TOPSIS
Tezcan et al.	2022	Temporary distribution warehouse location selection	AHP – VIKOR, TOPSIS, PROMETHEE
Bayram & Eren	2023	Emergency warehouse location selection	AHP – PROMETHEE, ELECTRE, TOPSIS

When the studies in the literature within the scope of disaster logistics are examined, it is seen that researchers mostly work on ES location selection. When Table 1 is examined, it is seen that AHP and TOPSIS methods are mostly used in these studies. Studies in the literature generally assume that service is provided to the location of the opened station and that no aid is sent to the surrounding provinces and districts from these depots. In addition, in the studies in the literature, it was determined that ESs were established only in city centers, and that no studies were conducted on the establishment of ESs in non-central districts. The Kahramanmaraş earthquakes that occurred on February 6, 2023 affected 10 provinces and revealed how important the aid from surrounding provinces is. It is thought that a possible Istanbul earthquake may also affect the surrounding provinces. Therefore, in this study, the locations of emergency stations planned to be opened in 16 districts outside the center of Ankara were tried to be determined. The assumption that the ESs to be opened will provide service to neighboring provinces and districts has been taken into account. Studies in the literature were used to determine the criteria to be taken into account in comparing the alternatives of 16 districts located outside the center of Ankara. Expert opinion was used to determine the criterion weights. These data may vary from person to person. In order to eliminate this change, fuzzy logic is used in the literature (Desticioglu et al., 2023). Since more reliable and realistic results are obtained with Pythagorean fuzzy numbers (PFNs) (Bulut & Ozcan, 2023), PFAHP and PFTOPSIS methods were used in this study. In the study, 16 district alternatives were compared and the districts where emergency stations could be established were listed. In the next section, PFAHP and PFTOPSIS method are discussed.

Method

The importance of the criteria used in evaluating alternatives in MCDM problems varies from person to person and from region to region. To eliminate this change, fuzzy numbers are used in the literature. Since more realistic data is obtained with PFNs compared to other fuzzy numbers (Bulut and Özcan, 2023), PFNs was used in this study. In the study, PFAHP was first used to determine the criterion weights and the PFTOPSIS method was used to compare the district alternatives where emergency facilities will be established.

Pythagorean Fuzzy Sets (PFSs)

Intuitive fuzzy numbers were first introduced by Atanassov (1986), and fuzzy numbers with different properties have been introduced to the literature by many researchers. Yager (2013) developed Pythagorean fuzzy sets (PFSs). These sets provide better results in cases where intuitive fuzzy sets are insufficient to eliminate uncertainty. PFSs provides flexibility in solving models containing uncertainty and obtains stronger results (Ilbahar et al., 2018; Gul & Ak, 2018). As in other intuitive fuzzy sets, it is assumed that PFSs values will not exceed 1. PFS definitions are presented below.

Definition 1: Let X denote a set of constants. P, PFS can be defined as an object that satisfies the following condition:

$$P = \{< x, P(\mu_p(x), v_p(x)) > x \in X\} \quad (1)$$

Here, $\mu_p(x): X \rightarrow [0,1]$ and $v_p(x): X \rightarrow [0,1]$, define the degree of membership and non-ownership of objects xϵX and p respectively.

$$0 \leq \mu_p(x)^2 + v_p(x)^2 \leq 1 \quad (2)$$

The degree of hesitation is given in equation number 3.

$$\pi_p(x) = \sqrt{1 - \mu^2{}_p(x) - v^2{}_p(x)} \quad (3)$$

Definition 2: Let $\beta_1 = P(\mu_{\beta_1}, v_{\beta_1})$ and $\beta_2 = P(\mu_{\beta_2}, v_{\beta_2})$, be two Pythagorean fuzzy numbers, γ>0. These PFNs can be defined by the following operators (Zeng et al., 2016):

$$\beta_1 \oplus \beta_2 = P\left(\sqrt{\mu_{\beta_1}^2 + \mu_{\beta_2}^2 - \mu_{\beta_1}^2 \mu_{\beta_2}^2}, v_{\beta_1} v_{\beta_2}\right) \quad (4)$$

$$\beta_1 \otimes \beta_2 = P\left(\mu_{\beta_1} \mu_{\beta_2}, \sqrt{v_{\beta_1}^2 + v_{\beta_2}^2 - v_{\beta_1}^2 v_{\beta_2}^2}\right) \quad (5)$$

$$\gamma\beta_1 = P\left(\sqrt{1 - (1 - \mu_{\beta_1}^2)^{\gamma}}, (v_{\beta_1})^{\gamma}\right) \quad (6)$$

$$\beta_1^{\gamma} = P\left((\mu_{\beta_1})^{\gamma}, \sqrt{1 - (1 - v_{\beta_1}^2)^{\gamma}}\right) \quad (7)$$

Definition 3: Let $\beta_1 = P(\mu_{\beta_1}, v_{\beta_1})$ and $\beta_2 = P(\mu_{\beta_2}, v_{\beta_2})$, be two PFNs. The order of these two PFNs is shown as follows.

If $\beta_1 > \beta_2$ then $\mu_{\beta_1} \geq \mu_{\beta_2}$ and $v_{\beta_1} \leq v_{\beta_2}$.

The score function of the two PFNs is given in Equation 8.

$$s(\beta_1) = (\mu_{\beta_1})^2 - (v_{\beta_1})^2 \quad (8)$$

Definition 4: According to the score function given in Equation 8, the comparison of 2 PFNs is as follows (Zhang and Xu, 2014):

i. If s(β_1)< s(β_2) it is $\beta_1 \prec \beta_2$
ii. If s(β_1) > s(β_2) it is $\beta_1 \succ \beta_2$
iii. If s(β_1) = s(β_2) it is $\beta_1 \sim \beta_2$

Pythagorean Fuzzy AHP (PFAHP) Method

The algorithm steps of the PFAHP method are listed below (Bulut & Ozcan, 2021):

Step 1: Pairwise comparison matrices are created with the 1-9 scale developed by Saaty for the criteria used in comparison. Afterwards, these numbers are converted into the weight measure for PFAHP developed by Ilbahar et al. (2018).

Step 2: Using Equations 9 and 10, the lower and upper limits of the membership and non-membership functions and the difference matrices $D=(d_{ik})_{mxm}$ are calculated.

$$d_{ikL} = \mu_{ikL}^2 - v_{iku}^2 \quad (9)$$

$$d_{ikU} = \mu_{ikU}^2 - v_{ikL}^2 \quad (10)$$

Step 3: Using Equations 11 and 12, the range multiplication matrix $S = (s_{ik})_{mxm}$ is calculated.

$$s_{ikL} = \sqrt{1000^{d_L}} \quad (11)$$

$$s_{ikU} = \sqrt{1000^{d_U}} \quad (12)$$

Step 4: Using the equation given in Equation 13, the determination value $\tau = (\tau_{ik})_{mxm}$ is calculated.

$$\tau_{ik} = 1 - (\mu_{ikU}^2 - \mu_{ikL}^2) - (v_{ikU}^2 - v_{ikL}^2) \quad (13)$$

Step 5: Multiply $S = (s_{ik})_{mxm}$ ile $\tau = (\tau_{ik})_{mxm}$ using Equation 14 to create the weight matrix before normalization.

$$t_{ik} = \left(\frac{s_{ikL} + s_{ikU}}{2}\right)\tau_{ik} \quad (14)$$

Step 6: The weighted normalized matrix is obtained by Equation 15:

$$w_i = \frac{\sum_{k=1}^{m} t_{ik}}{\sum_{i=1}^{m}\sum_{k=1}^{m} t_{ik}} \quad (15)$$

The AHP method can be a guide for the decision maker by taking into account both subjective and objective criteria. In addition, the AHP method enables evaluation of which criterion is more important by comparing each criterion in pairs (Desticioglu & Ayan, 2023). The AHP method is an MCDM method that allows the application of qualitative and nical criteria together, taking into account the opinions of individuals and groups (Omurbek & Simsek, 2014). In this study, since both quantitative and qualitative criteria are taken into account in comparing alternatives in the ES location selection problem, the AHP method was preferred in determining the criterion weights. Pairwise comparison of the determined criteria involves uncertainty as it will vary from person to person or from region to region. Fuzzy logic is used to eliminate this uncertainty (Desticioglu et al., 2023). More realistic and reliable results are obtained with PFNs compared to other fuzzy numbers (Bulut & Özcan, 2023). Therefore, in this study, it was preferred to compare the alternatives with PFAHP and PFTOPSIS methods.

Pythagorean Fuzzy TOPSIS (PFTOPSIS) Method

The TOPSIS approach, devised by Hwang and Yoon in 1979, is used to prioritize options. In the TOPSIS method, the closest and furthest alternatives to the ideal solution can be determined (Hwang & Yoon, 1979).

The TOPSIS method is an MCDM method that allows the evaluation of alternatives by taking into account both benefit criteria and cost criteria (Yıldırım et al., 2019). That's why it is one of the most preferred methods by researchers. In cases where the criteria to be used in comparing alternatives are uncertain, the TOPSIS method can be used with fuzzy numbers. In this study, fuzzy PFNs were used to reduce the uncertainty inherent in the criteria used. Due to the presence of uncertainty in the criteria used for evaluating alternatives in the study, and the fact that different individuals may have different evaluations of the options, the PFTOPSIS approach was employed to compare the alternatives. The application steps of the PFTOPSIS method are explained below (Oz et al., 2019):

Step 1: A decision matrix is created for the alternatives, taking into account PFSs (Bulut and Özcan, 2021). A decision matrix is created as shown in Equation 16 to show C_j (j=1, 2, …, n) alternatives and x_i (i= 1, 2, …, m) criteria.

$$R = \left(C_j(x_i)\right)_{mxm} = \begin{pmatrix} P(u_{11},v_{11}) & P(u_{12},v_{12}) & \cdots & P(u_{1n},v_{1n}) \\ P(u_{21},v_{21}) & P(u_{22},v_{22}) & \cdots & P(u_{2n},v_{2n}) \\ \vdots & \vdots & \ddots & \vdots \\ P(u_{m1},v_{m1}) & P(u_{m2},v_{m2}) & \cdots & P(u_{mn},v_{mn}) \end{pmatrix} \quad (16)$$

Step 2: Pythagorean fuzzy positive ideal and negative ideal solutions are calculated with Equations 17 and 18.

$$x^+ = \left\{C_j \max_i s\left(C_j(x_i)\right) \middle| j = 1,2,\dots,n\right\}$$
$$= \{\langle C_1, P(u_1^+, v_1^+)\rangle, \langle C_2, P(u_2^+, v_2^+)\rangle, \dots, \langle C_n, P(u_n^+, v_n^+)\rangle\} \quad (17)$$
$$x^- = \left\{C_j \min_i \langle s\left(C_j(x_i)\right)\rangle | j = 1,2,\dots,n\right\}$$
$$= \{\langle C_1, P(u_1^-, v_1^-)\rangle, \langle C_2, P(u_2^-, v_2^-)\rangle, \dots, \langle C_n, P(u_n^-, v_n^-)\rangle\} \quad (18)$$

Step 3: The distances to the positive and negative ideal solution are calculated with equations 19 and 20, respectively:

$$D(x_i, x^+) = \sum_{j=1}^{n} w_j\, d\left(C_j(x_i), C_j(x^+)\right)$$

$$= \frac{1}{2}\sum_{j=1}^{n} w_j \left(\left|(u_{ij})^2 - (u_j^+)^2\right| + \left|(v_{ij})^2 - (v_j^+)^2\right| + \left|(\pi_{ij})^2 - (\pi_j^+)^2\right|\right) \quad (19)$$

$$D(x_i, x^-) = \sum_{j=1}^{n} w_j\, d\left(C_j(x_i), C_j(x^-)\right)$$

$$= \frac{1}{2}\sum_{j=1}^{n} w_j \left(\left|(u_{ij})^2 - (u_j^-)^2\right| + \left|(v_{ij})^2 - (v_j^-)^2\right| + \left|(\pi_{ij})^2 - (\pi_j^-)^2\right|\right) \quad (20)$$

Step 4: Closeness values for each alternative are calculated according to Equation 21:

$$\xi(x_i) = \frac{D(x_i, x^-)}{D_{max}(x_i, x^-)} - \frac{D(x_i, x^+)}{D_{min}(x_i, x^+)} \quad (21)$$

Step 5: Alternatives are ranked from the one with the greatest closeness value to the alternative with the worst closeness value. The alternative with the highest Closeness value is the optimal choice.

Case Study

Disasters are events that destroy a certain region or a country. In order to reduce the negative effects caused by disasters, necessary planning must be made before the disaster. In order to reduce the negative effects of disasters, the locations of ESs that will serve after the disaster must be determined correctly. In the literature,

it is seen that researchers are working on determining the locations of ESs to be established in city centers to serve only that province. However, the Kahramanmaraş earthquakes that occurred on February 6, 2023 affected 10 provinces and revealed how important the aid from surrounding provinces is. Therefore, in this study, it is aimed to provide service to the surrounding provinces with the ESs to be opened. It is thought that the possible Istanbul earthquake may also affect the surrounding provinces. In this study, in order to reduce the effects of earthquakes, the locations of ESs that will be established in districts outside the center of Ankara and will serve neighboring provinces have been tried to be determined. In the studies in the literature, it is seen that MCDM methods are used in location selection problems based on many criteria among different alternatives. Therefore, in this study, PFAHP and PFTOPSIS methods, which are among the MCDM methods, were used in the location selection problem of ESs to be opened in the non-central districts of Ankara.

In the study, firstly, the criteria to be used in ES location selection were used by using studies in the literature. It is aimed to provide service to neighboring provinces and districts with the ESs to be opened in the study. Therefore, unlike the studies in the literature, the "Number of Provinces within Coverage Distance" and "Number of Districts within Coverage Distance" criteria were also taken into account in the evaluation of the alternatives. Once the criteria were established, views were sought from 10 AFAD employees who were experts in the field. They were then instructed to evaluate and compare the established criteria in pairs. Given the subjective nature of these opinions, fuzzy logic has been employed to mitigate this variability. Since more realistic solutions are obtained with PFNs compared to other fuzzy numbers (Bulut and Özcan, 2021), PFNs were also used in this study. First, criterion weights were calculated using pairwise comparison matrices received from experts with the PFAHP method. Afterwards, 16 districts located outside the center of Ankara were compared in terms of places where ESs would be opened according to the determined criteria, and the alternatives were listed using the PFTOPSIS method. In the last part of the study, calculations were made with FTOPSIS and FCOPRAS methods, which contain similar steps to PFTOPSIS, and the results were compared. The sensitivity analysis involved doing computations using binary changes in the criterion weights that were derived for the selection of ES locations. The resulting outcomes were then compared. The stages of this study regarding the location selection of ESs are shown in Figure 1.

Figure 1. ES location selection flow chart

Determination of Criteria

It is seen in the literature that there are studies on determining the locations of ESs using MCDM methods. In the studies on ES location selection in the literature, the most common criteria for comparing alternatives are "Population", "Earthquake / Disaster Risk", "Distance to the Center", "Transportation", "Land Cost", "Proximity to the Port / Airport / Highway", "Infrastructure", “Security” etc. criteria are used. Since the most preferred criteria in the studies in the literature are "Population", "Earthquake Risk" and "Distance to the Center", these criteria were used to compare the alternatives in this study. Unlike the studies in the literature, the aim of this study is to provide service to neighboring provinces and districts with the ESs opened.

Therefore, in this study, unlike the literature, the "Number of Provinces within the Coverage Distance" and "Number of Districts within the Coverage Distance" criteria, which are within the specified coverage distance to the ES to be opened, were also used among the evaluation criteria to compare the alternatives. The criteria used and explanations of these criteria are given in Table 2.

Table 2 Criteria used in ES location selection and explanations

Criteria.	Explanation
Population (ESC_1) (Roh et al., 2013)	Population of the district where the Emergency Station is planned to be established
Earthquake Risk (ESC_2) (Peker et al., 2016, Hazırcı & Sahin, 2019)	Earthquake risk of the district where the Emergency Station is planned to be established
Distance to the Center (ESC_3) (Roh et al., 2013; Peker et al., 2016, Ergun et al., 2020))	Distance of the district where the Emergency Station is planned to be established to the city center
Number of Provinces within the Coverage Distance (ESC_4)	Number of neighboring provinces within the 300 km coverage area of the district where the Emergency Station will be established
Number of Districts within the Coverage Distance (ESC_5)	Number of neighboring districts within the 100 km coverage area of the district where the Emergency Station will be established

It is aimed to deliver aid to the disaster area within approximately 1 - 1.5 hours from the ES planned to be opened. Therefore, the coverage area for the ES planned to be opened was determined as 100 km according to the "Number of Districts in Coverage Distance" criterion. It is aimed to deliver aid to neighboring provinces within approximately 4 hours from the ES planned to be opened. Therefore, in the "Number of Provinces in Coverage Distance" criterion, the coverage distance was taken as 300 km, taking into account factors such as traffic and speed limits that may be encountered on the way from the ES planned to be opened to the disaster area. As a result, the number of districts 100 km away from that district was taken into account from the "Number of Districts in Coverage Distance" criterion. In the "Number of Provinces within Coverage Distance" criterion, the number of provinces within 300 km coverage distance from the district where the ES is planned to be established is taken into account. In calculating the distances between provinces and districts, the Distance from District to District tab of the General Directorate of Highways was used (KGM, 2024).

Calculation of Criterion Weights with PFAHP

The PFAHP approach was employed to determine the weights of the criteria for the purpose of selecting locations for ESs. In the previous section, the criteria to be used for ES location selection were determined as "Population", "Earthquake Risk", "Distance to the Center", "Number of Provinces within Coverage Distance" and "Number of Districts within Coverage Distance".

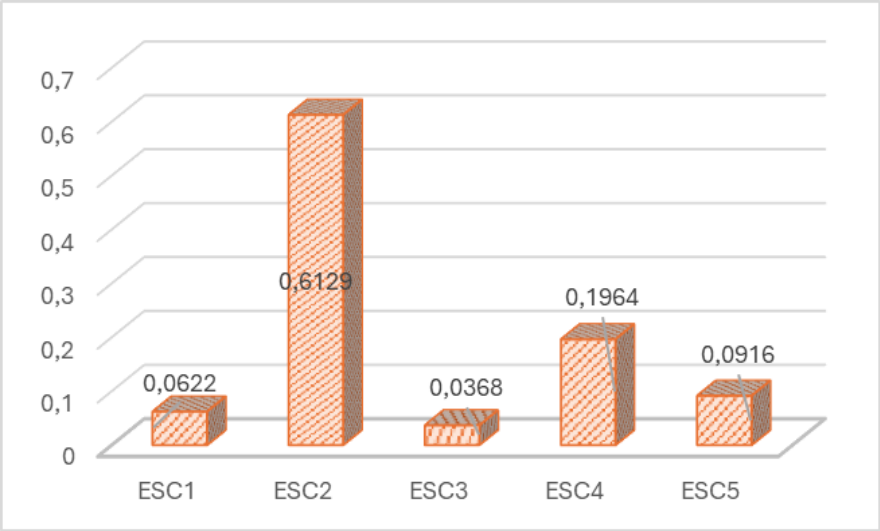

Figure 2. Criteria weights calculated with PFAHP

To establish the criterion weights in the study, 10 individuals employed at Ministry of Interior Disaster and Emergency Management Presidency (AFAD) were questioned. These individuals were requested to assess and compare the criteria using the 1-9 scale devised by Saaty. Afterwards, these comparison scores were converted into fuzzy Pythagorean numbers and calculations were made by following the steps of the PFAHP method. The criterion weights obtained as a result of the calculations are given in Figure 2.

When Figure 2 is examined, it can be seen that the most important criterion for ES location selection is earthquake risk with a weight of 0.6129. This shows that when choosing the location of ESs, the earthquake risk in the selected region is taken into account first. The second most important criterion for location selection was the "Number of Provinces within Coverage Distance" Criteria, which takes into account the aim of delivering aid to surrounding provinces from the station to be opened. The weights of other criteria are also given in Figure 2.

Ranking of Alternatives with the PFTOPSIS Method

In the study, the problem of determining the locations of ESs to be established in 16 districts outside the center of Ankara was examined. In addition, it is aimed to determine the locations of these ESs in a way that will serve neighboring provinces and districts. In the study, the PFTOPSIS method was used to evaluate 16 alternative districts where ESs were planned to be opened. First of all, data corresponding to the criteria were obtained for each district. Population, earthquake risk and distance to the center data of the districts are given in the Appendix. In the study, first the data corresponding to these criteria were scored according to the 1-9 scale, and then these scores were converted into PFNs. The PFTOPSIS method was used to do calculations, resulting in the determination of proximity values for each choice. In the calculations, "Population", "Number of Provinces within Coverage Distance" and "Number of Districts within Coverage Distance" were taken as benefit criteria, "Earthquake Risk" and "Distance to the Center" were taken as cost criteria and the calculations were made accordingly. Figure 3 was created with the calculated closeness values.

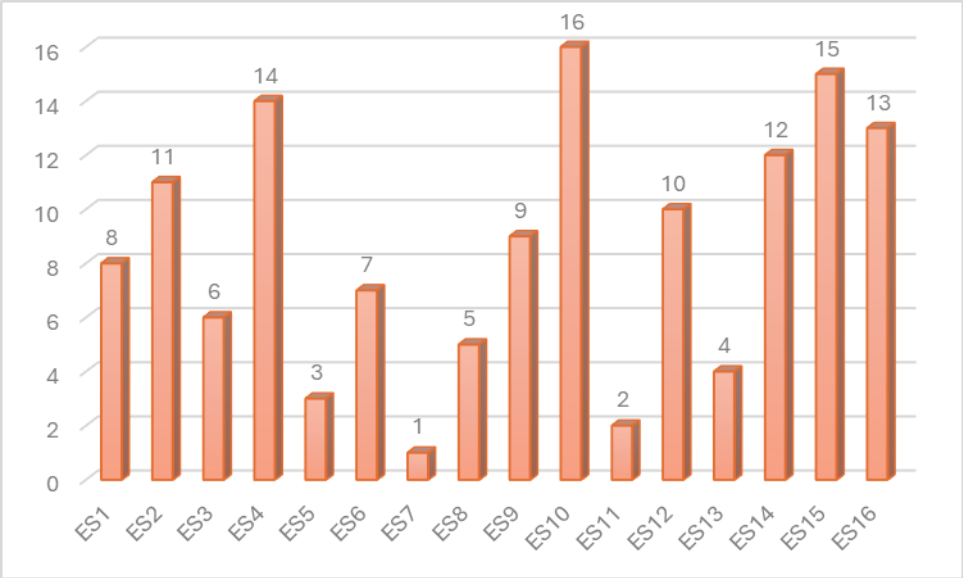

Figure 3. Ranking of alternative districts calculated with PFTOPSIS

When Figure 3 is examined, it is seen that ESs should first be established in Elmadağ, Kahramankazan and Çamlıdere districts, respectively. The most effective criterion in creating the ranking is the "Earthquake Risk" criterion, which has the highest weight. When the districts are compared according to the determined criteria, the order of the alternatives where ESs will be opened is ES7 – ES11 – ES5 – ES13 – ES8 – ES3 – ES6 – ES1 – ES9 – ES12 – ES2 – ES14 – ES16 – ES4 – ES15 – ES10. In this case, if ESs will be opened in more than one district, the districts where the stations will be opened can be determined by following this order.

Comparative Analysis

In this section, the results obtained with the PFAHP - PFTOPSIS method developed for ES location selection are compared with the results obtained with the PFAHP - FTOPSIS and PFAHP - FCOPRAS methods, which include similar algorithm steps. In the calculations made with all three methods, criterion weights calculated with PFAHP were used. During the comparison of alternatives, calculations were made using PFTOPSIS, FTOPSIS and FCOPRAS methods. First, the data of alternative ESs were converted into triangular fuzzy numbers. Afterwards, calculations were made by following the steps of the FTOPSIS and FCOPRAS methods. In the calculations made, it is seen that there are differences from the ranking obtained with the PFTOPSIS method, but a similar ranking is obtained in the calculations made with the FTOPSIS and FCOPRAS methods. Figure 4 was created using calculations made with the PFAHP – PFTOPSIS, PFAHP – FTOPSIS and PFAHP – FCOPRAS methods.

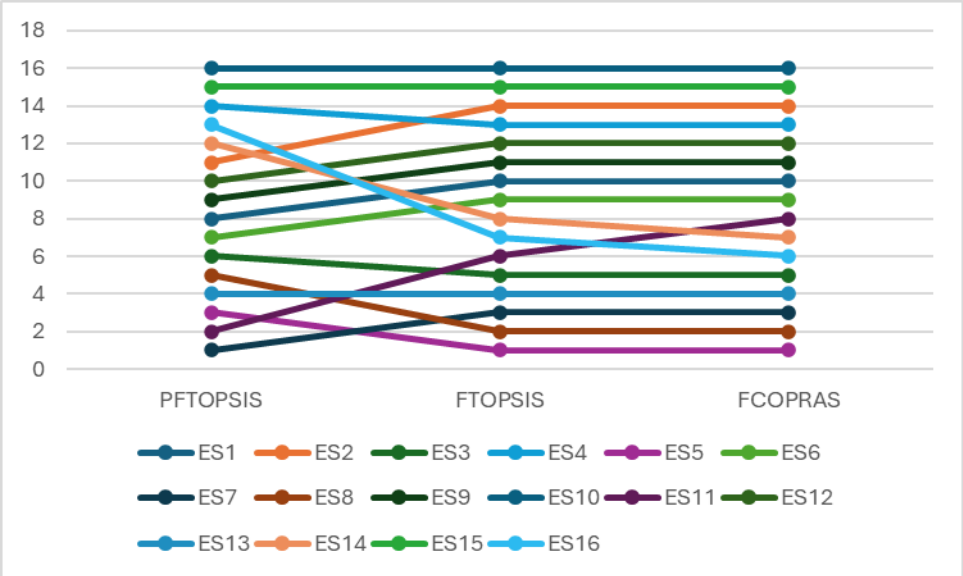

Figure 4. Comparison of calculations made with PFTOPSIS, FTOPSIS and FCOPRAS

When Figure 4 is examined, it is noted that the ranking obtained from the calculations made with PFTOPSIS is slightly different from the rankings obtained with the FTOPSIS and FCOPRAS methods, but the ranking does not change significantly. This is due to the use of different fuzzy numbers in these methods. It can be seen that the rankings obtained by calculations made with FTOPSIS and FCOPRAS methods are the same, except for a few alternatives. This is due to the fact that these methods involve similar steps and use the same fuzzy numbers. However, studies indicate that more realistic results are achieved with PFNs (Yager, 2014; Bulut & Ozcan, 2021). Therefore, it would be a more accurate approach to determine the locations of the ESs to be opened in the non-central districts of Ankara according to the order made by the PFAHP - PFTOPSIS method.

Sensitivity Analysis

The Kahramanmaraş earthquakes that occurred on February 6, 2023 affected a wide region and airports and highways suffered great damage in this earthquake. These earthquakes affected a large area and showed how important the aid to be delivered from surrounding provinces is. It is assumed that a possible Istanbul earthquake may also affect a wide area. Therefore, planning accordingly before the earthquake will be effective in reducing the negative effects of the earthquake on the region. Therefore, in this study, the problem of determining the locations of ESs to be established in the non-central districts of Ankara in order to deliver aid to the surrounding provinces that will be affected by a possible Istanbul earthquake was examined. Since more than one criterion will be effective in location selection, the integrated PFAHP – PFTOPSIS method of MCDM techniques was used to solve the problem. It is thought that there may be changes in the future periods, such as changes in the characteristics of the region and the opening of new ESs in the surrounding provinces, and it is assumed that this situation may also cause changes in the criterion weights. Therefore, in this section, sensitivity analysis of binary changes in criterion weights was conducted and the effect of the change in criterion weights on the alternative ranking was tried to be determined. The weights of the 5 criteria used in comparing the alternatives were changed in pairs and calculations were made for the 10 scenarios created. The rankings obtained in solving 10 different scenarios created within the scope

of sensitivity analysis are given in Figure 5. In Figure 5, the ranking obtained with the current criterion weights is shown as "S1", and in other scenarios, it is shown which criteria weights were obtained by changing.

	ES1	ES2	ES3	ES4	ES5	ES6	ES7	ES8	ES9	ES10	ES11	ES12	ES13	ES14	ES15	ES16
S1	8	11	6	14	3	7	1	5	9	16	2	10	4	12	15	13
C1-C2	5	7	11	6	13	2	4	16	9	14	3	10	8	15	1	12
C1-C3	8	11	6	14	3	7	1	5	9	16	2	10	4	12	15	13
C1-C4	9	15	6	12	2	4	1	3	14	16	5	13	7	11	8	10
C1-C5	8	13	7	14	2	6	1	4	9	16	3	12	5	10	15	11
C2-C3	4	5	7	12	13	3	2	16	10	11	1	6	8	15	9	14
C2-C4	6	2	11	9	10	5	3	13	4	16	1	8	7	14	12	15
C2-C5	4	3	6	12	13	7	2	14	8	10	1	5	9	15	11	16
C3-C4	6	11	4	12	3	5	1	8	13	16	6	9	7	14	15	10
C3-C5	6	11	4	12	3	5	1	8	13	16	2	9	7	14	15	10
C4-C5	7	12	4	13	3	8	1	5	10	16	2	9	6	11	15	14

Figure 5. Alternative rankings obtained by sensitivity analysis

In the calculations made with PFAHP, it was determined that the ESC2 criterion had the greatest criterion weight. This shows that the most effective criterion in creating the ranking is the ESC2 criterion. The criterion with the second highest weight in the calculations is the ESC4 criterion. When Table 3 is examined, it is noted that the rankings change significantly, especially when the ESC2 criterion weight is replaced with other criterion weights. This is due to the fact that the ESC2 criterion has a weight of 0.6129 and has a great impact on the creation of the ranking. It is seen that there is a change in the ranking when the weights of the ESC4 criterion, which ranks second with a weight of 0.1964, and the other criteria are changed. It is noteworthy that since the weight values of the other criteria are close to each other, there is no major change in the ranking when the weights of these criteria are changed.

Conclusion

Disasters can be defined as technology, nature or human-induced events that occur at unexpected times and negatively affect a part or all of the society physically, economically and socially. Although it is impossible to predict when disasters will occur, it is possible to minimize the negative effects of disasters with precautions and planning. In taking these precautions, it is necessary to know in advance how many people in that region may be affected by the disaster and which disasters are most likely to occur in that region. Studies carried out before disasters to reduce the negative effects that disasters may cause are defined as disaster logistics. Disaster logistics includes many activities such as planning, location selection, distribution, transportation and storage. One of the most important elements of disaster logistics is ESs. Determining the location of ESs correctly is of great importance as it will be effective in quickly delivering aid to the region after the disaster. Therefore, in this study, the problem of location selection of ESs was examined. More than one criterion is effective in the location selection of ESs. Therefore, AHP and TOPSIS methods, which are the most preferred MCDM methods, were used in determining the locations of ESs in the study. In determining the criterion weights, AFAD personnel were interviewed and asked to compare the criteria. This information contains uncertainty as it may vary from person to person. In order to eliminate this uncertainty, PFNs were used in the study and integrated PFAHP – PFTOPSIS methods were used to make the calculations.

In order to eliminate this uncertainty, PFNs were used in the study and integrated PFAHP – PFTOPSIS methods were used to make the calculations. However, the Kahramanmaras earthquakes that occurred on February 6, 2023 affected a wide geography and showed that the aid sent from surrounding provinces is of great importance. Therefore, it is aimed to provide service to the surrounding provinces with the ESs opened in this study. It is thought that the possible Istanbul earthquake will also affect a wide geography. Therefore, in this study, it is aimed to provide service to the neighboring provinces with a coverage distance of 300 km and the neighboring districts with a coverage distance of 100 km with the ESs that will be opened outside the center of Ankara. As far as is known, this is the first study in which the aim is to provide service to neighboring provinces and districts with ESs to be opened in out-of-center districts, and the integrated PFAHP - PFTOPSIS methods are used in the location selection of the ES. Since more than one criterion is taken into account when comparing alternative districts, MCDM methods were used to solve the location selection problem of ESs.

In the study, firstly, studies in the literature on ES location selection were examined and the criteria effective in location selection were determined. However, in this study, unlike the literature, it is planned to provide service to the neighboring provinces and neighboring districts from stations that will be opened. In comparing the alternative districts determined for ESs, the "Population", "Earthquake Risk" and "Distance to the Center" criteria, which are the most used in the literature, as well as the "Number of Provinces within the Coverage Distance" and "Number of Districts within the Coverage Distance" criteria were taken into account. Pairwise comparison matrices of the criteria were created through interviews with experts and the scores were converted into PFNs. Afterwards, the criterion weights were calculated with the PFAHP method and it was determined that the most effective criterion in location selection was Earthquake Risk with a weight of 0.6129. In this case, it seems that the earthquake risk is primarily effective in determining the locations of emergency stations. In this case, it seems that the earthquake risk is primarily effective in determining the locations of emergency stations. Accordingly, ESs should first be opened in Elmadağ, Kahramankazan, Camlıdere, Kızılcahamam and Evren districts.

In order to determine the effectiveness of the PHAHP – PFTOPSIS methods used for ES location selection, calculations were made with the FTOPSIS and FCOPRAS methods, which have similar application steps with the same criterion weights. When the rankings obtained as a result of the calculations were compared, it was determined that a ranking close to the ranking obtained with the PFTOPSIS method was obtained, and the rankings of some alternatives were changed. In the last part of the study, recalculations were made by taking the binary changes of the criterion weights and the resulting rankings were compared. In the calculations made, it was determined that the rankings changed greatly when the weights of the ESC2 and ESC4 criteria, which have the largest criterion weights, were changed in pairs. This shows that these criteria are primarily effective in determining the places where emergency facilities will be established. The weights of the other criteria vary between 0-0.1, and since these criteria have weights close to each other, it is noteworthy that the bilateral changes in the criterion weights do not affect the alternative rankings much.

Recommendations

In this study, the integrated PFAHP – PFTOPSIS method was used to determine the locations of ESs that will also serve the surrounding provinces. In future studies, the location selection problem of ESs can be examined by adding different criteria. The study examined the location selection problem of ESs planned to be opened outside the center of Ankara. In future studies, the problem can be expanded to include different provinces and regions. In addition, in future studies, the results obtained by solving this problem using spherical, neutrosophic and hesitant fuzzy numbers and different MCDM methods can be compared.

Scientific Ethics Declaration

The author declares that the scientific ethical and legal responsibility of this article published in EPSTEM journal belongs to the author.

Acknowledgements or Notes

* This article was presented as an oral presentation at the International Conference on Basic Sciences, Engineering and Technology (www.icbaset.net) held in Alanya/Turkey on May 02-05, 2024.

References

Atanassov, K. T., (1999). *Intuitionistic fuzzy sets* (pp. 1-137). Physica-Verlag HD.

Bayram, B., & Eren, T. (2023). Cok kriterli karar verme yontemleriyle afet sonrası gecici depo yeri seçimi. *Acil Yardım ve Afet Bilimi Dergisi*, *3*(2), 22-30.

Bulut, M., & Ozcan, E. (2021). Integration of battery energy storage systems into natural gas combined cycle power plants in fuzzy environment. *Journal of Energy Storage*, *36*, 102376.

Bulut, M., & Ozcan, E. (2023). Ranking of advertising goals on social network sites by Pythagorean fuzzy hierarchical decision making: Facebook. *Engineering Applications of Artificial Intelligence*, *117*, 105542.

Cetinkaya, C., Ozceylan, E., & Isleyen, S. K. (2021). Emergency shelter site selection in maar shurin community of Idlib (Syria). *Transportation Journal*, *60*(1), 70-92.

Derse, O. (2022). Dematel tabanlı TOPSIS yontemi ve kume kapsama modeli ile afet lojistigi icin depo yeri secimi: Ege bolgesi ornegi. *Kahramanmaras Sutcu Imam Universitesi Muhendislik Bilimleri Dergisi*, *25*(4), 702-713.

Desticioglu- Tasdemir, B., & Asilogullari Ayan, M. (2023). Sustainable supplier selection in the defense industry with multi-criteria decision-making methods. *International Symposium on Intelligent Manufacturing and Service Systems* (pp. 95-106). Singapore: Springer Nature Singapore.

Desticioglu - Taşdemir, B., Kumcu, S., & Ozyoruk, B., (2023). Comparison of e-commerce sites with pythagorean fuzzy AHP and TOPSIS methods. *Intelligent and Fuzzy Systems. INFUS 2023. Lecture Notes in Networks and Systems* (pp.327-335), Zurich: Springer Nature.

Durdag, C., Ergenecoşar, S., Kınık, Z., & Yılmaz, K. K. (2021). Afet bakış acısıyla lojistik depo yeri seçimi: İstanbul Beykoz ilçesi üzerine bir uygulama. *Beykoz Akademi Dergisi*, *9*(1), 98-107.

Ergun, M., Korucuk, S., & Memiş, S. (2020). Surdurulebilir afet lojistiğine yönelik ideal afet depo yeri seçimi: Giresun ili ornegi. *Canakkale On Sekiz Mart Universitesi Fen Bilimleri Enstitusu Dergisi*, *6*(1), 144-165.

Gul, M., & Ak, M. F. (2018). A comparative outline for quantifying risk ratings in occupational health and safety risk assessment. *Journal of Cleaner Production*, *196*, 653-664.

Hoyois, P., Scheuren, J. M., Below, R., & Guha-Sapir, D. (2007). *Annual disaster statistical review: Numbers and trends*. Retrieved from https://theisrm.org/.pdf

Hwang, C. L.& Yoon, K. (1981). Methods for multiple attribute decision making. In *Multiple attribute decision making: methods and applications a state-of-the-art survey* (pp.58-191). Springer.

Ilbahar, E., Karas, A., Cebi, S., & Kahraman, C. (2018). A novel approach to risk assessment for occupational health and safety using Pythagorean fuzzy AHP & fuzzy inference system. *Saf Sci., 103*, 124–136

KGM (2024). Karayolları Genel Mudurlugu Retrieved from https://www.kgm.gov.tr/sayfalar/Kgm/sitetr/uzakliklar/ilcedenilceyemesafe.aspx

Ofluoglu, A., Birdogan, B., & Ar, I. M. (2017). Multi-criteria decision analysis model for warehouse location in disaster logistics. *Journal of Management Marketing and Logistics*, *4*(2), 89-106.

Oz, N. E., Mete, S., Serin, F., & Gul, M. (2018). Risk assessment for clearing and grading process of a natural gas pipeline project: An extended TOPSIS model with Pythagorean fuzzy sets for prioritizing hazards. *Human and Ecological Risk Assessment: An International Journal*.

Omurbek, N., & Simsek, A. (2014). Analitik hiyerarşi süreci ve analitik ağ süreci yöntemleri ile online alişveriş site secimi. *Journal of Management and Economics Research*, *12*(22), 306-327.

Ozturk, F., & Kaya, G. K. (2020). Afet sonrası toplanma alanlarının promethee metodu ile değerlendirilmesi. *Uludag Universitesi Muhendislik Fakultesi Dergisi*, *25*(3), 1239-1252.

Peker, I., Korucuk, S., Ulutas, S., Okatan, B. S., & Yasar, F. (2016). Afet lojistigi kapsaminda en uygun dağitim merkez yerinin ahs-vıkor butunlesik yontemi ile belirlenmesi: Erzincan ili örneği. *Journal of Management and Economics Research*, *14*(1), 82-103.

Polat, E. G. (2022). Distribution centre location selection for disaster logistics with integrated goal programming-AHP based TOPSIS method at the city level. *Afet ve Risk Dergisi*, *5*(1), 282-296.

Roh, S. Y., Jang, H. M., & Han, C. H. (2013). Warehouse location decision factors in humanitarian relief logistics. *The Asian Journal of Shipping and Logistics*, *29*(1), 103-120.

Saaty, T. L. (1980). The analytic hierarchy process (AHP). *The Journal of the Operational Research Society*, *41*(11), 1073-1076.

Sahin, Y., & Hazırcı, M. (2019). Gecici iskân alanlarının seçimi için ahp temelli p-medyan modeli: Burdur ornegi. *Muhendislik Bilimleri ve Tasarım Dergisi*, *7*(2), 403-417.

Sekkeli, Z. H. (2020). Afet ve acil durum lojistigi kapsamında acil durum toplanma merkezi seçiminde AHP yontemi: Kahramanmaraş on iki subat belediyesinde bir uygulama. *Insan ve Toplum Bilimleri Arastırmaları Dergisi*, *9*(2), 903-930.

Sen, G., & Esmer, S. (2017). Afet lojistigi: Bir literatür taraması. *The International New Issues in Social Sciences*, *5*(5), 231-250.

Tezcan, B., Alakaş, H. M., Özcan, E., & Tamer, E. R. E. N. (2021). Afet sonrası geçici depo yeri seçimi ve çok araçlı araç rotalama uygulaması: Kırıkkale ilinde bir uygulama. *Politeknik Dergisi*, *26*(1), 13-27.

Thomas, A. S., & Kopczak, L. R. (2005). From logistics to supply chain management: the path forward in the humanitarian sector. *Fritz Institute*, *15*(1), 1-15.

Trivedi, A. (2018). A multi-criteria decision approach based on DEMATEL to assess determinants of shelter site selection in disaster response. *International Journal of Disaster Risk Reduction*, *31*, 722-728.

Yager, R. R. (2013). Pythagorean membership grades in multicriteria decision making. *IEEE Transactions on fuzzy systems*, *22*(4), 958-965.

Yıldırım, M., Karakaya, O., & Altan, İ. M. (2019). TOPSIS yöoteminde maliyet ve karlılık oranlarının kullanılmasıyla finansal performansın olcumu: Ana metal sanayi sektöründen bir şirket ornegi. *Gazi Iktisat ve Isletme Dergisi*, *5*(3), 170-181.

Yurek, Y. T., Ozyoruk, B., Ozcan, E., & Bulut, M. (2023). Socio-political evaluation of renewable energy resources under uncertain environment. *Engineering Applications of Artificial Intelligence*, *126*, 106881.

Zeng, S., Chen, J., & Li, X. (2016). A hybrid method for Pythagorean fuzzy multiple-criteria decision making. *International Journal of Information Technology & Decision Making*, *15*(02), 403-422.

Zhang, X., & Xu, Z. (2014). Extension of TOPSIS to multiple criteria decision making with Pythagorean fuzzy sets. *International Journal of Intelligent Systems*, *29*(12), 1061-1078.

Author Information

Beste Desticioglu -Tasdemir
National Defence University, Alparslan Defence Sciences and National Security Institute, Department of Operations Research, Ankara/ Türkiye
Contact e-mail: *bdesticioglu@kho.msu.edu.tr*

To cite this article:

Desticioglu -Tasdemir, B. (2024). Locating emergency stations using Multi-Criteria Decision-Making (MCDM) methods: Application of Ankara province. *The Eurasia Proceedings of Science, Technology, Engineering & Mathematics (EPSTEM), 28,* 448-461

Appendix

Alternative	Population	Earthquake Risk	Distance from Center	Number of province within coverage distance	Number of districts within coverage distance
Akyurt	40625	3	35	12	5
Ayaş	12998	4	57	12	7
Bala	20521	2	67	12	2
Beypazarı	48357	3	99	10	4
Çamlıdere	8100	1	103	8	3
Çubuk	95449	3	39	11	5
Elmadağ	44379	2	41	13	5
Evren	2952	1	175	8	1
Güdül	8079	3	91	10	6
Haymana	26016	4	76	11	1
Kahramankazan	59123	3	46	13	7
Kalecik	12794	3	68	12	4
Kızılcahamam	26872	2	78	10	5
Nallıhan	26553	2	158	8	2
Polatlı	128378	4	78	10	2
Şereflikoçhisar	33140	2	147	7	1

The Eurasia Proceedings of Science, Technology, Engineering & Mathematics (EPSTEM)
ISSN: 2602-3199

The Eurasia Proceedings of Science, Technology, Engineering & Mathematics (EPSTEM), 2024

Volume 28, Pages 462-469

ICBASET 2024: International Conference on Basic Sciences, Engineering and Technology

Establishing a Remote Area Network for an Automation System: A Case Study of Yeni Karpuzlu Drinking Water Automation

Aydin Gullu
Trakya University

M. Ozan Aki
Trakya University

Abstract: Yeni Karpuzlu is a town located in the Ipsala district of Edirne province. The drinking water needs of this town are supplied from a deep water well. Water is pumped from the deep well using a submersible pump and sent to a 500-m^3 capacity concrete water tank. Here, the water goes the town's water demand through natural flow. The water is then sent from the tank, which is located 30 meters above ground level, to the town. There is a distance of 800 meters between the well and the tank, and 6000 meters between the tank and the control center located in the town. A local network has been established using outdoor access points for communication between the industrial control devices located at these three points. Data from the instruments are collected at a speed of 300mbps. Additionally, it is sent to the video center via IP cameras for area security. All devices on this network communicate with each other and are controlled. This paper will discuss the operation of the automation system mentioned above. Operations include the pump operation based on tank levels, pressure control using an adjustable valve to maintain network pressure, and monitoring and control operations from the central unit.

Keywords: Automation system, Drinking water automation, Network

Introduction

Industrial automation is a rapidly evolving field that offers numerous benefits to various industries. Automation technologies have been shown to increase productivity, improve product quality, and increase production process efficiency (Atif et al., 2022). The adoption of automation in the manufacturing sector, catalyzed by Industry 4.0, has introduced new technologies that enable the automation of manufacturing processes (Bakar et al., 2021). This shift towards automation is driven by factors such as the need for higher productivity, increased quality, and a shortage of skilled labor (Lin et al., 2023). However, there are also difficulties in implementing industrial automation. The deployment of new complex technologies such as Cyber-Physical Systems (CPS) and the adoption of new manufacturing paradigms such as Computer Integrated Manufacturing (CIM) present challenges that must be addressed for successful automation (Lai et al., 2020). Additionally, the need for greater flexibility and reconfigurability of production facilities is crucial for the effective adoption of industrial robots in manufacturing sectors (Bader & Rahimifard, 2018). Moreover, the Industrial Internet of Things (IIoT) plays an important role in providing automation solutions for industrial processes by connecting sensors, actuators, and robotic devices, thereby enabling the automation of production processes through Factory Automation (Herrera et al., 2020). Integration of IoT with industrial automation technologies such as Raspberry Pi further enhances automation capabilities in industrial environments (Merchant & Ahire, 2017). The advantages of industrial automation are shown in Figure 1. Automated systems for drinking water management have truly transformed the way water quality is monitored and maintained. These systems utilize advanced technologies such as flow cytometry, optical coherence tomography and chlorination to ensure the safety and efficiency of drinking water networks.

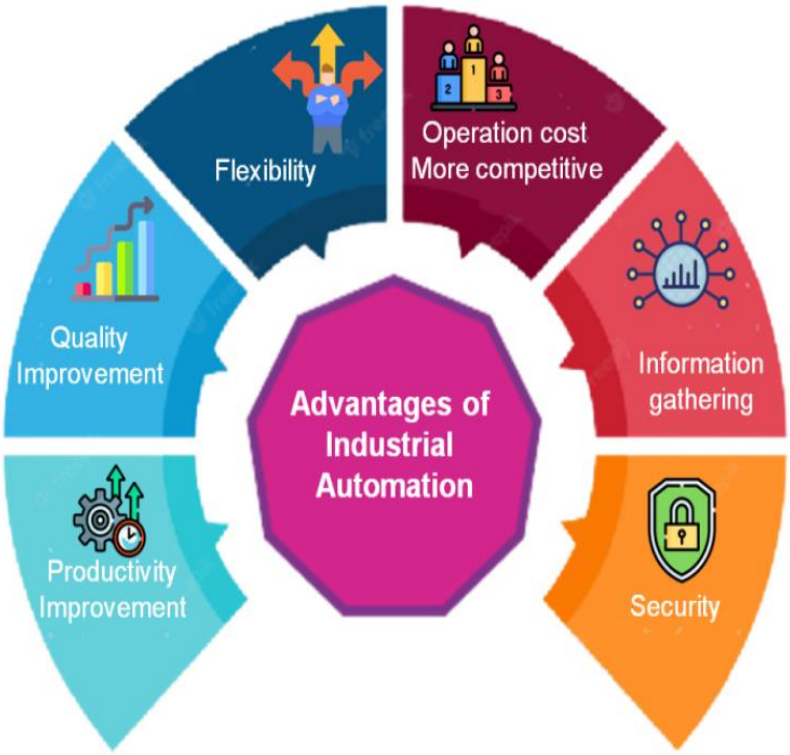

Figure 1. The advantages of industrial automation (Al Shahrani et al., 2022)

In addition to monitoring water quality, collecting water from the source, storing it and presenting it to users is also a separate process. In this study, an automation process of taking water from the well, storing it and presenting it to users will be discussed. An operator will manage the process from the SCADA system(Akı & Gullu, 2016).

SCADA (Supervisory Control and Data Acquisition) systems are crucial in various industrial applications such as water treatment and distribution networks. These systems operate in real-time environments such as water pumping stations, oil refining facilities and railway control centers (Musa et al., 2013). SCADA systems ensure efficient and safe operations by monitoring and controlling critical infrastructure (Shahzad et al., 2014). They are essential for supervisory control, data collection and automation processes, thus improving the reliability and performance of industrial systems (Hammouda et al., 2015).

The architecture and security of SCADA systems are critical to their implementation. SCADA systems provide real-time data about industrial processes, leading to increased efficiency and reduced operating costs (Ara, 2022). They play an important role in communication between devices in strategic industries such as power plants (Arifin et al., 2021). Additionally, SCADA systems aid in sensor fault detection due to their access to data and sensor information (Wang et al., 2020).

SCADA systems are widely used to monitor and control various processes, including controlling temperature control systems in stirred tank heaters (Bayusari et al., 2013). They are also vital for condition monitoring in wind turbines by utilizing SCADA data for performance monitoring (Tautz-Weinert & Watson, 2017). Additionally, SCADA systems are moving towards cloud-based solutions to improve industrial performance in IoT networks (Vilajosana et al., 2019).

In this study, 4 stations located at different distances from each other are configured to be wireless networks with each other. Control and monitoring were carried out with programmable controllers added to the stations. The stations consist of 2 deep water wells, 1 water tank and a control center. PLC was used to control the devices in wells and warehouses outside the center. The system is monitored and controlled from a computer located in the center. In addition, internet connection is available from the center and control of the facility is provided from anywhere. In the following sections, the network structure, characteristics of the stations, and the central control station will be explained.

Method

Yeni Karpuzlu Municipality is a town located in İpsala, Edirne. 3100 people live in the town. The town's drinking water needs are met by groundwater. For water needs, water is drawn with submersible pumps located in wells dug at a depth of 150 meters. The drawn water is sent to a water tank at a height of 30 meters. The tank with a capacity of 500m3 meets the water needs of the town. An automation system has been established to control and monitor this facility. Due to the possible distance between different stations and distances between them, a separate network installation was carried out. In the following sections, the network structure and stations will be discussed.

Remote End Units and Network Structure

There are 4 units for water automation. Three units controlled by PLC are close to each other from the center. There is a distance of 700m between the station where the main well and pump are located and the tank. There is a distance of 300m between the second well and the pump station and the tank. The distances and locations of the pumps and the water tank are shown in Figure 2.

Figure 2. Locations of the pumps and the water tank

Figure 3. Locations of the city center and the water tank

The pumps and the well are located 6km away from the city Centre. Water is pumped into the tank located 35m above the ground by pumps. There is a distance of 6km between the water tank and the city Centre. The center and tank layout are shown in Figure 3. From here, water is sent to the city via natural flow via pipes. Pump status, tank level and other information are sent to the control station at the center via wireless data transfer.

In Figures 2 and 3, 4 stations and their locations relative to each other are shown. Mains electricity is available at each station. Piping has been constructed for water transmission. The operation of the pumps at the stations is controlled by PLC. Water level in the water tank, amount of spent water, water pressure and mains pressure are measured by sensors and processed by PLC. Commands are sent for the pumps to operate according to the water level. The operation of the pumps, the level of the tank, and the water pressure are also monitored from the center. A wireless local network has been established for all this data transfer. Wireless outdoor antennas shown in Figure 4 and Figure 5 were used for wireless data transfer. These devices are also access points. Figure 4 is a long distance antenna with 23 dBi power. All of these antennas can work as AP, Client and repeater. The antenna in Figure 5 has a power of 13dBi.

Figure 4. Access points TP-LINK CPE710

Figure 5. Access points TP-LINK CPE510

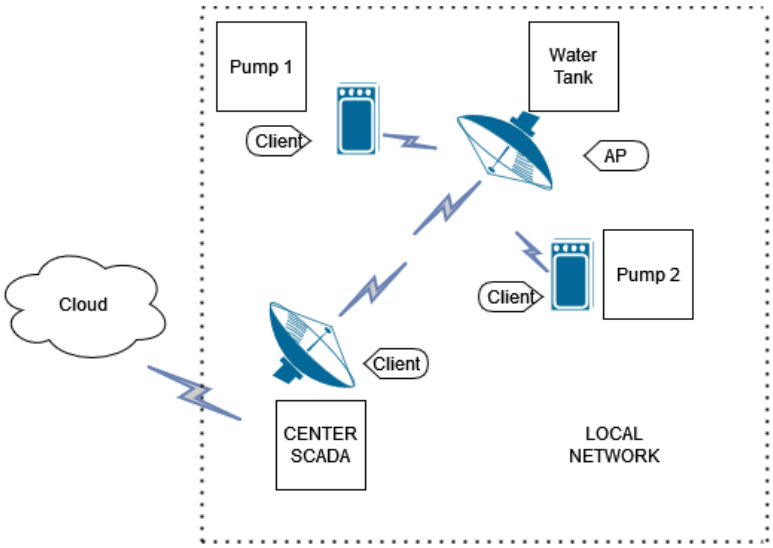

Figure 6. Network architecture of the system

Two high power antennas are connected to the center with water storage. The AP in Figure 5 was used for the communication of the pumps. 4 wireless devices transmitted data at the specified distances for system automation. This established lodge accesses the internet via the network center. A VPN network is also used for system security. The network structure of the automation system is shown in Figure 6.

Water Tank Automation

Pumps transport groundwater to the water tank located 35 meters above the ground. The tank has a water carrying capacity of 500m3. When it is fully filled, 3.5 Bar pressure is created on the pipe on the ground. When the water in the water tank, which is located higher than the city center, is sent to the city center by mountain flow, it creates a pressure between 3-7 bars. This pressure is expected to be around 4 bars. For this reason, the pressure was reduced with a valve at the pipe outlet. The number of liters of water sent to the city is monitored instantly per hour with a flow meter. In addition, 1 pulse was taken for each cubic meter and counted on the flowmeter. In this way, the amount of drained water is also monitored.

The water tank is located at an altitude of 35 meters. The tank, consisting of a concrete structure, has a circular cross-section and a height of 5 meters. The total height is 40 meters. The level is scaled between 0-100 and corresponds to 0-5 meters. A 4-20 mA 0-5 meter analog hydrostatic liquid level sensor was used. Additionally, a floater was used for the upper limit. PLC monitors all sensor and flowmeter data and transfers it to other PLCs and the center. 2 analog sensors were used for pressure. This station has a motorized valve as an outlet. The control of this valve is made according to pressure sensors. Additionally, security cameras have been installed in the station for station security and flow. All stations are connected to this center via clients. There is one access point here. The AP with 23dBi power is positioned 25 meters above the ground to see all stations. Polarization is adjusted to the main center. In this way, it can transfer automation data and camera data to the main center. Transfer speed was measured as 300mbs at a distance of 6km. Water storage automation is shown in figure 7.

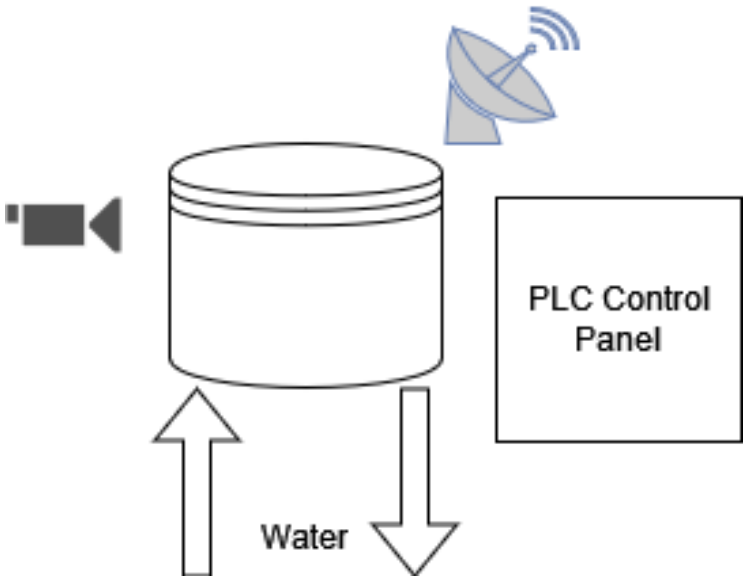

Figure 7. The water tank automation

Water Well - Pump Automation

Drinking water is sent to the water tank by a submersible pump from the well located at a depth of 150 meters. The pump is operated when needed, depending on the water level. The operation of the pump is done by a driver. Operations such as frequency control and overcurrent control are also performed and monitored with the driver. The operating modes are according to the level, according to the float and manually. In addition, pump operation can be done via the panel with a selector switch, independent of the PLC and automation system. Chlorination is also carried out at this station. The chlorine pump control is somehow operated at the appropriate dose according to the water level. An IP security camera is positioned for station security. Automation data and camera image are transferred wirelessly. Well automation is shown in figure 8. GLC-496T PLCs were used for the stations in the facility. A 7" HMI touch panel was used for the wells.

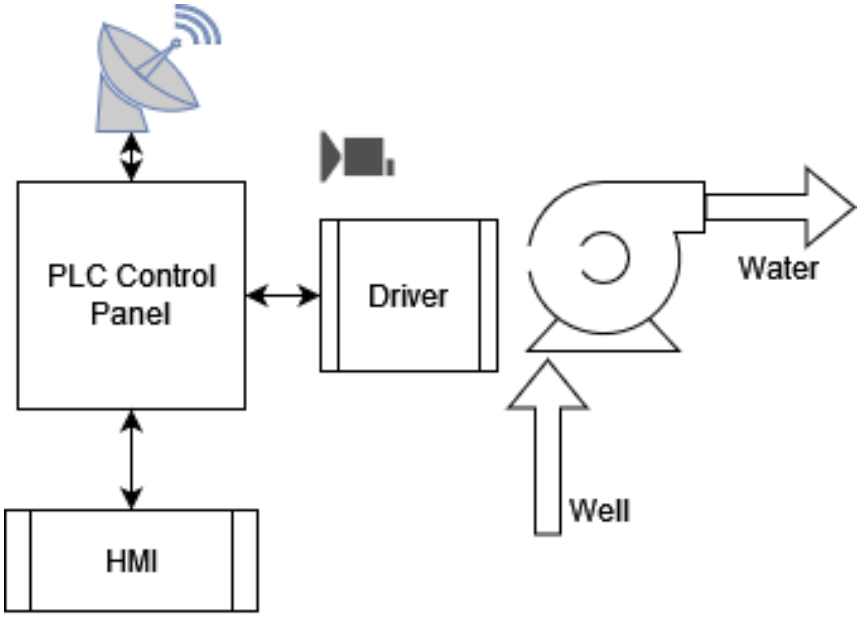

Figure 8. The pump automation

SCADA - Central Monitoring and Control

SCADA design has been made for central control of the facility. On this screen, data received from 3 PLCs were processed and visually reflected on the screen. Water level, pressures and water flow are monitored instantly. Additionally, operating modes are also controlled here. Automatic and manual control selection can be easily made by the operator. In addition, camera images at the stations are transferred to the center and monitored. All data is transferred wirelessly. At the farthest distance, the data rate to this unit is measured at 300mbp.

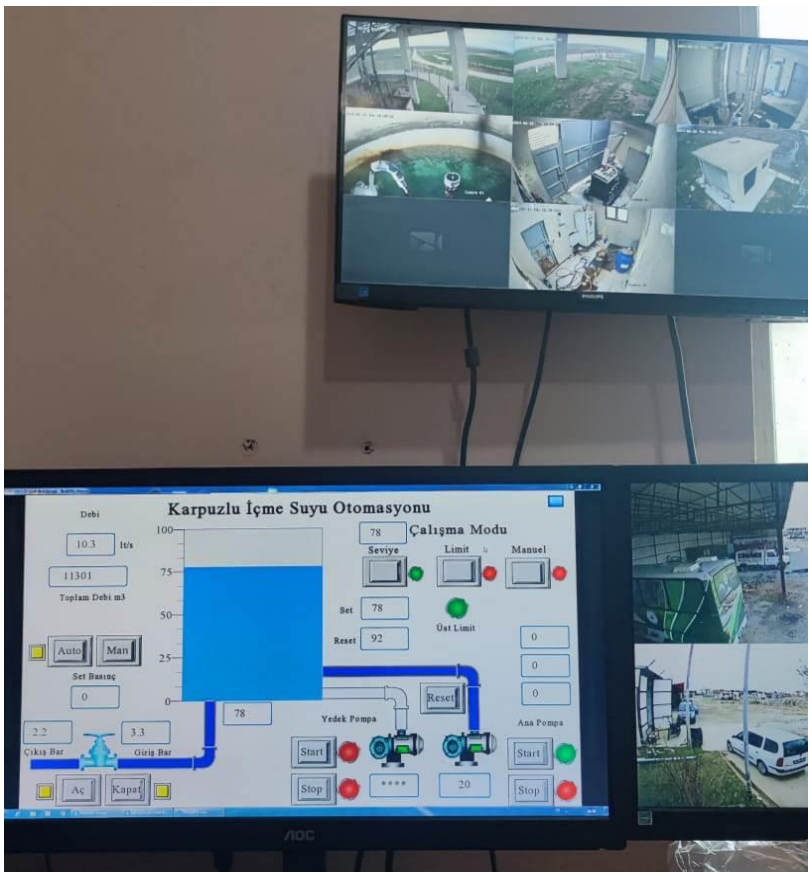

Figure 9. SCADA and camera view

Conclusion

In this study, an automation was established for the drinking water of a town. PLC and wireless network devices were positioned in 3 stations located in different locations, allowing the stations to communicate with each other. For remote control, another antenna was added to the control room located in the city center, allowing remote control by the operator. With the internet connection from this center, authorized personnel are allowed to monitor and control the facility from anywhere they want. 2 pumps are controlled in the facility. The level of the water tank, pressure and flow rates are monitored instantly. Both the water and the security of the facility are monitored with cameras. The operator displays the status of the equipment in the facility (operating, error, waiting) and the values of the sensors. Remote control function can be performed in different modes. Seamless data transfer between locations is ensured with the installed outdoor access points. In addition to transferring automation data, images of IP security cameras were also transferred.

Scientific Ethics Declaration

The authors declare that the scientific ethical and legal responsibility of this article published in EPSTEM journal belongs to the authors.

Acknowledgements or Notes

This article was presented as an oral presentation at the International Conference on Basic Sciences, Engineering and Technology (www.icbaset.net) held in Alanya/Turkey on May 02-05, 2024.

References

Akı, O., & Gullu, A. (2016). Solar pump project feasibility study for the village kumdere. *Unıtech16*, 3, 249-251.

Al Shahrani, A. M., Alomar, M. A., Alqahtani, K. N., Basingab, M. S., Sharma, B., & Rizwan, A. (2022). Machine learning-enabled smart industrial automation systems using internet of things. *Sensors*, *23*(1), 324.

Ara, A. (2022). Security in supervisory control and data acquisition (SCADA) based ındustrial control systems: Challenges and solutions. *IOP Conference Series: Earth and Environmental Science*, *1026* (1), 012030.

Arifin, M. A. S., Susanto, D. S., Idris, M. Y., & Budiarto, R. (2021). The trends of supervisory control and data acquisition security challenges in heterogeneous networks. *Indonesian Journal of Electrical Engineering and Computer Science*, *22*(2), 266-275.

Atif, M., Junejo, F., & Amin, I. (2022). 'Mover'a centralized job scheduling and rapid routing solution. *Research Square*, *1*, 1877006.

Bader, F., & Rahimifard, S. (2018). Challenges for industrial robot applications in food manufacturing. *Proceedings of the 2nd International Symposium on computer Science and Intelligent Contro*l, (pp. 1-8).

Bakar, M. A., Razali, N., Wook, M., Ismail, M. N., & Sembok, T. (2021). Exploring and developing an industrial automation acceptance model in the manufacturing sector towards adoption of Industry 4.0. *Manufacturing Technology*, *21*(4), 434-446.

Bayusari, I., Septiadi, R., & Suprapto, B. Y. (2013). Perancangan sistem pemantauan pengendali suhu pada stirred tank heater menggunakan supervisory control and data acquisition (SCADA). *Jurnal Rekayasa Elektrika*, *10*(3), 153-159.

Hammouda, M. B., Lakhoua, M. N., & El Amraoui, L. (2015). Dependability evaluation and supervision in thermal power plants. *International Journal of Electrical & Computer Engineering*, *5*(5), 905-917.

Herrera, J. L., Bellavista, P., Foschini, L., Galán-Jiménez, J., Murillo, J. M., & Berrocal, J. (2020). Meeting stringent qos requirements in iiot-based scenarios. *Globecom 2020-2020 IEEE Global Communications Conference* (pp. 1-6).

Lai, N. Y. G., Jayasekara, D., Wong, K. H., Yu, L. J., Kang, H. S., Pawar, K., & Zhu, Y. (2020). Advanced automation and robotics for high volume labour-intensive manufacturing. *2020 International Congress on Human-Computer Interaction, Optimization and Robotic Applications (HORA)* (pp.1-9). IEEE.

Lin, J.-H., Tjakrawinata, K. G., Jian, Y.-L., & Wun, Z. Y. (2023). Application on pcb defect detection system using multi-axis arm ıntegrated with optics and deep learning technology.

Merchant, H., & Ahire, D. (2017). Industrial automation using iot with raspberry pi. *International Journal of Computer Applications*, *168*(1), 44-46.

Musa, S., Shahzad, A., & Aborujilah, A. (2013). Simulation base implementation for placement of security services in real time environment. *Proceedings of the 7th International Conference on Ubiquitous Information Management and Communication*, (pp. 1-5).

Shahzad, A., Musa, S., Aborujilah, A., & Irfan, M. (2014). The scada review: system components, architecture, protocols and future security trends. *American Journal of Applied Sciences*, *11*(8), 1418.

Tautz-Weinert, J., & Watson, S. J. (2017). Using scada data for wind turbine condition monitoring–a review. *IET Renewable Power Generation*, *11*(4), 382-394.

Vilajosana, X., Watteyne, T., Vučinić, M., Chang, T., & Pister, K. S. (2019). 6TiSCH: Industrial performance for IPv6 ınternet-of-things networks. *Proceedings of the IEEE*, *107*(6), 1153-1165.

Wang, H., Wang, H., Jiang, G., Wang, Y., & Ren, S. (2020). A multiscale spatio-temporal convolutional deep belief network for sensor fault detection of wind turbine. *Sensors*, *20*(12), 3580.

Author Information

Aydin Gullu
Trakya University, Ipsala Vocational School, Mechatronics Program, Edirne, Türkiye
Contact e-mail: *aydingullu@trakya.edu.tr*

M. Ozan Aki
Trakya University, Ipsala Vocational School, Mechatronics Program, Edirne, Türkiye

To cite this article:

Gullu, A., & Aki, M.O. (2024). Establishing a remote area network for an automation system: A case study of Yeni Karpuzlu drinking water automation. *The Eurasia Proceedings of Science, Technology, Engineering & Mathematics (EPSTEM), 28*, 462-469.

The Eurasia Proceedings of Science, Technology, Engineering & Mathematics (EPSTEM)
ISSN: 2602-3199

The Eurasia Proceedings of Science, Technology, Engineering & Mathematics (EPSTEM), 2024

Volume 28, Pages 470-476

ICBASET 2024: International Conference on Basic Sciences, Engineering and Technology

Performance and Design Optimization of Solar Collectors

Marija Chekerovska
Goce Delcev University

Todor Chekerovski
Goce Delcev University

Sara Srebrenkoska
Goce Delcev University

Sasko Dimitrov
Goce Delcev University

Abstract: The objective of the present work was to conduct a comparative analysis of solar collectors. The experimental set-up consists of two flat plate solar collectors, the first collector was with a fixed surface tilted at 30o towards the South, and the second one was equipped with dual-axis rotation system. A programmable chronological tracker was used to control the motion of the moving collector. An experimental programme was performed to investigate the effect of the sun tracking system usage on the collector efficiency. The study includes development of a 3-D mathematical model of the system and extensive numerical simulation, based on the computational fluid dynamics (CFD) approach. The main aim of the modelling is to provide information on heat transfer, and to numerically simulate the heat transfer performances and the energy capture capabilities of the fixed and moving collectors in various operating modes. The comparative analysis shows that there is a good agreement between the experimental and numerically predicted results for different running conditions, and the presented modelling approach can be used for further investigations, including more complex problems.

Keywords: Solar collector, Solar energy, Heat transfer

Introduction

One of the simplest and most direct applications of the solar energy, which is cost effective, is its conversion into heat. It is also one of the ways the residential and other sectors can lessen their share in electricity consumption and impact on the environment. The cost effectiveness of solar thermal collectors depends on the cost of collector components, the efficiency and the thermal losses associated with the collector at the local operating conditions. Flat plate solar water heaters are traditionally in use in domestic hot water systems because of the low temperature requirement and low equipment cost (Sumathy, 1999). Conventional solar water heater systems and solar assisted heat pump systems for hot water production in specific local conditions are presented in (Li & Yang, 2009).

A 3-D numerical model for flat-plate solar collector that considers the multidimensional and transient character of the problem, the effect of the non-uniform flow on the collector efficiency was quantified and the degree of deterioration of collector efficiency was defined by Molero - Villar et al.(2009). Their analysis showed that this deterioration increases with the increase of the flow non-uniformity, although this effect is very limited. The model was verified with a steady-state conditions.

The model in time-dependent conditions, the properties of the working fluid, air gap and absorber are computed in real time, the heat transfer coefficients are also computed in the on-line mode and time-dependent boundary conditions are considered. The experimental verification showed a satisfactory convergence of the measured and calculated fluid temperatures at the collector outlet. This study relay heavily on the model developed by (Zima & Dziewa (2011). Yanjuan et al. (2015) presented numerical simulation method to solve the complex problem coupled with fluid flow, heat transfer and thermal stress in their system. The effects of the key operating parameters on the performances of the receiver are numerically investigated. Ramaswamy et al. (2020) worked on thermal and CFD analysis with different fluid air, water and different solar collector's i.e flat plate and parabolic trough was modeled by using CATIA design software. Thermal analysis were done with solar collectors with aluminum & copper).

Methodology of the Research

Experimental Research

The experimental set-up considered in this study was located in the town of Shtip, latitude 41^{o} 45' and longitude 22^{o} 12', (Figure 1). The system, consists of: moving collector equipped with a two-axis tracking device (a programmable chronological tracker is used to control the motion of the moving collector), static collector, horizontal water tank, circulating pumps, non-return valves, flow-meters, three-way valves, expansion vessel, manometers, air-vent devices, pressure-relief valves, drain valves, cold water entrance, automatics, temperature sensors, solar irradiation (heat flux) sensor etc.

Figure 1. Experimental set-up and a segment of the tracking system: electric drive (a), gear spindle (b), auxiliary mechanism (c)

a) b)

Figure 2. Installation of the a) movable collector and b) static collector

The main components of the experimental set-up enabling one of the collectors to move arround two axes of rotation can be seen in Figure 1. The main technical parameters of the flat solar collector is shown in Table 1. The collector consists of a transparent cover, absorber (absorber plate which absorbs heat), insulation (to protect against loss of heat), 10 copper pipes placed in pipe register with U-body construction and the collector body. The system is filled with working fluid which is a mixture of water and propylene glycol (in 50: 50% ratio), whose flow in the system is controlled by a differential thermostat. The differential thermostat has a direct communication with the pump, providing information and whether to switch-on or switch-off.

In this system there are two flow circles, one for the static and one for the movable collector, each one equipped with its own pump. Two circles are equipped with adequate equipment, shown in Figures 2, which includes a pipe line with appropriate fittings, valves - irreversible, spherical, valve for air relief, valves for filling and drenage, as well as flow-meters for hot water. The system has been equipped with an expansive vessel, safety valve and pressure gauge.

Table 1. Main technical parameters of the solar collector

Description	**Specification**
Collector annotation	Εκο Mag 2
Collector body	Aluminum
Dimensions, in mm	1500 x 970 x 81
Fluid content (water and propylene glycol)	1.76 liters
Vertical pipes: number, material, dimensions	10, Cu, 10.0/0.35 mm/mm
Manifolds (headers): number, material, dimensions	2, Cu, 22.0/0.8 mm/mm
Absorber plate	Aluminum, selective colour
Thermal insulation	Mineral wool, 50 mm
Transparent (glass) cover	Polycarbonate glass, 4 mm
Maximum temperature	165 ^{o}C
Weight	18 kg

For getting information from the collectors automatics UVR 61-3 was used, whose role is control of the system operation, as well as data storage. The installation contains temperature sensors at the movable and static collectors, at the cold water inlet in the tank, at the hot water tank, radiation sensor and water flow-meters. Appropriate information about the measured values of the sensors and pump work during the day are displayed on computer using the device D-LOGusb using the appropriate programs Winsol and Memory Manager. With the use of these programmes the data are continuously stored and can be displayed in tabular and graphical Excel.

Numerical Model Set-Up and Simulations

The flat-plate solar collector geometry considers the transient properties of its different zones. The numerical domain for the mathematical model comprises all functionally important parts of the collector, presented with their real geometry: manifolds (distributing and combining), vertical pipes, working fluid, transparent (glass) cover, absorber plate, air region and thermal insulation. The back and sides metal cover is also included in the model.

The geometry was created using Gambit pre-processor. The basic geometry of the collector pipe system used in the research, with the main dimensions, the outline of the computational domain and the mesh generated for calculations, are presented in (Figures 3) and (Figure 4). The numerical grid consists of 791033 volume cells and 171743 computational nodes. The grid independence was tested and verified using three different grids, in order to ensure that the grid resolution would not have a notable impact on the results: (1) 632800 volume cells, (2) 791033 volume cells, (with 171743 nodes) and (3) 949300 volume cells. Since the grid refinement changed the results by less than 0.5 %, which was previously decided as criteria, it was concluded that the influence of eventual further refinement would be negligible and, therefore, the mesh No. 2 was taken as appropriate for computation.

The numerical simulations were carried out using steady state implicit pressure based solver. The governing partial differential equations for mass and momentum are solved for the steady incompressible flow. The velocity-pressure coupling has been effected through the SIMPLEC algorithm. Second order upwind scheme was chosen for the solution scheme. The turbulence is covered with the RNG k-ε model and standard wall functions for the near-wall treatment. The considered case includes CFD modelling of solar irradiation, modes

of mixed convection and radiation heat transfer between the tubes surfaces, glass cover, absorber and side walls of the collector. It also covers mixed convection in the circulating water/propylene glycol mixture inside the tubes and conduction between the absorber plate, the tubes material, the insulation region and the collector cover.

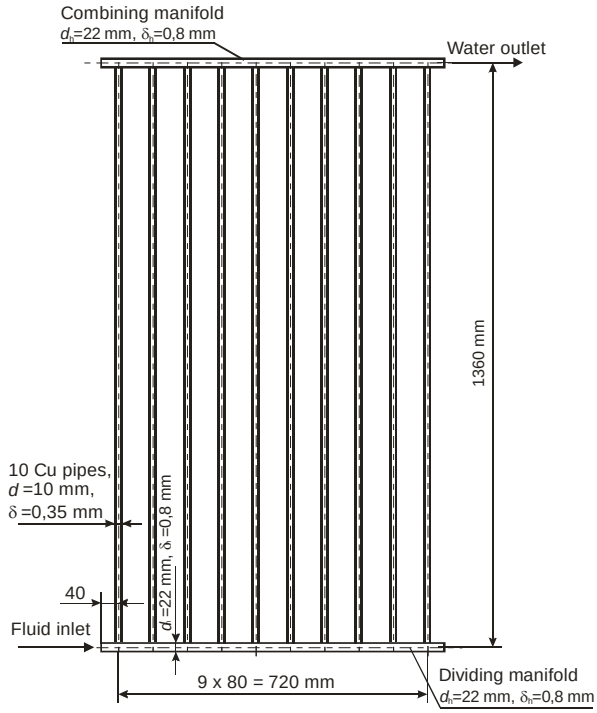

Figure 3. The collector pipeline system geometry

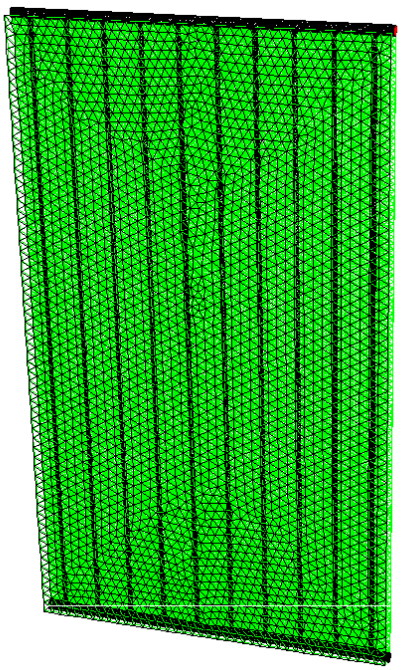

Figure 4. Numerical mesh

The selection of the most appropriate thermal radiation model in certain conditions depends on various factors, and in the case of solar collector modelling it becomes even more complex due to the necessity to include solar load model. The Discrete Transfer Radiation Model (DTRM) has been already proved as an efficient radiant transfer method in solar energy collector applications. In the present study, it was decided to correlate the experimental results with a mathematical model that incorporates the Discrete Ordinates (DO) radiation method, due to the opportunity of applying a solar load directly to the DO model (Saha & Mahanta, 2001). The DO radiation method considers the radiate transfer equation (RTE) in the direction **s** as a field equation:

$$\frac{dI(\mathbf{r},\mathbf{s})}{ds} + (a+s_s)I(\mathbf{r},\mathbf{s}) = an^2\frac{\sigma_0 T^4}{\pi} + \frac{\sigma_s}{4\pi}\int_0^{4\pi} I(\mathbf{r},\mathbf{s}')\Phi(\mathbf{s}\cdot\mathbf{s}')d\omega' \qquad (1)$$

where: $I_l(\mathbf{r},\mathbf{s})$ [W/m^{2}srad] is the spectral intensity, λ is the wavelength, a [m^{-1}] is the spectral absorption coefficient, **r** [-] is the location vector, **s** [-] is the direction vector (defined as $\mathbf{s}=\mu\vec{i}+\eta\vec{j}+\xi\vec{k}$), **s**' [-] is the vector of scattering direction, σ_s [m^{-1}] is the scattering coefficient at wavelength λ, σ_0 [W/m^{2}K^4] is the Stefan-Boltzmann constant, σ_0 =5,672·10^{-8} W/m^{2}K^4, ω' [-] is the solid angle, Φ is the phase function, which represents the probability that a ray with frequency v' from the direction **s** in a finite discrete solid angle $d\omega$' will veer in the direction **s**' inside the angle $d\omega$, with frequency v.

Results and Discussion

According to the CFD model and conducted numerical simulation, the fluid temperature change in the dividing and collecting manifolds, is presented in Figure 5. The change of the temperature of the working fluid versus the fluid velocity (wf,i) in proper working condition, according to the conducted CFD simulations are shown in (Figure 6). The values of the fluid velocity at this diagram are: wf,1 = 0.0001 m/s, wf,2 = 0.0005 m/s, wf,3 = 0,001 m/s, wf,4 = 0,005 m/s, wf,5 = 0,01 m/s. Temperature profiles of the air gap in three horizontal intersections along the collector height are shown in (Figure 7). The working fluid velocity vectors in the lower left part of the collector's pipe system is shown in (Figure 8).

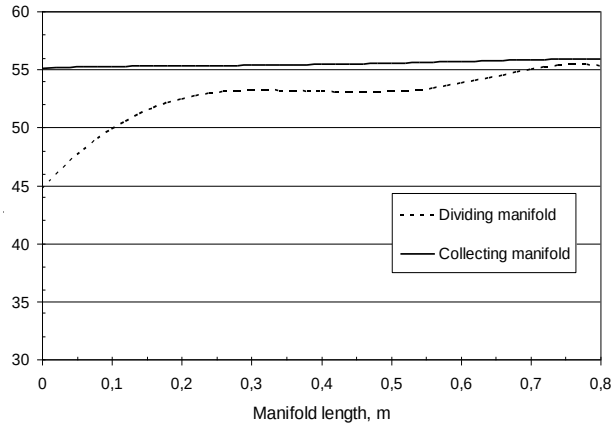

Figure 5. The change of the fluid temperature in the dividing and collecting manifolds

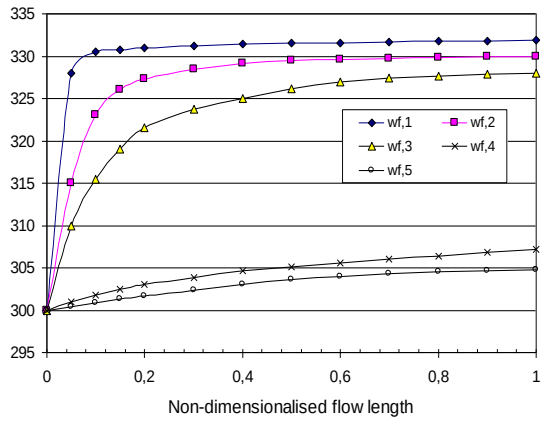

Figure 6. Change of the fluid temperature at different fluid velocities

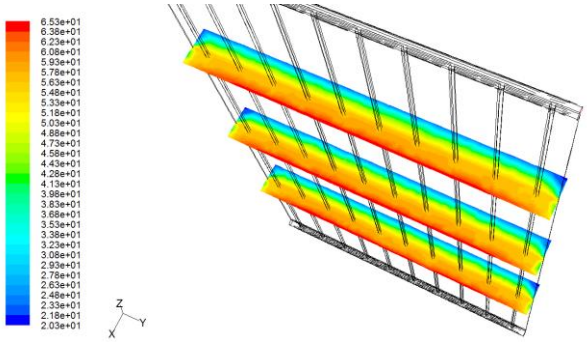

Figure 7. Temperature profiles in three intersections

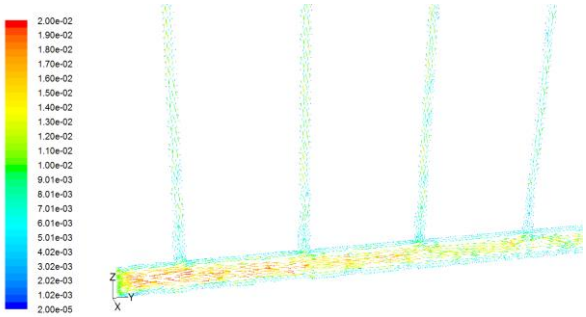

Figure 8. Velocity vectors at the bottom of the collector pipe system (dividing manifold)

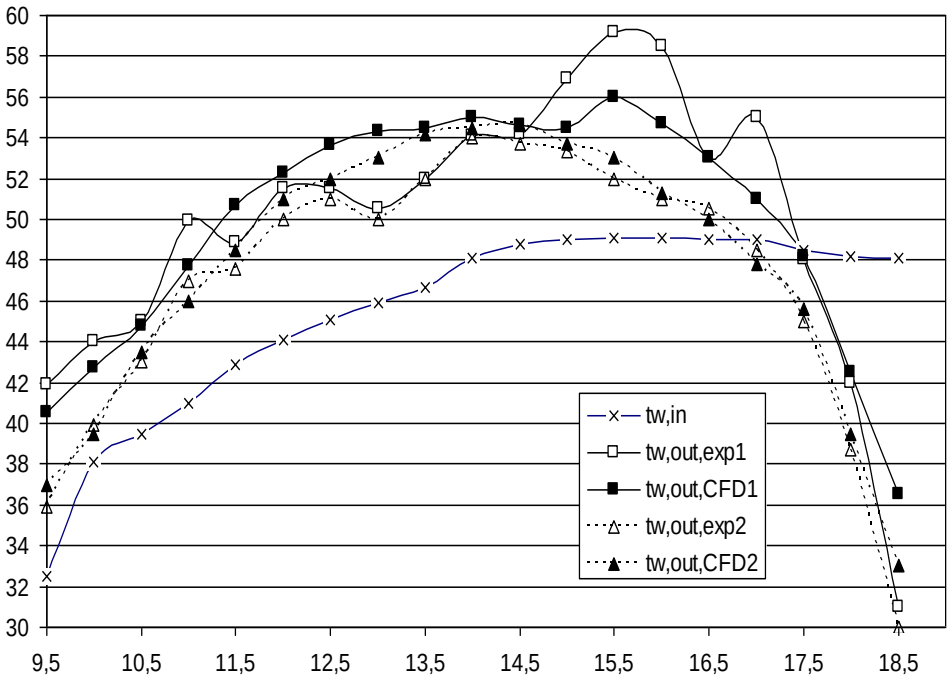

Figure 9. Working fluid temperature change, a comparison between the experimental and CFD results: 1 – experimental and CFD results, moving collector; 2 - experimental and CFD results, static collector

In order to draw up conclusions a comparison between the experimental and numerical simulation results has to be done. To accomplish this, while keeping other collector parameters fixed, the solar radiation flux for the simulation module is varied. An example of a comparison chart is shown in (Figure 9), indicating the measured and simulated outlet temperatures of the working fluid (propylene glycol/water mixture) versus time.

Conclusion

An experimental and CFD research has been conducted with the aim to assess the operation and to enhance the efficiency of a passive flat plate solar collector, by use of a controlled tracking system that could be easily applied in a typical (conventional) collector, without changing its shape. The efficiency of the proposed method was confirmed by experimental verification, showing significant increase, compared to the immobile collector unit. In order to provide a complete analysis in different operating conditions, a comprehensive CFD modelling and simulation is undertaken.

The analysis shows that there is a good agreement between the experimental and numerically predicted values for different running conditions and flow rates. In the present case, the outlet fluid temperature is the main parameter for comparison. It can be noticed that the CFD model results are much closer to the experimental data in the case of the static collector. Although there are some discrepancies, which may be explained by some experimental imperfectness matters, a conclusion can be drawn that the CFD modelling and simulation gives good results and can be used for more complex problems.

Recommendations

Given that the work establishes a model of a solar collector using CFD technology, together with the experimental analysis, the verified mathematical model can be applied for further research in order to gain a detailed insight into the thermal and fluid flow processes in thermal devices and plants, including other solar collectors' types and designs. The model will be a useful tool for improving the technical characteristics of the flat solar collectors and for comparative analysis of different collectors' configurations and technical solutions.

Scientific Ethics Declaration

The authors declare that the scientific ethical and legal responsibility of this article published in EPSTEM journal belongs to the authors.

Acknowledgements or Notes

This article was presented as a poster presentation at the International Conference on Basic Sciences, Engineering and Technology (www.icbaset.net) held in Alanya/Turkey on May 02-05, 2024.

References

Li, H., & Yang, H. X. (2009). Potential application of solar thermal systems for hot water production in Hong Kong. *Applied Energy, 86*(2), 175–180.

Molero - Villar, N., Cejudo - Lopez, J.M., Dominguez - Munoz F., Rodriguez Garcia, E., & Carrillo - Andres, A. (2009). Numerical 3-D heat flux simulations on flat plate solar collectors, *Solar Energy, 83*(7), 1086-1092.

Ramaswamy, R., Aravinda, K., & Pasha, S. K. (2020). CFD and thermal analysis of solar collectors by using Fea technique, *The International Journal of Analytical and Experimental Modal Analysis, 12* (8), 2404-2410.

Saha S. K., & Mahanta D. K. (2001). Thermodynamic optimization of solar flat-plate collector. *Renewable Energy, 23*(2), 181-193.

Sumathy, K. (1999). A study on the thermal performance of a flat-plate collector in Hong Kong. *International Journal of Ambient Energy*, *20*(2), 59-66.

Wang Y., Liu Q., Lei, J., Jin, H., (2015). Performance analysis of a parabolic ttrough solar collector with non-uniform solar flux conditions. *International Journal of Heat and Mass Transfer. 82*, 236–249.

Zima, W., & Dziewa, P. (2011). Modelling of liquid flat-plate solar collector operation in transient states, *Proc. IMechE Part A: Journal of Power and Energy, 225* (1), 3-62.

Author Information

Marija Chekerovska
Faculty of Mechanical Engineering, Goce Delcev University, Stip, Republic of N. Macedonia
Address Krste Misirkov no. 10-A, Shtip
Contact e-mail: *marija.cekerovska@ugd.edu.mk*

Todor Chekerovski
Faculty Od Electrical Engineering, Goce Delcev University, Stip, Republic of Macedonia

Sara Srebrenkoska
Faculty of Mechanical Engineering, Goce Delcev University, Stip, Republic of N. Macedonia
Address Krste Misirkov no. 10-A, Shtip

Sasko Dimitrov
Faculty of Mechanical Engineering, Goce Delcev University, Stip, Republic of N. Macedonia
Address Krste Misirkov no. 10-A, Shtip

To cite this article:

Chekerovska, M., Chekerovski, T., Srebrenkoska S., & Dimitrov, S. (2024). Performance and design optimization of solar collectors. *The Eurasia Proceedings of Science, Technology, Engineering & Mathematics (EPSTEM), 28*, 470-476.

The Eurasia Proceedings of Science, Technology, Engineering & Mathematics (EPSTEM)
ISSN: 2602-3199

The Eurasia Proceedings of Science, Technology, Engineering & Mathematics (EPSTEM), 2024

Volume 28, Pages 477-483

ICBASET 2024: International Conference on Basic Sciences, Engineering and Technology

Oxidation of Sintered Refractory Alloy (Ni_3Al)

Nacer Halem
University of Mouloud Mammeri-Tizi-Ouzou (UMMTO)

Zohra Halem
University Mohand Oulhadj of Bouira (UMOB)

Ouardia Halem
University of Mouloud Mammeri-Tizi-Ouzou (UMMTO)

Georgette Petot-Ervas
Centralesupélec, CNRS

Abstract: Ni_3Al is a superalloy which is of particular interest at high temperatures due to its high resistance to oxidation with the formation of a protective oxide layer that performs better than NiO and Cr_2O_3. Among the factors likely to affect the reaction mechanism and modification of the oxidation kinetics, the surface state appears to be a very important parameter. In the case of sintered materials, the surface condition will be linked to the porosity of the material and therefore to densification. This work essentially has two parts. The first consists of developing Ni_3Al sinters intended for oxidation, studying the densification mechanisms and bringing together the results obtained by dilatometry at variable temperature and by differential thermal analysis which made it possible to demonstrate sintering in a reactive liquid phase extremely fast SHS type, with instantaneous formation of the Ni_3Al phase. The second part is devoted to the isothermal oxidation between 1100 and 1350°C of cubic-shaped sinters (4mm edge) under a flow of oxygen for 24 hours. The shape of the parabolic curves is correlated with morphological and microstructural observations to deduce the diffusional kinetic regime which controls the speed of the reaction. On the other hand, these observations highlighted a very strong adhesion due to the indentations of the Al_2O_3 oxide in the metal at the oxide/metal interface. Various techniques (Density – XRD – SEM and Microanalysis) to characterize the sinters and the oxidation products complete our study.

Key words: Alloy, Ni_3Al, Sintering, Oxidation

Introduction

Nickel-based materials containing aluminum are used at high temperatures in aggressive environments (corrosion, irradiation, etc.). The choice of aluminum is motivated by the introduction of an element likely to lead to obtaining a refractory alloy. Aluminum is characterized by a high affinity for oxygen. However, it is practically unalterable in the air. This is due to the formation of a protective layer of alumina which has good corrosion resistance and constitutes a good electrical insulator. Various techniques have made it possible to develop the Ni_3Al phase by the SHS method (Mihelic, 1992), SRS (Thadani, 1992), reactive sintering (Bose, 1988; Hwang, 1992; Nashimura, 1993; Rabin, 1985), HIP (Chang, 1985), activation by grinding (Jang, 1991; Cardellini, 1994), or by infiltration (Dunand, 1994). However, certain authors such as (Bose, 1988 & Hwang, 1992), have developed the Ni_3Al alloy by natural sintering. The resistance to oxidation of alloys (Ni-Al) depends mainly on their composition (Rapp, 1984; Lacombe, 1984). Other scanning electron microscopy (SEM) and transmission microscopy (TEM) methods have been used to study the oxidation of Ni_3Al (Bobeth, 1992). It

appears from the bibliography that Ni_3Al has been widely studied in the bulk state, but little concerning sintered materials. So, it seemed interesting to us to study the influence of the microstructure and the addition of 13% by mass of aluminum on the oxidation of sintered nickel. According to the Ni-Al binary diagram (figure 1) (Singleton, 1986), the Al content of 13% predicts the Ni_3Al phase.

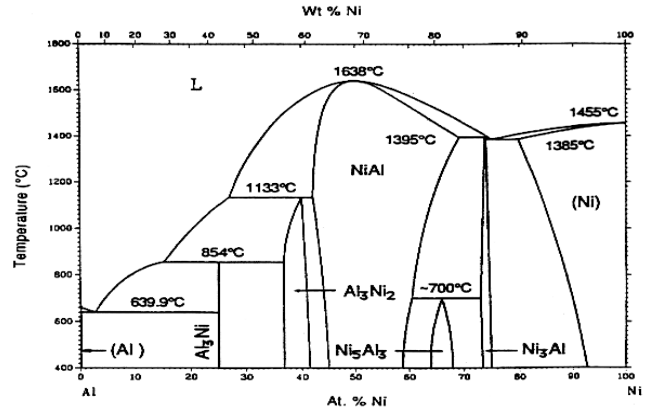

Figure 1. Ni-Al phase diagram.

Experimentation

The nickel and aluminum powders sold by Cerac have respective purities of 99.99% and 99.50%. Their respective average size is 5µm and 15µm. The powder mixtures (Ni-13% Al) by mass were carried out for 3 hours in a turbula. The agglomerates with a raw density of approximately 70% of the theoretical density were obtained by cold isostatic compression under 200 MPa for 2 minutes. The compacted bar obtained is cut into pellets (∅13mm and height 6mm) for the various heat treatments and characterizations. The shrinkage of the agglomerates was followed under dynamic argon U (3.5l/h) using a Setaram TMA92 type dilatometer at variable temperature, with heating and cooling rates of 5°C/min up to at 750°C. A differential thermal analysis (DTA) was carried out on the mixture up to 800°C under a flow of argon U (3.5l/h) at a rate of 10°C/min. The pellets were sintered under dynamic vacuum for 1 hour at a temperature of 750°C, with a heating and cooling rate equal to 20°C/min. Finally, various characterization techniques (XRD, Vickers density and microhardness measurements, and microstructural observations were implemented to characterize the sinters.

Isothermal oxidation was carried out on cubic samples (4mm edge) between 1100 and 1350°C, under oxygen flow for 24 hours, on polished surfaces up to 1µm. The evolution of the mass was monitored using a Setaram B85 thermobalance. The samples were characterized after oxidation by X-ray diffraction, scanning electron microscopy and microanalysis.

Results and Discussion

Sintering

The evolution of the linear shrinkage of the Ni-13%Al mixture presents a sudden shrinkage of amplitude of around 8%, manifests itself around 550°C, with an average expansion coefficient (between 20 and 550°C) of the order of $1.48.10^{-5}°C^{-1}$, calculated at cooling (figure 2). It is not preceded by any prior swelling and is followed by a regime of thermal expansion quite comparable to that which accompanies the initial heating stage. The densification curve is characteristic of liquid phase sintering. The shrinkage which occurs very suddenly is most certainly linked to the effect of this liquid phase which propagates at very high speed, leaving behind the solid compound Ni_3Al while causing the grains of Ni and Al to come together at the moment when they come into reaction. Undoubtedly linked to homogeneity problems, porosities can remain within the compound, as micrographic observation shows later.

The thermogram of the powder mixture (Ni-13%Al) by mass (figure 3) reveals the presence of a very energetic exothermic peak, reflecting the violence of the reaction corresponding to the stoichiometric composition of the Ni_3Al compound. However, preceding this reaction, we observe a small endothermic peak which could correspond to the formation of a molten aluminum phase but more probably to that of the eutectic liquid

(T=640°C). Indeed, some authors consider that the diffusion in the solid state of aluminum in nickel or in iron is already initiated even before its melting temperature is reached (Bose, 1988; Rabin, 1991; Gevanishvili, 2002), which seems to explain the sudden shrinkage at T=550°C on the shrinkage curve. It turns out that the formation of the liquid and the triggering of the reaction are almost concomitant.

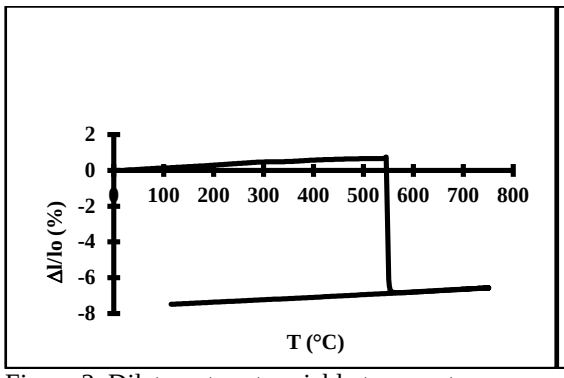

Figure 2. Dilatometry at variable temperature (Ni-13%Al) by mass.

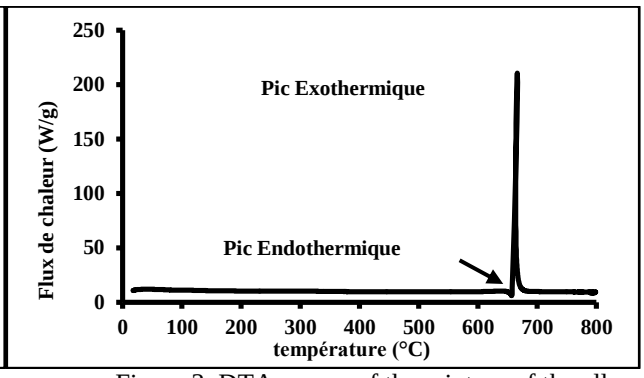

Figure 3. DTA curves of the mixture of the alloy (Ni-13%Al) by mass.

The diffractogram of the sintered alloy (Ni-13%Al) (figure 4) reveals only the single-phase compound Ni_3Al with a final density of 92% which would be consistent with the mechanism of reactive sintering described by (German, 1996). Morphological observations of the product formed (figure 5), after polishing and chemical attack, reveal the presence of pores and large grains of more or less rounded geometric shapes.

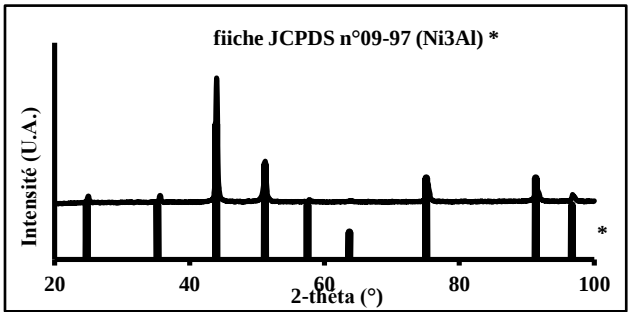

Figure 4. XRD spectrum of the sintered alloy (Ni-13%Al).

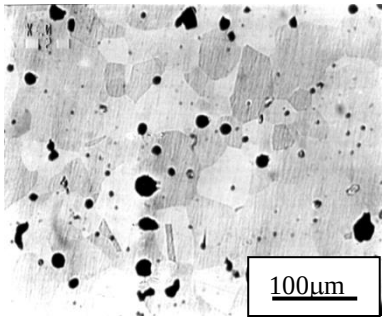

Figure 5. Microstructure of Ni_3Al

Oxidation

The isothermal changes in weight gain, per unit area and as a function of time, are shown in figure 6. These results show that the curves have a parabolic appearance whatever the oxidation temperatures between 1100 and 1350°C. They have low mass gain.

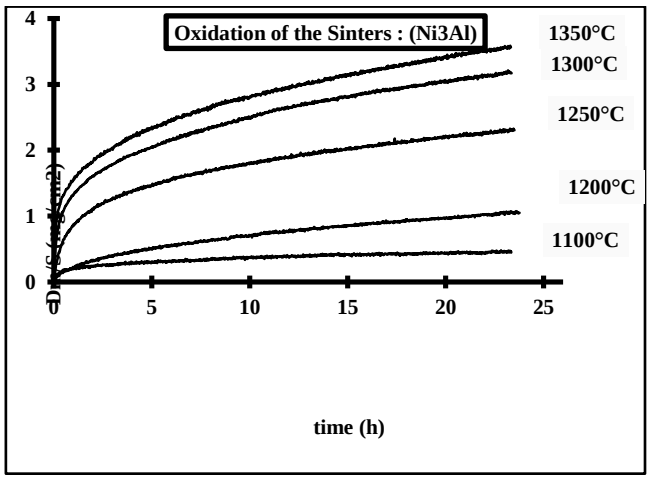

Figure 6. Mass gain per unit area of Ni_3Al.

From the oxidation temperature T=1200°C, X-ray diffraction analysis shows that the oxide formed on the surface of the sinters is alumina Al_2O_3. On the other hand, at T=1100°C, no oxide was revealed. Because at this temperature alumina is in an amorphous state and only crystallizes from1200°C (Castel, 1990). The oxide layer presents irregularities (non-uniform) which explains the presence of the two phases (Ni_3Al and Al_2O_3) by XRD (figure 7). To better exploit these results it is necessary to know the products formed by a morphological study on the surface and in cross sections as well as by microanalysis.

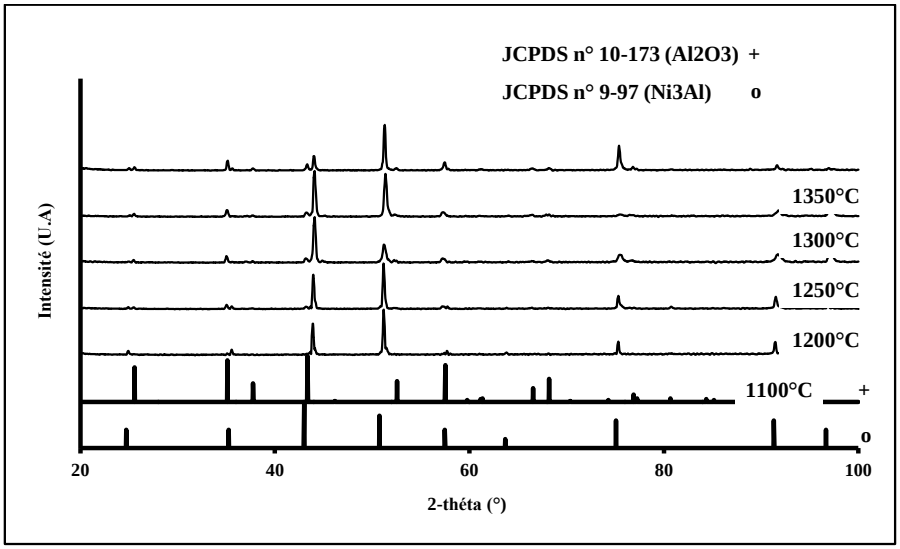

Figure 7. Diffractogram of Ni_3Al after 24 hours of oxidation.

The morphology of the oxidized frits changes very significantly with the oxidation temperature. The Ni_3Al sinter oxidized at T=1100°C (figure 8), shows the formation of two layers of oxide, one on the surface in the form of scales and the other underlying. They could be made of α-Al_2O_3 or $NiAl_2O_4$ spinel. But these compounds not having been identified by XRD, probably due to their low quantity and the limit of detection by X-rays, we have observed the oxide layer in cross section. Oxidation at T=1350°C seems to indicate a notable improvement from the recovery but porous point of view (figure 9).

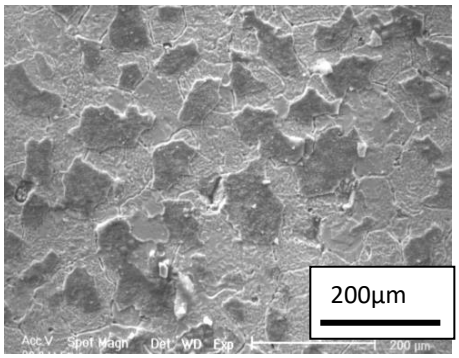

Figure 8. Scaled oxide (T=1200°C)

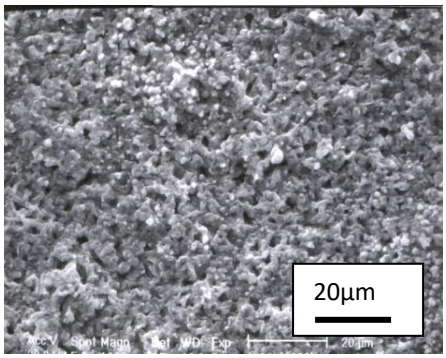

Figure 9. Porous Al_2O_3 (T=1200°C).

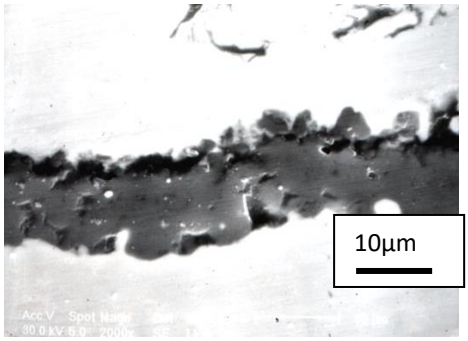

Figure 10. Oxide layer (T=1200°C).

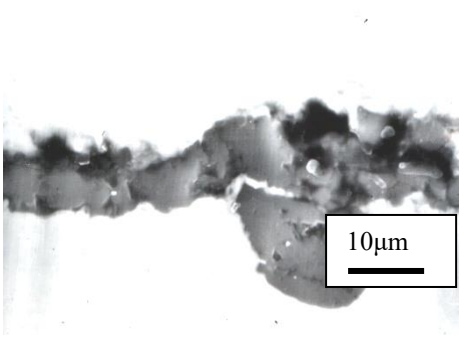

Figure 11. Oxide layer (T=1250°C).

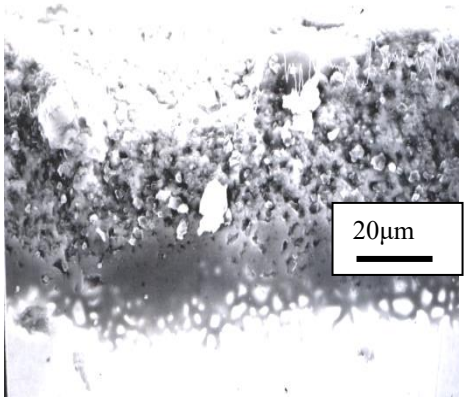

Figure 12. Oxide layer (T=1300°C).

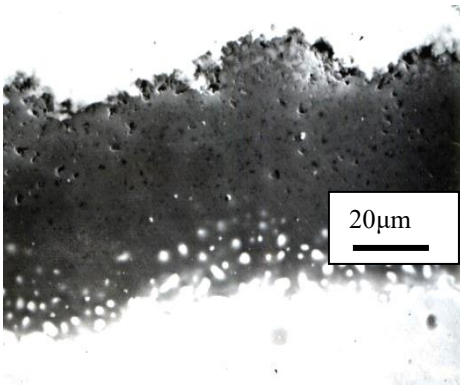

Figure 13. Oxide layer (T=1350°C).

The cross-sectional observation of the oxide layer at T=1100°C is very thin and cannot be detected by XRD, hence the difficulty in highlighting it in the cross section. On the other hand, on the other Ni_3Al sinters it highlights an internal growth of the oxide, 9at the grain boundaries of the metal. These inkings are the cause of good adhesion of the corrosion layer to the metal and confirm that the increase in temperature goes in the direction of an increase in the resistance to oxidation of the material (figures 10- 11-12-13). Overall, the oxide layer thickens with the percentage of aluminum, in accordance with the mass gain measured on the thermobalance.

By correlating the parabolic shape of the kinetic curves with microscopic observations, it seems logical to attribute the growth of the oxide layer to a diffusional process in the volume of Ni^{2+} which are mobile thanks to the nickel vacancies. The values of the rate constants kp deduced from the linear transforms at different temperatures (table 1) obey an Arrhenius law : $K_p = K_0.exp\left(-\frac{E_a}{RT}\right)$. The oxidation process is thermally activated with an energy of the order of $(160 \pm 10\frac{kJ}{mol})$ (figure 14). This value is lower than that of the nickel diffusion activation energy determined for single-crystalline NiO $\left(E_a \approx 247\frac{kJ}{mol}\right)$ (Atkinson, 1978). This difference can be attributed to the significant contribution of grain boundaries to the transport processes in the corrosion layer.

Table1. Rate constants of Ni_3Al oxidized.

Kp (mg.cm^2.s$^{-1/2}$)	0,065	0,2141	0,3295	0,4516	0,5259
T (°C)	1100	1200	1250	1300	1350

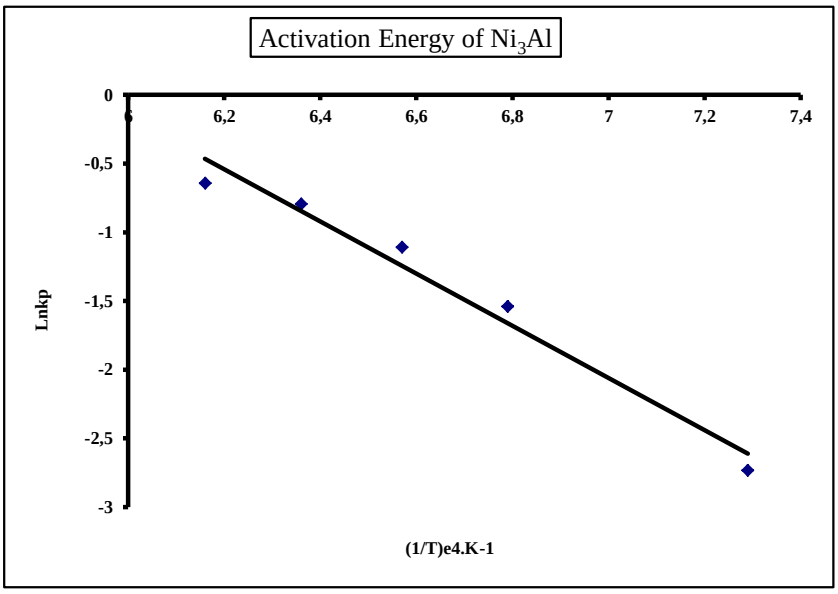

Figure 14. Arrhenius representation of the oxidation of Ni_3Al.

Conclusion

Ni_3Al sintering takes the form of liquid-reactive phase sintering, with a self-combustion type reaction, completely consuming both constituents. In this case, the transient liquid phase leads to the formation of the relatively dense intermetallic compound Ni_3Al. Regarding oxidation, given the low weight gain, Ni_3Al sinters have better resistance to oxidation. From 1200°C, there is the formation of an adherent and compact Al_2O_3 oxide layer in sufficient quantity which plays a protective role and is responsible for the best resistance to oxidation. The morphology of the oxide layer and the parabolic kinetics show that we are in the presence of a cationic diffusional process.

Scientific Ethics Declaration

The authors declare that the scientific ethical and legal responsibility of this article published in EPSTEM journal belongs to the authors.

Acknowledgements or Notes

* This article was presented as a poster presentation at the International Conference on Basic Sciences, Engineering and Technology (www.icbaset.net) held in Alanya/Turkey on May 02-05, 2024.

References

Atkinson, A., & Taylor, R.I. (1978). The self-diffusion of Ni in NiO and its relevance to the oxidation of Ni. *Journal of Materials Science, 13*,427-432.

Bobeth, M., Pompe, W., Schumann, E., & Ruhle, M., (1992). Out-diffusion of the noble component during the initial stage of the oxidation of γ'-Ni_3Al. *Acta Metallurgica Et Materialia, 40*(10), 2669-2676.

Bose, A., Rabin, B.H., & German R.M., (1988). Reactive sintering nickel-aluminide to near full density. *Powder Metallurgy International, 20*(3),25-30.

Cardellini, F., Mazzone, G., Montone, A., & Vittori-Antisari, M. (1994). Solid state reactions between Ni and Al powders induced by plastic deformation. *42*(7), 2445-2451.

Castel, B. (1990). *Les alumines et leurs applications* (p.54). Naathan.

Chang, K.M., Taub, A. J., & Huang, S.C. (1985). *High-temperature ordered intermetallic alloys* (Vol 38., p.335). *C*.C. Koch (Ed.). Pittsburgh, Pennsylvania: Cambridge University Press.

Dunand, D.C., (1994). NiAl formation by annealing of infiltrated aluminium-nickel precursors. *Journal of Materials Science*, (29), 4056-4060.

Gedevanishvili, S., & Deevi, S. C. (2002). Processing of iron aluminides by pressureless sintering through Fe+ Al elemental route. *Materials Science and Engineering : A, 325*(1-2), 163-176.

German, R.M. (1996). *Sintering theory and practice* (p.405). John Wiley & Sons.

Hwang, K.S., & Lu, Y.C. (1992). Reaction sintering of 0,1% B doped Ni3Al, *Powder, Metallurgy International, 24*(5), 279-283.

Jang, J.S.C., & Koch, C.C. (1990). Amorphization and disordering of the Ni3Al ordered intermetallic by mechanical milling. *Journal of Materials Research,5*(3), 498-510.

Lacombe, P., & Dabosi, F. (1984). Corrosion des matériaux à hautes temperatures, *Ecole d'hiver du CNRS Tome, 1*, 33-34.

Mihelic, B., Dahic, M., Djekic, R., & Uskokovic, D. (1992). Processing of compact materials by the use of self-propagating high-temperature synthesis and pseudo-hot isostatic pressing, *Materials Letters, 13, 391-395*.

Nishimura, C., & Liu, C.T. (1993). Reactive sintering of Ni3Al under compression. *Acta Metallurgica Et Materialia, 1*(1), 113-120.

Rabin, B. H., &Wright, R.N. (1991). Synthesis of iron aluminides from elemental powders, Reaction mechanism and densification behaviour, *Metallurgical Transactions A, 22*, 277-286.

Rabin, B. H., Bose, A., & German, R.M. (1988). Processing effects on densification in reactive sintering of nickel-aluminum powder mixtures. *Modern Development in Powder Metallurgy, 20*, 511-529.

Rapp, R. A. (1984). The high temperature oxidation of metals forming cation-diffusion scales. *Metall. Trans. A, 15*, 765-782.

Singleton, M.F., Murray, J.L., & Nash, P. (1986). *Binary alloy phase diagrams* (Vol 1., p.140). T.H. Massalski, J.L. Murray, L.H. Bennett, H. Baker (Eds.). ASM, Metals Park.

Thadani, N.N., Work, S., Graham, R.A., & Hammetter, W. F. (1992). Shock-induced reaction synthesis (SRS) of nickel aluminides. *Journal of Materials Research*, *7*(5), 1063-1075.

Author Information

Nacer Halem
University Mouloud Mammeri
Tizi-Ouzou, Algeria
Contact e-mail: *nacer.halem@ummto.dz*

Zohra Halem
University Mohand Oulhadj
Bouira, Algeria

Ouardia Halem
University Mouloud Mammeri
Tizi-Ouzou, Algeria

Georgette Petot-Ervas
Centralesupélec, CNRS,
Paris, France

To cite this article:

Halem, N., Halem, Z., Halem, O., & Petot-Ervas, G. (2024). Oxidation of sintered refractory alloy (Ni_3Al). *The Eurasia Proceedings of Science, Technology, Engineering & Mathematics (EPSTEM), 28*, 477-483.

The Eurasia Proceedings of Science, Technology, Engineering & Mathematics (EPSTEM)
ISSN: 2602-3199

The Eurasia Proceedings of Science, Technology, Engineering & Mathematics (EPSTEM), 2024

Volume 28, Pages 484-491

ICBASET 2024: International Conference on Basic Sciences, Engineering and Technology

Experimental Investigations on the Fabrication of Low Alloy Steels Using Wire Arc Additive Method

Pruthviraj Chauhan
Pandit Deendayal Energy University

Vatsal Vaghasia
Pandit Deendayal Energy University

Rakesh Chaudhari
Pandit Deendayal Energy University

Jay Vora
Pandit Deendayal Energy University

Abstract: Wire arc additive manufacturing (WAAM) has emerged as a transformational technology with the capacity to redefine the landscape of alloy steel component production. This method utilizes an electric arc to selectively fuse a continuous wire feed, progressively constructing intricate metal structures layer by layer. GMAW-based WAAM adaptability enables the creation of complex geometries and customized part designs, making it applicable across diverse industrial sectors. This paper investigates WAAM-specific applications in alloy steel fabrication, focusing on key process variables such as voltage, travel speed, and Gas mixture ratio. The experimental parameters for a single layer are examined with voltage ranging from 20 to 22, travel speed from 23, 25, and 27 mm/min, and Gas mixture ratio 1,5,9 mm/min. It utilizes materials like TM B9, a 1.2-diameter flux-cored wire. Additionally, the study considers the nominal composition (wt-%) of 9 Chromium, and 1 Molybdenum, with small additions of nitrogen and niobium to improve the creep resistance. Furthermore, the final findings of the study suggest that the optimal combination of process variables for achieving high-quality weld beads in WAAM of alloy steel components can be determined through Response Surface Methodology (RSM). RSM is a statistical method for analysing and modeling the relationship between the response of interest and some independent variables. In this case, the response variable would be the quality of the weld bead, which encompasses factors such as bead geometry, integrity, and absence of defects.

Keywords: Alloy steel fabrication, GMAW welding, Wire arc additive manufacturing (WAAM)

Introduction

In modern manufacturing, the pursuit of innovative techniques to enhance efficiency, flexibility, and product quality is ceaseless. One such cutting-edge methodology gaining significant traction is Gas Metal Arc Welding (GMAW)-Based Wire Arc Additive Manufacturing (Shah et al., 2023). This transformative process has become a potent tool for fabricating complex components with unprecedented precision and speed, revolutionizing traditional manufacturing paradigms. Within the realm of GMAW-based WAAM, a particular focus has been directed towards its application in the processing of low alloy steel, such as the renowned alloy TM B9. TM B9, recognized for its exceptional combination of strength, toughness, and corrosion resistance, stands as a prime candidate for a multitude of industrial applications, spanning from automotive to aerospace sectors (Suat et al., 2020). Integrating GMAW-based WAAM into the production of TM B9 components presents an exciting frontier, offering unparalleled opportunities to optimize manufacturing workflows, reduce material waste, and

expedite production cycles. This introduction sets the stage for a comprehensive exploration into the realm of GMAW-based WAAM for low alloy steel, specifically focusing on the exemplary properties of alloy TM B9. A critical aspect of this exploration involves the meticulous study and optimization of welding parameters, such as voltage, Gas mixture ratio, and travel speed (Vora et al., 2022). These parameters play a pivotal role in determining the quality and characteristics of the fabricated components. In addition to studying and optimizing welding parameters such as voltage, Gas mixture ratio, and travel speed. it is essential to investigate the bead geometry resulting from these parameters for achieving better wall structure in the fabricated components (Dinovitzer et al., 2019). Bead geometry, including bead width, height, and penetration depth, directly influences the structural integrity, mechanical properties, and overall quality of the weld.

Due to the presence of metals like Ni, Mo, and Cr, low alloy steel (TM B9) has excellent mechanical qualities and resistance to corrosion, making it extremely weldable(Rodrigues et al., 2020) . With its higher welding temperature, TM B9 in particular is perfect for WAAM procedures, guaranteeing greater layer fusion. Its primary attributes like high strength, resistance to corrosion, weldability, ductility, makes it ideal for use in a variety of industries, including the oil and gas, biomedical, maritime, and aerospace sectors(Jahns et al., 2023) . The best parameter settings for WAAM variables have been found through the use of optimization techniques, resulting in TM B9 single-layered structures that are clean. Research has shown that in order to build single-layered structures with minimal flaws and desired mechanical qualities, it is crucial to have sufficient control over the design parameters (Chaudhari et al., 2023). In the process of optimizing WAAM parameters for bead shape, research has revealed that voltage and gas mixture ratios are critical variables. Factors including filler type, welding parameters, and bead shapes affect the quality of WAAM components. Since GMAW-based WAAM produces thin-walled structures with ideal process variables, its higher deposition rate makes it superior to other approaches. WAAM technique creates metal additive structures using single-layer deposition.

Due to their unique characteristics and the subtleties of the AM process, different materials are affected by WAAM in different ways. The microstructure and mechanical characteristics of steel are significantly influenced by process factors, and WAAM enables efficient deposition suitable for large-scale manufacturing (Shah et al., 2023). Because of its high heat conductivity and tendency to crack, aluminum presents difficulties and requires exact parameter management to reduce flaws. WAAM is perfect for aerospace and medical applications because it provides titanium with fast deposition rates and meticulous parameter control, both of which are necessary to avoid contamination and guarantee the required mechanical qualities. For high-temperature and corrosion-resistant components, nickel-based alloys benefit from WAAM; nevertheless, careful process optimization is required to overcome cracking and distortion concerns.

Copper and its alloys have great thermal and electrical conductivity, making them valuable in WAAM. Strict parameter selection and shielding gas control are required to reduce oxidation and produce high-quality deposits for electrical components and heat exchangers. All things considered, WAAM offers both potential and challenges for a variety of materials, necessitating customized methods for the best fabrication results(Raut & Taiwade, 2021). Also examine various research papers that concentrate on focuses on bead geometries optimisation of GMAW-based WAAM variables. employs the single-layer deposition method with the Box-Behnken design methodology. uses ANOVA and multivariable regression methods to evaluate feasibility. Chaudhari et al. (2022) emphasises hardness, porosity, and mechanical characteristics. examines the alloy's potential for wire-arc additive fabrication. Thorough rundown of the difficulties, materials, development, and methodology of WAAM. Pay attention to the heat treatment, dimensional precision, microstructural homogeneity, and process parameters. Examines the latest advancements, materials, in-process procedures, difficulties, and WAAM technology (Zhou et al., 2020).

The present work focuses on the experimental analysis of TM B9 bead morphologies using GMAW-based WAAM single-layer deposition. Using WAAM variables (voltage, gas mixture ratio, travel speed) and output responses (BW, BH), experiments were conducted using Taguchi's L9 approach. To determine the significance of WAAM components on output qualities, ANOVA was employed. Main effect plots were made, and the optimal input set of WAAM variables was determined for each unique output variable, to better understand the influence of WAAM parameters on output features(IvánTabernero et al., 2018). To obtain desirable material properties and deposition rates, current research in GMAW-based WAAM concentrates on optimizing process variables such as Gas mixture ratio, voltage, and travel speed. Moreover, research is being done on multi-material deposition, hybrid methods, surface quality enhancement, and the metallurgical behaviour of deposited materials(Shah et al., 2023). Even though problems like surface roughness, porosity, and microstructure control are still present, research is being done to produce new materials, monitor sophisticated processes, and integrate Industry 4.0 technology to overcome these problems.

Materials and Methods

In the current study, bead-on-plate experiments were carried out utilising a 20 mm thick Mild Steel 2062 grade substrate and a 1.2 mm flux core wire (TM B9) employing the GMAW technique. The wire used, TM B9, has the following chemical composition, which is listed in Table 2. Testing was done using the WAAM Machine system. The substrate plate was carefully cleaned and allowed to dry before deposition. A GMAW torch, a wire feeder, shielding gas cylinders containing carbon dioxide and argon, a controller, and a specialised machine were among the apparatus used in the experiment (Chaudhari et al., 2022). The nozzle, which could deposit material on the restricted base metal in any direction, was manipulated by the controller. The torch was maintained in a vertical position, perpendicular to the deposition route. Before the programme began, shielding gas was supplied to prevent the material being deposited from coming into contact with ambient gases. The experimental setup is displayed in Fig. 1. By utilising an experimental matrix created by the Box-Behnken design (BBD) utilising the response surface methodology (RSM), single bead deposition was performed on the substrate plate.

Table 1. Experimental conditions

Variables	**Unit**	**Values**
Voltage	V	20; 21; 22
Travel speed	mm/min.	23; 25; 27
GMR	-	1; 5; 9

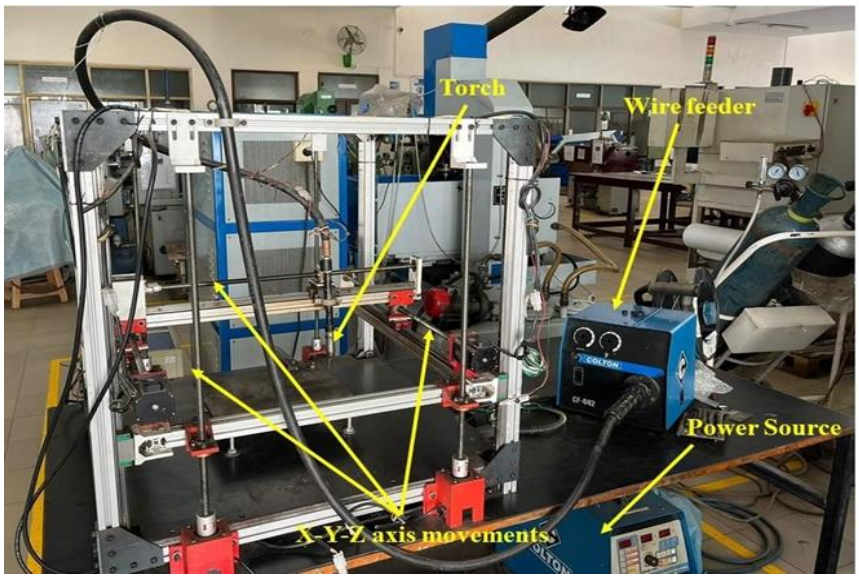

Figure 1. Experimental setup of WAAM

Three input variables were examined in the study: voltage, TS, and wire feed speed. The ratio of CO2 gas to argon is represented by GMR. Over 15 L/h of sustained flow rate were attained. Every bead had the same length, measuring 150 mm (Vora et al., 2022).). Throughout the experiment, a flux core wire with a diameter of 1.2 mm was used in conjunction with a GMAW torch. parameter utilised in the experiment setup is displayed in Table 1.

Table 2. Chemical composition of TM B9

Flux core wire (BM T90)						
Grade	C	Mn	Si	Ni	Cr	Mo
Wt.%	0.25	1.20	0.50	0.80	10.50	1.00
Substrate plate (mild steel 2062)						
Grade	C	Mn	Si	P	S	Fe
Wt.%	0.22	1.50	0.40	0.045	0.045	Balance

By establishing a link between solutions and machining factors, this approach lowers staff expenses and experimentation (Iván Tabernero et al., 2018).After the input variables were altered, nine experiments were produced. To ensure accuracy and reproducibility, each test was done three times. The average outcomes were

then chosen for more examination. Once the input variables were altered, fifteen experiments were produced. To guarantee accuracy and repeatability, each test was run three times. The average results were then analysed.

Testing and Characterizations

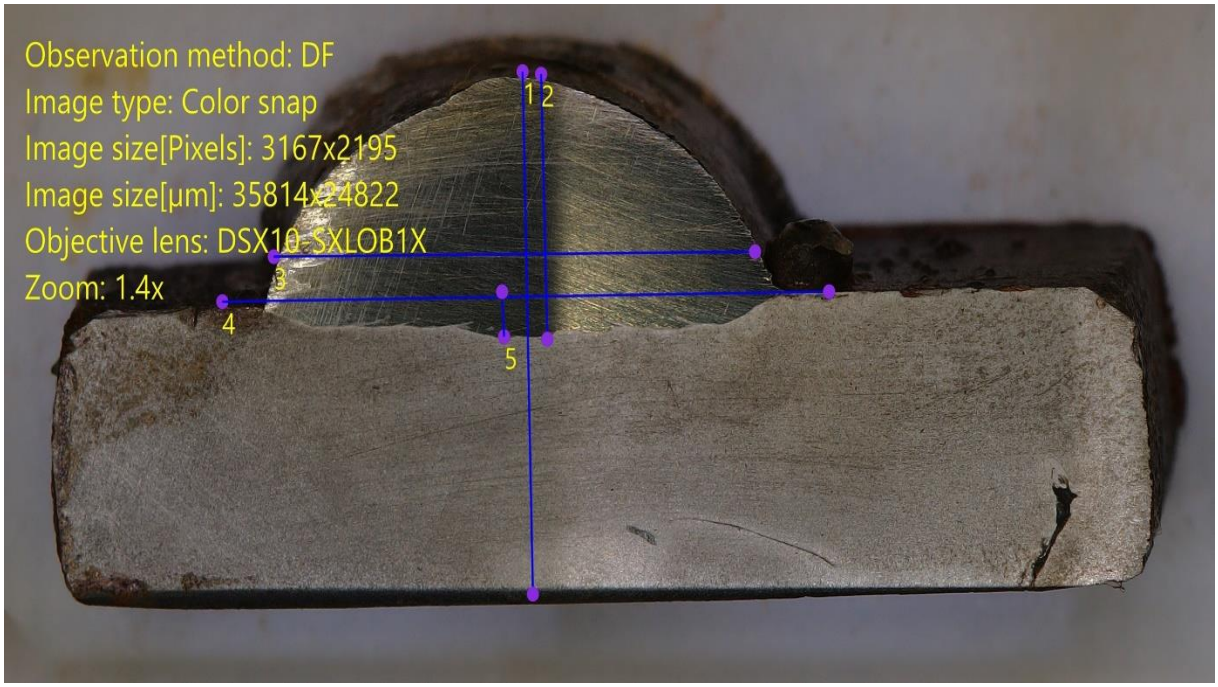

Figure 2. Measurement of output

The current study took into account output metrics such as BH and BW. Small cross-sections of each bead deposition were cut to measure the bead geometries. The band saw machine was used to make the specimens that were used to examine the output variables. All samples were first cleaned and polished with different abrasive sheets before being analyzed. Here, we define various parameters: total height (1), weld bead height (2), weld weight (3), base plate surface (4), and depth of penetration (5). Optical microscopy was utilized to analyse the weld bead height (BH), and weld weight (BW). To ensure precision, three measurements were taken across the cross-section of each deposited bead.

Results and Discussion

Taguchi's L9 array design with WAAM variables and the corresponding results for a subset of replies are shown in Table 3. Utilizing an optical microscope, the response values of BH and BW were examined(Vora et al., 2022). The biggest BH value and the shortest BW value among the nine trials that were performed were 7.41 mm and 8.99 mm, respectively

Table 3. Experiment results

Sr. No	Voltage (V)	GMR	Travel Speed (mm/min)	BH (mm)	BW (mm)
1	20	1	23	7.41	6.92
2	20	5	25	5.89	6.39
3	20	9	27	5.11	5.90
4	21	1	25	5.72	7.93
5	21	5	27	4.97	7.36
6	21	9	23	7.61	7.21
7	22	1	27	4.03	8.99
8	22	5	23	6.34	8.62
9	22	9	25	5.28	8.41

Table 4. ANOVA for BH, and BW

Source	DF	SS	MS	F	P	Significance
For BH						
Regression	3	10.1476	3.3825	28.56	0.001	Significant
TS	1	1.2696	1.2696	10.72	0.022	Significant
Voltage	1	0.1176	0.1176	0.99	0.365	Insignificant
GMR	1	8.7604	8.7604	73.97	0.000	Significant
Error	5	0.5921	0.1184			
Total	8	10.7398				
R-Sq. = 94.49 %; R-Sq. (Adj.) = 91.18 %						
For BW						
Regression	3	8.6596	2.8865	307.96	0.000	Significant
TS	1	7.7230	7.7230	823.96	0.000	Significant
Voltage	1	0.8956	0.8956	95.56	0.000	Significant
GMR	1	0.0409	0.0409	4.37	0.091	Insignificant
Error	5	0.0468	0.0093			
Total	8	8.7065				
R-Sq. = 99.46 %, R-Sq. (Adj.) = 99.14%						

Analysis of Variance for BH, and BW

Analysis of variance (ANOVA), a statistical approach utilized to ascertain the most significant elements for improving product or process quality, was applied to the findings obtained after Taguchi's array. To analyse the data of the response variables BH and BW, Minitab software was used(Chaudhari et al., 2022). In the regression analysis, a 95% confidence interval was taken into account. Accordingly, to show a significant influence on the chosen output response, the input variable's P-value should not be greater than 0.05. The travel speed (TS) and voltage terms had a considerable influence on the BH response, however, the gas mixture ratio (GMR) had no discernible effect on the output response variable. Changes in the level of TS had a significant impact on BH values, as evidenced by the greatest F-value for TS. All three WAAM factors were significant for the BW response; voltage had the greatest effect, followed by GMR and TS (Dinovitzer et al., 2019). It was discovered that the R^2 values of the BH and BW models were 94.49% and 99.46%, respectively, and that their adjusted R^2 values were 91.18% and 99.14%, respectively.

This indicates that the models effectively validated the whole selected design space. For wire arc additive manufacturing (WAAM) to achieve the required weld properties and overall process performance, the relationship between voltage, gas mixture ratio, and travel speed is essential(Jiang et al., 2022). Voltage and Travel Speed have a reciprocal relationship. As voltage increases, it can compensate for higher travel speeds by supplying more heat. Conversely, reducing voltage may be needed to prevent overheating at slower travel speeds to ensure proper fusion. The Gas Mixture Ratio also impacts arc stability and heat transfer, influencing the ideal voltage and travel speed settings. Adjusting the gas composition may be essential to achieve the desired bead shape, depth of penetration, and overall weld quality. In essence, optimizing the relationship between voltage, travel speed, and gas mixture ratio is vital for consistent and high-quality welds in wire arc additive manufacturing(IvánTabernero et al., 2018). Experimentation, analysis, and fine-tuning of these factors are typically necessary to strike the right balance for specific materials, deposition configurations, and process demands.

Main Effect Plots

Main effect plots have been employed to understand how various parameters in Wire Arc Additive Manufacturing (WAAM) affect the output characteristics. When fabricating thin multi-layered structures, Having maximum BH and minimum BW values is desirable. Figure 3 illustrates the impact of input factors on the BH response. Increasing the voltage tends to decrease the BH value as it leads to a longer arc length. Greater Metal Removal (GMR) doesn't significantly affect BH (Jahns et al., 2023). However, Travel Speed (TS) has the most significant impact on BH; increasing TS levels reduces BH because higher travel speeds don't allow sufficient time for molten metal deposition. Thus, to achieve higher BH values, it's advisable to use a lower voltage level of 20V, a higher GMR level of 9, and a lower TS level of 23 mm/s.

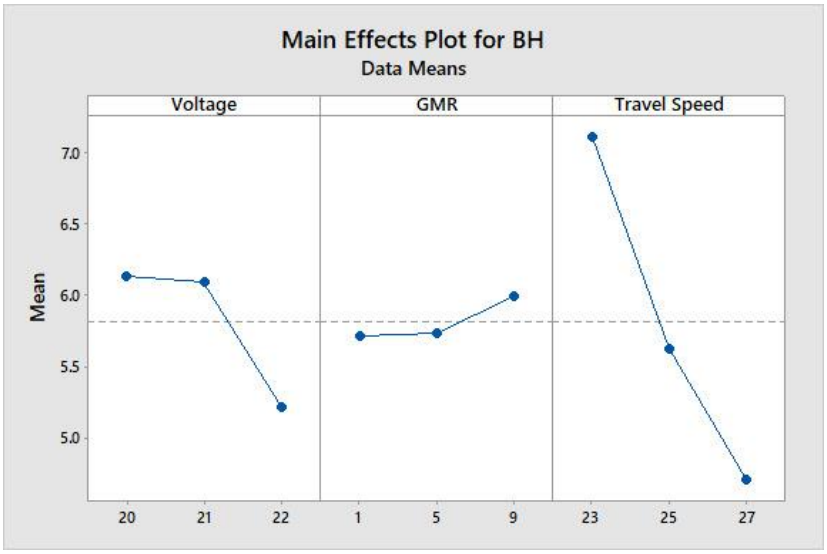

Figure 3. Influence of WAAM factors on BH

Figure 4 shows how different WAAM parameters affect the reaction of the bead width. As the voltage increased from 20 to 22 V, it demonstrated a greater BW response, which was explained by the longer arc length at higher voltages. Increasing Greater Metal Removal (GMR) was found to be beneficial for BW response as it led to a decrease in BW values(Chaudhari et al., 2023). Travel Speed (TS) had minimal impact on BW response; however, slightly decreased BW was observed with higher TS levels due to insufficient time for molten metal deposition at higher travel speeds(IvánTabernero et al., 2018). Thus, to achieve lower BW values, it is recommended to use a lower voltage level of 20V, a higher GMR level of 9, and a lower TS level of 27 mm/s.

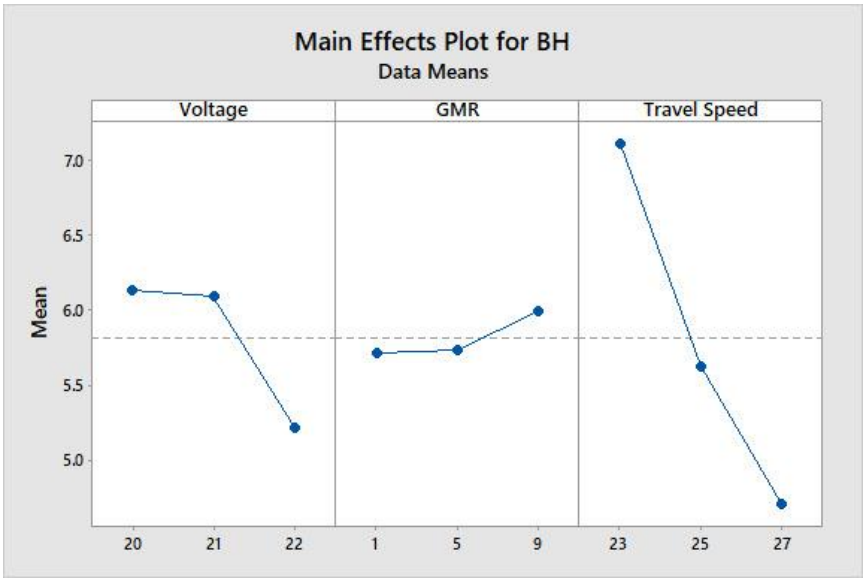

Figure 4. Influence of WAAM factors on BW

Conclusion

The study used TM B9 Flux cored wire with a 1.2 mm diameter to deposit a single bead on a mild steel 2062 substrate plate utilising a GMAW-based (WAAM) process. Bead width and bead height were the output responses of experimental trials that were carried out using Taguchi's L9 technique. The input WAAM variables were voltage, gas mixture ratio (GMR), and travel speed (TS). The biggest BH value and smallest BW value among the nine trials that were performed were 7.61 mm and 5.90 mm, respectively. The ANOVA results indicated that TS was the most important component for BH response, followed by voltage; GMR had no discernible effect on BH response. All three WAAM factors were shown to be significant for the BW response, with voltage having the most impact and GMR and TS following closely behind. To forecast response values

within the specified range of WAAM variables. To understand the effect of WAAM factors on output characteristics, main effect plots were created. It is recommended to use a lower voltage level of 20V, a higher GMR level of 9, and a lower TS level of 24 mm/s to get larger BH values. On the other hand, a lower voltage level of 20V, a higher GMR level of 9, and a lower TS level of 27 mm/s are advised to obtain lower BW values.

Scientific Ethics Declaration

The authors declare that the scientific ethical and legal responsibility of this article published in EPSTEM journal belongs to the authors.

Author Contribution

Mr. Pruthviraj Chauhan: Methodology, Formal analysis, Data curation, Writing original draft, Mr Vatsal Vaghasia:Visualization, Investigation, Formal analysis, Writing-review &editing, Dr. JayKumar Vora: Writing-review & editing, Supervision, Dr. Rakesh Chaudhari: Methodology, Formal analysis, Writing-review & editing, Supervision

Acknowledgement or Notes

* This article was presented as an oral presentation at the International Conference on Basic Sciences, Engineering and Technology (www.icbaset.net) held in Alanya/Turkey on May 02-05, 2024.

* The author, Pruthviraj Chauhan extend their heartfelt appreciation to Pandit Deendayal Energy University for facilitating the resources and conducive atmosphere for their research endeavors. especially grateful to the Mechanical Engineering Department for their indispensable support and counsel throughout this study.

References

Anand, M., Bishwakarma, H., Kumar, N., Ujjwal, K., & Kumar Das, A. (2022). Fabrication of multilayer thin wall by WAAM technique and investigation of its microstructure and mechanical properties. *Materials Today: Proceedings*, *56*, 927–930.

Chaudhari, R., Bhatt, R., Vaghasia, V., Raja, B. D., Patel, V. K., Khanna, S., Vora, J., & Patel, V. V. (2023). A parametric study and experimental investigations of microstructure and mechanical properties of multi-layered structure of metal core wire using wire arc additive manufacturing. *Journal of Advanced Joining Processes*, *8*, 100160.

Chaudhari, R., Parmar, H., Vora, J., & Patel, V. K. (2022). Parametric study and ınvestigations of bead geometries of GMAW-based wire–arc additive manufacturing of 316L stainless steels. *Metals*, *12*(7), 1232.

Dinovitzer, M., Chen, X., Laliberte, J., Huang, X., & Frei, H. (2019). Effect of wire and arc additive manufacturing (WAAM) process parameters on bead geometry and microstructure. *Additive Manufacturing*, *26*, 138–146.

Jahns, H., Unglaub, J., Muller, J., Hensel, J., & Thiele, K. (2023). Material behavior of high-strength low-alloy steel (HSLA) WAAM walls in construction. *Metals*, *13*(3), 589.

Jiang, B., Huang, J., Ma, H., Zhao, H., & Ji, H. (2022). Multi-objective optimization of process parameters in 6016 aluminum alloy hot stamping using Taguchi-Grey relational analysis. *Materials*, *15*(23), 8350.

Paskual, A., Álvarez, P., & Suárez, A. (2018). Study on Arc welding processes for high deposition rate additive manufacturing. *Procedia Cirp*, *68*, 358–362.

Raut, L. P., & Taiwade, R. V. (2021). Wire Arc Additive Manufacturing: A Comprehensive review and research directions. *Journal of Materials Engineering and Performance*, *30*(7), 4768–4791.

Rodrigues, T. A., Duarte, V. R., Tomás, D., Avila, J. A., Escobar, J. D., Rossinyol, E., Schell, N., Santos, T. G., & Oliveira, J. P. (2020). In-situ strengthening of a high strength low alloy steel during Wire and arc additive manufacturing (WAAM). *Additive Manufacturing*, *34*, 101200.

Shah, A., Aliyev, R., Zeidler, H., & Krinke, S. (2023). A Review of the recent developments and challenges in wire arc additive manufacturing (WAAM) process. *Journal of Manufacturing and Materials Processing*, *7*(3), 97.

Suat, Y., Koc, B., & Yilmaz, O. (2020). Building strategy effect on mechanical properties of high strength low alloy steel in wire + arc additive manufacturing. *Zavarivanje i Zavarene Konstrukcije*, *65*(3), 125–136.

Prakash, A., & Kore, S. D. (2024). Mechanical, metallurgical, and corrosion investigations on wire arc additively manufactured low carbon steel. *Journal of Adhesion Science and Technology*, 1–29.

Treutler, K., Gehling, T., Scheck, M., Richter, A., Bohn, C., Ehlers, R., Rembe, C., & Wesling, V. (2024). Properties oriented WAAM—microstructural and geometrical control in WAAM of low-alloy steel. *Welding in the World*, *68*(2), 247–257.

Vora, J., Parikh, N., Chaudhari, R., Patel, V. K., Paramar, H., Pimenov, D. Y., & Giasin, K. (2022). Optimization of bead morphology for GMAW-based wire-arc additive manufacturing of 2.25 Cr-1.0 mo steel using metal-cored wires. *Applied Sciences*, *12*(10), 5060.

Zhou, Y., Lin, X., Kang, N., Huang, W., Wang, J., & Wang, Z. (2020). Influence of travel speed on microstructure and mechanical properties of wire + arc additively manufactured 2219 aluminum alloy. *Journal of Materials Science & Technology*, *37*, 143–153.

Author Information

Pruthviraj Chauhan
Pandit Deendayal Energy University, Gandhinagar, India 382007
Contact e-mail: *pruthvi.chauhan108@gmail.com*

Rakesh Chaudhari
Pandit Deendayal Energy University, Gandhinagar, India 382007

Vatsal Vaghasia
Pandit Deendayal Energy University, Gandhinagar, India 382007

Jay Vora
Pandit Deendayal Energy University, Gandhinagar, India 382007

To cite this article:

Chauhan, P., Vaghasia, V., Chaudhari, R., & Vora, J. (2024). Experimental investigations on the fabrication of low alloy steels using wire arc additive method. *The Eurasia Proceedings of Science, Technology, Engineering &Mathematics (EPSTEM), 28,* 484-491.

The Eurasia Proceedings of Science, Technology, Engineering & Mathematics (EPSTEM)
ISSN: 2602-3199

The Eurasia Proceedings of Science, Technology, Engineering & Mathematics (EPSTEM), 2024

Volume 28, Pages 492-501

ICBASET 2024: International Conference on Basic Sciences, Engineering and Technology

Physicochemical, Morphological and Anticorrosive Properties of Electrodeposited ZnNi Alloy Coating

Baya Benfedda
Mouloud Mammeri University of Tizi- Ouzou

Salem Boudinar
Mouloud Mammeri University of Tizi -Ouzou

Zaina Mezine
Research Centre in Semiconductors Technology for Energetic

Abstract: Corrosion in its many forms is a major problem for many types of materials, extending from machining to manufacturing and daily use. In fact, it affects practically all engineering projects, from the biggest to the smallest: energy production, construction, transport, medical sector, electronics, etc. Consequently, corrosion generates both economic and environmental problems. To prevent corrosion and preserve materials' durability, several protection methods can be applied. These included protection by applying a coating on the metal surface. In this context, Zinc based alloy coatings have attracted much interesting scientific community because of their excellent mechanical and anti-corrosive properties. In the present work, ZnNi coatings were electrodeposited on steel substrates using a chloride bath containing ammonium salts. The effect of some experimental parameters, namely, potential and metal ion concentration ratio on the deposition kinetics of ZnNi system as well as on its physicochemical, morphological and anticorrosive properties has been investigated. For this purpose, an appropriate experimental work was performed by using both electrochemical (cyclic voltammetry, chronoamperometry, open circuit potential, potentiodynamic polarization) and non-electrochemical (SEM-EDX) analysis methods. Based on the obtained results, it has been revealed that simultaneous codeposition of both elements Zn and Ni is possible in our experimental conditions. However, deposition kinetics exhibited a strong dependence on explored parameters. Also, morphological aspect and chemical composition of deposits are strongly influenced by metal ion concentration ratio. Investigation of corrosion behaviour confirms the protective effect of coatings acted as a sacrificial anode. Furthermore, increasing Ni content in the deposits induces a significant enhancement in corrosion resistance. Thus, Zn-Ni alloy coatings prepared from the Ni(II)-rich bath exhibited better corrosion resistance.

Keywords: Corrosion, Steel, ZnNi alloy coating, Electrodeposition

Introduction

Nowadays, corrosion phenomena have taken a considerable importance due to the increasing use of metals and alloys in modern life. It is considered to be a major source of metal structures and industrial equipments failure. From an economic viewpoint, the corrosion consequences are quite heavy and may even be disastrous (Chevalier,2010). These include: work and manufacturing interruptions, higher maintenance costs, risk of injury or accident to personnel, environmental contamination (Rodriguez, 2021). To prevent corrosion and reduce damage, various protection methods have been developed, including application of coatings, cathodic protection, and inhibition protection, etc (Venkatesha, 2008).

Steel substrates are generally protected against corrosion by a sacrificial electrodeposited coating. Zinc-based alloys and cadmium coatings (Lin & Sriraman 2006), are some of the most commonly sacrificial coatings. Cadmium coatings are considered highly reliable due to their excellent corrosion resistance and engineering properties (Bashkov, 2005). However, they are highly toxic. So, their manufacturing processes require cyanide baths, which are also characterised by their high toxicity. Furthermore, cadmium plating induces a significant amount of hydrogen into the substrate which causes its weakening. In recent years, increasing environmental and ecological preoccupations requires the development of an alternative coating that can efficiently substitute cadmium. In this context, zinc deposits show excellent sacrificial behaviour (Pistofidis,2006). However, their application remains limited in the automotive industry because of their high dissolution rate and poor mechanical properties (Tomic, 2023)

To this end, the development of zinc-based alloys is a highly attractive strategy for enhancing pure zinc coatings' protective properties (Silva, 2010). This is therefore based on addition of some elements to zinc matrix, which can form a very wide range of metallic combinations of ZnX type, such as ZnCo (Bhat, 2022), ZnCu (Oulmas, 2019), ZnFe (Ebrahimi, 2003), ZnMn (Bedir, & Fashu, 2015). Among these coatings, ZnNi alloy appears to be a potential candidate due to its viability as an alternative to cadmium coatings. To this end, Zn-Ni alloys containing 15 to 20% weight of nickel exhibited a very high corrosion resistance compared to cadmium and titanium coatings.

Such coating is widely applied in the aerospace and energy production fields due to its excellent resistance at high temperatures and even under severe oxidation conditions (Abou-Krisha, 2007). In recent years, an extended research activity is focused on the electrodeposition and characterisation of ZnNi alloy coatings (Pedroza,2014), The goal is to optimise deposition parameters in order to develop new coatings which provide increasingly enhanced anticorrosion properties (Roventi, 2015).

This work is situated in this context of ideas. In particular, this study focuses on the electrodeposition of ZnNi alloy coatings from a chloride bath containing ammonium salts. The effect of some experimental parameters, such as potential and Ni^{2+} ion concentration on deposition kinetics of ZnNi alloys coatings, physicochemical properties, surface morphology and corrosion behavior were investigated.

Method

Electroplating Kinetic

The electrochemical experiments were carried out in a conventional three-electrode cell. A vitreous carbon rotating disk electrode (RDE) (0.2 cm^2) with a rotation speed fixed at 250 rpm was used as working electrode to investigate the kinetic of ZnMn electrodeposition. The counter electrode was a platinum wire immersed in a separate compartment containing solution without electroactive metallic cations. All potential values were measured with respect to a saturated calomel reference electrode $Hg/Hg_2Cl_2/Cl^-$ (SCE). All experiments were performed at ambient temperature in an aerated chloride bath containing ammonium chloride. The latter improves bath conductivity and also complexes metal cations (Zn^{2+} and Ni^{2+}), this avoids the formation of hydroxides during ZnNi electroplating. To carry out this work, three baths were used, which are differentiated by the metal ion concentration ratio, their compositions are shown in Table 1. The pH was adjusted to 2 by adding dilute hydrochloric acid solution. The solutions were prepared immediately prior to each experiment.

Table 1. The composition of electroplating baths

Bath	Ratio $[Ni^{2+}]/[Zn^{2+}]$	Species	Concentration (mol/l)
1	0.66	$NiCl_2$, H_2O	0.2
		$ZnCl_2$, 6 H_2O	0.3
		NH_4Cl	2.8
2	1	$NiCl_2$, H_2O	0.3
		$ZnCl_2$, 6 H_2O	0.3
		NH_4Cl	2.8
3	1.5	$NiCl_2$, H_2O	0.45
		$ZnCl_2$, 6 H_2O	0.3
		NH_4Cl	2.8

Preparation of Steel Substrates and Elaboration of ZnNi Coatings

Steel substrates with area of 1 cm^2 were used to elaborate Zn-Ni alloy coating. Prior to each experiment, steel substrates were polished mechanically with a METKON FORCIMAT polishing machine equipped with a rotating disk using abrasive paper with various granulometry (400, 600, 800, 1000, 2000, 4000) and then lustrated on a diamond-paste impregnated felt with different grains size (9 µm, 3 µm and 1 µm). Then, they were degreased with ethanol for 10 minutes using ultrasound. Finally, rinsed with distilled water and dried.

Corrosion Test Solutions

Corrosion behaviour of ZnNi alloy coatings was studied in 3% weight of NaCl solution

Characterizations Techniques

The electrochemical measurements were performed using an EG&G 273A Potentiostat/Galvanostat controlled by a microcomputer via GPIB interface operated by M352 EG&G software. Cyclic voltammetry was used to study deposition kinetics and chronoamperometry was employed to prepare ZnNi samples. The anti-corrosion properties of ZnNi coatings were evaluated by using various electrochemical methods, such as open circuit potential (OCP), linear polarization and Tafel curves.

The morphological properties of ZnNi alloy coatings were studied by scanning electron microscope (ESEM XL 30 Philips).The chemical compositions were measured by SEM-JEOL JSM-7610 scanning electron microscope coupled with X-ray microanalysis (EDX).

Results and Discussion

Electrochemical Study

Electrodeposition of Zn and Ni

Before investigating the electrochemical deposition kinetics of ZnNi, a voltammetric study of deposition kinetics for each element was performed separately. Figure 1.a shows the cyclic voltammograms recorded on a vtreous carbon electrode RDE from a zinc chloride bath ($[ZnCl_2]$ = 0,3 mol/l , $[NH_4Cl]$ = 2,8 mol/l , pH = 2). The results show a cathodic current starting at -1.08 V vs. SCE, it is attributed to the reduction of Zn^{2+} ions.(zinc metal deposit). By scanning toward more cathodic potential, an increase in current density is observed, suggesting the proton reduction (evolution of hydrogen) (Fashu, 2015).

So, the reduction current density increases with the potential, this indicates an increase of the deposit rate. In the reverse scan, one dissolution peak is observed at -1 V vs. SCE. It corresponds to zinc dissolution. This peak becomes more extensive and intense as the applied cathodic potential increases. This can be explained by a considerable increase in the amount of zinc deposited.

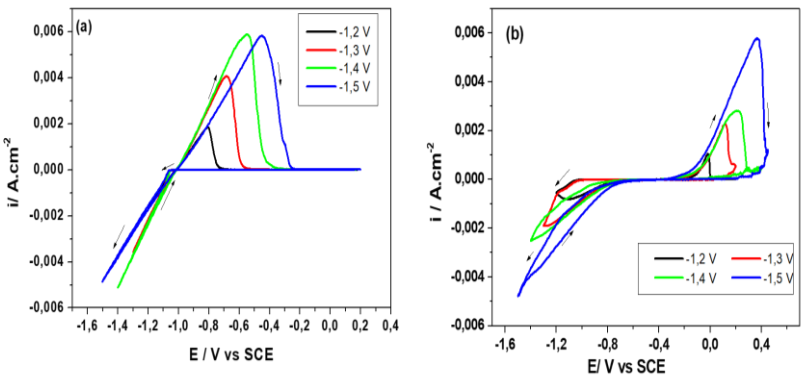

Figure 1. Cyclic voltammograms obtained on vitreous carbon RDE at various cathodic limit potentials, pH = 2, V_b = 20 mV/s, w = 250 rpm, (a) zinc voltammograms, (b) Ni voltammograms

The electrochemical study of nickel deposition kinetics from a nickel chloride bath ($[NiCl_2]$ = 0,3 mol/l , $[NH_4Cl]$ = 2,8 mol/l , pH = 2) was also performed on a vitreous carbon electrode RDE. Figure 1.b illustrates the cyclic voltammograms obtained at several cathodic limit potential. All recorded cyclic voltamperomograms show a cathodic current at -0.85 vs. SCE which corresponds to the Ni^{2+} reduction (formation of the nickel deposit). At more cathodic potentials, a strong increase in current density is noted, which can be explained by the appearance of hydrogen evolution, that occurs simultaneously with nickel deposition. In the anodic region of voltammograms, a quite symmetrical peak is observed around -0.3 vs. SCE, which is attributed to nickel dissolution. its intensity increases as the cathodic potential increases. This result is related to an increase in deposition rate and corroborates our discussions during cathodic scanning. Such results have been widely reported in the literature (Abou-Krisha, 2007).

Electrodeposition of ZnNi Alloys Coating

In order to study the effect of both potential and Ni^{2+} ion concentration on ZnNi electroplating, cyclic voltammetry analysis was performed at various Ni^{2+} ion concentrations and potentials by applying the same parameters (V_b = 20 $mV.s^{-1}$, w = 250 rpm). The results were shown in Figure 2. As we can see on Figure 2, the voltammograms curves have a similar pattern, where we observe a significant evolution of both anodic and cathodic processes as a function of the imposed potential. Indeed, in all recorded voltammogram curves, the reduction current density increases as the applied potential increases. Also, the dissolution peak intensities showed a similar behaviour, i.e. the anodic peak intensity increased with rising cathodic potential. In addition, all plots show several peaks, suggesting the presence of several phases in the alloys as deposited during cathodic scanning. Such a result suggests that the chemical composition of alloys changes with cathodic potential as well as Ni^{2+} concentration. The presence of such peaks confirms the simultaneous co-deposition of zinc and nickel. It is important to note that the anodic peak for pur zinc dissolution was higher compared to the ZnNi alloy dissolution (Fig.1.a). Several hypotheses can be proposed for this behaviour. It may be due to the small amount of zinc deposited in the alloy compared with pur metal, or it may be attributed to the adsorption phenomenon, which remains competitive between different electroactive species (Zn^{2+} and Ni^{2+}). It can also be associated to the formation of some phases with nickel (Shams, 2018) Based on these results, it is clear that formation of ZnNi alloys with different compositions is achievable in our experimental conditions. It is also important to note that the shape of anodic peaks strongly changes with Ni^{2+} ion concentration.

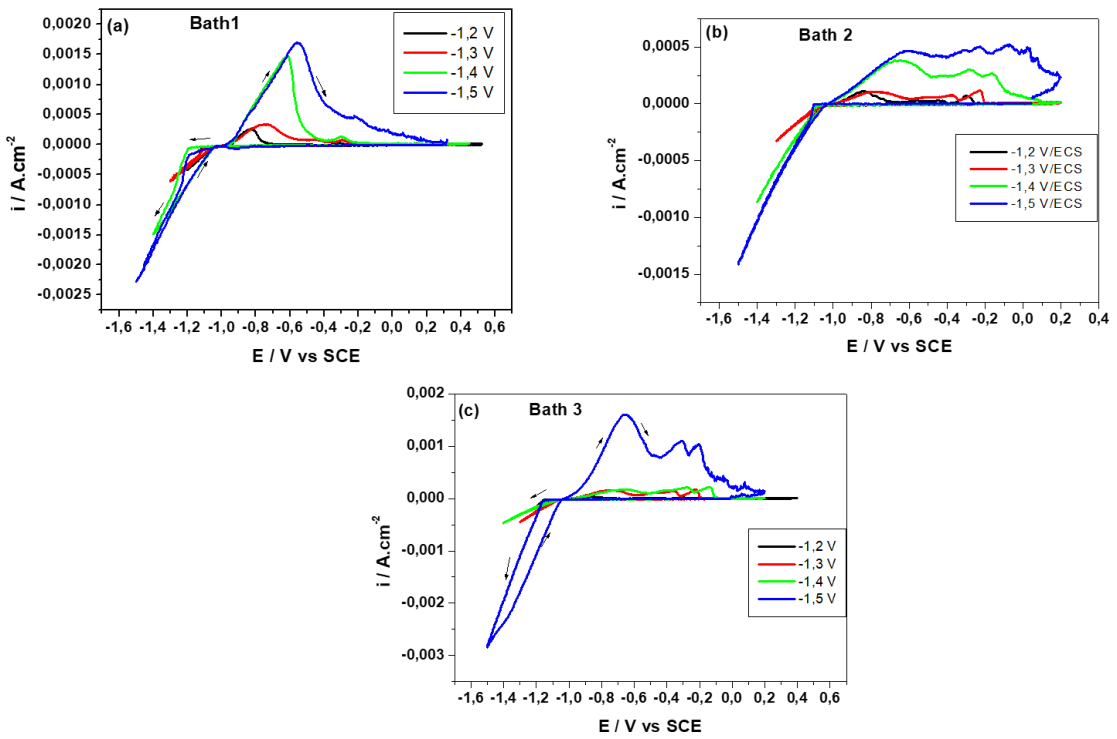

Figure 2. Cyclic voltammograms for ZnNi alloys deposition on vitreous carbon RDE at various Ni^{2+} concentration and cathodic limit potentials, (a) $[Ni^{2+}]$ = , (b) $[Ni^{2+}]$ = , (c) $[Ni^{2+}]$ = , pH = 2, Vb = 20 mV/s, w = 250 rpm

In the case of bath 1 with a concentration ratio ($\frac{[Ni^{2+}]}{[Zn^{2}]}$ = 0.66), we can see the emergence of a quite broad peak that is more pronounced around -1 V. It is attributed to zinc-rich phase compared with the kinetic study discussed of each element separately. In bath 2 (concentration ratio = 1), anodic peaks obtained at different potentials are flattened and not very symmetrical. They are attributed to ZnNi phases dissolution. As a result, their intensity remains similar and comparable, this may be due to the coexistence of several ZnNi phases with similar compositions. In such conditions, it is possible to consider the formation of the δ-ZnNi and γ-ZnNi phases, which has already been reported in the literature (Ghaziof, 2014)

For bath 3, with a concentration ratio of 2 , for potentials (-1,2, -1,3 et -1,4 vs. SCE), the anodic peaks are not changing with the imposed potentials. In this case, all peaks have a very flattened shape and low intensity, indicating the dissolution of different ZnNi phases. However, at the more cathodic potential (-1.5 V vs. SCE), a quite symmetrical anodic peaks were observed on the voltammogram. The first one is observed around the pure zinc potential and is more intense than the others. It is therefore attributed to the dissolution of a zinc-rich phase. Two other peaks, with low intensity compared to the first one, are located respectively at -0.42 and -0.27 V vs. SCE, which are quite close to the pure nickel dissolution potential. Obviously, these peaks can be attributed to ZnNi phases dissolution, which are probably rich in nickel.

Also, as we can see on the voltammogram, the peak intensities corresponding to zinc-rich phases are quite high compared with those of Ni-rich phases. This behaviour can be explained by the anomalous co-deposition phenomena, which means that the less noble metal is deposited preferentially compared to the noble metal. This phenomena has been widely reported and discussed in several research works related to ZnNi electroplating (Abou-Krisha,2007).

Current Efficiency of ZnNi Deposit

Based on the results as previously described, we can estimate the current efficiency of ZnNi deposited in each bath as a function of the applied cathodic potentials (figure 3). As shown in Figure 3, ZnNi current efficiency show almost identical evolution in all baths. In fact, deposition current efficiency increases as the potential becomes more cathodic. As a result, hydrogen evolution seems to be minimized under these conditions. These results clearly demonstrate the behaviour observed in the previously described voltammetric analysis, where a significant increase in anodic peak intensity was observed in all registered voltammograms. It is important to note that the current efficiency is strongly dependent on the Ni^{2+} ion concentration; the highest efficiencies were obtained for coatings produced from bath 2. In summary, ZnNi coatings obtained in different baths at highly cathodic potentials displayed a very considerable current efficiencies with an average value estimated at 80.8%.

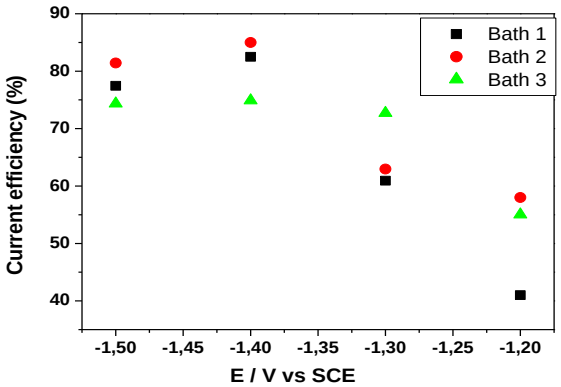

Figure 3. ZnNi current efficiency vs cathodic limit potentieals and different Ni^{2+} concentrations bath 1-[Ni^{2+}] = 0,2 mol/l , bath 2- [Ni^{2+}] = 0,3 mol/l , bath 3 - [Ni^{2+}] = 0,45 mol/l

Chronoamperometric Analysis

The obtained results from the previous sequence have allowed us to define the deposition parameters of ZnNi system and to confirm that ZnNi alloy deposition is possible in our experimental conditions. In this section, we will elaborate a series of ZnNi samples on steel substrates, from different baths (bath 1, bath 2, bath 3) with respectively Ni^{2+}/Zn^{2+} concentration ratios (0.66, 1 and 1.5) at -1.3V and -1,4 V vs. SCE during 600 s. The

chronoammograms shown in figure 4 have almost the same shape and similar evolution. However it should be noted that measured current density changes with both potential and Ni^{2+} ion concentration. Indeed, current density in increased with increasing cathodic potential. This can be attributed to an increase of deposition rate, which probably induces a significant increase in the amount of deposit. It is important to note that the recorded current densities in bath 2 are much higher than those obtained from other baths. This correlates perfectly with our previous hypotheses as described from voltammetric analysis.

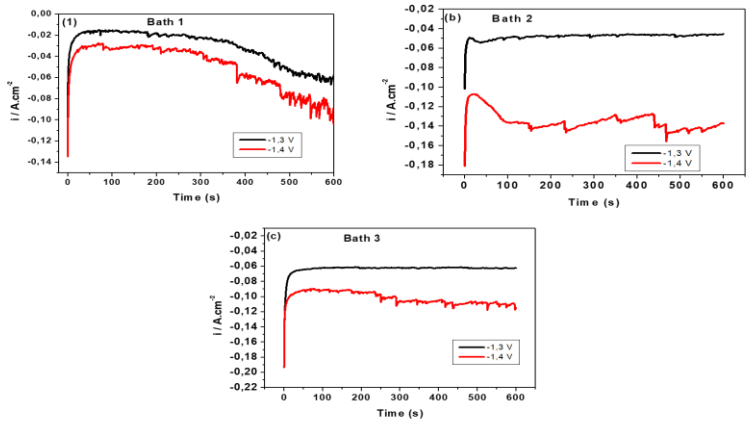

Figure 4. Current–time transients for ZnNi alloys coating deposited on steel substrate in différents baths and at various imposed potentials, pH = 2, t = 600 s, (a) bath 1, (b) bath 2, (c) bath 3

Surface Morphology of ZnNi Alloy Coatings

SEM micrographs of ZnNi alloy coatings produced from different baths at -1.3 V vs. SCE during 600 s are illustrated in Figure 5. As can be seen on Figure 5, the surface morphology of ZnNi coatings is stronbly dependend on the Ni^{2+} ion concentration in the electroplating bath. In the case of bath 1 (Figure 5.a), where the Ni(II) concentration is lower than that of zinc, the observed morphology is granular, and the coating consists of uniformly distributed grains as a background and some cauliflower-like microstructures growing on the surface of the deposit. According to some authors, the appearance of the cauliflower like morphology in the deposit suggests the formation of a nickel-rich ZnNi phase In addition, the presence of certain cavities (hollow shapes) in the deposit can be attributed to specific preferential sites of hydrogen evolution (Fashu, 2015)

Deposits formed from bath 2 with a concentration ratio = 1 (figure 5.b) , have a similar morphological aspect compared to bath 1 (figure 5.a), but there is a difference in grain size. In fact, the deposit exhibits a strong coalescence between grains, which have a tendency to form very fine cauliflower-like microstructures, which is uniformly distributed on the substrate surface. In this case, the coating is very compact with excellent coverage. In addition, some clear regions are uniformly distributed on the surface of deposit, this suggests the formation of different ZnNi phases with similar proportions.

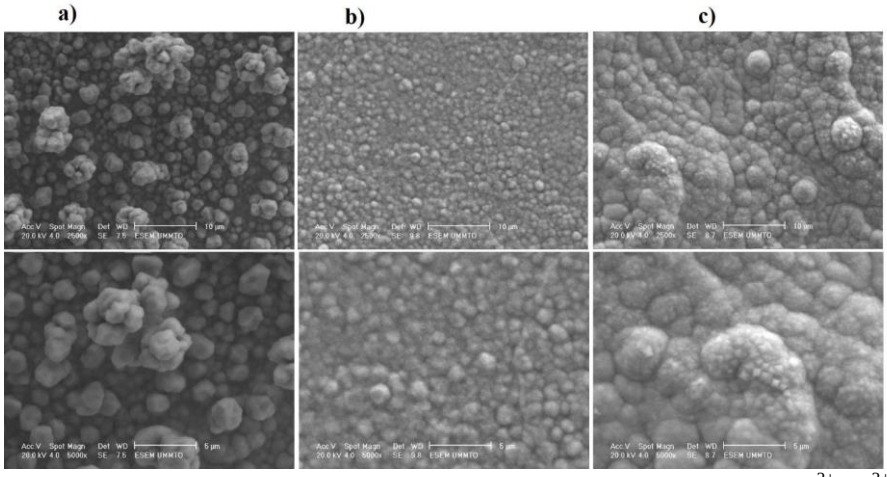

Figure 5. SEM Images of ZnNi alloys coating deposited on steel substrate at different Ni^{2+}/Zn^{2+} ion ratio in the bath , (a) bath 1 (ratio = 0,66), (b) bath 2 (ratio = 1), (c) bath 3 (ratio =) E = 1,3V vs SCE, pH = 2, t = 600 s

In the case of deposits obtained from bath 3 (concentration ratio = 1.5) figure 5.c, we can observe that the morphology is quite different from that observed in other baths (figure 5.a and figure 5.b). It consist of a fine pyramid-grains morphology. Globally, the deposit is compact but less homogeneous, with some areas highly agglomerated forming bumps with different sizes, which confers to the deposit a heterogeneous aspect. Such behavior can be explained by adsorption phenomena, which becomes competitive between H^+ and Ni^{2+} ions, leading a discontinuity in the deposit. Also, the presence of certain cracks in the coating is due to hydrogen evolution, which seems to be important in these conditions.

EDX Chemical Composition of Coating

In this work, we also performed a chemical composition analysis of ZnNi alloy coatings prepared in different baths at -1.3 vs. SCE. Figure 6 shows the obtained EDX spectra. As we can see on figure 6, all spectra show a characteristic peak of zinc and nickel. This confirms the simultaneous co-deposition of both zinc and nickel during ZnNi alloy coating electroplating. However, we note a difference in the peak intensities. In fact, all the recorded spectra show that the peak of zinc is more intense than the one of nickel, suggesting a high content of Zn in the deposits. Such behavior is probably explained by the anomalous co-deposition phenomena, which is widely discussed in the literature (Abou-Krisha, 2007). In this case, zinc is preferentially deposited compared to nickel. Other peaks with very low intensities are also observed, namely oxygen and carbon peaks. In this sequence, a semi-quantitative chemical composition analysis was also carried out on all deposits described above (Table 2).

It is clear that ZnNi deposits obtained at different Ni^{2+} ion concentrations have a high content of zinc. It should be noted that the content of each element evolves according to Ni^{2+} ions concentration. As a result, increasing the Ni(II) concentration in the bath induces a significant increase in Ni content and a slight rise in zinc content in the deposit.

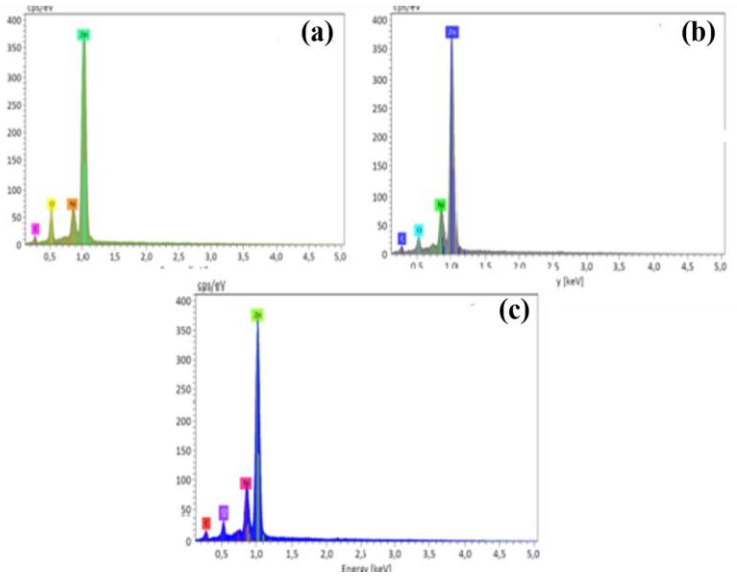

Figure 6. EDX spectra of ZnNi coatings prepared in different baths at -1,3 V vs SCE during 600 s, (a) bath 1, (b) bath 2, (c) bath 3

Table 2. Chemical compositions of ZnNi alloy coatings obtained by EDX analysis, E = -1,3 V vs SCE, t = 600 s

Element content (wt.%)	Zn	Ni	O
Bath 1	78.49	10.11	11,4
Bath 2	80.78	13.45	5,77
Bath 3	78.47	17.36	4,17

It is clear that ZnNi deposits obtained at different Ni^{2+} ion concentrations have a high content of zinc (Table 2). It should be noted that the content of each element evolves according to Ni^{2+} ions concentration. As a result, increasing the Ni(II) concentration in the bath induces a significant increase in Ni content and a slight rise in zinc content in the deposit.

Corrosion Behaviour of ZnNi Alloy Coatings

In this section, we are interested to investigate the corrosion behaviour of ZnNi coatings in a 3 wt.% NaCl solution.

Open Circuit Potential Measurements

Figure 7 shows ocp curves of steel and ZnNi-coated steel obtained from different baths at -1.3 V Vs.SCE. These measurements were performed in an aerated 3% wt NaCl solution during one hour's immersion. As can be seen on Figure 7 , the corrosion potential of coatings is more cathodic compared to the one of steel. This confirms the sacrificial" character of the coating. Also, the plots reveal that the corrosion potential shifts towards noble values as the Ni^{2+} ions concentration increases. This could be due to the increase of Ni content in the deposit. It is important to note that these results are widely reported in the literature (Pedroza, 2014).

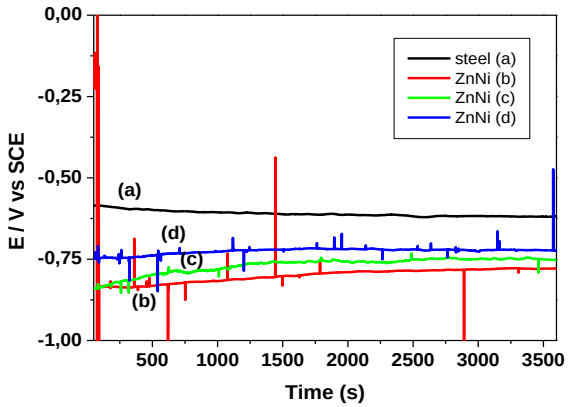

Figure 7. OCP curves of steel and ZnNi alloy coatings prepared from different baths at -1.3 V Vs.SCE after one hour's immersion in a 3% wt. NaCl solution.

Potentiodynamic Polarization Analysis

In order to highlight the electrochemical parameters which characterize corrosion behaviour of ZnNi alloy coatings, we carried out potentiodynamic polarization measurements of ZnNi alloys and steel in a 3% wt. NaCl medium, sweeping the potential of ± 250 mV around corrosion potential at a scan rate of 1 mV/s. The obtained curves are illustrated in figure 8. It is clear that the corrosion behavior of ZnNi alloy coatings is highly dependent on the Ni^{2+} concentration in the bath. it should be noted that the corrosion potential shifted to more positive value as Ni^{2+} ions concentration increased in the electrolytic bath Figure 8 (b, c and d). This can be explained by an increase of Ni content in the deposit, which corroborates the results of EDX analysis. The values of E_{corr} , i_{Corr}, b_a and b_c deduced from the previous curves (Figure 8) are shown in Table 3

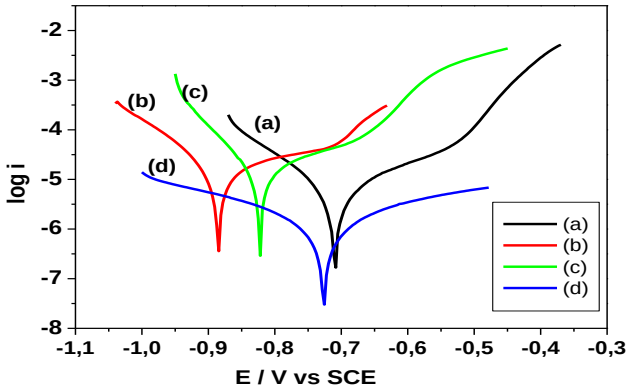

Figure 8. Potentiodynamic polarization curves for the teel and ZnNi alloy coating obtained in diffrent baths at -1,3 V vs. SCE, (a) steel, (b) ZnNi-bath 1, (c) ZnNi-bath2, (d) ZnNi-bath 3, after one hour's immersion in 3% wt. NaCl solution, V_b = 1 mV/s

Table 3. Electrochemical parameters determined from potentiodynamic polarization curves (Fig.8)

Sample	$E_{deposit}$ = -1,3 V vs.SCE			
	E_{corr} / V vs SCE	i_{corr} (A/cm^2)	ba (mV/dec)	bc (mV/dec)
Steel	-0.700	4.57 x10^{-6}	202	-101
ZnNi-bath1	-0.886	1.81 x 10^{-5}	406	-118
ZnNi-bath 2	-0.822	1.44 x 10^{-5}	237	-70
ZnNi-bath 3	-0.725	1.50 x 10^{-6}	392	-321

From the values reported in Table 3, it can be seen that corrosion current density of ZnNi coating decreases as the concentration of Ni^{2+} increases in the bath, which confirms a further increase of Ni content in the deposits. Coatings elaborated in baths 1 and 2 exhibit higher corrosion current densities compared to the pure steel, this suggests that coatings are less resistant than steel, which lends them a protective character as sacrificial anodes.

It is also noticeable from table 3 that the coating prepared in bath 3 has a low current density, which certainly reflects its high corrosion resistance, because it contains a higher Ni content (around 17%) compared to the other coatings. In the light of these results, it is clear that corrosion behaviour of ZnNi alloy coatings is highly dependent on their chemical composition, which can easily be controlled by modifying the metal ion concentration ratio.

Conclusion

In summary, the electrodeposition of ZnNi alloy coatings is quite feasible in our experimental conditions. Nevertheless, the deposition kinetics revealed a strong dependence on potential and ions concentration ratio. Indeed, both valtammogram processes (anodic and cathodic) evolve as a function of the imposed potential and Ni^{2+} concentration. In this case, the corresponding current densities increase with cathodic limit potential. In addition, voltammetric analysis has shown that the shape of anodic peaks changes considerably according to the ions concentration ratio, which due to the formation of several ZnNi phases. It has been revealed that ZnNi coatings obtained from batch 2 exhibited a better morphological aspect compared to those obtained from other baths. The EDX chemical analysis indicated that ZnNi coatings obtained in different baths have a high zinc content and low Ni content, which indicates that the electrodeposition of ZnNi is affected by the anomalous codeposition phenomena. The study of the corrosion behaviour of coatings developed at various Ni^{2+} concentrations has clearly confirmed their protective character as sacrificial anodes. In addition, Increasing Ni^{2+} ions concentration in the bath improved corrosion resistance of ZnNi alloys coating.

Scientific Ethics Declaration

The authors declare that the scientific ethical and legal responsibility of this article published in EPSTEM journal belongs to the authors.

Acknowledgements or Notes

* This article was presented as a poster presentation at the International Conference on Basic Sciences, Engineering and Technology (www.icbaset.net) held in Alanya/Turkey on May 02-05, 2024.

References

Abou-Krisha, M.M., Assaf, F.H., & Toghan, A. A. (2007). Electrodeposition of Zn–Ni alloys from sulfate bath. *Journal of Solid State and Electrochemistry, 11*, 244-252.

Bashkov. N., Petrov, K., & Kovacheva, D. (2005) Influence of the alloying component on the protective ability of some zinc galvanic coatings. *Electrochimica Acta, 51*(1) 77-87.

Bedir, M., Korkmaz, D., Bakkaloglu, O. F., Oztas, M., Karahan, I. H., & Hacıbrahimoglu, M. Y. (2015). Effect of pH values on the characterization of electrodeposited Zn–Mn coatings in chloride-based acidic environment. *International Journal of Electrochemical Science, 10*(6), 4513-4522.

Bhat, R. S., Manjunatha, K. B., Venkatakrishna, K., & Hegde, A. C. (2022). Electrodeposition of Zn–Co coating and its electrochemical performance. *Protection of Metals and Physical Chemistry of Surfaces*, *58*(1), 99-108.

Chevalier, S., (2010). *Cost of corrosion*: A *macro-economic* and *metallurgical approach.* Porquerollesp.7-9.

Ebrahimi, F., & Li, H. (2003). Structure and properties of electrodeposited nanocrystalline FCC Ni-Fe alloys. *Reviews on Advanced Materials Science, 5*(2), 134-138.

Fashu, S., Gu,C. D., Zhang, J. L., Zheng, H., Wang, X. L., & Tu,J. P. (2015). Electrodeposition, morphology, composition, and corrosion performance of Zn-Mn coatings from a deep eutectic solvent. *Journal of Materials Engineering and Performance, 24,* 434-444.

Ghaziof, S., & Gao, W. (2014). Electrodeposition of single gamma phased Zn-Ni alloy coatings from additive-free acidic bath. *Applied Surface Science, 311,* 635-642.

Lin, C. C., & Huang, C. M. (2006). Zinc-nickel alloy coatings electrodeposited by pulse current and their corrosion behavior. *Journal of Coating and Technology, 3*(2), 99-104.

Oulmas, C., Mameri, S., Boughrara, D., Kadri, A., Delhalle, J., Mekhalif, Z., & Benfedda, B. (2019). Comparative study of Cu–Zn coatings electrodeposited from sulphate and chloride baths. *Heliyon, 5*(7), e02058.

Pistofidis, N., Vourlias, G., Konidaris, S., Pavlidou, Stergiou, E. A., & Stergioudis, G. (2006). Microstructure of zinc hot-dip galvanized coatings used for corrosion protection. *Materials Letters,60,* 786-789.

Rodriguez, A. A., Miller, C. M., & Monty, C. N. (2021). Field testing and cost– benefit evaluation of corrosion-protective coatings on winter maintenance equipment in the state of Ohio. *Journal of Cold Regions Engineering, 35*(1), 04020031.

Roventi, G., Cecchini, R., Fabrizi, A., & Bellezze,T. (2015) Electrodeposition of nickel-zinc alloy coatings with high nickel content. *Surface and CoatingsTechnology, 276*, 1-7

Shams, A., Yahui, Z., & Khan, F. (2018). Electrochemical behaviour and analysis of Zn and Zn-Ni alloy anti corrosive coatings deposited from citrate baths. *RSC Advance, 8,* 28861.

Silva, F. L., Lago, G. D., D'Elia, E., & Senna, L.F. (2010). Electrodeposition of Cu-Zn alloy coatings from citrate baths containing benzotriazole and cysteine as additives. *Journal of Applied Electrochemistry, 40* (11), 2013-2022.

Sriraman, K. R., S., Brahimi., J. A., Szpunar, J. H., & Osborne, S. Y.(2013). Characterization of corrosion resistance of electrodeposited Zn-Ni Zn and Cd coatings, *Electrochimica Acta, 105*, 314-323

Tomić, M.V., Mitrović, M.G. (2023). Electrodeposition of Zn-Mn/CeO_2 composite coatings, evaluation of corrosion properties. *Journal of Solid State Electrochemistry, 27,* 1901-1910.

Rajappa, S. K., Venkatesha, T. V., & Praveen, B. M. (2008). Chemical treatment of zinc surface and its corrosion inhibition studies. *Bulletin of Materials Science, 31,* 37-41.

Author Information

Baya Benfedda
Mouloud Mammeri University of Tizi Ouzou, Algeria
Contact e-mail: *baya.mellil@ummto.dz*

Salem Boudinar
Mouloud Mammeri University of Tizi Ouzoui Algeria

Zaina Mezine
Research Centre in Semiconductors Technology for Energetic, Algeria

To cite this article:

Benfedda, B., Boudinar, S., & Mezine, Z. (2024). Physicochemical, morphological and anticorrosive properties of electrodeposited ZnNi alloy coating. *The Eurasia Proceedings of Science, Technology, Engineering & Mathematics (EPSTEM), 28,* 492-501.

The Eurasia Proceedings of Science, Technology, Engineering & Mathematics (EPSTEM)
ISSN: 2602-3199

The Eurasia Proceedings of Science, Technology, Engineering & Mathematics (EPSTEM), 2024

Volume 28, Pages 502-509

ICBASET 2024: International Conference on Basic Sciences, Engineering and Technology

Tin-Based Keggin-Type Phosphomolybdate and Silicomolybdate as Catalysts for the Green Synthesis of Adipic Acid

Lynda Mouheb
Mouloud Mammeri University of Tizi-Ouzou

Leila Dermeche
Mouloud Mammeri University of Tizi-Ouzou

Cherifa Rabia
University of Science and Technlogy Houari Boumediene

Abstract: The catalytic activity of two series of Keggin-type salts of formula $Cs_{4-x}Sn_xSiMo_{12}O_{40}$ (x: 0.5 and 1) and $Cs_{3-x}Sn_xPMo_{12}O_{40}$ (x: 0.25-1) was examined in the liquid phase cyclohexanone oxidation to adipic acid (AA) in the solvent absence. The materials were prepared and characterized by FTIR, UV-Vis and SEM. The adipic acid synthesis was carried out at 90°C in presence of hydrogen peroxide (30%), a green oxidant that produces only water as by-product. The effects of catalyst/substrate molar ratios and time reaction on dipic acid yields were studied. The results of this study showed that the POM-H_2O_2 system was found to be efficient for the production of adipic acid from the oxidation of cyclohexanone and the yields were closely dependent on the operating conditions. The highest AA yield (55%) was obtained with $Cs_2Sn_{0.5}PMo_{12}O_{40}$ using a catalyst/substrate molar ratio of 3.7×10^{-3} and a reaction time of 20h.

Keywords: Adipic acid, Phosphomolybdates, Silicomolybdates, Keggin-type, Cesium-tin salts.

Introduction

In recent decades, the use of Keggin-type polyoxometalates (POMs) as catalysts and photocatalysts in various types of reactions has developed very rapidly (Mizuno et al., 2006). These POMs are composed of a heteropolyanion of the general formula $[XM_{12}O_{40}]^{n-}$, made up of metal oxide groups containing transition metals in high oxidation states (M : W(VI), Mo(VI)... and X : Si(IV), P(V)...) (Pope et al., 1983) and a counter-ion which can be a proton, an organic group, a metal (alkaline, alkaline-earth, transition) and/or a non-metal. Their particularity resides in the structural and electronic characteristics and the acidic (Lewis and/or Bronsted) and redox properties (Mizuno et al., 2009). They also have the advantage of being able to undergo rapid and reversible redox transformations under mild conditions. In addition, the redox and acid properties of POMs can be adjusted according to the heteropolyanion composition and the counter-ion nature, making it possible to develop an effective strategy for a multifunctional catalysis (Mazari et al., 2013; Mouheb et al., 2018).

In this context, we chose to study two series of POMs with compositions $Cs_{4-x}Sn_xSiMo_{12}O_{40}$ (x: 0.5 and 1) and $Cs_{3-x}Sn_xPMo_{12}O_{40}$ (x: 0.25-1). These materials, prepared and characterised by several techniques, were tested in the oxidation of cyclohexanone to adipic acid (C_6 diacid) with the aim of examining the influence of their composition on their catalytic properties.

C_6 diacid is one of the most widely synthesised products in industry. It is mainly used as a precursor in the synthesis of nylon-6, polyamide 6 and other food and cosmetic products. The industrial process uses concentrated nitric acid as oxidant in the oxidation of both cyclohexanone and cyclohexanol, in the presence of

a Cu/V catalyst. In addition to the formation of adipic acid, this process also causes the formation of nitrogen oxides (NOx), in particular nitrous oxide (N_2O), which contributes to the destruction of the ozone layer and the greenhouse effect.

To overcome these drawbacks, several alternatives have been proposed for the adipic acid synthesis. Among these, the POM-H_2O_2 based system appears to be a promising alternative to the industrial process, as it is a non-polluting process. Unlike HNO_3, H_2O_2 produces only water as a by-product.

The POM-H_2O_2 system was first used by Nomiya et al. (1984) in the cyclohexanone oxidation to adipic acid. Many studies have subsequently been based on this system, using POMs of different compositions to improve the yield of adipic acid (Cavani et al., 2011; Idrissou et al., 2018., Tahar et al., 2015; Mazari et al., 2013; Benadji et al.,2013; Mouanni et al., 2018; Mouanni et al., 2019; Mouheb et al., 2018; Moudjahed et al., 2016; Guerroudj et al., 2019; Moudjahed et al., 2022).

Previous research has highlighted the effectiveness of Keggin and Dawson type POMs in the cyclohexanone oxidation to adipic acid, particularly those based on tin, antimony and cobalt. This performance was attributed to the presence of redox couples (Sn(IV)/Sn(II), Sb(V)/Sb(III) and Co(III)/Co(II)) and Mo(VI)/Mo(V), which favour the oxidation-reduction process.

In this work, the catalytic properties of two series of Keggin-type salts of formula $Cs_{4-x}Sn_xSiMo_{12}O_{40}$ (x: 0.5 and 1) and $Cs_{3-x}Sn_xPMo_{12}O_{40}$ (x: 0.25-1) were studied in the liquid phase oxidation of cyclohexanone to adipic acid (AA) at 90°C in the presence of hydrogen peroxide (30%) without solvent, with the aim of examining the effect of the heteroatom (P and Si) on the yield of adipic acid. The materials were prepared and characterised by FTIR, UV-Vis and SEM.

Experimental

Polyoxometalates Synthesis

$H_3PMo_{12}O_{40}.13H_2O$ and $H_4SiPMo_{12}O_{40}.14H_2O$, heteropolyacids, were prepared by the conventional method described in the literature (Copeaux et al.,1909; H. Copeaux et al., 1907; Rocchicioli-Deltcheff et al., 1976; Sanchez et al., 1982).

$Cs_{3-2x}Sn_xPMo_{12}$ (x: 0.25-1) and $Cs_{4-2x}Sn_xSiMo_{12}$ (x: 0.5 and 1), heteropolysalts were synthesized from the, $H_3PMo_{12}O_{40}$ and $H_4SiPMo_{12}O_{40}$ heteropolyacids, respectively, via cation exchange by adding of caesium and tin chlorides according to the stoichiometric coefficients (Eqs. 1 and Eqs. 2), as described in an earlier works (Mouheb et al., 2020).

$$H_3PMo_{12}O_{40} + (3\text{-}2x)\ CsCl + x\ SnCl_2 \rightarrow Cs_{3-2x}Sn_xPMo_{12}O_{40}\downarrow + 3HCl \quad \text{Eq.1}$$

$$H_4SiMo_{12}O_{40} + (4\text{-}2x)\ CsCl + x\ SnCl_2 \rightarrow Cs_{4-2x}Sn_xSiMo_{12}O_{40}\downarrow + 4HCl \quad \text{Eq.2}$$

Characterization

- Infrared spectroscopy was recorded on a Shimadzu IR Afdinity- 1S spectrometer.
- UV–Vis spectra were performed at room temperature on Thermo scientific Evolution 220 spectrometer between 200 and 800 nm.
- The SEM images were recorded on a Philips microscope Environmental ESEM X l30.

Catalytic Test

The liquid-phase oxidation of cyclohexanone was carried out at 90°C using a 100 mL round-bottomed flask under reflux according to method described by Nomiya et al. (Nomiya et al.,1984) as detailed in our previous studies (Mouheb et al., 2018; Mouanni et al., 2019; Mouheb et al.,2020). The catalytic oxidation of the substrate to adipic acid is closely controlled by the POM-H_2O_2 system. Hydrogen peroxide feeds this catalytic system by providing oxygen via the POM, which oxidizes the cyclohexanone to the diacid. The oxidant, H_2O_2, thus enables the POM to regenerate, according to the mechanism illustrated in the scheme in Figure 1.

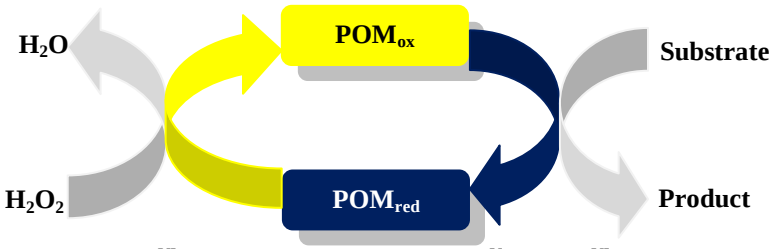

POM_{ox} (Mo^{VI}) + Substrate → POM_{red} (Mo^{V} and Mo^{VI}) + Product

POM_{red} (Mo^{V} and Mo^{VI}) + H_2O_2 → POM_{ox} (Mo^{VI}) + H_2O

Figure 1. Catalytic cyclohexanone oxidation principle in the presence of POM-H_2O_2 system

Keggin-type phosphomolybdates and silicomolybdates have a yellow colour, characteristic of molybdenum in the degree of oxidation (VI). After oxidation of the substrate, the reduced POM takes on a blue colour, characteristic of Mo (V). The addition of hydrogen peroxide drop by drop, each time the POM is reduced, restores the yellow colour of the POM, demonstrating the regeneration of the POM. Visualising the change in the oxidation state of the Mo by the change in colour helps to preserve the efficiency of the POM by maintaining the oxidising properties in each catalytic cycle until the substrate is exhausted. It should be noted that only two Mo (VI) atoms per Keggin anion can undergo reduction at any one time. The resulting homogeneous reaction mixture was cooled to 0°C overnight. Adipic acid (AA), one of the oxidation products, is the only one that can be isolated in the form of white crystals. AA is identified by HPLC chromatography and FTIR spectroscopy (Figure 2) . Its melting point is (~151°C). AA yield was calculated as follows:

AA yield (%) =AA recovered mass × 100 / theoretical AA mass

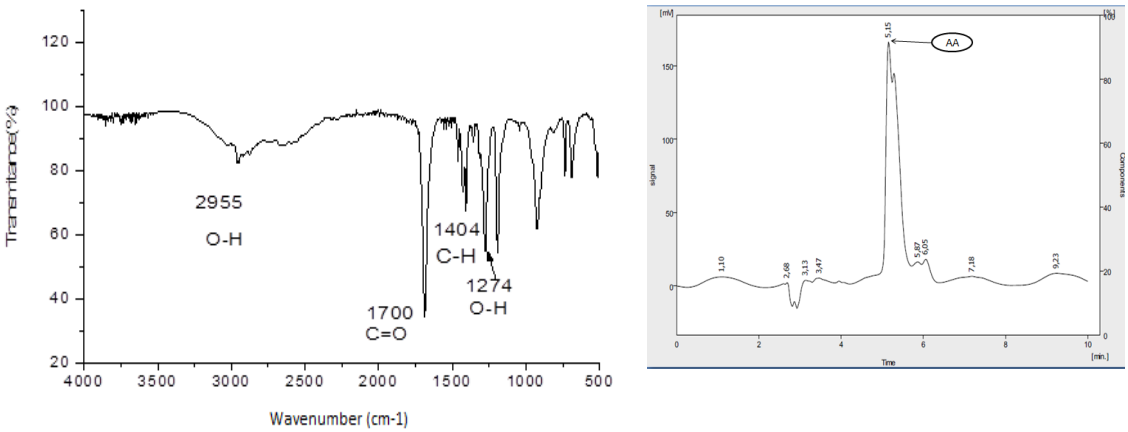

Figure 2. FTIR spectra and HPLC chromatogram of obtained adipic acid

Results and Discussion

Characterization

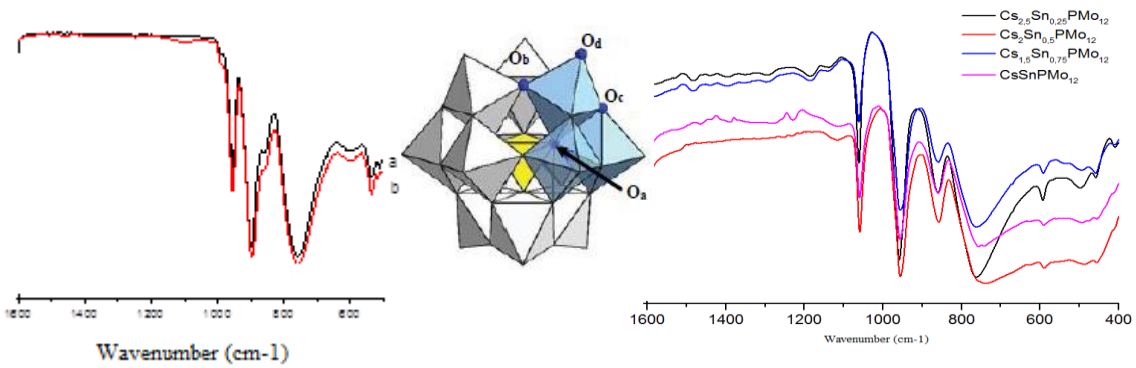

Figure 3. FT-IR spectra of (a): $Cs_2Sn_1SiMo_{12}O_{40}$, (b) $Cs_3Sn_{0,5}SiMo_{12}O_{40}$ and $Cs_{3-2x}Sn_xPMo_{12}O_{40}$ series

FTIR spectra (Figure 3) of prepared POMs have the characteristic vibration bands of the Keggin anion in the 1100-500 cm^{-1} spectral range (Rocchiccioli-Deltcheff et al., 1983) related to 4 oxygen types Oa, Ob, Oc and Od. These bands are located at 1060-1066cm^{-1}, 951-970cm^{-1}, 869-890cm^{-1} and 760-810cm^{-1} corresponding to ν_{as} (P-Oa), ν_{as} (M-Od), ν_{as} (M-Ob-M) and ν_{as} (M-Oc-M) respectively. Nevertheless, silicomolybdic salts (figure 3) $Cs_2Sn_1SiMo_{12}O_{40}$ and $Cs_3Sn_{0.5}SiMo_{12}O_{40,}$ show a weak intensity of the Si-Oa band at around 1000 cm^{-1} and a shoulder at around 850cm^{-1} with shift in the vibration band, as obtained in parent heteropolyacid spectrum. This change in vibration frequency probably corresponds to a symmetry defect in the Keggin anion. The FTIR results showed that the structure of the Keggin anion is not affected by Cs and Sn proton substitution.

The UV-Vis spectra of $H_3PMo_{12}O_{40}$ and $H_4SiMo_{12}O_{40}$ (Figure 4) show a broad metal-oxygen charge transfer (MOCT) band in the 200-500nm region made up of three components linked to the three types of oxygen Ob, Oc and Od of Keggin anion, a UV-Vis spectrum typical of a Keggin structure corresponding to a VI oxidation state of molybdenum. (Guerroudj et al., 2019). In addition to this band, another band around 700nm, attributed to the presence of molybdenum in an oxidation state (V), appears in the UV-Vis spectra of tin-substituted POMs. This result is justified by the dark blue colour of the tin-based salts, characteristic of the presence of Mo (V), in agreement with data from the literature (Dermeche et al., 2009). These results suggest that tin-containing POMs are partially reduced, which can be explained by the exchange of electrons between Sn(II) and Mo(VI) according to the following equation:

$$Sn^{II} + 2\,Mo^{VI} \Leftrightarrow Sn^{IV} + 2\,Mo^{V}$$

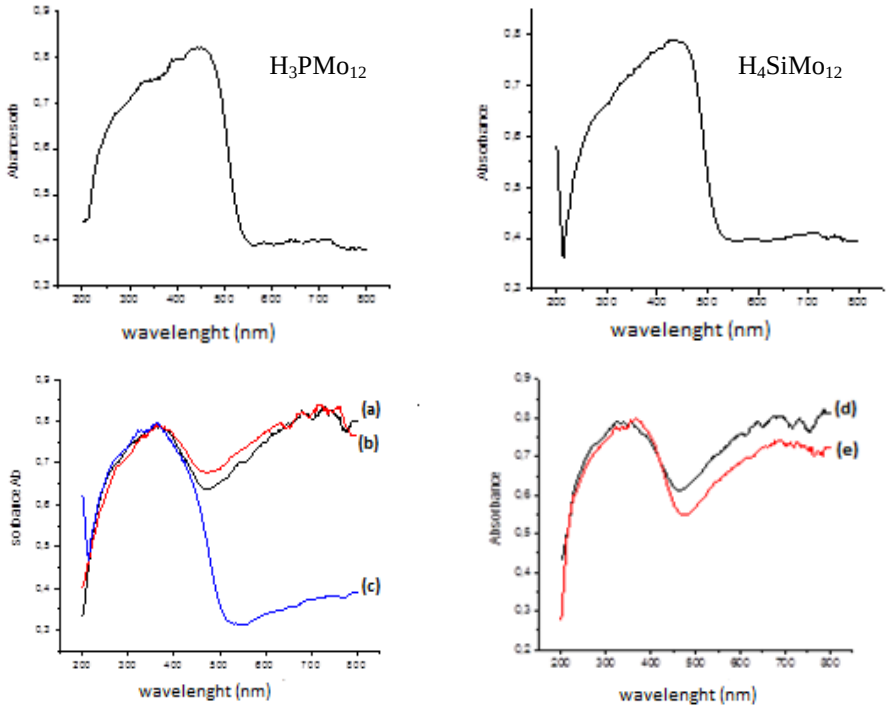

Figure 4. UV-Vis spectra of the two Keggin-type heteropolyacids, (a): $Cs_2Sn_{0.5}PMo_{12}$, (b): $CsSnPMo_{12}$, (c): $Cs_3PMo_{12}O_{40}$, (d): $Cs_3Sn_{0.5}SiMo_{12}$ and (e): $Cs_2SnSiMo_{12}$

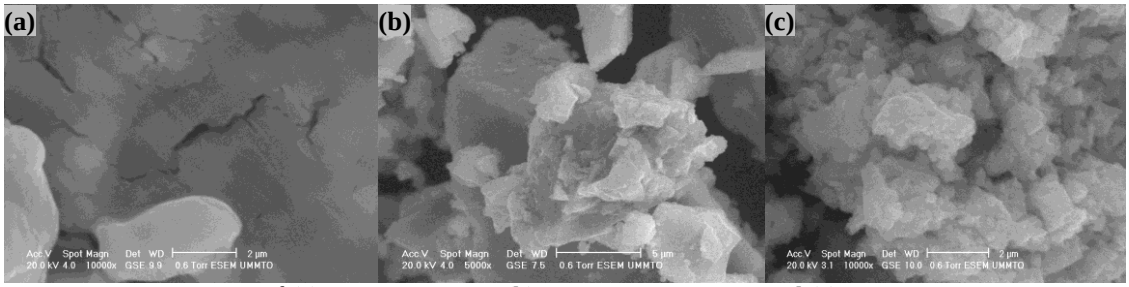

Figure 5. SEM images of (a): H3PMo12O40, (b): Cs1Sn1PMo12O40 and (c) Cs2Sn0,5PMo12O40

In order to compare the morphology of the catalysts, a SEM analysis was performed on $H_3PMo_{12}O_{40}$, $Cs_1Sn_1PMo_{12}$ and $Cs_2Sn_{0,5}PMo_{12}$. SEM images of $H_3PMo_{12}O_{40}$, $Cs_1Sn_1PMo_{12}O_{40}$ and $Cs_2Sn_{0,5}PMo_{12}O_{40}$ show a

POM morphology that is very sensitive to their chemical composition (Figure 5). The tin-based salts show a denser structure composed of small spherical particles compared with the $H_3PMo_{12}O_{40}$ morphology. On the other hand, an increase in the density of spherical particles is observed with increasing Sn content (this is clear from images (b) and (c) in Figure 5).

Cyclohexanone Oxidation

Table 1 displays the obtained AA yields, under the used operating conditions for the cyclohexanone oxidation (catalyst/substrate molar ratio = 10^{-3}), as a function of the chemical composition of the catalyst. The two acids $H_4SiMo_{12}O_{40}$ and $H_3PMo_{12}O_{40}$ have higher AA yields than those obtained with the salts (26 versus 16-24%). Among the salts, $Cs_3Sn_{0.5}SiMo_{12}O_{40}$ and $Cs_2Sn_{0.5}PMo_{12}O_{40}$ are more effective at forming adipic acid than $Cs_1Sn_1PMo_{12}O_{40}$ and $Cs_2Sn_1SiMo_{12}O_{40}$ with AA yields of 23-24 against 16-20%. The AA yield obtained with 0.5 atoms of Sn per Keggin unit, similar to that obtained with the two heteropolyacids, may be explained by the fact that the Bronsted acidity may be equivalent to the Lewis acidity introduced by the SnIV/SnII couple following electron exchange with Mo(VI) (Mouheb et al., 2020).

Table 1. AA yield as a function of chemical composition of catalyst.

Phosphomolybdates			Silycomolybdates		
Catalyst	AA yield (%)	Tf_{AA}*(°C)	Catalyst	AA yield (%)	Tf_{AA}*(°C)
H_3PMo_{12}	26	151	H_4SiMo_{12}	26	148
$Cs_2Sn_{0.5}PMo_{12}$	24	152	$Cs_3Sn_{0.5}SiMo_{12}$	23	152
$Cs_1Sn_1PMo_{12}$	16	151	$Cs_2Sn_1SiMo_{12}$	20	150

Reaction conditions : $n_{catalyst}/n_{-one} = 10^{-3}$; T=90°C ; t=20h ; agitation rate: 1000 rpm, H_2O_2 30%.

On the basis of the previous results (Guerroudj et al., 2019) and in order to improve the efficiency of the catalysts, a study of the variation catalyst/substrate molar ratio was carried out with $Cs_2Sn_{0.5}PMo_{12}O_{40}$ and $Cs_3Sn_{0.5}SiMo_{12}O_{40}$. The results (Figure 6 (A)) reveal that, the AA yield has increased from 16 to 40% and from 11 to 29% when the catalyst/substrate molar ratio increased from 0.50×10^{-3} to 1.83×10^{-3}, in the presence of $Cs_2Sn_{0.5}PMo_{12}O_{40}$ and $Cs_3Sn_{0.5}SiMo_{12}O_{40}$, respectively. This result shows that the cyclohexanone oxidation to adipic acid is very sensitive to catalyst/substrate molar ratio. This is probably due to increase of active sites.

In order to further investigate the influence of the catalyst/substrate molar ratio on AA performance, the best performing catalyst $Cs_2Sn_{0.5}PMo_{12}O_{40}$, was selected to examine this parameter (Figure 6 (B)). The results show a similar AA yield 21 and 27% for extreme ratios 1.0×10^{-3} and 4.7×10^{-3}, respectively and similar AA yield 40-46% for intermediate ratios 1.33×10^{-3} - 2.70×10^{-3}. It should be noted that the highest yield (55%) is obtained with a ratio of 3.70×10^{-3}. It can be seen that the yield of adipic acid is very sensitive to the catalyst/substrate molar ratio.

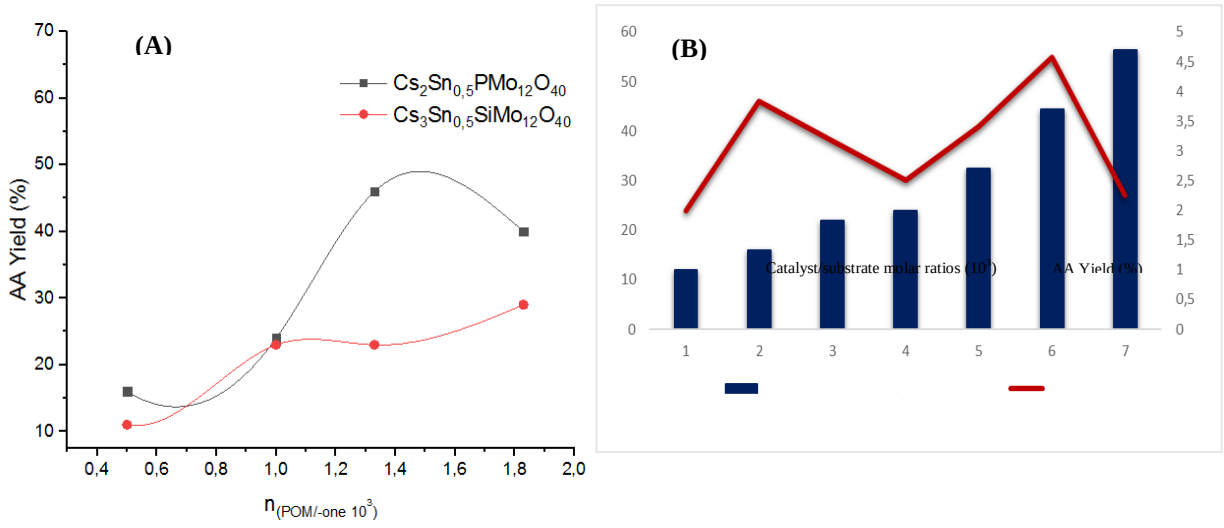

Figure 6. Evolution of AA yield as a function of the catalyst/substrate molar ratio: (A) comparative study between $Cs_2Sn_{0.5}PMo_{12}O_{40}$ and $Cs_2Sn_{0.5}SiMo_{12}O_{40}$. (B) $Cs_2Sn_{0.5}PMo_{12}O_{40}$

Table 2 shows the effect of tin steochiometric coefficient 'x' from the $Cs_{3-2x}Sn_xPMo_{12}O_{40}$ series (x: 0.25-1) on AA yields. The oxidation of cyclohexanone was carried out with an optimised catalyst/cyclohexanone molar ratio of 3.7×10^{-3} .The results show that an increase in tin atoms per Keggin unit from 0.25 to 0.5 led to an increase in AA yield from 31 to 55%. For values of x greater than 0.5, the AA yield decreases from 55% to 40-41% and subsequently appears to be independent of the value of x. These results show that the best formulation for obtaining the highest yield (55%) is $Cs_2Sn_{0,5}PMo_{12}O_{40}$.

Table 2. Adipic acid yields as a function of the Sn atoms number in $Cs_{3-2x}Sn_xPMo_{12}O_{40}$

Catalyst	Adipic acid Yields (%)
$Cs_{2.5}Sn_{0.25}PMo_{12}O_{40}$	31
$Cs_2Sn_{0,5}PMo_{12}O_{40}$	55
$Cs_{1.5}Sn_{0.75}PMo_{12}O_{40}$	40
$CsSnPMo_{12}O_{40}$	41

Reaction conditions: $n_{catalyst}/n_{\text{-one}} = 3.7 \times 10^{-3}$, T°=90°C, agitation rate :1000rpm,H_2O_2 30%.

Figure 7 illustrates the evolution of adipic acid yield as a function of reaction time in the presence of optimized catalyst $Cs_2Sn_{0.5}PMo_{12}O_{40}$ and under optimum conditions. The formation of adipic acid increases with reaction time, so the yield increases from 22 to 55% after 20h of reaction This result suggests that a time of 20 h is necessary to achieve the maximum AA yield, result in agreement with those reported in previous work which demonstrated a conversion of intermediates to adipic acid with time (Mouheb et al.,2020).

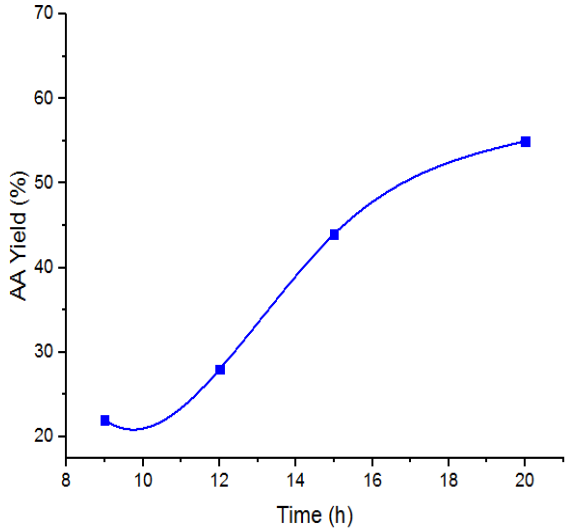

Figure 7. adipic acid yield as a function of reaction time.
Reaction conditions : $n_{catalyst}/n_{\text{-one}} = 3.7 \times 10^{-3}$, T°=90°C, agitation rate :1000rpm,H_2O_2 30%.

Conclusion

The non-soluble salts prepared, $Cs_{4-x}Sn_xSiMo_{12}O_{40}$ (x: 0.5 and 1) and $Cs_{3-x}Sn_xPMo_{12}O_{40}$ (x: 0.25-1) series well-characterised have a Keggin-type structure in a partially reduced state with the simultaneous presence of Mo(VI)/ Mo(V) and Sn(IV)/ Sn(II). Their morphology is particularly sensitive to chemical composition. Both series showed good catalytic activity, depending on the catalyst/substrate molar ratio, in the liquid phase cyclohexanone oxidation to adipic acid. The reaction was carried out without solvent and in the presence of hydrogen peroxide (30%). Among the different POMs, $Cs_2Sn_{0.5}PMo_{12}O_{40}$ was the most efficient with a 55% of adipic acid yield. The absence of solvent, a harmful product, and the use of hydrogen peroxide, that decomposes only into water, make the POM-H_2O_2 system clean.

Scientific Ethics Declaration

The authors declare that the scientific ethical and legal responsibility of this article published in EPSTEM journal belongs to the authors.

Acknowledgements or Notes

This article was presented as oral/poster presentation at the International Conference on Basic Sciences, Engineering and Technology (www.icbaset.net) held in Alanya/Turkey on May 02-05, 2024.

References

Benadji, S., Mazari, T., Dermeche, L., Salhi, N., Cadot, E., & Rabia, C. (2013). Clean alternative for adipic acid synthesis via liquid-phase oxidation of cyclohexanone and cyclohexanol over $H_{3-2x}Co_x$ $PMo_{12}O_{40}$ catalysts with hydrogen peroxide. *Catalysis Letters*, *143(8)*, 749-755.

Botto, I. L., Garcia, A. C., & Thomas, H. J. (1992). Spectroscopical approach to some heteropolymolybdates with the Anderson structure. *Journal of Physics and Chemistry of Solids*, *53*(8), 1075-1080.

Cavani, F., Etienne, E., Favaro, M., Galli, A., Trifiro, F., & Hecquet, G. (1995). Enhancement of catalytic activity of the ammonium/potassium salt of 12-molybdophosphoric acid by iron ion addition for the oxidation of isobutane to methacrylic acid. *Catalysis Letters*, *32*, 215-226.

Cavani, F., Ferroni, L., Frattini, A., Lucarelli, C., Mazzini, A., Raabova, K., ... & Babini, P. (2011). Evidence for the presence of alternative mechanisms in the oxidation of cyclohexanone to adipic acid with oxygen, catalysed by Keggin polyoxometalates. *Applied Catalysis A: General*, *391*(1-2), 118-124.

Copeaux, H. (1906). Ann. *Chim*, *7*, 118.

Copeaux, H. (1909). Ann. *Chim*, *17*, 21.7

Dermeche, L., Thouvenot, R., Hocine, S., & Rabia, C. J. I. C. A. (2009). Preparation and characterization of mixed ammonium salts of Keggin phosphomolybdate. *Inorganica Chimica Acta*, *362*(11), 3896-3900.

Guerroudj, M. R., Dermeche, L., Mouheb, L., Mazari, T., Benadji, S., & Rabia, C. (2019). Preparation, characterization, and catalytic activity of tin (antimony) substituted and lacunar Dawson phosphotungstomolybdates for synthesis of adipic acid. *Bulletin of Chemical Reaction Engineering & Catalysis*, *14*(2), 283-293.

Idrissou, Y., Mouanni, S., Amitouche, D., Mazari, T., Marchal-Roch, C., & Rabia, C. (2019). Cyclohexanone oxidation over $H_3PMo_{12}O_{40}$ heteropolyacid via two activation modes microwave irradiation and conventional method. *Bulletin of Chemical Reaction Engineering & Catalysis*, *14*(2), 427-435.

Mazari, T., Benadji, S., Tahar, A., Dermeche, L., & Rabia, C. (2013). Liquid-phase synthesis of adipic acid

Mizuno, N., Kamata, K., & Yamaguchi, K. (2006). Liquid-phase oxidations catalyzed by polyoxometalates. In *Surface and nanomolecular catalysis* (pp. 477-506). CRC Press.

Mizuno, N., Kamata, K., S. Uchida., S., & Yamaguchi, K. (2009). Modern heterogeneous oxidation. *Catal.*, *185*.

Molinari, J. E., Nakka, L., Kim, T., & Wachs, I. E. (2011). Dynamic Surface Structures and Reactivity of Vanadium-Containing Molybdophosphoric Acid (H3+ x PMo12–x V x O40) Keggin Catalysts during Methanol Oxidation and Dehydration. *ACS Catalysis*, *1*(11), 1536-1548.

Mouanni, S., Mazari, T., Amitouche, D., Benadji, S., Dermeche, L., Roch-Marchal, C., & Rabia, C. (2019). Preparation and characterization of $H_{3-2(x+y)}Mn_xCo_yPMo_{12}O_{40}$ heteropolysalts. Application to adipic acid green synthesis from cyclohexanone oxidation with hydrogen peroxide. *Comptes Rendus. Chimie*, *22*(4), 327-336.

Mouanni, S., Mazari, T., Benadji, S., Dermeche, L., Marchal-Roch, C., & Rabia, C. (2018). Simple and green adipic acid synthesis from cyclohexanone and/or cyclohexanol oxidation with efficient $(NH_4)_xH_yM_zPMo_{12}O_{40}$ (M: Fe, Co, Ni) catalysts. *Bulletin of Chemical Reaction Engineering & Catalysis*, *13*(2), 386-392.

Moudjahed, M., Dermeche, L., Benadji, S., Mazari, T., & Rabia, C. (2016). Dawson-type polyoxometalates as using Keggin-type phosphomolybdates Catalysts. *Journal of Materials Science and Engineering. B*, *3*(3B), 146.

Moudjahed, M., Dermeche, L., Idrissou, Y., Mazari, T., & Rabia, C. (2022). Oxidation of cyclohexanone and/or cyclohexanol catalyzed by Dawson-type polyoxometalates using hydrogen peroxide. *Journal of Chemical Sciences*, *134*(1), 31.

Mouheb, L., Dermeche, L., Essayem, N., & Rabia, C. (2020). Keggin-type mixed polyoxomolybdatescatalyzed cyclohexanone oxidation by hydrogen peroxide: In situ IR pyridine adsorption. *Catalysis Letters*, *150*, 3327-3334.

Mouheb, L., Dermeche, L., Mazari, T., Benadji, S., Essayem, N., & Rabia, C. (2018). Clean adipic acidsynthesis from liquid-phase oxidation of cyclohexanone and cyclohexanol using $(NH_4)_xA_yPMo_{12}O_{40}$ (A: Sb, Sn, Bi) mixed heteropolysalts and hydrogen peroxide in free solvent. *Catalysis Letters*, *148*, 612-620.

Mouheb, L., Dermeche, L., Mazari, T., Benadji, S., Essayem, N., & Rabia, C. (2018). Clean adipic acid synthesis from liquid-phase oxidation of cyclohexanone and cyclohexanol using $(NH_4)_xA_yPMo_{12}O_{40}$

(A: Sb, Sn, Bi) mixed heteropolysalts and hydrogen peroxide in free solvent. *Catalysis Letters*, *148*, 612-620.

Nomiya, K., Miwa, M., & Sugaya, Y. (1984). Catalysis by heteropolyacid—VII. catalytic oxidation of cyclohexanol by dodecamolybdate. *Polyhedron*, *3*(5), 607-610.

Popa, A., Sasca, V., Stefanescu, M., Kiš, E. E., & Marinković-Nedučin, R. (2006). The influence of the nature and textural properties of different supports on the thermal behavior of Keggin type heteropolyacids. *Journal of the Serbian Chemical Society*, *71*(3), 235-249.

Pope, M. T., Jeannin, Y., & Fournier, M. (1983). *Heteropoly and isopoly oxometalates* (Vol. 8). Berlin: Springer-Verlag.

Porta, P., Minelli, G., Pettiti, I., Botto, L. I., & Thomas, H. J. (1997). Anderson phases as precursors of nickel–molybdenum–tungsten oxides. *Journal of Materials Chemistry*, *7*(2), 311-313.

Rocchiccioli-Deltcheff, C., Fournier, M., Franck, R., & Thouvenot, R. (1983). Vibrational investigations of polyoxometalates. 2. Evidence for anion-anion interactions in molybdenum (VI) and tungsten (VI) compounds related to the Keggin structure. *Inorganic Chemistry*, *22*(2), 207-216.

Rocchiccioli-Deltcheff, C., Thouvenot, R., & Franck, R. (1976). Spectres ir et Raman d'hétéropolyanions α $XM_{12}O_{40}^{n-}$ de structure de type Keggin (X= B^{III}, Si^{IV}, Ge^{IV}, P^{V}, As^{V} et M= W^{VI} et Mo^{VI}). *Spectrochimica Acta Part A: Molecular Spectroscopy*, *32*(3), 587-597.

Sanchez, C., Livage, J., Launay, J. P., Fournier, M., & Jeannin, Y. (1982). Electron delocalization in mixed valence molybdenum polyanions. *Journal of the American Chemical Society*, *104*(11), 3194-3202.

Sasca, V., Ştefănescu, M., & Popa, A. (1999). Studies on the non-isothermal decomposition of H3PMo12O40·xH2O and H4PVMo11O40· yH2O. *Journal of Thermal Analysis and Calorimetry*, *56*(2), 569-578.

Tahar, A., Benadji, S., Mazari, T., Dermeche, L., Marchal-Roch, C., & Rabia, C. (2015). Preparation, characterization and reactivity of Keggin -type phosphomolybdates, $H_{3-2x}Ni_xPMo_{12}O_{40}$ and $(NH_4)_{3-2x}$Ni x PMo 12 O 40, for adipic acid synthesis. *Catalysis Letters*, *145*, 569-575.

Author Information

Lynda Mouheb
Mouloud Mammeri University of Tizi-Ouzou
Tizi-Ouzou, Algeria

Leila Dermeche
Mouloud Mammeri University of Tizi-Ouzou
Tizi-Ouzou, Algeria.
Contact E-mail: *leila.dermeche@ummto.dz*

Cherifa Rabia
University of Science and Technlogy ‘Houari Boumediene,
Bab Ezzouar,Algeria

To cite this article:

Mouheb, L., Dermeche L., & Rabia, C. (2024). Tin-based Keggin-type phosphomolybdate and silicomolybdate as catalysts for the green synthesis of adipic acid. *The Eurasia Proceedings of Science, Technology, Engineering & Mathematics (EPSTEM), 28,* 502-509.

The Eurasia Proceedings of Science, Technology, Engineering & Mathematics (EPSTEM)
ISSN: 2602-3199

The Eurasia Proceedings of Science, Technology, Engineering & Mathematics (EPSTEM), 2024

Volume 28, Pages 510-518

ICBASET 2024: International Conference on Basic Sciences, Engineering and Technology

Application of Methodology for Defining the Adjoining Lands and Flooding River Strips in Bulgaria in a GIS Environment Upon Bridge Facility Designing

Silvia Kirilova
University of Architecture

Kameliya Radeva
Bulgarian Academy of Sciences

Abstract: The "Methodology for defining the adjoining lands and flooding rivers stripes in Bulgaria" (MALFARS) has been developed in 2012 based on the requirements of the EU Water Framework Directive 2000/60. In this article we investigated another aspect of MALFARS application. We have reviewed the possibilities for methodology application upon designing of bridge facilities within the researched river section. The study presents the application of the Methodology for the designing of a bridge facility over the Dzherman River upon the maximum dimensional water quantities calculated for the studied section of the river. We have used GIS instruments to analyze and evaluate the results obtained for the parameters of the maximum runoff and the conductivity of the river section. The results present the defined flooding zones of the adjoining river areas/stripes, good conductivity of the road facility, hydraulic and geometric characteristics of the runoff in the investigated river section in cases of high water levels

Keywords: Floodable strips, Bridge equipment, Maximum streamflow, Dzherman river

Introduction

Determining the area of floodable riparian strips is a subject of research in engineering hydrology in the hydro technical design of bridge facilities, dikes, etc. Particularly prone to failure during high river levels are the riverine bridges and that is why it is important to determine the maximum streamflow of the river that crosses a given bridge (Vigil & Booker, 2023). The floods change river morphology (hydraulic and geometrical parameters of the riverbed), river depths, flow velocity, and load transport, negatively affecting the bridges as structurally and functionally impaired. (Sasidharan et al., 2023; Sasidharan et al., 2022). A lot of techniques can be applied like HEC-RAS (Popescu&Bărbulescu, 2023; Ghimire et al., 2022), FLO 2D, TELEMAC 2D, MIKE, etc. (Anees et al., 2016). Several studies analyze flood impact on bridges by flood-frequency analysis and hydraulic approach (Mondoro & Frangopol, 2018)

The aim of the present study is to apply a methodology for determining the floodable riverside areas (Methodology for Defining the Adjoining Lands and Flooding Rivers Stripes in Bulgaria – MALFARS) with GIS tools and suitable hydrological and hydraulic model for assessing the risk of flooding of the constructed bridge over the Dzherman river part of the "Struma" highway (Dupnitsa municipality). According to the regulations, the bridge is a Class I facility, which is dimensioned with a 1.0% probability of exceeding and hydraulically checked for 0.1% probability of exceeding. The methodology was applied in hydrological reports related to flooded river sections and mainly in the developed flood risk management plans of the basin regional directorates under the leadership of the Ministry of Environment and waters in Bulgaria. In the present research,

the methodology is applied for the first time in such a case with a view to be included in technical reports for a new bridge design facilities and for the rehabilitation of existing ones.

Study Area

The present study covers the watershed of the Dzherman River (a left tributary of the Struma River), from the source area to Highway "Struma" in the area of the Dzherman village. The drainage basin of the Dzherman River is part of the northwestern sections of the Rila mountain range. The river's source is a lake at an altitude of 2,535 m and it is 47.8 km long (Hristova, 2012). Dzherman River influences the Struma River at an altitude of 369 m (Fig. 1). According to the River basin management plans for river basin directorates upon the Ministry of Environment and waters the river is considered as water body BG4ST600R036, type R5.

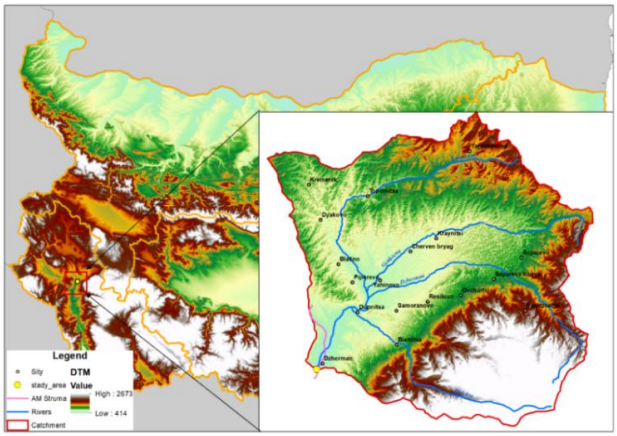

Figure 1. Location of the study area

Materials and Methods

The "Methodology for Defining the Adjoining Lands and Flooding River Stripes in Bulgaria" (MALFARS) is the official accepted methodology for assessing the boundary and the area of the river stripes. This approach includes nine steps – 1: digital input data provided in a GIS environment; 2: defining physio-geographical characteristics based on DEM (digital elevation model); short climate characteristics of the survived area; 4: hydrological calculation, etc. (Figure 2).

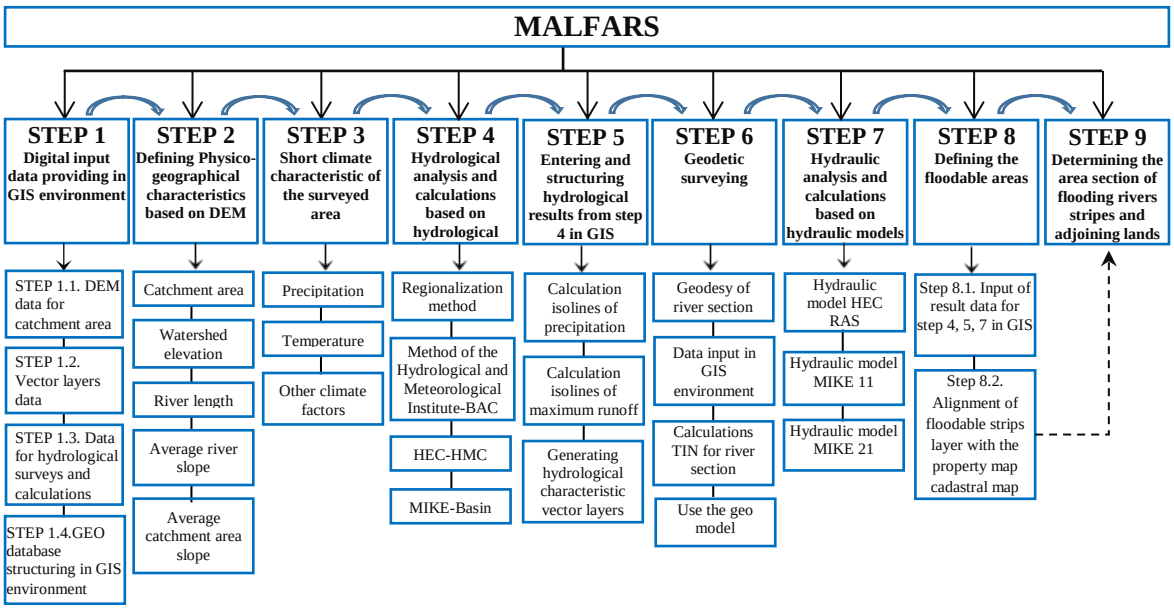

Figure 2. Methodology for defining the adjoining lands and flooding river stripes in Bulgaria" (MALFARS)

According to the first step of the methodology, input information is required to create a GIS database for the studied watershed, which is implemented with raster data - DEM and vector objects - rivers, springs and natural and artificial lakes, existing hydro-technical systems and facilities, forest cover, soil characteristics and others. The generated DEM of the studied watershed is the basis for the orographic characteristics (step 2): area (A, km^2) and altitude (H, m) of the river basin, length (L, km) and slope (i, ‰) of the river (river section) and others. The climatic characterization is performed on the basis of main climate data (air temperature and precipitation), as well as some features of the climate in the studied watershed (step 3). The selection of a hydrological model for the maximum runoff calculation (according to step 4 of MALFARS) is based on the availability of hydrometric and meteorological information in the study area. The studied section, a bridge facility part of Struma highway, does not coincide with a hydrometric station from the national reference hydrometric network. Therefore, the hydrological analysis and assessment is carried out under conditions of insufficient or total lack hydrological information. In this case, empirical relationships between the hydrological characteristics and the orographic characteristics of the studied watersheds are applied to estimate the maximum runoff to the studied area. In the present study, regressions between the modulus of the maximum runoff (M_{qmax}, $l/s/km^2$) and the mean altitude (H, m), between the coefficient of variation of the maximum runoff (Cv) and the catchment area (A, km^2) are used.

A logarithmic grid is used to plot the graphical dependencies. The resulting regressions were evaluated using the correlation coefficient (R) at a statistical significance level of 5.0% and evaluation criteria for the correlation coefficient. The information arrays of data on the maximum runoff observed in the hydrometric stations used in the study are subjected to processing through mathematical statistics. Parametric and non-parametric criteria for uniformity, representativeness and significance of hydrological series of maximum water quantities were used. The test was performed according to the Mann-Whitney, Pettit's test and Wilcoxon tests. The collateral curves for each HMS are calculated and constructed, on the premise of choosing the most appropriate theoretical distribution law based on minimal deviations of the empirical points from the theoretical ones (Mamdouh et al., 1993). The analysis was made to reach reliable results for the maximum runoff parameters used to construct regional dependencies. The method of analogy is applied to obtain maximum water quantities with characteristic probability of exceeding for the studied area. The adopted hydrometric station for analog is HMS 51430 on the Dzherman River, which is located about 6.5 km above the studied section. The station was opened in 1936 and has been operating until now and based on WMO requirements (WMO, 2017) a calculation period of 1961 to 2020 is assumed. The hydrological series of annual maximum water quantities is processed with the methods of mathematical statistics, the security curve is calculated and constructed, and the statistical parameters are calculated using the method of maximum likelihood under lognormal distribution. Based on the obtained ordinate deviations with a lognormal distribution at HMS 51430 and with the application of the method of moments, the theoretical probability curve for the studied section of the Dzherman River is obtained as

$$Q_{p,i} = \overline{Q_i}(\varphi_{p,i}.Cv + 1)$$

Where as

i is river section

$Q_{p,i}$ – annual maximum discharge with probability *P* for the river section

$\overline{Q_i}$ – average of the annual maximum discharges by the equation: $M_{max,av} = f(H)$;

C_v – coefficient of variation of the annual maximum discharge by the equation $C_v = f(A)$;

φ_p –conditional outflow coefficient of maximum runoff at probability of exceeding p%;

In step 5 of the methodology, the hydrological results are implemented in the developed GIS database. Thematic maps of the distribution of the annual maximum runoff, the coefficient of variation of the maximum runoff and others are created. In step 6, the topography of the studied river section is implemented in the developed database. Using AcrMap tools a digital terrain model of the river section is generated in TIN format. With the capabilities of HEC-geoRAS (HEC- GeoHMS, User's Mannual, 2013), based on the created TIN format, cross profiles along the length of the river bed are generated (Icaga et al., 2016). In step 7, a hydraulic model was selected. HEC-RAS was used for the purpose of the study. The results of step 6 and step 4 are implemented in the model and the bridge facility is designed (Ogras&Onen, 2020). The results of the hydraulic model, such as the water level elevation, the change in the average velocity and the depth of the water current, are implemented again in GIS to perform step 8 (8.1 and 8.2) of the methodology. From the processed information, thematic maps of the flooding river strips and the adjoining lands in the studied river section are prepared, and present the final result of the adopted methodology in step 9 (Figure 2).

Data Source

The DEM for the study catchment was generated from open-access raster data with a 30 m x 30 m grid cell size from the Advanced Spaceborne Thermal Emission and Reflectance Radiometer (ASTER) Global Digital Terrain Model Version 3 (GDEM 003). Linear objects are vectorized from topographic maps at a scale of 1:25000 (https://www.cadastre.bg). For land cover, data from Corine Land Cover was used for two years – 2018 and 2022 (Radeva&Kirilova, 2023). For the climatic characteristics of the river catchment, data from meteorological observations in the city of Dupnitsa are used (Table 1). The initial data for constructing the degree dependences for determining the maximum runoff to the studied section are maximum runoff values in the catchments of the Dzherman River - Dupnitsa (HMS 51430), the Blagoevgradska Bistrica River - Slavovo (HMS 51450) and the Rilska River - village. Pasta (HMS 51470). Data on the physio-geographical characteristics of the HMS were taken from NIMH - MOEW (Table 2)

Table 1. Meteorological data (Dupnitsa city)

Climate parameters	Month												Year
	I	II	III	IV	V	VI	VII	VIII	IX	X	XI	XII	
T_{av} (°C)	-0,9	1,3	4,7	10,6	15,3	18,8	21,0	20,5	16,7	11,4	6,5	1,5	10,6
T_{max} (°C)	3,1	6,2	10,5	16,7	21,5	24,9	27,6	27,8	24,1	18,1	11,3	5,3	16,4
T_{min} (°C)	-5,1	-3,3	-0,4	4,7	8,9	12,3	13,5	12,6	9,3	4,9	1,9	-2,3	4,8
Precip. (mm)	45	38	37	61	69	79	52	40	38	56	61	51	627

Table 2. HMS Physio-geographical characteristics

HMS №	River	A (km^2)	H (m)	L (km)	Average slope ‰	Average catchment slope
51430	Dzherman	396	1001	30	43.1	0.222
51450	Rilska	222	1918	24	50.3	0.519
51470	Blagoevgradska bistritza	105	1790	21	30,8	0,44

Results and Discussion

For the purpose of hydrological characteristics analysis and evaluation vector layers were generated and the physico-geographical characteristics of the studied watershed were calculated based on the developed DEM and with the help of the HEC-geoHMS modules in a GIS environment (Table 3)

Table 3. Orographic characteristics of the studied area

Section	River	A (km^2)	H (m)	L km	Average river slope ‰	Average catchment slope
Bridge from Highway Struma	Dzherman	492,8	955	37,2	40,8	0,2

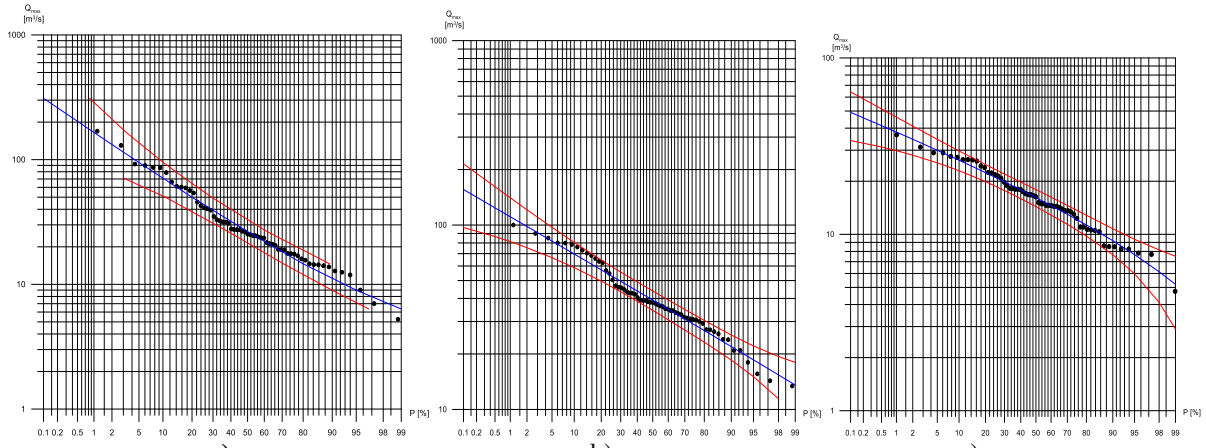

a). b). c)

Figure 6. Theoretical probability of exceeding curves for maximum runoff observed in HMS 51430 (a), HMS 51450 (b) and HMS 51470 (c)

To determine the characteristics of the maximum outflow of the Dzherman River to the studied section of the bridge over the Dzherman River, three HMS with a period of the observed magnitude from 1961 until 2020 were used. The hydrological series are checked for homogeneity according to the accepted criteria, which confirm their significance. The probability of exceeding curves for the maximum runoff with an assumed lognormal distribution in a logarithmic-probability network were calculated and constructed (Figure 6).

The statistical parameters of the hydrological series of the used HMS were calculated by the maximum likelihood method with an assumed lognormal distribution. The results of the calculations are given in Table 4. Based on data on the statistical parameters of the maximum runoff calculated in table 4 for the studied hydrometric stations, regression of type $Y = a.X^b$ were constructed, where Y is the hydrological variable, and X is the orographic characteristic (catchment area - A (km^2) or the mean altitude of the watershed H (m)), a and b are coefficients of the non-linear regression.

Table 4. Statistics of Q_{max}

HMS	**River**	$\boldsymbol{M_{qmax}}$, **(l/s/km²)**	**Statistics** Q_{max} (m^3/s)	σ	C_v	C_s
51430	Dzherman	0.09	36.0	29.8	0.83	3.35
51450	Rilska	0.192	42.6	20.4	0.48	1.16
51470	Blagoevgradska Bistritza	0.167	17.5	6.96	0.36	0.93

Figure 4a and 4b show the graphical relationships between the modulus of maximum runoff and mean elevation and coefficient of variation and catchment area.

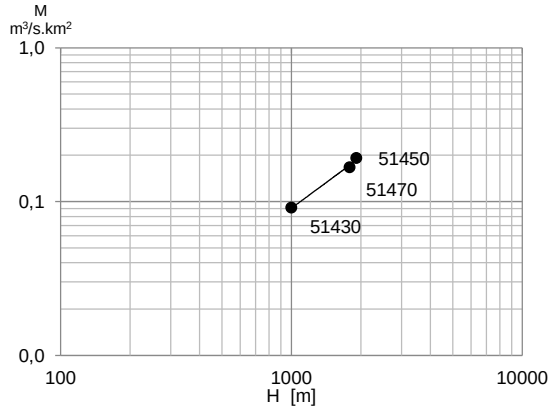

Figure 4a. Relationship between $M_{q\,max}$ and H

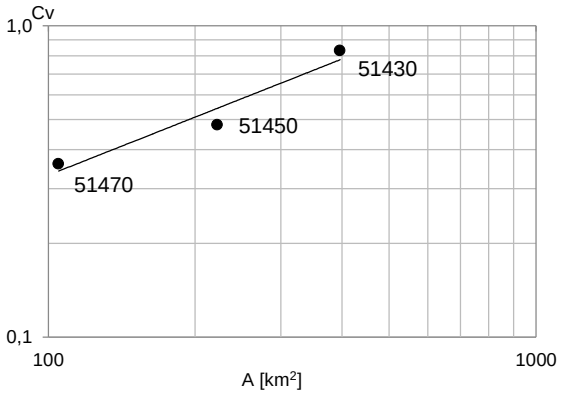

Figure 4b. Relationship between $C_{v\,max}$ and A

For each graphical dependence, the non-linear regression dependence for the individual hydrological parameter with the corresponding evaluation criteria is derived. For the maximum runoff modulus ($\boldsymbol{M_{qmax}}$), the following dependence was obtained:

$$\boldsymbol{M_{qmax}} = 4{,}32.10^5.H^{1{,}108}\ (m^3/s.km^2),$$

which is checked with the correlation coefficient $R = 0{,}997$ and reliability assessment of R by the probability error $E_R = 2{,}6\ \% < 3.0\%$ and by Fisher criteria $F_R = 5{,}55 > 3.0$. The following dependence was obtained for the coefficient of variation of the maximum runoff modulus:

$$C_{v,max} = 1{,}9.10^2.H^{0{,}62}$$

which is checked with the correlation coefficient $R = 0{,}968$ and estimate the reliability of R by the probability error $E_R = 2{,}43\ \% < 3.0\%$ and by Fisher criteria $F_R = 4{,}15 > 3$.

Applying the derived non-linear regression dependences for the studied section (the bridge over the Dzherman River), the maximum runoff Qmax, brige = 42.5 m^3/s and coefficient of variation Cv = 0.88 is obtained. To obtain the maximum water quantities with a specific probability of exceeding for the studied section, we have used the data on the maximum runoff from HMS 51430, which is accepted as an analogue. The calculation procedures carried out for the determination of the maximum water quantities with different probability of

exceedings for the section along Dzherman River, with the applied hydrological model, give the following results, accepted as final for input information in the hydraulic model (Table 5).

Table 5. Dimensional maximum water quantities for the studied section of Dzherman River

Section	River	A (km^2)	H (m)	$Q_{0.1\%}$ (m^3/s)	$Q_{1\%}$ (m^3/s)
Bridge from HW Struma	Dzherman	492,8	955	353,0	188,7

To create the digital terrain model for the studied river section in TIN format (Figure 6), a captured topography of the river section (Figure 5) is used, according to step 6 of MALFARS.

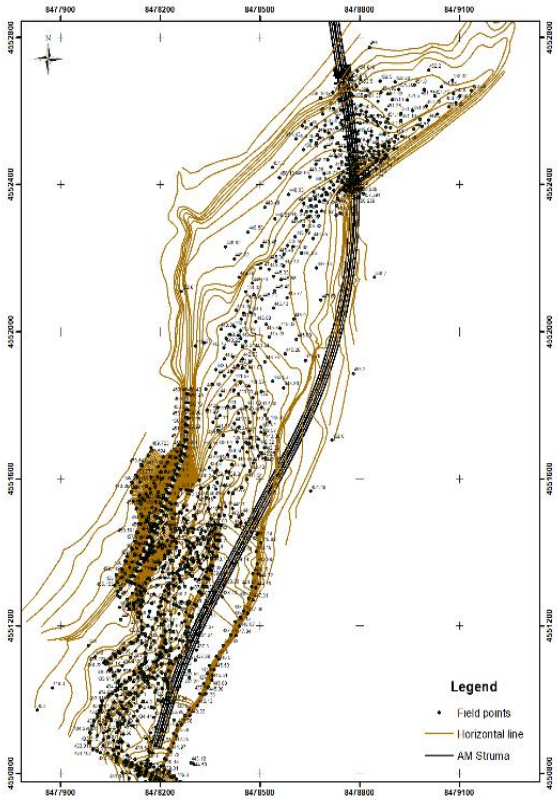

Figure 5. Geodetic surveying

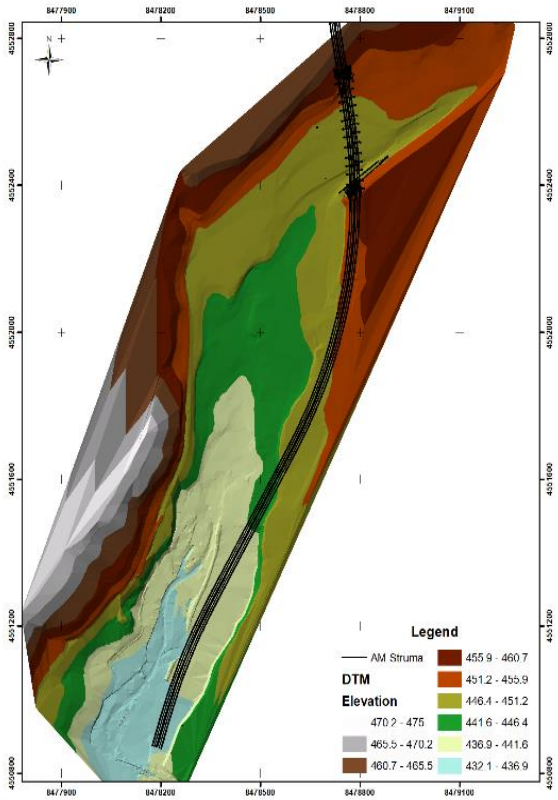

Figure 6. Digital terrain motel

With the capabilities of the HEC-geoRAS model, cross profiles along the length of the studied river section are generated (Figure 7). The results of the geometric characteristics of the river section of the Dzherman River are input information for the selected HEC-RAS hydraulic model, according to step 7 of the methodology. The selected hydraulic model make it possible to model the shape and dimensions of the bridge facility that is a subject of this study. The results of the hydraulic calculations for the modeled bridge structure over the Dzherman River and the position of the water level at the maximum water amount with 0.1% probability of exceding calculated in the hydrological model are presented in Figure 8. The obtained hydraulic parameters of the river current from the hydraulic model show that the calculated maximum water quantity with a 0.1% probability of exceeding does not create conditions for flooding the so designed bridge structure.

To create thematic maps representing the inundation strip and inundation area, hydraulic results such as flow depth change and average velocity change are implemented in the already designed DEM in a GIS environment. Figures 9 and 10 present thematic maps of the variation in river flow depth and variation in mean velocity at maximum water quantity with a 0.1%. probability of exceeding.

From figure 9 and 10, the outline of the water surface that shows the boundaries of the flooding strips has been defined. The outline of the water surface determines the area of the flooded territory. In the investigated computational section, the flooded area amounts to 0.28 km^2 at the maximum water quantity – $Q_{0.1\%}$ = 353 m^3/s.

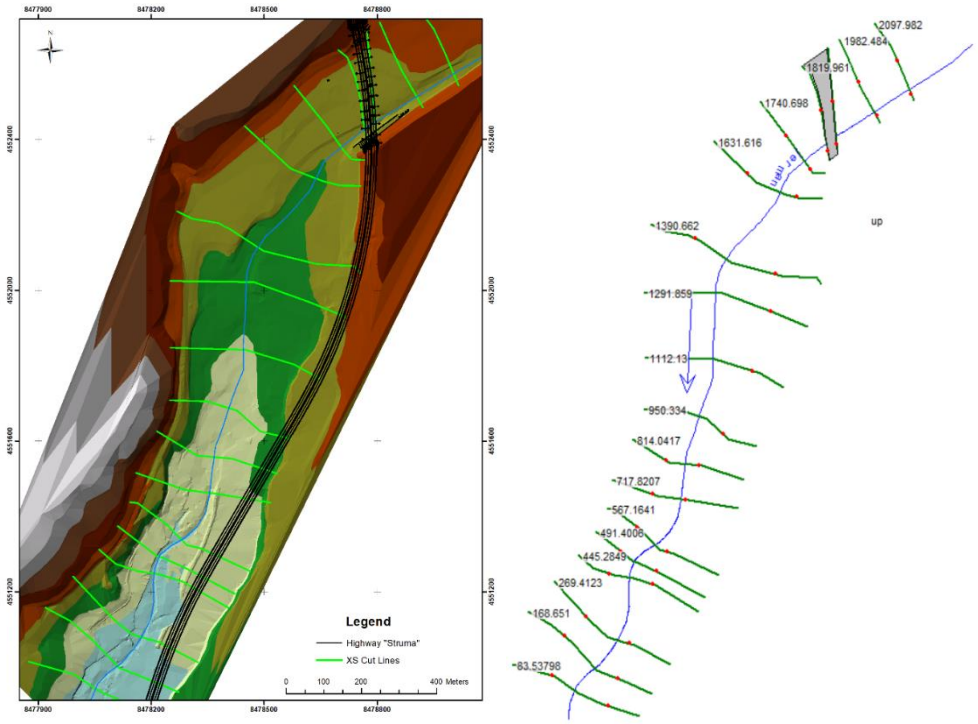

Figure 7. Location of the cross profiles along the river section (Dzherman River)

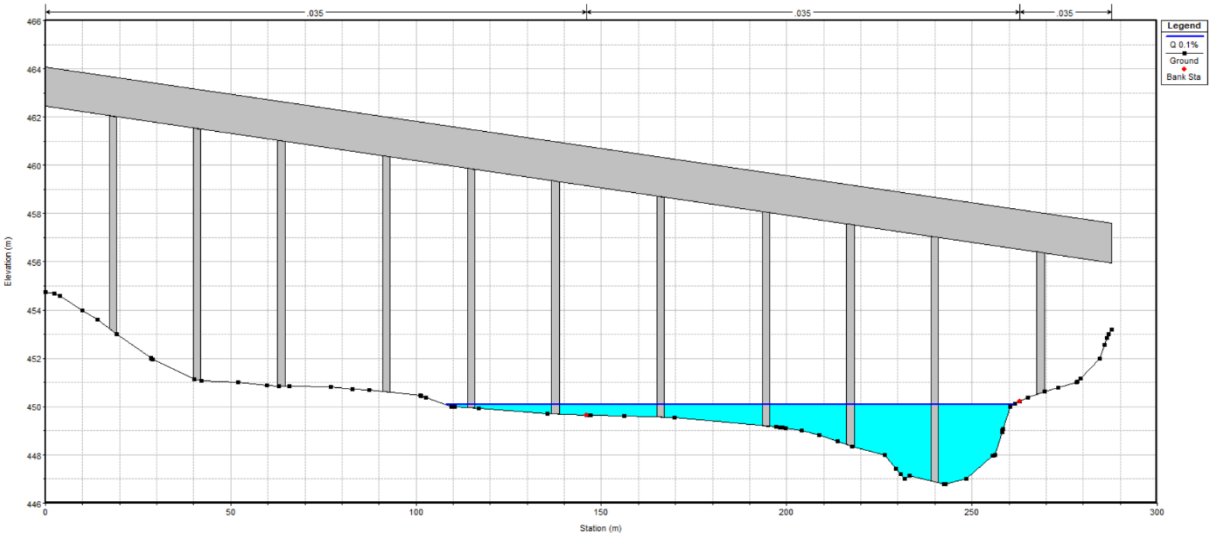

Figure 8. Cross profile of Dzherman river with longitudinally depicted the bridge facility part of HW Struma with a water quantity with a 0.1%. probability of exceeding

The obtained hydraulic parameters of the river current from the hydraulic model show that the calculated maximum water quantity with a 0.1% probability of exceeding does not create conditions for flooding the so designed bridge structure. To create thematic maps representing the inundation strip and inundation area, hydraulic results such as flow depth change and average velocity change are implemented in the already designed DEM in a GIS environment. Figures 9 and 10 present thematic maps of the variation in river flow depth and variation in mean velocity at maximum water quantity with a 0.1%. probability of exceeding. From figure 9 and 10, the contour of the water surface that shows the boundaries of the flooding strips has been difined. The water surface outline determines the area of the flooded territory. In the investigated computational section, the flooded area amounts to 0.28 km^2 at the maximum water quantity – $Q_{0.1\%}$ = 353 m^3/s.

The inspection carried out for the bridge, which is part of the Highway Struma, is not flooded and no destruction of the design structure of the bridge will be observed when the maximum amount of water passes with 0.1%

probability of exceeding in the Dzherman riverbed. In the lower section of the highway route, flooding of the roadway has been observed, which leads to taking construction measures for protection against flooding.

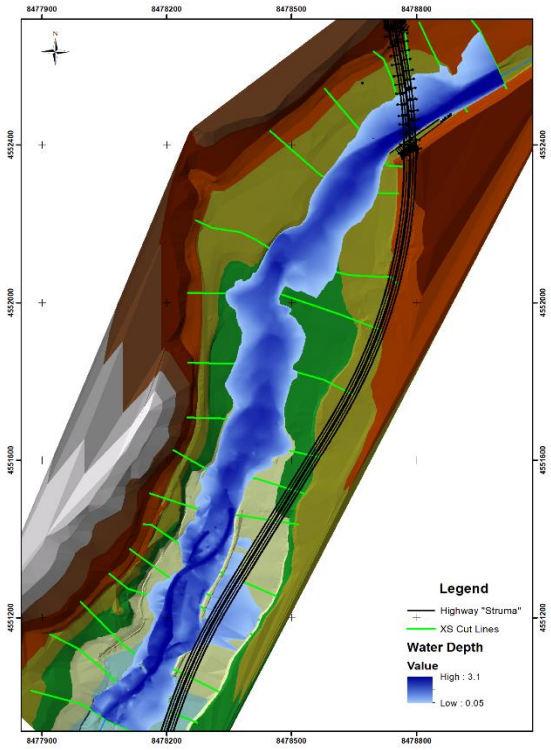

Figure 9. Water surface depth at $Q_{0,1\%}$ = 353 m3/s

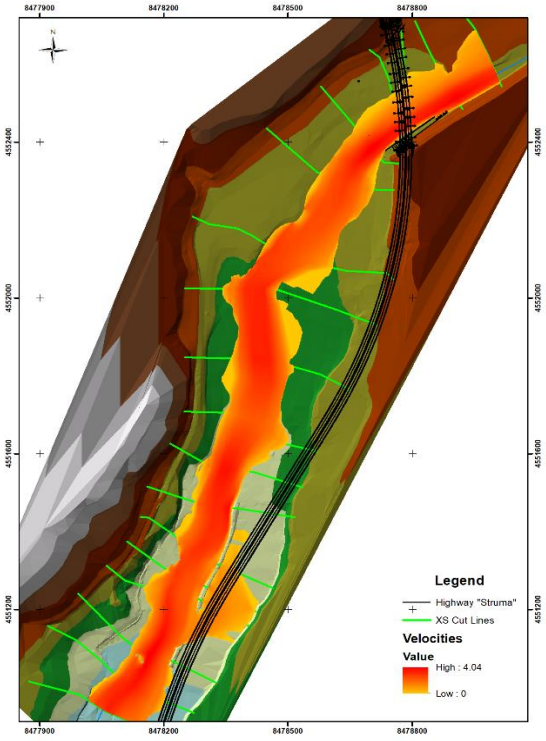

Figure 10. Average current speed at $Q_{0,1\%}$ = 353 m3/s

Conclusion

The results of the present study show that the "Methodology for Defining the Adoining Lands and Flooding River Stripes in Bulgaria" (MALFARS) is an important tool for assessing the risk of damage to bridge structures. The generated vector layers for the analysis and assessment of the hydrological characteristics based on the developed DEM and the HEC-geoHMS modules in a GIS environment provide objective information about the physicogeographical characteristics of the studied watershed. The Cross-sections in the surveyed river section are generated in a GIS environment using HEC geoRAS modules and the developed DEM derived from geodetic terrain surveying. The selected hydrological model and calculated maximum water quantities with 0.1% and 1.0% probability of exceeding based on the HEC-RAS model defines the accurate determination of water level elevations, bridge facility throughput and average river flow velocities at assumed maximum water quantities. According to the results of the present survey, a thousand-year high river wave is not possible to flood and destroy the built bridge over the Dzherman River. The methodology is applied for the first time to river bridges in the country and the results of the survey demonstrates its importance and contribution to define flooding riverside strips for other bridge structures built over water bodies.

Scientific Ethics Declaration

The authors declare that the scientific ethical and legal responsibility of this article published in EPSTEM journal belongs to the authors.

Acknowledgements or Notes

* This article was presented as an oral presentation at the International Conference on Basic Sciences, Engineering and Technology (www.icbaset.net) held in Alanya/Turkey on May 02-05, 2024.

References

Anees, M. T., Abdullah, K., Nawawi, M. N. M., Ab Rahman, N. N. N., Piah, A. R. M., Zakaria, N. A.,…& Omar, A. M. (2016). Numerical modeling techniques for flood analysis. *Journal of African Earth Sciences, 124,* 478–486.

Ghimire, E., Sharma, S., Lamichhane, N. (2022). Evaluation of one-dimensional and two-dimensional HEC-RAS models to predict flood travel time and inundation area for flood warning system. *ISH Journal of Hydraulic Engineering, 28*(1), 110–126.

HEC-GeoHMS (Geospatial Hydrologic ModellingExtension). (2013). *User's manual.* Retrieved from https://www.hec.usace.army.mil/software/hec-geohms/documentation/HEC-GeoHMS_Users _Manual_4.2.pdf

Hristova, N. (2012). *Hydrology of Bulgaria*. Sofia: Tip-Top Press.

Icaga, Y., Tas, E., & Kilit, M. (2016). Flood inundation mapping by GIS and a hydraulic model (HEC RAS): A case study of Akarcay Bolvadin subbasin, in Turkey. *Acta Geobalcanica*, *2*(2), 111-118.

Mahdouh, S., Van Oorschot, H. J. L., & De Lange, S. J. (1993). *Statistical analysis in water resources engineering*. Rotterdam: Aa Balkema.

Ministry of Environment and waters. (n.d). Retrieved from https://www.moew.government.bg/bg/vodi/planove-za-upravlenie/planoveza-upravlenie-na-riska-ot-navodneniya-purn/planove-za-upravlenie-na-riska-ot-navodneniya-2022-2027/

Ministry of Environment and waters (n.d). Retrieved from https://www.moew.government.bg/bg/vodi/planove-za-upravlenie/planove-za-upravlenie-na-rechnite-basejni-purb/planove-za-upravlenie-na-rechnite-basejni-2022-2027-g/

Mondoro, A., & Frangopol, D. M. (2018). Risk-based cost-benefit analysis for the retrofit of bridges exposed to extreme hydrologic events considering multiple failure modes. *Engineering Structures, 159,* 310–319.

Ogras, S., & Onen, F. (2020) Flood analysis with HEC-RAS: A case study of Tigris River. *Advances in Civil Engineering, 2020,* 6131982.

Popescu, C., & Bărbulescu, A. (2023). Floods simulation on the Vedea River (Romania) using hydraulic modeling and GIS software: A case study. *Water*, 15, 483.

Pregnolato, M., Winter, A. O., Mascarenas, D., Sen, A. D., Bates, P., & Motley, M. R. (2022). Assessing flooding impact to riverine bridges: an integrated analysis. *Natural Hazards and Earth System Sciences*, *22*(5), 1559-1576.

Radeva, K., & Kirilova, S. (2023) Remote sensing data upon application of methodology for defining the adjoining lands and flooding river stripes in Bulgaria In *Remote Sensing for Agriculture, Ecosystems, and Hydrology XXV* (Vol.12727, pp.23-40). SPIE.

Sasidharan, M., Parlikad, A. K., & Schooling, J., (2022). Risk-informed asset management to tackle scouring on bridges across transport networks. *Structure and Infrastructure Engineering, 18*(22), 1-17.

Sasidharan, M., Parlikad, A. K., Schooling, Hadjidemetriou, G. M., Hamer, M., Kirwan, A., & Roffe, J. (2023). A bridge scour risk management approach to deal with uncertain climate future. *Transportation Research Part D: Transport and Environment, 114,* 103567.

Vigil, A. J. E., Booker, J. D. (2023). Hydrological vulnerability assessment of riverine bridges: The Bajo Grau bridge case study. *Water, 15*(5), 846.

WMO. (2017). *Guidelines on the calculation of climate normals.* Retrieved from https://library.wmo.int/viewer/55797/download?file=1203_en.pdf&type=pdf&navigator=1

Author Information

Silvia Kirilova
University of Architecture, Civil Engineering and Geodesy, Hydraulics and Hydrology Department, 1164, 1 Hristo Smirnenski Blvd., Sofia, Bulgaria
Contact e-mail: *spacedgclima@gmail.com*

Kameliya Radeva
Space Research and Technology Institute, Bulgarian Academy of Sciences, 1113, str. "Acad. Georgy Bonchev" bl. 1, Sofia, Bulgaria

To cite this article:

Kirilova, S., & Radeva, K. (2024). Application of methodology for determining the adjoining lands and flooding river strips in Bulgaria in a GIS environment upon bridge facility designing. *The Eurasia Proceedings of Science, Technology, Engineering & Mathematics (EPSTEM), 28,* 510-518.

The Eurasia Proceedings of Science, Technology, Engineering & Mathematics (EPSTEM)
ISSN: 2602-3199

The Eurasia Proceedings of Science, Technology, Engineering & Mathematics (EPSTEM), 2024

Volume 28, Pages 519-525

ICBASET 2024: International Conference on Basic Sciences, Engineering and Technology

Design, Synthesis and in Silico Studies of New 2-MethylQuinazolin-4(3*H*)-Ones Derivatives

Karima Ighilahriz-Boubchir
Mouloud Mammerie University of Tizi-ouzou

Amina Benazzouz-Touami
Mouloud Mammerie University of Tizi-ouzou

Malika Makhloufi-Chebli
Mouloud Mammerie University of Tizi-ouzou

Abstract: The concept of the green chemistry consists in the development of an environmentally friendly approach for organic synthesis using ecological and efficient protocols. In order to develop a methodology that could fit into the green chemistry field, for the synthesis of new quinazolin-4(3*H*)-ones derivatives via benzoxazinone, the choice was made on the use of both as catalysts, known for their efficiency, and microwave irradiations for time saving.The quinazolinone core and its derivatives form an important class of compounds, as they are present in a large family of products with broad biological activities. They generally display useful therapeutic and pharmacological properties such as anti-inflammatory, anti-convulsant, antihypertensive and antimalarial activity.The derivatives of the 2-metylquinazolin-4(3*H*)-ones **3a-d** series was synthesized from 2-methyl benzoxazin-4(3*H*)-one **1** and aniline in the presence of $H_3PW_{12}O_{40}$ (PW_{12}) under microwave irradiation and solvent free conditions. The compound structures were established using IR, 1H-NMR, 13C-NMR and mass spectroscopy. The toxicity of the hydrazone derivatives was studied through ADMET (Absorption, Distribution, Metabolism, Excretion, and Toxicity) simulations using ADMET Lab 2.0 server.

Keywords: Keggin-type heteropolyacids, Quinazolin-4(3*H*)-ones, Benzoxazin-4(3*H*)-one

Introduction

Quinazolin-4(3*H*)-ones are versatile nitrogen heterocyclic compounds, displaying a broad spectrum of biological and pharmalogical activities such as anti-fungal (El-Hashash et al., 2015), anti-tumoral (Kumar et al., 2003), hypotensive (EI-Brollosy et al., 2003), anti-cancer (Khili et al., 1994), anti-HIV(Alagarsamy et al., 2003), analgesic (Alagarsamy et al., 2002), anti-inflammatory (Kumar et al., 2007) etc. Moreover, the quinazolin-4(3*H*)-one moiety is found in several bioactive natural products (Saleh et al., 2004). For these reasons their synthesis has received considerable attention (Rad- Moghadam & Khajavi, 2006). In this work, we have synthesized quinazoline-4(3*H*)-ones and we have studies in silico properties prediction.

In our previous work (Ighilahriz et al., 2017), we have shown that the addition of monosubstituted aniline to the benzoxazin-4-ones gives two zwitterionic intermediates respectively. These cyclic intermediates can give the open product 2, which is relatively stable, or directly the closed product 3. It should be noted that the main effect of this ring-opening competition is due to the transfer of the negative charge from nitrogen to oxygen to give the closed product or from oxygen to nitrogen to give the open compound. Given that oxygen is more electronegative than nitrogen, pathway (2) is therefore more favoured (in the case of R=Ph). The 2-aryl-benzoxazin-4-ones have two nucleophilic attack sites, which can either open the heterocycle to give compound

3 or form compound 2. The competition between the two nucleophilic attacks depends on a number of parameters, such as the size and the nature of the nucleophile. The mechanism, is given in the following:

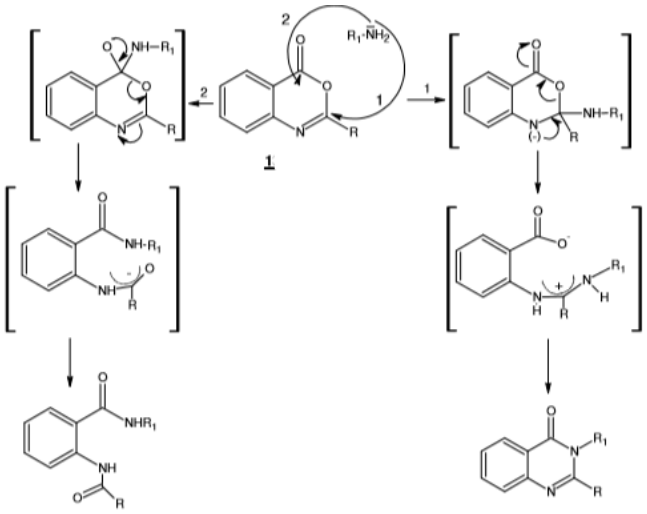

2 **3**

Scheme 1. Mecanisme for the condensation of anilines with benzoxazin-4-one reaction.

Method

Experimental Method

All melting points were measured on a Stuart Scientific SMP3 apparatus fitted with a microscope and uncorrected. The IR absorption spectra (KBr disks) were measured on a Nicolet Magna 550 series II IR Spectrophotometer. 1H-RMN (300.13 MHz) and 13C-RMN (75.47 MHz) spectra were recorded in deuterated chloroform ($CDCl_3$) on a Brucker DRX 300 spectrometer using tetramethylsilane (TMS) as an internal reference and results are expressed as δ values (ppm). Mass spectra were recorded on a Nermag R 10-10C quadruple mass spectrometer at 70 eV. All the compounds gave satisfactory elemental analyses. The multimode microwave reactor (a modified microwave oven Candy MGA 20M) has a single magnetron (2.45 GHz) with a maximum delivered power of 800 W. It was directly graduated in W (from 100 to 800 W). Experiments were carried out in a Pyrex reactor fitted with a condenser.

Computational Method

Prediction of the Pharmacokinetic Properties And Toxicological Properties Using ADMET

The pharmacokinetic properties of the compounds studied. The following properties, (i) absorption, Lipinski's rule of five, water solubility, Caco-2 permeability, intestinal absorption (human), skin permeability and P-glycoprotein interactions, (ii) distribution: VDss, Fu, Log BB and CNS permeability, (iii) metabolism and (iv) excretion were selected. Also, online pkCSM pharmacokinetics were used to predict the toxicity of the molecules, including skin sensitization, hepatotoxicity, etc. The results obtained were analyzed and compared with the reference values of the pkCSM pharmacokinetics prediction properties (Pires et al., 2015).

The Bioactivity Scores Prediction

The bioactivity scores of the quinazolin-4(3*H*)-ones toward G protein-coupled receptor (GPCR) ligand, ion channel modulator, a kinase inhibitor, nuclear receptor ligand, protease inhibitors, and enzyme inhibitor were predicted by using the Molinspiration bioactivity score v2018.03. The predicted results are written in Table 9. The rule for the bioactivity scores estimation is the following: when the bioactivity score was more than 0.00; the compound was considered active. While if the bioactivity score in the range between -0.50 and 0.00; the compound was moderately active. But if the bioactivity score was less than -0.50, the compound was inactive.

Synthesis

The action of aromatic amines on 2-methylbenzoxazin-4-ones in the presence of an aprotic solvent has been described in the literature (Kidwai, 2003). In the present work, we have replaced these aromatic amines with dichloanilines. The reaction of dichloroanilines with 2-methylbenzoxazin-4-ones was performed under microwave irradiation in the presence of PW_{12} catalyst and in the absence of solvent. The dichloroanilines and 2-methyl-benzoxazin-4-one, in the presence of PW_{12} in catalytic quantity, were ground and then subjected to microwave irradiation for 3 minutes at 300W and 9 minutes at 400W. The results obtained are summarized in Table 1.

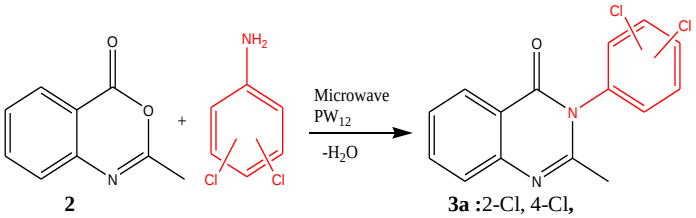

2

3a :2-Cl, 4-Cl**,**
3b : 2-Cl, 5-Cl,
3c : 2-Cl, 6-Cl,
3d : 3-Cl, 4-Cl.

Scheme 2. Synthesis of 3-(dichlorophenyl)-2-methylquinazolin-4(3*H*)-ones under solvent free conditions.

Results and Discussion

Caracterization

The compounds 3a-d were prepared in good yields (53-67 %). It was found that yields of products 3 depend on position of two chlorine atoms. In the 3,4-position of the chlorine, the yield of compound 3d is higher than that of compound 3c (53%). This difference in the yield is due to the steric hindrance of the chloro groups (Table 1).

Table 1. Melting points Mp and yields of compounds 3a-d

Compounds	ArNH	Yields (%)	Melting points (^{0}C)
3a	2,4-diCl_2-C_6H_3	59	142
3b	2,5-diCl_2-C_6H_3	60	128
3c	2,6-diCl_2-C_6H_3	53	130
3d	3,4-diCl_2-C_6H_3	70	219

The UV-Visible spectra of compounds 3a-d reveal two absorptions, with the most intense one attributed to the π→π* transition, and the weaker one characterizing the n→π* electronic transition (Table 2).

Table 2. UV-vis spectral analysis

Compounds	λ(nm)		Transition
		264.1	π→ π*
3a	306.0		π→ π*
	317.9		n→ π*
		255.0	π→ π*
3b	365.0		π→ π*
	305.0		n→ π*
		206.0	π→ π*
3c	305.0		π→ π*
	317.0		n→ π*
		267.0	π→ π*
3d	305.0		π→ π*
	317.0		n→ π*

The IR spectrum also confirms the structure of compounds 3a-d by the appearance of two characteristic bands at 1687.69-1692.20 cm^{-1} and 1602.14-1605.76 cm^{-1} corresponding to the carbonyl and imine functions, respectively.

Table 4. IR bands for the compounds 3a-d as KBr pellets.

Fonction / Compounds	ν C=O	υC=N
3a	1692.14	1602.14
3b	1687.69	1604.62
3c	1692.20	1605.76
3d	1689.00	1604.00

The structures of the synthesised compounds 3a-d were further confirmed by mass spectra and elemental analysis (Table 5). The mass spectrum of product 3b shows a molecular peak with even number (304) and even number (2) of nitrogens, satisfying the nitrogen rule. This peak is accompanied by two peaks at m/z=306 (3.11%) and m/z=308 (1.55%). This is due to the contribution of chlorine isotopes.

Table 5. Elemental analysis and mass spectrometry data.

Compounds	Chemical formula	Elemental analysis
3a	$C_{15}H_{10}Cl_2N_2O$	C 59.04, H 3.30, Cl 23.23, N 9.18, O 5.24
3b	$C_{15}H_{10}Cl_2N_2O$	C 59.04, H 3.30, Cl 23.23, N 9.18, O 5.24
3c	$C_{15}H_{10}Cl_2N_2O$	C 59.04, H 3.30, Cl 23.23, N 9.18, O 5.24
3d	$C_{15}H_{10}Cl_2N_2O$	C 59.04, H 3.30, Cl 23.23, N 9.18, O 5.24

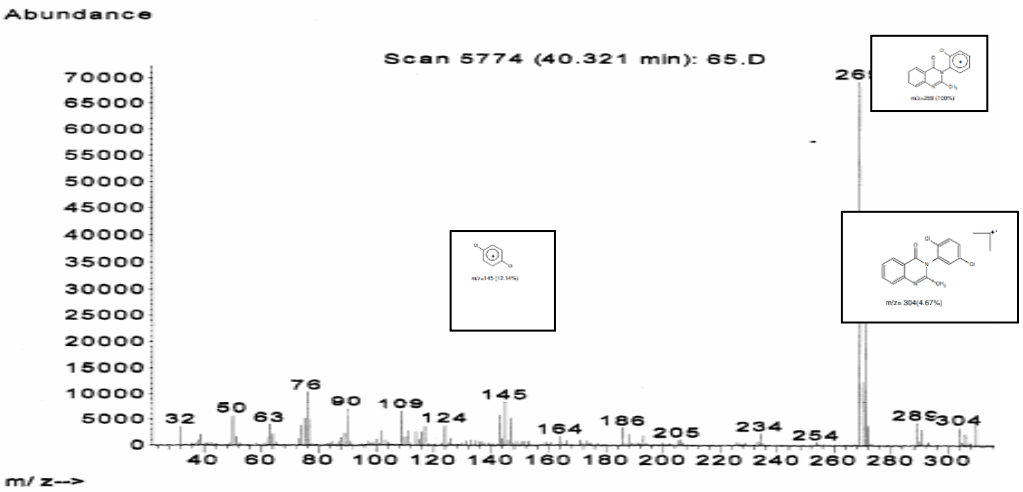

Figure 1. Mass spectra of 3-(2,4-dichlorophenyl)-2-methylquinazolin-4(3*H*)-one 3a.

The 1H-NMR spectrum of compound 3 shows six signals, whose integration is compatible with the total number of protons in the molecule and the presence of a singlet at 2.13 ppm, corresponding to the methyl group. This confirms the structure of our compound 3a-d.

Table 6. NMR data of the compounds 3a-d.

Compounds	1H-NMR (DMSO)	13C-NMR ($CDCl_3$)
3a	δppm = 8.12 (d, 1H), 7.95 (d, 1H); 7.85 (t , 1H); 7.66 (m, 3H); 7.53 (t, 1H), 2.13 (s, 1H).	δppm = 160.93; 154.15; 147.45; 135.61; 135.45; 134.61; 133.12; 132.49; 130.35; 129.50; 127.41; 127.15; 126.88; 120.40; 23.55.
3b	δppm = 8.46 (d, 1H); 7.13 (d, 1H); 7.93 (t, 1H), 7.66 (m, 3H), 7.55 (t, 1H); 2.14 (s, 3H).	δppm = 160.90; 153.92; 147.43; 136.66; 135.13; 133.17; 132.01; 131.68; 131.48; 130.95; 127.42; 127.16; 126.86; 123.02; 23.48.
3c	δppm = 8.12 (d, 1H); 7.94 (d, 1H); 7.80 (t, 1H); 7.55 (m, 3H); 7.12 (t, 1H); 2.11 (s, 1H).	δppm = 161.30; 153.52; 147.52; 135.97; 133.74; 132.70; 129.90; 129.05; 127.74; 127.47; 126.97; 120.06; 25.39.
3d	δppm = 8.12 (d, 1H) ; 7.81 (m, 3H) ; 7.72 (d, 1H) ; 7.63 (m, 2H), 2.20 (s, 1H).	δppm = 161.06; 156.41; 144.90 ; 137.24 ; 135.90, 132.91 ; 132.48 ; 132.10 ; 131.18 ; 129.51 ; 127.82 ; 127.12 ; 125.18 ; 120.32 ; 23.42.

Predication of the Pharmacokinetic Properties and Toxicological Properties via ADMET

In this study, the pharmacokinetic predictions of the quinazolinone 3a-d were estimated. The results revealed that all the investigated molecules show significant values for oral absorption. Compound 3d shows the highest water solubility value among the other analogues. All of the evaluated compounds are predicted to have high cellular permeability, especially for intestinal cells (95.994-96.444%) (Table 7). Generally, it is known that an orally available molecule that satisfies both Lipinski's and Veber's rules has a balance between lipophilicity and hydrophilicity. As shown from table 7, compounds 3a-d follow both Lipinski's and Veber's rules and thus qualify as possible drug-like molecules. The Caco-2 cell line is generally utilized as an in vitro example of the human intestinal mucosa to calculate drug absorption by assessing the log of the apparent permeability coefficient (log Papp; log cm/s). A chemical is considered to have high-level Caco-2 permeability for the pkCSM webserver if its log Papp value is more than 0.90 cm/s. Table 7 shows that all products 3a-d have high Caco-2 permeability.

In terms of the BBB, which determines a drug's capacity to enter the brain while boosting effectiveness (fewer adverse effects), a molecule is capable of moving across the blood-brain barrier quickly when log BB is greater than 0.3. As a result, because the log BB values of all examined derivatives are highest than 0.3, they can only cross the blood - brain barrier marginally. All of the synthesized compounds showed relatively high activity as they inhibit CYP1A2, CYP2C19, and CYP3A4. This can be positively correlated to the lipophilicNity of the compounds to metabolism related toxicity. These results show that these compounds could be involved in drug-drug interactions, and could initiate oxidative stress.

Table 7. ADMET proporties of the synthesis compounds.

Property		Compound **3a**	Compound **3b**	Compound **3c**	Compound **3d**
Absorption	Water solubility (log mol L^{-1})	-4.21	-4.545	-4.545	-4.625
	Caco2 permeability (log Papp in 10^{-6} cm s^{-1})	1.077	1.635	1.629	1.625
	Intestinal absorption (%)	95.994	95.994	96.244	96.444
	Skin permeability (log Kp)	-2.675	-2.339	-2.351	-2.335
	P-Glycoprotein substrate	No	No	No	No
	P-Glycoprotein I	No	No	No	No
	P-Glycoprotein II	Yes	Yes	Yes	Yes
Distribution	VDss (log L kg^{-1})	0.002	-0.133	-0.093	-0.076
	Fraction unbound (Fu)	0.221	0.179	0.181	0.149
	BBB permeability (log BB)	0.556	0.612	0.548	0.565
	CNS permeability (log PS)	-1.354	-1.338	-1.356	-1.328
Metabolism	CYP2D6 substrate	No	Yes	No	No
	CYP3A4 substrate	Yes	Yes	Yes	Yes
	CYP1A2 inhibitor	Yes	Yes	Yes	Yes
	CYP2C19 inhibitor	Yes	Yes	Yes	Yes
	CYP2C9 inhibitor	Yes	No	No	No
	CYP2D6 inhibitor	No	No	No	No
	CYP3A4 inhibitor	No	No	No	Yes
Excretion	Total clearance (log ml mim^{-1} kg^{-1})	0.154	0.205	0.327	0.27
	Renal OCT2 substrate	No	Yes	Yes	Yes
Toxicity	AMES toxicity	Yes	No	No	No
	Max. tolerated dose (log mg kg^{-1} day^{-1})	0.302	-0.123	-0.096	-0.055
	hERG I inhibitor	No	No	No	No
	hERG II inhibitor	No	No	No	No
	Oral rat acute toxicity (LD50) (mol kg^{-1})	2.527	2.132	2.135	2.165
	Oral rat chronic toxicity (LOAEL)	0.776	1.178	1.230	1.301
	(mol kg^{-1}	No	No	No	No
	bw day^{-1})	No	No	No	No
	Hepatotoxicity	0.463	0.885	0.850	0.909
	Skin sensitisation	-0.360	0.133	-0.045	-0.212
	T. pyriformis toxicity (log mg L^{-1})				
	Minnow toxicity (log mM)				

Table 8. Lipinski's and Veber's for the synthesis compounds

Property	Compound **3a**	Compound **3b**	Compound **3c**	Compound **3d**
log P	3.69	3.69	3.69	3.69
Molecular weight	391.14	391.14	391.14	391.14
H-bond acceptors	2	2	2	2
H-bond donor	0	0	0	0
No. of Lipinski's rule violations	0	0	0	0
TPSA	34.89	34.89	34.89	34.89

In conclusion, in this study, pkCSM software was used to predict the toxicological properties of the target compounds. Furthermore, this software has a system that performs predictions on the type of toxicity that a compound presents, such as mutagenicity, hepatotoxicity, cardiotoxicity, and skin sensitization. Herein, the bacterial mutagenic potential of the quinazoline derivatives through Ames toxicity testing showed that three analogues, namely 3b-d, could be considered as non-mutagenic agents. Yet, the toxicities of all of the compounds in T. pyriformis are high. Also, the investigated compounds were predicted for one of the important parameters regarding toxicity, which is cardiotoxicity, in the form of human ether-a-go-go-related gene I/II (hERG I/II), which was found to be at an acceptable level. G protein-coupled receptor (GPCR) ligand: The quinazoline (3a, 3b, and 3c) were found to be active with the bioactivity scores in the range from 0.02 to 0.04. the compound 3d was inactive.

• Ion channel modulator: the quinazoline 3a was found to be active with the bioactivity scores 0.01 while the other compounds were found to be moderately active with the bioactivity scores in the range from -0.04 to -0.13.

• Kinase inhibitor: all the quinazoline were found to be moderately active with the bioactivity scores in the range from -0.10 to -0.36.

• Nuclear receptor inhibitor: the two quinazoline 3a and 3d were found to be inactive with the bioactivity scores less than -0.50 (the range from -0.51 to -0.52). While the two compounds 3b-3c were found to be moderately active with the bioactivity scores -0.48.

• Protease inhibitor: all the quinazoline were found to be moderately active with the bioactivity scores in the range from -0.17 to -0.33.

Table 9. The bioactivity scores prediction of the compound 3a-d.

The bioactivity scores	Compound **3a**	Compound **3b**	Compound **3c**	Compound **3d**
GPCR ligand[a]	0.03	0.04	0.02	-0.05
Ion channel modulator	0.01	-0.13	-0.04	-0.13
Kinase inhibitor	-0.30	-0.18	-0.10	-0.36
Nuclear receptor ligand	-0.52	-0.48	-0.48	-0.51
Protease inhibitor	-0.50	-0.22	-0.46	-0.52
Enzyme inhibitor	-0.33	-0.33	-0.17	-0.28

[a]G protein-coupled receptor (GPCR) ligand

Conclusion

We developed an efficient synthesis of 2-methylquinazolin-4(3*H*)-ones using the 2-methylbenzoxazin-4-one and substituted anilines under PW_{12}-mediated catalysis, microwave irradiation and solvent-free conditions. Mildness of the catalysts, avoidance of solvents, short reaction times and good yields are the outstanding advantages of the present protocol. The structures of synthesized compounds were performed by UV-visible, IR, 1H-NMR, 13C-NMR and spectroscopy mass. Furthermore, ADMET and bioactivity scores properties were calculated and showed satisfactory pharmacokinetic and toxicological properties.

Scientific Ethics Declaration

The authors declare that the scientific ethical and legal responsibility of this article published in EPSTEM journal belongs to the authors.

Acknowledgements or Notes

* This article was presented as a poster presentation at the International Conference on Basic Sciences, Engineering and Technology (www.icbaset.net) held in Alanya/Turkey on May 02-05, 2024.

References

Alagarsamy, V., Pathak, U.S., Venkateshperumal, R., Meena, S., Thirumurugan, K., Solomon, V. R., & De Clercq, E. (2003). Anti-HIV and anti-bacterial activities of 2-substituted thiadiazolo quinazolines. *Indian Journal of Pharmaceutical Sciences*, *65*(3), 293-296.

Alagarsamy, V., Solomon, V. R., Vanikavitha, G., Paluchamy, V., Chandran, M.R., Sujin, A.A., Thangathiruppathy, A., Amuthalakshmi, S., & Revathi, R. (2002). Synthesis, analgesic, anti-inflammatory and anti-bacterial activities of some novel 2-phenyl-3-substituted quinazolin-4(3H)-ones, *Biological and Pharmaceutical Bulletin*, *25*(11), 1432-1435.

El-Hashash, M. A., Elshahawi, M. M., Ragab, E. A., & Nagdy, S. (2015). Synthesis and antifungal activity of novel quinazolin-4 (3 H)-one derivatives. *Synthetic Communications*, *45*(19), 2240-2250.

Ighilahriz-Boubchir, K., Boutemeur-Kheddis, B., Rabia, C., Makhloufi-Chebli, M., Hamdi, M., & Silva. M.S. A. (2007). Recyclable Keggin heteropolyacids as an environmentally benign catalyst for the synthesis of new 2-benzoylamino-*n*-phenyl-benzamide derivatives under microwave ırradiations at solvent-free conditions and the evaluation of biological activity. *Molecules*, *23*(1), 8.

Kidwai, M., Rastogi, S., & Mohan, R. (2003). Rudy. *Croatica Chemoca Acta*, *76*(4), 365.

Kumar, A., Singh, R.C., & Kumar, B.S. (2007). Synthesis of 3-[4'-(p-chlorophenyl)-thiazol-2'-yl]-2-[(substitutedazetidinone/thiazolidinone)-aminomethyl]-6-bromoquinazolin-4- ones as anti-inflammatory agent, *Bioorganic & Medcinal Chemistry*, *15*(8), 3089-3096.

Pires, D. E., Blundell, T. L., & Ascher, D. B. (2005). pkCSM: Predicting small-molecule pharmacokinetic properties using graph-based signatures, *Journal Medicinal Chemestry*, *58*(9), 4066-4072.

Rad-Moghadam, K., & Khajavi, M. (2006). One pot synthesis of substituted Quinazolin-4(3*H*)-ones under microwave irradiation. *Journal of Chemical Research*, (11), 702-703.

Saleh, M., Hafez, Y., Abdel-Hay, F., & Gad, G. (2004), Synthesis and biological activities of some new 3H-quinazolin-4-one derivatives derived from 3-phenylamino-2-thioxo-3H-quinazolin-4-one. *Phosphorus, Sulfur and Silicon*, *179*(2), 411-426.

Author Information

Karima Ighilahriz-Boubchir
Laboratory de Physic and Chemistry of Materials LPCM, Departement of Chemistry, Faculty of Sciences, University Mouloud Mammeri, 15000, TiziOuzou, Algeria
Contact e-mail: *karima.boubchir@ummto.com*

Amina Benazzouz-Touami
Laboratory de Physic and Chemistry of Materials LPCM, Departement of Chemistry, Faculty of Sciences, University Mouloud Mammeri, 15000, TiziOuzou, Algeria

Malika Makhloufi-Chebli
Laboratory de Physic and Chemistry of Materials LPCM, Departement of Chemistry, Faculty of Sciences, University Mouloud Mammeri, 15000, TiziOuzou, Algeria

To cite this article:

Ighilahriz-Boubchir, K., Benazzouz-Touami, A. & Makhloufi-Chebli, M. (2024). Design, synthesis and in silico studies of new 2-methyl quinazolin-4(3*h*)-ones derivatives. *The Eurasia Proceedings of Science, Technology, Engineering & Mathematics (EPSTEM), 28*, 519-525.

The Eurasia Proceedings of Science, Technology, Engineering & Mathematics (EPSTEM)
ISSN: 2602-3199

The Eurasia Proceedings of Science, Technology, Engineering & Mathematics (EPSTEM), 2024

Volume 28, Pages 526-532

ICBASET 2024: International Conference on Basic Sciences, Engineering and Technology

Influence of Digital Marketing Techniques on Consumer Behavior for Mobile Services

Iyad A.A Khanfar
Zarqa University

Abstract: The aim of this research was to explore how different digital marketing techniques, such as video marketing, internet advertising, email marketing, and SEO, impact consumer behavior regarding mobile services offered by Zain Telecom in Amman, Jordan. A simple random survey method was employed, with 445 questionnaires distributed to Zain Telecom customers in Amman. After excluding incomplete responses, 405 completed questionnaires were analyzed using multiple regression, descriptive analysis, and reliability testing. The findings indicate that all the independent variables significantly influence consumer behavior in purchasing mobile services, with email marketing exhibiting the strongest impact. Consequently, the study suggests an increased investment in email marketing techniques.

Keywords: Digital marketing, Business engineering, Mobile services

Introduction

Thanks to the advancements in the Internet and technology, individuals now have the ability to communicate and engage with people residing in different countries. These technological advancements have enabled companies to establish direct communication channels with their customers, a phenomenon commonly referred to as digital marketing. Digital marketing involves the presentation, promotion, or sale of products and services through various online platforms (Yasmin et al., 2015).

In contrast, traditional marketing encompasses older methods such as newspapers, television, brochures, etc., to inform consumers about products. Understanding customer needs and preferences has become more efficient and accessible due to technological advancements. Online polls and questionnaires facilitate surveys and market research, streamlining the process for businesses. Through digital marketing, companies can more effectively communicate with customers, fostering more fruitful and positive client relationships (Garg et al., 2020).

Digital marketing has demonstrated benefits for both customers and businesses. By implementing digital marketing strategies, businesses can enhance productivity and reduce costs simultaneously. It has been observed that companies adopting digital marketing practices have succeeded in reducing expenses while expanding their market reach and customer base.

Research Problems and Questions

Nowadays, there is stiff competition among telecommunications companies; therefore, Zain Telecom Company needs to develop effective digital marketing techniques to survive in this competition. These questions are addressed in this study with the aim of providing answers.

– Does the Video marketing technique used by Zain Telecom Company influence a Consumer behavior to purchase mobile services?
– Does the Internet advertising technique used by Zain Telecom Company influence a Consumer behavior to purchase mobile services??
– Does the email marketing technique used by Zain Telecom Company influence a Consumer behavior to purchase mobile services?
– Does the search engine optimization (SEO) technique used by Zain Telecom Company influence a Consumer behavior to purchase mobile services

Literature Review

Digital Marketing Techniques

Digital marketing has become increasingly significant in contemporary Jordan. Marketers employ this novel type of digital marketing tools to increase sales of goods and services. Businesses and brands increasingly use a variety of digital platforms and technologies for their marketing initiatives as a result of the growth of digital marketing.

People use digital devices rather than going to real stores. As a result, the most widespread and effective marketing campaigns are online (Rai, 2018.) This is a result of the gradual incorporation of digital platforms into advertising campaigns and everyday life.

Video Marketing

Video is defined as "an audiovisual technique for recording image and sound on a magnetic medium and reproducing this recording on a screen" by Le Robert's dictionary. Videos are a language that use visuals (and typically sounds), according to Costa-Sanchez (2017), who opts for a more straightforward description. For his part, Schwenzow (2021) references the Berkeley Institute of Design's (2012) definition of "video" and adds additional specific technical information to the description of "Le Robert." Indeed, the term "video" is used here to refer to "sequences of images, typically at a frame rate of 20 to 30 fps." The same Institute goes on to say that humans can only see a sequence of images moving fluidly up to a threshold of 20 frames per second. with this confirmation by pointing out that video marketing piques people's emotions.Finally, Scott (2017) describe s video marketing as a tool for companies to speak with customers directly.

Internet Advertising

The delivery of marketing messages to consumers over the internet is known as online advertising, sometimes known as online marketing, internet advertising, or web advertising. Globally, the number of internet users is rising quickly. This facility is being used by all kinds of people to pass the time or learn new information (Eshghi, Sarkar & Sarkar 2017). When a customer uses Google or another search engine, numerous organizations simultaneously offer identical products.

According to Sadia Afzal and Javed Rabbani Khan, "Impact of online and conventional advertising on consumer branded apparel purchasing behavior" (2015), there is no direct impact of online advertising. And generally, on consumer buying behavior of branded clothing, but there is a marked effect. The indirect effects of the two-advertising media on consumers' purchasing behavior due to the advertising characteristics and consumer attitudes are mediated and have a large mediating effect. He also mentioned that their purchasing decisions depend on previous experience with the product, brand loyalty and word of mouth. Therefore, it can be concluded that online advertising has a certain influence on the purchasing behavior of consumers. Some advertising agencies actively manage and control online media. If we review the latest research, we conclude that social media advertising has a significant influence on consumers and their purchasing decisions.

Email Marketing

In the early days of e-commerce, email was one of the first forms of communication that was extensively utilized, and despite the introduction of a number of new communication channels, it still plays a significant role for many multi-channel businesses. In fact, according to a number of industry surveys, email is not only among the most popular direct marketing methods, but it may also help businesses make more money (Zhang et al., 2017). Email answers are successful in general, however prior research has shown that they vary based on the consumer profile "Wu, Li and Liu, 2018".

The early forms of direct marketing, such conventional mailings and catalogues, which have been well studied, are where the present usage of email originated. For instance, Bult and Wansbeek (1995) came to the conclusion that clients with a history of making larger purchases have greater response rates. Email marketing has distinct qualities that can't be immediately translated from traditional direct marketing literature, according to Bronfer and Drèze's (2009) analysis. In addition, email differs from other digital mediums in a number of ways. Email, for instance, allows advertisers more control over message delivery dates and the environment in which messages are shown when it comes to online display advertising.

Email is a marketing channel that has inspired a lot of academic research. For instance, in 2014, the authors of the paper “The Impact of Electronic Message Personalization on Customers’ Perception of Privacy Risks” (Song, Kim, Han) examined the impact of email message personalization on consumers’ perception of privacy risks. In 2018, the authors of “Personalization and Business Metrics in Email Marketing” (Sahni, Wheeler, Chintagunta) looked at the impact of email personalization on business metrics, including sales and churn rates, in a series of studies. The authors found that personalization led to better performance. They also proposed several mechanisms that explain how personalization can help boost sales.

Search Engine Optimization (SEO)

The search engine is a component of software or a service which allows users to conduct searches for information on the Internet or in a particular database using keywords as well as phrases. To create an accessible database of information found on the World Wide Web, search engines utilize web crawlers, also known as spiders, for indexing web pages and other online material. A search engine that receives a user's search query provides a list of pertinent web pages or documents that match the query. Among the most used search engines are Bing, Google, Yahoo!, and Baidu. (Kritzinger & Weideman, 2013).

Consumer Behavior

Hollebeek (2019) defines consumer behavior as “the ever-evolving relationship between affect and cognition, behavior, and the environment in which people engage in the exchange-related activities of their lives.” How consumers respond to a marketing or advertising campaign depends on a number of factors. These factors become increasingly important in a digital environment, making the use of this medium more challenging. Some of the factors that influence consumer behavior include: Customer involvement Customer perception Schivinski (2016) Dabrowski (Schivinski & Dabrowski, 2016) Ethical considerations (Järvinen, 2015) Behavioral economics Dowling (2019).

Research Hypotheses

- The hypotheses were refined and developed based on a comprehensive review of literature and relevant theories:
- H1: Video marketing has a significant influence on consumer behavior regarding the mobile services provided by Zain Telecom Company in Amman city.
- H2: Internet advertising has a significant influence on consumer behavior regarding the mobile services provided by Zain Telecom Company in Amman city.

- H3: Email marketing has a significant influence on consumer behavior regarding the mobile services provided by Zain Telecom Company in Amman city.
- H4: Search engine optimization (SEO) has a significant influence on consumer behavior regarding the mobile services provided by Zain Telecom Company in Amman city.

Study Model

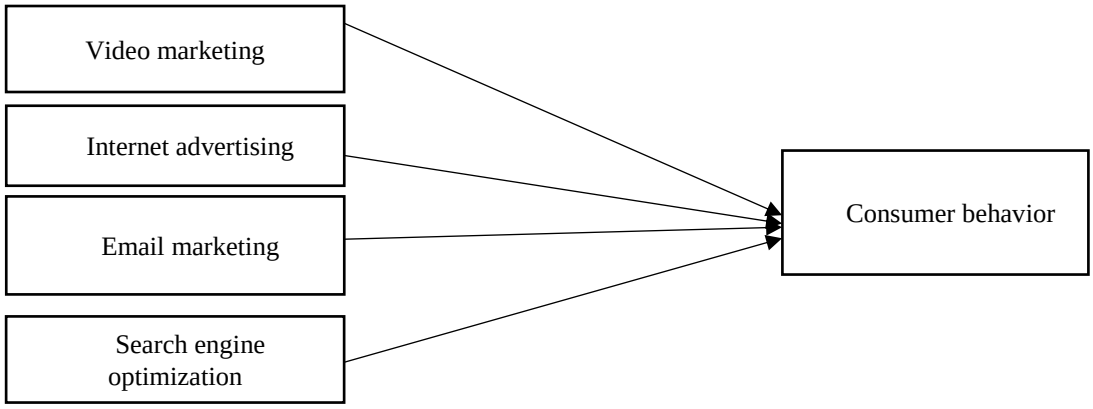

Study Methodology

This study contains a survey of people who purchase mobile services of Zain telecom Company at Amman city. The methodology of the study includes sections on survey design, reliability findings, sample size and method, population, and study design. The study will concentrate on the digital marketing techniques, particularly how video marketing, internet advertising, email marketing, and (SEO) influenced on consumer behavior of mobile services. These four hypotheses have been proposed to explain relationships between independent variables and the dependent variable of consumer behavior.

The study makes an effort to ensure that the survey is understandable. Customers of Zain Telecom Company were made aware of the goal of the study and asked for feedback on the questions; a few respondents pointed out that some words were unclear. Aside from these comments, the pre-test survey results indicate that the questions are factually correct, precise, and easy to understand. Unclear words were removed after the pre-test, according to (Hair et al 2006). Suitability samples are the most popular type of sample design in humanities research because it allows for the use of an accurate database and statistical system. This model design approach can also be used in service marketing. All customers of Zain Telecom's mobile services make up the study's population. Only 405 of the 445 questionnaires distributed to Zain telecom customers at Amman city were returned; the analysis was done using those 405 responses. The number 405 is regarded as suitable for data analysis (Sekaran, 2003).

Survey Designing

Surveys were crafted with three distinct sections to gather data. The initial section focused on gathering demographic details from respondents, encompassing gender, age, education, salary, and marital status. Utilizing a Likert scale, both independent and dependent variables were assessed, a common practice across diverse fields like marketing and humanities. The second section comprised 25 questions aimed at evaluating independent variables such as Video marketing, internet advertising, email marketing, and SEO. Meanwhile, the third section consisted of 8 questions tailored to measure the dependent variable, specifically customers' purchasing decisions. It's worth noting that, according to the findings of various researchers, utilizing a 5-point scale is considered as effective as any other method (Churchill, 2004).

Reliability Test

All calculated variables meet the reliability threshold of 0.70. Table 1 displays the Cronbach's Alpha for each variable, indicating a high level of reliability across all variables. Table 1 delineates five distinct categories.

Table 1.Reliability analysis

Variables	Item number	Cronbach alpha
Video marketing	6	0.84
Internet advertising	6	0.82
Email marketing	6	0.78
SEO	7	0.76
Consumer behavior	7	0.79

To evaluate the reliability of the gathered information, Cronbach's alpha was utilized, with a recommended range greater than 0.70. This technique serves as the final method for confirming the consistency of the overall scale under various conditions. The study employed Cronbach's alpha to assess item reliability. The computed Cronbach alpha, depicted in the table above, ranges from 0.750 to 0.840, indicating a very good result. Demonstrated in the discussion that follows by the "Mean value" of the respondents' responses.

Table 2.Means and standard deviations

Variables	Mean	Std. Deviation
Video marketing	5.13	0.673
Internet advertising	4.15	0.824
Email marketing	5.21	0.668
SEO	5.11	0.635
Consumer behavior	5.22	0.671

Descriptive analysis was utilized to analyze the data, focusing on participants' evaluative criteria. By examining participants' responses, both descriptively and through average value scores, their evaluation criteria were determined. Table 2 illustrates the calculated minimum and maximum scores, providing an interval evaluation. Mean and standard deviation values for each variable, based on 405 valid responses, were examined (see Table 2). The variable with the highest mean score, reflecting consumer behavior according to participant responses, was analyzed. The results highlight email marketing as the most significant factor influencing consumer behavior. The high mean scores suggest that the majority of respondents agreed on the impact of these factors. Overall, these findings indicate a significant relationship between consumer behavior and Zain Telecom customers' decision-making processes regarding mobile services.

Simple Regression

Simple regression analysis demonstrates the influence and contribution of each variable on the dependent variable, which is consumers' behavior. The coefficient of determination (R-squared) value is presented in Table (3).

Table 3. Simple regression

Variables	**R2**
Video marketing	0.169
Internet advertising	0.159
Email marketing	0.282
Search engine optimization	0.057

Video marketing explains 16.9% of the variance in consumer behavior. Internet advertising explains 15.9% of the variance. Email marketing has the highest impact, explaining 28.2% of the variance. SEO has a lower impact, explaining 5.7% of the variance.

Conclusion

This research investigates the influence of various online marketing techniques, such as Content Marketing, Email Marketing, Social Media Marketing, and SEO, on the purchasing decisions of internet services offered by Zain Telecom Company within the Jordanian market. The results indicate a positive effect of all independent variables on customers' purchasing decisions, with Email Marketing emerging as the most influential techniques among the four. The study suggests a reevaluation of marketing approaches targeting users, given that customers increasingly seek comprehensive information to compare products and alternatives before making a purchase. Nonetheless, it's crucial to acknowledge the study's limitation to Zain Telecom customers exclusively, emphasizing the need for future research encompassing larger sample sizes and exploring additional online marketing techniques to ensure more precise outcomes. Overall, this research significantly contributes to the understanding of online marketing dynamics and their impact on customers' purchasing behavior within the Jordanian market.

Scientific Ethics Declaration

The author declares that the scientific ethical and legal responsibility of this article published in EPSTEM journal belongs to the authors.

Acknowledgements or Notes

* This article was presented as an oral presentation at the International Conference on Basic Sciences, Engineering and Technology (www.icbaset.net) held in Alanya/Turkey on May 02-05, 2024.

References

Alnsour, M. (2018). Social media effect on purchase intention: Jordanian airline industry. *Journal of Internet Banking and Commerce*, *23*(2), 20-28.

Alzyoud, M. F. (2018). Does social media marketing enhance impulse purchasing among female customers: case study of Jordanian female shoppers. *Journal of Business and Retail Management Research, 13*(2), 135-151.

Al-Shaikh, M. S., & Khanfar, I. A. (2023). Delivery service via electronic applications and its impact on customers satisfaction at retail stores in Amman City/Jordan. In V. Reimers, C. Chao, & S. Gorman (Eds.), *The Implementation of Smart Technologies for Business Success and Sustainability* (pp. 827-837). Springer, Cham.

Bansal, R., Masood, R., & Dadhich, V. (2014). Social media marketing- a tool of innovative marketing. *Journal of Organizational Management, 3*(1), 1-7.

Budiman, S. (2021). The effects of social media on brand image and brand loyalty in generation y. *Journal of Asian Finance, Economics and Business, 8*(3), 1339-1347.

Berkeley Institute of Design. (2012). *Human information processing - CS 160 fall 2012*. Retrieved from https://bid.berkeley.edu/cs160-fall12/index.php/Human_Information_Processing.

Churchill, G., & Iacobucci, D. (2004). *Marketing research: Methodological foundations* (9th ed.). Ohio: Thomson South-Western.

Content Marketing Institute. (n.d.). *What is content marketing?* Retrieved from www.contentmarketinginstitute.com/what-is-content-marketing

Garg, M., Bansal, A., & Single, K. (2021). Impacts of digital marketing on consumer decision making. *International Journal for Scientific Research & Development, 8*(3), 213-218.

Iskandar, M., & Komara, D. (2018). Application marketing strategy search engine optimization (SEO). *IOP Conference Series: Materials Science and Engineering, 407*, 012011.

Kaukoranta, M. (2015). How to reach more target customers by search engine optimization (SEO) and search engine advertising (SEA). *Seinäjoki University of Applied Sciences,* 19-33.

Khanfar, I. A., Dalbah, I., Atteyh, A. A., & Al-Shaikh, M. S. (2023). The impact of choosing distribution channels factors during the coronavirus pandemic on the wholesaler's satisfaction. In V. Reimers, C. Chao, & S.

Gorman (Eds.), *The implementation of smart technologies for business success and sustainability* (pp. 65-79). Cham: Springer.

Kotler, P. H., & Keller, K. L. (2013). *Marketing management* (14th ed.). England :Pearson Education.

Lou, C., & Xie, Q. (2021). Something social, something entertaining? How digital content marketing augments consumer experience and brand loyalty. *International Journal of Advertising, 40*(3), 376-402.

Lopezosa, C., Codina, L., Díaz-Noci, J., & Ontalba, J. (2020). SEO and the digital news media: From the workplace to the classroom. *Comunicar, 28*(63), 65-75.

Lodhi, S., & Shoaib, M. (2017). Impact of e-marketing on consumer behavior: a case of Karachi, Pakistan. *Journal of Business and Management, 19*(1), 90-101.

Mohr, L. B. (1990). *Understanding significance tests*. Newbury Park, CA: Sage Publications.

Nur, E. (2021). The impact of social media on firm value: a case study of oil and gas firms in Indonesia. *Journal of Asian Finance, Economics and Business, 8*(3), 0987-0996.

Omar, A., & Atteya, N. (2020). The impact of digital marketing on consumer buying decision process in the Egyptian market. *International Journal of Business and Management, 15*(7), 120-132.

Rafiq, M., & Malik, A. (2018). Impact of social media on purchasing decision of consumer with special reference to Lahore, Pakistan. *Journal of Social Sciences, 4*(2), 268-273.

Pulizzi, J. (2014). *Epic Content Marketing - How to tell a different story, break through the clutter, and win more customers by marketing less*. McGraw Hill.

Reimers, V., Chao, C., & Gorman, S. (2016). Permission email marketing and its influence on online shopping. *Asia Pacific Journal of Marketing and Logistics, 28*(2), 308-322.

Stefan, S. (2019). Factors affecting purchasing decision and operation of alternative fuel powered heavy duty trucks in German. *Transportation Research, 5*(4), 87–107.

Saunders, M., & Lewis, P. (2012). *Doing research in business and management: an essential guide to planning your project*. Harlow, UK: Financial Times Prentice Hall.

Ugonna, J., Victor, O., & Jeft, O. (2017). Effects of online marketing on the behavior of consumers in selected online companies in owerri, imo state - Nigeria. *International Journal of Business and Management Invention, 6*(6), 32-43.

Author Information

Iyad A.A Khanfar
Empirical Study in Jordan, Faculty of Economics and Administrative Science, Zarqa University, Jordan
Contact e-mail: *i.khanfar@zu.edu.jo*

To cite this article:

Khanfar, I. A. A. (2024). Influence of digital marketing techniques on consumer behavior for mobile services. *The Eurasia Proceedings of Science, Technology, Engineering & Mathematics (EPSTEM), 28,* 526-532.

The Eurasia Proceedings of Science, Technology, Engineering & Mathematics (EPSTEM)
ISSN: 2602-3199

The Eurasia Proceedings of Science, Technology, Engineering & Mathematics (EPSTEM), 2024

Volume 28, Pages 533-553

ICBASET 2024: International Conference on Basic Sciences, Engineering and Technology

Software Project Management and Their Economic Evaluation in terms of Enterprise Sustainability

Ibrahim Krasniqi
University Haxhi Zeka

Naim Ismajli
AAB College

Ganimete Krasniqi
Ministry of Environment, Spatial Planning and Infrastructure

Abstract: Nowadays, we are witnessing that projects, computers and software as an integral part of them infiltrates or rather ruthlessly penetrates all spheres of business and daily life of a modern society and directs enterprise development, efficiency, productivity, competitiveness, image and ultimately in a way their very existence. In recent decades, the software industry and its products have become one of the factors without which the normal operation of contemporary economies cannot be imagined, however, software development often presents almost insurmountable difficulties.The research is related exactly to the analysis of software projects and their impact in the sustainability of enterprises. It is difficult to imagine any enterprise that claims to be competitive, to prepare, realize and monitor their projects without software support, be it standard software or specially developed for the needs of the enterprise, where software development comes into play. During the research combined methods are utilized. The methodology used includes the theoretical analysis which is based on the current literature from this field, followed by "case studies" that deal with the development of software projects in Kosovo by conducting interviews with their IT managers using face to face and semi structured interviews and finally based on gathered data the development of a concrete software project has been simulated. Finally the outcome from research is that always software development has to be identified with the project objectives of the project contractors and aims to meet their requirements and expectations. Software project team's work for years in the development of complex and professional software projects, where competence in the relevant field as well as motivation play a key role in the development of successful business projects.

Keywords: Project management, Software projects, Business engineering

Introduction

In the modern business environment, software projects play a pivotal role in the operations and success of enterprises across various industries. Effective software project management is essential for ensuring the timely delivery of high-quality products and services, meeting customer expectations, and maintaining competitive advantage (Aarseth et al., 2017). However, alongside the technical aspects of project management, there is an increasing recognition of the importance of economic evaluation in terms of enterprise sustainability (Acar, 2017). Enterprise sustainability encompasses the long-term viability and resilience of organizations in economic, social, and environmental dimensions. It goes beyond short-term profitability and considers the broader impact of business activities on stakeholders, society, and the planet (Albertao et al., 2010). In this context, evaluating software projects from an economic standpoint becomes crucial not only for financial performance but also for sustainable development. This study aims to explore the intersection of software

project management and economic evaluation within the framework of enterprise sustainability (Alharthi. et al., 2016). By examining the economic aspects of software projects, including costs, benefits, risks, and returns on investment, we seek to understand their implications for the overall sustainability of enterprises. Through rigorous analysis and empirical evidence, we aim to shed light on how organizations can optimize their software project management practices to enhance sustainability outcomes (Becker et al., 2017). The significance of this research lies in its potential to inform decision-making processes within organizations, guiding resource allocation, investment strategies, and project prioritization. By integrating economic evaluation into software project management practices, enterprises can not only achieve short-term objectives but also contribute to long-term sustainability goals (Beghoura et al., 2017). Moreover, by considering sustainability criteria in project decision-making, organizations can align their activities with societal values, regulatory requirements, and environmental stewardship *Calero and Piattini (2017). In the subsequent sections of this paper, we will delve into the theoretical foundations of software project management and economic evaluation, review relevant literature, propose a conceptual framework for analysis, and present empirical findings from case studies or data analysis (Calero et al., 2013). Ultimately, we aim to provide insights and recommendations that can support practitioners, policymakers, and scholars in advancing the sustainability agenda within the realm of software project management (Garcıa-Mireles et al., 2018).

Indeed, we are witnessing that computers and software as an integral part of them infiltrates or rather ruthlessly penetrates all spheres of life of a modern society and directs development, efficiency, productivity, competitiveness, image and ultimately in a way their very existence (Garcıa-Mireles et al., 2018). In recent decades, the software industry and its products have become one of the factors without which the normal operation of contemporary economies cannot be imagined, however, software development often presents almost insurmountable difficulties (Huemann, & Silvius, 2018). It is difficult to imagine any enterprise that claims to be competitive, without software support, whether it is standard software or specially developed for the needs of the enterprise, where software development comes into play. Software development is identified with the project objectives of the project contractors and aims to meet their requirements and expectations (Kern et al., 2015). Software project teams work for years in the development of complex and professional software projects, where competence in the relevant field as well as motivation play a key role in the development of successful business projects (Kern et al., 2013)

Statement of the Problem

The main objective of this study has been to analyze the problem of identification, planning and evaluation of software projects to give a modest theoretical contribution regarding the methods and their specifics. The research in this study is based on the fact that:

- The development of software projects, as well as many investments from the field of information technology, presents a high degree of risk, which is especially related to the change in user preferences and their unrealistic expectations. All this is related to the very nature of the software. It is a very specific, immaterial product and as such cannot be seen or touched. This makes the development and management of software projects much more complex than the development and management of classic projects. In fact, the software project manager can monitor and control the development of the project only based on a solid documentation of it. The chances that this determination / assessment of software project development is not objective are very high.
- The goal of software project management is to increase productivity, raise quality, and minimize costs during software creation. This requires the coordination of influential factors, the balance between which enables the development of the software project within the anticipated budget, anticipated time limits and planned expenses. In this paper, attention is focused on the identification and evaluation of software projects. Other phases in the project management cycle have been addressed as necessary.

Research Questions

1. What is the difference between other projects and software projects?
2. What is the most suitable method for evaluating the software project?
3. In Kosovo, which method is more efficient to use?

Literature Review

Sustainability is a multifaceted term; it has different meanings to different groups and contexts. A meaningful and reasonable understanding of sustainability implies collective efforts of socially responsible actions and their impact on others especially in the future. Huemann and Silvius, (2017), defined business sustainability as "meeting needs of the firm's direct and indirect stakeholders, such as shareholders, employees, clients, pressure groups, communities, without compromising its ability to meet future stakeholder needs as well" . Some research considered when organizations utilize recent IT/IS in favour of enhanced performance levels that last for longer time, is called sustainable IT. In this regard, information systems play an important role in improving the efficiency of firms' operations and supply chains, which links to sustainability (Lago et al., 2018). Researchers Marnewick, C. (2017), believe that sustainable IT is characterized by the application of IT practices and technologies for the benefit of different stakeholders to ensure long-term benefits in economic, social, and environmental sustainability pillars (Martens, M.L. and Carvalho, M.M. 2016), Previously, sustainability has been envisaged as a constraint in the business domain (Økland, A. 2015). The success of business organizations have been founded upon minimizing costs and increasing revenues. Software project management and its economic evaluation in terms of enterprise sustainability nowadays is becoming very popular and important in general. In order to understand the topic and aim the research will analyze the terms and bescribe their role in enterprice sustainalbility.

Software Project Management (SPM) Frameworks: Numerous SPM frameworks exist, such as Agile, Waterfall, and DevOps (Pohludka et al., 2018). These frameworks offer different methodologies for managing software development projects, each with its own set of advantages and challenges. Enterprise Sustainability: Enterprise sustainability encompasses the long-term viability and resilience of an organization in terms of economic, environmental, and social factors. In the context of software project management, sustainability involves ensuring that software projects are delivered efficiently, effectively, and in a manner that aligns with the organization's overall sustainability goals (Savitz. 2013).

Economic Evaluation of Software Projects: Economic evaluation techniques, such as Cost-Benefit Analysis (CBA) and Return on Investment (ROI), are commonly used to assess the financial viability of software projects (Silvius et al., 2018). These evaluations consider factors such as development costs, potential revenue or cost savings, and the overall economic impact on the organization. Alignment with Sustainability Goals: Researchers have highlighted the importance of aligning software project management practices with broader sustainability goals. This alignment involves considering factors such as resource efficiency, waste reduction, and the environmental impact of software development processes (Sumner, 2018).

Sustainable Software Development Practices: Adopting sustainable software development practices, such as green computing and energy-efficient programming techniques, can contribute to both economic savings and environmental sustainability (Statista.com. 2021). These practices aim to minimize the carbon footprint and ecological impact of software projects while optimizing resource utilization. Challenges and Opportunities: Despite the growing recognition of the importance of sustainability in software project management, organizations face various challenges in implementing sustainable practices (Turner et al., 2013). These challenges include balancing short-term economic concerns with long-term sustainability goals, overcoming resistance to change, and integrating sustainability considerations into existing project management processes (Yunis et al., 2013).

Future Directions: Future research in this area may focus on developing comprehensive frameworks and methodologies for integrating sustainability into software project management practices. Additionally, there is a need for empirical studies to assess the real-world impact of sustainable software development practices on enterprise sustainability metrics (Zerbino et al., 2021). This literature review provides an overview of the current state of research on software project management and its economic evaluation in the context of enterprise sustainability (Ziemba, 2019), It highlights the importance of aligning software project management practices with broader sustainability goals and identifies opportunities for future research and practice in this area.

Software Projects, Their Types and Features

It is difficult to imagine any enterprise that claims to be competitive, without software support, whether it is standard software or developed specifically for the needs of the enterprise. The software project represents that type of project where mainly or exclusively software is developed. However, it should be borne in mind that the types of projects dealing with software development are very different. According to Ziemba, E. (2019), software projects are of different types such as:

- development projects,
- prototype projects,
- evolutionary projects,
- migration projects,
- maintenance projects,
- projects for integration, and
- projects for installation.

There are major differences between the Software and other projects such as:

- software is immaterial, not physical,
- software is not produced, but developed,
- the software does not wear out,
- the development and delivery of the software, most often, is contracted as a whole and not as parts (unless it is developed with separate modules).

The software presents a summary of ideas, designs, instructions and formulas. Next, let's see what the project represents and what are the differences between software projects (Sumner, M. 2018). In addition to what was said above, there are also some other features that characterize software projects, such as:

- In most cases, the realization of an idea is done for the first time,
- Long duration,
- Great opportunities for presenting problems, respectively different risks.

Acordıng to Schieg, M. (2009), Features of the software projects are:

- Intangible product,
- It is not possible to accurately measure the development time of the project,
- Software development does not flow in a defined manner,
- The development process is not yet clearly defined,
- Distribution of tasks,
- Software engineering is not a natural science,
- High level of abstraction and at the same time low level of standardization.

In the literature, we will also come across a classification based on the size of the project, such as the size of the software project, depending on the hours committed to its development:

- small 1 – 250 hours
- medium 251 – 5,000 hours
- great over 5 000 hours

According to the application and the groups to which they are dedicated:

- Individual software (individual production, contract production)
- Standard software (standardized solutions, user groups)

Another division of software projects is the classification of software according to the degree of difficulty - its complexity; classification that when put in relation to the so-called maturity level of the process model (of software development) Capability Maturity Model - CMM, a very clear overview of the company's competitive capabilities in the software market will be obtained, and also indirectly reflects the state of development of the software industry.

Capability Maturity Model - CMM can be said to represent the level of experience achieved by the enterprise in the development of software projects, according to which there are five degrees of maturity of the development process, respectively of the enterprise's ability to develop software projects. The aforementioned division or classification is as follows:

Type "S" software can be fully described through a formal specification, which means that the generated software corresponds to the specification faithfully. Typical examples of "S" (Specification) software are programs for sorting data, or for calculating various mathematical functions.

"P" (Problem) type software represents that software that solves a defined and specific problem, while typical examples of "P" software represent programs that deal with different calculation models from the field of constructions (e.g. e.g. statics) or meteorological forecasts.

"E" type software (Embedded) represents such software or application that is embedded - Embedded (software installed on various devices). As we can see, "S" type software compared to "P" and especially "E" type software appears to be easier to develop and is more stable in terms of evolution.

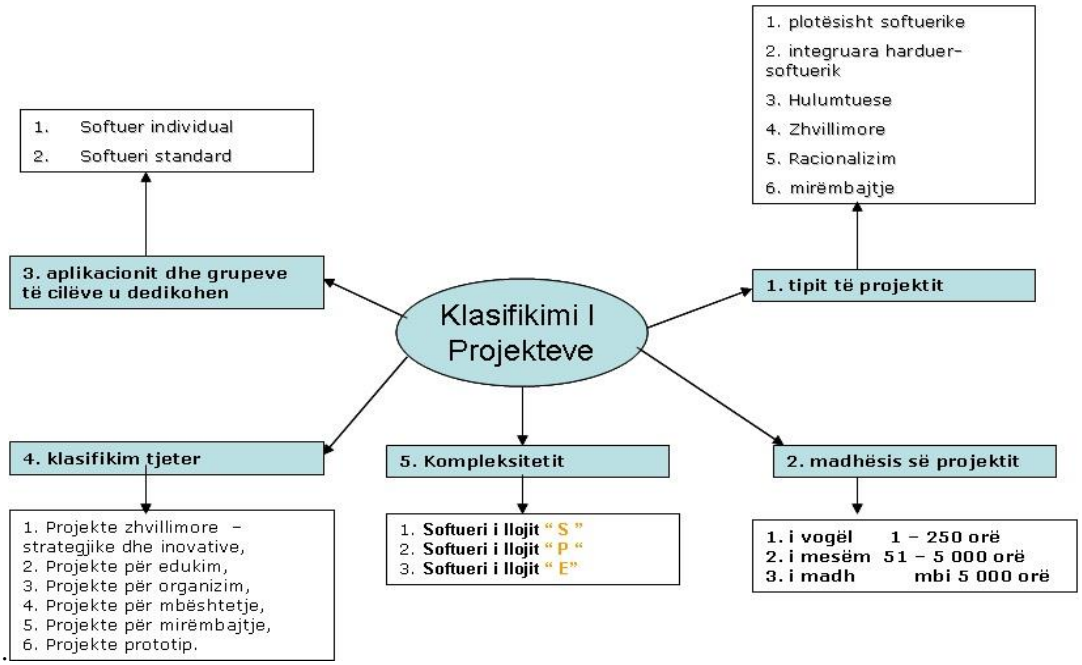

Figure 1. Classification of software projects

Software Project as an Investment

Ideas for investment projects can come from both the state and the private sector, while in terms of software projects, which can also apply to any other type of project, before the realization of these ideas it must be decided whether, in really, was the project in question carried out or not? In this part of the paper, we will examine only one of the three aspects of decision-making, namely the decision to implement the project, that is, we will examine only the types of expenses and the types of benefits related to software projects.

As a measure for the measurement of personnel expenses, it is presented M/NY month/person, while for the volume (size) of the product (product scope) it is Lines of Code - the number of lines without counting comments as well as Function Points - the number of functions separately . In various literature, we will come across the division of expenses, such as in personnel expenses, material expenses, expenses for foreign services, expenses for taxes and various taxes, etc., as well as capital expenses.

Software Market and Industry

The software industry is the collective name for the business that deals with the development and maintenance of software (Økland, 2015). This industry also includes activities, namely services that are related to software such as: training, consulting and maintenance. Market segmentation represents an essential step in the marketing planning process, because the main purpose of market segmentation is to enable the company to channel its commitments in those areas where the opportunities are greater and to find ways to differentiate its from the competition. As the first division of the software market, the so-called division into the primary and secondary branch (branch) is presented.

The primary branch includes those enterprises that specialize in software development or services in the market, related to both software and hardware (giving advice), while the secondary branch includes those enterprises that self-developed or software related services they offer within the company, while they do not offer either

software or software related services in the market. In fact, the secondary sector is considered to belong to all sectors of the economies of developed countries, because it is difficult to find any sector where software is not found as part of various products and services, such as:

- telecommunication,
- electrical engineering,
- automotive industry,
- pharmaceutical industry,
- financial services (banks, insurance companies),
- traffic, etc.

Another division of the overall software market is that of horizontal and vertical software products (Martens, M.L. and Carvalho, M.M. 2016). The vertical market deals specifically with specialized industries, while the horizontal market tends to serve a much broader and more general user base.

Table 1. Software project market division

Horizontal software	Vertical software
general calculation software	software for complex calculations (various enterprises)
word processors	software for managing different fuel pumps
project planning software	oil exploration management software
IP(Internet Protocol) network monitoring software	geological telemetry monitoring software

Success of Software Projects

Successful software development largely depends on the quality of software project management. The essential goals of software project management are related to increasing productivity, ensuring a defined quality, as well as reducing costs for achieving the objective during the development of the software project (Huemann, M. and Silvius, G. 2017).

According to Marnewick, C. (2017), three primary software project management strategies are distinguished:

- maximizing the satisfaction (fulfillment of requirements) of the users,
- minimizing costs and time for software development, and
- minimization of errors (bugs).

The management of software projects is different from the management of other projects, for the reasons mentioned earlier in this paper, and in the following we will focus in more detail on the factors that determine the level of success of software projects. There are numerous statistical reports related to the fate of software projects that contain the answer to the question "what happened to software projects?" The results were depressing.

- Delivered but not working 47%
- Paid but not used 29%
- Repaired, but not put into use 19%
- Repaired and put into use 3%
- 2% were put into use without major problems

The reasons for software project failures according to different authors are different, but in this paper we will present only a few that are mentioned by most authors.

- unclear requirements or inefficient planning,
- lack of process models or inadequate management information system,
- inefficient system of monitoring, evaluation and control,
- prices and unrealistic planning of objectives,
- insufficient communication and excessive documentation orientation,
- insufficient quality assurance as well as non-definition of "core functionality"

and the factors that determine the fate of software projects, according to the Standish Group, arE:

- user participation 15.9%
- implementation support 13.9%
- clear formulation of requirements 13.0%
- adequate planning 9.6%
- real expectation 8.2%
- finer project milestones 7.7%
- competent personnel (staff) 7.2%
- ownership 5.3%
- clear vision and objectives 2.9%
- intensively engaged personnel 2.4%

Management of Software Projects

The objective of software project management is to develop software on time, with quality, and at an acceptable budget, software that works, that is developed on time and on budget, and that can be maintained and reused. To achieve these goals, successful management is needed in the development of software projects. So, in order not to risk developing a low-quality software product, i.e. a product that will not meet the expectations and will not respond to the contractor's requirements, in order not to risk being delayed in the realization of the project, in order not to exceed the foreseen budget, in order not to engage unmotivated personnel (or to risk that they become demotivated) both in number and inadequate qualifications, and that all of this ends up with entropy of the so-called software project system, it is necessary to use the methods offered by the discipline of modern project management. So, with project management we coordinate the project's objectives, work and resources to achieve the goal we aim for, always accompanied by different definitions (in people, resources, time, etc.), while in terms of software project management, time of programming as "fun" that the weather has passed, while software development in a professional way is always, or almost always, accompanied by a lack of different definitions (time, tools, etc.). The generation of software until today has been managed to dominate only partially, and as evidence for this we have the various reports such as much quoted standish group report, with statistics for different years. The reasons for which project management is needed can best be seen from the so-called magic square, presented in Figure 4, where in order to achieve the appropriate cost of the project, quality, quantity, and duration are presented as influential factors. and expenses. The main problems arise from the task that project management has to balance between these factors, for the reason that quality, quantity and productivity must be increased, while expenses and duration must be reduced, respectively shortened. But in order to better understand the square in question, let's see the importance of the mentioned factors for the evaluation and management of software projects. Quality - refers to those characteristics of the software which will enable its use, respectively its operation in the required or suitable way. Quantity – is treated as a very important attribute or characteristic, which is expressed in measurement units such as Line Of Code - LOC, etc. which is used the most, but which, as we said, is not the only one, while the expenses caused by the same are often presented in Person Month- PM (Calero & Piattini, 2017).

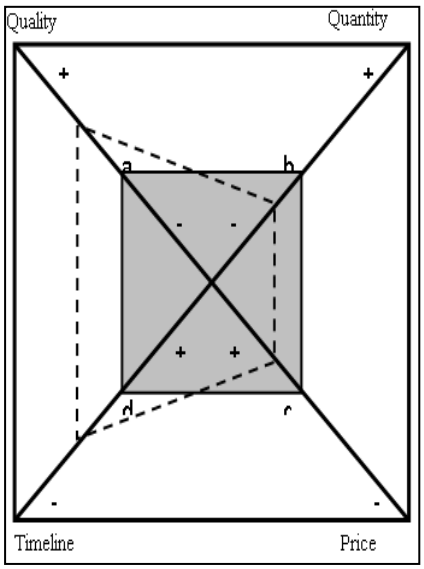

FigurE 2. Magic square

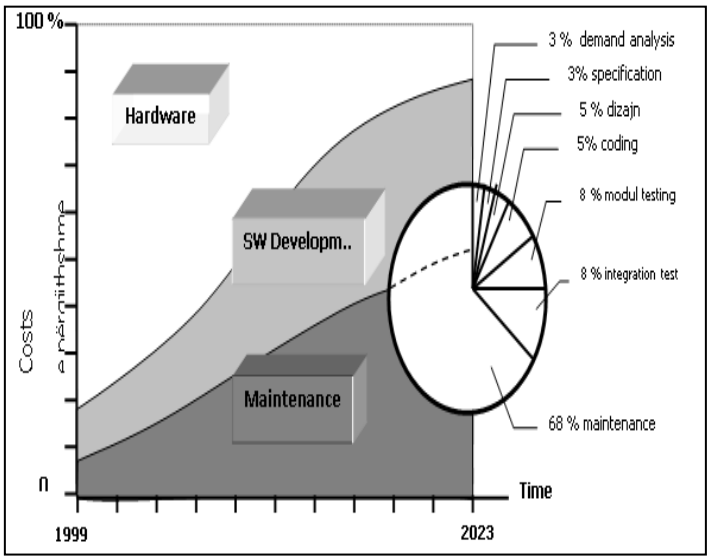

Figure 3. Software investment trend

The duration of the project - also represents a very important factor in the management of projects, especially software ones; for example, the correlation or relationship between the costs and the duration of the project is not linear as it might seem in advance, because in fact the costs will increase with the reduction or shortening of the duration of the Project

Software Project Management Process

Project processes can generally be divided into two main categories, namely:

- project management processes, and
- product-oriented processes.

Project management processes are concerned with the description and organization of work within the project, while product-oriented processes are concerned with the specification and creation of project products. Product-oriented processes are usually defined according to the Project life-cycle and are distinguished according to the field of application and consists of five phases of project management that we will mention below (Anaya, 2019).

- The planning phase of the project contains the creation and protection of the realized scheme for the fulfillment of the purpose and objective of the project.
- The implementation phase includes: training and management of the project team, realization of the project plan, recording of actual resources for use, modification of the project plan, collection and distribution of project information in progress, managerial relations and dispute resolution.
- The control phase of the project should ensure the continuation of the project according to the plans and the realization of the decisive goals.
- Project closure involves the formal acceptance of project results and includes the following activities: post-project status review, summary report preparation, project data archiving, project inventory sale, and project team distribution.
- Project audit and its commissioning.

Software Project Life Cycle (Software Life - Cycle)

The life cycle of system development represents the process of understanding how an information system can support business needs, designing the system, constructing it and delivering it to users Acar, H. (2017), In the standard IEEE Glossary of Software Engeering Terminology, Software Life Cycle presents: "The period of time that begins when the software product is conceived and ends when the product is no longer available for use (Anaya, 2019). A typical software life cycle contains: the requirements phase, the design phase, the implementation phase, the testing phase, the installation, testing and verification phase, the operation and maintenance phase, and sometimes the superstructure phase." To create such a software component, the following activities are carried out:

- task analysis, specification of requirements as well as documentation and control of requirements,
- conception of the solution, documentation and control of the concept,
- detailed design of the solution, documentation and control of the design,
- coding and testing that part of the program developed for the respective component,
- integration with parts of programs (codes) of other components (separately),
- installation and testing of the component as part of the overall system.

Definition of Goal and Objectives in Software Projects

Project objectives are derived from the project goal, which represents the highest level orientation point. They should describe the volume of the project, its breadth and specific goals (Sumner, M. 2018). The objectives and goal of the project must, before the start of the project, be clearly defined and there is full agreement about them, because the outputs of the project will be developed on the basis of these objectives and goals and not the other way around. The objectives of the software project are subject to the SMART framework, which means that when setting/defining the goal, care should always be taken that it - the goal fulfills some criteria that actually

make up the acronym SMART, (Specific - specific, Measurable - that can to be measured; Achievable, Realistic, Time-related).

Software Project Planning

In planning the development of software projects in the aforementioned source, three levels of the process are distinguished, including:

• Process architecture – shows how the software development flow should be specified, what standard process elements exist (should be taken into account) and how the mutual influence between them should be described,
• Process model – to establish the course of action (procedure) for the development of a software product.
• Project plan – a project plan is formed for each concrete software development. This plan is therefore formed by the project manager and is oriented towards one or more process models (incarnations of a Process Model).
Further along the process, software project development planning adopts the following activities (Marnewick, C. 2017). The basis for planning all activities is the WBS, or project hierarchy structure, which makes the hierarchical division of the project into clearly defined tasks or activities, thus identifying the work that must be done to complete the project. The structure of the project plan can be in the form of a table or graph.

Table 2. Software project development planning

Project definition	Evaluation	Risk evaluation
Definition of objectives and requirements.	Determination of product dimensions.	Risk analysis Categorization of risks
Selection of the development process.	Time planning (scheduling).	Risk assessment
Definition of work.	Cost estimation and budgeting.	Preparation of risk response plans

Planning Procedures

Planning and follow-up of the plan represent the most important tasks of project management, while quality control and assurance are closely related to them. In fact, a plan requires answers to these questions: what, how, how much (expenses), who, when and with what, while in planning procedures we have to answer the question how?

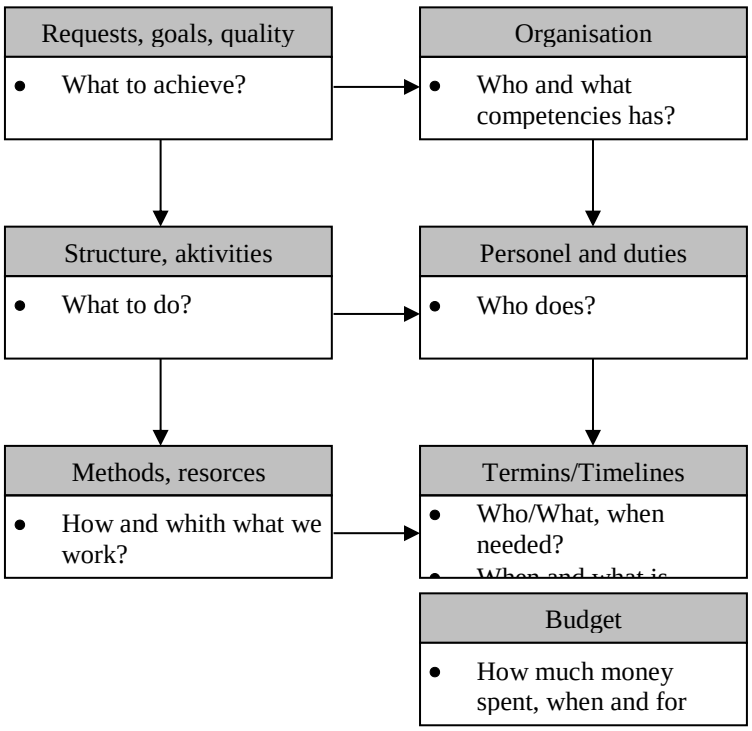

Figure 4. Plan flow formed by interdependence of plan parts

Process Models of Software Projects

Process models present concepts on which projects are based, and any software development must be done within defined organizational frameworks, whereas a process model describes such a framework.

Table 3. Software project process models

According to Balzert a defined process should define the following:	List of process models for software projects:
• sequence of work flow, • each activity that must be carried out separately, • defining the parts of the product, • product performance criteria (when it is a completed product), • necessary qualifications of collaborators, • responsibilities and powers, • applicable standards, directives, methods and tools.	• Code And Fix • Classic "Waterfall" model • "Spiral" model • "V" model • Evolutionary / Incremental Model

Evaluation of Software Projects

Types of Procedures

The evaluation of software projects represents an attempt to estimate the planned expenses for the development and maintenance of software projects, which is done through the analysis, determination and evaluation of factors influencing the software project, as a basis for evaluation (as inputs - input data) and also also in terms of the form of presentation of outputs (results), e.g. Line of Code, Function Point, Object Point, etc.).

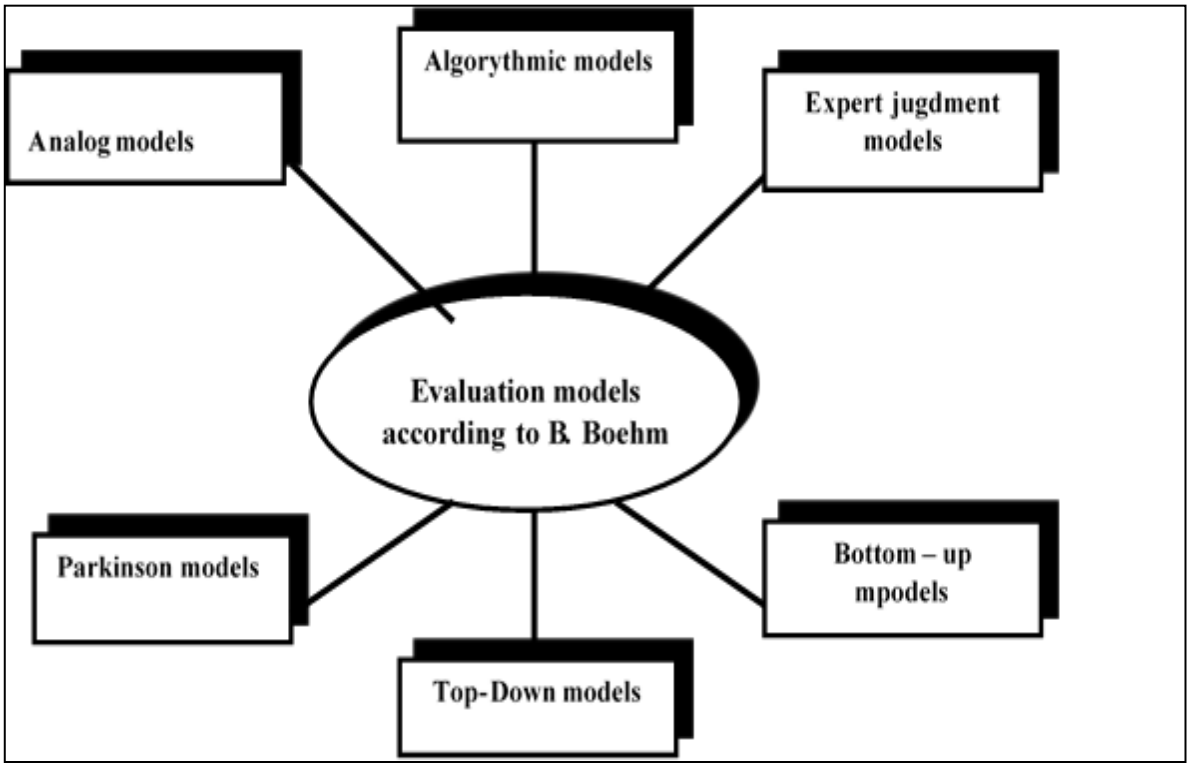

Figure 5. Project evaluation models

However, when it comes to the costs of a software project, the factors with influence in determining the costs of the development of the software project (cost-factors) should definitely be mentioned, such as Factors (performance) of the product, of the computer, of the personnel and of the project that we will explain in more detail when we talk about the Constructive Cost Model - Co Co Mo methods (constructive cost model, Funnctin Poin method and Object Point method. Methods of evaluation of software projects according to (Martens, M.L. and Carvalho, M.M. 2016) are:

- Algorithmic - parametric models.
- Expert Judgment
- Analogy
- Parkinson's
- Price to Win
- Top-Down
- Bottom-Up

Based on this, the author proposes seven basic steps in estimating the cost of software projects:

1. Establish Objectives
2. Plan for Required Data and resources
3. Pin down software requirements
4. Work out as much detail as feasible
5. Use several independent techniques and sources
6. Compare and iterate estimates
7. Follow up

B. Boehm in his work now most cited in this paper "Software Engineering Economics" writes "without data on productivity it is impossible to calculate the cost of a project because it (productivity) is the cornerstone or basis for any calculation (estimation) of the project".

Software Project Constructive Cost Modeling – COCOMO

In order for the investment decision to be as fair as possible, it is necessary to present the most accurate forecast of the costs of the development of the software project, these costs, to the greatest extent, are costs for personnel engagement. So at the beginning of every software project, questions such as:

- How high will be the overall project work costs,
- How long (Person Months) the project will last,
- What should be the number of engaged personnel,
- How much the project will ultimately cost.

In order for the method in question to be as efficient as possible, which means as accurate as possible in the evaluation, a distinction is made between types or models of projects (project modes).

Table 4. Software project cost modeling

COCOMO simple organic model	COCOMO organic model	COCOMO intermediar - semidetached mode	COCOMO detal - embedded mode
Small projects, respectively smaller than 50 000 DSI with a small number of connections (interfaces) with other systems (Stand Alone applications), stable environment for development, which means that every collaborator knows the whole project, respectively has experience in similar projects.	Projects with an average size between 50 000 and 300 000 DSI (delivered source instructions), each collaborator possesses special knowledge related to the development of the project in question, the team that is committed to the development of the project is not trained together, respectively in terms of projects with a degree of complexity or difficulty between Organic and Embedded Mode.	Projects with an average size between 50 000 and 300 000 DSI (delivered source instructions), each collaborator possesses special knowledge related to the development of the project in question, the team that is engaged for the development of the project is not trained together, respectively in terms of projects with a degree of complexity or difficulty between Organic and Embedded Mode	Large projects – over 300 000 DSI, high level of definition in development and the main characteristic is the close connection of the developed software with other hardware-software systems, e.g. flight control software systems and real-time systems etc.

COCOMO's life cycle consists of five stages and that

- Planning and definition of requirements,
- Product design,
- Detailed design,
- Coding and testing of modules,
- Integration and testing.

COCOMO – Base Model

Based on what was said above, the project costs in Person Months can be calculated based on the formula presented below, which the author of this method has arrived at after analyzing 63 completed projects.

PM=2.4(KDSI)1.05

while the duration per month (TDEV-time for development) of the project development is calculated according to the formula

TDEV=2.5(PM)0.38

which derives from the calculated expenses, e.g. if we will develop a software with 50 KDSI according to the above formula we will earn an expense of

PM = 2.4 * (50)1.05 = 145.9 Person Months and with a duration of
TDEV = 2.5 * (145.9) 0.38 = 16.6 Months

Also, with the above-mentioned formulas, we can, in addition to the expenses per Person Month and the duration of the project development, also calculate the productivity of the project development (expressed in lines of the source code for the entire project development process - DSI), if the we related the volume of the project in KDSI with the project development costs.

KDSI / PM = KDSI / 2.4(KDSI)1.05

and also besides the calculated productivity, e.g. for a volume of 50 KDSI with an expenditure of 145.9 PM with a duration of 16.6 months, we can calculate the number of personnel needed since this formula as an average comes out

PM=145.9PM / 16.6 Months = 8.8 People

To calculate the costs and duration of the software project development, CoCoMo uses the same formula for all three types of projects, but with different coefficients and exponents respectively (Table 2) and for this very reason the classification of the project is needed, which is the object of assessment, in one of the types of projects mentioned above.

Table 5. Formulas for calculating expenses and duration by project type

Project type	Expenses	Timeline
Organic	$PM=2.4(KDSI)^{1.05}$	$TDEV = 2.5(PM)^{0.3}$
Partialy integrated	$PM=3.0(KDSI)^{1.12}$	$TDEV =2.5(PM)^{0.35}$

As can be seen in partially integrated and detailed projects, development costs compared to Organic projects will be greater, thanks to the larger exponents and multipliers that are based on them, and as a result, they will have different costs for projects with the same volume and all this based on the type of project in question.

Table 6. Software project characteristics

Project volume = 100KDSI	Project volume = 100KDSI	Project volume = 100KDSI
Type = Organik $PM=2.4(100)^{1.05}$ = 302 PM	Lloji = partialy integrated $PM=3.0(100)^{1.12}$ = 521 PM	Type = Detailed $PM=3.6(100)^{1.20}$ = 904 PM

For the same volume, for partially integrated projects, the duration will be 23.3 and for the Detail 40.9. As we see from the big differences it brings in the evaluation method, the classification in different types of software projects results that, the more precise we will be in respecting the classification criteria, the more accurate our evaluations will be and in after all, this assessment will largely define the fate of the project.

Table 7. COCOMO base model

Phases	Products in KDSI	Participation	Request analysis	Product design	Programing	Testing plan	Verification	Project office	Project quality	Guide formulation
Plans and requests	7	8	48	14	2		2	6	16	5
	8	8	48	13	24	3	7	14	4	7
	32	8	46	14	6	4	8	12	4	6
	128	8	44	15	8	5	9	10	4	5
	512	8	42	16	10	6	10	8	3	5
Product design	2	18	10	42	10	4	6	15	4	9
	8	18	10	42	11	5	13	3	9	7
	32	18	10	42	12	6	8	11	3	8
	128	18	10	42	13	7	9	9	3	7
	512	18	10	42	14	8	10	7	2	7
Programing	2	60	3	6	55	4	8	9	8	7
	8	57	3	6	55	5	9	8	7	7
	32	54	3	6	55	6	10	7	7	6
	128	51	3	6	55	7	11	6	7	5
	512	48	3	6	55	8	12	5	6	5
Integration and testing	2	22	2	4	32	3	30	10	10	9
	8	25	2	4	36	3	28	9	9	9
	32	28	2	4	40	4	25	8	9	8
	128	31	2	4	44	4	23	7	9	7
	512	34	2	4	48	5	20	6	8	7

COCOMO – Intermediar Model

The intermediate CoCoMo model is an extension of the basic CoCoMo model. In the intermediate CoCoMo model, a total of 15 factors are considered (subject to a category that can be very low, low, normal high, very high and extra or extremely high), different in terms of influence, which are summarized in four categories or groups that too

Table 8. COCOMO intermediar model

Features of the software product	**Computer features**	**Personnel characteristics**	**Project characteristics**
RELY- required software reliability - siguria e kërkuar nga softueri, DATA- size of application database – vëllimi i bazës së të dhënave, CPLX – complexity of the product – kompleksiteti i produktit.	TIME – execution time constraint - definitions related to execution time, STOR - main storage constraints - definitions related to the main (operational) memory, VIRT - virtual machine volatility - the stability of the virtual machine, TURN – computer turnaround time – the time needed to restore the computer state	ACAP - analyst capability - system analyst capability, AEXP - applications experience - experience with the application, PCAP - programmer capability - the ability of the programmer, VEXP - virtual machine experience - experience with the virtual machine, LEXP - programming language experience - experience with the programming language.	MDOP - modern programming practices - the application of modern programming practices, TOOL - use of software tools - use of software tools for development, SCED - required development schedule - the appropriate duration of the project.

Table 9. Multipliers for constructive expenditure modeling – intermediate CoCoMo model

Features of the software product	**Computer features**	**Personnel characteristics**	**Project characteristics**
RELY-security required by software 0.75 0.88 1.00 1.15 1.40	TIME–executable time definitions. 1.00 1.11 1.30 1.66	ACAP–system analyzer ability 1.46 1.19 1.00 0.86 0.71	MDOP–application of modern programming language.
DATA–database volume 0.94 1.00 1.08 1.16	STOR–main (operational) memory related definitions	AEXP – experience with the application 1.29 1.13 1.00 0.91 0.82	1.24 1.10 1.00 0.91 0.82 TOOL – use of soft tools. for development
CPLX–product complex 0.70 0.85 1.00 1.15 1.30 1.65	1.00 1.06 1.21 1.56 VIRT – virtual machine stability 0.87 1.00 1.15 1.30	PCAP – programmer skill 1.42 1.17 1.00 0.86 0.70 VEXP – virtual machine experience	1.24 1.10 1.00 0.91 0.83 SCED – appropriate project duration
	TURN – the time needed to restore the state of the computer	1.21 1.10 1.00 0.90 LEXP – programming language experience	1.23 1.08 1.00 1.04 1.10
	0.87 1.00 1.07 1.15	1.14 1.07 1.00 0.95	

Corrected Expenditure Formulas

Project type	basic model	between model
Organic	PM=2.4(KDSI)1.05	PM=3.2(KDSI)1.05
Partially integrated	PM=3.0(KDSI)1.12	PM=3.0(KDSI)1.12
Detail	PM=3.6(KDSI)1.20	PM=2.8(KDSI)1.20

COCOMO –Final Model

The detailed model of the constructive expenditure modeling method differs from the intermediate model of the same method, respectively it is further detailed in two aspects; also in dividing the software project into a three-level hierarchy starting from the lowest, the level of modules, the level of subsystems (subsystems) and the system level.

Table 10. Attributes with their multiplier values by stages at module level

		Clasification					
Atributes	**Phases**	Very low	Low	Norml	High	Very high	Ekstra high
CPLX	Product design	0,70	0,85	1,00	1,15	1,30	1,65
	Detal design	0,70	0,85	1,00	1,15	1,30	1,65
	Coding	0,70	0,85	1,00	1,15	1,30	1,65
	Integration and testing	0,70	0,85	1,00	1,15	1,30	1,65
PCAP	Product design	1,00	1,00	1,00	1,00	1,00	
	Detal design	1,50	1,20	1,00	0,83	0,65	
	Coding	1,50	1,20	1,00	0,83	0,65	
	Integration and testing	1,50	1,20	1,00	0,83	0,65	
VEXP	Product design	1,10	1,05	1,00	0,90		
	Detal design	1,10	1,05	1,00	0,90		
	Coding	1,30	1,15	1,00	0,90		
	Integration and testing	1,30	1,15	1,00	0,90		
LEXP	Product design	1,02	1,00	1,00	1,00		
	Detal design	1,10	1,05	1,00	0,98		
	Coding	1,20	1,10	1,00	0,92		
	Integration and testing	1,20	1,10	1,00	0,92		

After dividing the project into three hierarchical levels, for each of them an assessment is made of their volume in DSI as well as of their attributes such as: CPLX - module complexity, PCAP - programmer skill, VEXP - experience with the virtual machine as well as LEXP – experience with programming language as well as in

case of partial development of the project also AAF and EDSI. Below are presented the attributes with the value of their multipliers according to the phases at the module level, while there is also an analogous table for the attributes located at the subsystem level.

Software Maintenance

The method of constructive expenditure modeling also enables the evaluation of the maintenance of software projects which is defined through the so-called annual change traffic ACT, i.e. we relate the participation of the volume of the source code of the developed software which during a year has undergone changes, respectively has been modified through introducing a new code or changing the existing one. EG a software project with a volume of 32 KDSI (32000DSI) has been developed, where the annual flow of changes is 5,000 new program lines are introduced, while 3,000 program lines are modified from the existing project, then we will have

ACT = 5000+3000*/32000=0.25 and now starting from the project development expenditure PMD (DEVELOPMENT) we calculate the annual maintenance expenditure PMAM (ANNUAL MAINTACE) through the formula

$$\mathbf{PM_{AM} = ACT * PM_D}$$

From the formula in question, we obtain the project maintenance costs per Person Month and for the whole year, and if we want to see the necessary number of personnel for maintenance - full-time software persons, then the amount obtained from the above formula must be divided by 12 month.

FSPM = PMAM/12 months

Table 11. RELY with changed values of multipliers for the maintenance phase

Categorisation	Multiplicators value per development phase	Multiplicators value er maintenance phase
Very low	0,75	1,35
Low	0,88	1,15
Normal	1,00	1,00
High	1,15	0,98
Very high	1,40	1,10

Below in the table are presented multipliers with changed values for MDOP during the maintenance phase.

Table 12. MDOP with changed multiplier values for the maintenance phase

Categorisation	Multiplicators value per development phase	Multiplicators value per maintenance phase				
		2 KIDS	8KIDS	32KIDS	128KIDS	512KIDS
Very low	1.24	1,25	1.30	1.35	1.40	1,45
Low	1.10	1.12	1.14	1.16	1.18	1,20
Normal	1,00	1,00	1,00	1,00	1,00	1,00
High	0.91	0.90	0.88	0.86	0.85	0,84
Very high	0.82	0.81	0.77	0.74	0.72	1,70

As we saw, the CoCoMo method of constructive expenditure modeling enables us, through different levels of detailing, to evaluate the software project, even at the macro level, through the fundamental or basic model, while through the in-between model and that detail we can also do assessment at the micro level. This method in its assessments takes into consideration the characteristics or attributes of the product, personnel, technology as well as the project, while for the objective evaluation of these influential factors the method in question gives us clear instructions even though the quantification of these influential factors does not follow without problems.

Testing the Software

Software and quality testing have the task of finding errors, respectively to see how well the quality requirements have been met. The importance of testing is best seen from the results presented on an empirical basis by Boehm42, according to which the costs of eliminating an error that is discovered after the delivery of the software are on average 100 times greater than when the error is discovered already at the analysis stage.

There are various methods for software testing. The main characteristic of static testing methods is that during testing, the software component is not launched, but the source code is analyzed to find errors, while the so-called manual testing methods such as inspections, reviews and walkthroughs are most often used. Testing is carried out by random selection. The purpose of dynamic testing methods is to detect differences between the actual operation of the developed software and the proper operation according to the specification. in the literature, the Black-Box and White-Box methods are most often mentioned as such testing methods. In Black-Box testing, the test software is treated as a " black box ". The tester is not interested in behavior and internal structure, but his area of interest is to find such circumstances that influence the behavior of the software to deviate from its proper behavior, that which is defined in the specification.Whereas in White-Box testing, the tester's interest is focused on the internal structure of the software being tested, and all of this considering the appropriate state or required by the specification. The goal is therefore to find errors in the program, while the testing is done with those data that will go through all the possible paths (branches) of the program. In conclusion, we can say that ensuring software quality is necessary from many aspects, but when it comes to commercial software, it (quality) ensures competitive (comparative) advantages just as the existence itself, or rather the presence of software in a product compared to the same product but without software e.g. automotive industry.

Research Methodology for Managing Software Projects in Organizations

First we have definen dhe research objectives where clearly articulated the goals and objectives of the research, such as improving software project management practices within trade organizations, enhancing efficiency, or reducing costs. Secondly we did the literature review, conducting a thorough literature review to understand existing methodologies and best practices in software project management, especially in the context of trade organizations. Identify relevant theories, frameworks, and case studies. İn next step the reserach has identified trade organization requirements. Gathering insights into the specific needs, challenges, and constraints faced by trade organizations regarding software project management. This involved interviews, surveys, or focus groups with stakeholders within these organizations.

Based on those we choose the appropriate research methodology based on the objectives, such as quantitative, qualitative, and mixed-method approaches. We considered case studies, surveys, interviews, and did design data collection instruments tailored to the chosen methodology. Before finalizing gthe methodology we did conduct a pilot test of the research instruments to ensure they are effective and valid. İn next step we did implement the research plan to collect relevant data from organizations. As well we ensure data collection methods align with ethical standards and address any privacy or confidentiality concerns. Further th reserach did analyze the collected data using appropriate techniques based on the research questions and methodology. This involved quantitative analysis (e.g., statistical tests, regression analysis) and/or qualitative analysis (e.g., thematic analysis, content analysis) followed by software development acording to requests of organization and finalized by software testing. The findings of the research was very promising and the developed and adopted sofware for the choosen company has function well. İn the end of research the recommendations and conclusions based on the findings, will be drawn regarding the management of software projects in organizations. The paper will provide practical recommendations for improving software project management practices, addressing challenges, and leveraging opportunities.

Case Study for This Research

In recent decades, the software industry and its products have become one of the factors without which the normal functioning of contemporary businesses and economies cannot be imagined. Therefore, it is difficult to imagine any company that claims to be competitive, without software support, whether it is standard software or developed specifically for the needs of the company. The paper has as a case study the development and evaluation of a software project in the company Elkos Group and describes the steps of how a software project is developed and implemented for the needs of the company.

Development of the Human Resources Software Project at Elkos Group

Considering the large capacity of work and the large number of workers that the Elkos Group company has, the need has arisen for the design and development of this project in order to increase work efficiency and for the administration in this company to be as functional as possible. With the implementation of this project, it will be

possible to manage the company's staff. With the implementation of this application, administrative procedures will be significantly reduced, thereby increasing work efficiency, we will have a clear overview of the company's staff.

Technical Solution and Description of the Database

This system enables easy and efficient management as well as easy services of Human Resources in the Company. The database of this application consists of several tables and their diagram looks like the following.

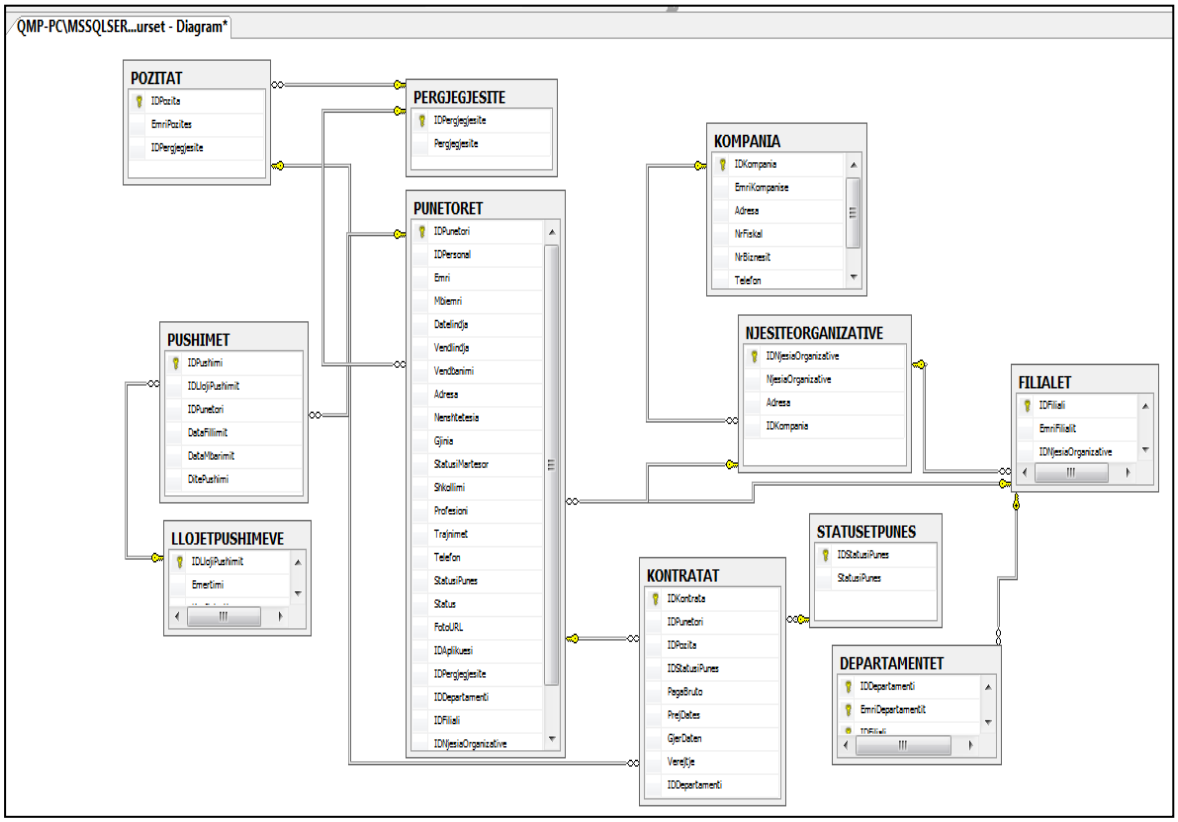

Figure 6. Human resources application software description

Table 13. Digitization and Registration of Departments

Field	Type of data	Description
ID Departament	int	Unique number that identifies the registered apartment and which is automatically increased by the system
Departament name	varchar (50)	Describes the Name of the Apartment
ID Branch	int	Unique number identifying the registered Fiialit

Table 14. Digitization and registration of subsidiaries

Field	Type of data	Description
ID Branch	int	Unique number identifying the registered Affiliate
Branch name	varchar (50)	Describes the Affiliate Name
ID org, unit	int	Unique number that identifies the registered Organizational Entity

Table 15. Digitization of the company

Field	Type of data	description
ID Company	int	Unique number that identifies the registered Company
Company name	varchar (50)	Describes the Company Name
Adress	varchar (50)	Describes the address of the Company
Fiscal nr	varchar (50)	Describes the fiscal number of the Company
Bussines nr	varchar (50)	Description of the Company's business number
Telefon	varchar(50)	Describes the Company's phone number

Table 16. Digitizing the registration of employee contracts

Field	Type of data	Description
ID Contrats	int	Unique number that identifies the registered contract and which is automatically increased by the system
ID Employee	int	Unique number that identifies the registered employee and which is automatically increased by the system
ID Position	int	Unique number that identifies the position of the registered employee and which is automatically increased by the system
ID Status	int	Unique number that identifies the status of the registered employee
Wage Bruto	float	It shows the gross payment that came out of the contract
From	datetime	Describes the start date of the contract
To	datetime	Describes the End Date of the contract
Remarks	text	Describe the murder, why the contract is over
ID Departament	int	Unique number that identifies the registered apartment and which is automatically increased by the system

Table 17. Digitizing the registration of the type of employees' vacations

Field	Type of data	Description
ID vacation type	int	Unique number that identifies the Type of Holiday registered and which is automatically increased by the system
Designation	varchar (50)	Describes the Vacation Type
Coefficient	float	Describes the coefficient of rest

Table 18. Digitization of registration of organizational units

Field	Type of data	Description
ID org. Unit	int	Unique number that identifies the registered Organizational Unit
Org. Unit	varchar (50)	Describes the Designation of the Organizational Unit
Adress	varchar (50)	Describes the address of the organizational unit
ID Company	int	Describes the ID of the Company in which the Organizational Unit is registered

Table 19. Digitizing the registration of human resources employees

Field	Type of data	Description
Worker ID	int	Unique number that identifies the registered employee and which is automatically increased by the system
Personal ID	varchar(50)	Describes the employee's personal number
Name	varchar(50)	Shows the name of the employee
LAST	varchar(50)	Shows the last name of the employee
Birthday	datetime	Shows the date
Birthplace	varchar(50)	It shows the place of birth
RESIDENCE	varchar(50)	Shows Residence
address	varchar(50)	Shows the address
Citizenship	varchar(50)	Shows the citizen
gender	varchar(50)	Describes gender
Marital Status	varchar(50)	Describes the marital status of the employee
SCHOOLING	varchar(50)	Describe the worker's education
OCCUPATION	varchar(50)	Describes the profession of worker
Training	varchar(50)	Describes the training that the employer has completed
phone	varchar(50)	Shows the phone number of the employee
Job Status	varchar(50)	Describes whether it is part-time or full-time
Status	varchar(50)	It describes the status whether it is Active or Passive
Photo URL	varchar(50)	It shows where the employee's photo is stored
Applicant ID	int	The unique number of the applicant who applied for the job
Responsibilities ID	int	The unique number of the employee's responsibilities
Department ID	int	Unique number that identifies the apartment where the employee works
Affiliate ID	int	Unique number that identifies the Branch where the employee works
Organizational Unit ID	int	Unique number that identifies the Organizational Unit where the employee works
Status	varchar(50)	It describes whether it is a worker or an applicant

Discusion and Description

This section demonstrates the key findings shown from the conducted investigations and will discuss the generated themes. In particular, to answer the research question about what organizations can do to enable software project systems drive their businesses towards growth and sustainability, we will show the activities undertaken by the firm taken as case study that assumed to be effective for software system role that enables business growth and sustainability. These activities are drawn based on the sustainability principles that have been suggested by Huemann and Silvius (2017). The Human Resources software management project ensures the management of Human Resources in a Company, the basic objectives of this Project are:

- Registers and manages the Company with Organizational Units and Branches of Organizational Units
- Registers and manages the Working Staff
- Records and manages Workers' Holidays
- Registers and manages Employee Contracts

Conclusion

Based on the literature review provided, and case study developed here are some conclusions and recommendations regarding software project management and its economic evaluation in terms of enterprise sustainability:

Integration of Sustainability into Project Management: There is a growing recognition of the importance of integrating sustainability considerations into software project management practices. This integration involves aligning project management frameworks and methodologies with broader sustainability goals to ensure the long-term viability and resilience of the organization.

Economic Evaluation for Sustainability: Traditional economic evaluation techniques, such as Cost-Benefit Analysis (CBA) and Return on Investment (ROI), need to be augmented to account for sustainability factors. Organizations should consider the economic impact of sustainable software development practices, such as resource efficiency and waste reduction, in their project evaluation processes.

Importance of Sustainable Practices: Adopting sustainable software development practices not only contributes to environmental sustainability but also offers economic benefits. Practices such as green computing and energy-efficient programming can lead to cost savings through reduced resource consumption and improved operational efficiency.

Challenges in Implementation: Despite the potential benefits, organizations face challenges in implementing sustainable software project management practices. These challenges include resistance to change, lack of awareness or understanding of sustainability issues, and the need for investment in new technologies and skill development.

Recommendations

Develop Comprehensive Sustainability Frameworks: Organizations should develop comprehensive frameworks and methodologies for integrating sustainability into software project management practices. These frameworks should provide guidance on incorporating sustainability considerations into project planning, execution, and evaluation processes.

Educate and Train Project Managers: Project managers play a crucial role in driving the adoption of sustainable software development practices. Organizations should invest in training and education programs to equip project managers with the knowledge and skills needed to integrate sustainability into their project management approach.

Incentivize Sustainable Practices: Organizations can incentivize the adoption of sustainable software development practices by incorporating sustainability metrics into project evaluation criteria. Recognizing and rewarding teams that achieve sustainability goals can help foster a culture of sustainability within the organization.

Collaborate with Stakeholders: Collaboration with stakeholders, including customers, suppliers, and regulatory bodies, is essential for advancing sustainability in software project management. Organizations should engage with stakeholders to identify sustainability priorities, share best practices, and address common challenges.

Invest in Research and Development: Continued research and development are needed to advance sustainable software development practices and technologies. Organizations should invest in R&D efforts aimed at developing innovative solutions for minimizing the environmental impact of software projects while maximizing economic value.

In conclusion, integrating sustainability into software project management practices requires a multi-faceted approach that considers economic, environmental, and social factors. By adopting sustainable practices, organizations can not only contribute to a more sustainable future but also realize economic benefits and enhance their long-term competitiveness

Scientific Ethics Declaration

The authors declare that the scientific ethical and legal responsibility of this article published in EPSTEM journal belongs to the authors.

Acknowledgements or Notes

* This article was presented as an oral presentation at the International Conference on Basic Sciences, Engineering and Technology (www.icbaset.net) held in Alanya/Turkey on May 02-05, 2024.

References

Aarseth, W., Ahola, T., Aaltonen, K., Økland, A., & Andersen, B. (2017). Project sustainability strategies: A systematic literature review. *International Journal of Project Management*, *35*(6), 1071-1083.

Acar, H. (2017). *Software development methodology in a Green IT environment* (Doctoral dissertation, Université de Lyon).

Albertao, F., Xiao, J., Tian, C., Lu, Y., Zhang, K. Q., & Liu, C. (2010). Measuring the sustainability performance of software projects. In *2010 IEEE 7th International Conference on E-Business Engineering* (pp. 369-373). IEEE.

Anaya, L. (2019). To what extent is it viable to apply benefits management approach for ERP systems?. *Procedia Computer Science*, *164*, 33-38.

Alharthi, A., Spichkova, M. & Hamilton, M. (2016), "Sustainability profiling of long-living software systems", in QuASoQ 2016: International Workshop on Quantitative Approaches to Software Quality, CEUR-WS, (pp. 12-19).

Becker, C., Betz, S., Chitchyan, R., Duboc, L., Easterbrook, S.M., Penzenstadler, B., Seyff, N. & Venters, C.C. (2016). Requirements: the key to sustainability. *IEEE Software, 33*(1), 56-65.

Becker, C., Betz, S., Chitchyan, R., Duboc, L., Easterbrook, S. M., Penzenstadler, B., & Venters, C. C. (2015). Requirements: The key to sustainability. *IEEE Software*, *33*(1), 56-65.

Beghoura, M.A., Boubetra, A. and Boukerram, A. (2017). Green software requirements and measurement: random decision forests-based software energy consumption profiling, *Requirements Engineering, 22*(1), 27-40.

Calero, C., & Piattini, M. (2017). Puzzling out software sustainability. *Sustainable Computing: Informatics and Systems*, *16*, 117-124.

Calero, C., Moraga, M., & Bertoa, M. F. (2013). Towards a software product sustainability model. *arXiv preprint arXiv:1309.1640*.

García-Mireles, G. A., Moraga, M. Á., García, F., Calero, C., & Piattini, M. (2018). Interactions between environmental sustainability goals and software product quality: A mapping study. *Information and Software Technology*, *95*, 108-129.

Huemann, M., & Silvius, G. (2017). Projects to create the future: Managing projects meets sustainable development. *International Journal of Project Management*, *35*(6), 1066-1070.

Kern, E., Naumann, S., & Dick, M. (2015). Processes for green and sustainable software engineering. *Green in Software Engineering*, 61-81.

Lago, P., Koçak, S. A., Crnkovic, I., & Penzenstadler, B. (2015). Framing sustainability as a property of software quality. *Communications of the ACM*, *58*(10), 70-78.

Marnewick, C. (2017). Information system project's sustainability capabality levels. *International Journal of Project Management*, *35*(6), 1151-1166.

Martens, M.L. and Carvalho, M.M. (2016a), "Sustainability and success variables in the project management context: an expert panel", Pro Martens, M. L., & Carvalho, M. M. (2016). Sustainability and success variables in the project management context: an expert panel. *Project Management Journal*, *47*(6), 24-43.

Økland, A. (2015). Gap analysis for incorporating sustainability in project management. *Procedia Computer Science*, *64*, 103-109.

Pohludka, M., Stverkova, H., & Ślusarczyk, B. (2018). Implementation and unification of the ERP system in a global company as a strategic decision for sustainable entrepreneurship. *Sustainability*, *10*(8), 2916.

Savitz, A. (2013). *The triple bottom line: how today's best-run companies are achieving economic, social and environmental success-and how you can too*. John Wiley & Sons.

Schieg, M. (2009). The model of corporate social responsibility in project management. *Verslas: Teorija ir Praktika*, *(4)*, 315-321.

Silvius, A. G., Kampinga, M., Paniagua, S., & Mooi, H. (2017). Considering sustainability in project management decision making: An investigation using Q-methodology. *International Journal of Project Management*, *35*(6), 1133-1150.

Zerbino, P., Aloini, D., Dulmin, R., & Mininno, V. (2021). Why enterprise resource planning initiatives do succeed in the long run: A case-based causal network. *Plos one*, *16*(12), e0260798.

Turner, J.R., Anbari, F. and Bredillet, C. (2013). Perspectives on research in project management: The nine schools, *Global Business Perspectives*, *1*(1), 3-28.

Yunis, M., Tarhini, A., & Kassar, A. (2018). The role of ICT and innovation in enhancing organizational performance: The catalysing effect of corporate entrepreneurship. *Journal of Business Research*, *88*, 344-356.

Zerbino, P., Aloini, D., Dulmin, R., & Mininno, V. (2021). Why enterprise resource planning initiatives do succeed in the long run: A case-based causal network. *Plos one*, *16*(12), e0260798.

Ziemba, E. (2018). The contribution of ICT adoption to sustainability: Households' perspective. *Information Technology & People*, *32*(3), 731-753.

Author Information

Ibrahim Krasniqi
University Haxhi Zeka
Rr. UCK, nn, 30000 Peje, Kosovo
Contact e-mail: *ibrahim.krasniqi@unhz.eu*

Naim Ismajli
AAB College Prishtina, Kosovo

Ganimete Krasniqi
MMPHI-GoK, Rilindja Building, Prishtina, Kosovo

To cite this article:

Krasniqi, I., Ismajli, N., & Krasniqi, G. (2024). Software project management and their economic evaluation in terms of enterprise sustainability, *The Eurasia Proceedings of Science, Technology, Engineering & Mathematics (EPSTEM)*, *28*, 533-553.

The Eurasia Proceedings of Science, Technology, Engineering & Mathematics (EPSTEM)
ISSN: 2602-3199

The Eurasia Proceedings of Science, Technology, Engineering & Mathematics (EPSTEM), 2024

Volume 28, Pages 554-564

ICBASET 2024: International Conference on Basic Sciences, Engineering and Technology

SCADA System for Process Data Exchange in Master Slave RF and Iot Network

Bilijana Citkuseva-Dimitrovska
University Goce Delcev Stip, R.N.Macedonia

Elena Zafirov
Onesky Flyght, Dallas, USA

Goce Stefanov
University Goce Delcev Stip, R.N.Macedonia

Abstract: In every aspect of our lives, we can observe how automation plays a facilitating role in the performance of responsibilities of a comprehensive rank. Thanks to the development of electronics, today's process measurement systems enable the measurement values of process quantities to be visualized on display, sent remotely, and stored in a file, compatible with future user processing. In this paper are represented results of the development, design and practical implementation of the SCADA system, which enables data exchange between SCADA screen, MASTER and SLAVE stations. The MASTER station is installed in one industrial plant and the SLAVE is installed in another plant. The SCADA monitoring system is built into the MASTER station. The SLAVE station is connected by RF (radio frequency connection) to the MASTER station. In the MASTER and SLAVE station two microcomputers units, as well as appropriate RF modules, are installed. The microcomputer in the MASTER station is serially connected to the IoT microcomputer, for the transfer of measurement data in the Internet network. The solution provides visualization, data log file, and transfer to the IoT network of process data from the two industrial plants.

Keywords: SCADA, Exchange data, RF Network, IoT network

Introduction

In real industrial processes there are standalone plants that represent a separate whole. Most often these plants are far from intra and internet network of the production companies. Therefore there is a need to automate and connect these plants in the intranet of the company and more widely in the Internet (IoT) network. Automation, control, management, and monitoring processes are of exceptional importance, especially for industrial use,(Bennett, 1982), (Hor, 2005). Efforts are made to ensure more reliable and simpler work, especially for operators who are directly exposed to the proper functioning of the entire industrial process. This approach to work is made possible by the so-called SCADA (**S**upervisory **C**ontrol and **D**ata **A**cquisition) system (Automation Community, 2023), (Myomron). On the other hand, a modern controlled system of an industrial process is fully rounded if in addition to SCADA, it is also connected to an IoT network. Such a concept enables process data to be transferred to any location, visualized in real-time, and stored on a cloud computer.

Commonly, some standalone industrial processes might represent a separate entity. Since these plants are far from the Intra and Internet network of manufacturing companies, the data distribution of analog and digital signals from sensors and actuators of some process quantities (eg voltage, current, pressure, flow, temperature, LEDs, relay, etc.) .) must be made from these remote entities to the master station via wireless communication, most likely a radio frequency (RF) connection (Stefanov, 2021), (nRF24L01), (Single-chip 2.4 GHz Transceiver

NRF24L01). There are various wireless communication technologies used in building IoT applications and RF is one of them. Usually, such radio communications are two-way or bidirectional (Single-chip 2.4 GHz Transceiver NRF24L01). In this paper, a prototype of SCADA system for bidirectional exchange of process data between two remote industrial plants is designed.

Design on SCADA System for Exchange Data in Master Slave RF and Iot Network

In Figure 1, a block diagram of a realized SCADA system for Data Exchange in MASTER SLAVE RF and IoT network is shown.

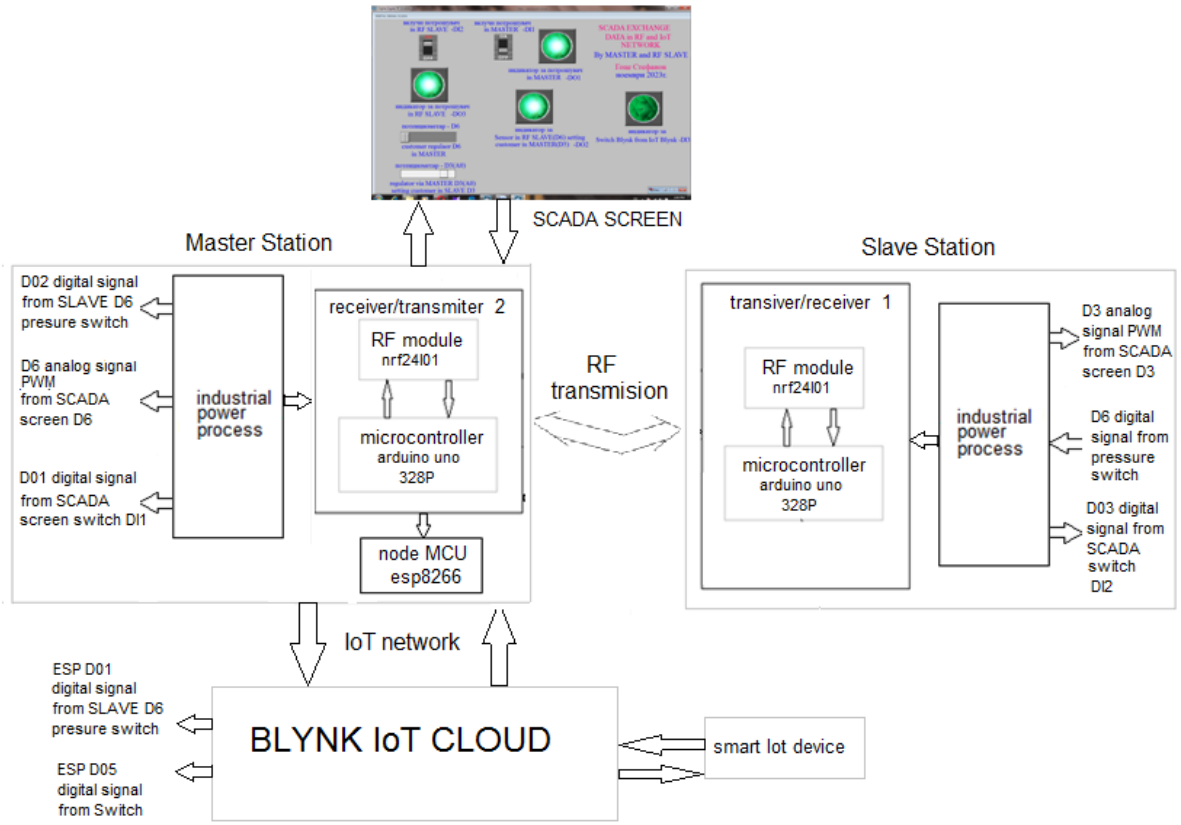

Figure 1. Block diagram of a SCADA system for bidirectional exchange of process data between two remote industrial plants implemented in IoT and RF network

SCADA system enables data exchange between SCADA screen, MASTER and SLAVE stations. The MASTER station is installed in one industrial plant and the SLAVE is installed in another plant. The SCADA monitoring system is built into the MASTER station. The SLAVE station is connected by RF (radio frequency connection) to the MASTER station. In the MASTER and SLAVE stations, two microcomputers units as well as appropriate RF modules are installed. The microcomputer in the MASTER station is serially connected to the IoT microcomputer for the transfer of measurement data in the IoT network.

In the designed SCADA system prototype, switches and LEDs were used as sensors and actuators to verify the correct operation of the solution. The microcomputers in the MASTER and SLAVE stations are 328P on arduino uno board (ATMEGA328P). The microcomputer that allows connecting the system to the IoT network is a nodeMCU esp8266-12E (ESP8266). The design of the prototype system consists of design of the SLAVE and MASTER stations and the design of the SCADA controll system.

Design of the MASTER and SLAVE Station

In real industrial plants there are parts that are remote from intra and internet network. In such standalone plants there is a problem with timely collection, visualization and analysis of signals from sensors that are important for proper functionality of industrial equipment. The designed RF MASTER SLAVE network in this paper

solves this problem and enables integration of signals from standalone plants in intra network of the company. In Figure 2 is shown block diagram of RF MASTER SLAVE network (which is part from Figure 1).

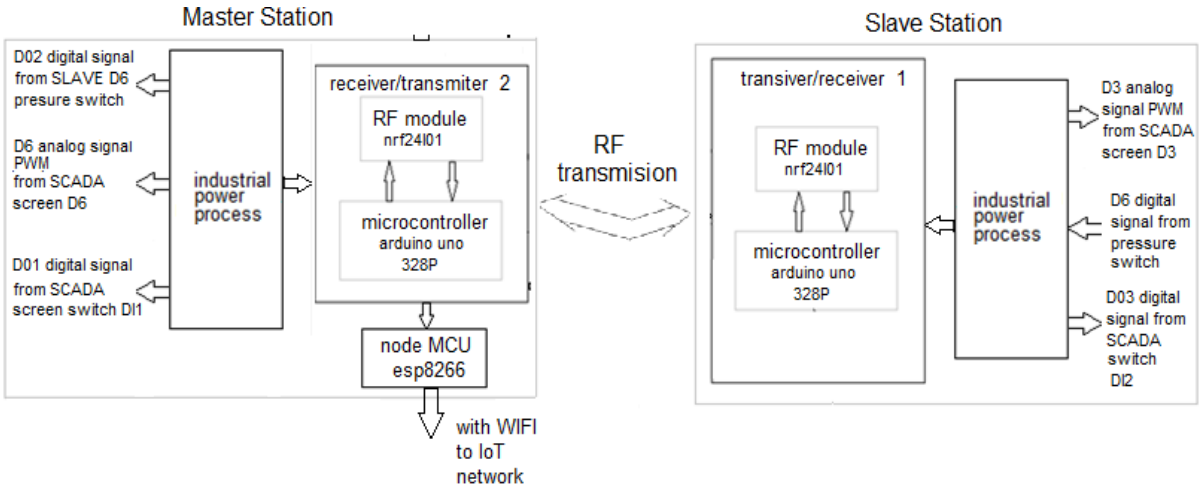

Figure 2. Block diagram of bidirectional RF MASTER SLAVE sensors network

SLAVE and MASTER station on both sides consist of sensors network and actuators, RF module and microcontroller. Such a solution provides the possibility to connect the process quantities of standalone plant in the intra network of the manufacturing company. From Figure 1 and 2 can be seen that this solve is based on microcomputer, RF modules and WIFI interface. The SLAVE microcomputer collects data for the quantities of the industrial process through the sensor network and with RF communication sends collected data to the MASTER microcontroller that is connected to IoT network with a WIFI interface (nodeMCU ESP8266-12e) (Stefanov, 2021). From other hand, the MASTER microcomputer is connected to a personal computer through UART port and sends collected data to SCADA screen and intra company network. This hardware architecture on the one hand provides data, adequate to the conditions in the industrial process to be collected and visualized on SCADA screen on a personal computer and on the other hand the possibility for distribution of data in the IoT network is created. The design of the RF MASTER SLAVE network consists of design of the RF SLAVE station and the design of the RF MASTER station.

The design of the SLAVE station consists of a microcomputer ATmega 328P on an arduino uno board, RF module nrf24l01 (Stefanov, 2021) and appropriate hardware components:
- *switches as sensors*
D6 digital input signal from pressure switch
-*LEDs as actuators*
D3 analog PWM output signal which is active with SCADA screen potentiometer D3
D03 digital output signal which is active with SCADA screen switch DI2

The design of the MASTER station consists of a microcomputer ATmega 328P on an arduino uno board, RF module nrf24l01, nodeMCU ESP8266-12e and SCADA Cx Supervisor design, and appropriate hardware components:
- *switches as sensors*
D6 digital input signal from pressure switch
-*LEDs as actuators*
D02 digital output signal which is active with pressure switch D6 from SLAVE
D6 analog PWM output signal which is active with SCADA screen potentiometer D6
D01 digital output signal which is active with SCADA screen switch DI1

Features of the Used Hardware

a.) *NRF24L01 Module*

NRF24L01 is a single-chip radio transceiver module that operates on 2.4 - 2.5 GHz (ISM band) (Stefanov, 2021). This transceiver module consists of a fully integrated frequency synthesizer, a power amplifier, a crystal oscillator, a demodulator, a modulator and Enhanced ShockBurs protocol engine. Output power, frequency channels, and protocol setup are easily programmable through an SPI interface. Built-in Power Down and

Standby modes makes power saving easily realizable. In the Figure 3 is shown electronic board on NRF24L01 module and his pinout.

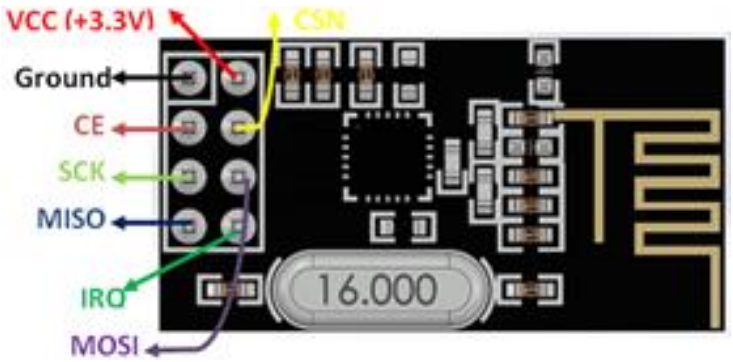

Figure 3. Electronic board of NRF24L01 module and his pinout

In the Table 1 are given pinout configuration on NRF24L01 module.

Table 1. Pinout configuration on NRF24L01 module

Pin Number	**Pin Name**	**Abbreviation**	**Function**
1	Ground	Ground	Connected to the Ground of the system
2	Vcc	Power	Powers the module using 3.3V
3	CE	Chip Enable	Used to enable SPI communication
4	CSN	Ship Select Not	This pin has to be kept high always, or else it will disable the SPI
5	SCK	Serial Clock	Provides the clock pulse using which the SPI communication works
6	MOSI	Master Out Slave In	Connected to MOSI pin of MCU, for the module to receive data from the MCU
7	MISO	Master In Slave Out	Connected to MISO pin of MCU, for the module to send data from the MCU
8	IRQ	Interrupt	It is an active low pin and it is used only if interruption is required

NRF24L01 Features:

- 2.4GHz RF transceiver Module
- Operating Voltage: 3.3V
- Nominal current: 50mA
- Range : 50 – 100 m
- Operating current: 250mA (maximum)
- Communication Protocol: SPI
- Baud Rate: 250 kbps - 2 Mbps.
- Channel Range: 125
- Maximum Pipelines/node : 6
- Low cost wireless solution

The NRF24L01 is a wireless transceiver module, meaning each module can both send, as well as receive data. The operating frequency is 2.4 GHz, which falls under the ISM band and hence it is legal to use in almost all countries for engineering applications. When the modules operate efficiently coverage can be in distance of 100 meters (200 feet), which makes it a great choice for all wireless remote controlled projects.!!!!!!

The module operates at 3.3V, hence can be easily used with 3.2V systems or 5V systems. Each module has an address range of 125 and each module can communicate with 6 other modules hence it is possible to have multiple wireless units communicating with each other in a particular area. Hence mesh networks or other types of networks are possible using this module. Therefore, this module is an ideal choice for practical applications.
The **NRF24L01module** works by means of **SPIcommunications**. These modules can either be used with 3.3V microcontroller or a 5V microcontroller with SPI port. The complete details of usage of this module through SPI

is given in the data sheet below. The circuit diagram in the Figure4 shows that the module should be interfaced with the microcontroller.On Figure 4 is shown the usage of 3.3V microcontroller, but it is applied in the same way for a 5V MCU. The SPI Pins (MISO<MOSI and SCK) are connected to the SPI pins of the microcontroller and the signal pins (CE and CSN) are connected to the GPIO pins of the MCU.There are ready made available libraries, like R24 Library, for interfacing this module with Arduino.

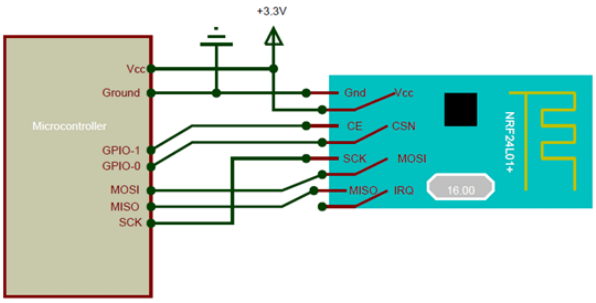

Figure 4. NRF24L01 module interfaced with a microcomputer

With help of these libraries N**RF24L01** can be easily interfaced with Arduino**,** with few lines of code. If using some other microcontroller, the datasheet has to be read in order to understand how to establish SPI communication. The **NRF24L01module** is a bit tricky to use especially since there are many cloned versions in the market. In case of troubleshoot, 10µF and 0.1µF capacitors should be added parallel to source Vcc and Ground pins. Also, the 3.3V supply should be clean and does not have any noise coupled in it.

b) Microcomputer ATmega 328P

The Arduino Uno is an open-sourcemicrocontroller board based on the Microchip ATmega328P microcomputer and developed by Arduino.cc. The board is equipped with sets of digital and analog input/output(I/O) pins that may be interfaced to various expansion boards (shields) and other circuits. The board has 14 digital I/O pins (six capable of PWM output), 6 analog I/O pins, and is programmable with the Arduino IDE (Integrated Development Environment), via a type B USB cable. It can be powered by the USB cable or by an external 9-volt battery, though it accepts voltages between 7 and 20 volts.

a.)

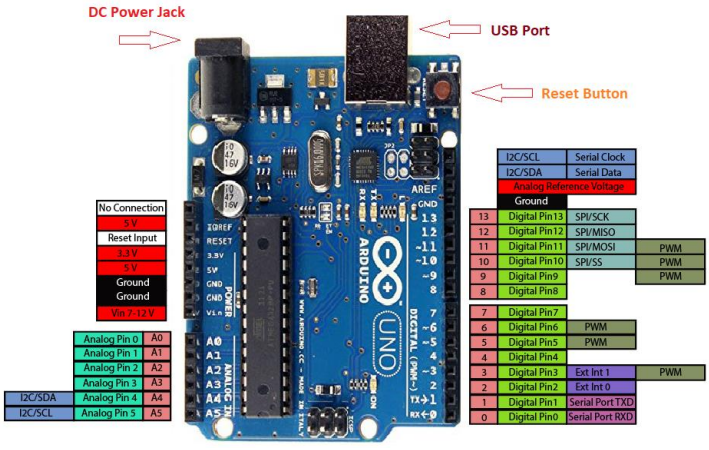

b.)

Figure 5. a.) Arduino Uno and b.) pinout

The word "uno" means "one" in Italianand was chosen to mark the initial release of Arduino Software. The Uno board is first in a series of USB-based Arduino boards; The Uno board and version 1.0 of the Arduino IDE were the reference versions of Arduino, which have now evolved to newer releases. The ATmega328P on the board comes preprogrammed with a bootloader that allows uploading new code to it, without the use of an external hardware programmer (Stefanov,2021). In Figure 5 a) is shown electronic board of Arduino Uno with build Atmega 328P microcomputer and in Figure 5 b) are shown its pinouts. The MASTER station, unlike the SLAVE station as seen in Figure 1 and 2, has yet NodeMCU 8266-12e node.

c.) Microcomputer NodeMCU ESP8266-12e

The NodeMCU ESP8266 development board comes with the ESP-12E module containing ESP8266 chip having Tensilica Xtensa 32-bit LX106 RISC microprocessor. This microprocessor supports RTOS and operates at 80MHz to 160 MHz adjustable clock frequency. NodeMCU has 128 KB RAM and 4MB of Flash memory to store data and programs. Its high processing power with in-built Wi-Fi / Bluetooth and Deep Sleep Operating features make it ideal for IoT projects.NodeMCU can be powered using Micro USB jack and VIN pin (External Supply Pin). It supports UART, SPI, and I2C interface. In the Figure 6 is shown NodeMCU ESP8266 and its pinout.

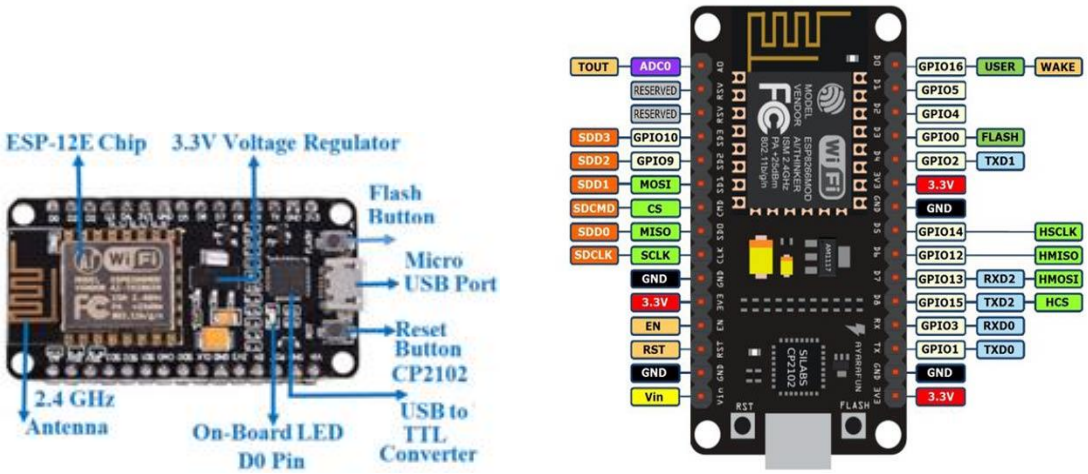

a.) b.)

Figure 6. a.) NodeMCU ESP8266 and b.) Pinout

NodeMCU is an open source based firmware and development board specially targeted for IoT based applications. It includes firmware that runs on the ESP8266 WIFI SoC from Espress Systems, and hardware which is based on ESP-12 module.

NodeMCU ESP8266 specifications &features

- Microcontroller: Tensilica 32-bit RISC CPU Xtensa LX106
- Operating Voltage: 3.3V
- Input Voltage: 7-12V
- Digital I/O Pins (DIO): 16
- Analog Input Pins (ADC): 1
- UARTs: 1
- SPIs: 1
- I2Cs: 1
- Flash Memory: 4 MB
- SRAM: 64 KB
- Clock Speed: 80 MHz
- USB-TTL based on CP2102 is included onboard, Enabling Plug n Play
- PCB Antenna
- Small Sized module to fit smartly inside your IoT projects

The NodeMCU ESP8266 board can be easily programmed with Arduino IDE since it is easy to use.

An essential part of the designed prototype SCADA system is the SCADA CDJ-Supervisor, so below follows a brief description of this software package, which is a product of Omron.

Design of the SCADA

The SCADA is made in Omron CX-Supervisor software, (Myomron). CX-Supervisor is dedicated to the design and operation of PC based visualization and machine control. It is not only simple to use for small supervisory and control tasks, but it also offers a wealth of power for the design of the most sophisticated applications. CX-Supervisor boasts powerful functions for a wide range of PC based HMI requirements. Simple applicationscan be created rapidly with the aid of a large number of predefined functions and libraries, and even very complex applications can be generated with a powerful programming language or VBScript. CX-Supervisor has an extremely simple, intuitive handling and high user friendliness. CX-Supervisor runs on standard PC desktop computers running Microsoft Windows. CX-Supervisor is intuitive and easy to use and allows the developer to rapidly configure, test and debug a project. CX-Supervisor comprises two separate executable Windows programs, CX-Supervisor Development environment and CX-Supervisor Runtime environment. Applications are created and tested using the development environment and then delivered as a final customer application with the runtime environment. The runtime-only environment may only be used for executing an application previously generated using the development environment. It is not possible to generate a new runtime application using the runtime environment. In the Figure 7 is shown connection between sensor hardware, microcontroller and CX-Supervisor SCADA.

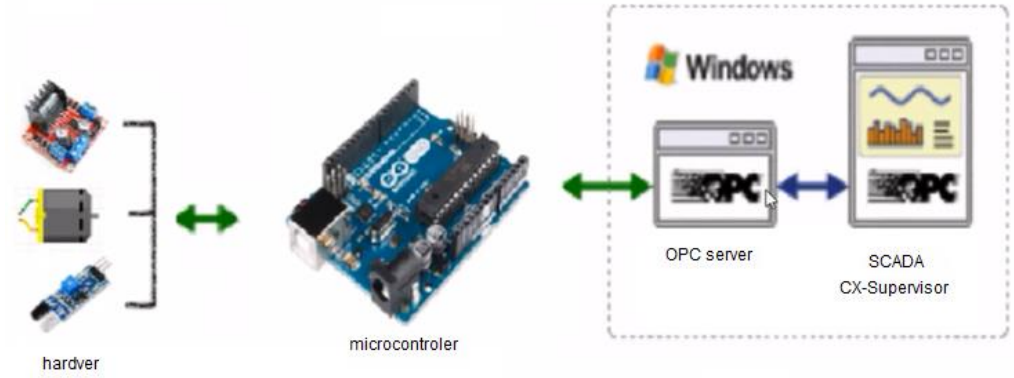

Figure 7. Connection between sensor hardware, microcontroller, and CX-Supervisor SCADA

a.) *Setting up Graphic Symbols*

The first thing to do is to set up graphic symbols. Now that the project exists with its own page, the graphic objects can be constructed and added to the page, Figure 8 a).

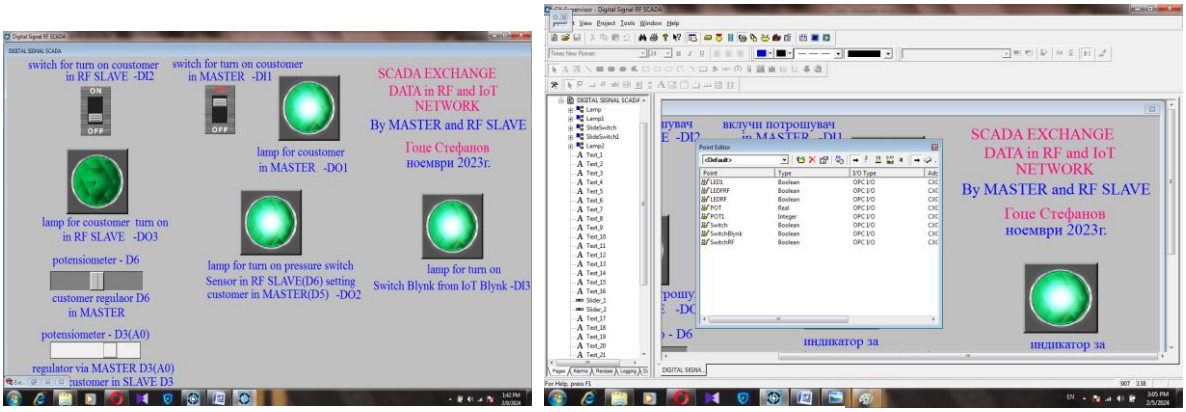

a.) b.)

Figure 8. a.) Setting graphic symbols, b.) Setting variables for graphical symbols

The graphics editor uses a Graphic Object toolbar and a floating window known as the Palette to construct and control objects on the page. These are very easy to use. Several small icons are visible on the Graphic Object toolbar - each one representing one of the graphical objects with which an application can be constructed. Some of the objects are graphical primitives - straight lines, ellipses, rectangles; some are rather more advanced - such as the gauge object, which has built-in functionality.

b.) *Setting up Variables for Graphical Symbols*

For each of the graphic symbols, a point variable with the appropriate size and unit is created, Figure 8 b). These variables correspond to the variables in the Arduino code.

c.) Setting Grafical Symbols with Variables

Finally, each graphic symbol is associated with a corresponding variable. In the Figure 9 is shown SCADA screen with defines variables.

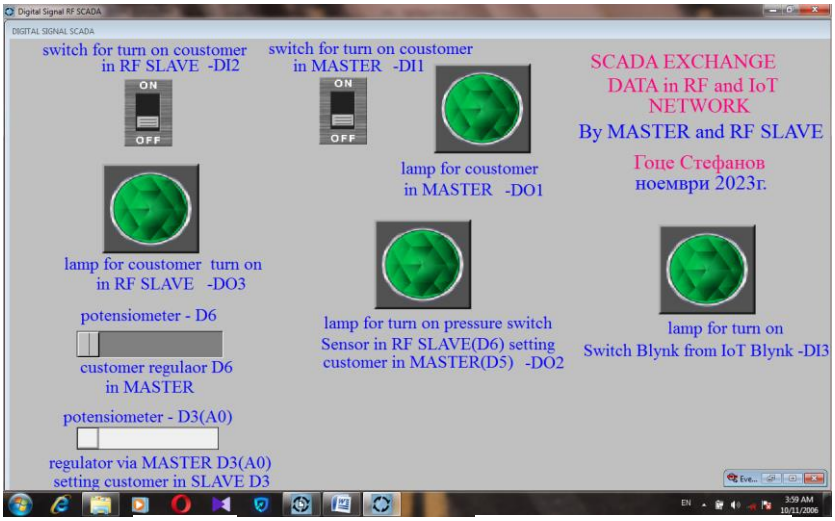

Figure 9. SCADA exchange data system screen with defines variables

SCADA screen for this prototype SCADA exchange data consists of the following elements:
Switch for turn on customer in RF SLAVE - DI2, switch for turn on customer in MASTER - DI1, lamp for indication turn on customer in MASTER - D01, lamp for indication turn on customer in RF SLAVE - D03, lamp for indication turn on pressure switch sensor in RF SLAVE D6 (causes turn on customer in MASTER - D02), lamp for turn on switch blynk from IoT Blynk - DI3, potentiometer - D6 which regulates analog PWM output signal D6 in MASTER station, potentiometer - D3 which regulates analog PWM output signal D3 in SLAVE station.

Experimental Results

Figure 10 a) shows the prototype on the SLAVE station, and Figure 10 b) shows the prototype on the MASTER station.

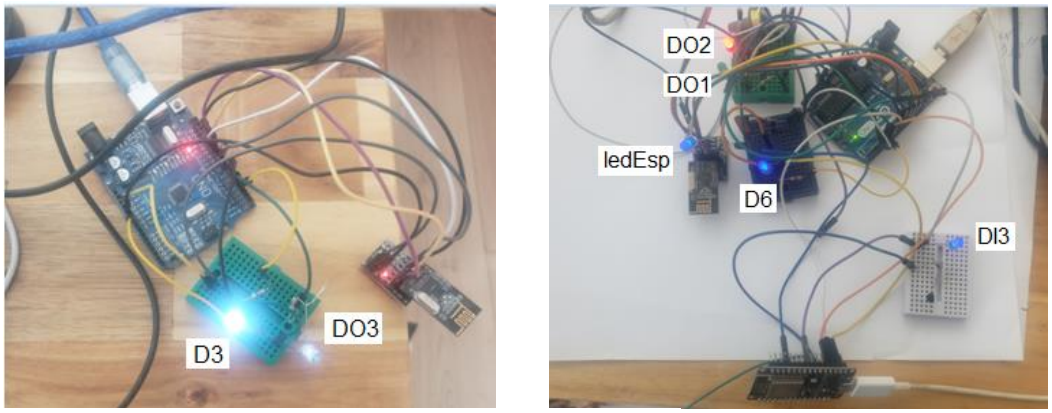

a) b)

Figure 10. Prototype on design SCADA exchange data system: a) prototype on SLAVE station, b) prototype on MASTER station

Figure 11a shows the screen of the design SCADA exchange data system and in Figure 11b is shown prototype on SLAVE and MASTER station when the SCADA screen is as in the figure 11a.

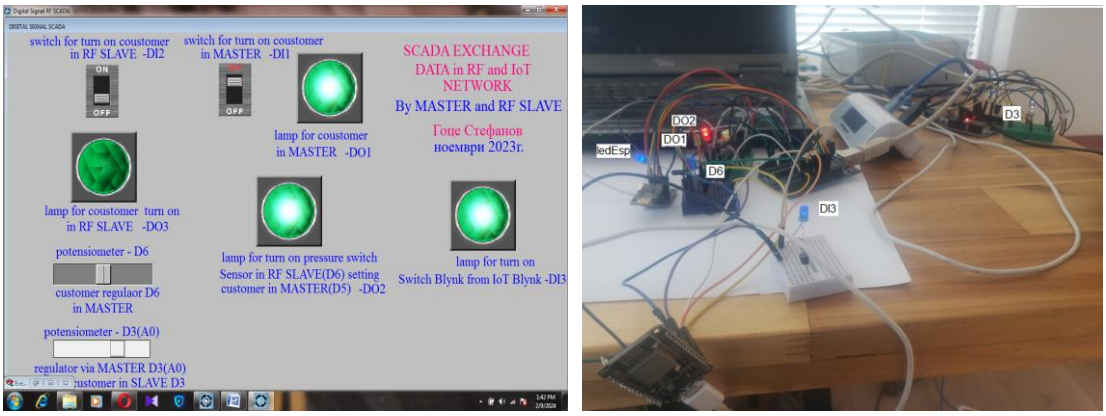

a.) b.)

Figure 11. a) Screen of the design SCADA exchange data system and b) prototypes on SLAVE and MASTER station when the SCADA screen is as in the figure 11 a)

In Figure 11 a) SCADA screen indicates that they are currently turn on: lamp for indication turn on customer in MASTER - D01, lamp for indication turn on pressure switch sensor in RF SLAVE D6 (causes turn on customer in MASTER - D02), lamp for turn on switch blynk from IoT Blynk - DI3, potentiometer - D6 which regulates analog PWM output signal D6 in MASTER station is is set to 50 % duty cycle, potentiometer - D3 which regulates analog PWM output signal D3 in RF SLAVE station is set to 50 % duty cycle.

A comparison of Figure 11 a) and b) shows that the LEDs in Figure 11 b) are in a state that is defined by the state of the elements of the SCADA screen. Figure 13 shows a routing diagram to illustrate the connection of the signal exchange between the SCADA screen, MASTER station, SLAVE station and the Blink Cloud.
On the Figure 12 a) are shown the regulated one analog PWM output signal D3 in RF SLAVE station, for illustrations for verification of the work of the designed SCADA system, when potentiometers in SCADA screen D3 is set to 50 % duty cycle, and Figure 12 b) the same thing when potentiometers in SCADA screen D3 is set to 90 % duty cycle.

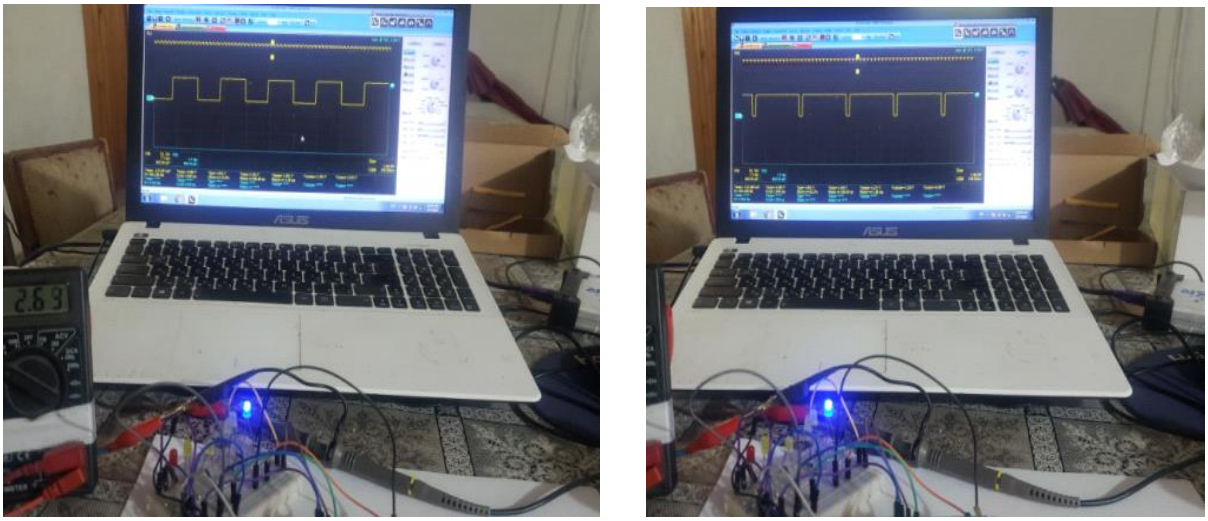

Figure 12. Verification the work of the designed SCADA system a.) when analog PWM output signal D3 in RF SLAVE station signal is 50 % and b.) when analog PWM output signal D3 in RF SLAVE station is 90 %

From Figure 12 a) also can be seen that led diode D03 (in RF SLAVE station) is on and is at medium brightness, the digital meter shows a value of 2.69 V, the waveform of the oscillogram is with a duty cycle 50 %. From Figure 12 b) it can be seen that D03 is on and is at high brightness, the digital meter shows a value of 4.57 V, the waveform of the oscillogram is with a duty cycle 90 %.

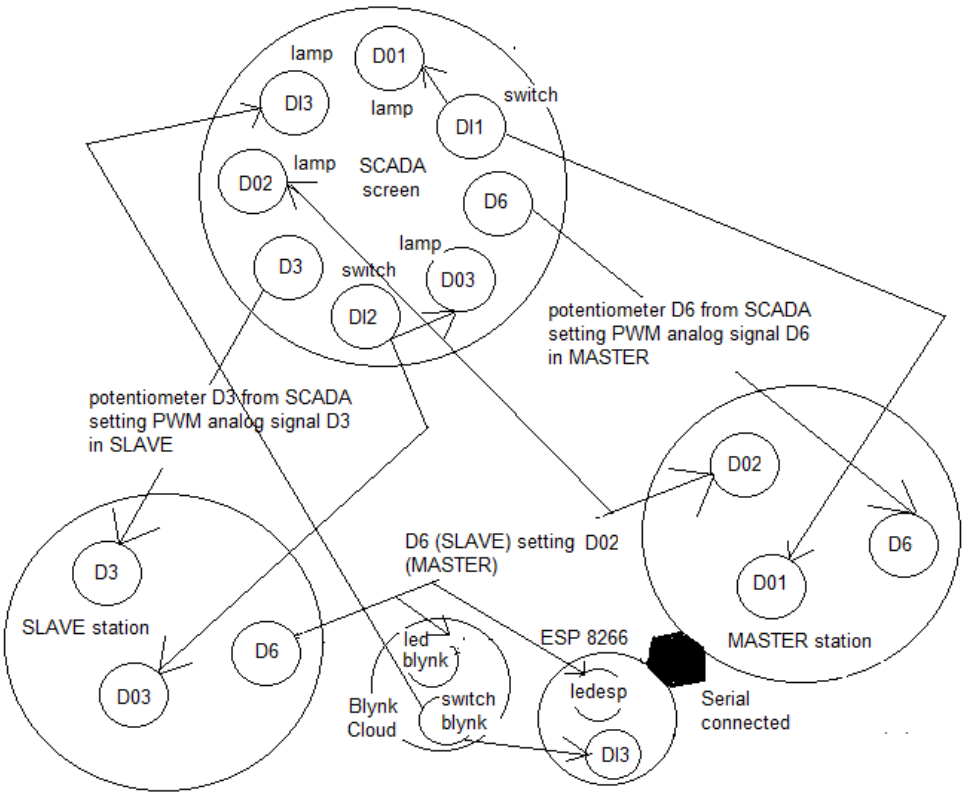

Figure 13. Routing diagram to illustrate the connection of the signal exchange between the SCADA screen, MASTER station, SLAVE station and the Blink Cloud

Figure 14 a) shows a data screen on a mobile device in which the data was transferred from a SCADA exchange data system in the IoT network, and Figure 14 b) represents a screen on the IoT Blynk cloud network (Stefanov, 2023).

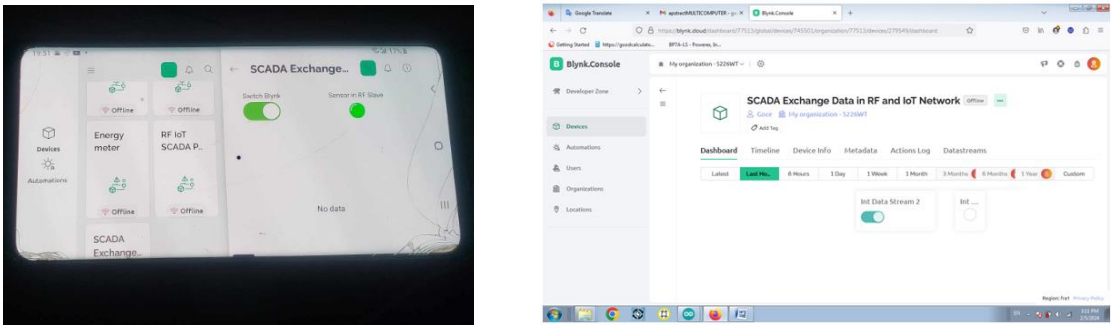

a) b)

Figure 14. The screen on the exchange data from SCADA system in IoT network: a) screen on mobile device, b) screen on IoT Blynk cloud network

Turn on Switch Blynk in the Figure 14 a) shows that the Blink cloud turns on the LED DI3 (Figure 11 b)) in the MASTER station and turn on LED Sensor in RF Slave in the same Figure 11 a) shows that the pressure switch D6 (Figure 2) in the RF SLAVE is turned on.

Conclusion

The paper is designed as an experimental prototype on SCADA system for exchange data between two remote industrial plants. One measuring point is marked as SLAVE, the other is marked as MASTER station. The two measuring points are connected to each other by RF communication. The tested nrf24l01 modules provide the possibility of remote transmission of signals up to 5 km in free air. SLAVE and MASTER stations accept digital and analog signals and exchange them among each other. SCADA system and WIFI interface are embedded in

the MASTER measuring point. The SCADA system participates in visualization and data exchange between SLAVE and MASTER stations, as well as data exchange in the IoT network. Such a solution provides the possibility of distribution and control of process data in remote industrial plants from any measuring point (SLAVE or MASTER station). Additionally, the proposed system also provides the possibility for the distribution of obtained data in IoT cloud computers and mobile smart devices (mobile telephone, tablet, etc.).

Scientific Ethics Declaration

The authors declare that the scientific ethical and legal responsibility of this article published in EPSTEM journal belongs to the authors.

Acknowledgements or Notes

* This article was presented as oral/poster presentation at the International Conference on Basic Sciences, Engineering and Technology (www.icbaset.net) held in Alanya/Turkey on May 02-05, 2024.

References

Atmel.(2015). 8-bit AVR microcontroller with 32K bytes ın-system programmable flash. Retrieved from *Atmel-7810-Automotive-Microcontrollers-ATmega328P_Datasheet. pdf*.

Bennett, S., & Linkens, D.A.(1982). *Computer control of industrial processes*. Stevenage: Peregrinus.

Citkuseva -Dimitrovska, B., Golubovski, R., Spasevska, H., Stefanov, G., & Kukuseva, M. (2021). Investigation of efficiency aspects in 3x3 photovoltaic plant using model of shading. *First International Conference ETIMA, 1*(1).

Hor, C. L., & Crossley, P. A. (2005). Knowledge extraction from intelligent electronic devices. In *Transactions on Rough Sets III* (pp. 82-111). Berlin, Heidelberg: Springer.

Stefanov, G., Kukuseva -Paneva, M., & Stefanova, S. (2023) 3-phase smart power meter implemented in RF network. *Balkan Journal of Applied Mathematics and Informatics, 6*(1), *25-37.*

Stefanov, G., Kukuseva, M., & Stefanova, E. (2021). Design of an intelligent Wi-Fi sensor network. *Balkan Journal of Applied Mathematics and Informatics, 4*(1), 17-26.

Author Information

Bilijana Citkuseva Dimitrovska
Faculty of Electrical Engenering
Goce Delcev University Stip
Krste Misirkov, 10A, 2000 Stip
North Macedonia
Contact e-mail: *bilijana.citkuseva@ugd.edu.mk*

Elena Zafirov
One Sky Flight 7777 Lemmon Ave
Dallas, TX 75209 , USA

Goce Stefanov
Faculty of Electrical Engenering
Goce Delcev University Stip
Krste Misirkov, 10A, 2000 Stip
North Macedonia

To cite this article:

Citkuseva-Dimitrovska, B., Zafirov, E., & Stefanov, G. (2024). SCADA system for process data exchange in master slave RF and Iot network. *The Eurasia Proceedings of Science, Technology, Engineering & Mathematics (EPSTEM), 28,* 554-564.

The Eurasia Proceedings of Science, Technology, Engineering & Mathematics (EPSTEM)
ISSN: 2602-3199

The Eurasia Proceedings of Science, Technology, Engineering & Mathematics (EPSTEM), 2024

Volume 28, Pages 565-574

ICBASET 2024: International Conference on Basic Sciences, Engineering and Technology

Optimization of Properties of Iron Oxide Nanoparticles Synthized by Sol-Gel Method

Gulten Sadullahoglu
Istanbul Health and Technology University

Abstract: In this study, the effects of pH value and capping agent on the morphology, pore structure and size of iron oxide nanoparticles were investigated systematically to obtain optimum properties. Iron oxide nanoparticles were synthized by sol-gel method. Polyvinyl alcohol (PVA) was used as capping agent by adding to the solution at 70 °C. After the drying process the powders were heat treated at 250 °C for 2 h under air atmosphere. Particle size of each sample was determined by using ZetaSizer instrument. X-ray diffraction (XRD) technique was employed for structural properties of iron oxide nanoparticles, FE-SEM (Field Emmision Scanning Electron Microscopy) was used to analyze the morphology of the powders. Magnetic properties of the nanoparticles were measured by VSM (Vibrating Sample Magnetometer) under air atmosphere at room temperature. Spesific surface area, porosity and pore size distribution of iron oxide nanoparticles were calculated by Brunauer-Emmett-Teller (BET) instrument. The results indicated that formation of the γ-Fe_2O_3 is sensitive to either the pH value of the solution or the capping agent, for the uncoated samples when pH value of the solution is adjusted to 2.5, α-Fe_2O_3 phase was detected as a single phase. When the solution was neutralized, γ-Fe_2O_3 was formed as the major phase in the microstructure, γ-Fe_2O_3 phase was formed as the major phase in the PVA coated samples leading to highest value of 50.33 emu/g measured in the sample of PVA8.5. For the PVA coated samples, specific surface area is in the range of 15.73 – 20.81 m^2/g, the intervals of pore volume and average pore width are increased to 0.099 – 0.121 cm^3/g and 23.19 – 23.07 nm respectively.

Keywords: Magnetic nanoparticles, Sol–Gel method, Capping agent, Pore structure, X-Ray diffraction

Introduction

Because of their chemical stability, cheap, and non-toxic nature iron oxide nanoparticles have attracted tremendous interest from researchers. Iron oxide, in nature has many phases like α-Fe_2O_3, β-Fe_2O_3, γ-Fe_2O_3, and Fe_3O_4. Out of all these polymorphic forms, α-Fe_2O_3 nanoparticles are most stable at ambient conditions (Ramasami et al., 2023). α-Fe_2O_3 nanoparticle is more popular than others due to its cost-effective synthesis, non-toxic nature, stability at room temperature, environment friendliness, a reusable and a wide range of applications such as catalysts, contrast agents in Magnetic Resonance Imaging (MRI), anticancer therapeutics (Behera et al., 2020; Ghosh et al., 2020; Rasheed et al., 2018;), drug delivery, pigments, gas sensors and biosensors (Guardia et al., 2000; Katsuki & Komarneni, 2003; Tedeschi & Enders, 2001). Different methods have been reported for the synthesis of iron oxide nanoparticles that includes, hydrothermal, co-precipitation, microemulsion, thermal decomposition, green synthesis, sol-gel, high-energy ball milling, etc, (Bhavani et al., 2017; Bhuiyan et al., 2020; Gonzalez-Moragas et al., 2015; LaGrow et al., 2019; Lemine et al., 2010; Okoli et al., 2012; Ravikumar & Bandyopadhyaya, 2011; Woo et al., 2003). But there are some challenges in controlling the particle size, shape, monodispersity, and morphology due to the high surface energy of iron oxide nanoparticles leading to aggregation under normal reaction condition (Jain et al., 2005; Mahmoudi et al., 2010; Mornet et al., 2005). To overcome these limitations scientists have applied different annealing temperature, reaction pH and capping agents (Woo et al., 2003; Predescu et al., 2018; Sharma, et al., 2019; Kumari et al., 2018; Sharma et al., 2021).

A. Bandhu at. Reported that when molarity of citric acid was between 0.05 and 0.2 M and at 400 °C annealing temperature α-Fe_2O_3 and γ-Fe_2O_3 phases were detected in XRD analysis however, at 210 °C, only α-Fe_2O_3 was observed and particle size changed from 22 nm to 56 nm when citric acid concentration decreased to 0.05 M in the solution. When some chemicals were added to the solution in stead of citric acid pore structure changed considerably and γ-Fe_2O_3 phase was formed in the structure. When iron oxide nanoparticles were coated with pepsin, high saturation magnetization was obtained as magnetic biomaterial for magnetically controlled drug delivery (Bandhu et al., 2015). Capping agents have clinical a significance to produce biocompatible nanoparticles. The covalent bonding between the chains of capping ligands and the nanoparticles' surface leads to steric hindrance providing stability to the nanocomposite (Javed et al., 2020). In this study, to investigate the effects of pH value of solution and application of Polyvinyl Alcohol (PVA) as capping acent on particle size, pore structure, magnetic properties, phase formation and microstructure to reach optimum properties.

Experimantal

All chemicals including iron nitrate nonahydrate ($Fe(NO_3)_3.9H_2O$), citric acid ($C_6H_8O_7$), polyvinylalcohol (PVA), were obtained from Merck and used as received, without further purification. Uncoated and PVA coated samples were prepared by the sol–gel method. $Fe(NO_3)_3.9H_2O$ was disolved in distilled water by using magnetic stirrer at 400 rpm. Citric acid ($C_6H_8O_7$) was added to the solution with molar ratio of citrate to nitrate 1:1. pH value of the solution are adjusted as 2.5, 7, 8.5 and 10 by adding NH_4OH dropwise to the solution. The mixture was simultaneously mixed and heated at 70 °C, when gel was obtained samples were dried at gradually increasing temperatures from 135 °C to 185 °C 135. Dried powders were heat treated at 250 ° for 2 h under air atmosphere. For the production of the coated samples, Polyvinyl alcohol (PVA) was added to the solution slowly over about 45 minutes while the precursers were mixed in a magnetic stirrer, Fe:PVA ratio is 1:1, followed by the same procedure as for the uncoated sample.

X-ray diffraction patterns of all the samples were recorded in powder X-ray diffractometer, Malvern PANalytical X'Pert PRO model, using Cu Kα radiation (α = 0.15425 nm) in the range of 2θ from 3° to 90°. The microstructure of the samples was observed by field-emission scanning electron microscopy by Thermo Scientific Apreo 2 S LoVac. Surface area, porosity and adsorption capacity are measured using the Brunauer, Emmett and Teller (BET) method in a 77 K liquid nitrogen environment, based on nitrogen (N_2). Particle size of the samples were measured by Malvern Nano ZS. Magnetic properties of the samples were measured at room temperature between -10000 - +10000 Oe external magnetic field by using Dexing Magnet VSM 550.

Results and Discussion

XRD Analysis

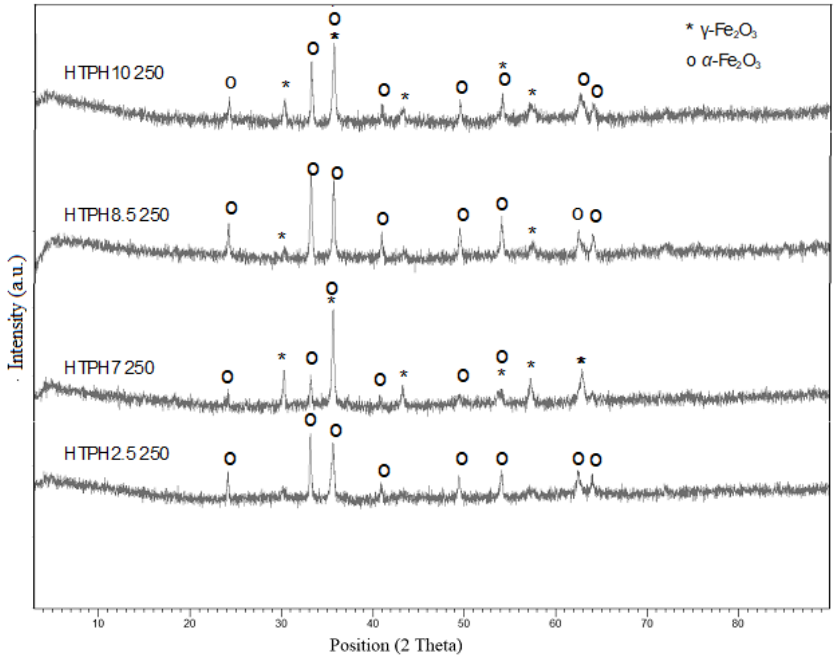

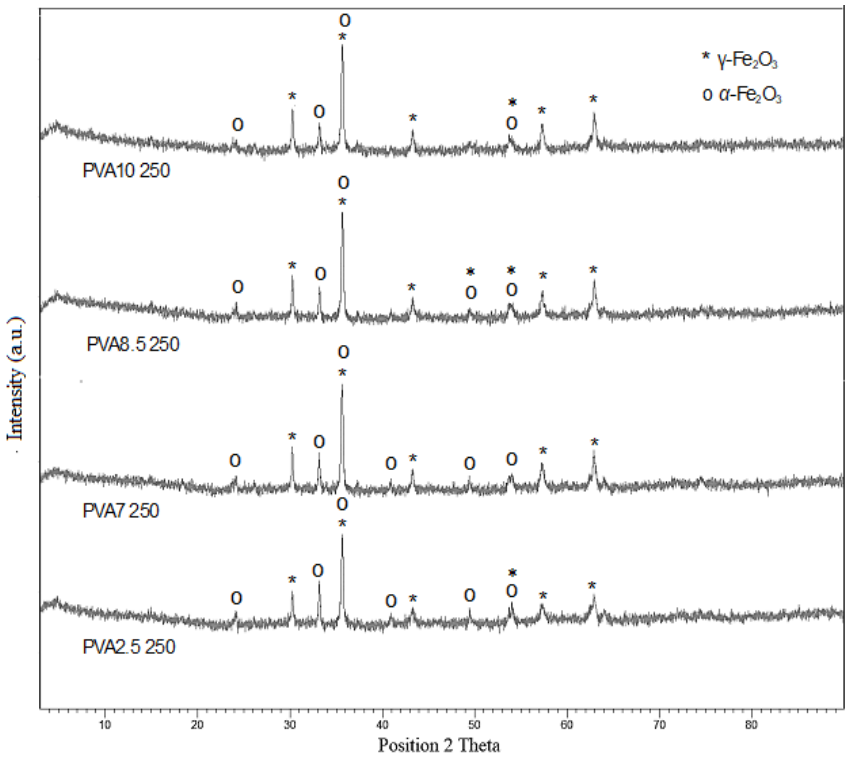

Figure 1. XRD patterns of the uncoated and PVA coated samples.

Figure 1 shows the diffraction patterns of the samples, for the sample of HTPH2.5 diffraction peaks detected belongs to α-Fe_2O_3 (hematite) phase. in the material. Diffraction peaks of α-Fe_2O_3 were found at 24.13° , 33.13° , 35.59° , 40.85° , 49.43°, 54.05°, 62.47° and 63.79° of 2θ and were correlated with Miller indices of (0 1 2), (1 0 4), (1 1 0), (1 1 3), (0 2 4), (1 1 6), (2 1 4) and (3 0 0) having ICSD file No. 89-2810.

When the pH value of the solution for the uncoated sample was increased to 7, the diffraction peaks corresponding to ferromagnetic γ-Fe_2O_3 phase were detected as a major phase Diffraction peaks of γ-Fe_2O_3 were found at 30.24° , 35.6° , 43.25° , 53.82° , 57.27° and 62.85° of 2θ and were correlated with Miller indices of (2 2 0), (3 1 1), (4 0 0), (2 1 1), (5 1 1) and (4 4 0) respectively having ICSD file No. 39-1346.

SEM Analysis

The micrographs of the uncoated and PVA coated samples are presented in Figure 1. In the SEM microstructure images of coated and uncoated samples, nanoparticles are of different shapes and sizes, and it has been observed that these particles form aggregates. mesoporous structure between in stuck nanoparticles provides a hysteresis in adsorption and desorption isotherm. In Figure 2(g)-(h), PVA coated samples show a distribution of spherical nanoparticles which were stuck together.

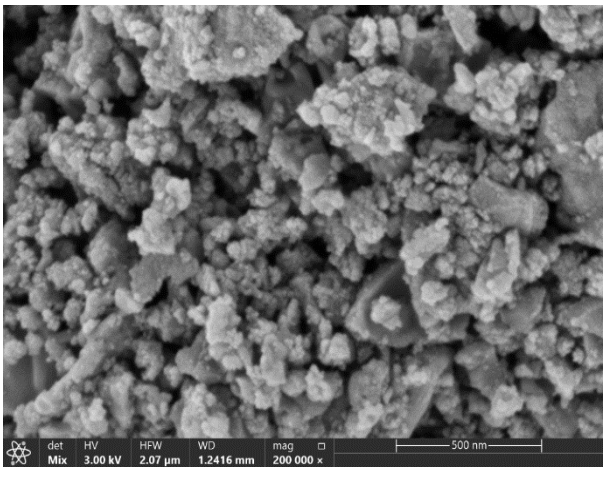

(a)

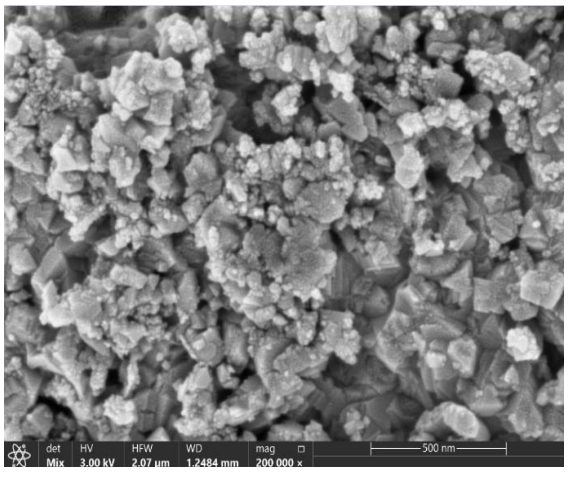

(b)

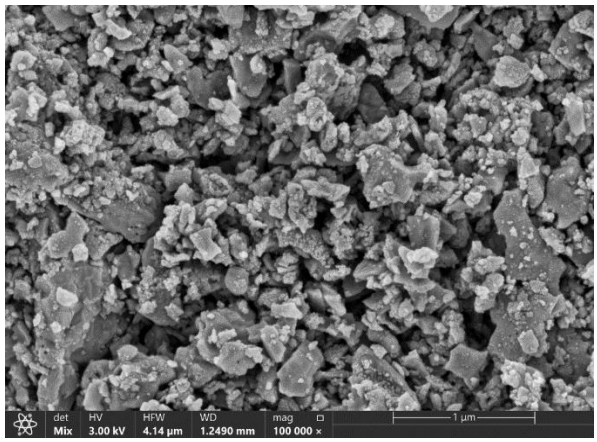

(c)

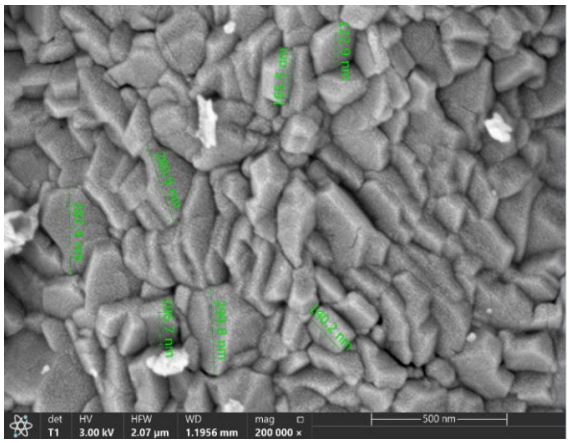

(d)

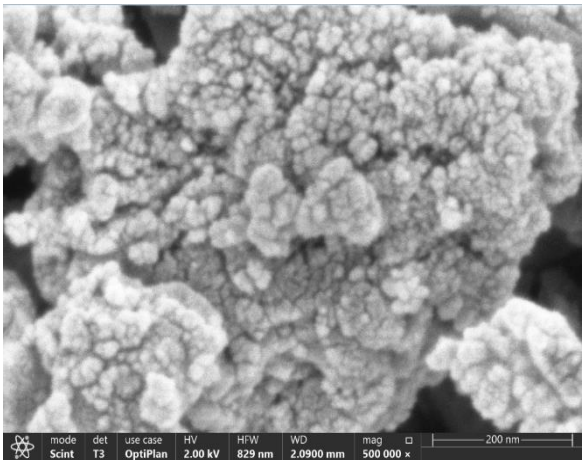

(e)

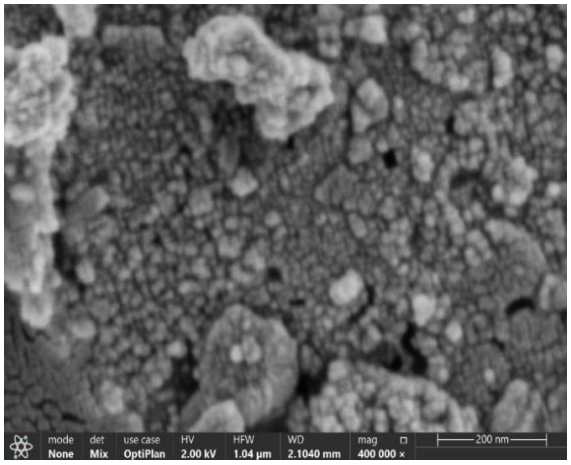

(f)

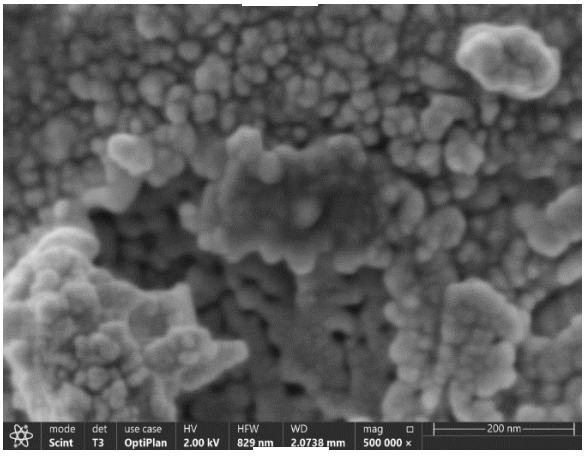

(g)

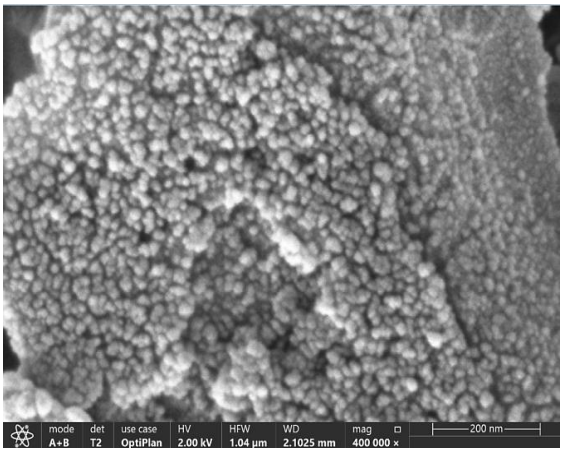

(h)

Figure 2. HRSEM images of the uncoated (a -d) and PVA coated (e -h) samples.

Nitrogen Gas Adsorption Analysis

Structure of Fe_2O_3 Samples were Determined by BET Analysis

The low-temperature liquid nitrogen adsorption experiment includes the adsorption/desorption curve and pore size change. The experimental results of the samples are compared with the results of samples which have

processed at different pH value and the coated samples to obtain the effect of nanoparticle adsorption on the pore structure (Table 2).

Figure 1. shows the adsorbtion and desorption isotherms of the samples. Adsorption/desorption curves are determined by the Barrett–Joyner Halenda (BJH) method through analyzing the desorption branch of adsorption data. It can be seen from the curves of the coated and uncoated samples that the adsorption curves belong to type III isotherms are concave, and the amount of adsorbed gas increases with the increase of the component relative pressure.

In such cases, the adsorbent—adsorbate interaction is weak as compared with the adsorbate—adsorbate interactions.The hysteresis loops of the samples belong to H3 hysteresis loops. Type H3 loop, which does not exhibit any limiting adsorption at high relative pressure is observed with aggregates of plate-like particles giving rise to slit-shaped pores. Also if the pore network consists of macropores which are not completely filled with pore condensate (Wang et al., 2022).

In Figure 2 (a), (b) and (d) desoption isotherms have steep clousers at about 0,4 relative pressure this is due to the cavitation – induced evoporation. In the case of the sample HTP8,5 and all the coated samples (Figure (c), (e)-(h)) desorption isotherms of changes smoothly when the relative pressure decreases in the removing of adsorbate process. This may referred that adsorbate molecules can be desorbed easer from pores than that of other samples.

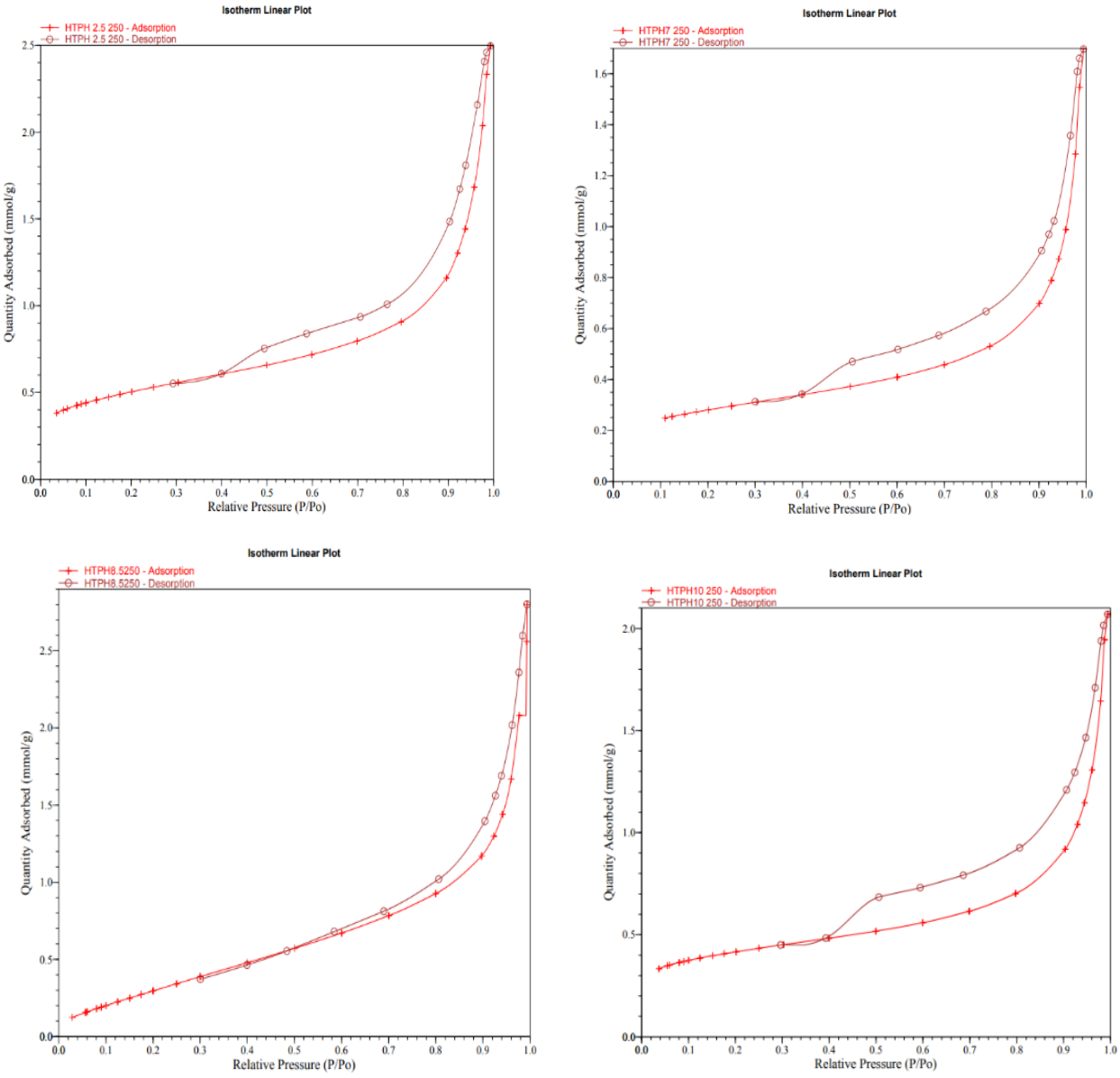

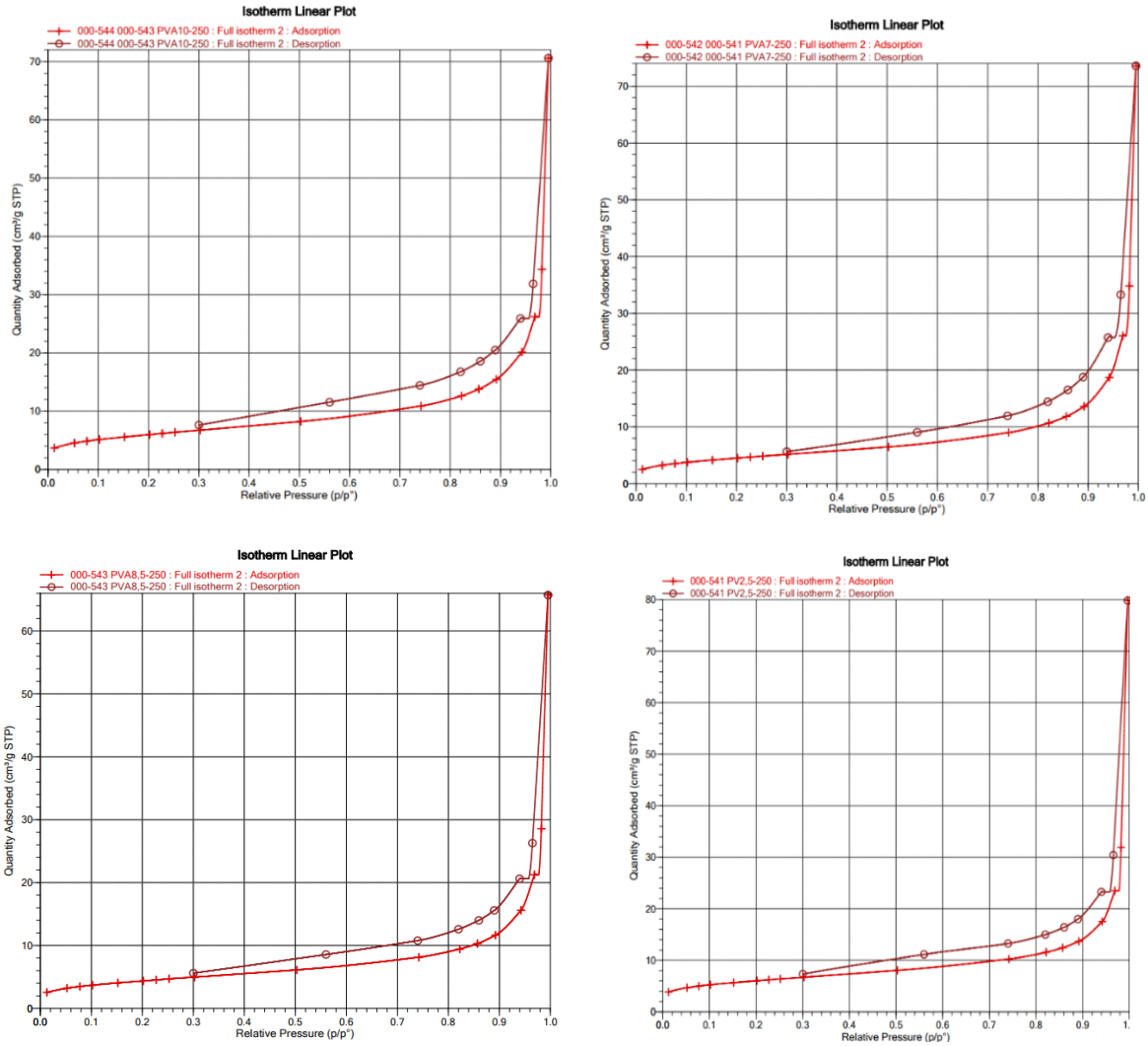

Figure 3. Adsorption and desorption isotherms of the uncoated and PVA coated nanoparticles**.**

The average pore diameter and specific surface data in Table 2 are determined by the Brunauer–Emmett–Teller (BET) method in the low-temperature liquid nitrogen adsorption experiment.The specific surface area, pore volumes and average pore diameters of the uncoated iron oxide samples varied between 22.2-40.1 m^2 /g, 0.055-0.097 cm^3 /g and 9.536-13.873 nm, respectively.

Table 1. Surface area (m^2/g), pore volume (cm^3/g), average pore diameter (nm) and particle size (nm) of the uncoated and PVA coated samples.

Sample	Surface Area (m^2/g)	Pore Volume (cm^3/g)	Average Pore Diameter (nm)
HTPH2.5250	40.1075	0.0827	9.53620
HTPH7250	22.2038	0.0556	13.8736
HTPH8.5250	28.4509	0.0973	9.4389
HTPH10250	32.6688	0.0667	11.2474
PVA2.5250	20,8158	0,1209	29,0750
PVA7250	15,7323	0,1123	27,4403
PVA8.5250	15,7747	0,0999	28,0846
PVA10250	20,7509	0,1069	23,1963

In the case of the samples capped with PVA, the pore volume of the samples were significantly increased and the spesific surface area of the PVA coated samples were lower than the uncoated samples. The specific surface area, pore volumes and average pore diameter of the PVA coated samples between 15.73-20.81 m^2 /g, 0.0999-0.1209 cm^3 /g and 23.196-29.075 nm, respectively.

Particle Size Measurements

The average particle size is between 1166 nm and 1473 nm for uncoated samples, a homogeneous distribution in the microstructure was observed only for the HTP2.5 sample. Different size distributions are observed in PVA coated samples, the average particle size is between 1066 nm and 1711 nm.

Figure 4. Particle size measurements of the uncoated and PVA coated samples.

Magnetic Properties

The effect of pH value of solution and PVA coating on the magnetic properties has been studied at room temperature. Figure 5 highlights the magnetization measurements as a function of the applied external magnetic field. Various magnetic parameters such as saturation magnetization (M_S), remanent magnetization (M_R), and

coercivity (H_c) have been evaluated using the M − H loops and are shown in Table 2. For the uncoated samples, the saturation of magnetization calculated using the M − H loop was found between 13.75 - 44.85 emu/g (Table 2).

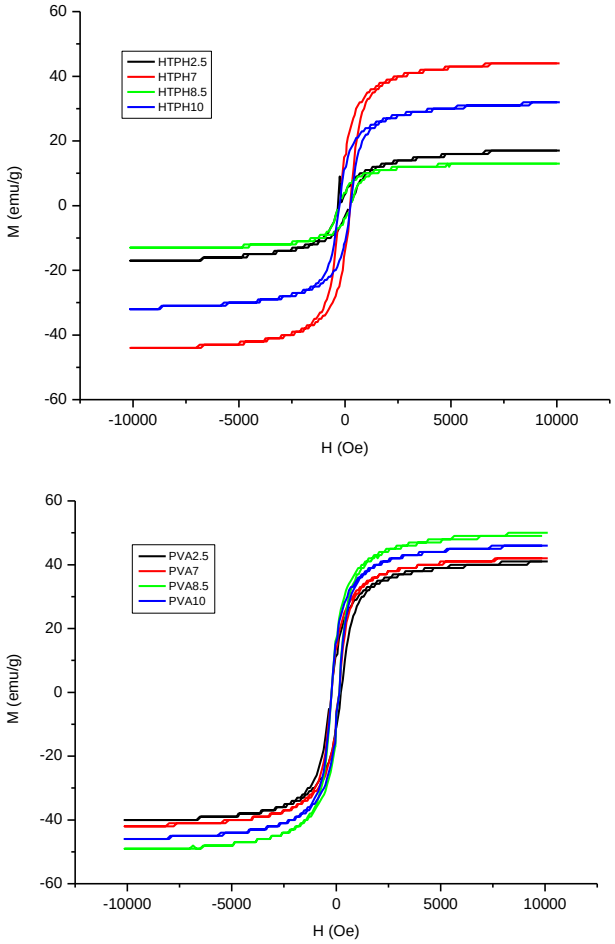

Figure 5. Hysteresis loops of the uncoated and PVA coated samples.

The magnetization of the samples increased on the formation of ferrimagnetic γ-Fe_2O_3 phase in the microstructure depending on the pHvalue of the solution fort he uncoated samples.

Table 2. Magnetic properties of the uncoated and PVA coated samples.

Sample	M_s (emu/g)	M_R (emu/g)	H_c (Oe)
HTPH-2.5	18.89	4.08	250.70
HTPH-7	44.85	15.94	247.65
HTPH-8.5	13.75	4.65	250.70
HTPH-10	32.33	11.91	267.05
PVA-2.5	41.60	12.05	239.06
PVA-7	42.46	14.04	224.22
PVA-8.5	50.33	17.39	226.72
PVA-10	46.61	15.85	219.96

PVA coated samples have higher saturation magnetization values between 41.60 – 50.33 emu/g, because ferrimagnetic γ-Fe_2O_3 phase was detected as major phase in the XRD diffraction patterns.

Conclusions

In this study, iron oxide nanoparticles have been produced by sol-gel method, in the X-Ray diffraction patterns ofthe samples, for the uncoated samples when pH value of the solution is adjusted to 2.5, α-Fe_2O_3 phase was detected as a single phase. When the solution was neutralized, γ-Fe_2O_3 was formed as the major phase in the

microstructure for the further increament of pH value, γ-Fe_2O_3 was formed as the secondary phase. In PVA coated samples, the γ-Fe_2O_3 phase was formed as the major phase. In this case, it can be concluded that the formation of the γ-Fe_2O_3 is sensitive to either the pH value of the solution or the capping agent.

The existence of ferromagnetic γ-Fe_2O_3 phase in the materials caused the M_s value to reach the highest value of 44.85 emu/g for the uncoated samples. This value increased to 50.33 emu/g measured in the sample of PVA8.5. For the uncoated samples, BET measurement indicated that specific surfase area, pore volume and average pore width are in the range of 40.10 – 32.2 m^2/g, 0.082 – 0.056 cm^3/g and 9.43 – 13.87 nm respectively. In the adsorption and desoption isotherms, desorption curves have steep clousers at about 0.4 relative pressure except for the sample HTPH8.5. Because pores are larger and open ended in the particles which causes adsorbate molecules to be desorbed easily from pores.

For the PVA coated samples, specific surface area is in the range of 15.73 – 20.81 m^2/g, the intervals of pore volume and average pore width are increased to 0.099 – 0.121 cm^3/g and 23.19 – 23.07 nm respectively. In the drug delivery, increase in pore volume provides carrying more drug in the particles.

Scientific Ethics Declaration

The author declares that the scientific ethical and legal responsibility of this article published in EPSTEM journal belongs to the author.

Acknowledgements or Notes

* This article was presented as an oral presentation at the International Conference on Basic Sciences, Engineering and Technology (www.icbaset.net) held in Alanya/Turkey on May 02-05, 2024.

References

Bandhu, A., Sutradhar, S., Mukherjee, S., Greneche, J.M., & Chakrabarti, P. K. (2015). Synthesis, characterization and magnetic property of maghemite (γ-Fe_2O_3) nanoparticles and their protective coating with pepsin for bio-functionalization. *Materials Research Bulletin, 70,* 145–154.

Behera, B. Pradhan, S., Samantaray, A., & Pradhan, D. (2020) Antiproliferative and cytotoxic activity of Hematite (α-Fe2O3) nanoparticles from Butea monosperma on MCF-7 cells. *African Journal of Pharmacy and Pharmacology*. *14,* 29–40.

Bhavani, P., Rajababu, C., Arif, M., Reddy, I.V.S., & Reddy, N.R. (2017). Synthesis of high saturation magnetic iron oxide nanomaterials via low temperature hydrothermal method. *Journal of Magnetism and Magnetic Materials, 426,* 459–466.

Bhuiyan, S.H., Miah, M.Y., Paul, S.C., Das Aka, T., Saha, O., Rahaman, M., Sharif, Habiba, J.I., & Ashaduzzaman O. (2020). Green synthesis of iron oxide nanoparticle using Carica papaya leaf extract: Application for photocatalytic degradation of remazol yellow RR dye and antibacterial activity. *Heliyon, 6*, e04603.

Ghosh, D., Majumder, S., & Sharma, P. (2020) Anticancerous activity of transition metal oxide nanoparticles. in: S.K. Saxena, S.M.P. Khurana (Eds.), *NanoBioMedicine,* 107–137.

Gonzalez-Moragas, L., Yu,S.-M., Murillo-Cremaes, N., Laromaine, A., & Roig, A. (2015). Scale-up synthesis of iron oxide nanoparticles by microwave-assisted thermal decomposition. *Chemical Engineering Journal, 281,* 87–95.

Guardia, P., Batlle-Brugal, B., A Roca,.G. Iglesias, O., Morales, M.D.P., Serna, C., Labarta, A., & Batlle, X. (2007). Surfactant effects in magnetite nanoparticles of controlled size. *Journal of Magnetism and Magnetic Materials, 316*, e756–e759.

Jain, T.K., Morales, M.A., Sahoo, S.K., Leslie-Pelecky,D.L., & Labhasetwar, V. (2005). Iron oxide nanoparticles for sustained delivery of anticancer agents. *Molecular Pharmaceutics, 2,* 194–205.

Javed, R., Zia, M., Naz, S., Aisida, S. O. Ain, N.ul & Ao. Q. (2020). Role of capping agents in the application of nanoparticles in biomedicine and environmental remediation: recent trends and future prospects. *Journal of Nanobiotechnology, 18*, 172.

Katsuki, H., & Komarneni, S. (2003). Role of α-Fe2O3 morphology on the color of red pigment for porcelain. *Journal of the American Ceramic Society, 86,* 183–185.

Kumari, S., Yadav, N., Ghosh, D., Srivastava, C., & Majumder, S. (2018). Role of polyvinyl pyrrolidone as a capping agent in the synthesis of magnetite (Fe3O4) nanoparticles. *Indian Journal of Chemistry A, 57*, 1151–1155.

LaGrow, A.P., Besenhard, M.O., Hodzic, A., Sergides, A., Bogart, L.K. Gavriilidis, A., & Thanh, N.T.K. (2019). Unravelling the growth mechanism of the co-precipitation of iron oxide nanoparticles with the aid of synchrotron X-Ray diffraction in solution. *Nanoscale, 11,* 6620–6628.

Lemine, O.M., Sajieddine, M., Bououdina, M., Msalam, R., Mufti, S., & Alyamani, A. (2010). Rietveld analysis and Mossbauer ¨ spectroscopy studies of nanocrystalline hematite α-Fe_2O_3. *Journal of Alloys and Compounds, 50*(2), 279–282.

Mahmoudi, M., Simchi, A., & Imani, M. (2010). Recent advances in surface engineering of superparamagnetic iron oxide nanoparticles for biomedical applications. *Journal of Iranian Chemical Society, 7*, 1–27.

Mornet, S., Portier, J., & Duguet, E. (2005). A method for synthesis and functionalization of ultrasmall super-paramagnetic covalent carriers based on maghemite and dextran. *Journal of Magnetism and Magnetic Materials, 293*, 127–134.

Okoli, C., Sanchez-Dominguez, M., Boutonnet, M., Järås, S., Civera, C., Solans, C., & Kuttuva,G.R. (2012). Comparison and functionalization study of microemulsion-prepared magnetic ıron oxide nanoparticles. *Langmuir, 28*(22), 8479–8485.

Predescu, A. M., Matei, E., Berbecaru, A. C., Pantilimon, C., Drăgan, C., Vidu, R., Predescu C., & Kuncser V. (2018). Synthesis and characterization of dextran-coated ıron oxide nanoparticles. *Royal Society Open Science, 5,* 171525.

Ramasami, P., Baabu S., Kumar, H. K., Gumpu, M. B., J. Babu, K, Kulandaisamy, A. J., & Rayappan, J. B. B. (2023). Iron oxide nanoparticles: a review on the province of ıts compounds, properties and biological applications. *Materials*, *16*(1), 59.

Rasheed, R.T., Al-Algawi, S.D., Kareem, H.H., & Mansoor, H.S. (2018). Preparation and characterization of hematite ıron oxide (α-Fe_2O_3) by sol-gel method. *Chemical Sciences Journal, 9*(4), 1000197.

Ravikumar, C., & Bandyopadhyaya, R. (2011). Mechanistic study on magnetite nanoparticle formation by thermal decomposition and coprecipitation routes. *The Journal of Physical Chemistry C*, *115* (5), 1380–1387.

Sharma, P., Dhiman,S., Kumari, S., Rawat, P., Srivastava, C., Sato, H., Akitsu, T., Kumar, S., Hassan, I., & Majumder, S. (2019). Revisiting the physiochemical properties of Hematite (α-Fe2O3) nanoparticle and exploring its bio-environmental application. *Materials Research Express*, *6*(9), 095072.

Sharma, P., Kumari, S., Ghosh, D., Yadav, V., Vij, A., Rawat, P., Kumar, S., Sinha, C., Saini, S., Sharma, V., Hassan, M. I., Srivastava, C. M., & Majumder, S. (2021). Capping agent-induced variation of physicochemical and biological properties of α-Fe_2O_3 nanoparticles. *Materials Chemistry and Physics*, *258*, 123899,

Tedeschi, L., & Enders, D. (2001). Asymmetric synthesis of β-phosphono malonates via Fe2O3- mediated phospha-michael addition to knoevenagel acceptors. *Organic Letters, 3*, 3515–3517.

Wang, L., Li, Z., Mao, G., Zhang, Y., & Lai, F. P. (2022). Effect of nanoparticle adsorption on the pore structure of a coalbed methane reservoir: A Laboratory Experimental Study. *ACS Omega, 7,* 6261−6270,

Woo, K., Lee, H.J., Ahn, J.P., & Park, Y.S (2003). Sol–gel mediated synthesis of Fe_2O_3 nanorods. *Advanced Materials, 15,* 1761–1764.

Author Information

Gulten Sadullahoglu
Mechatronics Engineering Department, Istanbul Health and Technology University, Türkiye
Contact e-mail: *gulten.sadullahoglu@istun.edu.tr*

To cite this article:

Sadullahoğlu, G. (2024). Optimization of properties of iron oxide nanoparticles synthized by Sol-Gel method. *The Eurasia Proceedings of Science, Technology, Engineering & Mathematics (EPSTEM), 28,* 565-574.

The Eurasia Proceedings of Science, Technology, Engineering & Mathematics (EPSTEM)
ISSN: 2602-3199

The Eurasia Proceedings of Science, Technology, Engineering & Mathematics (EPSTEM), 2024

Volume 28, Pages 575-580

ICBASET 2024: International Conference on Basic Sciences, Engineering and Technology

Investigation of the Antioxidant Capacity of *Taraxacum Officinale L.* Leaf Extract

Mehmet Erdem
Gaziantep University

Mehmet Ozaslan
Gaziantep University

Abstract: The aim of this study is to investigate the potent antioxidant capacities of *Taraxacum officinale* leaf extract. Asteraceae family, the genus Taraxacum is widespread in the Mediterranean countries, with approximately 2000 species worldwide. *Taraxacum officinale*, a species that stands out in phytotherapy, is a perennial plant with yellow flowers commonly found in the warm regions of Asia and Europe. Initially used in folk medicine for liver diseases, it has been observed over time that it is also used for various diseases such as dyspepsia and urinary system disorders. *T. officinale* contains numerous phenolic compounds contributing to antioxidant, anti-inflammatory, and antimicrobial activities. This research aimed to evaluate the antioxidant capacities of aqueous and ethanol-water extracts prepared from *T. officinale* leaves. Antioxidant capacities were assessed using spectrophotometric methods in DPPH, FRAP, and CuPRAC forms. The results showed that the DPPH, FRAP, and CuPRAC values were higher in the 50% ethanol extract of T. officinale leaves: 137.1 mg Trolox/g (DPPH method), 132.7 mg Trolox/g (FRAP method), and 409.9 mg Trolox/g (CuPRAC method). In conclusion, *Taraxacum officinale* leaves clearly demonstrate to be a rich source of polyphenols with high antioxidant properties. It has no seious side effect or toxicity. Considering its lack of serious side effects and toxicity, when formulated into herbal medicine, it could be effective in the treatment of various diseases, especially common liver and bile diseases, based on its biological activity studies.

Keywords: Taraxacum officinale, In vivo antioxidant, DPPH, FRAP, CUPRAC.

Introduction

The Asteraceae family is one of the largest families of flowering plants, comprising almost 1000 genera and approximately 20,000 species (Tanker et al., 1993). The genus Taraxacum consists of approximately 2000 species and is a member of the Asteraceae family. In a study, it was found that many subspecies belong to this genus, divided into approximately 30-57 varieties (Schutz et al., 2006). There are 45 species of this genus in Türkiye (Soest, 1975).

Traditionally used for many diseases for years (Schutz et al., 2006), it has also been observed clinically used (Blumenthal, 1998; ESCOP Monographs, 2003; WHO Monographs, 2007; PDR for Herbal Medicines, 2008) in diseases such as dyspepsia, liver, gallbladder, and urinary tract diseases, and *Taraxacum officinale* is seen to enter our lives today only as a dietary supplement in various forms. However, it is a plant with many bioactivities, especially strong anti-inflammatory, antioxidant, and hepatoprotective properties. When considering its side effects and toxicity, it no serious side effects or toxicity reported. In light of this information, it is evaluated that if it is converted into herbal medicine format, it can be effective in the treatment of many diseases, especially cancer, liver, and bile duct diseases, which are commonly seen today, due to its strong antioxidant, anti-inflammatory, anti-cancer, and hepatoprotective effects. According to the results of bioactivity studies conducted on the plant, *Taraxacum officinale* has been reported to have analgesic, antiallergic (Schutz et al., 2006), antidepressant (Li et al., 2014) , anti-inflammatory (ESCOP Monographs, 2003; Schutz et al., 2006 ;

WHO Monographs, 2007; Jeon et al., 2008; Koh et al., 2010; Awortwe et al., 2011; Zhang et al., 2012; Park et al., 2014, Piao et al., 2015), anti-hyperglycemic (ESCOP Monographs, 2003; Schutz et al., 2006), anticarcinogenic (Schutz et al., 2006; Sigstedt et al., 2008; Choi & Kim, 2009), antimicrobial (ESCOP Monographs, 2003; Astafieva et al., 2012; Astafieva et al., 2015; Rehman et al., 2016), antimutagenic (Di Giorgio et al., 2015), antioxidant (ESCOP Monographs, 2003; Schütz et al., 2006; Park et al., 2011; Colle et al., 2012; Park et al., 2014; Kenny et al., 2015; Yang et al.,2015; Lis and Olas, 2019;Majewski et al., 2020), antispermic (Tahtamouni et al., 2011; Tahtamouni ve ark., 2016), antithrombotic (ESCOP Monographs, 2003; Schutz et al., 2006), diuretic (ESCOP Monographs, 2003; Schütz et al., 2006 ; WHO Monographs, 2007;Clare et al., 2009), hypolipidemic(Zhang et al., 2008; Choi et al., 2010; Gonzalez et al., 2014; Kim et al., 2014), immunological(WHO Monographs,2007; Jinchun & Jie, 2011; Lee et al., 2012), choleretic (ESCOP Monographs, 2003; Schutz et al., 2006) , and prebiotic effects (Schutz et al., 2006), as well as hepatoprotective (Domitrović et al., 2010; Mahesh et al.,2010; Park et al., 2010; Colle et al., 2012;Gulfrazl et al., 2014; Hfaiedh et al.,2016), nephroprotective and neuroprotective properties it is used in hepatitis treatment. Extracts contain lipotropic substances that can improve the functionality of hepatocytes. Many other health benefits have been attributed to the use of T. officinale extracts or the plant itself.

T. officinale contains many phenolic compounds that contribute to antioxidant, anti-inflammatory, and antimicrobial activities (Park et al., 2011; Colle et al., 2012; Kenny et al., 2015; Martinez et al., 2015). In a study by Williams and colleagues, the flavonoid and phenolic fractions responsible for the bioactivity of *Taraxacum officinale* were comprehensively addressed (Williams et al., 1996). The main phytochemicals found in the plant can be listed as follows: carotenoids; flavonoids (e.g., quercetin, luteolin-7-glucoside); phenolic acids (e.g., caffeic acid, chlorogenic acid, chicoric acid); polysaccharides (e.g., inulin); sesquiterpene lactones (e.g., taraxinic acid, taraxacoside, 11p,13-dihydrolactucin, ixerin D); sterols (e.g., taraxasterol, β-sitosterol, stigmasterol); triterpenes (e.g., α-amyrin) (Singh et al., 2008; Amin Mir et al., 2013).

The aim of this study is to investigate the potent antioxidant capacity of *Taraxacum officinale* leaf extract using two different methods and to contribute to the natural prevention of oxidative stress, which is implicated in many diseases, in the future.

Materials and Methods

Plant Material: *Taraxacum officinale* in the leafy stage were collected from the Gaziantep Region, Türkiye, and the above-ground parts were harvested and washed before being dried in the shade.

Extraction Procedure: The dried plant samples were ground in the laboratory at room temperature using a laboratory grinder. The powdered sample (50 g of dandelion leaves) was weighed and extracted in 1 L of ethanol (96%) for two weeks at room temperature. The mixture was occasionally shaken during the waiting period. Then, it was filtered (Whatman No. 4 filter) and strained. After removing the solvent using a rotary evaporator, the extracts were stored at +4°C in a refrigerator (Colle et al., 2012).

Antioxidant Activity (AOA): Firstly, a DPPH solution was prepared for DPPH detection. For this purpose, 0.002 mg of DPPH was weighed and dissolved in 50 ml of methanol to prepare a DPPH solution with a final concentration of 0.2 mM.

The scavenging capacities of the extracts for the 1,1-diphenyl-2-picrylhydrazyl (DPPH) free radical were determined (Hatano et al., 1988). Addition of DPPH solution to the extracts results in a decrease in optical density absorbance at 517 nm, and the discoloration of the extracts indicates their radical scavenging activity (Baydar et al., 2011).

To test tubes containing 0.1 mg/100µl of extract solution, prepared DPPH solution (final concentration 0.2 mM) was added. For the control, 1.0 ml of dH_2O was added to the test tube instead of the extract. After incubating the samples at room temperature and in darkness for 30 minutes, absorbances were measured at 517nm. The free radical scavenging activity was calculated using the following equation:results were expressed as mM Trolox® equivalent (TE) per mg Trolox/g.

Percentage Inhibition was calculated using the following formula:

% Inhibition = [(AControl 517 nm - ASample 517 nm) / AControl 517 nm) x 100].
(AControl: absorbance of control and ASample: absorbance of the sample)

Ferric Reducing Antioxidant Power (FRAP):

The FRAP assay was performed according to Benzie and Strain (1996). The FRAP reagent was prepared by mixing 300 mM acetate buffer (pH 3.6), 10 mM 2,4,6-tripyridyl-s-triazine (TPTZ) solution, and 20 mM $FeCl_3 \cdot 6H_2O$ in a ratio of 10:1:1 immediately before use. The 300 mM acetate buffer was prepared by mixing 0.31 g sodium acetate trihydrate ($C_2H_3NaO_2 \cdot 3H_2O$) with 1.6 mL acetic acid and diluting to a final volume of 100 mL with distilled water. The TPTZ solution was prepared by dissolving 10 mM TPTZ in 40 mM HCl.

For the assay, 100 µL of extract was mixed with 900 µL of water and 2 mL of FRAP reagent. After incubating the mixture at room temperature in the dark for 30 minutes, the absorbances were measured against a blank at 593 nm. The results were expressed as mg Trolox equivalent (TE) per gram of sample.

Cupric Ion Reducing Antioxidant Capacity (CUPRAC):

The CUPRAC analysis was conducted according to the method described by Apak et al. (2004). In a test tube, 1 mL of $CuCl_2$ solution (0.01 M), neocuproine (7.5 mM), and 1 M ammonium acetate buffer (pH 7.0) solutions were added. After adding 0.1 mL of extract to the test tube, 1 mL of distilled water was added. All samples were then incubated in the dark at room temperature for 1 hour, and the absorbance values were measured at 450 nm. The results were expressed as mg Trolox equivalent (TE) per gram of sample.

Results

In our study, we decided to evaluate the antioxidant activities of T. officinale leaf ethanol extracts using two methods: a complex method based on both hydrogen atom transfer (HAT) and single electron transfer (SET) mechanisms (DPPH), and two methods based solely on the SET mechanism (FRAP and CUPRAC) (Table 1). The antioxidant activities of plant extracts are generally attributed to the presence of phenolic acids. Therefore, T. officinale's 50% ethanol extracts exhibited the highest antioxidant activities. Data regarding the DPPH radical scavenging activity and metal reduction activity of extracts obtained from T. officinale and their antioxidant activities determined in vitro are presented. These results express the total antioxidant capacity for each extract in mg Trolox/g (Table 1).

Table 1. Antioxidant activity in different extracts from *T. officinale*.

Extracts	Radical scavenging activity		Metal reducing activity	
	DPPH mg Troloks/g	EC_{50}, mg/ml	FRAP mg Troloks/g	CuPRAC mg Troloks/g
96% ethanol extract	28.8 ± 0.6	16.7	27.1 ± 0.6	95.9 ± 0.2
50% ethanol extract	137.1 ± 3.7	3.9	132.7 ± 2.3	409,9± 5.6
Water extract	57.1 ± 1.4	8.6	43.9 ± 3,4	186.7 ± 2.5
Standart				
Gallic acid		0.198		

Discussion

Extraction yield is a measure of the efficiency of the solvent in extracting specific components from raw materials. Considering our radical scavenging activity and EC50 values, it can be concluded that T. officinale exhibits strong antioxidant activity. Similarly, Paduret et al. found an inhibition capacity of 80.664% for T. officinale methanolic extract in a 50% DPPH solution. The ethanol extract of T. officinale flowers recorded 90.27 ± 0.5% inhibition at a concentration of 100 g/mL (Padureţ et al., 2016). In another study, an aqueous extract showed an IC50 value of 4.48 µg/mL, lower than our findings (Hu & Kitts, 2005). Tettey et al. reported T. officinale as a potent antioxidant in their study. García-Carrasco et al. detected the highest DPPH radical scavenging activity in leaf extract with an EC50 value of 1.9 µg/mL, consistent with our findings. Leaf extract provided the highest antioxidant capacity with a value of 302.3 ± 26.3 µmol TE/g, indicating good antioxidant activity in the FRAP assay (García-Carrasco et al., 2015). Furthermore, findings from González-Castejón et al. are consistent with our results (González-Castejón et al., 2012). The antioxidant activity of T. officinale is attributed to phenolic hydroxyl groups and activation of endogenous antioxidant enzymes (Park et al., 2014). Specifically applying Taraxacum officinale roots and leaves to rats leads to the development of an endogenous antioxidant profile (Kuntz & Kuntz, 2008; Harvey & Ferrier, 2017). Our results for antioxidant capacities using

the DPPH, FRAP, and CuPRAC methods for *Taraxacum officinale* leaf parts are consistent with previous findings.

Conclusion

In conclusion, Taraxacum officinale leaves clearly demonstrate being a rich source of polyphenols with potential application in scavenging free radicals and reducing metal. Upon consideration of side effects and toxicity, it appears to have no serious adverse effects or toxicity. Given the biological activity studies of this plant, if formulated into a herbal medicine, it could be effective in treating various diseases, particularly common liver and bile diseases.

Scientific Ethics Declaration

The authors declare that the scientific ethical and legal responsibility of this article published in EPSTEM journal belongs to the authors.

Acknowledgements or Notes

* This article was presented as an oral presentation at the International Conference on Basic Sciences, Engineering and Technology (www.icbaset.net) held in Alanya/Turkey on May 02-05, 2024.

References

Amin Mir M, Sawhney SS, &:Jassal MMS (2013). Qualitative and quantitative analysis of phytochemicals of Taraxacum ofcinale Wudpecker. *J. Pharm. Pharmocol*, *2* (1),001–005.

Apak, R., Guclu, K., Ozyurek, M., & Karademir, S. E. (2004). Novel total antioxidant capacity index for dietary polyphenols and vitamins C and E, using their cupric ion reducing capability in the presence of neocuproine: CUPRAC method. *Journal of Agricultural and Food Chemistry, 52*(26), 7970-7981.

Astafieva, A. A., Rogozhin, E. .A, Odintsova, T. I., Khadeeva, N. V., Grishin, E. V., & Egorov, T. A. (2012). Discovery of novel antimicrobial peptides with unusual cysteine motifs in dandelion taraxacum officinale Wigg. flowers. *Peptides, 36*(2), 266-271.

Astafieva, A. A., Enyenihi, A. A., Rogozhin, E. A., Kozlov, S. A., Grishin, E. V., Odintsova, T. I., Zubarev, R. A. , & Egorov, T. A. (2015). Novelproline-hydroxyproline glycopeptides from the dandelion (Taraxacum officinale Wigg.) flowers: de novo sequencing and biological activity. *Plant Science, 238,* 323-329.

Awortwe, C., Sackeyfio, A. C., Osei-Safo, D., Bugyei, K. A., & Asiedu-Gyekye, I. J. (2011). Dual effect of Taraxacum officinale leaves: Anticholinergic and inhibitory effect on inflammatory cells in ovalbumin-sensitized guinea-pigs. *African Journal of Pharmacy and Pharmacology, 5*(23), 2613-2619.

Baydar, N.G., Babalık Z, Türk, F.H., Cetin, E.S.(2011). Phenolic composition and antioxidant activities of wines and extracts of some grape varieties grown in Turkey. *Journal of Agricultural Sciences, 17*, 67-76.

Benzie, I. F. F., & Strain, J. J. (1996). The ferric reducing ability of plasma (FRAP) as a measure of "antioxidant power": The FRAP Assay. *Analytical Biochemistry, 239*(1), 70–76.

Blumenthal, M. (1998). *The complete german comission e monographs*. Boston:Theraupeutic Guide to Herbal Medicines, 118-120.

Choi, E. J.,& Kim, G. H. (2009). Dandelion (Taraxacum officinale) flower ethanol extract inhibits cell proliferation and induces apoptosis in human ovarian cancer SK-OV-3 cells. *Food Scıence and Bıotechnology, 18*(2), 552-555.

Choi, U. K., Lee, O. H., Yim, J. H., Cho, C. W., Rhee, Y. K., Lim, S. I., & Kim, Y. C. (2010). Hypolipidemic and antioxidant effects of dandelion (Taraxacum officinale) root and leaf on cholesterol-fed rabbits. *Internatıonal Journal of Molecular Scıences, 11*(1), 67-78.

Clare, B. A., Conroy, R. S., &Spelman, K. (2009). The diuretic effect in human subjects of an extract of Taraxacum officinale folium over a single day. *Journal of Alternative and Complementary Medicine, 15*(8), 929-934.

Colle, D., Arantes, L. P., Gubert, P., da Luz, S. C. A., Athayde, M. L., Teixeira Rocha, J. B., & Soares, F. A. A. (2012). Antioxidant properties of Taraxacum officinale leaf extract are involved in the protective effect against hepatoxicity induced by acetaminophen in mice. *Journal of Medicinal Food, 15*(6), 549-556.

Colle, D., Arantes, L. P., Rauber, R., de Mattos, S. E. C., da Rocha, J. B. T., Nogueira, C. W., & Soares, F. A. (2012). Antioxidant properties of Taraxacum officinale fruit extract are involved in the protective effect against cellular death induced by sodium nitroprusside in brain of rats. *Pharmaceutıcal Biology, 50*(7), 883-891.

Didier, F., Catherine, F., Odile, T., & Jean-Louis, L. (2011). Caffeoyl derivatives: major antioxidant compounds of some wild herbs of the Asteraceae family. *Food and Nutrition Sciences*, *2*(3), Article ID: 4889

Di Giorgio C, Boyer L, De Meo M, Laurant C, Elias R, Ollivier E. (2015).In vitro and in vivo antimutagenic effects of DIG, a herbal preparation of Berberisvulgaris, Taraxacum officinale and Arctium lappa, against mitomycin C. *Journal of Natural Medicines, 69*(3), 267-277.

Domitrović, R., Jakovac, H., Romić, Z., Rahelić, D., & Tadić, Z. (2010). Antifibrotic activity of Taraxacum officinale root in carbontetrachloride-induced liver damage in mice. *Journal of Ethnopharmacol, 130*(3), 569-577.

ESCOP Monograph. (2003).*The scientific foundation for herbal medicinal products* (2nd ed., pp. 499-502). Stuttgard: Thieme.

García-Carrasco, B., Fernandez-Dacosta, R., Dávalos, A., Ordovás, J. M., & Rodriguez-Casado, A. (2015). In vitro hypolipidemic and antioxidant effects of leaf and root extracts of Taraxacum officinale. *Medical Sciences, 3*(2), 38-54.

González-Castejón, M., Visioli, F., & Rodriguez-Casado, A. (2012). Diverse biological activities of dandelion. *Nutrition Reviews, 70*(9), 534-547.

Gulfrazl, M., Ahamd, D., Ahmad, M. S., Qureshi, R., Mahmood, R. T., Jabeen, N., & Abbasi, K. S. (2014). Effect of leaf extracts of *Taraxacum officinale* on CCl4 induced hepatotoxicity in rats, in vivo study. *Pakıstan Journal of Pharmaceutıcal Sciences, 27(4),* 825-829.

Han, H., He, W., Wang, W., & Gao, B. (2011) Inhibitory effect of aqueous dandelion extract on HIV-1 replication and reverse transcriptase activity. *BMC Complement Altern Med 11*:112

Harvey, R. A., & Ferrier, D. R. (2017). *Lippincott's illustrated reviews: biochemistry*. Lippincott Williams & Wilkins.

Hatano, T., Kagawa, H., Yasuhara, T., & Okuda, T. (1988). Two new flavonoids and other constituents in licorice root; their relative astringency and radical scavenging effects. *Chemical and Pharmaceutical Bulletin, 36,* 2090–2097.

Hfaiedh, M., Brahmi, D., & Zourgui, L. (2016). Hepatoprotective effect of taraxacum officinale leaf extract on sodium dichromate-induced liver injury in rats. *Envıronmental Toxıcology, 31*(3), 339-349.

Hu, C., & Kitts, D. D. (2005). Dandelion (Taraxacum officinale) flower extract suppresses both reactive oxygen species and nitric oxide and prevents lipid oxidation in vitro. *Phytomedicine, 12*(8), 588-597.

Jeon, H. J., Kang, H. J., Jung, H. J., Kang, Y. S., Lim, C. J., Kim, Y. M., & Park, E. H. (2008). Anti-inflammatory activity of Taraxacum officinale. *Journal of Ethnopharmacology, 115*(1), 82-88.

Jinchun, Z., & Jie, C. (2011). The effects of Taraxacum officinale extracts (TOE) supplementation on physical fatigue in mice. *African Journal of Traditional, Complementary and Alternative Medicines*, *8*(2).

Kenny, O., Smyth, T.J., Hewage, C.M., & Brunton, N. P. (2015). Quantitative UPLC-MS/MS analysis of chlorogenic acid derivatives in antioxidant fractionates from dandelion (Taraxacum officinale) root .*Internatıonal Journal of Food Scıence and Technology, 50*(3), 766-773.

Kim, J. J., Park, C. M., Kim, M. J., Cho, C. W., & Song, Y. S. (2014). Hypolipidemic effect of dandelion (Taraxacum officinale) extracts via fecal lipid excretion in C57BL/6 mice fed an atherogenic diet. *Food Scıence and Bıotechnology, 23*(3), 841-847.

Koh, Y. J., Cha, D. S., Ko, J. S., Park, H. J., & Choi, H. D. (2010). Anti-ınflammatoryeffect of taraxacum officinale leaves on lipopolysaccharide-ınduced ınflammatory responses in RAW 264.7 cells. *Journal of Medıcınal Food, 13*(4), 870-878.

Kuntz, E., & Kuntz, H. D. (2009). *Hepatology: Textbook and atlas*. Springer Science & Business Media.

Li, Y. C., Shen, J. D., Li, Y. Y., & Huang, Q. (2014). Antidepressant effects of the water extract from taraxacum officinale leaves and roots in mice. *Pharmaceutical Biology, 52*(8), 1028-1032.

Lis, B., & Olas, B. (2019). Pro-health activity of dandelion (Taraxacum officinale L.) and its food products–history and present. *Journal of Functional Foods, 59,* 40-48.

Mahesh, A., Jeyachandran, R., Cindrella, L., Thangadurai, D., Veerapur, V.P., & Rao, D. M. (2010). Hepatocurative potential of sesquiterpenelactones of Taraxacum officinale on carbontetrachloride induced liver toxicity in mice. *Acta Bıologıca Hungarıca, 61*(2), 175-190.

Majewski, M., Lis, B., Juśkiewicz, J., Ognik, K., Borkowska-Sztachańska, M., Jedrejek, D., & Olas, B. (2020). Phenolic fractions from dandelion leaves and petals as modulators of the antioxidant status and lipid profile in an in vivo study. *Antioxidants, 9*(2), 131.

Martinez, M., Poirrier, P., Chamy, R., Prufer, D., Schulze-Gronover, C., Jorquera, L., & Ruiz, G. (2015). Taraxacum officinale and related species-an ethnopharmacological review and its potential as a commercial medicinal plant. *Journal of Ethnopharmacology, 169,* 244-262.

Pădureţ, S. E. R. G. I. U., Amariei, S., Gutt, G., & Piscuc, B. (2016). The evaluation of dandelion (Taraxacum officinale) properties as a valuable food ingredient. *Romanian Biotechnological Letters, 21*(3), 11569-11575.

Park, C. M., Cho, C. W., & Song, Y. S. (2014). Top 1 and 2, polysaccharides from taraxacum officinale, inhibit NF kappa B-mediated inflammation and accelerate Nrf2-induced antioxidative potential through the modulation of PI3K-Akt signaling pathway in RAW 264.7cells. *Food and Chemıcal Toxıcology ,66*,56-64.

Park, C. M., Park, J. Y., Noh,. K. H., Shin, J. H., & Song, Y. S. (2011a).Taraxacum officinale weber extracts inhibit lps-induced oxidative stres and nitric oxide production via the nf kappa b modulation in RAW 264.7 cells. *Journal of Ethnopharmacology, 133*(2), 834-842.

Park, C. M., Youn, H .J., Chang, H. K, & Song, Y. S. (2010). TOP 1 and 2 polysaccharides from Taraxacum officinale, attenuate CCl4-induced hepatic damage through the modulation of NF kappa B and its regulatory mediators. *Food and Chemıcal Toxıcology,48*(5), 1255-1261.

Anonymous. (2008).*PDR for herbal medicines* (2nd ed., pp.252-254). Montvale, New Jersey: Medical Economics Company.

Piao, T., Ma, Z., Li, X., & Liu, J. (2015). Taraxasterol inhibits IL-1β-induced inflammatory response in human osteoarthritic chondrocytes. *European Journal of Pharmacology, 756,* 38-42.

Rehman, M. U., & Rather, I. A. (2019). Myricetin abrogates sisplatin-induced oxidative stress, inflammatory response, and goblet cell disintegration in colon of wistar rats. *Plants, 9*(1), 28.

Schütz, K., Carle, R., Schieber, A. (2006). Taraxacum--a review on its phytochemical and pharmacological profile. *Journal of Ethnopharmacology,107*(3), 313-323.

Singh,. A, Malhotra, S., Subban, R. (2008) Dandelion (Taraxacum officinale) - hepatoprotective herb with therapeutic potential. *Pharmacogn Rev. 2* (3), 163–167.

Sigstedt, S. C., Hooten, C. J., Callewaert, M. C., Jenkins, A. R., Romero, A. E., Pullin, M. J., Kornienko, A., Lowrey, T. K., Slambrouck, S. V., & Steelant, W. F. (2008). Evaluation of aqueous extracts of taraxacum officinale on growth and invasion of breast and prostate cancer cells. *International Journal of Oncology, 32*(5), 1085-1090.

Soest J. L. Van, (1975).Taraxacum wiggers. D. PH.(Ed.). In *Flora of tTurkey and the East Aegean islands* (Vol. 5, pp.788-812). Univeristy Press: Edinburg.

Tahtamouni, L. H., Alqurna, N. M., Al-Hudhud, M. Y., & Al-Hajj, H. A. (2011). Dandelion (Taraxacum officinale) decreases malerat fertility in vivo. *Journal of Ethnopharmacol, 135*(1), 102-109.

Tahtamouni, L. H., Al-Khateeb, R. A, Abdellatif, R. N., Al-Mazaydeh, Z. A., Yasin, S. R., Al- Gharabli, S., & Elkarmi, A. Z. (2016). Anti-spermatogenic activities of Taraxacum officinale whole plant and leaves aqueous extracts. *Veterinary Research Forum, 7*(2), 89-97.

Tanker, N., Koyuncu, M., & Coşkun, M. (1993). *Farmasötik botanik*. Ankara Üniversitesi Eczacılık Fakültesi Yayınları, No.70.

Tettey, C. O., Ocloo, A., Nagajyothi, P. C., & Lee, K. D. (2014). Antioxidant activity of solvent fractions of taraxacum officinale (dandelion) leaves. *Journal of Herbs, Spices & Medicinal Plants, 20*(4), 329-340.

Trojanova, I., Rada, V., Kokoška, L., & Vlkova, E. (2004). The bifidogenic effect of Taraxacum officinale root. *Fitoterapia, 75*(7-8), 760-763.

Williams, C. A., Goldstone, F., & Greenham, J. (1996). Flavonoids, cinnamic acids and coumarins from the different tissues and medicinal preparations of taraxacum officinale. *Phytochemistry, 42*(1), 121-127.

WHO Monographs on Selected Medicinal Plants. (2007). *Spain,* (Vol. 3 ,pp.328-338).

Zhang, J., Kang, M. J., Kim, M.J., Kim, M. E., Song, J. H., Lee, Y. M., Kim, J. I. (2008). Pancreatic lipase inhibitory activity of taraxacum officinale in vitro and in vivo. *Nutrition Research and practice, 2*(4), 200-203.

Zhang, X., Xiong, H., & Liu, L. (2012). Effects of taraxasterol on inflammatory responses in lipopolysaccharide-induced RAW 264.7 macrophages. *Journal of Ethnopharmacology, 141*(1), 206-21

Author Information

Mehmet Erdem
Department of Health Services Vocational School, Gaziantep University, 27310, Gaziantep-Türkiye,
Contact e-mail: *merdem@gantep.edu.tr*

Mehmet Ozaslan
Department of Biology, Gaziantep University, 27310, Gaziantep-Türkiye,
Contact e-mail: *ozaslanmd@gantep.edu.tr*

To cite this article:

Erdem, M. & Ozaslan, M.. (2024). Investigation of the antioxidant capacity of *Taraxacum officinale l.* leaf extract. *The Eurasia Proceedings of Science, Technology, Engineering & Mathematics (EPSTEM), 28,* 575-580.

The Eurasia Proceedings of Science, Technology, Engineering & Mathematics (EPSTEM)
ISSN: 2602-3199

The Eurasia Proceedings of Science, Technology, Engineering & Mathematics (EPSTEM), 2024

Volume 28, Pages 581-585

ICBASET 2024: International Conference on Basic Sciences, Engineering and Technology

A Comparative Analysis of the Opportunities and Challenges Associated with Building Information Modeling Implementation in Jordan and Kuwait

Samaher Asaad
Al-Zaytoonah University of Jordan

Akram Suleiman
Al-Zaytoonah University of Jordan

Abstract: Building Information Modeling (BIM) utilizes a multifaceted computer software data model to document building designs, simulate construction, and manage the operations of new facilities. This research aims to investigate the adoption of BIM in the Jordanian and Kuwaiti construction sectors. To achieve this objective, the research commenced with a comprehensive literature review on global and Middle Eastern BIM adoption, identifying the benefits and challenges of BIM in the construction industry. Subsequently, an exploratory study was conducted using an online survey to assess the current level of BIM expertise and characterize the perceived advantages and barriers associated with BIM implementation. The current state of BIM implementation in Jordan and Kuwait can be characterized as lagging behind. The study shows there is more awareness of BIM applications, programmes, and benefits in Jordan than Kuwait. The study identified and compared several barriers to BIM adoption in Jordan and Kuwait, including: Lack of government support, Lack of effective collaboration among project stakeholders, Lack of demand for BIM.

Keywords: Building Information Modeling (BIM), Construction industry, Civil engineering

Introduction

Building information modelling, or BIM, is a quickly developing idea in the field of building project management, and its development has had a significant impact on the highly fragmented construction sector. Even if there are many software programmes available today that support the idea of BIM, an increasing number of businesses are turning to applied research fields in order to profit from the use of BIM (Gerges et al., 2016). Even while utilising BIM for a project has many advantages, there are still a lot of obstacles preventing its widespread adoption in the construction sector. The cost of implementation, a lack of client demand, a lack of confidence in the integrity of BIM, a lack of standards for the description of BIM objects and a coding system, contract/legal issues and uncertainties, skills shortages, and the inability of firms to adapt to such a change due to cultural and financial factors are some of the barriers that Aibinu and Venkatesh (Aibinu and Venkatesh, 2014) identified in their research on the status of BIM adoption and the BIM experience of cost consultants in Australia.

Few studies have also looked into the obstacles that the Jordanian building industry faces when implementing BIM. Al Awad (2015) looked into the process, technical, and human factors that prevent SMEs from using BIM. These factors include poor educational attainment, a lack of knowledge and skills, training, and culture. According to Matarneh and Hamed (2017), the major obstacles impeding the adoption of BIM in the Jordanian building industry are the lack of incentives and support from construction policymakers, the unavailability of BIM standards and codes, lack of awareness, lack of client demand, resistance to change, lack of a BIM

specialist in Jordan, lack of necessary training, and the cost of BIM, which includes software, hardware upgrades, training, and time. Matarneh and Hamed (2017) did not, however, look at the connections between BIM barriers.

In Kuwait, the need for housing is growing, and this is turning into one of the main problems the nation is facing. In order to address Kuwait's housing crisis, effective building designs and construction techniques are essential (Nawari & Alsaffar, 2017). Gerges et al. (2016) showed that by promoting cooperation between project participants, practitioners saw enhanced communication and reduced project risks. It was also noted that in order for BIM to be fully implemented in the State of Kuwait, there will need to be a concentrated effort made to persuade clients to want BIM, overcome reluctance to change among construction industry professionals, and provide additional training for design team members. According to Umar (2022) the four primary areas of "organisation," "technical," "government and legal," and "environment" comprise the top challenges. Nawari and Alsaffar (2016) navigated Kuwaiti universities' and institutes' present BIM education situation. Additionally, an educational framework for the introduction of BIM courses in Kuwait was designed. The study also concentrated on establishing goals and content specifications for different college course levels. Previous study Nawari and Alsaffar (2017) proposed a new BIM-based permitting procedure. By utilising building information found in structural and architectural models, as well as programming tools found in BIM software applications, the proposed approach demonstrates how a BIM-based compliance checking framework holds the potential to optimise and streamline Kuwait's residential building codes conformance checks.

In order to enable the construction industry to concentrate on these barriers and guarantee that BIM is accepted efficiently, this article focuses on identifying the major obstacles to the adoption of BIM in Jordan and Kuwait. In addition, this article conducts a critical investigation to determine the obstacles facing BIM using a survey, and a review of the literature throughout the Jordanian and Kuwaiti construction sector. The selection of these two countries was based on the fact that they reflect different economic environments in the Middle East. Jordan is categorised as a low-income country under the 2021 IWA Country Classification, which puts Kuwait, a high-income country, in sharp contrast (Asaad & Suleiman, 2023).

Materials and Methods

The purpose of this study is to look into how BIM is currently used in Jordan and Kuwait construction sector. In order to determine the present degree of BIM expertise and to characterise the perceived value, benefits, and obstacles facing BIM deployment, an exploratory study was subsequently carried out utilising a structured online survey that was created based on the literature analysis. In order to capture the present state of practice in Jordan and Kuwait on the use and implementation of BIM, the questionnaire was created to be straightforward, easy to understand, and specific.

Results and Analysis

The study's sample comprises architects, engineers, and contractors who work in the Jordanian and Kuwaiti AEC construction sectors. The questionnaire results are shown in the following subsections.

Respondents' Profiles

Table 1. The survey participants' demographics.

Demography	Respondents	Frequency
Type of respondents organization	Clients	17
	Consultants	33
	Contractors	37
	Others	7
Qualification of respondents	Civil Engineer	55
	Mechanical Engineer	8
	Architecture	13
	Electrical Engineer	14
	Others	4
Country of respondents	Jordan	58
	Kuwait	36

As shown in Table 1, there were 94 full replies to the survey. A total of 13 architects (13.8%), 55 Civil engineers (58.5%), 14 Electrical engineers (14.8%) and 8 Mechanical engineers (8.5%); 37 contractors (39.4%), 33 consultant (35.1%), and 17 clients (18.1). Thus, the survey's respondent distribution was not normally distributed, indicating that Engineers especially civil engineers are the group most interested in take part in surveys and increase your BIM knowledge.

Respondents' Experience of BIM

By asking respondents about their Knowledge about using the BIM application, the level of BIM awareness among the respondents was ascertained. As shown in table 2 only 29.8% of respondents' were answered with ''very strong'' and ''strong'', the bulk of respondents (41.5%) had < 25% ratio of BIM use during work, indicating that the present experience with BIM is still quite low. The responders who have worked with BIM with 25% to 50% (25.5%), came after these. According to the data, the responders with over 50% ratio of BIM use during work the lowest response rate (20.8%). Evidently, Jordan and Kuwait are still in the very early stages of BIM adoption. This result was consistent with the finding that the majority of respondents have little awareness of BIM.

Table 2. BIM awareness among the respondents.

''Ratio of BIM use during work''						
	<25%	25%TO 50%	50% to 75%	>75%%	Total	
Jordan	25	12	13	7	57	
Kuwait	14	12	5	4	35	
Total	39	24	18	11	92	
consultant	11	8	9	5	33	
Contractor	19	8	7	2	36	
Client	4	6	2	4	16	
Others	5	2			7	
Total	39	24	18	11	92	
''Knowledge about using the BIM application''						
	Very weak	Weak	Average strength	Strong	Very Strong	Total
Jordan	17	7	15	9	10	58
Kuwait	9	6	12	5	4	36
Total	26	13	27	14	14	94
consultant	5	5	9	8	6	33
Contractor	13	5	11	4	4	37
Client	5	2	5	2	3	17
Others	3	1	2		1	7
Total	26	13	27	14	14	94

Table 3. The mean of BIM awareness questions.

Question/ Country	Ratio of BIM use during work ''1.00 = "<25%" , 2.00 = "25%TO 50%"; 3.00 = 50% to 75%; 4.00= >75%	Knowledge about using the BIM application''1.00 = "very weak" , 2.00 = "weak"; 3.00 = ''average strength'';, 4.00= ''strong'', 5:00= ''very strong''
Jordan	2.04	2.79
Kuwait	1.97	2.69
Total	2.01	2.76
Type of organization or company		
consultant	2.24	3.15
Contractor	1.78	2.49
Client	2.38	2.76
Others	1.29	2.29
Total	2.01	2.76

The mean ratio of BIM use during work in Jordan is 2.04, or "25% - 50%," as table 3 illustrates for the question "Ratio of BIM use during work", this implies that a sizable fraction of Jordanian respondents are utilizing BIM technology at work. Conversely, Kuwait's mean ratio for using BIM in construction is 1.97, or "less than 25%". This implies that Kuwait does not use BIM technology to the same extent as Jordan does. The mean level of

knowledge about using BIM applications in Jordan is 2.79, which is equivalent to "weak". This suggests that respondents in Jordan have a moderate level of knowledge about using BIM applications. The mean level of knowledge about using BIM applications in Kuwait is 2.69, which is equivalent to "weak". This suggests that respondents in Kuwait have a similar level of knowledge about using BIM applications as respondents in Jordan. It's interesting to note that when various business types are examined, general contractors have the least amount of ratio of BIM use during work, according to type of organization or company, The mean ratio of BIM use during work for the clients was have the maximum mean followed by the consultants with values 2.38 and 2.24 respectively which is equivalent to "25%- 50%", where the contractor mean was 1.78 which is equivalent to'' <25%''. The mean level of knowledge about using BIM applications in Consultants group is 3.15, which is equivalent to "average strength". This suggests that respondents in Consultants group a moderate level of knowledge about using BIM applications. The mean level of knowledge about using BIM applications in Client and contractor groups are 2.76 and 2.49 respectively, which is equivalent to "weak".. This suggests that respondents in consultants group have higher level of knowledge about using BIM applications as respondents other groups.

Jordan and Kuwait's Barriers and Difficulties with BIM Implementation

Every new technology has various difficulties during introduction before being fully utilised. This study also looked into obstacles to BIM implementation in Jordanian and Kuwaiti AEC construction projects. As seen in Table 4, respondents cited a number of obstacles that are crucial for BIM adoption in Jordan and Kuwait, ranging from technical problems to more subjective considerations. Table 4 demonstrates that three of the top five factors that have the greatest impact on the deployment of BIM were the same in both nations. Inadequate government legislation to fully support BIM implementation was one of the top three barriers for both nations that concurred with the results of study was performed in Jordan by Matarneh and Hamed (2017). Matarneh and Hamed, (2017) smaller business owners typically don't have these demands, even if the Jordanian government is currently implementing BIM for specific public projects. In fact, smaller enterprises are more likely to oppose technological advancements (Matarneh and Hamed, 2017). The other two common barriers were related to shortage of BIM expertise and the shortage of effective communication among project stakeholders, The Jordanian construction industry has to enhance its current communication status because poor communication is a common problem in the sector (Suleiman et al., 2023). '' Clients' lack of desire and interest in utilising BIM technology for project design and construction'' was top one in Jordan, but ranked nine in Kuwait. '' Small businesses lack the funding to establish a new workflow, which is essential for the successful implementation of BIM'' was ranked 2 and 9 in Kuwait and Jordan respectively.

Table 4. A ranking of barriers to using BIM.

Country	Jordan		Kuwait	
Barriers	Mean	Rank	Mean	Rank
Clients' lack of desire and interest in utilising BIM technology	3.48	1	2.62	9
lack of effective communication among project stakeholders	3.47	2	2.69	5
Inadequate government legislation to support BIM implementation	3.43	3	3.11	1
Lake of participants with expertise in BIM application	3.29	4	2.81	3
The absence of concern for the building's long-term maintenance	3.27	5	2.63	8
Organisations may oppose any changes to new technology.	3.17	6	2.67	6
Engineers often hesitant to learn new applications.	3.14	7	2.53	11
Absence of BIM-savvy architects and engineers	3.13	8	2.81	4
Small businesses lack the funding to establish a new workflow	3.09	9	2.94	2
A lack of understanding of BIM among relevant parties	3.04	10	2.50	12
not providing BIM instruction or training in universities	2.96	11	2.67	7
Experts believe that various traditional programmes fulfil the requirement and finishing the project.	2.91	12	2.57	10

Conclusion

The Design, Construction, and Operation (DECO) industry, as well as the Architectural and Construction Engineering industry, share a vast amount of knowledge regarding Building Information Modelling (BIM). In the Middle East, BIM adoption and implementation have grown more slowly than in previous studies. The study determined the awareness and the main obstacles to BIM adoption in Jordan and Kuwait, including: "The lack of government support"; "Lack of communication between the stakeholders"; and "Lack of demand for BIM. In

a similar vein, therefore, it follows that the Jordanian and Kuwaiti government ought to make a concerted effort to develop a roadmap and establish regional BIM standards and regulations at the procedural as well as organisational levels The study shows there is more awareness of BIM applications, programmes, and benefits in Jordan than Kuwait.

Recommendations

This study is an initial step towards comprehending Jordan's and Kuwait present state of BIM deployment. However, it offers a standard for upcoming research that should address other avenues further. Also, for the both countries consultants group have higher level of knowledge about using BIM applications than the contractor and clients groups.

Scientific Ethics Declaration

The authors declare that the scientific ethical and legal responsibility of this article published in EPSTEM Journal belongs to the authors.

Acknowledgements or Notes

* This article was presented as an oral presentation at the International Conference on Basic Sciences, Engineering and Technology (www.icbaset.net) held in Alanya/Turkey on May 02-05, 2024.

References

Aibinu, A., & Venkatesh, S. (2014). Status of BIM adoption and the BIM experience of cost consultants in Australia. *Journal of Professional Issues in Engineering Education and practice*, *140*(3), 04013021.

Al Awad, O. (2015). *The uptake of advanced IT with specific emphasis on BIM by SMEs in the Jordanian construction industry.* (Doctoral dissertation, University of Salford United Kingdom).

Asaad, S., & Suleiman, A. (2023). Socio-demographic factors and treated wastewater reuse in the MENA region: Insights and implications. *Desalination*, *565*, 116830.

Gerges, M., Ahiakwo, O., Jaeger, M., & Asaad, A. (2016). Building Information Modeling and its application in the state of Kuwait. *International Journal of Civil, Environmental, Structural, Construction and Architectural Engineering*, *10*(1), 81-86.

Matarneh, R., & Hamed, S. (2017). Barriers to the adoption of building information modeling in the Jordanian building industry. *Open Journal of Civil Engineering*, *7*(3), 325-335.

Nawari, N. O., & Alsaffar, A. (2017). The role of BIM in simplifying construction permits in Kuwait. In AEI 2017 (pp. 855-866).

Nawari, N. O., & Alsaffar, A. (2016). Planning and development of bim curriculum for Kuwait. *Journal of Civil Engineering and Science (JCES)*, *5*(1), 15-32.

Suleiman, A., Almasaeid, H., Hussein, N., & Abahre, J. (2023). Addressing the causes and effects of poor communication in the jordanian construction industry: a study on improving project performance. *Civil and Environmental Engineering*, *19*(1), 156-166.

Umar, T. (2022). Challenges of BIM implementation in GCC construction industry. *Engineering, Construction and Architectural Management*, *29*(3), 1139-1168.

Author Information

Samaher Asaad
Al-Zaytoonah University of Jordan, Amman, Jordan
Contact e-mail: *2968@zuj.edu.jo*

Akram Suleiman
Al-Zaytoonah University of Jordan, Amman, Jordan

To cite this article:
Asaad, S.A. & Suleiman, A.S. (2024). A comparative analysis of the opportunities and challenges associated with building information modeling implementation in Jordan and Kuwait. *The Eurasia Proceedings of Science, Technology, Engineering & Mathematics (EPSTEM)*, *28*, 581-585.